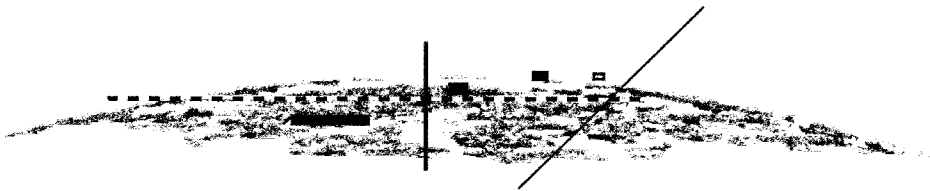


GEOFORSCHUNGSZENTRUM POTSDAM
STIFTUNG DES ÖFFENTLICHEN RECHTS

Scientific Technical Report

ISSN 1610-0956



GEOFORSCHUNGSZENTRUM POTSDAM
STIFTUNG DES ÖFFENTLICHEN RECHTS

Peter Bormann (Editor)

International
Training Course 1999 on

**Seismology
Seismic Hazard Assessment
and Risk Mitigation**

Lecture and exercise notes

Volume I

Scientific Technical Report STR99/13

Imprint

Edited by:

Peter Bormann
GeoForschungsZentrum Potsdam
Telegrafenberg
D-14473 Potsdam, Germany

Printed in Potsdam, Germany
August 1999

The International Training
Course on "Seismology, Seismic Hazard
Assessment and Risk Mitigation" was
held in Beijing, China
26 September to 30 October, 1999

It was sponsored by:

- GeoForschungsZentrum
Potsdam (GFZ)
- China Seismological Bureau
(CSB)
- Federal Foreign Office (AA), Bonn
- Federal Ministry of Economical
Co-Operation and Development
(BMZ), Bonn
- Carl Duisberg Gesellschaft (CDG),
Regional Office of the State of
Brandenburg in Berlin
- Secretariat of the International
Decade for Natural Disaster
Reduction (IDNDR), Geneva
- United Nations Educational, Scientific
and Cultural Organization (UNESCO),
Paris
- International Association of Seismology and
Physics of the Earth's Interior (IASPEI)

Lecture and exercise notes, Volume I

International
Training Course 1999

on

**Seismology, Seismic Hazard Assessment
and Risk Mitigation**

Beijing, China, 26 September to 30 October

jointly organized by
GeoForschungsZentrum Potsdam (GFZ)
China Seismological Bureau (CSB)

Supported by
Carl Duisberg Gesellschaft (CDG)

co-sponsored by
AA (Bonn), BMZ (Bonn), CDG (Berlin), IASPEI,
IDNDR Secretariat (Geneva), UNESCO (Paris)

Peter Bormann
Editor

Scientific Technical Report STR99/13

CONTENTS

	Page
Foreword by the editor	1
 1. <u>Basics of seismometry, seismic data acquisition and exchange</u>	
Fundamentals of seismometry	Ch. Teupser † 3
Constructing response curves - an introduction to the Bode-diagram	J. Bribach 18
Exercise on plotting seismograph response (Bode-diagram)	J. Bribach 25
Exercise on estimating seismometer parameters by STEP transition	J. Bribach 26
Calibration by harmonic drive	Ch. Teupser † 31
Influence of the frequency characteristic of the seismograph on its seismic recordings	P. Bormann 32
Principles of acquisition, handling and storage of digital seismological data	J. Bribach 40
Seismic data acquisition and analysis	M. Baumbach 57
Demonstration of different digital data acquisition systems together with seismometers for mobile and stationary use - strong-motion recordings and display of the collected data	Zhang Wenbo 77
Trends and requirements in strong-motion data acquisition, management analysis and exchange	Lilie Xie 87
Data processing and analysis for strong-motion accelerograms	Lilie Xie 96
Understanding and setting STA/LTA trigger algorithm and associated parameters	114
WCDs and access to data sources via Internet and CD-ROM	Zhao Zhonghe 136
How to retrieve data from IRIS / USGS stations	S. Mc Lafferty 148

2. Seismic stations and networks: Planning, site selection, installation and operation

Seismic network, planning, procurement, installation, organisation and tuning	A. Trnkoczy	158
Seismic site quality and selection of surface seismic stations	A. Trnkoczy P. Bormann	195
Surface vault seismic station preparation	A. Trnkoczy	215
Radio-link transmission of seismic data and feasibility study	A. Trnkoczy	232
Bandwidth-dependent transformation of noise data from spectral into time domain and vice versa Part I: Introduction and methodology	P. Bormann	244
Bandwidth-dependent transformation of noise data from spectral into time domain and vice versa Part II: Exercises and solutions	P. Bormann	251

3. Seismic sources and source parameters

Introduction to seismic sources and source parameters	P. Bormann, H. Grosser	254
Magnitude of seismic events	P. Bormann	271
Seismic scaling relations	P. Bormann	316
Determination of fault plane solutions	M. Baumbach, P. Bormann	331

4. Seismological observatory practice: Analysis of records

Identification and analysis of longitudinal core phases: Requirements and guidelines	P. Bormann, S. Wendt	346
Exercise on local event localisation	P. Bormann, M. Baumbach, K. Wylegalla	367
Exercise on 3 - component seismogram interpretation	P. Bormann, K. Wylegalla	372
Exercise on magnitude determination	P. Bormann, K. Wylegalla	377

Exercises on event location and magnitude determination by means of seismic core phases	S. Wendt, P. Bormann	381
Exercise on fault-plane solution	M. Baumbach, P. Bormann H. Grosser	388
Exercise on take-off angle calculations	P. Bormann	395
Exercise on the determination of source parameters derived from seismic spectra	M. Baumbach, P. Bormann	401
"SEISAN" introductory training course	J. Havskov, L. Ottemöller	407
SEIS 89: A PC-tool for seismogram analysis	M. Baumbach	423

5. Seismicity, seismic hazard, risk assessment and disaster management

Introduction to natural disasters and disaster mitigation	P. Bormann	453
Seismicity and seismotectonics in Asia	Zhang Peizhen, Chen Yong	482
Seismic hazards in Asia: What do we know after GSHAP ? What remains to be done ?	Chen Yong, Li Juan	492
Earthquakes in China: A brief introduction	Z. L. Wu, Y.-T. Chen, R.F. Liu	509
Macroseismic and strong-motion parameters	G. Grünthal	521
Methodology of seismic hazard assessment	G. Grünthal	538
Exercise on assigning seismic intensities	G. Grünthal	544
Exercise on incompleteness of a catalogue with respect to the determination of the parameters of the Gutenberg-Richter relation	G. Grünthal	547
Exercise on the determination of the parameters of the Gutenberg-Richter relation $\log N = a - b \cdot m$	G. Grünthal	548
Exercise on earthquake occurrence in time (Poisson distribution)	G. Grünthal	550

Exercise on the application of extreme value statistics	G. Grünthal	551
Exercise on seismic hazard assessment: a simplified approach	G. Grünthal, Ch. Bosse	552
Exercise on PC assisted hazard assessment	Ch. Bosse, G. Grünthal	553
Approaches to seismic hazard assessment in China: Methodology. Part I: Assessment of seismic hazard based on area source and seismicity data	Chen Yong	555
Approaches to seismic hazard assessment in China: Methodology. Part II: Analysis of earthquake loss based on macroeconomic indicators	Chen Yong, Chen Qifu	568
Introduction to CAPSeis	Li Minfeng, Li Shengqiang	581
PC assisted exercises in seismic hazard assessment based on data from the countries of participants	Chen Yong, Chen Qifu, Chen Ling	585
Seismic risk assessment and disaster management	Yuxian Hu	594
Method on physical damage prediction of brick buildings	Feng Quimin	666

Foreword by the editor

The International Training Courses on "Seismology and Seismic Hazard Assessment" are organised by the Division of Solid Earth Physics and Disaster Research of the GeoForschungsZentrum Potsdam (GFZ), Germany, every second year in co-operation with hosting institutions in developing regions. The German lecturers co-operate closely with experts invited from both advanced industrial nations and developing countries. While the basic tutorial lectures and exercises on fundamentals of seismometry, seismic data acquisition and analysis as well as on earthquake source processes, statistics, hazard assessment and microzonation are covered by lecturers from Germany, France, Norway, Slovenia/Switzerland and sometimes also Japan and USA, lecturers from developing countries contribute their special regional expertise. Special thanks to all sponsors who render these courses possible.

The contents and approach of the courses have been constantly adapted to changing needs, conditions and expertise available in earthquake prone developing regions. E.g., during the course in 1993 at the University of Roorkee, India, local experts covered the lectures on regional seismotectonics and earthquake monitoring as well as aspects of earthquake engineering. When the Instituto Nicaragüense de Estudios Territoriales (INETER) invited the course to be run in 1995 in Managua to the benefit of participants from Latin American and the Caribbean countries it became clear, that besides problems of earthquake seismology those related to volcano and tsunami monitoring and warning had to be covered too. Accordingly, experts from Colombia, Costa Rica, Mexico, Nicaragua and Japan were invited to cover these aspects besides the topics related to regional tectonics, seismic hazard and risk. As an extra asset the nearby volcano Cerro Negro erupted fiercely in the middle of the course and provided a unique opportunity for close-up field inspections and demonstrations of effective seismological volcano monitoring. Similarly, geoscientists and earthquake engineers from Algeria, Ethiopia, Kenya, South Africa and Zimbabwe were involved when the course was run in 1997 in Kenya on the invitation of the University of Nairobi.

This year, having been invited by the China Seismological Bureau to run a course for participants from Asian and Pacific countries in Beijing, we can benefit from the vast experience of Chinese experts in seismology and earthquake engineering. Thus, for the first time, extensive lectures related to vulnerability assessment, risk evaluation and disaster management are on the course agenda. They are complemented by field excursions into the Tangshan area where the most devastating earthquake of this century occurred in 1976. The participant will also benefit from extensive demonstrations of China's achievements in earthquake monitoring and analysis as well as in instrument design and manufacturing. Accordingly, a new lecture material had to be produced with many contributions from both Chinese and German instructors which appear for the first time in the course volumes.

With this flexible approach and constant up-dating of the course contents we hope to make a valuable contribution to the development of needed expertise and self-reliance in developing countries and to lay a solid and stimulating foundation, both in scientific and human terms, for closer regional and global co-operation. In this context we should be aware that natural phenomena causing disasters to man do not observe political borders. They also completely ignore our religious, social or other quarrels and misconceptions. A deeper understanding of our still living planet Earth and thus improved response to its phenomena with hazard potential to man requires the pooling of all human intellectual, scientific, spiritual and economic-technical resources. Therefore, we have only the choice to either live in harmony and co-operatively with nature and each other on a regional and global scale or to perish.

What is applicable between nations is valid on a smaller scale within nations and communities as well. Often we forget that our own contribution to the tackling of pressing problems can be only very limited even when it is based on the best motivation and specialised expertise. Problems of disasters prevention and mitigation, as most other problems affecting a whole society, are much too complex as to be handled successfully by specialists alone. On the other hand even the most honourable decisions of politicians or other generalists will be in vain or counterproductive if they are not based on solid scientific-technical and sociological expertise and social responsibility.

The training course aims at developing interdisciplinary problem understanding and sensitive "interfaces" towards other disciplines. This will help you in critically assessing the limits of your knowledge with respect to the problems to be tackled, to better judge whom you have to consult, with whom you have to co-operate and where you have more courageously to interfere in order to bring your specialised knowledge better into play to the benefit of your country and community (cf. Fig. 13 in the lecture *Introduction to natural disasters and disaster mitigation*). This also requires to develop a mutually understandable language, to be able to translate our expert "slang" into words which make sense to other people as well, both to the ordinary public and to have to use of your results in their own specialised fields of activities but also to ordinary public. The training course strives to make a contribution in this respect too. Therefore, be inquisitive, do question any concept, statement, term, notion, fact or formula which you do not understand !

We will focus on introducing you to the very fundamentals of seismological observatory practice, as well as to seismic hazard, vulnerability and risk assessment, hopefully to an extent which will enable you to set up respective programs in your countries, if not yet available, or to accomplish your related job more efficiently when coming home. And the course should motivate you to follow-up the topics covered more thoroughly in future by consulting the specialised literature. On more fancy subjects such as earthquake prediction research, which are still far from being operational and yet forefront science, also from a sociological and managerial point of view, will only brief you shortly. Our comments on these issues should make you both curious and sober in your own decisions when setting priorities on why, when and where to spend the limited human, financial and technical resources at your disposal in investigating and combating geological disasters in your home countries.

Please note that several of our course lectures and exercises, complemented by many more detailed information on all aspects of seismological observatory practice will become part of the New Manual of Seismological Observatory Practice of the International Association of Seismology and Physics of the Earth Interior (IASPEI). This manual will also be developed, step by step, during the next few years as an Internet home page which can be accessed via <http://www.seismo.com>. This will enable us to update relevant information and instructions easily.

Finally, I wish to express my sincere thanks to all colleagues who contributed to the new course volumes with new or revised manuscripts and to Ms. Heike Gerighausen and Ms. Angela Sachse who assisted me in the technical preparations for this publication.

Potsdam, 20 August 1999

Prof. Dr. Peter Bormann
Chairman of the training course

FUNDAMENTALS OF SEISMOMETRY

Christian Teupser †

1. The mechanical receiver

The most common procedure of measuring the ground motion is to suspend a mass with a minimum of attachment to the earth and depend upon its inertia to keep it fixed in position as the earth moves. The simplest type of seismometer uses a pendulum having only one degree of freedom. It is usually designed to measure one component of ground motion especially the translation in N-S, E-W or Z direction. Due to the gravity different constructions are necessary for the horizontal and the vertical component.

The horizontal component consists in principle of a pendulum swinging around a nearly vertical axis (Fig. 1). If the inclination of the axis is the angle ν to the vertical, the natural period will be

$$(1) \quad T_S = 2\pi \sqrt{\frac{l}{g \sin \nu}}$$

where l is the reduced pendulum length and g the acceleration due to gravity [TEUPSER and ULLMANN, 1964]. The motion of such a pendulum can be described by the following linear differential equation [TEUPSER, 1962]

$$(2) \quad \frac{d^2 \eta}{dt^2} + 2D_{s0} \omega_s \frac{d\eta}{dt} + \omega_s^2 \eta = \frac{1}{I} \left(\frac{d^2 x}{dt^2} + g\zeta \right) - \frac{G_s}{K_s} i_s$$

where D_{s0} is the open damping, $\omega_s = 2\pi/T_S$ the natural angular frequency, G_s the electrodynamic constant of the magnet and coil assembly, K_s the inertial moment, and η the angular deflection of the centre of mass. x is the ground displacement in the direction of the free motion of pendulum, ζ a small tilt against an axis perpendicular to the axis of rotation through the centre of mass, and i_s the current in the coil.

The vertical motion can be detected by a pendulum swinging about a horizontal axis. The pendulum is supported against gravity by a helical spring fixed at the frame in A and at the boom in B (Fig. 2). In order to obtain a long-period seismograph with negligible non-linear effects, the principle of LaCOSTE [1934] is the best solution using a so-called 'zero-length' spring. As the centre of mass is not generally situated in the horizontal plan through the axis of rotation ($\varepsilon \neq 0$), the natural period of a pendulum will be

$$(3) \quad T_S = 2\pi \sqrt{\frac{l \sin \gamma}{g \cos(\gamma + \varepsilon)}}$$

where η is the angle between the ends of the spring [TEUPSER, UNTERREITMEIER, 1977]. The equation of motion is

$$(4) \quad \frac{d^2\eta}{dt^2} + 2D_{so}\omega_s \frac{d\eta}{dt} + \omega_s^2\eta = -\frac{1}{l} \left(\frac{d^2y}{dt^2} + g\beta\sin\varepsilon \right) - \frac{G_s}{K_s} i_s$$

where β is a small tilt about the axis of rotation. y is the ground displacement in a direction inclined against the vertical by the angle ε . If $\varepsilon = 0$, the pendulum is sensitive about vertical motions only. This is the condition for an exact vertical seismograph [MALISCHEWSKY et al., 1970]. If $\varepsilon = 54.7^\circ$, a homogeneous triaxial equipment can be constructed using three such inclined vertical pendulums.

2. The response of mechanical receiver

A pendulum with low damping responds to a forced oscillation with an oscillation of the same period superposed by the free oscillation of the pendulum with his own period T_s . The unwanted free oscillation distorts the wanted forced one. To make satisfactory use of pendulums in seismometry, it is necessary to diminish the effects of the transient free oscillations. This will be obtained by introducing sufficient damping, by which we mean any force opposing the pendulum motion and increasing with its velocity. The ideal equipment for this purpose is a magnet and coil assembly. As the boom motion induces the voltage $e_s = G_s d\vartheta/dt$ in the coil, the current i_s will be

$$(5) \quad i_s = \frac{G_s}{R_s + R_{as}} \frac{d\vartheta}{dt}$$

when the coil with the resistance R_s is terminated by R_{as} . Neglecting tilts, the differential equation of a vertical or horizontal seismograph is

$$(6) \quad \frac{d^2\vartheta}{dt^2} + 2D_s\omega_s \frac{d\vartheta}{dt} + \omega_s^2\vartheta = -\frac{1}{l} \frac{d^2x}{dt^2}$$

where D_s is the total damping

$$(7) \quad D_s = D_{so} + \frac{G_s^2}{2\omega_s K_s (R_s + R_{as})}$$

The differential equation (6) can be solved using the Laplace transform

$$(8) \quad F(s) = \int_0^{\infty} f(t) e^{-st} dt$$

where $f(t) = 0$ for $t < 0$. The inverse transform is given by

$$(9) \quad f(t) = \frac{1}{2\pi j} \int_{-j\infty}^{+j\infty} F(s) e^{st} ds.$$

As the Laplace transform of the derivate $f^{(n)}(t)$ equals $s^n F(s)$, the differential equation (6) becomes an algebraical equation

$$(10) \quad (s^2 + 2D_s \omega_s s + \omega_s^2) \theta(s) = - \frac{s^2 X(s)}{1}$$

where $X(s)$ is the Laplace transform of the ground displacement. If the deflection of the centre of inertia $l \vartheta(t)$ is linearly magnified by mechanical, optical, or electronic devices with the factor V_0 , the recorded amplitude $a(t)$ is obtained using (6)

$$(11) \quad a(t) = V_0 l \vartheta(t) = \frac{V_0}{2\pi j} \int_{-j\infty}^{+j\infty} U_s(s) X(s) e^{st} ds.$$

The transfer function function of the mechanical receiver $U(s)$ included in (11) is

$$(12) \quad U_s(s) = \frac{s^2}{s^2 + 2D_s \omega_s s + \omega_s^2}.$$

Let $s = j\omega$ with denoting ω angular frequency, the Laplace transform changes into the Fourier transform and the transfer function (12) can be written

$$(13) \quad U_s(j\omega) = V_s(\omega) e^{j\varphi_s(\omega)}$$

where $V_s(\omega)$ is the amplitude and $\varphi_s(\omega)$ the phase response of the mechanical receiver

$$(14) \quad V_s(\omega) = \frac{\omega^2}{\sqrt{(\omega^2 - \omega_s^2)^2 + 4D_s^2 \omega_s^2 \omega^2}},$$

$$(15) \quad \tan \varphi_s(\omega) = \frac{2D_s \omega_s \omega}{\omega^2 - \omega_s^2}.$$

Amplitude and phase responses for different dampings are given in Fig. 3 and 4. If at $t = 0$ a harmonic ground motion suddenly starts, the formulas (8) and (11) yield

$$(16) \quad X(s) = \frac{\omega x_0}{s^2 + \omega^2}$$

and $a(t) =$

$$(17) = -V_0 x_0 U_S(\omega) \left[\sin(\omega t + \varphi_S) - \frac{\omega_S}{\omega \beta_S} e^{-D_S \omega_S t} \sin(\beta_S \omega_S t + \zeta_S) \right]$$

$$\text{where } \beta_S = \sqrt{1 - D_S^2} \quad \text{and} \quad \sin \zeta_S = 2D_S \beta_S V_S(\omega) .$$

As mentioned above the recorded motion consists of two terms, a steady state one with the frequency of the forced motion and negative exponential one, the so-called transient response, with the frequency of the pendulum. The steady state part is associated with the poles and zeros of $U_S(s)$ and the transient one is obtained from the poles and zeros of $X(s)$.

The amplitude and the phase angle of the forced motion is given by the responses (14) and (15), respectively. Neglecting the transient response, the mechanical receiver can record the displacement, the velocity, and the acceleration of ground motion in certain frequency intervals. These three special cases are:

1. For $\omega \geq \omega_S$ and $0.4 < D_S < 0.7$ is $V_S(\omega) \approx 1$. The response of the seismograph is proportional to the displacement of the ground motion.
2. A heavy damping $D_S \gg 1$ gives $V_S(\omega) \approx \omega / 2D_S \omega_S$ in the range $\omega_S / 2D_S < \omega < 2D_S \omega_S$. The response is proportional to the velocity of the ground motion.
3. For $\omega \leq \omega_S$ and $0.4 < D_S < 0.7$ is $V_S(\omega) \approx \omega^2 / \omega_S^2$. The response is proportional to the acceleration of the ground motion.

3. The electromagnetic seismographs

In these instruments the coil of the mechanical receiver is connected to a galvanometer through a network of resistances (Fig. 5). The equation of motion of the galvanometer is

$$(18) \quad \frac{d^2 \psi}{dt^2} + 2D_g \omega_g \frac{d\psi}{dt} + \omega_g^2 \psi = \frac{G_g}{K_g} i_g$$

where ψ is the angular deflection of the galvanometer. The other values are defined like those of the mechanical receiver. As in the receiver coil a voltage $e_g = -G_g d\psi/dt$ will be induced in the galvanometer coil opposite to the galvanometer motion. In the theory of electromagnetic seismographs the transference factor k_g and the coupling factor σ are defined as

$$(19) \quad k_g = \frac{G_S G_g R_3}{K_g [(R_S + R_1)(R_g + R_2) + R_3(R_S + R_g + R_1 + R_2)]} ,$$

$$(20) \quad \sigma = \frac{k_g}{2} \sqrt{\frac{K_g}{D_s \omega_s D_g \omega_g K_s}} .$$

It can be shown that the coupling factor describing the galvanometer reaction lies between the limits $0 < \sigma < 1$. [EATON, 1957 and TEUPSER, 1958]

Applying Kirchhoff's laws for the coupling network (Fig. 5) and the Laplace transform for eq. (6) and (18), the transfer function of the electromagnetic seismograph becomes

$$(21) \quad T(s) = \frac{2D_m \omega_m s^3}{(s^2 + 2D_s \omega_s s + \omega_s^2)(s^2 + 2D_g \omega_g s + \omega_g^2) - 4D_s D_g \omega_s \omega_g \sigma^2 s^2}$$

where D_m is defined like D_s (eq. 7) and

$$(22) \quad D_m \omega_m = \text{Max}(D_s \omega_s, D_g \omega_g) .$$

If L_g is the optical lever arm of the galvanometer the magnification factor will be defined as

$$(23) \quad V_o = \frac{L_g k_g}{D_m \omega_m l} .$$

Neglecting the galvanometer reaction ($\sigma = 0$), the amplitude response $W(\omega)$ and the phase angle $\varphi(\omega)$ are

$$(24) \quad W(\omega) = \frac{2D_m \omega_m U_s U_g}{\omega} ,$$

$$(25) \quad \varphi = \varphi_s + \varphi_g - \frac{\pi}{2} .$$

Special tuning of the 4 parameters of the electromagnetic seismograph, the two natural frequencies and the two dampings, enables the registration of the integral, the displacement, the velocity, the acceleration, and the third derivate of ground motion. The conditions for this tuning and the operating range is shown in Table 1. $V_n \approx V_o W(\omega)/\omega^n$ is the magnification of the n^{th} derivate of the ground motion in the operating range. The schematic response curve are shown in Fig. 6. Detailed theoretical treatment shows that any response characteristic which includes the galvanometer can be produced by the so-called equivalent parameters of the mechanical receiver and the galvanometer [GRENET, COULOMB, 1935].

4. The electronic seismographs ~~~~~

The possibility to built up long-life electronic amplifiers enables the installation of a new generation of seismological instruments. The output of such a seismograph with conventional moving-coil transducer or displacement transducer delivers a high-level electronic signal suitable for registration on magnetic tape or electronic data processing.

The signals of the transducers are led to combinations of low-, band-, and high-pass filters. The transfer functions of second-order low-pass are given by

$$(26) \quad U_L = \frac{\omega_L^2}{s^2 + 2D_L\omega_L s + \omega_L^2},$$

those of band-pass filters by

$$(27) \quad U_B = \frac{2D_B\omega_B s}{s^2 + 2D_B\omega_B s + \omega_B^2}$$

and those of high-pass filters by

$$(28) \quad U_H = \frac{s^2}{s^2 + 2D_H\omega_H s + \omega_H^2}.$$

Such second-order filters can be easily built up using operational amplifiers. Therefore, the transfer function of such a seismograph is given by

$$(29) \quad T(s) = \frac{N(s)}{D(s)}.$$

This function is described by the roots of the numerator, the zeros of $T(s)$, and the roots of the denominator $D(s)$, the poles of $T(s)$.

Important new classes of seismograph can be constructed by feeding the output signal into an auxiliary transducer attached to the pendulum. In this way, the output signal generates a force acting on the mass. If this feedback is negative, the relative motion between the seismometer boom and the frame is reduced. This invokes the well-known general properties of negative feedback systems, which are to improve stability, linearity, and dynamic range as compared with open-loop systems using components of similar quality.

The schematic diagram of such a feedback seismograph shows Fig. 7. The Laplace transform of the transfer function is

$$(30) \quad T_f(s) = \frac{s^2 Q(s)}{s^2 + 2D_s \omega_s s + \omega_s^2 + kG(s)Q(s)}$$

where $Q(s)$ and $G(s)$ are the transfer functions of the transducer or the filter in the feedback loop, respectively. Using different filters in the feedback loop one can modify the transfer function. In general, the feedback is negative

and the loop consists of a parallel connection of a low-pass, a direct way, a one-stage high-pass, and a two-stage high-pass [PLESINGER, 1973]

$$(31) \quad G(s) = \frac{\beta_0 \omega_0}{s + \omega_0} + \beta_1 + \frac{\beta_2 \omega_h s}{s + \omega_h} + \frac{\beta_3 \omega_H^2 s^2}{s^2 + 2\alpha_H \omega_H s + \omega_H^2} .$$

If there is only the direct way, the natural frequency will be increased to

$$(32) \quad \omega'_s = \sqrt{\omega_s^2 + k\beta_1} .$$

Such devices measure the acceleration for frequencies $\omega < \omega'_s$ and are called force-balance accelerometers [MELTON, 1976]. These in modern seismometry often mentioned force-balance systems, therefore, sense the ground motion after the same inertial principle explained above, but provide an additional restoring force. The electric signal generating this force is nearly proportional to ground acceleration and is used as output signal. The precision to which the ground motion can be measured is rised as in well-known potentiometric meters.

Using a low-pass the same effect will be obtained but only for long periods. The co-called centering factor is [SUTTON and LATHAM, 1969]

$$(33) \quad F = \frac{\omega_s^2 + k\beta_0}{\omega_s^2} .$$

A high-pass in the feedback loop increases the apparent damping of the pendulum. As shown above the seismograph acts as a velocity meter. A more subtle benefit is that the elimination of dissipative elements from the electromechanical system removes the primary source of Brownian motion of the seismometer mass, and therefore opens the door to the development of very small seismometers. A least, the second-stage high-pass simulates an increasing of the inertial moment. This lengthen the period and the range in which the seismograph measure the displacement. Such a feedback must be combined with velocity feedback because the increased inertia requires more damping.

Looking again at the response of the feedback seismograph one can see that it is controlled entirely by the feedback network if the last term in the denominator dominates the other ones. In this case the response is independent of the parameters of the mechanical receiver. Using a proportional, integral and differential feedback (PID) [WIELANDT and STRECKEISEN, 1982]

$$(34) \quad G(s) = a + \frac{b}{s} + cs ,$$

a conventional electromagnetic seismograph can be simulated. With a displacement transducer the response will be

$$(35) \quad T_f(s) = \frac{s^3}{s^3 + (2D_s \omega_s + kc)s^2 + (\omega_s^2 + ka)s + kb}$$

Apart from the term with s^3 in the denominator this equation represents the transfer function of an electromagnetic seismograph. As the natural period of this system can be chosen much greater than the period of the mechanical receiver, a velocity response can be obtained in broad frequency band. Such seismographs are called Very-Broad-Band (VBB) seismographs [STEIM, 1986]. They will be recommended as a new standard in global seismic networks. With high resolution A/D converters such broad-band seismographs are able to record the whole spectrum and dynamic range of seismic signals.

5. The strainseismographs

The seismographs discussed up till now uses the inertia of a suspended mass. Therefore, they are called inertia seismographs contrary to the strainseismographs which measure the variation of the distance between two points during the passage of seismic waves [BENIOFF, 1935 and AGNEW, 1986]. In other words, these instruments are excited by the phase difference of the propagating wave. They also measure as so-called extensometers the ground deformation caused by earth tides, meteorological influences, and tectonic processes. Their main field of application is the recording of long-period events reaching from seismic waves to secular variations.

The terminals of the strainseismograph are usually piers inbedded in the soil. For measuring the variation of the distance three methods are mainly used (Fig. 8). In the first suitable instrument one pier was lengthened by a rigid rod, so that a transducer can be fixed between its free end and the second pier. Instead of the rod an invar wire can be used as length normal, too. The third possibility is the light beam strainseismograph constructed by the aid of lasers. As the strainseismographs using rods or wire are not longer than 30 m, laser strainseismographs of 1000 m length have been developed.

References

- AGNEW, D.C.: Strainmeters and tiltmeters. Rev. of Geophysics 24 (1986) 3, 579-624.
- ARANOVICH, Z.I.; D.P. KIRNOS; V.M. FREMD: Apparatura in metodika sejsmometriceskich nabljudenij v SSSR. NAUKA, Moskva 1974.
- BENIOFF, H.: A linear strain seismograph. Bull. Seism. Soc. Am. 25 (1935), 283-309.
- BORMANN, P.: Registrierung und Auswertung seismischer Ereignisse. Veroeff. Inst. Geodyn. (1966) 1, 158 S.
- EATON, J.P.: Theory of the electromagnetic seismograph. Bull. Seism. Soc. Am. 47 (1957), 37-75.
- GRENET, G.; J. COULOMB: Nouveaux principes de construction des seismographes electromagnetiques. Annales de Physique, Paris, 11. serie, 3 (1935), 321-369.
- LACOSTE, L.J.B.: A new type long period vertical seismograph. Physics 5 (1934), 178-180.
- MALISCHEWSKY, P.; CH. TEUPSER; W. ULLMANN: Der Vertikalseismograph unter besonderer Beruecksichtigung des Typs VSJ-I. Veroeff. des Inst. f. Geodynamik Jena (1970) 15, 77 S.
- MELTON, B.S.: The sensitivity and dynamic range of inertial seismographs. Rev. Geophys. and Space Physics 14 (1976) 1, 93-116.
- PLESINGER, A.: Synthesis of feedback controlled broadband modifications of conventional seismograph systems. Zeitschr. Geophys. 39 (1973) 4, 573-596.
- SAWARENSKI, E.F.; D.P. KIRNOS: Elemente der Seismologie und Seismometrie. Berlin: Akademie-Verlag, 1960. 512 S.
- STEIM, J.M.: The very-broad-band seismograph. Harvard University Cambridge, Massachusetts, Doctoral Thesis, 1986.
- SUTTON, G.H.; G.V. LATHAM: Analysis of a feedback-controlled seismometer. Journ. Geophys. Res. 69 (1969) 18, 3865-3882.
- TEUPSER, CH.: Der Rueckwirkungsfaktor bei elektrodynamischen Erschuetterungsmessern. Freiburger Forschungshefte C 51 (1958), 64 S.
- TEUPSER, CH.: Die Eichung und Pruefung von elektrodynamischen Seismographen. Freiburger Forschungshefte C 130 (1962), 103 S.
- TEUPSER, Ch.; W. ULLMANN: Der neue Jenaer Horizontalseismograph HSJ-I. Veroeff. Inst. fuer Bodendynamik und Erdbebenf. (1964) 76, 147 S.

TEUPSER, CH.; E. UNTERREITMEIER: Der elektronische Dreikomponentenseismograph EDS-1, Theorie, Aufbau, Wirkungsweise. Veroeff. Zentralinst. Physik d. Erde (1977) 51, 114 S.

WIELANDT, E.; G. STRECKEISEN: The leaf-spring seismometer: Design and performance. Bull. Seism. Soc. Am. 72 (1982), 2349-2367.

WILLMORE, P.L.: Manual of seismological observatory practice. World Data Center A for Solid Earth Geophysics, Report SE-20 (1979) Boulder, Colorado USA.

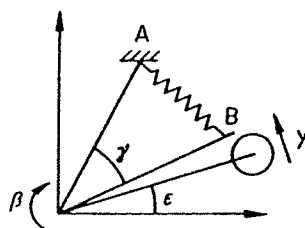
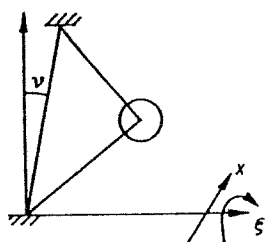


Fig. 1 Horizontal seismograph

Fig. 2 Vertical seismograph

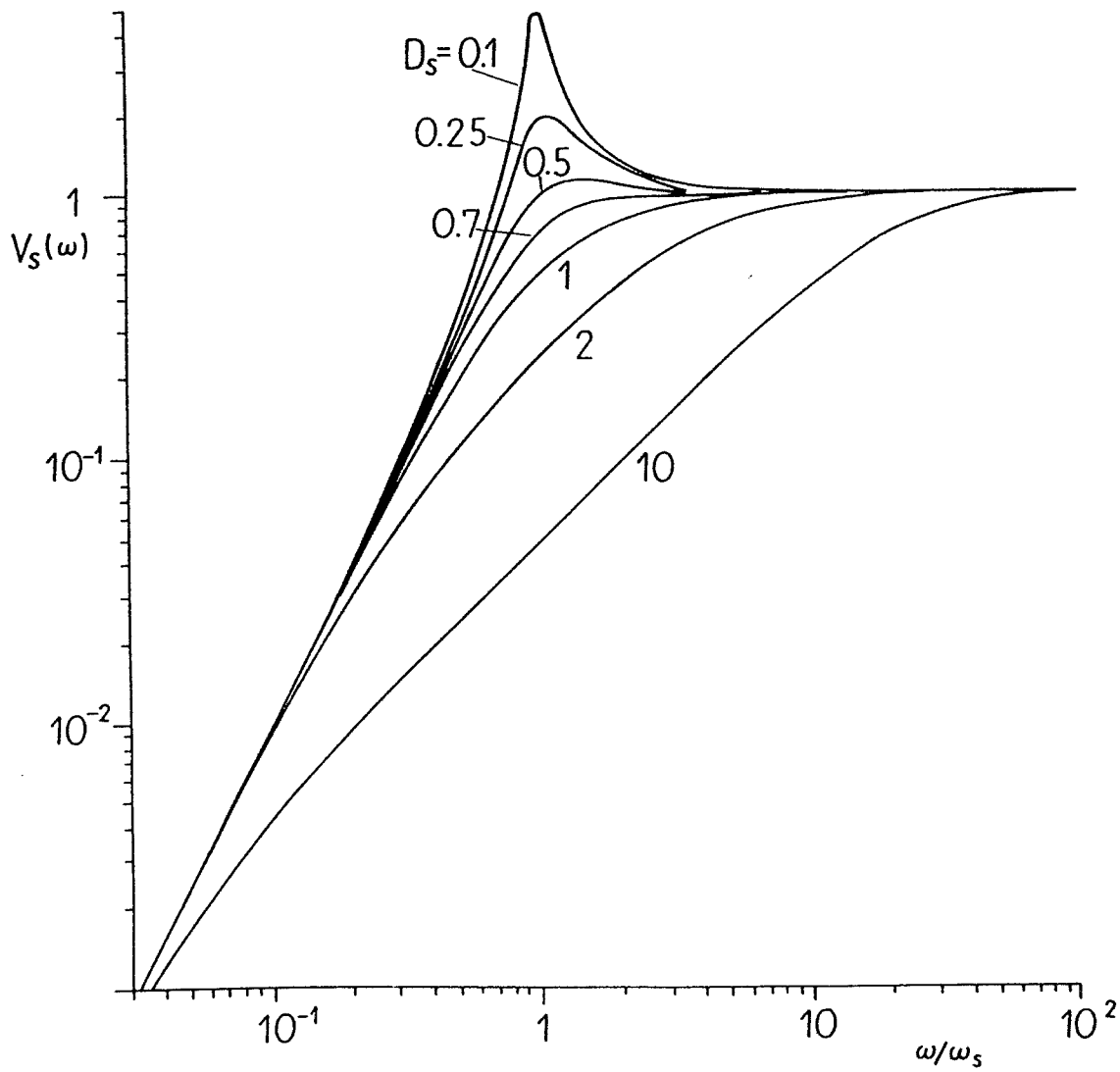


Fig. 3 Amplitude response

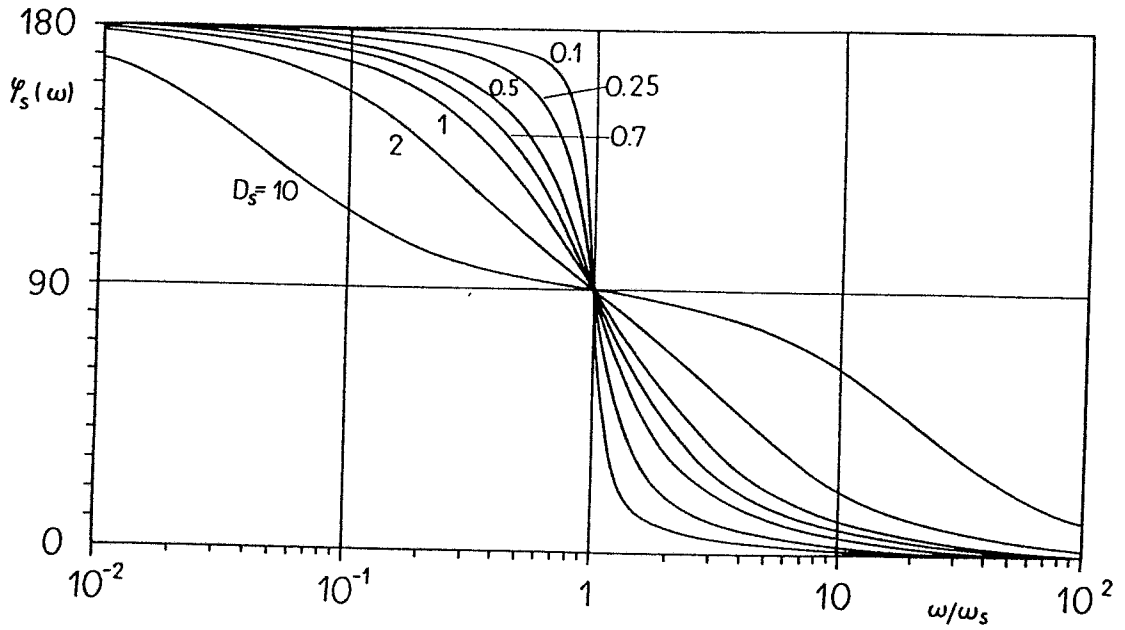


Fig. 4 Phase response

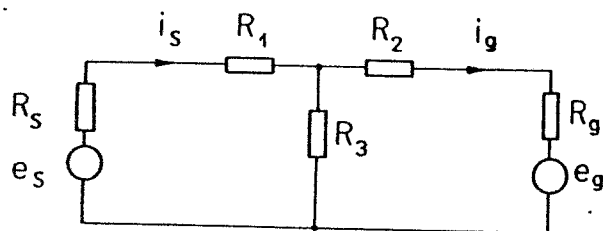


Fig. 5 Circuit diagram of electromagnetic seismograph

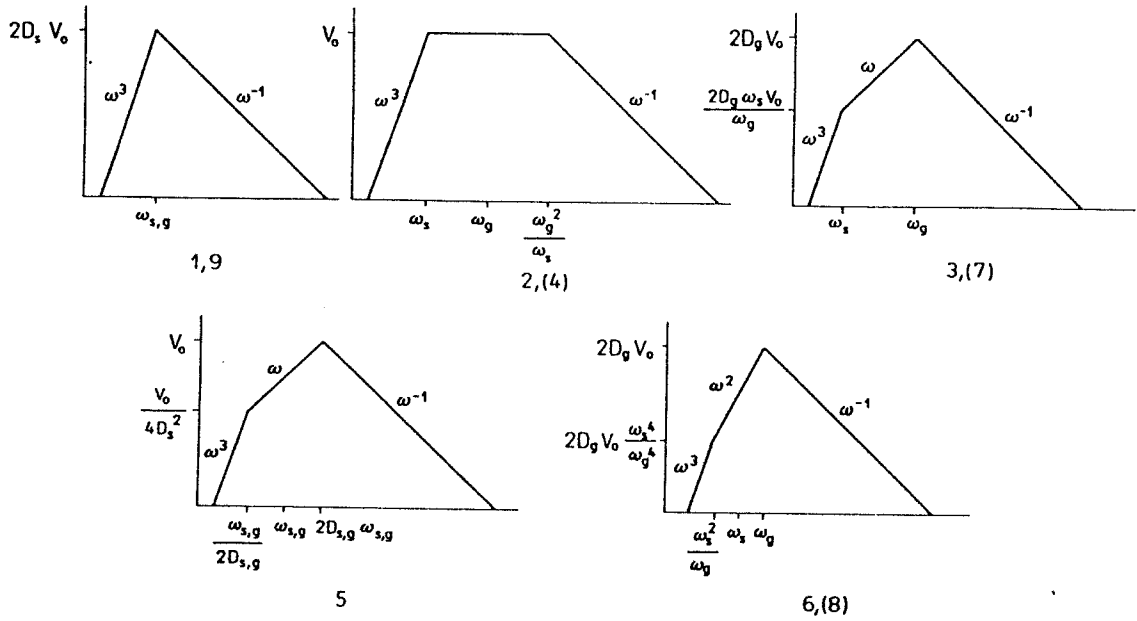


Fig. 6 Schematic responses of electromagnetic seismograph

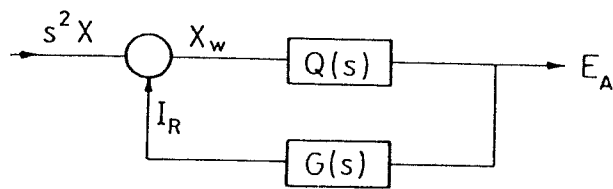


Fig.7 Circuit diagram of electronic seismograph

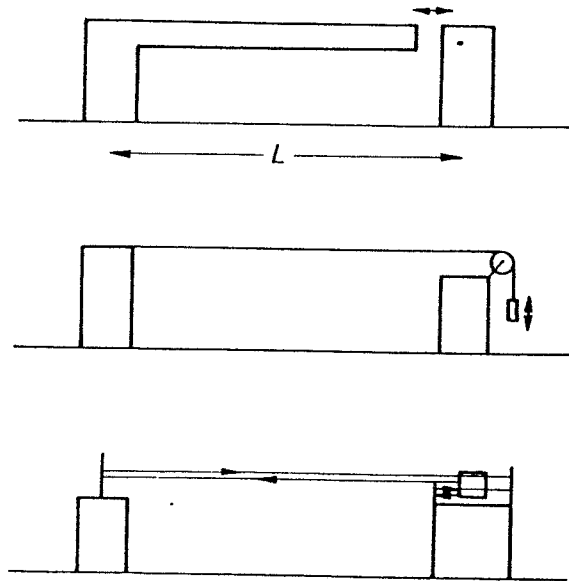


Fig. 8 Principles of strainseismograph

Table 1

case	tuning	$\frac{\omega_B}{\omega_S}$	D_B	D_S	operational range	V_n
1	integral	≈ 1	$0.47 \leq D_{S,B} \leq 0.6$		$\omega \geq \omega_{S,B}$	$\frac{2L k}{\omega_S^2}$
2	displacement I	< 1	0.5	$\frac{\omega_B}{2\omega_S}$	$\omega_B \leq \omega \leq \frac{\omega_B^2}{\omega_S}$	$\frac{L k}{D_S \omega_S^2}$
3	velocity I	< 1	$0.4 \leq D_{S,B} \leq 0.7$		$\omega_B \leq \omega \leq \omega_S$	$\frac{2L k}{\omega_S^2}$
4	displacement II	> 1	$\frac{\omega_B}{2\omega_S}$	0.5	$\omega_S \leq \omega \leq \frac{\omega_B^2}{\omega_S}$	$\frac{L k}{D_S \omega_S^2}$
5	velocity II	≈ 1		$D_{S,B} > 1$	$\frac{\omega_B}{1.3D_S} \leq \omega \leq 1.3D_S \omega_S$	$\frac{L k}{2D_S \omega_S^2}$
6	acceleration I	< 1	$\frac{\omega_B}{2\omega_S}$	0.5	$\frac{\omega_B^2}{\omega_S} \leq \omega \leq \omega_S$	$\frac{2L k}{\omega_S^3}$
7	velocity III	> 1	$0.4 \leq D_{S,B} \leq 0.7$		$\omega_S \leq \omega \leq \omega_B$	$\frac{2L k}{\omega_S^2}$
8	acceleration II	> 1	0.5	$\frac{\omega_B}{2\omega_S}$	$\frac{\omega_B^2}{\omega_S} \leq \omega \leq \omega_B$	$\frac{2L k}{\omega_S^3}$
9	3 rd derivate	≈ 1	$0.47 \leq D_{S,B} \leq 0.6$		$\omega \leq \omega_{S,B}$	$\frac{2L k}{\omega_S^4}$

CONSTRUCTING RESPONSE CURVES - AN INTRODUCTION TO THE BODE DIAGRAM

Jens Bribach

Geoforschungszentrum Potsdam, Division 2: Solid Earth Physics and Disaster Research,
Telegrafenberg, D-14473 Potsdam, Germany
Fax: +49 331 288 1266; E-mail: brib@gfz-potsdam.de

1. THE BODE DIAGRAM

True Ground Motion is of main interest in seismology. On the other hand any measuring device will alter the incoming signal as well as any amplifier, and as any output device. Working in the frequency domain, the quotient of input signal and output signal is called RESPONSE. This response is complex, and to get a more handy result it can be split into two terms: amplitude response and phase response (see FOURIER Transform). Amplitude response means the output amplitude divided by the input amplitude at a given frequency. Phase response is the difference between output phase and input phase, or the phase shift. A graphical expression of this splitting is known as BODE-diagram. One part shows the logarithm of amplitude A versus the logarithm of frequency f (or angular frequency ω , or period T , see figure 1a). The other part depicts the (linear) phase ϕ versus the logarithm of frequency f (or $\omega = 2\pi f$, or $T = 1/f$, cf. Fig. 1b). For A also the terms *Amplification* or *Magnification* are used.

1.1. The signal chain

The signal passes a chain of devices. Any single element of this chain can be described by its response. It is useful to split any response into elements of first or second order. At the end the *Overall Amplitude Response* of the complete chain can be constructed by multiplying all single amplitude responses, and the *Overall Phase Response* by adding all single phase shifts.

1.2. First and second order elements

For the amplitude response the double logarithmic scale of the amplitude diagram facilitates an easy and fast construction. Any element can be approximated by two straight lines. One horizontal line leads to the element corner frequency, and one line dropping from that point with a slope depending on the order of this element.

A first order element is completely described by its amplification A and by its corner frequency f_c . The slope beyond f_c is one decade in amplitude per decade in frequency. The real amplitude value at f_c is dropped to 0.707 of maximum amplitude (see figure 2, dotted line), for our fast construction we do not take this dotted line into account.

A second order element inhibits the slope of two decades in amplitude per amplitude in frequency. Additionally it needs another parameter called *Damping D*, describing the amplitude

behaviour at frequencies near f_c (compare figure 3).

2. THE SEISMOLOGICAL SIGNAL CHAIN

The seismological signal passes the chain

- mechanical receiver
- transducer
- preamplifier
- filter
- recording unit (to be recognised separately)

Note! In sections 2.1 and 2.2 we discuss amplitude responses related to ground displacement. Therefore, the ordinate axis of the BODE-diagram (amplitude A) for the mechanical receiver has no unit (or the unit $[m/m]$), and for the transducer the unit is $[V/m]$. Changing to other types of movement, being proportional to ground velocity or to ground acceleration, will be described in section 3.

2.1. The mechanical receiver

The mechanical receiver is a second order system. It describes the relative movement of the pendulum (i.e. a seismic mass attached to a frame by a spring) with respect to the frame. Damping D is set mostly to 0.707 . Only at this damping value the amplitude value at f_c is also 0.707 (Fig. 3, dotted curve). For higher values of damping one obtains a more flat curve (dashed). For lower values of D the dash-dot curve strongly exceeds the amplification level at f_c , signalling low-damped resonance oscillations of the pendulum, which can be stimulated by any signal.

The amplification of the mechanical receiver is $A = 1$. That means for frequencies $f > f_c$ the amplitude of the pendulum movement with respect to the frame is similar to the ground amplitude. For the phase shift see Fig. 7b (HIGH Pass 2).

2.2. The transducer

The transducer transforms the relative movement of the pendulum into an electrical signal, i.e. in a voltage. The *Transducer Constant* G gives the value of the output voltage U depending on the relative pendulum movement z . There are three main types of transducers, distinguished by their proportionality to ground motion and its derivatives:

- Displacement $U \sim z$ $G_d[V/m]$
(capacity or inductivity bridges)

- Velocity $U \sim dz/dt$ $G_v[Vs/m]$
(magnet-coil systems)

- Acceleration $U \sim d^2z/dt^2$ $G_a[Vs^2/m]$
(piezo-electric systems, $U \sim F = m a$)

The above proportionality of the transducer voltage to ground motion (i.e. to displacement, velocity or acceleration, respectively) is, of course, only given for frequencies $f > f_c$, i.e. for the horizontal line of the mechanical receiver response (cf. Fig. 3).

All transducer amplitude responses can be drawn as straight lines over the full considered frequency range (Fig. 4). They differ only in their slope.

The phase responses have a constant phase shift over the whole frequency range at values of 0° (displacement), 90° (velocity), or 180° (acceleration).

2.3. The preamplifier

The preamplifier is a first order LOW Pass. Its corner frequency is beyond the signal range of seismology - up to several 10 kHz . Thus, only the amplification is of interest (Fig. 5). The response is a horizontal line drawn at the amplification level A .

The phase shift is $\phi = 0^\circ$, but one should keep in mind that, if using the inverting input, the phase shift will be $\phi = -180^\circ$ over the whole frequency range.

2.4. First and second order LOW Passes

LOW Passes have constant amplifications A for frequencies lower than their corner frequencies f_c . For frequencies higher than f_c the amplification drops with a slope depending on the order of the filter (Fig. 6a). LOW Passes cut the high frequencies, therefore, also the term High Cut is in use. The phase shift for $f < f_c$ is about 0° and for $f > f_c$ it turns to -90° (first order, LP1) respectively -180° (second order, LP2; see Fig. 6b), passing half of the phase shift exactly at f_c .

Of course, the given amplitude and phase values are approximations. In reality we would obtain $\phi = 0^\circ$ only if inserting a frequency of 0 Hz , and $\phi = -90^\circ$ (-180°) for infinite frequency values. But the accuracy is sufficient for our fast construction.

2.5. First and second order HIGH Passes

HIGH Passes have constant amplifications A for all frequencies higher than their corner frequency f_c . For frequencies lower than f_c the amplification drops with a slope depending on their order (Fig. 7a). It cuts the low frequencies, so one can also find the term Low Cut.

The phase shift for $f > f_c$ is about 0° , and for $f < f_c$ it turns to $+90^\circ$ (first order, HP1) respectively $+180^\circ$ (second order, HP2; see Fig. 7b), passing half of the phase shift exactly at f_c .

Comparable to the description of LOW Passes the given amplitude and phase values are an approximation.

2.6. Second order BAND Pass

The second order BAND Pass (BP2) can be explained as a combination of a first order LOW

Pass and a first order HIGH Pass. It suppresses all frequencies, except f_c , with a slope of one decade in amplitude per decade in frequency (Fig. 8a). The top at f_c can be turned into a horizontal line (symmetrical to f_c) by increasing the damping to values $D > 1$. Thus it is possible to construct a BAND Pass by combining a HIGH Pass with a LOW Pass.

The phase shift for $f < f_c$ is about $+90^\circ$, and for $f > f_c$ it turns to -90° (see Fig. 8b), passing half of the phase shift at f_c .

3. THE OVERALL RESPONSE

The construction of the overall response should be divided into two steps:

- from mechanical receiver to the final filter stage;
- adding the recorder response.

The first result, the electrical output, is useful for fitting the signal to the recorder input. It has to be fixed, i.e. changes in magnification (or signal resolution) should be done only when setting up the recorder.

3.1. From the mechanical receiver to the final filter

As defined in section 2, the amplitude response is constructed related to ground displacement. Multiplying all the units of our signal chain, we get the unit [V/m] for the axis of ordinates. All elements, mechanical receiver, transducer, and filter stages can be implemented into the same sheet of a double logarithmic grid, each element with its magnification and its corner frequency. Then the resulting amplitude response has to be constructed point by point at certain frequencies. It can be done by multiplying the amplitude values of all elements at these frequencies. This is the more accurate method. Another way is to add in the double logarithmic diagram the distances (e.g. in millimetres) of all element amplitudes to the amplitude level line of $A = 1$ (i.e. $\log A = 0$). Note that distances above this line are positive and below it negative and also that linear adding in a logarithmic scale means multiplication of the amplitude values while subtraction means division. This graphical method is faster. The final amplitude response curve can be drawn on the same sheet, together with the single elements.

3.2. Adding the recorder

At the real end of our signal chain we will find a commercially available recorder, transforming the obtained voltage back into movement (drum recorder) or into computable digital values (Analogue-to-Digital Converter = ADC). Their main parameter is the input sensitivity H .

In case of a drum recorder, H is the pen deflection per Volt (in units [m/V]).

For an ADC H is the digital count per Volt (in units [digit/V]).

Thus the overall amplitude response needs a separate BODE-diagram for each recorder type. Multiplying the units we obtain the units [m/m] for the drum recorder, and [digit/m] for the

ADC. You will find also derivatives of this unit, like [digit/nm] or [counts/nm].

3.3. Introducing ground velocity and ground acceleration

If the amplitude response curve has to be constructed related to ground velocity (or ground acceleration), it is sufficient to redraw either the response of the mechanical receiver or this of the transducer. The more simple method is to change the transducer response. Each slope will change one order if turning from displacement to velocity, or from velocity to acceleration. The unit of the ordinate turns from [V/m] (displacement) via [Vs/m] (velocity) to [Vs²/m] (acceleration). These units will also be the units of the amplitude response from the mechanical receiver to the final filter stage. Beyond this the construction of the overall amplitude response is similar to section 3.1. The units of the recorder amplitude response will alter to [m·s/m] (velocity) or [m·s²/m] (acceleration) for the drum recorder. For the ADC we obtain [digit·s/m] (velocity) or [digit·s²/m] (acceleration).

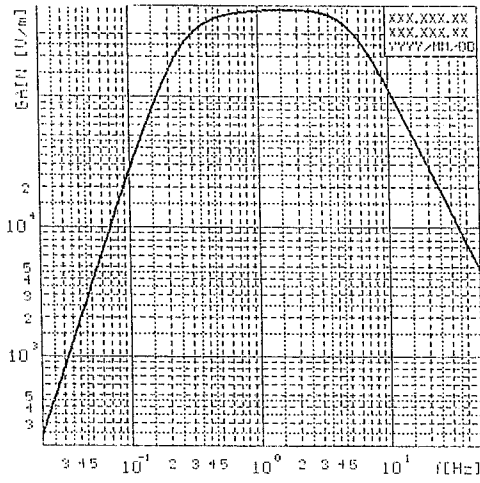


Fig. 1a: Amplitude Response

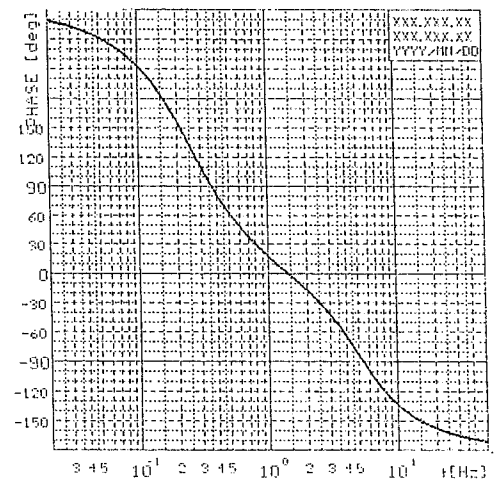


Fig. 1b: Phase Response

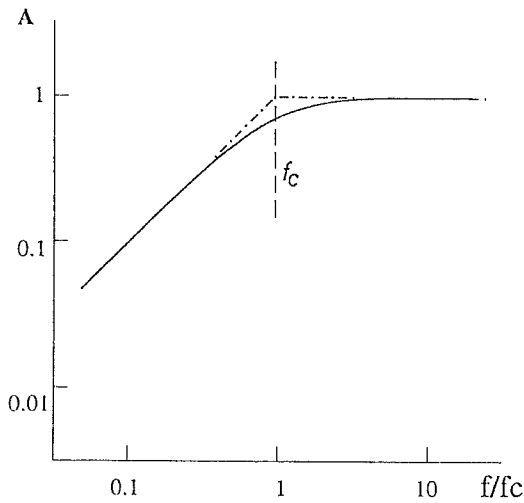


Fig. 2: First order HIGH Pass (HP1)

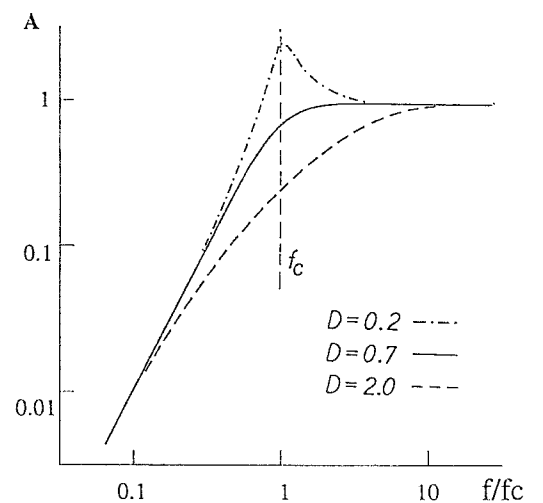


Fig. 3: Second order HIGH Pass (HP2) or Mechanical Receiver

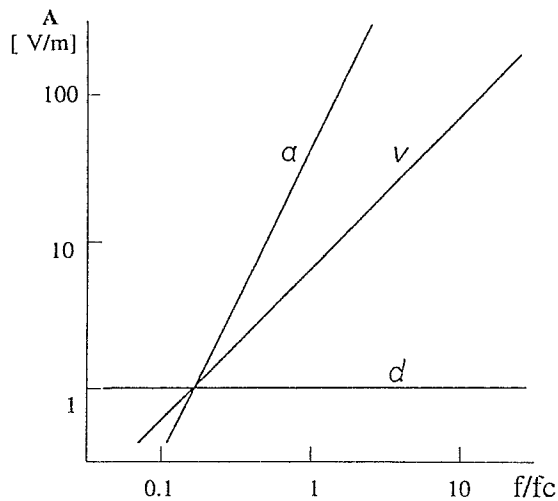


Fig. 4: Transducer Amplitude Response

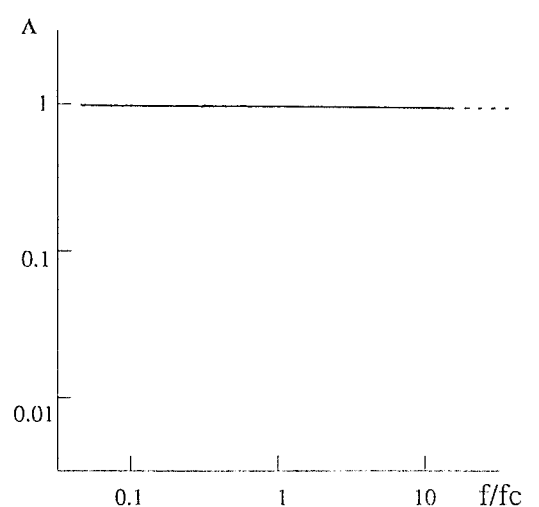


Fig. 5: Preamplifier Amplitude Response

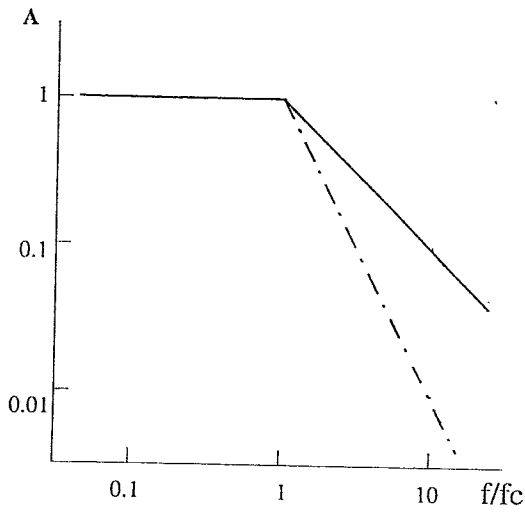


Fig. 6a: LOW Pass Amplitude Response

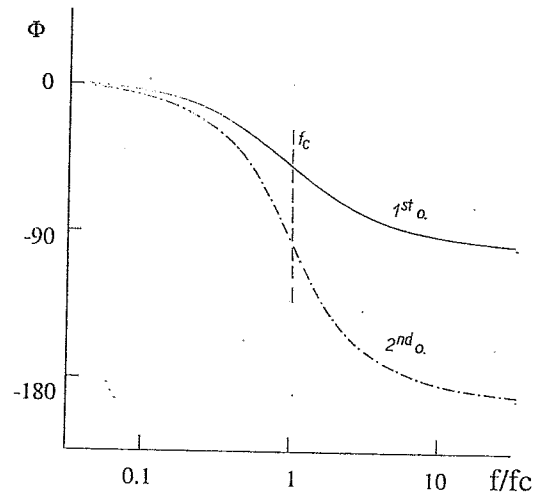


Fig. 6b: LOW Pass Phase Response

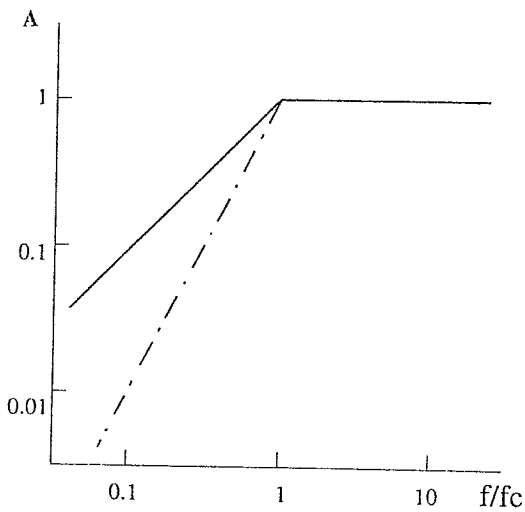


Fig. 7a: HIGH Pass Amplitude Response

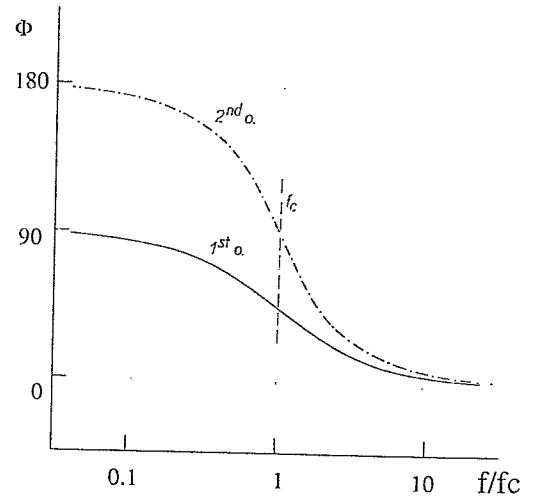


Fig. 7b: HIGH Pass Phase Response

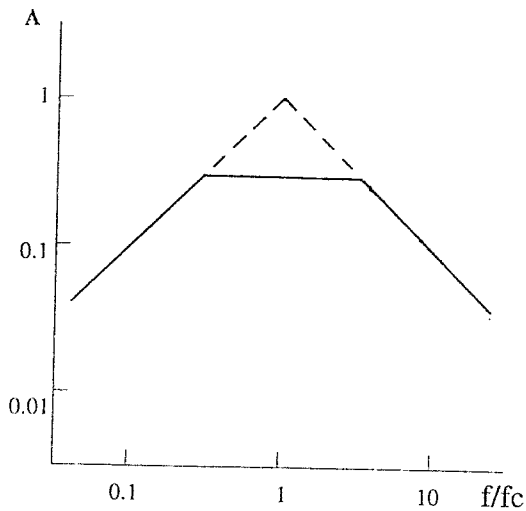


Fig. 8a: BAND Pass Amplitude Response

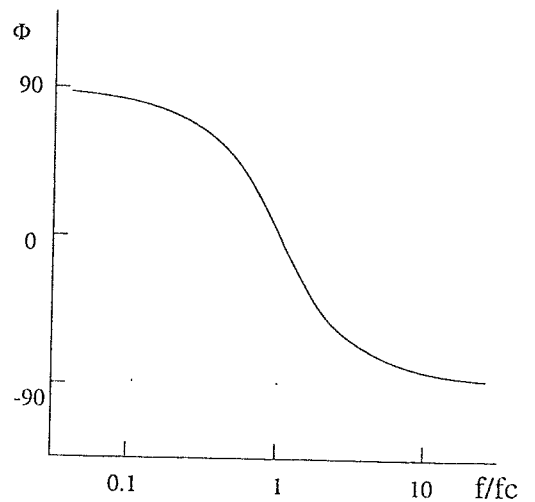


Fig. 8b: BAND Pass Phase Response

EXERCISE ON PLOTTING SEISMOGRAPH RESPONSE (BODE-DIAGRAM)

Jens Bribach

Geoforschungszentrum Potsdam, Division 2: Solid Earth Physics and Disaster Research,
Telegrafenberg, D-14473 Potsdam, Germany
Fax: +49 331 288 1266; E-mail: brib@gfz-potsdam.de

The BODE-diagram displays the transfer function of a given device as a plot of logarithmic amplitude A and of linear phase shift ϕ versus logarithmic frequency f (or period $1/f$) scales. Its main advantage consists of an easy construction of response curves which can be approximated by straight lines:

- any Pole in the transfer function generates an amplitude decay proportional to frequency f (20 dB per decade or 6 dB per octave) and a phase shift ϕ of -90° ;
- any Zero causes a slope of 1:1 too and a phase shift of $+90^\circ$;
- corner frequencies (e.g. of filters) correspond to the point of interception of two straight lines.

All stages of a signal transfer chain can be constructed component by component. It is recommended to decompose all functions into parts of 1st or 2nd order. One gets the complete transfer function by multiplying these individual functions. In the logarithmic amplitude scale as well as in the linear phase scale this is done by adding of the related individual curves.

Task 1: Plot the BODE-diagrams (amplitude only) of the following devices:

Seismometer

Transducer Constant	$G_S = 15.915$ Vs/m
Natural Period	$T_S = 5$ s
Attenuation	$D_S = 0.707$

HIGH Pass HP1 (1st order)

Magnification	$A_{HI} = 10$
Corner Frequency	$f_{HI} = 0.01$ Hz

LOW Pass LP1 (1st order)

Magnification	$A_{L1} = 2$
Corner Frequency	$f_{L1} = 0.2$ Hz

LOW Pass LP2 (2nd order)

Magnification	$L_2 = 2$
Corner Frequency	$f_{L2} = 10$ Hz
Attenuation	$D_{L2} = 0.707$

Task 2: Plot the systems overall amplitude response approximated by straight lines.

EXERCISE ON ESTIMATING SEISMOMETER PARAMETERS BY STEP FUNCTION

Jens Bribach

Geoforschungszentrum Potsdam, Division 2: Solid Earth Physics and Disaster Research,
Telegrafenberg, D-14473 Potsdam, Germany
Fax: +49 331 288 1266; E-mail: brib@gfz-potsdam.de

1. BACKGROUND

Transition Function means the response of a system versus time caused by a STEP Function input. Applying a step in any way to a seismometer allows to derive the main seismometer parameters by analysing the generated time series. In the absence of expensive calibration equipment (e.g. shaking table) or in case of sealed seismometers this simple method is very suitable and can also be used under field conditions.

2. STEP TRANSITION: PROCEDURES AND RELATIONSHIPS

2.1. Applying STEPs to the seismometer

Applying steps is the oldest calibration method in seismology. Teupser (1962) describes three main types:

- a) pulling a thin block (thickness max. 0.01 mm) off the seismometer bottom;
- b) applying a heavy weight upon the seismometer platform;
- c) applying a constant current to the coil of an electrodynamical system (if available; for driving current see *Exercise on calibration by harmonic drive*).

Because a) is the most rough method one should use it for field or for portable seismometers only and never for sensitive station sensors. In case a) and b) the seismometer mass will return to the former position after deflection, in case c) the seismometer mass will move to an offset position which will depend on the applied current. To assure linearity the mass deflection - or the seismometer displacement - should not exceed several 100 micrometers.

2.2. Evaluating STEP-transition time series

2.2.1. All types of seismometers ($D_S < 0.5$)

Fig. 1 shows the time series of a low-damped seismometer ($D_S = 0.1$). The time section A represents the time from the moment of step input up to the transition to a real harmonic movement of the mass. The moment of step causes odd signals. Mechanical application of a

step impulse generates additional vibrations because of hitting effects. An electrical step can induce an electrical pulse if the calibration coil and the signal coil are mounted to the same core (the so-called transformer effect). Therefore the analysis of generated time series should start only beyond section A with:

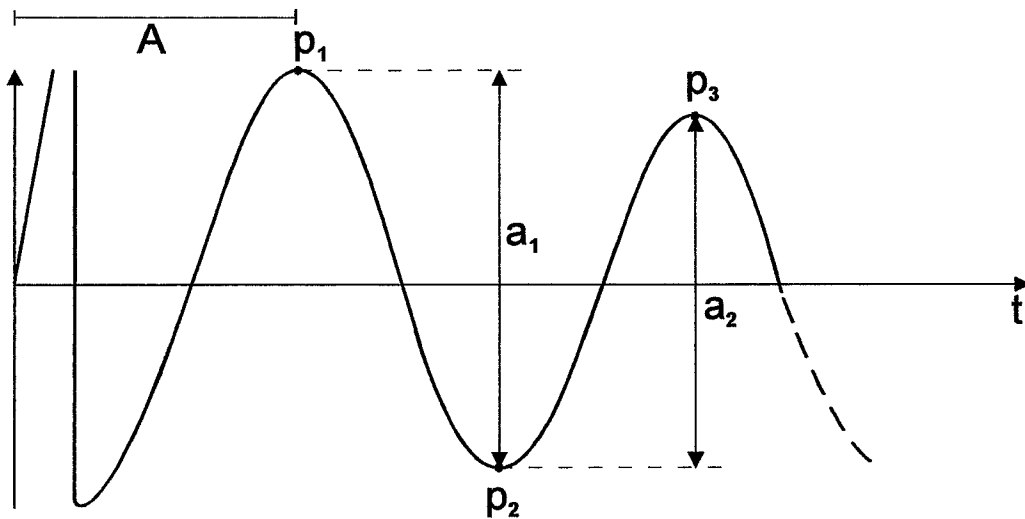


Fig. 1: Response of a low-damped seismometer to a step pulse.

First step: Measuring of the period and damping of the time series

The period T should be measured by averaging over as many cycles as possible (10 or more) to get an accuracy better than 99% .

Note! The measured period is larger than the natural period because of the seismometer damping.

The damping D is calculated from the equation

$$D = \frac{1}{\sqrt{\left(\frac{(N-1)\pi}{\ln(a_1/a_N)}\right)^2 + 1}} \quad (1)$$

with a_1 as the double amplitude between the first two oscillation peaks (p_1 and p_2) and a_N as the double amplitude between the peaks (p_N and p_{N+1}). N should be selected so as to get an $a_N \approx 0.2 \dots 0.4 a_1$.

Second step: Estimation of the seismometers natural period T_S

If possible switch off all external attenuators (e.g. resistors) to decrease the measuring error. For example: with a damping $D = 0.2$ the measured period is $T = 1.02 T_S$. The natural period of the seismometer is

$$T_S = T\sqrt{1-D^2} \quad (2)$$

2.2.2. Electro-dynamical system (moving coil)

The electrodynamical constant (or generator constant) G_S of moving coil systems can also be estimated by step transition via its relation to damping D . The complete seismometer damping D_S is

$$D_S = D_{S0} + D_G \quad (3)$$

with D_{S0} as the natural damping of the seismometer (mostly mechanical effects), and with D_G as the moving coil damping. The latter is caused by an external resistor R_a shorting the coil (electromagnetical force), i.e.:

$$D_G = \frac{G_S^2 T_S}{4\pi m_S (R_a + R_S)} \quad (4)$$

Except R_a and T_S all other parameters in eq. (4) are documented by the manufacturer and will not change over time. While for pendulum seismometers usually the parameters

- | | |
|----------------------|-------------------------|
| - K_S [$kg.m^2$] | inertial moment |
| - l_0 [m] | reduced pendulum length |

are given instead of m_S one gets for geophone systems

- | | |
|-----------------------------------|------------------|
| - m_S [kg] = $K_S l_0^{-2}$ | seismic mass and |
| - R_S [$Ohms$] | coil resistance. |

Note! When measuring coil resistance don't forget to lock the seismometer.

The evaluation again starts as above with: measuring of the period and damping of the time series as the first step and the estimation of the seismometers natural period T_S as the second step.

This is followed by:

Third step: Estimation of the seismometers natural damping D_{S0}

The external damping resistor must be removed (open circuit). Then we get, similarly to (1),

$$D_{S0} = \frac{1}{\sqrt{\left(\frac{(N-1)\pi}{\ln(a_1/a_N)}\right)^2 + 1}} \quad (1)$$

Fourth step: External damping

The external resistor must be set to a value that causes an damping down to 20 ... 50% per period. Then we measure the neighbouring amplitudes a_1 (between p_1 and p_2) and a_2 (between p_2 and p_3 ; p_2 is used twice to reduce measuring error) and get

$$G_S [Vs/m] = \sqrt{(D_S - D_{S0}) \frac{4\pi}{T_S} m_S (R_a + R_S)} \quad (6)$$

This constant can also be used when calibrating a system by harmonic drive.

Note! For pendulum seismometers there are different notations of this constant

- 1) force/current $[N/A]$ = $[Vs/m]$ and
- 2) torque/current $[Nm/A]$ = $[Vs]$

They are transferable via the reduced pendulum length l_0 as

$$G_{S_1} [V_s] = G_{S_2} [V_s / m] \cdot l_0 [m] \quad (7)$$

3. APPLICATION TO A SPECIFIC SEISMOMETER

3.1 Parameter list

Below a typical seismometer parameter list is given.

Mechanical constants:

Natural Period	T_S s
Open Damping (Attenuation)	D_{S0}
Reduced Pendulum Length	l_0	0.0785 m
Inertial Moment	K_S	0,0201 kg m ²
(Seismic Mass	m_S kg)

Transducer constants 1 (signal coil):

Coil Resistance	R_{S1}	6030 Ω
Electrodynamical constant	G_{S1} Vs/m

Transducer constants 2 (calibration coil):

Coil Resistance	R_{S2}	835 Ω
Electrodynamical constant	G_{S2} Vs/m

3.2 Exercise tasks

- Task 1: Mark those seismometer parameters which are absolutely necessary for calculating the seismometer response curve (Bode-diagram)
- Task 2: Complete the list below by analysing the related time series plots in Fig. 2a - c
- Task 3: Calculate the current through the calibration coil which is necessary to deflect the seismometer mass by $1\ \mu\text{m}$ at a frequency $f = 1\ \text{Hz}$ (see *Exercise on calibration by harmonic drive*)

REFERENCES

- Teupser, Ch. (1962). Die Eichung und Prüfung von elektromagnetischen Seismographen, Freiburger Forschungshefte C130, 103 pp.

EXERCISE ON CALIBRATION BY HARMONIC DRIVE

after a manuscript by Christian Teupser

If the seismometer possesses an auxiliary magnet and coil assembly, the calibration can be carried out by the aid of an electric current. The equation of motion (see Fundamentals of seismometry) shows that a current i_s acts in the same way as a ground acceleration

$$\frac{d^2 x_e}{dt^2} = \frac{G_{S2} l_0}{K_S} i_s . \quad (1)$$

where G_{S2} is the electrodynamic constant of the auxiliary coil (given in $[Vs/m]$). For other constants see *Exercise on STEP function*. It corresponds to a harmonic drive of frequency f with an equivalent ground displacement

$$x_e = \frac{G_{S2} l_0}{4\pi^2 f^2 K_S} i_s . \quad (2)$$

For a translational seismometer, for example a geophone, with the seismic mass m_s the equivalent seismic displacement is

$$x_e = \frac{G_{S2}}{4\pi^2 f^2 m_s} i_s . \quad (3)$$

Since the output voltage of a geophone with electromagnetic transducer is

$$E_s = G_{S1} \frac{dz}{dt} , \quad (4)$$

where z is the displacement of the seismic mass, G_{S1} is the electrodynamic constant of the signal coil, and f_s the natural frequency, one obtains for a harmonic excitation

$$E_s = \frac{G_{S1} G_{S2} f}{2\pi m_s \sqrt{(f^2 - f_s^2)^2 + 4D_s^2 f^2 f_s^2}} . \quad (5)$$

Changing the frequency of the exciting current the output voltage attains a maximum at $f = f_s$. This can be used to determine the natural frequency and the damping using an oscilloscope.

INFLUENCE OF THE FREQUENCY CHARACTERISTICS OF THE SEISMOGRAPH ON ITS SEISMIC RECORDINGS

Peter Bormann

Geoforschungszentrum Potsdam, Division 2: Solid Earth Physics and Disaster Research,
Telegrafenberg, D-14473 Potsdam, Germany
Fax: +49 331 288 1293 or 1204; E-mail: course@gfz-potsdam.de

1. Introduction

Quantifiable instrumental recordings of the ground motion are a precondition for deriving quantitative scientific information from the analysis of seismic data. Seismologically relevant ground motions cover a wide range of periods ($0,03 \text{ s} < T < 3200 \text{ s}$). Within this range the frequency characteristic of the seismographs, i. e. the frequency dependence of their magnification is normally designed such as to ensure the best possible signal - to-noise ratio. This requires to consider the selection of frequency characteristics in the context of predominating spectra of seismic signals as well as noise. On the other hand misconceptions are widespread as to the proper meaning and use of the frequency characteristics or instrumental response curves derived from the calibration of seismographs. From this a number of systematic errors result when standard procedures of deriving the so-called "true ground motion" from instrumental recordings are applied. This will be illustrated both from a theoretical as well as a phenomenological point of view.

2. Frequency and phase characteristics of electrodynamic seismographs

A mechanical seismic receiver with galvanometric recording forms a coupled vibration system. Assuming small deflections of the pendulum and the galvanometer mirror the magnification of this system results from the solution of a linear differential equation of the 4th order. The solution consists of a time-dependent negative exponential term describing the transient response and of a time-independent stationary term. In case of a stationary harmonic ground oscillation the frequency and phase characteristics of the system ($\bar{U}(\omega)$ and $\varphi(\omega)$, respectively) are unambiguously defined by the eigenperiods T_s and T_g of seismometer and galvanometer, respectively, their damping factors D_s and D_g , the coupling factor σ^2 between seismometer and galvanometer and the magnification factor V_0 . These parameters can be determined by various calibration methods. The resonance factor \bar{U} results as the product of the individual resonance factors of seismometer (fig. 1) and galvanometer (fig. 2), i. e. $\bar{U} = U_s \cdot U_g / \omega$ with $\omega = 2\pi/T$ and T - period of ground motion. The amplitude-magnification characteristic of the coupled system is $V(\omega) = V_0 \cdot \bar{U}$. In case of galvanometric recordings and under the conditions $T_s > T_g$ and $D_s < D_g$, V_0 and \bar{U} can be determined from the following formulas /1/:

$$(1) \quad V_0 = \frac{2l_L}{l_{\text{red}}} \sqrt{\sigma^2 \frac{D_s T_g K_s}{D_g T_s K_g}} \quad \text{and}$$

$$(2) \quad \bar{U} = \frac{2 D_g}{\pi T_g} \frac{1}{\sqrt{T^{-2} + a + b T^2 + c T^4 + d T^6}}$$

with l_L - length of the light indicator, l_{red} - reduced length of the pendulum, K_s and K_g - moments of inertia of the seismic pendulum and galvanometer, respectively,

and

$$(3) \begin{cases} a = m^2 - 2p, & b = p^2 - 2mq + 2s, & c = q^2 - 2ps, & d = s^2, \\ m = 2 \left(\frac{D_s}{T_s} + \frac{D_g}{T_g} \right), & p = \frac{1}{T_s^2} + \frac{1}{T_g^2} + \frac{4 D_s D_g}{T_s T_g} (1 - \sigma^2), \\ q = \frac{2 D_s}{T_s} \cdot \frac{1}{T_g^2} + \frac{2 D_g}{T_g} \cdot \frac{1}{T_s^2}, & s = \frac{1}{T_s^2 T_g^2} \end{cases}$$

Because of the symmetry of these formulas one obtains identical frequency characteristics when permuting the respective parameters of the seismometer and galvanometer and observing the conditions $T_s < T_g$ and $D_s > D_g$. This option is very important for the recording of very long-period seismic waves since it is relatively easy to operate galvanometers even at periods $T_g > 100$ s while seismometers with $T_s > 30$ s tend to be unstable. In this case the recorded ground motion is displacement proportional when the conditions $T_s \approx T < T_g$, $D_g < 1$ and $D_s \gg 1$ are observed.

The recorded harmonic motion $y(t) = Y \sin(\omega t + \varphi)$ shows a phase shift φ when compared with a harmonic ground motion $x(t) = X \sin \omega t$. The phase characteristic $\varphi = \varphi(\omega)$ can be determined from the relationship

$$(4) \quad \tan \varphi = \frac{p T^2 - s T^4}{m T - q T^3} - 1$$

when taking the relations given under (3) into account.

The amplitude X of the true ground motion could be determined from the recorded amplitude Y if V_0 and $\bar{U}(\omega)$ are known and the presupposition of stationary harmonic oscillations holds true:

$$(5) \quad X = \frac{Y}{V_0 \bar{U}(\omega)} .$$

3. Influence of the seismograph's transient response

But seismic waves are more complicated. In particular body wave onsets cannot be described by a stationary harmonic oscillation but rather by wavelets with modulated amplitudes corresponding to a generalized BERLAGE function

$$(6) \quad x(t) = \begin{cases} 0 & \text{for } t < 0 \\ t^a e^{-b\omega t} \sin \omega t & \text{for } t \geq 0 \end{cases}$$

with a and b - wavelet parameters, t - time (cf. /2/).

In this case the transient response of the seismograph has to be taken into account. Its duration and character depend on the duration and form of the seismic signal as well as on the vibration parameters of the seismograph. The transient response results in a systematic distortion of the amplitude and period of the recorded signal, i. e. the effective magnification $\bar{U}_1^B(\omega, a, b)$ is different from the frequency characteristic $\bar{U}(\omega)$ for stationary harmonic oscillations. This difference is largest for the first half-cycle. While in this case the distortion shows no strong dependence on the wave form the latter has a significant influence on the effective magnification of later half-cycles. The period of the incoming wave - particularly that of the first cycle - is also distorted due to the seismograph's phase shift. On the other hand the true and recorded onset time as well as the direction of first motion are always identical as long as the condition $x(t) = 0$ for

$t < 0$ is fulfilled (i. e. if there is no movement of the seismograph prior to the onset-time due to noise or any preceding ground motion.

The transient response is largest for narrow-band peak - like frequency characteristics. This resonance type of frequency response is realized if for $T_g \approx T_s$, D_s and $D_g \ll 1$ and $\sigma^2 \gg 0,1$. In this case the seismograph reacts strongly only to ground periods close to the eigenperiod of the system. But the maximum amplification is only reached after the system has absorbed the energy of many ground oscillation, i. e. the transient response will take a long time. At the same time owing to its small attenuation the system will respond rather unspecifically with a long mono-frequency wave train to any kind of ground motion containing frequencies identical or close to the resonance frequency. In case of zero attenuation this wave train - once excited - would be of infinite duration. On the other hand a broad-band characteristic with a flat top is originated by combining a seismometer and galvanometer with very different eigenperiods and highly overcritical damping of at least on component of this coupled system, normally that with the shorter eigenperiod. This means that the resonance peak has to be truncated at the expense of the system's magnification. The strong damping of the individual reaction of the seismograph results in a small phase shift between ground motion and seismograph response for ground periods T between T_s and T_g and consequently in a very short transient response. The seismograph thus follows the ground motion very closely with minimum distortion. A seismograph with infinite attenuation would be equivalent to a rigid body that follows exactly the ground motion for all frequencies without magnification or distortion and thus, without transient response. Besides this physical explanation there is a very illustrative one from the point of view of FOURIER-transformation. A needle impulse in the time-domain is equivalent to an infinite spectrum in the frequency domain while a single spectral line in the frequency domain corresponds to an infinite wave train of one definite period in the time domain. Therefore a ground deformation in form of a needle impulse can only be reproduced properly on the record if the frequency characteristic of the seismograph corresponds to a filter of infinite band-width. If, on the contrary, the band-width of the frequency characteristic is infinitesimal small the seismograph picks up only one of the infinite number of endless mono-frequent wavetrains that form the needle impulse. Its reaction, therefore, will be an undamped wave train of that given filter frequency.

But natural phenomena as well as technical possibilities for constructing real seismographs lie between these extremes of mathematical and physical abstraction. For illustration fig. 3, shows various short-period frequency characteristics used at Moxa station of the Central Institute for Physics of the Earth as well as examples of their recordings (figs.4, 5 and 6). Although the narrow-band characteristic A' is the optimal fit to the inverse short-period noise spectrum observed at Moxa station with a maximum magnification at $T = 1$ s 4times that of the standard type A the amplitude of the recorded first motions is not larger than in records of type A. Even the maximum ground motion of body wave onsets as calculated by using formula (5) is still generally lower when records of type A' are used (fig. 7). This partly explains the systematically lower magnitude estimates from records of narrow-band peak characteristics such as the ones installed at WWNSS stations as compared with the medium - to broad - band records typical for basic stations in most socialist countries. Geophones used in exploration geophysics and deep seismic sounding normally have narrow-band resonance characteristics, too, resulting in limited frequency content of the recorded signals and significant distortion of their character with respect to the true ground motion. The longer wavelets in narrow-band records make the discrimination and exact determination of onset-times of closely spaced successive onsets generally more difficult and sometimes impossible. These effects are detrimental for both quantitative amplitude studies as well as detailed travel-time

analyses of later arrivals (depth phases of shallow events, intersections and triplifications of travel-time curves).

4. Deconvolution of seismograms

Seismological interpretation methods leading to physically more informative results require in most cases the knowledge of true ground motion and/or high-resolution travel-time data. The true ground motion can be restored by deconvolving the seismogram.

In principle the deconvolution of the seismographic record means its transformation to the record of a seismograph with the band width $(2T_0, \infty)$ by means of calculation. This can be accomplished in the frequency domain by a two-fold Fourier transformation or in the time domain by applying the exact or the approximate inverse filter operator of the seismograph (cf. NEUGEBAUER /9/). But the exact restoration of the true ground movement is possible only in case of perfect unbiased seismograms.

The presence of noise as well as random and truncation errors can falsify the result to uselessness. Another independent approximate method was proposed by NEUNHÖFER /10/ who accomplished the deconvolution by repeated convolution of suitable wavelets using a generalized Monte-Carlo-technique and trial and error until the residuals between the recorded seismogram and the seismogram for the synthesized approximate ground movement become smaller than a given figure. This method allows the recognition and elimination of disturbing drifts and jumps and cannot be applied on a routine basis. KORČAGINA and MOSKVINA /8/ outline in their paper, too, the difficulties and uncertainties involved in practical attempts to restore the true ground motion from classical analog recordings. Therefore, to avoid all these problems, the easiest and best way of deconvolution is to avoid convolution. But this means that one should give preference to broad-band seismographs, to guarantee that the primary information has been recorded with minimum distortion. This is all the more so if one has facilities for analog or digital recording on magnetic tape which, by means of computers, will later allow the application of desirable operations such as the determination of other derivatives of the ground displacement (ground velocity and acceleration), spectral analysis, band-pass, multi-channel and noise prediction filtering.

The only significant problem when recording teleseismic signals of both very weak as well as strong seismic events with an extremely broad displacement proportional frequency characteristic is the very large dynamic range to be coped with (some 120 dB). It can be reduced by some 20 dB when using a pass-band magnification proportional to ground acceleration. At the same time such a characteristic fits best the overall trend of the inverse noise spectrum thus ensuring a good signal-to-noise ratio with a minimum dynamic range. Frequency characteristics of this type have for the first time been recommended for world-wide use by BERCKHEMER /4/. In case of digital recordings ground displacement and velocity can easily be derived from these data by one- or two-fold integration, very stable records presupposed.

5. Conclusions

Broad-band frequency characteristics give a better picture of the true ground motion than small-band ones. The expected gain in magnification when fitting a frequency characteristic into a small noise window might be lost completely in case of short wavelets owing to the reduced effective magnification during the transient response. This fact also explains partly the discrepancy between so-called "Eastern" and "Western" body wave magnitudes.

Broad-band characteristics are particularly suitable for the determination of the direction of first motion and the identification and onset-time determination of successive body wave groups, e. g. in connection with a multiple rupture process in

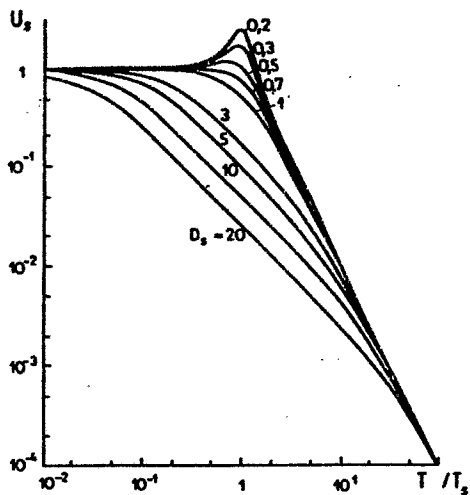


Fig. 1 Resonance factor U_s of the seismometer as a function of the ratio T/T_s for different values of the seismometer damping D_s (after /6/)

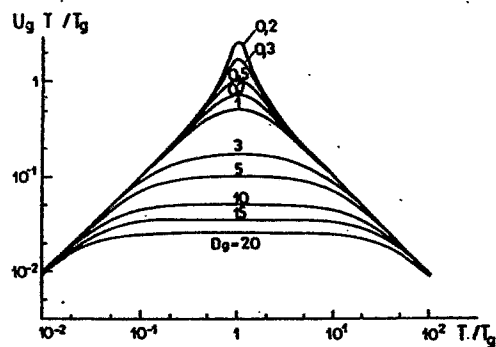


Fig. 2 Normalized resonance factor $U_g T/T_g$ of the galvanometer as a function of the ratio T/T_g for different values of the galvanometer damping D_g (after /6/)

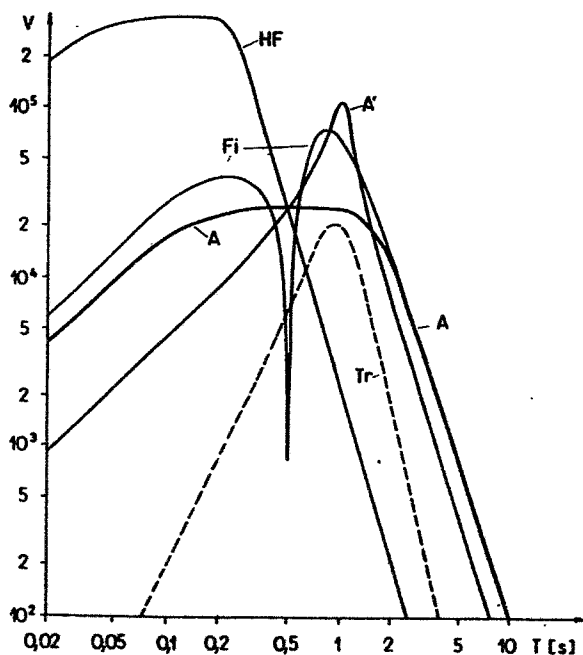


Fig. 3 Frequency characteristics of various short-period seismographs at Moxa station

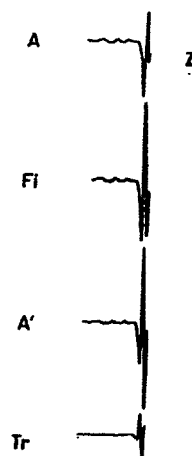


Fig. 4 Vertical records of types A, Fi, A' and Tr from a deep earthquake under the Sea of Okhotsk (29 Jan 1971, $D=72.3^\circ$, $h=544$ km, $MPV=6.1$)



Fig. 5 Vertical records of types A, Fi, A' and Tr from an earthquake in Honshu, Japan (7 Oct 1970, $D = 88.0^\circ$, $h = 179$ km, $MP1V = 5.8$, $MP3V = 6.4$).

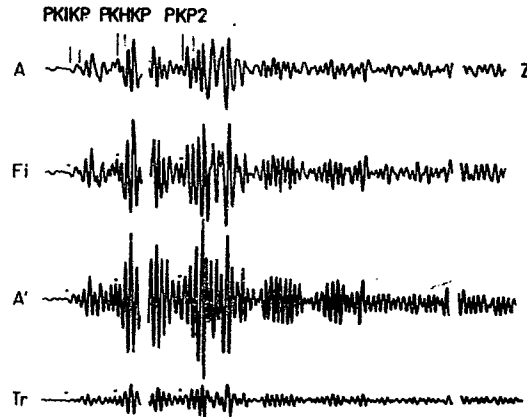


Fig. 6 Vertical records of types A, Fi, A' and Tr from a deep earthquake in the Fiji Island region ($D = 152.6^\circ$, $h = 584$ km, $MPV = 5.7$).

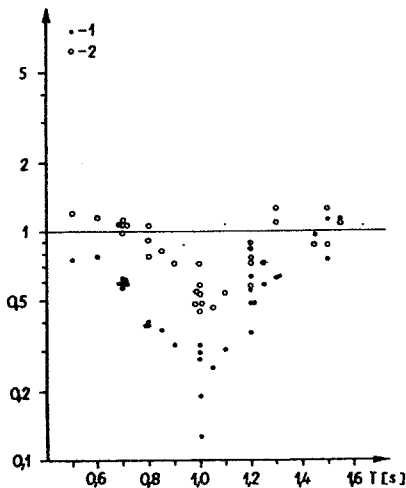


Fig. 7 Amplitude ratio of the first onsets and of the maximum amplitude of P, respectively, in records of type A' and A, normalized to the same magnification for stationary harmonic oscillations. 1 - first onsets, 2 - maximum amplitude of P

the focal region or with closely spaced travel-time curves in case of triplications, depth phases of shallow events etc.

While narrow-band frequency characteristics distort strongly the character of true ground motion extreme broad-band characteristics show minimum convolution. In case of velocity or acceleration proportional characteristics a good fit with the general trend of the inverse noise spectrum is achieved thus insuring a good signal-to-noise ratio over the whole period range and a dynamic range still manageable with modern digital records.

Selected references

- /1/ ARCHANGEL'SKIJ, V.T. et al.: Apparatura i methodika nabljudenij na sejsmičeskich stancijach SSSR. Izdat. Akad. Nauk SSSR, Moskva (1962).
- /2/ ARONOVIC, Z.I.; VIL'KOVIC, E.V.; DOLGOPOLOV, D.V.: Amplitudnye karakteristiki sejsmografa pri nestacionarnych vhodnyh signalach i ocenka pogresnostej, svjazannyh s primeneniem amplitudnyh charakteristik dlja stacionarnyh garmoničeskich kolebanij. Analiz seismičeskich nabljudenij na elektronnyh mašinach. Vyčislitel'naja sejsmologija, Vypusk 1, Izdatel'stvo "Nauka", Moskva (1966), p. 73 - 91.
- /3/ BANERJIA, K.N.: Response characteristics of electrodynamic seismographs. Proc. nat. Inst. Sci. India 26 (1960) 4, Part A, Phys. Sci., p. 348 - 354.
- /4/ BERCKHEMER, H.: The concept of wide-band seismometry. Proc. XII Ass. Gén. CSE, Obs. Roy. Belg. Comm. Sér A, 13, Sér Geophys., 101, Bruxelles (1971).
- /5/ BORMANN, P.: Standardization and optimization of frequency characteristics at Moxa station (GDR). Proc. XIIIth General Ass. European Seismological Comm., Technical and Economical Studies, D. Series, No. 10, Bucharest (1974), p. 133 - 145.
- /6/ DUCLAUX, F.: Seismoetric théorique. Gauthier-Villiar, Paris (1960), 129 pp.
- /7/ KONDORSKAJA, N.V.; ARANOVIC, Z.I.: Metodiceskie osnovy optimizacii sistemy sejsmičeskich nabljudenij. Izv. AN USSR, Fiz. Zemli (1971) 7.
- /8/ KORČAGINA, O.A.; MOSKVINA, A.G.: O vosstanovlenii istinnogo dvizenija povvy po sejsmogramme. Izv. Akademija Nauk, Fiziki Zemli (1975) 7, p. 27 - 42.
- /9/ NEUGEBAUER, H.-J.: Application of elastic network theory in seismometry. Proc. XII. Ass. Gén CSE, Obs. Roy. Belg. Comm. Sér A, 13, Sér Geophys., 101, Bruxelles (1971), p. 224 - 238.
- /10/ NEUNHÖFER, H.: Deconvolution by reiterated convolution. Zeitschrift für Geophysik, Würzburg 29 (1973) 4, p. 513 - 514.
- /11/ SAWARENSKI, E.F.; KIRNOS, D.P.: Elemente der Seismologie und Seismometrie. Akademie-Verlag Berlin (1960), 512 pp.
- /12/ TEUPSER, Ch.: Die Eichung und Prüfung von elektrodynamischen Seismographen. Freiburger Forschungshefte C 130, Akademie-Verlag Berlin (1962), 103 pp.
- /13/ TEUPSER, Ch.: Verallgemeinerung der Theorie elektrodynamischer Seismographen durch frequenzabhängige Koppelung. Veröff. des Inst. für Geodynamik der DAW zu Berlin, Nr. 2, Akademie-Verlag (1965), 127 pp.
- /14/ TEUPSER, Ch.: Die kurzperiodischen Seismographen Typ VSJ-II und HSJ-II. Veröff. des Zentralinstituts für Physik der Erde Nr. 12 (1971), 59 pp.
- /15/ TEUPSER, Ch.; UNTERREITMEIER, E.: Der elektronische Dreikomponenten-seismograph EDS-1. Theorie, Aufbau und Wirkungsweise. Veröff. des Zentralinstituts für Physik der Erde Nr. 51 (1977), 144 p.

- /16/ ULLMANN, W.: Analytische Seismometrie.
Veröff. des Inst. für Geodynamik Jena, Akademie-Verlag Berlin (1971), 339 pp.
- /17/ UNTERREITMEIER, E.: Zur Erhöhung der Störfreiheit langperiodischer Seismographensysteme.
Veröff. des Zentralinstituts für Physik der Erde Nr. 12 (1971), 199 pp.
- /18/ WILLMORE, P.L. (Editor): Manual of seismological observatory practice.
World Data Centre A for Solid Earth Geophysics, Report SE-20, Sept. 1979.

Mitteilung des Zentralinstituts für Physik der Erde Nr. 1046

PRINCIPLES OF ACQUISITION, HANDLING AND STORAGE OF DIGITAL SEISMOLOGICAL DATA

by Jens Bribach

Geoforschungszentrum Potsdam, Division 2: Solid Earth Physics and Disaster Research,
Telegrafenberg, D-14473 Potsdam, Germany
Fax: +49 331 288 1266; E-mail: brib@gfz-potsdam.de

1. SIGNAL TERMS

This lesson deals with terms related to technical realisations of signal acquisition. It covers the signal path from the seismic sensor to the computer final memory. Generally, a signal can be described by its dynamic range and its bandwidth. Dynamic range means the relation between available resolution and (estimated) maximum amplitudes in the logarithmic form of

$$20 \lg \frac{\text{max. amplitude}}{\text{resolution}} [dB] = \text{deciBel.} \quad (1)$$

But any technical solution will limit both resolution and maximum amplitudes which can be recorded or processed. Analogue records on paper, on film or on magnetic tape have a dynamic range less than 45 dB.

Example: Direct writing paper record

$$\left. \begin{array}{l} \frac{\text{max. pen deflection } 20 \text{ mm}}{\text{resolution } 0.2 \text{ mm}} \end{array} \right\} 40 \text{ dB.} \quad (2)$$

Digital records permit to realise a significantly larger dynamic ranges (up to about 140 dB, see section 4.). When estimating the achievable or reasonable resolution one has to take into account the Signal-to-Noise Ratio (SNR). The smallest signal to be processed should have an SNR = 5 ... 10 with respect to the instrumental noise. On the other hand, especially for investigations of the ambient seismic noise, it might be required that the latter is still well resolved, i.e. that the record resolution is several times smaller than the smallest ambient noise amplitude of interest and that the instrumental noise is still well below the ambient noise.

Bandwidth means the frequency range $B = f_{\text{CL}} - f_{\text{HL}}$ with f_{CL} and f_{HL} as the corner frequencies of the related lowpass and highpass filters, respectively (cf. Fig. 1). Technical solutions by means of a seismic sensor, filters etc. necessarily limit the overall bandwidth of the whole acquisition unit.

The corner frequency is defined as the point at which the amplitude A of the response function has dropped by -3 dB ($= 0.707$). Under real conditions the recorded minimum and maximum frequencies, f_{min} and f_{max} , are different from the related corner frequencies because

technical filters cannot realise an infinite slope. Alternatively, one sometimes finds in literature the definition $B = f_{\max} - f_{\min}$ which is larger than $f_{CL} - f_{CH}$ (cf. Fig.1).

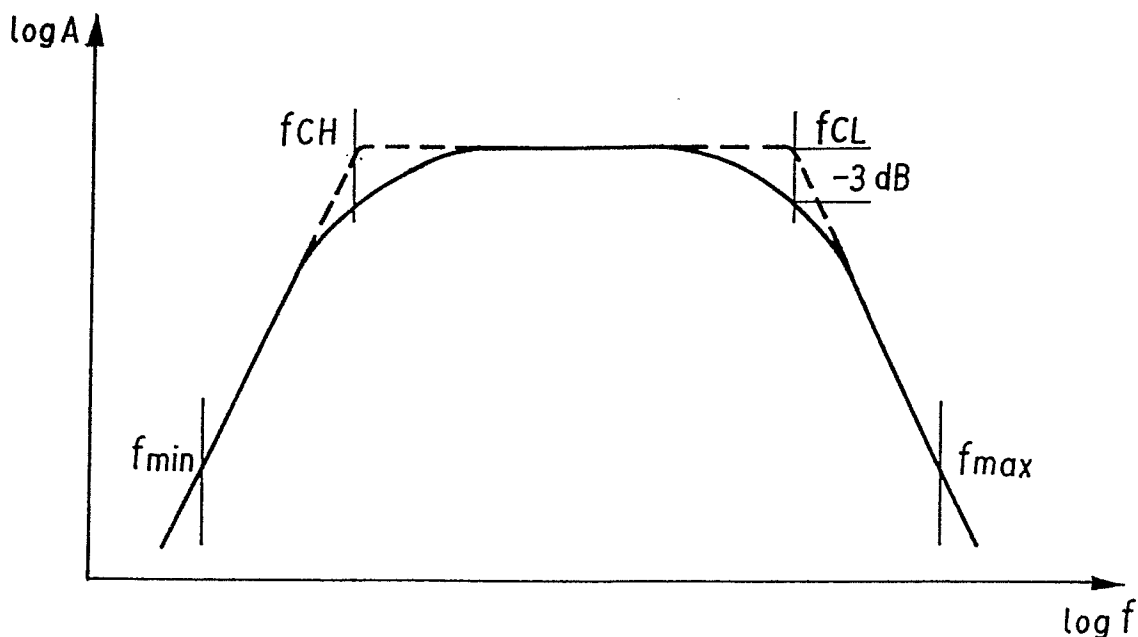


Fig. 1: Amplitude-frequency response of a bandpass filter. f_c - corner frequency; index H - highpass, L - lowpass

Note: The noise power density is proportional to the square of bandwidth. Therefore, the signal-to-noise ratio *SNR* can be improved by bandpass filtering before processing. This is relevant also for the selection of the appropriate resolution.

2. THE SEISMIC SIGNAL

The bandwidth of the seismic signal covers approximately the frequency range from about 1mHz to 1kHz (i.e. about 7 decades or 20 octaves). Tab. 1 gives a rough estimate of maximum possible frequencies which can be recorded depending on distance from the source.

Tab. 1: Maximum seismic signal frequencies as a function of source distance.

Distance	Max. signal frequencies
0.1 km	1000 Hz
10 km	100 Hz
100 km	10 Hz
1000 km	5 Hz
10000 km	1 Hz

The dynamic range of both seismic noise and seismic signal is in the first instance a function of bandwidth. But the amplitudes of noise and signal vary also by more than 3 decades as a function of frequency (cf. Fig. 2 and chapter *Bandwidth-dependent transformation of noise data ...*).

Narrowband short-period measurements ($f > 1 \text{ Hz}$) at quiet places show ambient noise amplitudes less than 1 nm (nanometer) (cf. Fig. 2). In order to resolve this seismic noise a resolution of about 0.1 nm is required in this frequency range.

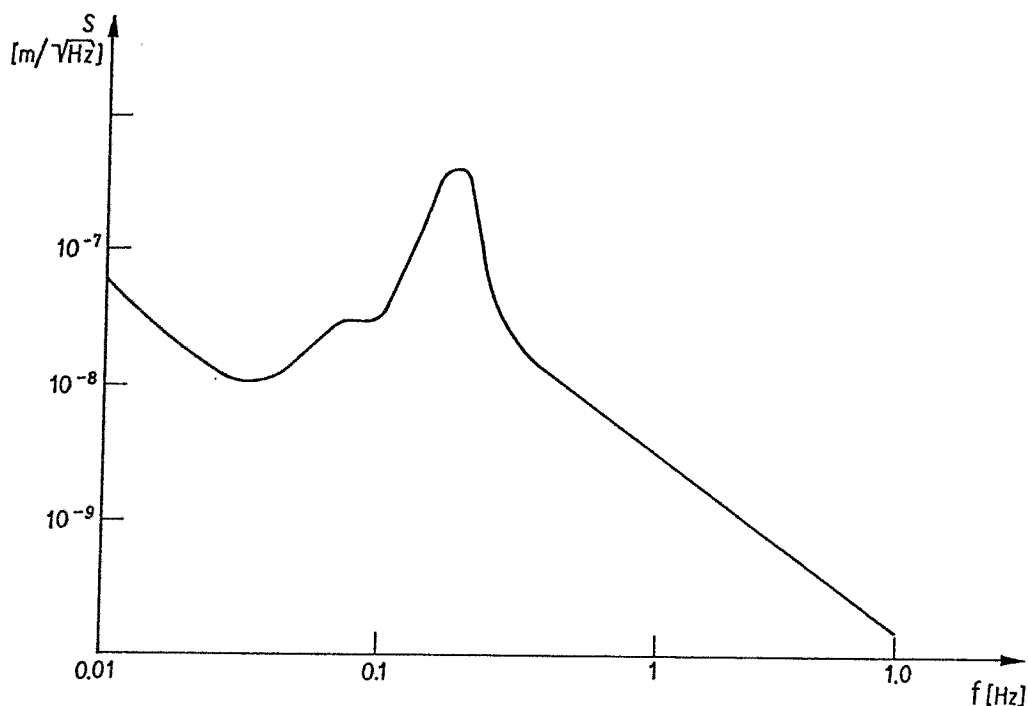


Fig.2: Amplitude spectra of minimum noise at global low-noise sites according to Peterson (1976).

On the other hand, both events of magnitude $M_L = 5.5$ and of $M_s = 8.5$ produce at an epicentral distance of 10 km and 40° (about 4500 km), respectively, ground motion displacement amplitudes of about 10 mm. With a resolution of 10^{-7} mm this would correspond to a dynamic range of 160 dB.

3. INSTRUMENT RESPONSE

Mechanical seismic sensors (spring-mass-system) follow the earth displacement for signal frequencies higher than the natural frequency of the sensor. Their bandwidth is in the range of 2 to 3 decades between their natural frequency at the lower end and spurious resonances at the upper end, e.g. due to the natural frequency of the spring. Tab. 2 summarises the bandwidth of

several types of seismic sensors, i.e. the frequency range between their natural frequency and the maximum frequencies which can still be recorded undisturbed by spurious resonances

Tab. 2: Bandwidth of seismic sensors.

Sensor	Natural frequency	Max. "clean" freq.
geophone (G.)	2.0 ... 20. Hz	300 ... 3000 Hz
short period seismometer (SP)	0.2 ... 2. Hz	50 ... 200 Hz
long period seismometer (LP)	0.01 ... 0.1 Hz	1 ... 20 Hz
broad band seismometer (BB)	(0.003) ... 0.1 Hz	10 ... 50 Hz

The transducer transforms the mechanical movement of the sensor into an electrical signal. Depending on the type of transducer the electrical output is proportional to acceleration, velocity or displacement (Tab. 3).

Tab. 3: Types of transducers.

Transducer	Sensor type	Output prop. to
piezoelectrical	G; SP	Acceleration a
electrodynamical	G; SP; LP	Velocity v
capacitive/inductive	SP; LP; BB	Displacement d

The frequency dependence of both noise amplitudes and signal amplitudes is, in a wide range, approximately proportional to f^{-1} up to f^{-2} . Therefore, the use of a velocity proportional output reduces the necessary dynamic range from 160 dB to 120 dB.

But common mechanical systems as transducers can perform either with high linearity or with high dynamics. This problem was solved by feedback systems which always force the mechanical sensor back to zero position (Fig. 3). Thus high linearity of both sensor and trans-

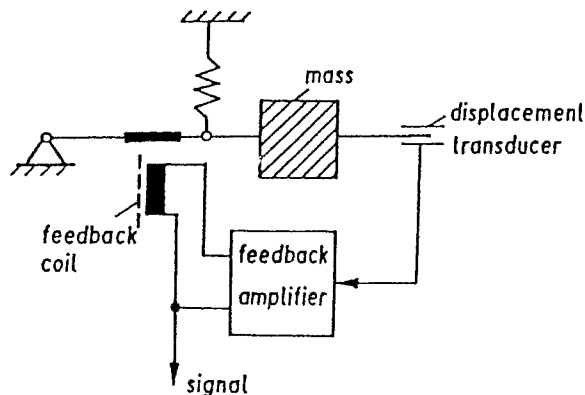


Fig. 3: Scheme of a force-balance feedback system.

ducer can be assured together with high resolution of the transducer, and independent of the dynamic range. The system output of a force-balance system is proportional to acceleration (down to $f \rightarrow 0$). By additional integration a velocity proportional response can be generated within a rather broad frequency range (according to Wielandt 1986 between about 3 mHz and 10 Hz).

Fig. 4 shows typical response curves of short-period (SP), long-period (LP) and broadband (BB) seismographs. The steep slope of all response curves for $f > f_c$ is necessary to prevent aliasing effects due to digitisation.

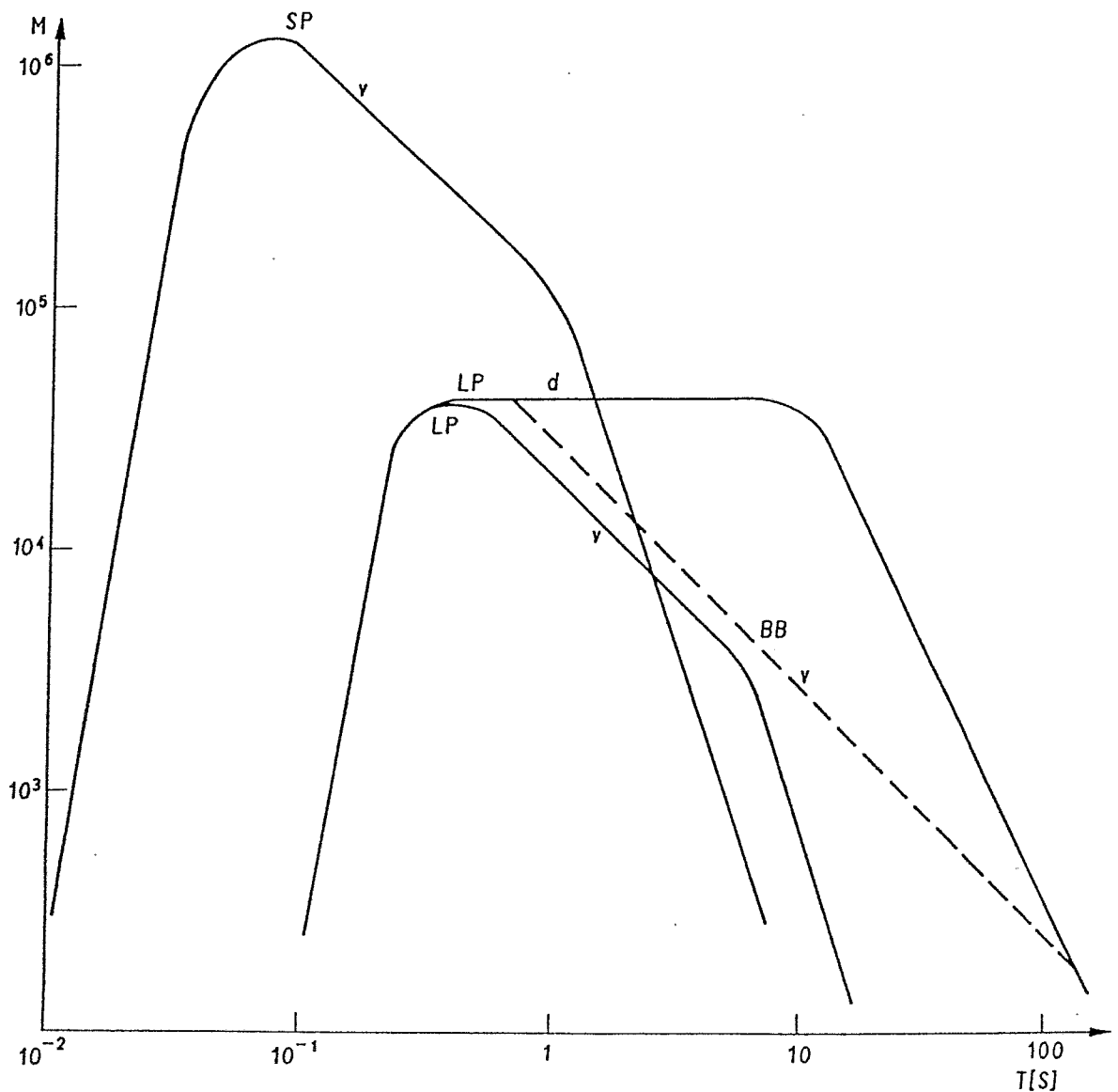


Fig. 4: Typical response curves of seismographs. *v* - velocity proportional and *d* - displacement proportional response. *M* stands for magnification of ground-motion displacement amplitudes.

4. DIGITISING ANALOGUE SIGNALS

4.1. Sampling

Sampling means to get probes of the analogue signal. The sampling time T_s has to take into account the speed of possible signal changes. It should be chosen according to the relation

$$T_s < \frac{\text{resolution}}{2\pi f_{\max} \cdot \text{max. amplitude}} \quad (3)$$

Accordingly, in order to prevent errors due to digitisation the $1/T_s$ has to be much higher than the maximum frequency f_{\max} to be recorded. On the other hand the Analogue-to-Digital Converter (ADC) needs as much time as possible for digitising the probe. This is performed by a Sample-and-Hold Circuit (S & H; cf. Fig. 5). To get probes an electronic switch S is closed for the time T_s only. The input voltage U remains on the capacitor C .

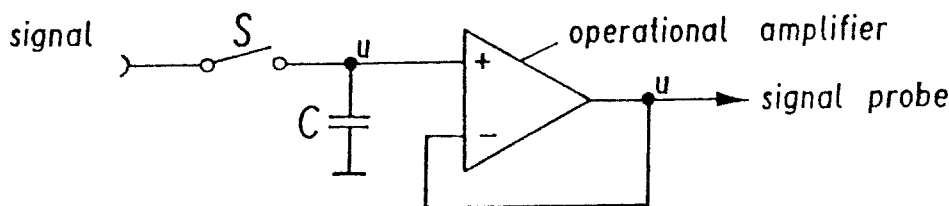


Fig. 5: Sample-and-hold circuit

The necessary sampling frequency (digitisation rate) f_D is defined by Shannon's sampling theorem:

$$f_D = 2 f_{\max} \quad (4)$$

with f_{\max} - maximum frequency to be recorded.

Often f_{\max} is named the *Nyquist frequency* ($f_{Ny} = 0.5 f_D$) which is related to the avoidance of the second kind of digitisation errors, namely *aliasing*. Because of the structure of real filters any analogue signal will still contain components of $f > f_{Ny}$. But spectral lines of those frequencies will then be presented as spectral lines of $f < f_{Ny}$ (periodical repetition of the spectrum; cf. Fig. 6). The size of the *aliasing* effect depends on how much the signal amplitudes can be reduced for frequencies $f < f_{Ny}$ with respect to the main amplitude-frequency level. But the possible error range due to *aliasing* can only be estimated; no information on the real amplitude and real phase of *aliasing* can be obtained.

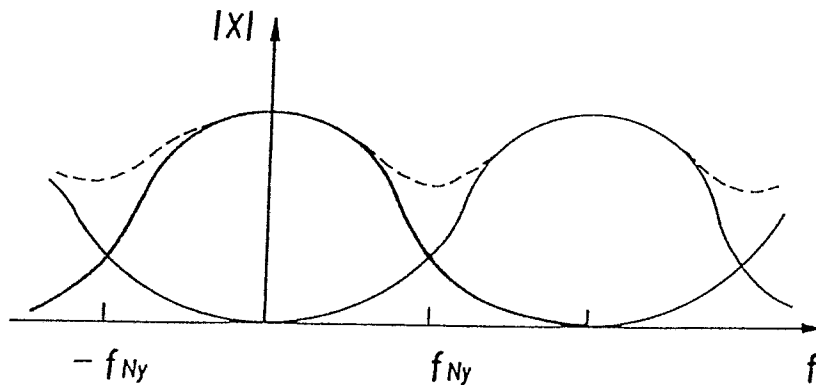


Fig. 6: Spectral aliasing:

1. Original spectrum —————
2. Periodic repetition ————
3. Aliasing effect - - - - -

In seismology the corner frequency of anti-aliasing LOW PASS filters is mostly set at $f_c = 0.5 f_{\max} = 0.5 f_{Ny}$. In this case a 6th or a 7th order low pass is sufficient for analogue recordings and visual data analysis. The related amplitude decay for $f \gg f_c$ is then 6 or 7 octaves per one octave of frequency. This corresponds to a factor of $2^6 = 64$ or 36 dB, respectively.

When using digital data acquisition and analysis the amplitude reduction at f_{Ny} has to cover the dynamic range of the Analogue-to-Digital-Converter (ADC). But analogue filters should not exceed 8th order (i.e. 48 dB per octave). This problem can be solved by *oversampling*, i.e. by setting:

- the input sampling rate f_i more than 10 times higher than the wanted sampling or acquisition rate f_D ;
- the corner frequency of the analogue input low pass at $f_c = 0.5 \dots 0.1 f_D$.

Thus, e.g., with an *oversampling* of $f_i = 20 f_D$ and a 6th order low pass of $f_c = 0.5 f_D = 0.025 f_i$ the signal is reduced at $f_{Ny} (f_i) = 0.5 f_i$ by -156 dB. This would be sufficient even for a (still theoretical) 27-bit-ADC.

The final filtering to reduce the sampling rate to f_D is done digitally, mostly by special signal processors fast enough to process real time filtering up to 64th order. This steep slope allows low-pass corner frequencies closer to the originally wanted sampling rate f_D , commonly up to $f_{Cdig} = 0.8 f_{Ny} (f_D)$. For the given example (64th order, $0.08 f_{Ny}$) the low pass performs a damping of -124 dB at $f_{Ny} = 0.5 f_D$.

When using such steep slope low passes one should process frequencies up to f_{Cdig} only. Re-calculating the filter influence for $f_{Cdig} > f > f_{Ny}$ would increase digital noise and would re-magnify the just damped aliasing effects too.

4.2. Analogue-to-digital conversion

The Analogue-to-Digital Converter (ADC) turns the values of given samples into a number of quantified values. The smallest digitisation step is called *digit* or *count*. The ADC counts in steps of powers of 2 (2^n). Every cipher is called *bit* as an abbreviation of *binary digit*.

Example: The 4 bit number H H L H ;

H → High or present (i.e. current on)

L → Low or absent (i.e. current off)

binary number	H	H	L	H	
binary values	2^3	2^2	2^1	2^0	
decimal value	8	+ 4	+ 0	+ 1	= 13

The smallest unit of a digital value or word is Byte (= 8 bit). 12 bit and 16 bit ADC are sold as personal computer plug-in boards including S & H interface and multiplexer for 8 or 16 input channels. Their dynamic range is insufficient for some applications and can be extended by switchable amplification levels depending on signal level (so called gain-ranging). A widespread solution uses a 12-bit ADC in the form of

mantissa	11 bit	16 bit = 2 Byte
sign	1 bit	
exponent	4 bit	

The exponent represents the gain level in powers of 2 or 4 or 8. But nowadays more and more 24-bit ADCs are used in modern data loggers. Tab. 4 gives the dynamic range which be realised with common ADCs

Tab. 4: Dynamic ranges of common ADCs

bits (incl. sign)	digits	dyn. range
12	2,048	66 dB
16	32,768	90 dB
24	8,338,608	140 dB

5. SIGNAL TRANSMISSION

Analogue transmission is still often used for short or non-expensive connections. Typical distances are given in Tab. 5.

Tab. 5: Distances for analog transmission lines.

Signal	Link	Distance
direct connection	wire	some 100 m
amplitude modulation	wire	some 10 km
	telephone line	direct conn. 40 ... 100 km
frequency modulation	radio link	via relays > 1000 km

The most often used analogue method is frequency modulation. The instrument analogue output controls a Voltage Controlled Oscillator (VCO). Instrument voltage changes cause frequency changes in the range of the speech band of 300 ... 3400 Hz. you have only to take into account the modulation condition: carrier frequency $> 3f_{\max}$.

The VCO output can be switched immediately to commercial transmitters (cf. Tab. 6).

Tab. 6: Available commercial transmitters

Transmitter	Carrier [Hz]	Dyn. range [dB]	Power supply
telephone	300 ... 3400	60 ... 90	... 10 mW
walkie-talkie	300 ... 3400	40 ... 60	... 10 W

A typical analog data transmission-acquisition chain is depicted in Fig. 6. For a larger number of channels one should hire whole carrier groups. A carrier group of 24 telephone channels can be switched via one galvanic coupled telephone wire, e. g. in local networks.

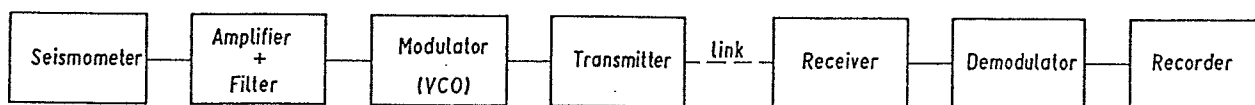


Fig. 7: General scheme of an analog data transmission-acquisition system.

The same links are available for digital transmission. The digital information is converted bit by bit into frequency or phase jumps of the carrier frequency by help of a MODEM (MODulator/DEMulator).

Digital transmission allows connections in both directions via one line either simultaneously (full duplex) or alternately (half duplex). Fig. 7 depicts the general scheme of a digital data acquisition-transmission system.

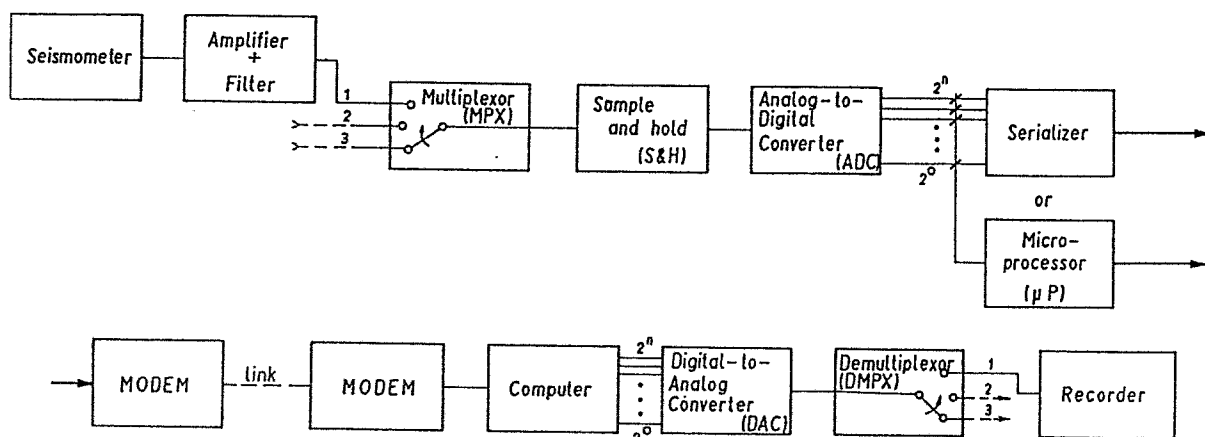


Fig. 8: General scheme of a digital data transmission-acquisition system.

6. DATA TRANSMISSION

Data rates depend on sampling rates. In the following explanations we count on the base of a 16-bit-word (= 2-Byte-word) per sample. The sampling rate is the number of samples per second (sps). Seismology commonly uses sampling rates f_D of

$$f_D = 2.5 \dots 4 f_C \quad (5)$$

with f_C as the filter's upper corner frequency. For evaluating the slope of the signal spectrum f_C should be up to two times higher than the expected signal corner frequency. Common sampling and data rates are given in Tab. 7. Note that sampling rates are generally a compromise with respect to transmission and storage capacity.

Tab. 7: Common sampling and data rates at seismic stations.

Problem	Sampling rate [sps]	Components per station	Data rate [bit/s]
near field investigation	1000	1	16,000
local networks	200	1 (3)	3,200 (9,600)
territory monitoring	20	3	960
global monitoring	1 (20)	3	48
Example of single 3-component broadband station	1 * 200	Vertical	3200
	3 * 20	vert.; N-S; E-W	960
	3 * 1	vert.; N-S; E-W	48
Sum of single BB station	263	3-component	4208

Line or channel transmission rates (capacity) are given in *Baud* (1 Bd = 1 bit/s). Transmission procedures reduce this values to 90 ... 80 %. On the other hand the statistical behaviour of the information allows bit coding to run 4800 and 9600 bit/s on 2400 Bd lines. This coding is part of the MODEM transmission procedure, and it does not touch computer input or output routines (MNP5-protocol: compression factor 2; V42: factor 4). Tab. 8 summarises typical data transmission rates.

Tab. 8: Transmission rates (brutto)

Transmission rate	Telephone	Data network	Radio
65,000 Bd		ISDN narrow band	
9,600 Bd		Datex	
4,800 Bd		Datex	
2400 or 1200 Bd	leased lines		walkie-talkie
300 Bd	acoustic coupling		

7. DATA STORAGE

According to transmission rates storage capacity forms the second limitation. Tab. 9 summarises storage media and capacities commonly used in seismological applications.

Tab. 9: Storage media used in seismological applications. Storage duration is based on the assumption of a single broadband station as in Tab. 7 with 1×200 sps + 3×20 sps + 3×1 sps. *) for data no commercial solution available

Medium	Capacity	Storage of 263 sps for	Access time
Tapes			
- tape ½"	25 ... 200 MByte	13 ... 100 h	several min.
- Video*)	13 GByte	280 d	several min.
- R-DAT	3 GByte	65 d	several min.
- EXABYTE/video8	5 GByte	110 d	several min.
Discs			
- floppy disc	... 3 MByte	... 2.5 h	some 10 ms
- hard disc	... 30 GByte	... 2 years	some 10 ms
- optical disc	... 5 GByte	... 100 d	some 100 ms
Solid state			
- 1-Mbit-chips	4 MByte/board	2 h/board	some 100 ns
- 4-Mbit-chips (C-MOS-SRAM)	16 MByte/board	8 h/board	(for all solid state memories)
- Flash-RAM (PCMCIA)	... 440 MByte	... 200 h	

Storage of triggered records will reduce the data amount down to about 5...10 %. The same can be achieved by daily or weekly inspection of the whole time series and selection of event record sections. This has the additional advantage of minimising false alarms and non-detections.

In field measurements solid state memories (Integrated Circuits *IC*) have replaced older audio tape cassette technique. But also floppy disc drives can be used under rough field conditions. Data processing demands quick access and will run within the computer's main solid state memory supported by discs. In data archiving the trend is from high density tape to optical disc (*MOD*) and to compact disk (*CD*).

Before storing data their formats should be standardised, both for sampled data for complementary guiding (header) information. But there is no dominating international standard. Note, that data of time series should be stored in dual form (i.e. in powers of 2) and that any group of data (file, data set) has to be opened with a guiding information named 'header'.

The header should contain at least the following:

- time beginning of the record (year, month, date, hour, min, sec)
length
time correction if no absolute time base is available
- order of channels
stations
station components (vertical, N-S, E-W ...)
- station information station code and co-ordinates
status(e.g. out-times of station or components)
sampling rates
response curves
- event information location
origin time
magnitude
comments

The multiplex structure defines the order or the arrangement of data from different sources within a data file. Sampling of different components generates

time multiplex:	first	sample	of	component	1
	first	sample	of	component	2
	first	sample	of	component	3

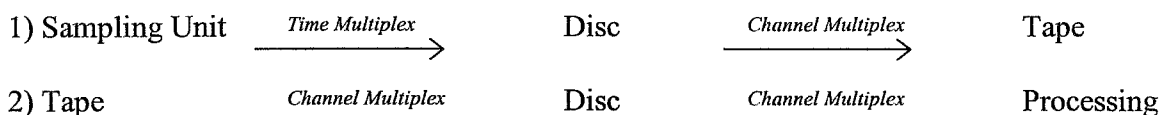
					1
	second	sample	of	component	1
	second	sample	of	component	2
	second	sample	of	component	3

Also transmission and immediate storage are done in this structural form. But before processing and archiving the data file should be converted into:

channel multiplex:	first	sample	of	component	1
	second	sample	of	component	1
	third	sample	of	component	1

	first	sample	of	component	2
	second	sample	of	component	2
	third	sample	of	component	2

Because data transformation and filtering are carried out channel-wise. The following scheme is run inside the processing system:



8. TIME SIGNAL

The time signal is the main guiding information of time series. Its accuracy should be better than $t = 0.1$ s for global and better than $t = 0.01$ s for local evaluations. In case of digital data acquisition the required time accuracy depends on the sampling rate f_D and should be roughly:

$$t = \frac{1}{10 f_D} \quad (6)$$

Crystal clocks run with an error of 10^{-6} to 10^{-8} for temperature compensated crystals (TCXO). This corresponds to about 0.1 ... 0.001 s per day.

Radio time signal errors occur on the receiver side only. Their first relevant component is due to the finite travel time which depends on the station distance. A distance of 300 km causes a delay of 1 ms. Weather induced time errors are not relevant in seismological applications. The second relevant cause of time errors occurs within the receiver (filters). They are in the order of 1 ms up to several 10 ms depending on the receiver type. Because of different receiving conditions a radio controlled crystal clock is the most widely used device. Advanced solutions use computer controlled compensation of the crystal behaviour due to ageing, temperature changes etc. Corrections are derived from average time signal differences.

Absolute time signals are distributed by national and world-wide services. National time service signals are transmitted by radio stations (hourly pulse groups), time transmitters (pulse coded signal: year ... sec) and by television transmitters: On several well defined times the start time of a (picture) frame synchronising pulse is controlled by the atomic clock of the national time service.

World-wide time signals are available from satellite positioning systems such as the United States Global Positioning System (GPS). Its signals can be received continuously around the world for 24 hours per day. Limitations for non-military users do not affect seismological time signal requirements. In 1988 also the former Soviet Union opened its similar GLONASS system for civil use. One gets satisfying results also by using world-wide long wave transmission systems such as the Omega time service. But needed technical efforts and receiver costs are meanwhile higher than for the mentioned satellite time services.

The absolute time signals should be related to the recorded time series in two ways:

- In order to find archived data the header should give the exact date of the record down to minute or second;
- Within the time series additional time pulses (e.g. 1 bit per word) allow precise data synchronisation and correlation and ease the orientation in long data blocks.

Time synchronisation is necessary for block-wise digital transmission because outside sampling happens at a time different from centralised storage time and secondly, transmission procedures change the length of a data block dependent on information structure.

Figure 9 shows schematically various components and options of seismological data acquisition systems. The solution depicted in the upper part (seismometer to paper record) is the cheapest one (if no expensive special recording paper is required) but expensive in evaluation. In the middle part the one-way transmission of frequency modulated analogue or hardware coded digital signal is shown. The lower part represents computer based acquisition which allows data transmission in both directions for additionally automatic checking and control of the outside station. This can be used for clock correction, seismometer and amplifier calibration, and for changing of station parameters.

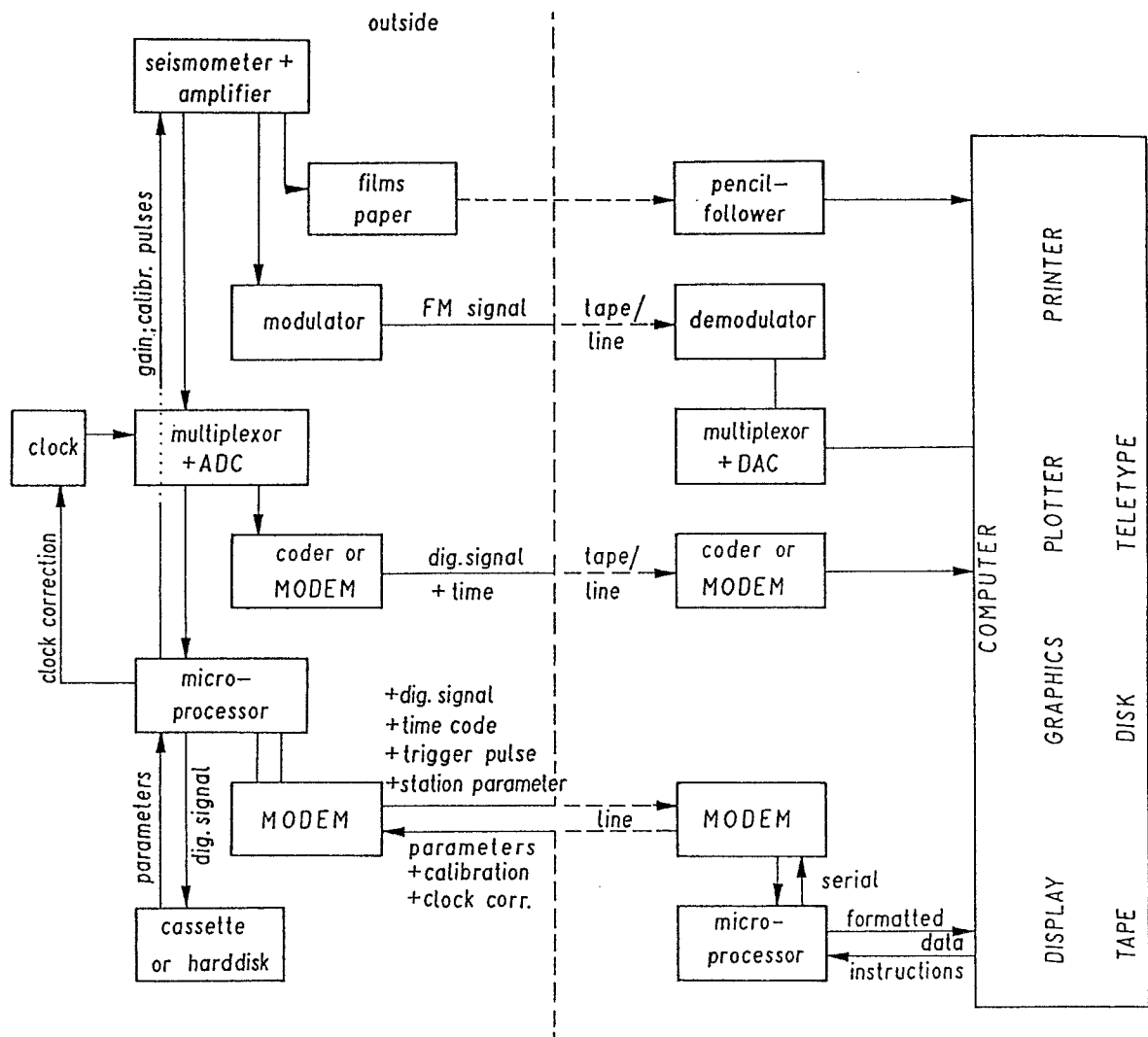


Fig. 9: Components and links of seismological data acquisition systems (from seismometer to computer).

9. TRIGGER CRITERIA

Amplitude criteria are non-expensive in analogue hardware or in computer software realisation. The most simple one consists of a threshold level fixed at 3 ... 5 times of maximum noise amplitudes. But noise level is proportional to bandwidth. This problem can be solved by passband filtering at the expected maximum of the signal-to-noise ratio *SNR*:

local events	higher than 5 Hz
regional events	2 ... 5 Hz
global events	lower than 1 Hz

Additionally, the amplitude threshold level can be adapted to current noise conditions by relating average long-time changes of natural (weather) or human noise (traffic) to short-time changes (*STA/LTA*: Short-Term Average / Long-Term Average). The latter differ strongly from the *LTA* in case of the onset of transient seismic signals of sufficient *SNR*.

Fig. 10 shows an analogue realisation of an *STA/LTA* trigger.

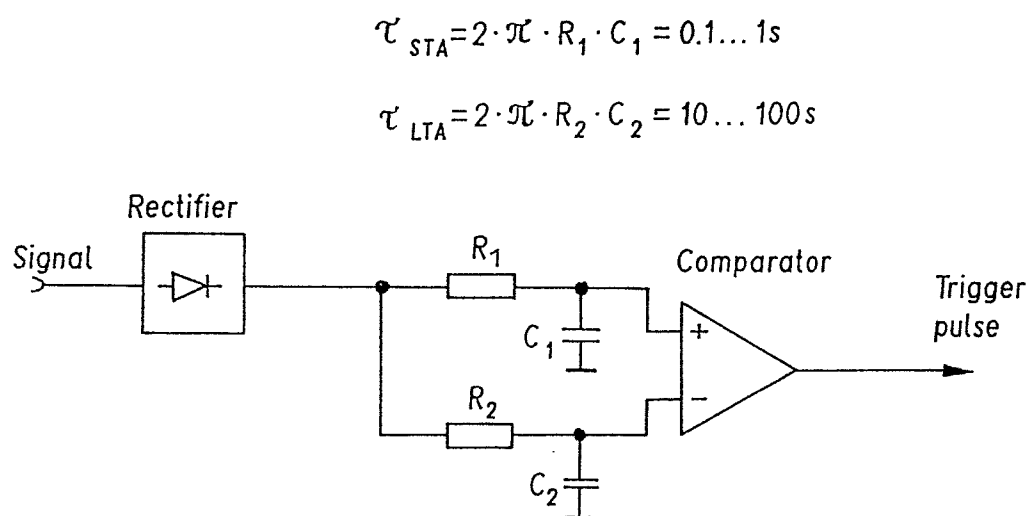


Fig. 10: Analogue realisation of an *STA/LTA* trigger. τ - time interval of averaging.

The signal is rectified, and its absolute values are integrated by first order low passes of different integration times τ :

<i>STA</i> \approx 0.1 s ... 1 s
<i>LTA</i> \approx 10 s ... 100 s

Commonly the amplitude threshold level is set to *STA/LTA* = 3 ... 5. A digital software solution of an *STA/LTA* trigger requires first order recursive low passes only. It can be run on-line in background processing of any PC.

The functioning of STA/LTA triggers and the setting of the most suitable parameters depending on the task and type of seismic signals to be monitored are described in detail in chapter *Understanding and setting STA/LTA trigger algorithm and associated parameters*.

Frequency criteria are more sensitive and they cover a broad signal band simultaneously. The less expensive ones use periodogram analysis to monitor some main spectral lines via *STA/LTA*. More sophisticated trigger algorithms, some of them including also pattern recognition, are described by Murdock and Hutt (1983) and Joswig (1990, 1993, 1995).

Fourier transformation of a given time window is also used for identification. Spectral analysis can not be run on-line without additional signal processors. To reduce calculation expense often the Walsh transform is applied (cf. Gofforth and Herrin, 1981). It needs addition and subtraction procedures only, but calculated Walsh spectral lines are different from signal frequencies. Thus evaluation becomes more difficult.

Error prediction filters use the difference between the (predicted) model and the true signal. Models can be Fourier or Walsh spectra or the statistical behaviour of random variables. The trigger compares model coefficients with signal coefficients or model generated time series with origin time series.

Lowering the threshold level will increase the false alarm rate exponentially. Checking criteria will reduce this effect. The most widespread criteria are postdetector and voting.

The postdetector checks the signal behaviour after triggering, e. g. the signal envelope. For short period measurements the signal duration should be longer than 3 seconds to exclude pulses generated by disturbances within the device.

Voting means that an event must be triggered by 3 ... 5 stations of a network within given time window depending on signal travel times through the network.

REFERENCES

- Bath, M. (1974). *Spectral Analysis in Geophysics*. Elsevier Science Publ. Company, Amsterdam-Oxford-New-York.
- Gofforth, T. and Herrin, E. (1981) An automatic seismic signal detection algorithm based on the Walsh transform, *BSSA*, **71**, 1351-1360.
- IASPEI/CCSS (1983). *Proceedings of the workshop on portable digital seismograph development*. 30.Nov.- 2. Dec., Los Altos, California.
- Joswig, M. (1990). Pattern recognition for earthquake detection. *Bull. Seism. Soc. Am.*, **80**, 170-186.

- Joswig, M. (1993). Single-trace detection and array-wide coincidence association of local earthquakes and explosions. *Computers and Geosciences*, **19**, 207-221.
- Joswig, M. (1995). Artificial intelligence techniques applied to seismic signal analysis. *Consel de Léurope, Cahiers du Centre Européen de Géodynamique et de Séismologie*, Vol. 9, Proceedings of the Workshop: Dynamic systems and artificial intelligence applied to data banks in geophysics, 5-15.
- Lee, W.H.K.; Stewart, S.W. (1981). Principles and applications of micro-earthquake networks. Academic Press New York-London-Toronto-San Francisco Sidney.
- Murdock, J. N. and Hutt, C.R. (1983) A new event detector designed for the seismic research observatories, USGS, Open File Report 83-7851
- Peterson, J.; Hutt, C.R.; Holcomb, L.G. (1980). Test and Calibration of the Seismic Research Observatory. Open-File Report 80-187, Albuquerque, New Mexico
- Stearns, Samuel D. (1975). Digital Signal Analysis. Hayden-Verlag, Reochelle Park, New York, 280pp.
- Wielandt, E. (1986). Design Principles of Electronic Inertial Seismometers. Inst. of Geophysics, Publ. No. 384, Zurich.

SEISMIC DATA ACQUISITION AND ANALYSIS

Michael Baumbach

GeoForschungsZentrum Potsdam, Division 2: Solid Earth Physics and Disaster Research,

Lecture presented at the Advanced Study Course on Seismic Risk („SERINA“)
September 21-27, 1997, Thessaloniki, Greece

1. THE RECORDING SYSTEM

Time series recorded by seismic stations depend on the source mechanism of the earthquake considered, on the velocity and attenuation structure of the propagation medium and on the recording system used. Additionally, they might be superimposed by ambient seismic noise. The recording system includes the seismometer and the data recorder. When we try to derive information about the earthquake source, the Earth structure, or local site effects we have to be aware, that the results may be affected by the recording system. One has to know, therefore, the basic properties of the recording system in order to correct the recorded time series or the derived source or medium parameters accordingly.

The first part of the lecture deals with the seismometer and the different techniques used for digitising the analogue output signal of the seismometer. Further, methods for estimating the quality of recording systems are described.

1.1 The Seismometer

In order to understand how the recorded signal can be related to the ground motion we analyse the equation of motion of a vertical pendulum seismometer (figure. 1).

Its equation of motion is:

$$kx + D\dot{x} + m(\ddot{x} + \ddot{y}) = 0 \quad (1)$$

x - displacement of the suspended mass relative to the ground

y - displacement of the ground (true ground motion)

k - spring constant

D - friction coefficient

m - suspended mass

When applying the Fourier transform to equation (1) we get

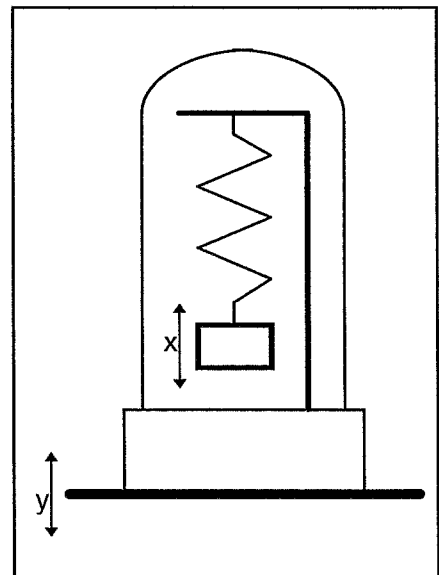


Fig. 1: Pendulum seismometer without transducer

$$X(\omega) = Y(\omega) \omega^2 / (\omega_0^2 + 2 i h \omega \omega_0 - \omega^2) = Y(\omega) T(\omega) \quad (2)$$

with $\omega_0^2 = k/m$ $\omega_0 = 2 \pi f_0$ - angular eigenfrequency of the seismometer
and $h = D/(2 m \omega_0)$ - damping constant

The expression

$$T(\omega) = \omega^2 / (\omega_0^2 + 2 i h \omega \omega_0 - \omega^2) \quad (3)$$

is denoted as frequency response function and its inverse Fourier transform as impulse response function of the system. Indeed, a Delta impulse $\delta(t)$ has a flat spectrum $\delta(\omega) = 1$. Therefore, the inverse Fourier transform of (2) gives the response of the seismometer to an impulse input. According to (2) the seismometer output can be calculated either by multiplying the ground motion spectrum with the frequency response function and subsequent Fourier transformation of $X(\omega)$ into the time domain or by convolving the ground displacement $y(t)$ with the impulse response function $T(t)$, i.e. $x(t) = y(t) * T(t)$.

The general shape of the frequency response of a seismometer can be derived from (3): at small frequencies ($\omega \ll \omega_0$) the response is proportional to ω^2 , at high frequencies ($\omega \gg \omega_0$) the response is -1 . The behaviour in the vicinity of the eigen- or corner frequency ω_0 depends strongly on the seismometer damping constant h .

The motion of the pendulum can be measured by a capacitive or inductive transducer. In case of a capacitive transducer the measured voltage is proportional to the displacement of the suspended mass. In case of an inductive transducer a coil, connected to the seismometer mass, is moving through a permanent magnetic field. The induced voltage is proportional to the velocity of the seismometer mass. This introduces an additional $i\omega$ in the numerator of the seismometer frequency response function. Further, the generator constant G of the seismometer coil has to be taken into account. The transducer resists to the motion of the seismometer mass and therefore changes the damping constant h . For an electromagnetic sensor, we finally get the frequency response function

$$T(\omega) = G i \omega^3 / (\omega_0^2 + 2 i h \omega \omega_0 - \omega^2). \quad (4)$$

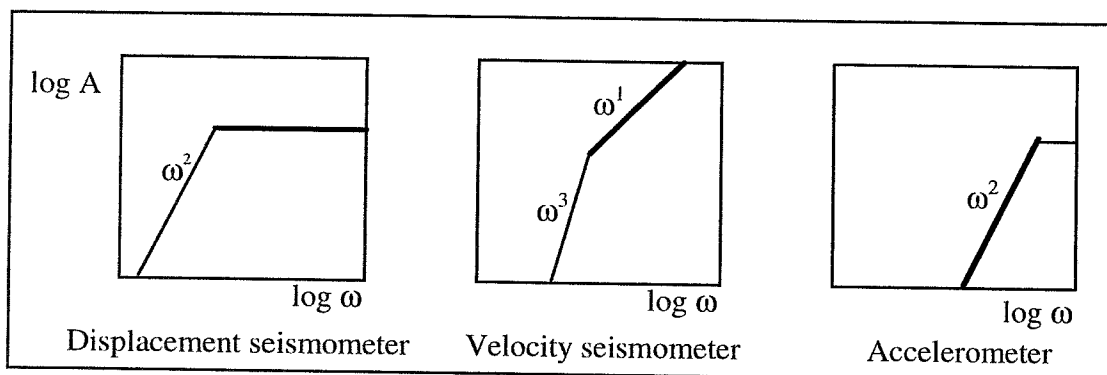


Fig.2: Response curves for different seismometer types, A: displacement amplitude
 ω : angular frequency

Usually, the damping constant h is set to 0.7. For $h \geq 1$ the pendulum returns to the resting state (zero position) after initial elongation (release test, zero initial velocity) without oscillations ($h = 1$: critical damping).

Figure 2 shows the frequency response curves of displacement and velocity seismometers and an accelerometer. Below the corner frequency a displacement seismometer records acceleration. Therefore, accelerometers usually consist of sensors with high eigenfrequencies (e.g. 60-100 Hz).

Equation 3 is a specific example for the calculation of the system response of general linear time invariant systems, which will be described by linear differential equations (Scherbaum, 1994). The general expression for the frequency response function of such a systems is:

$$T(\omega) = C \frac{(i\omega - z_1)(i\omega - z_2)(i\omega - z_3) \dots (i\omega - z_m)}{(i\omega - p_1)(i\omega - p_2)(i\omega - p_3) \dots (i\omega - p_n)} \quad (5)$$

where C is a constant and p_j and z_j are the so called poles and zeros of the system. They are complex numbers and describe the system completely.

The poles and zeros of equation (3) are

$$p_{1,2} = (-h\omega_0, \pm \omega_0 \sqrt{1-h^2}) \quad z_{1,2,3} = (0, 0). \quad (6)$$

1.2 Digital data recorder

Before sampling the analogue data they have to pass through an ant-alias lowpass filter which should remove all signal energy above the so-called Nyquist frequency f_n , that is half the sampling frequency f_s . Otherwise, the sampling process would map this energy into the frequency band from 0 to f_n and distort the digitised time series. Therefore, anti-alias filtering has to be done using analogue filters. Analogue filters of course influence the recorded trace what has to be taken into account when analysing the data. They change both the amplitude and the phase spectrum. The corner frequency of the analogue filters is usually about 30% f_n , what means, that a significant portion of the frequency range is lost or its spectral amplitudes being distorted.

Over the last years the dynamic range of the analogue to digital converters has been permanently improved. Nowadays, 24 bit converters are becoming a standard, although there are still 16 bit systems on the market and a lot of 12 bit systems are still in use in many countries. The theoretical dynamic range DR of digital systems is being calculated in Decibels [db] as

$$DR = 20 \log(A_{max} / A_{min}) = 20(n - 1) \log 2 \approx 6(n - 1). \quad (7)$$

n is the number of bits of the AD-converter and -1 takes into account, that one bit is used for storing the sign of the sample.

Methods for increasing the dynamic range of AD-converters

1. Gain ranging

Gain ranging AD-converters sample the same analogue signal from different channels with amplifications differing by $i = 2^k V$ (k - integer constant, V is the voltage corresponding to 1 count at the lowest amplification). The sample to be stored will be selected by a logic unit from the AD-board that has the highest amplification and is not yet off-scale. The data are usually stored in gain ranging format which consists of the mantissa m (output of the converter) and an exponent n of i which shows the gain amplification. The amplitude in counts can then be derived as

$$A = m i^n . \quad (8)$$

Other more recent gain ranging systems use instead of AD-boards with different preamplifiers one single programmable preamplifier which checks the input voltage of the AD-converter and reduces, if required, the preamplification. It should be underlined, that the use of gain ranging AD-converters increases the dynamic range but decreases the internal resolution (larger amplitude steps for greater amplitudes compared with smaller ones).

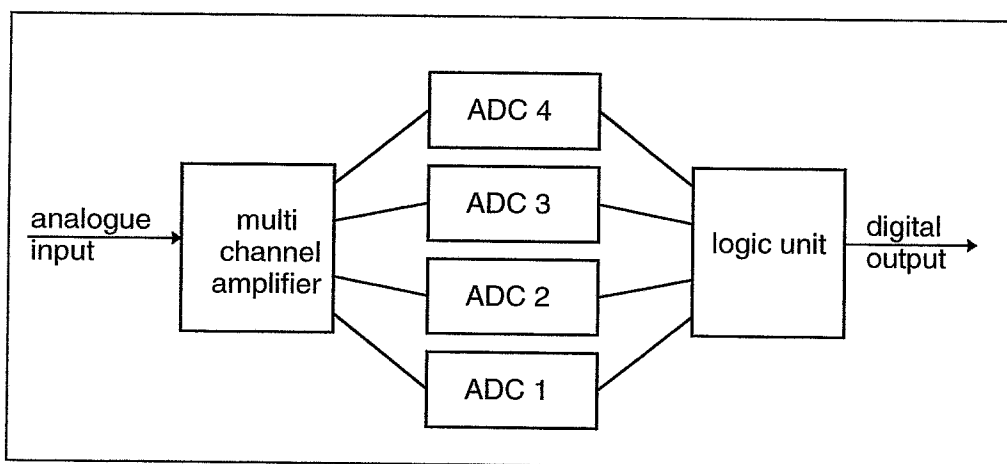


Fig. 3: Schema of a gain ranging ADC

2. Oversampling

Oversampling means, that the primary sampling rate is larger than the final sampling rate desired. The method (Oppenheim and Schaffer, 1989) is based on the assumption, that the quantization noise has a variance that is independent of the sampling rate. This is true if the quantization noise has a probability density function which is flat between $\pm Q / 2$, where Q is the quantization step. The variance of the quantization noise equals $Q^2 / 12$. When applying the Parseval theorem, which states that the energy in the time domain equals the energy in the frequency domain, we get for two different Nyquist frequencies f_1 and f_2 and a given time series of quantization noise

$$\int_{t_1}^{t_2} n(t)^2 dt = \int_{-\omega_1}^{\omega_1} N_1(\omega) N_1^*(\omega) d\omega = \int_{-\omega_2}^{\omega_2} N_2(\omega) N_2^*(\omega) d\omega. \quad (9)$$

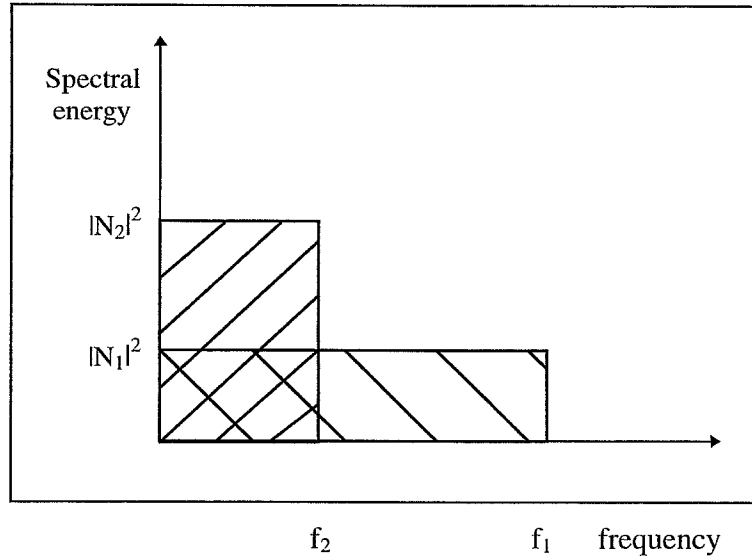


Fig. 4: Principle of oversampling

N_1 and N_2 are the spectral noise amplitudes for Nyquist frequencies $\omega_1=2\pi f_1$ and $\omega_2=2\pi f_2$, N_1^* and N_2^* are the complex conjugates of N_1 and N_2 . The time integral does not depend on the sampling rate and therefore on the Nyquist frequency. This results in a different spectral noise amplitude $N(\omega)$ for different Nyquist frequencies ω_1 and ω_2 .

$$|N_1|/|N_2| = \sqrt{(f_2/f_1)} \quad (10)$$

Digital lowpass filtering of an oversampled time series with full floating point accuracy (decimation filter) and subsequent resampling with a lower sampling rate decreases the noise level by $\sqrt{(f_2 / f_1)}$ and therefore increases the dynamic range of the recording system. For example, a recording system with an oversampling ratio f_1 / f_2 of 16 (PDAS-100, TELEDYNE Geotech) increases the dynamic range by a factor of 4 what corresponds to an enhancement of the number of bits by 2.

1.3 Properties of modern recording systems

There are several seismic recorders with different parameters on the market. When selecting a recorder for a specific purpose one has to check what system has the optimum parameters for the data to be recorded. This chapter describes the most important parameters and shows, how to derive them.

1. Dynamic range

According to equation 7 we have to find the the maximum and minimum signal amplitude for computing the dynamic range of a data recorder. The maximum amplitude for the given recorder can be simply derived from its clipping level in counts. The minimum amplitude of a seismic signal that can be identified in a record depends on the eigennoise of the recorder in counts. A comparison of sinus oscillations with different amplitudes (model of a seismic trace) superimposed by normally distributed noise with standard deviation σ (eigennoise of the recording system) shows, that a seismic signal can be detected starting from an amplitude of $\sqrt{2} \sigma \approx 1.4 \sigma$ (figure 5), which is assumed as minimum amplitude for the computation of the dynamic range of the recorder ($DR=20 \log (A_{max}/A_{min})$ in db).

For checking the dynamic range in the frequency domain we have to compare the spectra of the sinus signal and the noise. For the transformation into the frequency domain we use the discrete Fourier series. The length of the time series was selected as a multiple of the period of the test signal. In this case the sinus test function is orthogonal to all basis functions so that only one Fourier coefficient describes the test signal in the frequency domain. In order to compare the noise and signal parameters we apply the Parseval theorem to the given time series f_i . In order to get power instead of energy we divide the equation by the length of the time series T.

$$N^{-1} \sum_{i=1}^N f_i^2 = 1/2 \sum_{k=1}^{N/2} |F_k|^2 \quad (11)$$

N is the number of samples f_i and F_k are the complex Fourier coefficients.

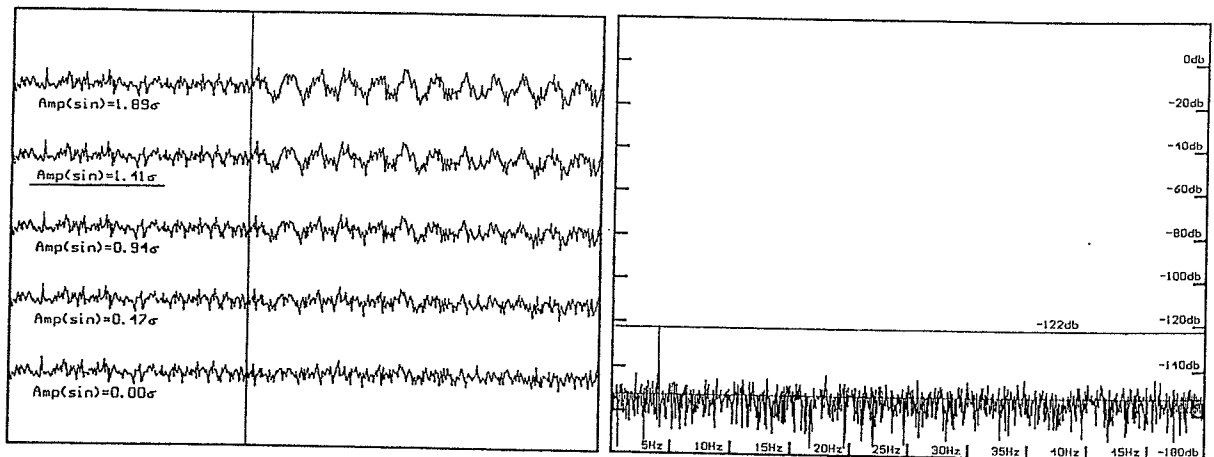


Fig. 5: Synthetically generated noise ($\sigma = 3.6$, typical for a REFTEK 72A07 Recorder) with superimposed sinus oscillations of different amplitudes (left) and corresponding spectrum for noise and sinus oscillations with amplitude of 1.4σ . The spectrum is displayed in db relative to the clipping amplitude of the recorder (0 db). The single peak in the spectrum is due to the sinus test signal.

The ratio of the power of the noise n_i to the power of the sinus signal $s_i = A_0 \sin(\omega t_i)$ can be derived in the time and frequency domain as

$$\sum_{i=1}^N n_i^2 / \sum_{i=1}^N s_i^2 = 2 \sigma^2 / A_0^2 \quad \text{and} \quad \sum_{i=1}^{N/2} |R_i|^2 / A_0^2 \quad (12)$$

respectively. R_i are the Fourier coefficients of noise. For the assumed minimum signal amplitude of $A_0 = 1.4 \sigma \approx \sqrt{2} \sigma$ we get, that the signal power equals the noise power. From (12) we conclude, that the amplitude of the minimum detectable seismic signal can be computed simply from the noise spectrum:

$$A_0 = \sqrt{(\sum |R_i|^2)} \quad (13)$$

Expression (13) shows, that there is a simple way to compute the dynamic range of a recording system from the spectrum of the eigennoise and the clipping amplitude in counts.

$$DR = 20 \log (A_{clip} / \sqrt{(\sum |R_i|^2)}) \quad (14)$$

Figure 5 displays the minimum spectral amplitude calculated according to (13) as a solid line at -122db. It well agrees with the spectrum peak, caused by the minimum detectable sinus signal. When using the spectral noise level as the minimum spectral amplitude one would significantly overestimate the dynamic range (e.g. by 30 db for the given example according to figure 5). All tests were done with a sampling frequency of 100 Hz. One has to keep in mind that the dynamic range changes with sampling frequency for recorders with oversampling.

2. Recorder noise

The eigennoise of the recorder has to be measured with shorted input. For a given AD-converter the usable dynamic range depends on the standard deviation of the eigennoise measured in units of counts. Three high gain recorders were tested:

- REFTEK 72A07, Refraction Technology, 24 bit AD-Converter
- PDAS100, TELEDYNE Geotech, 16 bit ADC, gain ranging, oversampling
- MARS88 Lennartz Electronic, 16 bit ADC, oversampling.

The standard deviation of the noise ranges between 1.2 and 22.1 counts, what corresponds to a difference of about 4 bits. Figure 6 shows the noise spectrum and the distribution of noise amplitudes. The least significant bit was best selected for the MARS88, in order to get the highest dynamic range for the given system.

Some recorders for temporary field installations are optimised for low power consumption (REFTEK 72A07). This may result in a step-like baseline shift if external devices (hard disk, GPS) are temporarily switched on. Further, temperature changes may cause a low frequency base line drift. These effects introduce additional noise.

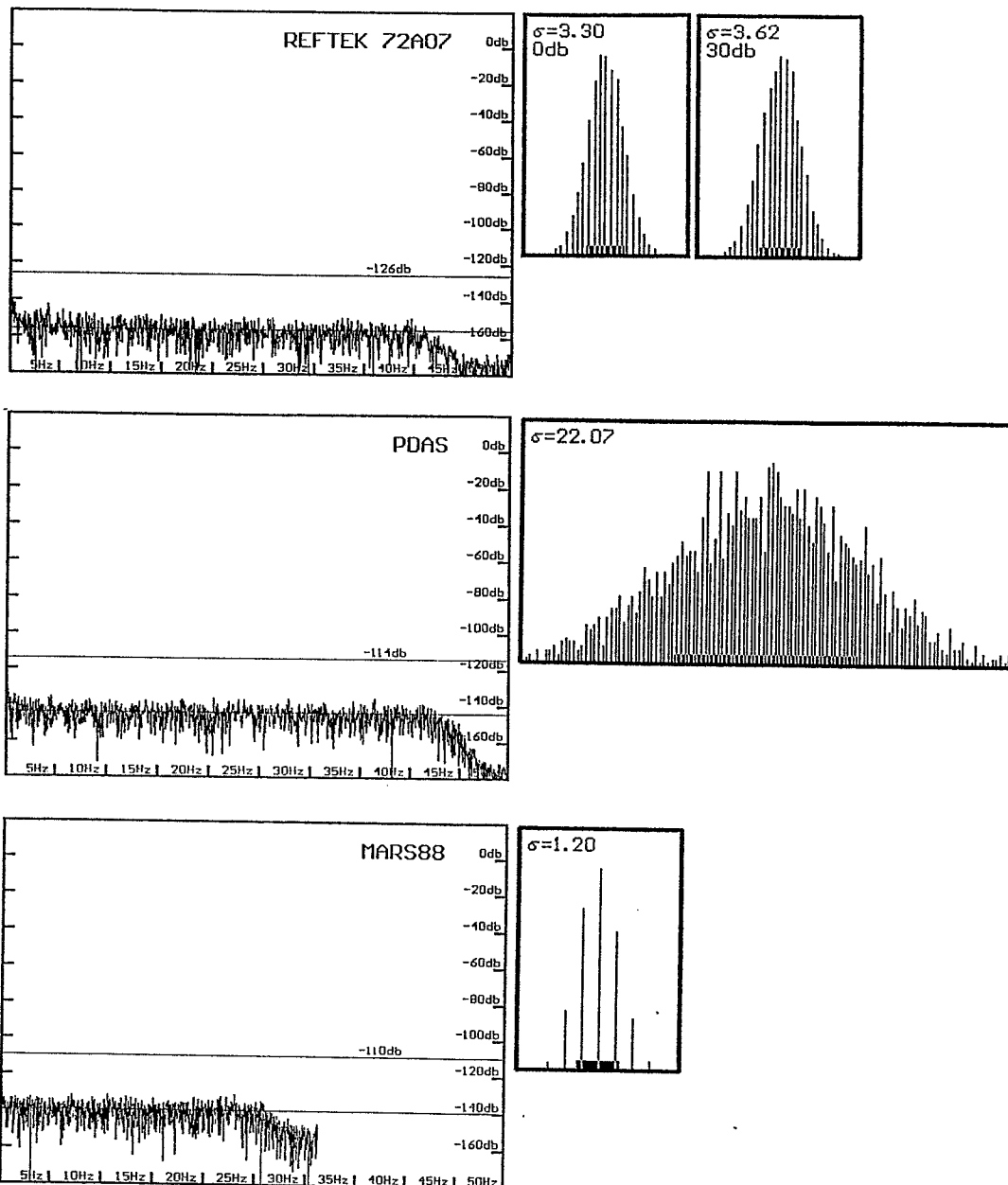


Fig. 6: Spectra of recorder noise for shorted input, usable dynamic range and amplitude distribution of noise samples, σ – standard deviation of noise in counts.

3. Resolution

Recorders without gain ranging do not show resolution changes for different amplitudes (no change of quantization step). Figure 7 shows the spectra of two records with a 4 Hz- sinus signal and amplitudes close to the clipping level and 60 db below the clipping level, respectively. The overtones are due to the limited stability of the sinus generator. Remarkable is the different noise level. Although the MARS88 uses oversampling (no gain ranging ADC), the resolution decreases as a result of storing the data in a gain ranging format. The data quantization step therefore increases with amplitude and decreases the system resolution, what results in a higher noise level for signals with large amplitudes (30 db for the given example).

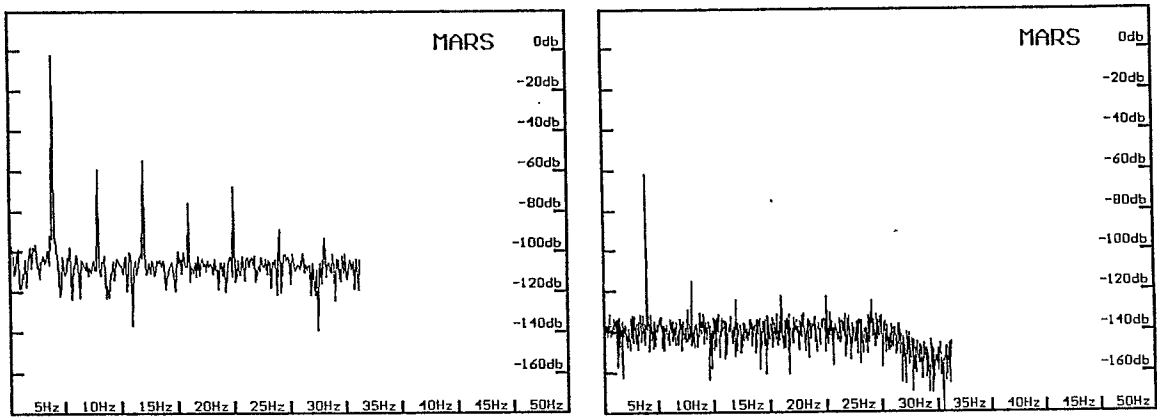


Fig. 7: Spectra of noise records superimposed by sinus oscillations of different amplitudes. The data were stored in gain ranging format.

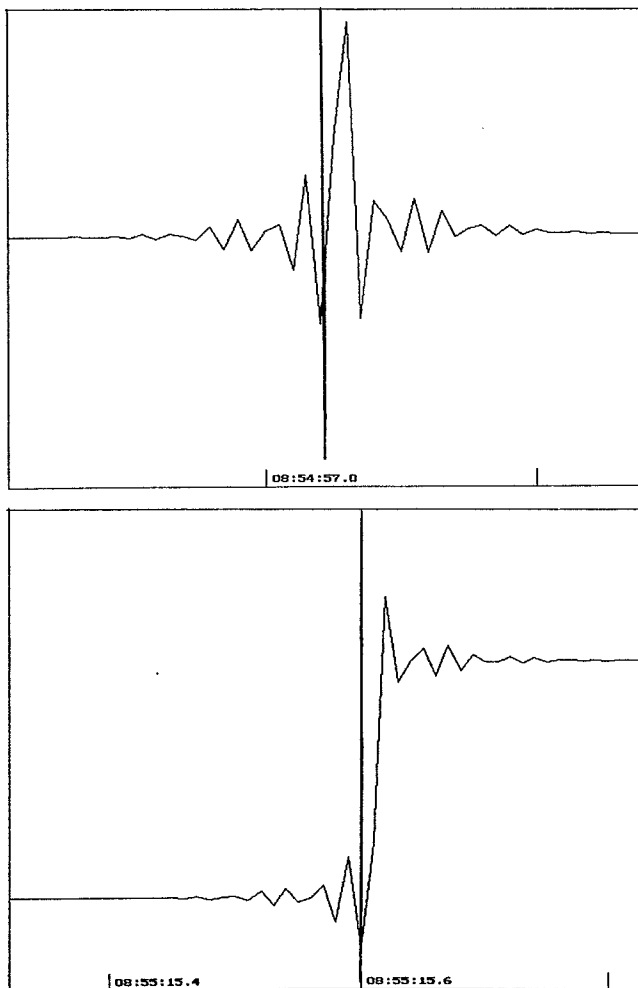


Fig. 8: Records, showing acausal effects for impuls (above) and step test functions (below). The exact time of the beginning of the impuls and step, respectively, is marked by the vertical bar.

4. Anti-alias filter

In modern high gain seismic recorders are usually linear phase finite impulse response (FIR) filters implemented (Scherbaum and Bouin, 1997a). They are used as digital anti-alias filters and sampling noise decimation filters for recorders using the oversampling technique. They are very steep stable filters and expand the usable frequency range up to 80% of the Nyquist frequency f_n in contrast to analogue filters which have a passband approximately up to 30% of f_n . Analogue filters are always causal filters and cause a phase distortion of the input signal within the passband of the filter. Linear phase filters pass signals within the passband undistorted, except for a constant time shift. A filter which additionally corrects this time shift is called zero phase filter. These filters are acausal and produce oscillations before the onset approximately with the Nyquist frequency. This is a result of the two-sided impulse response of the linear or zero phase filters. Figure 8 shows records of step and impulse functions with remarkable precursory signals. In case of seismic records they might be misinterpreted as earlier arrivals. In general, onset times picked from linear or zero phase filtered traces will be always too early.

Zero phase filters are implemented in most high gain recorders (QUANTERRA, REFTEK, MARS, PDAS, ORION). There is one strong motion recorder on the market (ALTUS K2 from Kinematics) with a linear phase filter which produces a time shift, depending on the sampling rate: shift of 0.38 sec for 100 Hz, 0.156 sec for 250 Hz. This shift has to be taken into account when data of different recorder types are processed and analysed together. The acausal effects can be removed by post filtration (Scherbaum, 1997a). For some recorders the corresponding programs can be requested (Scherbaum, 1997b).

2. SEISMOMETER SIMULATION

For the estimation of some seismological parameters (e.g. arrival times, amplitudes, periods) records with a specific seismometer response are more suitable or even required to make them comparable with related readings from standardized seismic networks (e.g. WWSSN stations). Further, the estimation of source parameters of earthquakes in the time domain requires the simulation of a broadband displacement record.

Figure 9 shows the displacement spectrum of a vertical component P-wave of an $M_s=5.8$ rockburst (Teutschenthal, Germany) as derived from a velocity broadband record at station TNS of the German Regional Seismograph Network (GRSN). The source spectrum, corrected for wave propagation effects, shows the typical shape: at low frequencies a constant amplitude and at high frequencies an ω^{-3} decay. The high frequency decay usually ranges between ω^{-2} and ω^{-3} . The seismic moment $M_0 = \mu A \bar{D}$ (μ - shear modulus, A - area of the rupture plane, \bar{D} average static dislocation) can be derived in the frequency domain from the low-frequency amplitude level ($\omega \rightarrow 0$) of the P- or S-wave or in the time domain from the P- or S-displacement integral. Additionally, the corner frequency of the P- or S-wave spectrum (figure 9: 1.5 Hz for P) or the duration of the P- or S-pulse in the time domain allow to estimate the size of the rupture plane. Figure 9 displays a noise spectrum in addition to the P-wave ground motion spectrum. At a frequency of 0.1 Hz the noise spectrum exceeds the P-spectrum. In the given case, for $f < 0.15$ Hz no signal can be recovered from the record because of the high noise level. The usable frequency range increases with increasing magnitude and decreasing epicentral distance.

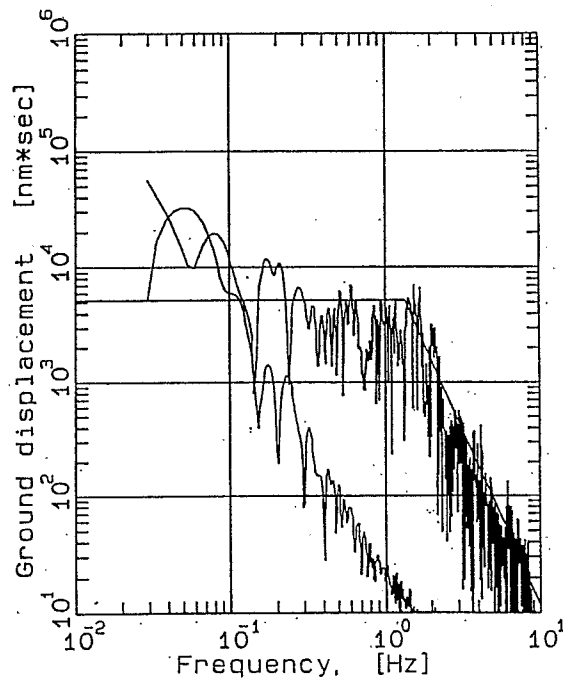


Fig. 9: Source spectrum of a P-wave record (rockburst) and related noise spectrum

Simulation theory starts with the Laplace transform L which transforms the time function $f(t)$ into a function of the complex variable $s = \sigma + i\omega$ (for complete theory see Plesinger et al., 1996)

$$L(f(t)) = F(s) = \int_{-\infty}^{+\infty} f(t) e^{-st} dt \quad (15)$$

As physical model linear time invariant systems (LTI) are adopted. They can be described by a differential equation of the general form (14) with x as input- and y as output (see equation 1 as example)

$$\sum_{m=0}^M b_m y^{(m)} = \sum_{n=0}^N a_n x^{(n)} \quad (16)$$

(m) and (n) denote the m -th or n -th derivative. The ratio of the Laplace transform of the output signal to the Laplace transform of the input signal gives the system transfer function $H(s)$.

$$H(s) = \frac{\sum_{n=0}^N a_n s^n}{\sum_{m=0}^M b_m s^m} = C \frac{\prod_{n=0}^N (s - z_n)}{\prod_{m=0}^M (s - p_m)} \quad (17)$$

z_n and p_m , the roots of the numerator and denominator are called zeros and poles of the transfer function, respectively. When replacing s by $i\omega$ we get the Fourier spectrum of the transfer function (compare with equation 5).

A practical example is the transfer function of a seismometer (3) as derived above. For deriving a simulation filter $H(s)$ one has to divide the transfer function $V(s)$ of the desired seismometer by that of the seismometer, which was used for recording, $U(s)$

$$H(s) = V(s) / U(s) \quad (18)$$

and check the result for stability. According to Plesinger et al. (1996) a transfer function is stable, if

- the number of zeros is less than or equal to the number of poles
- there are no pure imaginary poles or poles at the origin of the co-ordinate system
- the real part of all poles is negative
- both complex poles and zeros occur in conjugate pairs.

There are different methods of transition from a continuous to a sampled record. One of them is the bilinear Z-transform

$$s = \frac{2}{\Delta t} \frac{z-1}{z+1}, \quad \Delta t \text{ is the sampling interval, } z \text{ is a complex variable.} \quad (19)$$

When replacing s according to (19) in the transfer function $H(s)$, derived for seismometer simulation according to (18), we get an expression like

$$H^*(z) = \frac{V^*(z)}{U^*(z)} = \frac{c_0 + c_1 z^{-1} + c_2 z^{-2} + \dots + c_n z^{-n}}{1 + d_1 z^{-1} + d_2 z^{-2} + \dots + d_m z^{-m}} \quad (20)$$

c_i and d_i are real numbers, $V^*(z)$, $U^*(z)$, and $H^*(z)$ are the bilinear Z-transforms of the transfer functions of the seismometer to be simulated, as well as of the seismometer which was used for recordings and of the simulation filter. The shifting theorem of the Z-transform

$$W^*(z) z^{-k} \equiv w_{l-k} \quad (21)$$

states, that the multiplication of a Z-transform with z^{-k} results in a time shift of the corresponding discrete time series w_l by k samples. The application of this shifting theorem (21) converts equation (20) into a difference equation

$$v_l = c_0 u_l + c_1 u_{l-1} + c_2 u_{l-2} + \dots + c_n u_{l-n} - d_1 v_{l-1} + d_2 v_{l-2} + \dots + d_m v_{l-m}. \quad (22)$$

(22) is the equation of an ARMA-filter (auto regressive moving average filter): The new filtered sample is computed from the weighted average of the current and the last n samples of the original time series u_l and the last m samples of the filtered time series v_l . Such type of filter is rather easy to program.

The bilinear Z-transform produces non-linear distortions of the frequency scale. By prewarping (inverse predistortion) the corner frequencies ω_i of the seismometers or filters using the formula (23) this effect can be corrected.

$$\omega_i = \frac{2}{\Delta t} \tan(\Delta t \omega_i / 2) \quad \Delta t \text{ is the sampling interval} \quad (23)$$

The simulation can be stabilised by limiting the frequency range to the one within which the simulation is exact. This bandwidth depends on the noise level and on the steepness of the simulation filter. There is a complete software package for simulation filtering available (PREPROC, Plesinger et al., 1996)

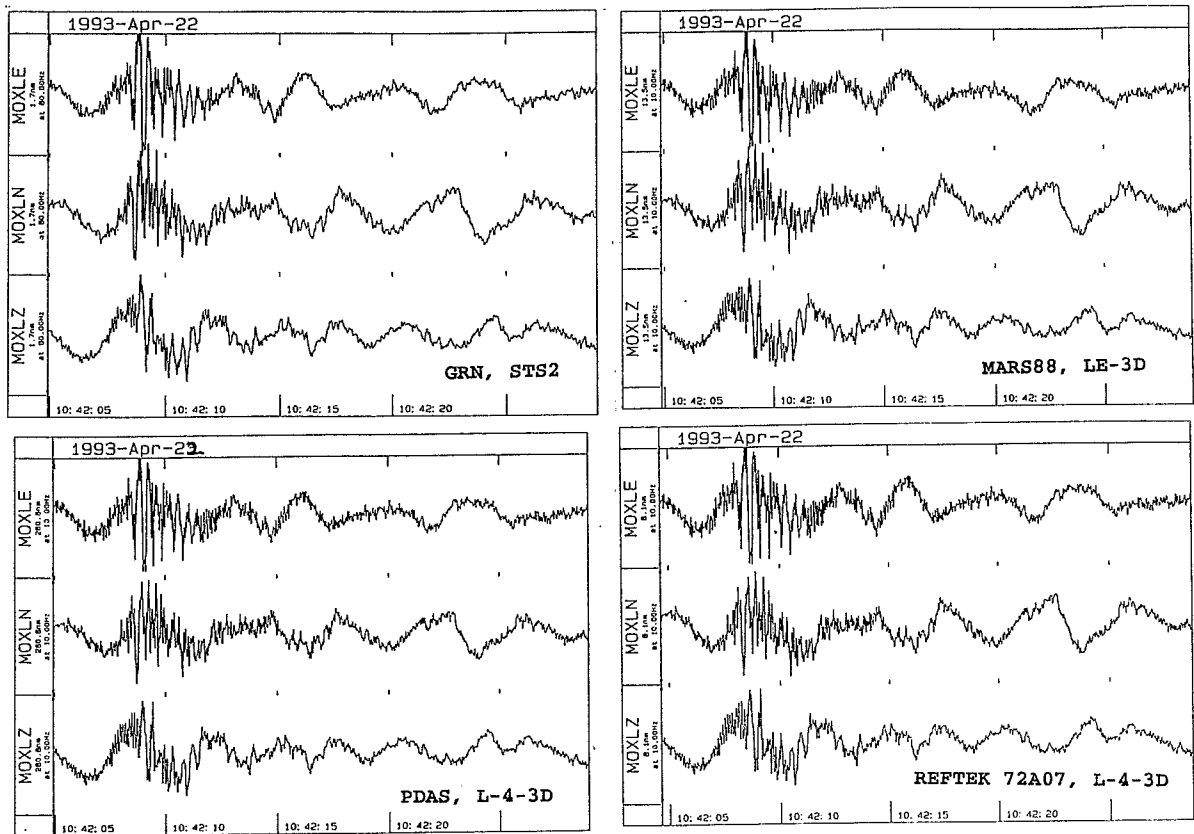


Fig. 10: Simulated records of a seismometer with an eigenperiod of 5 sec derived from records of a GRSN broadband station (200 sec)(upper left) and 2 short period (1 sec) stations left and right below. A primary record of the same event from a station with an intermediate period seismometer (5sec) is shown for comparison (upper right).

Figure 10 shows a quarry blast, recorded by 4 different systems at the same location:

1. permanent station MOX, German Regional Seismograph Network, seismometer STS2 (T=100 sec), recorder: Quanterra
2. field stations: MARS88, seismometer LE-3D (T=5sec)
 PDAS100, L4-3-D (T=1sec)
 REFTEK 72A07 L4-3-D (T=1sec).

For comparison the STS2 and L4-3-D-records were transformed into a record of a LE-3D seismometer (T=5sec). The simulated records do not show any remarkable difference.

Figure 11 shows records of an Mb=6.4 Alaska earthquake (13.5.1993) from a virtual velocity seismometer with an eigenperiod of 20 sec (damping: 0.7 of critical), derived from a broadband record (left: German Regional Seismograph Network, station BRG, seismometer

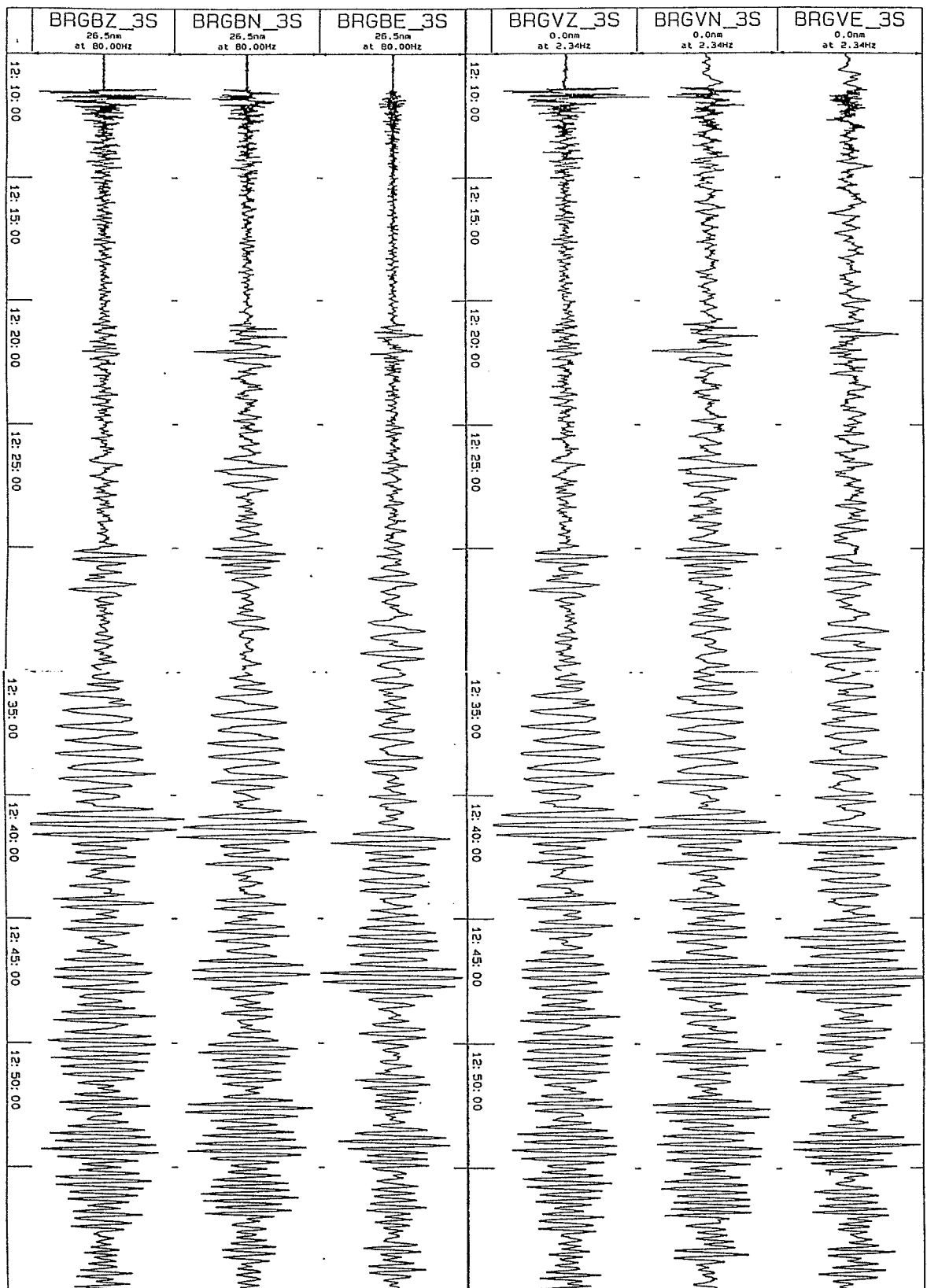


Fig. 11: Comparison of two simulations of intermediate period seismometer records (eigen-period 20 sec) derived from records of a broadband (200 sec),(left) and a short period (1 sec) seismometer (right), respectively. (Alaska earthquake, 13.5.1993, Mb=6.4)

STS2, T = 200 sec) and from a PDAS-recorder, equipped with a short period seismometer (right: Mark L4-3-D, T = 1sec). This example shows, that at least for the vertical component a good short-period seismometer can be used for simulating intermediate period records. The horizontal components of a MARK L4-3-D seismometer are mechanically less stable than the vertical component. This results in a higher noise level compared with the vertical component. The simulation of seismometers becomes important, when in the course of large projects different seismometers and data loggers are used together and the scientific objectives require a uniform station response. Further, parameter estimations in routine seismological analysis have to be derived from seismometers with internationally agreed dedicated response curves which remain unchanged over long time spans.

3. COMPARISON OF RECORDED AND SYNTHETIC SEISMOGRAMS

The normal way of deriving models of the earth structure is to extract arrival time, period and amplitude information from seismograms in order to use these data in inversion procedures (e.g. derivation of velocity models from travel time data). Waveform methods, which fit theoretical seismograms to records are usually limited to low frequencies and small velocity perturbations because of the problem to find analytical solutions for heterogeneous media with large velocity contrasts. Further, one should have rather dense station networks. The standard nowadays for calculating theoretical seismograms for local earthquakes is a horizontally layered velocity model. Programs based on the original Thompson-Haskell matrix method show instabilities at high frequencies. Wang (1997) derived a new stabilisation method which allows fast and correct computation of high frequency seismograms for point sources with a given source mechanism. This method was applied to aftershock records of the Mb=6.3 Killari intraplate earthquake of September 29, 1993.

The factors contributing to the strong damage and the high death toll (12000 people) caused by the Killari earthquake were:

1. high population density
2. occurrence at night time
3. the area was assumed to have the lowest seismic risk in India
4. traditional building style (basalt stones without cement or concrete)
5. strong ground motion amplification.

Figure 12 shows the epicentre distribution of the Killari aftershocks (Baumbach et al. 1994). They were recorded with 3 digital PDAS-stations, 4 strong motion stations and 9 analogue stations (magnetic tape records). The velocity recordings have a rather monofrequent character (Fig. 13). This is a first hint for ground motion amplification caused by a thin low-velocity surface layer. The resonance frequencies for a vertically incident S-wave are $f_n = (2n+1)V_s / 4H$. H is the thickness of the surface layer and V_s is the S-velocity, $n=0,1,2,\dots$. The coda of the records is very long. This could be caused by high crustal scattering and low attenuation. The geological underground consists of granite, covered by a 300 m basalt layer and few meters of black soil. The depth of the basalt could be estimated at some places from wells. Figure 14 displays spectra at PDAS station sites with epicentre distances of 5 to 10 km. They show typical spectral peaks with an amplification of 5-8 due to the surface layer. Some of the spectra display overtones. The amplification peaks are within the frequency range of the corner frequencies of the P- and S-waves from low magnitude aftershocks. Therefore, it is impossible to estimate reliably their source parameters from the P- or S-spectrum.

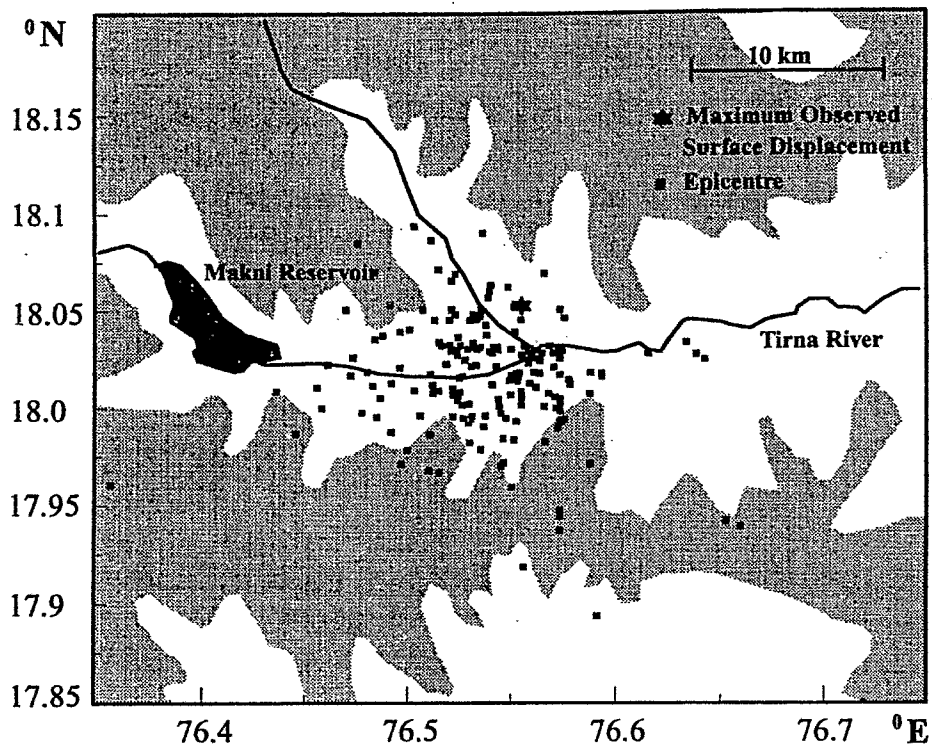


Fig. 12: Epicentres of Killari aftershocks

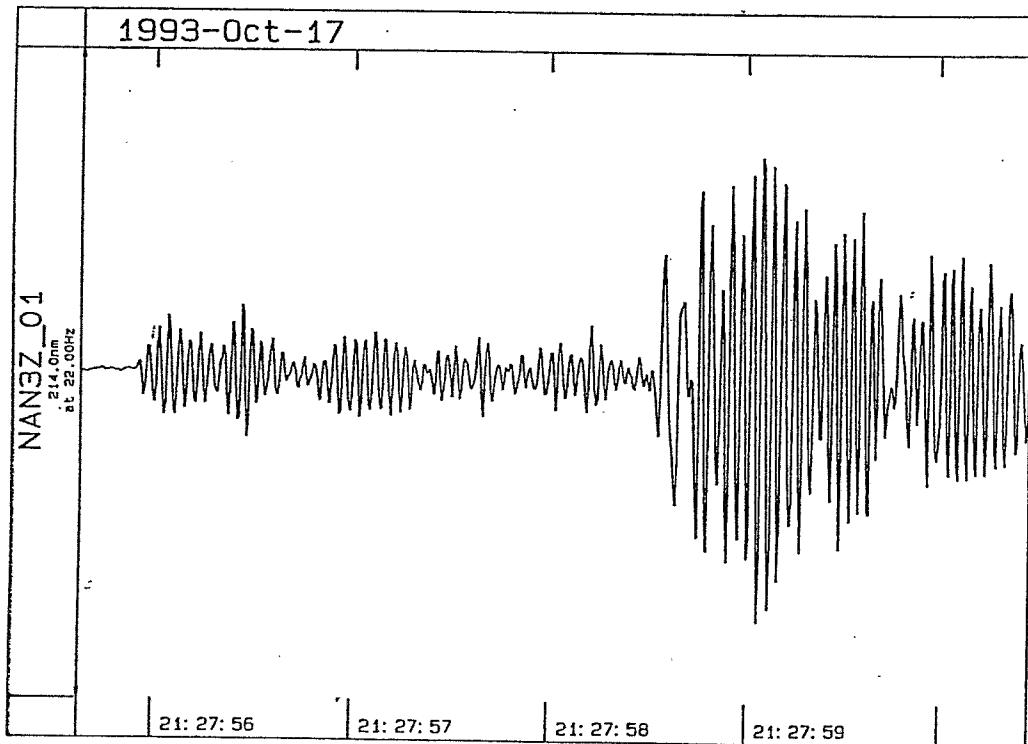


Figure 13: Velocity record of a Killari aftershock

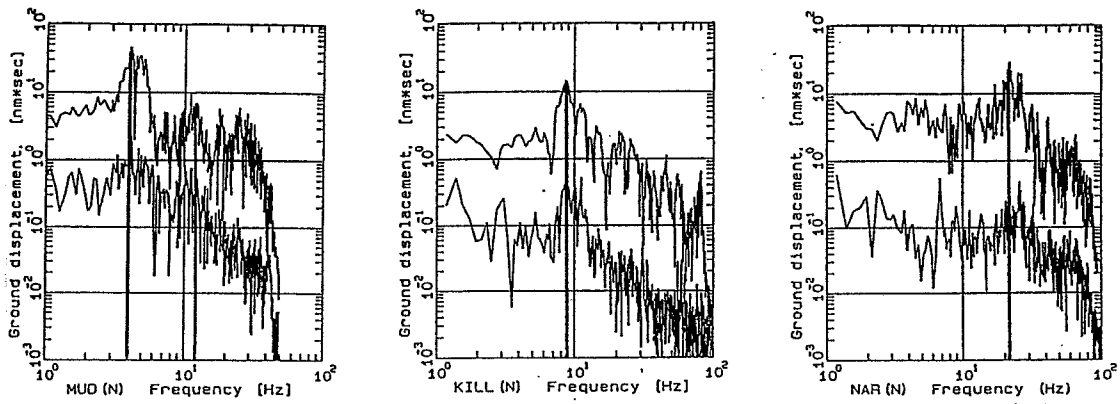


Fig. 14: Spectra of aftershocks (upper trace, horizontal components) showing soil amplification effects. Noise spectra are indicated for comparison (lower trace).

To analyse the ground motion amplification in detail theoretical seismograms were calculated for the following velocity model:

Layer	thickness [km]	ρ [g / cm ³]	V_p (km / sec)	V_s (km / sec)	Q_p	Q_s
1	0.005	1.3	1.2	0.2	80	20
2	0.300	2.5	4.5	2.6	500	220
3	∞	2.7	6.0	3.5	800	270

The assumed layer thicknesses coincide well with the results from drillings in the epicentre area of the Killari earthquake, carried out in 1996 (Gupta, 1996, personal communication).

Figure 15 shows the synthetic displacement seismograms for an epicentral distance of 20 km and a thrust mechanism. The upper three traces (radial, transversal and vertical) show the displacement at the surface, the lower ones at a depth of 5 m (soil-basalt boundary). Remarkable are the high frequency oscillations after the P- and S-onsets caused by the surface soil layer. The second onset after the P-wave at 00:00:04 could be misinterpreted as reflection from a deep crustal boundary. Both, travel time and amplitude studies showed that this is an inhomogeneous P-wave, guided at the 300 m deep basalt/granite boundary.

Finally, theoretical seismograms were computed for an aftershock and a small 3-station network with an aperture of 8 km. The 3-component seismograms were recorded by PDAS-stations. For analysis they were converted into Wood-Anderson records. The typical spectra of the stations MUD, KIL and NAR (figure 14) show different resonance frequencies: 4 Hz, 10 Hz and 20 Hz, respectively. These differences are caused by different thickness of the surface layer and result in different periods of the S-wave onset (fig. 16). The above shown velocity model gives a resonance frequency of 10 Hz and is therefore typical for station KIL. The fault plane solution was calculated from polarity readings only, because the amplitudes are strongly influenced by the surface layer. The S-wave periods and amplitudes of the Killari (KIL) radial component record are in good agreement with the corresponding synthetic seismogram. The amplitudes of the recorded and calculated transversal and vertical component records differ remarkably. The other stations show differences in periods because of the wrong model

thickness of the uppermost layer. Because of the dominant influence of the uppermost layer, a better fit could be expected when using models with different soil thickness for different stations.

The P-polarities of records and synthetics coincide for all stations. Differences in the amplitudes show that the fault plane solution calculated with only 12 P-polarities is less accurate. Further modelling with different source mechanisms, different source duration and different surface and intermediate layers could probably improve the fit.

The calculations show, that the analysis of dense network recordings of aftershocks of strong earthquakes could contribute to the estimation of ground motion amplification caused by low velocity surface layers. The results could be used for microzonation studies.

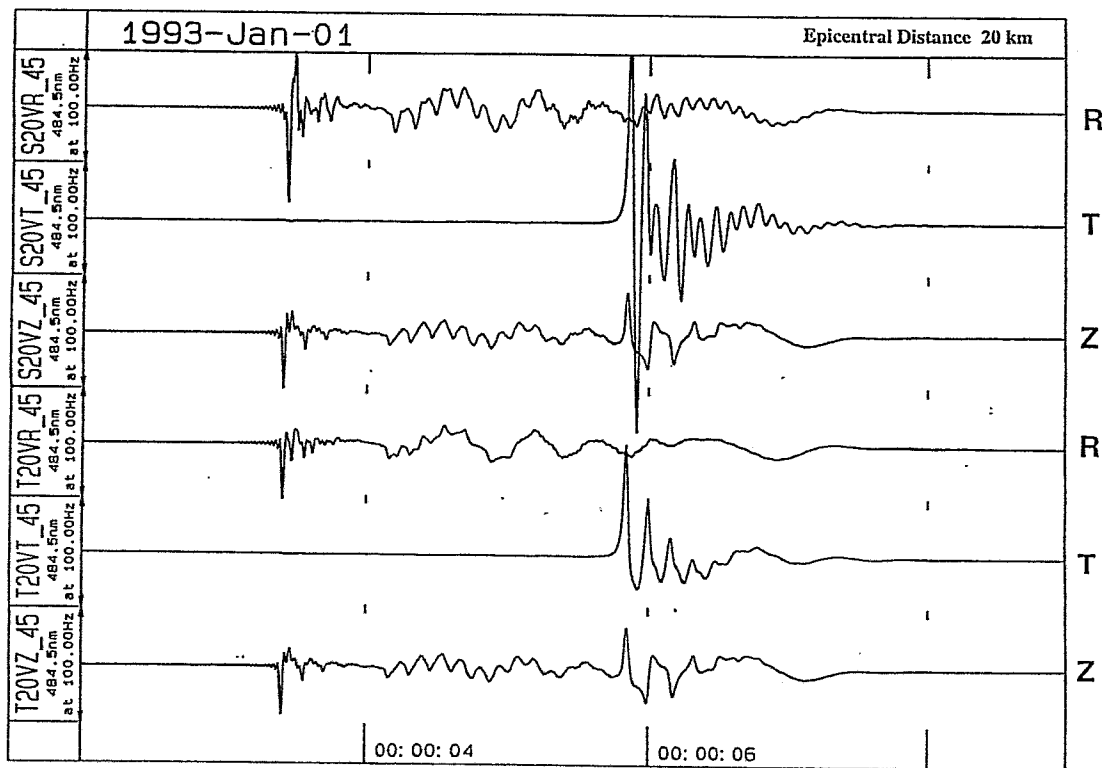


Fig. 15: Synthetic seismograms for a Killari aftershock with thrust mechanism. Upper traces: surface displacement, lower traces: displacement at 5 m depth

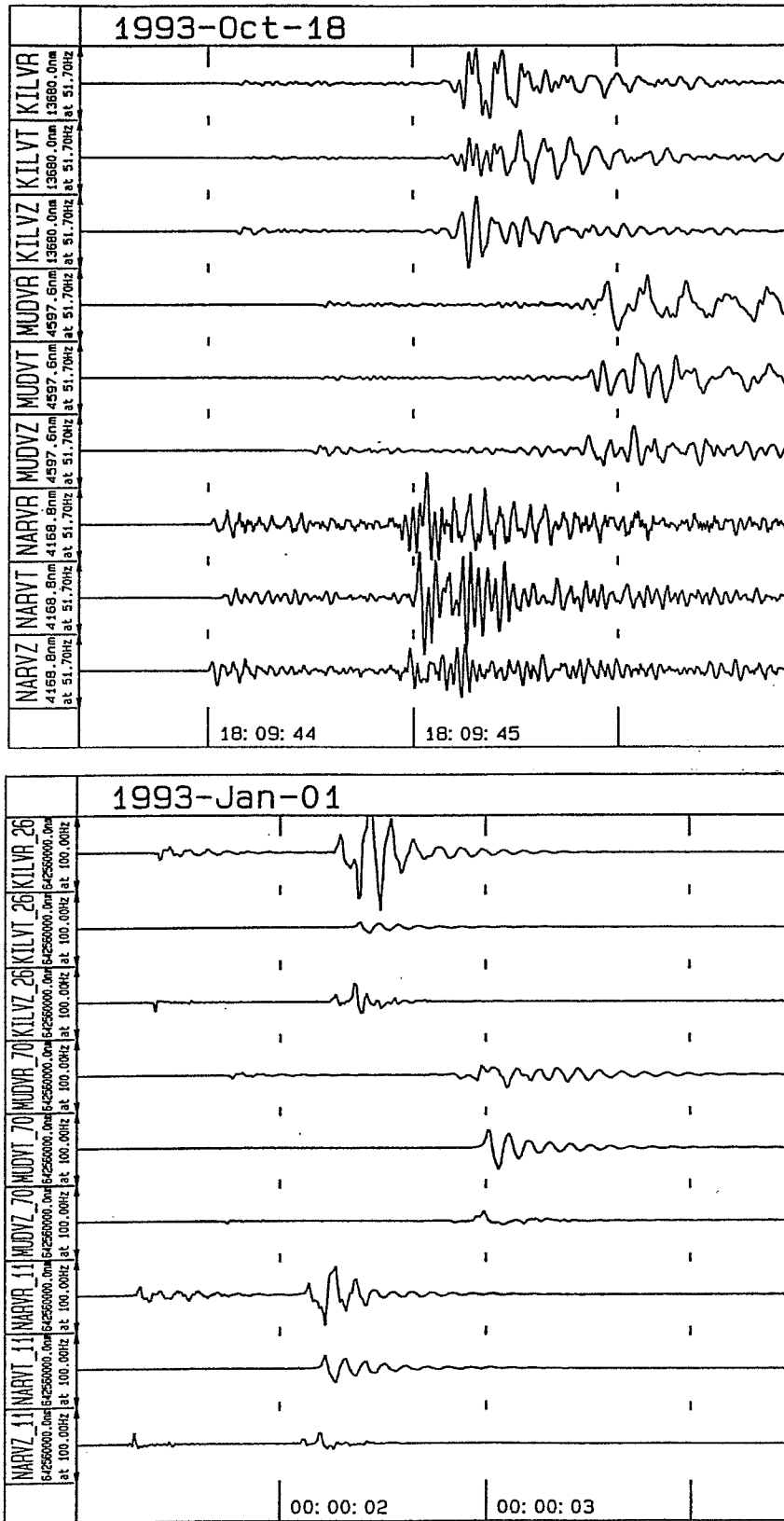


Fig. 16: Comparison of records (top) and synthetics (bottom) for a 3 station network

References

- Baumbach, M., H. Grosse, H.G. Schmidt, A. Paulat, A. Rietbrock, C.V.Ramakrishna Rao, P. Solomon Raju, D. Sarkar and Indra Mohan. Latur earthquake, Memoir 35, 1994, Geological Society of India, pp. 33-63.
- Baumbach, M., H. Grosse: Erprobung von Registrierapparaturen für die Task Force Erdbeben. GFZ Potsdam, 1994.
- Oppenheim, A.V., R.W. Schaffer, Discrete time signal processing. Prentice Hall, 1989
- Plesinger, A., Zmeskal, M. and J. Zednik: Automated preprocessing of digital seismograms: Principles and software, Version 2.2, E. Bergman, ed, Prague & Golden, 1996.
- Scherbaum, F.: Basic concepts in digital signal processing for seismologists. Lecture notes in Earth sciences, Vol. 53. Springer Verlag, Berlin Heidelberg, 1994.
- Scherbaum, F. and M.-P. Bouin: FIR filter effects and nucleation phases. Submitted to Geophys. J. Int.: 1997a February 18.
- Scherbaum, F.: Zero phase filters in digital seismic acquisition systems: blessing or cure ? Submitted to EOS: 1997b February 25.
- Wang, R.: A new algorithm of wavenumber integration method for synthesising high frequency seismograms. 57. Annual meeting of the German Geophysical Society, Potsdam, March 3-7, 1997, Programme and abstract volume.

DEMONSTRATION OF DIFFERENT DIGITAL DATA ACQUISITION SYSTEMS TOGETHER WITH SEISMOMETERS FOR MOBILE AND STATIONARY USE—STRONG-MOTION RECORDINGS AND DISPLAY OF THE COLLECTED DATA

ZHANG Wenbo

Beijing Strong Motion Observation Center Institute of Engineering Mechanics,
China Seismology Bureau, P.O. Box 2722, Beijing 100080, China, E-mail: wenbo@public.east.cn.net

1. STRONG MOTION RECORDERS USED IN CHINA

SMA-1, analog accelerograph

Recording medium: 70mm Estar base photo film
Recording traces: Total of seven traces: three active acceleration tracks,
Two timing traces, and two fixed traces for reference.
Timing marks: Two marks per second ($\pm 0.2\%$)
Charts speed: 10 mm/second
Recording time: 25 minutes
Start-up time: Full operation within 50 milliseconds
Dynamic range: 0.01g to 1.0g
Sensor: Three flexure-type accelerometers in an
orthogonal arrangement
Natural frequency: 25 Hz
Damping: 60% critical
Range: $\pm 1g$ full scale. Full scale deflection on film is 18.5 mm
Bandwidth: 1 to 10 Hz

PDR-1/FBA-13, digital accelerograph, made by Kinometrics, USA

Number of channels: 3
Input signal: $\pm 25 \mu V$ min to $\pm 2.5 V$ max
Input filtering: Selectable 2.5, 12.5, 25, 50 Hz
Gain-ranging: $\pm 36dB$ up and down during event
Dynamic range: 102dB
Resolution: 12 bit
Recording medium: Digital cassette tape
Digital recording: Phased encoded; 4-track: three-data, one parity
Bit density: 1280 bits/inch/track
Recording time: 22.5 or 45 minutes with 300 ft. Tape
Tape speed: 1.25 or 2.5 inches/second
Start-up time: 150 millisecond
Sample rate: 100 or 200 sps
Trigger: STA/LTA selectable ratios or differences
Full scale: 2g
Natural frequency: 50 Hz
Damping: 70% critical
Timing system: Quartz crystal clock is standard
(3×10^{-7} over temperature range of 0-50 °C)

SCQ-1/WLJ-100, digital accelerograph, tape recorder, made by IEM, China

Number of channels:	3
Input filtering:	Selectable 25, 50 Hz
Gain-ranging:	±36dB up and down during event
Dynamic range:	102dB
Resolution:	12 bit
Recording medium:	Tape
Sample rate:	100 or 200 sps
Trigger:	STA/LTA selectable ratios or differences
Full scale:	2g
Natural frequency:	70±2 Hz
Damping:	70% critical
Timing system:	Quartz crystal clock is standard (1×10^{-5} over temperature range of 0-40 °C)

SSA-2, SSR-1, K2, solid state accelerograph, made by Kinometrics, USA.**SSA-2**

Sensor:	Internal, orthogonally oriented triaxial accelerometer.
Full scale:	2g
Natural frequency:	50 Hz
Damping:	70% critical
Bandwidth:	DC to 50 Hz
Sample Rate:	200 sps
Anti-alias filter:	2 pole, 50 Hz, Butterworth
Frequency response:	Dc to anti-alias filter cutoff
Sensitivity:	±2.5 volts full scale
Resolution:	12 bits
Trigger:	Programmable threshold trigger, 0.1 to 10% of full scale, bandwidth 1Hz to 12 Hz
Recording medium:	256 kilobytes of CMOS static RAM standard (with battery back-up)
Timing system:	Internal clock standard (Accuracy approx. $\pm 5 \times 10^{-5}$ from 0-50 °C)

SSR-1

Number of channels:	3, Optional 6
Dynamic range:	16 bits
Converter resolution:	16 bits
Full scale:	±2.5 V at 0 dB gain
Sensor interface:	3 channel general purpose sensor interface. Compatible with FBA-23, WR-1 and SS-1. Additional 3 channel input for optional channels.
Sample rate:	1000 sps for 1 channel, 500 sps for 3 channels, 200 sps for 6 channel.
High-Pass filter:	0.01 Hz, each channel individually in or out
Anti-alias filter:	3 plug-in filter modules provide 1 corner frequency each for 3 channels. Standard 5, 15 and 50 Hz. Additional 250 Hz filter is standard. Response is 6-pole Butterworth.
Bandwidth:	DC to anti-alias filter corner frequency
Preamplifier gains:	0 to 60 dB software selectable in 20 dB steps.

Trigger:	Each channel independent. 1) Band-pass filter threshold; 2) STA vs. LTA, ratio or difference; 3) Pre-programmed experiment windows; 4) External
Recording medium:	1 megabyte of CMOS RAM. Expandable to 4 megabyte
Timing system:	a) keyboard; b) armed with keyboard, started with TICK plus; c) continuous and automatic decoding and synchronization to external IRIG time code; d) optional internal OMEGA receiver.

K2

Sensor channels:	3 standard; 6 and 12 optional
Input level:	Standard $\pm 2.5V$
Gain:	User selectable of X1, X3, X10, X100 (opt)
Damping:	Provision for internal resistor (opt)
Anti-alias filter:	Brickwall FIR filter. Cut-off at 80% of output Nyquist; 120 dB down at output Nyquist
Dynamic range:	>114 dB
Frequency:	DC to 80 Hz @ 200 sps
Sampling rate:	20, 40, 50, 100, 200, 250 sps
Trigger selection:	Independently selected for each channel. Threshold: selectable from 0.01% to 100% of full scale Voting: internal, external and network trigger votes with arithmetic combination. Additional: STA/LTA
Recording medium:	6 MB ScanDisk; optional 20 MB ScanDisk; Optional 170, 340 or 520 MB hard disk.
Timing system:	Free running disciplined oscillator (standard); GPS (opt)
Timing accuracy:	5 microseconds of UTC

2. K2 – DEMONSTRATION FOR STRONG MOTION RECORDINGS AND DISPLAY OF THE COLLECTED DATA

2.1 Introduction

K2 is a high dynamic range accelerograph. Technical advances and innovative engineering have increased performance and flexibility of this recorder to offer a dynamic range greater than 114 dB. The high dynamic range and superior resolution offer significant advantages for applications where signal fidelity and data integrity are vital. Developed for Microsoft Windows™, QuickTalk® and QuickLook® software provide a user-friendly environment, making system setup, communications and rapid analysis. Up to now there are about ten K2s deployed in China. They are distributed in structural monitoring arrays, borehole array and regional seismic networks and arrays.

2.2 Getting started

- Connecting PC ➔ Connecting the internal battery (make sure *OPER/STBY* switch is in the **STBY** position)
- ➔ Connecting the power supply
 - ➔ Turning on the power (turn the *OPER/STBY* switch to the **OPER**)

- position)
- ➔ Running **QuickTalk**
 - ➔ Zero-Adjusting an internal FBA

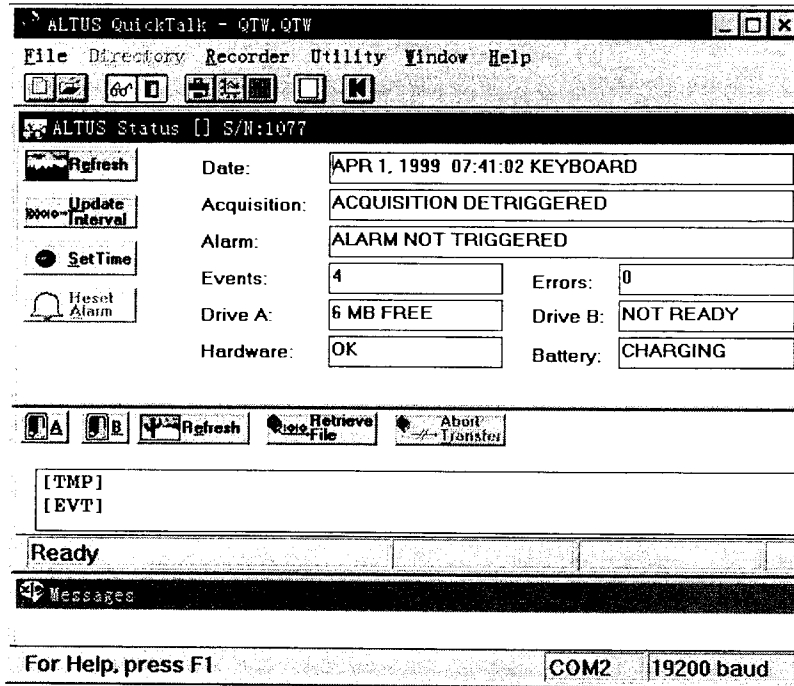
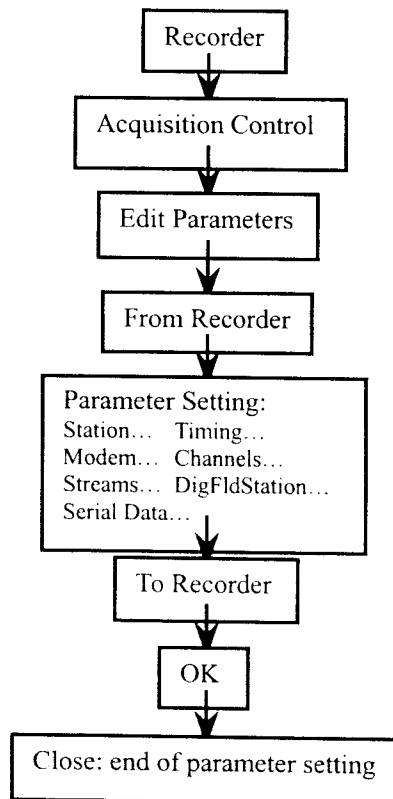


Fig. 1: QuickTalk Window

2.3 Configuring instrument

- Parameters setting: Fig. 2 (below): Flowchart showing parameter setting



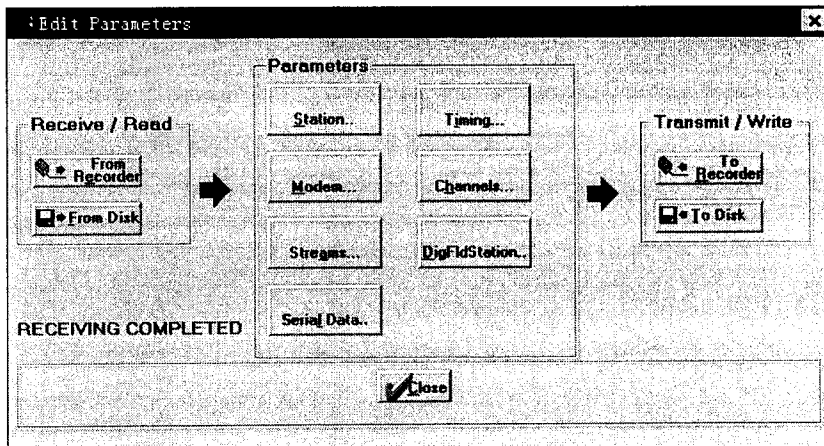


Fig. 3: Window for parameter editing

- Station parameters – They determine which channels are recorded and provide information on the instrument.

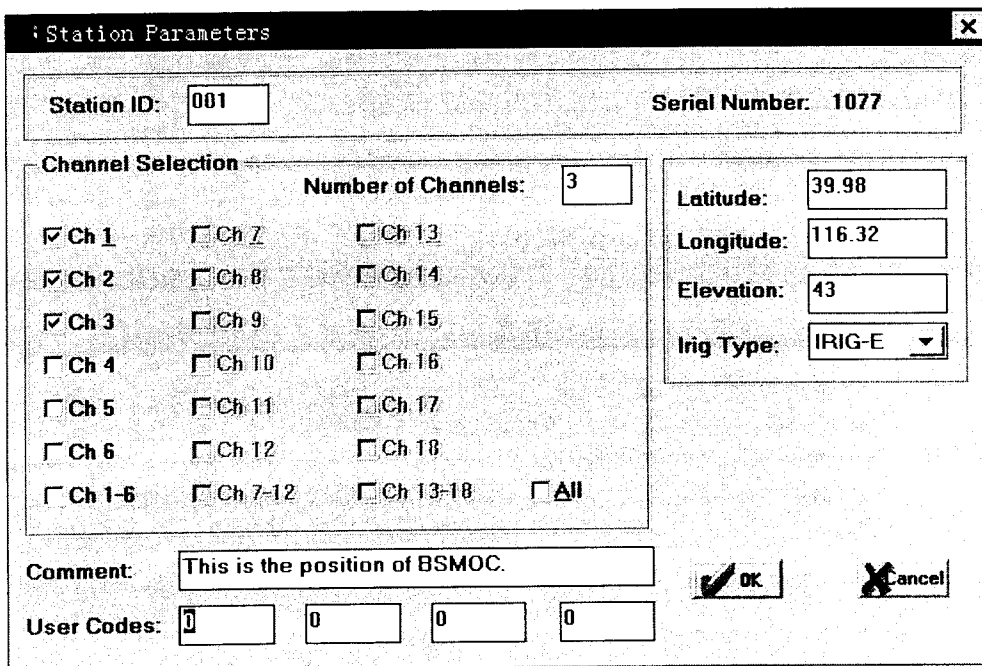


Fig. 4: Window for station parameters

- Timing parameters – They edit timing-related parameters.

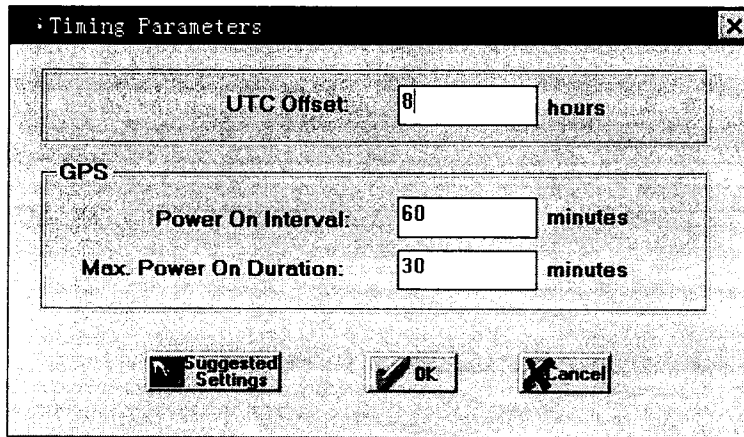


Fig. 5: Window for editing timing parameters

- Modem parameters – They determine the modem settings, how power to a cellular phone is controlled, and when the K2 calls you.

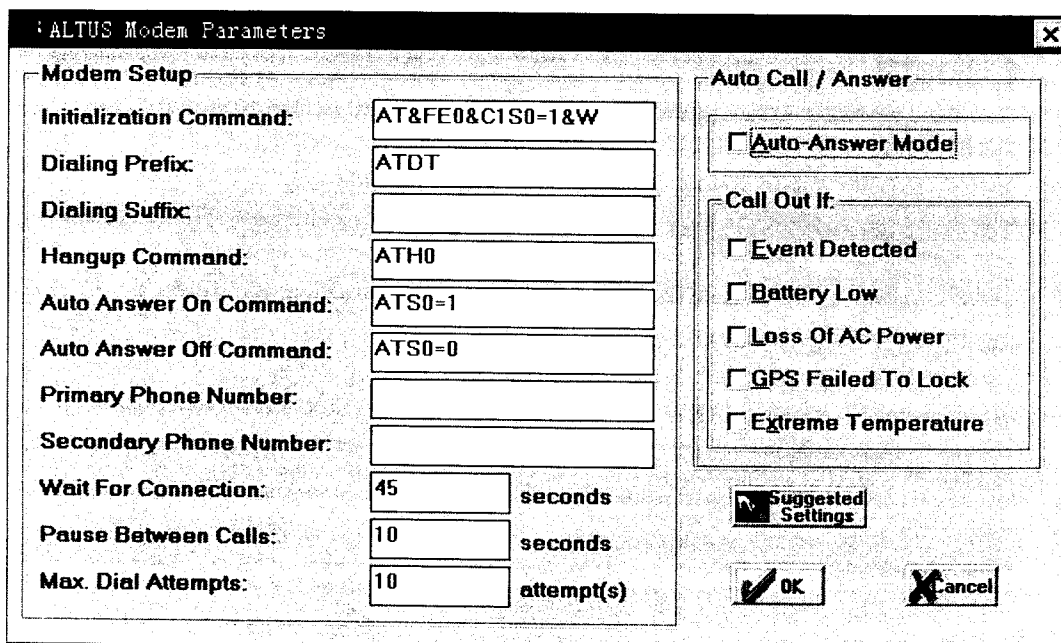


Fig. 6 Modem Parameters Window

- Channel trigger parameters – They determine what type of seismic signal will cause the triggering of an individual channel.

Fig. 7: Window for setting channel parameters

- Stream parameters – They determine at what sampling rate the instrument will record, and how long the unit will record before the trigger and after the de-trigger.

Stream Trigger Sources and Weights								
Ch 1:	1	Ch 7:	1	Ch 13:	0	Network:	1	Total Weight: 15
Ch 2:	1	Ch 8:	1	Ch 14:	0	Keyboard:	1	
Ch 3:	1	Ch 9:	1	Ch 15:	0	External:	1	
Ch 4:	1	Ch 10:	1	Ch 16:	0	Detrigger Weight:	1	
Ch 5:	1	Ch 11:	1	Ch 17:	0	Trigger Weight:	1	
Ch 6:	1	Ch 12:	1	Ch 18:	0			

Fig. 8: Window for setting stream parameters

- Digital field station configuration – It determines whether and what data is sent on the auxiliary digital output port.

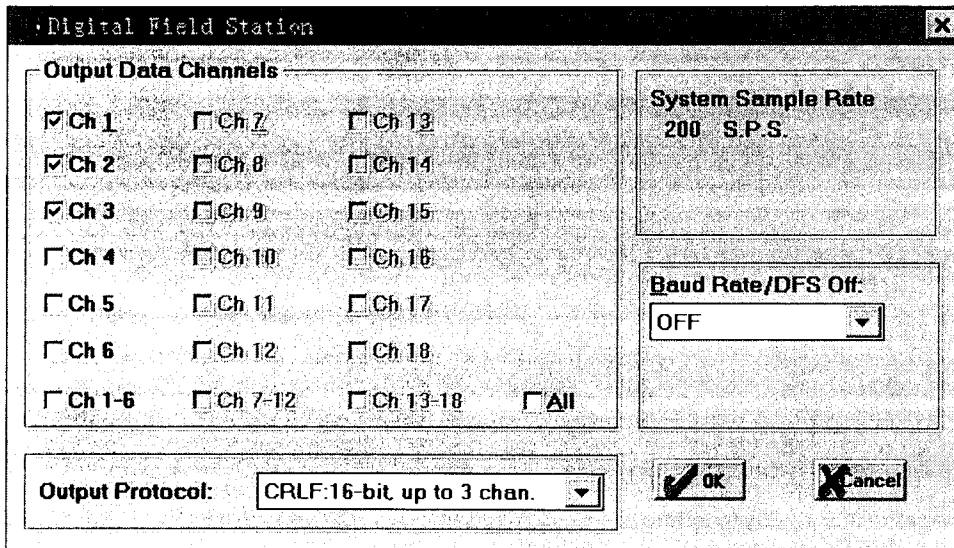


Fig. 9: Digital field station configuration window

- Serial data stream configuration – It determines if real time packetized data is sent out on the RS232 port.

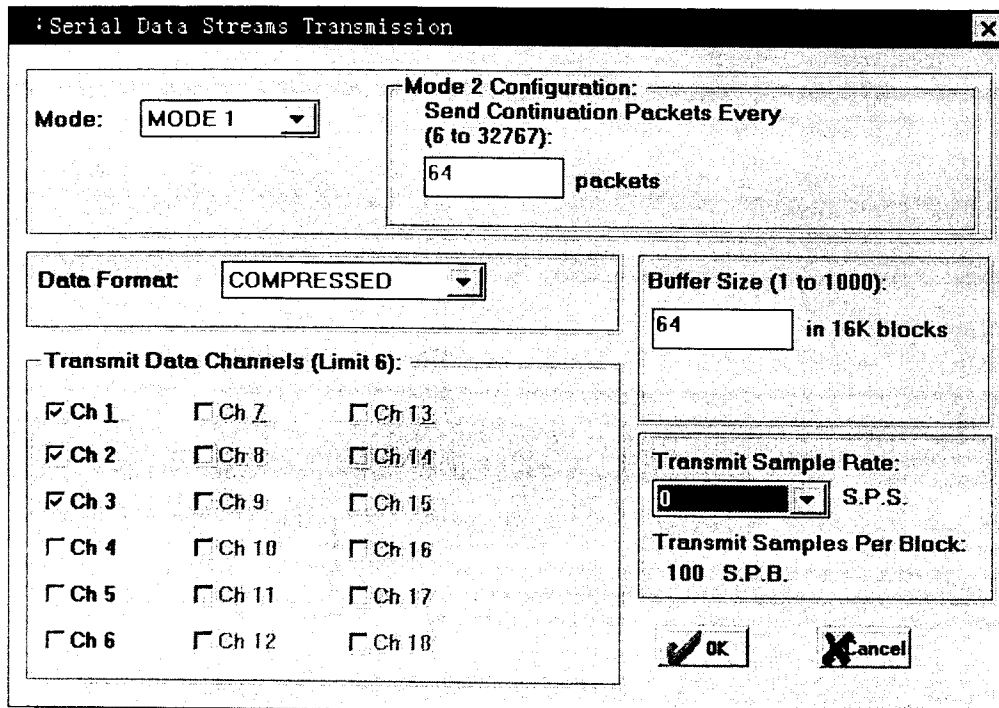
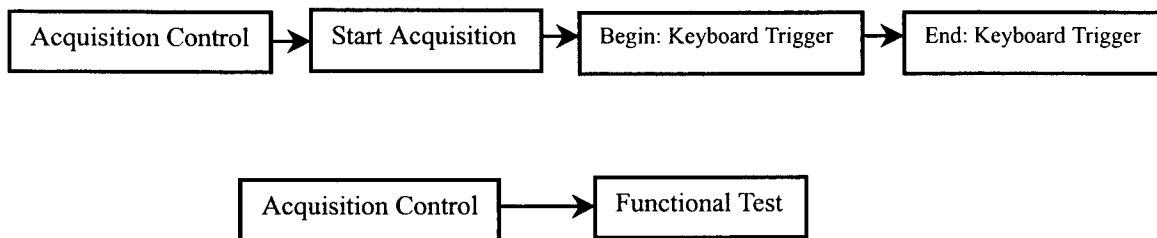


Fig. 10: Serial data stream configuration window

2.4 Trigger- and functional tests



2.5 Receive files

To use Quick Talk to download event files from K2 to PC:

1. From Quick Talk, go to the desired drive by clicking on A: or B: button in the **Directory** window.
2. Double click on the directory entry to change to that directory.
3. Double click on the filename to download that file. After download the files the K2 clears the archive bit in the file's directory entry.
4. Use QuickLook for Windows or another communication program to view K2 event files.

2.6 Displaying event files

Use the QuickLook software to view event files retrieved from a K2 recorder.

■ Starting & exiting QuickLook

To start QuickLook from within QuickTalk, select **Window** and **QuickLook Window**. The Run QuickLook dialog opens, as shown in Figure 11.

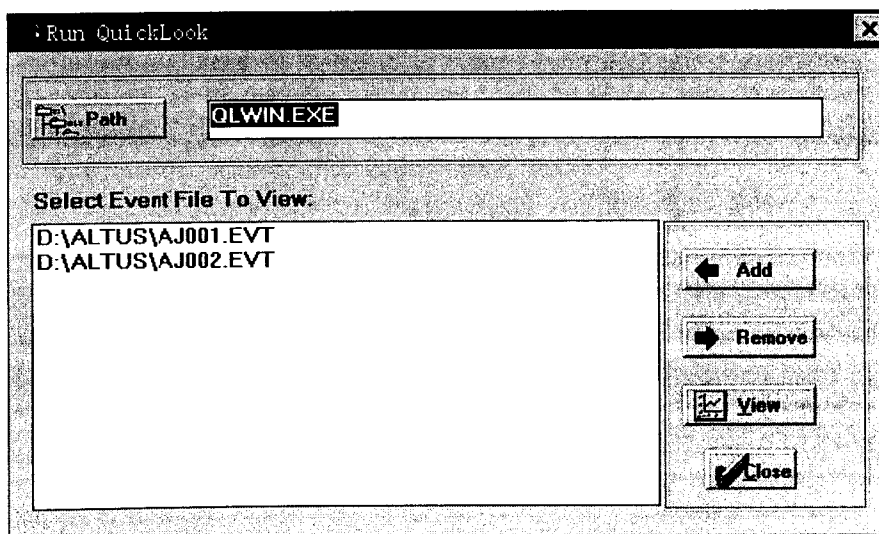


Fig. 11: Run QuickLook window

Exit QuickLook just to double-click in the upper left-hand corner of the window, or select **File and Exit**.

■ Opening an event file

When QuickLook starts, the Run QuickLook dialog box makes accessible event files recently from the K2 recorder. In Figure 11, there are two event files named AJ001.Evt and AJ002.EVT.

Use the **Add** button to add previously retrieved event files to *Select Event File to View* list.

Changing the Path: click on the **Path** button to change the event file path.

Removing Files from the List: select the name of the event file to remove from the list, then click the **Remove** button.

Viewing an Event File: Select an event filename and click the **View** button. Or, double-click on the filename. The QuickLook window opens displaying the trace.

■ The QuickLook window

Figure 12 shows the QuickLook window and its components.

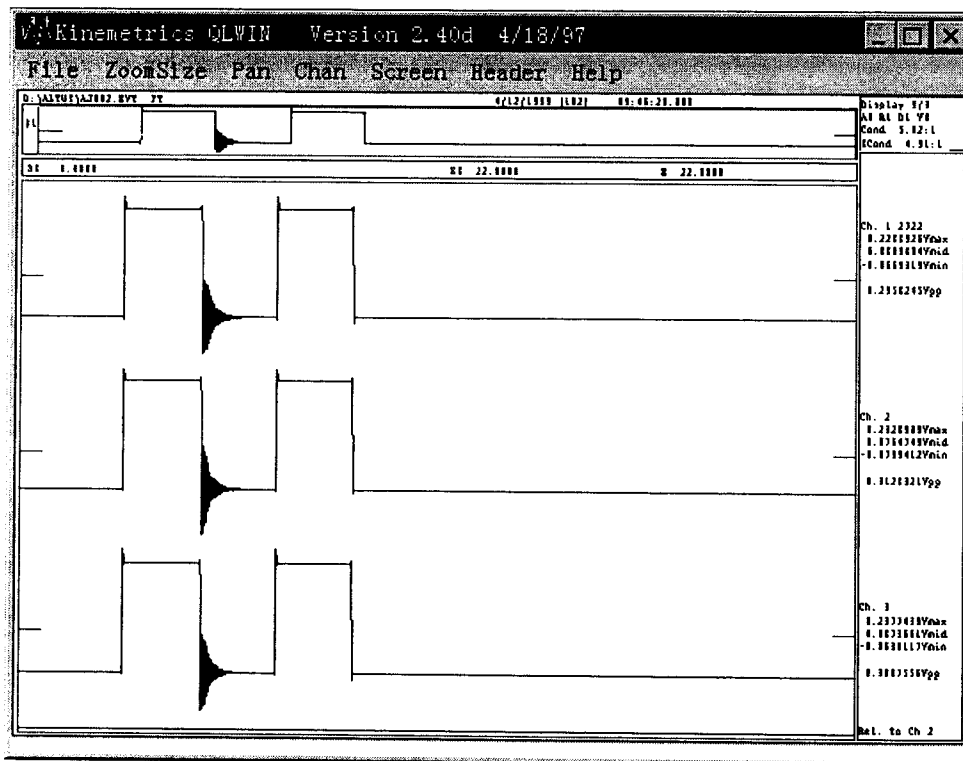


Fig. 12: QuickLook Window

REFERENCES

Altus K2 Digital Recorder User Manual, Kinematics, Inc., Document 302200, Revision E, April 1998.

QuickTalk & QuickLook Communications Software for Altus Recorder Systems User's Guide, Kinematics, Inc., Document 302208, August 1997.

TRENDS AND REQUIREMENTS IN STRONG-MOTION DATA ACQUISITION, MANAGEMENT, ANALYSIS AND EXCHANGE

Li-Li Xie

Institute of Engineering Mechanics, China Seismological Bureau
29 Xuefu Road, Harbin, 150080, China,
Fax: +86-451-666 4755; Email: llxie@public.hr.hl.cn

1. INTRODUCTION

Safeguarding life and property from the destructive effects of earthquakes is a serious world-wide problem. The ultimate goal of any earthquake hazard mitigation effort is to devise and implement socially and economically acceptable strategies for minimizing the loss of life and property resulting from earthquakes. For designing safe and economical structures and facilities in earthquake-prone regions, it is necessary to understand both the nature of the ground motion that these systems may experience and the nature of their responses to the motions. Much can be learned from lessons of seismic damage, and analytical, experimental and theoretical results by computer and mathematical modeling of fault-mechanisms, wave propagation, structural response, soil-structure interaction, and other factors. But a complete and reliable understanding of the phenomena involved can only be obtained from direct measurements of the various aspects of the overall processes. This requires measurements of both the near-field strong ground motion and of the response of structures during actual earthquakes. The **Strong-Motion Instrumentation Program (SMIP)** is defined here as a general title of the totality of activities related to strong earthquake motion data acquisition, data management (i.e. archiving, storage, dissemination etc.), data processing and data application.

The SMIP plays an essential role to improving public earthquake safety. Its primary purpose is to create new knowledge on strong earthquake ground motion and the seismic response of structures. The fundamental task of SMIP is to record each damaging earthquake on ground and in man-made structures in densely urbanized areas by using strong-motion instruments such as analog or digital strong-motion accelerograph. The program usually covers a cooperative instrumentation network, a data center, and a supporting strong-motion data analysis and research center at the national, regional, or local level in support of this task.

1. OBJECTIVES OF SMIP

The SMIP aims at improving public earthquake safety by implementing its task of coordination, acquisition, rapid dissemination and interpretation of strong-motion recordings of each damaging earthquake in the area concerned. Strong-motion recordings of damaging earthquakes in densely urbanized areas are critical for improvements in the design of earthquake-resistant structures and efforts to reduce potentially catastrophic losses of property and lives in future earthquakes. The recordings are fundamental for understanding and characterizing the physics of seismogenic failure, the generation and propagation of damaging ground motions, and the shaking performance of structures. The program's consistency of strong-motion recordings and long-term effectiveness are well-illustrated by a immense collection of accelerograms, which were recorded during significant earthquakes that occurred

all over the world, but mainly in the United States, since 1933.

2. HISTORY AND SCOPE OF SMIP

Strong-motion recording was initiated in the United States and rooted in the World Engineering Congress that convened in Tokyo in 1929. American engineers returned from these meetings convinced that there was an immediate need for the United States to develop a rugged seismograph able to record potentially damaging ground motions and to monitor the response of critical structures during strong local earthquakes. In 1931, the US Congress allocated additional funds to the Coast and Geodetic Survey for the establishment of an engineering seismology program, including the development of a strong-motion seismograph (accelerograph), and the implementation and operation of a national strong-motion network.

The first U.S. accelerographs were installed in southern California in the summer of 1932; by 1972 the network included 575 accelerographs at permanent stations located throughout the United States and in Central and South America. The U.S. Geological Survey's National Strong-Motion Program (NSMP) has evolved over more than six decades. The NSMP's National Strong-Motion Network (NSMN) currently operates over 900 strong-motion recorders at approximately 570 permanent stations located in 33 States and the Caribbean. As a rough estimate, there are now about ten thousands strong-motion recorders installed all over the world, among them one third in the United States, one third in Japan and one third in remaining parts of the world.

A complete SMIP should encompass the following components: a strong-motion instrument network for data acquisition, a data center for data routine analysis, data management and data interpretation and utilization. The data management is responsible for archiving, dissemination and quick reporting of data and for preparing also the relevant complementary data needed for data interpretation such as geological, seismological and geotectonic data.

3. DATA ACQUISITION AND STRONG-MOTION NETWORKS

Strong-motion networks may be **permanent** or **mobile**. Besides this there exist **integrated borehole** and portable **strong-motion arrays**, which are instrumented with high-fidelity, wide-dynamic range recorders (General Earthquake Observation System, GEOS). They can be used both for array operations and for critical post-earthquake response studies. Analysis is conducted as data becomes available.

Besides data on seismic strong-motion **complementary data** are required which are crucial for the interpretation of existing strong-motion recordings of damaging earthquakes. This requires the compilation of seismic, geotechnical and geologic borehole data on the near-surface lithology and for seismic site characterization.

Additionally, there exist programs for development and installation of special-purpose instrumented arrays for soil-structure interaction studies (**Structure and Soil-Structure Interaction (SSI) Arrays**). Such programs require the cooperation of many agencies.

Another important aspect are **near-real time strong-motion measurements for emergency response and warnings**. They necessitate the configuration and implementation of modern

telecommunication which allows rapid retrieval and interpretation of on-scale (strong-motion) measurements in urbanized areas for near-real time damage assessment and quick effective decision-making on emergency response and the deployment of relief and reconstruction forces.

4. DATA MANAGEMENT

The acquisition of large amounts of strong-motion data by a variety of organizations results in an increasing need to develop data archiving, management, and retrieval procedures that will increase data accessibility for research and engineering applications. A user-friendly data-management system permitting ready access to complete strong-motion time series and spectral data bases is a fundamental need of both the scientific and engineering communities. A prime consideration is that strong-motion accelerograms be made available without delay after an earthquake to designers, researchers, and others who have a need to see the recordings.

The volume of digital data requires a data archiving and retrieval system which involves two components. One component should provide a catalog of information regarding station, event, and data parameters. A second component, comprising a much larger volume of information, should provide the actual time series and spectral values. The first component should be interfaced with the second one so as to facilitate archiving and retrieval of the time series. The first component of the system should be maintained by appropriate data-collection agencies which should also maintain the second component depending on resources and objectives of the agency. These two interactive components suggested a database management system which is consistent with present uses of strong-motion data.

Based on the above observations, the following three points should be emphasized in order to improve the management of strong-motion data :

1. An operational strong-motion data center should be established with the following major activities:
 - 1) digitizing, processing, archiving and disseminating analog strong-motion records recorded by the Strong-Motion Network;
 - 2) implementing a modern data base for rapid data retrieval and dissemination via Internet, ftp sites, CD-ROM, etc.;
 - 3) developing and implementing hardware and software for rapid incorporation of near-real time strong-motion data into a data base for rapid dissemination at a web site;
 - 4) preparing specific guidelines for effective coordination and unification of all program efforts towards archiving, cataloging and disseminating strong-motion data.
2. Strong-motion data should be archived and cataloged so that these data can easily and readily be obtained by users and a commitment should be made to continuously update the catalog of strong-motion data so as to keep it current.
3. A minimum standard of documentation should be developed for existing and future strong-motion data collected by various agencies and organizations. The strong-motion data refers to the strong-motion records (processed and unprocessed) and to information pertaining to these records that is relevant for research purposes. For each record three general categories

of information can be identified: accelerogram, recording station, and causative earthquake. In each of these categories the following information should be documented:

Accelerogram

- Date and time of earthquake
- Location (address) and identification (I.D.) number of recording station
- Earthquake magnitude and site intensity
- Source-site distances (epicentral, hypocentral)
- Accelerogram characteristics (uncorrected peak acceleration, corrected peak acceleration, velocity and displacement, and RMS acceleration)

Recording Station

- Location, coordinates, and I.D. number
- Structure which houses the instrument (size and type)
- Type of instrument and location within the structure
- Local geology (description and classification)

Earthquake

- Date and time
- Location description and hypocentral coordinates (including location uncertainty if known)
- Magnitudes (M_L , M_S , M_W , M_b , M_{JMA} , etc.)
- Maximum intensity
- Source dimension (length, width, radius, area)
- Seismic moment and stress drop
- Source rupture characteristics (fault type, strike, dip, displacement, slip and rupture directions, rupture velocity)

Each organization maintaining strong-motion instruments should document the above information for every accelerogram digitized. It is recognized that some of this information, such as earthquake source parameters, may not become available for some time. However, organizations should attempt to maintain this documentation to the best of their ability in an organized manner.

5. DATA UTILIZATION

Applications of strong ground-motion data take a variety of forms. For the purposes of this written lecture, they are arbitrarily divided into (1) basic seismological and engineering seismology research, (2) basic earthquake engineering research, and (3) engineering practice and code development.

5.1 Basic seismological and engineering seismology research

Strong motion data contribute to the understanding of source mechanisms and propagation of seismic waves from the source to the point of interest, including local site effects (see Figures

7 and 8 in the chapter *Data processing and analysis of strong-motion accelerograms*). The characteristics of the source mechanism that can be examined using strong-motion data include: rupture velocity, point of initiation of the rupture, asperities or irregularities on the fault that produce strong radiation of high-frequency seismic waves, the direction of fault rupture and the resultant pattern of wave radiation, spectral content, stress drop, fault-rupture dimensions, time sequence or slip rate of fault-rupture dimensions, time sequence or slip rate of fault motion, amount of energy release or seismic moment, type of ground rupture, and possible regional differences in these parameters. An enhanced knowledge of the physics of the source is valuable not only to the science of seismology but also for the estimation of strong ground motion for engineering application.

Strong ground-motion data also contribute to a better understanding of wave propagation characteristics, such as geological and physical characteristics of the wave path (e.g., velocities, density, and rigidity); attenuation along the path, both geometric and that from anelasticity; scattering effects; near-source parameters topography or other structural elements; and site effects caused by variations in soil type, water table, and neighboring geologic structure and topography. The resultant strong-motion duration and frequency content are strongly affected by the characteristics of the propagation path as well as the duration of the earthquake source. Strong regional differences have been observed in high-frequency wave propagation in various parts of the United States.

Adequate strong-motion instrumentation, including two- and three-dimensional arrays, is required to obtain the basic data for a better understanding of the seismological source and propagation parameters. This enhanced understanding will significantly improve the capability to predict strong ground motions in a given geologic environment.

5.2 Basic earthquake engineering research

Over the past 40 years, the specialized field of earthquake engineering has grown from infancy to its current advanced state, allowing the design and construction of buildings with greatly improved safety and cost-effectiveness. This progress could not have taken place without the availability of strong-motion accelerograms and high-speed digital computers that together enabled the development and implementation of the current methodologies of analysis and design.

The research that played a major role in the development of these methodologies can be classified into four areas: (1) strong ground motions, (2) mathematical modeling and dynamic analysis, (3) structural performance, and (4) seismic design.

5.2.1 Strong Ground Motions

Understanding the nature of strong ground motions, i.e., intensity, frequency content, phase relations, duration, and spatial variations, is fundamental to achieving good earthquake-resistant design of critical structures based on economic and safety considerations. These structures include buildings, bridges, dams, offshore platforms, liquefied natural gas storage tanks, and nuclear power plants.

Through the improved strong-motion instrumentation program, much valuable information

has been recorded that has led to a better understanding of the expected ground motions which are required in the design process (see figure 8 in chapter *Data processing and analysis of strong-motion accelerograms*). The ground-motion criteria used for earthquake-resistant design of critical structures have undergone major revisions in recent years because of recorded ground motions. Further revisions can be expected as new knowledge is gained through the strong-motion instrumentation program.

5.2.2 Mathematical modeling and dynamic analysis

Because of the availability of high-speed digital computers, it is possible to perform the numerical work required by detailed mathematical models of critical structures. Twenty-five years ago the practicing engineering profession was very limited in its ability to calculate seismic response. Presently, however, detailed dynamic analysis are routinely carried out for important structures. For example, seismic response analysis of nuclear power plants containing a multitude of piping systems, equipment, and secondary structures are made, including soil-structure interaction effects. These design activities set up a demand in modelling which, in turn, creates a demand for improved knowledge of strong motion.

5.2.3 Structural performance

Because of economic considerations, controlled damage must be allowed to take place in many structures, such as buildings, offshore platforms, and bridges during maximum credible earthquake conditions. This requirement necessitates an understanding and an ability to predict the resisting forces developed under large deformation cyclic conditions and the failure mechanisms likely to take place under extreme conditions. With the availability of modern electronically controlled, hydraulically powered testing equipment and shaking tables, high-speed data acquisition and processing equipment, and computers and associated computer programs for control and analysis, much knowledge has been recently gained regarding structural performance under seismic conditions. The validity of this knowledge is, of course, highly dependent upon the ability to prescribe realistic seismic excitations, which is dependent upon information gained through the strong-motion instrumentation program.

5.2.4 Seismic Design

The practice of earthquake engineering in the design and construction of structural facilities has undergone major changes during the past 25 years as a result of advances made in the areas of seismic ground motions, mathematical modeling, dynamic analysis, and structural performance. Codes have been modernized, requiring the designs to be based on more realistic seismic ground-motion criteria, better detailing of structural components and systems, and improved control of materials. Considering that basic earthquake engineering research leads to economic and safety improvements in seismic design and construction, it is very clear that every effort should be made to strengthen the strong-motion instrumentation program, which is fundamental to this development.

5.3 Engineering practice and code development

Accelerogram data have also led to improvements in building codes. For example, the evolution of the lateral force provisions in these codes is based on the accelerograms recorded during major earthquakes. More accelerogram data are required, however, because of the need for further improvements in engineering practice and building codes. Few accelerograms have been recorded near the fault ruptures of earthquakes greater than magnitude 7, although these pose the largest threat to many urban environments. Engineers rely on extrapolations of the existing data base to predict the motions of these potentially destructive events. As a result, the uncertainty in these estimates is greater than those where little or no extrapolations are involved. Consequently, the design of future structures may not be optimal and the evaluation of existing ones may be inaccurate in some cases.

6. DATA PROCESSING

The recorded strong-motion data usually need to be processed to eliminate and /or correct various of effects or errors from recording system, digitizing process and so on. As a standard data processing procedure the processed data usually are provided in uncorrected and corrected form with also calculated velocity, displacement, response spectra and Fourier spectra.

6.1 Uncorrected and corrected data

The term "uncorrected" indicates that a digitized (or digitally recorded) time series has received no processing that involves any hypotheses as to the character or frequency content of the ground motions or recording instruments. An "uncorrected" analog-recorded time series has been corrected only for uneven film transport with time and for transverse motion of the film as it moved longitudinally through the recorder; it has been shifted to have zero mean; and it has been translated from digitization units to units of cm/sec/sec (ordinates) and seconds (abscissas).

The "correction" process applies bandpass filters (removing noise contamination) and instrument correction (removing the effects of frequency-dependent instrument response) to a time series. A software developed by the US Geological Survey located at the Menlo Park, California USA named BAP, that will correct the time series, is available from the NSMP web site (<http://nsmp.wr.usgs.gov>).

6.2 Basic Strong-Motion Accelerogram Processing (BAP) software

The Basic Strong-Motion Accelerogram Processing (BAP) computer program was developed at the U.S. Geological Survey (USGS) to process and plot digitized strong-motion earthquake records. BAP will calculate velocity and displacement from an input acceleration time series or it will calculate acceleration and displacement from an input velocity time series. The program will make linear baseline corrections, apply instrument correction, filter high frequency and/or low frequency content from the time series, calculate the Fourier amplitude spectrum, and calculate response spectra. It will also plot the results after each processing step. A paper copy of the BAP manual: "BAP: Basic Strong-Motion Accelerogram Processing

Software; Version 1.0" by April M. Converse and A. Gerald Brady, 1992 (USGS Open-File Report 92-296A) is available upon request by contacting Kent Fogleman fogleman@usgs.gov (telephone: 650-329-4745) or by ordering a copy from the USGS Information Services (Internet: [http:// mapping.usgs.gov/esic/to_order.html](http://mapping.usgs.gov/esic/to_order.html)).

6.3 Strong Motion Analyst (SMA)

Recently the Kinematics developed a software package for strong motion data routine processing. This Strong Motion Analyst (SMA) software package is a tool designed for earthquake engineers, seismologists and academic researchers to process strong motion accelerograms. It is a Windows™-based interactive processing tool that features instrument correction, data editing, filtering, ground motion integrations, Fourier and Response Spectra calculations, and .V1, .V2, .V3, file format output. Its key features are to support up to 18 data channels, up to 5 damping values, and up to 100 period values and to produce uncorrected acceleration (.V1 files), corrected acceleration, velocity and displacement (.V2 files), Fourier and response spectra (.V3 files), power spectral density and FFT graphs. For more information contact sales@kmi.com .

In China, rather sophisticated software for data processing was developed. It can be applied for recording systems with a single degree of freedom (such as pendulum systems) and also for systems of a pendulum coupled with a galvanometer. This software can provide all results as BAP does and takes more factors into consideration such as limitation of record length, uncertainties in baseline and restriction on the cut-off frequencies for band-pass filter.

7. DATA EXCHANGE AND DISSEMINATION

As a consequence of the large number of strong-motion programs throughout the world, a number of data management and distribution problems have arisen. There is a growing concern that, as the number of participating organizations and the strong-motion data base continues to increase, a significant amount of the data may not get into the hands of the user on a timely basis. This problem already exists to some extent and is likely to become worse. The major reason for it is the fragmentation of existing programs and the lack of coordination among them. However, with the rapid development of the internet web technology, many organizations have put their data onto their specially designed web site. The users can easily access most of the data recorded so far through the internet.

At present, there are many efforts dedicated to the dissemination of strong motion data in a variety of forms, such as:

7.1 Publications

The U.S. Geological Survey (USGS) National Strong-Motion Program (NSMP) routinely publishes a variety of reports related to strong-motion recordings from U.S. earthquakes, such as the GEOS Reports - USGS Open-File Reports of earthquake and aftershock data collected by the NSMP General Earthquake Observation System (GEOS) project. In Japan, the Port and Harbour Research Institute of the Ministry of Transport and the Abiko Research Laboratory of the Central Research Institute of Electric Power Industry (CRIEPI) also publish their strong

motion data reports, namely the “Annual Report on Strong-Motion Earthquake Records in Japanese Ports” and the “Strong Motion Earthquake Records Obtained by the CRIEPEI Observation Network”, respectively. In China, about 10 big volumes of strong-motion data as well as the results of their routine analysis, such as calculated velocity, integrated displacement, response spectra and Fourier spectra, have been published since 1980.

Preliminary Data Reports: These are compilations of strong-motion records from individual earthquakes, aftershocks, or related series of earthquakes.

Catalogues of Strong-Motion Records: These are summaries of the accelerograms recovered from the U.S. National Strong-Motion Network and from the strong-motion accelerograph stations of cooperating agencies. From 1974-1980 these reports were issued quarterly and titled "Seismic Engineering Program Reports". Beginning in 1981, the reporting period switched to an annual cycle. From 1981 to 1985 the reports were called "Strong-Motion Program Reports, January-December [year]"; since 1986 the title has been "Catalogue of U.S. Geological Survey Strong-Motion Records, [year]".

CD-ROMs: The National Oceanic and Atmospheric Administration of the United States Department of Commerce has prepared a CD-ROM Strong Motion Data Collection which contains more than 15,000 digitized and processed accelerograph records dating from 1933 to 1994.

7.2 Online Database

The USGS Publications database is now online and available at "<http://usgs-georef.cos.com/>. This database provides access to the publications of the USGS and includes references to U.S. Geological Survey reports and maps published from 1880 to date, references to non-USGS publications with USGS authors published from 1983 to date, and 225 references to reports produced by the Hayden, King, Powell, and Wheeler surveys.

A very similar database titled: “ON-LINE WORLD-WIDE STRONG GROUND MOTION DATABASE (SMDB) ” is also available at the web-site: <http://www.wdcb.rssi.ru/CGDS/>.

DATA PROCESSING AND ANALYSIS FOR STRONG MOTION ACCELEROGRAMS

Lili Xie

Institute of Engineering Mechanics, China Seismological Bureau
29 Xuefu Road, Harbin, 150080, China,
Fax: +86-451-666 4755; Email: llxie@public.hr.hl.cn

1. INTRODUCTION

At the present time (1998) there are about 10,000 recording strong-motion earthquake accelerographs distributed very unevenly throughout the seismic regions of the world. In a typical year, these instruments will generate several dozen records of strong earthquake ground motion to be added to the several thousands of important records which already exist. Practically, all of these accelerographs produce records as a digital data set or as an analog trace of acceleration versus time, either in a computer-compatible format in a RAM, or as photographic trace on film or paper, or as a scratch on waxed paper.

The object of the present report is to explain to the non-specialist in instrumentation and data processing the way in which the information contained in these analog traces can be as accurately and completely recovered as is practically feasible. Emphasis will be on the records of mechanical-optical-photographic type of accelerographs which have been standard for more than 50 years. Most of the basic ideas and theory will apply with only minor modifications to other types of recording, such as the modern digital accelerographs with state RAM as well as to the older waxed paper system used in some standard Japanese accelerographs.

The analog photographic trace acceleration-time record of the current standard accelerograph is of special significance in that it yields a great deal of information of immediate practical importance by inspection and by simple scaling without the need for more elaborate data processing. Any engineer with a modest amount of special knowledge and experience will be able to learn much from such records. The first main chapter of this paper will be devoted to the simplified type of data analysis using only dividers and scales without trace digitization or calculations. In the second main chapter it will be shown that additional information of importance can be derived from the record by special data processing techniques.

2. DIRECTLY -SCALED INFORMATION FROM ACCELEROGRAMS

2.1 The accelerogram

A typical accelerogram will be an analog trace of acceleration versus time in the form of (1) a 35 or 70 mm film negative, (2) a photographic enlargement or copy on film or paper, positive or negative, of a 35 or 70 mm film, (3) a 12-inch wide photographic paper record or a copy thereof, (4) a computer plot perhaps derived from either a digital magnetic tape, or play-backed from the RAM system of a digital instrument, or (5) a reproduction in a book or report which maybe photographed from an original, a copy, a tracing or a computer plot. For the

simplified analysis discussed in this chapter, any of these basic formats normally will provide satisfactory accuracy. For more accurate analysis involving digitized records, it will be necessary to use original records or carefully prepared film copies made on dimensionally stable materials on equipment of known distortion characteristics.

Fig. 1 is a copy of a typical accelerogram of the most complete form likely to be encountered in practice. The seven traces can be identified as follows:

- (1) absolute time code for reading absolute time (received on a special radio included in some accelerographs, more commonly, this first trace is a duplicate of trace 7;
- (2) horizontal linear acceleration in direction of the long dimension of the accelerograph case;
- (3) fixed trace for digitization purposes;
- (4) linear acceleration in the vertical direction;
- (5) fixed trace;
- (6) horizontal linear acceleration in direction transverse to the long dimension of the accelerograph case, and
- (7) relative time marks, a certain number of pulses per second, generated by an internal timing circuit.

Time on the record is in effect measured directly from the recorded internal time marks rather than deriving it from the record speed. The internal time marks, calibrated to an accuracy of 0.2 percent in case with time marks of two pulses per second, provide a means for correcting non-uniformities in the recording speed if they should occur. Relative time intervals on the acceleration traces themselves, such as periods of predominant waves or duration times of strong shaking, can usually be determined to a sufficient accuracy using dividers placed directly on the timing trace opposite the features being timed. For an example of the use of the time marks, note that on trace 2 the length of one period of a prominent sinusoidal component of the waveform has been indicated. By scaling this directly against the time scale of trace 7 with dividers and a millimeter scale, the period of the wave is ascertained to be about 0.07 second (14 Hz). Direct scaling from trace 7 also indicates that the duration of strong shaking on Traces 2 and 6 is about 2 seconds.

The absolute time marks of trace 1 are not present on most accelerograms and are not essential for most engineering applications. They do, however, serve two potentially useful purposes. First, they make possible a positive identification of the earthquake event being measured, since it can be compared with data from seismological observatories. Secondly, they provide an accurate way of synchronizing various accelerographs located at any distance so that exact phase relationships can be established. Where suitable standard time radio transmissions are available, this radio link is the best way to provide synchronization between accelerographs hundreds of kilometers apart, being usually less expensive than hardwire of telephone line links.

The two fixed traces (3 and 5) which record the position of light beams reflected from mirrors attached to the instrument case provide a means for correction for certain types of spurious trace motion. Should small transverse motions of the whole film occur during transport, as could happen if the perforation holes were oversize, the fixed and variable traces would be affected alike, and the difference between them would be free of such an error. Such fixed traces are sometimes missing from older accelerograms and in such cases the base of a timing pulse mark can often be used as a substitute. These fixed traces are not needed for the simplified analysis of the record and play a role only for the more detailed computer processing of the accelerograms.

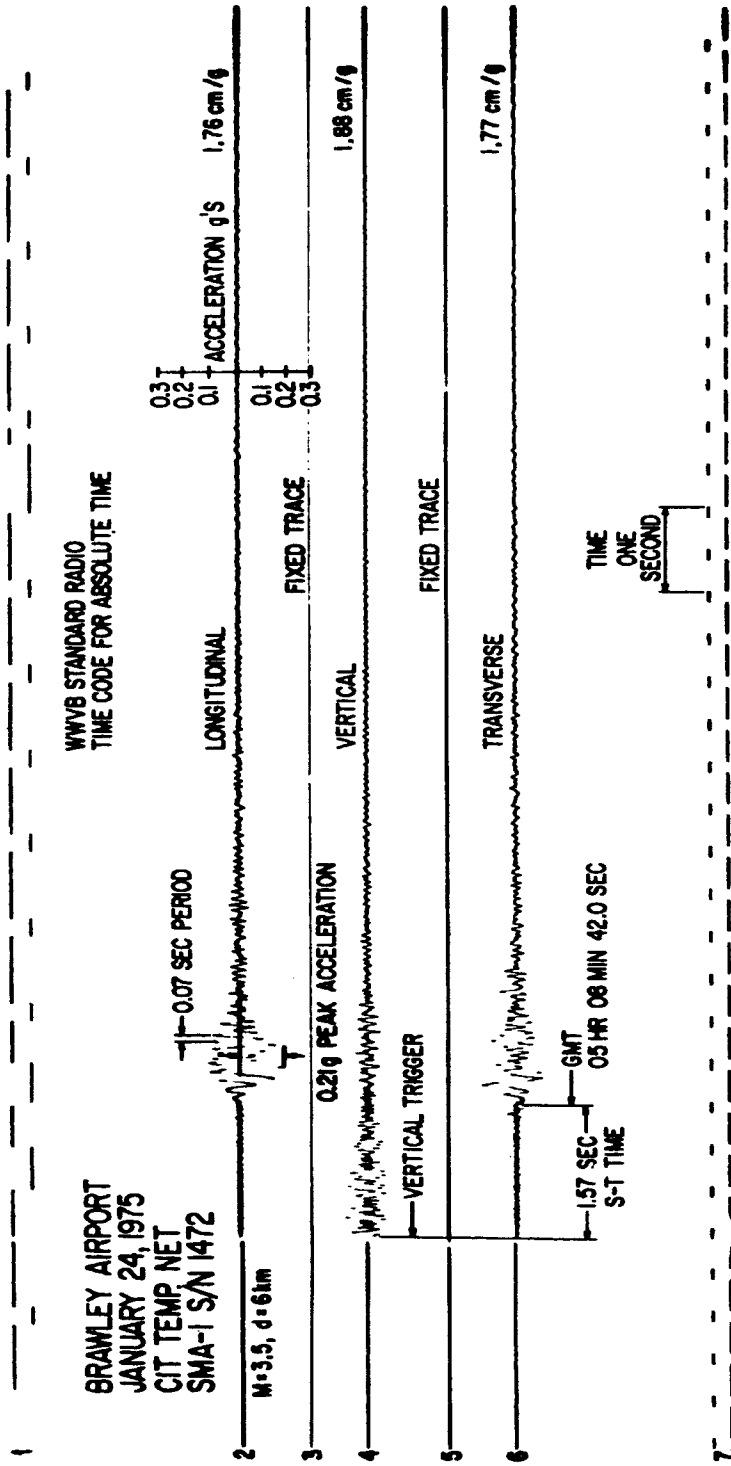


Fig. 1: Typical strong-motion earthquake accelerogram.

2.2. The acceleration-time traces

For the acceleration traces (2, 4 and 6), the most important information required for interpretation is the transducer sensitivity, expressed as cm/g trace displacement on the original film. The instrument manufacturer supplies with each accelerograph a calibration sensitivity for each accelerometer trace. In Fig. 1, for accelerograph serial No. 1472, the manufacturer's calibrations (shown at the right of Fig. 1) are: trace 2, longitudinal, 1.76 cm/g; trace 4, vertical, 1.88 cm/g; trace 6, transverse, 1.77 cm/g. These calibrations are carried out on special fixtures in the manufacturer's laboratories, and are specified to be accurate to 0.5 percent. An overall calibration can also be carried out in the field by the user on the complete assembly by rotating the whole accelerograph in the earth's gravitational field through a measured angle and noting the corresponding trace deflections. With care, such tilt calibrations can be made to an accuracy of about 1%. The relative ease with which an absolute calibration of the whole instrumentation system can be carried out is one of the main advantages of the current types of strong-motion accelerographs.

It should be noted that the measured sensitivities can depart significantly from the "nominal" sensitivity which is given in the manufacturer's data sheet for the instrument type as 1.9 cm/g. For this particular serial number, there is a 6 percent variation in sensitivity between the various components and a 7 percent departure from the nominal value. Since acceleration values can be directly scaled from the record with an accuracy greater than these figures, it is clear that the individual trace sensitivity figures should always be used for quantitative work.

Given the 1.9 cm/g nominal sensitivity of the transducer system and the overall width of the recording medium, which for standard 70 mm perforated film is 60 mm space between perforations, it is clear that for full scale 1 g readings these may be a large overlap of the three acceleration traces. The accelerograph specifications call for a positioning of the traces on the film to minimize this overlapping while keeping full-scale deflections on the film. In practice it is usually not difficult to distinguish the individual traces and their peak values, but for some high frequency, high amplitude records this may require special attention.

The general instrument specifications call for a maximum photographic trace width on the original film of 0.2 millimeters. Considering that the full scale 1g acceleration value gives a trace deflection of about 2 centimeters, this means that the trace width is 1 percent of full scale. By direct scaling by eye a resolution of 0.01 g is the best that can be expected. As will be seen later, this resolution can be improved by an order of magnitude with modern digitization techniques.

Note that instrument sensitivity figures are always expressed in terms of the original film record. In working with copies from the original record, care must be used to take account of possible scale changes and distortions. In particular, great care should be exercised with copies made on office duplication machines which may involve uncertain magnifications and serious distortions. The numerical values shown in Fig. 1, for example, can be accurately checked only on the original film record. Where it is expected that various copies may be made from an accelerogram representation of the type shown in Fig. 1, it would be good practice to include a small scale as shown at the right of trace 2.

With the above precautions, values such as peak accelerations can be determined by direct measurement with dividers and linear scale and the application of the appropriate sensitivity. From Fig. 1, trace 2, it can be seen that the peak horizontal acceleration is about 0.21 g.

A visual inspection of the acceleration trace will also reveal many significant features of the frequency content and wave shape. Fig. 1, trace 2 shows a relatively simple wave form with predominant periods of 0.07 second (14 Hz) with some preceding lower frequency motions and some succeeding higher frequencies. The vertical motions of trace 4 have distinctly higher frequencies, as is always the case with strong earthquake motions, and have somewhat lower amplitudes. As a rough average for past earthquakes, vertical motions are usually about two-thirds the amplitude of horizontal components.

It will be seen that the vertical motion record of trace 4 begins considerably ahead of the horizontal motions of traces 2 and 6. At most stations, particularly those very near to the epicenter or on soft low-velocity ground, earthquake waves emerge at near vertical angles and therefore, since the longitudinal waves travel faster than the transverse shear waves, the first motions are usually predominantly vertical. If the starting mechanism of the accelerograph is arranged to respond to vertical rather than horizontal motion, the more rapidly arriving longitudinal P-waves will start the instrument well ahead of the arrival of the larger horizontal motions. In this way, the complete initial sequence of the first horizontal arrivals corresponding to shear waves can be recorded. The vertical trigger is set to operate at an acceleration threshold which can be adjusted from 0.005 g to 0.05 g, with a flat frequency response from 1 to 10 Hz and a rapid cutoff above 10 Hz to eliminate false starts caused by high frequency machinery and vehicle vibrations in the immediate vicinity of the accelerograph. The total time elapsing from triggering to full operating capability is specified to be not greater than 0.1 second, which means that the initial P-wave arrival time is known to within one-tenth of a second and the initial S-wave arrival time to a somewhat better accuracy. This S-T time (shear wave arrival time minus trigger time) is thus nearly equal to the S-P time (shear wave arrival time minus longitudinal wave arrival time). Once the values of the shear wave and the longitudinal wave velocities or just the differential travel-time curves in the region are known, the distance from the recording site to the earthquake hypocenter can be determined.

2.3. Summary of directly-scaled information

The information which has been directly obtained from the accelerogram by visual inspection and simple scaling without digitization or further processing can be summarized as: (1) peak acceleration, (2) time duration of strong shaking, (3) frequency of predominant waves and rough idea of frequency range, (4) amplitude and frequency relationships between vertical and horizontal motions, and (5) approximate distance from recording site to earthquake hypocenter. Information of this kind is sufficient to relate the given earthquake to past recorded earthquakes in many significant ways.

2.4. Typical earthquake accelerograms

Fig. 2 shows a collection of representative acceleration-time records for earthquake ground motions in the epicentral region close to the source. One typical horizontal component is given for each event. All have been plotted to the same acceleration and time scale so that direct comparison can be made. It is obvious that earthquakes produce acceleration records of rather different shape and size. It is also evident that the eye is a sensitive pattern recognition instrument. Various acceleration peak distributions or envelope shapes can be distinguished which might be difficult to describe quantitatively through simplified representations such as frequency spectra, threshold duration, or peak distribution statistics.

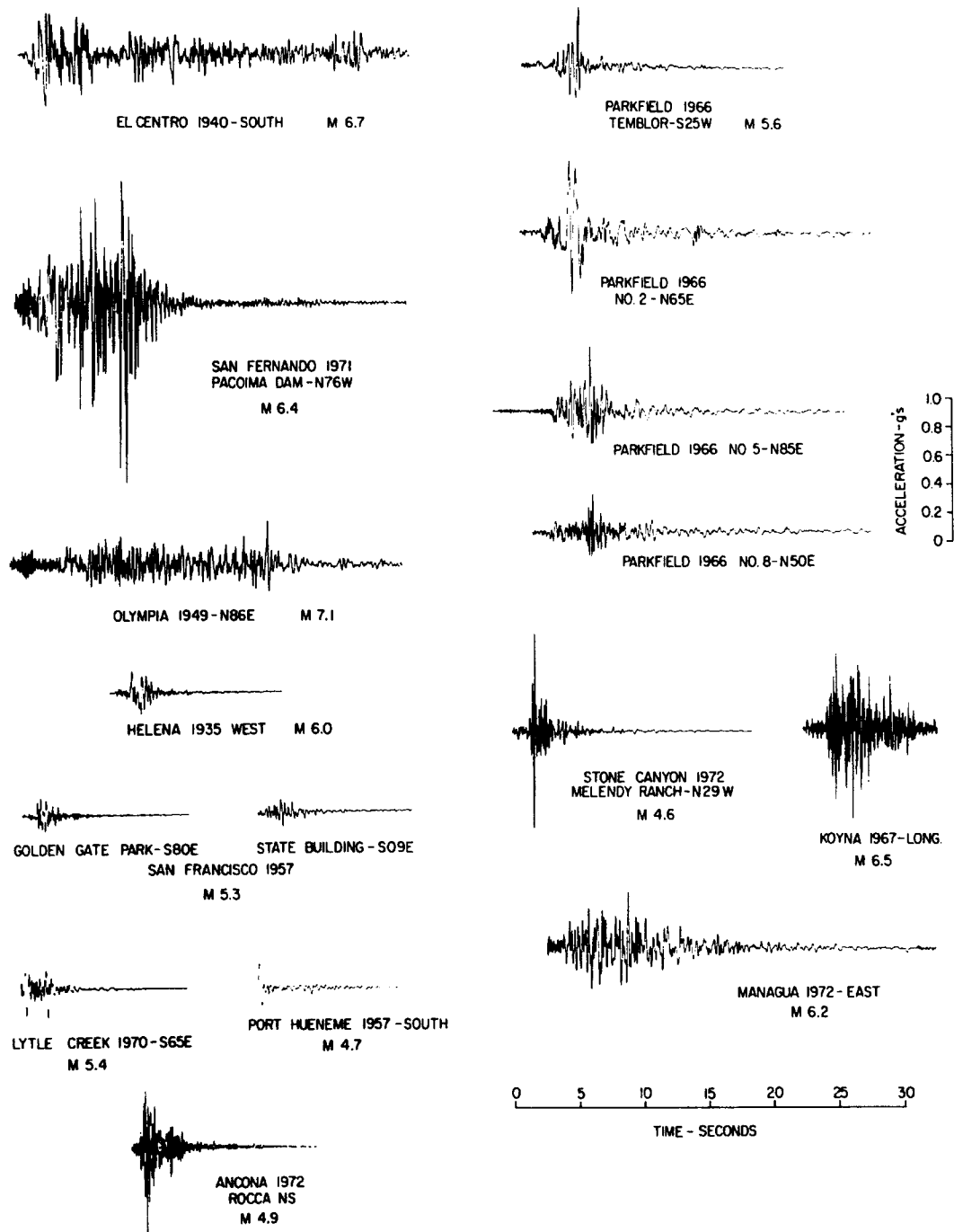


Fig. 2: Earthquake ground acceleration recorded in different epicentral regions

The present world data bank of strong motion accelerograms contains about thousands of important three-component records of strong ground motion from several hundred different earthquakes, recorded under many different conditions of distance, site geology, transmission path, etc. For each of these earthquakes a considerable amount of information is available on the effects of the earthquake on structures, on people, and on nature. One way in which the kind of information obtained above from scaling and inspection of the accelerograms can be

used is to infer additionally similar properties of the event as compared to those contained in the data bank whose accelerograms resemble most the new record. This comparison of similarity should be based on criteria such as amplitudes of peak value, duration of strong shaking, approximate frequency characteristics, and general envelope shape. The latter indicates the way in which the peak amplitudes vary over the length of the record. These similarly appearing past earthquake records as judged by the eye should then point the way to several past earthquakes for which considerable information as to damage and so forth might be available which could be assumed to share some of the practical characteristics of the new event.

To make meaningful visual comparisons, it is almost essential that the accelerograms be plotted to the same scale. When comparing, e.g., Fig. 1 with records in Fig. 2, the nearest resemblance would appear to be the San Francisco 1957 State Building record. However, noting that the time scale in Fig. 2 is about five times that of Fig. 1 it will be seen that the duration of the Fig. 1 record is much less than that of the State Building record, although the peak accelerations are about twice as big. One can thus conclude that the Fig. 1 record was recorded closer to a smaller earthquake. This is in fact supported by seismological measurements. They give magnitudes $M = 5.3$ for the 1957 San Francisco earthquake and $M = 3.5$ for the earthquake producing Fig. 1 and indicate that the State Building record was made at about 18 kilometers distance as compared to about 6 kilometers only for the record in Fig. 1. In both cases the ground motion was not of a damaging size.

The practical usefulness of the above approach depends on the availability of past accelerograms in a suitable form and on conveniently summarized data for past earthquakes. As the number of well recorded earthquakes increases, such correlations should become more and more valuable.

Information such as that derived above by direct scaling and inspection of uncorrected and unprocessed accelerograms is often sufficient to answer many of the important practical questions which arise immediately after an earthquake. Decisions as to the need to evacuate a damaged building, to empty a reservoir, or to carry out expensive inspection procedures need not await a detailed analysis of the record, but can usually be given with a satisfactory accuracy from the above simplified analysis. Subsequent processing will refine the answers and add significant additional information, but it is not likely that it will alter such practical decisions. This is one of the main advantages of the ready availability of analog accelerograms from the current types of photographic recording field accelerographs.

3. DIGITIZED ACCELEROGRAMS AND ADVANCED DATA PROCESSING

3.1 Introduction

The more detailed problems of accelerogram processing to recover additional information from the record will be considered now. The main advantages to be gained are:

- (1) resolution is improved and yields an increased dynamic range by an order of magnitude;
- (2) it is possible to introduce corrections for transducer characteristics so that the frequency range of the measurements can be extended;
- (3) digital computations permit accurate integration of accelerograms to find ground velocities and ground displacements, quantities which can be correlated in a significant

- way with various geophysical and geological parameters;
- (4) calculation of frequency spectra, response spectra, and structural responses becomes relatively simple with the input information in digital computer-compatible format, and
 - (5) the existence of the digitized data makes it feasible to carry out many statistical studies and to prepare various plots in any desired form or scale.

Unless the data have already been collected by modern digital accelerometers these advantages can in case of primary analog recordings only be realized by digitizing them so as to produce the basic data in a computer-compatible format. Although very few engineers who wish to use accelerograms will need to understand the details of digitization and data processing but can simply use the results of standard procedures, there are several advantages in knowing in a general way what these procedures are. First, a knowledge of the limitations of the measurements and of the data processing will ensure against misinterpretation. For example, the data processing procedures impose definite high and low frequency limits on the calculated spectrum curves, depending on the characteristics of the record. Secondly, the extent to which additional refinements in data processing might be justified for special research purposes can be assessed. Thirdly, a knowledge of the care with which the data processing has been carried out will enhance the confidence with which the information is used.

3.2 Digitizing method and digitizing noise

In the Institute of Engineering Mechanics (IEM)/China Seismological Bureau, analog accelerograms are digitized on a flat table of a semi-automatic digitizer. The table is $\sim 55 \text{ cm} \times 123 \text{ cm}$. The cross hairs are manually set to successive x, y coordinates on the record trace. The coordinates are converted to digital form by means of two separate potentiometers and are stored in a four-digit accumulator system from which they are readout to a four-digit Digitron-Displayer and a tape puncher. The maximum range along which the cross hairs can move on the table, is 72 cm in the x-direction and 30 cm in the y-direction. The finest resolution of this system is 100 digital counts per centimeter on the abscissa and 500 digital counts per centimeter on the ordinate.

The accelerograms are sampled in an unequal interval, which seems to give the best definition of the trace for a given sampling rate. All significant peaks and inflection points are picked, along with as many intermediate points as are needed for an accurate definition of shape. The average number of sampled points per second of record in the rapidly oscillating part are $\sim 70\text{-}80$.

If the record is too long to be digitized in one position, every two consecutive sections should include an overlapped part of $\sim 5 \text{ cm}$ in length. On each overlapped part, two cross straight lines should be drawn arbitrarily and then digitized along with digitizing of the acceleration traces, fixed traces and time marks on the same section. It means that these two drawn straight lines would be digitized twice and have two different sets of digital coordinates. Then, two sets of fitted straight lines (each set consists of two fitted lines) could be obtained for the two drawn lines by making the sum of the squares of the coordinate deviations from the assumed fitting line a minimum. By the coordinate converter, two sets of fitted lines could be translated and rotated to coincide with each other. Thus, by means of the same coordinate converter, the digital coordinates of acceleration trace, fixed lines and time marks on the following section are easily transformed into the coordinate system used in the previous section and then the

digital coordinates of traces, fixed lines and time marks on two consecutive sections are connected.

It has been shown that the digitizing error, consisting of systematic and random errors, is introduced to digitized results during digitization. Ten sets of digital results independently obtained from digitizing the same straight nylon line 0.2 mm in diameter by seven operators are shown in Fig. 3. The curve on the bottom of Fig. 3 which is obtained by averaging the ten digitizations, represents the systematic errors of the specified digitizing equipment. The difference $Y_i = Z_i - \bar{Z}$ between the average result and individual digitization represents the random digitizing noise.

Fig. 4 shows several typical random errors and Fig. 5 the standard histograms, constructed by the total random noise points of individual digitization, which approximate well the probability density distribution function. All the distribution functions are very close to the normal Gaussian distribution with zero mean, and variance equal to unity. The Fourier amplitude spectra of digitizing noise displacements (computed from twice integrating the random digitizing noise) are given in Fig. 6.

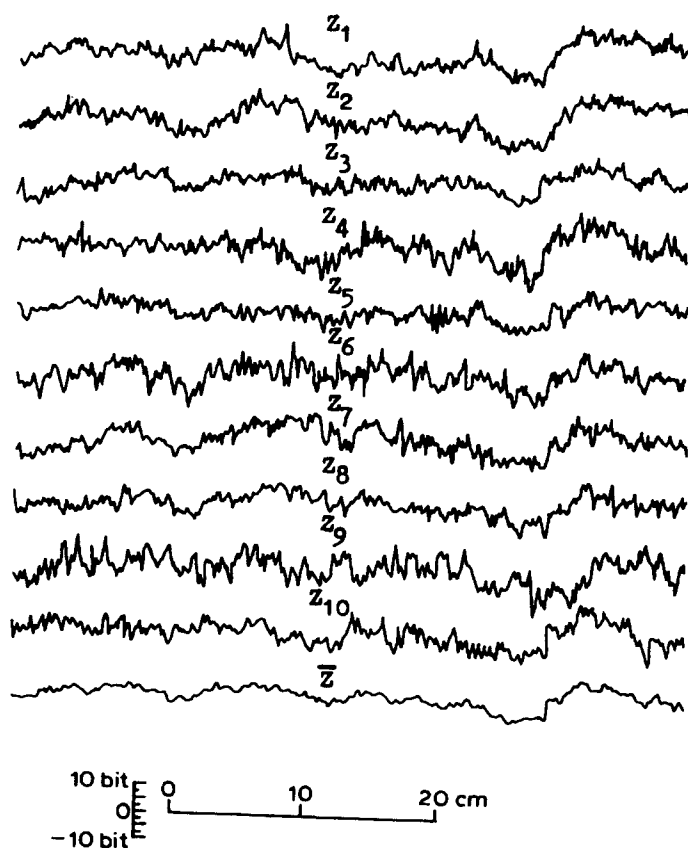


Fig. 3: Ten digital results independently obtained from digitizing a straight line and their average.

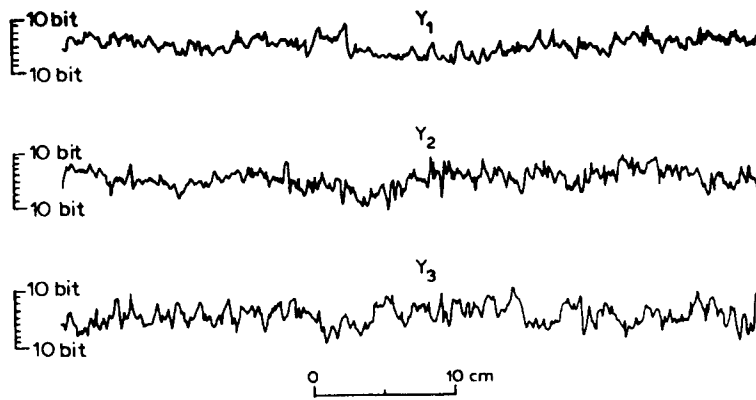


Fig. 4: Several typical random digitizing noise

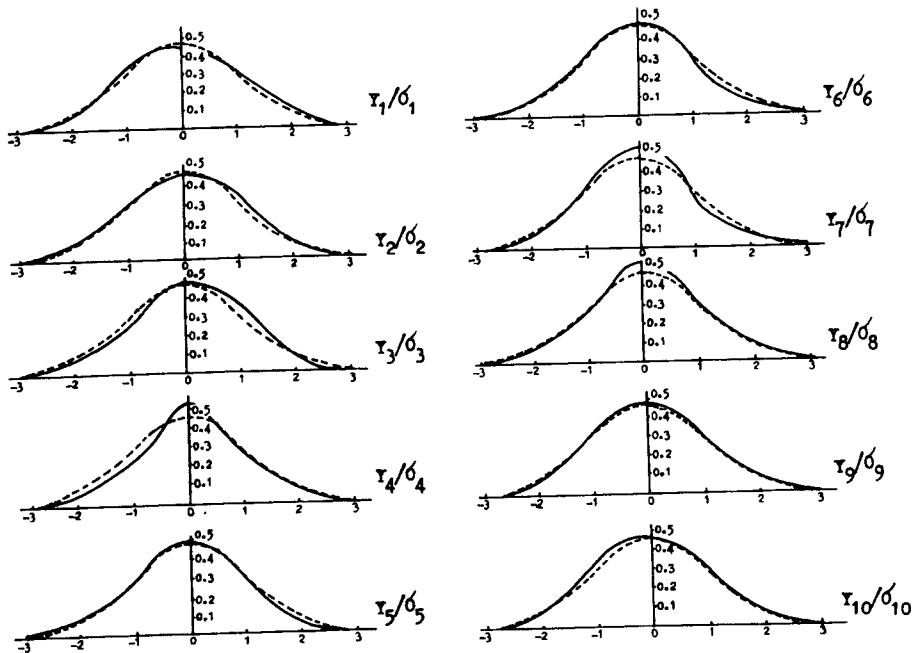


Fig. 5: Statistical distribution of random digitization noise.

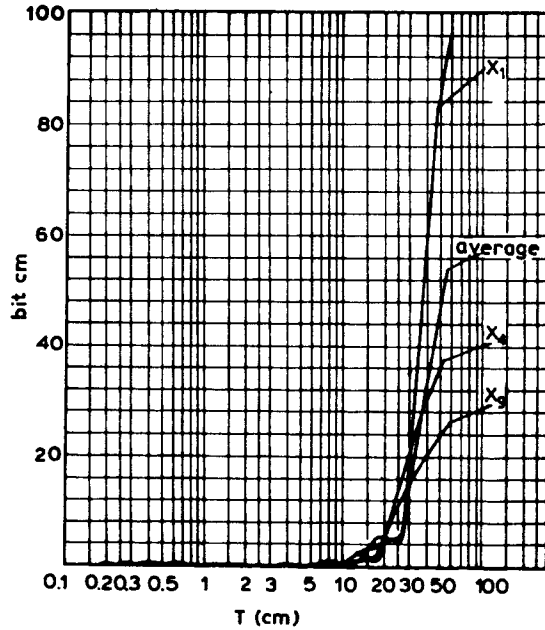


Fig. 6: Fourier amplitude spectra of digitizing noise displacement

From Figs. 3 to 6 the characteristics of digitizing noise can be summarized as follows:

- (1) the random noise due to manual digitization is an ergodic stationary random process with the amplitude of normal Gaussian distribution;
- (2) the standard deviation of digitizing noise is about 3 bits which corresponds to the real acceleration of $0.015/A$ (cm s^{-2}) with the instrument sensitivity of A (cm gal^{-1}) for the record; and
- (3) the energy of digitizing noise displacement is predominantly distributed at long periods. It has been found that at the period shorter than $25/V$ s. (V is the recording speed at which records are produced), the amplitude of digitizing noise displacement becomes so large that it may significantly distort the actual displacement record. Therefore, a cut-off frequency $f_{LC} \geq V/25$ Hz (or $T_{LC} \leq 25/V$ s) for high-pass filtering is suggested for the zeroline correction of the accelerograms. In such a case an equivalent maximum displacement error of $0.15/AV^2$ (cm s^{-2}) will be left in actual displacements. If a strict requirement is needed for a particular research, it would be possible to choose a higher cut-off frequency. Then an acceptable small displacement error could be expected. Table I lists the recommended cut-off frequencies f_r for high-pass filter and the appropriate values of possible displacement errors.

Table I Recommended cut-off frequencies and possible displacement errors

Recommended cut-off frequency f_r	(Hz)	$V/25$	$V/10$	$V/5$
Possible max. Displacement error	(cm)	$0.15/AV^2$	$0.045/AV^2$	$0.025/AV^2$

V-----recording speed, cm s^{-1} . A-----sensitivity of instrument, cm gal^{-1} .

4. INSTRUMENT RESPONSE CORRECTION

As mentioned above, the 12-channel accelerograph of model RDZ1 designed by IEM engineers and manufactured in Beijing Geological Instruments Factory are mostly used in the strong-motion instrument network in China.

The essential part of this kind of strong motion instrument is composed of 12 velocity-sensing pendulums separately coupled with 12 galvanometers through an attenuation circuit. The dynamic differential equation of motion of the pendulum-galvanometer system can be written as:

$$\ddot{\theta}(t) + 2n_1 D_1 \dot{\theta}(t) + n_1^2 \theta(t) = -\ddot{X}(t)/l_o + 2n_1 D_1 \sigma_1 \dot{\varphi}(t) \quad (1)$$

$$\ddot{\varphi}(t) + 2n_2 D_2 \dot{\varphi}(t) + n_2^2 \varphi(t) = 2n_2 D_2 \dot{\theta}(t) \quad (2)$$

This is a coupled dynamic differential equation of a system with two degrees of freedom. Equations (1) and (2) can be further combined together as a single fourth order differential equation with constant coefficients such as

$$\begin{aligned} & d^4 \varphi(t) / dt^4 + 2(n_1 D_1 + n_2 D_2) d^3 \varphi(t) / dt^3 \\ & + (n_1^2 + n_2^2 + 4n_1 n_2 D_2 D_1 (1 - \sigma^2)) d^2 \varphi(t) / dt^2 \\ & + 2n_1 n_2 (n_1 D_2 + n_2 D_1) d \varphi(t) / dt + n_1^2 n_2^2 \varphi(t) \\ & = -2D_2 n_2 \sigma_2 / l_o \cdot d^3 X(t) / dt^3 \end{aligned} \quad (3)$$

where, $\theta(t), \varphi(t)$ are the angular displacement of coils of pendulum and galvanometer, respectively; n_1, n_2 are the natural circular frequency of pendulum and galvanometer, respectively; D_1, D_2 are the critical damping ratio of pendulum and galvanometer, respectively; $d^3 X(t) / dt^3$ is the first derivative of measured acceleration with respect to time; l_o is the reduced pendulum; $\sigma^2 = \sigma_1 \cdot \sigma_2$ is coupling coefficient which is a dimensionless quantity used as a measure of the coupling relation between a pendulum and a galvanometer, where σ_2 is the coefficient reflecting the action of a pendulum-galvanometer and σ_1 is the coefficient reflecting the reaction of galvanometer-pendulum.

In fact, the recorded accelerograms are directly proportional to $\varphi(t)$, which is the response of the galvanometer of the coupling system under the action of input acceleration $\ddot{X}(t)$. The extent to which the response $\varphi(t)$ could be considered as the exact input acceleration depends on the parameters n_1, D_1, n_2, D_2 and σ^2 of the coupling system. In the case of RDZI system, a flat frequency response range is from 0.5 Hz to 30 Hz. But out of this range, the recorded accelerogram will be seriously distorted not only in the high frequency band but also in the low frequency band. In such a case, an instrument correction in both amplitudes and phases for recovering the exact input seismic motion from distorted accelerograms is necessary.

It is not straight forward to understand the relation between response $\varphi(t)$ and input acceleration $\ddot{X}(t)$ by solving eq. (3) or eqs. (1) and (2) directly. But for most pendulum-galvanometer accelerographs, coupling coefficient σ^2 are generally very small, so that it could be neglected. Thus the differential eq. 3 will take the form as:

$$\begin{aligned}
& d^4 \bar{\varphi}(t) / dt^4 + 2(n_1 D_1 + n_2 D_2) d^3 \bar{\varphi}(t) / dt^3 \\
& + (n_1^2 + n_2^2 + 4n_1 n_2 D_1 D_2) d^2 \bar{\varphi}(t) / dt^2 \\
& + 2n_1 n_2 (n_1 D_2 + n_2 D_1) d \bar{\varphi}(t) / dt + n_1^2 n_2^2 \bar{\varphi}(t) \\
& = -2D_2 n_2 \sigma_2 / l_o \cdot d^3 X(t) / dt^3
\end{aligned} \tag{4}$$

Or, it could be rewritten as an equivalent form

$$\ddot{\bar{\theta}}(t) + 2n_1 D_1 \dot{\bar{\theta}}(t) + n_1^2 \bar{\theta}(t) = -\ddot{X}(t) / l_o \tag{5}$$

$$\ddot{\bar{\varphi}}(t) + 2n_2 D_2 \dot{\bar{\varphi}}(t) + n_2^2 \bar{\varphi}(t) = 2n_2 D_2 \sigma_2 \dot{\bar{\theta}}(t) \tag{6}$$

where, the quantities $\bar{\theta}(t)$ and $\bar{\varphi}(t)$ denote the effects of neglecting σ^2 on responses $\bar{\theta}(t)$ and $\bar{\varphi}(t)$. Obviously, eqs. (5) and (6) are simplified to a decoupled second order differential equation set. It is expected that eqs. (5) and (6) could be used in instrument correction instead of eqs. (1) and (2) or eq. (3). But the important point is to verify the reasonableness of such substitution.

Let $\varepsilon(t)$ denote the errors coming from substitution of $\bar{\varphi}(t)$ for $\varphi(t)$, i.e.

$$\varepsilon(t) = \varphi(t) - \bar{\varphi}(t) \tag{7}$$

By subtracting eq. (4) from eq. (3) a differential equation on $\varepsilon(t)$ could be derived as

$$\begin{aligned}
& d^4 \varepsilon(t) / dt^4 + 2(n_1 D_1 + n_2 D_2) \cdot d^3 \varepsilon(t) / dt^3 \\
& + (n_1^2 + n_2^2 + 4n_1 n_2 D_1 D_2) d^2 \varepsilon(t) / dt^2 \\
& + 2n_1 n_2 (n_1 D_2 + n_2 D_1) d \varepsilon(t) / dt + n_1^2 n_2^2 \varepsilon(t) \\
& = 4D_1 D_2 n_1 n_2 \sigma^2 \ddot{\varphi}(t)
\end{aligned} \tag{8}$$

where n_1, D_1, n_2, D_2 and σ^2 are the instrument parameters as demonstrated above, and $\ddot{\varphi}(t)$ is the second derivative of the angular displacement response of the galvanometer, i.e., the second derivative of the distorted accelerograms recorded by accelerographs. It has been proved (Xie Lili et al., 1981) that under the assumption of zero initial conditions, the maximum error $|\sigma(t)|_{\max}$ could be evaluated as

$$|\varepsilon(t)|_{\max} \leq 8n_1 D_1 D_2 \sigma^2 \varphi_{\max} / n_2$$

and the relative error will be

$$|\varepsilon(t)|_{\max} / \varphi_{\max} \leq 8n_1 D_1 D_2 \sigma^2 / n_2$$

Where φ_{\max} is the maximum recorded acceleration.

For RDZ1 accelerographs, $D_1 = 6\sim 11$, $D_2 = 0.6$, $n_1 = 8\pi \text{ s}^{-1}$, $n_2 = 240\pi \text{ s}^{-1}$ and the value of coupling coefficient σ^2 depends on the resistance of attenuation circuit and the parameters of the pendulum-galvanometer system which usually varies between $10^{-3}\sim 10^{-5}$. Therefore the maximum relative error will be $\varepsilon_{\max} / \varphi_{\max} \leq 1.6 \times (10^{-3} \sim 10^{-5})$.

It could be concluded that the effect neglecting σ^2 on instrument response $\varphi(t)$ in eq. (3) is small enough to use eq. (4) or eqs. (5) and (6) as a substitution for eq.(3) or eqs. (1) and (2). In case the natural frequency of galvanometer, $f_2 = n_2 / 2\pi$ is much higher than that is significant in normal engineering practice, it is reasonable to convince that $\bar{\varphi}(t)$, the response of the galvanometer governed in eq. (6), is almost directly proportional to $\dot{\bar{\theta}}(t)$, in a rather wider frequency range starting from zero Hz, that means

$$\bar{\varphi}(t) = 2D_2\sigma_2\dot{\bar{\theta}}(t)/n_2 \quad (9)$$

would not bring any errors to the solution of eq.(6) and no correction is needed for $\bar{\varphi}(t)$ as a first derivative of $\bar{\theta}(t)$, the solution of eq. (5).

From the theory of seismometers and eq. (5), it is known that $\bar{\theta}(t)$, the response of pendulum is almost directly proportional to the measured acceleration $\ddot{X}(t)$ in a limited frequency range centered at the natural frequency of the pendulum, i.e., a relationship between $\dot{\bar{\theta}}(t)$ and $\dot{X}(t)$ in this given frequency range could be expressed as

$$\dot{\bar{\theta}}(t) = -\dot{X}(t) / 2n_1D_1l_0. \quad (10)$$

As an example, the velocity sensing pendulum of the Model RDZ1 accelerograph has $n_1 = 8\pi \text{ s}^{-1}$ and $D_1 = 6\sim 11$, thus, formula 10 is acceptable only in the frequency range from 0.5 Hz to 30 Hz, and will result in significant errors both at lower and higher frequencies beyond this range (cf. Fig.7). In this case, the instrument correction of the recorded accelerogram is important for retrieving the exact signal from a distorted record. For such correction the Imaginary Pendulum Method and the Differential-Integral Method are used.

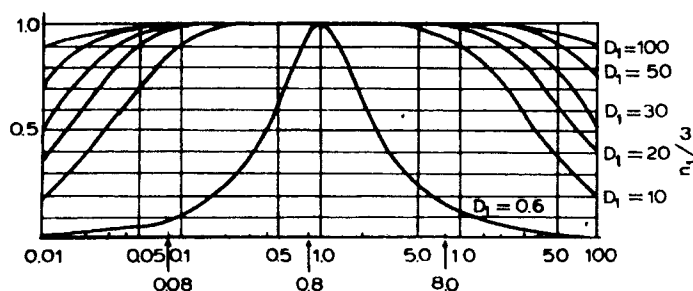


Fig. 7. The frequency response of the velocity sensing pendulum

4.1 Imaginary Pendulum Method

It is supposed that there exist an ideal velocity sensing pendulum which has an appropriate natural circular frequency Ω and a large enough damping ratio Z . Therefore, it will have a sufficiently wide frequency range with flat response to make formula (10) effective in a wide range from low to high frequencies. The response velocity of this imaginary pendulum, $\dot{\xi}(t)$, with respect to a real input acceleration $\ddot{X}(t)$, can be derived as follows:

$$\dot{\xi}(t) = \ddot{\theta}(t) + (n_1 D_1 - z\Omega) \cdot \zeta(t) / n_1 D_1 + (n_1^2 - \Omega^2) / 2n_1 D_1 \quad (11)$$

It shows that, the response velocity of an imaginary pendulum is composed of three parts: (1) a distorted accelerogram $\ddot{\theta}(t)$ recorded by the real pendulum (n_1, D_1); (2) the term including the response velocity $\dot{\zeta}(t)$ of imaginary pendulum (Ω, Z) with respect to the distorted accelerogram; and (3) the term including the response displacement $\zeta(t)$ of imaginary pendulum (Ω, Z) for the same distorted accelerogram.

The second term $\dot{\zeta}(t)$ will give a much larger correction to the high frequency signal than to the low one while this is opposite for the third term $\zeta(t)$. Also, if a lower (higher) Ω is selected, a more exact signal at lower (or higher) frequency will be retrieved.

4.2 Differential- Integral Method

The fundamental idea of this method could be described as follows: differentiate and integrate the distorted accelerogram $\ddot{\theta}(t)$ to get $\ddot{\theta}(t)$ and $\bar{\theta}(t)$. The corrected accelerogram could then be obtained by summing up all the three terms as indicated on the left side of eq. (5). Fig. 8 describes the flow-chart of these two methods.

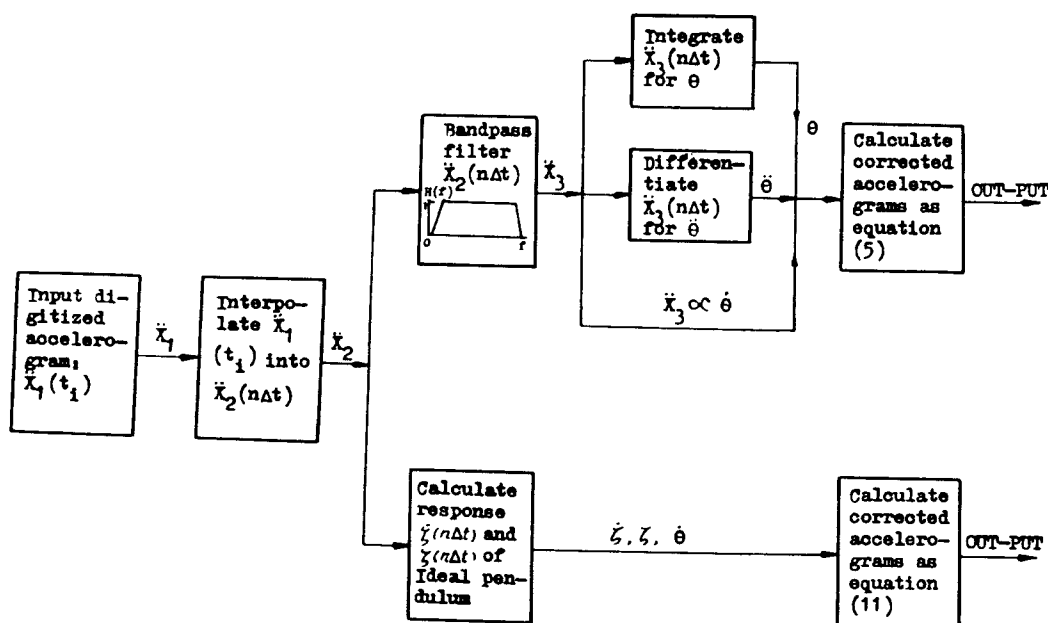


Fig. 8: Flow chart for the instrument distortion correction.

5. DETERMINATION OF THE CUT-OFF FREQUENCY FOR BAND-PASS FILTER

In the program of a data processing routine developed in the California Institute of Technology, the acceleration data should be low-pass filtered at the corner frequency of 25 Hz to reduce digitization noise, and are then corrected for the instrument response. Then, high-pass filtering is performed on acceleration, computed velocity and displacement, respectively, for base line correction and corrected records. But, in the routine processing procedure used in IEM the acceleration data should be high-pass filtered as well as low-pass filtered before the instrument correction of the accelerogram is executed. After instrument correction, high-pass filtering should still be performed on acceleration, computed velocity and displacement for baseline correction. Taking into account the transducer characteristics, recording speed at which records are produced, digitization noise and application of the records, different cut-off and terminated frequencies for low-pass and high-pass filters are selected.

5.1 Selection of cut-off frequency f_{LC} for low-pass filter

In the IEM routine procedure, a cut-off frequency of 35 Hz is selected for low-pass filters. This is based on the following reasons:

- (1) the acceleration instrument used in IEM has a flat response at high frequency up to 30 Hz and the response falls down ~20% at even 35 Hz;
- (2) equally spaced data with an interval of 0.01 s are prepared for instrument correction and the Nyquist frequency of 50 Hz is greater than the selected cut-off frequency; and
- (3) no significant noise exists in the high frequency up to 35 Hz.

Obviously, it is reasonable to set the cut-off frequency as 35 Hz for low-pass filter. This upper limit is also agreeable with the needs of earthquake engineering.

5.2 Selection of cut-off frequency f_{HC} for high-pass filter

It is a rather sophisticated problem to select the cut-off frequency of the high-pass filter for the base-line correction of the accelerograms, especially for those records with a short duration. Several effects mentioned below should be taken into consideration in selecting the cut-off frequency f_{HC} of the high-pass filter (Fig. 9):

(1) *Background of digitization for specified digitizer.* In general cases, the cut-off frequency f_{HC} for a high-pass filter could be taken from recommended values f_r given in Table I, based on the permitted maximum noise displacement.

(2) *Errors from uncertainties in the baseline of accelerograms.* This error originates mainly from the uncertainties in the parameters by which a baseline is defined. The baseline of a given accelerogram is usually determined by fitting the “closest: curve to the data by the least-squares method. In this case, for a given accelerogram, values of the baseline parameters strongly depend on the particular selection of digitized data points along the length of the record. It has been reported that the uncertainties of baseline parameters significantly affect the low-frequency components of the amplitude as well as phase spectra of displacements and the long period limits due to such errors can be expressed as

$$T_u = 2.69 + 0.194L \quad (12)$$

where T_u is the long period limit due to the error rising from the uncertainties in baseline parameters, L is the duration or the length of the record. This relation shows that the long period limit increases with the record length.

It is suggested that the bigger one of such two low frequency limits as f_r and f_u would be finally selected as the cut-off frequency for the high-pass filter, i.e. $f_{HC} = \max(f_r, f_u)$ where $f_u = 1/T_u$.

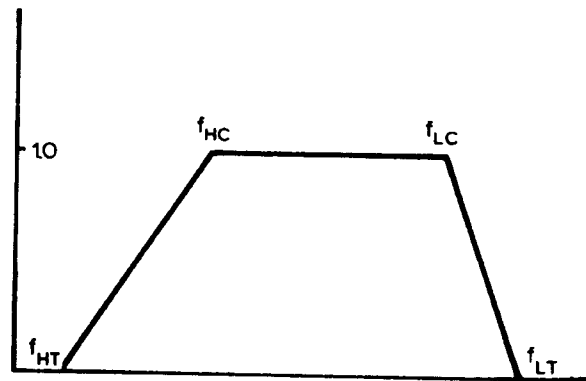


Figure 9. Selection of cut-off frequency for high-pass filter

5.3 Selection of the width of transition zone

According to the theory of Ormsby filter (Ormsby, J.F.A., 1961), a relation between the width Df of the transition zone and the error δ of the transfer function, when a finite number of weights are used, is given experimentally by

$$\delta = 0.012 / Df \cdot N \cdot \Delta t \quad (13)$$

where N is the number of weights on one side of symmetric filter, Δt is the time sampling interval for the record and the filter function.

For the low-pass filter, if an error δ of 1.2% is permitted and Δt is usually taken as 0.01 s, Df is then the reciprocal of N . Generally, $N = 50$ can assure economical computing time and $Df = 2$ Hz, i.e., a terminated frequency of $f_{HT} = 37$ Hz is adopted.

For the high-pass filter, the selection of the terminated frequency f_{HT} could be determined in the following two ways:

(1) if the duration of the record is very long, the value of f_{HC} and also the width Df of transition zone are very small. It could be known from eq. (13) that the value of N becomes very large and the consumption of computation time is then inevitable. For solving this

problem, a running mean filtering and the decimation of data are used before the high-pass filtering. This can extend the value of Df and improve computing-time economy. But it should be pointed out that the decimation will introduce the aliasing error into records unless the procedure of running-mean filter is performed successively on the velocity and the displacement as well as the acceleration before their decimation in the step to high-pass filter of the data; and

(2) for most accelerograms produced by near earthquakes, records are characterized by short duration. In such cases, a higher cut-off frequency f_{HC} is always required, and a larger value of the width of transition zone such as 0.3-0.6 Hz and a moderate N could then be selected. Thus, it may provide a possibility to eliminate all decimation in filtering and to ensure that no aliasing errors would be introduced to integrated displacements.

References

- Hudson, D.E. Reading and Interpreting Strong Motion Accelerograms, Earthquake Engineering Research Institute, 1979.
- Iwan, W.D. (Edited), U.S. Strong-Motion Earthquake Instrumentation, Proceedings of the U.S. National Workshop on Strong-Motion Earthquake Instrumentation, held at Santa Barbara, California, USA, April 12-14, 1981
- Ormsby, J.F.A., Design of numerical filters with application to missile data processing, Assoc. Comp. Machinery J., 8: 440-460.
- Panel on Strong-Motion Instrumentation/Committee on Earthquake Engineering, Recommendations for the Strong-Motion Program in the United States, National Academy Press, Washington, D.C. 1987.
- Xie, Li-Li, The Main Features of Data Processing Procedure for Strong-Motion Records in China, Physics of the Earth and Planetary Interiors, 38(1985), 134-143, Elsevier Science Publishers B.V., Amsterdam-Printed in The Netherlands.
- Xie, Li-Li, Li Shabai and Qian Jukang, Study on the Instrument Correction of Accelerograms Recorded by Accelerograph Coupled with Galvenometers, Journal of Earthquake Engineering and Engineering Vibration, 1: 106-116 (in Chinese). 1981.
- Xie, Li-Li, Peng Kezhong and Yu Shuangjiu, An Overview of Chinese Strong Motion Instrumentation and Data Processing Program, Earthquake Research in China, Vol.4, No.1, 1990.

UNDERSTANDING AND SETTING STA/LTA TRIGGER ALGORITHM AND ASSOCIATED PARAMETERS

Amadej Trnkoczy

Kinematics SA, Z.I. Le Trési 3, CH-1028 Prévèrenge, Switzerland,
E-mail: amadej.trnkoczy@quantum.si

1. INTRODUCTION

By introducing the digital seismic data acquisition, long term continuous recording and archiving of seismic signals became a demanding technical problem. A seismic network or even a single seismic station operating continuously at high sampling frequency produce an enormous amount of data, which is often difficult to store (and analyze) locally or even at the recording center of a network. This situation forced seismologists to invent triggered seismic data acquisition. In a triggered mode a seismic station or a seismic network still process all incoming seismic signals in real time (or in near-real-time) but incoming data is not stored continuously and permanently. Processing software - a trigger algorithm - serves for the detection of typical seismic signals (earthquakes, controlled source seismic signals, underground nuclear explosion signals, etc.) in the constantly present seismic noise signal. Once an assumed seismic event is detected, recording and storing of all incoming signals starts. It stops after trigger algorithm 'declares' the end of the seismic signal.

Automatic trigger algorithms are relatively ineffective when compared to a seismologist's pattern recognition ability during reading of seismograms, which is based on years of experience and on the enormous capability of human brain. There are few exceptions, where the most complex detectors, mostly dedicated to a given type of seismic signals, approach to human ability. In all practical cases automatic trigger algorithms are losing some data on one side and generate falsely triggered records, which are not seismic signals, on the other. Small amplitude seismic signals are often not resolved from seismic noise and are therefore lost for ever, and, if the trigger algorithm is set sensitive, false triggers are recorded due to irregularities and occasionally excessive amplitude of seismic noise. False triggers burden off-line data analysis later and unnecessarily occupy data memory of seismic recording system. As a result, any triggered mode data acquisition impairs the completeness of the recorded seismic data and produce some additional work to clean-out false records.

Several trigger algorithms are presently known and used - from a very simple amplitude threshold type to the sophisticated pattern recognition, adaptive methods, and neural network based approaches. They are based on the amplitude, the envelope, or the power of the signal(s) in time domain, or on the frequency or sequency domain content of seismic signal. Among the more sophisticated ones. Allan's (1978; 1982) and Murdock and Hutt's (1983) trigger algorithms are probably the most commonly known. Many of these algorithms function in association with the seismic phase time picking task. Seismic array detection algorithms fall into a special extensive field of research, which will not be discussed here. For more advanced algorithms see e.g. Joswig (1990; 1993; 1995). However, in practice, only

relatively simple trigger algorithms have been really broadly accepted. and can be found in seismic data recorders in the market and in most network's real time processing packages.

The simplest trigger algorithm is the amplitude threshold trigger. It simply detects any amplitude of seismic signal exceeding a pre-set threshold. The recording starts whenever this threshold is reached. This algorithm is rarely used in weak-motion seismology but it is a standard in strong motion seismic instruments, that is in the systems where high sensitivity is mostly not an issue, and where consequently man-made and natural seismic noise amplitudes are much smaller than the signals which are supposed to trigger the instrument.

The root-mean-square (RMS) threshold trigger is similar to the amplitude threshold algorithm, except that the RMS values of the amplitude in a short time window are used instead of 'instant' signal amplitude. It is less sensitive to spike-like man-made seismic noise, however it is rarely used in practice.

Today, the 'short-time-average through long-time-average trigger' (STA/LTA) is the most broadly used algorithm in weak-motion seismology. It continuously calculates the average values of the absolute amplitude of seismic signal in two consecutive moving-time windows. The short time window (STA) is sensitive to seismic events while the long time window (LTA) provides information about the temporal amplitude of seismic noise at the site. When the ratio of both exceeds a pre-set value, an event is 'declared' and data starts being recorded in a file.

Several more sophisticated trigger algorithms are known from literature (e.g. Joswig 1990; 1993; 1995) but they are rarely used in the seismic data loggers currently in the market . Only some of them are employed in the network's real time software packages available. When in the hands of an expert, they can improve the events/false-triggers ratio significantly, particularly for a given type of seismic events. However, the sophisticated adjustments of operational parameters to actual signals and seismic noise conditions at each seismic site that these triggers require, has proven unwieldy and subject to error in practice. This is probably the main reason why the STA/LTA trigger algorithm still remains the most popular.

Successful capturing of seismic events depends on proper settings of the trigger parameters. To help with this task, this document explains the STA/LTA trigger functioning and gives general instructions on selecting its parameters. Technical instructions on setting the trigger parameters depend on particular hardware and software and are not given here. Refer to the corresponding manuals for details.

2. PURPOSE

The short-time-average/long-time-average STA/LTA trigger is usually used in weak-motion applications that try to record as many seismic events as possible. These are the applications where the STA/LTA algorithm is most useful. It is nearly a standard trigger algorithm in portable seismic recorders, as well as in many real time processing software packages of the weak-motion seismic networks. However, it may also be useful in many strong motion applications, except when the interest is limited to the strongest earthquakes.

The (STA/LTA) trigger significantly improves the recording of weak earthquakes in comparison with amplitude threshold trigger algorithms. At the same time it decreases the number of false records triggered by natural and man-made seismic noise. To some extent it also allows the discrimination among different types of earthquakes.

The STA/LTA trigger parameter settings are always a tradeoff among several seismological and instrumental considerations. The goal of searching for optimal parameter settings is the highest possible seismic station sensitivity for a given type of seismic signals (which includes 'all earthquakes' target as well) at a still tolerable number of false triggers.

The STA/LTA trigger is most beneficial at seismically quiet sites where natural seismic noise (marine noise) is the dominant type of seismic noise. It is also effective in case of changes of 'continuous' man-made seismic noise. Such changes, for example, occur due to day/night variation of human activity close to or in urban areas. The STA/LTA algorithm is less effective in the presence of irregular, high amplitude man-made seismic noise which is often of burst and/or spike type.

3. HOW IT WORKS - BASICS

The STA/LTA algorithm continuously keeps track of the always-present changes in the seismic noise amplitude at the station site and automatically adjusts the seismic station's sensitivity to the actual seismic noise level. As a result, a significantly higher sensitivity of the system during seismically quiet periods is achieved and excessive number of falsely triggered records is prevented, or at least mitigated, during seismically noisy periods. Calculations are repeatedly performed in real time. This process is usually taking place independently in all seismic channels of a seismic recorder or of a seismic network.

The STA/LTA algorithm processes filtered seismic signals (more in the section 5.1 'Selection of trigger filters') in two moving time windows – a short-time average window (STA) and a long-time average window (LTA). The STA measures the 'instant' amplitude of the seismic signal and is watching for earthquakes. The LTA takes care of the current average seismic noise amplitude.

First, the absolute amplitude of each data sample of incoming signal is calculated. Next, the average of absolute amplitudes in both windows is calculated. In a further step a ratio of both values — STA/LTA ratio—is calculated. This ratio is continuously compared to a user selected threshold value - STA/LTA trigger threshold level. If the ratio exceeds this threshold, a channel trigger is declared. A channel trigger does not necessarily mean that a multi-channel data logger or a network actually starts to record seismic signals. All seismic networks and most seismic recorders have a 'trigger voting' mechanism built in that defines how many and which channels have to be in a triggered state before the instrument or the network actually starts to record data (more in the section 5.4 'Selection of voting scheme parameters'). To simplify the explanation, we shall, for the moment, observe only one signal channel. We will assume that a channel trigger is equivalent to a network or a recorder trigger.

After the seismic signal gradually terminates, the channel detriggers. This happens when the current STA/LTA ratio falls below another user selectable parameter - STA/LTA detrigger threshold level. Obviously, the STA/LTA detrigger threshold level should be lower (or rarely equal) than the STA/LTA trigger threshold level.

In addition to the data acquired during the 'trigger active' time, seismic networks and seismic recorders add a certain amount of seismic data to the event file before triggering – pre-event-

time (PEM) data. After the trigger active state terminates, they also add post-event-time (PET) data.

For better understanding, Fig. 1 shows a typical local event and the trigger variables (simplified) during STA/LTA triggering. Graph a) shows an incoming continuous seismic signal (filtered). Graph b) shows an averaged absolute signal in the STA and LTA windows respectively as they move in time toward the right side of the graph and graph c) shows the ratio of both. In addition, the trigger active state (solid line rectangle), the post-event time (PET), and the pre-event time (PEM) (dotted line rectangles) are shown. In this example, the trigger threshold level parameter was set to 10 and detriger threshold level to 2 (two short horizontal dotted lines). One can see that the trigger became active when the STA/LTA ratio value exceeded 10. It was deactivated when the STA/LTA ratio value fell below 2. At the bottom on graph d) the actually recorded data file is shown. It includes all event phases of significance and a portion of the seismic noise at the beginning.

In reality, the STA/LTA triggers are usually slightly more complicated. However the details are not essential for the understanding and proper setting of trigger parameters.

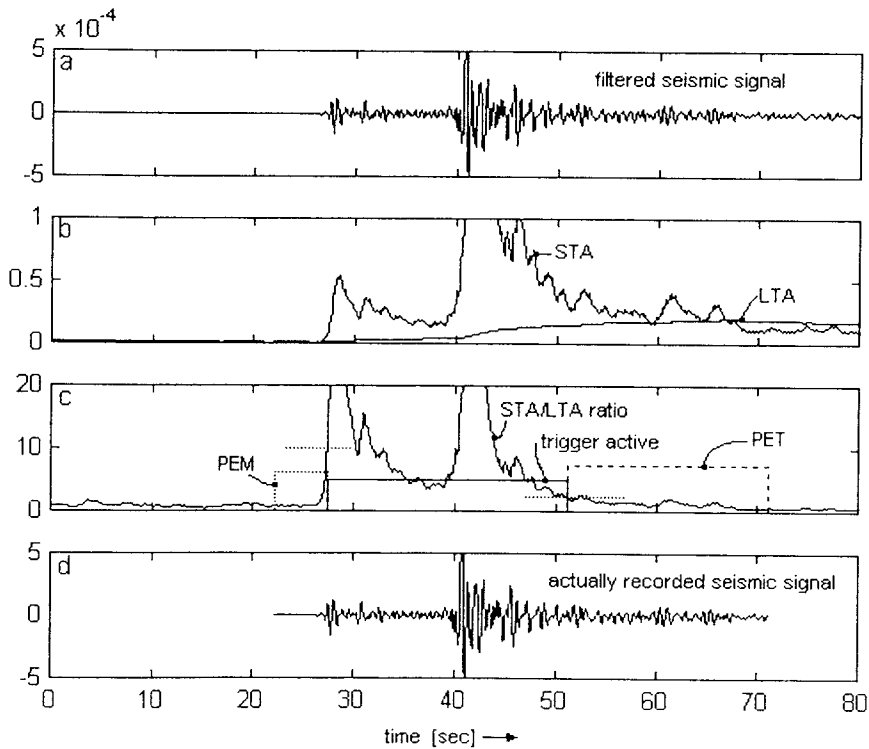


Fig. 1: Function and variables of STA/LTA trigger calculations.

4. HOW TO ADJUST STA/LTA TRIGGER PARAMETERS

To set the basic STA/LTA trigger algorithm parameters one has to select the following:

- STA window duration
- LTA window duration
- STA/LTA trigger threshold level
- STA/LTA dettrigger threshold level.

However, optimal triggering of a seismic recorder or a seismic network does not depend only on these parameters. There are usually four additional associated parameters which, only if well tuned with the trigger parameters, guarantee optimal data recording. These parameters are:

- trigger filters
- pre-event time (PEM)
- post-event time (PET)
- trigger voting scheme.

Although not directly related to the STA/LTA trigger algorithm, these additional parameters are also discussed in this document in order to provide a complete information.

The STA/LTA trigger parameter and associated parameters settings depend on the goal of the application, on the seismic noise condition at the site, on the properties of seismic signals at a given location, and on the type of sensor used. All these issues vary broadly among applications and among seismic sites. Obviously, there is no general, single rule on setting them. Each application and every seismic site requires some study, since only practical experiences enable the determination of really optimal trigger settings.

Note that seismic recorders and network software packages come with a set of default (factory set) trigger and trigger associated parameter values. They are rarely optimal and must therefore be adjusted to become efficient in a particular application. For best results, changing these parameters and gradually finding the best settings is a process which requires a certain amount of efforts and time.

4.1 Selection of short time average window (STA) duration

Short time average window measures the 'instant' value of a seismic signal or its envelope. Generally, STA duration must be longer than a few periods of typically expected seismic signal. If the STA is too short, the averaging of the seismic signal will not function properly. The STA is no longer a measure of the average signal (signal envelope) but becomes influenced by individual periods of the seismic signal. On the other hand, STA duration must be shorter than the shortest events we expect to capture.

To some extent the STA functions as a signal filter. The shorter the duration selected, the higher the trigger's sensitivity to short lasting local earthquakes compared to long lasting and lower frequency distant earthquakes. The longer the STA duration selected, the less sensitive it is for short local earthquakes. Therefore, by changing the STA duration one can, to some extent, prioritize capturing of distant or local events.

The STA duration is also important with respect to false triggers. By decreasing the duration of the STA window, triggering gets more sensitive to spike-type of man-made seismic noise, and vice versa. Although such noise is usually of instrumental nature, it can also be seismic. At the sites highly polluted with spike-type noise, one will be frequently forced to make the STA duration significantly longer than these spikes, if false triggers are too numerous. Unfortunately, this will also decrease the sensitivity of the recording to very local events of short duration. Fig. 2 explains the effect of STA duration on local events and spike-type noise.

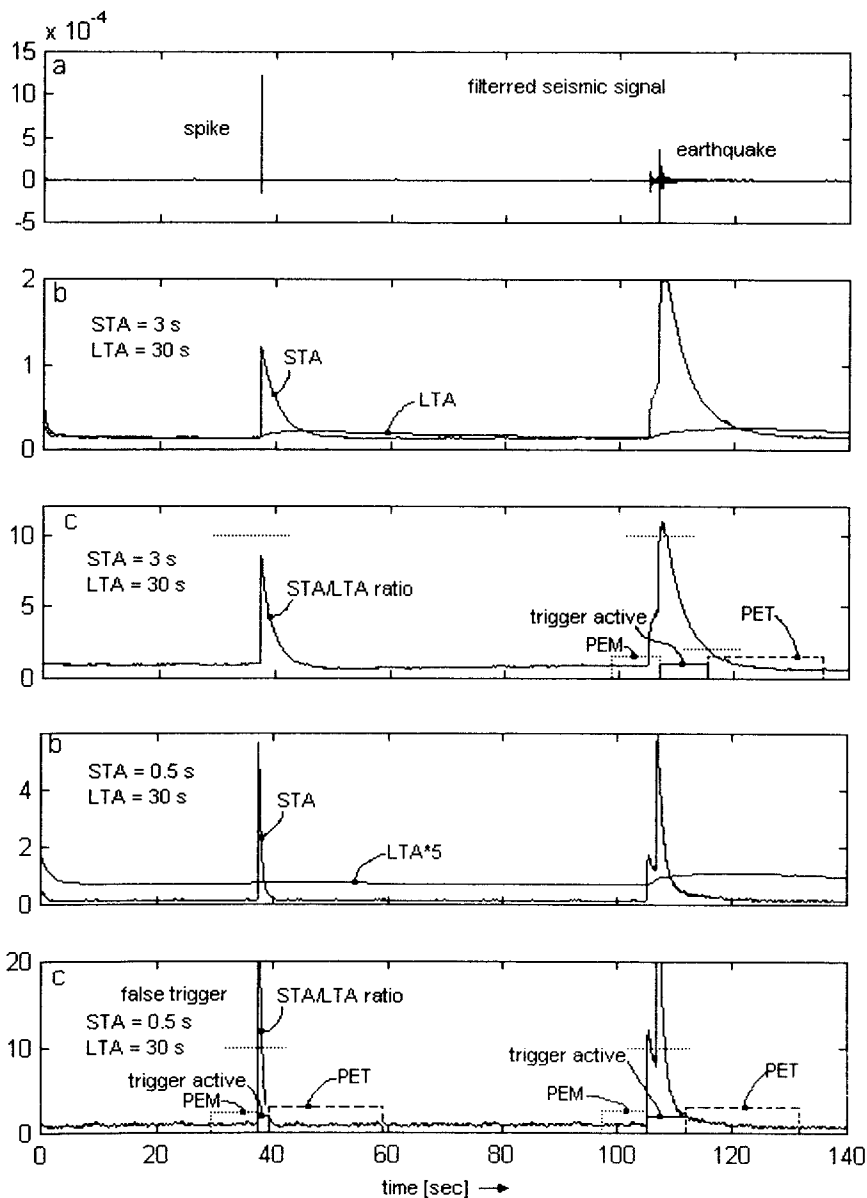


Fig. 2: Influence of STA duration on trigger sensitivity to short local events and 'spiky' and 'spiky' noise in seismic signals.

On graph a) a signal with an instrumental spike on the left and with a short, very local earthquake on the right side is shown. Graphs b) and c) show STA, LTA, STA/LTA ratio, and trigger active states along with PEM and PET. The STA/LTA trigger threshold was set to 10 and dettrigger threshold to 2. One can see that when using a relatively long STA of 3 sec, the earthquake did trigger the system, but only barely. However, a much bigger amplitude (but shorter) instrumental spike did not trigger it. The STA/LTA ratio did not exceed the STA/LTA threshold and there was no falsely triggered record due to the spike. The lower two graphs show the same variables but for a shorter STA of 0.5 sec. The spike clearly triggered the system and caused a false record. Of course, the earthquake triggered the system as well.

For regional events, a typical value of STA duration is between 1 and 2 sec. For local earthquakes shorter values around 0.5 to 0.3 s are commonly used in practice.

4.2 Selection of long-time average window (LTA) duration

The LTA window measures average amplitude seismic noise. It should last longer than a few 'periods' of typically irregular seismic noise fluctuations. By changing the LTA window duration, one can make the recording more or less sensitive to regional events in the 'Pn'-wave range from about 200 to 1500 km epicentral distance. These events typically have the low-amplitude emergent Pn- waves as the first onset. A short LTA duration allows that the LTA value more or less adjusts to the slowly increasing amplitude of emergent seismic waves. Thus the STA/LTA ratio remains low in spite of increasing STA (nominator and denominator of the ratio increase). This effectively diminishes trigger sensitivity to such events. In the opposite case, using a long LTA window duration, trigger sensitivity to the emergent earthquakes is increased because the LTA value is not so rapidly influenced by the emergent seismic signal, allowing Sg/Lg waves to trigger the recording.

Fig. 3 explains the described situation. In graph a) an event with emergent P waves is shown. Graphs b) and c) show the time course of trigger parameters for a relatively long LTA of 60 sec. The LTA does not change fast, allowing the STA/LTA ratio to exceed the STA/LTA trigger threshold (short horizontal dotted line) and a normal record results. Graphs d) and e) show the same situation with a shorter LTA of 30 s. The LTA value increases much faster during the initial phase of the event, thus decreasing the STA/LTA ratio value which does not exceed the STA/LTA trigger threshold. No triggering occurs and the event is missed forever.

Similarly, efficient triggering of recording of events with weak P waves compared to S waves requires a longer LTA for two reasons. First, if P waves do not trigger, they 'contaminate' true information about seismic noise prior to the event measured by LTA, since their amplitude exceeds the amplitude of seismic noise before the event. This results in diminished trigger sensitivity at the moment when S waves arrive. This 'contamination' is decreased if a longer LTA duration is selected. Second, longer LTA makes the trigger more sensitive to P waves as well, if they are not strictly of impact type.

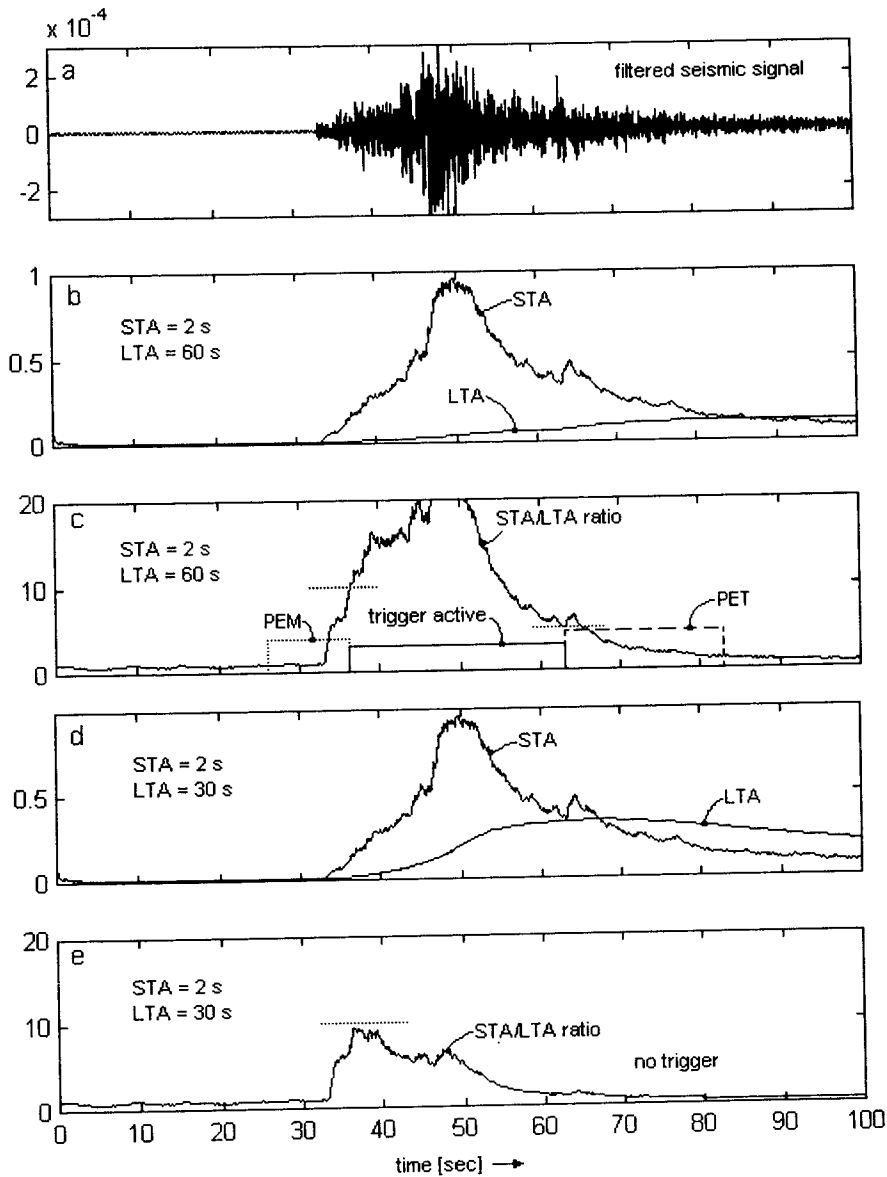


Fig. 3: Influence of LTA duration on trigger algorithm sensitivity to earthquakes with emergent seismic signals.

Fig. 4 represents such a case. Graph a) shows a typical event with significantly bigger later phase waves than P waves. Graphs b) and c) show trigger parameters for a long LTA of 100 s. P wave packet as well as S wave packet trigger the recorder. Appropriate PEM and PET assure that the event is recorded as a whole in a single file with all its phases and a portion of seismic noise before them. Graphs d) and e) show the same situation but for a shorter LTA of 45 sec. One can see that the P waves did not trigger at all, while the S waves barely triggered. The STA/LTA ratio hardly exceeds the STA/LTA trigger threshold. As the result, the recorded data file is much too short. P waves and information about seismic noise before them are missing in this record. A slightly smaller event would not trigger at all.

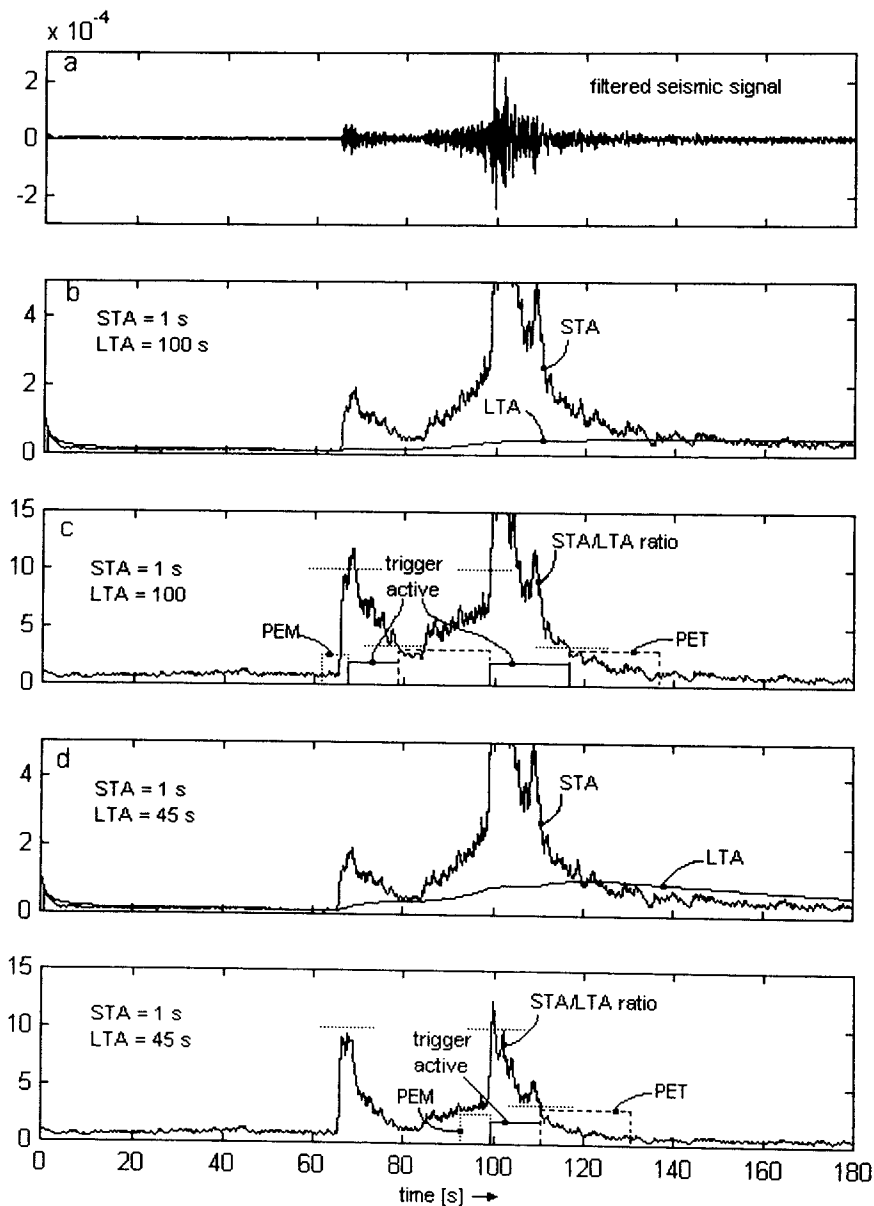


Fig. 4: Influence of LTA duration on trigger algorithm sensitivity to earthquakes containing weak P waves.

On the other hand, a short LTA will successfully accommodate recorder sensitivity to gradual changes of 'continuous' man-made seismic noise. Such 'transition' of man-made seismic noise from low to high is typical for night-to-day transition of human activity in urban areas. Sometimes, using a short LTA can mitigate false triggers due to traffic. Examples of such cases could be a single heavy vehicle approaching and passing close to the seismic station on a local road, or trains on a nearby railway. A short LTA can 'accommodate' itself fast enough to such emerging disturbances and prevent false triggers.

Fig. 5 shows an example of the LTA response on increased seismic noise. Graph a) shows seismic noise, which gradually increased in the middle of the record. Note that the change of

its amplitude is not sudden but lasts about 20 to 30 sec. Graphs b) and c) show the situation at a short LTA of 30 sec. One can see that the LTA value more or less keeps track of the increased noise amplitude. The STA/LTA ratio remains well below the STA/LTA trigger threshold and there is no false trigger in spite of significantly increased seismic noise at the site. Graphs d) and e) show the situation with a longer LTA of 60 s. In this case, the LTA does not change so rapidly, allowing a higher STA/LTA ratio during noise increase. As the result, a false trigger occurs and a false record unnecessarily occupying data memory is generated.

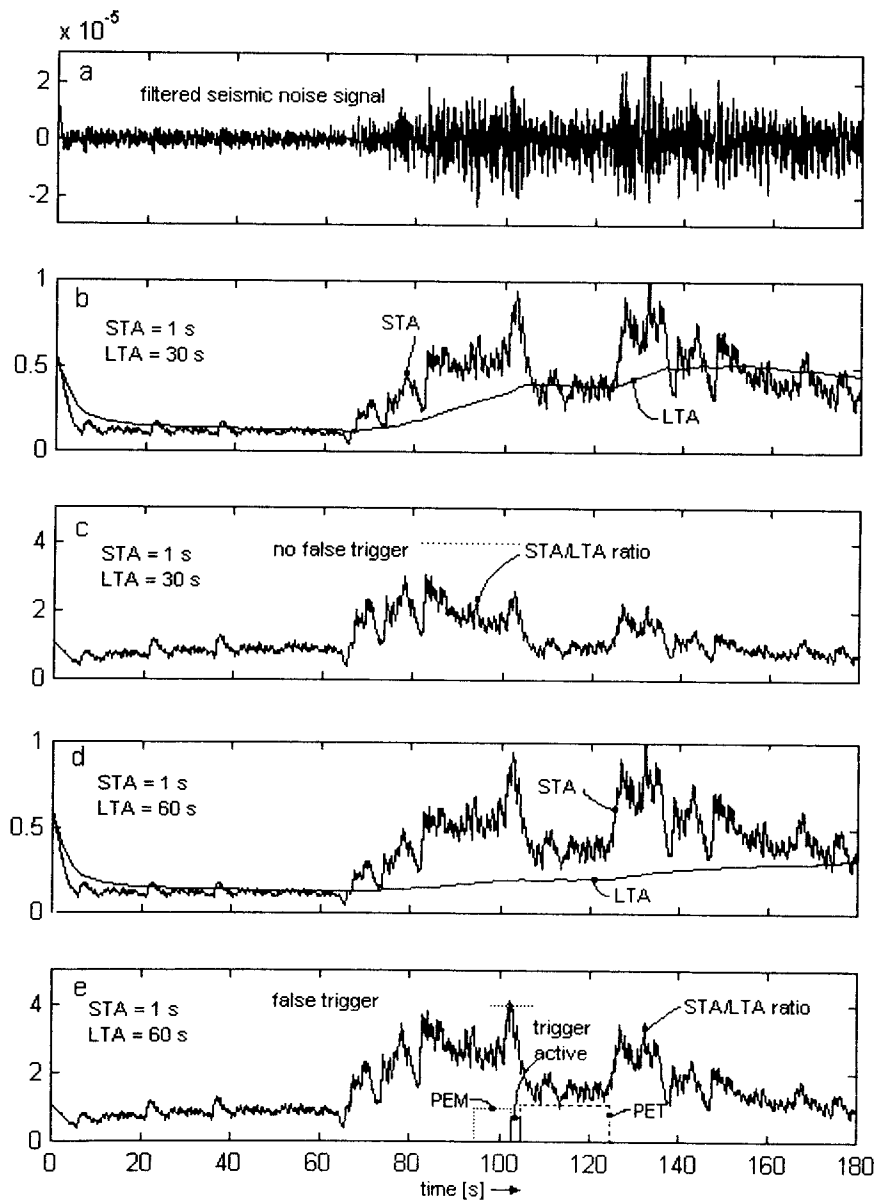


Fig. 5: Influence of LTA duration on false triggering when seismic noise conditions change.

Natural seismic noise (marine noise) can change its amplitude by a factor exceeding the value of twenty. However, these changes are slow. Significant changes can occur only during a few hours period, or at worst, in several tens of minutes. Therefore even the longest LTA duration is short enough to allow LTA to accommodate completely to marine noise amplitude variations.

The LTA duration of 60 seconds is a common initial value. A shorter LTA duration is needed to exclude emergent regional events from triggering, if desired, or if quickly changing man-made noise is typical for the site. A longer LTA can be used for distant regional events with very long S-P times and potentially emergent P waves.

4.3 Frozen versus continuously updated LTA during events

Calculations of the LTA value during an event, that is after a channel trigger is declared, can be performed in the first approximation in two different ways.

Either the LTA value is continuously updated and calculated during the event as usual, or the LTA value is kept frozen at the moment when channel trigger is declared. In this case the LTA is not allowed to change (increase) during an event at all. Most of seismic recorders available in the market have both frozen or continuously updated LTA user selectable options. However, each approach has its good and bad points.

The 'frozen' LTA window (the word 'clamped' is also used in literature) can force the unit into a permanently triggered state in case of a sudden increase of man-made seismic noise at the site. The situation is illustrated in Fig.6.

Graph a) shows an earthquake during which seismic noise increases and remains high even after the termination of the event. Such situation can, for example, happen if a machinery is switched on in the vicinity of the recorder. In such case a completely frozen LTA (graph b) would never again allow the STA/LTA ratio to fall below the STA/LTA detrigger threshold level (graph c) and a continuous record would result. The result is that the seismic recorder's memory soon gets full and blocks further data recording.

A continuously updated LTA (the word 'unclamped' is also used in literature), on the other hand, frequently terminates records too early. Graphs d) and e) of Fig. 6 explain this situation. Very often records with truncated coda waves result because the LTA increases rapidly if the beginning portion of large earthquake signal is included in its calculation. Thus the STA/LTA ratio decreases too rapidly and terminates recording prematurely. Coda waves of the event on Fig. 6 are lost. This undesired result could be much more distracting for lasting regional events as it is shown in the Fig. 6.

Some seismic recorders work with a special calculation of LTA. The LTA value is, to the first approximation, 'frozen' after a trigger. However, this 'freezing' is not made complete. Some 'bleeding' of event signal into the LTA calculation is allowed. Such algorithm tries to solve both problems. It does not cause endlessly triggered records in case of a rapid permanent increase of seismic noise and, at the same time, it does not cut coda waves too early.

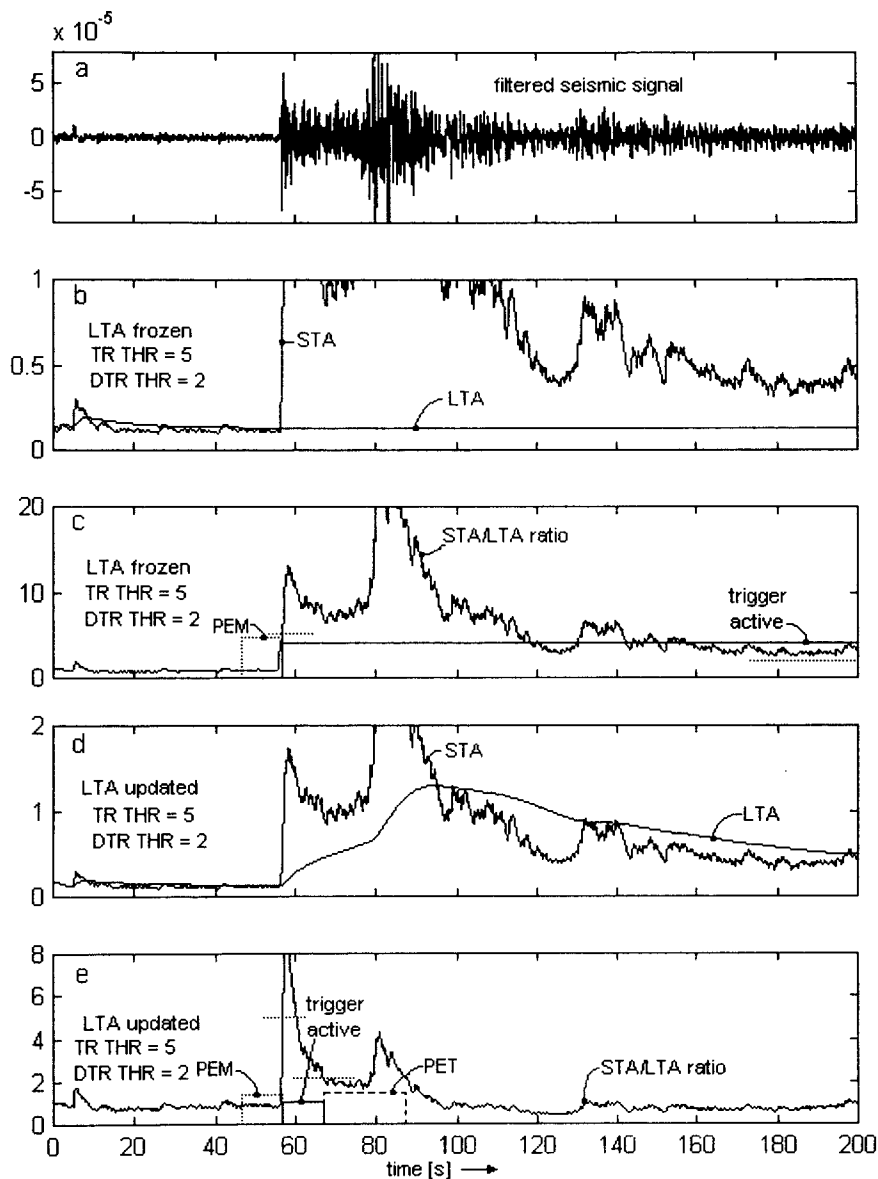


Fig. 6: Potential problems with two conventional ways of calculating the LTA: an endless record with a completely frozen LTA and cut coda waves with updated LTA calculations.

4.4 Selection of STA/LTA trigger threshold level

The STA/LTA trigger threshold level to the greatest extent determines which events will be recorded and which not. The higher value one sets, the more earthquakes will not be recorded, but the fewer false-triggers will result. The lower the STA/LTA trigger threshold level is selected, the more sensitive the seismic station will be and the more events will be recorded. However, also more frequent false triggers will occupy data memory and burden the analyst. Optimal STA/LTA trigger threshold level depends on seismic noise conditions at the site and

on one's tolerance to falsely triggered records. Not only the amplitude but also the type of seismic noise influence optimal STA/LTA trigger threshold level setting. A statistically stationary seismic noise (with less irregular fluctuations) allows lower STA/LTA trigger threshold level, completely irregular behavior of seismic noise demands higher values.

Note that some false triggers and some missed earthquakes are an inevitable reality whenever recording seismic signals in an event-triggered mode. Only a continuous seismic recording, if affordable, completely solves the problem of false triggers and incompleteness of seismic data.

It is a dangerous trap to select a very high STA/LTA trigger threshold level and a high channel gain simultaneously. Many recorders in the market allow this setting without any warning messages. This situation is particularly dangerous in extremely noisy environments, where, due to too many false triggers, the instruments are usually set to record only the strongest events.

Suppose one has set the STA/LTA trigger threshold level to 20. Suppose also that one has set the gain of the channel in such a way that he has about 150 mV of average seismic noise signal at the input of the recorder and that the input full scale voltage of the channel is ± 2.5 V. Obviously, this setting would require a $0.15 \text{ V} \times 20 = 3 \text{ V}$ signal amplitude to trigger the channel. Since its maximum input amplitude is limited to 2.5 V, it can never trigger, no matter how strong an earthquake occurs. Note that this error is not so obvious, especially in low seismicity regions with rare events. One can operate an instrument for very long time without records and forever wait for his first recorded earthquake.

With certain products in the market, this potential danger of erroneously setting is solved in the following way: Whenever one uses the STA/LTA algorithm, an additional threshold trigger algorithm remains active in the 'background'. Because of it the channel triggers whenever its input amplitude exceeds 50% of channel input voltage range for example, in no relation to the STA/LTA trigger setting. In this way the strongest, and therefore the most important events are still recorded, no matter how carelessly the STA/LTA trigger algorithm parameters are set.

An initial setting for the STA/LTA trigger threshold level of 4 is common for an average quiet seismic site. Much lower values can only be used at the very best station sites with no man-made seismic noise. Higher values about 8 and above are required at less favorable sites with significant man-made seismic noise. In strong-motion applications higher values are more common due to the usually noisier seismic environments and generally smaller interest in weak events.

4.5 Selection of STA/LTA detrigger threshold level

The STA/LTA detrigger threshold level determines the termination of data recording (along with the PET parameter - more information about it in the section 5.3 'Selection of post-event time (PET) parameter').

The STA/LTA detrigger threshold level determines how well the coda waves of recorded earthquakes will be captured in data records. To include as much coda waves as possible, a

low value is required. If one uses coda duration for magnitude determinations, such setting is obvious. However, a too low STA/LTA dettrigger threshold level is occasionally dangerous. It may cause very long or even endless records, for example, if a sudden increase in seismic noise does not allow that the STA/LTA ratio falls below the STA/LTA dettrigger threshold level. On the other hand, if one is not interested in coda waves a higher value of STA/LTA dettrigger threshold level enables significant savings in data memory and/or data transmission time. Note that coda waves of distant earthquakes can be very long.

In general, the noisier the seismic site, the higher the value of the STA/LTA dettrigger threshold level should be used to prevent too long or continuous records. This danger is high only at sites heavily polluted by man-made seismic noise.

A typical initial value of the STA/LTA dettrigger threshold level is 2 to 3 for seismically quiet sites and weak motion applications. For noisier sites higher values must be set. For strong-motion applications, where coda waves are not of the highest importance, higher values are frequently used.

5. HOW TO ADJUST ASSOCIATED PARAMETERS FOR PROPER TRIGGERING AND DATA RECORDING

5.1 Selection of trigger filters

Nearly all seismic recorders and networks have adjustable band-pass trigger filters. They continuously filter the incoming seismic signals prior to the trigger algorithm calculations. Selection of these filters is important for a proper functioning of the STA/LTA trigger algorithm (as well as for amplitude threshold trigger algorithm). The purpose of these filters is three-fold:

- They remove DC component from incoming seismic signals. Namely, all active seismic sensors have some DC offset voltage at the output. This DC offset, if too high, deteriorates the STA/LTA ratio calculation. The calculation of the absolute value of the signal becomes meaningless if the DC component is higher than the seismic noise amplitude. This results in malfunction of the STA/LTA trigger algorithm and drastic reduction of trigger sensitivity for weak seismic events.
- Their frequency band-pass can prioritize frequencies corresponding to the dominant frequencies of seismic events one wants to record.
- Their stop-band can attenuate dominant frequencies of the most distracting seismic noise at a given site.

The trigger filter pass-band should generally accommodate the frequencies of the maximum energy of expected seismic events. It should, at the same time, have a band-pass that does not coincide with peak frequency components of typical seismic noise at the site. If this is possible, a significant improvement of the event-trigger/false-trigger ratio results. Obviously, one can understand that if the peak amplitudes of seismic noise and the dominant frequencies of the events of most interest coincide, the trigger filter becomes inefficient.

One should not forget that the frequency response function of the seismic sensor used with a recorder or in a network channel also modifies the frequency content of events and noise signals at the input of trigger algorithm. Therefore the sensor used is an important factor in the choice of a trigger filter. The type of sensor output - proportional to either ground displacement, velocity or the acceleration - has a similar effect. Sensors with ground acceleration proportional output - accelerometers - emphasize high frequencies. They usually require a filter protection against excessive high-frequency man-made seismic noise. Ordinary seismometers have typically an output proportional to ground velocity, sometimes also to ground displacement. They are less influenced by high-frequency man-made seismic noise.

The adjustment flexibility of high- and low-corners of these filters varies among different products. The same is true for the steepness of the filter flanks. Generally, one does not need very steep (high order) filters and a lot of flexibility, because events, similar to the seismic noise, are highly variable. It is generally impossible to determine very precisely where exactly to set the frequency limits of these filters.

5.2 Selection of pre-event time (PEM) parameter

Ideally, the triggered earthquake records should include all seismic phases of an event and, in addition, a portion of the seismic noise signal prior to it. Selection of an appropriate pre-event time (PEM) assures that the earthquake records are complete. For the majority of weak events, the trigger algorithm usually does not trigger at the beginning of the event but sometimes during the event, when the waves with the maximum amplitude of ground velocity reach the station. This happens very often with the earthquakes, which have emergent onset waves, and with most of the weak local and regional events where the S phase amplitudes can be much bigger than the P phase. In practice, triggering on the S waves of the weak local and the regional earthquakes is actually more frequent than triggering on the P waves. But for seismological reasons, the P onset waves plus some seismic noise prior to them should be included in the record. A proper PEM should take care about this.

Technically this is solved in the following way. In seismic recorders and in a network's central recording computer a portion of seismic signal prior to the instrument trigger time is temporally stored in a pre-event ring buffer (abbreviation PEM denotes 'pre-event-memory') and prepend to the data recorded.

PEM must surmount the following periods of time:

- the desired record duration of seismic noise prior to the event;
- the maximal expected S-P time of earthquake records, and
- time needed to calculate the STA/LTA ratio, which, in the worst case, equals one STA window duration,

Add these three time periods and the result is the appropriate PEM value.

The effect of a too short PEM is shown in Fig. 7. Graph a) shows an event approximately 400 km away from the station with weak P waves partly buried in the seismic noise. On graph b) the STA and the LTA values are shown. Graph c) shows the STA/LTA ratio and the trigger and dettrigger thresholds (short horizontal dotted lines). The trigger threshold is set to 6. One

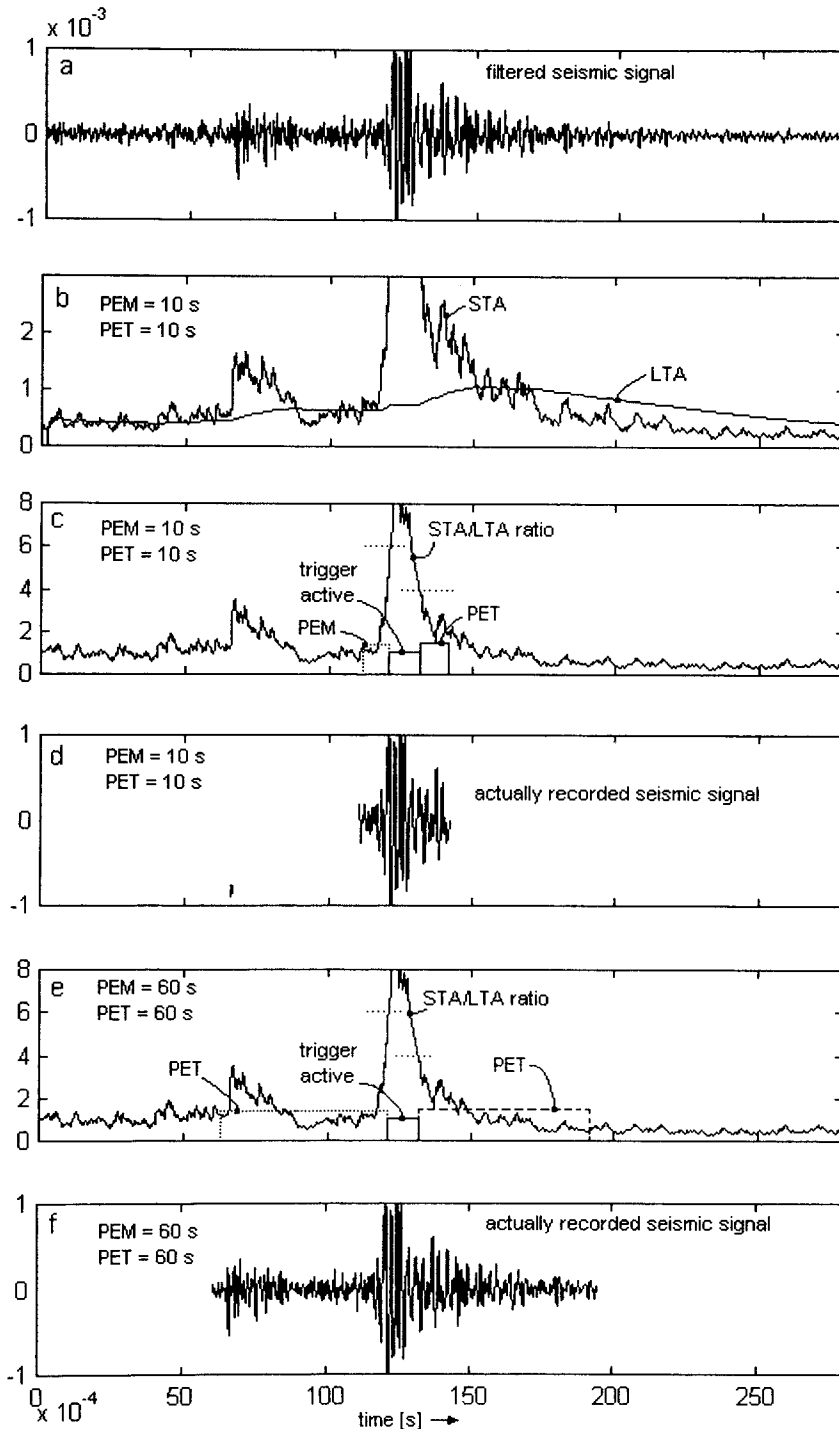


Fig. 7: Proper and improper setting of the pre-event time (PEM) and the post-event time (PET)

can see that the channel triggers on the S waves. However, a PEM of 10 seconds is much too short to catch the P waves. Graph d) shows the actually 'recorded' event. It starts much too late and contains no seismic noise record. Graphs e) and f) show the same event but with a properly set PEM parameter. Seismic noise as well as the P waves are properly recorded.

The maximal expected S-P time depends on maximal distance of relevant earthquakes from the station and on seismic wave velocity in the region. For practice and for local and regional events, accurate enough results can be gained by dividing the maximum station-to-epicenter distance of interest by 5 (distance in miles) or by 8 (distance in km) to get the required maximum S-P time in seconds.

The application dictates the choice of the desired pre-event noise record duration. At least a few seconds are usually required. Note that if one wants to study spectral properties of weak events, seismic noise spectra are usually required to calculate signal-to-noise ratio as a function of frequency. This, however, requires a significant length of noise records depending on the lowest frequency of interest. The PEM must be set accordingly.

As an example, let us calculate a required PEM parameter value for a temporal local seismic network with 50 km aperture, where 0.5 sec is set for the STA duration. Suppose that no coincidence trigger exists and all stations run independent trigger algorithms. The owner is interested in the seismicity 200 km around the center of the network. He would also like to have a 10 sec long record of seismic noise before the P waves. We need 0.5 sec for STA calculation, 10 sec for seismic noise, and $\approx (200 \text{ km} + 50/2\text{km})/8 \approx 28$ sec to cover the maximal expected S-P time. Note that the most distant station from the epicenter in the network still has to record P waves — that is why we added one half of the network aperture to the maximal epicentral distance of interest. The PEM should therefore be set to $0.5 + 10 + 28 \sim 40$ sec. Obviously, smaller networks and shorter ranges of interest require shorter PEM and vice versa.

5.3 Selection of post-event time (PET) parameter

The post-event time parameter assures complete recording of seismic events after a dettrigger. The main purpose of PET is catching the remaining earthquake coda waves that are smaller in amplitude than the STA/LTA dettrigger threshold level. Functionally PET is simply a fixed recording time added to the event file after an instrument or a network (not individual channels!) dettriggers. It has a similar effect on coda waves as the STA/LTA dettrigger threshold level parameter. However, its effect is event-size independent. This makes it a less effective coda wave 'catcher' than a low STA/LTA dettrigger threshold level. It is most suitable for local events. Practical values of PET are usually too short to be of any help for large distant earthquakes with very long coda waves. Contrary to a very low STA/LTA dettrigger threshold level that may cause re-triggering problems, a long PET is safe in this respect (see section 4.5 'Selection of STA/LTA dettrigger threshold level').

Optimal PET duration depends mostly on the application. If coda waves are important, a long PET should be selected. If coda waves have no significance, use a short PET. Obviously, the short local events require only a short PET, regional and teleseismic events, on the other hand, would require much longer PET.

A reasonable value for local seismology would be 30 sec, and 60 to 90 sec for regional seismology, assuming one wants the coda waves well recorded. To find optimal value, observe coda waves of your records and adjust the PET accordingly.

There are usually no practical instrumental limitations on selection of the longest PET. However, note that very long PET use up the recorder's data memory easily. So, do not exaggerate, particularly in seismically very active areas or if a high rate of false triggers is accepted.

5.4 Selection of voting scheme parameters

The coincidence trigger algorithm, available either in seismic networks or within a multi-channel stand-alone seismic recorder, or in a group of interconnected seismic recorders, uses voting scheme for triggering. The voting scheme parameters are actually not directly related to the STA/LTA trigger algorithm. However, inappropriate setting of voting scheme prohibits efficient functioning of overall triggering of a network or a recorder. For that reason we also deal with the voting scheme parameters in this section.

In section 4 'How to adjust STA/LTA trigger parameters,' we described how each individual channel would trigger if it were the only one in an instrument or in a network. In the following section we describe how the individual channel triggers are combined to cause the system to trigger in a multi-channel recorder or in a seismic network. We call this 'voting', as a number of votes or weights can be assigned to each seismic channel so that it may cast towards getting the system to trigger. Only if the total number of votes exceeds a given pre-set value, the system actually triggers, a new data file opens, and data acquisition begins.

How this voting system is set up depends on the nature of the signals that one is trying to record and on the seismic noise conditions at sensor sites. The noisy channels, which would frequently falsely trigger, will obviously have less 'votes' or assigned weights than the quiet, 'reliable' channels. Obviously one will need some first-hand experience of the conditions at the sites before optimizing this voting scheme. The voting mechanism and the terminology differ to some extent among products. However, there are usually four basic terms associated with the voting scheme parameters

- Channel weights (votes).

A channel weight defines the number of votes the channel contributes to the total when it is triggered. If the channel has a good signal/noise ratio, assign it some positive number of votes. The more 'reliable' the channel in terms of the event trigger/false trigger ratio is, the higher number should be selected. If a channel is noisy and frequently falsely triggers, give it lesser or even zero weight. In case you want a channel to inhibit triggering (a rare case indeed), give it negative weights.

- Trigger weight

This is the total number of weights required to get the seismic recorder or the network to trigger.

- Detrigger weight

The Detrigger weight is a value below which the total trigger weights (sum of all individual weights) must fall in order to cause a recorder or a network to detrigger. The

Detrigger weight of 1 usually means that all voting channels must be dettriggered before the recorder will dettrigger. However, other definitions are also possible.

- External channel trigger weight

This value represents the number of weights one assigns to the 'external trigger channel' source. This parameter is most useful in networks of interconnected stand-alone seismic recorders. In this configuration every triggered recorder 'informs' all other units in the network that it triggered. If one wants to ensure that all recorders in the network trigger when one unit triggers, the external trigger channel should have the same weight as the Trigger weight. If one wants to use a combination of an external trigger with other internal criteria, one should set the weights accordingly.

Understanding of the voting scheme parameters is best gained through examples. The following section gives a few examples of various voting schemes.

- A classic strong-motion seismic recorder set at a free-field site has no interconnected units and normally has a three-component internal FBA accelerometer. One would set all three Channel weights to 1 and also set Trigger weight to 1. Consequently any channel could trigger the system. At noisier sites a Trigger weight set to 2 would be more appropriate. In the latter case, two channels must be in a triggered mode simultaneously (or within a time period usually named aperture propagation window (APW) time, which is an additional parameter available with seismic networks) for the beginning of data recording.
- A small weak motion seismic network around a mine is designed for monitoring local micro-earthquakes. It consists of 5 surface seismic stations with vertical component short-period seismometers and one three-component down-hole accelerometer. An 8-channel data logger is used at the network's center. One of the surface stations is extremely noisy due to nearby construction works. All others have approximately the same seismic noise amplitudes. One can temporarily set a Channel weight 0 to the noisy station to exclude its contribution to triggering and channel weights of 1 to all other surface stations. The down-hole accelerometer is very quiet but less sensitive than surface stations (accelerometers). Select Channel weight 2 for each of its components. For this network a trigger weight of 3 would be an adequate initial selection. The system triggers either if at least three surface stations trigger, or two components of the accelerometer trigger, or one surface station and one component of the accelerometer trigger. Suppose also that there are frequent blasts in the mine. If one wishes, one can use an External trigger channel weight set to -8 and manually (with a switch) prevent seismic network recording of these blasts (down-hole: 3x2 channel votes + surface stations: 4x1 channel vote - 8 External votes < 3 Trigger votes).
- Let us suppose that an interconnected strong motion network of two seismic recorders with the internal three-component FBA accelerometers is installed in a building, one in the basement and one on the roof. Initially one can set the Channel weights to 1 for each signal channel, as well as for the External trigger channel. Suppose the Trigger weight is set to 1 as well. As a result each channel of the system can trigger both units in the system.

After a while one discovers that the seismic recorder on the roof triggers the system much too frequently, due to the sway of the building in the wind. Changing the voting scheme of the roof unit so that Trigger weight is 3, its channels have 1 weight, while the External trigger channel has 3 weights, can compensate for this action. Now, the recorder installed on the roof triggers only if all its three channels trigger simultaneously or if the 'quiet' recorder in the basement triggers. The number of falsely triggered records will be drastically reduced.

- A small regional radio-frequency (RF) FM modulated telemetry seismic network, with a coincidence trigger algorithm at the central recording site, has 7 short period three-component seismic stations. The three stations, #1 west of the center and #2 and #3 east, not far from the center, have a low seismic noise and are connected to the center via three independent reliable RF links. The two stations north to the center, #4 and #5, are linked with the center via a joined RF repeater. The link between this repeater and the center is, unfortunately, frequently influenced by RF interference, resulting in frequent and simultaneous spikes and glitches in all six transmitted seismic signals. Due to unfavorable geology these two stations have a relatively high seismic noise. The two stations south of the center, #6 and #7, are also connected to the center via another common RF repeater. The station #6 is very quiet and the station #7 is influenced by traffic on a nearby new busy freeway. The RF link from this repeater to the center is less RF interference prone.

In such situation (apart from trying to technically solve the RF link problem with the northern stations and repositioning of the station #7) an appropriate initial voting scheme would be as follows. A Trigger weight set to 7 (to disable otherwise much too frequent false triggering of the system due to RF interference on all 6 channels of the two northern seismic stations) and a Channel weight 1 to all channels of the northern stations (their total Channel weight should not exceed the Trigger weight), a channel weight 3 to all three channels of the station #1 (to allow independent triggering of the system if all three channels of this good station are triggered), a channel weight 2 to all channels of the stations #2 and #3 (to allow triggering of the whole system if at least four channels of these two closely situated stations are activated), a channel weight 2 to all channels of the station #6 (to accentuate its low seismic noise characteristics but to prevent independent triggering of the system due to occasional RF interference), and a weight 0 to all channels of the station #7 (to exclude its partition in triggering due to excessive man-made seismic noise).

These examples should give enough insight into the flexibility of the coincidence triggering options and about some of the ways in which this flexibility can be used for a particular application. Note also that any initial voting scheme can be significantly improved after more experience with seismic noise conditions at the sites is gained.

6. PRACTICAL RECOMMENDATIONS FOR FINDING OPTIMAL TRIGGERING PARAMETERS

A systematic approach is required for successful adjustment of the optimal triggering and the associated parameters. First, the goals of the seismic installation must be carefully considered and a priori knowledge about seismic noise (if any) at the site(s) must be taken into account. Based on this information, the initial parameters are set. Information about them must be saved for documentation purpose. Start with rather low trigger threshold level settings than with a too high setting. Otherwise one can wait too long to get sufficient number of records for a meaningful analysis required for further adjustment steps.

Then the instrument or the network is left to operate for a given period of time. The required length of operation without changing recording parameters depends strongly on the seismic activity in the region. At least several earthquakes and/or falsely triggered records must be recorded before the first readjustment of parameters is feasible. Judgements based on a single or a few records rarely lead to improvements. Such work simply doesn't converge to any meaningful adjustment.

Afterwards, all records, including those falsely triggered, must be inspected. The completeness of the event records is checked (seismic noise, the P arrivals, the coda waves), and the causes of the false triggers are analyzed. The ratio of event-records/false-records is calculated and compared to the target level. If the number of false triggers does not reach the accepted level, increase the trigger sensitivity by lowering the STA/LTA trigger threshold level(s). Basically, one will acquire more seismic information for nearly the same price and effort. If the number of false triggers is too high, find the reasons for that and try to mitigate them by changing STA/LTA and/or voting scheme parameters. Only if this doesn't help, decrease trigger sensitivities.

After the analysis is finished, the parameters are changed according to its findings and the new settings archived for documentation purposes. Again the instrument or the network is left active for a certain period of time, the new records are analyzed, and other changes made if needed. By repeating this process one will gradually find the best parameter setting.

7. REFERENCES

- Allen, R.V. (1978) Automatic earthquake recognition and timing from single traces, *BSSA*, **68**, 1521-1532.
- Allen R.V. (1982) Automatic phase pickers: Their present and future prospects, *BSSA*, **72**, S225-242.
- Goforth, T. and Herrin, E. (1981) An automatic seismic signal detection algorithm based on the Walsh transform, *BSSA*, **71**, 1351-1360.
- Joswig, M. (1990). Pattern recognition for earthquake detection. *Bull. Seism. Soc. Am.*, **80**, 170-186.
- Joswig, M. (1993). Single-trace detection and array-wide coincidence association of local earthquakes and explosions. *Computers and Geosciences*, **19**, 207-221.

- Joswig, M. (1995). Artificial intelligence techniques applied to seismic signal analysis. *Consel de Léurope, Cahiers du Centre Européen de Géodynamique et de Séismologie*, Vol. 9, Proceedings of the Workshop: Dynamic systems and artificial intelligence applied to data banks in geophysics, 5-15.
- Murdock, J. N. and Hutt, C.R. (1983) A new event detector designed for the seismic research observatories, USGS, Open File Report 83-7851
- Veith, K.F. (1977) A digital event detector, *EOS*, **58**, 1190

WDCs AND ACCESS TO DATA SOURCES VIA INTERNET AND CD-ROM

Zhao Zhonghe

National Centre for Seismic Data and Information, China Seismological Bureau, 56 Sanlihe
Road, Beijing 100045, China;
Fax: +86 10 68530226; E-mail: zhzhao@sdb.csdi.ac.cn

1. INTRODUCTION TO THE WORLD DATA Centres

1.1 The World Data Centre system

The World Data Centre system was a product of the International Geophysical Year of 1957-1958. Planning of the IGY was co-ordinated by CSAGI, the Special Committee for the IGY set up by the International Council of Scientific Unions. CSAGI established the World Data Centre system to serve the IGY, and developed data management plans for each IGY scientific discipline. The data specifications were published in a series of Guides to Data Exchange originally issued in 1957 and updated in 1963, 1973, 1979 and 1987. The 1955 recommendation mentioned that Data Centres should be prepared to handle data in machine-readable form, which at that time meant punched cards and punched tape.

National IGY Committees were invited to establish and to operate World Data Centres at national expense, abiding by the CSAGI rules. The USA and USSR established complex centres, known respectively as WDC-A and WDC-B, to serve most IGY disciplines. In many disciplines there was a third or even a fourth centre, known as WDC-C1 if in Western Europe and WDC-C2 if in Asia or Australia (the European centres being known simply as WDC-C if there was no corresponding WDC-C2). Multiple centres were deemed advisable to guard against catastrophic loss of data, and for the convenience of data providers and users.

Because of its success, the WDC system was made permanent and used for post-IGY data. New programs evolved, based on the IGY structure as a general framework, such as the International Quiet Sun Year of 1964-1965, the International Magnetospheric Study of 1976-1979, the Solar Maximum Year of 1979-1981 and the Middle Atmosphere Program of 1982-1985. Most of the sponsoring national bodies agreed to continue the WDCs to serve these programs, and the data collections have remained accessible to users.

Since the IGY, the gathering and exchange of data has been transformed by technological advances, such as the replacement of analogue with digital instruments, the networking of digital instruments to simplify collection and exchange of data, and unstaffed automatic observatories. Personal computers and compact disc readers are ubiquitous. Many WDCs publish collections of digital data sets on compact discs for easy distribution. Digital communication networks make it possible to transfer large data files by electronic mail, reducing much of the routine work of WDC staff, who are now largely engaged in developing new data compilations and new tools for data display and analysis.

The environmental WDC disciplines make use of map-based data and information on natural

features and human activities that differ in character from the numerical data sets of the older disciplines and require new analytical techniques.

Over the years the tally of WDCs has changed because of scientific, technical and economic factors. A comprehensive set of WDC-D was established in China in 1988. WDC-A in the USA has expanded; many of its discipline centres are collocated with national data centres. WDC-B in Russia is now operated by three different organisations. Some of the C, C1 and C2 centres in Europe and Asia have moved or have closed (especially those that depended on the expertise of a particular research group), but new centres have opened. All centres now have computer facilities and most use electronic networks to meet requests, to exchange catalogue information and to transfer data.

Following, all WDCs, including their homepage addresses are listed:

WDC-A for Atmospheric Trace Gases (Oak Ridge)

<http://cdiac.esd.ornl.gov/cdiac/wdca/wdcinfo.html>

WDC-A for Glaciology (Boulder)

<http://www-nsidc.colorado.edu/NOAA/wdc-a.html>

WDC-A for Human Interactions in the Environment (Saginaw)

<http://www.ciesin.org/home-page/WDC.html>

WDC-A for Marine Geology and Geophysics (Boulder)

<http://www.ngdc.noaa.gov/mgg/wdcamgg>

WDC-A for Meteorology (Asheville)

<http://www.ncdc.noaa.gov/wdcamet.html>

WDC-A for Oceanography (Silver Spring)

<http://www.nodc.noaa.gov/NODC-dataexch.html>

WDC-A for Paleoclimatology (Boulder)

<http://www.ngdc.noaa.gov/paleo/paleo.html>

WDC-A for Remotely Sensed Land Data (Sioux Falls)

<http://edcwww.cr.usgs.gov/doc/edchome/world/wdcguide.html>

WDC-A for Rockets and Satellites (Greenbelt)

http://nssdc.gsfc.nasa.gov/about/about_wdc-a.html

WDC-A for Rotation of the Earth (Washington)

<http://maia.usno.navy.mil>

WDC-A for Seismology (Golden)

<http://wwwneic.cr.usgs.gov>

WDC-A for Solar Terrestrial Physics (Boulder)

<http://www.ngdc.noaa.gov/stp/WDC/wdcstp.html>

WDC-A for Solid Earth Geophysics (Boulder)

<http://www.ngdc.noaa.gov/seg/wdca/wdcaseg.shtml>

WDC-B General Page (Moscow)

<http://www.wdcb.rssi.ru/WDCB>

WDC-B for Marine Geology and Geophysics (Gelendzhik)

<http://www.sea.ru/cmgd/wdc.html>

WDC-B for Meteorology (Obninsk)

<http://www.meteo.ru/>

WDC-B for Oceanography (Obninsk)

<http://www.meteo.ru/>

WDC-B for Rockets and Satellites (Obninsk)

<http://www.meteo.ru/>

WDC-B for Rotation of the Earth (Obninsk)

<http://www.meteo.ru/>

WDC-B for SolarTerrestrial Physics (Moscow)

http://www.wdcb.rssi.ru/WDCB/wdcb_stp.shtml
 WDC-B for Solid Earth Physics (Moscow)
http://www.wdcb.rssi.ru/WDCB/wdcb_sep.html
 WDC-C for Earth Tides (Brussels)
<http://www.oma.be/KSB-ORB/ICET>
 WDC-C1 for Geomagnetism (Copenhagen)
<http://www.dmi.dk/projects/wdcl/>
 WDC-C1 for Geomagnetism (Edinburgh)
<http://ub.nmh.ac.uk>
 WDC-C for Glaciology (Cambridge)
<http://www.spri.cam.ac.uk/wdcc.htm>
 WDC-C for Recent Crustal Movements (Prague)
 WDC-C for Soils (Wageningen)
<http://www.isric.nl>
 WDC-C for Solar Activity (Meudon)
<http://www.obspm.fr/departement/dasop/dasop.html>
 WDC-C1 for Solar Terrestrial Physics (Chilton)
<http://www.wdc.rl.ac.uk>
 WDC-C for Sunspot Index (Brussels)
http://www.oma.be/KSB-ORB/SIDC/sidc_txt.html
 WDC-C2 for Airglow (Mitaka)
<http://www.nao.ac.jp>
 WDC-C2 for Aurora (Tokyo)
<http://www.nipr.ac.jp/english/aurora.html>
 WDC-C2 for Cosmic Rays (Mito)
<http://www.env.sci.ibaraki.ac.jp/Sun/sun15-eng.html>
 WDC-C2 for Geomagnetism (Bombay)
 WDC-C2 for Geomagnetism (Kyoto)
<http://swdcd.db.kugi.kyoto-u.ac.jp>
 WDC-C2 for Ionosphere (Tokyo)
<http://wdc-c2.crl.go.jp>
 WDC-C2 for Nuclear Radiation (Tokyo)
 WDC-C2 for Solar Radio Emission (Nagano)
<http://solar.nro.nao.ac.jp>
 WDC-C2 for Solar-Terrestrial Activity (Sagamihara)
<http://www.isas.ac.jp>
 WDC-D for Astronomy (Beijing)
<http://www.bao.ac.cn/wdc>
 WDC-D for Geology (Beijing)
 WDC-D for Geophysics (Beijing)
 WDC-D for Glaciology and Geocryology (Lanzhou)
 WDC-D for Meteorology (Beijing)
 WDC-D for Oceanography (Tianjin)
<http://www.coi.gov.cn>
 WDC-D for Renewable Resources and Environment (Beijing)
<http://www.CERN.AC.CN/wdc-d>
 WDC-D for Seismology (Beijing)
<http://www.eq.csi.ac.cn/wdcds>
 WDC-D for Space Sciences (Beijing)

The WDC homepages are rapidly expanding, and the addresses are subject to change. Up-to-date information is maintained on the WDC System homepages at WDC-A in Boulder,

Colorado, which are mirrored in Europe by the WDC-C1 for Solar Terrestrial Physics at Chilton, England, and by WDC-B at Moscow, Russia. At the time of writing, these addresses are:

<http://www.ngdc.noaa.gov/wdc/wdcmain.html>

<http://www.wdc.rl.ac.uk/wdcmain>

<http://plato.wdcb.rssi.ru/wdc>

1.2 Activities of WDCs

The following list given by WDCs guide summarises the general activities of WDCs.

- (1) Collecting and cataloguing data and information in co-operation with other WDCs.
- (2) Maintaining the data in good condition.
- (3) Providing data to users, at minimum costs of copying and distribution.
- (4) Working with originators of data to improve documentation of the data.
- (5) Preserving important old data sets by converting them from tabular to digital form.
- (6) Compiling specialised data sets for small-scale, regional and global geophysical research.
- (7) Making data sets available on such media as compact discs, enabling users to search large data collections and transfer them to their home laboratory.
- (8) Assessing technical issues of ageing, error growth and lifetimes of data storage media.
- (9) Combining data from various sources to derive data products, such as indices of solar or geomagnetic activity.
- (10) Compiling numerical models to describe the time-varying and space-varying geophysical environment, such as the geomagnetic field and the upper atmosphere.
- (11) Maintaining on-line information services related to the above activities.
- (12) Operating visitor programs to enable scientists to work on WDC data holdings with the assistance of the WDCs professional staff.
- (13) Assisting scientists to locate and access related data not held in the WDC System.

Exercise:

Access the WDCs homepage with a Web browser to find the WDC Guide and read the brief description of WDCs for seismology and for solid earth geophysics, including WDC-A for Seismology, WDC-A for Solid Earth Geophysics, WDC-B for Solid Earth Geophysics, WDC-D for Geophysics and WDC-D for Seismology. The Web site is

<http://www.ngdc.noaa.gov/wdc/wdcmain.html>

2. ACCESS TO DATA SOURCES VIA INTERNET

2.1 Brief introduction to the Internet

The Internet, with a capital "I" as the first letter, is a wide area network supported by TCP/IP protocol. The Internet has developed very fast. Actually, it appeared in 1960s, during the time of the "cold war". At that time, there was a strange question in the United States: "What would happen after a nuclear war?" The U. S. authorities thought about the so-called "post nuclear situation". They needed a network to command and control the country. So some people were asked to develop a computer network. It was assumed that the network on the whole is unreliable. But it was needed, for instance, to transmit a message from one node, the

source node, to another node, the destination node. If some part of the network was blown down, the information could be transmitted through another route to the destination. With this idea, a communication protocol called TCP/IP (Transmission Control Protocol / Internet Protocol) was developed. With TCP protocol, a message is divided into several packages; each one is transmitted individually from one node to another, roughly along the direction to the destination. So the particular route is not important, just the destination, the result, is important. Then the IP protocol is for handling the address, the routing. With this TCP/IP protocol, it is easy for other computers or networks to join into the network. That is why this network developed very fast. At the beginning, this network was sponsored by the Advanced Research Project Agency of the U.S. Department of Defence. So it was named as ARPANET after its sponsor's name. Then, with the fast development of the network, the ARPANET, though it was still a part of the network, became smaller and smaller in the midst of the networks. Finally, people call this network as Internet, a network of networks.

At present the Internet has become a worldwide computer network. Human created the Internet and, in turn, the Internet has changed humans life. Also the Internet has become a useful and easy way for scientific data collection and distribution all over the world. The Internet makes the world much smaller.

2.2 E-mail

E-mail, the electronic mail, is the most widely used service of the Internet and it is the main way to transmit messages between the Internet and other networks, such as OMNET. In addition to the usual usage of E-mail for exchanging information, there are several other applications.

(1) Subscribed E-mail data services

Some data centres or research groups offer their data to users by E-mail based on the subscription of the users. For example, U.S. National Earthquake Information Centre/World Data Centre-A for Seismology has two E-mail data services that provide earthquake information rapidly. You may subscribe by sending a specially formatted e-mail message.

The first service, known as BIGQUAKE, sends a message whenever a large earthquake release is issued (the criteria varies depending on the location of the event). To subscribe, send an e-mail message to:

majordomo@ghmail.cr.usgs.gov

In the body of the message (not the subject line) put

subscribe bigquake

The second service, QEDPOST, sends a daily message of the earthquakes located 7 days behind the current day taken from the Quick Epicentre Determinations (QED) listing. It is a preliminary publication and typically contains 10-30 events per day. To subscribe, send an e-mail message to the same address as mentioned above and in the body of the message (not the subject line) put

subscribe qedpost

For these two kinds of subscription, you will receive an e-mail message with instructions on how to confirm your subscription.

To REMOVE your address from the mailing list, send a mail message to majordomo@ghgmail.cr.usgs.gov

In the body of the mail message (not the subject line), put

unsubscribe bigquake for BIGQUAKE
or
unsubscribe qedpost for QEDPOST

(2) autoDRM

An AutoDRM (Automatic Data Request Manager) is a software package that allows anyone with access to electronic mail to retrieve data from the site where such an AutoDRM is installed.

AutoDRM is now a widely used method to retrieve earthquake information from seismological observatories, including earthquake catalogues, station information, waveform data and the information. It should be noted that when you send a request to an AutoDRM system you must carefully fill in the body of your mail message, following the format given by the AutoDRM guide. Otherwise the AutoDRM system would return an error message to you.

You can get a list of urgently available AutoDRMs providing seismic data from Web site of:

http://seismo.ethz.ch/autodrm_list.html

You may obtain instructions by sending an e-mail to any AutoDRM listed above with the text 'HELP' in your mail. For instance, you may send an e-mail to the address: autodrm@seismo.ifg.ethz.ch with the text 'HELP'.

An example of the use of AutoDRM is to get an earthquake catalog for June 29,1999 from Swiss Seismological Service:

E-mail address: autodrm@seismo.ifg.ethz.ch

No subject

Text of your e-mail:

BEGIN

DATE1 199906290000

DATE2 199906300000

DETEC

EMAIL your e-mail address

STOP

Then you will get an answer from the AutoDRM of Swiss Seismological Service like this:

Below follows what you requested
(unless your request contained a severe error!):

DETECTIONS OF THE SWISS SEISMOLOGICAL SERVICE

Recording Date & Time may be used for specific waveform requests!

Q: quality remark (A = very good, B = good, C = fair, D = poor)

L: type of location (A = automatic, M = 'manually' by an analyst)

Recorded at	Origin	Location	Region (or
YYYYMMDDHHMM	Date Time	Lat Lon Dep Mag Q L	Azim/Slown if PKP)
199906290812:29	Jun1999 08:12:46.5	46.3N 8.0E 3	Ml=1.6 B M Brig / Switzerland
199906291356:29	Jun1999 13:56		A not located
199906291512:29	Jun1999 15:12:44.6	45.2N 9.3E 10	Ml=2.6 D A Northern Italy
199906291514:29	Jun1999 15:14		A not located
199906292325:29	Jun1999 23:18:12.7	37.2N 67.4E 10	M>=6.4 A A Afghanistan-Tajikis
199906292328:29	Jun1999 23:28		A not located
199906292332:29	Jun1999 23:32:35.0	46.4N 10.2E 10	Ml=2.2 C A Bormio / Italy

If you want to install AutoDRM in your data centre as a tool for providing data to other people, you can get the complete AutoDRM software package from its original designer, Dr. U. Kradolfer of Swiss Seismological Service, with a WWW browser. The URL is:

<http://seismo.ethz.ch/autodrm.html>

or you can use anonymous ftp account as described in section 2.3.

Exercise:

- (1) Send an e-mail to NEIS for subscribing a BIGQUAKE service, confirming the subscription, and then removing the subscription.
- (3) Make an AutoDRM request for getting an earthquake catalog from Swiss Seismological Service.

2.3 File Transfer Protocol

File Transfer Protocol (FTP) is one of the members of TCP/IP family, which includes more than one hundred protocols. With FTP, many ftp servers are established for providing information and data. There is a kind of FTP servers called anonymous ftp. When you use an anonymous ftp, usually you can use "anonymous" as the user name and use your E-mail address as password, so that the ftp server can know who are interested in those data.

Following example shows how to get AutoDRM software package from Swiss Seismological Service with ftp command in a UNIX system. But here the user name is ftp and password is also ftp.

```
ftp seismo.ethz.ch
login as user=ftp and password=ftp
cd pub/gse
binary
get README
get INSTALL_autodrm.readme
get autodrm_2.9.tar.Z .
```

Now there are some softwares for ftp which work on MS windows. And most WWW browsers have incorporated the ftp function into WWW system. So it is much easier to use ftp function than ever before.

Exercise:

Download a file from the anonymous FTP server of CSDInet Centre (at National Centre for Seismic Data and Information, CSB)

<ftp://sdb.csdi.ac.cn>

2.4 Finger

As an easy way to provide earthquake catalogues to the public, people use a function given by UNIX operating system called "finger". (At present there is special software for other operating systems to realise "finger" function.) Actually, this function is to give information of the status of people with a given E-mail address. There is a file ".plan" in his/her directory, which content will be returned to you, if you "finger" his/her E-mail address. File ".plan" is usually used for telling you his/her plan for the next few days. With this function, many seismic networks put their earthquake catalogue for the recent days in file ".plan", and anyone can use a finger command to get such catalogue like this:

finger quake@machine.domain

For instance, to get IRIS DMC catalogue of 10 recent large earthquakes, for which waveform data are available, you may

finger spyder@iris.washington.edu

Following is a part of the answer from IRIS DMC as an example:

[iris.washington.edu]

The following are the most recent events (as reported by the USGS NEIC) for which Spyder(R) has retrieved data:

DATE-TIME	SEC	LAT	LON	DEPTH	MAG	REGION	NUMBER	VBB	LP
9906101507	21.	36.26 N	71.28 E	113	5.3	AFGHANISTAN-USSR BORDER	RE	70	56
9906152042	01.	18.33 N	97.39 W	33	6.5	CENTRAL MEXICO		67	62
9906152152	18.	17.20 N	95.50 W	100	4.5	OAXACA, MEXICO		12	11
9906161835	59.	17.04 S	173.36 W	79	5.6	TONGA ISLANDS		17	09
9906161932	33.	14.54 S	176.15 W	33	5.5	FIJI ISLANDS REGION		09	09
9906181055	25.	5.46 N	126.66 E	33	6.2	MINDANAO, PHILIPPINE ISLAN		67	52
9906190903	08.	5.41 S	146.77 E	210	5.2	EAST PAPUA NEW GUINEA REGI		26	24
9906211743	01.	18.33 N	101.40 W	33	5.7	GUERRERO, MEXICO		29	24
9906211737	27.	36.45 N	70.61 E	229	5.6	HINDU KUSH REGION		68	57
9906220047	42.	4.49 S	133.81 E	33	5.8	WEST IRIAN REGION		22	21

Exercise:

Get a rapid earthquake catalogue by using "finger" function:

Finger quake@andreas.wr.usgs.gov

2.5 Bulletin Board

IRIS's Bulletin Board represents a kind of application of the Internet. As a matter of fact, it is a "telnet" function. You can use "telnet" to login into a remote host computer, by using a proper user name and password, which are recognized by the host computer. IRIS Bulletin Board is an interactive data service system, which requires a user name of "bulletin" and a password of "board". Here is an example showing how to get into IRIS's Bulletin Board.

```
wdcds:~> telnet dmc.iris.washington.edu
Trying 128.95.166.129...
Connected to dmc.iris.washington.edu.
Escape character is '^'].
```

SunOS 5.6

```
login: bulletin
Password:
Last login: Thu Jun 24 01:55:25 from 210.72.96.80
```

Though, with the development of World Wide Web system, many functions of IRIS's Bulletin Board have been moved to the WWW server, it is still a useful way for users to retrieve near real-time waveform data from IRIS DMC (Data Management Centre).

Exercise:

Login to IRIS DMC Bulletin Board system and get some data from IRIS DMC.

2.6 World Wide Web

The World Wide Web is an on-line information delivery system with the so-called hypertext and hyper-media documents. That means, these documents are specially coded texts or multimedia documents. If you want to put your information to the Internet world with WWW, you may run your own Web server or put your web pages onto a Web server run by others. Each Web server has a Uniform Resource Locator. The URL is the address on the web with that people can visit the pages on the Web server. Web pages can include text information, pictures, sounds, video, FTP links for downloading software, and much more. You can create living documents that are updated weekly, daily, or even hourly to give web surfers a different experience every time they visit your pages. As the technology develops, even more amazing applications will be possible.

A web browser is a program that is used to visit web pages. The two most well known web browsers are Netscape Navigator and Microsoft Internet Explorer, which are used by the vast majority. Other browsers are available as well. Most web browsers need you to include `http://` at the beginning of the URL so the program knows that you want to visit a web page. Thus, you will need to tell your web browser to open, for instance, <http://www.eq-csi.ac.cn> to get to the pages of CEQinfo, the Chinese Earthquake Information Service.

The web does not look the same to everyone. Some people use Netscape, Internet Explorer, Mosaic or other browsers that support graphics. Others can only make a connection through lynx, which supports the text and the links, but no pictures.

Even though the European Laboratory for Particle Physics, CERN, can be credited for laying the foundation of the Web, the National Centre for Supercomputing Applications, NCSA, developed many of the tools that made the Web usable to mere mortals. The very first web browser was written by Tim Berners-Lee, while at CERN the first web browser to capture the public's imagination was Mosaic, which was written by Marc Andreessen and other undergraduate students at NCSA.

2.7 Surfing the Internet for earthquake data

Dr. Steven Malone of Washington University maintains a list of Internet type connections where original seismic data or seismic research information is available. You may use this list as a guide to surf the Internet for earthquake data. And from the following Web sites you can get this list:

<http://www.geophys.washington.edu/seismosurfing.html>

or

<http://seismo.ethz.ch/seismosurf/seismobig.html>

If you do not remember these addresses, you may search the Web site by using an Internet search engine, e.g., Yahoo (<http://www.yahoo.com>), and then you may type "Surfing the Internet for Earthquake Data" in the search window. Yahoo will give you the connection to the list.

A similar list for surfing the Internet for strong motion data is provided by Dr. Dave Wold at his site:

<http://www-socal.wr.usgs.gov/smdata.html>

With these lists as beginning, you can find much many more data centres and institutions on the network, which may provide you with significant volume of useful data and information.

Exercise:

Access the Web site of the list of strong motion data.

3 CD-ROM FOR DATA SHARING

3.1 An example of CD-ROM usage

Here we take the first CD-ROM prepared by the International Seismological Centre (ISC) as an example, which contains data from the ISC Bulletin for 1992-93. This disk was requested by ISC Council as a method of supplying the complete Bulletin to subscribers. In addition to ISC Bulletin files, the CD contains an explanatory note (README.TXT) and a program (ISCBUL.EXE) which will run under MS-DOS, together with its FORTRAN source. The ISCBUL program will extract earthquake data by origin times and positions of events. This CD-ROM contains:

\1992\ Twelve monthly bulletin files
e.g. 199201.FFB for 1992 January

\1993\ Twelve monthly bulletin files
 e.g. 199310.FFB for 1993 October
\USEFUL\FFORM.TXT Details of format of .FFB files
\USEFUL\PROGRAM\ All FORTRAN source files for ISCBUL.EXE, compiled at
ISC with Microsoft FORTRAN, Compiler Version 5.00.03.
ISCBUL.EXE Simple program to list ISC bulletin files.
README.TXT An explanation of how to use this CD-ROM

ISCBUL.EXE should be copied to a directory on your hard disk before use, as it will create temporary files in the directory from which it is run.

ISCBUL is run by typing `iscbul` at the command prompt followed by at least one keyword and value pair.

e.g. `iscbul time 1993`

This command should cause the program to begin listing the prime estimates of the events in the ISC bulletin for 1993 January. Once a full screen of information has been displayed a prompt will be shown. Hitting the 'Enter' key at this point will display a further screen. The process can be stopped by entering ^C (Control-C) or 'n' at the prompt.

Exercise:

Read an ISC data disk and display a part of earthquake catalogue by using a program given by the disk.

3.2 CD-ROM products for earthquake data

Up to now, ISC has published 6 CD-ROMs. They are:

- (1) Bulletin (events and phases) 1964-1977
- (2) Bulletin (events and phases) 1978-1985
- (3) Bulletin (events and phases) 1986-1991
- (4) Bulletin (events and phases) 1992-1993
- (5) Bulletin (events and phases) 1994, Catalogue (events only) 1964-1993, `iscbul`, `Seisan` (a seismic data manipulation program from the University of Bergen)
- (6) Bulletin (events and phases) 1994-1995
Catalogue (events only) 1964-1993
`iscbul`, a program to search the Bulletin and Catalogue
International Registry of Seismic Station Codes
Bibliography of Seismology

U.S. National Geophysical Data Centre (NGDC)/ NOAA National Data Centres maintains an online store. You can order their CD-ROM with geophysical data products on the Internet. A list of the CD-ROM products can be found at the Web site:

<http://www.ngdc.noaa.gov/seg/fliers/products.shtml>

There are also many CD-ROM data products available at the Orfeus (Observations and Research Facilities for European Seismology) Data Centre (ODC). The ODC is a regional data centre funded by corporate founders and participants in the European-Mediterranean region with the aim to gather and redistribute broadband waveform data. ODC primarily

serves its participants. Participants receive the CD-ROMs with ODC volumes, containing quality controlled waveform event data from the European-Mediterranean region, as the data has been processed. The ODC acts also as the regional distributor for waveform data published by NEIC and the FDSN on CD-ROM. Relevant seismological software is available from ODC's Seismological Software Library. You can get a complete updated list of those CD-ROM products from following Web site:

<http://orfeus.knmi.nl/>

There are many other data centres or institutions that produce CD-ROM products for data distribution. And you may make your own CD-ROMs for data archive and/or distribution.

Exercise:

Find CD-ROM products for earthquake data available at Orfeus Data Centre by browsing the Web page at

<http://orfeus.knmi.nl/>

REFERENCES

- International Council of Scientific Unions (1996), Guide to the World Data Centre system, Produced by World Data Centre A, NOAA/NGDC, Boulder.
- Kradolfer, U. (1996), AutoDRM - The First Five Years, *Seism. Res. Let.*, 67, pp. 30-33.
- National Centre for Seismic Data and Information (1996), A guide to the Internet Resources in earth sciences (in Chinese), Seismological Press, Beijing.

HOW TO RETRIEVE DATA FROM IRIS/USGS STATIONS

Sue McLafferty

Albuquerque Seismic Lab, Kirtland AFB East, Bldg. 10002, Albuquerque,
New Mexico 87115, U.S.A., Fax: +1-505-846-6973, Email: sue@asl.cr.usgs.gov

1. OVERVIEW

Data can be retrieved from the IRIS/USGS stations in either decompressed ASCII format or in compressed binary (SEED) format.

Choices of ASCII format data include "Expanded variable record length ascii", "Expanded fixed record length ascii" and "SAC ascii digital counts". There is a limit of 10,000 samples per request (8.3 minutes of 20 sample/second data). SEED data is a much more efficient way to transfer and store data than ascii data but requires a program that will decode the data (such as DIMAS or rdseed). The limit per request varies from hours to days of data depending on the sample rate of the data. The method of data retrieval depends both on the desired data format and the type of connection available between the analysis computer and the IRIS/USGS station computer.

To access the IRIS/USGS computer at the user's station, the user can set up either a direct serial connection or a LAN (Local Area Network) connection. The direct serial connection requires that a cable be connected from a serial port on the analysis computer to a serial port which is configured as a spare terminal on the IRIS/USGS computer. The LAN connection requires that network software (including TCP/IP programs telnet and ftp) be running on the analysis computer and that the appropriate ethernet cable and transceiver are available.

Remote IRIS/USGS stations can be accessed either by dial-up (telephone) connection or by an Internet connection depending on the station. The dial-up connection requires that the analysis computer be connected via a modem to a phone line. The Internet connection requires that you have access to the Internet and that the analysis computer has the programs telnet and ftp. For a current list of station phone numbers and network addresses, contact the Albuquerque Seismic Labs (a list current to 10/97 is attached to this handout). The list is also available on the web site <http://aslwww.cr.usgs.gov/stations/dialup.html>.

2. HOW TO RETRIEVE DECOMPRESSED ASCII DATA

The basic method for retrieving ASCII format data is to capture/log a retrieve session to a file on the analysis computer. A retrieve session entails connecting to the IRIS/USGS station and logging in as user=seed and password=data. This starts a program called retrieve which allows the user to select and transmit the requested data.

The method that is used to log the retrieve session and connect to the station computer will depend on the type of analysis computer and the software running on the computer. For a PC running Windows95, the program Hyperterminal will allow the user to connect to the station computer through a direct serial connection or by dial-up connection. The Transfer menu option "Capture Text" will allow to user to log the retrieve session. The Windows95 program Telnet will allow the user to make a network connection to the station (either a LAN or Ineternet connection). The Terminal menu option "Start Logging" will allow the user to log the retrieve session.

Once the user is connected to the station computer, the retrieve session will be the same no matter what method was used to connect to the computer. The following is an example of a retrieve session to request SAC ascii data. The session is annotated with comments delimited by asterisks (*comment*):

OS-9/68K V2.4 Motorola VME147 - 68030 97/10/03 19:52:49

User name?: seed *Enter seed for the User name*
Password: *Enter data - the Password will not be displayed*
Process #29 logged on 97/10/03 19:52:53
Welcome!

WELCOME to the Global Telemetered Seismograph Network (GTSN) - DP

...please wait

Data Retrieval System / GTSN - DP / GT1X

Please type your name and organization - up to 50 characters:

sue mclafferty - asl *Enter your name and organization*

Data Retrieval System / GTSN - DP / GT1X

Copyright 1986-1994 by Joseph M. Steim & Quanterra, Inc.

Retrieve (C) 1986-1994 - Release 35/06-1213- 68020- FPU

type ? for help

Command? ? *Enter ? to display the help menu shown below*

Data Retrieval System / GTSN - DP / GT1X

Retrieve (C) 1986-1994 Quanterra, Inc. - Release 35/06-1213- 68020- FPU

"C <C/E>" = Change buffer from/to continuous/event data

"T <V/F/C/CS/S/P>" = select Transmission file format

"F <W/S/L/V...>" = select optional Filters

"E [ALL]/<DATE> <DATE> [<SEEDNAMES>]" = Examine available data or logs
 "S <SEEDNAME> <DATE>" = Setup single data channel to retrieve
 "G" = start or resume sending selected segment
 "G P[LOT]" = Plot selected segment on 4014 terminal
 "G <S/B>" = Store selected segment to local/backup file
 the following 4 methods are available for SEED binary transfer:
 "K <SEEDNAMES> <DATE> <DATE> [MAXREC] [TIMETOL]" = via Kermit
 "X <SEEDNAMES> <DATE> <DATE> [MAXREC] [TIMETOL]" = via STP
 "V <SEEDNAMES> <DATE> <DATE> [MAXREC] [TIMETOL]" = archiVe local file
 "I <SEEDNAMES> <DATE> <DATE> [MAXREC] [TIMETOL]" = via uuencode
 "R" = send station description
 "L[|B|C] [ALL]" = view entries in event, caliB, or Clock Log
 "P" = display active Processes
 "U <N>" = view User log <N> entries backward
 "Y[T] <N> [<M>]" = view [<M>] activitY log <N> entries backward
 "M <message text>" = send Message to station operator
 "Q" = Quit on-line session. CTL-"C" is ABORT key.
 <SEEDNAMES> supports wildcards (i.e. BH?,?LZ,???) and DET|CAL|TIM|MSG

Command? t *Enter t to select the transmission format*

Possible transmission formats are:

"C" - Compressed hexadecimal ascii
 "CS" - Compressed hexadecimal ascii SEED
 "V" - Expanded variable record length ascii
 "F" - Expanded fixed record length ascii
 "S" - SAC ascii digital counts
 "X" - Exit to main command menu

Transfer mode? s *Enter s to select SAC ascii digital counts*

Current transmission mode is SAC ascii

Transmit card numbers with each line of data? (y/n): n *Enter n for no*
 card numbers

Command? s bhz 97/10/2 1:00:00 *Select the channel and start time for*
 data retrieval

...scanning available channels

Search requested starting at 1997/10/02 01:00:00

Time window begins in segment 4 at buffer record 14419

Maximum number of samples to transfer? 25 *Select number of samples*
 limit=10000 samples

Buffer server is processing your request

skipping first 1759 samples...

transmission will begin at requested starting time within -0.009113 sec

...event detector on in record starting at 1997/10/02 00:58:32

Use the "G" command to begin transmission
or to re-transmit data received incorrectly.

Command? g *Enter g to transmit the data*

Start (31) and end (35) cards to transmit?<CR> *Enter <CR> for all cards*

```

0.0500000 -12345.0000000 -12345.0000000 -12345.0000000 -12345.0000000
-0.0091130 1.1908870 0.0000000 0.0000000 2.0000000
-12345.0000000 -12345.0000000 -12345.0000000 -12345.0000000 -12345.0000000
-12345.0000000 -12345.0000000 -12345.0000000 -12345.0000000 -12345.0000000
-12345.0000000 -12345.0000000 -12345.0000000 -12345.0000000 -12345.0000000
-12345.0000000 -12345.0000000 -12345.0000000 -12345.0000000 -12345.0000000
-12345.0000000 40.5800018 -122.5400009 300.0000000 -12345.0000000
-12345.0000000 -12345.0000000 -12345.0000000 -12345.0000000 -12345.0000000
-12345.0000000 -12345.0000000 -12345.0000000 -12345.0000000 -12345.0000000
-12345.0000000 -12345.0000000 -12345.0000000 -12345.0000000 -12345.0000000
-12345.0000000 -12345.0000000 -12345.0000000 -12345.0000000 -12345.0000000
-12345.0000000 -12345.0000000 -12345.0000000 -12345.0000000 -12345.0000000
-12345.0000000 -12345.0000000 0.0000000 0.0000000 -12345.0000000
-12345.0000000 -12345.0000000 -12345.0000000 -12345.0000000 -12345.0000000
-12345.0000000 -12345.0000000 -12345.0000000 -12345.0000000 -12345.0000000
1997 275 1 0 0
0 6 0 0 25
-12345 -12345 -12345 -12345 -12345
1 1 11 -12345 -12345
-12345 -12345 40 -12345 -12345
-12345 -12345 -12345 -12345 -12345
-12345 -12345 -12345 -12345 -12345
1 1 1 1 0

```

GT1X H972750100ZVBB

```

-12345 -12345 -12345
-12345 -12345 -12345
-12345 -12345 -12345
-12345 -12345 -12345
-12345 -12345 -12345
-12345 -12345 -12345
-12345 -12345 -12345
2649.0 2649.0 2649.0 2649.0 2649.0
2650.0 2649.0 2649.0 2650.0 2649.0
2649.0 2649.0 2650.0 2649.0 2649.0
2649.0 2649.0 2649.0 2649.0 2649.0
2650.0 2649.0 2650.0 2649.0 2649.0

```

Command? q *Enter q to quit the retrieve session*

...normal termination

...vbb data retrieval system logged out

IMPORTANT NOTE: Do not close the Hyperterminal or Telnet window before entering "q" to quit the retrieve session.

Once disconnected from the computer, the user should close the log session file. Depending on the analysis application, the file will probably need to be edited to remove all extraneous command lines (non-data).

The following is an example of expanded variable length ascii format data:

```
GT1X 1997/10/02 01:00:00 -0.009113 SEC Z VBB 20.00 SPS UNFILTERED 25
```

```
2649 2649 2649 2649 2649 2650 2649 2649 21193
2650 2649 2649 2649 2650 2649 2649 2649 21194
2649 2649 2649 2649 2650 2649 2650 2649 21194
2649 0 0 0 0 0 0 2649
```

The following is an example of the expanded fixed length ascii format data:

```
GT1X 1997/10/02 01:00:00 -0.009113 SEC Z VBB 20.00 SPS UNFILTERED 25
```

```
2649    2649    2649    2649    2649    13245
2650    2649    2649    2650    2649    13247
2649    2649    2650    2649    2649    13246
2649    2649    2649    2649    2649    13245
2650    2649    2650    2649    2649    13247
```

3. HOW TO RETRIEVE SEED DATA

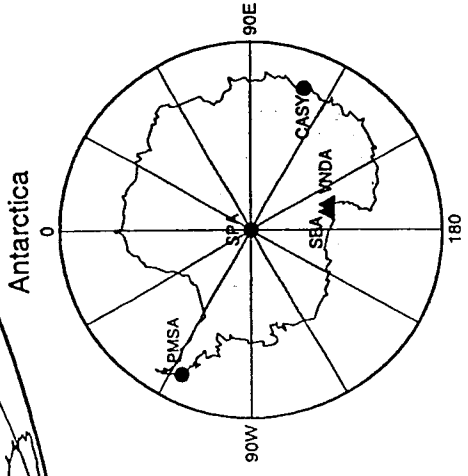
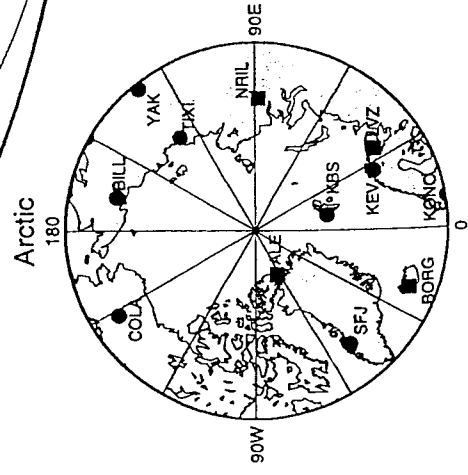
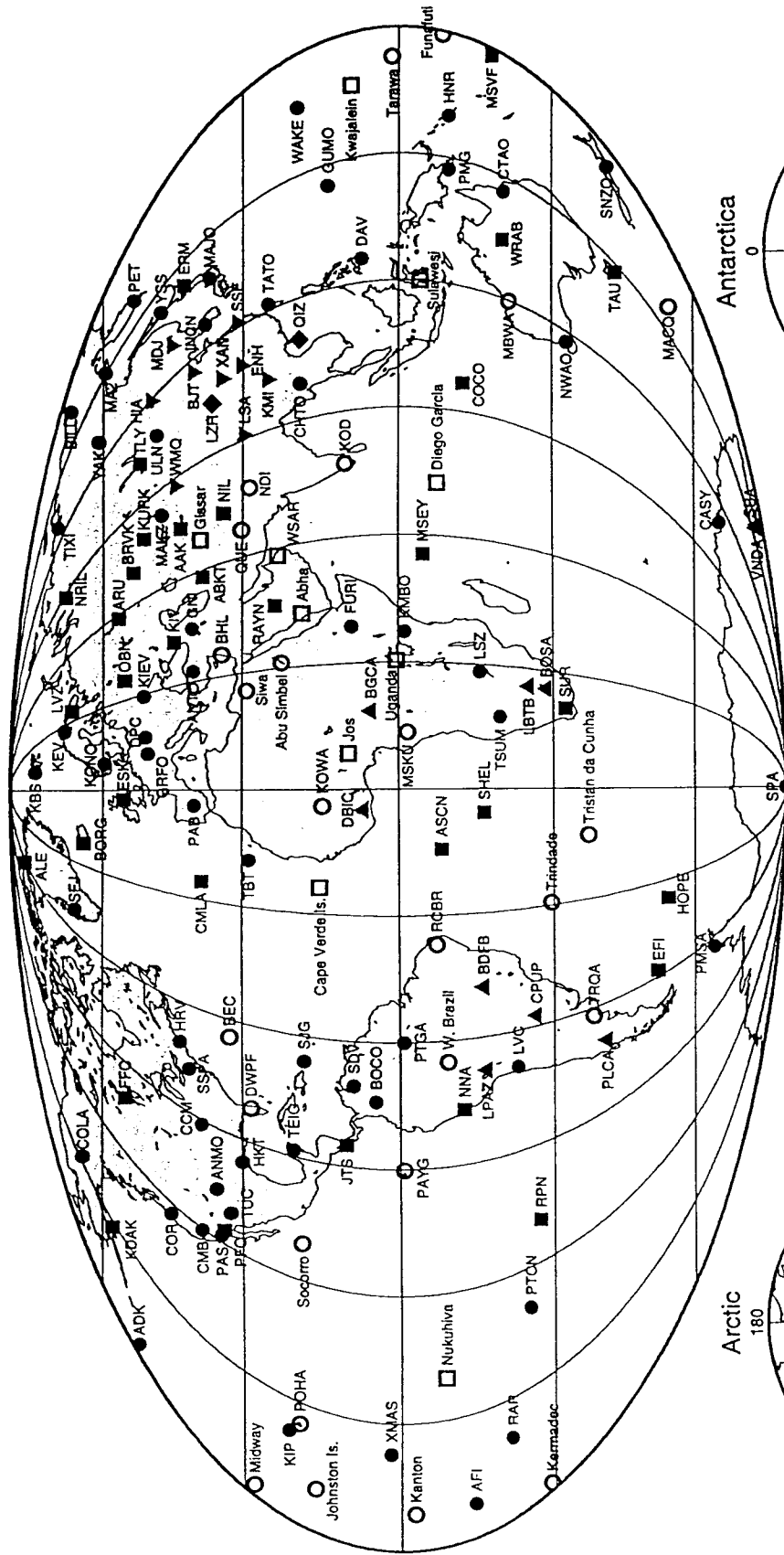
Since SEED data is in binary rather than ascii format, the procedure to log a retrieve session will not work. Two of the available procedures entail making a file on the IRIS/USGS computer and then transferring the file

For data requests using a direct serial connection or dial-up connection, the Windows95 program Hyperterminal will allow the user to connect to the station computer. The retrieve program option "K" is used to generate a file which is then transferred to the analysis computer using Kermit protocol. See the "Procedure to retrieve data using Kermit" in the DIMAS (Display, Interactive Manipulation and Analysis of Seismograms) operations manual for the details.

For data requests using a network connection, the telnet program will allow the user to connect to the station computer. The retrieve program option "V" is used to create an archive local file. The program ftp (on the analysis computer) is used to transfer the file to the analysis computer and delete the file from the IRIS/USGS computer. See the "Procedure to create and copy a SEED data file via the network" in the DIMAS manual for details.

If the user is running the DIMAS software on the analysis computer, the DIMAS program NETRD will also allow the user to retrieve SEED data using a network connection. This is the preferred method as it does not create files on the IRIS/USGS computer disk.

Global Seismograph Network



- installed 60 ● 26 ○
- planned 9 ▼ 10 ▲
- IRIS/USGS Stations 33 ■ 2 ◆
- NCDSN Stations (IRIS/USGS)
- GTSN Stations (AFTAC/USGS)
- IRIS/IDA Stations (UCSD)
- CDSN Stations (China/USGS)

USGS Albuquerque Seismological Laboratory
September 1997 (RLW/CRH)

Station Phone numbers and Internet Addresses

A phone line or internet connection enables many IRIS/USGS Global Seismic Network stations to provide users data recorded within minutes of a data request. The table below contains the current phone number and/or internet addresses available for digital data retrieval from IRIS/USGS GSN stations. The Data Collection Center updates the table whenever changes or additions occur.

Contact the Data Collection Center, webmasters@asl.cr.usgs.gov or (505) 846-5646, for information regarding accounts and passwords for data retrieval from stations.

The most recent change to the table occurred on 2 Sep 1997, 11:27:13 MDT.

Station	Location	Phone Number	Internet Address	Notes
ADK	Adak, Alaska	907-592-3724	-	-
AFI	Afiamalu, Western Samoa	685-27-028	-	-
ANMO	Albuquerque, New Mexico	505-846-0384	anmo.cr.usgs.gov	-
ANTO	Ankara, Turkey	90-312-210-1273	-	-
BILL	Bilibino, Russia	4217-62-25742	-	NOTE: limited success with the dialup at present time.
BOCO	Bogota, Colombia	5-71-338-4537	200.3.149.8	-
CASY	Casey, Antarctica	672-12-846	-	-
CCM	Cathedral Caves, Missouri	314-245-6555	-	-
CHTO	Chaing Mai, Thailand	66-53-220-506	-	-
COLA	College, Alaska	907-474-5913	cola.giseis.alaska.edu	-
COR	Corvallis, Oregon	541-737-0853	-	-
CTAO	Charters Towers, Australia	61-7-3365-2374	ctao.seis.uq.edu.au	-
DAV	Davao, Philippines	63-82-97-1290	-	-
GNI	Garni, Armenia	-	194.67.210.253	-
GUMO	Guam, Marianas Islands	671-637-4647	202.128.5.75	-
HNR	Honiara, Solomon Islands	677-25-165	-	-
HRV	Harvard, Massachusetts	508-456-3099	hrv.harvard.edu	NOTE: The telnet connection is not working at this time.
HKT	Hockley, Texas	512-346-3292	129.116.194.225	-
INCN	Inchon, Republic of Korea	82-273-46988	incn.kma.go.kr	-
KBS	Ny-Alesund, Spitzbergen	47-79-027129	193.156.10.249	-

KEV	Kevo, Finland	358-16-678550	-	-
KIEV	Kiev, Ukraine	380-41-222-7206	-	-
KIP	Kipapa, Hawaii	808-689-7413	140.90.183.151	-
KMBO	Kilima Mbogo, Kenya	254-2-445896	-	-
KMI	Kunming, Yunnan Province, China	86-871-5212583	-	NOTE: limited success with the dialup at this time
KONO	Kongsberg, Norway	47-55-32-6101	kono.ifjf.uib.no	-
LSA	Lhasa, Tibet, China	86-89163-39567	-	-
LSZ	Lusaka, Zambia	260-1-250-774	-	-
LVC	Limon Verde, Calama, Chile	56-55-322-407	165.182.34.175	-
MAJO	Matsushiro, Japan	81-262-78-9393	-	-
MA2	Magadan, Russia	7-413222-0154	194.87.56.194	-
MDJ	Mudanjiang, China	86-453-652-8858	-	-
NWAO	Narrogin, Australia	61-9-295-2880	-	-
PAB	San Pablo, Spain	34-2-541-6132	-	-
PET	Petropavlovsk, Russia	7-415-22-59136	195.9.105.45	-
PMG	Port Moresby, New Guinea	675-326-0864	-	-
PTGA	Pitinga, Brazil	55-92-723-1194	-	-
RAR	Rarotonga, Cook Islands	6-82-27-446	-	-
SDV	Santo Domingo, Venezuela	57-61-840	-	NOTE: The dialup does not work presently, this may be problem with local telephone company VSAT.
SFJ	Sondrestrom Fjord, Greenland	299-113-69	-	-
SJG	San Juan, Puerto Rico	787-263-5934	-	-
SNZO	South Karori, New Zealand	64-4-472-3833	131.203.44.28	-
SPA	South Pole, Antarctica	-	199.4.250.15	NOTE: The satellite is only visible for about 6 hours a day - expect a large failure rate.
SSE	Sheshan, Shanghai, China	86-21-57654170	-	-
SSPA	Standing Stone, Pennsylvania	814-667-4486	-	-
TSUM	Tsumeb, Namibia	264-672-20717	-	-
TATO	Taipei, Taiwan	886-2-783-9920	140.109.80.44	-

TBT	Taburiente, Canary Island, Spain	34-22-24-4679	-	-
TIXI	Tiksi, Yakutia, Russia	7-41167-53434	-	NOTE: Dialup is currently inoperative
TUC	Tucson, Arizona	520-621-1733	-	-
ULN	Ulanbatar, Mongolia	-	202.131.1.100	-
WAKE	Wake Island	808-424-2148	-	-
WMQ	Urumqi, Xinjiang Province, China	86-991-2625262	-	-
XAN	Xian, China	86-29-5954447	-	-
YAK	Yakutsk, Russia	7-41122-6-28-21	194.87.244.5	-
YSS	Yuzhno Sakhalinsk, Russia	75-0441-62518	193.124.51.66	-

SEISMIC NETWORK PLANNING, PROCUREMENT, INSTALLATION, ORGANISATION, AND TUNING

Amadej Trnkoczy

Kinematics SA, Z.I. Le Trési 3
CH-1028 Préverenges, Switzerland

1. INTRODUCTION

In the last two decades of the 20th century, several developing countries have set numerous seismological projects into motion. Unfortunately, viewing many of them from the end of the 1990s, one must realise that many have not fulfilled the expectations. As to the reasons that would adequately explain this situation, probably the greatest factor is the shortage of seismometry knowledge in the developing countries that began these projects. Yet such specialised knowledge is unquestionably required if one expects to establish and operate a truly beneficial seismic network. Misunderstandings of the process of establishment of a new network and unrealistic expectations have led quite a few seismic network purchasers to disappointments.

Purchasing seismic equipment is neither the first nor the last step necessary to establish an effective seismic network.

It is clear that every newcomer in seismometry, as well as every serious manufacturer of seismic equipment wants the purchased system to operate at the best benefit for the community. For that reason this document will outline the following to the less experienced:

- procedures for establishing a seismic network,
- criteria for a proper allocation of the available finances among all the various tasks essential for establishing and operating a successful seismic network, and
- some conceptual and technical aspects of seismic system selection which several less experienced purchasers have neglected or have been unaware of.

2. PLANNING AND FEASIBILITY STUDY

2.1. Goal-setting and feasibility study

The very first step toward establishing a new seismic network is understanding and setting the network's goals. These goals can differ significantly. The same applies to the seismic system requirements. One will not have an optimal system unless one clearly defines the projects unique goals.

Just as each country has unique seismicity, seismo-tectonic and geological formations, so every seismological project has unique contextual combinations that one must consider in order to find the optimal system design for that project.

Accordingly, several issues must be addressed:

- the main purpose of setting up a network, usually either monitoring a region's general seismicity; or to perform special studies (monitoring of special seismo-tectonic features, of important civil engineering structures, chemical or nuclear explosions, man-induced seismicity, etc.)
- the purchaser's interest in ranked order in: local seismology (epicentral distances < 140 km), regional seismology (epicentral distances between 140 and 2.000 km), and/or global seismology (epicentral distances > 2.000 km)
- relative importance to the project: of the network's alarm function for civil defence purposes; of the seismological research aimed at either the long-term mitigation of the country's seismic risk; and/or at the scientific research of the Earth's deep structure.

Many countries that have little or no seismic equipment first consider buying a system to monitor the region's general seismicity. With good arguments they expect the new system to help mitigating the region's seismic risk over a longer period. Nevertheless, even for a project of such well-defined scope, several questions must still be answered. Country's needs as well as countries financial, personal, and infrastructural abilities must be realistically assessed:

- how big is the country or region to be monitored?
- what is the seismicity level in the country or region?
- what is the country's existing level of seismology and seismometry knowledge, and considering the country's financial and academic realities, what are its resources for improving that knowledge?
- how developed is the country's infrastructure, particularly in telecommunications?
- how much is the country willing to pay, per year, long term, to operate the system, and to support research work using the recorded data?
- how much is the country willing to pay to establish the system?

Having realistically quantified the above facts, one can then begin 'shopping' for a seismic system that meets those criteria. This is always a trade off between desires and reality. This procedure ensures that the new network will perform successfully in the existing environment, if carried out realistically.

If there are few or even no seismology experts employed in the country, definitely get help from seismic equipment business independent consultants in the international academic world. In this early phase, focus on your country's specific socio-economic needs and seismic-awareness, and do not worry too much about specific equipment. In the later phases of network establishment,

contact also sales and system engineers from seismic-equipment manufacturers, who can help you defining the technical details of your system.

2.2. Realistic awareness of finances

Often newcomers in seismometry do not know how to allocate the finances in a way that the network would gain optimal effectiveness. Too often they spend majority of their seismic network funds purely on buying equipment (boxes), even though an identically important expenditure is to make sure it meets the conditions for proper operation of this complex equipment. To make sure one has correctly prepared for the purchase of seismic network equipment, one's budget must include money for:

- a feasibility study that examines potential network layouts, site selection, and potential seismic systems,
- preparation of a remote station and a central recording site,
- purchase of the network equipment,
- payment of manufacturer's services such as installation, training, maintenance, and long term support,
- new scientific and technical personnel usually required and their training,
- network operating costs (personnel, data transmission cost, consumables, and spare parts), and
- network technical servicing and maintenance cost.

The five figures on the following pages show examples of funding apportionment among several different already established seismic network projects. The numbers in the figures show the amounts allocated to different tasks (normalised per single station), both in thousands of US dollars and as a percentage of the project's total cost.

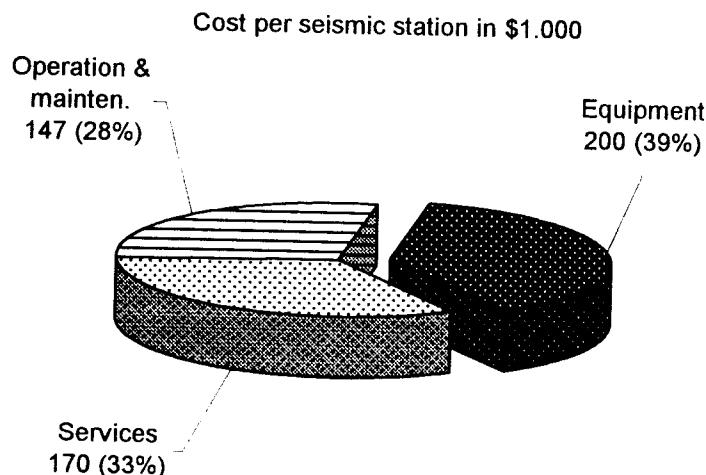


Fig 1: Cost distribution of establishment and 5-year operation of global seismic network (GSN).

Figure 1 shows an approximate cost distribution (per station) for establishing and operating the global seismic network (GSN) during five years according to IRIS plan 1990-1996 (IRIS consortium is composed of about 70 leading universities in USA with research program in seismology). Not only did this network use the most demanding and expensive equipment available, also expensive site preparations and world-wide maintenance were often required which increased costs per station.

Figure 2 shows details of the IRIS GSN system's establishment costs (excluding all operational costs; again, costs are averaged per station). Cheaper surface vault seismic stations are considered only. IRIS constructed many of the sites as deep expensive bore-hole installations. Even if they are not taken into account in this figure, IRIS still allocated substantial funds for the vaults and to tasks other than equipment-buying.

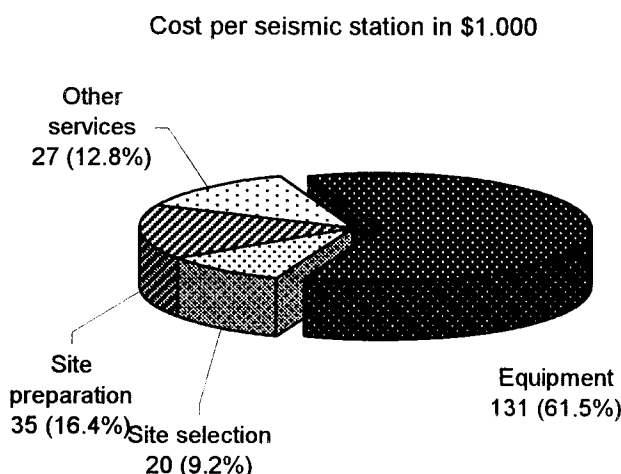


Fig. 2: Cost distribution of establishment of IRIS GSN surface vault seismic stations.

Figure 3 shows a distribution of the finances, which a developing country spent to establish a reasonably large seismic network, using analogue RF telemetry. The country's significant investment in services (21.6%) paid for training at the factory and during installation, as well as one year of the manufacturer's full-time engineer support led to the successful start and operation of this network.

Figure 4 shows a negative example of cost distribution, for a small, yet technologically demanding seismic network. Note the small amount invested into tasks other than equipment-buying. Particularly the site preparation works; 4.1% is surely not sufficient, making it difficult to believe that these sites could provide ample working conditions for such demanding sensors as very broad band (VBB) STS-1 and STS-2 seismometers. The relatively high amounts spent for services (9.3%) came mostly because the purchasers desired a turn-key type of system. With no experiences in seismometry, the chances of efficiently using the installed equipment seem small.

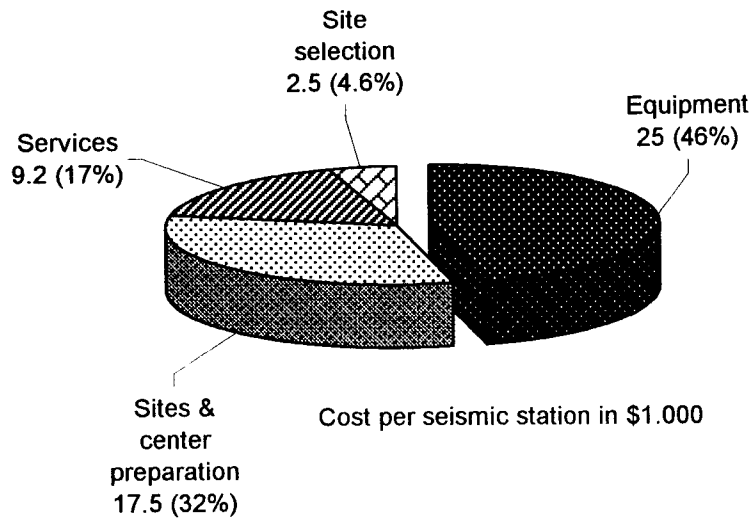


Fig. 3: Cost distribution of a relatively large national seismic network with 20 SP seismic stations, strong-motion instrumentation, and analogue FM telemetry.

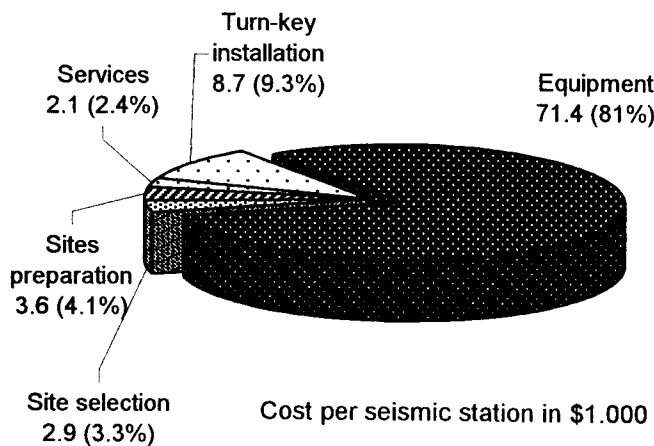


Fig. 4: Cost distribution of a small, technologically high-end seismic network with an inappropriate allocation of funds.

Figure 5 shows another example of a large seismic network - a national, high-end technology, duplex-digital telemetry system - installed in a large country. But again, despite the network's size, the most modern equipment, and the central recording equipment for two centres, the country only invested about 60 % of its total project funds in the equipment. The other half of the money was spent on follow-up services, including a great deal of training and two years of full-time engineer support provided by the equipment's manufacturer.

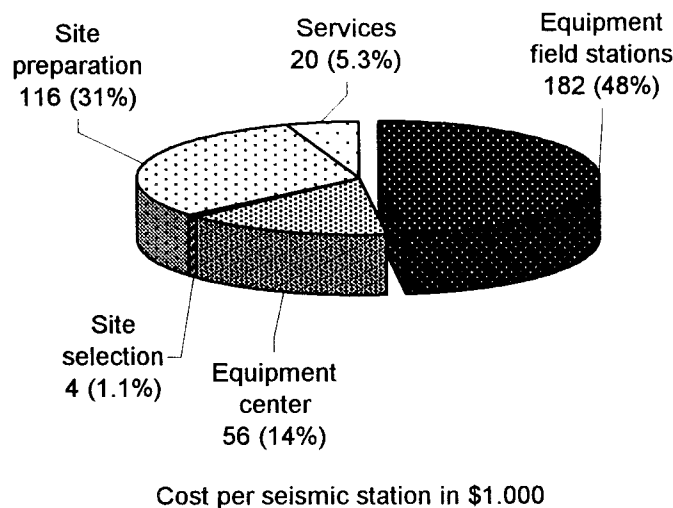


Fig. 5: Cost distribution of a very large national, high-end technology, duplex-digital RF and phone line telemetry seismic network with two recording centres.

The funding distributions shown in Figures 1 through 5 are approximate and for illustration purpose only. Actual conditions (including the type of network, the level of existing local technical knowledge, local labour prices, and the type of seismic site preparation works), will change from country to country, thus significantly influencing dispersion of the funds. But despite deviations and the differences in absolute cost, these figures seem to indicate that the percentages of the total cost for each task remain in the similar proportions from network to network. The main message of these figures is the same:

**Do not spend nearly all of the allocated funds for buying equipment!
 Save at least one-third of the money for feasibility study, for site selection, for establishing of the proper working conditions, and for gaining seismic expertise necessary to fully exploit the equipment.**

2.3. Basic system engineering parameters

Once the goals are clear and the funds are properly allocated, one has to clarify the entire project's interrelated seismological and technological aspects. One should pay attention to:

- the size and the layout of the proposed seismic network (this should affect the choice of the type of transmission links for transmission of seismic data from the remote stations to the centre),
- the seismicity level to be monitored - in other words, the amount of data one will deal with (this should effect data transmission equipment, central processing site's real-time and off-line capabilities, whether the system will need continuous or triggered data recording capabilities, if and what type of the trigger algorithm it will use, the type of data archive system; this should also affect one's choices of the equipment's weak-motion versus strong-motion partitioning),

- how accurate one wants the network's event determination to be (this should effect the number of stations and the network's layout),
- how wide a dynamic range and resolution are desired for the data acquired from the network, (this should influence the choice of technology for data acquisition, as well as the sensor type and data-logger designs),
- the importance of the new system having alarm capabilities for civil defence purposes and the expected response time (this should influence which data-transmission links will be chosen, as well as how much real-time processing power will be needed at the central recording site),
- the amount of technical reliability one expects from the system (this should affect the choice of data transmission links, how much hardware-system redundancy one can afford, like auto-duplicating memory drives, double computers, etc., as well as decision between 'office-grade' and industrial grade computers),
- the desired robustness of the system in terms of functioning throughout damaging earthquakes (this should influence the selection of data-transmission links, of power back-up utilities for the remote stations and the central recording site, and last but not least, of seismic risk safe civil-engineering designs for the building of the central processing site).

After reasonably assessing these aspects and making a decision for each unique situation, one can then choose a coarse system engineering approach and begin selecting equipment which best matches one's idealised needs. Obviously everybody, almost certainly, has to agree to certain trade-offs.

2.4. Determining the network's layout.

Determining a layout for one's seismic network requires two steps:

- articulating one's preferred estimates for the number of stations and their approximate positions, and
- determining the exact final station sites for the actual installation.

Since the first stage closely relates to the goals of the network and available funds, the purchaser of the network should carry it out, delineating how many stations he wants and can afford to set up and where approximately he would locate them.

Since the second stage typically requires knowledge of seismometry, seismo-geology, and data transmission technology (if applicable), and good knowledge of seismic equipment capabilities and limitations, the customer may want to have it performed by the manufacturer of the network.

2.4.1. Number of stations in the network

The number of seismic stations should be based on the goals of the network, on the size of the region of the network, and, of course, on the available funding. For space reasons we will not go into details on the minimum number of stations that are technically required for a given seismological goal, but here is a short overview:

For determination of an event location (based on phase readings), the theoretical minimum is three to four stations (depending on whether one also wants to determine the event depth). However, remember that such results, due to their uncertainty, usually have little value. For a more-accurate determination of location, six stations acquiring good records of an event should provide scientifically credible evidence of an event's location, and ten to fifteen stations acquiring good-quality records of an event should provide an acceptable basis for more-sophisticated studies of the earthquake's source parameters. A waveform analysis of digital, high dynamic range, three-component records leads to good results with lesser stations.

Larger countries or regions will require a greater number of stations, of course - unless their interest is only in the strongest earthquakes. Note that seismic researchers do not care much about the total number of stations in a network; what counts is the number of stations in the network that adequately record a given event ('record' meaning that they trigger data acquisition and the records have large enough signal-to-noise ratio). In large regions, long epicentral distances often prevent the triggering of distant stations, or the earthquake signals get buried in the seismic noise. Thus the total information available for a given event, unless strong one, typically comes from only a portion of the total network.

2.4.2. Seismic network layout geometry

Although the spatial distribution of the stations in a seismic network is very important for the network's capabilities of event determination, for space reasons we will only give some very brief recommendations.

On a map, subdivide the region to be monitored into a series of reasonably irregular triangles having approximately equal areas. Avoid too narrow and long triangles. Avoid thinking in rigid patterns, locating the stations into perfect triangles, circles or straight lines, because such rigidity may result in "blind spots" - that is regions with poor event-location determination (note: seismic arrays are not discussed here.) The corners of these triangles are the approximate points where one will try to locate seismic stations. Take into account any existing seismic stations in neighbouring countries or regions as well. If there are none, push some of seismic stations as close as possible to the borders of the region being monitored.

Have realistic expectations concerning the earthquake depth determination based on phase readings. Here is the rule of thumb for a reliable depth determination. First, we need to estimate the average depth of the earthquakes in the network's region. Then make sure that the average distance between stations in the seismic network does not exceed twice that average event depth. The latter is admittedly a tough requirement, especially in the large regions and in the regions where the events are typically shallow! Only a few small countries and practically none of the larger countries can afford such a dense network.

Yet one can still temporarily afford to make the network denser in places. Buy a few portable seismic stations, and then temporarily install them in any sub-region of particular interest at the time. For example, such temporal networks are regularly established in the epicentral region right after a strong event to perform aftershock studies. At least for a time, this will drastically increase the seismic network's density in the region of interest, allowing much better detectability and locations, including depth, and more detailed studies.

Have realistic expectations also about the system's earthquake epicenter determinations. For events outside the seismic network, expect large errors in determining their epicenters. Generally, do not expect reliable determination of events, unless the "seismic gap" (the largest of all angles among the lines connecting a potential epicenter with all the stations in the network, which recorded the event) is more than 200° . Thus, to increase the accuracy of epicenter determinations,

especially for the events outside the seismic network, one needs to include data in the analysis from seismic stations in neighbouring countries, as well as from any other available national or international sources. Acquiring this wider database is nearly necessary for determining reliable event locations on the border and outside any seismic network.

3. SELECTING THE RIGHT SYSTEM

In this chapter only a very brief description of seismic systems will be given with the aim to help the very beginners in seismometry. It is intended to provide an overview on basic ideas in seismometry and describe the existing possibilities on the market. Much more thorough information about particular elements of a seismic system and concepts in seismometry may be found elsewhere.

3.1. Seismic sensors

The most important factors in selecting seismic sensors suitable for a particular application are:

- the type of the sensors - accelerometers versus seismometers,
- the number of sensor components per seismic station,
- the sensor's sensitivity, and
- the sensor's frequency range of operation.

3.1.1. Seismometers and/or accelerometers?

The new network purchaser will need to decide whether weak-motion sensors - seismometers or strong-motion sensors - accelerometers, or a combination of both types of instruments are best suited to his needs. Note that, in the high seismic-risk countries and in the networks whose main goal is future seismic risk mitigation, strong motion instrumentation plays a very important role. During most damaging earthquakes, weak motion records recorded with seismometers installed close to the epicentre are usually clipped. This is much less true for modern high dynamic range seismic data recording compared to old analogue recording, however, it still remains a relevant issue. For large regional or national projects, a portion of the budget should be set aside for strong motion equipment, which, if properly selected, will never be clipped.

Although there are significant technical differences in strong and weak motion network designs, both types of sensors are nowadays frequently integrated into a single system. Six-channel data loggers with three weak and three strong motion channels are a state of the art product and very cost effective choice of today. They are capable of covering the whole dynamic range of seismic events, down from seismic noise to the biggest damaging events.

The relative merits of these systems, as well as specific technical details of strong motion networks are not addressed in this document.

3.1.2. One-component and three-component seismic stations

Historically, many seismic stations and networks used single component sensors - usually vertical seismometers. Many of them still operate. This had been the case because the equipment

was analogue and required paper-recording for seismic data. If three components were used, then exactly three times more equipment was required but three times more valuable information was not gathered. It was also very difficult, if not impossible, to generate a vector of ground motion from three separate paper seismograms.

Today, in the era of digital recording and processing of seismic data, the situation is different. The price/performance ratio is much more favourable for three-component stations. Most data recorders and data transmission links are capable of accepting at least three channels of seismic data. The costs for upgrading the central processing facilities for an increased number of channels due to three-component sensor are relatively small. Generating vector-of-ground-motion is easy with computers.

Since ground motion is essentially a vector containing all seismic information, and considering the fact that many modern seismological analyses require this vector as input information, one component stations are no longer a sensible choice for new installations. Only very rarely can a one-component seismic station be of real use.

3.1.3. Sensitivity of seismic sensors

Strong motion accelerometers are relatively insensitive since they are designed to record the strongest events at small hypocentral distances. Their maximal acceleration measuring range is usually expressed in g-s. However, modern accelerometers will produce valuable records of smaller events within epicentral region as well, where seismometer records may still be clipped. Accelerometers with 0.25, 0.5, 1, 2, and 4 g full-scale sensitivity are available today. One should, of course, order full-scale sensitivity, fitting to the maximal expected acceleration at the sites of the new network. Ordering too sensitive accelerometers may result in clipped records of the strongest and most important events in the region. Installation of accelerometers with too high full-scale range causes diminished sensitivity and needlessly reduces data acquisition resolution of all future records.

Weak motion sensors - seismometers - are usually orders of magnitude more sensitive. They can record very weak and/or very distant events, which produce ground motion of comparable amplitudes to natural seismic noise. Some seismometers can measure ground motion smaller than the amplitudes of the lowest natural seismic noise found anywhere in the world. Their sensitivity is from hundred to several thousand V/m/s. If one plans to purchase very sensitive sensors, he must be willing and able to find the appropriate low seismic noise sites for their installation. If the sites are not appropriately chosen and have high seismic noise (natural and/or man made), this very high sensitivity of the modern seismometers is of little use.

3.1.4. Frequency range of seismic sensors

Today's weak motion sensors are roughly divided into three categories:

- the short-period (SP) seismometers that measure signals from approximately 0.1 to 100 Hz, with corner frequency around 1 or 2 Hz and flat, ground velocity proportional output above this corner frequency (a typical example: Kinematics' SS-1 seismometer with a corner frequency at 1 Hz and flat response up to 100 Hz),
- the broadband sensors (BB) with flat ground velocity proportional response from approximately 0.01 to 50 Hz (a typical example: Guralp CMG40T seismometer with frequency range from 0.03 to 50 Hz),
- the very broadband seismometers (VBB) measuring frequencies from below 0.001

Hz to approximately 10 Hz (a typical example: Streckeisen STS-1 seismometer with frequency range from 0.0028 to 10 Hz). By definition, they should be able to resolve Earth tides.

The frequency limits shown above are the corner frequencies of sensors' frequency response function. This means that analysis below low-frequency and above high-frequency corner is still possible to some extent. How much we can extend this range depends on the sensor design, instrumentation noise, and, in many cases, on seismic noise conditions at the seismic station site.

The choice of the right sensor depends on its seismological application. In general, the flat portion of frequency response function (FRF) should cover the range of frequencies, which are generated by particular seismic events of interest or which are important in a particular phenomenon studied.

The strong motion sensors (accelerometers) measure seismic signals between DC to up to 200 Hz (a typical example: Kinematics EpiSensor from DC to 200 Hz). However, they differ from the weak motion sensors in their output voltage, which is proportional to ground acceleration and not to ground velocity as it is usual for seismometers.

Some strong motion sensors in the market have no DC response but a low frequency high-pass corner at around 0.1 Hz. These sensors have an important drawback: their records can hardly be used for residual displacement calculations, either of the ground in the near field of very strong earthquakes, or of the permanently damaged civil engineering structures after strong events. They are considered as less appropriate for seismic applications where low frequency signals are also important.

The following table should help in selection of appropriate sensors. It shows some typical seismological applications and their approximate frequency range of interest.

Application description and approximate frequency range of interest	from [Hz]	to [Hz]
Seismic events associated with mining process	5	2,000
Very local and small earthquakes, water pond induced seismicity	1	100
Local seismology	0.2	80
Strong motion applications	0.0	100
General regional seismology	0.05	20
Frequency dependence of seismic wave absorption	0.02	30
Energy calculations of distant earthquakes	0.01	10
Scattering and diffraction of seismic waves on core boundary	0.02	2
Studies of dynamic process in earthquake foci	0.005	3
Studies of crust properties	0.02	1
Dispersion of surface waves	0.003	0.2
Free oscillations of the Earth, silent earthquakes	0.0005	0.01

3.1.4.1. SP seismometers

The SP sensors (as well as long period LP seismometers), called also the "narrow-band" sensors, were historically developed as 'mechanical filters' for mitigating distracting natural 0.2 - 0.3 Hz seismic noise peak which heavily blurred small seismic signals on paper seismograms. However, with today's digital and high-resolution data recording and processing, this rigid 'hardware filtering' can easily be replaced by much more flexible computer processing. A need for sensors that filter seismic signals by themselves does not exist any more. In addition, when filtering seismic signal with sensors, we irreversibly lose a portion of seismic information and we introduce undesired signal phase distortion.

Nevertheless, the SP seismometers are still, and will remain in the future, a valid selection for several seismological applications, particularly for local seismology where low frequencies of seismic signal are not of major interest or do not exist at all.

Most SP seismometers are passive sensors and are therefore easy to install and operate. They require no power, which allows use of smaller back-up batteries for the rest of the equipment at remote station sites. They are relatively stable in a broad range of temperatures, which allows less exacting (and inexpensive) vault design. The electronic drift and mass position instability usually associated with active sensors are not a problem. They are, in short, a very practical solution for all applications where seismic signals of interest are not expected to contain significant components below 0.1 Hz.

3.1.4.2. Broadband seismometers

Today, the broadband sensors are a very popular choice. They provide complete seismic information from below 0.01Hz to 50 Hz and therefore allow a much broader range of studies than the SP records.

A single high performance BB seismic station can determine as much, if not more information as several conventional SP seismometers measuring arrival time and first motion.

However, the BB seismometers are significantly more expensive and demanding for installation and operation than SP seismometers. The BB seismometers require a higher level of expertise in regard to instrumentation and analytical methods. They are active feedback sensors and require a stable single or double polarity power supply. They also require very careful site-selection in a seismo-geological sense, better controlled environment in seismic vaults, and they are sometimes a bit "tricky" to install.

Since they do not attenuate 0.2 - 0.3 Hz natural seismic noise peak, their raw output signal contains much more seismic noise than signals from a SP seismometer. Consequently, small but useful seismic signals are often buried in seismic noise and can be resolved and analysed only after digital processing. In principle, their raw signals are not viewed directly in routine work but should be pre-processed to reveal their full content. A simple phase reading from broad band raw signal is far more difficult than phase reading from the traditional SP traces.

3.1.4.3. Very broadband seismometers

The VBB sensors are utilised in global seismology studies. They are able to resolve the lowest

frequencies, as they occur due to Earth tides and free oscillations of the Earth. Their primary purpose is the research of the deep interior of the Earth. Their only, however important, advantage, compared to the BB seismometers, is their ability to record frequencies around and below 0.001 Hz. They are expensive, require very elaborate and expensive seismic shelters, and are, as a rule, tricky to install. They are ineffective for seismic-risk mitigation projects and some also lack frequency response high enough for local/regional seismology.

However, data from a VBB station is very useful to the international scientific seismological community. It is also excellent for educational purposes. For a large national project, we recommend the installation of one VBB station, or perhaps two in a very large country or region. Such a station could serve as a very attractive "meeting point" with seismologists from the developed countries who can, through these contacts, transfer expertise and knowledge to a less experienced owner of a new seismic network.

Site selection and preparation for a VBB station requires extensive studies and often expensive civil engineering works. The cost of a single, good VBB site preparation works can sometime exceed \$100,000.

3.1.4.4. LP passive seismometers

The long-period passive sensors are not a suitable choice for new installations. These sensors are clearly inferior to the BB equivalents and more or less of historical value.

3.2. Seismic data acquisition

The two most important decisions about data acquisition system one will need to make are:

- digital versus analogue data acquisition and
- continuous versus triggered mode of operation.

The third technical decision is a choice of data transmission from the remote stations to the central recording facility. This will be briefly discussed in the next chapter.

3.2.1. Digital versus analogue data acquisition

There exist three primary types of seismic systems with respect to the technology of data acquisition: analogue, mixed, and digital.

3.2.1.1. Analogue seismic systems

The analogue seismic systems include analogue sensors, analogue signal conditioning, usually frequency modulated (FM) telemetry through radio (RF) or phone lines, analogue demultiplexers, and analogue drum recorders. Paper seismograms are the final result of a completely analogue system. The two primary drawbacks of such systems are:

Low dynamic range and resolution of data acquired (about 40-45 dB with single and about 60-65 dB with double, low-and high-gain data transmission channels) lead to modest completeness of seismic data. On one hand, many events are of too weak amplitude to be resolved on paper records and on the other hand, many records of strong events are clipped because their amplitude is too large to be recorded undistorted. In fact, only a very small "window" of the full dynamic

range of earthquakes that interest seismologists is actually recorded distortion-free.

Their second disadvantage is the incompatibility of paper records with computer analysis. This is a fatal drawback today because modern seismic analysis is almost entirely based on computer processing.

For these reasons such systems are no longer built.

3.2.1.2. Mixed analogue/digital seismic systems

Mixed systems, frequently erroneously called digital, have analogue sensors, analogue signal conditioning, FM telemetry, analogue demultiplexers, but digital data acquisition in the central recording site, digital processing, and digital data archiving.

Such systems also have a low dynamic range (FM data transmission links are the limiting factor) and therefore, they have the same disadvantage as the analogue systems regarding data completeness and quality. However, they can accommodate off-line as well as automatic near-real time computer analysis. One can use most modern analysis methods, except those, which require very high-resolution raw data. Such systems are still useful for some applications when the high dynamic range of recorded data is not of prime importance and the purpose of the seismic network is limited to a specific goal.

3.2.1.3. Digital seismic systems

In digital systems only the seismometers are analogue. All other equipment is digital. The dynamic range and the resolution are much higher than that of analogue and mixed type systems. It depends mainly - but not only - on the number of bits of analogue-to-digital (A/D) converters used in the digitizers. With converters available from 12 to 24 bit A/D today, the obtainable dynamic range is approximately from 72 to 140 dB. In practice, however, the total dynamic range and the resolution of data acquisition is usually somewhat less than the number of bits an A/D converter would theoretically allow. There are two known design principles that can further increase the dynamic range and/or the resolution of seismic data recording.

The gain-ranging method automatically adjusts the analogue gain of the system according to the amplitude of the seismic signal and thus prevents clipping of the strongest events. In this way, the dynamic range of data acquisition can be dramatically increased, however, the resolution remains roughly unchanged. Unfortunately, even modern electronics is imperfect and gain-ranging amplifiers induces 'gain-ranging errors' in the data. Therefore, the resolution of gain-ranged recording is actually decreased. These errors depend on data itself, which makes them hard to detect. For this reason, many seismologists are reluctant to use the gain-ranging systems. They have been mostly replaced by straightforward, multi-bit A/D conversion, which nowadays allows nearly as wide dynamic range.

The over-sampling principle is another approach, which helps improving the dynamic range and resolution of digital data acquisition. The data is sampled at a much higher rate than it is required in seismology and then the value of each sample of the final (lower sampling rate) output data stream is calculated by a statistical model. The increase in the resolution is significant. However, the efficiency of over-sampling depends on the ratio between the over-sampling frequency and final sampling rate of actual seismic data. The higher the final sampling rate used, the less benefit is gained from over-sampling. Therefore, for example, in local seismology, which frequently requires 200 Hz sampled data, the benefit of over-sampling is quite modest with some data logger designs.

Buyers of digital seismic networks from the developing countries often ask for additional paper drum recorders because they wish to 'continuously monitor' incoming signals and/or they believe drum recorders will serve as an excellent educational tool. However, there are a number of problems with paper drum recorders in digital systems. "Hardware-wise" they are fundamentally incompatible with digital systems. This requires additional digital-to-analogue converters. Being mechanical devices, they are and will continue to be expensive. They require continuous and specialised maintenance and consumables. On the other hand, nearly all modern observatory seismic software packages allow continuous observation of the incoming signals in (near) real time and some even simulate the traditional appearance of paper seismograms. In our experience, once the user becomes familiar with the digital system, expensive paper drum recorders soon prove to be of little use and come out to be a false investment. There is not much benefit in purchasing drum recorders with digital systems.

3.2.2. Continuous versus triggered mode of data acquisition

Continuous digitally acquired seismic signals by their very nature provide a huge amount of data. A reasonably sized digital weak motion seismic network operating in continuous mode will produce a volume of data so large that most people would find it implausible to store for any length of time. Yet, only a small portion of that data is in fact useful earthquake information.

This storage problem has frequently led seismic network users to operate their systems on a "triggered" basis (particularly the local and regional seismic networks that require a high frequency of data sampling). Triggered systems still do continuous, real-time acquisition and processing of seismic signals, but for trigger purpose only. They begin storing those signals only if the system's trigger algorithm recognises a seismic event. Such systems do not generate continuous time histories of seismic signals, but rather produce "event files".

However, the inexperienced users often do not sufficiently understand the data-producing limits of the triggered mode of operation of seismic networks, and many have felt disappointed at the results. Note that a decision between a continuous and a triggered mode of operation usually means a decision between a high network event-detectability and significantly reduced detectability. The difference in detectability is not small - approximately one event magnitude scale. And it easily becomes drastic if man-made seismic noise at the remote station sites is high due to poorly selected sites.

Note that:

Continuous seismic signal recording provides the most complete data, but storing and processing of all that data can become difficult, expensive, or even impossible. But systems in triggered mode will lose many weak events and produce a certain number of false triggers. The completeness of data is inevitably impaired because the efficiency of today's widely used trigger algorithms is far inferior to the seismologist's pattern recognition ability.

However the quality of data, recorded either in continuous or in triggered mode, is in both cases the same.

3.2.2.1. Trigger algorithm types

Triggered seismic systems can have various trigger algorithms:

- The amplitude threshold trigger simply searches for any amplitude exceeding a pre-set threshold. Recording starts whenever this threshold is reached. This algorithm is normally used in strong motion seismic instruments. That is in the systems where high sensitivity is not an issue, and where consequently man-made and natural seismic noise is not critical.
- The root-mean-square (RMS) threshold trigger is similar to the amplitude threshold algorithm, but the RMS value of the amplitude in a short time window is used instead of 'instant' signal amplitude. It is less sensitive to spike-like man-made seismic noise, however it is rarely used in practice.
- The short-time average through long-time average trigger (STA/LTA) is the most frequently used trigger algorithm in weak-motion seismology (cf. chapter *Understanding and setting STA/LTA trigger algorithm and associated parameters*). It continuously calculates the average values of the absolute amplitude of seismic signal in two consecutive moving-time windows. The short time window (STA) is 'sensitive' to seismic events, while the long time window (LTA) provides information about temporal amplitude of seismic noise at the site. When the ratio of both exceeds a pre-set value (usually set between 4 and 8), an event is 'declared' and data starts being recorded in a file. The STA/LTA trigger algorithm is well suited to cope with fluctuations of natural seismic noise, which are slow in nature. It is less effective in situations where man-made seismic noise of a bursting or spiky nature is present. At sites with high, irregular man-made seismic noise, the STA/LTA trigger usually does not function well.
- Several more sophisticated trigger algorithms are known from the literature. They are frequently used in seismic networks but rarely in the seismic data loggers currently on the market. In the hands of an expert they can improve the events/false triggers ratio over STA/LTA algorithm, particularly for a given type of seismic events. However, the sophisticated adjustments of operational parameters to actual signal and seismic noise conditions at each seismic site that these triggers require, has often been proven unwieldy and subject to error.

Every triggered seismic system must have an adjustable band-pass filter in front of the trigger algorithm. This is particularly important with BB seismometers where small earthquake signals are often buried in dominant 0.2-0.3 Hz seismic noise. The adjustable pass-band filter allows the trigger algorithm to be sensitive to the frequency band of one's most interest. In this way it allows that such events may still be resolved and acquired.

3.2.2.2. Stand-alone, coincidence triggered, and ring buffered systems

Trigger algorithms are generally implemented in two ways.

In seismic networks with stand-alone stations, each remote station has its own independent trigger. In such networks data is usually transferred to the central recording site on request-only or it is collected in-person. These seismic networks have the lowest effectiveness of triggering and consequently the smallest detectability and/or the highest rate of falsely triggered records. The completeness of data is modest because not all stations in the network trigger simultaneously for each event. This approach requires a good deal of routine maintenance work in order to "clear" numerous false records from the local data memory (if trigger thresholds are set low – if

not, the network has a lower detectability). Remote stations may come across 'memory full' problems because they evidently have a limited local memory. Such networks absolutely require a very careful selection of station sites with as low as possible man-made seismic noise. If low noise is not assured, such observatory seismology type networks become very insensitive and may frequently be considered a serious project failure. Nevertheless, such networks are frequently used as temporal networks. They also function well where high sensitivity is not desired at all - for example in most strong motion networks.

Seismic networks, which use the coincidence trigger algorithm, are much better at detectability and completeness of acquired data. In these systems, data is transmitted continuously from all remote stations to the central recording site (or at least trigger status information) where a complex trigger algorithm discriminates between earthquakes and excessive seismic noise. The coincidence trigger takes into account not only signal amplitudes in all incoming channels but also their correlation - the number of simultaneously 'activated' stations and potentially their spatial distribution. This results in an algorithm which is much more robust against false-triggers. Thus, the trigger threshold level can be significantly lowered, resulting in a better detectability by the whole network. Each network station's signals are recorded for every trigger. This greatly improves completeness of the recorded data.

An even better solution is provided by systems which temporally store continuous signals in their memory (ring buffers) for a given period of time. This time can range from several hours to several days. After the specified time, these systems erase the old data replacing them by the new incoming data. However, during the designated time a seismologist can detect, associate, and analyse events far better than any automatic algorithm. While this method requires prompt analysis of seismic signals, excellent completeness of data and detectability is obtained. In addition, for the most interesting periods, like aftershock sequences or earthquake swarms, the data can be stored in a continuous manner, thus keeping permanently all information contained in the signals. Such systems may still have an automatic trigger algorithm operating simultaneously which enables automatic processing and a short reaction time in the case of large events. Modern high capacity and very affordable hard disks enable the use of the ring buffer approach by the relatively inexpensive systems. Probably this approach is presently the best compromise between a triggered and a fully continuous seismic system.

3.3. Seismic data transmission from remote stations to central processing site

3.3.1. General considerations

While data transmission may seem like a less important task of a seismic network, poorly selected or designed data transmission capacities are the most frequent cause of disappointments and technical failures. The technical quality of a telemetry seismic network operation rests largely on the reliability and the quality of data transmission.

Another very important but frequently over-looked factor is the cost of data transmission. Note that these costs may largely determine the budget for long-term seismic network operation. Many seismic networks all over the world (also in some very developed countries) have been forced to change their data transmission links to cheaper solutions after some years of operation. Note that data transmission costs per year in a network that was established just after a damaging earthquake, seem completely acceptable but may no longer seem acceptable after five years of relative seismic silence.

The three key technical parameters in data transmission related decision making are:

- the required Baud rate (the amount of data which must be transmitted in a second),
- the distances to which data must be transmitted, and
- the desired reliability (acceptable time unavailability of the links, that is the maximum time per year where signal-to-noise ratio is lower than required (analogue links) or bit error-rate (BER) is higher than allowed (digital links).

These parameters must fit to the available data transmission infrastructure in the country and to the acceptable long-term cost of seismic network operation.

Conditions in a particular country are a very important factor in the selection of an appropriate data transmission system and therefore require the user to be actively involved. It is essential to get information about the availability, reliability, and cost of different approaches from local communication experts. The manufacturers of seismic equipment are generally not familiar with the local conditions and may be unable to correctly advise the best solution for a particular country. The responsibility for finding the optimal solution for a given country lies on the buyer. At least, he must acquire realistic information about the communication infrastructure and is obligated to discuss the situation with the potential network manufacturer.

Technical considerations, reliability, initial price, and operational costs of data transmission links vary widely from country to country. It is the responsibility of the seismic system buyer to find the optimal solution for a given country.

3.3.2. Basic concepts

From the aspect of data transmission to the central processing site there are several basic concepts applying to the design of seismic networks.

In the simplest case a seismic network is a group of stand-alone seismic stations with local recording medium. The majority of older networks, particularly analogue, are still of this type. The information is gathered in person, either by collecting paper seismograms, or by downloading digital data from stations into a lap top computer. Data can be stored on a removable memory medium, like memory cards, DAT tapes, or removable hard or CD disks.

Such networks are suitable for low seismicity regions and are often used in strong motion seismology. Often such networks are temporally established for aftershock studies or similar special research purposes. As a permanent, national or regional observatory seismic network, such networks are rarely suitable.

The next level of network sophistication is enabling real time or near-real time data transfer from the remote stations to the central processing site. Data may be stored in the 'event file' form or in the form of continuous data streams. Networks in this group differ significantly in their capabilities, depending mainly on trigger algorithm (if applicable) and communication links used. At present these are the most frequently used designs.

The latest, most modern design concept of seismic networks is the so-called Intranet concept. Data transmission is done through computer networks. At the moment Internet/Intranet solution seems the most promising where the tools found on Internet are used in the Intranet. These networks work in an open architecture client/server environment. Data transmission itself is done

by commercially available and standardised software and by off-the-shelf hardware components. This significantly reduces the cost of network ownership, increases reliability, and guarantees flexibility. With such systems 'central processing site' loses much of its meaning since data can be processed and/or archived in every authorised node of the network.

However, the so-called 'last-mile' problem remains acute at the time being, particularly in the developing countries. The availability of computer network 'tabs' and the indispensable remoteness of seismic stations conflict. This conflict can be efficiently solved by short distance spread spectrum RF links from the stations to the nearest network 'tabs'. Also a certain time latency (data can be transmitted only in a near-real time manner with delays up to several tens of seconds) may represent a drawback in the applications with emphasised seismic alarm purpose.

Below we give a short summary of types of data transmission links used in seismology. More on this can be found in the chapter *Radio-link transmission of seismic data and feasibility survey*.

3.3.3. Types of data transmission links used in seismology

In seismometry there are several different kinds of data transmission in use, from simple short wire lines to satellite links on global distances. They differ significantly in respect to data throughput, reliability of operation, maximal applicable distances, robustness against damaging earthquakes, and in cost of establishment, cost of operation, and required maintaining. A table in the Worksheet: 'Seismic data transmission links used in seismometry in brief', which is added to this document, enumerates the most common types, their major advantages and drawbacks, and potential applications.

Note that strong-motion seismic networks generate far less data than weak-motion networks and therefore, their designs differ significantly. Seismic data transmission links that are fully acceptable for strong-motion data may be totally inadequate for weak-motion data and data transmission links used in weak-motion field may be an absolute overkill and too expensive for strong motion networks.

3.3.4. Simplex versus duplex data transmission links

There are two basic types of digital data transmission links.

The simplex type links transmit data one-way only - usually from remote stations to the centre. These links are relatively error prone. Radio interference or fading may corrupt data during transmission and there is no way of recovering data, unless the forward error correction (FEC) methods are used. However, the FEC methods are rarely used except with satellite links. They require a significant bandwidth overhead, which is sometimes hard to provide using standard, low cost 3.5 kHz bandwidth RF channels. The simplex links usually use only different types of error-checking methods that allow recognition of corrupted data. They allow recognising errors, but not also correcting them. The error recognition methods practically used range from very simple parity check and check-sum (CS) error detection, to more efficient cyclic redundancy check (CRC) error detection.

The duplex type links allow data flow in both ways – from the remote station to the centre and vice versa. Different types of error-checking methods are used, ranging from the simple parity check, the CS error detection, to the CRC error detection. Also the error-correction methods are regularly used. They are usually based on repeated re-sending of corrupted data blocks until they are received correctly. In this way a very significant increase of reliability of data transmission is

achieved. However, these links require nearly double amount of the RF equipment and are therefore expensive compared to the simplex-links.

Another very important benefit of the duplex links is that they allow remote access to data acquisition parameters and their control as well as remote use of various diagnostic commands at the remote seismic stations from central facilities. This ability significantly reduces the maintaining costs of such seismic networks.

3.3.5. Notes on dial-up phone lines and selection of modems.

Dial-up phone lines are very often proposed for seismic data transmission because they are readily available and apparently cheap. However, they have important limitations that one must be aware of.

First, continuous seismic data transmission is not possible via dial-up lines. This makes coincidence triggers hardly applicable or at least very clumsy and slow. Second, their throughput is in practice, in spite of the high baud-rate capabilities of modern modems, frequently limited. Even the fastest modems do not help if the public phone system in a country is of low quality, unreliable, or overused. Especially in the developing countries, public phone system reliability is often over-estimated by seismic network purchasers. This easily results in inefficient data transmission and tedious re-transmitting of data files. A public phone system must be very reliable for comfortable transmission of sometimes very big seismic event files.

In practice, dial-up phone lines based networks cannot 'digest' earthquake swarms and the numerous after-shocks after strong events. Therefore, they are an appropriate choice for low seismicity regions only. In addition, they often do not function at all for several hours after strong events, due to either especially high usage of public phone system or technical difficulties. They are certainly not the right choice for networks whose important or even predominant purpose is seismic alarm.

In many countries, public phone networks have specific properties and special 'tricks'. Therefore it is advisable to purchase modems locally. Obviously one has to choose a modem type, which is attested in the country and which performs best under local circumstances. Modems react differently to each phone system's particular weak points. A modem, which works perfectly in one country, may not be the optimal solution for another country. We strongly recommend the purchase of modems locally and only after a consultation with local communication experts who have practical experience with digital data transmission over local phone lines in a particular country.

4. SEISMIC STATION SITE SELECTION

The matter of seismic site selection is too often not given sufficient depth of study and attention in spite of the fact that:

... any weak motion seismic network can have a detectability only as good as its site conditions allow, no matter how technologically advanced and expensive its equipment is.

If seismic noise at the sites is high, all or a part of the benefits of a modern, high-dynamic range equipment are lost. A professional site selection procedure is therefore essential for success of any weak motion seismic network. For good results, many factors at the sites must be taken into consideration.

Generally, it is best to begin the process of site selection by choosing two to three times as many potential sites as one actually plans to use. Then we study each one and see which sites meet as many of the criteria as possible. Gradually, selecting the most promising, one will eliminate certain sites and get down to the number of sites required plus two or three. By computer modelling of a few most likely network layouts and by comparing the results, one will be able to make an informed decision about which sites will record and locate seismic events best. Only the basic steps of the site selection procedure will be presented here. For more details see chapter *Seismic site quality and site selection of surface seismic stations*. The site selection procedure encompasses office and field studies.

Off-site, "office" studies are relatively inexpensive and are therefore the first to perform. From an office, one can study maps and contact local authorities to gather information about the potential sites. The first step is defining the geographical region of interest. We gather and examine existing geological faults, seismo-tectonic features, and all available information about seismicity in the area. If the main goal of the new network is monitoring general seismicity in an entire country, this stage is, of course, trivial. Then we prepare a simplified map of regional seismo-geological conditions showing the quality of bedrock. The rule is: the higher the acoustic impedance of the bedrock, the less seismic noise and the higher the maximum possible gain of seismic station. Next we study the topographical aspects of the possible locations. Moderately changing topography is desired. To study man-made and natural seismic noise sources in the region, one should evaluate road traffic, railway traffic, heavy industry, mining and quarry activities, agricultural development of the region, and any other source of man-made seismic noise around the potential sites, along with the natural sources like oceans and lakes, rivers, waterfalls etc. Refer to the *Manual of Seismological Observatory Practice, Ed. Willmore (1979)* for details. Much of the information we need can be found on maps and obtained by asking questions to the local authorities.

If the new network is a radio-frequency (RF) telemetry system, one has to correlate RF data transmission requirements with seismological requirements. Topographic profiling of RF paths based on topographical maps and link budget calculation is performed. The result is known as link availability, which is compared with the desired one. If one plans the use of phone lines for data transmission, their availability and the distances to which new phone lines would have to be laid have to be checked. If one plans to power future stations by main power, the availability of main power lines and the distances to which new power lines would have to be laid must be checked - or one must decide for solar panels.

It is also very important to research land ownership and future land use plans for the potential sites. It makes no sense to undertake extensive studies if one will be unable to use certain sites because of property ownership issues or if it appears that future development will make the site unsuitable for seismic stations.

The climate at the sites also influences site selection and preparation. Temperatures, wind, precipitation, insulation data (for solar panels powered stations), lightning treat etc. may all influence site selection.

Once one has gathered all this information, it is likely that half or more of initially proposed sites will be eliminated for one reason or another.

The **field studies** are the next step in the site selection process. Expect to make several visits to each site. A seismologist familiar with seismic noise measurements, a seismo-geologist, and a communication expert (if we are considering a telemetry network) should all visit the sites. They should verify the ease of access to the site, search for very local man-made seismic noise sources adjacent to the site, which may not be visible from the maps, perform seismic noise measurements, study the local seismo-geological conditions at the site, investigate the local RF data transmission conditions (if applicable), and on site verify power and phone line availability.

Local geology should be studied to determine its complexity and variations as well as seismic coupling between local seismic noise sources and the potential station site. To the extent that is possible, uniform local geology is preferred for seismic stations. The degree of weathering that local rocks have undergone is another important parameter - it can give the first, however highly unreliable, estimate of the required depth of the seismic vault. Better approach is to make shallow profiling at the sites. Shallow profiles are an important part of high-quality site selection procedure. If profiles from any reason are not made, then expect surprises when you begin digging seismic vaults. Many times it is really a matter of almost pure chance what one might run into. Note that the seismic vault must reach hard bedrock.

After all these studies we end up with a two or three potential sets of the best suitable seismic stations. The resulting network layouts are now studied for the best network performance by computer modelling. By comparing the results, one will be able to make an informed decision about the final seismic network layout.

5. SEISMIC STATION SITE PREPARATION

5.1. Purpose of seismic shelters

Civil engineering structures at seismic stations assure a good mechanical contact between seismic sensors and non-weathered, solid bedrock. They protect equipment from temperature and humidity impact, dust and dirt, lightning treat and from small animals. The shelter should also provide a good, low-resistance electric ground for sensitive electronic equipment and lightning-protection system grounding, and easy and safe access to maintain and service the equipment. The well-engineered seismic shelter structure must also minimise distortion of seismic signals due to structure-soil interaction and man-made and wind-generated seismic noise. seismic sensors generally require a stable thermal environment for operation. With passive sensors, mass position may change too much and with active sensors temperature changes result in an output voltage drift, which cannot be resolved from low frequency seismic signals. This ruins signal-to-noise ratio of recording at low frequencies or even clip the sensor completely. Also many active sensors require mass centring if temperature 'slips' outside a few degree C.

Less than 0.5 degree C peak-to-peak temperature changes in a few days must be assured for good results with broad band sensors. This is, of course, not a trivial requirement in a shelter. Extremely demanding non-vault VBB shelters assure even better temperature stability down to ~30 m degree C peak-to-peak in two months (Uhrhammer at all, 1998).

The passive SP seismometers and accelerometers are less demanding than BB and VBB seismometers in respect to thermal stability of sensor environment.

Two vital, but often overlooked issues, leading to potentially fatal consequences if neglected, are lightning protection and grounding system.

Note that lightning is the most frequent cause of seismic equipment failures. One needs to research the best lightning protection for each particular situation and then invest in its purchase, installation and maintenance. We have known of several seismic networks that lost half or more of their equipment in less than two years after installation because people simply neglected adequate lightning protection measures.

Good, low impedance grounding system keeps instrument-noise low, allowing proper grounding and shielding of equipment and cables. It is a pre-requisite for lightning protection system functioning and is also absolutely required for an interference-free VHF or UHF RF telemetry.

We also suggest raising a light fence around the vault to minimise man- and animal-made seismic noise and to some extent protect stations against vandalism. The size of the fence, ranging from 5 x 5 m to 100 x 100 m, depends on what kind of activities go on around the site, on the population density in the vicinity, the ground quality, natural seismic noise levels, and the depth of the vault. Note that fencing often represents a significant portion of the site and structure preparation costs.

Inadequate site preparation and seismometer placement can easily wipe out all the benefits of expensive, high-sensitivity, high dynamic-range seismic equipment. For example, a too shallow seismic vault, which sits on unconsolidated alluvial deposits instead of bedrock can, due to thermal and wind effects, make broad-band recording useless. It is pointless to invest money in expensive seismic equipment only to have its benefits wasted because of improper site conditions.

5.2. Types of seismic shelters

The three main types of seismic shelters are:

- the surface vaults; these are the least expensive and by far the most frequently used, however they suffer the greatest level of natural and man-made seismic noise (for more details and figures related to this type of installation see chapter *Surface vault seismic station site preparation*);
- the deep vaults placed in abandoned tunnels, old mines or natural caves; these are usually the best locations with respect to the price/seismic-noise-performance ratio, however, they are not easily available and sometimes require extensive cabling, which may increase their cost;
- the bore-hole seismic stations with depths from 10 to 2000 m; these are best from the perspective of seismic noise. Signal/noise ratio improvement up to 30 dB in ground velocity power density at about 0.01 Hz can be obtained by a 100 m deep hole. For high frequencies above 1 Hz the greatest gains in noise level reduction are realised within the first 100 m of hole depth. Wind generated high frequency noise can be attenuated as well, however a complete shielding from it is possible only by a very deep bore-hole (Young et al. 1996). Bore-holes are expensive. They may cost from \$5,000 to \$200,000 for the bore-hole itself, plus the cost of bore-hole type sensors, which cost as much as three-times more than regular surface sensors. Bore-holes are used principally in regions entirely covered by alluvial deposits where no sites with good bedrock outcroppings are available, or for the most demanding research work.

5.3. Civil engineering works at vault type seismic stations

Today, seismic stations are most often in the ground vault-form. The massive, solid concrete, "seismic piers" traditionally found in old seismic observatories are no longer built. Above-ground buildings or shelters are not desired at all. In fact, above-ground structures are far less suitable than under-ground vaults because of potential structure-soil interaction problems and due to wind-generated seismic noise caused by the above-surface structural elements. (Bycroft 1978, Luco at all, 1990). Also sufficient thermal stability of the environment is much easier to achieve in an underground vault. If small buildings of any kind already exist at the selected location, make sure the seismometer vault is placed far enough to minimise wind-generated noise and according to the recommendations of the Manual of Seismic Observatory Practice (Willmore, ed. 1979). The structure of the vault should be light and above-ground parts kept to minimum, therefore creating as little wind resistance as possible.

Surface seismic vaults usually measure between 1 and 2 m in diameter, depending on their depth, the quantity of installed equipment and the desired ease of maintaining. They are from 1 to 10 m deep, depending on the depth, the quality, and the weathering of bedrock at the site. Round or rectangular cross-sections are equally suitable.

5.4. Organisation of civil engineering works

Whatever construction work is needed to prepare the sites, it is usually arranged and paid for by the customer of the new network rather than the manufacturer of the seismic equipment. Very large national projects may be an exception to this rule. Site construction will require a great deal of preparation and involvement by the system buyer. There is generally a number of good design alternatives from which to choose and we suggest to hire a local civil engineering contractor to design the best solution for a particular system and specific circumstances in the country. A seismo-geologist and a civil engineer should supervise the construction works. Their main responsibility is assuring that the enclosure is watertight and that the sensors have a good contact with solid bedrock. The system's manufacturer can provide sketches and suggestions about the procedure, he can also supervise the works, but usually he does not provide true structural drawings for seismic shelters. Working in tandem with a local civil engineer is usually a more efficient solution because he is familiar with all local circumstances, which are generally unknown to the manufacturer of seismic equipment. Local builders know best what materials and construction methods are available and workable in a particular developing country. Do not "over-engineer" the project; it is usually not necessary that a big civil engineering firm designs in every detail, builds, and oversees seismic site preparation.

6. DATA TRANSMISSION USING VHF, UHF, AND SPREAD-SPECTRUM RF LINKS

6.1. The need for a professional RF network design

In practice, the most frequent technical problems with radio-frequency (RF) telemetry seismic networks origin in inadequately designed data transmission links. Therefore we are discussing this topic separately.

The design of RF telemetry links in a seismic network is a specialised technical matter, therefore guessing and "common sense" approach usually cause problems or even complete project failure. There are quite a few common misunderstandings and over-simplifications

regarding the amount of data that must be transmitted, the degree of reliability required for successful transmission of seismological data, the significance of "open line of sight" between transmitters and receivers as a required and sufficient condition for reliable links, as well as regarding the over-simplified methods of link verification. However, the real issues in the RF link design and reliability calculations are the frequency of operation, Fresnel ellipsoid obstructions by topographic obstacles, the curvature of the Earth, the gradient of air reflectivity in the region, expected fading, potential wave diffraction and/or reflections, time dispersions of the RF carrier with digital links, etc. All these are specialised technical issues. More details on this are given in chapter *Radio-link transmission of seismic data and feasibility survey*.

In any event, to prevent failures, a professional RF survey is strongly recommend which should be a part of the seismic network planning procedure. It includes the calculation of RF links based on topographical data and only seldom field measurements. A professional RF survey provides several benefits for the customer:

- Assurance that the links will provide the desired reliability of operation.
- The minimum number of required links and RF repeaters in the network. Note that, in most designs, every RF repeater degrades data quality to some extent and obviously increases the probability of link-down time and the price of the system.
- A minimum number of licensed frequencies required.
- Optimal distribution of RF frequencies over the network, which minimises the probability of RF interference problems.
- Less polluted RF space in the country.
- Minimised antennae size and mast heights, resulting in potential savings on antennae and antenna mast cost.
- Significantly increased robustness to technical failures due to proper RF layout design.

The cost of a professional RF survey represents generally a few percent of the total investment. We believe that the combined benefits of an RF survey are well worth the investment. It is a major step toward the reliable operation of the seismic network.

6.2. Problems with RF interference

Radio-frequency interference caused by other users of VHF or UHF RF space in the developing countries is quite a common and difficult problem. There are several reasons for that. In some countries, the lack of discipline and confusion in RF space where army, police, security authorities, and civil authorities all operate under different (or no) rules causes unforeseen interference. In others, poor maintenance of high power communication equipment results in strong stray radiation from the side-lobes of powerful transmitters that interferes with seismological links. Extensive, unauthorised use of walkie-talkies can also be the cause of problems.

The best, and more or less the only solution is to work closely with local experts who are familiar with true RF space conditions in the country during the design phase of a seismic

network. Note that RF interference problems are generally beyond control of seismic system manufacturers. All RF equipment, no matter who manufactures it, is designed to be used in an RF space where everybody strictly obeys the rules. Therefore, the interference problem can be solved - or at least mitigated - only by employing local experts in the network buyer's seismic team while designing a network.

6.3. Organisation of RF data transmission network design

A RF layout design is always an integral part of a seismic site selection procedure. It can be performed by the seismic system purchaser if he has adequate knowledge in this field. Practice shows that this is rarely the case, not only in the developing countries. However, even if the RF survey is purchased from an independent company or from a seismic equipment manufacturer as a part of services, the process still requires involvement of the seismic system buyer. For efficient office and fieldwork the customer has to prepare an approximate initial seismic network layout, road and topographic maps, and climatic data beforehand. He has to make available knowledgeable staff members and well informed local people acquainted with local conditions at the sites, who will join the site selection field team. Usually he has to assure also efficient logistics during the field work.

A detailed list of what to prepare is given in section 5 of chapter *Seismic site quality and site selection*. Note that the maps sent to the RF survey provider are working copies. They are normally not returned to the customer.

7. PURCHASING SEISMIC SYSTEM

7.1. The bidding process

While sending out a Request for Proposal and asking for bids on a new seismic system may be a good way to get started, there are a number of important issues one must be aware of when requesting bids or proposals. First, certain technical requirements and business standards must be met in order to be able to compare "apples-to-apples" when it is time to analyse received system proposals. Second, in order to find the most suitable system, one needs to invest a fair amount of additional time in research and investigation before sending out the bid specifications. Namely, many very important issues are hard to define in the Request for Proposal. The proposals can easily give unclear information regarding the following crucial issues:

- the actual reliability of the equipment,
- the actual user friendliness of the system,
- the availability of long-term support by the manufacturer including true availability of spare parts in next years, and
- the financial stability of the manufacturer.

In the Request for Proposal one should not forget to state clearly the goals of the new seismic network and rate their relative importance. Too often what one wants to accomplish with the new system is not clearly described and the goals are not prioritised, resulting in vague instructions to manufacturers and hence, potentially disappointed customers.

In the Request for Proposal one should include all relevant basic technical information, so that the manufacturer can put together the corresponding technical solution. However, we recommend that the Request for Proposal does not contain an over-detailed technical description of the desired system - unless one already decided who should win the bidding process (which is illegal, but not so uncommon practice). With too many technical details one can end up limiting one's choices and even disqualifying the most suitable system just because a relatively unimportant technical detail can not be fulfilled.

We strongly recommend not to push manufacturers to design a new system specifically for your needs. The majority of seismic equipment manufacturers is willing to design such 'custom made' systems. However there is a high price for this commodity. Such systems will often be expensive, and as a 'prototype', obviously less tested than 'standard products' and more difficult to support in the long run. Avoid buying brand new systems in the market unless you are really assured with an excellent support from the manufacturer. Simply, try not to be a 'guinea pig'. Any brand new system obviously has more technical imperfections and 'kid's illnesses' than others. It obviously requires a higher level of existing knowledge of the system buyer and a really good co-working relationship with the manufacturer while solving these problems. Some countries are required by law to accept the lowest bid. Unfortunately, crucial qualities like services, equipment reliability, user-friendliness of the system, amount of factory testing, set-up and long-term support might be easily lost if one bases his choice solely on the lowest price and fulfilment of 'all' stated requirements (but practically never really sufficient) of the bid. In a legitimate desire to keep the price as low as possible, manufacturers will most probably cut difficult 'to measure' qualities, particularly short and long-term support, and services. This is a dangerous situation, particularly for less experienced customers. One way of avoiding this danger is spelling out explicitly all services required in the Request for Proposal. This is the place to be exacting; specify services and support type, their goal, technical level expected, place and duration, parts and labour warranties; pricing structure after warranties expire, timeliness requirements, etc.

7.2. Selecting a manufacturer

When evaluating the proposals, one should assess not only the technical qualities of the system, but also the quality of every manufacturer. What is their reputation? How long have they been in seismological equipment business? Obviously ask for references from users of the same or similar systems and learn about how well the company served them. As you get close to decision-making time, make a personal visit to the manufacturers whose offers you are considering seriously; meet their employees and tour their facilities. The company that serves you well before you have bought their product is more likely to continue to serve you well after you will have bought and paid for their product. Often manufacturers will pay at least some of the expenses for new potential clients of realistic projects to visit their facilities and meet their staff.

Carefully select the people who will participate in these visits. In addition to a member fully responsible in financial issues, one member of the team should be the individual responsible for future operation of the network. Other members of the team should be those most knowledgeable and experienced in seismology, no matter what their position in the hierarchy is or which power structure of the institution they belong to. Of course, all members should be fluent in the pertinent foreign language or technically competent translator should be included in the team.

Also take into consideration the size of the company. The relatively small ones may simply not have the "man-power" for long-term customer support of big projects, no matter how strongly they actually want to support you. They may manufacture good, technically most advanced

equipment, however their ability to support large national projects, their longevity and system-testing capacities may cause problems later.

Generally, one would not expect the best results from companies that merely assemble systems but they are not experts themselves in seismology. On one hand, the assembler of the system is incapable of providing profound seismological-technical support and on the other hand, the actual manufacturer of seismic equipment is not able and willing to spend much of his time in supporting you, because he was not paid for it. Experience shows that such projects rarely result in a happy end. Ask for visits with manufacturer's sales or system engineers. Data sheets themselves never give enough technical information about seismic systems. Sales and system engineers can provide all the details of a particular technical solution. Such visits, however, are less appropriate during the early stage of the project when one's goals are not yet specifically set. It is understandable that the sales representatives might be biased toward the equipment of the manufacturer they represent.

7.3. Equipment selection

As already mentioned, data sheets of seismic equipment alone seldom provide enough information. In addition, it is not easy to compare the data sheets of various manufacturers because each one to some extent uses a different system of specifications, measurement units, and definitions of technical parameters. There are at least ten different ways of expressing intrinsic noise and dynamic range of sensors or data recorders in use, for example. All of these factors must be well understood for a fair and accurate comparison. This can be best accomplished through in-depth contact with the manufacturers and with help of additional written information. Be sure to ask for all possible information about the system including the copies of the user manuals (the customer can examine the quality of technical documentation provided with the system, which is also an important element) and the published results of independent testing.

Ideally, we recommend buying one piece of key equipment such as a sensor, a data logger, processing software with demo data or an RF link and testing the product by yourself. In the case of large projects with adequate financing, manufacturers will often loan equipment for testing purposes free of charge. While it is ideal to get some first-hand experience before settling on which new system to purchase, this approach requires personnel who are knowledgeable about seismology and instrumentation. In reality, however, in many developing countries it is difficult or impossible to find such personnel and money for such apparently "unproductive experiments".

Be cautious about assembling products from different manufacturers in one system. It is not a simple or easy task to interface between different products in terms of the dynamic range, the signal-to-noise ratio, the full scale ranges, the baud rates, the processing power and the power supply sources. Stay with one manufacturer if possible, or, when that is not feasible, arrange to have one manufacturer who will be explicitly, contractually responsible also for interface problems and the functioning of the system as a whole. Understand also that the time spent for solving equipment interfacing problems specially for a given customer also has its price.

Each technical system, or element in it, properly operates within a certain set of parameters, or "range". One should be familiar with these ranges and know where within this range the system or its parts will actually operate. If one or more of the elements of the system are to operate at the extreme end of their operation range on a regular basis, the system or its element is most probably not the right choice. Note that there is always a price to pay for operating equipment under extremes. The results will often be disappointing if, for example, one plans on using the maximum possible number of channels in a FM radio-frequency link, or would like to acquire

data with the maximum possible number of channels in a seismic system, or exploit the maximum number of channels in seismic data analysis software, or operate the hardware at extreme temperatures, etc. In such case it is often better to find another system or system element, whose mid-range parameters can accommodate one's needs. Always make sure you have a given safety margin in your system and do not expect it to operate continuously, efficiently, and reliably in the extreme ranges.

7.4. Seismic equipment market is small

The global market for seismic systems and equipment is naturally quite limited. With very few exceptions, instruments are produced in small numbers. Inevitably, this sets a limit to the quantity and thoroughness of testing of the newly developed equipment. This is not a result of a lack of quality or commitment on the part of manufacturers in this field, but a simple, economic reality. Compared to industries with a far broader and more powerful economic base, like computer and electronic companies, seismic equipment moves into the field with relatively little testing, even by the most reputable manufacturers. In general, this equipment arrives with a higher-than-average number of bugs and technical imperfections that will need to be solved by the manufacturer and the user working in tandem. Currently, most seismic equipment is less user-friendly than most of us would like it to be and the technical documentation frequently falls far short from the glory of the Lord. Customers are rarely given comprehensive and easy-to-follow instructions on how to set-up and use the system. The reputed manufacturers of seismic equipment compensate for this situation with a committed and effective customer support services. Due to the fact that in the developing countries there is often a lack of knowledgeable experts who can cope with the technical problems by themselves, it is truly necessary to maintain a long-term working relationship with the maker of the purchased seismic system. The manufacturer's support and a reliable, knowledgeable and friendly relationship thereafter is one of the most important and crucial issues for success.

8. INSTALLATION

There are four ways of installing a new seismic system:

- The user installs the new system. Only 'boxes' are purchased. In this option, the customer is responsible for the proper functioning of the system as a whole and the manufacturer remains responsible for proper functioning of the elements, unless they are improperly used or installed. In practice, especially in the developing countries that are inexperienced with seismic equipment, this approach is very rarely satisfactory.
- The manufacturer demonstrates installation on a subsystem (a few stations, a sub-network). In this case, the manufacturer and the user, depending on who installs which portion of the system share responsibility for the system functioning. This approach is often successful. However, a certain amount of customer's experience with seismic, computer, and communication equipment is required for this method to work.
- The manufacturer installs the whole system with the full assistance from local technical and/or seismological staff that will be responsible for running, maintaining and servicing the network in the future. Responsibility for making sure the system functions well lies with the manufacturer. It is highly advantageous if local staff works alongside the manufacturer when

installing the system. The main benefit of this approach for the users is that they learn an enormous amount during the hands-on installation and associated problem-solving time. This is an efficient way of training and therefore the user should not expect savings and potential shortening of the installation time. To our experience, this seems to be the best way of installing a seismic network in the developing countries.

- If a customer orders a turnkey installation without his assistance, the manufacturer has complete responsibility for seeing that the system functions adequately. In this case, the network will no doubt be successfully installed, but local staff members will learn nothing about its actually operating and about solving potential future problems. This approach is adequate only for the countries having high level of seismological and technical knowledge.

Two technical details relating to system installation should also be mentioned here.

In case the system buyer will install the system or its parts, do not accept the 'standard length' cables offered sometimes by some seismic system manufacturers. The 'standard' cables rarely work well in the field - they are, according to Murphy's laws, always too short or too long. Do not loop or coil extra cable length because that will increase the threat of lightning damage and unnecessarily increase system noise (and, at the end, nobody will get 'extra' cable for free). Rather, ask for bulk cables with separate connectors or cables of a reasonable length margin and one-side mounted connectors only. You can then cut them to precisely the desired lengths in the field during installation. However, note that reliable, high quality soldering of connectors requires experience. Newcomers in soldering have no chance of performing the job correctly. Note that badly installed connectors are among the most frequent problem makers.

Note also that, in case of purchased installation, the seismic station sites must be completely prepared before the manufacturer arrives to install the system. All construction works must be finished, logistics organised, and access permits prepared (if applicable). Time and time again, manufacturers are faced with unprepared sites when arriving for the installation. A significant loss of time results and forces both parties to accept undesirable "last-minute" technical improvisations and compromises during installation. This generally leads to less reliable functioning of the system. Note that services are usually paid by time, and that an efficient use of this time is customer's direct benefit.

9. TUNING OF SEISMIC NETWORK

Before a seismic network can function with its full capacity, it must be tuned to local seismo-geological and system conditions. Tuning is especially important for networks that run in 'triggered mode'.

Unfortunately, many inexperienced customers are not aware of the fact that they will need to tune the system by themselves. Many think that the manufacturer can do this at the factory or during installation. But, it is a matter of fact that neither hardware, neither real time processing, nor off-line analysis software purchased can function properly immediately after hardware installation of a new seismic network. For best results, all new seismic networks require fine-tuning of many recording and computational parameters to local conditions. And only the user of the network can perform these adjustments because this process requires time and on site experience.

In addition to region's Earth structure, the seismic network dimension and layout, seismicity in the region, seismic noise levels and spectra at station sites, seismic signal attenuation in the region and local earth structure at the sites, all play a role in these adjustments. One will not be able to correctly tune the system's recording and processing parameters until he has acquired sufficient experience with natural and man-made seismic noise and earthquake signals at all the sites in the network and until he fully understands parameters, which have to be tuned. Therefore, tuning a network takes normally months of systematic work. Because of the long time required to accomplish this task, the system's manufacturer simply can not do it. Only network operator can correctly tune the network. Moreover, since seismic noise conditions at the sites may change in time, new stations may be added, the goals of the network may drift, etc., re-tuning of the network will probably be required from time to time. In reality, tuning a seismic network is an on-going task, which cannot be done 'once and for all'.

We will just enumerate the most common hardware and real-time processing parameters that need to be adjusted. They are:

- seismic gain at individual stations,
- signal-conditioning filter parameters,
- pre-trigger band-pass filter parameters,
- trigger algorithm parameters, which usually include:
 - trigger threshold values,
 - de-trigger thresholds values,
 - trigger time windows duration and other parameters,
 - weights of individual stations in coincident trigger algorithm,
 - grouping of stations in sub-regions in the coincidence trigger algorithm organisation.
- Pre-event time duration,
- post-event time duration,
- minimum run-time and/or maximum run-time duration, and
- propagation window length adjustment.

Note that not all enumerated parameters exist in every seismic network and that some adjustments may be missing from this list. Detailed discussion of individual parameters is above the scope of this text. More on trigger parameter setting is given in chapter *Understanding and setting STA/LTA trigger algorithm...*

The following are some of the off-line seismic analysis software issues that must be studied and prepared for efficient routine observatory work, or parameters, which have to be adjusted for correct analysis of seismic records:

- files with data acquisition parameters (data acquisition configuration file(s)),
- parameter files containing sensor calibration data,
- files containing data about geometrical configuration of seismic stations (network configuration file(s)),

- earth model parameters of event location program(s) (ground layer's thickness, seismic wave velocities, seismic station weights, epicenter distance weighing function, and similar parameters depending on the program used),
- automatic phase-picker parameters,
- magnitude-determination algorithm calibration parameters, and
- preparation of different macros and forms for routine, every-day analysis of seismic signals.

Some parameters, for example Earth model parameters, are often insufficiently known at the time of network installation and require a long term seismological research work, which results in gradual refinement of the model and increasingly better location of events.

No manufacturer can optimally pre-adjust all these parameters to the specific ground and network conditions. Truly, seismic networks come with a set of default values for all these parameters (factory pre-selected values based on 'world averages'). These values may work sufficiently well for the beginning of network operation in some cases, however, optimum seismic network performances require reconsidering most of them.

10. RUNNING A SEISMIC NETWORK

10.1. Organising the routine network operation tasks

Keeping one's network failure-free and in perfect working order, waiting to record earthquakes year after year requires hard and responsible work and a lot of discipline. High standard working habits are inevitable required. This goal is generally not simple to achieve. Seismic observatory staff will have to operate in a highly professional and reliable manner with:

- clearly defined personal responsibility for each task associated with the routine operation of the network and for other every-day analysis and archiving activities,
- a regular and well defined maintenance procedures of hardware and software,
- a continuous verification of all tasks and hardware operation, and
- a precise record-keeping of all activities, network operational parameters, their changes, all maintenance works and repair activities and in the seismic data archives.

Well-defined personal responsibility with respect to altering network operation parameters and strict obedience to the established procedures is an absolute must. Generally, network recording parameters should be changed only if there is an important and well thought through reason for this. Any change of recording parameters changes also network's detectability. Therefore generally the changes are avoided as much as possible. For general seismicity monitoring aspect reasons, ideally, there should be no changes for years after the network is fully adjusted. Nevertheless, real life is different, and some changes are inevitable from time to time. However, one should keep them in reasonable limits and document and archive them very carefully.

Careful and continuous documentation of network operation parameters in a logbook, log-file, or in the seismic database itself, is essential. This back-log information should contain all information about data acquisition parameters and their changes, a documentation of all station calibrations, a precise stations' down-time, a descriptions of technical problems and solutions, and descriptions of maintenance and service works. The exact times of parameters setting changes activation must be thoroughly recorded. This information must become an integral part of seismic data archive because only those signals, recorded along with the precise conditions at the time of the recording, can be properly interpreted.

Usually seismic network team is divided into a seismological and a technical group. This is fine if it relates to every day network operation activities and responsibilities. However, as much as possible, the basic technical as well as basic seismological knowledge should be 'evenly' distributed among the members of both groups. This favourably influences the general quality of the work of a seismic observatory. It also helps very much in a lot of critical situations, such as usually follow a severe unexpected technical problem with the network, a strong event in rapid deployment of portable stations, and during aftershock sequences, when the amount of work dramatically increases for a limited period of time.

The technical group must accept that no matter how modern and sophisticated seismic network they operate, they are actually services to the seismological group and therefore subordinated to seismologists. Seismologists define the goals of seismic network operation and its working parameters. Frequently personal frictions may appear because this issue is not clearly defined by the management.

Many national seismological observatories experienced the problem with organising around the clock, 24 hours per day, presence of their personnel at the central recording site. Usually governments more or less explicitly require such working regime in order to shorten reaction time to public and civil defence authorities in case of strong, potentially damaging earthquakes. But no matter how understandable such desire may be, it is the fact that this working regime is really feasible only in a few, very large seismological institutions. Only they have enough seismologists, which are capable of interpreting seismic data fast and competently. Even fully automated central recording and processing facility still requires verification and confirmation of automatically determined earthquake parameters by educated personnel. Also interpretation of automatically determined earthquake parameters in terms of expected intensities in a given region and probability of potential fatalities and damages is still a matter of experience and not a matter of automatic calculations.

In practice often the around the clock human presence at the observatory is achieved using all available, but mostly incompetent, personnel in order to formally fulfil higher authorities' requirements. Of course, practical value of such solution is highly questionable. If the country is a high seismic risk country and if the importance of the alarm purpose of a new network is expected to be high, one should rather consider a system of electronic pagers, which automatically alarms all available seismologists in the institution in the event of strong earthquakes. It is the nature of his profession that every seismologist must be made available and hurries up to the observatory at any time in case of earthquakes with macroseismic effects.

10.2. System maintenance

Maintaining a seismic network's hardware and software is a continuous activity that inevitably requires well-trained technical personnel capable to cope with mechanical, electrical, electronic, and computer problems. Nowadays, many vital operational parameters at the remote seismic stations can be remotely monitored by modern, high-end seismic systems with duplex data

transmission links. Such parameters are for example: back-up battery voltage, presence of charging voltage, potential software and communication problems, absolute time keeping equipment's health, remote stations vault and/or equipment temperature, potential water intrusion, etc. These utilities significantly reduce the need for field service work and therefore lower the cost of network operation. However, regular visits to the stations are still necessary, though far less frequently than in the past. Note that it is a mistake to simply put off in-person checks of remote seismic stations until something goes wrong. Periodic visual checks of cables and equipment, of potential corrosion problems on equipment and grounding and lightning system, of intrusion of water and small animals, and particularly regular change of batteries and cleaning the vaults and solar panels will help to eliminate potential technical problems before they occur.

And when something does go wrong, technical staff must be certain that they can respond immediately with the right personnel, action, and spare parts. One should always maintain a good stockpile of the most common spare parts and have a well-trained technician(s) with a pager on duty around the clock. Having technical personnel, in addition to seismological one, on duty 24 hours a day for potential action is a common practice in the observatory seismology.

Batteries require special attention. If the lightning damages are the most frequent source of technical failures during normal operation of a network, then battery failures are the number one reason for failures during main power failure and unusual high-seismicity periods. It should be noted that the output voltage alone of a battery provides little information about its overall health and capacity. Many types of batteries may still have adequate output voltage while at the same time their charge capacity is reduced to a small fraction of its original strength. Batteries in this condition will not do the job in case of a longer duration power failure, which is almost certain to occur after damaging earthquakes.

Once a year all the batteries in the seismic system must be laboratory-tested for remaining charge capacity. The batteries should be fully discharged, then fully charged, and again discharged in a controlled manner and their true charge capacity determined. Once the measured charge capacity is less than 60% - 70% of their nominal capacity, they should be replaced with new ones. Relying solely on measurements of battery voltage will certainly lead to technical failures on long run. We should never forget that we need fully operational batteries after big events since it is very likely that regular power source will be non-functional, often for quite a long time. The most important moment in the life-time of the seismic network may happen only once a decade - or less. One certainly does not want to miss it because of old batteries with insufficient charge capacity! Non-chargeable batteries, particularly the lithium type, must be replaced regularly according to the manufacturer's instructions, regardless of their output voltage at the moment of life time expiration.

10.3. Sensor calibration

Seismological observatories should calibrate all the sensors in their seismic system regularly - ideally, once a year. Strictly speaking, only the seismic signals recorded between two successive system calibrations that show no significant change in frequency response function are completely reliable.

Seismic sensor calibration requires knowledge that is seldom available in the developing countries. In most cases, special training is required. A useful approach is to include the first re-calibration of one or more sensors after one year of service in the purchase agreement with the manufacturer. The manufacturer and the local staff should perform this first one-year calibration service together. Hands-on practice under the close supervision of a specialist is the best way of

learning sensor calibration. If an inexperienced user calibrates the seismic sensors by himself, inadequate understanding of underlying physics and Murphy's Laws easily lead to errors, which are, in addition, sometimes difficult to detect. Practice shows that mere "book learning" is often not enough when trying to calibrate seismic sensors.

In the time of digital seismology, sensor transfer function representation in the 's' or 'z' plane is most commonly used. An excellent and comprehensive description of basics is given in Scherbaum (1996). A description of a popular seismometer calibration program UNICAL is given in Plesinger et al. (1995).

10.4. Archiving data

After several years, or even decades of operation of a seismic network, the scientific and financial value of a related national seismic archive is extremely high. Therefore, full attention must be paid to data archiving and a fail-safe back-up for that data. Seismology is a typical non-experimental science and lost or corrupted seismic data can never be re-generated. It is therefore an absolute must to provide a complete and reliable back-up archive. The back-ups should be kept in a different physical location, no matter whether they are on paper, tape, disk, CD or other memory medium.

When one first sets up a seismic network, he needs to think thoroughly about organising the data that he records in light of the fact that eventually he will have many, many years of accumulated records. Often, this crucial aspect of seismic system organisation is overlooked or left to on-the-spot decision by whoever is starting archiving records at the beginning of a new network operation. This may work fine for a while, but eventually everybody will run into serious problems if the archiving system chosen is inappropriate. It is necessary to carefully consider, from the very beginning, file coding and archive organisation and their long-term perspective.

In a small, weak-motion network in a low seismicity region that generates only a small number of records each year, or in a small or medium size strong-motion network one can probably get by with a DOS or Windows-type directory tree organisation for the data archive. Nevertheless, file-name coding of events must be thoroughly thought out to avoid confusion and/or file name duplications. Fortunately, due to long file names, UNIX, Windows 95, Windows 98, or NT operating systems are much more flexible than DOS in this respect

Larger networks in moderate to high seismicity regions require true relational database for archiving purposes. One should carefully consider different options in the market before one begins to log records. It is usually very painful to change the data coding or archiving method after several years of network operation, once thousands upon thousands of records are already stored.

Very powerful professional databases may not be the most suitable choice for seismology, primarily due to their high initial and maintaining cost, and secondly, due to too many utilities which will never be used in seismology (but which have to be paid for, of course). Special data bases which have been developed in seismological community for the needs of seismology, thoroughly tested in several existing applications, and accepted by many, seem to be the best choice at the moment.

Always keep the raw, unprocessed seismic data (raw event files, or sequences of continuous data) in the archive along with the full documentation about the recording conditions (data acquisition parameters and accompanying information). Processing and seismic analysis methods will change and evolve as time passes. Future generations will appreciate having unprocessed seismic data available to further their research and knowledge.

10.5. Dissemination of seismic data

International co-operation in the dissemination of seismic data is another pre-requisite for high-quality operation of any new seismic network in the developing countries. Broad-minded data sharing is

- the best way for a less experienced institution to get feedback about the quality of its own work and also
- a widely accepted international obligation.

Everyone can greatly improve their own work, for example, by observing and comparing the phase reading residuals, the event locations, the magnitude determinations and the source mechanism results, with the results of others published in international seismological bulletins. Any seismic study should also include as much seismic information as possible from the neighbouring regions and countries. Not only one's own data, but also all available pertinent data from others should be used in seismic research work. Disseminating one's own data will, in turn, facilitate easy and fast accessibility of other seismologists' data. It is very important to establish a generous data-sharing relationship with other seismological institutions.

Traditionally, seismic observatories of national seismic networks or larger regional networks regularly publish preliminary seismological bulletins (weekly, bi-weekly, or monthly), final seismological bulletins (yearly), and earthquake catalogues of the country or region (yearly, but with a few years delay so that the data from all other external sources can be included in the analysis). These catalogues are one of the bases for earthquake risk mitigation studies.

Immediate dissemination of data from strong events is another international obligation. Internet, fax, or phone are familiar forms of seismic data exchange in such cases. The Internet is used more and more often for sharing not only short information about strong events but also other publications like seismic bulletins and also earthquake waveform data. Actually Internet has nearly replaced all other seismic information exchange channels. In all developing countries where Internet access is not yet easy to get, seismological institutions have to undertake every possible effort to get it as soon as possible.

11. LITERATURE

- Beauduin, R. at all (1996) The Effect of the Atmospheric Pressure Changes on the Seismic Signals or How to Improve the Quality of a Station, BSSA, **86**, 1760.
- Bycroft, G.N. (1978) The effect of soil-structure interaction on seismometer readings, BSSA, **68**, 823.
- Lee, W.H.K and Steward, S.W. (1981) Principles and Applications of Micro-earthquake Networks, Advances in Geophysics, Supplement 2, Academic Press, NY, USA.
- Luco, J.E., Anderson, J.G., and Georgevich, M. (1990) Soil-structure interaction effects on strong motion accelerograms recorded on instrument shelters, Earth. Eng. & Struct. Dyn., **19**, 119.
- Plesinger, A., Zmeskal, M., and Zednik, J. (1995) PREPROC - Software for automated preprocessing of digital data, Ver.2.1, Ed. Bergman, E., NEIC Golden/FI, Prague.

- Scherbaum, F. (1996) *Of poles and zeros; Fundamentals of Digital Seismometry*, Kluwer Academic Publisher, Boston.
- Trnkoczy, A. and Zivcic, M. (1992) Design of Local Seismic Network for Nuclear Power Plant Krsko, *Cahiers du Centre Europeen de Geodynamique et de Seismologie*, Luxembourg, **5**, 31-41.
- Uhrhammer, R.A., Karavas, W., and Romanovicz, B. (1998) Broadband Seismic Station Installation Guidelines, *Seismo. Res. Letters*, **69**, 15-26.
- Understanding The Earth's Dynamics and Structure, The IRIS.
- Proposal 1991-1995 to The National Science Foundation, (1990), IRIS Consortium.
- Willmore, P.L. (Ed.) (1979) *Manual of Seismological Observatory Practice*, Report: SE-20, World Data Center A for Solid Earth Geophysics.
- Young C.J. et al. (1996) A Comparison of the High-Frequency Surface and Subsurface Noise Environment at Three Sites in the US, *BSSA*, **86**, 1516.

SEISMIC SITE QUALITY AND SITE SELECTION OF SURFACE SEISMIC STATIONS

Amadej Trnkoczy
Kinematics SA, Z.I. Le Trési 3
CH-1028 Préverenges, Switzerland

Peter Bormann
GeoForschungsZentrum Potsdam, Division 2
Telegrafenberg, D-14473 Potsdam, Germany
E-mail: course@gfz-potsdam.de

1. INTRODUCTION

Several factors affecting the quality of seismic stations or seismic network operation depend on seismic site selection. This matter is often not given the required attention. It is a fact that any new weak motion seismic network today can have high earthquake detectability and record representative event waveforms only to the extent that its sites allow, no matter how technologically advanced and expensive equipment is used. If seismic noise at the sites is too high, all or a part of the benefits of a modern, high-dynamic range equipment are lost. If the noise is of an excessive burst- or spike-type and large amplitude man-made seismic noise is present, high trigger thresholds and therefore poor network detectability will result. If a station is situated on soft ground, very broadband (VBB) or even broadband (BB) recording can be useless and short-period (SP) signals may be unrepresentative due to local ground effects. If network layout is inappropriate, the location of events will be inaccurate, systematically biased, or even impossible. A professional site selection procedure is therefore essential for the success of any new weak-motion seismic station or network.

Generally, it is best to begin the process of site selection by choosing two to three times as many potential sites as we actually plan to build. Then we can study each one and chose the sites that meet as many desired criteria as possible. Gradually, selecting the most promising, we eliminate certain sites and get down to the target number of sites plus two or three. Potentially, we may model system performance of a few most likely network layouts and by comparing the results we will be able to make an informed decision about which layout will record and locate seismic events best.

In this text, relevant parameters are discussed and the site selection process is demonstrated by seeking the best placement for six seismic stations of a permanent local seismic network around a nuclear power plant. The main goals of this particular project (Trnkoczy and Zivcic, 1992) were monitoring local seismicity, high network's detectability, and ability to accurately locate local events. Therefore chiefly, but not exclusively, the placement of short-period seismometers and surface seismic vaults are discussed.

2. OFF-SITE STUDIES

Site selection procedures encompass off-site studies and fieldwork. Off-site "office" studies are relatively inexpensive and are therefore performed first. From an office, we can study maps and gather information about the potential sites from local and regional authorities. Once we have gather all this information, it is likely that many of initial potential sites will already be

eliminated for one reason or another. This will obviously minimize future fieldwork and the cost of the feasibility study as well. A list of parameters usually studied covers:

- geographical region of interest
- seismo-geological conditions
- topographical conditions
- accessibility
- seismic noise sources in the region
- data transmission and power considerations
- land ownership and future land use issues
- climatic conditions

2.1. Definition of geographical region of interest

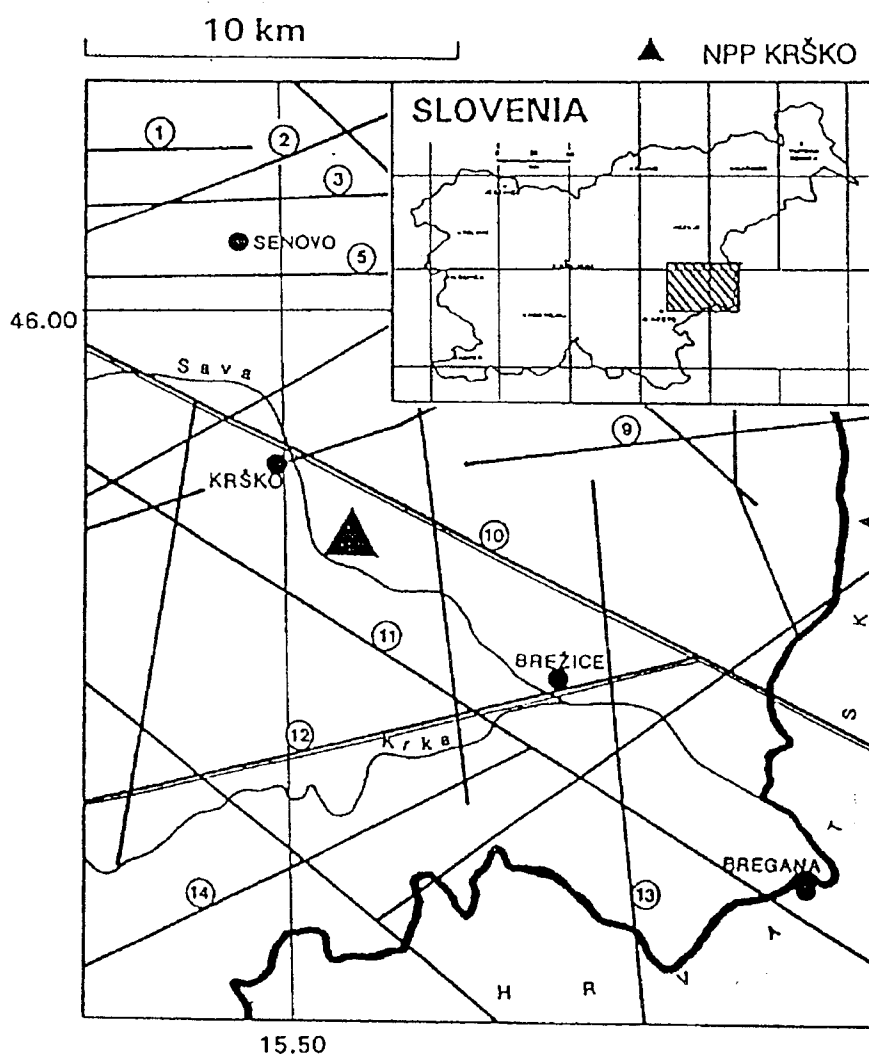


Fig. 1: The broader region of the network with its main geological faults (9-Artice fault, 10-Brestanica fault, 11-Sava fault, 12-Podbočje fault, 13-Brežice fault, 14-Orehovec fault).

The first step is defining the geographical region in which we are most interested. In this step our goals, socioeconomic and seismic information are important. We examine all known major geological faults from geological maps with a view to assess their neotectonic activity and potential, identify seismo-tectonic features from seismo-tectonic maps, if available, and compile all accessible information about the seismicity in the area. We compile historical and instrument-recorded events in the broader region from earthquake catalogs and other sources. The results of such a study are shown in the following figures. Fig. 1 shows the broader region chosen for our example and the main geological faults within it. Fig. 2 shows earthquake epicenters plotted from seismic catalogs and Fig. 3 shows the map of released seismic energy during the time span of the catalogues and the final choice of the specific region we wish to study in detail. If the main goal of the new seismic network is monitoring of the general seismicity in an entire country, this stage can be, of course, simplified.

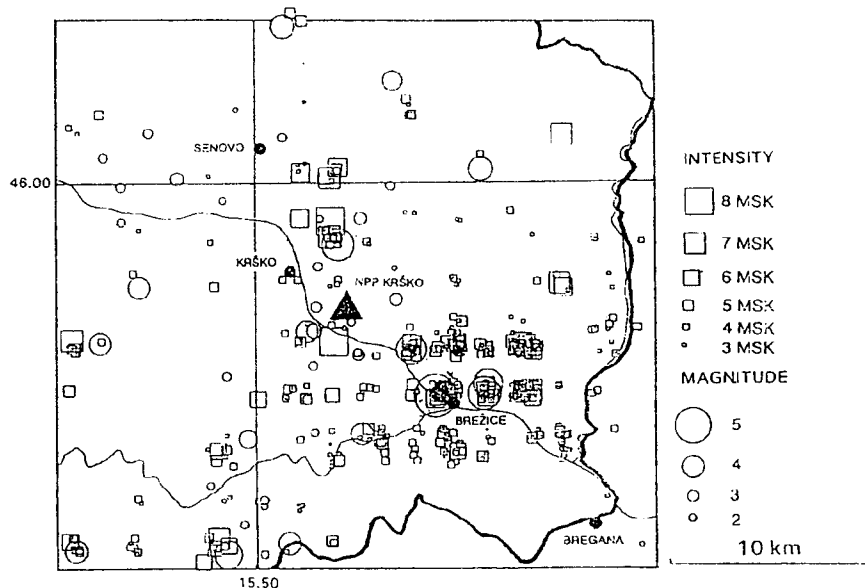


Fig. 2: Earthquakes in the broader explored region. Data compiled from all available earthquake catalogues.

2.2. Seismo-geological considerations

The quality of bedrock at seismic stations is a very important parameter for seismic signal and seismic noise relations and therefore significantly contributes to potential seismic station sensitivity. Usually, the higher the acoustic impedance of the bedrock, the less seismic noise and the higher the maximum possible gain of a seismic station. Therefore, for each new seismic network, we should prepare a map showing simplified seismo-geological conditions in the region. We determine the quality of bedrock in terms of acoustic impedance of the rock shown on geological maps for each type of bedrock in the region. We divide the region into three or four quality grades and draw a map similar to the one in Fig.4. The table below gives an example of classifying different bedrock into 'quality' categories, grade five being the best rock.

Grade		
1	Unconsolidated clastic sediments (clays, sands, mud)	Alluvial sediments
2	Consolidated clastic sediments (sandstone, marls)	Schist
3	Less compact carbonatic rocks (limestone, dolomite) and less compact metamorphic rocks	Conglomerates, breccia, ophiolit
4	Compact metamorphic rocks and carbonatic rocks	
5	Magmatic rocks (granites, basalts), very compact metamorphic rocks	Marbles, quartzite

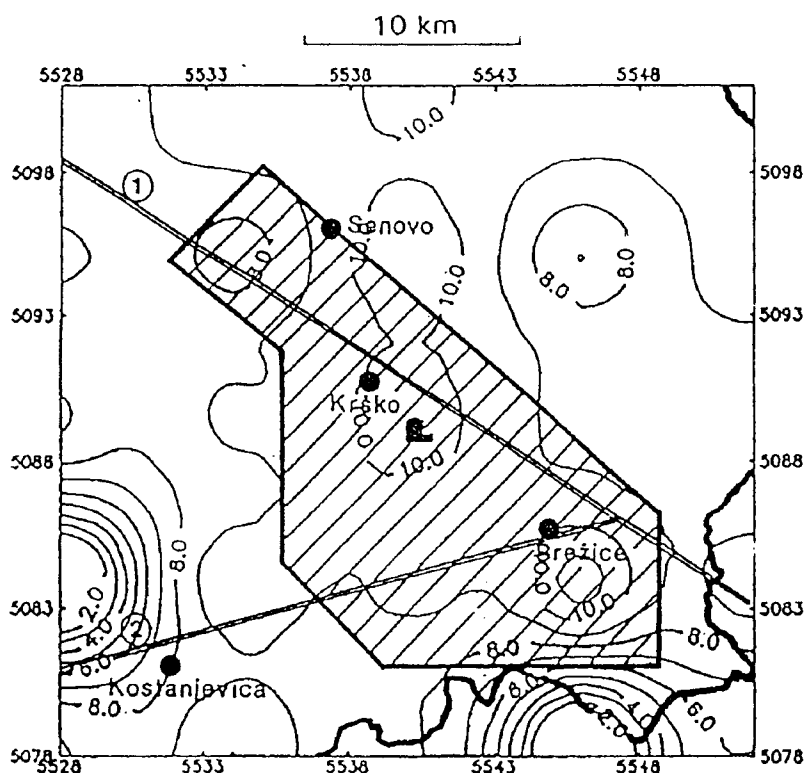


Fig. 3: Final choice of the region to be studied in detail by the seismic network (dashed area). Isolines show released log-seismic energy (for the time span of the catalogues) in J/km^2 .

2.3. Topographical considerations

Rough topography at seismic station sites may undesirably modify seismic event waveforms due to local effects. From this reason we should take into consideration topographical aspects of seismic sites as well. Seismic sites that are located in a moderately changing topography are preferred. Extreme steep mountain peaks or deep valleys may unpredictably and unfavorably influence recorded event waveforms and signal amplitudes.

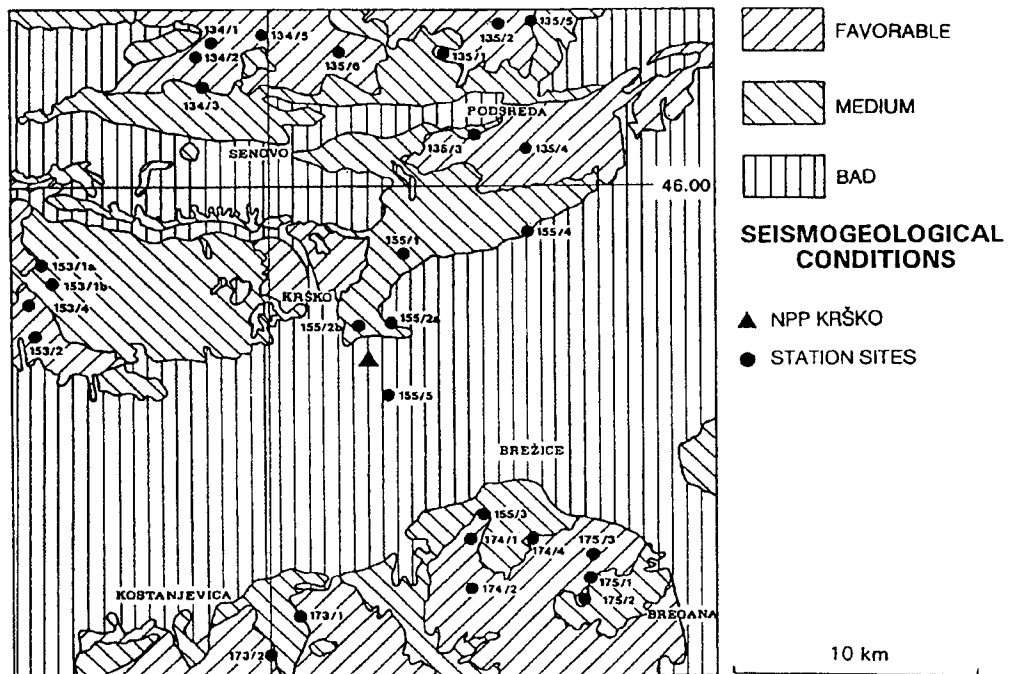


Fig. 4: The region of interest divided into three grades of bedrock quality and potential station sites.

There are also other undesirable effects of the topography around seismic stations. Mountain peaks are usually much more susceptible for wind-generated seismic noise, lightning damages, and sometimes also for icing of the equipment. Therefore, if possible, it is wise to mitigate them.

For radio-frequency telemetry networks, topographical aspects are extremely important. The choice of the sites is frequently based on RF link requirements rather than on seismological considerations, which are often over-compromised.

2.4. Station access considerations

Seismic stations are generally placed in remote places and as far as possible away from any human activity. This obviously results in a relatively difficult access. Public roads do not directly reach most good seismic stations. Walking a certain distance is more or less inevitable. Practice shows that newcomers often want to compromise too much in this respect .

Nevertheless, it is always possible to find a reasonable tradeoff between remoteness and ease of access. Stations which are very easy to access are usually noisy. Stations which are too difficult to access are expensive to establish and maintain. Accordingly they often suffer inadequate maintenance and long repair times.

Road maps and 1:25.000 scale topographic maps usually allow an easy estimate of the difficulties and time needed to access the potential station sites. In mountain regions not only the distance from the nearest road accessible by a four-wheel drive car is important. The height difference between the station site and the last point accessible by car should be considered too. One should take into account between 15 and 30 min (25 to 50 min) of cross-country walking time for each km of distance depending on vegetation and between 20 and 30 min for each 100

m height difference. Stations, which require more than half an hour cross-country walking, are rare. However, sometimes we have to accept even longer walking distances, particularly if data transmission using RF telemetry is involved.

Manufacturers frequently encounter an absurd desire to establish seismic stations at existing meteorological stations. This happens in the countries, which are new in seismometry and where meteorological institutions are appointed to take care about seismology in future. Note however that criteria for selection of meteorological and seismological stations are completely different. Such 'symbiosis' is rarely successful.

2.5. Evaluation of seismic noise sources

The assessment of man-made and natural seismic noise sources in the region from maps is the first stage of seismic noise study. Road traffic, railway traffic, heavy industry, mining and quarry activities, extensively exploited agricultural areas, and many other source of man-made seismic noise around the potential sites, along with natural sources like ocean and lake shores, rivers, waterfalls etc. can be evaluate in a qualitative manner from the maps and by asking questions to local authorities. The Manual of Seismological Observatory Practice, Willmore (Ed.), (1979) (Chapter: 'The organization of station networks', Subchapter: 'The siting of stations') gives valuable information about the minimum recommended station-site-to-noise-source distances. This information is given for three levels of sensitivity of seismic stations (A - very sensitive, B - moderately sensitive, and C - modestly sensitive), two geological conditions (hard rock and hardpan), and high and low seismic coupling between noise source and station site (condition a and b). The corresponding table is presented in Annex 1 to this lecture.

Note that these recommendations were designed for analogue paper seismogram technology of the sixties and seventies and are therefore most useful for seismic signal frequencies above 0.1 Hz; i.e. for medium- and high-frequency range of seismic signals. Seismic noise at low frequencies is mostly influenced by seismo-geological and environmental conditions at the sites and much less by some of seismic noise sources dealt with in this table.

Note also that map studies can give only a preliminary information about noise sources around the sites. "Paper work" should be obviously complemented by field measurements.

To demonstrate the evaluation of noise-source-to-station-site distances, we prepared a table (Fig.5) valid for a particular site. We should prepare a similar table for each station in a network and determine actual distances of the site from relevant seismic noise sources (the right most column) and compare them with the recommended minimum distances. The sites, which satisfy all or most of the recommendations, are the best. Local seismic noise sources like trees, buildings, fences, etc. require site visit, but this information can be added in the table later.

Once we have gathered this information about all potential sites in a network, we draw a map similar to Fig. 6. In this map all potential station sites and minimum recommended distances from known seismic noise sources are shown (circles around point noise sources and bands of appropriate width along with the roads or railways, for example). The minimum recommended distances in this figure correspond to a SP station with the gain around 25.000 at 1 Hz placed on hard clay, hardpan, or similar ground (Willmore, 1979). It is easy to get an overview over all noise sources at once from this figure and to see which and how many of them influence a particular potential seismic site.

STATION SITE NAME: Loma Palo Bonito COORDINATES: N 18° 46' 58.4" W 70° 13' 20.1"		SITE #: 7			DATE OF VISIT: 02/14/1998			ACTUAL DISTANCE
		HARD ROCK, GRANITE, ETC.			HARDPAN HARD CLAY, ETC.			
		RECOMMENDED MINIMAL DISTANCES [km]						
		A	B	C	A	B	C	
1. Oceans, coastal mountains system		300	50	1	300	50	1	75
2. Large lakes		150	25	1	150	25	1	22
3. Large dams, waterfalls	a	40	10	1	150	25	5	22
	b	60	15	5	50	15	10	
4. Large oil pipelines	a	20	10	5	30	15	5	
	b	100	30	10	100	30	10	
5. Small lakes	a	20	10	1	20	10	1	20
	b	50	15	1	50	15	1	
6. Heavy machinery, reciprocating machinery	a	15	3	1	20	5	2	25
	b	25	5	2	40	15	3	
7. Low waterfalls, rapids of a large river, intermittent flow over large dams	a	5	2	0.1	15	5	1	
	b	15	3	1	25	8	2	6
8. Railway, frequent operation	a	6	3	1	10	5	1	40
	b	15	5	1	20	10	1	
9. Airport, air traffic		6	3	1	6	3	1	
10. Non-reciprocating machinery, balanced industrial machinery	a	2	0.5	0.1	10	4	1	25
	b	4	1	0.2	15	6	1	
11. Busy highway, large farms		1	0.3	0.1	6	1	0.5	2.3
12. Country roads, high buildings		0.3	0.2	0.05	2	1	0.5	2.0
13. Low buildings, high trees and masts		0.1	0.03	0.01	0.3	0.1	0.05	0.03
14. High fences, low trees, high bushes, large rocks		0.05	0.02	5 m	0.06	0.03	0.01	0.02

LEGEND:

- A Seismic station with a gain of 200,000 or more at 1 Hz
- B Seismic station with a gain from 50,000 to 150,000 at 1 Hz
- C Seismic station with a gain of approximately 25,000 at 1 Hz
- a Source and seismometer on widely different formations or that mountain ranges or valleys intervene
- b Source and seismometer on the same formation and with no intervening alluvial valley or mountain range

Shaded cells: The actual distance from a source of disturbance to seismometer is smaller than the recommended distance for a particular gain of seismic station, ground quality, and seismic coupling.

Fig. 5: Minimum recommended station-site-to-noise-source distances according to Willmore (1979) and actual distances for seismic site Loma Palo Bonito, Dominican Republic, which is placed on hard granite rock. We see that for this particular station site all minimal distance requirements are fulfilled for a station with an approximate gain 50,000 to 150,000. Six criteria are not fulfilled (gray cells) for a station with 200,000 or more gain at 1 Hz.



Fig. 6: Map of the seismic network region with all potential station sites (full dots) and seismic noise sources – roads, railway, cities, villages, industrial facilities, quarries, etc – with minimum recommended distances drawn around them (for the case of gain 25.000 SP seismic stations at 1 Hz set on hard clay, hardpan and similar ground - case C,d according to Willmore, 1997).

2.6. Seismic data transmission and power considerations

For radio telemetry seismic networks we correlate RF data transmission requirements with the topography around the sites. Topographical 1:50.000-scale maps are most commonly used for this purpose. We seek for a topography, which enables reliable direct radio frequency (RF) links from the remote stations to the central recording site, or which assures the minimum number of RF repeaters if topography and/or distance do not allow direct connection. For details see chapter *Radio-link transmission of seismic data and feasibility survey*.

If we wish to use telephone lines for seismic data transmission, we check for phone line availability and the distances to which new phone lines would have to be laid. This information can be gathered from local phone companies. New phone lines are often a significant expense in the total cost of site preparation works. To avoid surprises it is wise to collect this information well in advance of the final selection of the sites.

If we plan to power seismic stations by main power, we have to check the availability of main power lines and the distances to which new power lines would have to be laid - or to decide for solar panels. The same comment as above applies to the cost of the new phone lines.

2.7. Land ownership and future land use

During planning of a new network it is also very important to clarify land ownership and future land use plans for the potential sites. It makes no sense to undertake extensive studies if one is actually unable to use certain sites because of property ownership issues or if it is probable that future development will make the site unsuitable for a seismic station in near future. This information should be gathered from local (land ownership) and regional (future land use) public offices and authorities.

If the land is privately owned, one should contact the owner as soon as possible and take every effort to agree on a renting or purchasing contract to both parties satisfaction. It is very important to have 'friends' rather than 'enemies' around the future seismic stations. In many developing countries this may be decisive for future safety of the installed equipment.

2.8. Climatical considerations

Several climatic parameters influence seismic site selection. Regional or national meteorological surveys provide this information. It is also found in yearly or longer-term bulletins, which are published by nearly every meteorological institution. It is true that in developing countries it is sometimes not easy to get the complete information. Nevertheless, we do not need precise values for these parameters. Even rough estimates help in proper site selection and proper design of seismic shelters.

The following parameters have important significance:

- Minimum and maximum temperatures determine how much thermal insulation is needed for the seismic vault and instruments. Below zero centigrade temperature may cause icing of antennae. Special antennae shielding is often required in very high mountains and polar regions.
- We need to know the frequency and maximum wind speeds at station sites. Wind is a primary source of seismic noise, so sites with less wind are much preferable than sites placed on windy mountain ridges.
- Insolation data determines the minimum size required for solar panels if the station is to be powered by solar panels. Number of sunny days in the worst month and the longest uninterrupted cloudy period in a year expected can serve as a measure.
- The frequency and amount of precipitation (total precipitation per year and maximal precipitation per hour) will determine what waterproofing measures are required to keep the seismic vaults dry.
- In colder climate annual snowfall levels determine how accessible a station will be during the winter, the waterproofing measures required, and optimal solar panel installation angle and size (if we are using solar panels).
- Considering information about lightning threat is very important and has a significant direct financial impact. Based on it, we decide on how extensive (and how expensive) lightning protection measures have to be taken or - how much lightning damages we will have to anticipate if these measures will not be implemented. The best is to obtain isokeraunic isolines, which are related to the probability of lightning strike. However, this data is rarely available. It is easier to obtain a less accurate but generally available meteorological parameter – number of stormy days per year. Lightning threat varies enormously from one region to another and locally depending on the topography. Serious consideration of this parameters pays off.

3. FIELD STUDIES

Field studies are the next step in the site selection process. Expect to make several visits to each potential site. A seismologist familiar with seismic noise measurements, a seismo-geologist, and a communication expert (if a telemetry network is considered) should all visit the sites. If site selection is purchased as a part of services (cf. section 5. below) manufacturer's experts will need from one to three days per site to accomplish the fieldwork. This assumes that all required maps and other information are prepared and logistics is well organized. Much depends also on country's infrastructure and the size of the network. If the network is an RF telemetry system, add 20% of time for topographical profiling and RF link calculations (cf. chapter *Radio-link transmission of seismic data and feasibility survey*). Experts visiting the sites should:

- verify the ease (in any weather) of access to the site;
- search for very local man-made seismic noise sources adjacent to the site, which may not be visible on the maps;
- perform seismic noise measurements;
- study the local seismo-geological conditions;
- investigate the local RF data transmission conditions (if applicable);
- verify power and phone line availability.

3.1. Station access verification

Station access should generally be guaranteed throughout the year. However, a few days of inaccessibility due to snow or high water per year can normally be tolerated. One should check this by talking to the local people.

If non-public dirt roads are used to access the sites, we should check about the future of such road. Sometimes roads owned by private, military, or forest authorities are built and then abandoned. If there is no guaranty that such remote dirt road will be maintained in future, it is better to reposition the seismic site. Rarely 'seismology' is financially strong enough to maintain such roads.

3.2. Local seismic noise sources and seismic noise measurements

During fieldwork we should explore the vicinity of the potential sites for local man-made sources of seismic noise which may not be resolvable from the available maps. A single small private 'industrial' facility too close to the site may ruin its seismic noise performances completely. Talking with as many as possible local people is the best source of information.

Measuring seismic noise at the site is an important task. Seismic noise varies greatly, depending on the season of the year, weather conditions, and innumerable daily occurrences. Seasonal variability of seismic noise has mainly natural causes and is clearly developed for $T > 2$ s only. It may be as large as 20 dB at the spectral peak for ocean storm microseisms around $T \sim 7$ s. Contrary to this, high-frequency noise is mostly man-made (traffic, machinery). At not very remote sites it often shows pronounced diurnal variations in the order of 10 to 20 dB as well. Ideally, to accurately weigh all these factors, it is best to take measurements at each site over a long period of time - long enough, in fact, to record a number of earthquakes too. This allows a comparison of the sites based on the signal-to-noise ratio. This is more relevant since sometimes higher noise at a site may be compensated by systematically larger signal amplitudes.

However, ideal long-term measurements are often not performed for financial reasons. But some measurements are much better than none. While short-lasting measurements can not provide complete information about the noise levels at the site, they are still very useful to identify man-made noise sources and to access the daily noise fluctuations in the crucial detection window for small and high-frequency local and teleseismic events (i.e. from 0.5 Hz to 20 Hz).

To weigh the influence of potential long-term natural seismic noise variation during fieldwork, we should obtain noise data from existing seismic stations in the region. If there are none we have to purposely set up a temporal reference seismic station, which is not moved from site to site. By comparing noise records taken at the same time at such stationary reference station(s) and the potential new site locations we can, at least with respect to the long-period natural seismic noise, weigh the representativeness of the noise data sampled at the potential sites. We can roughly scale it to the reference site(s). This assures that variations in natural seismic noise levels over time will not effect a fair comparison of different potential sites.

Records of seismic noise are usually re-calculated into noise spectra. In combination they may reveal much more information about the nature and importance of various seismic noise sources around the site than time-domain records or spectra alone (cf. Bormann (1998) and chapter *Bandwith dependent transformation of noise data from spectral into time domain and vice versa*). Fig. 7 shows a typical noise spectrum. One can easily see high contamination of the site by man-made seismic noise (frequencies around 15 Hz). Spectral spikes from 3 to 5 Hz shown in this spectrum originated in heavy machinery working in a 4 km distant quarry.

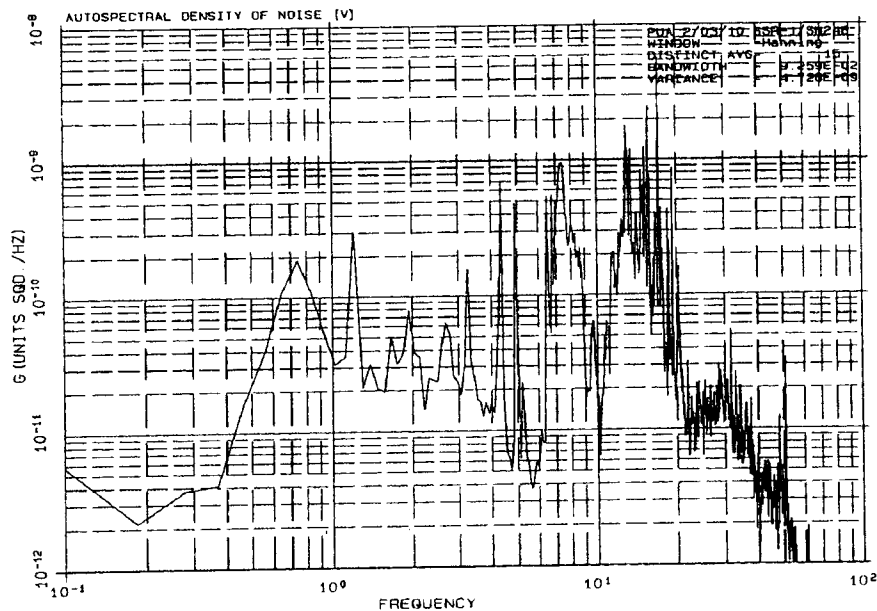


Fig. 7: A typical seismic noise spectrum (ground velocity power density in $\text{m}^2/\text{s}^2/\text{Hz}$) at a potential seismic station site showing man-made seismic noise generated by a nearby city and heavy machinery working in a 4 km distant quarry.

But at any event noise spectra should not be determined unless the related time-domain records have been inspected beforehand and cleaned from not representative spurious or transient events. The analysis of the noise conditions should never be made on the basis of the calculated spectra alone but always in conjunction with the related time-domain records.

At a minimum, make a few minutes long records of seismic noise to allow calculation of stable seismic noise spectra in the frequency range from 0.1 to 50 Hz for future SP seismic stations. Make a minimum of twenty to thirty minute records for noise spectra calculations from 0.01 to 50 Hz for BB seismic stations. Sampling rate should be 200 Hz or at least 100 Hz. In order to minimize, at least to some extent, the possible biasing influence of diurnal noise variations on the site quality assessment, the measurements at the various sites should be taken at about the same time of the day. Whenever possible, use the similar equipment and processing methods at your potential sites and at the reference station(s). This simplifies normalization procedure.

Note also that assessment of seismic noise quality for a future (V)BB seismic station requires much more effort. Days or even months of measurements are often required to get a full insight in seismic noise conditions at the potential site (Uhrhammer et al., 1998). A quiet short-period station site is not necessarily also a good low-frequency noise site. Seismic noise may behave differently in both frequency ranges.

In summary, in order to ease the interpretation of noise records and spectra and to put the assessment of site quality on a more objective footing one has to observe the following general rules with respect to the measurements:

- When searching for high-quality sites one has to be aware that one is measuring extremely weak ground motions at the resolution limit of the seismic sensor and recorder. Accordingly, one has to determine the level of internal instrumental and digitization noise first because it might be strong enough to seriously bias the records and calculated spectra at sites with very low ambient noise;
- The observer should stay-off (or better sit-off) very quietly and sufficiently far away from the seismic sensor while making noise measurements so as to avoid recording his own noise;
- Careful notes should be taken about all relevant environmental features and potential noise sources in the surroundings of the measurement site, best accompanied with photographic documentation of the area and of the installation of the equipment in the field. Particularly important are notes on geology, topography, vegetation cover, nearby rushing waters, weather conditions at the time of measurements, type and proximity of roads or railways and kind of traffic at the time of recording, nearby human settlements and on-going activities etc.;
- Stay far-enough away (several 100 m) from major power lines or transformer stations;
- Whenever possible, arrange for reference measurements at the same time (synchronize internal recorder clocks with your watches!);
- Whenever possible, measure at several alternative potential locations in the area of your planned site, at different times of the day (or season) and, if affordable, long enough so as to record not only ambient noise but also useful seismic signals (explosions, earthquakes);

3.3. Field study of seismo-geological conditions

During site visit a seismo-geologist studies the geology to determine its local complexity. As much as possible, uniform local underground conditions should be preferred for seismic stations. He also verifies the actual quality of bedrock as compared to that given in geological maps. He tries to estimate the degree of weathering that local rocks have undergone. This can sometimes give a rough estimate of the required depth of the seismic vault for placing the seismometers on unweathered rock. Unfortunately, many times it is highly unreliable to judge about the required vault depths in this way. At most of the sites only a shallow profiling, drilling, or actual digging

of the vault can reliably reveal how deeply the rock is weathered and how deep the seismic vault must be.

If there are local sources of seismic noise around the site, a seismologist should carefully consider seismic coupling between them and the seismic site, both by field inspection and interpretation of measured seismic noise. Local geological conditions and seismic coupling determine to a great extent how distracting such sources are. Sometimes the transition from soft-soil cover to an outcropping hard rock may effectively decouple high-frequency local noise travelling in the soft soil (Bormann et al., 1997). If shallow profiling is planned, the seismo-geologist should precisely determine the position of the shallow profiles.

3.4. Field survey of radio frequency (RF) conditions

A communication expert visiting the site examines potential local radio wave obstacles. He also examines the immediate topography surrounding the site because it can frequently not be resolved from the 1:50.000 scale maps, which are normally used in RF topographical profiling. These conditions define, to an important extent, the minimum required antenna height for reliable data transmission (cf. chapter *Radio-link transmission of seismic data and feasibility survey*).

3.5. Shallow profiling

Shallow profiling is the last step in the site selection process because it is the most expensive. It is normally done only at the most likely sites. Shallow refraction profiles reveal quantitative parameters of the rheological quality of the bedrock and enable determination of the depth of rock weathering. The results of shallow profiling determine the best "micro" position of the seismic vault as well as its required depth.

We usually make two approximately perpendicular profiles. Each should be about 100 meters long. Such profiles determine seismic wave velocity to the depth of 20 to 30 meters, which is enough even for the deepest seismic vaults.

If one chooses not to do profiling from any reason (most likely financial), then one has to expect surprises when digging seismic vaults. Often it is a matter of almost pure chance what one might run into. We need to dig until we reach bedrock and that can sometimes be very deep. Expect that vaults will have to be repositioned and re-dug if weathered bedrock happens to be too deep. These possibilities often make the relatively high cost of profiling a wise investment.

4. MODELING NETWORK LAYOUT CAPABILITIES

Once we have decided on the final number of seismic stations and we are very close to the final layout of the system, meaning that we have chosen two or three possible network layouts, the next useful step is to make a computer model of the network. The modeling should answer the question, which particular network layout performs best from different aspects of network performances. We can then choose competently the best one among the results from each possible network layout. Among the parameters we may wish to study are:

- network detectability in terms of distribution of minimum magnitude of events for a given number of records with a given earthquake signal-to-seismic-noise ratio (Fig. 8);
- precision (i.e. internal calculated accuracy) of event epicenter determinations in the region (Fig. 9);

- precision of event hypocenter determination in the region (Fig. 10);
- maximum magnitude of events that can be recorded without clipping (this presumes gain and dynamic range of the recording equipment used in the future network).

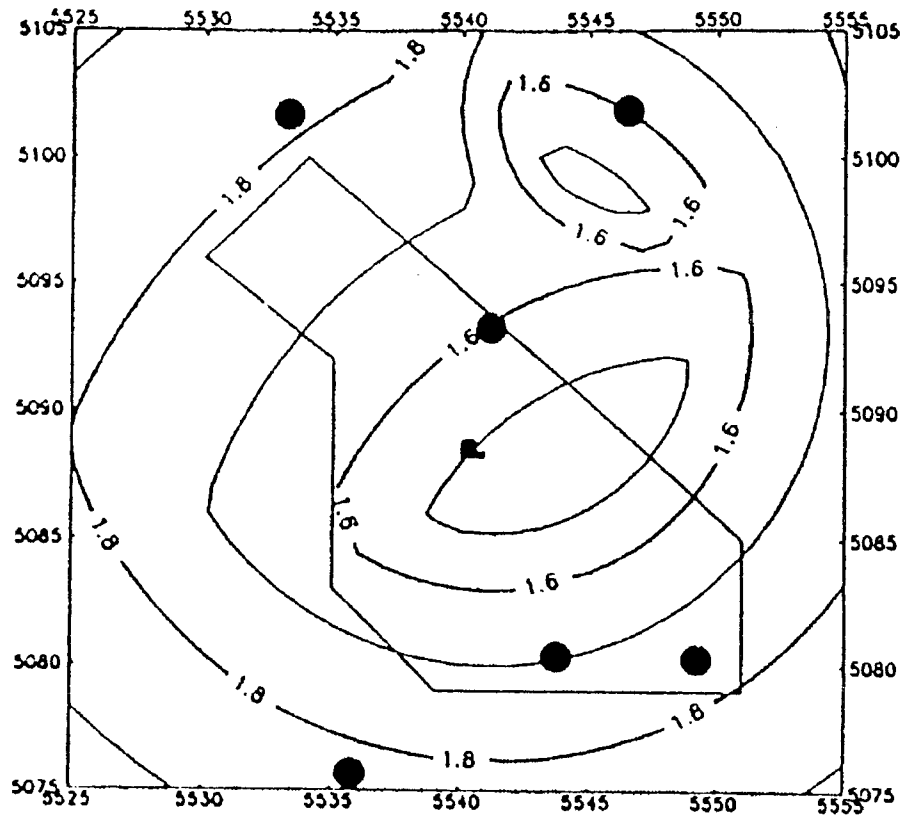


Fig. 8: An example of computer modeling of network capabilities. Isolines of minimum magnitude of events detected on 5 seismic stations (from six in the network) with signal to noise ratio >20 dB for the best of the alternative network layouts are shown.

Several methods of computer modeling of seismic networks are described in the literature, but an examination of each of them is beyond the scope of this paper. For our purpose simple methods suffice because the point is only the comparison of results between the various layout options. Determination of network's performances in absolute sense requires much more sophisticated approach.

Estimated uncertainties of P-phase readings, uncertainties of S-wave readings, uncertainties of P-wave and S-wave velocities, and predicted sensitivity of seismic stations based on the measured seismic-noise amplitudes at the sites are taken into account. A simplified and uniform seismic wave attenuation law in a homogeneous half-space or in a single or double layer ground model applies well for this purpose.

Note that the results of computer modeling based on such simplified model are almost never useful in an absolute sense. In general, an oversimplified seismic-wave velocity model, regional variations and anisotropy of ground, incomplete information about seismic noise at the sites, imprecise wave attenuation model, etc. prevent the results from being useful in an absolute sense. However, comparison of the performance between different layouts is still valuable and allows selecting the most suitable one among the potential options.

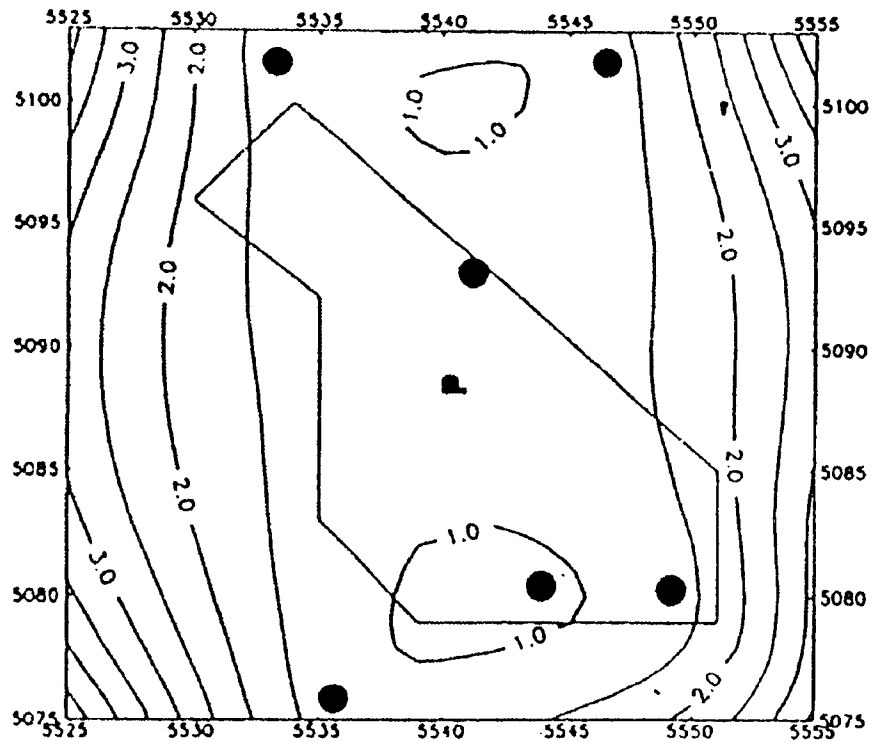


Fig. 9: An example of computer modeling of network capabilities. Isolines of uncertainty of epicenter determination in km (± 1 standard deviation) for the best of the alternative network layouts are shown.

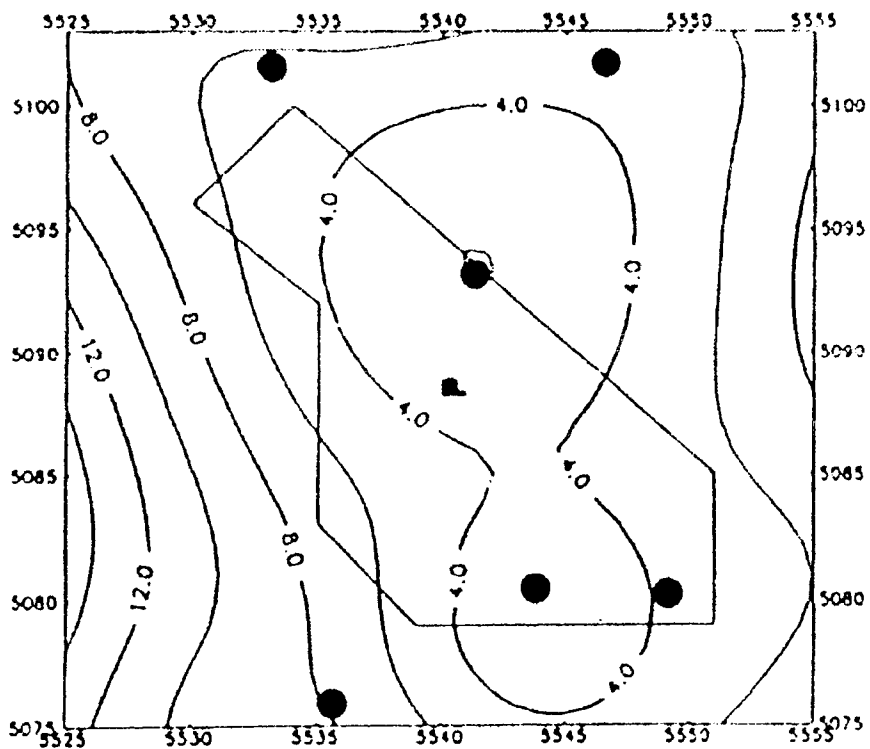


Fig. 10: An example of computer modeling of network capabilities. Isolines of uncertainty of hypocenter determination in km (± 1 standard deviation) for the best of the alternative network layouts are shown.

Several methods for direct computer calculation of optimal network's geometry can also be found in the literature (e.g. Kijko 1977; Rabinowitz and Steinberg 1990; Steinberg et al, 1995). However, practical limiting conditions with respect to infrastructure, topography and accessibility usually outweigh such theoretical approaches to the optimal network layout. Also, with these methods, sensitivity of the calculated 'optimal' layout to the initial conditions (like predicted gain of stations) is very high. This often makes their results questionable for practice. It is a fact that, in addition to theory, choosing the seismic network layout always involves making good, educated guesses based on experience. Also, site selection procedure is always a selection of potentially the best among available, and not so much good/bad type decision making.

5. WHAT TO PREPARE AND PROVIDE IF SEISMIC SITE SELECTION IS PURCHASED?

If seismic station site selection procedure is purchased as a part of services along with the seismic network equipment, the purchaser should prepare several logistic things to assure efficient work of manufacturer's experts. Note that these services are usually paid by the time the experts work on site selection for a new seismic network and that site selection is a 'stretchable' process. The more time (read money) he spends on it or the more efficiently he works during a given time period, the better resulting the station sites and consequently network performances will be. Therefore, it is a direct benefit of the customer that all required issues are taken thoughtfully and the needed working material and information is gathered as much as possible in full, as conditions in the particular country allow. The seismic network purchaser should prepare the following:

- A preliminary and approximate proposal of seismic network layout based on the goals of the network.
- A general-purpose 'high school type' topographical map of the whole region of the future network with color representation of terrain altitude (basic topographical display of the region).
- Regional (and local, if available) geological maps covering the region of the network.
- Map of past seismic activity in and around the region where the network is planned. Instrumental (if any) and historic data should be included.
- Seismo-tectonic map of the region (if available).
- 1:50.000 or 1:25.000 scale topographic maps covering the entire network region for RF profiling purpose for telemetry seismic systems. 1:50.000 scale maps are the best. 1:25.000 maps are better for fieldwork if there is no RF telemetry planned in the network. Get the permission to export such maps if they are under export restriction. The site selection provider will need them before fieldwork starts for initial studies, particularly if the network is an RF telemetry system.

- A state-of-the-art roadmap of the country for finding easy access to potential sites during fieldwork. Try to find the latest edition of such map. Road infrastructure changes fast in many developing countries.
- 1:5.000 scale maps (or at least 1:25.000 if 1:5.000 are not available) of the area surrounding the sites in case shallow seismic profiling of potential seismic sites is planned.
- Climatic data in the form of maps or tables published in annual or decade reports from the country's meteorological survey. Data should include precipitation, wind, insolation (if seismic stations will be solar panel powered), and lightning threat information (isokeraunic maps or number of storm days per year).
- Knowledgeable staff among the members of the institution, which will operate the network, and among well informed local people who are acquainted with local conditions at each potential station site. The member(s) of the responsible institution working in field together with the manufacturer's experts should obviously have full competency to make 'on spot' decisions regarding acceptability of access difficulties, land ownership issues, and other issues, which may have financial consequences during network establishment and future network operation. This person should be full-time and continuously with the manufacturer's experts until the site selection procedure is finished. If the region of the network is large, several different local persons may be needed. They can be members of local authorities (municipals, land use planing authorities, etc.) and should be familiar with local development conditions and present and future land use.
- One or two obviously four-wheel-drive vehicles in technically perfect condition. At least one car should be big enough to comfortably transport four people and measuring equipment in their original packing (two PC notebooks, seismometer, seismic recorder, cables and, in case of telemetry system, RF spectrum analyzer, provisory antenna mast, and Yagi antennae). Fairly roomy car is required. Enough cash, coupons or whatever document is required to purchase gasoline. Two or three customer's staff members (plus driver) are the best size team working with usually two manufacturer's experts.
- Air-conditioned working room with three tables, main power, and safe storage place for measuring equipment. If the network is an RF telemetry system, one of the tables must be large enough, minimum 1.5 x 3 m (5 x 10 feet), to allow working with several topographical maps stuck together while taking topographical profiles.
- Permits to enter restricted areas (army camps and training land, private land, natural reserves, state border regions, etc.) for local staff and foreign experts.

The maps sent to the site selection provider and used in the field are working copies. They are normally not returned to the customer. The maps are used when preparing the final report. If color maps are code protected against copying, two copies are needed (one for fieldwork and one for the final report).

Expect from one to three days of work for each station site of the network. Time spent widely depends on the dimensions of the network, infrastructure in the country, and general site accessibility. An efficient day of fieldwork usually lasts from sunrise to sunset.

Hint: Print this form and put check marks in appropriate bullets while preparing on site selection procedure.

REFERENCES

- Bormann, P., Wylegalla, K. and Klinge, K. (1997). Analysis of broadband seismic noise at the German Regional Seismic Network and search for improved alternative station sites. *Journal of Seismology*, **1**, 357-381.
- Kijko, A. (1977) An algorithm for optimal distribution of a regional seismic network. *PAGEOPH* **115**, 999-1009.
- Rabinowity N. and Steinberg D.M. (1990) Optimal configuration of a seismographic network: A statistical approach, *BSSA*, **80**, 187-196
- Steinberg, D.M. Rabinowitz, N., Shimshoni, Y., and Mizrachi (1995) Configuring a seismographic network for optimal monitoring of fault lines and multiple sources, *BSSA* **85**, 1847-1857
- Trnkoczy, A. and Zivcic, M. (1992) Design of a local seismic network for nuclear power plant Krsko. *Cahiers du Centre Europeen de Geodynamique et de Seismologie, Luxembourg*, **5**, 31-41.
- Urhammer, R.A., Karavas, W., Romanovicz, B. (1998). Broadband seismic station installation guidelines. *Seismol. Res. Letters*, **69**, 15-26.
- Willmore, P.L. (Editor) (1979). *Manual of Seismological Observatory Practice*, Report: SE-20, World Data Center A for Solid Earth Geophysics,

Annex 1

Recommended minimal distances from sources of seismic noise to seismic site after Willmore (Editor), 1979

STATION SITE NAME: _____ COORDINATES: N _____° _____' _____" W _____° _____' _____"		SITE #: _____			DATE OF ANALYSIS: ____/____/____			ACTUAL DISTANCE	
					DATE OF VISIT: ____/____/____				
		HARD MASSIVE ROCK, GRANITE, QUARTZITE, ETC.			HARDPAN HARD CLAY, ETC.				RECOMMENDED MINIMAL DISTANCES [km]
		A	B	C	A	B	C	[km]	
1. Oceans, with coastal mountains system		300	50	1	300	50	1		
2. Oceans, with broad coastal plains		1000	200	10	1000	200	20		
3. Inland seas, bays, very large lakes, with coastal mountain system		150	25	1	150	25	1		
4. Inland seas, bays, very large lakes, with broad coastal plains		500	100	5	500	100	5		
5. Large dams, high waterfalls, large cataracts		a	40	10	1	50	15	5	
		b	60	15	5	150	25	10	
6. Large oil or gas pipelines		a	20	10	5	30	15	5	
		b	100	30	10	100	30	10	
7. Small lakes		a	20	10	1	20	10	1	
		b	50	15	1	50	15	1	
8. Heavy reciprocating machinery, machinery		a	15	3	1	20	5	2	
		b	25	5	2	40	15	3	
9. Low waterfalls, rapids of a large river, intermittent flow over large dams		a	5	2	0.5	15	5	1	
		b	15	3	1	25	8	2	
10. Railway, frequent operation		a	6	3	1	10	5	1	
		b	15	5	1	20	10	1	
11. Airport, air ways heavy traffic			6	3	1	6	3	1	
12. Non-reciprocating power plant machinery, balanced industrial machinery		a	2	0.5	0.1	10	4	1	
		b	4	1	0.2	15	6	1	
13. Busy highway, mechanized farms			1	0.3	0.1	6	1	0.5	
14. Country roads, high buildings			0.3	0.2	0.05	2	1	0.5	
15. Low buildings, high trees and masts			0.1	0.03	0.01	0.3	0.1	0.05	
16. High fences, low trees, high bushes, large rocks			0.05	0.03	5 m	0.06	0.03	0.01	

LEGEND:

- A SP seismic station with a gain of about 200,000 or more at 1 Hz
- B SP seismic station with a gain from 50,000 to 150,000 at 1 Hz
- C SP seismic station with a gain of approximately 25,000 or less at 1 Hz
- a Source and seismometer on widely different geological formations or that mountain ranges or valleys intervene
- b Source and seismometer on the same geological formation and with no intervening alluvial valley or mountain range

Instructions for use of the form:

1. Get the information about all potential sources of seismic noise around the site and write the distances to them in the most right column of the table.
2. From geological maps and by visiting the site decide on the quality of the bedrock at the site. Decide either for 'good' rock (left three columns with minimal recommended distances) or for 'less suitable' ground (right three columns with the minimal recommended distances).
3. For each seismic noise source (where applicable) decide about seismic coupling between seismic site and the noise source. Select the appropriate horizontal line a) or b) with minimal recommended distance.
4. Mark appropriate cells in the table based on the steps #2 and #3 and compare their content with the actual minimal distances in the right most column.
5. Shade all cells where the minimal recommended distances to a noise source is bigger than the actual distance in the right most column. Find the most left column, C, B, or A, where no shaded cells appear. This column roughly denotes the approximate expected maximum gain of a SP seismic station at this site and 1 Hz at the site.
6. Make such table for all potential seismic sites studied and compare the results among alternatives.

SURFACE VAULT SEISMIC STATION SITE PREPARATION

Amadej Trnkoczy

Kinematics SA, Z.I. Le Trési 3
CH-1028 Préverenges, Switzerland

1. INTRODUCTION

Civil engineering work at remote seismic observatory stations should insure that modern seismic instruments can be used to their fullest potential by sheltering them in an optimal working environment.

Today's high dynamic range, high linearity seismic equipment is of such quality and sensitivity that seismic noise conditions at the site and the environment of the sensors have become much more important than in the past. Apart from site selection itself, the design of seismic shelters is the determining factor in the quality of seismic data acquisition.

Seismic vaults are today the most often built type of seismic stations. They are the least expensive, however they suffer seismic noise the most. A variety of factors must be considered before the optimal technical and financial solution of the seismic vaults can be reached: type of equipment installed, geological conditions, variety of available construction materials, accessibility of the remote stations, and climate at the site, for example.

Various solutions can be employed with equal success. Much depends on potentially planned future upgrades of the instrumentation and site, how comfortable the working conditions are desired for maintenance and service personnel, and, of course, on the funds available. Because of these diverse considerations, no firm design and civil engineering drawings are provided in this document. Instead, the general requirements that must be satisfied are described in detail so that any qualified civil engineer can design the shelter for optimal performance, taking into consideration local conditions in a given country and at a specific site. A design example of a seismic vault for a three-component short period (SP) station is also shown and its upgrade for broad band (BB) and potentially very-broad band (VBB) seismic sensors.

Vault shelter for seismic data acquisition and transmission equipment should satisfy the following general requirements:

- Provide adequate environmental conditions for the equipment.
- Assure the proper mechanical contact of seismic sensors with bedrock.
- Prevent seismic interaction between the seismic shelter and the surrounding ground.
- Mitigate seismic noise generated by wind, people, animals, and by potential noise sources within the vault.
- Assure a suitable electric ground for sensitive electronic equipment.
- Provide sufficient space for easy access and maintenance of the instruments.

These requirements will be discussed in detail. Some technical hints are given at the end of this document. Drawings and photos of a seismic vault with some technical details are also included.

2. CONTROLLING ENVIRONMENTAL CONDITIONS

Adequate shelter for seismic equipment should:

- Prevent large temperature fluctuations in the equipment due to day/night temperature differences or because of weather changes,
- Prevent large temperature fluctuations in the construction elements of the vault, resulting in seismometer tilts,
- Assure adequate lightning protection,
- Mitigate electromagnetic interference (EMI),
- Prevent water, dust and dirt from entering the shelter,
- Preventing small animals from entering the shelter.

At very low seismic frequencies and in VBB seismometers, air pressure changes also influence seismometer output. Special installation measures and processing methods can be used to minimize the effect of air pressure. However this issue will not be treated in here. See Beauduin, R. et al, 1996 for more information. A documentation of typical 'classic' design of seismometer vault is given in the 1979 edition of the Manual of Seismological Observatory Practice, Willmore while installation guidelines for BB and VBB stations are given by Uhrhammer et al. (1998).

2.1. Mitigating temperature changes

In general, seismic equipment can operate in quite a broad temperature range. Data sheets guarantee that most of the equipment on the market today functions properly between -20° to $+50^{\circ}$ C. However, this range is merely operational – that is, guaranteeing only that the equipment functions at a given (constant) temperature within these limits.

Variations of temperature in time, particularly diurnal, are far more important than the high or low average temperature in itself. Many broadband seismometers require mass centering if the temperature “slips” more than a few degrees C, although their operating range is much wider. Frequently even small temperature changes cause problems with mechanical and electronic drifts, which may seriously deteriorate the quality of seismic data at very low frequencies. Unfortunately, the practical sensitivity of the equipment to temperature gradients is rarely provided in data sheets. Very broadband (VBB) and some broadband (BB) seismometers require very stable temperature conditions. They are sometimes difficult or impossible to assure in a vault-type seismic shelter for VBB seismometers and require special installations (see Uhrhammer et al. 1998). Short period (SP) seismometers, particularly passive ones, and accelerometers are much less sensitive to temperature changes.

Certain elements, for example, some computer disk drives, diskette drives, and certain time-keeping equipment may also require narrower operating temperature tolerances.

In general, thermal drifts should be kept acceptably small by thermal insulation of the vault. However, the requirements differ significantly. Maximum $\pm 5^{\circ}$ C short-term temperature changes can be considered a target for passive SP seismometers and force feedback active accelerometers. To fully exploit the low frequency characteristics of a typical BB seismometer with a 30-sec period, the temperature must be kept constant within less than one degree C. To fully exploit VBB sensors with several-hundred-seconds period, only a few tens of milli-degrees C per month are recommended.

Data loggers, digitizers can tolerate less stable temperatures – on average, ten times greater changes than BB seismometers for the same output voltage drift. The best of them, for example, change their output voltage less than ± 3 counts in room temperature conditions. If daily temperature changes are less than 1°C , their output voltage changes less than ± 1 count (Quanterra, 1994).

The most effective way to assure stable temperature conditions is an underground vault that is well thermally insulated (Fig.1 and Fig.2). Underground installations are also best for a number of other reasons.

Thermal insulation of active seismic sensors is usually made in two places. First, the interior of the vault is insulated from external temperatures, and second, the sensors themselves are insulated from residual temperature changes in the vault. In the most critical installations, the seismic pier itself is also insulated along with the sensors.

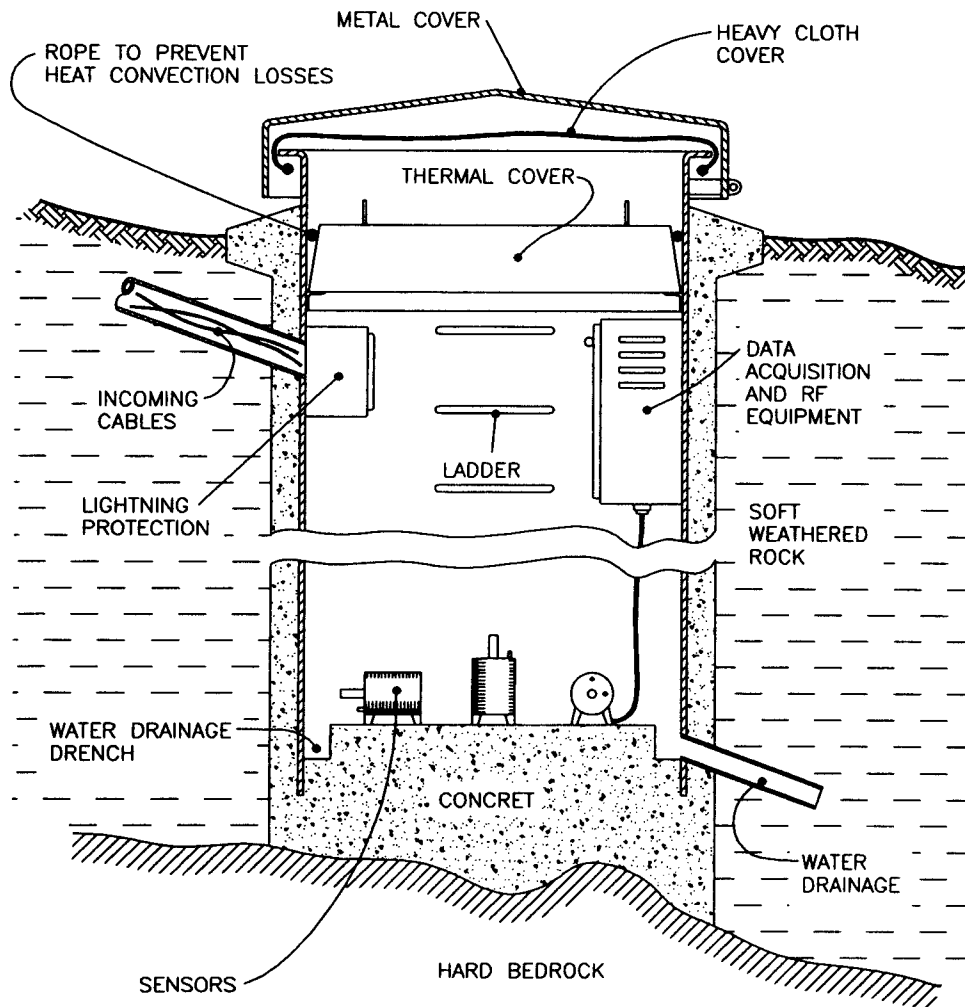


Fig. 1: An example of a vault of a short-period three-component seismic station made of a large-diameter metal pipe with thin concrete walls.

Underground vaults are usually insulated with a tight thermal cover made of styrofoam, foam rubber, polyisocyanuratic foam, or other similar, non-hygroscopic insulation material (Fig. 1, 3, and 4). Such materials are usually used in civil engineering for thermal insulation of buildings. They come in various thicknesses, often with aluminum foil on one or both sides. This aluminum layer additionally prevents heat exchange by blocking heat transfer through radiation. Thinner sheets can be glued together to make thicker ones. Casein-based glues are appropriate for styrofoam and expanding polyurethane resin is used to glue polyisocyanuratic foam sheets.

In continental climates, a 20 cm (8") layer is considered adequate but in extreme desert climates, up to 30 cm (12") of styrofoam is recommended. In equatorial climates a 10 cm (4") layer is considered sufficient.

There are two thermal cover design issues that are particularly important.

Special care must be taken to assure a tight contact between the vault's walls and the thermal cover. If it is not tight, then heat transfer due to convection through the gaps can be easily larger than heat transfer through the thermal cover by conduction. In such cases, the thermal cover becomes inefficient.

One way to achieve a tight thermal cover is shown in Fig 5. A "rope" is pressed into the gap between the vault's walls and the thermal cover. This "rope" is made of insulating fibers and is usually used for industrial hot water pipe insulation. It is available in different sizes and is inexpensive. The rope insulation must be tightly packed into all the gaps between the cover and the walls, otherwise heat convection will undo the insulating effects of the cover itself.

The cover should be placed at or below the level at which the ground heats up during the day – not on the top of the vault. In desert areas, surface ground temperatures can exceed 80° C. At 30 cm (12") depth, temperatures of 50° C is not unusual. In such conditions the thermal cover must be placed 40 - 50 cm (16" - 20") below ground level. A thermal cover of any thickness at the top of the vault, particularly if the vault's rim stands significantly above the surface, has almost no effect.

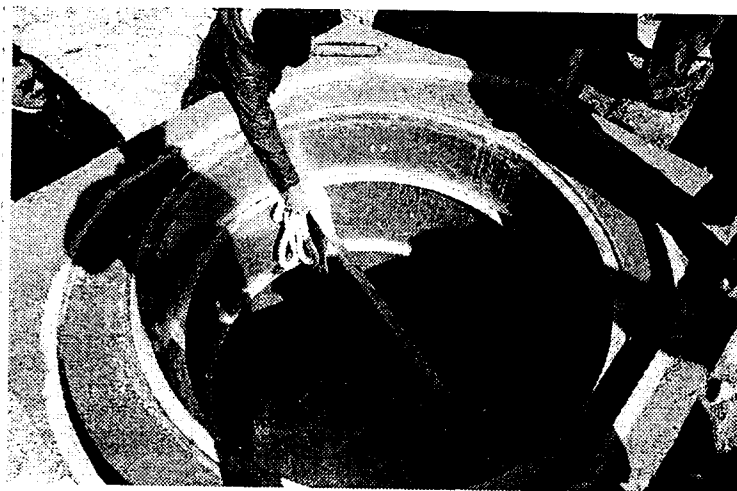


Fig. 2: Interior of a seismic vault made of welded metal sheets. The vault is big enough to accept weak and strong motion instrumentation as well as data acquisition and transmission equipment.

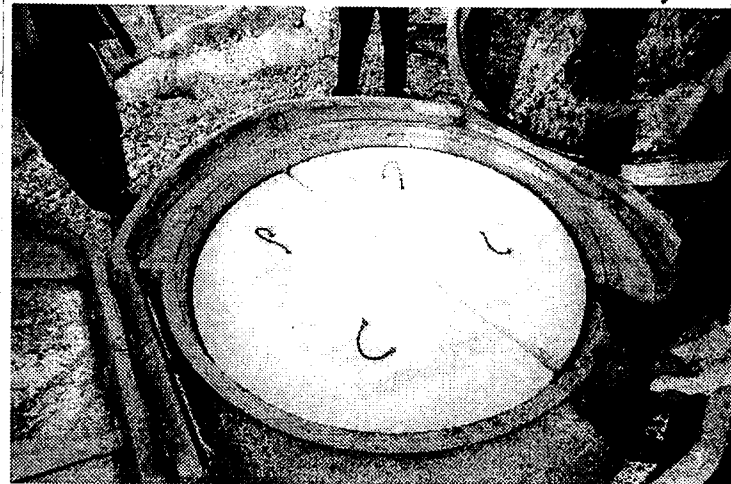


Fig. 3: The thermal cover of a seismic vault in two pieces made of thick styrofoam. The gaps between the cover and the vault walls and between both pieces must be made tightly sealed.



Fig. 4: Installing thermal cover in a seismic vault. In climates with big diurnal temperature changes the cover should be positioned lower in the vault where external ground temperature does not change significantly.

If vaults are used for BB or even VBB stations (see Wielandt, 1990), it is advisable to make a second inner thermal cover just above the sensors but below the floor where all other equipment is installed (Fig. 6). Since the most of maintenance work relates to batteries, data recording, and data transmitting equipment, the thermal- and mechanical-sensitive BB/VBB sensors are not disturbed at all during service and maintenance and additionally isolated.

A thermal isolation box is usually put around the sensors to additionally insulate them. Thermal insulation of the seismic pier itself, together with the seismometer, is the best method of insulation (Fig. 7). This method keeps the heat transfer between seismometer and vault interior

as low as possible, while at the same time assuring good thermal contact with the thermally very stable ground. Thus, the thermal inertia of the system is very large, limiting the rate if temperature changes to minimum.

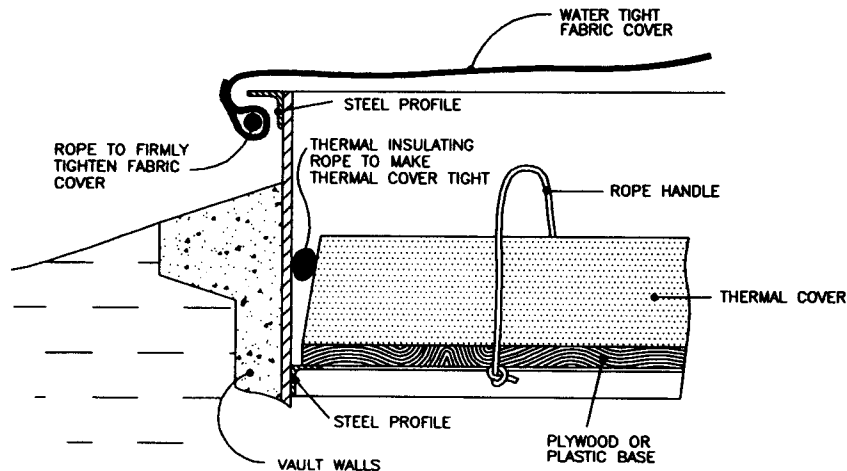


Fig. 5: Detail of making thermal cover effective by filling up the gaps between the cover and vault walls with insulation material and making the vault tight against dust, dirt, and rain during windy periods with a fabric cover.

The seismometer box and the entire exposed seismic pier are typically covered by a 10 - 20 cm (4" - 8") thick sheets of insulating material. The seams between the insulation sheets should be well filled with liquid foam. For details see Uhrhammer et al. (1998).

2.2 Thermal tilt mitigation

To study extremely low frequency range with VBB seismometers, special measures are required to prevent thermal deformations and tilts of the seismic pier in the vault. Modern VBB sensors, horizontal components in particular, can detect tilts of a few nanoradians. A human hair placed under the corner of a level football field would cause such a tilt or an air pressure difference of only 0.1 mbar over a distance of several km.

According to Wielandt (1990) a tilt of $\sim 10^{-9}$ rad would result in a noise ground acceleration amplitude of 10^{-9} g in the horizontal components but only of 10^{-11} g in the vertical one.

Homogeneity of the seismic pier and surrounding soil, and civil engineering details of vault design become very important. Uhrhammer and Karavas (1997) recommend the physical separation of the seismometer pier and the vault walls (Figs. 6 and 7). This separation assures that minute changes in the dimensions of the vault walls due to temperature change do not tilt the seismic pier. However, since such seismic vaults are not constructed "in one piece," one has to be particularly careful that the contact between the pier and vault walls is made watertight.

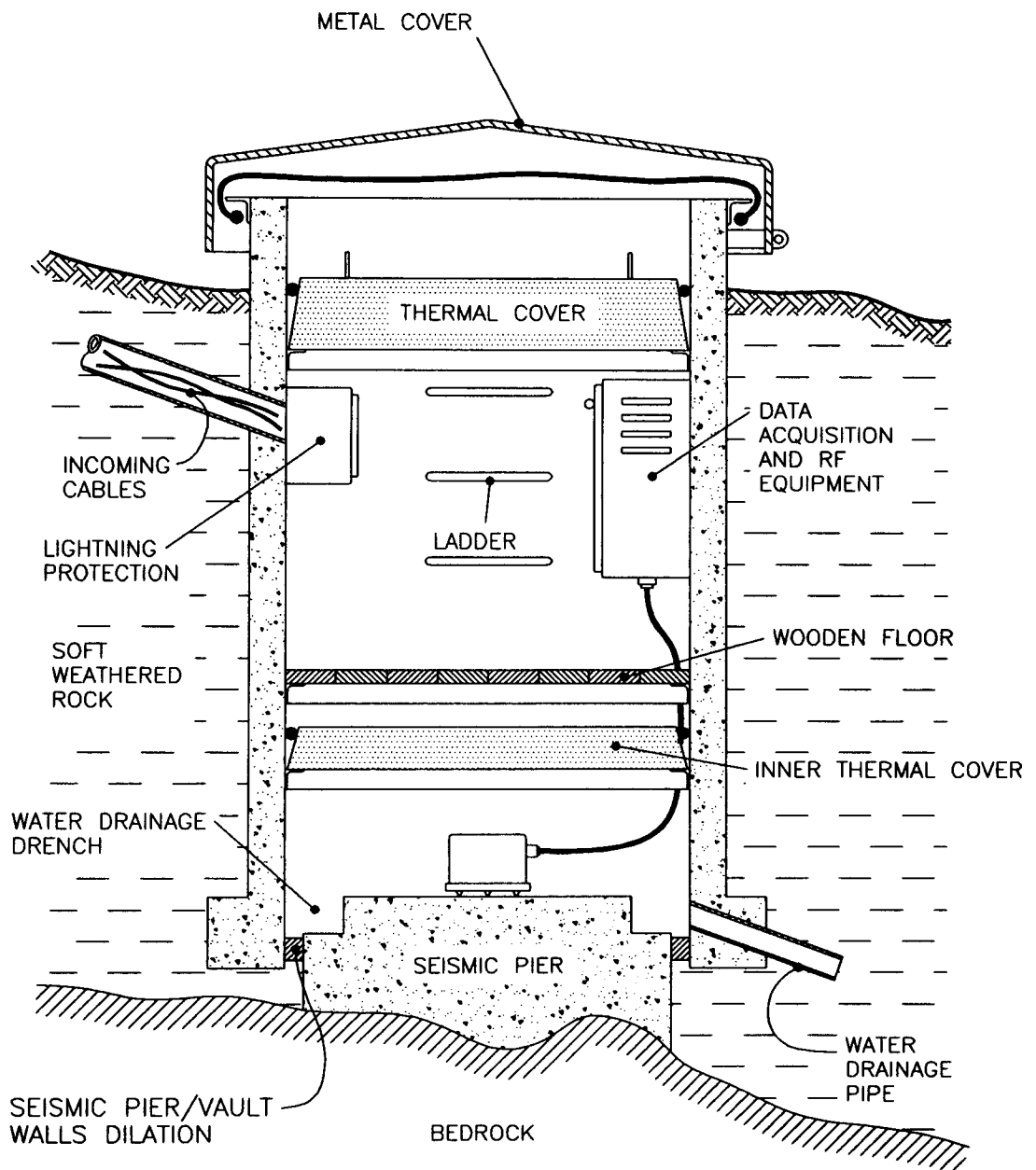


Fig. 6: An example of a BB or VBB seismic vault with a separate compartment for sensors and double thermal cover. Usually the sensor itself is additionally isolated.

The seismic pier should be made of homogenous material and neither it nor vault's walls should use any steel reinforcement. Steel and concrete have different temperature expansion coefficients, which cause stress and unwanted minute deformation of the structure of the vault

if temperature changes. Steel is unnecessary anyhow because structural strength is practically never an issue except in the very deepest of vaults. Sand aggregates used for concrete should be homogenous, fine-grain, and of similar sizes rather than different sizes as in the usual concrete mixture. Uhrhammer et al. (1998) recommend sieved sand with 50% Portland cement. After the pier is poured, the concrete must be vibrated to remove any trapped air.

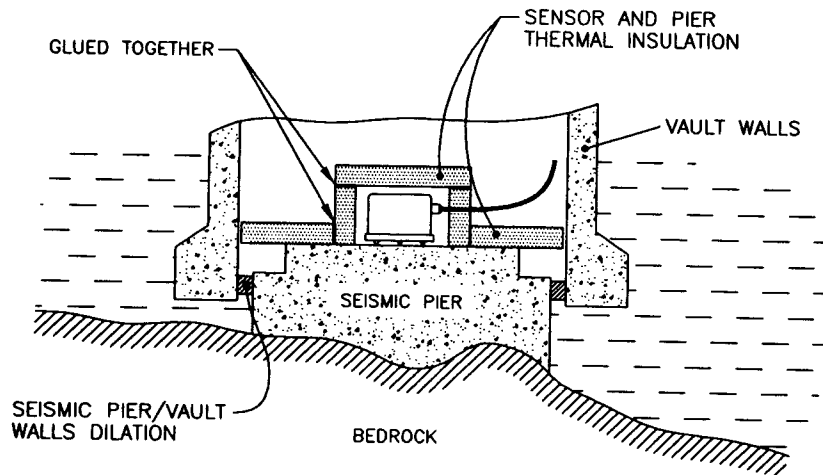


Fig. 7: Thermal isolation of a VBB sensor and surrounding seismic pier and mechanical separation of the pier from the vault walls for the most demanding applications.

2.3. Lightning protection

Lightning protection is probably the most important factor in preventing seismic station failures. Lightning causes most of the damage to seismic equipment around the world. We have known of several seismic networks that lost half or more of their equipment less than two years after installation because of inadequate lightning protection measures. Of course a direct hit of lightning will cause equipment damage despite the best protection. Fortunately, this rarely happens. However, lightning, even some distance from the station, can cause severe damage. The vast majority of lightning damage is a result of voltage induction surges in cables. Many high quality seismic instruments already have internal lightning protection circuitry, however these measures are sometimes not enough for high lightning threat regions. Such lightning protection may include gas-discharge elements, transorbs, voltage dependant resistors, and similar protection components.

Climactic and topographical conditions at every site vary greatly and determine the degree to which one should protect his system from lightning. Tropical countries and stations on top of mountains are the most vulnerable and therefore require maximum lightning protection measures.

Lightning protection includes the following measures:

- Enclose the equipment in a “Faraday cage,” either by making a metal shielded seismic vault or a loose mesh of ground metal strips around the vault. This creates as great as possible an equipotential electric field around the equipment, thus decreasing voltage drops on equipment and cables during lightning strikes,

- A good grounding system (no practical lightning protection measure works without grounding),
- Protection of all cables entering the seismic vault from voltage surges,
- Proper cabling that minimizes voltage induction during lightning.

If any of these measures are not taken, the others become largely ineffective.

The best lightning protection is a metal seismic vault. The metal walls can be very thin to protect against lightning. The exterior of the vault should not be painted so that good electrical contact can be made with the surrounding soil, thereby lowering grounding impedance. If the main cover or any other part of the vault is metal, it should be connected to the vault's walls by a thick flexible stranded wire.

In any case it is necessary to protect all cables entering the seismic vault. The lightning protection equipment of the cables must be installed at the point where they enter the vault. It must be grounded at the same point with a thick copper wire or strip that is as short and straight as possible. The unprotected part of any cable within the vault must be kept to an absolute minimum. All cables entering the vault must be protected if one wish to protect his equipment from lightning damage. Voltage surges usually occur in all cables at a station, so leaving a single long cable unprotected is virtually the same as leaving all cables unprotected.

All metal equipment boxes should be grounded with a thick copper grounding wire or strip (> 25 mm² cross-section) to the same point where lightning protection equipment of incoming cables is grounded. Follow a tree-shaped scheme of grounding wires. All these wires should be as short as possible and without sharp turns. All cables in a vault should be kept at a minimum length. No superfluous cables or even coiled lengths of excess cables are acceptable. These are true lightning catchers.

Usually telephone line and main power line companies can install lightning protection equipment of their lines. This should be required from them when asking for these utilities. However, manufacturer of seismic equipment also can provide and install such equipment if asked for.

Note that there is no 100% safe lightning protection system in the world. The money invested in it only reduces the probability of damage to an acceptable level. However, for high lightning risk regions and for expensive and delicate seismic equipment, long years of practice show that these investments pay off very well.

2.4. Electro-Magnetic Interference (EMI) protection

The EMI problem is normally not a very important issue because seismic stations are generally situated in very remote rural locations. However, in such regions the main power lines are frequently of low quality. We recommend using main power voltage stabilizing equipment in these cases. This equipment usually incorporates EMI filters and voltage surge protection, which further protects seismic equipment from failures and EMI-generated noise. In general, metal seismic vaults protect equipment from EMI very effectively.

Some passive seismometers with moving magnets and separate seismic components radiate EMI during mass motion. Since this may influence surrounding sensors, do not install such seismometers too close to each other. A minimum distance of 0.5 m (1½ feet) between them is recommended. A very simple test can assure you that any cross talk is insignificant. Disconnect and un-damp one component, move the seismometer mass by shaking slightly and measure the output of both other components. There should be no cross-talk. The

seismometers should not be placed too close to the metal walls of the vault either. A minimum distance of 0.3 m (1 foot) is recommended. This prevents potential changes in the static magnetic field, which may slightly influence the generator constant of some seismometers.

Data recording equipment with main power transformers should not be installed next to sensors on the same pier. The transformer may cause noise in the seismometer signals either through its magnetic field or due to direct mechanical vibrations at 50/60 Hz. Place such equipment in a metal housing and install it on the wall of the vault away of the sensors.

2.5. Water intrusion protection

Water entering seismic vaults is the second most frequent cause of seismic station failures.

The most effective way to prevent water damage is vault drainage (Fig. 8). Use a hard plastic tube of about 3 cm (1") diameter for water drainage. Such tubes are used for water pipelines. The drainage pipe must have a continuous and at least 3% grade, particularly in regions where the ground freezes. In some places drainage is impossible, particularly with deep vaults. In these cases the water tightness of the seismic vault is of the utmost importance. Note that a high ground water level and porous concrete vault walls more or less guarantee water intrusion.

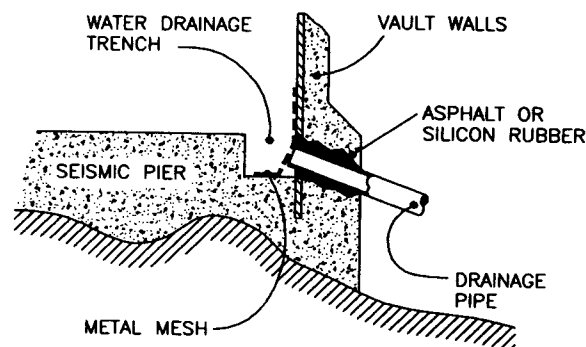


Fig. 8: Water drainage pipe and vault trench around the seismic pier.

Water tightness is easy to achieve if the vault's walls are made of metal welded from plain or corrugated iron sheets or from large-diameter metal tubes, providing the welds are good quality.

If the vault is made of concrete and has no water drainage, the concrete should be of a very good, uniform quality. Water-resistant chemicals should be added to the mixture to help keep it watertight. The concrete must be vibrated during construction to assure homogeneity of the walls.

The bottom of the seismic vault - seismic pier - is always made of concrete. Once again, use good quality, uniform-aggregate concrete with water-resistant additives. The bottom should have a water drainage ditch (Figs. 1 and 8) around the flat central pier on which the sensors are installed. For vaults with external water drainage, the ditch should be at least 5 cm (2") deep and 10 cm (4") wide. For the vaults without drainage the ditch should be larger (at least 15-cm by 15-cm or 6"x 6") that it can collect more water.

Making the vault walls/floor joint watertight requires a special care. Use asphalt to seal any cracks by heating the concrete with a hot-air fan and then pour hot asphalt into them. The cables entering the vault also require some special care. They are normally installed in a plastic or metal tube that should fit very snugly into the appropriate hole in the vault wall. Use silicon rubber or asphalt to seal any gaps.

In vaults designed for VBB seismometers whose seismic pier is mechanically separated from the walls, water tightness represents a special challenge. Once again use soft asphalt to make the gap between the walls and the pier watertight.

The upper rim of the vault must be at least 30 cm (1 foot) above the ground. At sites where a lot of snow is expected, this dimension should be higher, up to 60 cm (2 feet). Slush is particularly dangerous in regard to keeping vaults watertight. If possible, the surrounding terrain descends radially from the top of the vault.

One practical detail is to create a small “overhang” at the top edge of the vault (see Fig. 5). This ledge should be about 5 cm (2”) out from the vault wall. A thick, watertight fabric cover can be hooked over this metal edging. The cover is pulled tight to the vault by rope and prevents water from entering the vault during windy, rainy periods. It also protects against dust and dirt and provides some additional thermal insulation.

To minimize the danger of equipment flooding, install all equipment except for the sensors on the wall of the vault.

2.6. Protection from small animals

On first glance this issue may seem amusing. However, animals frequently use seismic vaults as dwellings. We have seen some very strange “seismic” records of ants, grasshoppers, lizards, and mice. Ants, reptiles, mice, rats, etc., can cause not only mysterious seismic records but also severe damage to cables and other plastic parts of the equipment.

Tight metal (particularly effective), fabric or thermal vault covers usually prevent animals from entering the vault from above. Plastic tubes for cables and drainage should be protected by metal mesh. Placing metal, wool or glass shards in the free space in these tubes also helps. Insecticides can be used to drive away ants and other insects.

3. CONTACT WITH BEDROCK

Good contact between seismic sensors and bedrock is a basic seismological requirement. Underlying soil and/or weathered rock layers will modify seismic signals without this vital contact between bedrock and sensor. Today it is well known that the interaction of soft superficial soil can significantly modify seismogram amplitudes, waveforms, and their spectral properties.

The depth of bedrock (which is effectively equivalent to the depth of the vault) and the degree of weathering of layers beneath the surface can be determined by shallow seismic profiling of the site, by drilling (most often too expensive), or by actually digging the vault. Except for the sites where the solid bedrock is evidently outcropped, will a local surface geological survey provide enough information about the required depth of the seismic vault.

If one chooses not to do shallow seismic profiles, then he has to expect surprises. It is often a matter of pure chance what we run into. We will need to dig until we reach bedrock and that

can sometimes be very deep; vaults have to be repositioned and re-dug if weathered bedrock is extremely deep. These risks make the relatively high cost of shallow profiling a wise investment.

A definition of “good” bedrock is necessary during digging vaults without profiles. Unfortunately, the definition is fairly vague, especially because some recent studies show that even an apparently hard rock site may still have significant amplification compared to true solid bedrock. As a rule of thumb, “good” bedrock is rock hard enough to prevent any manual digging. If profiles are available, P velocities measured should be higher than 2 km/s.

Seismic vaults are on average 2 to 6 m (7 to 20 feet) deep. At sites where the solid, non-weathered bedrock is outcropping, the required depth is defined solely by the space required for the equipment. One meter (3 feet) or even less may be adequate if the temperature stability requirement can be fulfilled under the given local climate conditions. On some highly weathered rock sites the required vault depth may exceed 10 m (30 feet). In some places a reasonably deep seismic vault cannot reach bedrock at all. Borehole seismic stations are required there. Sometimes, however rarely, vaults are still used at such places. A decision for such station must be firmly based on other seismological factors like network geometry, lack of bedrock anywhere in the region, and special interest in certain places. The number of these stations in a network should be kept at a very minimum.

4. SEISMIC SOIL -STRUCTURE INTERACTION AND WIND-GENERATED NOISE

The theories behind design and construction of seismic stations has greatly evolved in the last few decades. The increased sensitivity of seismic stations and the complexity of seismic research, based more and more on waveforms, require very quiet sites and distortion free records. Eighty, sixty years ago, seismic stations were usually situated in houses and observatories. Sensors were installed on large, heavy concrete piers, mechanically isolated from structural elements of the buildings, sometimes well above the ground (see see chapter *Organization of Station Networks* in Willmore, 1979).

However, scientists increasingly observed that the interaction between surrounding soil and civil engineering structures in such installations substantially modified seismic signals during seismic events (particularly if the site is on relatively soft ground). Structures swinging in the wind also caused undesired seismic noise and strong unilateral wind load or insolation on building's walls or the rock face of seismometer tunnel entries caused intolerable drifts in long-period or VBB records.

More and more evidence arose (Bycroft 1978, Luco et al., 1990) proving that every structure at the site modifies seismic waves to some extent. Therefore, today's seismic stations are mostly ground vaults, light constructions, and jutting only a few decimeters (about a foot) above ground. All buildings, antenna and other masts are built well away from the vault to minimize interaction.

Ideally, there is no seismic signal modification by the soil-vault structure interaction if vault's average density (taking into account the empty space in the vault as well) equals the density of the surrounding soil. However, in practice, seismic station design is never based on calculated average densities. The most important factors are that:

- the design is not too heavy, particularly if the surrounding soil is soft,
- all potential buildings and masts are placed away from the seismic vault,
- the vault rises above ground level as little as possible to minimize wind-generated seismic noise.

5. OTHER NOISE SOURCES

We recommend that seismic stations are fenced, despite the fact that fences usually represent a significant expense. There are a few exceptions, like stations in extremely remote desert or mountain sites. The fence minimizes seismic noise caused by human activities or by animals that graze too close to the vault. It also contributes to the security of the station to some limited extent. At least the undesired effects of too strong curiosity of people are limited.

The optimal size of the fence depends on several factors:

- Density of population around the site and human activity in close vicinity of the station,
- Potential agricultural activity in close vicinity,
- The probability of animal interference,
- General seismic noise amplitudes at the site. Quiet stations require bigger fenced area,
- Seismic coupling between ground surface and bedrock. Non-consolidated surface ground and seismometers installed on a very hard bedrock allow a smaller fence. A very deep vault has a similar effect.

The decision about the size is therefore heuristic. The smallest recommended fenced area is 10 x 10 m (30 x 30 feet). In the least favorable case, a fence could be 100 x 100 m (300 x 300 feet). A height of about 2 m (6 - 7 feet) is sufficient. Light construction with little wind resistance is preferable so that wind-generated seismic noise is minimized.

The equipment and the vault itself can also generate seismic noise. Equipment that includes main power transformers or rotating electromechanical elements like disk drives, diskette drives, cooling fans, etc. should be installed on the vault wall rather than on the seismic pier.

If the vault cover is not firmly attached, it can swing and vibrate in strong winds, which can totally ruin seismic records. Be sure that the cover is very firmly fixed to the top of the vault, as its own weight may not be sufficient to prevent vibration in strong wind. When closed and strongly shaken by hand, there should be no play whatsoever between the vault and the cover. If there is, it will cause seismic noise during strong wind conditions.

If a seismic station uses an antenna mast, place it well away from the vault to prevent seismic noise from being generated by the antenna swinging in the wind. The required distance is usually between 5-50 m, depending on a number of factors:

- Maximum expected wind speed and probability of windy weather at the site – the higher the speeds and the more often they appear, the greater the required distance,
- The antenna's height – the higher the antenna mast, the greater the required distance,
- The vault's depth – the deeper the vault, the smaller the distance,
- The type of seismic coupling between sensors and antenna base – strong couplings require larger distances,
- General seismic noise at the site – very quiet sites require larger distances.

6. ELECTRICAL GROUNDING

A grounding system is required for the proper functioning of electronic equipment. Grounding keeps the system's instrument-noise low, allowing proper grounding and shielding of equipment and cables. It is a prerequisite for proper functioning of lightning protection equipment and for interference-free functioning of RF telemetry (if applicable). The grounding system design is usually a part of the RF link design in telemetry seismic systems.

Generally, ground impedance below 1 ohm is desired. The total length of the required grounding metal strips depends a great deal on climate, local soil type, and humidity. Generally, a radial star configured system, of five to six "legs" with 15 to 20 m (45 - 60 feet) length each, is required for a grounding system (Fig. 9). The strips made of zinc plated iron or copper, 3 x 30 mm (1/8" x 1 1/4") in cross-section, should be buried from 25 to 35 cm (~1 foot) deep in the soil. In dry regions they should be deeper. The strips should be laid straight. No sharp turns (around rocks, for example) are allowed, because this decreases lightning protection efficiency as a result of increased inductivity of the grounding system.

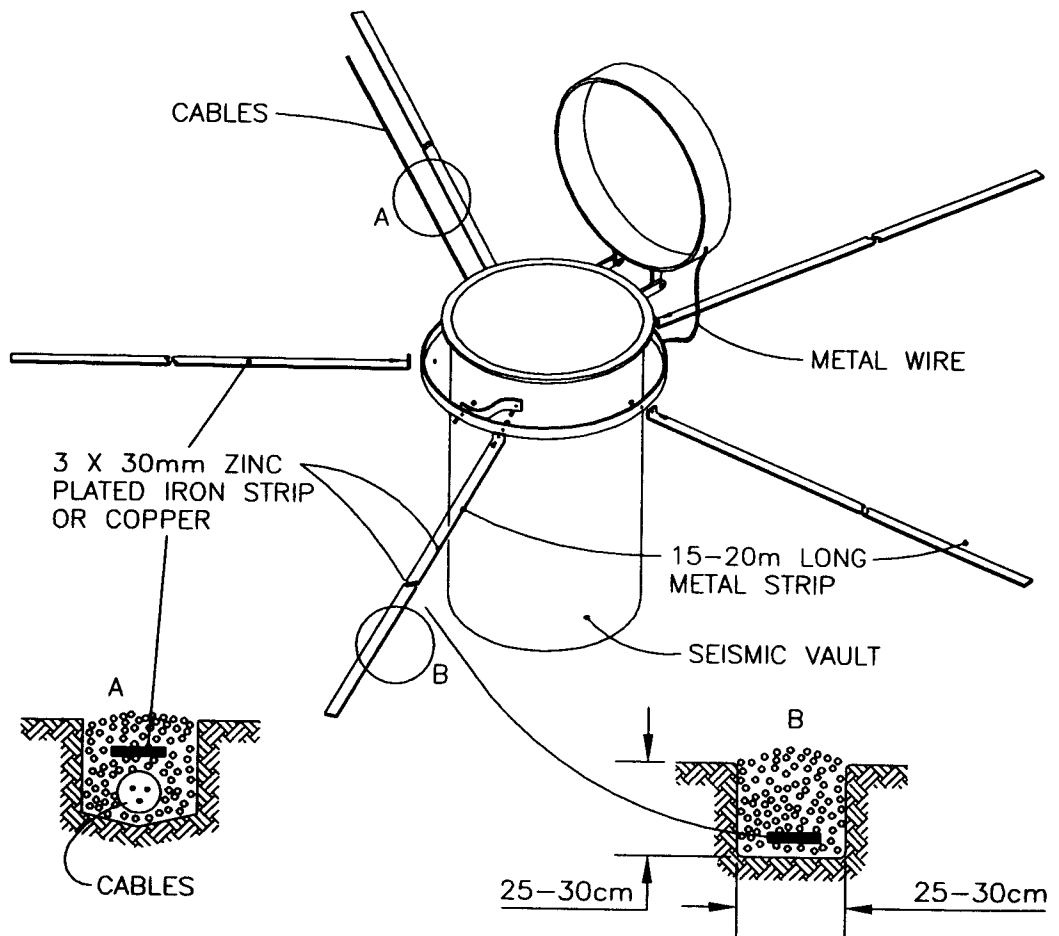


Fig. 9: Typical grounding system of a seismic vault. Its dimension depends on local soil humidity conditions.

In arid regions, high deserts, or completely stony areas, longer and thicker strips are required. In these cases, a different approach to grounding and lightning protection is sometimes taken by trying to obtain an electric equipotential plane all around the station during lightning

strikes. Grounding impedance is no longer the most important issue. High lightning threat regions and very dry or rocky ground usually require a specially-designed grounding system.

In seismic vaults without metal walls, bury a loose mesh made of grounding strips around the vault and connect them to the rest of the grounding system. Grid dimension of this mesh should be around 60 to 100 cm square (~2 to 3 feet square).

At seismic stations with RF data transmission and antenna masts, the star-configured grounding system should be centered on the antenna mast, not on seismic vault. The seismic vault is included in one of the legs of the grounding system. One of grounding strips must be laid exactly above the cables connecting the antenna mast and seismic vault (Fig. 9, detail A.). This assures a minimum voltage drop along the cables during lightning strikes and therefore a minimum voltage surge induced in the cables.

The antenna mast itself should be grounded as well and equipped with a lightning protection system. Its highest point should be at least 1 m (3 feet) above the highest antenna or solar panel installed on the mast.

Note that any grounding system requires periodic service checks because contacts between the metal parts may eventually corrode. It is generally recommended that the grounding impedance of the system be checked once every two years. Regular maintenance visits should always include a check of the lightning protection system and equipment and replacement of any burned elements.

7. VAULT CONSTRUCTION

Seismic vaults can be made with metal walls. Plain iron sheets welded together, of corrugated iron, or of pieces of large-diameter metal pipes can be used. For durability, we recommend zinc-plated metal. It is not necessary to make them very strong and heavy. Water tightness is relatively easy to assure with this design.

If the vaults are made from thinner sheet metal (a few mm), then pour relatively thin, 15 - 20 cm (6 - 8") concrete walls around the metal to add strength. The quality and homogeneity of this concrete is not necessarily high because water tightness is usually not a problem due to metal walls. Locally-available sand aggregates can be used in most cases. Such vaults may cause problems in the applications where deformation and tilts of the vault due to external temperature changes are important and is therefore not recommended for VBB stations.

The walls can also be made of concrete only – in this case it is the easiest to make the vault rectangular. Note that the quality of the concrete must be good to make the vault watertight, as explained earlier. Strength is, apart from very deep vaults, not a problem and therefore no steel reinforcement is needed.

At sites where accessibility allows, vaults can be made of the prefabricated concrete pipe sections used in sewerage system construction. They are cheap and can be obtained in different diameters and lengths. In deeper vaults you can simply stack them, as the depth of the vault requires. Care must be taken to make the joints between sections water tight.

The bottom of the seismic vault - seismic pier - is always made of high-quality, watertight concrete. Special requirements must be fulfilled for VBB sensors. More details are given in the 2.5. 'Water Protection' section.

The depth of seismic vaults is determined by seismo-geological parameters. But apart from providing adequate space to put all the equipment, the diameter is primarily a matter of the desired ease of installation, maintenance and service.

For three-component stations with single component sensors, from 1 to 1.5 m² (10 to 15 square feet) of space on the seismic pier is required. Less space suffices for three-component seismometers, three-component accelerometers, or a single component sensor. If the vault contains (or will contain in future) three-component weak motion and strong motion sensors, about 1.5 - 2 m² (15 - 20 square feet) is required.

We have found that a minimum for installation and maintenance is a 1.4 m (4 ½ feet) diameter vault. If the vault is deeper than 1 m (3 feet), a 1.5 to 1.6 m (5 to 5 ½ feet) diameter is recommended. Deep vaults (> 4 m (13 feet) require at least a 1.6 to 1.7 m (5 ½ to 6 feet) diameter. Vaults deeper than 1.2 m (4 feet) require a ladder.

8. MISCELLANEOUS HINTS

8.1. Vault cover design

A seismic vault cover should:

- Have a minimum of 5% slope so water drains quickly
- Have vertical siding all around that extends at least 15 cm (6") below the upper rim of the vault to prevent rain from entering in windy conditions
- Have a mechanism, which firmly fixes the cover to the ground and a lock to mitigate vandalism
- Have handles for easy opening and closing
- Be painted a light color, preferably white, that will reflect as much sun as possible, particularly in hot and dry desert regions.

The metal cover and thermal insulation cover of the vault should not be too heavy. They should be designed in such a way that a single person can open and close the vault smoothly. Otherwise, maintenance visits will require two people in the field. For large vaults, the cover can be designed in two parts or a simple pulley system may help.

8.2. Alternative materials

Metal, as material for a vault cover, is less appropriate in very hot and very cold climates as it becomes difficult to handle and work with under extreme temperature conditions. In dry regions, UV light-resistant plastic or water-resistant plywood is a better alternative. Plywood also has less thermal conductivity, which improves thermal insulation, and less weight, making handling the cover easier.

8.3. Mitigating vandalism

Experience shows that, apart from political instability in a country, most vandalism on seismic stations is driven by people's curiosity. Therefore, we believe that a large sign with a

short and easy to understand explanation of the purpose of the station posted at the entrance to the fenced area may significantly mitigate vandalism.

8.4. Fixation of the seismometers to the ground

In regions where earthquakes with 0.5 g or more peak acceleration can occur, seismometers must be firmly fixed to the seismic pier, exactly as is a common practice with strong motion sensors. Obviously, sensitive seismometers are clipped during very strong earthquakes. However, they should not shift or move during such events. Numerous aftershocks must still be recorded with the sensors properly oriented.

9. REFERENCES

- Beauduin, R. (1996) et al. The Effect of the Atmospheric Pressure Changes on Seismic Signals or How to Improve the Quality of a Station, *BSSA*, **86**, p 1760.
- Bycroft, G.N. (1978) The Effect of Soil-Structure Interaction on Seismometer Reading, *BSSA*, **68**, p 823.
- Luco, J.E., Anderson, J.G., and Georgevich, M. (1990) Soil-Structure Interaction Effects on Strong Motion Accelerograms Recorded on Instrument shelters, *Earthq. Engng. & Structural Dynamics*, **19**, p 119.
- Uhrhammer, R.A., Karavas, W. ,and Romanovicz, B. (1998), *Broadband Seismic Station Installation Guidelines*, *Seismo. Res. Letters*, **69**, 15-26.
- Quanterra, INC. FAQ letters, June 1994.
- Wielandt, E. (1990) Very broad-band seismometry, In: Boschi, E, Gardini, D. and Morelli, A. (eds), *Proc. of 1st Workshop on MEDNET*, Sept. 10–14, 1990, CCSEM, Erice, Il Cigno Galileo Galilei, Roma, 222-234(Wielandt, E. (1990) Very broad-band seismometry, In Boschi, E, Gardini, D. and Morelli, A. (eds), *Proc. of 1st Workshop on MEDNET*, September 10 – 14, 1990, CCSEM, Erice, Il Cigno Galileo Galilei, Roma, 222-234).
- Willmore, P.L. (ed) (1979) *Manual of Seismological Observatory Practice*, World Data Center A for Solid Earth Geophysics, Report SE-20.

ACKNOWLEDGEMENT

The author expresses his sincere gratitude to Dr. Frank L. Vernon of UC San Diego, USA and Prof. Peter Bormann from GeoForschungsZentrum Postdam, Germany for their valuable suggestions, comments, and time spent on reviewing the manuscript.

RADIO-LINK TRANSMISSION OF SEISMIC DATA AND FEASIBILITY SURVEY

Amadej Trnkoczy

Kinematics SA, Z.I. Le Trési 3, CH-1028 Préverenges, Switzerland
E-mail: amadej.trnkoczy@quantum.si

1. INTRODUCTION

Radio links are often used in seismology for data transmission. Compared to other means of data transmission, radio links offer a real-time, continuous, independent, robust to damaging earthquakes, and usually reasonable cost solution. However, practice shows that the most frequent technical problems with radio frequency (RF) telemetry seismic networks originate in the RF links themselves. Unfortunately, this is frequently a result of a carelessly designed RF system. Many seismic networks in the world experience unreliable and noisy data transmission. There are even reports of some complete failures. Therefore, this chapter gives some general advises on how to approach the design of a seismic telemetry system. VHF (usually around 180 MHz for seismology) and UHF (usually around 450 MHz for seismology) frequency band FM modulated links, as well as spread spectrum (around 900 MHz or 2.4 GHz) RF data transmission and satellite links will be discussed. The need for professional RF survey will be explained.

UHF and VHF frequency bands are still most frequently used today, however spread spectrum and satellite links are sharply gaining in importance in seismology too. Annex 1 summarizes the essential features of the various options for seismic data transmission links in seismology

2. TYPES OF RF DATA TRANSMISSION USED IN SEISMOLOGY

Most of today's RF telemetry seismic networks still use VHF or UHF frequency band using frequency modulation (FM) of the carrier. Both bands can be used for analog frequency modulated signal transmission or digital data transmission with different modulation schemes. Both technologies usually use standard 3.5 kHz bandwidth 'voice' channels. It is easier to obtain permission for them than for the special channels with higher bandwidth. Direct connection distances up to 150 km (100 miles) are possible with less than one watt RF power transmitters if topography allows.

VHF band is almost completely occupied in most countries. It is usually very difficult or even impossible to get permission to use this band. In addition, this band is more susceptible for interference of other users of RF space than higher frequencies. Therefore, it is rarely used for new seismic networks.

UHF band is presently the most popular. However, in many countries it is not easy to obtain permission for new frequencies even within this band.

Spread spectrum RF links are a new modern alternative. They operate at around 900 MHz or 2,4 GHz. Their use is relatively recent in seismological applications. Spread spectrum RF links do not use a single carrier frequency, but their transmitters transmit in the whole frequency band dedicated for such links. Many users use the same frequency band. The corresponding transmitter and receiver discriminate each other from other users using special code common to a particular link.

The practical advantage of spread spectrum links is that usually no permission is needed for operation and that they are very robust against RF interference (for this reason this technology was first developed for defense purposes). The only limitation, which applies, is maximum RF power of transmitters. Where this limit is set depends on country's regulations and varies very much. To our knowledge maximum transmitter power can be limited by law from 100 mW to 4 W. This limitation unfortunately seriously limits the maximum direct connection distance. In the countries where this limit is set to a few hundred milliwatts (100 mW in West European countries for example) this limitation poses an important drawback of spread spectrum links for seismology. Not much more than 20 (12) or 30 km (20 miles) can be reliably covered with them in such case. Direct connection distances around 100 km (62 miles) can be covered using stronger transmitters in the countries where their use is allowed.

Satellites links are also becoming more and more useful and in the reach of seismometry. No doubt they represent the future for seismic data transmission. However, presently (1998) their cost is still a severe problem.

Most of the commercially available satellite links are the high throughput type. Usually, the frequency band can be purchased (and is paid accordingly) in 110 kHz band increments. Prices for this band are around \$1.000/month (1999). Frequently, the smallest available bandwidth (and consequently the baud rate) is higher than usually required in a small seismic network. Presently this makes satellite links even more expensive for small networks.

However, if the size of the network and its total required bandwidth is equal or slightly smaller than any multiple of the bandwidth increments purchasable, the cost of satellite data transmission may become acceptable. This is easier to achieve in large national or big regional seismic networks than in smaller networks. How many seismic stations can transmit data in a 110 kHz frequency band depends on several parameters like seismic data sampling rate, the number of bits per data sample (resolution or dynamic range of the channels), whether single direction (simplex) or bi-directional (duplex) links are used, and on overhead bits required for data error detection, error correction, and link management.

One of the important issues which varies from county to country relates to central satellite recording site (hub). In some countries, mostly in such where the communication market is liberal, a seismic network owner may have its own 'private' hub directly at seismic central recording site. The cost of equipment of such local hub varies from \$100.000 to about \$250.000 (1998). In countries with less liberal communication market only shared-hubs, owned by a (many times monopolistic) communication company, are available. In this case the cost of communication is usually higher and also the cost of the communication lines from the shared-hub to the seismological central recording site must be counted in. These leased lines can significantly increase the total cost of data transmission particularly if the distance from the hub

to the seismological institution is large. Cost analysis of different satellite systems is generally complex and the prices vary significantly from country to country.

Another problem of satellite links is relatively high power consumption of RF equipment at remote seismic stations. One has to count to around 50W of power consumption for data transmission equipment at each site. This exceeds significantly the requirements of seismic equipment, which is usually built to be low power as much as possible. It poses inconveniences like large solar panels at the stations without main power and much bigger back-up batteries for a given station autonomy.

Nevertheless, the costs of satellite communications are constantly decreasing. Increasing liberalization in the communication market also speaks in favor of future use of satellite links. No other communication can serve better and with higher reliability the most remote and distant seismic stations.

3. THE NEED FOR PROFESSIONAL RADIO FREQUENCY (RF) SURVEY

The design of VHF, UHF or spreads spectrum RF telemetry links in a seismic network is a specialized professional technical matter. Practice shows that guessing and 'common sense' approach usually lead to problems or even complete project failure. The following misunderstandings and over-simplifications are commonly encountered:

The amount of data that must be transmitted in weak-motion seismology is often underestimated. Seismology requires an incomparably larger information flow (baud rate) than most other geophysical disciplines - several orders of magnitude more than meteorology, for example.

The degree of required reliability for successful data transmission in seismology is also frequently underestimated. Missing data due to interruptions on the links, excessive noise, spikes, and data errors are particularly destructive for networks operating in triggered mode and/or having any kind of automatic processing. With old paper seismograms and analogue technology, spikes, glitches, interruptions and other 'imperfections' are relatively easily 'filtered out' by the seismologist's pattern recognition ability during the analysis. However, the same errors, if too frequent, can make the results of an automatic computer triggering and/or analysis unacceptable.

Frequently, a false comparison with voice RF channels is experienced. People try to verify a seismological RF link between two points using walkie-talkies. If they can communicate, they expect that transmission of seismic data will also be successful. Note that voice channels allow a much lower signal-to-noise ratio while still being fully functional because human speech is highly redundant. Also the RF equipment parameters in walkie-talkies and in seismic telemetry are different. Such 'testing' of RF links is therefore meaningless.

Another widely spread belief is that an open 'line of sight' between transmitter and receiver is a sufficient guaranty for a reliable RF link. This may or not be true. It is true only for very short and direct links up to about 5 km length with absolutely no obstructions between transmitter and receiver. Such links may happen in some small size local seismic networks. For longer links, fading, that is the variation of the intensity or phase of RF signal due to changes in the characteristics of the RF signal propagation path with time, become a major consideration. Therefore, in most cases the real issues in link reliability calculations are equipment's gains and losses, RF signal attenuation (transmission loss calculation) based on Fresnel ellipsoid obstruction, and required fading margin.

The resultant reliability of the link is then expressed as a time availability (or probability of failure or time unavailability) in percent of time in the worst month of the year (or per year). During 'time unavailability' the signal-to-noise ratio at the output of the receiver is lower than required or the bit error rate (BER) of digital data transmission link is higher than required. Many parameters are involved in the RF path analysis starting with transmitter power, frequency of operation, the various losses and gains from the transmitter outward through the medium, receiving antenna system to the input of the far end receiver and its characteristics. In link attenuation calculation, curvature of the Earth, the regional gradient of air refractivity, potential wave diffraction and/or reflections, time dispersions of the RF carrier with digital links, processing gain and background noise level with spread spectrum links, etc. all play an important role.

Therefore, we strongly recommend a professional RF survey in the seismic network planning procedure.

4. BENEFITS OF A PROFESSIONAL RF SURVEY

The benefits of a professional RF survey are manifold:

- Professional RF survey assures that the links will actually *provide a desired reliability*, which has to be decided upon beforehand. During the RF survey the design parameters of the links in a network are varied until the probability of an outage in the worst month of a year fits or falls below the desired value. This may require some additional investment in the equipment (but it will prevent unreliable operation) or may save some money by loosening the requirements where appropriate.
- Professional RF survey guaranties *the minimum number of RF repeaters* in a network. This results in a direct benefit for the user because of less equipment, less spare parts, and cheaper and easier maintenance. The result will also be less instrumental noise in the recorded signals in RF frequency modulated (FM) analogue networks and a better BER performance of digital networks. Note that, in most designs, every additional repeater degrades data quality to some extent and always decreases the network reliability.
- Professional RF survey will determine a *minimum number of licensed frequencies required* in a network without sacrificing data transmission reliability. Note that required number of different carrier frequencies in VHF and UHF telemetry can be significantly smaller than the total number of the links in a network. This prevents unnecessary pollution of RF space in the country. Fewer frequencies are aimed also to user direct benefit since they are easier to obtain and fewer different RF spare parts (transmitters and receivers) are required due to more uniform RF equipment.
- *Robustness of the whole seismic network to technical failures and lightning treat is significantly increased* by proper RF layout. For example, one should always avoid repeaters, which transmit data from too many seismic stations, because any technical failure of such repeater results in non-proportionally severe consequences.
- *Diminished power consumption* of RF transmitters is achieved by calculating their minimum sufficient RF output. This results in less pollution of RF space in the country. The possibility to minimize output power of transmitters is also to user direct benefit because lesser power

consumption enables remote stations to operate independently longer and/or require smaller back-up batteries and solar panels for a given autonomy.

- Antennae mast heights and antennae minimum-required gain (that is their size and price) are minimized and most effective polarization is determined, resulting in *potential savings*.

5. RADIO-FREQUENCY (RF) SURVEY PROCEDURE

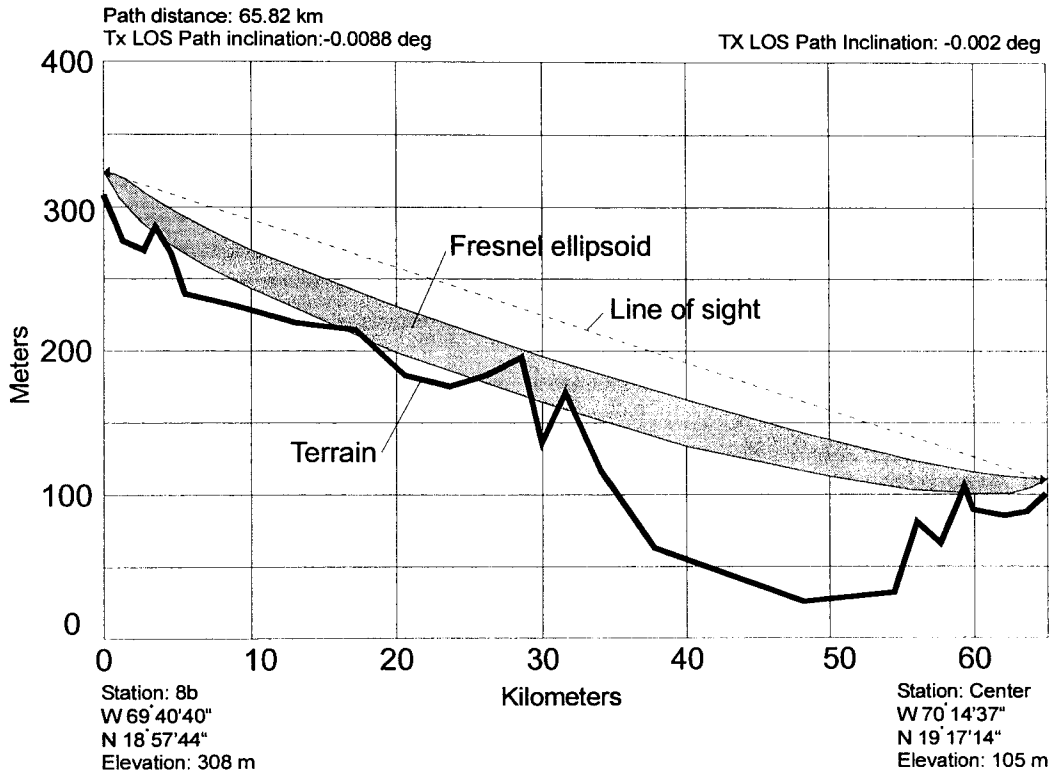
RF survey usually encompasses a go-no-go decision making for a given RF equipment, topographical profile from a transmitter site (remote seismic station) to a receiver site (central recording site or a repeater), local RF path conditions, and desired reliability of the link. It is based on decades of experience on transmission conditions' statistics all around the world and computer modeling using specialized software. Field RF measurements are rarely performed. First, they are much more time consuming and expensive and second, they are also less reliable than calculations. Namely, RF transmission conditions vary with time (diurnal, seasonal, weather dependent). These conditions vary unpredictably and within climatic zones. Theoretical calculations encompass full statistics of these variations, but practical one-time measurements suffer unpredictable variations in fading. Nevertheless, even if the measurements are not made, a communication expert still has to visit all potential seismic sites during seismic site selection procedure to acquire local topographical parameters and to check the existence of other potential RF obstacles which may not be evident from topographical maps.

If the RF link calculation based on a given set of input parameters does not assure the desired reliability, some of the input parameters must be changed. We can change topographical profile. This means we re-position the remote seismic station or we introduce a new RF repeater. We can change the antennae type and/or increase their gain. We can increase antenna masts height or increase transmitter output power (the last measure is actually hardly efficient) or we can change the RF equipment completely (significantly more powerful transmitters and/or more sensitive receivers).

Topographical profiles are usually taken from 1:50.000 scale topographical maps. In most cases many more profiles than stations in the network are usually taken and links calculated before we find the final RF layout of a network. A great deal of this work can be done before actual fieldwork starts, however, profiling is always needed also during the fieldwork.

A result of an RF link calculation is shown in Fig. 1 with input parameters on the left and output parameters on the right. The figure intentionally shows an example where there exists a 'direct line of sight', but the profile doesn't guaranty an acceptable link operation. Note the curved path of the first Fresnel ellipsoid where the RF energy actually travels from the transmitter to the receiver. This curvature is mostly due to regional gradient of air refractivity. In the shown example this ellipsoid hits the mountain ridge and causes a significant loss of energy or even the link failure.

For analogue VHF or UHF telemetry usually a time availability around 99.95% in the worst month (this is equivalent to about 15 minutes of outage of each link per month) is considered as marginally acceptable and 99.99% as a good one. If we use an RF repeater between the seismic station and central recording site we have to increase the required reliability of individual sub-sections.



Frequency: 900 Mhz
Distance: 65.82 km
Antenna height TX: 18 m
Antenna Height RX: 18 m
TX antenna type: Yagi
RX antenna type: Yagi
Effective isotropic radiation power: 38.0 dB
TX power: 30 dBm
TX antenna gain: 10 dB
TX connector loss: 0.05 dB
TX line loss: 2 dB
RX antenna gain: 10 dB
RX connector loss: 0.05 dB
TX site totals - gain/loss: 40.0/2.0 dB
RX site totals - gain/loss: 40.0/2.0 dB
RX threshold level: -110.0 dB
Profile: K =4/3, F = 0.6*F1

Free space path loss: 128.21 d
Diffraction loss: 0.0 dB
Total system loss: 132.2 dB
Total system gain: 50.0 dB
Unfaded receiver
signal level: -82.16 dBm
Fade margin: 27.8 dB
Outage: 23412 sec/year
Time availability: 99.926 %

Fig. 1: A result of an RF link calculation. Input parameters are given on the lower-left and the output results are on the lower-right side. For demonstration, a case where the line of sight between the transmitter and the receiver exists, was chosen, however, the link performance doesn't fit to the desired link availability of 99.99%. The Fresnel ellipsoid is too much obstructed by a mountain approximately in the middle of the link path.

In digital data transmission the bit error rate (BER) is usually used as a measure of data link reliability. BER strongly depends not only on physical reliability of the RF link but also on error detection and error correction methods used in RF equipment (modems). So, for example, one-directional (simplex) links are generally far less reliable than bi-directional (duplex) links, even if the RF links themselves are of the same quality in terms of analogue RF signal to noise ratio. This is because duplex links allow repeated transmission of corrupted data blocks until they are received error free while simplex links end with corrupted data (unless forward error correction methods are used). Due to high complexity of the problem a precise targeting of desired BER is usually beyond the scope of seismic network projects.

Something similar is true for spread spectrum links where another factor complicates the situation. Spread spectrum receivers incorporate so-called 'processing gain'. Based on the receiver's code processing these receivers are capable of resolving very weak RF signals, which may be even a certain number of dB below the RF noise at the receiver site. However, the problem is in the generally unknown amplitude of the RF noise at the receiver site. Note that every new spread spectrum transmitter increases the background noise in the band of operation of the spread spectrum system and since this band is 'open to public' it is difficult to predict its actual noise. From practical measurements' aspect, specialized spread spectrum measuring equipment is extremely expensive. Also algorithms, which are used to resolve the sub-noise level RF signals in the receivers, represent a problem. They are mostly proprietary and therefore not generally accessible. Both facts significantly reduce the practicability of measurements of the reliability of spread spectrum links for seismological purposes.

Fortunately, some spread spectrum equipment manufacturers can provide a special software, which allows easy but approximate link reliability measurements using their equipment. Taking into account a safety margin due to temporal variation of RF transmission conditions, one can successfully use these measurements for a course link quality estimate. It is difficult to relate these proprietary 'reliability scales' with standard parameters like probability of link outage or BER. Nevertheless, classical RF signal attenuation calculations still give valuable information about RF energy propagation over a given topographical profile. These results, combined with measurements using manufacturer's proprietary 'reliability scales' and practical experience, suffice in almost all seismometric projects.

The cost of a professional RF survey is generally around a few percent of the total investment in a new seismological network. Practice shows that its combined benefits are well worth the investment. RF survey is a major step toward the reliable operation of any future telemetry seismic network.

6. ARE EXISTING COMMUNICATION TOWER SUITABLE SEISMIC SITES?

Very often less experienced newcomers in seismometry consider mountain peaks with existing communication towers as potential seismic station sites, particularly if they are building an radio frequency (RF) telemetry seismic network. Such places appear to be an easy and inexpensive solution. Access problem is solved, RF communication paths to the central

recording site, which is usually situated in the capital or other bigger city, is supposed free, main power lines, and even phone lines are readily available.

Unfortunately, such sites also have several serious drawbacks and are in fact rarely suitable for seismic stations. The most important reasons for that are:

- Existing high towers that sway during windy periods cause high-amplitude, low-frequency seismic noise and may cause large number of false triggers with triggered seismic systems and deteriorate low frequency seismic signals. Consequently a diminished seismic station gain is used resulting in a low detectability of the station.
- There is usually a very high probability of RF interference between seismic RF telemetry system and other users. RF interference may easily impair seismic data transmission and consequently seismic system reliability. Several 'high power' parties (compared to one watt or less of RF power used in seismic telemetry) are potentially polluting the RF space at such places. In addition, if other users do not maintain their RF equipment properly, the RF energy radiated within uncontrolled side lobes worsens this danger. This happens quite frequently in developing countries.
- If such sites are inhabited, it is likely there will be too high man-made seismic noise due to human activities.
- The topography of such mountain peaks is rarely suitable for a seismic station. Communication antennae towers usually try to cover an area as large as possible. Therefore, as a rule, they are placed on the highest mountains in a country or region.

Nearly all such sites have powerful diesel generators to support communication equipment during power outages. When in operation, these generators are a major source of man-made, high frequency seismic noise. Of course, these generators will surely be running after a strong earthquake because that is precisely when it is most likely that the main power lines will fail. Since the periods during strong earthquakes and following aftershock sequence are the most important for seismic network, clearly the existing communication towers are not at all suitable for seismic sites.

6. THE PROBLEM OF RADIO-FREQUENCY INTERFERENCE

While spread spectrum links are fairly robust, radio-frequency interference between a seismological system and other RF space users is quite a common and difficult problem with VHF or UHF links in many developing countries. In some countries, the lack of discipline and a disorder in RF space cause unforeseen interference. In others, insufficient maintenance of high power communication equipment results in strong radiation from the side-lobes of powerful transmitters that also may interfere with seismological links. Army facilities (particularly if they operate 'out of civil law'), particularly different types of radars, easily interfere with seismological links. This danger is very high if seismic stations are installed at the sites, which are used by other high power RF communication users. See attached Work Sheet 'Using existing communication tower sites as seismic station sites'. Extensive, unauthorized use of walkie-talkies can also cause problems.

To make the situation even worse, in some developing countries, for security reasons, the use of RF spectrum analyzers, which can frequently reveal the origin of interfering signals, is often prohibited, particularly for foreigners. Nevertheless, even if a foreigner is allowed to use a RF spectrum analyzer during a certain period, short-term monitoring of RF space does not necessarily guarantee success because some interfering sources may appear only very intermittently and are, therefore, difficult to detect.

Note that RF interference problems due to a disorder in the RF space are generally beyond the control of a seismic equipment manufacturer and/or foreign RF survey provider. They can be solved - or at least mitigated - only by involving local RF communication experts during the early phase of the network planning. They are familiar with the real RF space conditions in the country and can advice much better than any foreign expert. If a new seismic network already experiences interference problems only very tedious and time consuming try-and-error procedures (swapping frequencies of the links or even VHF/UHF bands, changing antenna orientation and polarization, or even re-positioning of stations or repeaters) may help. However, the results are to an important degree unpredictable.

Annex 1:

Seismic data transmission links used in seismology in brief

Following issues are discussed:

- cost of data transmission equipment and its installation,
- cost of operation of data transmission lines,
- required maintaining of the data transmission links,
- data throughput,
- reliability of data transmission,
- continuous versus event file data transmission capability,
- applicability in respect to high/low seismicity regions and strong/weak motion networks,
- remote seismic station-to-recording center distance capability,
- robustness against strong earthquakes, and
- special issues.

Type of links	Description
Wire lines	<ul style="list-style-type: none"> ▪ inexpensive establishment if not too long, ▪ inexpensive operation; ▪ little in-house maintaining; ▪ relatively high throughput with modern modems; ▪ high reliability of data transmission links; ▪ continuous and event file data transmission possible; ▪ appropriate for high and low seismicity regions and weak and strong motion seismology, ▪ useful for very short distances only (a few km maximum); ▪ robust against damaging earthquakes
Leased phone lines	<ul style="list-style-type: none"> ▪ inexpensive establishment (unless high installation taxes required); ▪ very expensive operation in the long-run, operation cost usually proportional to the total length of the lines; ▪ no in-house maintaining, ▪ relatively high throughput with modern modems; ▪ reliable data transmission; ▪ capability to transmit data continuously and less efficient in event files; ▪ appropriate for high and low seismicity regions and weak motion networks, rarely used in strong motion networks, ▪ appropriate for short and long distances; ▪ medium robust against damaging earthquakes
Dial-up phone lines	<ul style="list-style-type: none"> ▪ inexpensive establishment, ▪ medium expensive operation, cost of data transmission is proportional to the amount of data transmitted, that is to the seismicity in the region; ▪ no in-house maintaining; ▪ usually low effective throughput despite of modern high-throughput modems; ▪ medium data transmission reliability; ▪ only event file data transmission feasible; ▪ applicable for strong motion networks and weak motion networks but in low seismicity regions only, ▪ applicable from short to very long distances;

	<ul style="list-style-type: none"> ▪ not robust against damaging earthquake, temporally fail to work after stronger earthquakes with macroseismic effects due to overloading or even break down of public phone system (an exception are seismic systems with several input phone lines and with the remote equipment which grabs the lines automatically at the moment of triggering to large events); ▪ reliability of data transmission highly depends on the overall quality of public phone system in a country; in many developing countries this is a serious obstacle for dial-up phone line systems; ▪ incapable to serve alarm and civil defense purposes
Radio-frequency links on VHF or UHF RF band	<ul style="list-style-type: none"> ▪ medium expensive establishment, ▪ inexpensive operation; ▪ require in-house maintaining; ▪ moderate but mostly sufficient throughput for digital data transmission on standard 3.5 kHz bandwidth 'voice' channels; ▪ medium reliable; ▪ continuous and event data transmission possible; ▪ applicable for high and low seismicity regions; ▪ used mostly in weak motion networks, rarely used in strong motion applications, ▪ applicable for distances up to 150 km (100 miles) with direct point-to-point connection and about three times that much using repeaters; ▪ robust to strong damaging events; ▪ have limited low-dynamic-range of data acquisition for analog FM telemetry; ▪ free frequencies are often difficult to obtain; ▪ frequently subject to RF interference in developing countries; ▪ RF survey required
RF spread spectrum links	<ul style="list-style-type: none"> ▪ medium expensive establishment, ▪ inexpensive operation; ▪ require in-house maintaining; ▪ medium high data throughput; ▪ medium reliability of data transmission; ▪ continuous and event file data transmission possible; ▪ useful in high and low seismicity regions and for weak and strong motion networks, ▪ useful for relative short point to point distances from 20 to 100 km maximum; ▪ robust to damaging earthquakes; ▪ insensitive to RF interference; implies the reduction of multi-path effects compared to VHF and UHF telemetry; ▪ permission to operate is easy to obtain or not required at all; ▪ maximum point-to-point distances depend on regulations limiting the maximum transmitter output power in a particular country; ▪ RF survey required
Microwave RF links	<ul style="list-style-type: none"> ▪ expensive establishment, ▪ expensive operation; ▪ maintaining usually beyond the scope of seismological institutions; ▪ high throughput; ▪ high reliability; ▪ continuous and event file data transmission possible;

	<ul style="list-style-type: none"> ▪ used in high and low seismicity regions and weak motion networks; ▪ appropriate for long distances; ▪ medium robust against earthquakes, ▪ usually these lines are hired from a second party communication company; they are often a part of public phone system in the country
Computer networks	<ul style="list-style-type: none"> ▪ medium expensive establishment (if connection points readily available), ▪ medium expensive operation; ▪ no in-house maintaining; ▪ high data throughput; ▪ reliable; ▪ semi-continuous and event file data transmission possible; ▪ used in high and low seismicity regions and strong and weak motion networks; ▪ convenient for medium to very long (even global) distances; ▪ allow reduced ownership cost; ▪ allow 'portable' central recording site anywhere in the network; ▪ frequently unavailable computer 'tabs' at remote seismic station sites (so called 'last mile problem'); ▪ different protocols can be used, Internet with TCP/IP protocol is increasingly gaining popularity
Satellite links	<ul style="list-style-type: none"> ▪ very expensive establishment, ▪ expensive operation; ▪ maintaining usually above the scope of most seismological institutions; ▪ high data throughput; ▪ reliable; ▪ continuous and event file data transmission possible; ▪ appropriate for high and low seismicity regions and weak and strong motion networks, ▪ medium to very large distances can be covered; ▪ robust to damaging earthquakes; ▪ convenient for extremely remote sites and large regional and national seismic networks; ▪ rarely used at present due to high cost, however satellite data transmission cost is constantly decreasing; ▪ for shared satellite hubs additional links from the hub to the seismological center required; ▪ high cost of the hub in systems with 'private' local hub; ▪ high power consumption of remote stations poses problem to solar panel powered stations

BANDWIDTH-DEPENDENT TRANSFORMATION OF NOISE DATA FROM SPECTRAL INTO TIME DOMAIN AND VICE VERSA. PART I: INTRODUCTION AND METHODOLOGY

Peter Bormann

GeoForschungsZentrum Potsdam, Division 2: Solid Earth Physics and Disaster Research
Telegrafenberg, D-14473 Potsdam, Germany

1. INTRODUCTION

Noise data for site quality assessment are collected with a wide range of instruments, both analog and digital, of different bandwidth, resolution and transfer functions. Accordingly, noise appearance in seismic records, amplitude- and frequency-wise, differs as do the various kinds of noise spectra derived therefrom. They are not easily comparable amongst each other and with older presentations of noise "spectra" derived from analog records. This is illustrated by the following figures. Fig. 1 represents a kind of classical noise spectrum as derived by visual amplitude and period readings in analog seismic records. Depicted are the envelopes of the maximum and minimum peak amplitudes of seismic noise that might be expected on land in rural environment over a rather long interval of time (about one year).

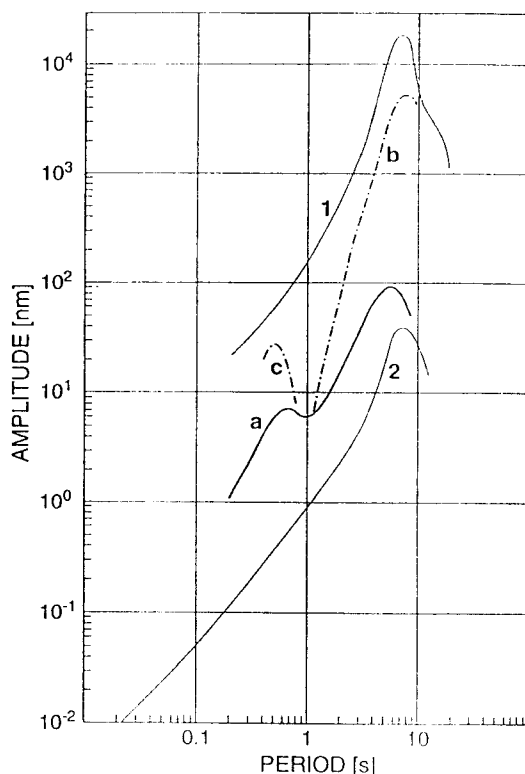


Fig. 1: Envelopes of maximum and minimum peak amplitudes for rural environments as determined from analog records of different type over a long time-span according to Brune and Oliver (1959) (curve 1 for high-noise sites and curve 2 for very low-noise sites) together with envelope curves of peak noise amplitudes at station MOX in Germany at times of minimum (curve a) and maximum noise (curves b and c). Taken from Bormann (1998) (with permission from Kluwer Academic Publishers).

The new global high noise and low noise models (NHNM and NLNM) published by Peterson (1993) in units of dB referred to $1 \text{ (m/s}^2\text{)}^2/\text{Hz}$ are depicted in Fig. 2. They represent the upper and lower bound envelopes of a cumulative compilation of representative ground acceleration power spectral densities P_a determined for noisy and quiet periods at 75 world-wide distributed digital stations. Peterson's original curves have been complemented by us with the respective curves P_v and P_d calculated according to equation (8) below.

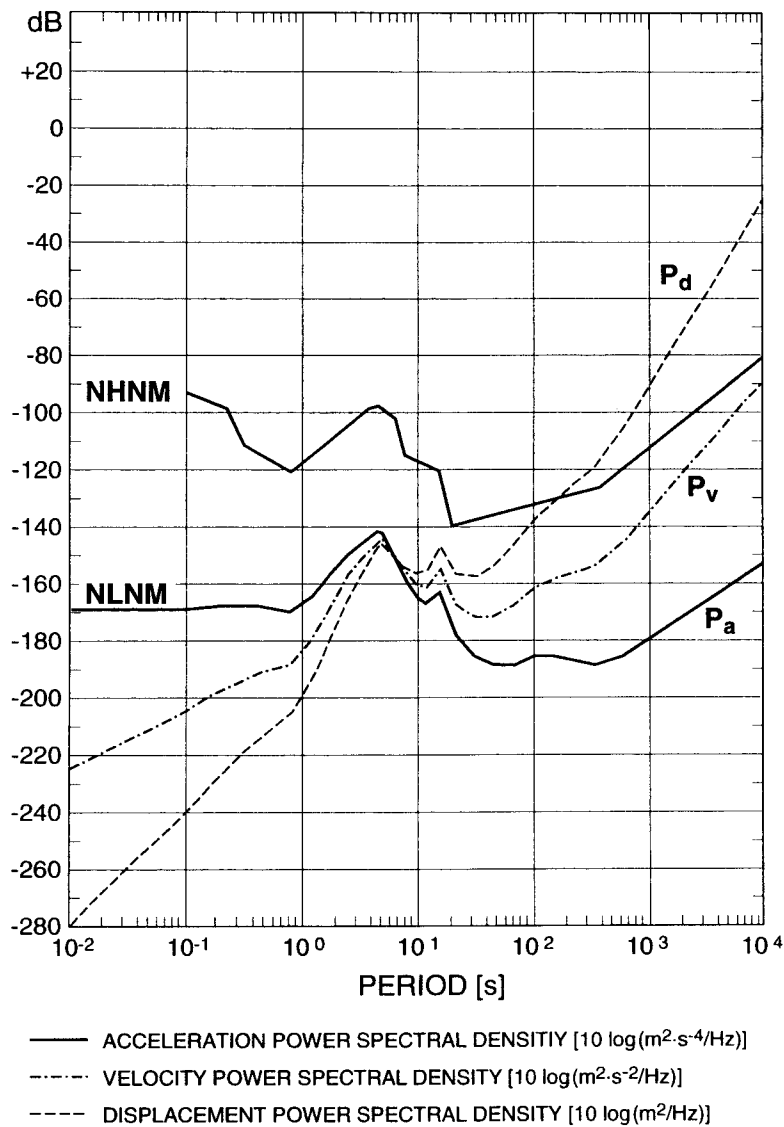


Fig. 2: Envelope curves of the new global high (NHNM) and low noise model (NLNM) according to Peterson (1993) in units of dB related to $1 \text{ (m/s}^2\text{)}^2/\text{Hz}$ and the respective curves calculated by the author for the displacement and velocity power spectral density P_d and P_v in dB related to $1 \text{ (m/s)}^2/\text{Hz}$ and $1 \text{ m}^2/\text{Hz}$, respectively. According to Bormann (1998) (with permission of Kluwer Academic Publishers).

Other presentations of global ambient seismic noise and signal conditions were presented by Aki and Richards (1980) in form of ambient noise velocity power density spectra (Fig. 3) and of amplitude spectral density for seismic waves and noise (Fig.4).

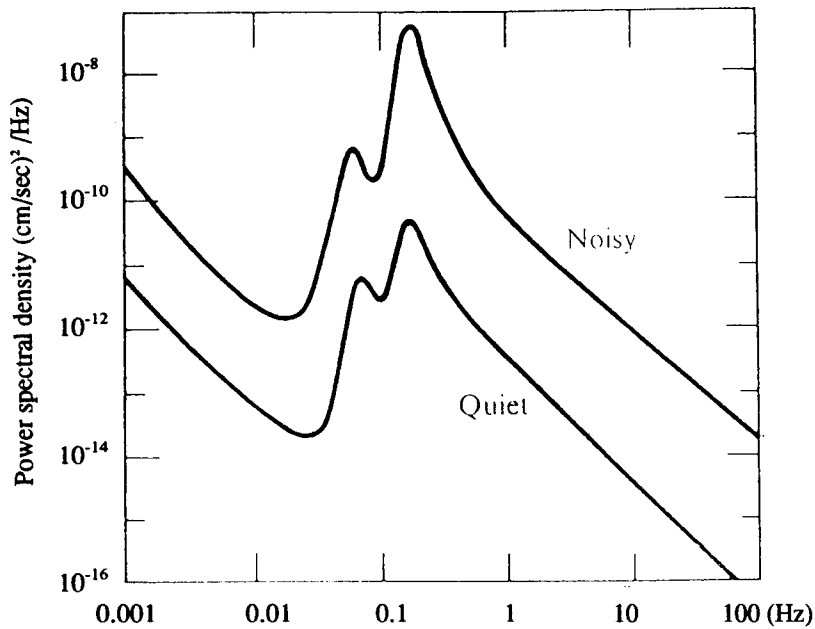


Fig. 3: Velocity power spectra of ambient seismic noise at noisy and quiet conditions for a typical station on hard basement rock (according to Aki and Richards 1980; with kind permission of the authors).

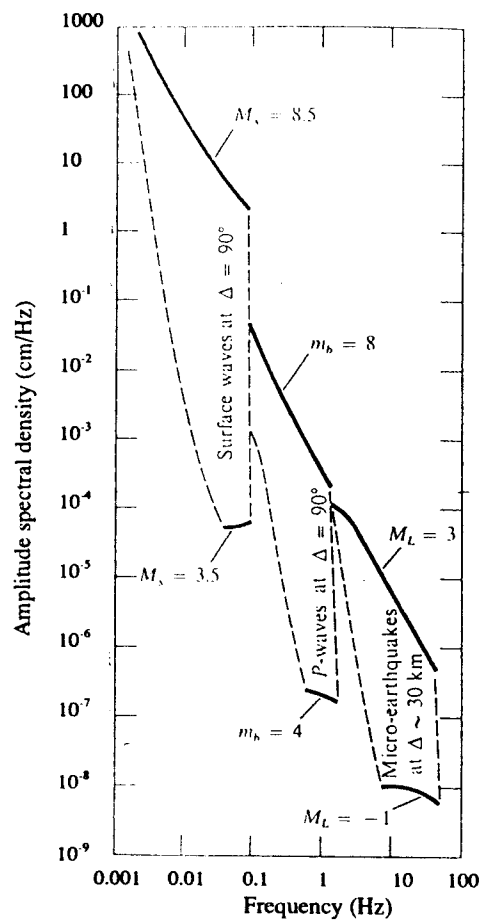


Fig. 4: Ranges of amplitude spectral densities for seismic waves. The lower bound is limited due to ambient seismic noise (according to Aki and Richards 1980; with kind permission of the authors).

Finally, we present in Fig. 5 a 15 s record segment of ambient seismic noise from a local seismic station site investigation carried out in NW Iran (left) together with the related displacement power density spectrum (right).

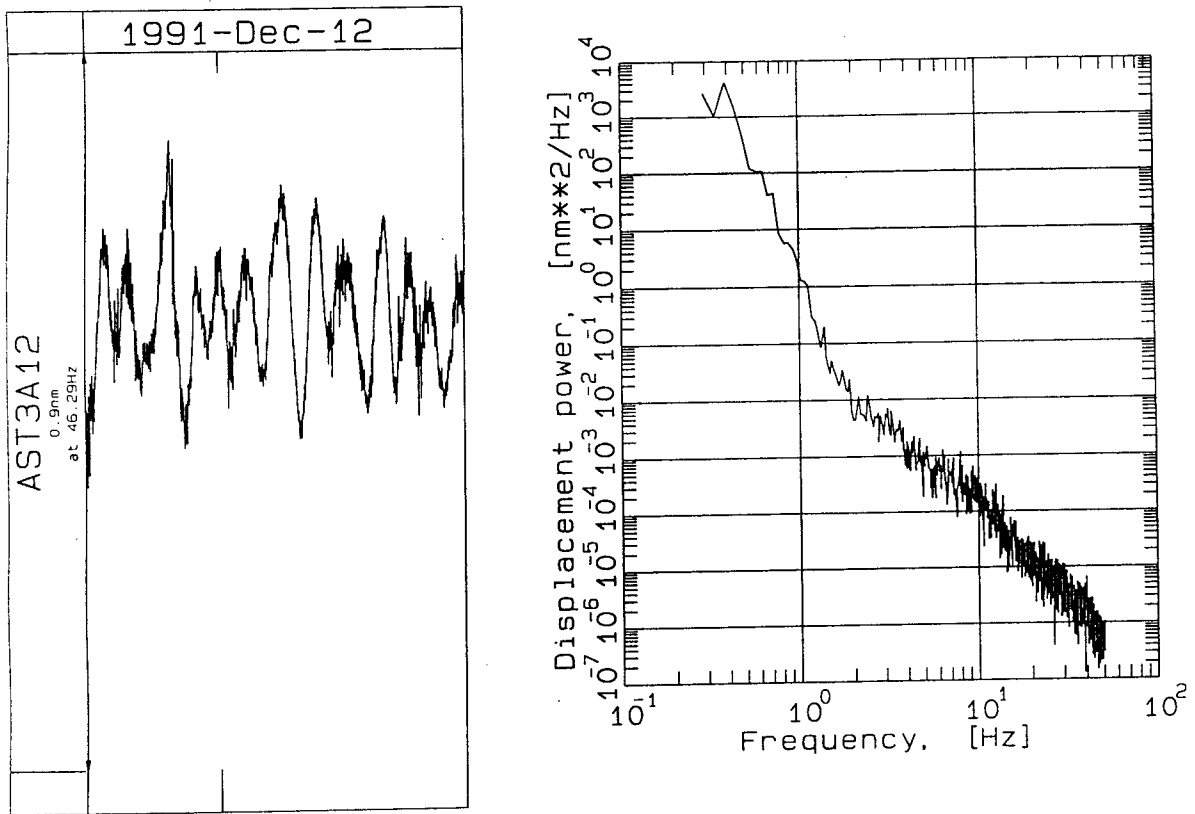


Fig. 5: Record section of seismic background noise at a quiet site in NW Iran (left) together with the related displacement power spectral density spectrum (right). The latter was calculated from 6 moving and 50% overlapping intervals, 4096 samples long each, i.e. from a total record length of about 80 s.

With the following exercise we want to demonstrate that characteristic values from all these different spectral presentations can be transformed into one another and that both old „classical“ noise presentations and modern ones derived from digital data correspond to each other rather well within the limits of accuracy and representativeness.

But having determined noise power density spectra from digital records it is not so obvious what this means in terms of ground motion amplitudes and appearance of noise in records of different bandwidth and vice versa. Therefore, we present below not only the relationships to be used for the conversion of power and amplitude spectra into different kinematic units but also for calculating from spectral representations of seismic noise for different bandwidth the related frequency-dependent root-mean-square (RMS) or average peak amplitudes (APA). These relationships will then be practiced in the following exercises.

2. CONVERSION OF SIGNAL AND NOISE SPECTRA INTO DIFFERENT UNITS

Nowadays digital recordings allow proper computational spectral analysis. For a transient signal $f(t)$ the Fourier transform $F(\omega)$ exists with

$$F(\omega) = \int_{-\infty}^{\infty} f(t) \exp(i\omega t) dt = |f(\omega)| \exp^{i\phi(\omega)} \quad \text{and} \quad (1)$$

$$f(t) = (2\pi)^{-1} \int_{-\infty}^{\infty} F(\omega) \exp(-i\omega t) d\omega. \quad (2)$$

$|F(\omega)|$ is the *amplitude spectral density* with the unit m/Hz and $\phi(\omega)$ the *phase-delay spectrum* with the units deg, rad or 2π rad. But contrary to *coherent transient seismic signals* $f(t)$ of finite length, as in seismograms from explosions or earthquakes, irradiated by defined localized sources, *ambient seismic noise* is a more or less *stationary stochastic process* without a defined phase-delay spectrum. Therefore, a more suitable spectral presentation of seismic noise is the *power spectral density* $P(\omega)$. It is the Fourier transform of the autocorrelation function $P(\tau) = \langle f(t) f(t + \tau) \rangle$, i.e.

$$P(\omega) = \int_{-\infty}^{\infty} P(\tau) \exp(i\omega\tau) d\tau. \quad (3)$$

The symbol $\langle \rangle$ indicates averaging over the time t . Depending on whether $f(t)$ is a displacement (d), velocity (v) or acceleration (a) record, $P(\omega)$ is given in units m^2/Hz , $(m/s)^2/\text{Hz}$ or $(m/s^2)^2/\text{Hz}$.

When converting displacements $x = a_d \sin\omega t$ into the related velocities dx/dt or accelerations d^2x/dt^2 then one has to consider that the respective velocity and acceleration amplitudes are $a_v = a_d \omega$ and $a_a = a_d \omega^2$, respectively, with $\omega = 2\pi f$ (f - frequency in Hz). Consequently, knowing the displacement power spectral density value $P_d(\omega)$ one can calculate the respective values of the velocity (P_v) or acceleration power spectral density (P_a), i.e.

$$P_v(\omega) = P_d \omega^2 = 4\pi^2 f^2 P_d \quad (4)$$

and

$$P_a(\omega) = P_d \omega^4 = 16\pi^4 f^4 P_d = 4\pi^2 f^2 P_v \quad (5)$$

or vice versa.

If the power spectral density is expressed in units of dB referred to $1 (m/s^2)^2/\text{Hz}$ it can be written as:

$$P_a[\text{dB}] = 10 \log (P_a / 1 (m/s^2)^2/\text{Hz}). \quad (6)$$

When substituting in (4) and (5) the frequency f by the period $T = 1/f$ in s we get:

$$P_v[\text{dB}] = P_a[\text{dB}] + 20 \log (T/2\pi) \quad (7)$$

and

$$P_d[\text{dB}] = P_a[\text{dB}] + 40 \log (T/2\pi) = P_v[\text{dB}] + 20 \log (T/2\pi). \quad (8)$$

Accordingly, $P_a = P_v = P_d$ applies for period $T = 2\pi = 6.28$ s and $(P_d - P_a) = 2 \times (P_v - P_a) = \text{const.}$ for any given period and negative for $T < 2\pi$ and positive for $T > 2\pi$ (cf. Fig. 2).

3. CONVERSION OF SPECTRAL AMPLITUDES OR POWER DENSITIES INTO RECORDING AMPLITUDES

According to Aki and Richards (1980) the amplitude of a wavelet $f(t)$ at $t = 0$ can be *roughly approximated* by the product of the amplitude spectral density and bandwidth of the wavelet, i.e.

$$f(t)_{t=0} = |F(\omega)| \cdot 2 (f_u - f_l) \quad (9)$$

with f_u and f_l as the upper and lower corner frequencies of the band-passed signal. Likewise, if the power spectral density defined for noise is $P(\omega) = P$ within the frequency band $f_l < f < f_u$ and $P(\omega) = 0$ otherwise, then the *mean square amplitude* is

$$\langle f^2(t) \rangle = 2P (f_u - f_l). \quad (10)$$

Thus, for a given bandwidth, we can approximately relate the noise *power spectral density* to its *root mean square (RMS) amplitude*:

$$a_{\text{RMS}} = \{2P (f_u - f_l)\}^{1/2}. \quad (11)$$

Proper determination and comparability of PSD at different frequencies require octave filtering. Increasing the frequency of a signal by one octave means doubling its frequency. Accordingly, a band-passed signal (or filter) with n octaves of bandwidth has corner frequencies

$$f_u = 2^n f_l \quad (12)$$

and a *geometric center frequency* f_0 of

$$f_0 = (f_u \times f_l)^{1/2} = f_l \times 2^{n/2}. \quad (13)$$

From this follows for the *relative bandwidth RBW*

$$(f_u - f_l) / f_0 = (2^n - 1) / 2^{n/2}. \quad (14)$$

and (11) becomes

$$a_{\text{RMS}} = (P \times f_0)^{1/2} \times \left\{ 2 (2^n - 1) / 2^{n/2} \right\}^{1/2} = (P \times f_0)^{1/2} \times (2 \text{ RBW})^{1/2} \quad (15)$$

Accordingly, the relative bandwidth for a 2-octave filter is 1.5 and for a 2/3-octave filter 0.466.

Aki and Richards (1980, vol.1, p. 498) converted PSD into ground motions by putting the bandwidth of the noise signal half the considered (center) frequency, i.e. by assuming $f_u - f_l = 0.5 f_o$. This is equivalent to the assumption of a bandwidth of approximately 2/3-octaves. For this special case one gets:

$$\langle \dot{f}^2(t) \rangle^{1/2} = a_{\text{RMS}} = (P \times f_o)^{1/2}. \quad (16)$$

Other authors (e.g. Fix, 1972; Melton, 1978) have used an integration bandwidth of 1/3-octave only for computing RMS amplitudes from PSD. Melton reasoned that this is nearly $\pm 10\%$ about the center period in width and thus close to the tolerance with which an analyst can measure the period on an analog seismogram. Therefore, using a 1/3-octave bandwidth seemed to him a reasonable convention for calculating RMS noise amplitudes from PSD. The differences as compared to RMS values based on 1/4- or 1/2-octave bandwidths are less than 20%. But 1/3-octave RMS amplitudes will be only about 70% or 50% of the respective RMS amplitudes calculated for 2/3- or 1-octave bandwidth, respectively. Typical response curves of narrowband seismographs well suited for recording of transient body-wave onsets have bandwidths between about 1 and 3 octaves. Choosing a constant one octave filter bandwidth for comparing amplitudes of noise and transient seismic signals seems to be rather appropriate, therefore.

For RMS amplitudes determined according to (11) or (15) there is a 95% probability that the *instantaneous peak* amplitudes of a random wavelet with Gaussian amplitude distribution will lie within a range of $2a_{\text{RMS}}$. Peterson (1993) could show, that both broadband and long-period noise amplitudes follow indeed very closely a Gaussian probability distribution. In that case the absolute peak amplitudes of the narrowband filtered signal envelopes should follow closely a Rayleigh distribution. In case of an ideal Rayleigh distribution the theoretical *average peak amplitudes* (APA) are $1.253 a_{\text{RMS}}$. Peterson (1993) measured from test samples of narrowband filtered VBB and LP noise records APA values between 1.194 and 1.275.

The exercises below aim at transforming data values from these different spectral presentations into the related other forms, to compare their mutual comparability and representativeness and to calculate for different signal bandwidth the RMS ground amplitudes corresponding to selected spectral density values.

REFERENCES

- Aki, K. and Richards, P.G. (1980). Quantitative seismology - theory and methods. W.H. Freeman and Company, San Francisco, Vol.1, chapter 10: principles of seismometry, 477-524
- Bormann, P. (1998). Conversion and comparability of data presentations on seismic background noise. *Journal of Seismology* .2, 37-45
- Brune, J.N. and Oliver, J. (1959). The seismic noise of the Earth's surface. *BSSA* 49, 349-353
- Fix, J.E. (1972). Ambient Earth motion in the period range from 0.1 to 2560 sec. *BSSA*, 62, 1753-1760
- Peterson, J. (1993). Observations and modeling of seismic background noise. U.S. Geol. Survey Open-File Report 93-322, 95p

BANDWIDTH-DEPENDENT TRANSFORMATION OF NOISE DATA FROM SPECTRAL INTO TIME DOMAIN AND VICE VERSA. PART II: EXERCISES

Peter Bormann

GeoForschungsZentrum Potsdam, Division 2: Solid Earth Physics and Disaster Research
Telegrafenberg, D-14473 Potsdam, Germany

Note:

- *The equation and figure numbers given below refer to Part I: Introduction and methodology !*
- *The solutions to the exercises below will be handed out to you for comparison **after** you have finished the exercise on your own!*

Exercise 1: Determine the relative bandwidth (RBW) of an

- a) 1-octave filter
- b) 1/2-octave filter
- c) 1/3 octave filter
- d) 1/4-Octave filter

using equation (14).

Exercise 2: Calculate for the noise maximum in Fig. 3 the corresponding RMS particle velocity and displacement.

- a) Estimate the velocity power maximum from Fig. 3 (Note logarithmic scale!)
- b) Give this value also in units of $(\text{m/s})^2/\text{Hz}$
- c) Estimate the frequency f_0 related to this maximum
- d) Calculate the RMS particle velocity amplitude by considering eq. (15) and a relative bandwidth of 2/3 octaves
- e) Transform this RMS particle velocity determined under d) into the corresponding RMS particle displacement considering eq. (4)
- f) Give the *amplitude spectral density* for the displacement amplitude determined under e) considering eq. (9)
- g) Compare the value calculated under f) with Fig. 4 and discuss the reason for the „notch“-shaped lower boundary of the range of seismic signal-amplitude spectral

density shown in this figure.

Exercise 3: Transform the displacement power values of Fig. 5 at $f = 1$ Hz and $f = 10$ Hz in

- a) units of m^2/Hz
- b) acceleration power values with units $(\text{m/s}^2)^2/\text{Hz}$
- c) the values determined under b) in units of dB referred to $1 (\text{m/s}^2)^2/\text{Hz}$ according to eq. (6) and compare the result with the respective values in Fig. 2 for the New Low Noise Model (NLNM).

Exercise 4: Determine from Fig. 2 the NHNM-values in units of $(\text{nm/s}^2)^2/\text{Hz}$ for

- a) $f = 1$ Hz
- b) $f = 0.1$ Hz

Exercise 5: Transform the values determined under 4. into the corresponding RMS displacement amplitudes considering a signal of 1/3 octave bandwidth and compare the result with the respective amplitudes in Fig. 1. Discuss possible discrepancies.

Exercise 6: Transform the *peak noise* amplitude in Fig.1 for curve 1 at $T \approx 6$ s into the respective acceleration power spectral density in units of $(\text{nm/s}^2)^2/\text{Hz}$ assuming a bandwidth of the signal of 1/3 octave.

Exercise 7: Express the result of 6. in dB referred to $1 (\text{m/s}^2)^2/\text{Hz}$.

Exercise 8: Compare the result of 7. with the respective value for the NHNM in Fig. 2 and discuss possible discrepancies.

SOLUTIONS

Note: Reading errors may result in slight deviations. But they should not be > 10%!.

1. a) 0,7071
 b) 0.3483
 c) 0.23156
 d) 0.1735

2. a) $5 \times 10^{-8} \text{ (cm/s)}^2/\text{Hz}$;
 b) $5 \times 10^{-12} \text{ (m/s)}^2/\text{Hz}$;
 c) 0.16 Hz;
 d) $a_{\text{orMS}} \approx 9 \times 10^{-7} \text{ m/s}$;
 e) $a_{\text{orMS}} \approx 9 \times 10^{-7} \text{ m}$;
 f) $|F(\omega)| \approx 5.6 \times 10^{-6} \text{ m/Hz}$

3. a) $2 \times 10^{-18} \text{ m}^2/\text{Hz}$ at 1 Hz and $1.5 \times 10^{-22} \text{ m}^2/\text{Hz}$ at 10 Hz;
 b) $3.12 \times 10^{-15} \text{ (m/s}^2)^2/\text{Hz}$ at 1 Hz and $2.3 \times 10^{-15} \text{ (m/s}^2)^2/\text{Hz}$ at 10 Hz;
 c) - 145 dB for 1 Hz and -146 dB for 10 Hz, i.e. the noise power at this station is about 20 dB higher than for the NLNM.

4. a) and b) $\approx -117 \text{ dB}$, i.e. $\approx 2 \times 10^6 \text{ (nm/s}^2)^2/\text{Hz}$;

5. $a_{\text{orMS}} = 24 \text{ nm}$ at 1 Hz and 770 nm at 0.1 Hz. These amplitudes are about 4 to 6 times smaller than those in Fig. 1. The reason is that the latter are RMS and not peak amplitudes. Besides this, the amplitudes in Fig. 1 were most probably measured with seismographs of typically 1 to 2 octaves bandwidth. According to eq. (11) their amplitudes would then be 1.8 to 2.5 times larger than those recorded with 1/3 octave bandwidth only.

6. $P_{\text{acc}} = 1.65 \times 10^9 \text{ (nm/s}^2)^2/\text{Hz}$;

7. - 87.8 dB referred to $1 \text{ (m/s}^2)^2/\text{Hz}$;

8. The value under 7. is about 9 dB larger than for the NHNM ($\approx -97\text{dB}$). This corresponds to a factor of almost 3 in amplitude. The reason is that the NHNM represents RMS and not maximum peak amplitudes! With 95% probability the latter are within the range of about $2 \times \text{RMS}$! Additionally, the assumed bandwidth of the noise signals in Fig. 1 of 1/3 octaves only was not correct (cf.. answer to 5.).

INTRODUCTION TO SEISMIC SOURCES AND SOURCE PARAMETERS

Peter Bormann and Helmut Grosser

GeoForschungsZentrum Potsdam, Division of Solid Earth Physics and Disaster Research,
Telegrafenberg, D-14473 Potsdam, Federal Republic of Germany;
Fax: +49-331 288 1204; E-mail: course@gfz-potsdam.de

1. TYPES AND PECULIARITIES OF SEISMIC SOURCE PROCESSES

Fig. 1 depicts the main kinds of sources which generate *seismic waves*. These are oscillatory deformations which propagate through the earth's medium and can be recorded by *seismic sensors*. These sources are of different *intensity* and *magnitude* and thus of radiated *seismic energy*.

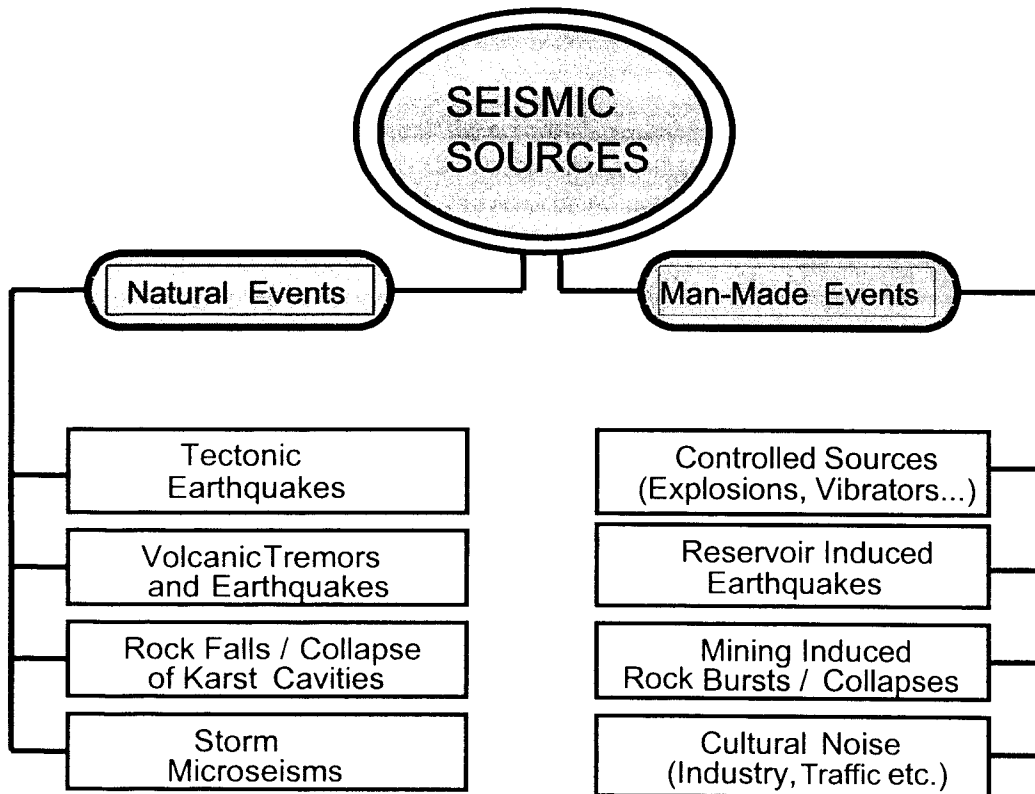


Fig. 1: Schematic classification of various kinds of events which generate seismic waves.

1.1 Earthquakes

Natural earthquakes are caused by the fracturing of brittle rock when it is deformed under stress load beyond its breaking strength. Sudden rupture will occur, either along pre-existing faults or by breaking up a new fault. The crustal blocks "snap" into a new position. For very large earthquakes, the length of the ruptured zone is up to 1000 km and the slip along the fault can reach several meters.

Laboratory experiments with homogeneous consolidated rocks under surface conditions show that, depending also their porosity, a volume strain in the order of 10^{-2} - 10^{-3} (i.e. about 0.1 % to 1% volume change) will break them. The strength of rocks in tension or shearing is generally much less. Shear strains in the order of about 10^{-4} rad or even less may already cause fracturing of solid brittle rock. But the Earth crust is already highly fractured and faulted. The strength of pre-fractured rock is much less than that of unbroken competent rock and is mainly controlled by the frictional resistance of the faults. The latter depends on the orientation of the faults with respect to the stress field and other conditions (cf. Scholz 1990) and varies in a wide range. Accordingly, deformations in the order of only 10^{-5} rad to 10^{-7} rad, i.e. the bending of a lithosphere plate by about 0.1 mm to 1 cm over a distance of 1 km, may already cause shear faulting along pre-existing zones of weakness. But the shear strength depends also on the composition and fabric (anisotropy) of rock, the temperature, the containing pressure, the deformation velocity etc. and not only on the total cumulative strain. More details on the physics of earthquake faulting and related geological and seismotectonic conditions in the real earth can be found in Scholz (1990) and in the chapter on *Physical and mathematical models of seismic source processes*. Further recommended overview articles on lithosphere rheology stratification and their relation to crustal composition, age and heat flow were published by Meissner and Wever (1988), Ranalli and Murphy (1987) and Wever et al. (1987). They also explain the influence of these parameters on the thickness and maximum depth of the seismogenic zone in the earth crust.

The relative motion and related interaction, deformation and stress loading of the earth's lithosphere plates is considered to be the main cause of tectonic earthquakes. The plates are driven, pushed and pulled by the slow motion of convection currents in the more plastic hot material of the earth mantle beneath the lithosphere. These relative motions are in the order of several cm per year. Fig. 2 show the global pattern of earthquake belts and the related major lithosphere plates. Besides this there exist many smaller sub- or micro-plates, in continental regions in particular. While earthquakes within major plates and along the mid-oceanic ridges or continental rifts do generally occur within the (mostly upper) earth's crust deep earthquakes down to a maximum of about 700 km depth may occur along ocean trenches, mainly of the Circum-Pacific earthquake and volcanic belt (e.g. along the Peru-Chile Trench, the Mexico Trench, the Ryukyu-Japan-Kurile-Aleuten Trenches, the New Hebrides Trench, the Tonga-Kermadec Trench) but also locally at some other places such as the Tyrrhenian Sea and the Aegean Sea in the Mediterranean Sea.

It is obvious that most earthquakes occur along the main plate boundaries. These boundaries constitute either zones of extension (e.g. in the up-welling zones of the mid-oceanic ridges or intra-plate rifts), transcurrent shear zones such as the west coast of North America with the famous San Andreas fault or the North Anatolian fault in Turkey, or zones of plate collision (e.g. the Himalaya thrust front) or subduction, the latter mostly along deep sea trenches. Accordingly, tectonic earthquakes may be of very different faulting type (strike-slip, normal, reverse or thrust faulting and mixed types (cf. Figs. 10 and 11 in the chapter *Determination of fault-plane solutions*)).

The largest strain rates are observed near active plate boundaries (about 10^{-8} to 3×10^{-10} per year). They are significantly less in active plate interiors (about 5×10^{-10} to 3×10^{-11} per year) or within stable continental platforms (about 5×10^{-11} to 10^{-12} per year; cf. Giardini 1994). Accordingly, a critical cumulative strain in the pre-fractured/faulted seismogenic zone of the brittle lithosphere in the order of about 10^{-6} to 10^{-7} is reached roughly after some 100, 1000 to 10.000 or 10.000 to 100.000 years of loading, respectively. This agrees well with the order of

time of so-called seismic cycles, i.e. the mean return period of the largest possible events, in these different plate environments (Muir-Wood 1993; Scholz 1990).

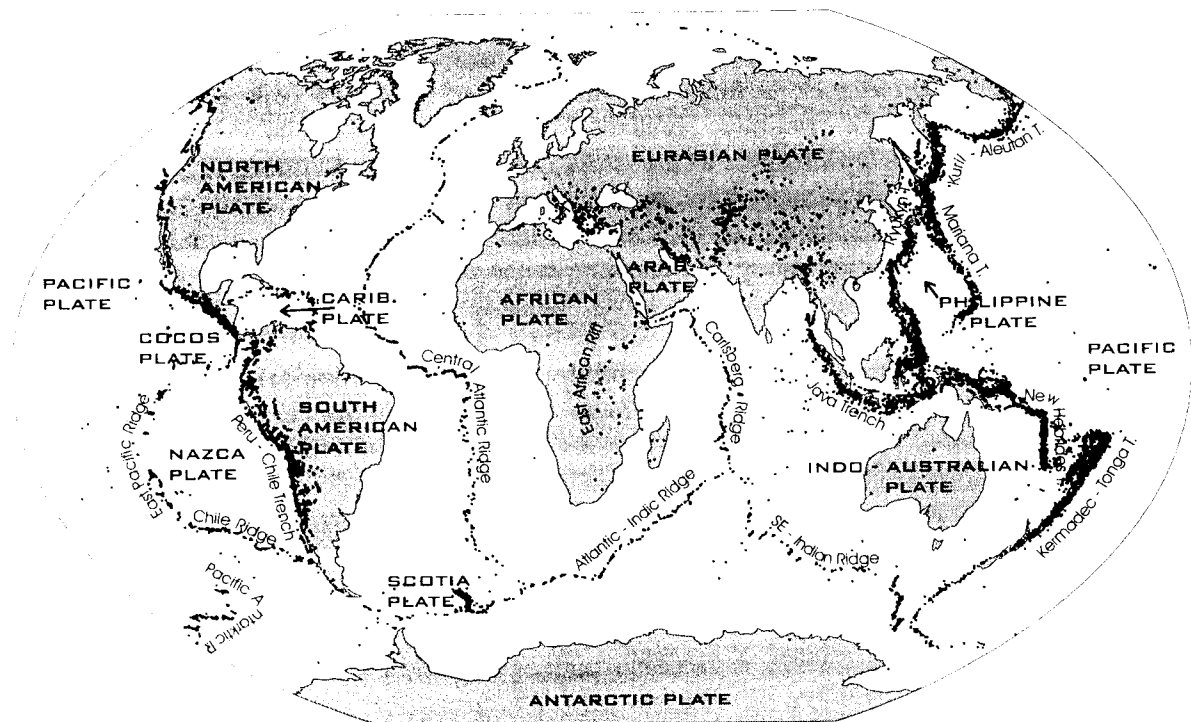


Fig. 2: Global distribution of earthquake epicentres according to the data catalogue of the United States National Earthquake Information Center (NEIC) 01/1977 - 07/1997 and the related major lithosphere plates.

Although there are hundreds of thousands to millions of weak tectonic earthquakes (EQs) globally every year most of them can be recorded by sensitive instruments only. But in the long-term global statistical average about 50,000 EQs are strong enough to be potentially perceptible by the local population (if there is any!) in the near-source area. Some 10,000 may even cause slight damage, some 100 of them (magnitude $M \geq 6$) may result in strong damage in nearby settlements and built-up areas while about 1 event every year ($M > 8$) may result in wide-spread devastation and disaster (Neumann et al. 1989; Lay and Wallace 1995). During the 20th century the 1995 Great Hanshin/Kobe earthquake caused the greatest economic losses (about 100 billion US\$), the 1976 Tangshan earthquake the most terrible human losses (about 243,000 people killed) while the Chile EQ of 1960 released the largest amount of seismic energy E_s of about 10^{19} Joule. This corresponds to about 50 to 100 years of the long-term annual average of global seismic energy release of about $1 - 2 \times 10^{17}$ J (Lay and Wallace 1995) and to about half a year of the total kinetic energy contained in the global lithosphere plate motion (Neumann et al. 1989). The total seismic moment (cf. 3. below) of the Chile EQ was about 3×10^{23} Nm. It ruptured about 800 - 1000 km of the subduction zone interface at the Peru-Chile trench in a width of about 200 km (Boore 1977; Scholz 1990).

It should be noted that most of the faulting energy E_f is required to power the growth of the earthquake fracture and the production of heat and not primarily to produce seismic waves. Accordingly, the seismic efficiency, i.e. the ratio of E_s/E_f is perhaps only about 10 % to less than 1%. It depends both on the stress drop during the rupture as well as on the total stress in the source region (Spence 1977; Scholz 1990).

Although the total energy released by the strongest historically known volcanic eruptions, may be even larger than the total faulting energy of the Chile EQ their seismic efficiency is generally much smaller, also due to the long duration of such eruptions. Nevertheless, in some cases, also volcanic earthquakes may locally reach the shaking strength of destructive EQs (e.g. *magnitudes* of about 6; cf. sub-chapter 2 below). Most of the seismic oscillations produced in conjunction with sub-surface magma flows are of the so-called tremor type, i.e. long-lasting non-coherent and more or less monochromatic oscillations which come from a two- or three-phase (liquid- and/or gas-solid) source process which is not narrowly localised in space and time. They cannot be analysed in the traditional way of seismic recordings from tectonic earthquakes or explosions and their source parameters be determined (cf. chapter *Volcano seismology*). In summary: About 85 % of the total world-wide *seismic moment* release by earthquakes occurs in subduction zones and more than 95 % by shallow earthquakes along plate boundaries. The other 5 % are distributed between intraplate events and deep and intermediate focus earthquakes. The single 1960 Chile event accounts for about 25 % of the total seismic moment release between 1904 and 1986. Volcanic earthquakes contribute only an insignificant amount to the global seismic moment release (see Scholz 1990).

1.2 Explosions

Explosions are mostly man-made (although natural explosions in conjunction with volcanic eruptions or meteorite impacts, such as the Tunguska meteorite of 30.06.1908 in Siberia, may occur) and mostly controlled, i.e. with known location and source time. While in exploration seismology aimed at (uppermost) crustal investigations explosion yields Y of a few kg to tons are sufficient to produce seismic waves which can be recorded from several km to hundreds of km distance, underground nuclear explosions of kt up to Mt TNT (Trinitrotoluol) equivalent may be seismically recorded even world-wide ($1 \text{ kt TNT} = 4.2 \times 10^{12} \text{ J}$). Nevertheless, even the strongest of all fired underground nuclear tests of an equivalent yield of about 5 Mt TNT produced body-waves of magnitude $m_b \approx 7$ only. This corresponds to roughly 0.1% of the seismic energy released by the Chile EQ of 1960. After 1974 underground tests with only $Y \leq 150 \text{ kt}$ were carried out. Only well contained underground chemical or nuclear explosions have a sufficiently good seismic coupling factor ϵ ($\epsilon \approx 10^{-2}$ to 10^{-3} , i.e. only 1 % to 0.1 % of the total released explosion energy is transformed into seismic energy). The coupling factor of explosions on the surface or in the atmosphere (depending on the altitude), is much less ($\epsilon \approx 10^{-3}$ to 10^{-6}) (cf. Griggs and Press 1961; Pomeroy and Olliver 1960).

Fig. 3 depicts schematically an idealised sub-surface explosion and tectonic earthquake (of pure strike-slip type) in a homogeneous medium. It is obvious that the explosion produces in its initial phase a homogeneous outward directed compressional motion in all directions while the tectonic earthquake produces first motions of different amplitude and polarity in different directions which are again different for longitudinal (P-) and transversal (S-) waves. These characteristics can be used to identify the type of source processes (cf. sub-chapter 4) and to discriminate between explosions and tectonic earthquakes. Implosions, e.g. of a karst caves or mining galleries produce a similar "first motion pattern" like an explosion but with opposite sign (i.e. dilatational - first motion). Contrary to this, mining induced tectonic rock bursts or tectonic events triggered/induced by high dam reservoir load and pore-pressure changes or by fluid/gas injections into or rapid withdrawal from underground reservoirs may look more similar to tectonic earthquakes. As compared to tectonic earthquakes the *duration* of the source process of explosions and the so-called *rise time* to the maximum level of displacement is much shorter (milliseconds as compared to seconds up to a few minutes) and

more impulsive (Fig. 4). Accordingly, explosions of comparable body wave magnitude excite more high-frequent oscillations (cf. *seismic source spectra*).

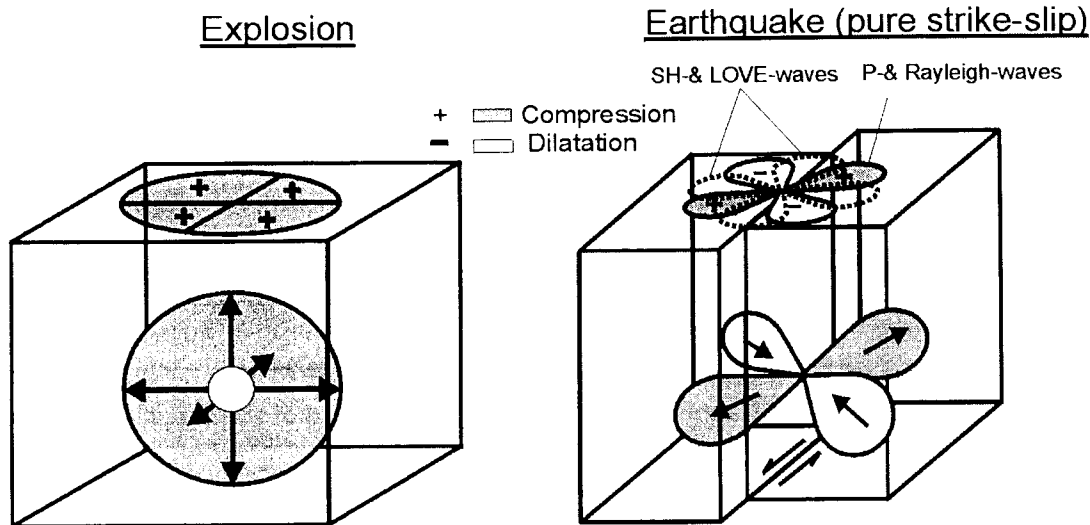


Fig. 3: Schematic sketches of an idealised underground explosion and of a pure strike-slip earthquake along a vertically dipping fault. The fault motion is "left-lateral", i.e. counter-clockwise. The arrows show the directions of compressional (outward, +, grey shaded) and dilatational (inward, -, white areas) motions. The patterns shown on the surface indicate the azimuthal variation of observed amplitudes at seismic stations and their polarity in seismic records. While point-like explosions in an isotropic medium should show no azimuth-dependent amplitudes and compressional first motions only, amplitudes and polarities vary for a tectonic earthquake. The dotted amplitude lobes in Fig. 3, right side, indicate qualitatively the different azimuth dependence of shear (S-) waves as compared to longitudinal (P-) waves (rotated by 45°) but their absolute values are much larger (about 5 times) than that of P-waves.

Explosion

Earthquake

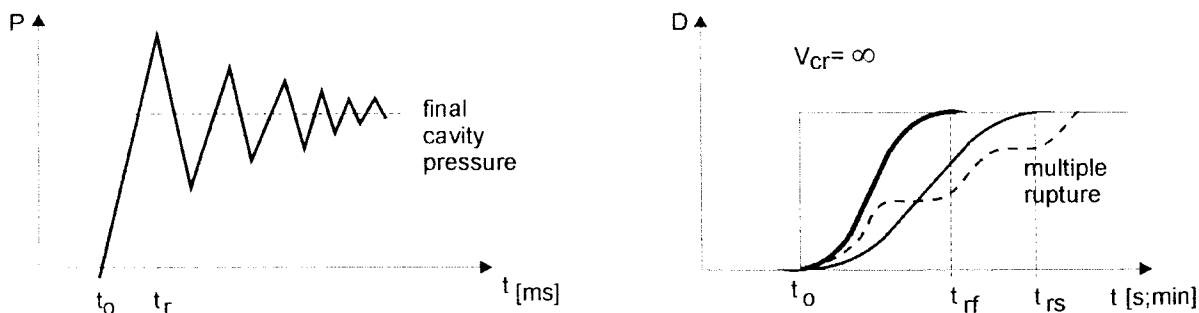


Fig. 4: Schematic diagrams of the different source functions of explosions (left) and earthquakes (right). P - pressure in the explosion cavity, D - fault displacement, t - time, t_0 - origin time of the event, t_r - rise time of P or D to its maximum (or in case of multiple events intermediate max.) values, t_{rf} - rise time of fast rupture, t_{rs} - rise time of slow rupture; the step function in the right diagram would correspond to an earthquake with infinite velocity of crack propagation v_{cr} . Current rupture models assume v_{cr} to be about 0.6 to 0.9 of the velocity V_s of shear wave propagation.

1.3 Microseisms

Very different seismic signals are produced by storms over oceans or large water basins (seas, lakes, reservoirs) as well as wind action on the topography and vegetation or built-up surface cover, so-called storm *microseisms*, and due to human activities such as rotating or hammering machinery, traffic etc., so-called *cultural seismic noise*. Rushing waters or gas/steam (in rivers, water falls, dams, pipelines, geysers) may be additional sources of natural or man-made *seismic noise*. They are mostly not well localised in space and fixed to a defined *origin time*. Accordingly, they produce more or less permanent on-going non-coherent interfering signals of more or less random amplitude fluctuations in a very wide frequency range of about 16 octaves (about 50 Hz to 1 mHz) which are often controlled in their intensity by the season (natural noise) or day time (man-made noise). Despite of the large variation of noise amplitudes world-wide by about 6 to 10 orders of magnitude they are generally much smaller than those of earthquakes and not felt by men. Because of all these significant differences to coherent seismic sources microseisms and seismic noise are not dealt with in this chapter (see chapter: *Seismic signals and noise*).

1.4 Other seismic events

Rock falls may last for several minutes and cause seismic waves but generally with less distinct onsets and separation of wave groups.

The collapse of karst caves, mining induced rock bursts or collapses of mining galleries are generally of an *implosion* type. Accordingly, their first motion patterns should show dilatation in all azimuth directions if not a secondary tectonic event has been triggered by the collapse. The strongest events may reach magnitudes up to about $M = 5.5$ and be recorded world-wide (e.g. Bormann et al. 1992).

Reservoir induced (not caused!) earthquakes have been frequently observed in conjunction with the impoundment or rapid water level changes of high dams. Since they are triggered events along pre-existing and pre-stressed tectonic faults they show the typical polarity patterns of tectonic earthquakes. The strongest events reported so far reached magnitudes up to 6.5 (e.g. Koyna earthquake in 1967). But strong events of this type are very rare.

2. PARAMETERS WHICH CHARACTERISE THE SIZE AND STRENGTH OF SEISMIC SOURCES

2.1 Macroseismic intensity

The size of a seismic source may be characterised via its *macroseismic intensity I*. The latter describes the strength of the resulting shaking in terms of human perceptions, damages to buildings and other structures as well as changes in the surrounding environment. *I* depends on the distance from the source and the underground conditions and is mostly classified according to scales of 12 degrees (e.g. Grünthal 1998). From an analysis of the areal distribution of perceptions and damages one can estimate the intensity I_0 in the (epicentral) source area as well as the source depth h . There exist correlation relationships between I_0 and other instrumentally determined measures of the earthquake size such as the *magnitude* as well as between *I* and ground acceleration. For more details see the chapter *Macroseismic and strong-motion parameters*.

2.2 Magnitude and seismic energy

The *magnitude* is a logarithmic measure of the size of an earthquake or explosion based on instrumental measurements. The magnitude concept was first proposed by Richter (1935). Magnitudes are derived from instrumental recordings of ground motion amplitudes and periods or from *signal duration*. There is no a-priori scale limitation or classification of magnitudes as for macroseismic intensities. Therefore, magnitudes are often incorrectly referred to in the press as "... according to the open-ended RICHTER scale...". In fact, nature limits the maximum size of tectonic earthquakes which is controlled by the maximum size of a brittle fracture in the lithosphere. The largest moment magnitude M_w observed so far was that of the Chile earthquake in 1960 ($M_w \approx 9.5$; Kanamori 1977). On the other hand, the magnitude scale is open to the lower end. Since nowadays high sensitive instrumentation close to the sources may record much smaller events than those with zero-magnitude according to Richter's original definition their magnitude values become negative. Via empirical *energy-magnitude-relationships* the *seismic energy* E_s irradiated by the seismic source as seismic waves can be estimated. Common relationships are those given by Gutenberg and Richter (1954, 1956) between E_s and the so-called surface wave magnitude M_s and the body-wave magnitude m_B , $\log E_s = 11.8 + 1.5 M_s$ and $\log E_s = 5.8 + 2.4 m_B$, respectively, with E_s in erg ($1 \text{ erg} = 10^{-7} \text{ J}$). According to the first relationship, a change of M by two units corresponds to a change in E_s by a factor of 1000. Nowadays, based on the analysis of digital recordings, there exist also direct procedures to estimate E_s (e.g. Purcaru and Berckhemer 1978; Boatwright and Choy 1986; Kanamori et al. 1993, Choy and Boatwright 1995) and to define an "energy magnitude" M_E (see chapter *Magnitude of seismic events*). Since most of the seismic energy is concentrated in the higher frequency part around the corner frequency of the spectrum M_E is a suitable measure of the earthquakes potential for damage. Contrary to this, the seismic moment (see below) is related to the final static displacement after an earthquake and consequently, the moment magnitude M_w to the tectonic effects of an earthquake.

2.3 Seismic spectrum, seismic moment and size of the source area

Another quantitative measure of the size and strength of a seismic shear source is the so-called scalar static *seismic moment*:

$$M_0 = \mu \bar{D} A \quad (1)$$

with μ - Young or shear modulus of the medium, \bar{D} - average final static displacement after the rupture earthquake, A - the surface area of the rupture. M_0 is a measure of the irreversible inelastic deformation in the rupture area. This inelastic strain is described in (1) by the factor $\bar{D} A$. On the basis of reasonable average assumptions about the Young modulus μ and the stress drop $\Delta\sigma$ and assuming $\Delta\sigma/\mu = \text{constant}$ Kanamori (1977) derives the relationship $E_s = 5 \times 10^{-5} M_0$. More information about the deformation in the source is described by the seismic moment tensor (see chapter *Physical and mathematical models of seismic source processes*). Its determination is nowadays a standard routine in the analysis of strong earthquakes by means of waveform inversion of digital broadband records (cf. chapter on *Source parameters and moment tensor solutions derived from seismic wave forms*).

M_0 can be determined from the spectra of seismic waves observed at the Earth surface by using the relationship:

$$M_0 = 4\pi d \rho V_{p/s}^3 u_0 / R_{\theta,\phi} \quad (2)$$

with: d - hypocentral distance between the event and the seismic station; ρ - average density of the rock and $V_{p/s}$ - velocity of the P- or S-waves around the source; $R_{\theta,\phi}$ - a factor correcting the observed seismic amplitudes for the influence of the radiation pattern of the seismic source (cf. Fig. 3 above and Fig. 3 and 4 in chapter *Determination of fault plane solutions*), u_0 - the low-frequency amplitude level as derived from the seismic spectrum of P- or S-waves, corrected for the instrument response and wave propagation effects (geometrical spreading, wave attenuation, boundaries, surface amplification). For more details see *Exercise on the determination of source parameters derived from seismic spectra*.

A simple seismic shear source with linear rupture propagation according to Aki (1967) shows in the far-field smooth displacement and velocity spectra. When corrected for the effects of geometrical spreading and attenuation we get so-called "source spectra" similar to the generalised ones shown in Fig. 5.

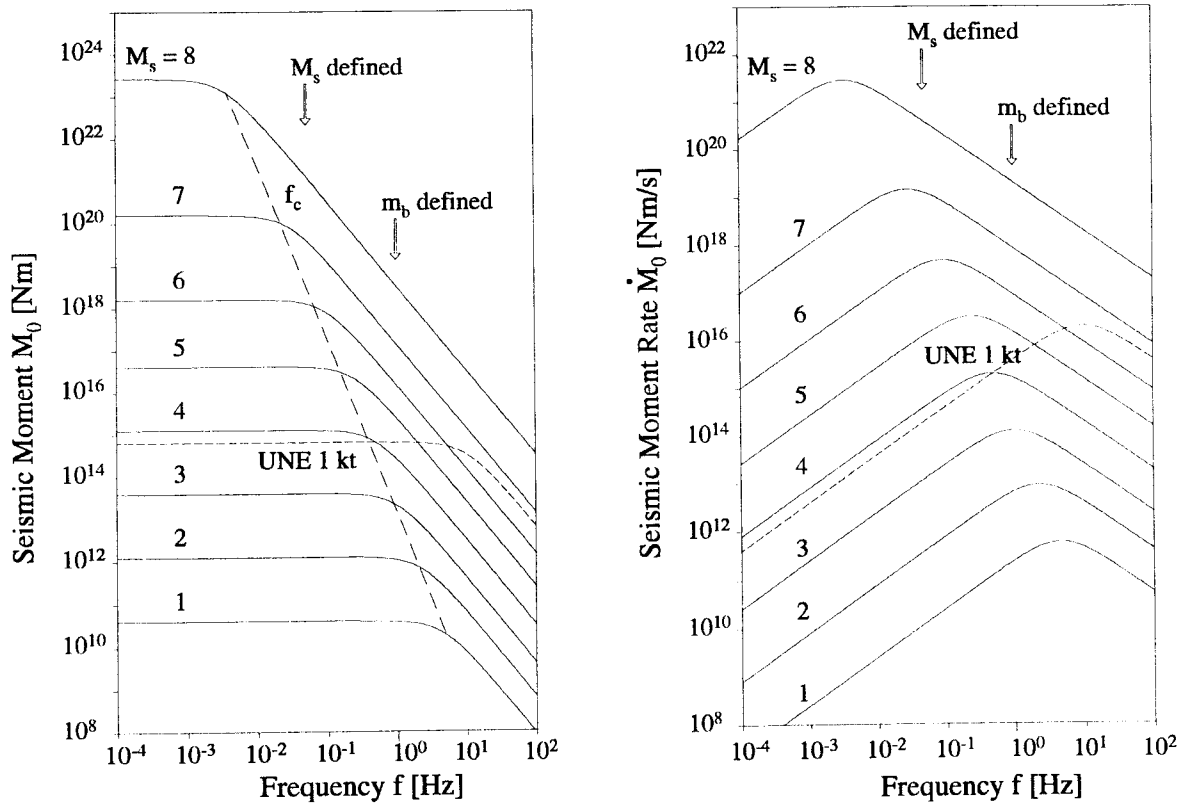


Fig.5: "Source spectra" of ground displacement (left) and velocity (right) for a seismic shear source. The broken line shows the increase of corner frequency with decreasing seismic moment of the event while the dotted line gives the approximate source spectrum for a well contained underground nuclear explosion of an equivalent yield of 1 kt TNT.

In Fig. 5 the low-frequency values have been scaled to the scalar seismic moment M_0 (left) and moment rate dM_0/dt (right), respectively. The given magnitude values M_s correspond to the related *linear* M_s - $\log M_0$ relationship given by Kanamori (1977). Note, that there exist other, non-linear empirical M_s - $\log M_0$ relationships (e.g. Gellert, 1976; Purcaru and

Berckhemer, 1978). They correspond to even stronger saturation effects than the one shown in Fig. 5. According to them the curve shown in Fig. 5 for $M_s = 8$ would correspond to $M_s \approx 8.5$, the largest surface wave magnitude ever determined, e.g. for the Chile earthquake 1960. The latter had a seismic moment M_0 of about $2 - 5 \times 10^{23}$ Nm.

The following general features are obvious from Fig. 5:

- "Source spectra" are characterised by a "plateau" of constant displacement spectral amplitudes for frequencies smaller than the so-called "corner frequency" f_c ;

The spectral displacement amplitudes decay rapidly for $f > f_c$ proportional with f^{-2} ;

- The plateau amplitudes increase with seismic moment M_0 and magnitude, respectively, while at the same time f_c decreases proportional to M_0^{-3} (cf. Aki, 1967).
- The surface wave magnitude M_s , which is, according to the original definition by Gutenberg (1945), determined from displacement amplitudes with frequencies around 0.05 Hz, is not linearly scaled with M_0 for $M_s > 6$ due to the beginning of the so-called saturation effect for spectral amplitudes with frequencies $f > f_c$.
- This saturation occurs already much earlier for P-wave magnitudes m_b which are determined from amplitude measurements around 1 Hz. No $m_b > 7$ is determined from *narrowband* short-period recordings, even for the largest events;
- Since wave energy is proportional to the square of ground motion particle velocity, i.e. $\sim (2\pi f u)^2 = (\omega u(\omega))^2$, the latter has its maximum at f_c .
- As compared with an earthquake of about the same magnitude the corner frequency f_c of an underground nuclear explosion (UNE) is about ten times larger. This means that an underground explosion of the same m_b as an earthquake produces much more high-frequency energy and has accordingly a significantly larger E_s . And since the seismic efficiency of explosions is about one order less than that of earthquake ruptures (cf. 1.1 and 1.2 above) the total energy related to the explosion yield Y is about two orders of magnitudes larger than the tectonic faulting energy E_f for events of equal m_b .

The main causes for this difference in E_s and high-frequency content between UNE and earthquakes are:

- The *duration* of the source process or *rise time* t_r to the final level of static displacement is much shorter in case of explosions than for earthquakes (cf. Fig. 4).
- The shock wave front of an explosion, which causes the deformation and fracturing of the surrounding rocks and thus the generation of seismic waves, propagates with approximately the P-wave velocity V_p while the velocity of crack propagation along a shear fracture/fault is only about 0.5 to 0.9 of the S-wave velocity, i.e. about 0.3 to 0.5 times that of V_p .
- The equivalent wave radiating surface area in case of an explosion is a sphere $A = 4\pi r^2$ and not a plane $A = \pi r^2$. Accordingly, the equivalent source radius in case of an explosion is smaller and thus the related corner frequency larger.

Note: Details of calculated "source spectra" depend on the model assumptions of the rupture process. E.g., when the rupture is propagating not one- but bi-directional and the spectrum of the source-time function is - more realistically - proportional to f^{-2} , then the high-frequency

decay for $f \gg f_c$ is proportional to f^{-3} . On the other hand, when the linear dimensions of the fault rupture differ in length and width then two corner frequencies will occur. A third one is related to the specifics of the source time function. Whether the two or three corner frequencies are separable will depend on their difference and, in case of real spectra derived from data limited in both time and frequency domain, mainly on the signal-to-noise ratio. Normally, real data are too noisy as to allow the discrimination between different types of rupture propagation and geometry.

The general shape of the seismic source spectra can be understood as follows: We know from optics that under a microscope no objects can be resolved and details of it seen anymore when its size becomes smaller than the wavelength λ of the light with which it is observed. In this case it appears just as a blurred point or dot. In order to resolve more details, electron microscopes are used which operate with much smaller equivalent wavelength. Similarly, the reverse is true in seismology. When observing at some distance a seismic source of radius r with wavelengths $\lambda \gg r$ then these do not carry any information about the details of the source process but only of the overall (integral) source process. They all "see" the source only as a point source. Accordingly, their spectral amplitudes are all constant forming the spectral plateau. On the other hand, wavelength $\lambda \ll r$ can resolve internal details of the rupture process. In case of an earthquake they correspond to smaller and smaller elements of the rupture processes or of the fault roughness (asperities and barriers). Accordingly, their spectral amplitudes decay rapidly with higher frequencies. Thus, the corner frequency f_c marks a critical position in the spectrum which is obviously related to the size of the source. According to Brune (1970) and Maderiaga (1976), who assumed both a circular fault model, the corner frequency in the P- or S-wave spectrum, respectively is $f_{c\ p/s} = c_m V_{p,s} / \pi r$ while according to Haskell (1964), who assumed a rectangular fault, $f_{c\ p/s} = c_m V_{p,s} / (L \times W)^{1/2}$ with L the length and W the width of the fault. The values c_m are model dependent constants. Accordingly, the critical wavelength $\lambda_c = V / f_c$, beyond which the source can be realised as a point source only, is $\lambda_c = c_m \pi r$ or $\lambda_c = c_m (L \times W)^{1/2}$, respectively.

Thus, when being able to determine both the source area (based on model assumption of the shape of the rupture!) and the seismic moment from seismic spectra, one can estimate from (1) the average total displacement \bar{D} . Knowing it other parameters such as the *stress drop* in the source area due to the faulting can be inferred too. More details are given in the chapter *Physical and mathematical models of seismic source processes* and in the related exercise *Determination of source parameters derived from seismic spectra*.

2.3 Orientation of the fault plane and the fault slip

Assuming that the earthquake rupture occurs along a plane fault surface the orientation of this plane in space can be described by the angles of its *strike* ϕ (against north) and *dip* δ (against the horizontal) and additionally the direction of slip on the fault by the *rake angle* λ . Fig. 8 and 9 in chapter *Determination of fault plane solutions* define these angles and how to determine them from a stereographic (Wulff net) or equal area (Lambert-Schmidt net) projection of first motion polarity observations. It can be shown that a rupture along a plane perpendicular to the above mentioned fault plane with a slip vector perpendicular to the slip on the first plane causes an identical angular distribution of first motions. Therefore, on the bases of first motion analysis alone one cannot decide which of the two planes is the true acting plane.

Note that the fault plane solution (i.e. the information about the orientation of the fault plane and of the fault slip in space) forms, together with the information about the static seismic moment M_0 (c.f. 2.3), the seismic moment tensor. Its principal axes coincide with the direction of the so-called pressure axis P and the tension axis T given with fault plane solutions. They should not be mistaken for the principal axes σ_1 , σ_2 and σ_3 (with $\sigma_1 > \sigma_2 > \sigma_3$) of the acting stress field in the earth which is described by the stress tensor. Only in case of a fresh crack in a homogeneous isotropic medium in a full space with no pre-existing faults and vanishing internal friction P is in the direction of σ_1 and T opposite to σ_3 . P and T are perpendicular to each other and form, under the above conditions, an angle of 45° with the two possible conjugate fault planes (45° -hypothesis) which are in this case perpendicular to each other (cf. Figures 2 and 11 in the chapter *Determination of fault-plane solutions*). The orientation of P and T is also defined by two angles each, the azimuth and the plunge. They can be determined by knowing the respective angles of the fault plane (cf. *Exercise on fault plane solutions*). If the above model assumptions hold true, one can, knowing the orientation of P and T in space determine that of σ_1 and σ_3 . Most of the data used for compiling the global stress map (Zoback 1992) come from earthquake fault-plane solutions calculated under these assumptions.

In reality, the internal friction of rocks is not zero. This results, according to Anderson's theory of faulting (1951) for most rocks in conjugate pairs of faults which are oriented at about $\pm 30^\circ$ to σ_1 . In this case, the direction of P and T, as derived from fault plane solutions, will not coincide with the principal stress directions. Near to the surface of the earth one of the principal stresses is almost always vertical. In case of a compressive regime, the minimum stress σ_3 is vertical while σ_1 is horizontal. This results, when fresh faults are formed in unbroken rock, in about 30° dipping thrust faults striking parallel or anti-parallel to σ_2 . In an extensional environment, σ_1 is vertical and the resulting dip of fresh normal faults is about 60° . When both σ_1 and σ_3 are horizontal, vertical strike-slip faults will develop, striking with $\pm 30^\circ$ to σ_1 . But most earthquakes are not due to fresh faulting but associated with the reactivation of pre-existing faults. Since the frictional strength of faults is generally less than that of unbroken rock, faults may be reactivated also at angles between σ_1 and fault strike different from 30° (cf. Mohr-Coulomb failure diagram, chapter *Physical and mathematical models of seismic source processes*). In a pre-faulted medium this mostly prevents failure on a new fault. Accordingly, there is no straight forward way to infer from the P and T directions determined for an individual earthquake the directions of the acting principal stress. On the other hand it is possible to infer the regional stress based on the analysis of many earthquakes in that region since the possible suite of rupture mechanisms activated by a given stress regime is constrained. This method aims at finding an orientation for σ_1 and σ_3 which is consistent with as many of the actually observed fault plane solutions as possible (e.g. Gephart and Forsyth 1984; Reches 1987; Rivera 1989).

3. DETAILED ANALYSIS OF RUPTURE KINEMATICS AND DYNAMICS IN SPACE AND TIME

Above we have considered suitable parameters for describing the size and faulting parameters of earthquakes and to some extent also of explosions. As a matter of fact, earth ruptures in real nature, as geological faults in general, are no planes, neither circular nor rectangular, neither homogeneously nor unilaterally slipping etc. All these are simplifying zero or at best first order model approximations to the truth in order to make the problem with limited data tractable at all. Real faults show jogs, steps, branching, splays etc. both in their horizontal and vertical extent (Fig. 6). Such jogs and steps, depending on their severity, are impediments

to rupture, so-called asperities or barriers, as are bumps or roughness features along the contacting fault surfaces. More illustrating examples can be found in Scholz (1990). Since these features exist at all scales, which implies the self-similarity of fracture and faulting processes and their fractal nature, this will necessarily result in heterogeneous dynamic rupturing and finally also in rupture termination.

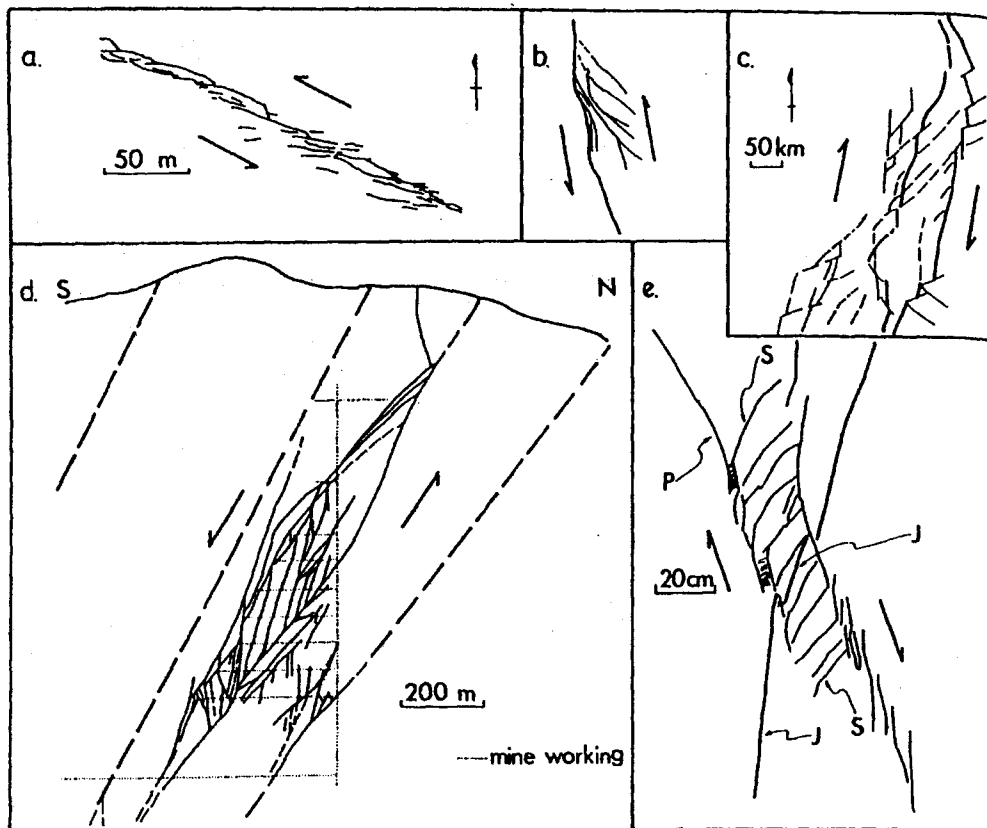


Fig. 6: Several fault zones mapped at different scales and viewed approximately normal to slip (taken from Scholz, 1990, with permission of Cambridge University Press).

According to Fig. 7 the complexity of the rupture process in time is very common to earthquakes, i.e. they are mostly multiple ruptures. This holds not only for very large earthquakes but is often observed even for small ones (Kikuchi and Ishida, 1993). And obviously, each event has its own "moment rate fingerprint".

Only in a few cases dense seismic strong-motion networks exist in the very source region of strong earthquakes which permit a detailed analysis of the rupture history in space and time described by the moment-rate density. As an example, Fig. 8 depicts data by Mendez and Anderson (1991) on the rupture process of the 1985 Michoacán Mexico earthquake. Shown are snapshots, 4 s apart from each other, of the dip-slip velocity field. One recognises two main clusters of maximum slip velocity being about 120 km and 30 s apart from each other. The related maximum cumulative displacement was more than 3 m in the first and more than 4 m in the second main cluster at about 55 km and 40 km depth, respectively. About 90 % of

the total seismic moment was released within these two main clusters which ruptured each within 8 s only while the total rupture lasted for about 56 s (Mendez and Anderson, 1991).

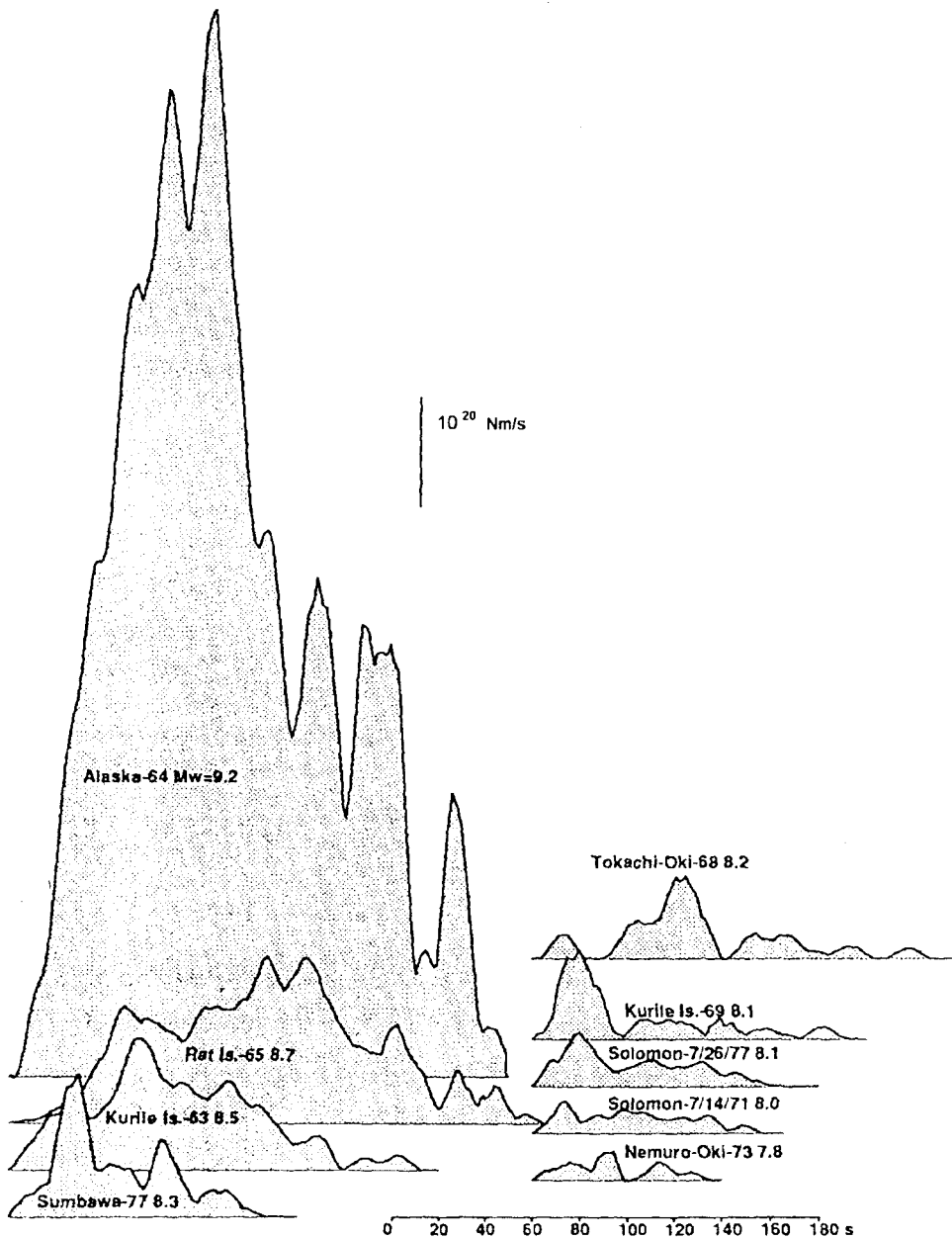


Fig. 7: Moment-rate (velocity source time) functions for the largest earthquakes in the 1960s and 1970s as obtained by Kikuchi and Fukao (1987). (Reproduced, with slight modification, from Kikuchi and Ishida, 1993, with permission of the Seismological Society of America).

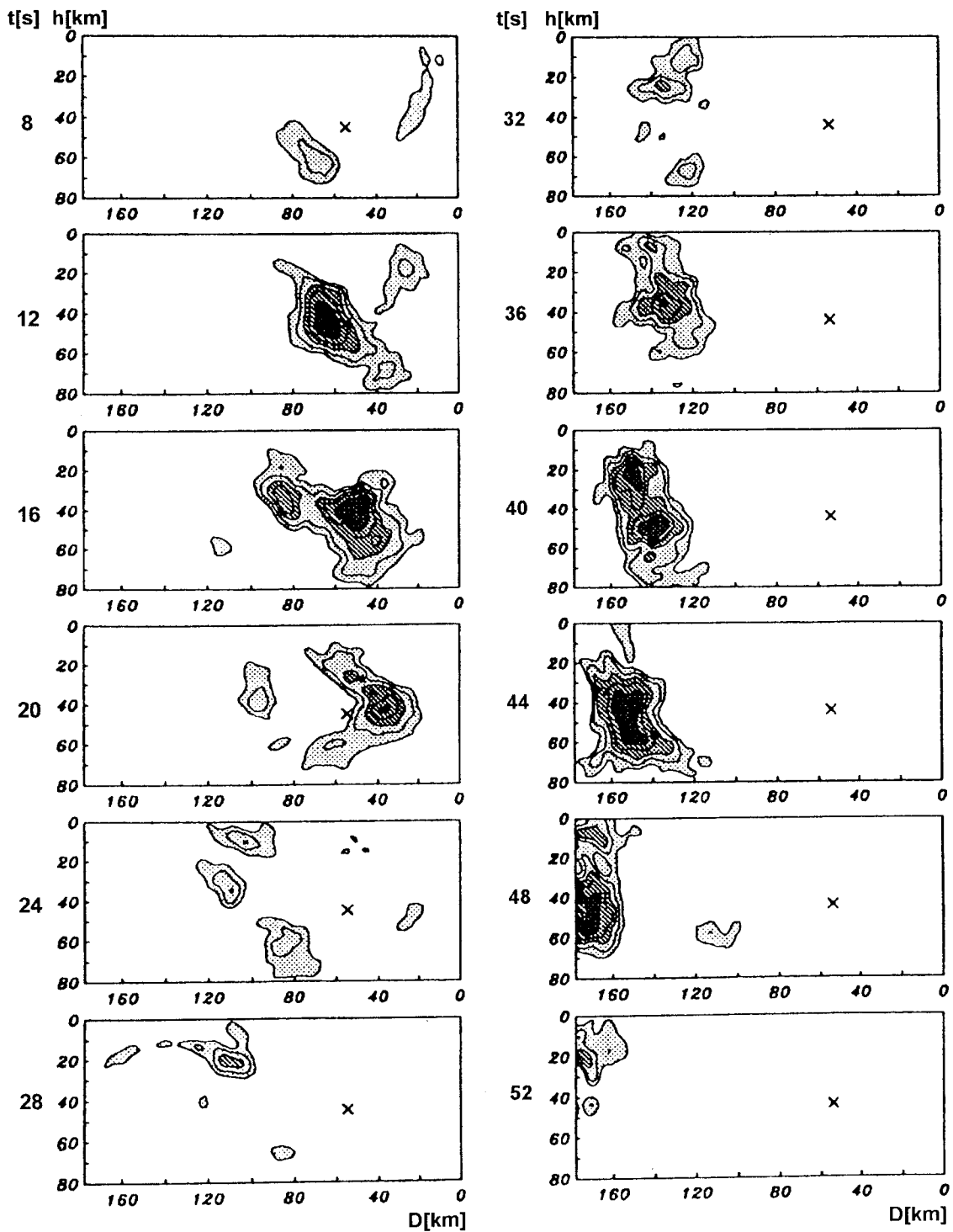


Fig. 8: Snapshots of the development in space and time of the inferred rupture process of the Michoacán earthquake in 1985. The contours represent dip-slip velocity at 5 cm/s interval, the cross denotes the NEIC hypocenter. Three consecutively darker shadings are used to depict areas with dip slip velocities in the range: 12 to 22, 22 to 32, and greater than 32 cm/s, respectively. t - snapshot time after the origin time of the event, h - depth, D - distance in strike direction of the fault (redrawn from Mendez and Anderson, 1991).

This sequential rupturing of local asperities produces most of the high-frequency content of earthquakes. Accordingly, they contribute more to the cumulative seismic energy release than to the moment release. This is particularly important for engineering seismological assessments of expected earthquake effects. Damage to (the multitude of low-rise) structures is mainly due to frequencies > 2 Hz. They are grossly underestimated when analysing strong earthquakes only in teleseismic records on the basis of medium and long-period seismic records or when calculating model spectra assuming smooth rupturing along big faults of large earthquakes. This problem can be overcome only with detailed strong-motion networks in source areas of potentially large earthquakes and by complementary field investigations and related modelling of the detailed rupture process in case of clear surface expressions of the earthquake fault. But this is beyond the scope of seismological observatory practice. But observatory seismologists need to be aware of these problems and the related limitations of their simplified standard procedures. Nevertheless, they have a value on their own by allowing a rough first order analysis of the dominating types and orientation of earthquake faulting in a given region and their relationship to regional tectonics and stress field. The latter can also be inferred from other kind of data such as overcoring experiments, geodetic data or field geological evidence. Their comparison with independent seismological data, which are mainly controlled by conditions at larger depth, may provide a deeper insight into the nature of the fields observed.

4. SUMMARY CONCLUSIONS

The detailed understanding and quantification of the physical processes and geometry of seismic sources is one of the ultimate goals of seismology, be it in relation to tectonics, the improved assessment of seismic hazard or with the aim of identifying the type of source and discriminating between natural and man-made events. Earthquakes can be quantified with respect to various geometrical and physical parameters such as time and location of the (initial) rupture and orientation of the fault plane and slip, earthquake size with respect to fault length, rupture area, amount of slip, magnitude, seismic moment, stress drop and radiated energy, duration and time-history (complexity) of faulting, particle velocity and acceleration of fault motion etc.. It is impossible, to represent this complexity in just a single number or a few parameters.

There are different approaches to tackle the problem. One aims at the detailed analysis of a given event, both in the near- and far-field, analysing waveforms and spectra of various kinds of seismic waves in a broad frequency range up to the static displacement field as well as looking into macroseismic data. Such a detailed and complex investigation requires a lot of time and efforts. It is affordable only for selected important events. The second simplified approach describes the seismic source only by a limited number of parameters such as the origin time and (initial rupture) location, magnitude, intensity or acceleration of observed/measured groundshaking, sometime also the fault plane solution. They can more easily be obtained and have the advantage that rough but quick information can be given to the public and concerned authorities. Further, this approach provides standardised mass data for comprehensive earthquake catalogues which are fundamental for other kinds of research such as earthquake statistics and seismic hazard assessment. But we need to be aware, that these simplified, often purely empirical parameters can not give a full description of the true nature and geometry, time history and energy release of a seismic source. In the following we will describe only the most common procedures in seismological (more or less routine) practice for simple and more complex parameter determinations such as magnitude and

energy, fault plane solutions, rupture area, displacement vector, stress drop and seismic moment.

REFERENCES

- Anderson, E.M. (1951). The dynamics of faulting and dyke formation with applications to Britain. 2nd ed. rev., Oliver & Boyd Publishers, Edinburgh
- Aki, K. (1967). Scaling law of seismic spectrum. *J. Geophys. Res.*, **72**, 4, 1217-1231.
- Berckhemer, H. and Purcaru, G. (1978). A magnitude scale for very large earthquakes. *Tectonophysics*, **49**, 189-198.
- Boatwright, J. L. and Choy, G. L. (1986). Teleseismic estimates of the energy radiated by shallow earthquakes. *J. Geophys. Res.*, Vo. 91. No. B6, 2095-2112.
- Bolt, B. A. (1993). Earthquakes and geological discovery. The Scientific American Library, W.H. Freeman and Company, New York, 220 pp.
- Boore, D. M. (1977). The motion of the ground in earthquakes. *Scientific American*, December 1977, W.H. Freeman and Company, San Francisco, 1-19.
- Bormann, P., Wylegalla, K. and Grosser, H. (1992). The strong mining event of March 13, 1989: Analysis of the multiple event. Proc. of the XXII. General Assembly of the European Seismological Commission (ESC), Barcelona, 17-22 Sept. 1990, Proceedings and Activity Report 1988-1990, Servei Geològic de Catalunya, 153-158.
- Brune, J. N. (1970). Tectonic stress and the spectra of shear waves from earthquakes. *J. Geophys. Res.* **75**, 4997-5009.
- Choy, L.G. and Boatwright, J.L. (1995). Global patterns of radiated seismic energy and apparent stress. *Journal Geophys. Res.*, **100**, B9, 18,205-18,228.
- Gellert, R.J. (1976). Scaling relations for earthquake source parameters and magnitudes. *Bull. Seism. Soc. Am.*, **66**, 1501-1523.
- Gephart, J.W. and Forsyth, D.W. (1984). An improved method for determining the regional stress tensor using earthquake focal mechanism data: application to the San Fernando earthquake sequence. *J. Geophys. Res.* **89**, B11, 9305-9320.
- Giardini, D. (1994). Personal communication.
- Griggs, D. and Press, F. (1961). Probing the earth with nuclear explosions. *J. Geophys. Res.* **66/1**, 237-258.
- Grünthal, G. (Editor) (1998). European Macroseismic Scale 1998. Conseil de l'Europe, Cahiers du Centre Européen de Géodynamique et de Séismologie, Vol. 15, Luxembourg, 99 pp.
- Gutenberg, B. (1945). Amplitudes of surface waves and magnitudes of shallow earthquakes. *Bull. Seism. Soc. Am.*, **35**, 57-69.
- Gutenberg, B. and Richter, C.F. (1954). *Seismicity of the Earth*. Princeton University Press, 2nd ed., 310 pp.
- Gutenberg, B. and Richter, C.F. (1956). Magnitude and energy of earthquakes. *Annali di Geofisica*, **9**, 1, 1-15.
- Haskell, N. A. (1964). Total energy and energy spectral density of elastic wave radiation from propagating faults. *Bull. Seism. Soc. Am.* **54**, 1811-1841.
- Kanamori, H. (1977). The energy release in great earthquakes. *J. Geophys. Res.* **82**, 2981-2987.
- Kanamori, H. (1980). The size of earthquakes. *Earthquake information bulletin*. Vol. 12, No. 1, 10-15.
- Kanamori, H., Mori, J., Hauksson, E., Heaton, Th. H., Hutton, L. K. and Jones, L. M. (1993). Determination of earthquake energy release and M_L using TERRASCOPE. *Bull. Seism. Soc. Am.*, Vol. 83, No. 2, 330-346.

- Kikuchi, M. and Ishida, M. (1993). Source retrieval for deep local earthquakes with broadband records. *Bull. Seism. Soc. Am.*, **83**, 6, 1855-1870.
- Kikuchi, M. and Fukao, Y. (1987). Inversion of long-period P-waves from great earthquakes along subduction zones. *Tectonophysics*, **144**, 231-247.
- Madariaga, R. (1976). Dynamics of an expanding circular fault. *BSSA* **66**, 639-666.
- Meissner, R. and Wever Th. (1988). Lithosphere rheology: Continental versus oceanic unit. *Journal of Petrology*, Oxford University Press, Special Lithosphere Issue, 53-61.
- Mendez, A. J. and Anderson, J. G. (1991). The temporal and spatial evolution of the 19 September 1985 Michoacan earthquake as inferred from near-source ground-motion records. *Bull. Seism. Soc. Am.*, **81**, 3, 1655-1673.
- Muir Wood, R. (1993). From global seismotectonics to global seismic hazard. *Annali di Geofisica*, **36**, 3-4, 153-168.
- Neumann, W., Jacobs, F. und Tittel, B. (1989). *Erdbeben* (in German). B.G. Teubner Verlagsgesellschaft, 212 pp.
- Pomeroy, P. W. and Oliver, J. (1960). Seismic waves from high altitudes nuclear explosions. *J. Geophys. Res.* **65/10**, 3445-3457.
- Purcaru, G. and Berckhemer, H. (1978). A magnitude scale for very large earthquakes. *Tectonophysics*, **49**, 189-198.
- Ranalli, G. and Murphy, D. C. (1987). Rheological stratification of the lithosphere. *Tectonophysics* **132**, 281-295.
- Reches, Z. (1987). Determination of the tectonic stress tensor from slip along faults that obey the Coulomb yield condition. *Tectonics*, **6**, 6, 849-861.
- Richter, Ch. (1935). An instrumental earthquake magnitude scale. *Bull. Seism. Soc. Am.* **25**, 1-31.
- Rivera, L. (1989). Inversion du tenseur des contraintes et des mécanismes au foyer à partir des données de polarité pour une population de séismes. Thèse de doctorat, Université Louis.Pasteur de Stasbourg.
- Scholz, Ch. H. (1990). *The mechanics of earthquakes and faulting*. Cambridge University Press, Cambridge, 439 pp.
- Spence, W. (1977). Measuring the size of an earthquake. *Earthquake Information Bulletin* **9/4**, 21-23.
- Wever, Th., Trappe, H., Meissner, R. (1987). Possible relations between crustal reflectivity, crustal age, heat flow, and viscosity of the continents. *Annales Geophysicae*, **87/03 B**, 255-266.
- Zoback, M.L. (1992). First- and second-order patterns of stress in the lithosphere: The World Stress Map Project. *J. Geophys. Res.*, **97**, B8, 11,703-11,728.

MAGNITUDE OF SEISMIC EVENTS

Peter Bormann

GeoForschungsZentrum Potsdam, Division of Solid Earth Physics and Disaster Research,
Telegrafenberg E428, D-14473 Potsdam, Federal Republic of Germany;
Fax: +49-331 288 1204; E-mail: course@gfz-potsdam.de

1. HISTORY, SCOPE AND LIMITATIONS OF THE MAGNITUDE CONCEPT

The concept of magnitude was introduced by Richter (1935) to provide an objective instrumental measure of the size of earthquakes. Contrary to *seismic intensity* I which is based on the assessment and classification of shaking damage and human perceptions of shaking and thus depends on the distance from the source the *magnitude* M uses instrumental measurements of earth ground motion adjusted for epicentral distance and source depth. Standardised instrument characteristics were originally used so as to avoid instrumental effects on the magnitude estimates. Thus it was hoped that M could provide a single number measure of earthquake size which is related to the released seismic energy E_s . But as outlined in the chapter *Introduction to seismic sources and source parameters*, such a simple empirical parameter is not directly related to any physical parameter of the source. Rather, the magnitude scale aims at providing a quickly determined simple "... parameter which can be used for first-cut reconnaissance analysis of earthquake data (catalog) for various geophysical and engineering investigations; special cautions should be exercised in using the magnitude beyond the reconnaissance purpose" (Kanamori, 1983).

The original Richter magnitude M_L is suitable for the classification of local shocks in Southern California only. It used data from the standardised short-period Wood-Anderson seismometer network. Gutenberg and Richter (1936) and Gutenberg (1945a, b and c) extended then the magnitude concept so as to be applicable also to ground motion measurements from medium- and long-period seismographic recordings of both surface waves (M_s) and different types of body waves (m_B) in the teleseismic distance range. Although they tried to scale them with each other so as to match at certain magnitude values it was realised that these different magnitude scales are only imperfectly consistent with each other. Therefore, Gutenberg and Richter (1956a and b) provided correlation relationships between the various magnitude scales (cf. section 3 below).

After the deployment of the World Wide Standardized Seismic Network (WWSSN) in the 1960s it became customary to determine m_b on the basis of short-period narrow-band P-wave recordings only, thus increasing the inconsistency between the magnitude estimates from body and surface waves. The main reasons for these inconsistencies are:

- Different magnitude scales use different periods and wave types which carry different information about the complex source process;
- The spectrum irradiated from a seismic source does not increase linearly with the size of the event in all frequency ranges. While long-period displacement amplitudes continue to increase, the corner frequency f_c , beyond which the spectral amplitudes decay with about f^{-2} to f^{-3} , decreases with increasing size. This changes the balance between high- and low-frequency content in the radiated source spectra as a function of event size;
- The maximum seismic energy is released around the corner frequency of the displacement spectrum because this relates to the maximum of the ground-velocity spectrum (cf. Fig. 5 in the chapter *Introduction to seismic sources and source parameters*). Accordingly, M ,

which is supposed to be a measure of seismic energy released, strongly depends on the position of the corner frequency in the source spectrum with respect to the pass-band of the seismometer used for the magnitude determination;

- For a given level of long-period displacement amplitudes the corner frequency is controlled by the stress drop in the source. High stress drop results in the excitation of more high frequencies. Accordingly, seismic events with the same long-period magnitude estimates may have significantly different corner frequencies and thus ratios between short-period/long-period energy or m_b/M_s , respectively;
- Seismographs with different transfer functions sample the ground motion in different frequency bands with different bandwidth. Accordingly, no general agreement of the magnitudes determined on the basis of their records can be expected.
- Additionally, band-pass recordings reduce systematically the recording amplitudes of *transient seismic signals*, the more so the narrower the bandwidth is (e.g. Scherbaum 1996; Bormann 1973 and 1998,). This cannot be fully compensated by correcting for the frequency dependent magnification of different seismographs based on their amplitude-frequency response. Although this is generally done in seismological practice in order to determine "true ground motion" amplitudes for magnitude calculation it is not fully correct. The reason is that the instrument magnification or amplitude-frequency response curves are valid only for steady-state oscillation conditions, i.e. after the decay of the seismographs transient response to an input signal (chapters *Seismic signals and noise; Seismic sensors and sensor calibration*).

There have been several efforts (in vain) (e.g. Gutenberg and Richter, 1956a; Christoskov et al. 1985) to unify or homogenise the results obtained by different methods of magnitude determination into a common measure of earthquake size or energy while others, aware of the above mentioned reasons for systematic differences have used them for better understanding the specifics of various seismic sources, e.g. for discriminating between tectonic earthquakes and underground nuclear explosions on the basis of the ratio m_b/M_s (e.g. Bormann 1972). Duda and Kaiser (1989) recommend instead the determination of different *spectral magnitudes*, based on measurements of the spectral amplitudes from one-octave bandpass filtered digital broad-band velocity records (cf. section 2.4.2).

Another effort to provide a single number measure of the earthquake size was made by Kanamori (1977). He developed the seismic moment magnitude M_w . It is tied to M_s but does not saturate for big events because it is based, as the seismic moment M_0 itself, on measurements of the (constant) level of low-frequency spectral displacement amplitudes for $f \ll f_c$. This level increases linearly with M_0 . According to eq. (1) in *Introduction to seismic sources and source parameters*, M_0 is proportional to the average static displacement and the area of the fault rupture and thus a good measure of the total deformation in the source. On the other hand it is (see the above discussion on corner frequency and high-frequency content) neither a good measure of earthquake size in terms of seismic energy release nor a good measure of seismic hazard since earthquake damage is mainly caused by high frequent strong ground motion with $f > 0.5$ Hz. Consequently, there is no single number parameter available which could serve as a good estimate of earthquake size in its different aspects. What is needed in practice are at least two parameters to characterise roughly both the size and related hazard of a seismic event, namely M_0 and f_c or M_w and m_b or M_L (based in short-period measurements), respectively, or a comparison between the moment magnitude M_w and the energy magnitude M_E of an event. The latter can today be determined from direct energy calculations based on the full integration of digital broadband records (Seidl and Berckhemer, 1982; Boatwright and Choy 1986; Kanamori et al. 1993; Choy and Boatwright 1995) (cf. section 2.4.3).

Despite of their limitations, standard magnitude estimates have proved to be suitable also for getting, via empirical correlation relationships, first rough estimates of other seismic source parameters such as the seismic moment M_0 , stress drop, amount of seismic energy E_s irradiated, length L , radius r or area A of the fault rupture, but also of the intensity of ground shaking I_0 in the source area and the probable extent of the area of felt shaking (see chapter *Seismic scaling relations*).

Magnitudes are also crucial for the quantitative classification and statistical treatment of seismic events aimed at assessing seismic activity and hazard, studying variations of seismic energy release in space and time etc. Accordingly, they are also relevant in earthquake prediction research. All these studies have to be based on well defined and stable long-term data. Accordingly, magnitude values - inherent systematic biases as discussed above notwithstanding - have to be determined over decades and even centuries by applying rigorously clear and well documented stable procedures and well calibrated instruments. Any changes have to be precisely documented in station log-books or event catalogues and need to be corrected for. Otherwise, serious mistakes may result from any research based on these data. After re-examining the earthquake catalogue for southern California between 1932 and 1990 Hutton and Jones (1993) concluded:

- magnitudes M_L had not been consistently determined over that period;
- amplitudes of ground velocities recorded on Wood-Anderson instruments and thus M_L were systematically overestimated prior to 1944 compared to present reading procedures;
- in addition, changes from human to computerised estimation of M_L led to slightly lower magnitude estimates for the time after 1975;
- these changes contributed to an apparently higher rate of seismicity in the 30s and 40s and a later decrease in seismicity rate which was attributed to the 1952 Kern County ($M_w = 7.5$) earthquake;
- variations in the rate of seismic activity have often been related to precursory activity prior to major earthquakes and therefore been considered as suitable for earthquake prediction;
- the re-determination of M_L in the catalogue for southern California does not confirm any changes in seismicity rate above the level of 90% significance for the time interval considered.

This and similar experience with other local and global catalogues led Habermann (1995) to the statement: "... the heterogeneity of these catalogues makes characterising the long-term behaviour of seismic regions extremely difficult and interpreting time-dependent changes in those regions hazardous at best. ...Several proposed precursory seismicity behaviours (activation and quiescence) can be caused by simple errors in the catalogues used to identify them. ... Such mistakes have the potential to undermine the relationship between the seismological community and the public we serve. They are, therefore, a serious threat to the well-being of our community."

Being aware now on the one hand of the inherent problems and limitations of the magnitude concept in general and specific magnitude estimates in particular and of the urgent need to strictly observe reproducible long-term standardised procedures of magnitude determination on the other hand we will review below the magnitude scales most commonly used in seismological practice. An older comprehensive review of the complex magnitude issue was given by Bath (1981), a more recent one by Duda (1989). Various special volumes with selected papers from symposia and workshops on the magnitude problem appeared in *Tectonophysics* (Vol. 93, No.3/4 (1983); Vol. 166, No. 1-3 (1989); Vol. 217, No. 3/4 (1993)).

2. MAGNITUDE SCALES

2.1 General assumptions and definition of magnitude

Magnitude scales are based on a few simple assumptions, e.g.:

- for a given source-receiver geometry "larger" events will produce wave arrivals of larger amplitudes at the seismic station;
- the decay of ground displacement amplitudes with epicentral distance Δ and their dependence on source depth h , i.e. the effects of geometric spreading and attenuation of the considered seismic waves, is known at least empirically in a statistical sense. It can be compensated by a so-called calibration function $\sigma(\Delta, h)$. The latter is the log of the inverse of the reference amplitude $A_0(\Delta, h)$ of an event of zero magnitude, i.e. $\sigma(\Delta, h) = -\log A_0(\Delta, h)$. The logarithm is used because of the enormous variability of earthquake displacement amplitudes;
- magnitudes should be a measure of seismic energy released and thus be proportional to the velocity of ground motion, i.e. to A/T with T as the period of the considered wave;
- the maximum value $(A/T)_{\max}$ in a wave group for which $\sigma(\Delta, h)$ is known should provide the best and most stable estimate of the event magnitude;
- the effects of prevailing azimuth dependent source directivity can be corrected by a regional source correction term C_r and the influence of local site effects on amplitudes depending on local crustal structure, near-surface rock type, soft soil cover and/or topography may be accounted for by a station correction C_s .

Accordingly, the general form of all magnitude scales based on measurements of ground displacement amplitudes A and periods T is:

$$M = \log(A/T)_{\max} + \sigma(\Delta, h) + C_r + C_s. \quad (1)$$

Note: calibration functions used in common practice do not consider a frequency dependence of σ . This is not fully correct. Theoretical calculations by Duda and Janovskaya (1993) show that differences in $\sigma(\Delta, T)$ for P-waves may become > 0.6 magnitude units for $T < 1$ s but they are < 0.3 for $T > 4$ s, i.e. more or less negligible for magnitude determinations in the medium- and long-period range.

2.2 General rules and procedures for magnitude determination

Magnitudes can be determined on the basis of eq. (1) by reading $(A/T)_{\max}$ for any wavelet or wave group of body (e.g. P, S, Sg, PP) or surface waves (L or Lg, R or Rg) for which calibration functions for either vertical (V) and/or horizontal (H) component records are available. In case of seismographic recordings with velocity proportional frequency response $(A/T)_{\max} = A_{v\max}$, i.e. it can be directly determined from the maximum trace amplitude of this wave or wave group, corrected for the velocity magnification in the considered period range. Contrary to this, in case of displacement records, one may not get for sure $(A/T)_{\max}$ were the displacement amplitude is largest! Sometimes smaller amplitudes associated with smaller periods may yield larger $(A/T)_{\max}$. Check it!

In measuring A and T from seismic records for magnitude determinations and reporting them to national or international data centres, the definitions and respective instructions given in the *Manual of Seismological Observatory Practice* (Willmore, 1979) as well as in the

recommendations by the IASPEI Commission on Practice from its Canberra meeting in 1979 (slightly modified and amended below) should be observed:

- The trace amplitude B of a seismic signal on a record is defined as its largest peak (or trough) deflection from the base-line of the record trace;
- For many phases, surface waves in particular, the recorded oscillations are more or less symmetrical about the zero line. B should then be measured either by direct measurement from the base-line or - preferably - by halving the peak-to-trough deflection (Figs. 1 a and c - e). For phases that are strongly asymmetrical (or clipped on one side) B should be measured as the maximum deflection from the base-line (Fig. 1b);
- The corresponding period T is measured in seconds between those two neighbouring peaks (or troughs) - or from (doubled!) trace crossings of the base-line - were the amplitude has been measured;
- The trace amplitudes B measured on the record should be converted to ground displacement amplitudes A in nanometres (nm) or some other stated SI unit, using the A-T response (magnification) curve $\text{Mag}(T)$ of the given seismograph (cf. Fig. 2); i.e. $A = B / \text{Mag}(T)$. (Note: In most computer programs used nowadays for the analysis of digital seismograms the measurement of period and amplitude is done automatically after marking the respective position in the record from where A and T should be determined);
- Amplitude and period measurements from the vertical component (V) are most important. If horizontal components (N - north-south; E - east-west) are available, readings from both records should be made at the same time (and noted or reported separately) so that the amplitudes can be combined vectorially, i.e. $A_H = \sqrt{(A_N^2 + A_E^2)}$;
- When several instruments of different frequency response are available (or in case of the analysis of digital broadband records filtered with different standard responses), A_{\max} and T measurements from each should be reported separately and the type of instrument used be stated clearly (short-, medium- or long-period, broadband, Wood-Anderson etc or give related abbreviations for instrument classes with standardised response characteristics; cf. Fig.2 and Tab. 1). For this, the classification given in the Manual of Seismological Observatory Practice (Willmore 1979) may be used;
- Broadband instruments are preferred for all measurements of amplitude and period;
- Note that earthquakes are often complex multiple ruptures. Accordingly, the time t_{\max} at which a given seismic body wave phase has its maximum amplitude may be quite some time after its first onset. Accordingly, in case of P- and S-waves the measurement should normally be done within the first 25 s and 40-60 s, respectively, but in case of very large earthquakes this interval may need to be extended to even more than a minute. For subsequent earthquake studies it is essential to measure and report also the time t_{\max} that measurement is made (cf. Figs. 1c-d and Tab. 1);
- For teleseismic ($\Delta > 20^\circ$) surface waves the procedures are principally the same as above for body waves but A_{\max} should normally occur and be measured in the period range between 16 and 24 s. On the other hand, in displacement proportional records of a dispersive surface wave train $(A/T)_{\max}$ may occur not at B_{\max} but at a smaller trace amplitude associated with a smaller period. Then, besides $(A/T)_{\max}$, also A_{\max} for the above period range should be reported. In order to find $(A/T)_{\max}$ it might be necessary to calculate A/T for several amplitudes and select the largest vectorially combined value. In records proportional to ground-motion velocity the maximum trace amplitude is related to $(A/T)_{\max}$!;

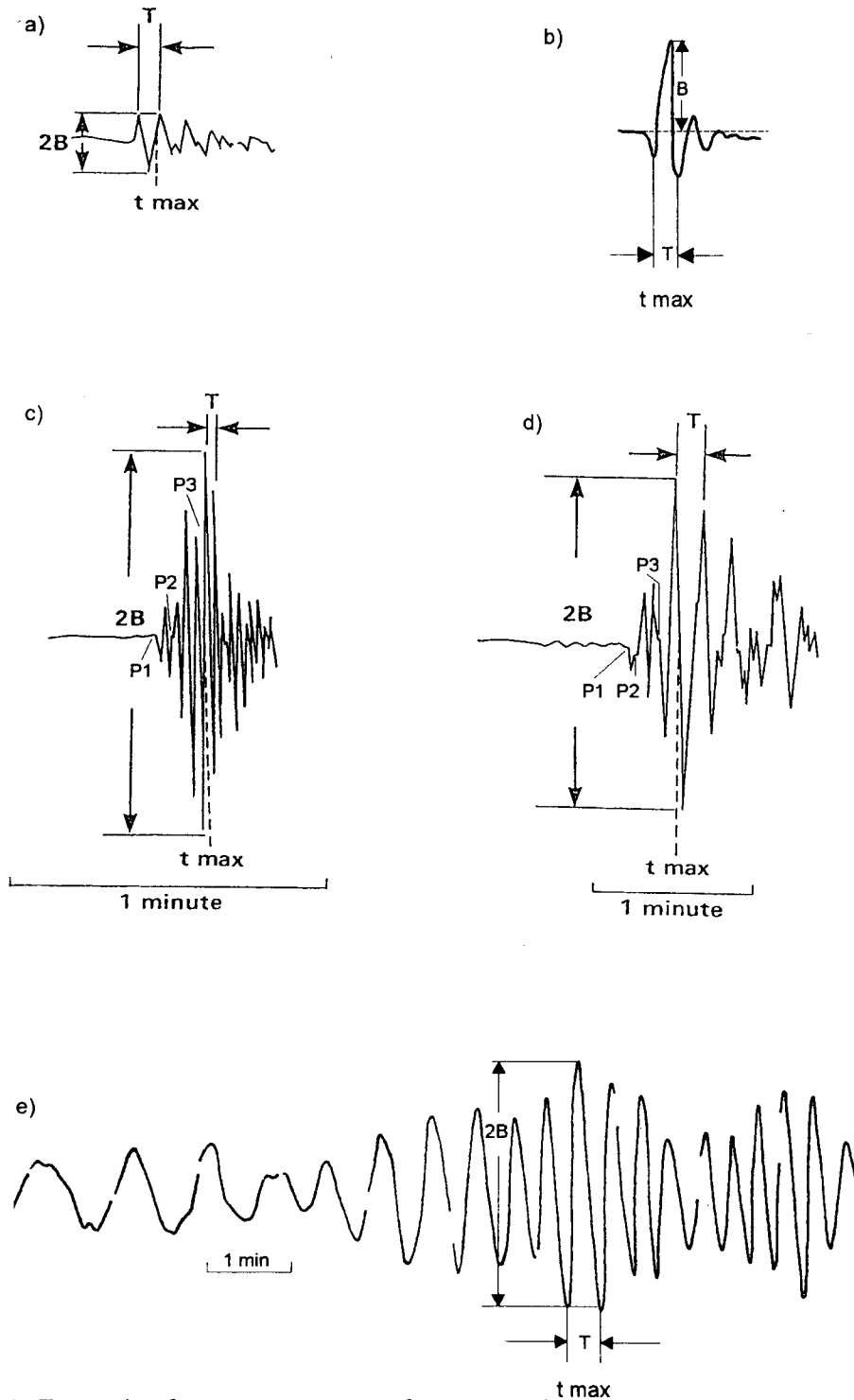


Fig.1: Examples for measurements of trace amplitudes B and periods T in seismic records for magnitude determination: a) in case of a short wavelet with symmetric and b) with asymmetric deflections, c) and d) in case of a more complex P-wave group of longer duration (multiple rupture process) and e) in case of a dispersive surface wave train. Note: c) and d) are seismogram cut-outs of the same event but recorded with different seismographs (classes A4 and C, respectively) while e) has been recorded by a seismograph of class B3; cf. Fig. 2).

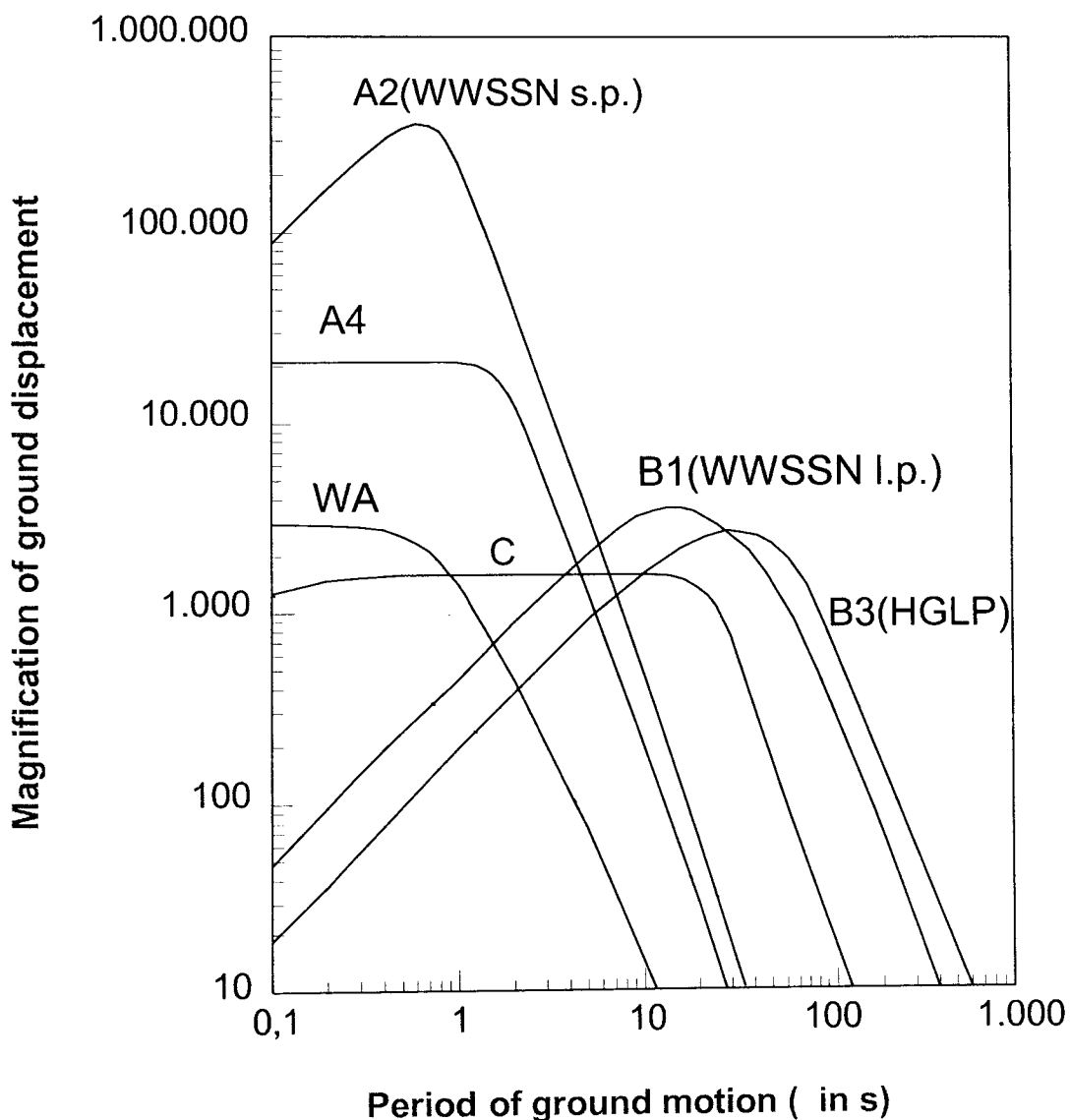


Fig.2: Relative magnification curves for ground displacement for various classes of standardised analogue recordings (redrawn and complemented from the Manual of Seismological Observatory Practice, Willmore 1979). A4 and C are the magnification curves of the standard short-period and broadband seismographs of the basis network of seismological stations in the former Soviet Union and Eastern European states while A2 and B1 were the standard characteristics for short- and long-period recordings at stations of the World Wide Standardized Seismograph Network (WWSSN) which was set up by the United States Geological Survey (USGS) in the 1960s and 70s. The other magnification curves are: WA - Wood-Anderson torsion seismometer, which was instrumental in the definition of the magnitude scale; HGLP - High Gain Long Period system.

- For large earthquakes, when mantle penetrating surface waves are often recorded, amplitude and periods of the vertical and horizontal components with the period in the neighbourhood of 200 s should also be measured (cf. section 2.4.3);
- On some types of short-period instruments (in particular analogue) with insufficient time resolutions it is not possible to measure the period of seismic waves recorded from nearby local events and thus to convert trace deflections properly to ground motion. In such cases magnitude scales should be used which depend on measurements of maximum trace amplitudes only;
- Often local earthquakes will be clipped in (mostly analog) records of high-gain short-period seismographs with insufficient dynamic range. This makes amplitude readings impossible. In this case magnitude scales based on record duration (cf. section 2.3.3) might be used instead, provided, that they have been properly scaled with magnitudes based on amplitude measurements.

When determining magnitudes according to more modern and physically based concepts such as seismic moment, mantle or energy magnitudes, special procedures have to be applied (cf. 2.4.3 and chapter *Determination of seismic moment, moment tensor and energy from digital broadband records*).

Tab. 1: Example from the former bulletin of station Moxa (MOX), Germany, based on the analysis of analogue photographic recordings. The event occurred on January 1967. Note the clear annotation of the type of instruments used for the determination of onset times, amplitudes and periods. Multiple body wave onsets of distinctly different amplitudes, which are indicative for a multiple rupture process, have been separated. Seismographs of type A, B and C were nearly identical with the response characteristics A4, B3 and C in Fig. 2. V - vertical component; H - vectorially combined horizontal components; Lm - maximum of the long-period surface wave train. Note the distinct differences in the individual magnitude determinations and the clear saturation effect (underestimation) of short-period (type A) magnitudes.

Day	Phase	Seismograph	h m s	Remarks
5.	+eiP1	A	00 24 15.5	<u>Mongolia</u> 48.08°N 102.80°E
	iP2	A	24 21.5	H = 00 14 40.4 h = normal MAG = 6.4
	iP3	A,C	24 28.0	$\Delta = 55.7^\circ$ Az = 309.6° (USCGS)
	Pmax	C	24 31	
	ePP2	C	26 27.5	PV1 A 1.2s 71.8nm MPV1(A)=5.6
	ePP3	C	26 34	PV2 A 1.8s 1120nm MPV2(A)=6.6
	eS2	C	32 04	PV3 A 1.6s 1575nm MPV3(A)=6.8
	i S3	C	32 11	PV3 B 8s 16.3 μ m MPV3(B)=7.1
	eiSS	B	35 56	SH3 B 18s 60 μ m MSH3(B)=7.3
	iSSS	B	36 44	LmV B 17s 610 μ m MLV(B)=7.8
	LmH	C	48.0	Note: P has a period of about 23s in the long-period seismograph of type B!

Global or regional data analysis centres calculate mean event magnitudes on the basis of many A/T or M data reported by seismic stations in different distance and azimuth with respect to the source. This will more or less average out the influence of regional source and local station conditions. Therefore, A/T or M data reported by individual stations to such centres should not yet be corrected for C_r and C_s . These correction can be determined best by network centres themselves when comparing the uncorrected data from many stations (e.g.

Hutton and Boore, 1987; Strauch and Wylegalla, 1989). They may then use such corrections for reducing the scatter of individual reportings and thus improve the average network estimate.

When determining new regional calibration functions for M_L than station corrections have to be applied before the final data fit in order to reduce the influence of systematic biases on the data scatter. According to the procedure proposed by Richter (1958) these station corrections for M_L have to be determined independently for readings in the N-S and E-W components. When calculating network magnitudes some centers prefer the median value of individual station reportings of M_L as the best network estimate. As compared to the arithmetic mean it minimises the influence of widely diverging individual station estimates due to outliers or wrong readings (Hutton and Jones, 1993).

2.3 Local magnitude scales

2.3.1 The original Richter magnitude scale for local earthquakes (M_L)

Following a recommendation by Wadati, Richter (1935) plotted the logarithm of maximum trace amplitudes A_{\max} measured in records of a standard Wood-Anderson (WA) horizontal component torsion seismometers as a function of epicentral distance Δ . The WA seismometers had the following parameters: natural period $T_s = 0.8$ s, damping factor $D_s = 0.8$, maximum magnification $V_{\max} = 2800$. Richter found that $\log A_{\max}$ decreases with distance along more or less parallel curves for earthquakes of different size. This led him to propose the following definition for the magnitude as a quantitative measure of earthquake size (Richter 1935, p. 7):

"The magnitude of any shock is taken as the logarithm of the maximum trace amplitude, expressed in microns, with which the standard short-period torsion seismometer ... would register that shock at an epicentral distance of 100 km".

This local magnitude was later given the symbol M_L (Gutenberg and Richter 1956b). In order to be able to calculate M_L also for other epicentral distances Δ between 30 and 600 km Richter (1935) provided attenuation corrections. They were later complemented by respective values for $\Delta < 30$ km assuming a focal depth h of 18 km (Gutenberg and Richter 1942) and published together in tabulated form by Richter (1958) as correction factor $-\log A_o(\Delta)$ (cf. Tab. 2). Accordingly, one gets

$$M_L = \log A_{\max} - \log A_o. \quad (2)$$

Note 1: As compared with the general magnitude formula (1), eq. (2) considers only the maximum displacement amplitudes but not their periods. Reason: WA instruments are relatively narrow-band and short-period and their traditional analogue recorders had a limited paper speed. Proper reading of the period of high-frequent waves from local events was rather difficult. It was assumed, therefore, that the maximum amplitude phase (which corresponds in case of local events generally to S_g , L_g or R_g) has always roughly the same predominant period. Also, $-\log A_o$ does not consider the above discussed depth dependence of $\sigma(\Delta, h)$ since seismicity in southern California is always shallow (mostly less than 15 km). (2) does not give regional or station correction terms but they had been taken into account when determining $-\log A_o$ for southern California.

Note 2: The original definition of the magnitude scale is not based on Richter's (1935) tabulated attenuation corrections but on amplitude measurements at 100 km distance, with $M_L = 0$ for $A_{\max} = 1 \mu\text{m}$ trace amplitude in a standard WA record! Richter's attenuation corrections are valid for southern California only. Their shape and level may be different in other regions of the world with different velocity and attenuation structure, crustal age and composition, heat-flow conditions etc. Accordingly, when determining M_L calibration functions for other regions, the amplitude attenuation law has to be determined first and then this curve has to be scaled to the original definition of M_L at 100 km epicentral distance in order to yield magnitudes compatible with the original definition (cf. Fig. 3).

Note 3: According to Hutton and Boore (1987) the *distance corrections developed by Richter for local earthquakes ($\Delta < 30 \text{ km}$) are incorrect*. This leads to magnitudes estimates from nearby stations to be smaller than those from more distant stations. Bakun and Joyner (1984) came to the same conclusion for weak events recorded in Central California at distances less than 30 km.

Tab. 2: Calibrating function $\sigma_L(\Delta) = -\log A_0$ for local magnitudes M_L according to Richter (1958). A_0 are the trace amplitudes in mm recorded by a Wood-Anderson Standard Torsion Seismometer from an earthquake of $M_L = 0$. Δ - epicentral distance in km.

Δ (km)	$\sigma_L(\Delta)$	Δ (km)	$\sigma_L(\Delta)$	Δ (km)	$\sigma_L(\Delta)$	Δ (km)	$\sigma_L(\Delta)$
0	1.4	90	3.0	260	3.8	440	4.6
10	1.5	100	3.0	280	3.9	460	4.6
20	1.7	120	3.1	300	4.0	480	4.7
30	2.1	140	3.2	320	4.1	500	4.7
40	2.4	160	3.3	340	4.2	520	4.8
50	2.6	180	3.4	360	4.3	540	4.8
60	2.8	200	3.5	380	4.4	560	4.9
70	2.8	220	3.65	400	4.5	580	4.9
80	2.9	240	3.7	420	4.5	600	4.9

Note 4: In 2.2 above it was said that, as a general rule, in case of horizontal component recordings, $A_{H\max}$ is the maximum *vector sum amplitude* measured at t_{\max} in both the N and E component. Deviating from this, Richter (1958) says: "... In using ...both horizontal components it is correct to determine magnitude independently from each and to take the mean of the two determinations. This method is preferable to combining the components vectorially, for the maximum motion need not represent the same wave on the two seismograms, and it even may occur at different times." In some investigations aimed at deriving local M_L scales $A_{H\max} = (A_N + A_E)/2$ has been used instead to calculate M_L (e.g. Kiratzi and Papazachos, 1984; Chávez and Priestley, 1985) although this is not fully identical with $M_L = (M_{LN} + M_{LE})/2$ and might give differences in magnitude up to about 0.1 units.

Note 5: The Richter M_L from arithmetically averaged horizontal component amplitude readings will be smaller by at least 0.15 as compared to M_L from $A_{H\max}$ vector sum! In case of significantly different amplitudes $A_{N\max}$ and $A_{E\max}$ this difference might reach several tenth magnitude units. Amplitude differences in the N and E component will be more controlled by (changing) radiation patterns of the sources with respect to a given station than by differences in wave type. It might be more correct, therefore, when $A_H = \sqrt{(A_N^2 + A_E^2)}$ was used in new studies for deriving local calibration functions as well as in later routine M_L determinations

based on these functions. Then, for a given station, only one station correction would be required instead of two for amplitude readings in N-S and E-W recordings, respectively. Such a practice would also be more consistent with that common in calculating teleseismic magnitudes from horizontal records and the above mentioned relevant recommendations of the IASPEI Commission on Practice.

Note 6: The smallest events recorded in local micro-earthquake studies have negative values of M_L while the largest M_L is about 7, i.e., also the M_L scale suffers *saturation* (cf. Fig. 11 in section 3 below and Fig. 5 in the chapter *Introduction to seismic sources and source parameters*). Despite of the above mentioned limitations M_L estimates of earthquake size are relevant for earthquake engineers and risk assessment since they are closely related to earthquake damage. The main reason is that many structures have natural periods close to that of the WA seismometer (0.8s) or are within the range of its pass-band (about 0.1 - 1 s). A review on the development and use of the Richter scale for determining earthquake source parameters is given by Boore (1989).

2.3.2 Other M_L scales based on amplitude measurements

The problem of vector sum amplitudes in horizontal component records or of arithmetic averaging of independent M_L determinations in N and E components can be avoided by using A_{Vmax} from vertical component recordings instead, provided that the respective $-\log A_0$ curves are properly scaled to the original definition of Richter for $\Delta = 100$ km. Several new formulas for M_L determinations based on readings of A_{Vmax} have been proposed for other regions (Alsaker et al. 1991; Kim 1998; Greenhalgh and Singh 1986, Wahlström and Strauch 1984). They mostly use Lg waves, sometimes well beyond the distance of 600 km for which $-\log A_0$ was defined by Richter (1958). Alsaker et al. (1991) and Greenhalgh and Singh (1986) showed that A_{Vmax} is ≈ 1 to 1.2 times $A_{Hmax} = 0.5 (A_{Nmax} + A_{Emax})$ and thus yields practically the same magnitudes.

Since Richters $\sigma(\Delta) = -\log A_0$ for southern California might not be correct for other regions, local calibration functions have been determined for other seismotectonic regions (e.g. for shield areas by Alsaker et al. 1991, Greenhalgh and Singh 1986, Kim 1998; for continental rift areas by Chávez & Priestley 1985 and Langston et al. 1998; for different Alpine Mediterranean countries by Kiratzi and Papazachos 1984 and Muco and Minga 1991). Those for continental shield areas revealed significantly lower wave attenuation when compared with southern California. Despite scaling them to the Richter M_L at 100 km deviations may become larger than one magnitude unit at several 100 km distances (cf. Fig. 3).

Note: Hutton and Boore (1987) proposed that local magnitude scales be defined in future such that $M_L = 3$ correspond to 10 mm of motion on a Wood-Anderson instrument at 17 km hypocentral distance rather than 1 mm of motion at 100 km. While being consistent with the original definition of magnitude in southern California this definition will allow more meaningful comparison of earthquakes in regions having very different wave attenuation within the first 100 km.

This proposal has already been taken into consideration when developing a local magnitude scale for Tanzania, East Africa (Langston et al. 1998). Calibration functions for Lg waves could sometimes be extended up to 1500 km distance, e.g. for Norway by Alsaker et al. (1991). At this distance $-\log A_0$ differs by 1.7 magnitude units from the extrapolated calibration curve for southern California!. These authors had also chosen a smaller reference distance (of 60 km) with respect to the original Richter scale.

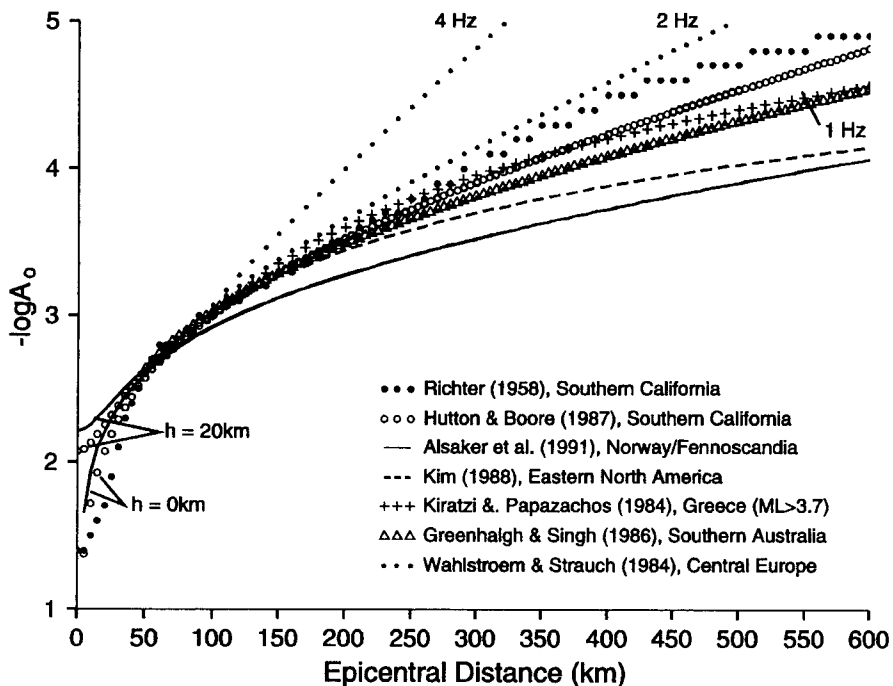


Fig. 3: Calibration functions for M_L determination for different regions. Note that $-\log A_0$ for Central Europe according to Wahlström and Strauch (1984) is frequency dependent. Although clipped here for epicentral distances > 600 km some of the curves shown are defined for much larger distances (cf. Tab. 3).

Station corrections determined in some of these studies varied between -0.6 to $+0.3$ magnitude units (Bakun and Joyner, 1984; Greenhalgh and Singh, 1986; Hutton and Jones, 1993) and correlated broadly with regional geology. This points to the urgent need to determine both calibration functions and station corrections for M_L on a regional basis. Also, since in other regions sources may be significantly deeper than in southern California, either $\sigma(\Delta, h)$ should be determined or at least the epicentral distance Δ should be replaced in the magnitude formulas by the "slant" or hypocentral distance $R = \sqrt{(\Delta^2 + h^2)}$. The latter is common now.

Nowadays procedures are available to synthesise precisely the response characteristic of Wood-Anderson seismographs from digital broadband recordings (e.g. Plesinger et al., 1996). Therefore, WA seismographs are no longer required for carrying out M_L determinations. Savage and Anderson (1995) and Uhrhammer et al. (1996) demonstrated the ability to determine an unbiased measure of local magnitude from synthetic WA seismograms. Thus, a seamless catalogue of M_L could be maintained at Berkeley. In a first approximation (although not identical!) this can also be achieved by converting record amplitudes from another seismograph with a displacement frequency response $\text{Mag}(T_i)$ into respective WA trace amplitudes by multiplying them with the ratio $\text{Mag}_{\text{WA}}(T_i)/\text{Mag}(T_i)$ for the given period of A_{max} (e.g. Greenhalgh and Singh, 1986; Wahlström and Strauch, 1984). Also, sufficient time resolution of high-frequency records is no longer a problem. There have been efforts, therefore, to develop frequency-dependent calibration functions matched to the Richter scale at 100 km distance (e.g. Wahlström and Strauch 1984; cf. Fig. 3). Tab. 3 summarises several formulae for M_L determination in other regions.

Tab. 3: Selected regional calibration functions $\sigma_L(\Delta) = -\log A_0$ for M_L determinations. Δ - epicentral distance in km; h - hypocentral depth in km; R - hypocentral ("slant") distance with $R = \sqrt{(\Delta^2 + h^2)}$; T - period in s; Com. - recording component.

Region	$\sigma_L(\Delta) = -\log A_0$	Com.	Range (km)	Reference
Southern California	$1.110 \log(R/100) + 0.00189(R - 100) + 3.0$	horiz.	$10 \leq R \leq 700$	Hutton&Boore (1987)
Central California	$1.000 \log(R/100) + 0.00301(R - 100) + 3.0$	horiz.	$0 \leq \Delta \leq 400$	Bakun&Joyner (1984)
Great Basin, Western USA	$1.00 \log(R/100) + 0.0069(R - 100) + 3.0$ $0.83 \log(R/100) + 0.0026(R - 100) + 3.0$	horiz. horiz.	$0 \leq \Delta \leq 90$ $90 \leq \Delta \leq 600$	Chávez&Priestley (1985)
Eastern N-America	$1.55 \log \Delta - 0.22$ $1.45 \log \Delta + 0.11$	horiz. vertic.	$100 \leq \Delta \leq 800$ $100 \leq \Delta \leq 800$	Kim (1998)
Greece	$1.58 \log(R/100) + 3.0$; for $M_L \leq 3.7$ $2.00 \log(R/100) + 3.0$; for $M_L > 3.7$	horiz.	$100 \leq \Delta \leq 800$	Kiratzi&Papazachos (1984)
Albania	$1.6627 \log \Delta + 0.0008 \Delta - 0.433$	horiz	$10 \leq \Delta \leq 600$	Muco&Minga (1991)
Central Europe	$0.83 \log R + (0.0017/T)(R - 100) + 1.41$	vertic.	$100 \leq \Delta \leq 650$	Wahlström&Strauch (1984)
Norway/Fennoskan.	$0.91 \log R + 0.00087 R + 1.010$	vertic.	$0 < R \leq 1500$	Alsaker et al. (1991)
Tanzania	$0.776 \log(R/17) + 0.000902(R - 17) + 2.0$	horiz.	$0 < R \leq 1000$	Langston et al. (1998)
South Australia	$1.10 \log \Delta + 0.0013 \Delta + 0.7$	vertic.	$40 < \Delta < 700$	Greenhalgh&Singh (1986)
Japan	$1.098 \log(R/100) + 0.0003(R - 100) + 3.0$			In: Hutton&Boore (1997)

Another local magnitude formula applicable in the distance range where P_g and S_g are still the first arrivals (up to about 130 to 250 km, depending on crustal thickness) had been given by Iida (1967):

$$M_L = \log A + 1.5 \log(t_s - t_p) + 1.2 \quad (3)$$

with A - maximum ground amplitude in μm and $t_s - t_p$ the time between the S and the P onset which is proportional to the slant direction R . The advantages of this formula are that it does not require prior localisation and distance determination of the events, that $t_s - t_p$ is not very sensitive to variations in the velocity model and independent on the availability of a precise absolute time base. This was, prior to the availability of digital data loggers with very accurate (now mostly GPS controlled) timing, often a big problem, especially in micro-earthquake studies with temporary networks. Therefore, this formula has been widely applied in such studies also outside of Japan (e.g. Neunhöfer and Güth 1989; Grosser et al. 1998). Although in European applications this Iida formula yielded systematically too low magnitudes (up to about 1 unit) it nevertheless allowed for the bulk of the data internally consistent relative estimates of event size which could later easily be scaled, on the basis of a few stronger regionally or globally recorded events, to more representative magnitudes published by the world data centres.

The increasing availability of strong-motion records and their advantage of not being clipped even in case of very strong nearby events has led to the development of (partially) frequency dependent M_L^{SM} scales from strong-motion data (Trifunac 1990; Lee et al. 1990; Hatzidimitriou et al., 1993). The technique to calculate synthetic Wood-Anderson seismograph output from strong-motion accelerograms was first introduced by Kanamori and Jennings (1978).

2.3.3 Duration magnitudes M_D

Analogue paper or film recordings have a very limited dynamic range of only about 40 dB and analogue tape recordings of about 60 dB. For many years widely used digital recorders with 12 or 16 bit A-D converters enabled already amplitude recordings with about 66 or 90 dB, respectively. Nevertheless, even these records are often clipped in case of strong near seismic events. Then magnitude determinations based on measurements of A_{max} are not possible. Therefore, alternative magnitude scales M_D have been developed. They are based on event signal duration. With nowadays 24 bit A-D converters and ≈ 140 dB usable dynamic range, this clipping problem is no longer pressing, rare extreme events not considered.

Bistricsany (1958) proposed the use of the duration of the surface-wave train for the determination of teleseismic magnitude. He obtained the following formulae for Wiechert seismographs at the Budapest station which were scaled to the equivalent surface-wave magnitudes M_s determined at Praha station:

$$M_D = 2.12 \log (F - eL) + 0.0065 \Delta + 2.66 \quad \text{for shallow events} \quad (4)$$

and

$$M_D = 1.58 \log (F - eL) + 0.0020 \Delta + 0.0007 h + 4.02 \quad \text{for deeper events} \quad (5)$$

with F the end and eL the commencement times (in minutes) of the recorded surface waves, Δ - epicentral distance in degrees and h - hypocentral depth in km.

In case of near seismic events the total signal duration D is mainly controlled by the length of the coda which follows the S_g onset. A theoretical description of the coda envelopes as an exponentially decaying function with time was presented by Herrmann (1975). He proposed a duration magnitude formula of the general form:

$$M_D = a_0 + a_1 \log D + a_2 \Delta \quad (6)$$

Real and Teng (1973) have noted for events with $M_L > 3.5$ a divergence between local magnitudes M_L and duration magnitudes calculated according to a formula like (6). They proposed a non-linear equation instead:

$$M_D = b_0 + b_1 \log D + b_2 (\log D)^2 + b_3 \Delta. \quad (7)$$

M_D scales according to (7) had been developed by Klinge (1989) for both local seismic stations in the Vogtland swarm earthquake region of Germany and more distant stations of the Potsdam seismic network. For each local station own coefficients had to be determined.

Different procedures have been proposed by various authors how to determine signal or coda duration (e.g. Wahlström 1979; Kiratzi and Papazachos 1985; Klinge 1989; Michaelson 1990, Eaton 1992) such as:

- duration from the P-wave onset to the end of the coda, i.e. where the signal disappears in the seismic noise of equal frequency;
- duration from the P-wave onset to that time when the coda amplitudes have decayed to a certain threshold level, given in terms of average signal-to-noise ratio or of absolute signal amplitudes or signal level in mV;
- total lapse time = coda threshold time minus origin time of the event.

An early formula for the determination of local magnitudes based on signal duration was developed for earthquakes in Kii Peninsula in Central Japan by Tsumura (1967) and scaled to the magnitudes M_{JMA} reported by the Japanese Meteorological Agency:

$$M_D = 2.85 \log (F - P) + 0.0014 \Delta - 2.53 \quad \text{for } 3 < M_{JMA} < 5 \quad (8)$$

with P as the onset time of the P wave and F the end of the signal above the noise level. Another duration magnitude equation of the same structure was defined by Lee et al. (1972) for the Northern California Seismic Network (NCSN). The event duration D is measured from the onset of the P wave to the point on the seismogram where the coda amplitude diminished to 1 cm on the Develocorder film viewer screen with its 20 times magnification:

$$M_D = 2.00 \log D + 0.0035 \Delta - 0.87 \quad \text{for } 0.5 < M_L < 5. \quad (9)$$

The location program HYPO71 (Lee and Lahr 1975) employs eq. (9) to compute duration magnitudes, called FMAG. But it was found out that (9) yields seriously underestimated magnitudes of events $M_L > 3.5$. Also, improved recording conditions and dynamic range within the Californian network had changed the network calibration for duration magnitudes. Therefore, several new duration magnitude formulae have been developed for the NCSN, all scaled to M_L . One of the latest versions by Eaton (1992) uses short-period vertical-component records, a normalisation of instrument sensitivity, different distant correction terms for $\Delta < 40$ km, $40 \text{ km} \leq \Delta \leq 350 \text{ km}$ and $\Delta > 350 \text{ km}$ as well as a depth correction for $h > 10 \text{ km}$.

According to Aki and Chouet (1975) coda waves from local earthquakes are commonly interpreted as back-scattered waves from numerous heterogeneities uniformly distributed in the earth crust. For a given local earthquake at epicentral distances shorter than 100 km the total duration of a seismogram is therefore almost independent of distance and azimuth and of structural details of the direct wave path from source to station. Also the shape of coda envelopes, which decay exponentially with time, remains practically unchanged. The dominating factor controlling the amplitude level of the coda envelope and signal duration is the earthquake size. This allows to develop duration magnitude scales without a distance term, i.e.:

$$M_D = a_0 + a_1 \log D \quad (10)$$

and thus quick magnitude estimates from local events even without knowing yet the exact distance of the stations to the source.

Note: Crustal structure, scattering and attenuation conditions vary from region to region. No generally applicable formula and coefficients can therefore be given. They have to be determined locally for any given station or network and be properly scaled to the best available amplitude-based M_L scale. Additionally, the resulting specific equation will also depend on the chosen definition for D, the local noise conditions and the sensor sensitivity at the considered seismic station(s) of a network.

2.3 Teleseismic magnitude scales

2.4.1 Surface wave magnitude scale M_S

Gutenberg (1945a) developed the magnitude scale M_S for teleseismic surface waves:

$$M_S = \log A_{H\max}(\Delta) + \sigma_S(\Delta). \quad (11)$$

It is based on measurements of the maximum *horizontal* "true" ground motion displacement amplitudes $A_{H\max} = \sqrt{(A_N^2 + A_E^2)}$ of the surface wave train at periods $T = 20 \pm 2$ s. This maximum corresponds to the so-called Airy phase which is related to a local minimum in the group velocity dispersion curve of surface waves due to the existence of a low-velocity layer in the upper mantle (asthenosphere). The velocity minimum in the dispersion curve causes the arrival of seismic energy of different period at about the same time. This results in an interference and amplification of amplitudes. No calibration function for vertical component surface waves had been determined since no comparably sensitive and stable vertical component long-period seismographs were available in these days.

As compared to body waves, the amplitude-distance relationship for surface waves is rather simple and smooth (Fig. 4). It is also obvious that for a given magnitude the surface wave amplitudes are about two orders of magnitude larger. The calibration function $\sigma_S(\Delta)$ is the *inverse* of an semi-empirically determined A - Δ -relationship scaled to an event of $M_S = 0$, thus compensating for the decay of amplitude with distance. Richter (1958) gave tabulated values for $\sigma_S(\Delta)$ in the distance range $20^\circ \leq \Delta \leq 180^\circ$. They are valid if the ground motion amplitudes are given in micrometer (μm) (Tab. 4). The increase of amplitudes (or decrease of σ_S) for very large Δ (cf. Fig. 4 and Tab. 4) is due to the increased geometric focussing towards the antipode of the spherical Earth's surface which then overwhelms the amplitude decay due to attenuation.

Tab. 4: Calibration values $\sigma_S(\Delta)$ for M_S determinations according to equation (11) corresponding to $-\log A_{H\max}$ in μm of surface waves with periods 20 ± 2 s from a standard shock of $M_S = 0$ (as published in Richter, 1958)

Δ (degrees)	$\sigma_S(\Delta)$	Δ (degrees)	$\sigma_S(\Delta)$	Δ (degrees)	$\sigma_S(\Delta)$
20	4.0	60	4.8	120	5.3
25	4.1	70	4.9	140	5.3
30	4.3	80	5.0	160	5.35
40	4.5	90	5.05	170	5.3
45	4.6	100	5.1	180	5.0
50	4.6	110	5.2		

This relationship was further developed by Eastern European scientists. Soloviev (1955) proposed the use of the maximum ground particle velocity $(A/T)_{\max}$ instead of the maximum ground displacement A_{\max} since it is more closely related to seismic energy. Collaboration between research teams in Prague and Moscow resulted in the proposal of a new standardised M_S scale and calibration function (so-called Moscow-Prague formula) by Karnik et al. (1962)

$$M_S = \log (A/T)_{\max} + 1.66 \log \Delta + 3.3 \quad (12)$$

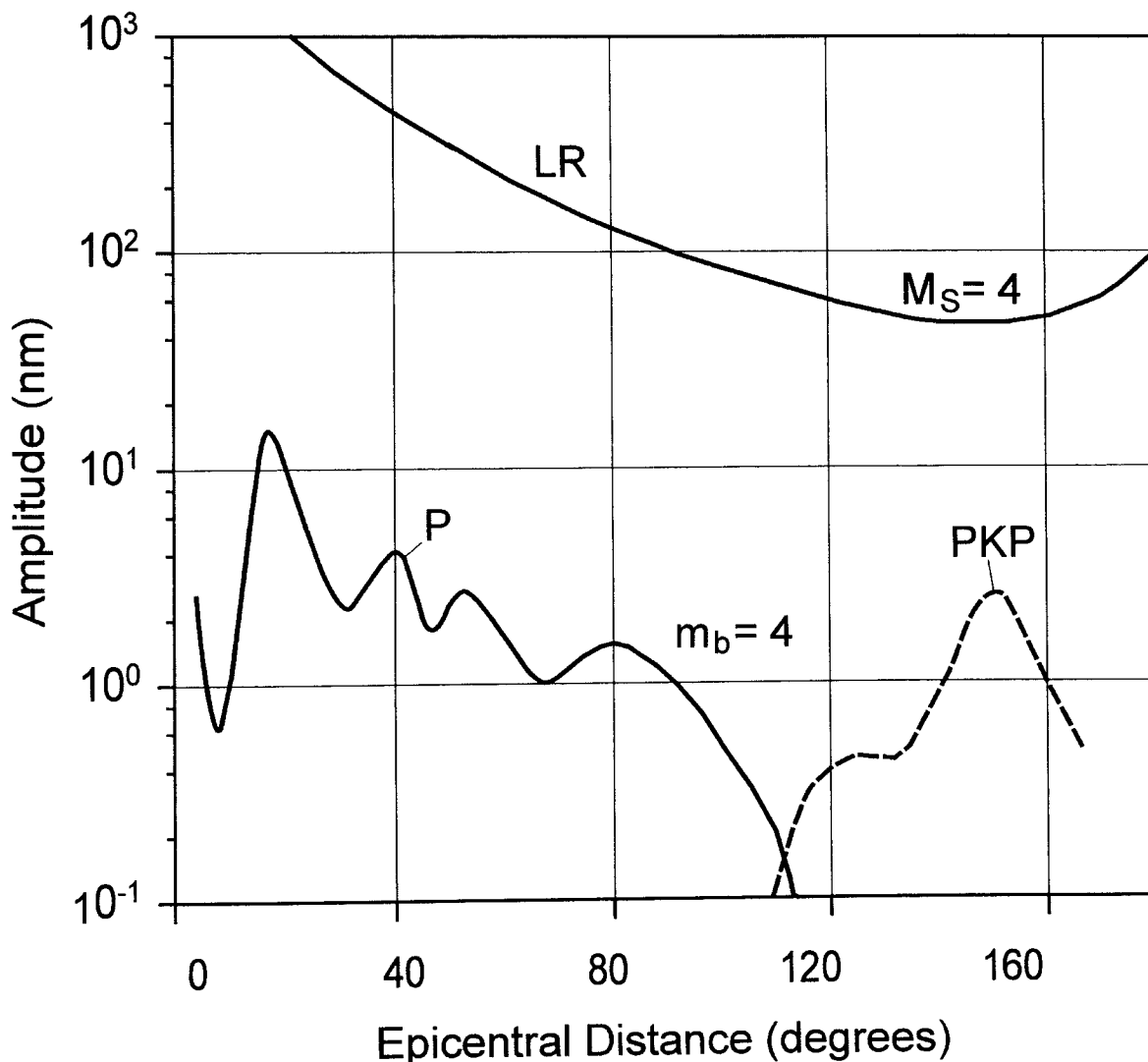


Fig. 4: Approximate smoothed amplitude-distance functions for P and PKP body waves (at about 1 Hz) and of long-period Rayleigh surface waves (Airy phase, $T \approx 20$ s) from an event with $m_b = M_S = 4$.

for epicentral distances $2^\circ < \Delta < 160^\circ$ and source depth $h < 50$ km. The IASPEI Committee on Magnitudes recommended in Zürich 1967 the use of this formula and gave mean periods corresponding to the maximum amplitudes of surface waves to be used for M_S determination. (Tab. 5) gives the smallest periods observed in the maximum of the surface wave train as a function of distance. But the periods observed in the Airy phase depend not only on distance but also on the crustal and upper mantle structure along the ray path. The largest periods observed for continental paths do not exceed 28 s but may be somewhat higher for oceanic paths. In any event, it is obvious, that the observed periods may significantly deviate from the very narrow (almost constant) period range of 20 ± 2 s originally proposed by Gutenberg (1945a). Therefore, using $(A/T)_{\max}$ instead of A_{\max} at periods near 20 s is in any event a better, more stable and more widely usable estimate of the seismic surface wave energy released by an earthquake.

Tab.5: Minimum periods observed in the maximum of the surface wave train (Airy phase) as a function of distance (taken from Willmore 1979)

Δ°	T(s)	Δ°	T(s)	Δ°	T(s)
10	7	30	10	80	16
15	8	40	12	100	16
20	9	60	14	140	18

The 1979 edition of the Manual of Seismological Practice (Willmore 1979) *recommends to use the standard formula (12) for both horizontal and vertical components*. That this is justified Bormann and Wylegalla (1975) and Bormann and Khalturin (1975) had shown for a large global data set of long-period surface wave magnitudes MLH and MLV determined at station MOX, Germany. They used $(A/T)_{\max}$ surface wave readings in the horizontal (H) and vertical (V) components of instruments of typ C (cf. Fig. 2) in the magnitude range $3.7 < M_s < 8.2$ and adjusted them with the calibration function given in (12). They got the orthogonal regression relationship

$$MLV - 0.97 MLH = 0.19 \quad (13)$$

with a correlation coefficient 0.98 and a standard deviation of ± 0.11 only.

NEIC adopted the vertical component as its standard in May 1975 (Willmore 1979), i.e. M_s is determined from the Rayleigh-wave maximum. Tab. 6 may aid in finding the appropriate part of the record.

Tab. 6: Time interval ($t_{R\max} - t_p$) between the arrival of the maximum phase of the Rayleigh wave and the first onset of P waves as a function of Δ according to Archangelskaya (1959) and Gorbunova and Kondorskaya (1977).

Δ°	$t_{R\max} - t_p$ (min)	Δ°	$t_{R\max} - t_p$ (min)	Δ°	$t_{R\max} - t_p$ (min)
10	4-5	55	26	100	45-46
15	6-8	60	28-29	105	47-48
20	9-10	65	31	110	48-50
25	10-12	70	33	115	53
30	13-14	75	35	120	55
35	15-16	80	37	125	57
40	18-19	85	39-40	130	60
45	21	90	42	140	64
50	24	95	43	150	70

When calculating M_s for 20 s surface waves of the same amplitudes according to eqs. (11) and (12) then (12) yields, on the average, magnitudes which are numerically by about 0.2 units larger than the original Gutenberg-Richter M_s .

Nowadays, both the ISC and NEIC use (12) for the determination of M_s from events with focal depth $h < 60$ km without specifying the type of waves or components considered. The ISC accepts both vertical or resultant horizontal amplitudes of surface waves with periods between 10 - 60 s from stations in the distance range $5^\circ - 160^\circ$ but calculates the representative average M_s only from observations between $20^\circ - 160^\circ$. Contrary to this NEIC

calculates M_S only from vertical component readings of stations between $20^\circ \leq \Delta \leq 160^\circ$ and for reported periods of $18 \text{ s} \leq T \leq 22 \text{ s}$. Recently, there has been a tendency to determine the surface-wave magnitude by specifying the type of the waves and/or components used, e.g. M_{LRH} or M_{LRV} from Rayleigh waves and M_{LQH} from Love waves or simply MLH and MLV as practiced already in the 60s in Germany (cf. Tab. 1). Note that M_S determined from vertical component records is based on Rayleigh waves only

Herak and Herak (1993) noted that $\sigma_S(\Delta)$ in the Moscow-Prague formula does not yield consistent magnitude estimates independent of Δ . They proposed another formula instead:

$$M_S = \log (A/T)_{\max} + 1.094 \log \Delta + 4.429. \quad (14)$$

It provides distance-independent estimates of M_S over the whole distance range $4^\circ < \Delta < 180^\circ$: M_S values according to (14) are equal with those from (12) at $\Delta = 100^\circ$, larger by 0.39 magnitude units at $\Delta = 20^\circ$ and smaller by 0.12 units for $\Delta = 160^\circ$. (14) is practically equal to the magnitude formula earlier proposed by von Seggern (1977) and similar to the results obtained by Christoskov et al. (1983) and more recently by Rezapour and Pearce (1998). When additionally taking appropriate values for geometrical spreading and attenuation into account (14) also agrees very well with the theoretical amplitude-distance function for Love waves obtained by Panza et al. (1989) which shows an increase beyond $\Delta > 140^\circ$ by about half an order of magnitude (cf. Fig. 4). **Note:** The Moscow-Prague formula (12) does not account for the amplitude increase beyond 140° and is defined up to $\Delta = 160^\circ$ only!

The introduction of (14) as a new standard calibration function for M_S has not yet been discussed or recommended by the IASPEI Commission on Practice. The same applies to necessary depth corrections for σ_S . Empirically derived corrections for intermediate and deep earthquakes were published by Bath (1985). They range between 0.1 and 0.5 magnitude units for focal depths of 50 - 100 km and between 0.5 and 0.7 units for depths of 100 - 700 km. But theoretical calculations by Panza et al. (1989) indicate that the depth correction may already exceed one magnitude unit even for shallow sources ($h \leq 60 \text{ km}$).

Karnik and Christoskov (1977) showed that $\sigma_S(\Delta)$ according to (12) lays in the distance range $4^\circ < \Delta < 10^\circ$ just in the middle of several $\sigma(\Delta)$ curves used at various European stations for amplitude or duration based M_L scales while Evernden (1971), Marshall and Basham (1973) and others argued that the distance correction term in (12) does not meet the amplitude decrease with distance of Rayleigh waves for $\Delta < 25^\circ$. Very recently Yacoub (1998) presented a method for accurate estimation of Rayleigh-wave spectral magnitudes M_R by velocity and frequency window analysis of digital records. He applied it to records of underground nuclear explosions in the distance range 5° to 110° and compared M_R with the classical time-window magnitude estimates M_S according to (12). While both agreed well in general M_R had smaller standard deviations. Another advantage is that the procedure for M_R determination can easily be implemented for on-line automated magnitude measurements.

Another scale, said to be equivalent to the Gutenberg and Richter M_S scale, is used by the Japan Meteorological Agency (with Δ in km and A ground amplitudes in μm ; Tsuboi, 1954):

$$M = \log \sqrt{(A_N)^2 + (A_E)^2} + 1.73 \log \Delta - 0.83, \quad (15)$$

in case of earthquakes deeper 60 km with the depth-distance factor K given by Katsumata (1964):

$$M = \log \sqrt{(A_N^2 + A_E^2)} + K(\Delta, h). \quad (16)$$

There are two more very important issues to be aware of in magnitude determinations by means of surface waves: Firstly, there may be significant regional biases due to surface-wave path effects. Lateral velocity variations in the crust and upper mantle as well as refraction at plate boundaries may result in significant focussing and de-focussing effects and related regional over- or underestimation of M_S (Lazareva and Yanovskaya, 1975). According to Abercrombie (1994) this seems to be the main cause for the anomalously high surface-wave magnitudes of continental earthquakes relative to their seismic moments and not so much differences in the source process. Therefore, in order to obtain reliable, unbiased estimates of regional seismic strain rate and hazard, local/regional moment-magnitude relationships should be preferred to global ones.

Secondly, according to Fig. 5 in the *Introduction to seismic sources and source parameters* surface wave spectra from events with $M_S > 7$ and a seismic moment $M_0 > 10^{20}$ Nm will have their corner period at $T > 20$ s. Accordingly, all M_S scales based on $(A/T)_{\max}$ measurements for periods $T \approx 20$ s will systematically underestimate M_S of larger events and saturate around $M_S = 8.5$ such as the strongest earthquake of this century in Chile 1960, which had according to Kanamori and Cipar (1974) $M_0 = 2\text{-}3 \times 10^{23}$ Nm for the main shock and $M_S = 8.5$ only (cf. Lay and Wallace, 1995). Several efforts have therefore been made to develop non-saturating magnitude scales (cf. 2.4.3 below).

2.4.2 Magnitude scales for teleseismic body waves

Gutenberg (1945b and c) developed a magnitude relationship for teleseismic body-waves such as P, PP and S in the period range 0.5 s to 12 s. It is based on theoretical amplitude calculations corrected for geometric spreading and attenuation and then adjusted to empirical observations from shallow and deep-focus earthquakes:

$$m_B = \log (A/T)_{\max} + Q(\Delta, h). \quad (17)$$

Gutenberg and Richter (1956a) published a table with $Q(\Delta)$ values for P, PP and S waves observations in vertical (V) and horizontal (H) components for shallow shocks (cf. Tab. 7), complemented by diagrams $Q(\Delta, h)$ for PZ, PPZ and SH ($Z = V$; Figs. 5a-c) which enable also magnitude determinations from intermediate and deep earthquakes.

These calibration functions are correct when ground displacement amplitudes are measured in medium-period records and given in $\mu\text{m} = 10^{-6}$ m. Gutenberg and Richter (1956a) proposed the so-called *unified magnitude* m as an weighted average of the individual m_B values determined for these different types of waves. The latter are observed with different dominating periods, leave the source at different take-off angles and their amplitude radiation characteristics differ. This significantly reduces the effect of the source mechanism on the magnitude estimate. Gutenberg and Richter (1956a) also scaled m_B and m to the earlier magnitude scales M_L and M_S so as to match these scales at magnitudes between about 6 to 7. But since m_B is based on amplitude measurements at shorter periods than those observed in the Airy phase of surface waves the m_B scale saturates somewhat earlier than M_S (cf. Fig. 11 in section 3 below).

Tab.7: Values of $Q(\Delta)$ for P, PP and S waves (V - vertical and H - horizontal component) for shallow shocks according to Gutenberg and Richter (1956a)

Δ°	PV	PH	PPV	PPH	SH	Δ°	PV	PH	PPV	PPH	SH	Δ°	PV	PH	PPV	PPH	SH
16	5.9	6.0			7.2	56	6.8	7.1	6.9	7.0	6.6	96	7.3	7.6	7.2	7.4	7.1
17	5.9	6.0			6.8	57	6.8	7.1	6.9	7.0	6.6	97	7.4	7.8	7.2	7.4	7.2
18	5.9	6.0			6.2	58	6.8	7.1	7.0	7.1	6.6	98	7.5	7.8	7.2	7.4	7.3
19	6.0	6.1			5.8	59	6.8	7.1	7.0	7.2	6.6	99	7.5	7.8	7.2	7.4	7.3
20	6.0	6.1			5.8	60	6.8	7.1	7.1	7.3	6.6	100	7.4	7.7	7.2	7.4	7.4
21	6.1	6.2			6.0	61	6.9	7.2	7.2	7.4	6.7	101	7.3	7.6	7.2	7.4	7.4
22	6.2	6.3			6.2	62	7.0	7.3	7.3	7.4	6.7	102	7.4	7.7	7.2	7.4	7.4
23	6.3	6.4			6.2	63	6.9	7.3	7.3	7.4	6.7	103	7.5	7.9	7.2	7.4	7.3
24	6.3	6.5			6.2	64	7.0	7.3	7.3	7.5	6.8	104	7.6	7.9	7.3	7.5	7.3
25	6.5	6.6			6.2	65	7.0	7.4	7.3	7.5	6.9	105	7.7	8.1	7.3	7.5	7.2
26	6.4	6.6			6.2	66	7.0	7.4	7.3	7.4	6.9	106	7.8	8.2	7.4	7.6	7.2
27	6.5	6.7			6.3	67	7.0	7.4	7.2	7.4	6.9	107	7.9	8.3	7.4	7.6	7.2
28	6.6	6.7			6.3	68	7.0	7.4	7.1	7.3	6.9	108	7.9	8.3	7.4	7.6	7.2
29	6.6	6.7			6.3	69	7.0	7.4	7.0	7.2	6.9	109	8.0	8.4	7.4	7.6	7.2
30	6.6	6.8	6.7	6.8	6.3	70	6.9	7.3	7.0	7.2	6.9	110	8.1	8.5	7.4	7.6	7.2
31	6.7	6.9	6.7	6.8	6.3	71	6.9	7.3	7.1	7.3	7.0	112	8.2	8.6	7.4	7.6	
32	6.7	6.9	6.8	6.9	6.4	72	6.9	7.3	7.1	7.3	7.0	114	8.6	9.0	7.5	7.7	
33	6.7	6.9	6.8	6.9	6.4	73	6.9	7.2	7.1	7.3	6.9	116	8.8		7.5	7.7	
34	6.7	6.9	6.8	6.9	6.5	74	6.8	7.1	7.0	7.2	6.8	118	9.0		7.5	7.7	
35	6.7	6.9	6.8	6.9	6.6	75	6.8	7.1	6.9	7.1	6.8	120			7.5	7.7	
36	6.6	6.9	6.7	6.8	6.6	76	6.9	7.2	6.9	7.1	6.8	122			7.4	7.6	
37	6.5	6.7	6.7	6.8	6.6	77	6.9	7.2	6.9	7.1	6.8	124			7.3	7.5	
38	6.5	6.7	6.7	6.8	6.6	78	6.9	7.3	6.9	7.1	6.9	126			7.2	7.4	
39	6.4	6.6	6.6	6.7	6.7	79	6.8	7.2	6.9	7.1	6.8	128			7.1	7.4	
40	6.4	6.6	6.6	6.7	6.7	80	6.7	7.1	6.9	7.1	6.7	130			7.0	7.3	
41	6.5	6.7	6.5	6.6	6.6	81	6.8	7.2	7.0	7.2	6.8	132			7.0	7.3	
42	6.5	6.7	6.5	6.6	6.5	82	6.9	7.2	7.1	7.3	6.9	134			6.9	7.2	
43	6.5	6.7	6.6	6.7	6.5	83	7.0	7.4	7.2	7.4	6.9	136			6.9	7.2	
44	6.5	6.7	6.7	6.8	6.5	84	7.0	7.4	7.3	7.5	6.9	138			7.0	7.3	
45	6.7	6.9	6.7	6.8	6.5	85	7.0	7.4	7.3	7.5	6.8	140			7.1	7.4	
46	6.8	7.1	6.7	6.8	6.6	86	6.9	7.3	7.3	7.5	6.7	142			7.1	7.4	
47	6.9	7.2	6.7	6.8	6.6	87	7.0	7.3	7.2	7.4	6.8	144			7.0	7.3	
48	6.9	7.2	6.7	6.8	6.7	88	7.1	7.5	7.2	7.4	6.8	146			6.9	7.2	
49	6.8	7.1	6.7	6.8	6.7	89	7.0	7.4	7.2	7.4	6.8	148			6.9	7.2	
50	6.7	7.0	6.7	6.8	6.6	90	7.0	7.3	7.2	7.4	6.8	150			6.9	7.2	
51	6.7	7.0	6.7	6.8	6.5	91	7.1	7.5	7.2	7.4	6.9	152			6.9	7.2	
52	6.7	7.0	6.7	6.8	6.5	92	7.1	7.4	7.2	7.4	6.9	154			6.9	7.2	
53	6.7	7.0	6.7	6.8	6.6	93	7.2	7.5	7.2	7.4	6.9	156			6.9	7.2	
54	6.8	7.1	6.8	6.9	6.6	94	7.1	7.4	7.2	7.4	7.0	158			6.9	7.2	
55	6.8	7.1	6.9	7.0	6.6	95	7.2	7.6	7.2	7.4	7.0	160			6.9	7.2	
												170			6.9	7.2	

Later, with the introduction of the WWSSN short-period 1s-seismometers (c.f. Fig. 2, type A2) it became common practice at NEIC to use the calibration function $Q(\Delta, h)$ for short-period PZ only. Additionally, it was recommended to take the largest amplitude within the

first few seconds (5 half cycles) instead of measuring the maximum amplitude in the whole P-wave train. One should be aware that this practice was due to the focussed interest on discriminating between earthquakes and underground nuclear explosions. The resulting short-period m_b values strongly underestimated the body wave magnitudes for $m_B > 5$ (cf. Tab. 1) and, as a consequence, overestimated the annual frequency of small earthquakes in the magnitude range of kt-explosions. Also, m_b saturates much earlier than the original Gutenberg-Richter m_B for medium-period body waves or M_S for long-period surface (cf. Fig. 5 in chapter *Introduction to seismic sources and source parameters* and Fig. 11 in section 3 below). Later, following the recommendations of the IASPEI Commission on Practice (cf. 2.2 above), the restriction to amplitude measurements within the first few seconds was abandoned. This somewhat reduced the discrepancy between m_B and m_b but in any event both are differently scaled to M_S .

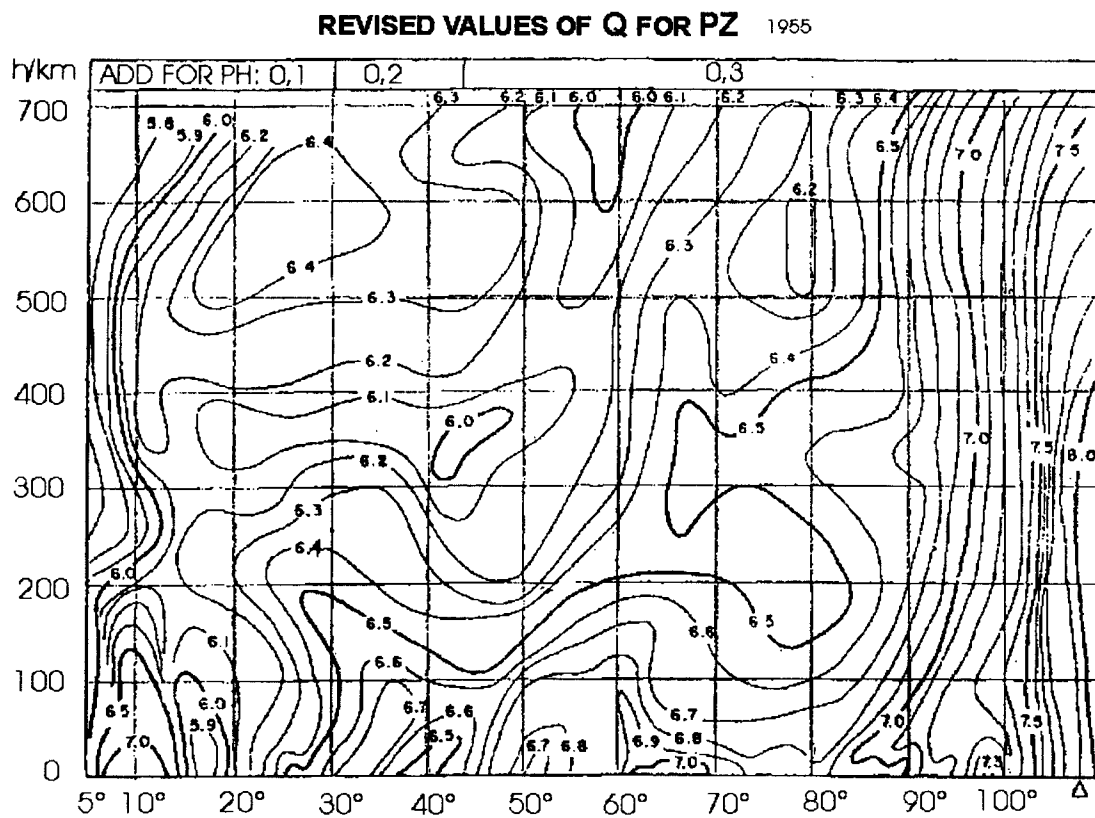


Fig. 5a

Fig. 5: $Q(\Delta, h)$ calibration functions for m_B determinations according to Gutenberg and Richter (1956a): a) for PZ, b) PPZ and c) SH.

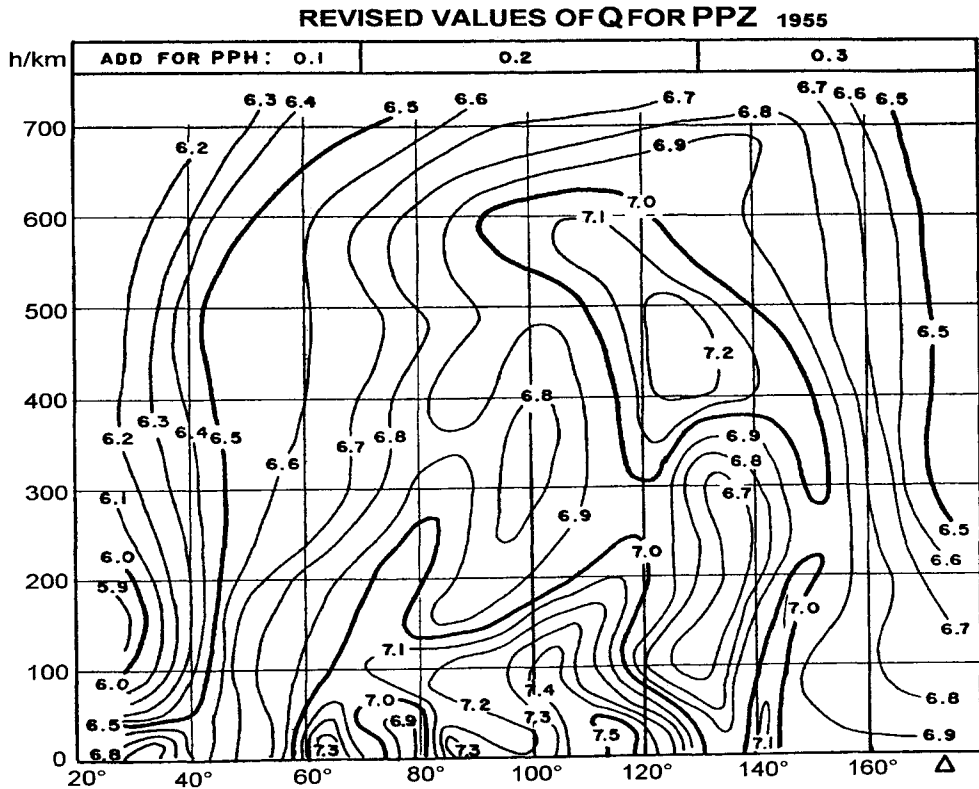


Fig. 5b

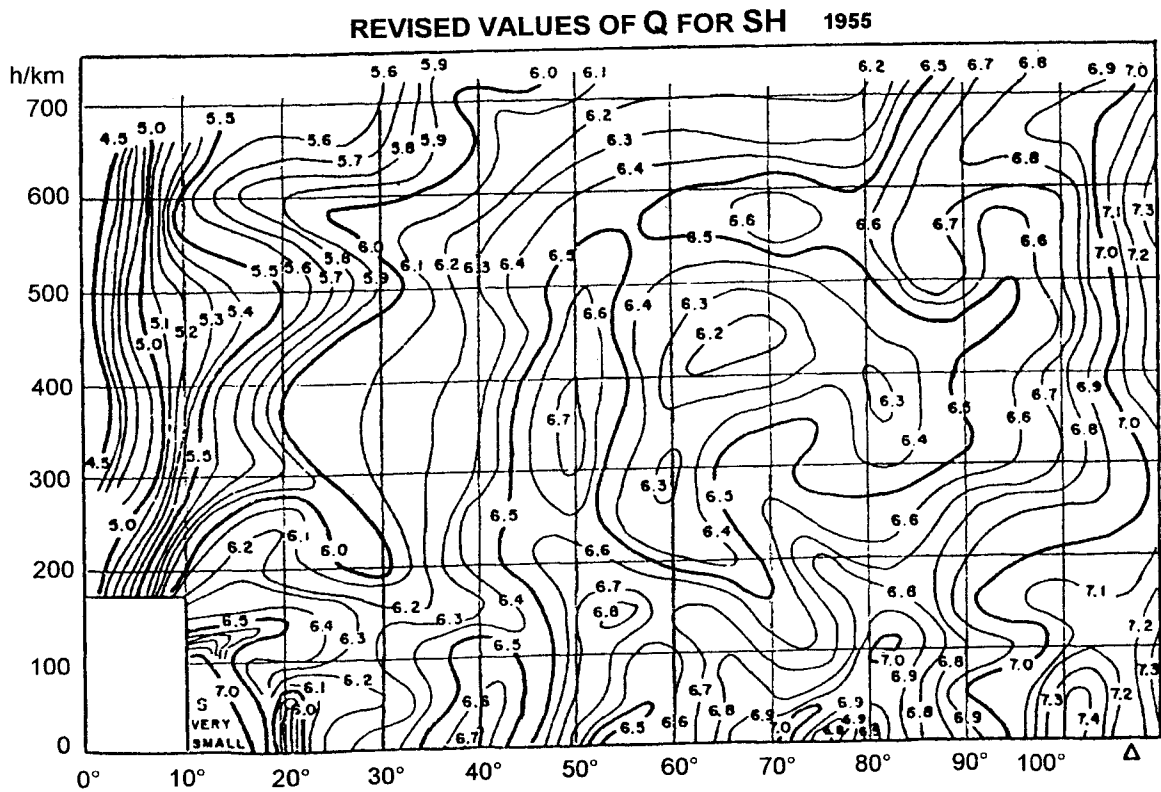


Fig. 5c

Veith and Clawson (1972) developed another calibration function $P(\Delta, h)_{SP}$ for short-period P-waves (Fig. 6) using data from underground nuclear explosions. It is consistent with observations and present-day concepts of attenuation. As compared to Fig. 5a it looks much smoother and resembles more the inverse of the short-period P-wave $A-\Delta$ relationship in Fig. 4. The values (also in Fig. 5a) are smallest around $\Delta = 20^\circ$. This coincides with the epicentral distance of large amplitudes due to the focussing effect of the strong positive velocity gradient at about 410 km depth in the upper mantle (so-called 20° discontinuity) while the upper-mantle discontinuity at 660 km depth produces the secondary maximum in the amplitude distance curve at $\Delta \approx 40^\circ$ (cf. Fig. 4). The rapid increase of $Q(\Delta, h)$ beyond $\Delta = 90^\circ$ is related to the strong amplitude decay in this distance range due to the strong refraction of the seismic rays into the outer earth core with its strongly reduced P-wave velocity as compared to the lower mantle ("core shadow"). In the average, m_P according to this calibration function is about 0.2 magnitude units smaller than m_b for short-period P-waves calibrated with $Q(\Delta, h)_{PZ}$. Due to a different attenuation model used this difference is particularly significant for deep earthquakes (up to 0.5 magnitude units). But both NEIC and ISC still use the Gutenberg-Richter Q functions, and for short-period PZ only, i.e. they determine in fact no m_B but m_b .

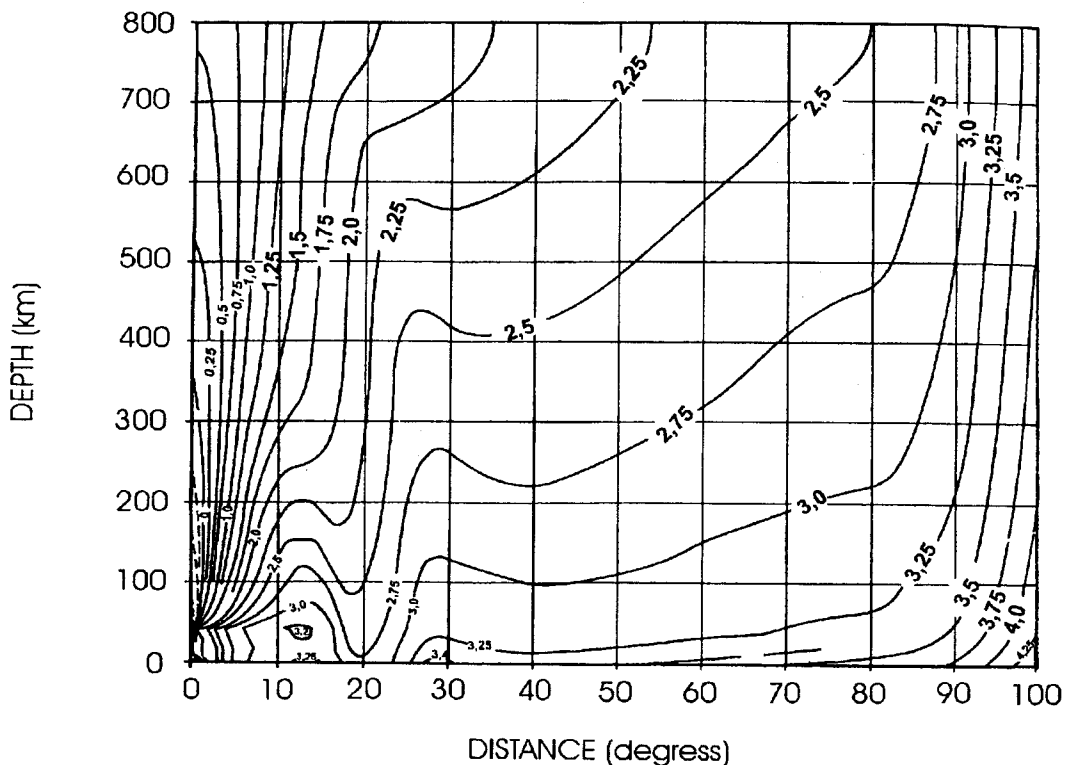


Fig. 6: Calibration function $P(\Delta, h)$ for short-period m_b determinations according to Veith and Clawson (1972). Note that these values are valid only if amplitudes are given in nanometers, $1 \text{ nm} = 10^{-9} \text{ m}$! (Modified from Veith and Clawson, 1972).

Another $Q_b(\Delta, h)$ function based on broadband recordings of P-waves (bandpass between 0.01 and 2 Hz) was derived recently by Nolet et al. (1998). It differs markedly from $P(\Delta, h)_{SP}$.

Duda and Kaiser (1989) recommend instead the determination of *spectral magnitudes* based on measurements of spectral amplitudes from one-octave bandpass filtered digital broadband records of P waves. As seen from Fig. 7, earthquakes of about the same magnitude m_b recorded in about the same distance range may have, depending also on focal depth and the

type of rupture mechanism, very different amplitudes in different spectral ranges. This is due to regional differences in ambient stress conditions and related stress drop.

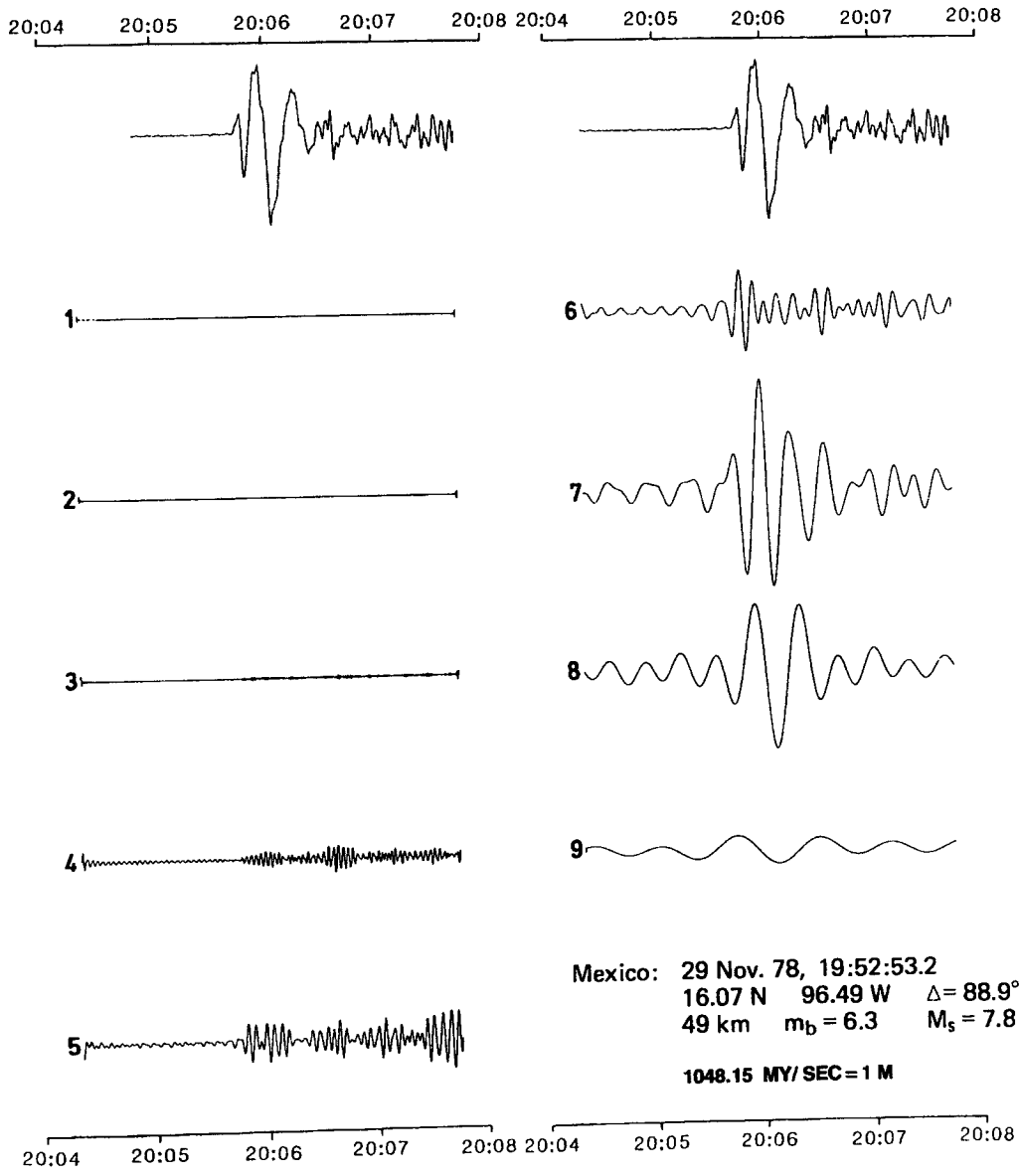


Fig. 5-12

Fig. 7a

Fig. 7: Examples of broadband digital records proportional to ground velocity of the P-wave group from two earthquakes of similar magnitude m_b in different source regions (uppermost traces in Figs. 7a and b, respectively) and their one-octave bandpass filtered outputs. The numbers 1 to 9 on the filtered traces relate to the different center periods between 0.25 s (1) and 64 s (9). Note that example a) on this page has its maximum ground velocity (or max A/T) at trace 7 which corresponds to a centre period of 16 s while it is at 1 s in example b) on the next page (trace 3). (copied from Duda, 1986, with permission of the BGR Hannover).

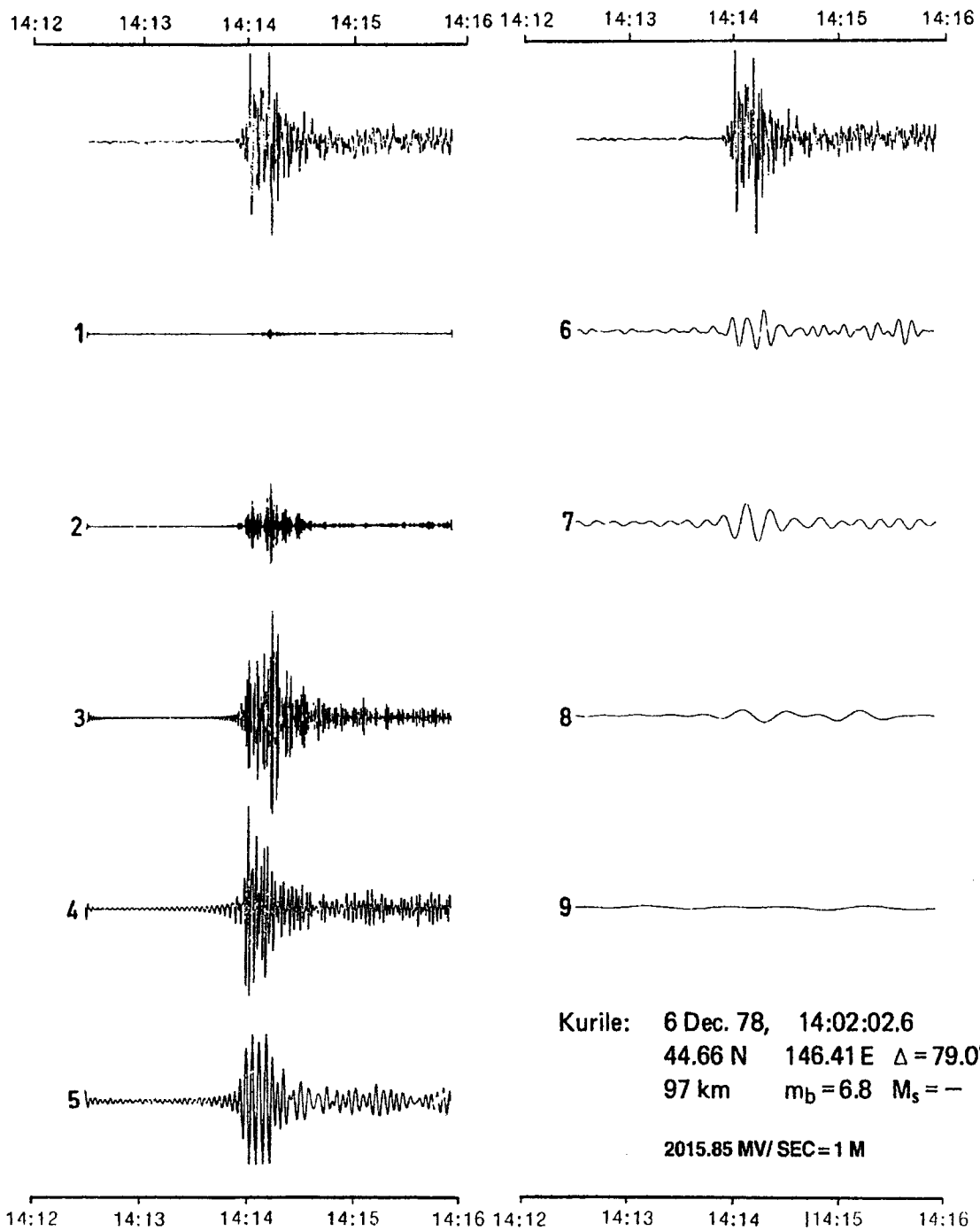


Fig. 7b:

Duda and Janovskaya (1993) also provide related theoretical spectral amplitude-distance curves based on the IASP91 velocity model and two different attenuation models so as to allow the magnitude calibration of spectral amplitude measurements (Fig. 8).

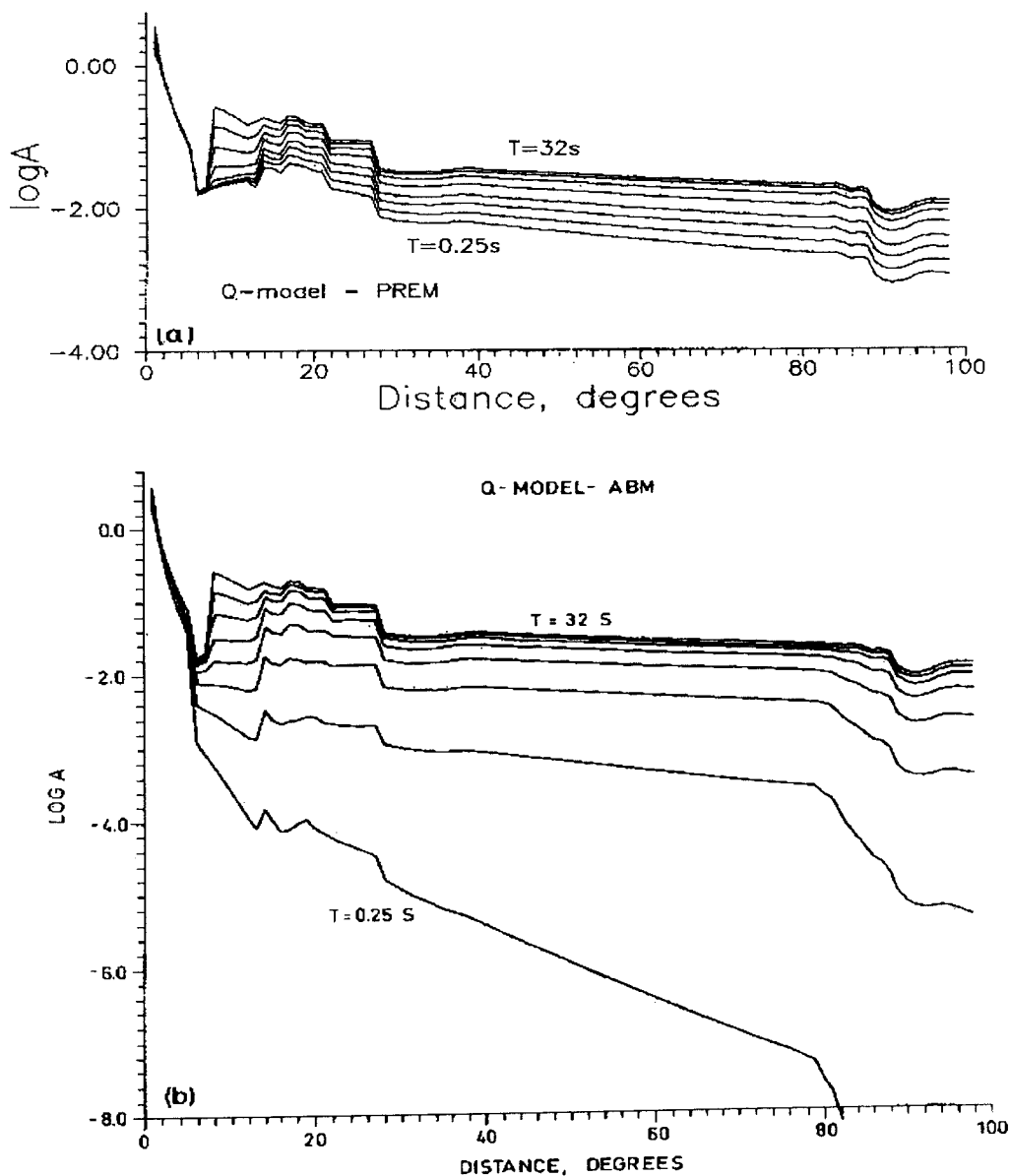


Fig. 8: Spectral amplitude-distance curves (in one octave steps) as calculated for the IASP91 velocity model and two alternative Q-models according to Liu et al. (1976) as in the PREM model (upper diagram) and according to the ABM-model of Anderson and Given (1982) (lower diagram). (Reprinted from Tectonophysics, Vol. 217, Duda and Janovskaya, 1993, p. 263; with permission from Elsevier Science).

In its essence, the effort of these authors is a response to the problems discussed above. It yields smoothed averaged estimates of the radiated seismic spectrum, its spectral plateau, corner frequency and high-frequency decay and thus of M_0 and stress-drop of the given event. By investigating the ratio of short- to long-period spectral magnitude estimates for different source regions one can also draw inferences on systematic differences in the prevailing source processes (e.g. low-, normal or high stress-drop events) and related ambient stress conditions. But this is not so much the concern of seismological routine practice aimed at providing a

simple one (or two) parameter size-scaling of seismic events for general earthquake statistics and hazard assessment. Rather, this is more a research issue. And this can be tackled best, as the proper quantification of earthquake size too, by determining and analysing both M_0 and the shape of the overall source spectrum instead of their smoothed estimates via spectral magnitudes. Therefore, no broad routine application of a strict spectral magnitude concept for seismological practice is yet in sight although it is a rather consequent approach to the complicated spectra-dependent magnitude issue itself.

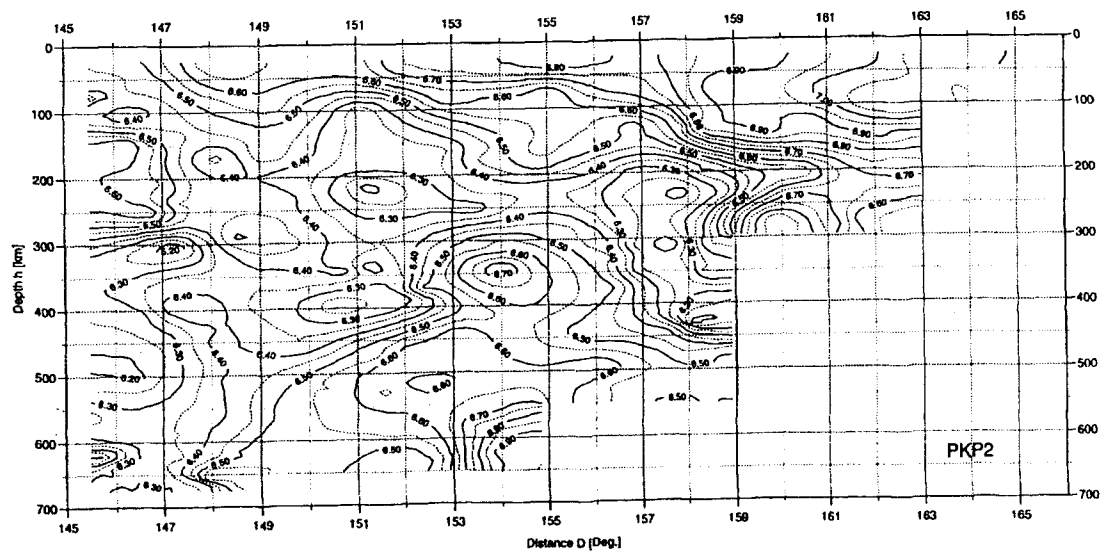
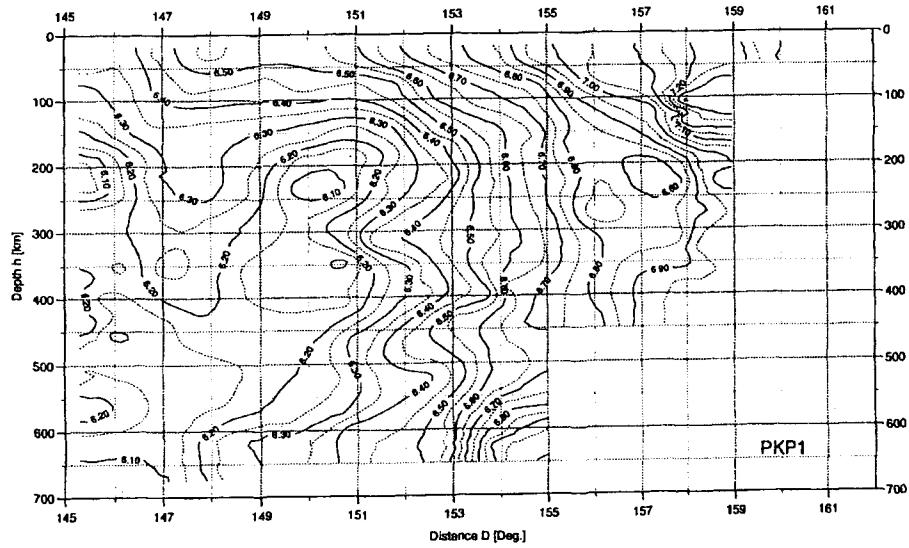
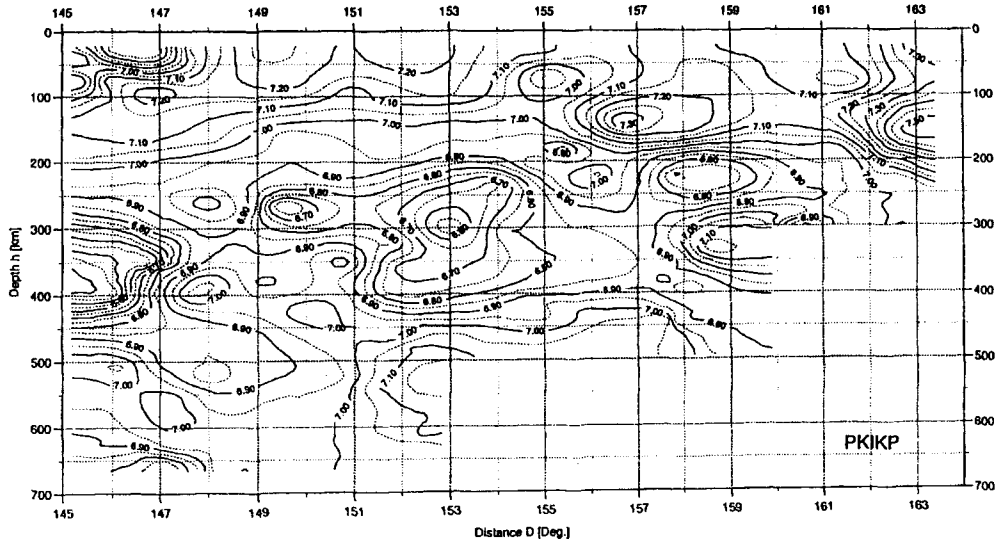
Both the ISC and NEIC continue to use the $Q(\Delta, h)$ functions derived by Gutenberg and Richter (1956a) for PZ for determining m_b by using P waves of $T \leq 3$ s. No body-wave magnitudes from PP or S waves are determined despite of the merits discussed above. Observations less than 21° or more than 100° are also ignored. The latter neglects the availability of both good PP readings far beyond 100° and also the fact, that PKP amplitudes increase significantly in the distance range of the core caustic around 145° . They reach amplitude levels comparable to those of P waves in the distance range $25^\circ < \Delta < 80^\circ$ (cf. Fig. 4). Many earthquakes, especially in the Pacific (e.g. Tonga-Fiji-Kermadec Islands) occur in areas with no good local or regional seismic networks. Often these events, especially the weaker ones, are also not well recorded by more remote stations in the P-wave range but often excellently observed in the PKP distance range, e.g. in Central Europe. This applies to several other event-station configurations too. Therefore, it is a waste of available seismic information not to use good PKP wave recordings for improved magnitude estimates of events not well covered by P-wave observations.

As a consequence, several efforts have been made to derive calibration functions for PKP waves but no generally accepted calibration functions for core phases do exist until now. Miyamura (1974) considered only shallow earthquakes. Janský et al. (1977) were the first to publish preliminary depth-dependent calibration functions. They allow magnitude determinations based on measurements of the maximum A/T ratio (A - amplitude in nm, T - period in s) from the whole PKP-wave group regardless of what branch of the travel-time curve it is related to. Kowalle et al. published Q functions for the first PKP onset measured at station MOX, Germany, and for CLL single phase measurements for source depth $h < 100$ km and $h > 500$ km. Wendt and Tittel (1991) used 26 Tuamotu underground nuclear explosions and the Homogeneous Magnitude System (HMS), developed by Christoskov et al. (1978 and 1985) to determine station corrections and a calibrating function for PKP (maximum amplitudes of the group only) for the rather limited distance interval 143° to 148° .

Below we present $Q(\Delta, h)_{PKP}$ functions for all three types of direct core phases (PKIKP, PKP1 and PKP2) which appear in the distance range $\Delta = 145^\circ - 164^\circ$ (Fig. 9). These calibration functions have been determined by S. Wendt in analogy to Fig. 5a for P waves on the basis of about 4000 A/T-readings in short-period vertical component recordings at station CLL, Germany.

Fig. 9: (next page) Calibration functions for the determination of $m_b(\text{PKP})$ for PKIKP, PKP1 and PKP2 (according to Wendt and Bormann, 1998)

Magnitude Calibrating Functions for Core Phases



The following relationship is used:

$$m_b(\text{PKP}) = \log_{10} (A/T) + Q(\Delta, h)_{\text{PKP}} \quad (18)$$

with amplitude A in μm (10^{-6} m), period T in s, epicentral distance Δ in degree and source depth h in km. Extensive use of this relationship at station CLL proved that m_b determinations from core phases are possible with a standard deviation $< \pm 0.2$ magnitude units as compared to P-wave m_b determinations by NEIC and ISC. If more than one PKP phase can be identified and A and T been measured then the average value from all individual magnitude determinations provides a more stable estimate. The general applicability of these calibration functions should be tested with data from other stations of the world-wide network.

2.4.3 Moment magnitude M_w , energy magnitude M_E and other non-saturating magnitude scales

Already Brune and King (1967) could show, that surface wave amplitudes at $T = 100$ s may be a better measure of the energy rating for very large earthquakes. Prozorov et al. (1977) modified (12) for very long-period surface waves ($80 \text{ s} < T < 250 \text{ s}$) from shallow events in order to avoid saturation:

$$M'_s = \log (A/T) + (1.66 - 0.91 \log (T/20)) \log \Delta + 3.95 + 2.88 \log (T/20). \quad (19)$$

According to eq. (2) and Fig. 5 in the *Introduction to seismic sources and source parameters* the seismic moment $M_0 = \mu \bar{D} A$ is determined from the plateau of the displacement amplitude spectrum for frequencies $f \rightarrow 0$ Hz and does not saturate. Kanamori (1977) proposed, therefore, a so-called moment magnitude M_w which is tied to M_s and will not saturate either. He reasoned as follows: According to Kostrov (1974) the radiated seismic strain energy is proportional to the stress drop $\Delta\sigma$, namely $E_s \approx \Delta\sigma \bar{D} A/2$. With the above definition of M_0 one can write $E_s \approx (\Delta\sigma/2\mu) M_0$. Assuming a reasonable value for the shear modulus μ in the brittle earth crust and upper mantle (about $3\text{-}6 \times 10^4$ MPa) and taking into account that according to Kanamori and Anderson (1975) and Abe (1975) the stress drop of large earthquakes is remarkably constant, ranging between about 2 and 6 Mpa (cf. Fig. 3 in *Seismic scaling relations*), one gets as an average $E_s \approx 5 M_0 \times 10^{-5}$. Inserting this into the relationship proposed by Gutenberg and Richter (1956c) between the released seismic strain energy E_s and M_s , namely

$$\log E_s = 4.8 + 1.5 M_s \quad (\text{in IS units Joule } J = \text{Newtonmeter Nm}) \quad (20)$$

it follows:

$$\log M_0 = 1.5 M_s + 9.1. \quad (21)$$

Resolving (21) for the magnitude one gets

$$M_w = 2/3 \log M_0 - 6.07. \quad (22)$$

According to Kanamori (1977) M_w agrees very well with M_s for many earthquakes with a rupture length of about 100 km. Therefore, he suggested, that (20) gives a correct value also of the seismic wave energy for earthquakes up to rupture dimensions \leq about 100 km. Thus,

he considered the M_w scale to be a natural continuation of the M_s scale for larger events. Inserting into the $\log E_s$ - M_s relationship the value $M_w = 9.5$ for the Chile 1960 earthquake (Kanamori, 1977) instead of the saturated value $M_s = 8.5$ one gets a 30 times larger seismic energy release! A simple, fast and robust method of M_w determination from broadband P waveforms has been developed by Tsuboi et al. (1995) with a view to rapid evaluation of the tsunami potential of large earthquakes.

Nowadays, digital broadband recordings and fast computer programs permit to determine directly the seismic energy E_s by integrating the radiated energy flux in velocity-squared seismograms over the duration of the source process and correcting it for the effects of geometric spreading, attenuation and radiation pattern. A method developed by Boatwright and Choy (1986) is now routinely applied at NEIC to compute radiated energies for shallow earthquakes of $m_b > 5.8$. The resulting correlation relationship E_s - M_s for almost 400 events derived by Choy and Boatwright (1995) is

$$\log E_s = 1.5 M_s + 4.4. \quad (23)$$

It indicates that (20) slightly overestimates E_s . But when using (20) further in the interest of continuity, resolving it for M_s and calling it energy magnitude M_E (since the direct determination of E_s now permits to define a related M_E) one gets

$$M_E = 2/3 \log E_s - 3.2 \quad (24)$$

and with Kanamori's condition $E_s/M_0 \approx 5 \times 10^{-5}$ and (22)

$$M_E = 2/3 \log M_0 - 6.0 = M_w. \quad (25)$$

Purcaru and Berckhemer published the same result already in (1978). But, as Choy and Boatwright (1995) showed, apparent stresses (and related stress drop) may vary even for shallow events only in a wide range between about 0.03 and 20.7 MPa with a tendency of higher stress drop for strike-slip than for thrust mechanisms. Accordingly, the former excite more high-frequency waves than the latter and their M_E will mostly be larger than M_w . The opposite will be true for the majority of thrust-fault earthquakes. Riznichenko (1992) gave a correlation relation on the basis of data from various authors which predicts (despite of large scatter) an average increase of $\Delta\sigma$ with source depth h according to $\Delta\sigma = 1.7 + 0.2 h$, i.e. stress drops of more than 100 MPa can be expected for very deep earthquakes. On the other hand, Kikuchi and Fukao (1988) got for 35 large earthquakes in all depth ranges $E_s/M_0 \approx 5 \times 10^{-6}$ only, i.e. one order of magnitude less than the Kanamori condition for deriving M_w . Therefore, M_E and M_w might be rather different.

Another strong argument to use M_E instead of M_w is that it follows more closely the original intent of the Gutenberg-Richter formula by relating magnitude to the velocity power spectrum and thus to energy. Differently, M_w is related to the seismic moment which is derived from the low-frequency asymptote of the displacement spectrum. Consequently, M_E is more closely related to the seismic potential for damage while M_w is related to the final static displacement and thus more to the tectonic consequences of an earthquake.

Kanamori et al. (1993) apply the direct determination of energy release to regional data from the very broadband recordings from the TERRASCOPE network and derive a relationship between M_L and E_s . It is linear between $1.5 < M_L < 6.0$ but M_L saturates for $M_L > 6.5$.

Another concept is the so-called mantle magnitude, M_m . It was introduced by Okal and Talandier (1989 and 1990), first for Rayleigh waves and later extended to Love waves. M_m is a magnitude scale which is firmly related to the seismic moment M_0 too and thus avoids saturation. On the other hand, it is closer to the original philosophy of a magnitude scale and allows quick, even one-station automated measurements (Hyvernaud et al., 1992) that do not require the knowledge of either the earthquake's focal geometry, or its exact depth, parameters which are crucial for a good moment estimate and require (global) network recordings. M_m is defined as

$$M_m = \log X(\omega) + C_S + C_D - 0.90 \quad (26)$$

with $X(\omega)$ as the spectral amplitude of a Rayleigh wave in $\mu\text{m-s}$, C_S a source correction, and C_D a frequency-dependent distance correction. For details, also with respect to the correction terms, see Okal and Talladier (1989 and 1990). Applications of M_m to the reassessment of the moment of shallow, intermediate and deep historical earthquakes are extensively described by Okal (1992 a and b). M_m is an estimate of $(\log M_0 - 13)$ (when M_0 is given in Nm). For the Chile 1960 earthquake Okal (1992a) gets values $M_m \approx 10$ to 10.3 and for $M_0 = 3.2 \times 10^{23}$ Nm. M_m determinations were extensively verified and are said to be accurate by about ± 0.2 magnitude units (Hyvernaud et al., 1992).

2.5. Other Magnitude scales

2.5.1 Lg-wave magnitudes

Sometimes S_g and L_g waves, recorded at shorter distances and with periods $T < 3$ s are used for magnitude determinations. These waves propagate well in continental platform areas and are most prominent at regional distances up to about 20° (e.g. Nuttli 1973). They allow rather stable magnitude estimates with small scatter. Ambraseys (1985) published related Q-functions for S_g , L_g (Q_g) and higher mode Rayleigh waves (Q_R) applicable for northwestern European earthquakes in the distance range $0.5^\circ < D < 11^\circ$ when using the relationship

$$M_{L_g, S_g, R} = \log (A/T)_{L_g, S_g, R} + Q_{g, R} \quad (27)$$

Street (1976) recommended on the basis of L_g recordings a unified m_b magnitude scale between central and northeastern North America. Ebel (1994) even proposed a frequency dependent scale $m_{L_g}(f)$, calibrated to m_b , to become the standard for regional seismic networks in northeastern North America. Stable single-station estimates of magnitudes from Nevada test site underground nuclear explosions have been made by Mayeda (1993) using 1-Hz L_g -coda envelopes. As compared with L_g magnitude estimates using third peak or rms amplitudes, these coda magnitudes have generally a five times smaller scatter (0.03 to 0.04 magnitude units only!).

2.5.2 Macroseismic magnitudes

Other efforts are directed to develop magnitude scales which are best suited for earthquake engineering assessment of potential damage and thus seismic risk. These efforts go in two directions by either relating M to macroseismic intensity and/or shaking area or by focussing on the high-frequency content of seismic records. So-called *macroseismic magnitudes* M_{ms} are particularly important for the analysis and statistical treatment of historical earthquakes. There are three main ways to compute them:

- (1) M_{ms} is derived from the epicentral intensity I_0 (or the maximum reported intensity I_{max}) assuming that the earthquake effects in the epicentral area are more or less representative of the strength of the event;
- (2) M_{ms} is derived from taking into consideration the whole macroseismic field, i.e. the size of the shaking is related to different degrees of intensity or the total area of perceptibility A ;
- (3) M_{ms} is related to the product $P = I_0 \times A$ which is nearly independent on the focal depth h which is often not reliably known.

Accordingly, formulae for M_{ms} have the general form of

$$M_{ms} = a I_0 + b , \quad (28)$$

or, whenever the focal depth h is known

$$M_{ms} = c I_0 + \log h + d , \quad (29)$$

or, when using the shaking area A_{fi} instead,

$$M_{ms} = e \log A_{fi} + f \quad (30)$$

with A_{fi} in km^2 shaken by intensities I_i with $i \geq \text{III}, \dots, \text{VIII}$, respectively. Sometimes the mean radius R_{fi} of the shaking area related to a given isoseismal intensity is used instead of the area A_i and (29) is then written (e.g. by Greenhalgh et al. 1989 and with M_{ms} scaled to M_L) as

$$M_{ms} = g \log R_{fi}^2 + h \log R_{fi} + j. \quad (31)$$

In these relationships a to j are different constants. They have to be determined independently for different regions. Most often M_{ms} is scaled to M_L which has proven to be best related to earthquake damages and engineering applications. Examples for regionally best fitting relationships according to equation (27) to (30) have been published for California and Western Nevada by Topozada (1975), for Italy by Tinti et al. (1987) and for Australia by Greenhalgh et al. (1989). For Europe, the relationship by Karnik (1969) yields the best results:

$$M_{ms} = 0.5 I_0 + \log h + 0.35. \quad (32)$$

Another M_{ms} scale based on $P = I_0 \times A$ had been published by Galanopoulos (1961):

$$M_{ms} = \log P + 0.2 (\log P - 6). \quad (33)$$

Another macroseismic magnitude scaled to the body wave magnitude of Central United States earthquakes in the range $2.7 \leq m_b \leq 5.5$ was developed by Nuttli and Zollweg (1974):

$$m_b = 2.65 + 0.098 \log A_f + 0.054 (\log A_f)^2. \quad (34)$$

It is applicable for magnitude estimates of central United States earthquakes with felt areas of shaking $A_f \leq 10^6 \text{ km}^2$ for which there are intensity maps but no instrumental data available. As the limit of perceptibility these authors give vertical component ground motion particle velocities of about $22 \mu\text{m/s}$ on sustained hard-rock. A respective relation given by Gutenberg and Richter (1956b) for California yields significantly smaller shaking areas for equal magnitudes. This has been confirmed by a more recent study of Frankel (1994). He compared felt area and moment magnitudes for California with its young mountain ranges and for a

global data set of earthquakes in stable continental regions (SCRs) such as central USA (Fig. 10). The main reason is that average attenuation at frequencies around 2-4 Hz, which correspond to the natural frequency of the thorax-abdomen system of an average human being (according to Goldman and Gierke, 1961, 3-4 Hz) and thus to the range of best human perceptibility of ground shaking, is very different in these regions (after Frankel, 1994, Q about 490 and 1600, respectively). As the lower limit of perceptibility Frankel (1994) gives a high-frequency acceleration spectral level at a distance of 100 km of 0.35 cm/s.

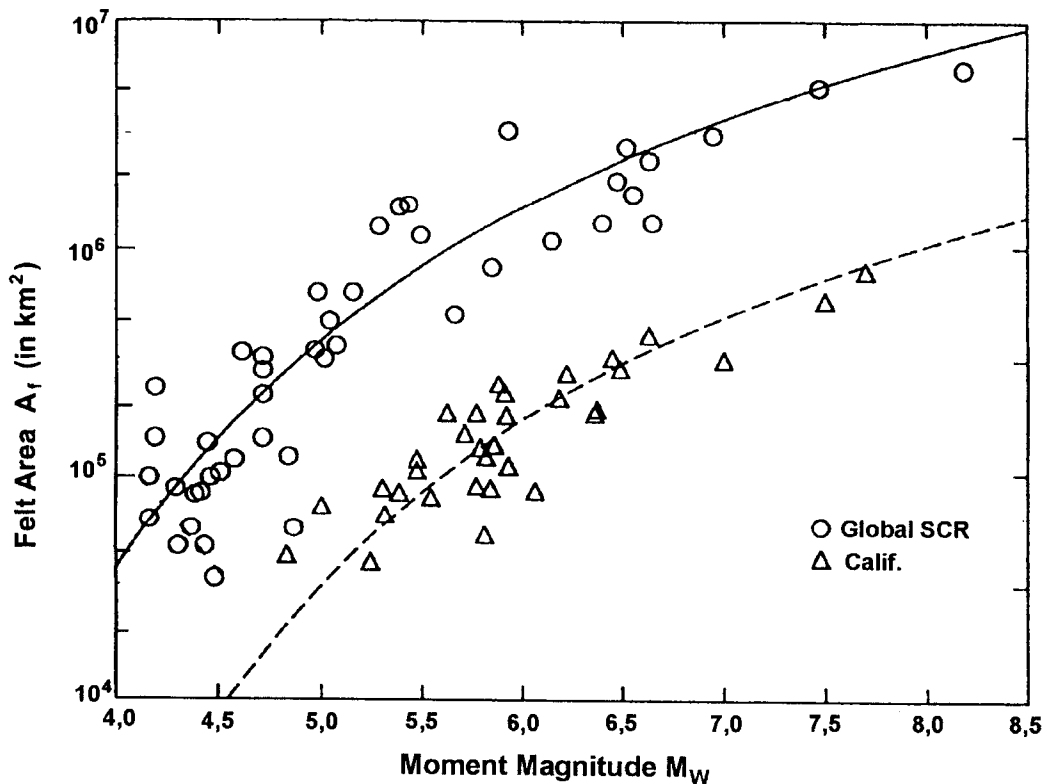


Fig. 10: Felt area A_f (in km^2) plotted against moment magnitude M_w for global data from stable continental regions (SCR; open circles; from Johnston, 1993) and California data (triangles, from Hanks et al., 1975; Hanks and Johnston, 1992). Solid and dashed lines are fits according to an equation given by Frankel (1994). (Modified from Frankel (1994).)

A related problem is the determination of magnitudes of prehistoric and historic (pre-instrumental) earthquakes from dimensions (length L , width W and/or dislocation D) of observed seismo-dislocations (e.g. Khromovskikh, 1989; Wells and Coppersmith, 1994; Mason, 1996) based on correlation relationships between magnitudes and respective field data from recent events (cf. chapter *Seismic scaling relations*).

2.5.3 High-frequency moments and magnitudes

Koyama and Zheng (1985) developed a kind of short-period seismic moment M_1 which is related to the source excitation of short-period seismic waves and scaled to m_b according to

$$\log M_1 = 1.24 m_b + 10.9 \quad (\text{in } J = \text{Nm}). \quad (35)$$

They determined M_1 from WWSSN short-period analogue recordings by applying an innovative approximate estimate of spectral amplitudes

$$Y(f) = 1.07 A_{\max} (\tau/f_0)^{1/2} \quad (36)$$

with A_{\max} - maximum amplitude, f_0 - dominant frequency and τ - a characteristic duration of the complicated wave-packets. They analysed more than 900 short-period recordings from 79 large earthquakes throughout the world in the moment range $7.5 \times 10^{17} \leq M_0 \leq 7.5 \times 10^{22}$ Nm. M_1 did not saturate in this range!

More recently, Atkinson and Hanks (1995) proposed a *high-frequency magnitude* scale

$$m = 2 \log a_{\text{hf}} + 3 \quad (37)$$

with a_{hf} as the high-frequency level of the Fourier amplitude spectrum of acceleration in cm/s, i.e. for $f \gg f_c$. They use average or random horizontal component accelerometer amplitudes at a distance of 10 km from the hypocenter or from the closest fault segment. m has been scaled to the moment magnitude $M = M_w$ for events of average stress drop in eastern North America and California. When M is known, m is a measure of stress drop. For large pre-instrumental earthquakes m can more reliably be estimated than M from the felt area of earthquake shaking (see 2.5.2). When used together, m and M provide a good index of ground motion over the entire engineering frequency band, allow better estimates of response spectra and peak ground motions and thus of seismic hazard.

2.5.4 Tsunami magnitudes

A different kind of magnitude is the *tsunami magnitude* scale M_t . According to Abe (1989)

$$M_t = \log H_{\max} + a \log \Delta + C \quad (38)$$

where H_{\max} is the maximum single (crest or trough) amplitude of tsunami waves in m as measured by tide-gages records and /or as derived from maximum inundation height, Δ - epicentral distance in km to the respective tide station and a and C - constants; a was found to be almost 1. In case of the long-wave approximation, i.e. with tsunami wavelengths being much larger than the bathymetric depths, the maximum tsunami height is strictly related to the maximum *vertical* deformation of the ocean bottom, $D_{\perp\max}$, and thus to the seismic moment M_0 . M_t was calibrated, therefore, with the average condition $M_t = M_w$ for the calibration data set. This resulted in:

$$M_t = \log H_{\max} + \log \Delta + 5.8. \quad (39)$$

(39) shows no saturation. For the Chile earthquake 1960 $M_t = 9.4$ while $M_w = 9.5$. Sometimes, very slow but large ruptures with a large seismic moment cause much stronger tsunami than it would have been expected from their surface wave, energy or body wave magnitudes M_s , M_E or m_b , respectively. Such events are called "tsunami earthquakes". A striking example is the Aleuten earthquake of 01.04.1946 with $M_s = 7.3$ and $M_t = 9.3$. Such strong but very slow earthquakes may have negligibly small energy in the high-frequency range relevant for seismic hazard, earthquake engineering and human perception of ground shaking.

2. CORRELATION RELATIONS BETWEEN MAGNITUDE SCALES

Gutenberg and Richter (1956a and b) provided correlation relationships between the various magnitude scales:

$$m_B = 2.5 + 0.63 M_s \quad (40)$$

$$m = 1.7 + 0.8 M_L - 0.01 M_L^2 \quad \text{and} \quad (41)$$

$$M_s = 1.27 (M_L - 1) - 0.016 M_L^2. \quad (42)$$

These relations were derived by a single random-variable parameter regression analysis assuming that the independent variable X (on the right side of the equation) is known and not afflicted with random errors and that the data scatter observed is due to random errors in the Y - (ordinate) direction only. Often they are wrongly applied, e.g. by solving (40) for M_s and calculating M_s for short-period m_b values as published by international data centers and finally calculating seismic energy E_s via E_s - M_s relationships (cf. section 3 below). Note that (40) is an optimal estimator for m_B but not for M_s ! In fact, both m_B and M_s determinations are afflicted with random errors and both account for the data scatter in an empirical m_B - M_s diagram. Therefore, only a two random-variable parameter regression (so-called "orthogonal regression") analysis yields equations which can be used both ways for optimal parameter estimation (Bormann and Khalturin, 1975; Bormann and Wylegalla, 1975, Ambraseys, 1990).

When using medium-period P-wave records and single random parameter regression almost identical relationships to (40) were found both by Bune et al. (1970) on the basis of records of the former Soviet station network and by Bormann and Wylegalla (1975) for a single station in Germany (MOX; magnitude range 4.7 to 8.5). The latter is

$$MPV = 2.5 + 0.60 MLH. \quad (43)$$

Note, that the related orthogonal regression to (43) calculated for the same data set by Bormann and Wylegalla (1975) is rather different:

$$MPV - 0.70 MLH = 1.83 \quad (44)$$

and that the respective best fitting single random-parameter regression with respect to MLH is

$$MLH = - 1.54 + 1.25 MPV. \quad (45)$$

This is clearly different from

$$MLH = - 4.17 + 1.67 MPV \quad (46)$$

which one gets when solving incorrectly (43) for MLH. As compared to (45) eq. (46) results in an overestimation of MLH by about 1.2 magnitude units for $m_B = 8$ and an underestimation of 0.8 units for $m_B = 5$.

The single random-parameter regression relationship between short-period m_b and M_s is very different from (40), namely, according to Gordon (1971),

$$m_b = (0.47 \pm 0.2) M_s + (2.79 \pm 0.09) \quad (47)$$

for a global station-earthquake data set. This agrees very well with the single station average formula derived by Karnik (1972) for the Czech station Pruhonice (PRU):

$$m_b(\text{sp, PRU}) = 0.47 \text{ MLH} + 2.95. \quad (48)$$

The orthogonal correlation between surface wave magnitudes determined from vertical and horizontal component recordings using the so-called Prague-Moscow calibration function (cf. eq. (12)) is, according to Bormann and Wylegalla (1975), nearly ideal, namely:

$$\text{MLV} - 0.97 \text{ MLH} = 0.19 \quad (49)$$

with a standard deviation of only 0.11 and a correlation coefficient of $r = 0.98$. This clearly justifies the use this calibration function, which was originally derived from horizontal amplitude readings, for vertical component (Rayleigh-wave) magnitude determinations too.

When using medium-period broadband data only, the orthogonal regression relation between magnitude determinations from PV and PPV or SH waves, respectively, are almost ideal. Gutenberg and Richter (1956a) had published Q-functions for all three phases (cf. Figs. 5a-c and Tab. 7 above). Bormann and Wylegalla (1975) found for a global earthquake data set recorded at station MOX the orthogonal fits:

$$\text{MPPV} - \text{MPV} = 0.05 \quad \text{and} \quad (50)$$

$$\text{MSH} - 1.1 \text{ MPV} = -0.64. \quad (51)$$

This confirms the good mutual scaling of these original body-wave calibration functions with each other, provided that they are correctly applied to medium-period data only. Therefore, it is not understandable why the international data centres until now hesitate to determine the proper m_B from PPV and SH waves too.

Kanamori (1983) summarised the relationship between the various magnitude scales in graphical form (Fig. 11). It also gives the ranges of uncertainty for the various magnitude scales due to observational errors and intrinsic variations in source properties related to differences in stress drop, complexity, fault geometry and size, source depth etc. The range of periods for which these magnitudes are determined are for m_b : ≈ 1 s; for M_L : $\approx 0.1 - 3$ s; for m_B : $\approx 0.5 - 15$ s; for M_s : ≈ 20 s and for M_w : $\approx 10 \rightarrow \infty$ s. Accordingly, these different magnitude scales saturate differently, the earlier, the shorter the dominating periods are: m_b around 6.5, M_L around 7, m_B at about 8 and M_s at about 8.5 while M_w does not saturate. This is in good agreement with the general conclusions one can draw on the basis of seismic source spectra (cf. Fig. 5 in the chapter *Introduction to seismic sources and source parameters*).

In an effort of uniform magnitude re-evaluation for European earthquakes in the magnitude range $3 < M < 8$ Ambrasseys (1990) published the following *orthogonal regression relationships* between the various common magnitude scales which can be solved for either one of the two variables:

$$0.75 m_b - 0.66 m_{BP} = 0.21 \quad (52)$$

$$0.77 m_b - 0.64 M_L = 0.73 \quad (53)$$

$$0.86 m_b - 0.49 M_s = 1.94 \quad (54)$$

$$0.80 M_L - 0.60 M_s = 1.04 \quad (55)$$

with m_b being determined according to the ISC procedure from short-period P-wave recordings and m_{BP} using medium-period P-wave records.

Other relationships have been published by Nuttli (1985) which allow to estimate for plate-margin earthquakes M_s when m_b is known. For $m_b > 5$ their results differ less than 0.2 magnitude units from those of (15) when solved for M_s .

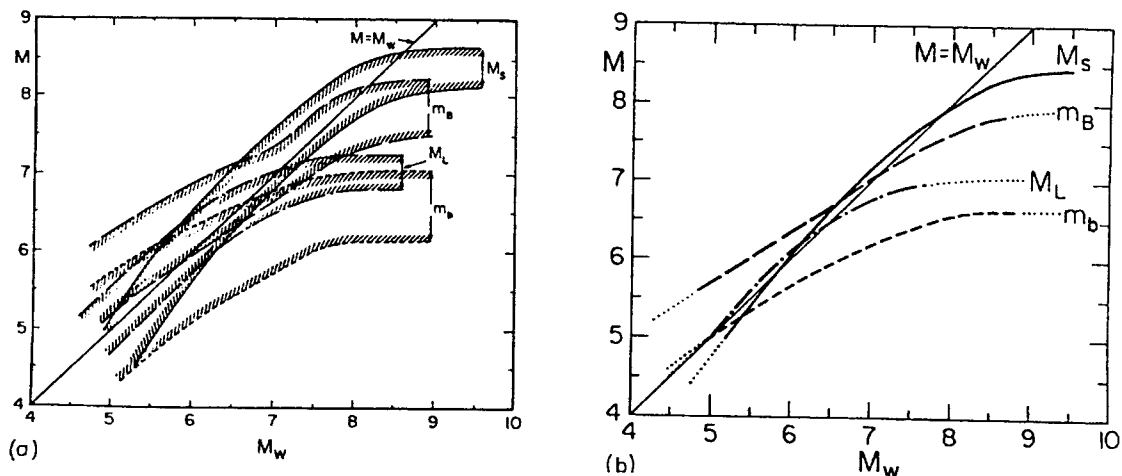


Fig. 11: Relations between magnitude scales (Reprinted from Tectonophysics, Vol. 93, Kanamori 1983, p.193, with permission from Elsevier Science).

4. SUMMARY

The lecture introduces into the history, foundations, scope and principal limitations of the magnitude concept, defines the various magnitude scales in current use, outlines the general procedures to be followed in magnitude determination and discusses the issue, what kind of magnitude scale is best suited for what kind of application in earthquake statistics, research, engineering seismology and hazard assessment, event discrimination etc. The related calibration functions are given for all standard magnitude scales as diagrams, tables or formulae and the correlation relationships between various types of magnitude scales are presented in equations and diagrams.

For practising the determination of magnitudes some *Exercises on magnitude determination* with solutions have been added. Related problems of the scaling of magnitudes with released seismic energy or with geometric, kinematic and dynamic parameters of the seismic source are dealt with in the chapter *Seismic scaling relations*.

REFERENCES

- Abe, K. (1975). -Reliable estimation of the seismic moment of large earthquakes. *J. Phys. Earth*, **23**, 381-390.
- Abe, K. (1989). Quantification of tsunamigenic earthquakes by the M_t scale. *Tectonophysics*, **166**, 27-34.
- Abercrombie, R.E. (1994). Regional bias in estimates of earthquake M_s due to surface-wave path effects. *Bull. Seism. Soc. Am.*, **84**, 2, 377-382.
- Aki, K and Chouet, B. (1975). Origin of coda waves: Source, attenuation and scattering effects. *J. Geophys. Res.*, **80**, 3322
- Alsker, A., Kvamme, L.B., Hansen, R.A., Dahle, A. and Bungum, H. (1991). The M_L scale in Norway. *Bull. Seism. Soc. Am.*, **81**, 2, 379-389.
- Ambraseys, N.N. (1985). Magnitude assessment of northwestern European earthquakes. *Earthquake Engineering and Structural Dynamics*, **13**, 307-320.
- Ambraseys, N.N. (1988). Magnitude-fault length relationships for earthquakes in the middle east. In: *Historical seismograms and earthquakes of the world*. Academic Press, 309-310.
- Ambraseys, N.N. (1990). Uniform magnitude re-evaluation of European earthquakes associated with strong-motion records. *Earthquake Engineering and Structural Dynamics*, **19**, 1-20.
- Ambraseys, N.N. and Bommer, J.J. (1990). Uniform magnitude re-evaluation for the strong-motion database of Europe and adjacent areas. *European Earthquake Engineering*, **2**, 3-16.
- Anderson, D.L. and Given, J.W. (1982). Absorbtion band Q model for the Earth. *J. Geophys. Res.*, **87**, 3893-3904.
- Archangelskaya, V.M. (1959). The dispersion of surface waves in the earth's crust. *Izv. Akad. Nauk SSSR, Seriya Geofiz.* **9** (in Russian).
- Atkinson, G.M. and Hanks, Th. (1995). A high-frequency magnitude scale. *Bull. Seism. Soc. Am.*, **85**, 3, 825-833.
- Bakun, W.H. and Joyner, W. (1984). The M_L scale in Central California. *Bull. Seim. Soc. Am.*, **74**, 5, 1827-1843.
- Bath, M. (1981). Earthquake magnitude - recent research and current trends. *Earth Science Reviews*, **17**, 315-398.
- Bath, M. (1984). Earthquake magnitudes based on PKP and SKP waves. In: *The O.G.S. Silver Anniversary Volume, O.G.S. Trieste*, p.93-108
- Bath, M. (1985). Surface-wave magnitude corrections for intermediate and deep earthquakes. *Physics Earth Planet. Interiors*, **37**, 228-234.
- Bisztricsany, E. (1958). On the problem of magnitude determination. *Zeitschr. f. Geophysik*, **24**, 153-160.
- Boatwright, J. and Choy, G. (1986). Teleseismic estimates of the energy radiated by shallow earthquakes. *J. Geophys. Res.*, **91**, B2, 2095-2112.
- Boore, D.M. (1989). The Richter scale: its development and use for determining earthquake source parameter. *Tectonophysics*, **166**, 1-14
- Bormann, P. (1972). Identification of teleseismic events in the records of Moxa station. *Gerlands Beitr. Geophysik* **81**,1/2, 105-116.
- Bormann, P. (1973). Standardization and optimization of frequency-characteristics at Moxa station (GDR). *Proceed. XII Assembly of ESC, Bukarest, Technical and Economic Studies, D-Series, No. 10*, 133-145.

- Bormann, P. and Khalturin, V.I. (1975). Relations between different kinds of magnitude determinations and their regional variations. Proceed. XIVth General Assembly of the European Seismological Commission, Trieste, 16-22 September 1974. Nationalkomitee für Geodäsie und Geophysik, AdW der DDR, Berlin 1975, 27-39.
- Bormann, P. and Wylegalla, K. (1975). Investigation of the correlation relationships between various kinds of magnitude determination at station Moxa depending on the type of instrument and on the source area (in German). Public. Inst. Geophys. Polish Acad. Sci., Vol. 93, 160-175.
- Bormann, P.(Ed.) (1989). Monitoring and analysis of the earthquake swarm 1985/86 in the region Vogtland/Western Bohemia. Akademie der Wissenschaften der DDR, Zentralinstitut für Physik der Erde Potsdam, Veröffentlichung No. 110, Potsdam, 282 pp.
- Bormann, P. (1998). Conversion and comparability of data presentations on seismic background noise. *Journal of Seismology*, **2**, 37-45.
- Brune, J.N. and King, C.Y. (1967). Excitation of mantle Rayleigh waves of period 100 seconds as a function of magnitude. *Bull. Seism. Soc. Am.*, **57**, 1355-1365.
- Bune, V.J., Vvedenskaya, N.A., Gorbunova, J.V., Kondorskaya, N.V., Landyрева, N.S., Fedorova, J.V. (1970). Correlation of M_{LH} and M_{PV} by data of the network of seismic stations of USSR. *Geophys. J. R. Astr. Soc.*, **19**, 533-542.
- Chávez, E. and Priestley, K.F. (1985). M_L observations in the great basin and M_0 versus M_L relationships for the 1980 Mammoth Lakes, California, earthquake sequence. *Bull. Seism. Soc. Am.*, **75**, 6, 1583-1598.
- Choy, G.L. and Boatwright, J.L. (1995). Global patterns of radiated seismic energy and apparent stress. *J. Geophys. Res.*, **100**, B2, 18205-18228.
- Christiskov, L., Kondorskaya, N.V. and Vanek, J. (1978). Homogeneous magnitude system of the Eurasian continent. *Tectonophysics*, **49**, 131-138.
- Christoskov, L., Kondorskaya, N.V. and Vanek, J. (1983). Homogeneous magnitude system of the Eurasian continent: S and L waves. Report SE-34, World Data Center A for Solid Earth, Boulder.
- Christoskov, L., Kondorskaya, N.V. and Vanek, J. (1985). Magnitude calibration functions for a multidimensional homogeneous system of reference stations. *Tectonophysics*, **118**, 213-226.
- Duda, S.J. (1986). The spectra and magnitudes of earthquakes. In: Buttkus, B. (Ed.). Ten years of the Gräfenberg Array: Defining the frontiers of broadband seismology. *Geologisches Jahrbuch Reihe E, Heft 35*, 71-79.
- Duda, S.J. (1989). Earthquakes: Magnitude, energy, and intensity. In: James, D.E. (Ed.). *The Encyclopedia of Solid Earth Geophysics*. Van Nostrand Reinhold Company, New York, 272-288.
- Duda, S.J. and Kaiser, D. (1989). Spectral magnitudes, magnitude spectra and earthquake quantification: the stability issue of the corner period and of the maximum magnitude for a given earthquake. *Tectonophysics*, **166**, 205-219.
- Duda, S.J. and Yanovskaya, T.B. (1993). Spectral amplitude-distance curves for P-waves: effects of velocity and Q-distribution. *Tectonophysics*, **217**, 255-265.
- Eaton, J.P. (1992). Determination of amplitude and duration magnitudes and site residuals from short-period seismographs in Northern California. *Bull. Seism. Soc. Am.*, **82**, 2, 533-579.
- Ebel, J.E. (1994). The $M_{Lg}(f)$ magnitude scale: A proposal for its use for northeastern North America. *Seismological Research Letters*, **65**, 2, 157-166.
- Evernden, J.F. (1971). Variation of Rayleigh-wave amplitude with distance. *Bull. Seism. Soc. Am.*, **61**, 231-240.

- Frankel, A. (1994). Implications of felt area-magnitude relations for earthquake scaling and the average frequency of perceptible ground motion. *Bull. Seism. Soc. Am.*, **84**, 2, 462-465.
- Galanopolous, A.G. (1961). On magnitude determination by using macroseismic data. *Ann. Geofis.*, **14**, 225-253.
- Goldman, D.E. and Gierke, H.E. (1961). Effects of shock and vibration on man. Chapter 44 in: Harris, C.M. and Crede, C.E. (Editors): *Shock and Vibration Handbook*, McGraw-Hill, New York.
- Gorbunova, I.V. and Kondorskaya, N.V. (1977). Magnitudes in the seismological practice of the USSR. *Izv. Akad. Nauk SSSR, ser Fizika Zemli*, No. 2, Moscow (in Russian).
- Gordon, D.W. (1971). Surface-wave versus body-wave magnitude. *Earthquake Notes*, **42**, 3/4, 20-28.
- Greenhalgh, S.A. and Singh, R. (1986). A revised magnitude scale for South Australian earthquakes. *Bull. Seim. Soc. Am.*, **76**, 3, 757-769.
- Greenhalgh, S.A., Denham, D, McDougall, R. and Rynn, J.M. (1989). Intensity relations for Australian earthquakes. *Tectonophysics*, **166**, 255-267.
- Grosser, H., Baumbach, M., Berkhemer, H., Baier, B., Karahan, A., Schelle, H., Krüger, F., Paulat, A., Michel, G., Demirtas, R., Gencoglu, S. and Yilmaz, R. (1998). The Erzincan (Turkey) earthquake (M_s 6.8) of March 13, 1992 and its aftershock sequence. *Pure appl. Geophys.*, **152**, 3, 465-505.
- Gutenberg, B. (1945a). Amplitudes of surface waves and magnitudes of shallow earthquakes. *Bull. Seism. Soc. Am.*, **35**, 3-12.
- Gutenberg, B. (1945b). Amplitudes of P, PP, and S and magnitude of shallow earthquakes. *Bull. Seism. Soc. Am.*, **35**, 57-69.
- Gutenberg, B. (1945c). Magnitude determination of deep-focus earthquakes. *Bull. Seim. Soc. Am.*, **35**, 117-130.
- Gutenberg, B. and Richter, C.F. (1936). On seismic waves (third paper). *Gerlands Beiträge zur Geophysik*, **47**, 73-131.
- Gutenberg, B. and Richter, C.F. (1942). Earthquake magnitude, intensity, energy and acceleration. *Bull. Seism. Soc. Am.*, **32**, 163-191.
- Gutenberg, B. and Richter, C.F. (1954). *Seismicity of the Earth*. Princeton University Press, 2nd ed., 310 pp.
- Gutenberg, B. and Richter, C.F. (1956a). Magnitude and energy of earthquakes. *Annali di Geofisica*, **9**, 1, 1-15.
- Gutenberg, B. and Richter, C.F. (1956b). Earthquake magnitude, intensity, energy and acceleration. *Bull. Seism. Soc. Am.*, **46**, 105-145.
- Gutenberg, B. and Richter, C.F. (1956c). The energy of earthquakes. *Q. J. Geol. Soc. London*, **112**, 1-14.
- Habermann, R.E. (1995). Opinion. *Seism. Res. Letters*, **66**, 5, p.3.
- Hanks, T.C. and Johnston, A.C. (1992). Common features of the excitation and propagation of strong ground motion for North American earthquakes. *Bull. Seism. Soc. Am.*, **82**, 1-23.
- Hanks, T.C., Hileman, J.A. and Thatcher, W. (1975). Seismic moments of the larger earthquakes of the southern California region. *Soc. Bull. Geol.*, **86**, 1131-1139.
- Hatzidimitriou, P., Papazachos, C., Kiratzi, A. and Theodulidis, N. (1993). Estimation of attenuation structure and local earthquake magnitude based on acceleration records in Greece. *Tectonophysics*, **217**, 243-253.
- Herak, M. and Herak, D. (1993). Distance dependence of M_S and calibrating function for 20 s Rayleigh waves. *Bull. Seism. Soc. Am.*, **83**, 6, 1881-1892.
- Herrmann, R.B. (1975). The use of duration as a measure of seismic moment and magnitude. *Bull. Seism. Soc. Am.*, **65**, 899-913.

- Hutton, L.K. and Boore, D.M. (1987). The M_L scale in Southern California. *Bull. Seism. Soc. Am.*, **77**, 6, 2074-2094.
- Hutton, L.K. and Jones, L.M. (1993). Local magnitudes and apparent variations in seismicity rates in Southern California. *Bull. Seism. Soc. Am.*, **83**, 2, 313-329.
- Hyvernaud, O., Reymond, D., Talandier, J., and Okal, E.A. (1993). Four years of automated measurement of seismic moments at Papeete using the mantle magnitude M_m : 1987-1991. *Tectonophysics*, **217**, 3-4, 175-193.
- Iida, K (1967). Determination of the magnitude of microearthquakes. C.R. des Séances de la 14. conf. réunie a Zuerich du 25.09. au 06.10.1967 (XIV General Assembly of IUGG). Abstract volume.
- Janský, J., Ruprechtová, L. and Tittel, B. (1977). Magnitude determination based on short-period core waves. *Studia geoph. et geod.*, **21**, 267-273.
- Johnston, A.C. (1993). The stable continental region data base. In: The earthquakes of stable continental regions: Assessment of large earthquake potential. EPRI report TR-102261, Electric Power Research Institute, Palo Alto, California.
- Kanamori, H. (1977). The energy release in great earthquakes. *J. Geophys. Res.*, **82**, 2981-2987.
- Kanamori, H. (1983). Magnitude scale and quantification of earthquakes. *Tectonophysics*, **93**, 185-199.
- Kanamori, H. and Cipar, J.J. (1974). Focal process of the great Chilean earthquake May 22, 1960. *Phys. Earth Planet. Inter.*, **9**, 128-136.
- Kanamori, H. and Anderson, D.L. (1975). Theoretical basis of some empirical relations in seismology. *Bull. Seism. Soc. Am.*, **65**, 1073-1095.
- Kanamori, H. and Jennings, P.C. (1978). Determination of local magnitude, M_L , from strong motion accelerograms. *Bull. Seism. Soc. Am.*, **68**, 471-485.
- Kanamori, H., Mori, J., Hauksson, E., Heaton, Th.H., Hutton, L.K. and Jones, L.M. (1993). Determination of earthquake energy release and M_L using TERRASCOPE. *Bull. Seism. Soc. Am.*, **83**, 2, 330-346.
- Karnik, V., Kondorskaya, N.V., Riznichenko, Yu.V., Savarensky, Ye.F., Soloviev, S.L., Shebalin, N.V., Vanek, J. and Zatopek, A. (1962). Standardisation of the earthquake magnitude scales. *Studia Geophysica et Geodaetica*, **6**, 41-48.
- Karnik, V. (1969). Seismicity of the European area. Part I. Reidel Publishing Company, Dordrecht, 364 pp.
- Karnik, V. (1972). Differences in magnitudes. *Vorträge des Soproner Symposiums der 4. Subkommission von KAPG 1970, Budapest*, 69-80.
- Karnik, V. and Christoskov, L. (1977). Magnitude determinations at short epicentral distances in Europe. *Publ. Inst. Geophys. Pol. Acad. Sc.*, A-5, 116, 51-60.
- Katsumata, M. (1964). A method to determine the magnitude of deep focus earthquakes in and near Japan. *Zisin (J. Seism. Soc. Japan)*, Ser. II, **17**, 152-165.
- Khromovskikh, V.S. (1989). Determination of magnitudes of ancient earthquakes from dimensions of observed seismodislocations. *Tectonophysics*, **166**, 269-280.
- Kikuchi, M. and Fukao, Y. (1988). Seismic wave energy inferred from long-period body wave inversion. *Bull. Seism. Soc. Am.*, **78**, 5, 1707-1724.
- Kim, W.-Y. (1998). The M_L scale in Eastern North America. *Bull. Seism. Soc. Am.*, **88**, 4, 935-951.
- Kiratzi, A.A. and Papazachos, B.C. (1984). Magnitude scales for earthquakes in Greece. *Bull. Seism. Soc. Am.*, **74**, 3, 969-985.
- Kiratzi, A.A. and Papazachos, B.C. (1985). Local Richter magnitude and total signal duration in Greece. *Ann. Geophys.* **3**, 4, 531-537.
- Klinge, K. (1989). Duration magnitude. In: Bormann, P. (Editor). *Monitoring and analysis of the earthquake swarm 1985/86 in the region Vogtland/Western Bohemia*. Akademie der

- Wissenschaften der DDR, Veröffentlichung Nr. 110 des Zentralinstituts für Physik der Erde, Potsdam 1989, 109-115.
- Kostrov, B. (1974). Seismic moment and energy of earthquakes, and seismic flow of rock. *Izv. Acad. Sci., USSR, Phys. Solid Earth (Engl. Transl.)*, **1**, 23-40.
- Kowalle, G., Tittel, B. and Bormann, P. (1983). Determination of a magnitude calibration function using short-period readings of PKP. *Tectonophysics*, **93**, 289-294.
- Koyama, J. and Zheng, S.-H. (1985). Excitation of short-period body-waves by great earthquakes. *Physics Earth Planet. Int.*, **37**, 108-123.
- Langston, C.A., Brazier, R., Nyblade, A.A. and Owens, T.J. (1998). Local magnitude scale and seismicity rate for Tanzania, East Africa. *Bull. Seism. Soc. Am.*, **88**, 3, 712-721.
- Lay, T. and Wallace, T.C. (1995). *Modern global seismology*. Academic Press, 521 pp.
- Lazareva, A.P. and Yanovskaya, T.B. (1975). The effect of the lateral velocity on the surface wave amplitudes. *Proceed. Intern. Symposium on Seismology and Solid-Earth Physics, Jena, April 1-6, 1974. Veröff. Zentralinstitut Physik der Erde No. 31, Vol. 2*, 433-440.
- Lee, W.H.K., Bennet, R. and Meagher, K. (1972). A method of estimating magnitude of local earthquakes from signal duration. *U.S. Geol. Surv. Open-File Rep.*, 28 pp.
- Lee, W.H.K. and Lahr, J.C. (1975). HYPO71 (revised): A computer program for determining hypocenter, magnitude, and first motion pattern of local earthquakes. *U.S. Geol. Surv. Open-File Rep. 75-311*, 113 pp.
- Lee, V., Trifunac, M., Herak, M., Zivcic, M. and Herak, D. (1990). M_L^{SM} computed from strong motion accelerograms recorded in Yugoslavia. *Earthquake Engineering and structural dynamics*, **19**, 1167-1179.
- Liu, H.-P., Anderson, D.L. and Kanamori, H. (1976). Velocity dispersion due to anelasticity; implications for seismology and mantle composition. *Geophys. J. R. Astron. Soc.*, **47**, 41-45.
- Marshall, P.D. and Basham, P.W. (1973). Rayleigh wave magnitude scale M_S . *Pure and Appl. Geophys.*, **103**, 237-434.
- Mason, D.B. (1996). Earthquake magnitude potential of the intermountain seismic belt, USA, from surface-parameter scaling of Late Quaternary faults. *Bull. Seism. Soc. Am.*, **86**, 5, 1487-1506.
- Mayeda, K. (1993). Mb(LgCoda): A stable single station estimator of magnitude. *Bull. Seism. Soc. Am.*, **83**, 3, 851-861.
- Miamura, S. (1974). Determination of body-wave magnitudes for shallow earthquakes in the New Zealand and Macquarie Loop regions using PKP data. *Phys. Earth Planet. Int.*, **8**, 167-176.
- Michaelson, C.A. (1990). Coda duration magnitudes in central California: an empirical approach. *Bull. Seism. Soc. Am.*, **80**, 1190-1204.
- Muco, B. and Minga, P. (1991). Magnitude determination of near earthquakes for the Albanian network. *Bolletino di Geofisica Teorica ed Applicata.*, **XXXIII**, 129, 17-24.
- Neunhöfer, H. and Güth, D. (1989). Detailed investigation of the great earthquake swarm in Western Bohemia by the local Vogtland network. In: Bormann, P. (Ed.) (1989). *Monitoring and analysis of the earthquake swarm 1985/86 in the region Vogtland/ Western Bohemia*. Akademie der Wissenschaften der DDR, Zentralinstitut für Physik der Erde Potsdam, Veröffentlichung No. 110, Potsdam, 282 pp.
- Nolet, G., Krueger, S., Clouser, R. M. (1998). Empirical determination of depth-distance corrections for m_b and M_w from Global Seismograph Network stations. *Geophysical Res. Letters*, **25**, 9, 1451-1454.
- Nuttli, O.W. (1985). Average seismic source-parameter relations for plate-margin earthquakes. *Tectonophysics*, **118**, 161-174.
- Nuttli, O. (1993). Seismic wave attenuation and magnitude relations for eastern North America. *J. Geophys. Res.*, **78**, 876-885.

- Nuttli, O.W. and Zollweg, J.E. (1974). Reh relation between felt area and magnitude for central United States earthquakes. *Bull. Seism. Soc. Am.*, **64**, 1, 73-85.
- Okal, E.A. and Taladier, J. (1989). M_m : A variable-period mantle magnitude. *J. Geophys. Res.*, **94**, B4, 4169-4193.
- Okal, E.A. and Taladier, J. (1990). M_m : Extension to Love waves of the concept of a variable-period mantle magnitude. *Pure and Appl. Geophys.*, **134**, 3555-384.
- Okal, E.A. (1992a). Use of the mantle magnitude M_m for the reassessment of the moment of historical earthquakes. I: Shallow events. *PAGEOPH*, **139**, 1, 17-57.
- Okal, E.A. (1992b). Use of the mantle magnitude M_m for the reassessment of the moment of historical earthquakes. II: Intermediate and deep events. *PAGEOPH*, **139**, 1, 59-85..
- Panza, J.F., Duda, S.J., Cernobori, L. and Herak, M. (1989). Gutenberg's surface-wave magnitude calibrating function: theoretical basis from synthetic seismograms. *Tectonophysics*, **166**, 35-43.
- Plesinger A., Zmeskal, M. and Zednik, J. (1996). Automated preprocessing of digital seismograms: Principles and software. Version 2.2, E. Bergman, ed., Prague & Golden.
- Purcaru, G. and Berckhemer, H. (1978). A magnitude scale for very large earthquakes. *Tectonophysics*, **49**, 189-198.
- Real, C.R. and Teng, T.L. (1973). Local Richter magnitude and total signal duration in Southern California. *Bull. Seism. Soc. Am.*, **63**, 1809.
- Rezapour, M. and Pearce, R.G. (1998). Bias in surface-wave magnitude M_S due to inadequate distance corrections. *Bull. Seism. Soc. Am.*, **88**, 1, 43-61.
- Richter, C.F. (1935). An instrumental earthquake magnitude scale. *Bull. Seism. Soc. Am.*, **25**, 1-32.
- Richter, C.F. (1958). *Elementary Seismology*. Freeman, San Francisco, Calif., 578 pp.
- Savage, M.K. and Anderson, J.G. (1995). A local-magnitude scale for the Western Great Basin-Eastern Sierra Nevada from Wood-Anderson seismograms. *Bull. Seism. Soc. Am.*, **85**, 4, 1236-1243.
- Scherbaum, F. (1996). *Of poles and zeros: Fundamentals of digital seismology*. Kluwer Academic Publishers, Dordrecht/Boston/London, 257 pp.
- Seidl, D. and Berckhemer, H. (1982). Determination of source moment and radiated seismic energy from broadband recordings. *Phys. Earth Planet. Inter.*, **30**, 209-213.
- Soloviev, S.L. (1955). Classification of earthquakes in order of energy (in Russian). *Trudy Geofiz. Inst. AN SSSR*, **39**, 157, 3-31.
- Strauch, W., Wylegalla, K. (1989). POTSDAM network magnitudes of the 1985/86 Vogtland earthquakes and determination of Q from Sg-amplitudes and coda waves. In: Bormann, P. (Editor). *Monitoring and analysis of the earthquake swarm 1985/86 in the region Vogtland/Western Bohemia*. Akademie der Wissenschaften der DDR, Veröffentlichung Nr. 110 des Zentralinstituts fuer Physik der Erde, Potsdam 1989, 282 pp.
- Street (1976). Scaling northeastern United States/southeastern Canadian earthquakes by their Lg waves. *Bull. Seism. Soc. Am.*, **66**, 5, 1525-1537.
- Tinti, S., Vittori, T. and Mulargia, F. (1987). On the macroseismic magnitudes of the largest Italian earthquakes. *Tectonophysics*, **138**, 159-178.
- Tittel, B. (1977). Zur Bestimmung von Erdbebenmagnituden aus longitudinalen Kernwellen. *Gerlands Beitr. Geophysik*, **86**, 79-85.
- Topozada, T.R. (1975). Earthquake magnitude as a function of intensity data in California and Western Nevada. *Bull. Seism. Soc. Am.*, **65**, 5, 1223-1238.
- Trifunac, M.C. (1990). M_L^{SM} . Computational Mechanics Publications, 17-25.
- Tsuboi, C. (1954). Determination of the Gutenberg-Richter's magnitude of earthquakes occurring in and near Japan. *Zisin. (J. Seism. Soc. Japan)*, Ser. II, **7**, 185-193.
- Tsuboi, S., Abe, K., Takano, K. and Yamanaka, Y. (1995). Rapid determination of M_w from broadband P waveforms. *Bull. Seism. Soc. Am.*, **85**, 2, 606-613.

- Tsumara, K. (1967). Determination of earthquake magnitude from total duration of oscillation. *Bull. Earthq. Res. Inst., Tokyo*, **45**, 7-18.
- Uhrhammer, R.A., Loper, S.J. and Romanovicz, B. (1996). Determination of local magnitude using BDSN broadband records. *Bull. Seism. Soc. Am.*, **86**, 5, 1314-1330.
- Veith, K.F. and Clawson, G.E. (1972). Magnitude from short-period P-wave data. *Bull. Seism. Soc. Am.* **62**, 2, 435-452.
- von Seggern, D. (1977). Amplitude-distance relation for 20-second Rayleigh waves. *Bull. Seism. Soc. Am.*, **67**, 405-411.
- Wahlström, R. (1979). Duration magnitudes for Swedish earthquakes. Seismological Institute Uppsala, Report No. 5-79, 22 pp.
- Wahlström, R. and Strauch, W. (1984). A regional magnitude scale for Central Europe based on crustal wave attenuation. Seismological Dep. University of Uppsala, Report No. 3-84, 16 pp.
- Wells, D.L. and Coppersmith, K.J. (1994). New empirical relationships among magnitude, rupture length, rupture width, rupture area, and surface displacement. *Bull. Seism. Soc. Am.*, **84**, 4, 974-1002.
- Wendt, S. and Tittel, B. (1991). Calibration function and station corrections for PKP waves in the vicinity of a caustic. *Studia geoph. et geod.*, **35**, 213-220.
- Wendt, S. and Bormann, P. (1998). Identification and analysis of short-period core phases. Part II: Exercises. In: Bormann, P. (1998). Regional International Training Course 1997 on Seismology and Seismic Hazard Assessment. Lecture and exercise notes, Vol. 1, GeoForschungsZentrum Potsdam, Scientific Technical Report STR98/05, 141-155.
- Willmore, P.L. (1979). Manual of Seismological Observatory Practice. World Data Center A for Solid Earth Geophysics, Report SE-20, September 1979, Boulder, Colorado, 165 pp.
- Yacoub, N.K. (1998). Maximum spectral energy for seismic magnitude estimation. Part I: Rayleigh-wave magnitude. *Bull. Seism. Soc. Am.*, **88**, 4, 952-962.

SEISMIC SCALING RELATIONS

Peter Bormann

GeoForschungsZentrum Potsdam, Division of Solid Earth Physics and Disaster Research,
Telegrafenberg E428, D-14473 Potsdam, Federal Republic of Germany;
Fax: +49-331 288 1204; E-mail: course@gfz-potsdam.de

1. DEFINITION AND USE OF SEISMIC SCALING RELATIONS

Empirical or semi-empirical seismic scaling relations relate measured parameters such as magnitudes or seismic moment to each other or to independently measured or calculated, often model-dependent physical or geometrical parameters of earthquake size such as released seismic energy, intensity, stress drop, duration of rupture, area or length of rupture, fault dislocation, area of felt shaking etc. For most earthquakes these parameters appear to be related in a systematic and predictable manner and the faulting parameters are mostly inferred from theoretical "scaling laws" and similarity conditions (cf. chapter *Physical and mathematical models of seismic source processes*). Thus, seismic scaling relations and laws allow to roughly estimate seismic energy or faulting parameters from measured magnitudes or seismic moments or the latter two from field evidence of faulting parameters such as surface rupture length and/or displacement. Therefore, the knowledge of theoretically well founded scaling laws or (semi-) empirical scaling relationships is of crucial importance for both probabilistic and deterministic seismic hazard analyses. They aim at assessing the future earthquake potential of a region on the basis of data from past events, dating back as far as possible and therefore often lacking instrumental measurements of magnitude, seismic energy or moment. Specifically, one often has to make reasonable estimates of the size of the largest earthquake that might have occurred at or could be generated by a particular fault or fault segment and of the kind of seismic spectrum it might (have) irradiate(d).

In this context one has to be aware that seismic sources differ not only in their geometrical size and average slip. Also ambient stress conditions and related dominating modes of faulting, ranges of stress drop and related seismic source spectra may differ significantly from region to region. Accordingly, events of the same seismic moment may release seismic energies which differ by 2 to 3 orders. Therefore, the use of global scaling relations may not be appropriate at all for some areas. Regional scaling laws should be used therefore whenever available, particularly when inferences have to be drawn on regional seismic strain rates or on seismic hazard, the latter being mainly controlled by the frequency of occurrence and the potential of earthquakes to generate strong high-frequency motions.

2. ENERGY-MAGNITUDE-MOMENT RELATIONS

Gutenberg and Richter (1956a) gave the following relationship between seismic energy E_s (in Joule ; $1 \text{ J} = 10^7 \text{ erg}$) and the so-called unified magnitude m which is related to m_B (cf. chapter *Magnitude of seismic events*):

$$\log E_s = 2.4 m - 1.2. \quad (1)$$

(1) is supposed to have minimum of observation errors and yields, together with the relationship $m_B = 2.5 + 0.63 M_s$ in the same publication,

$$\log E_s = 1.5 M_s + 4.8. \quad (2)$$

After many revisions, Gutenberg and Richter (1956c) finally published (2) which is now most widely applied. It was also used by Kanamori (1977) in developing the seismic moment magnitude M_w (cf. section 2.4.3 in chapter *Magnitude of seismic events*). Recently, Choy and Boatwright (1995) found

$$\log E_s = 1.5 M_s + 4.4 \quad (3)$$

as the best fit to a global data set of 397 earthquakes for which they had determined E_s directly by integration of squared velocity-proportional broadband records of P-waves.

From theoretical considerations Randall (1973) derived a relationship between E_s and the local magnitude M_L which was later confirmed empirically by Seidl and Berckhemer (1982) as well as by Berckhemer and Lindenfeld (1986). On the basis of direct energy calculations for earthquakes from the Friuli region, Italy, using digital broadband records of the Gräfenberg array in Germany, the latter got:

$$E_s \sim 2.0 M_L. \quad (4)$$

This is very close to the early empirical findings by Gutenberg and Richter (1956a) ($E_s \sim 1.92 M_L$) for southern California and the more recent one by Kanamori et al. (1993). The latter got

$$\log E_s = 1.96 M_L + 2.05 \quad (5)$$

for the magnitude range $1.5 < M_L < 6.0$. For $M_L > 6.5$ M_L saturates.

For short-period body wave magnitudes m_b Sadovsky et al. (1986) found the relationship

$$\log E_s = 1.7 m_b + 2.3 \quad (6)$$

which is said to be applicable for both earthquakes and underground explosions.

Note: According to the coefficient in the above eqs. one unit of magnitude increase in M_s , m_b , M_L and m_B , respectively, corresponds to an increase of E_s by a factor of about 32, 50, 100 and 250 times!

In this context one should mention that in the USSR the so-called Rautian (1960) energy scale $K = \log E_s$ (with E_s in J) is widely used and given in the catalogues. It is based on the same elements as any other magnitude scale such as an empirical calibration function and a reference distance (here 10 km). K relates to magnitude M via

$$K = 1.8 M + 4. \quad (7)$$

Riznichenko (1992) summarised data and relationships published by many authors (cf. Fig. 1) between magnitude M and K on the one hand and $\log M_o$ on the other hand. Depending on the range of distance and size M stands here for M_L , m_b , m_B or M_s .

Kanamori (1983) published linear relationships between $\log E_s$ and $\log M_0$ for both shallow and intermediate to deep events (cf. Fig. 2). They are rather similar and correspond, in the average, to the relationship $E_s/M_0 = 5 \times 10^{-5}$ which he used in the development of the moment magnitude scale M_w (Kanamori 1977).

But it had been mentioned earlier in section 2.4.3 of the chapter on *Magnitude of seismic events* that later investigations have revealed sometimes significant deviations from this average E_s/M_0 - relationship (e.g. Kikuchi and Fukao, 1988). This is due to local and regional differences in source mechanism, stress drop, time history of the rupture process etc. It makes global correlation relationships of this type often unsuitable for drawing inferences on regional differences in long-term regional tectonic deformation and stress accumulation rates on the one hand or on seismic hazard in the range of higher frequencies, which cause most of the earthquake damages and are more relevant for earthquake engineers, on the other hand.

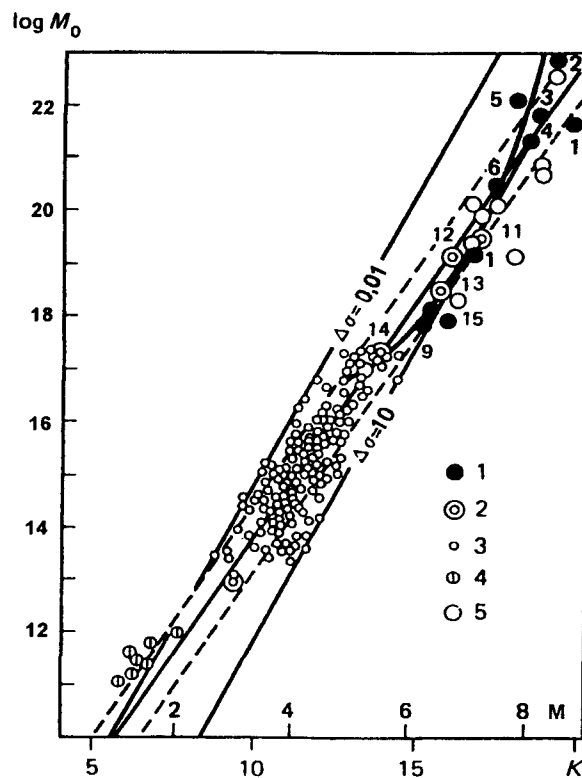


Fig. 1: Correlation between seismic moment M_0 (in $\text{Nm} = \text{J}$), magnitude M and Rautian's (1960) energetic class K according to a compilation of data from many authors. Related stress drop $\Delta\sigma$ has been given in MPa (full straight lines). Broken lines mark the 68% confidence interval. 1 - large global earthquakes; 2 - average values for individual regions; 3 - earthquakes in the western USA; 4 - microearthquakes in Nevada; 5 - M_0 determinations from field data; 6 to 15 - individual values from earthquakes in different regions. (Modified from Riznichenko, 1992.)

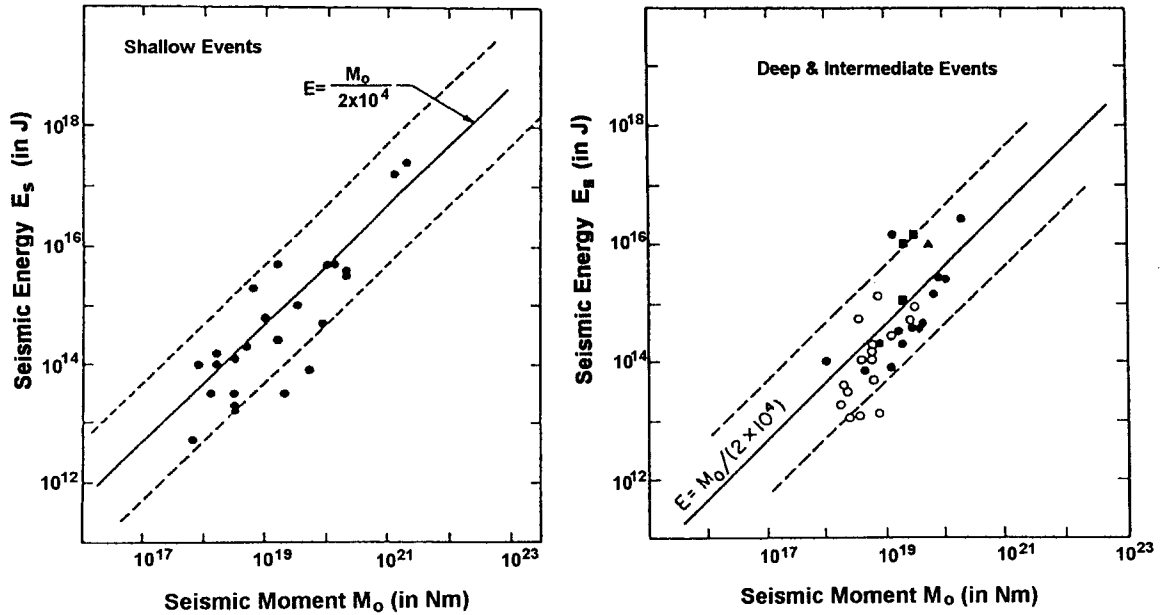


Fig. 2: Relations between seismic moment M_0 and energy E_s for shallow events (left) and intermediate to deep events (right) according to Vassiliou and Kanamori (1982). The solid line indicates the relation $E_s = M_0 / (2 \times 10^4)$ suggested by Kanamori (1977) on the basis of elastostatic considerations. (Modified from Kanamori, 1983 in *Tectonophysics*, Vol. 93, p. 191 and 192, with permission from Elsevier Science).

3. MOMENT-MAGNITUDE RELATIONS

Global relations between M_s and M_0 were derived by Ekström and Dziewonski (1988) from high quality determinations of M_0 from the Global Digital Seismic Network (GDSN). They are given below, as for all other relations with M_0 , in $\text{Nm} = \text{J}$ ($1 \text{ Nm} = 10^7 \text{ dyn cm} = 10^7 \text{ ergs}$):

$$M_s = \log M_0 - 12.24 \quad \text{for} \quad M_0 < 3.2 \times 10^{17}, \quad (8)$$

$$M_s = -19.24 + \log M_0 - 0.088 (\log M_0 - 24.5)^2 \quad \text{for} \quad 3.2 \times 10^{17} \leq M_0 < 2.5 \times 10^{19}, \quad (9)$$

$$M_s = -10.73 + 0.667 \log M_0 \quad \text{for} \quad M_0 \geq 2.5 \times 10^{19}. \quad (10)$$

Note that all these relations are single random parameter regression solutions. Solving them for $\log M_0$ may overestimate moments for the larger events and underestimate M_0 for smaller earthquakes.

Chen and Chen (1989) published detailed global relations between M_0 and M_s , m_b and M_L , respectively, based on data for about 800 earthquakes in the magnitude range $0 < M < 8.6$. These authors also showed, that their empirical data are well fitted by theoretical scaling relations derived from a modified Haskell model of a rectangular fault which produces displacement spectra with three corner frequencies. Similar global scaling relations had been derived earlier by Geller (1976), also based on the Haskell (1964 and 1966) model. In both papers these relations show saturation for M_L at about 6.3, for m_b between about 6.0 and 6.5 and for M_s between about 8.2 and 8.5.

Other global relationships between M_o and M_s were derived from Chen and Chen (1989) from a theoretical scaling law based on a modified Haskell source model. They fit well a set of global data with a standard deviation of individual values $\log M_o$ of about ± 0.4 and confirm the saturation of M_s at about 8.5:

$$\log M_o = 1.0 M_s + 12.2 \quad \text{for} \quad M_s \leq 6.4, \quad (11)$$

$$\log M_o = 1.5 M_s + 9.0 \quad \text{for} \quad 6.4 < M_s \leq 7.8, \quad (12)$$

$$\log M_o = 3.0 M_s - 2.7 \quad \text{for} \quad 7.8 < M_s \leq 8.5, \quad (13)$$

and $M_s = 8.5 = \text{const.}$ for $\log M_o > 22.8 \text{ Nm}$.

Also M_s - M_o relations (and vice versa) show regional variability. Ambraseys (1990) could show, that the global relations (8) - (10) underestimate systematically M_s determinations for events in the Alpidic region of Europe and adjacent areas by about 0.2 magnitude units in the average. Abercrombie (1994) discussed possible reasons for the anomalously high surface-wave magnitudes of continental earthquakes relative to their seismic moment. This illustrates the need for regional scaling of moment-magnitude relationships even in the relatively long-period range.

For M_o and body-wave magnitudes m_b (of 1s period) Chen (1989) give the following global scaling relations (with saturation at $m_b = 6.5$ for $\log M_o > 20.7$):

$$\log M_o = 1.5 m_b + 9.0 \quad \text{for} \quad 3.8 < m_b \leq 5.2, \quad (14)$$

$$\log M_o = 3 m_b + 1.2 \quad \text{for} \quad 5.2 < m_b \leq 6.5, \quad (15)$$

and for M_o and M_L for California (with saturation at $M_L = 6.3$ for $\log M_o > 20.1$):

$$\log M_o = M_L + 10.5 \quad \text{for} \quad M_L \leq 3.6, \quad (16)$$

$$\log M_o = 1.5 M_L + 8.7 \quad \text{for} \quad 3.6 < M_L \leq 5.0, \quad (17)$$

$$\log M_o = 3 M_L + 1.2 \quad \text{for} \quad 5.0 < M_L \leq 6.3. \quad (18)$$

Average scaling relations between m_b , M_s and M_o for plate-margin earthquakes have been derived by Nuttli (1985). They yield practically identical values as the equations (11)-(13) for M_o when M_s is known while the deviations are not larger than about a factor of 2 when using m_b and eqs. (14) and (15).

The need for regional relationships between M_o and magnitudes is particularly evident in case of M_L . When calculating M_o according to (16) and (17) for California and comparing them with the values calculated for a relationship given by Kim et al. (1989) give for the Baltic Shield

$$\log M_o = 1.01 M_L + 9.93 \quad \text{for} \quad 2.0 \leq M_L \leq 5.2 \quad (19)$$

then we get for $M_L = 2.0, 4.0$ and 5.0 , respectively, values for M_o which are 3.5, 5.4 and 16.6 times larger for California than for the Baltic Shield. Using instead an even more local

relationship for travel paths within the Great Basin of California (Chávez and Priestley, 1985), namely

$$\log M_0 = 1.2 M_L + 10.49 \quad \text{for} \quad 1 \leq M_L \leq 6 \quad (20)$$

then we get for the same magnitudes even 9, 21 and 32 times larger values than for the Baltic Shield according to (19).

4. SCALING RELATIONS OF M , M_0 AND E_s WITH FAULT PARAMETERS

Scaling relations of magnitudes, seismic moments and energy with fault parameters are used in two ways:

- 1) to get a rough estimate of relevant fault parameter when M , M_0 or E_s of the event are known from the evaluation of instrumental recordings or
- 2) in order to get a magnitude, moment and/or energy estimates for historic or even prehistoric events for which no recordings are available but some fault parameters such as (maximum possible) length of surface rupture and/or amount of surface displacement can still be determined from field evidence.

The latter is particularly important for improved assessment of seismic hazard and of the maximum possible earthquake, especially in areas with long mean return periods for strong seismic events. Of particular importance for hazard assessment are also relationships between macroseismic intensity I and magnitude M on the one hand (cf. eqs. (28) to (34) in chapter *Magnitude of seismic events*) and between ground acceleration and I or M , on the other hand (cf. chapter *Macroseismic and strong-motion parameters*). Unfortunately, the measured maximum accelerations for equal values of intensity I scatter in the whole range of $I = \text{III}$ to IX by about two orders of magnitude (Ambraseys, 1975). The reason for this scatter is many-fold, e.g. human perception is strongest for frequencies around 3 Hz while acceleration and damage might be strongest for more high frequent ground motions. Also, damage is not strictly related to peak acceleration only but also depends its frequency with respect to the natural period of the shaken structures and on the duration of strong ground shaking. For some structures damage is also more closely related to strong ground-motion displacement or velocity and not to acceleration.

Respective relationships, especially those between the various source parameters, are mostly based on model assumptions on the fault geometry, rupture velocity and time history, ambient stress and stress drop etc. But sometimes they can, at least partially, be confirmed or constrained by field evidence or petrophysical laboratory experiments. As for other scaling relations discussed above, global relationships can give only a rough orientation since the scatter of data is considerable due to the many influencing factors and their regional variability. Whenever possible, regional relationships should be developed.

Sadovsky et al. (1986) found that for both crustal earthquakes and underground explosions the following relationship holds between seismic energy E_s (in erg) and the seismic source volume V_s (in cm^3):

$$\log E_s = 3 + \log V_s \quad (21)$$

with V_s for earthquakes being estimated from the linear dimensions of the aftershock zone. This means, that the critical energy density in sources of both natural and artificial crustal

earthquakes is about equal and roughly 10^3 erg/cm^3 or 100 J/m^3 , that it does not depend on the energy released by the event and that E_s increases only on the account of volume increase of the source. Accordingly, not the type of seismic source but the properties of the medium play the decisive role in the formation of the seismic wave field. With respect to this the modifying influence of ambient stress and related stress drop $\Delta\sigma \approx 2\mu E_s/M_0$ had been mentioned already earlier (cf. sections 2.4.2 and 2.4.3 in chapter *Magnitude of seismic events*).

Fig. 4 shows the relation between seismic moment M_0 and the area A_r of fault rupture as published by Kanamori and Anderson (1975). It is controlled by the stress drop $\Delta\sigma$; the larger $\Delta\sigma$ the greater is M_0 for a given rupture area. One recognises that intraplate earthquakes have in the average a higher stress drop (around 10 MPa = 100 bars) than interplate events (around 3 MPa).

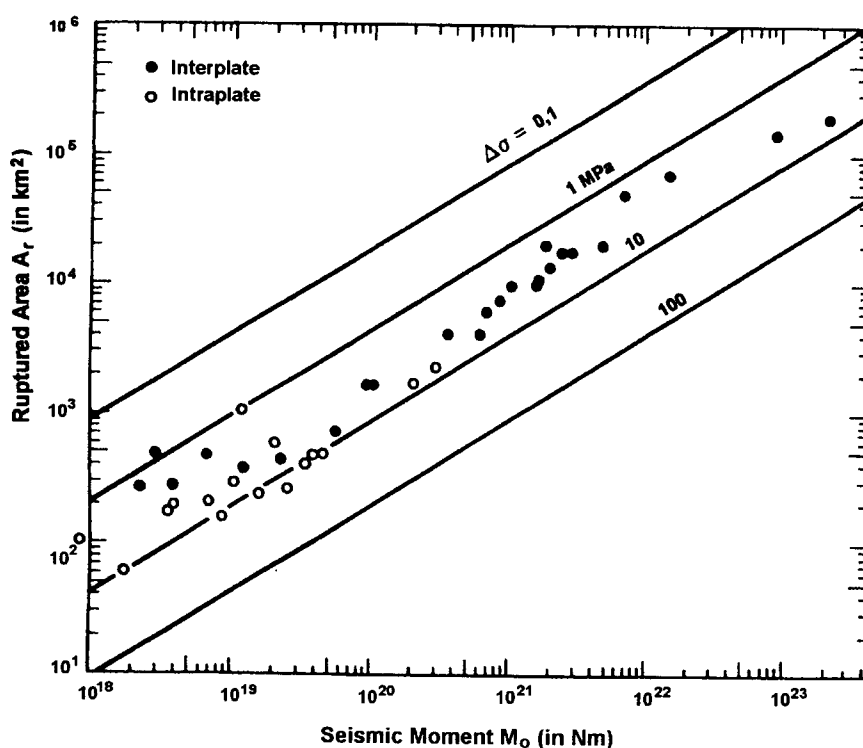


Fig. 4: Relation between area of fault rupture A_r and seismic moment M_0 for inter- and intraplate earthquakes. The solid lines give the respective relationships for different stress drop $\Delta\sigma$ (in MPa; $1 \text{ Pa} = 10^5 \text{ bars}$). (Modified from Kanamori and Anderson, 1975.)

The data in Fig. 4 are well fitted by the average relationship suggested by Abe (1975):

$$M_0 = 1.33 \times 10^{15} A_r^{3/2} \quad (22)$$

which is nearly identical with the correlation relation by Purcaru and Berckhemer (1982):

$$\log M_0 = (1.5 \pm 0.02) \log A_r + (15.25 \pm 0.05) \quad (23)$$

with M_0 in Nm and A_r in km^2 . (23) corresponds to the theoretical scaling relation derived by Chen and Chen (1989) for a modified Haskell model with the assumption $L = 2W$ (L - length and W - width of fault rupture, $A_r = LW = 0.5 L^2$) and an average displacement $\bar{D} = 4.0 \times 10^{-5} L$. Note that experimental data indicate also other aspect ratios L/W up to about 30 (e.g. Purcaru and Berckhemer, 1982). Wells and Coppersmith (1994) gave another relation between moment magnitude and A_r :

$$M_w = (0.98 \pm 0.03) \log A_r + (4.07 \pm 0.06) \quad (24)$$

derived from a very comprehensive data base of source parameters for historical shallow-focus earthquakes ($h < 40$ km) in continental interplate or intraplate environments.

There also exists a log-log-linear relation between L and M_0 . Interestingly, for a given seismic moment L is in the average about 6 times larger for interplate (strike-slip) events than for intraplate ones (cf. Fig. 5). The ratio α between average fault displacement (slip) \bar{D} and fault length L is according to Scholz et al. (1986) $\alpha \approx 1 \times 10^{-5}$ for interplate and $\alpha \approx 6 \times 10^{-5}$ for intraplate events. Since this result is independent of the type of fault mechanism this implies that intraplate faults have a higher frictional strength (and thus stress-drop) than plate boundary faults but smaller length for the same seismic moments.

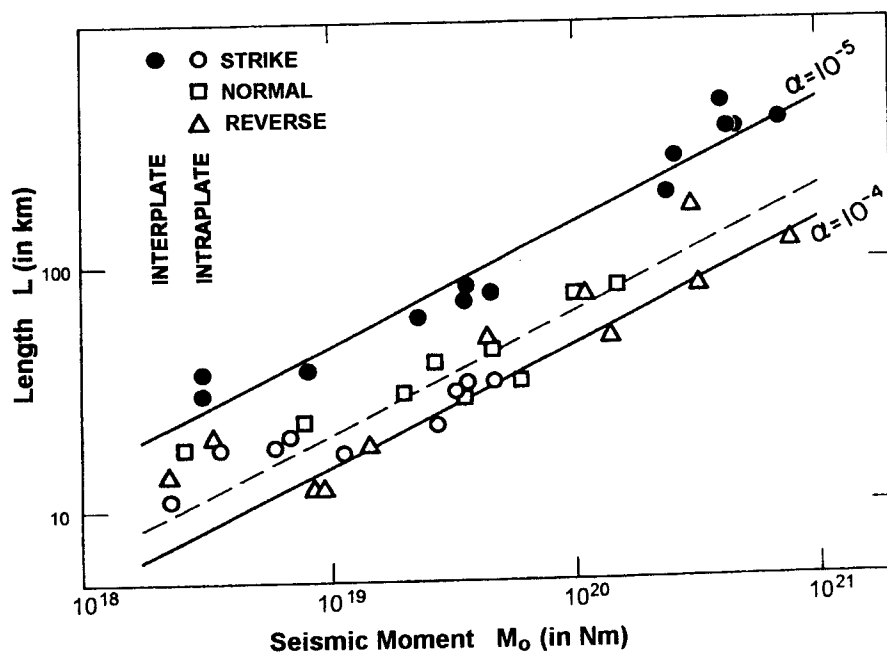


Fig. 5: Fault length L versus seismic moment M_0 for large inter- and intraplate earthquakes. The solid lines give the respective relationship for the ratio $\alpha = \bar{D}/L$. (Modified from Scholz et al., 1986.)

The slope of the curves in Fig. 5 is 0.5. This corresponds to a relation $M_0 \sim L^2$ (Scholz 1982; Pegeler and Das, 1996) which is valid for large earthquakes only ($M >$ about 6.5 to 7). Then the width W of the fault is already saturated, i.e. equal to the thickness of the brittle fracturing zone in the lithosphere. Depending on heat flow and composition this seismogenic zone in the

earth crust is about 10 to 30 km thick. Accordingly, for large earthquakes, the fault area growth with increasing M_0 in length direction only.

Recently, there has been some serious debate on the scaling of large earthquakes and their ratio α (Scholz, 1994 and 1997; Romanowicz 1994; Romanowicz and Rundle, 1993 and 1994; Sornette and Sornette, 1994; Wang and Ou, 1998). Romanowicz (1992), who prefers to scale slip not with length but with width, even gives a relationship of $M_0 \sim L$ in case of very large earthquakes. Contrary to this, Hanks (1977) showed that earthquakes with rupture dimensions smaller than this seismogenic thickness scale according to $M_0 \sim L^3$ which is equivalent to (21).

According to an older data compilation shown in Fig. 6 the correlation between source length L , magnitude M and energetic class K is not very good. Relations given by various authors for events in different environment differ often strongly.

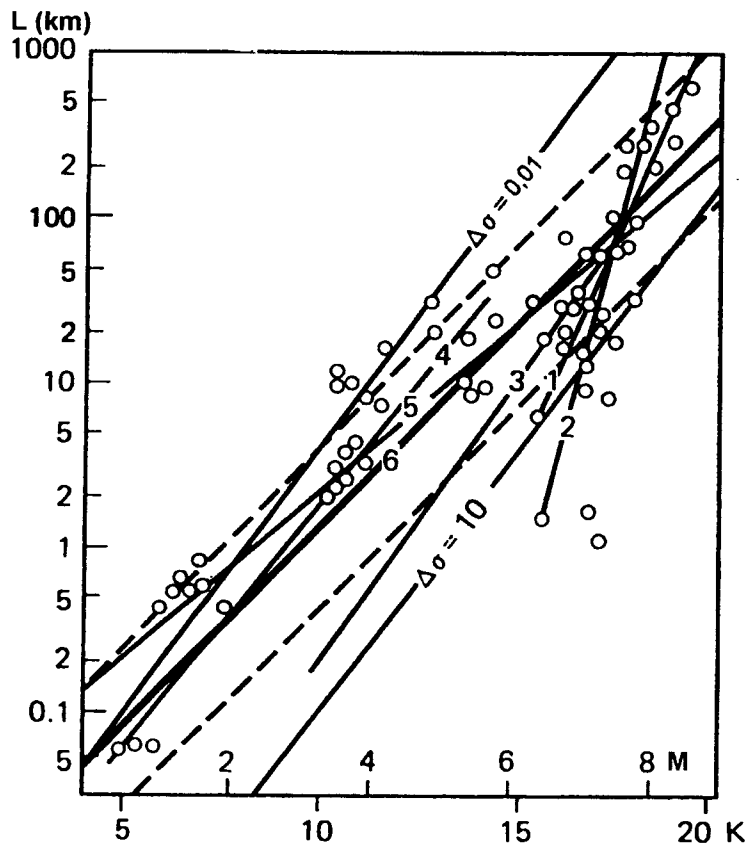


Fig. 6: Correlation of source length L with magnitude M and energetic class K according to data from various sources (e.g. curve 1 by Tocher, 1958, curve 2 by Iida, 1959; curve 6 average by Riznichenko, 1992). Thin straight lines: related stress drops $\Delta\sigma$ are given in MPa; broken lines mark the limits of the 68% confidence interval with respect to the average curve 6). (Modified from Riznichenko, 1992).

Ambraseys (1988) published relationships derived from the dimensions of fault surface ruptures for Eastern Mediterranean and Middle Eastern earthquakes (with L - observed fault length in km, \bar{D} - relative fault displacement in cm, M_{SC} - predicted surface wave magnitudes):

$$M_{SC} = 1.43 \log L + 4.63 \quad (25)$$

and

$$M_{SC} = 0.4 \log (L^{1.58} \bar{D}^2) + 1.1. \quad (26)$$

They yield results which are in good agreement with those by Nowroozi (1985) for Iran but they differ significantly from the respective relations given by by Tocher (1958) for Western USA and from Iida (1959) for Japan (cf. curves 1 and 2 in Fig. 6).

Khromovskikh (1989) analysed available data for more than 100 events of different faulting type and from different seismotectonic regions of the earth and derived from them 7 different relationships between magnitude M and the length L of the rupture zone, amongst them those for the following regions:

a) the Circum-Pacific belt: $M = (0.96 \pm 0.25) \log L + (5.70 \pm 0.34)$ (27)

b) the Alpine fold belt: $M = (1.09 \pm 0.28) \log L + (5.39 \pm 0.42)$ (28)

c) rejuvenated platforms: $M = (1.25 \pm 0.19) \log L + (5.45 \pm 0.28)$ (29)

and compared them with respective relationships of other authors for similar areas.

Other relationships which allow to estimate L (in km) when M_s is known were derived by Chen and Chen (1989) on the basis of their general scaling law based on the modified Haskell source model. These relationships clearly show the effect of width saturation:

$$\log L = M_s/3 - 0.873 \quad \text{for} \quad M_s \leq 6.4 \quad (30)$$

$$\log L = M_s/2 - 1.94 \quad \text{for} \quad 6.4 < M_s \leq 7.8 \quad (31)$$

$$\log L = M_s - 5.84 \quad \text{for} \quad 7.8 < M_s \leq 8.5. \quad (32)$$

The same authors also gave similar relations between the average dislocation \bar{D} (in m) and M_s , namely:

$$\log \bar{D} = M_s/3 - 2.271 \quad \text{for} \quad M_s \leq 6.4 \quad (33),$$

$$\log \bar{D} = M_s/2 - 3.34 \quad \text{for} \quad 6.4 < M_s \leq 7.8 \quad \text{and} \quad (34)$$

$$\log \bar{D} = M_s - 7.24 \quad \text{for} \quad 7.8 < M_s \leq 8.5 \quad (35)$$

while Chinnery (1969) derived from still sparse empirical data a linear relation between magnitude M and $\log \bar{D}$ (with \bar{D} in m) for the whole range $3 < M < 8.5$

$$M = 1.32 \log \bar{D} + 6.27 \quad (36)$$

which changes to

$$M = 1.04 \log \bar{D} + 6.96 \quad (37)$$

when only large magnitude events are considered.

Probably best established are the respective correlation relations which Wells and Coppersmith (1994) have determined for shallow-focus (crustal) continental interplate or intraplate earthquakes on the basis of a rather comprehensive data base of historical events. Since most of these relations for strike-slip, reverse and normal faulting events were not statistically different (at a 95% level of significance) their average relations for all slip types are considered to be appropriate for most applications. Best established are the relationships between moment magnitude M_w and rupture area (cf. eq. (24)), surface rupture length (SRL) and subsurface rupture length (RLD) (both in km). They have the strongest correlations ($r = 0.89$ to 0.95) and the least data scatter:

$$M_w = (1.16 \pm 0.07) \log (\text{SRL}) + (5.08 \pm 0.10) \quad (38)$$

$$M_w = (1.49 \pm 0.04) \log (\text{RLD}) + (4.38 \pm 0.06) \quad (39)$$

$$\log (\text{SLR}) = (0.69 \pm 0.04) M_w - (3.22 \pm 0.27) \quad (40)$$

$$\log (\text{RLD}) = (0.59 \pm 0.02) M_w - (2.44 \pm 0.11) \quad (41).$$

Comparing (40) and (41) it follows that in general the surface rupture length is only about 75% of the subsurface rupture length.

The correlations between M_w and \bar{D} as well as \bar{D} and SLR are somewhat smaller ($r = 0.71$ to 0.78):

$$M_w = (0.82 \pm 0.10) \log \bar{D} + (6.693 \pm 0.05) \quad (42)$$

$$\log \bar{D} = (0.69 \pm 0.08) M_w - (4.80 \pm 0.57) \quad (43)$$

$$\log \bar{D} = (0.88 \pm 0.11) \log (\text{SLR}) - (1.43 \pm 0.18) \quad (44)$$

$$\log (\text{SLR}) = (0.57 \pm 0.07) \log \bar{D} + (1.61 \pm 0.04). \quad (45)$$

Wells and Coppersmith (1994) reason that the weaker correlation may reflect the wide range of displacement values for a given rupture length (differences up to a factor 50 in their data set!). These authors also give relations between SLR and the maximum surface displacement which is, in the average, twice the observed average surface displacement while the average subsurface slip ranges between the maximum and average surface displacement.

Chen and Chen (1989) derived from their scaling law also the following values:

- rupture velocity $v_r = 2.65$ km/s;
 - total rupture time T_r (in s) = 0.35 (s/km) \times L (km)
 - slip velocity $dD/dt = (2.87 - 11.43)$ m/s.
- (46)

As does slip also slip velocity varies strongly. From teleseismic studies we can obtain only spatially and temporally averaged values of fault motion but the actual co-seismic slip is largely controlled by spatial heterogeneities along the fault rupture (cf. Fig. 8 in chapter *Introduction to seismic sources and source parameters*). Large slip velocities over 10 m/s suggest very high local stress drop of more than 10 MPa. (cf. Yomogida and Nakata, 1994).

On the other hand, sometimes very slow earthquakes may occur with very large seismic moment but low seismic energy radiation (e.g. "tsunami earthquakes"). This has special relevance when deriving scaling relations suitable for the prediction of strong ground motions (e.g. Fukushima, 1996).

Scaling relationships between fault parameters, especially between D and L , are also controlled by the fault growth history and age and whether the event can be considered to be a single and rare or a composite and frequent one (e.g. Dawers et al., 1993; Tumarkin et al., 1994). There exist also scaling relations between fault length and recurrence interval which are of particular relevance for seismic hazard assessment (e.g. Marrett, 1994).

Using eqs. (25), (27), (28), (29) and (38) one gets for a surface rupture length of 100 km magnitudes $M = 7.5, 7.7, 7.6, 7.95,$ and $7.4,$ respectively. Knowing the M_s or M_w and calculating L and \bar{D} according to eqs. (31)-(35), (40) and (43) one gets for magnitude 7.0 $L = 36.3$ km and 40.7 km, $\bar{D} = 1,4$ m and $1,07$ m and for magnitude 8.0 $L = 144.5$ km and 199.5 km, $\bar{D} = 3,8$ m and 5.2 m. The good agreement of the calculated values for magnitudes 7 and the stronger disagreement for magnitudes 8 are obviously due to the growing difference between M_s (used in the relations by Chen and Chen, 1989) and M_w (used in the relations by Wells and Coppersmith, 1994) for $M_s > 7$ (saturation effect).

For the rupture duration we get according to (61) for $M_s = 7$ and 8 approximately 13 s and 51 s, respectively.

5. SIMILARITY CONDITIONS

Under certain assumptions there exist several conditions of static (geometric) and dynamic similarity. With the assumption of a constant stress drop one gets

$$W/L = k_1 \quad \text{i.e. a constant fault aspect ratio} \quad \text{and} \quad (47)$$

$$\bar{D}/L = k_2 \quad \text{i.e. constant strain } \alpha. \quad (48)$$

One can combine (47) and (48) with the definition of the seismic moment $M_o = \mu \bar{D} W L = \mu k_1 k_2 L^3$ and gets $M_o \sim L^3$ which is valid for source dimensions smaller than the thickness of the seismogenic layer. Besides this there is a dynamic similarity, namely, the rise time t_r required for reaching the total displacement, i.e. the duration of the source-time function, is

$$t_r = k_3 \times L/v_{cr} \quad (49)$$

with v_{cr} the crack or rupture velocity (cf. Fig. 4 in chapter *Introduction to seismic sources and source parameters*). This is equivalent to the relationship (48) of constant strain. Lay and Wallace (1995) showed that this results in period-dependent amplitudes of seismic waves which scale with the fault dimension. For periods $T \gg t_r$ the amplitude does not depend on fault length L . This corresponds to the plateau of the "source displacement spectrum". But if $T \ll t_r$ then the amplitudes scale as $1/L^2$ or f^{-2} (cf. Fig. 5 in the same chapter). This explains the saturation effect when analysing frequencies higher than the corner frequency of the source spectrum.

REFERENCES

- Abe, K. (1975). Reliable estimation of the seismic moment of large earthquakes. *J. Phys. Earth*, **23**, 381-390.
- Abercrombie, R.E. (1994). Regional bias in estimates of earthquake M_s due to surface-wave path effects. *Bull. Seism. Soc. Am.*, **84**, 2, 377-382.
- Ambroseys, N.N. (1975) The correlation of intensity with ground motion. Proc. XIV General Ass. ESC 1974 in Trieste, Published by Nationalkomitee für Geodäsie und Geophysik, Akademie der Wissenschaften der DDR, Berlin 175, 335-341.
- Ambraseys, N.N. (1985). Magnitude assessment of northwestern European earthquakes. *Earthquake Engineering and Structural Dynamics*, **13**, 307-320.
- Ambraseys, N.N. (1988). Magnitude-fault length relationships for earthquakes in the middle east. In: *Historical seismograms and earthquakes of the world*. Academic Press, 309-310.
- Ambraseys, N.N. (1990). Uniform magnitude re-evaluation of European earthquakes associated with strong-motion records. *Earthquake Engineering and Structural Dynamics*, **19**, 1-20.
- Berckhemer, H. and Lindendorf, M. (1986). Determination of source energy from broadband seismograms. In: Buttkus, B. (Ed.). *Ten years of the Gräfenberg Array: Defining the frontiers of broadband seismology*. Geologisches Jahrbuch Reihe E, Heft 35, 79-83.
- Bormann, P. and Khalturin, V.I. (1975). Relations between different kinds of magnitude determinations and their regional variations. *Proceed. XIVth General Assembly of the European Seismological Commission, Trieste, 16-22 September 1974*. Nationalkomitee für Geodäsie und Geophysik, AdW der DDR, Berlin 1975, 27-39.
- Chen, P. and Chen H. (1989). Scaling law and its applications to earthquake statistical relations. *Tectonophysics*, **166**, 53-72.
- Chinnery, M.A. (1969). Earthquake magnitude and source parameters. *Bull. Seism. Soc. Am.*, **59**, 5, 1969-1982.
- Choy, G.L. and Boatwright, J.L. (1995). Global patterns of radiated seismic energy and apparent stress. *J. Geophys. Res.*, **100**, B2, 18205-18228.
- Dawers, N.H., Anders, M.H. and Scholz, C.H. (1993). Growth of normal faults: Displacement-length scaling. *Geology*, **21**, 1107-1110.
- Fukushima, Y. (1996). Scaling relations for strong ground motion prediction models with M^2 terms. *Bull. Seism. Soc. Am.*, **86**, 2, 329-336.
- Geller, R.J. (1976). Scaling relations for earthquake source parameters and magnitudes. *Bull. Seism. Soc. Am.*, **56**, 5, 1501-1523.
- Gutenberg, B. and Richter, C.F. (1956a). Magnitude and energy of earthquakes. *Annali di Geofisica*, **9**, 1, 1-15.
- Gutenberg, B. and Richter, C.F. (1956b). Earthquake magnitude, intensity, energy and acceleration. *Bull. Seism. Soc. Am.*, **46**, 105-145.
- Gutenberg, B. and Richter, C.F. (1956c). The energy of earthquakes. *Q. J. Geol. Soc. London*, **112**, 1-14.
- Hanks, T.C. (1977). Earthquake stress drops, ambient tectonic stress, and the stresses that drive plate motion. *Pure Appl. Geophys.*, **115**, 441-458.
- Haskell, N.A. (1964). Total energy and energy spectral density of elastic wave radiation from propagating faults. *Bull. Seism. Soc. Am.*, **54**, 1811-1841.
- Haskell, N. A. (1966). Total energy and energy spectral density of elastic wave radiation from propagating faults. Part II. A statistical fault model. *Bull. Seism. Soc. Am.*, **56**, 125-140.
- Iida, K. (1959). Earthquake energy and earthquake fault length. *J. Earth Sci., Nagoya Univ.*, **7**, 98-107.

- Kanamori, H. (1977). The energy release in great earthquakes. *J. Geophys. Res.*, **82**, 2981-2987.
- Kanamori, H. and Anderson, D.L. (1975). Theoretical basis of some empirical relations in seismology. *Bull. Seism. Soc. Am.*, **65**, 1073-1095.
- Kanamori, H. and Jennings, P.C. (1978). Determination of local magnitude, M_L , from strong motion accelerograms. *Bull. Seism. Soc. Am.*, **68**, 471-485.
- Kanamori, H. (1983). Magnitude scale and quantification of earthquakes. *Tectonophysics*, **93**, 185-199.
- Kanamori, H., Mori, J., Hauksson, E., Heaton, Th.H., Hutton, L.K. and Jones, L.M. (1993). Determination of earthquake energy release and M_L using TERRASCOPE. *Bull. Seism. Soc. Am.*, **83**, 2, 330-346.
- Kikuchi, M. and Fukao, Y. (1988). Seismic wave energy inferred from long-period body wave inversion. *Bull. Seism. Soc. Am.*, **78**, 5, 1707-1724.
- Kim, W.-Y., Wahlström, R. and Uski, M. (1989). Regional spectral scaling relations of source parameters for earthquakes in the Baltic Shield. *Tectonophysics*, **166**, 151-161.
- Lay, T. and Wallace, T.C. (1995). *Modern global seismology*. Academic Press, 521 pp.
- Marrett, R. (1994). Scaling of intraplate earthquake recurrence interval with fault length and implications for seismic hazard assessment. *Geophys. Res. Letters*, **21**, 24, 2637-2640.
- Nowroozi, A. (1985). Empirical relations between magnitudes and fault parameters for earthquakes in Iran. *Bull. Seism. Soc. Am.*, **75**, 1327-1338.
- Nuttli, O.W. (1985). Average seismic source-parameter relations for plate-margin earthquakes. *Tectonophysics*, **118**, 161-174.
- Pegeler, G. and Das, S. (1996). Analysis of the relationship between seismic moment and fault length for large crustal strike-slip earthquakes between 1977-92. *Geophys. Res. Letters*, **23**, 905-908.
- Purcaru, G. and Berckhemer, H. (1982). Quantitative relations of seismic source parameters and a classification of earthquakes. *Tectonophysics*, **84**, 57-128.
- Randall, M.J. (1973). The spectral theory of seismic sources. *Bull. Seism. Soc. Am.*, **63**, 1133-1144.
- Rautian, T.G. (1960). In: *Methods of the detailed study of seismicity (in Russian)*. Moscow, Izd. AN SSSR, **176**, 75-114.
- Riznichenko, Yu. V. (1992). *Problems of seismology*. Mir and Springer Publishers, Moscow and Berlin-Heidelberg-New York, 445 pp. (English translation of the original Russian publication of 1985).
- Romanowicz, B. (1992). Strike-slip earthquakes on quasi-vertical transcurrent faults: inferences for general scaling relations. *Geophys. Res. Letters*, **19**, 481-484.
- Romanowicz, B. (1994). *Comment and Reply*: Comment on "A reappraisal of large earthquake scaling" by C. Scholz. *Bull. Seism. Soc. Am.*, **84**, 5, 1675-1676.
- Romanowicz, B. and Rundle, J.B. (1993). On scaling relations for large earthquakes. *Bull. Seism. Soc. Am.*, **83**, 1294-1297.
- Romanowicz, B. and Rundle, J.B. (1994). Reply to comment on "On scaling relations for large earthquakes by Romanowicz and Rundle" from the perspective of a recent non-linear diffusion equation linking short-time deformation to long-time tectonics. *Bull. Seism. Soc. Am.*, **84**, 5, 1684.
- Sadovsky, M.A., Kedrov, O.K. and Pasechnik, I.P. (1986). On the question of energetic classification of earthquakes (in Russian). *Fizika Zemli*, Moscow, **2**, 3-10.
- Scholz, C.H. (1982). Scaling laws for large earthquakes: consequences for physical models. *Bull. Seism. Soc. Am.*, **72**, 1-14.
- Scholz, C.H. (1986). Scaling differences between large interplate and intraplate earthquakes. *Bull. Seism. Soc. Am.*, **76**, 1, 65-70.

- Scholz, C.H. (1994). Reply to comment on "A reapraisal of large earthquake scaling" by C. Scholz. *Bull. Seism. Soc. Am.*, **84**, 5, 1677-1678.
- Scholz, C.H. (1997). Size distributions for large and small earthquakes. *Bull. Seism. Soc. Am.*, **87**, 4, 1074-1077.
- Scholz, C.H., Aviles, C.A. and Wesnousky, S.G. (1986). *Bull. Seism. Soc. Am.*, **76**, 1, 65-70.
- Seidl, D. and Berckhemer, H. (1982). Determination of source moment and radiated seismic energy from broadband recordings. *Phys. Earth Planet. Inter.*, **30**, 209-213.
- Sornette, D. and Sornette, A. (1994). Comment on "On scaling relations for large earthquakes by Romanowicz and Rundle" from the perspective of a recent non-linear diffusion equation linking short-time deformation to long-time tectonics. *Bull. Seism. Soc. Am.*, **84**, 5, 1679-1683.
- Tocher, D. (1958). Earthquake energy and ground breakage. *Bull. Seism. Soc. Am.*, **48**, 147-153.
- Tumarkin, A.G., Archuleta, R.J. and Madariaga, R. (1994). Scaling relations for composite earthquake models. *Bull. Seism. Soc. Am.*, **84**, 4, 1279-1283.
- Vassiliou, M.S. and Kanamori, H. (1982). The energy release in earthquakes. *Bull. Seism. Soc. Am.*, **72**, 371-387.
- Wang, J.-H. and Ou, S.-S. (1998). On scaling earthquake faults. *Bull. Seism. Soc. Am.*, **88**, 3, 758-766.
- Wells, D.L. and Coppersmith, K.J. (1994). New empirical relationships among magnitude, rupture length, rupture width, rupture area, and surface displacement. *Bull. Seism. Soc. Am.*, **84**, 4, 974-1002.
- Yomogida, K. and Nakata, T. (1994). Large slip velocity of the surface rupture associated with the 1990 Luzon earthquake. *Geophysical Res. Letters*, **21**, 17, 1799-1802.

DETERMINATION OF FAULT PLANE SOLUTIONS

Michael Baumbach, Peter Bormann and Helmut Grosse

GeoForschungsZentrum Potsdam, Division 2: Solid Earth Physics and Disaster Research
Telegrafenberg, D-14473 Potsdam, Germany

1. INTRODUCTION

The direction (polarity) and amplitude of motion of a seismic wave arriving at a distant station depends both on the wave type considered and the position of the station relative to the motion in the earthquake source. This is illustrated by Figs. 1a and b.

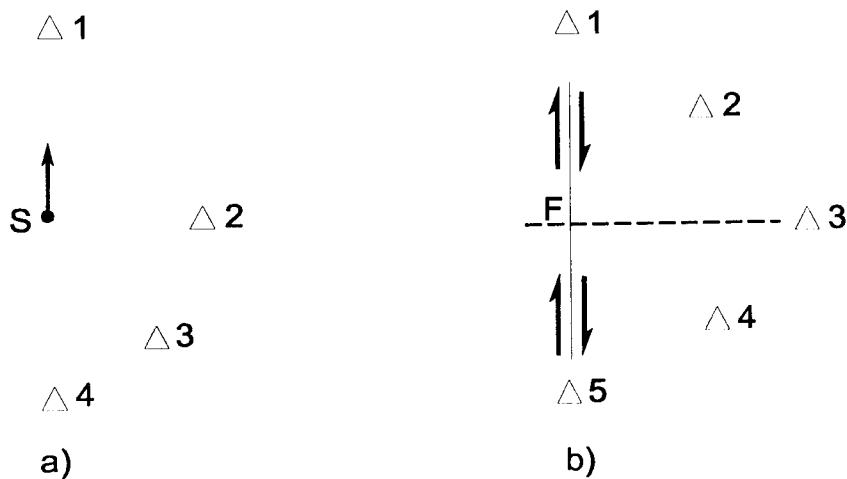


Fig. 1: Direction of source displacement with respect to seismic stations Δ_i for a) a dislocation point source S and b) a fault rupture F. Note that in the discussion below we consider the source to be a point source with an extension much smaller than the distance to the stations.

Fig. 1a represents a linear displacement of a point source S while Fig. 1b stands for a right lateral (dextral) shear dislocation along a fault plane F. Shear dislocations are the most common model to explain earthquake fault ruptures. Note that in the discussion below we consider the source to be a point source with an extension much smaller than the distance to the stations. First we look into the situation depicted in Fig. 1a. When S moves towards Δ_1 than this stations will observe a *compressional* (+) first P-wave arrival (i.e. the first motion is away from S), Δ_4 will record a P-wave of opposite sign (-, *dilatation*, i.e. first motion towards S), and station Δ_2 will receive no P-wave at all. Contrary to this, S-waves, which are polarized parallel to the displacement of S and perpendicular to the direction of wave propagation, will be recorded at Δ_2 but not at Δ_1 and Δ_4 while station Δ_3 will receive both P- and S-waves.

Somewhat different is the situation in case of a fault rupture (Fig. 1b). At stations Δ_1 and Δ_5 , which are positioned in the strike direction of the fault, the opposite signs of motion on both side of the fault will cancel, i.e. no P-waves will be observed. The latter also applies for station Δ_3 which is sited perpendicular to the fault. On the other hand, stations Δ_2 and Δ_4 ,

which are positioned at an angle of 45° with respect to the fault, will record the P-wave motions with maximum amplitudes but opposite sign. This becomes clear also from Fig. 3a. It shows the different polarities and the amplitude "lobes" in the four quadrants. The length of the displacement arrows is proportional to the P-wave amplitudes observed in different directions from the fault. Accordingly, by observing the sense of first motions of P-waves at many stations in different azimuth with respect to the source it will be possible to deduce a "fault-plane solution". But because of the symmetry of the first-motion patterns, two potential rupture planes, perpendicular to each other, can be constructed. Thus, on the basis of polarity data alone, an ambiguity will remain as to which one was the acting fault plane. This can only be decided by taking into account additional data on azimuthal amplitude and frequency or wave-form patterns, which are controlled by the Doppler effect of the moving source, and/or field data on the orientation and nature of seismotectonic faults.

According to the above said, the amplitude distribution for a pure double-couple shear mechanisms is described in a spherical co-ordinate system (θ, ϕ) (cf. Fig. 2) by

$$A_P(\theta, \phi) = \cos \phi \sin 2\theta. \quad (1)$$

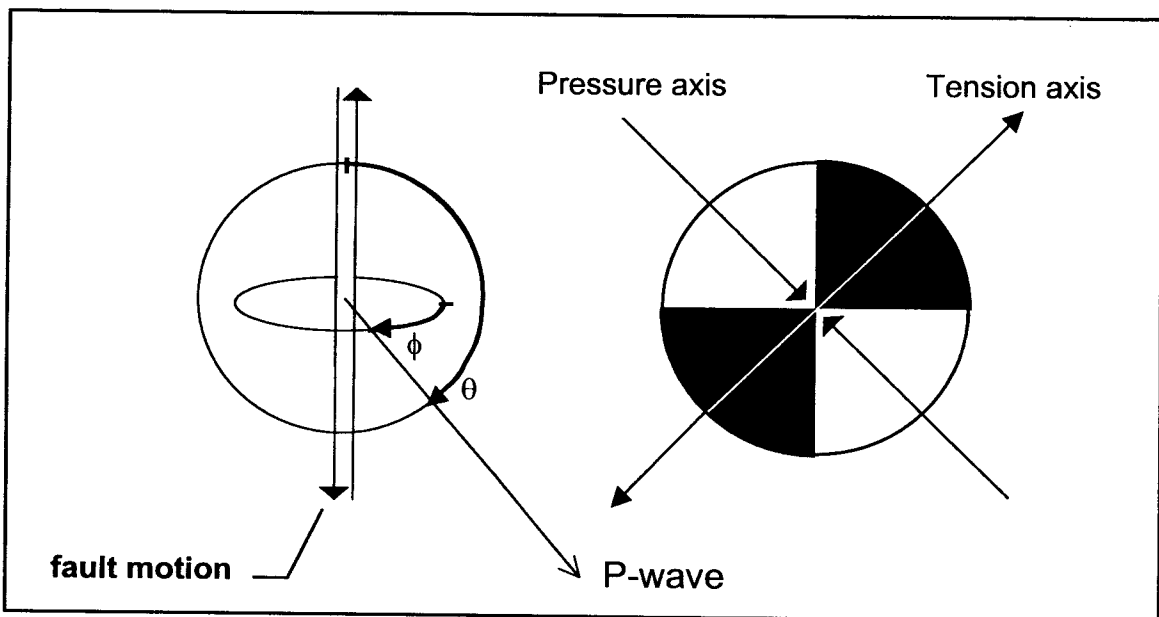


Figure 2: P-wave radiation pattern for a shear fault. Black areas: polarity +, white areas - .

This expression divides the focal sphere into 4 quadrants. The focal sphere for a seismic point source is an imaginary sphere of arbitrarily small radius centered on the source. Within each quadrant the sign of the P-wave first motion (polarity) does not change but amplitudes are large in the center of the quadrant and small (or zero) near to (or at) the nodal lines which separate the quadrants. The nodal lines for P-waves coincide with the horizontal projection of the cut-traces of the two orthogonal fault planes through the focal sphere. Opposite quadrants have the same polarity, neighbouring quadrants different polarities. Note that *compression* is observed at stations falling in the *tension quadrant* (force directed away from the point source) while *dilatation* is observed at stations falling in the *compression quadrant* (force directed towards the point source).

The position of the quadrants on the focal sphere depends on the orientation of the active fault and the slip direction. Therefore, the estimation of the P-wave first motion polarities and their back-projection onto the focal sphere allows to find the focal mechanism of a shear event (fault-plane solution). The only problem is, that the hypocentre and the seismic ray path from the source to the individual stations must be known. This may be difficult for a heterogeneous model with 2D or 3D-velocity structure.

2. COMPUTER-ASSISTED FAULT PLANE SOLUTIONS

In most applications for local earthquakes 1D-layered velocity models are accepted, i.e. layers with constant velocities and velocity discontinuities at the boundaries. The majority of location programs (e.g. HYPO71 by Lee and Jahr, 1975; HYPOELLIPSE by Lahr, 1989; HYPOINVERS by Klein, 1985) are based on this type of velocity model. Additionally, HYPOINVERS and HYPOELLIPSE do accept layers with linear velocity gradients. Moreover, HYPOELLIPSE may locate local events with predefined travel-time tables too. During the location procedure the ray paths to the stations are calculated. The azimuth AZM and the take-off angle AIN at which the P-wave, arriving at a given station, leaves the focal sphere are listed in the output files. The remaining problem to be solved is to find the distribution of P-polarities on the focal sphere and to estimate the angles, describing the focal mechanism.

The computer program FPFIT (Reasenberger and Oppenheimer, 1985) calculates double couple fault plane solutions based on P-wave polarity readings. It accepts as input the output files of the localisation programs HYPO71, HYPOELLIPSE and HYPOINVERSE. The inversion is accomplished through a grid-search procedure that finds the source model by *minimising a normalised weighted sum of first-motion polarity discrepancies*. Two weighting factors are incorporated in the minimisation. One of them reflects the estimated variance of the data while the other one is based on the absolute value of the P-wave radiation amplitude (cf. Fig. 3). In addition to the minimum-misfit solution, FPFIT finds alternative solutions corresponding to significant relative misfit minima. The existence of several minima may be due to insufficient number of polarity readings, localisation errors, polarity mis-readings or an inadequate velocity model (e.g. not modelled refractions) resulting in an incorrect position of the P-wave first-motion polarities on the focal sphere. One has also to be aware that it sometimes may even happen that the seismometer component outputs have been wrongly plugged at a given station, resulting in systematically wrong polarity reportings by such a station. In case of models which perfectly fit the data FPFIT applies an additional constraint. Its effect is to maximise the distance sum between the observation points and the nodal planes on the focal sphere. The display program FPLOT shows the final fault plane solution and the estimated uncertainty in terms of the range of possible orientation of the pressure and tension axes which is consistent with the data.

While the above programs accept only the output files of the hypocenter localisation programs for local events another widely used program package for seismogram analysis, SEISAN (Havskov, 1996; version 1.2 now available as CD-ROM from the International Seismological Center in Thatcham, UK) uses a modified version of the program HYPOCENTER (Lienert et al., 1986; Lienert, 1991; Lienert and Havskov, 1995). The main modifications are that it can also accept secondary phases and locate teleseismic events too. The output files are used in conjunction with the FOCMEC program (Snoke et al., 1984) for the determination of the fault plane parameters but currently on the basis of polarity readings only. The implementation of the additional use of S-P amplitude ratios is intended.

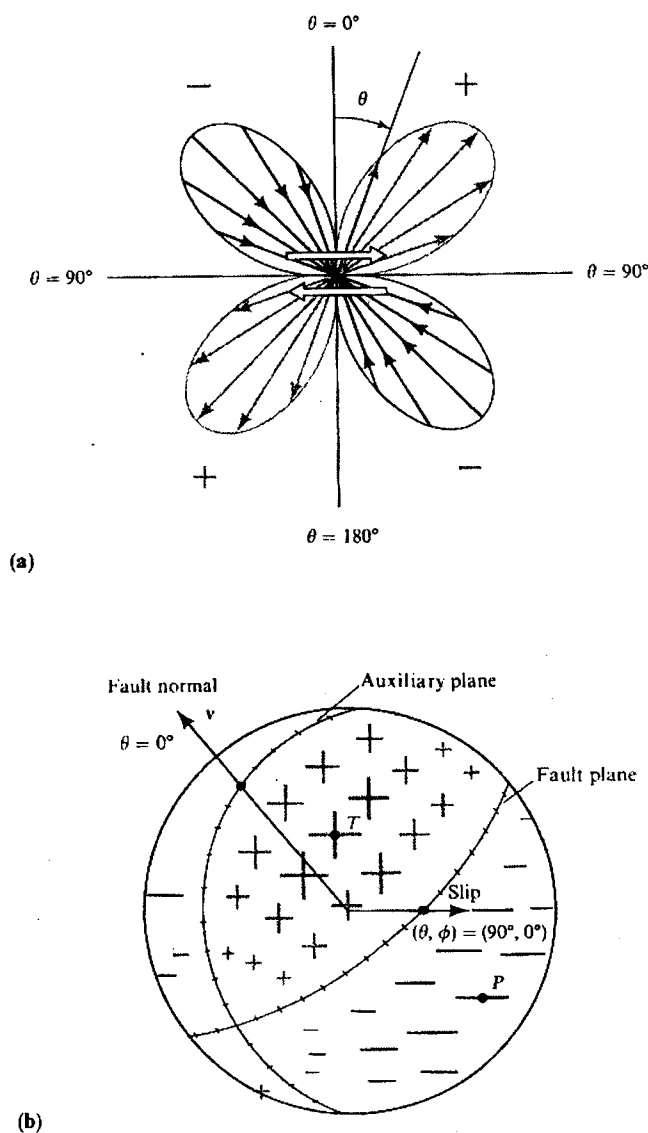
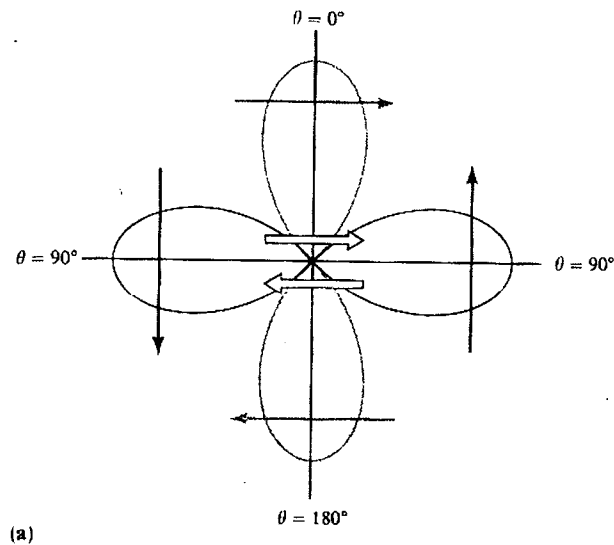
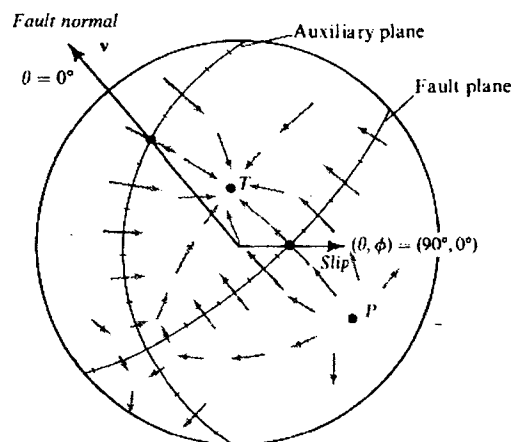


Fig. 3: Radiation pattern of the radial displacement component (P-wave) due to a double-couple source: a) for a plane of constant azimuth (with lobe amplitudes proportional to $\sin 2\theta$) and b) over a sphere centered on the origin. Plus and minus signs of various sizes denote amplitude variation (with θ and ϕ) of outward and inward directed motions. The fault plane and auxiliary plane are nodal lines on which $\cos\phi \sin 2\theta = 0$. The pair of arrows in a) at the center denotes the shear dislocation. Note the alternating quadrants of inward and outward directions. (according to Aki and Richards 1980 ; with kind permission of the authors)

In case of sparse networks or weak events the number of polarity data may be too small for reliable estimation of fault plane solutions. In this case P, SV and SH amplitudes can be used besides polarities in order to get more stable and better constrained, i.e. less ambiguous fault plane solutions. This is due to the difference in P-wave (Fig. 3) and S-wave (Fig.4) polarity and angular amplitude pattern for a given source mechanism.



(a)



(b)

Fig. 4: Radiation pattern of the transverse displacement component (S-wave) due to a double-couple source. a) in the plane $\{\phi = 0, \phi = \pi\}$ and b) over a sphere centered on the origin. Arrows imposed on each lobe in a) show the direction of particle displacement associated with the lobe while the arrows with varying size and direction in the spherical surface in b) indicate the variation of the transverse motions with θ and ϕ . There are no nodal lines as in Fig. 3 but only nodal points where there is zero motion. Note that the nodal point for transverse motion at $(\theta, \phi) = (45^\circ, 0^\circ)$ at T is a maximum in the pattern for longitudinal motion (cf. Fig. 3) while the maximum transverse motion (e.g., at $\theta = 0$) occurs on a nodal line for the longitudinal motion. The pair of arrows in a) at the center denotes the shear dislocation. (according to Aki and Richards 1980; with kind permission of the authors).

In case of a double-couple mechanism according to Fig. 2 the S-wave amplitude pattern follows the relationship

$$A_S = \cos 2\theta \cos \phi - \cos \theta \sin \phi \quad (2)$$

with θ and ϕ - unit vectors in θ and ϕ direction, A_S - shear-wave displacement vector.

The program FOCMEC (Snoke, 1984) allows to calculate fault plane solutions from P, SH and SV polarities and SV/P, SH/P or SV/SH amplitude ratios provided that the ratios are corrected to the focal sphere by taking into account geometrical spreading, attenuation and free-surface effects. For surface correction the program FREESURF, which is supplied together with FOCMEC, can be used. The applied Q-model has to be specified according to the regional attenuation conditions or related corrections. When adopting a constant V_p/V_s velocity ratio the geometrical spreading is the same for P- and S-waves and absolute changes in amplitude cancel each other in the above amplitude ratios. Head waves and amplitude changes at velocity boundaries require special treatment. The programme FOCPLT, also provided together with FOCMEC, allows to plot upper or lower hemisphere projections of the focal sphere and to show the data, fault planes, pressure P and tension T axes and the nodal points for SH and SV-waves.

While the program HYPO71 is available as part of Vol.1 of the IASPEI software library (Lee, 1995) the programs FOCMEC, FPFIT, HYPOELLIPSE and HYPOINVERSE are freely available through the Internet under the following addresses:

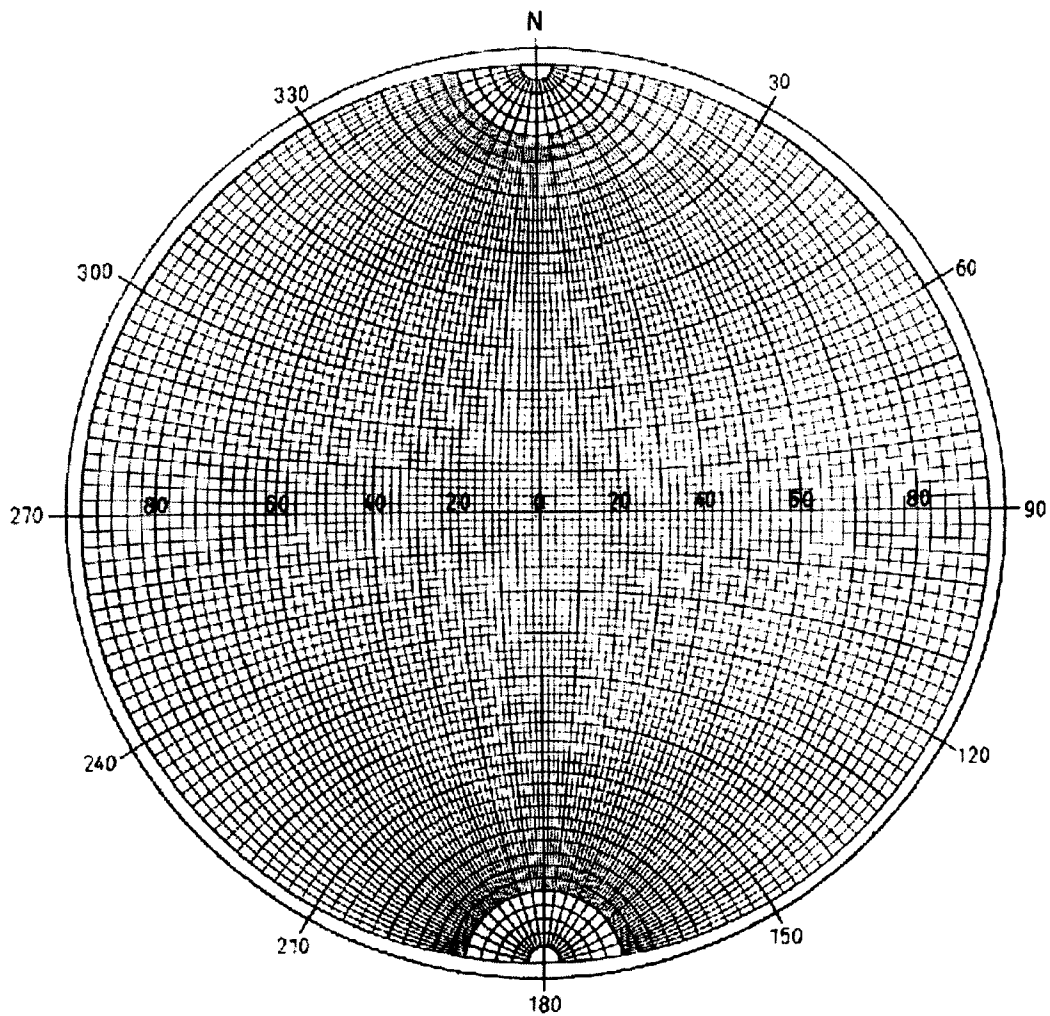
FOCMEC: <http://www.iris.washington.edu>
 FPFIT: <http://orfeus.knmi.nl/other.services/software.links.html#focalmech>
 HYPOELLIPSE: <http://giseis.alaska.edu/pub/SOFTWARE/hypoel/>
 HYPOINVERSE: <http://orfeus.knmi.nl/other.services/software.links.html#location>

3. MANUAL DETERMINATION OF FAULT-PLANE SOLUTIONS

Manual fault plane solutions are normally based on P-wave polarity readings only. To obtain a fault plane solution basically three steps are required:

- (1) Calculating the positions of the penetration points of the seismic rays through the focal sphere which are defined by the ray azimuth AZM and the take-off angle AIN of the ray from the source.
- (2) Marking these penetration points through the upper or lower hemisphere in a horizontal projection of that sphere using different symbols for compressional and dilatational first arrivals. Usually, lower hemisphere projections are used. Rays which have left the upper hemisphere have to be transformed into their equivalent lower hemisphere ray. This is possible because of spherical symmetry of the radiation pattern (cf. Figs. 6 and 7).
- (3) Partitioning the projection of the lower focal sphere by two perpendicular great circles which separate all (or at least most) of the + and - arrivals in different quadrants.

Two kinds of projections can be used, either the equal-angle Wulff net or the Lambert-Schmidt equal area projection (Figs. 5a and 5b; see also Aki and Richards, 1980, Vol. 1, p. 109-110.). The latter provides a less cluttered plot of data with take-off angles less than 45° but in principle the procedure of constructing the fault planes is the same (cf. *Exercise on faults plane solutions* and *Exercise on calculation of take-off angles*)



The Wulff Net

Fig. 5a: The equal angle Wulff net.

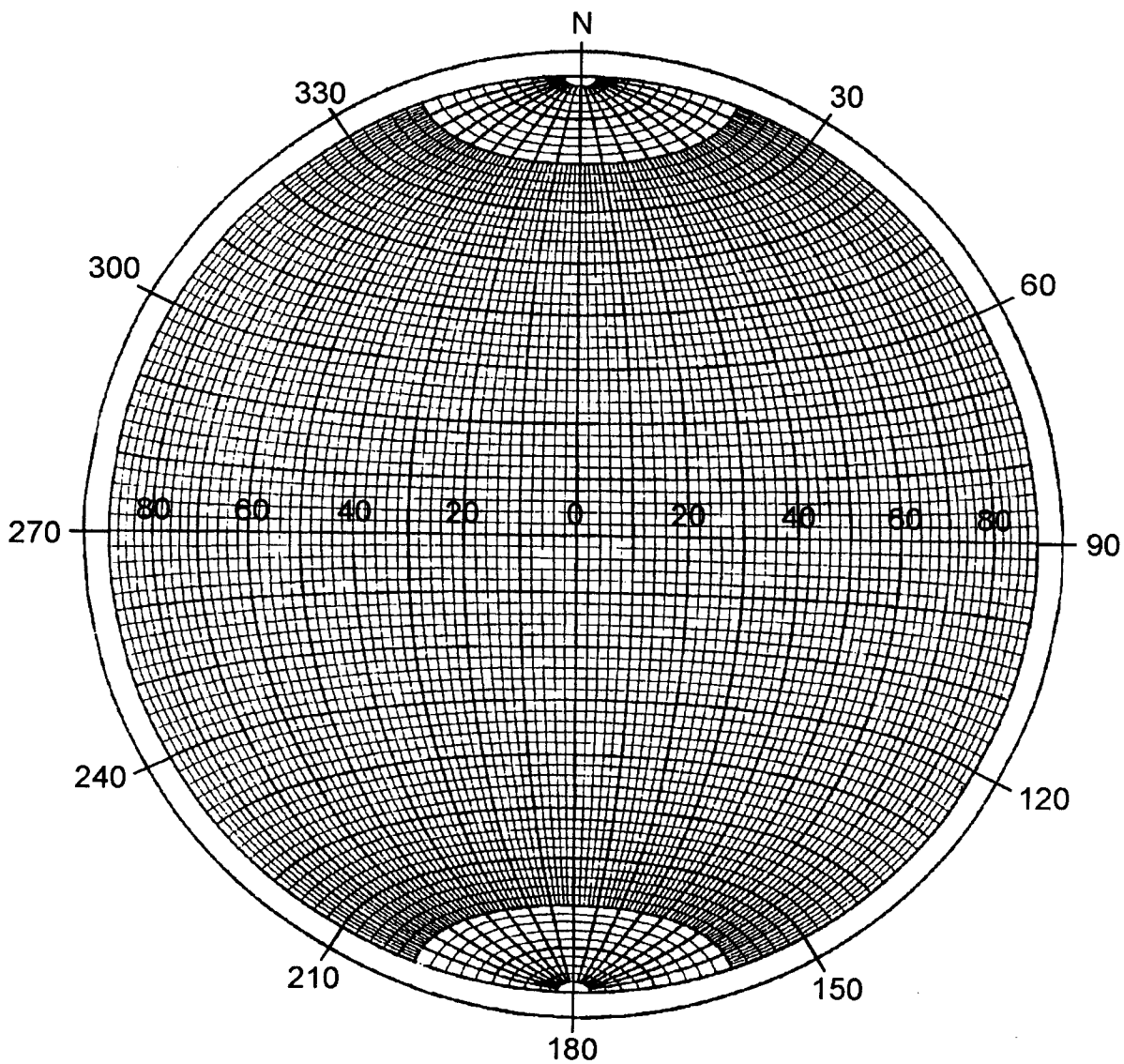


Fig. 5b: The equal area Lambert-Schmidt net.

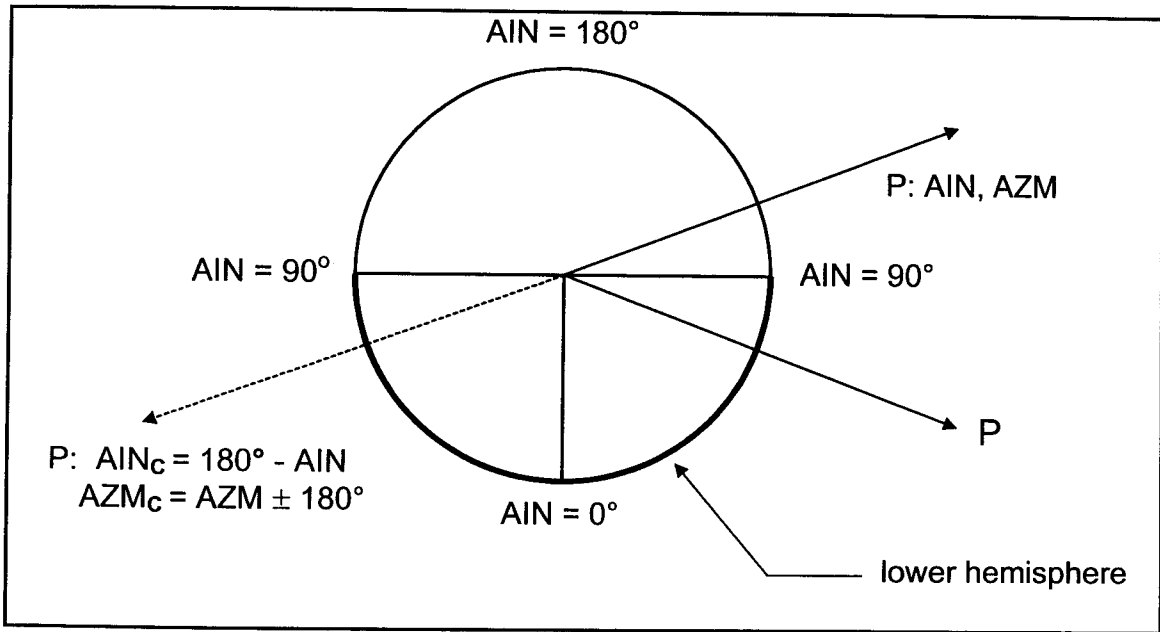


Fig. 6: Transformation of a ray leaving the focal sphere upwards into a downward ray with same polarity and changed incidence angle and azimuth.

Fig. 7 (below): Two rays, leaving the focal sphere in opposite directions, reach - because of the symmetry of radiation pattern - the stations 1 and 2 with the same polarity. The crossing point of the upgoing ray with the focal sphere can, therefore, be remapped according to the formulae given in Fig. 5 into a crossing point with the lower hemisphere which coincides with the ray crossing-point for station 2.

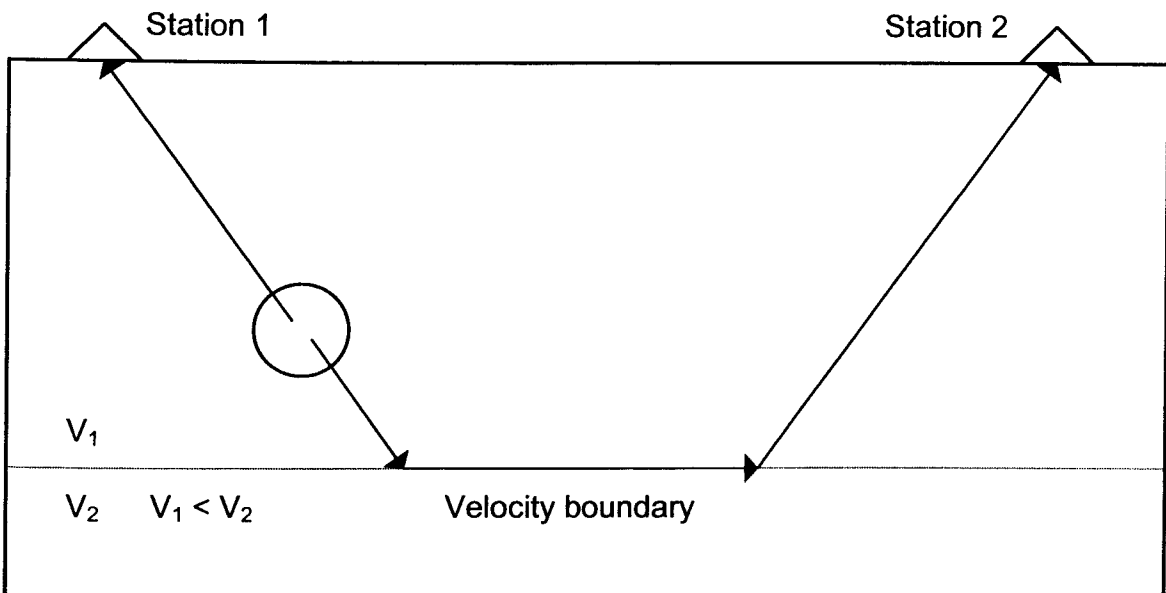


Fig. 8 shows the angles which describe the orientation and motion of a fault plane and Fig. 9 shows their determination in the net projections. The **strike angle** ϕ is measured clockwise against North ($0^\circ \leq \phi \leq 360^\circ$). To resolve the 180° ambiguity, it is assumed that when looking into the strike direction the fault dips to the right hand side (i.e. its fault-trace projection is towards the right of the net centre). The **dip angle** δ describes the inclination of the hanging wall against the horizontal ($0^\circ \leq \delta \leq 90^\circ$). The **rake angle** λ describes the displacement of the hanging wall relative to the foot wall ($-180^\circ \leq \lambda \leq 180^\circ$). $\lambda = 0$ corresponds to slip in strike direction, $\lambda > 0$ means upward motion of the hanging wall (i.e. *reverse or thrust faulting component*) and $\lambda < 0$ downward motion (i.e. *normal faulting component*).

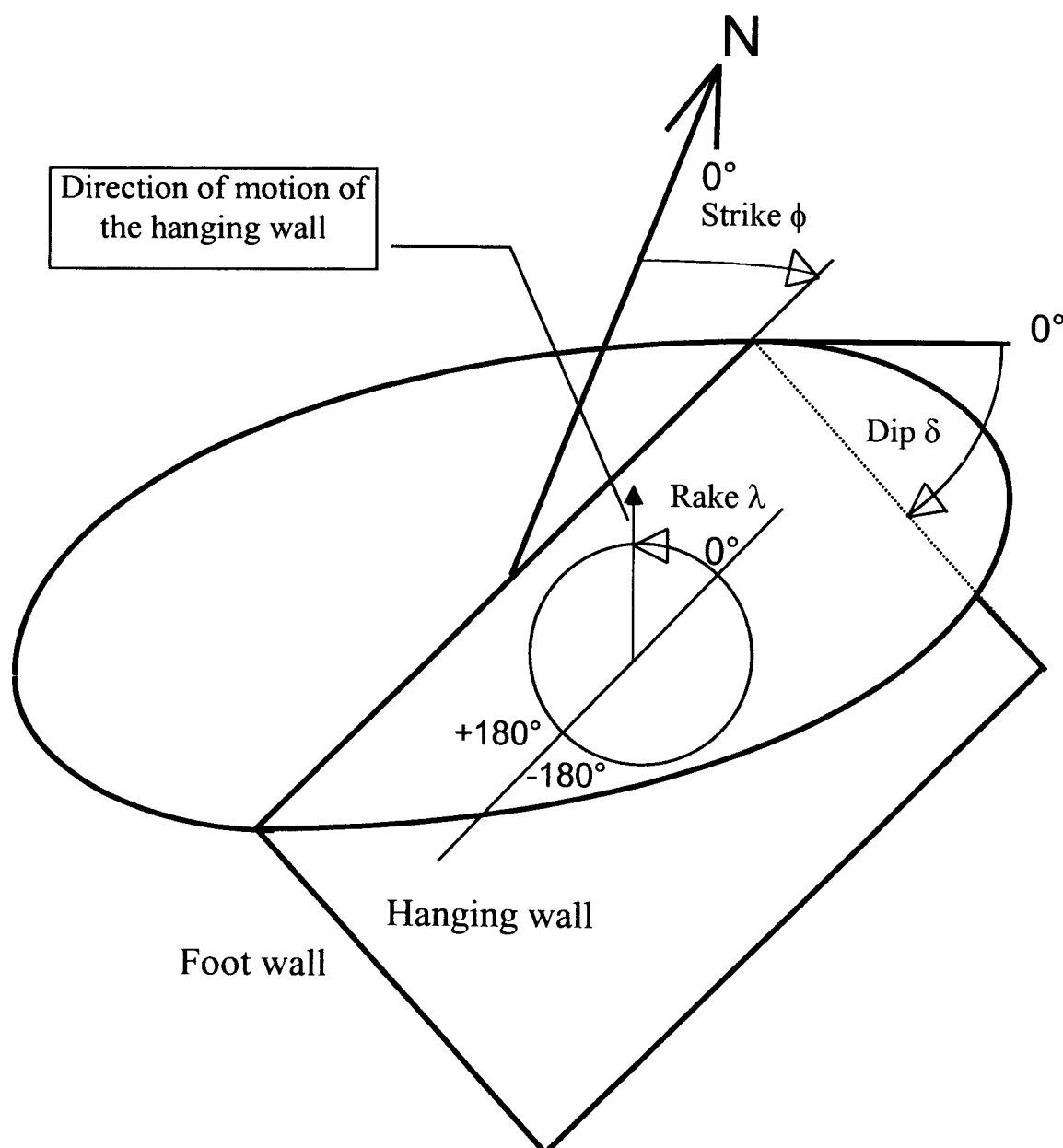


Fig. 8: Angles describing the orientation and motion of faults (cf. text).

In Fig. 9 P1, P2 and P3 mark the positions of the poles of the planes FP1 (fault plane), FP2 (auxiliary plane) and EP (equatorial plane) in their net projections. From Fig. 8 it is obvious that all three planes are perpendicular to each other (i.e. 90° apart) and intersect in the poles of the respective third plane, i.e. FP1 and FP2 in P3, FP1 and EP in P2 etc. Note that on the basis of polarity readings alone it can not be decided whether FP1 or FP2 was the really acting fault. A discrimination from seismological data alone requires additionally a study of the azimuth dependence of frequency (*Doppler effect!*), amplitudes and/or waveforms. These effects can more easily be studied in low-frequency teleseismic recordings while in the local distance range high-frequency waveforms and amplitudes may be strongly influenced by resonance effects due to low-velocity near-surface layers. Seismotectonic considerations or field evidence from surface rupture in case of strong earthquakes may allow to resolve this ambiguity too. Figs. 10 and 11 depict several basic types of earthquake faulting and their related fault-plane solutions in so-called "beach-ball" presentations of the net projections.

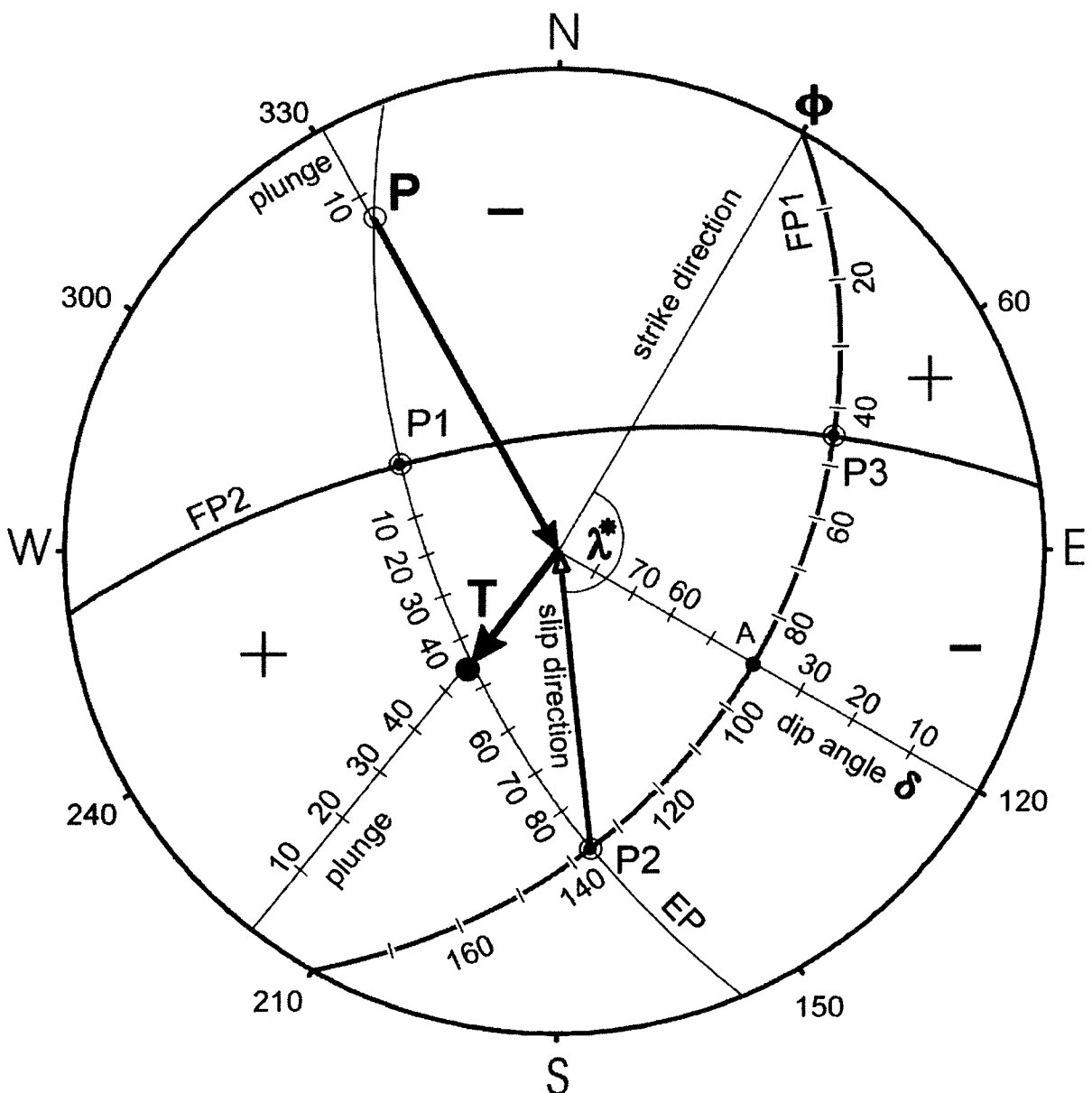


Fig. 9: Determination of the fault plane parameters ϕ , δ and λ in the net diagrams. The polarity distribution, slip direction and projection of FP1 shown do qualitatively correspond to the faulting case depicted in Fig. 8. For abbreviations used see text.

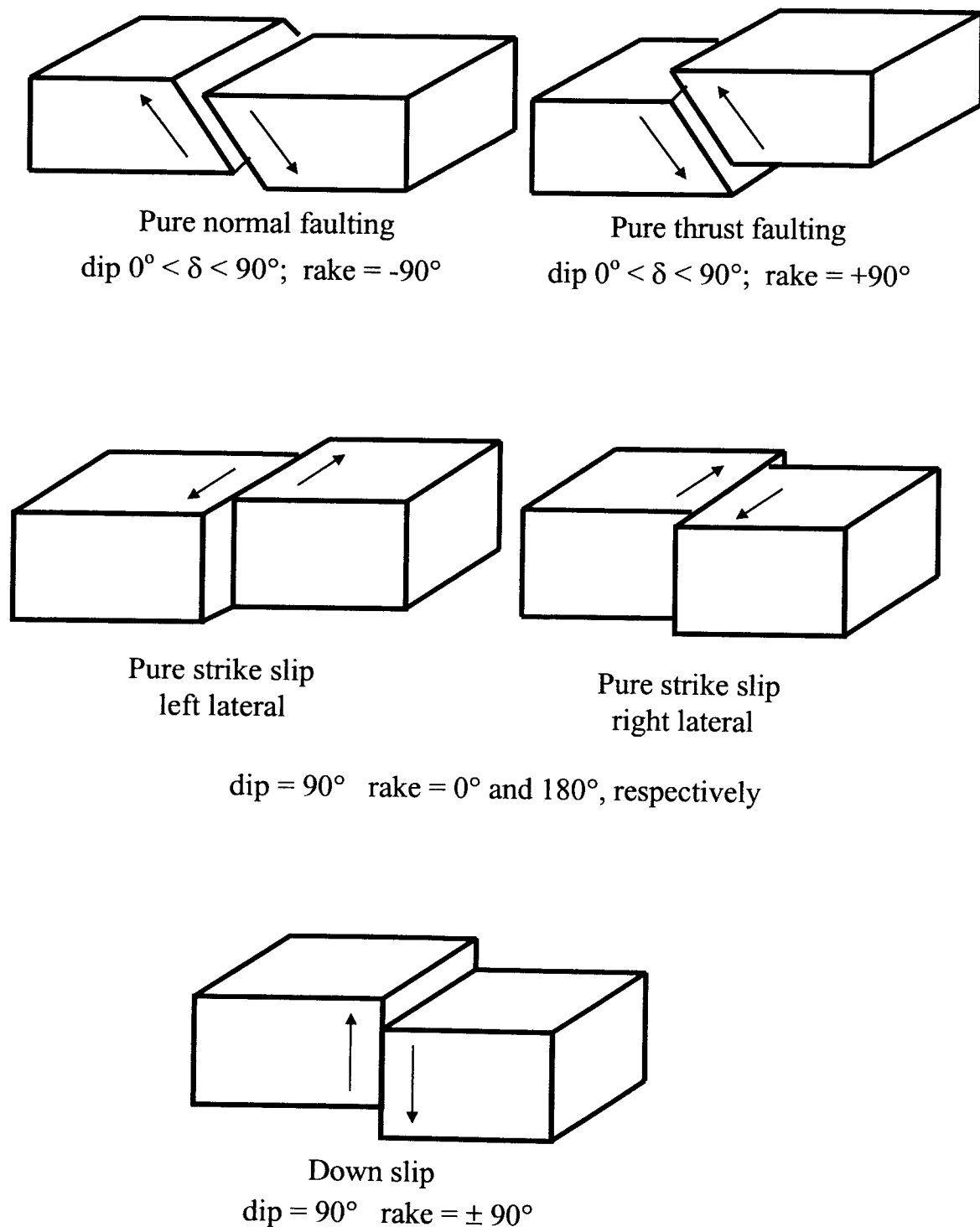


Fig. 10: Basic types of earthquake faulting for some selected dip and rake angles. Note that mixed types of faulting do occur when $\lambda \neq 0, 180^\circ$ or $\pm 90^\circ$., e.g. normal faulting with strike-slip component or strike-slip with thrust component. Also, dip angles may vary between $0^\circ < \delta \leq 90^\circ$. For fault plane traces and polarity distributions of these faulting types in their "beach-ball presentation" see Fig. 11.

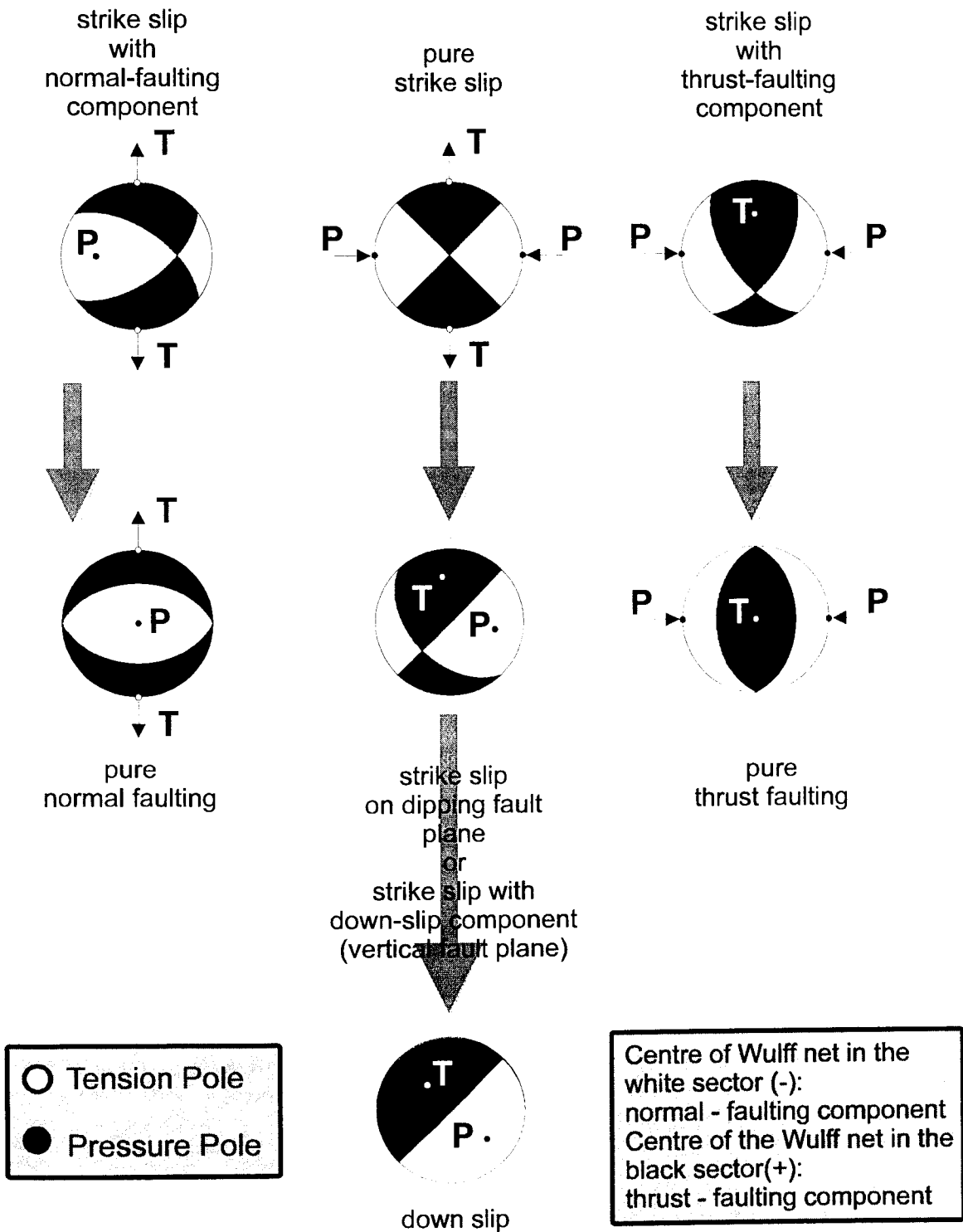


Fig. 11: Beach-ball presentation of the net projections of the fault plane cut-traces and of the penetration points of the T-and P-axes through the lower focal hemisphere for different faulting mechanisms. White sectors correspond to negative and black sectors to positive first-motion polarities.

4. ACCURACY OF FAULT PLANE SOLUTIONS

Fault plane angles determined by eye-fit to the polarity data may be uncertain by about $\pm 10^\circ$. This is acceptable. Even computer assisted best fits to the data will produce different acceptable solutions within about the same error range with only slightly different standard deviations (cf. Fig. 1 in the exercise on take-off angle calculations, NEIC and HRVD solutions, respectively).

Additionally, one has to be aware, that even different fitting algorithm/error-minimisation procedures may produce for the same data results within this range of uncertainty. Uncertainties due to not ideal distribution of seismic stations and thus available polarity data in the net diagram, erroneous polarity readings and differences in model assumptions (e.g. in the velocity models used) may even result in still larger deviations between the model solution and the reality in nature. One should also be aware that the assumed constant angular (45°) relationship between the fault plane on the one hand and the pressure and tension axis on the other hand, which is true in fact only in case of a fresh rupture in a homogeneous isotropic medium, may not be correct in the given stress environment and tectonic situation.

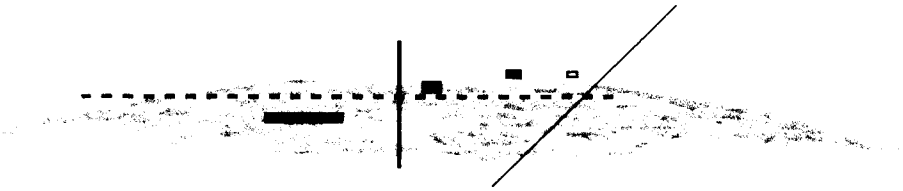
REFERENCES

- Aki, K. and P.G. Richards (1980). Quantitative seismology. Theory and methods. Vol. 1. W.H. Freeman and Company, San Francisco, ISBN 0-7167-1058-7, 557 pp.
- Havskov, J. (Editor) (1996). The SEISAN earthquake analysis software for the IBM PC and SUN, Version 5.2. Institute of Solid Earth Physics, Univ. of Bergen, August 1996
- Klein, F.W. (1985). HYPOINVERSE, a program for VAX and professional 350 computers to solve the earthquake locations. U.S. Geological Survey Open-File Report 85-515, 53 pp.
- Lahr, J.C. (1989). HYPOELLIPSE/Version 2.0: A computer program for determining local earthquakes hypocentral parameters, magnitude, and first motion pattern. U.S. Geological Survey Open-File Report 89-116, 92 pp.
- Lee, W.H.K. and J.C. Lahr (1975). HYPO71 (revised): A computer program for determining hypocenter, magnitude, and first motion pattern of local earthquakes. U.S. Geological Survey Open-File Report 75-311, 100 pp.
- Lee, W.H.K. (1995). Realtime seismic data acquisition and processing. IASPEI Software Vol.1, 2nd Edition. (Can be ordered from Seismological Society of America, 201 Plaza Professional Building, El Cerrito, CA 94530, USA; Fax: +1 510 525 7204)
- Lienert, B.R.E., E. Berg and L.N. Frazer (1988). HYPOCENTER: An earthquake location method using centered, scaled, and adaptively least squares. Bull. Seism. Soc. Am. 76, 771-783.
- Lienert, B.R.E. (1991). Report on modifications made to Hypocenter. Institute of Solid Earth Physics, University of Bergen.

Lienert, B.R.E., J. Havskov (1995). A computer program for locating earthquakes both locally and globally. *Seismological Research Letters*. 66, 26-36

Reasenber, P.A. and D. Oppenheimer (1985). FPFIT, FPLOT and FPPAGE: Fortran computer programs for calculating and displaying earthquake fault-plane solutions. U.S. Geological Survey Open-File Report 85-739.

Snoke, J.A., J.W. Munsey, A.G. Teague and G.A. Bollinger (1984). A program for focal mechanism determination by combined use of polarity and SV-P amplitude data. *Earthquake Notes* **55**, No. 3, p. 15



GEOFORSCHUNGSZENTRUM POTSDAM
STIFTUNG DES ÖFFENTLICHEN RECHTS

Peter Bormann (Editor)

International
Training Course 1999 on

Seismology
Seismic Hazard Assessment
and Risk Mitigation

Lecture and exercise notes

Volume II

Scientific Technical Report STR99/13

Imprint

Edited by:

Peter Bormann
GeoForschungsZentrum Potsdam
Telegrafenberg
D-14473 Potsdam, Germany

Printed in Potsdam, Germany
August 1999

The International Training
Course on "Seismology, Seismic Hazard
Assessment and Risk Mitigation" was
held in Beijing, China
26 September to 30 October, 1999

It was sponsored by:

- GeoForschungsZentrum
Potsdam (GFZ)
- China Seismological Bureau
(CSB)
- Federal Foreign Office (AA), Bonn
- Federal Ministry of Economical
Co-Operation and Development
(BMZ), Bonn
- Carl Duisberg Gesellschaft (CDG),
Regional Office of the State of
Brandenburg in Berlin
- Secretariat of the International
Decade for Natural Disaster
Reduction (IDNDR), Geneva
- United Nations Educational, Scientific
and Cultural Organization (UNESCO),
Paris
- International Association of Seismology and
Physics of the Earth's Interior (IASPEI)

Lecture and exercise notes, Volume II

International
Training Course 1999

on

**Seismology, Seismic Hazard Assessment
and Risk Mitigation**

Beijing, China, 26 September to 30 October

jointly organized by
GeoForschungsZentrum Potsdam (GFZ)
China Seismological Bureau (CSB)

Supported by
Carl Duisberg Gesellschaft (CDG)

co-sponsored by
AA (Bonn), BMZ (Bonn), CDG (Berlin), IASPEI,
IDNDR Secretariat (Geneva), UNESCO (Paris)

Peter Bormann
Editor

Scientific Technical Report STR99/13

CONTENTS

	Page
Foreword by the editor	1
1. <u>Basics of seismometry, seismic data acquisition and exchange</u>	
Fundamentals of seismometry	Ch. Teuper † 3
Constructing response curves - an introduction to the Bode-diagram	J. Bribach 18
Exercise on plotting seismograph response (Bode-diagram)	J. Bribach 25
Exercise on estimating seismometer parameters by STEP transition	J. Bribach 26
Calibration by harmonic drive	Ch. Teuper † 31
Influence of the frequency characteristics of the seismograph on its seismic recording	P. Bormann 32
Principles of acquisition, handling and storage of digital seismological data	J. Bribach 40
Seismic data acquisition and analysis	M. Baumbach 57
Demonstration of different digital data acquisition systems together with seismometers for mobile and stationary use - strong-motion recordings and display of the collected data	Zhang Wenbo 77
Trend and requirements in strong-motion data acquisition, management analysis and exchange	Lilie Xie 87
Data processing and analysis for strong-motion accelerograms	Lilie Xie 96
Understanding and setting STA/LTA trigger algorithm and associated parameters	114
WCD's and access to data sources via Internet and CD-ROM	Zhao Zhobghe 136
How to retrieve data from IRIS / USGS stations	S. Mc Lafferty 148

2. Seismic stations and networks: Planning, site selection, installation and operation

Seismic network, planning, procurement, installation, organisation and tuning	A. Trnkoczy	158
Seismic site quality and selection of surface seismic stations	A. Trnkoczy P. Bormann	195
Surface vault seismic station preparation	A. Trnkoczy	215
Radio-link transmission of seismic data and feasibility study	A. Trnkoczy	232
Bandwidth-dependent transformation of noise data from spectral into time domain and vice versa Part I: Introduction and methodology	P. Bormann	244
Bandwidth-dependent transformation of noise data from spectral into time domain and vice versa Part II: Exercises and solutions	P. Bormann	250

3. Seismic sources and source parameters

Introduction to seismic sources and source parameters	P. Bormann, H. Grosser	254
Magnitude of seismic events	P. Bormann	271
Seismic scaling relations	P. Bormann	316
Determination of fault plane solutions	M. Baumbach, P. Bormann	331

4. Seismological observatory practice: Analysis of records

Identification and analysis of longitudinal core phases: Requirements and guidelines	P. Bormann, S. Wendt	346
Exercise on local event localisation	P. Bormann, M. Baumbach, K. Wylegalla	367
Exercise on 3 - component seismogram interpretation	P. Bormann, K. Wylegalla	372
Exercise on magnitude determination	P. Bormann, K. Wylegalla	377

Exercises on event location and magnitude determination by means of seismic core phases	S. Wendt, P. Bormann	381
Exercise on fault-plane solution	M. Baumbach, P. Bormann H. Grosser	388
Exercise on take-off angle calculations	P. Bormann	395
Exercise on the determination of source parameters derived from seismic spectra	M. Baumbach, P. Bormann	401
"SEISAN" introductory training course	J. Havskov, L. Ottemöller	407
SEIS 89: A PC-tool for seismogram analysis	M. Baumbach	423

5. Seismicity, seismic hazard, risk assessment and disaster management

Introduction to natural disasters and disaster mitigation	P. Bormann	453
Seismicity and seismotectonics in Asia	Zhang Peizhen, Chen Yong	483
Seismic hazards in Asia: What do we know after GSHAP ? What remains to be done ?	Chen Yong, Li Juan	492
Earthquakes in China: A brief introduction	Z. L. Wu, Y.-T. Chen, R.F. Liu	509
Macroseismic and strong-motion parameters	G. Grünthal	521
Methodology of seismic hazard assessment	G. Grünthal	538
Exercise on assigning seismic intensities	G. Grünthal	544
Exercise on incompleteness of a catalogue with respect to the determination of the parameters of the Gutenberg-Richter relation	G. Grünthal	547
Exercise on the determination of the parameters of the Gutenberg-Richter relation $\log N = a - b \cdot m$	G. Grünthal	548
Exercise on earthquake occurrence in time (Poisson distribution)	G. Grünthal	550

Exercise on the application of extreme value statistics	G. Grünthal	551
Exercise on seismic hazard assessment: a simplified approach	G. Grünthal, Ch. Bosse	552
Exercise on PC assisted hazard assessment	Ch. Bosse, G. Grünthal	553
Approaches to seismic hazard assessment in China: Methodology. Part I: Assessment of seismic hazard based on area source and seismicity data	Chen Yong	555
Approaches to seismic hazard assessment in China: Methodology. Part II: Analysis of earthquake loss based on macroeconomic indicators	Chen Yong, Chen Qifu	568
Introduction to CAPSeis	Li Minfeng, Li Shengqiang	581
PC assisted exercises in seismic hazard assessment based on data from the countries of participants	Chen Yong, Chen Qifu, Chen Ling	585
Seismic risk assessment and disaster management	Yuxian Hu	594
Method on physical damage prediction of brick buildings	Feng Quimin	666

IDENTIFICATION AND ANALYSIS OF LONGITUDINAL CORE PHASES: REQUIREMENTS AND GUIDELINES

Peter Bormann¹⁾ and Siegfried Wendt²⁾

¹⁾ GeoForschungsZentrum Potsdam, Division 2: Solid Earth Physics and Disaster Research, Telegrafenberg, D-14473 Potsdam, Germany; E-mail: course@gfz-potsdam.de

²⁾ Universität Leipzig, Institut für Geophysik und Geologie, Geophysikalisches Observatorium Collm, D-04779 Wernsdorf, Germany; E-mail: wendt@rz.uni-potsdam.de

1. WHY SHOULD WE LOOK FOR CORE PHASES?

Oldham (1899) was the first to identify in records of the $M = 8.7$ Assam earthquake of 1897 the three main types of waves predicted by Poisson and Rayleigh, namely longitudinal (P-), transversal (S-) and long period surface waves (LR). He surmised from the substantial delay of P-waves beyond epicentral distances of 120° and the then missing S-waves the probable existence of a molten core, which Wiechert had hypothesised the year before to consist of iron. Gutenberg (1913) then determined the depth of the core-mantle boundary (CMB) with rather high accuracy (2900 km below the earth surface) and to inferred a drop in the velocity of longitudinal waves by almost 40% beneath the CMB. Such a two-shell earth causes refraction phenomena analogous to the optical caustic formed by a spherical lens. Such a caustic was found to exist indeed at $D \approx 145^\circ$. Later, Inge Lehman (1936) identified a phase named by her P' . It arrived before the caustic within the shadow zone for primary mantle P-waves. Its existence and observed travel times let her conclude "... that inside the core there is an inner core in which the velocity is larger than in the outer core".

Since that time detailed investigations of refracted, reflected and converted core phases have revealed more details of the CMB, the discontinuity between the outer and inner core (ICB) and of the transition layers above them. Indications for the existence of negative velocity gradients above and scattering irregularities at the CMB, for attenuation anomalies and anisotropy etc. have been found. The identification, verification and quantification of such phenomena provides crucial clues for a more realistic parameterisation of these boundary layers and for deeper insights into their nature. This will result in improved modellings which are crucial for understanding the interaction and coupling between the inner and outer core as well as between core and mantle. They govern the thermal, compositional, kinematic and dynamic history of the earth, the driving forces for the episodic cycles of increased orogenic and magmatic activities throughout the earth history, the origin and drift of the geomagnetic field and of many other fundamental geophysical processes.

Improving existing earth models requires to identify more comprehensively related seismic phases and to determine more precisely their travel times. Currently, more than 10% of all first onsets published by the World Data Center A (NEIS) in Earthquake Data Reports (EDR) are core phases. To look for first arrivals only is, regrettably, still the prevailing practice at seismological observatories. But model improvements require urgently to identify and report

secondary arrivals too which sometimes follow very closely. Only by this way we will be able to verify with real data the precise position of focal points, cusps and receding branches in travel-time curves as they can be calculated from earth models. These characteristic features respond very sensitive to changes in the model parameters. Additionally, one has to study the amplitudes and waveforms too. They depend not only on the geometry and velocity distribution but also on the attenuation structure of the earth. Its anelastic part is closely related to the rheology and thus to the thermal and compositional properties of the earth.

Besides this, one should look not only for the various direct core phases but also for reflected and converted ones. They often sample parts of the earth which are not passed by recorded direct refracted waves. This may be due to the inhomogeneous distribution of seismic sources and receivers or because of the specifics of the velocity distribution. The uppermost outer core, e.g., is not sampled by any of the direct core phases. The reason is, that their rays are refracted towards the deeper parts of the core because of the strong velocity decrease below the CMB (cf. Fig. 1). Consequently, only core phases which are reflected back into the core at the CMB will sample those parts of the uppermost outer core (cf. Fig. 15).. Comparing the spectral amplitudes from multiple reflections of this type is well suited for better constraining the attenuation properties in those parts and the acoustic impedance contrast at the CMB.

Thus, a detailed identification and analysis of the various types of core phases on a global scale by seismic observatories may yield unique data for verifying or improving existing earth models. Besides this, a more careful analysis and reporting of such phases to international data centres may also help to improve their routine determination of basic source parameters of seismic events such as magnitudes and hypocentral co-ordinates. This applies, in particular, when the events occur in regions which are not well covered by local or regional stations while in other parts of the world, at "core phase distances", good seismic networks with low detection thresholds may exist. This is true, e.g., for seismic stations in central and northern Europe with respect to events in the SW Pacific. Many seismic stations in Africa record, besides earthquakes from the SW Pacific, also those from the seismically very active regions of the Aleutian Islands, Alaska and California and stations in South America those from the Hindukush, Himalaya and China earthquake region within the PKP distance range.

Until now, it is standard practice at the international seismological data centres to use only P-wave onsets up to epicentral distances of 100° for the determination of body-wave magnitudes m_b . But there are several seismic stations such as Collm (CLL) in Germany, which are reporting to the EDR of NEIS almost as many period (T) and amplitude (A) readings for PKP core phases between $110^\circ < D < 160^\circ$ as for teleseismic P-waves. Thus, not using PKP for magnitude determinations, is a waste of potentially useful information. Often NEIS is unable to give m_b values because of lacking suitable P-wave data although reliable A and T values reported for PKP were readily available. Therefore, from data of CLL, calibration functions for magnitude determination from PKP phases have been derived which should also be used and checked with data from other stations in order to test their general applicability or to introduce required modifications on the basis of a global data set collected by the seismological world data centres.

In case of strong earthquakes or underground nuclear explosions, reflected core phases such as PKPPKP, PKKP or their multiples (up to P7KP has already been observed!) may appear in seismic records as small but rather distinct short-period onsets. They are well separated in time (about 10 to 80 min.) from P, PKP, PP, PcP or other short-period phases related to the main

event. Therefore, station operators frequently interpret them as P-wave onsets from another event (cf. Fig. 14 below). Although this misinterpretation is mostly recognised by the automatic data association procedures at the international data centres, often enough this has not been the case. Ambraseys and Adams (1986) reported, that misinterpreted PKKP arrivals at the LASA array in Montana, USA, resulted in the location and reporting to the International Seismological Center (ISC) of spurious events in western and central Africa with magnitudes between 4 to 6. They had nothing to do with real seismicity there and thus could have biased significantly hazard assessments based on uncorrected catalogue data.

This highlights the importance of a priori correct phase identification at seismic observatories. Guidelines for the identification of core phases in short-period seismic records are given below (see also *Exercises on the analysis of short-period core phases*). Although modern interactive data analysis programs allow to call for all travel-time curves theoretically expected at a given distance and to overlay them on the records, thus aiding a correct phase identification, we prefer to demonstrate the sequence of logic steps to be followed when interpreting a seismic record without knowing beforehand the source parameters of the event.

Our emphasis is on short-period core phases because only high-gain short-period (or accordingly filtered broadband) records provide sufficient world-wide data of these mostly weak phases with good time-resolution. The stronger direct core phases may appear distinct in long-period or broadband records too but the different PKP onsets appearing beyond the caustic within a few seconds to each other are then often integrated to a more or less complex long-period wavelet which does not allow precise onset time determinations of these individual phases without special processing (Fig. 2). The much weaker reflected or converted core phases can be recognised usually in short-period narrow-band (filtered) records only. They may occur in practically all teleseismic distance ranges.

2. RAY PATHS AND TRAVEL TIMES OF PKP PHASES

Fig. 1 shows the ray paths and travel-time curves for PKP phases according to the IASPEI 1991 velocity model (IASP91 for short; Kennett 1991). Recommended by the International Association of Seismology and Physics of the Earth Interior (IASPEI) the latter is the currently most often used one-dimensional earth model. The caustic effect due to this velocity structure is clearly to be seen. The three different core phases PKP1, PKP2 and PKIKP reach the point B at a distance of about 145° at the same time while being more or less clearly separated for larger distances. The symbol P stands for ray segments travelled as a longitudinal wave through the earth mantle while the symbols K and I stand for travelling as a longitudinal wave through the outer or inner core, respectively. PKP2 forms the receding travel-time branch between the points A and B (focus). From thereon PKP1 exists up to the point C, forming a prograde branch. - According to IASP91, the ray which was totally reflected due to the velocity increase at the inner core boundary arrives at nearly 155° . This gives rise to the formation of a cusp at point C with the receding branch of the inner core reflection PKiKP going back to point D at about 114° . Since the branch CD follows within ≤ 2 s after PKP1, PKP2 or PKIKP, respectively, and since, according to Fig. 3, the theoretically expected related wave amplitudes are for $D > 135^\circ$ smaller than for the other three phases and thus normally not recognisable, this branch has not been

Ray paths and travel-time curves of core phases PKIKP, PKP1, PKP2

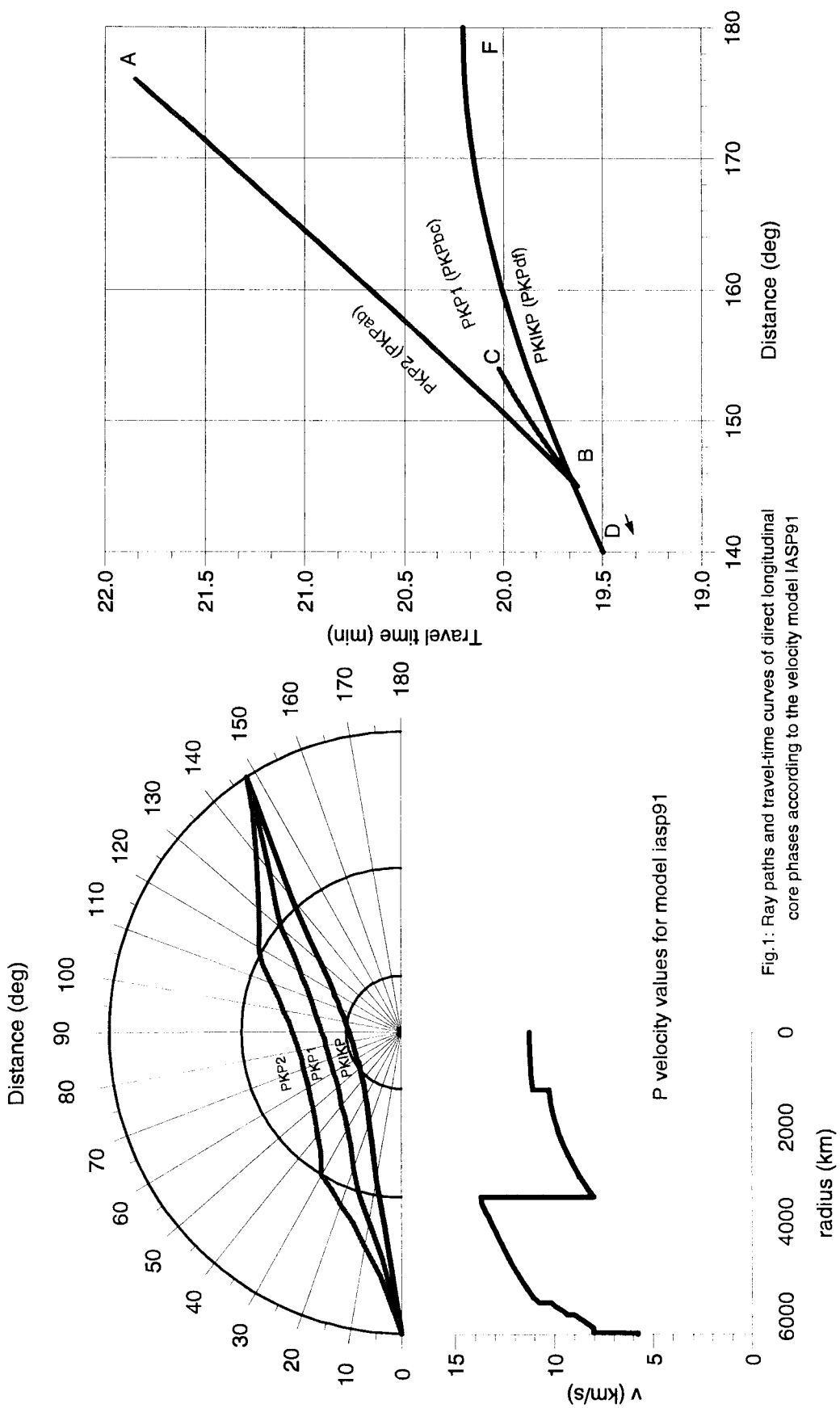


Fig.1: Ray paths and travel-time curves of direct longitudinal core phases according to the velocity model IASP91

depicted in Fig. 1. PKIKP forms, from the cusp at point D up to 180°, the prograde travel-time branch DF. Accordingly, these three considered PKP-phases are nowadays often discerned by adding the branch symbols (mostly as lower case letters) instead of using the classical notation given above, i.e. PKIKP = PKP_{df}, PKP1 = PKP_{bc}, PKP2 = PKP_{ab}.

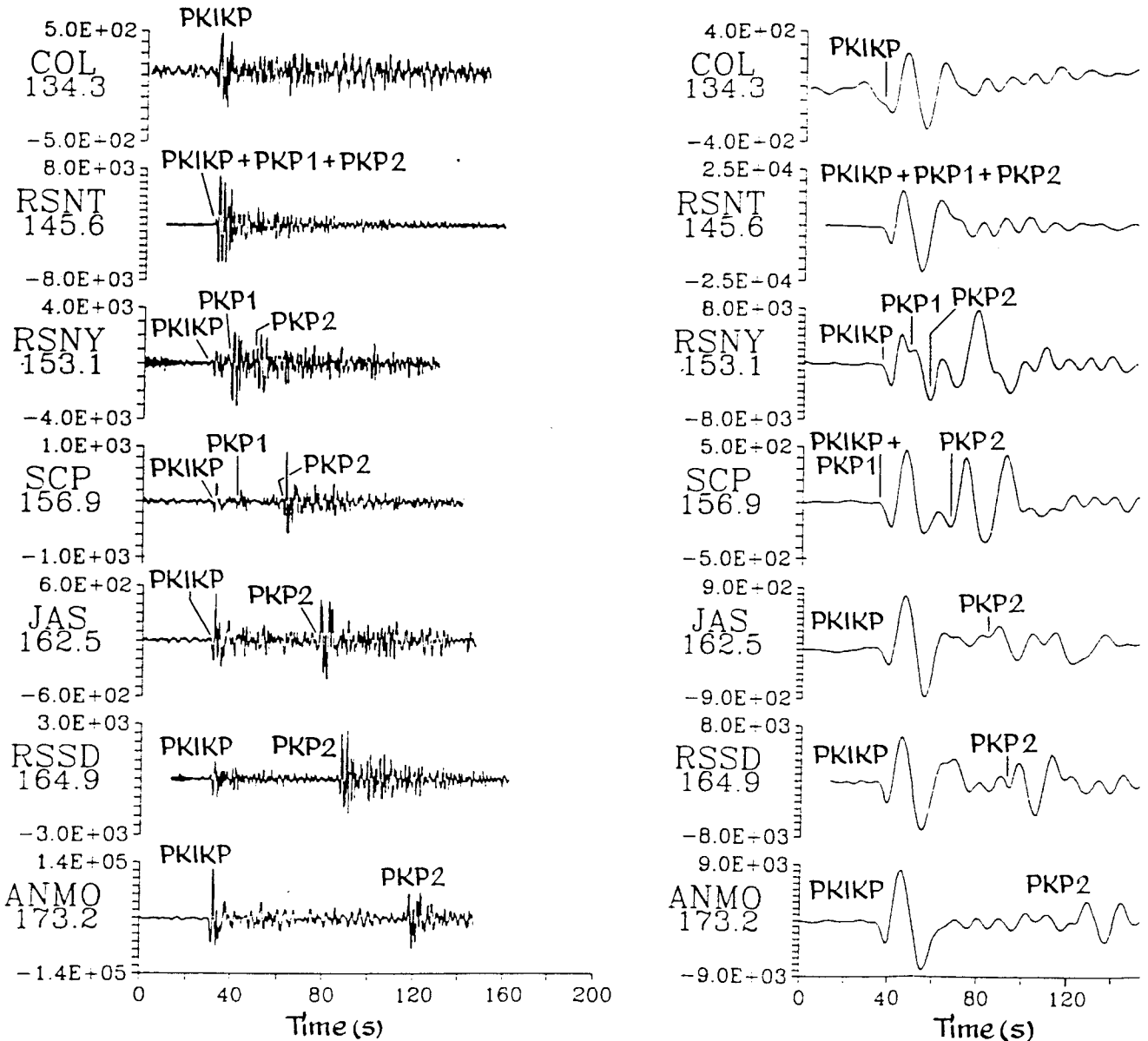


Fig. 2: Seismograms from Mid-Indian Rise earthquake on May 16, 1985 ($M = 6.0$, $h = 10$ km) at epicentral distances between 134.2° and 173.2° . Left: short-period records, right: long-period records (Reprint from Kulhánek, *Anatomy of Seismograms*, Copyright 1990; with permission from Elsevier Science).

3. AMPLITUDE-DISTANCE RELATIONSHIPS FOR PKP PHASES

Besides the systematic, distance-dependent travel-time differences the amplitude ratio of the different direct longitudinal core phases is another important identification criterion. According to the normalised theoretical amplitude-distance curves shown in Fig. 3 PKIKP is the weakest phase for $D < 155^\circ$. Exceptions may be sometimes observed weak amplitude forerunners. These phases, annotated PK(P) by Hales, 1995 and PKHKP in the initial publication by Bolt (1964), are due to energy scattered from the CMB. These rather incoherent phases may arrive between about 130° and 144° up to 17 s before PKIKP (cf. Fig. 4).

For $D < 135^\circ$ PKiKP, following PKIKP within a second, may have several times larger amplitudes. Between $143^\circ < D < 155^\circ$ the intermediate phase PKP1(PKP_{bc}) is theoretically expected to have amplitudes about 2 to 10 times larger than that of PKIKP, followed by PKP2(PKP_{ab}) with about 1.5 to 4 times larger amplitudes than PKIKP (cf. Fig. 3).

According to ray theory PKP1 is supposed not to exist beyond $D = 155^\circ$ for the models IASP91 (Fig. 1) and 1066B (Fig. 3), but due to diffraction around the inner core this phase is often observed up to about 160° (Fig. 5) but then generally as the weakest of the direct core phases.

According to Fig. 3 PKP2 is expected to become somewhat smaller than PKIKP beyond about 155° . This does not agree with our observations up to about 165° . They show PKP2 generally with 2-4 times, sometimes even more larger amplitudes than PKIKP (Figs. 5 - 7). This is also reflected in the magnitude calibration functions Q of these 3 phases as depicted in Fig. 9 of the chapter *Magnitude of seismic events*, with Q being smaller when the relative amplitude is larger.

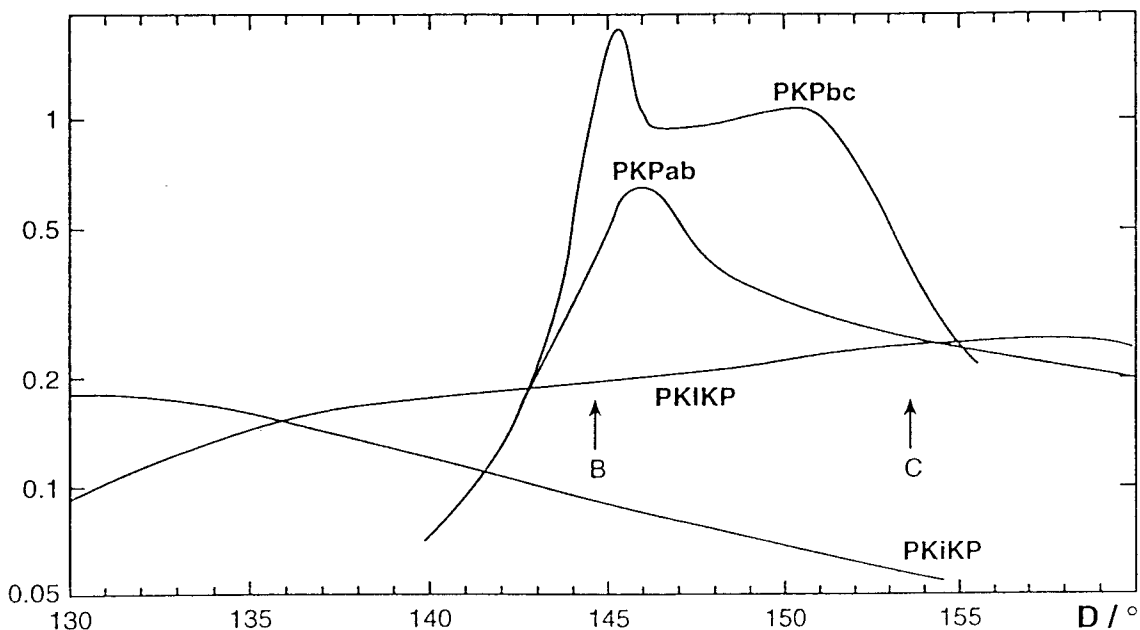
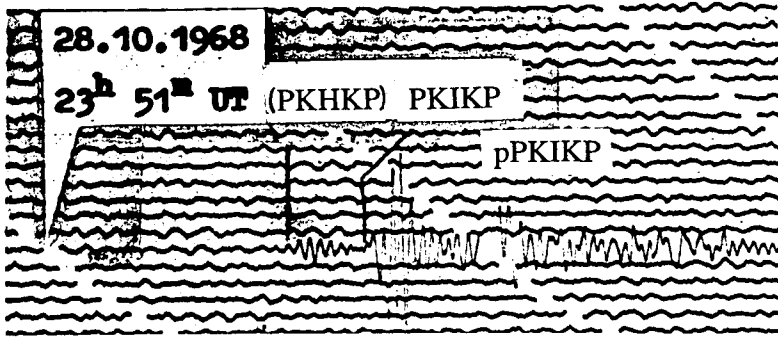


Fig. 3: Smoothed amplitude-distance relationships for the core phases PKIKP, PKiKP, PKP1 and PKP2 as calculated for the model 1066B (modified according to Houard et al. 1993).



D = 135.5°
h = 60 km
m_b = 5.9
Santa Cruz
Islands

Fig. 4: Short-period, vertical component, at station Moxa (MOX), Germany, of an event underneath Santa Cruz Islands. The (PKHKP) forrunner is clearly to be seen.

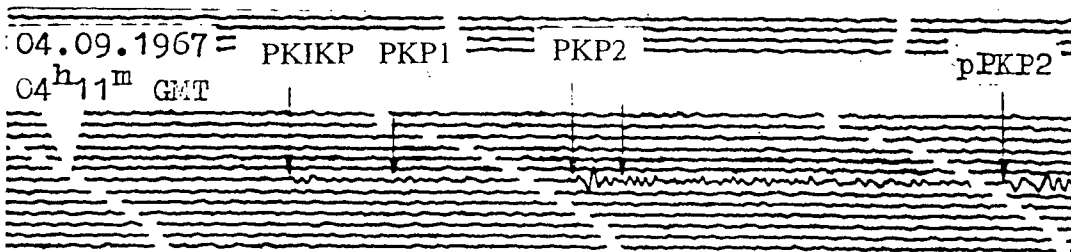


Fig. 5: Short-period, vertical component, at station Moxa (MOX), Germany, of an event underneath of the Kermadec Islands (D = 159.1°, h = 231 km, m_b = 5.5). PKP1 is still clear.

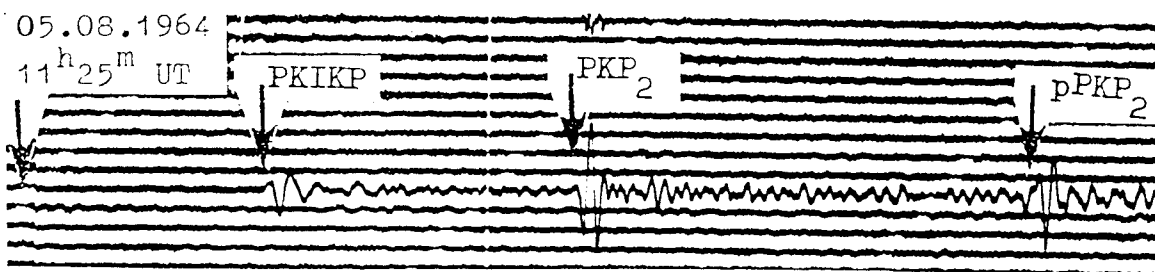


Fig. 6: Short-period, vertical component, at station Moxa (MOX), Germany, of an event south of the Kermadec Islands (D = 159.5°, h = 235 km, m_b = 5.5). PKP2 is still much stronger than PKIKP.

Fig. 7 below shows the average relative experimental A-D relationships for two ranges of source depth h as determined from data of station CLL. It provided the basis for the new PKP magnitude calibration functions in Fig. 9 of the chapter *Magnitude of seismic events* were. Fig. 8 depicts a typical short-period band-pass-filtered record section for PKP observations at the digital broadband German Regional Seismograph Network (GRSN). It illustrates essential amplitude features and travel-time relationships of the core phases discussed above.

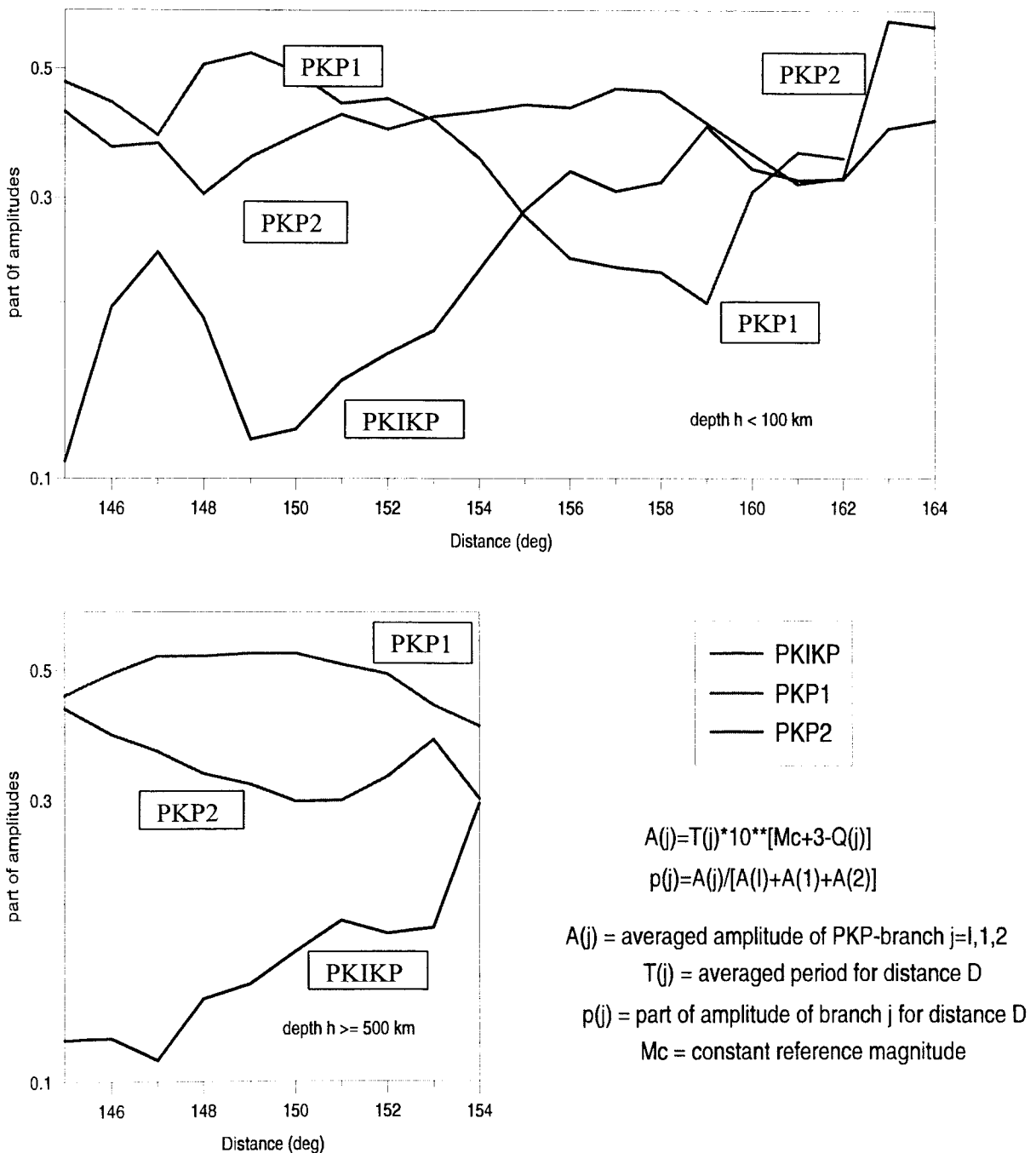


Fig. 7: Experimental A-D relationships for PKIKP, PKP1 and PKP2 as derived from experimental data observed at station Collmberg (CLL), Germany, for focal depths $h < 100$ km (above) and $h > 500$ km (below).

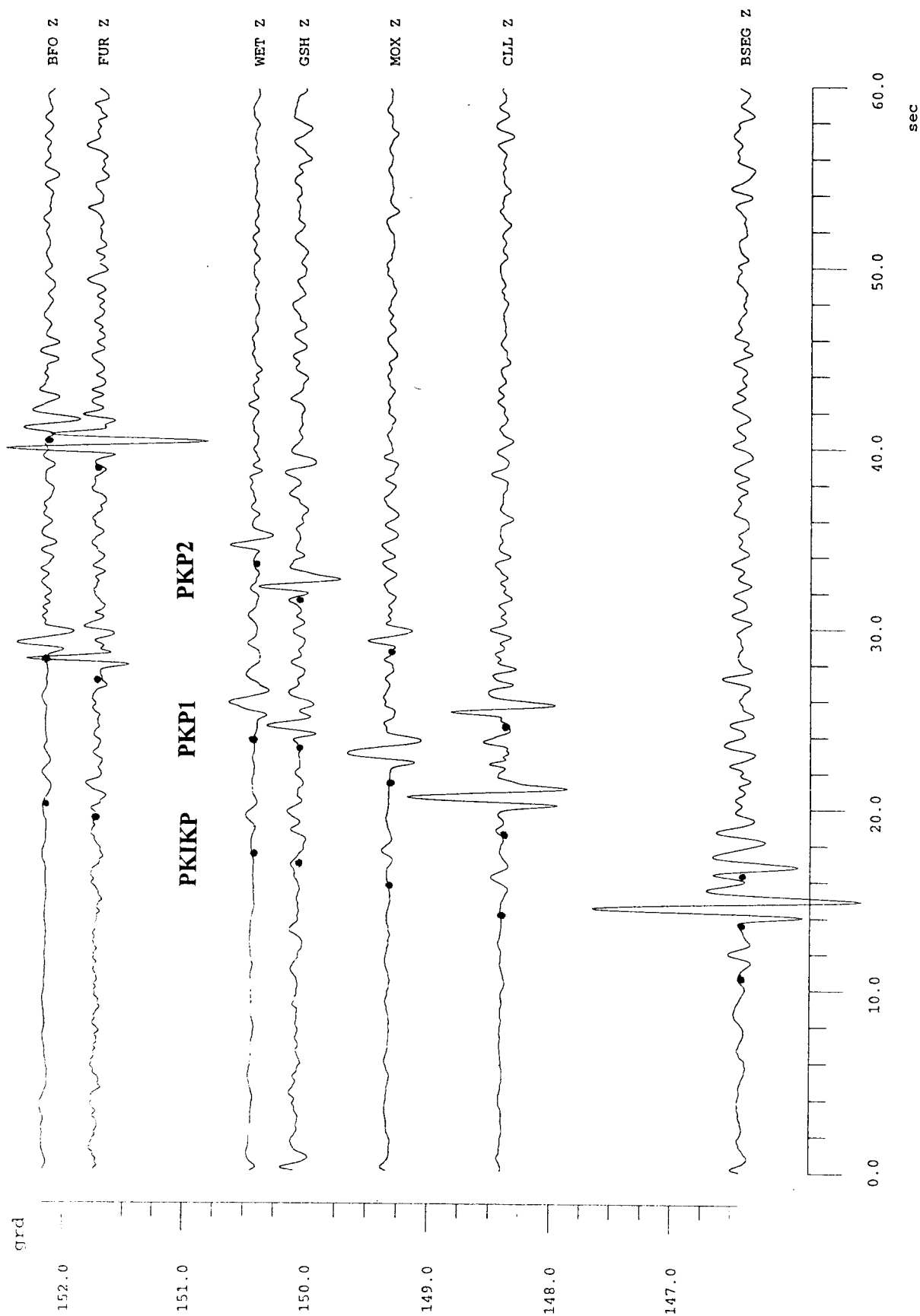


Fig. 8: Short-period band-pass filtered record section (WWSSN-SP) of core phases from an earthquake underneath the Fiji Islands (29 November 1997, $O = 02:42:27,3$ UT, $h = 581$ km, $m_b 5.2$; the record starts at $03:00.50$ UT) at stations of the German Regional Seismograph Network (GRSN). The full dots mark the theoretically expected onset times for PKIKP, PKP1 and PKP2 according to the IASP91 travel time table.

4. MAGNITUDE DETERMINATION FROM DIRECT LONGITUDINAL CORE PHASES

Although several versions of magnitude calibration functions Q for PKP waves have already been proposed earlier, no generally accepted calibration functions for core phases do exist until now. Miyamura (1974) considered only shallow earthquakes. Janský et al. (1977) were the first to publish preliminary depth-dependent calibration functions. They allowed magnitude determinations based on measurements of the maximum A/T ratio (A - amplitude in nm, T - period in s) from the whole PKP-wave group regardless of what branch of the travel-time curve it is related to. Kowalle et al. published Q functions for the first PKP onset measured at station MOX, Germany, and for CLL single phase measurements for source depth $h < 100$ km and $h > 500$ km (Tittel, 1977). Wendt and Tittel (1991) used 26 Tuamotu underground nuclear explosions and the Homogeneous Magnitude System (HMS), developed by Christoskov et al. (1978 and 1985) to determine station corrections, magnitudes and a calibrating function for PKP (maximum amplitudes of the group only) for the rather limited distance interval 143° to 148° .

Detailed depth- and distance-dependent functions $Q(D, h)$ have been determined by S. Wendt on the basis of amplitude and period measurements of short-period vertical component recordings at station CLL, Germany, for all three direct core phases which appear in the range $D = 145^\circ - 164^\circ$. The isoline plots of $Q(D, h)$ are shown in Fig. 9. They were derived from a total of about 4000 A/T -readings between 1970 and 1994. The following relationship applies for determining the core-phases body wave magnitude $m_b(\text{PKP})$:

$$m_b(\text{PKP}) = \log_{10}(A/T) + Q(D, h)$$

with amplitude A in μm (10^{-6} m), period T in s, epicentral distance D in degree and source depth h in km.

These depth-dependent magnitude calibration curves allow m_b determinations from core phases with a standard deviation of $< \pm 0.2$ magnitude units as compared to m_b determinations from teleseismic P waves at the international data centres such as ISC or NEIC. If more than one PKP phase can be identified and amplitudes and periods been measured the average value from all individual magnitude determinations should be calculated which is a more stable estimate. The general applicability of these calibration functions should be tested with data from other stations of the world-wide seismic network.

Fig. 9 (next page): Magnitude calibration functions $Q(D, h)$ for PKIKP, PKP1 and PKP2 as derived from data of the seismological observatory Collm (CLL), Germany, by S. Wendt.

Magnitude Calibrating Functions for Core Phases

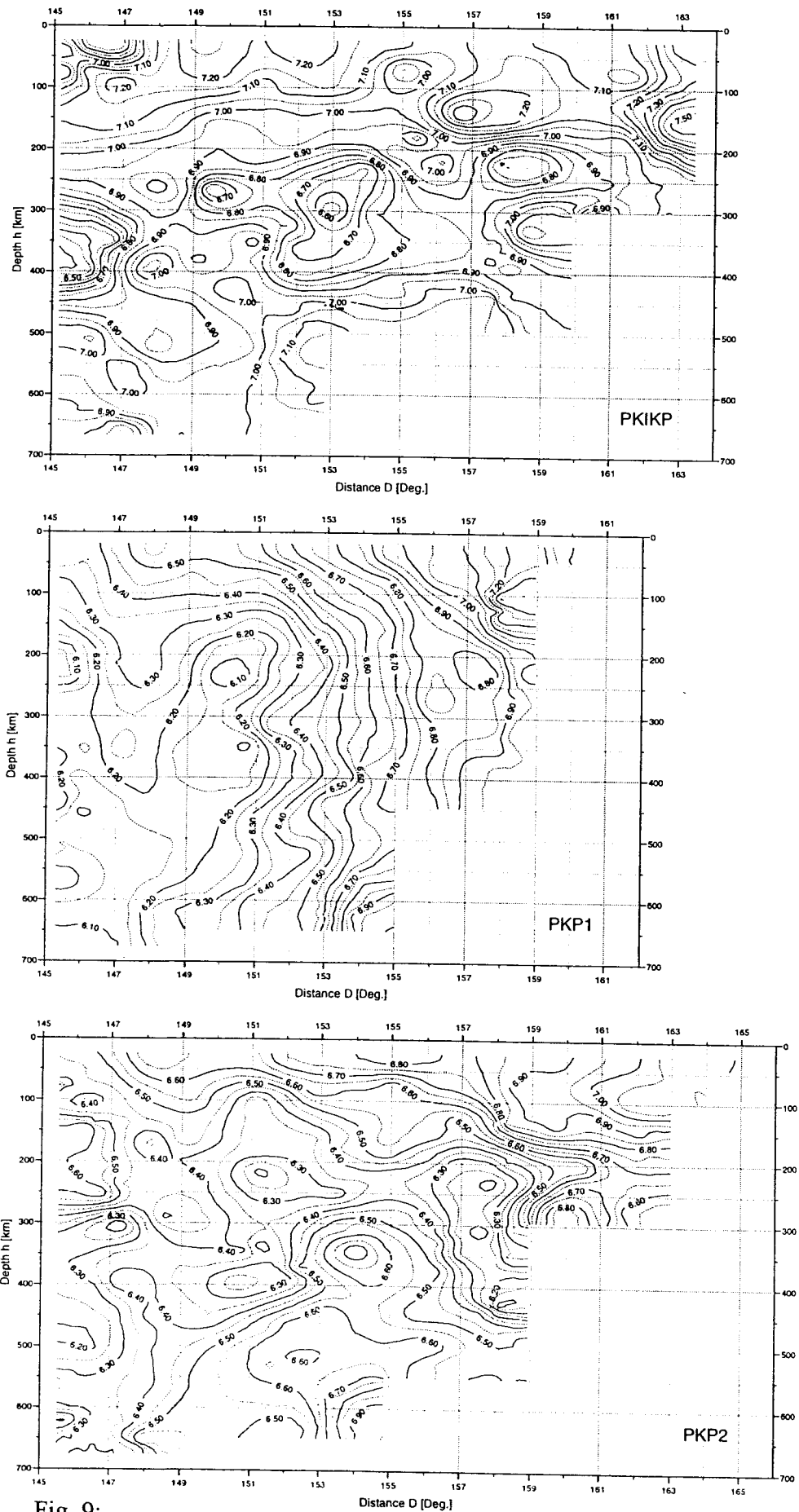


Fig. 9:

5. ADDITIONAL CHARACTERISTICS OF PKP-ONSETS

As can be inferred from Fig. 1 above, PKP-onsets have much larger amplitudes in vertical components than in horizontal ones (cf. also Fig. 10 below). This is equivalent to a rather small slowness ranging between 0 s° (in case of PKIKP at $D = 180^\circ$) and 4.44 s° for PKP2 at the same epicentral distance. The latter value corresponds to that of mantle P-waves diffracted around the CMB for $D > 98^\circ$. The slowness values near the caustic vary between 1.7 s° for PKIKP and $< 4 \text{ s}^\circ$ for PKP2. Awaiting of data from a *station network* (e.g. Fig. 8) or *array* one can determine the slowness from the onset-time differences and use the slowness values both for event location as well as an additional identification criterion (e.g. Schlittenhardt, 1996).

The differential time pPKP - PKP (i.e. depth phase - direct core phase) is, in a first approximation, nearly independent of the epicentral distance (Fig. 11). This allows to determine D with rather good accuracy (better than about 1.5°) from the travel-time differences of the 2 or 3 pronounced direct core phases in records of a single station only even without knowing the source depth (Fig. 12). In case of clearly developed depth phases one may sometimes be able to recognise the same sequence of onsets with different amplitudes as for the direct core phases (Fig. 10). If this is not the case, one should determine the focal depth always from the time difference between pPKP and the strongest PKP-onset.

In case of rather clear first motion polarities in 3-component records of core phases such as for PKP1 in Fig. 10 the azimuth of the event can be determined too, with an accuracy of about 5 to 10° .

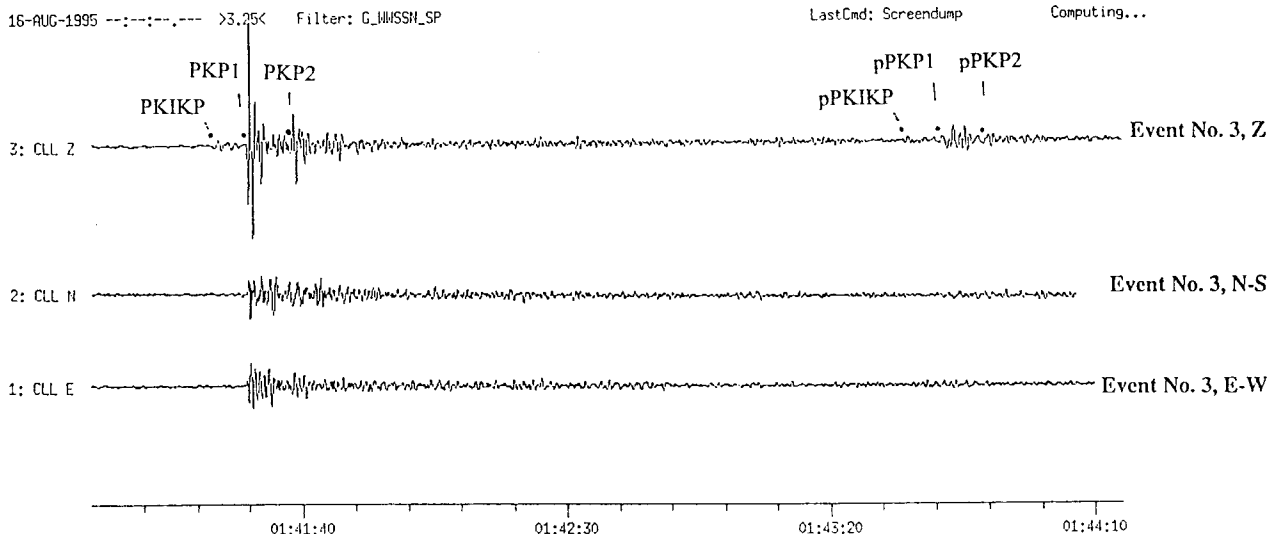


Fig. 10: Example of a three component short-period recordings of direct longitudinal core phases and related depth phases at station CLL from an event underneath Fiji Islands ($D = 150.0^\circ$, $H = 540 \text{ km}$, $m_b = 5.3$).

IASPEI 91: pPKP - PKP for 150 deg

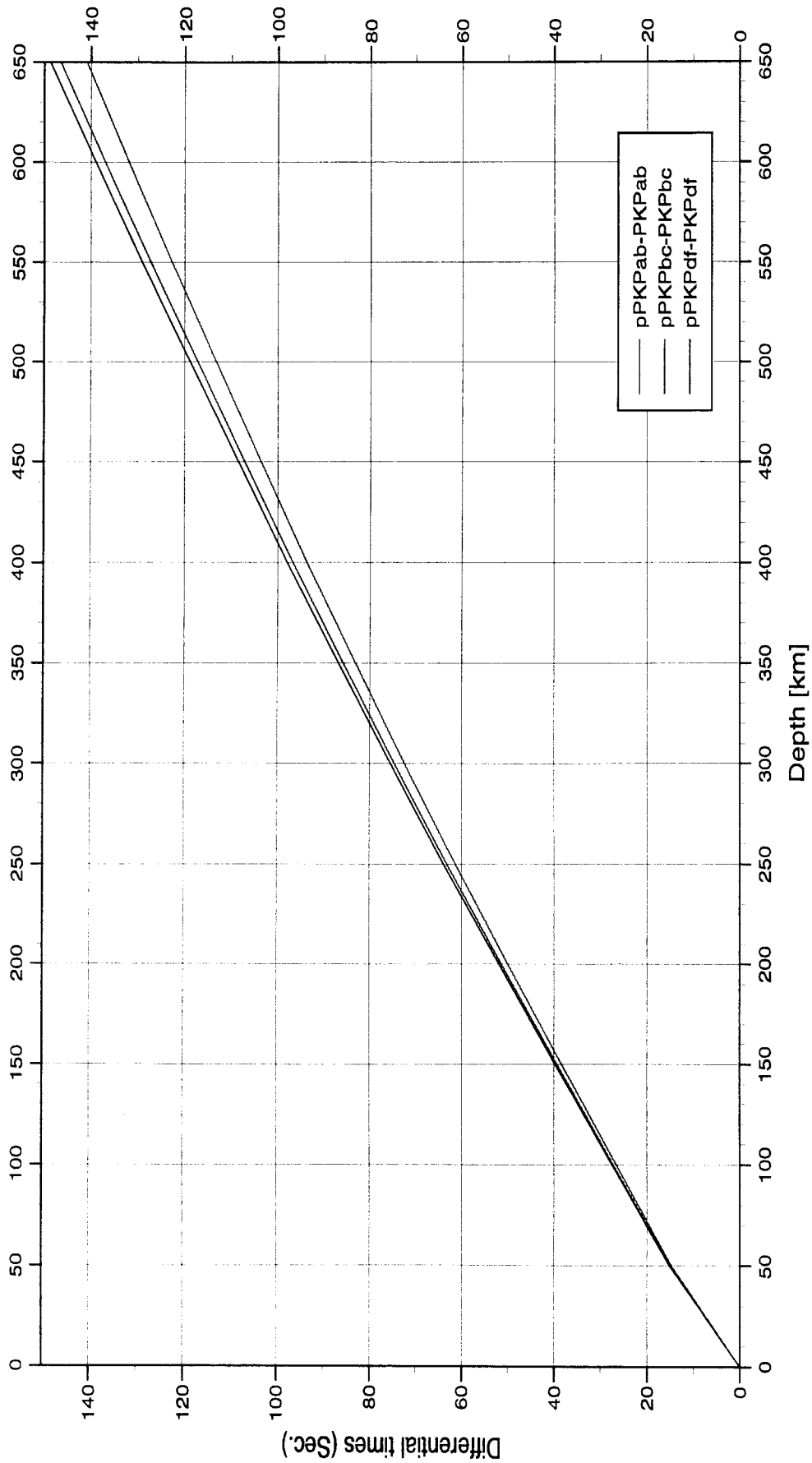


Fig. 11: Differential travel-times pPKP-PKP for the branches ab, bc and df according to the travel-time tables IASP91 (Kenneth, 1991) at the epicentral distance 150°.

IASPEI 91: PKPbc - PKPdf and PKPab - PKPdf (PKP1 - PKIKP and PKP2 - PKIKP)

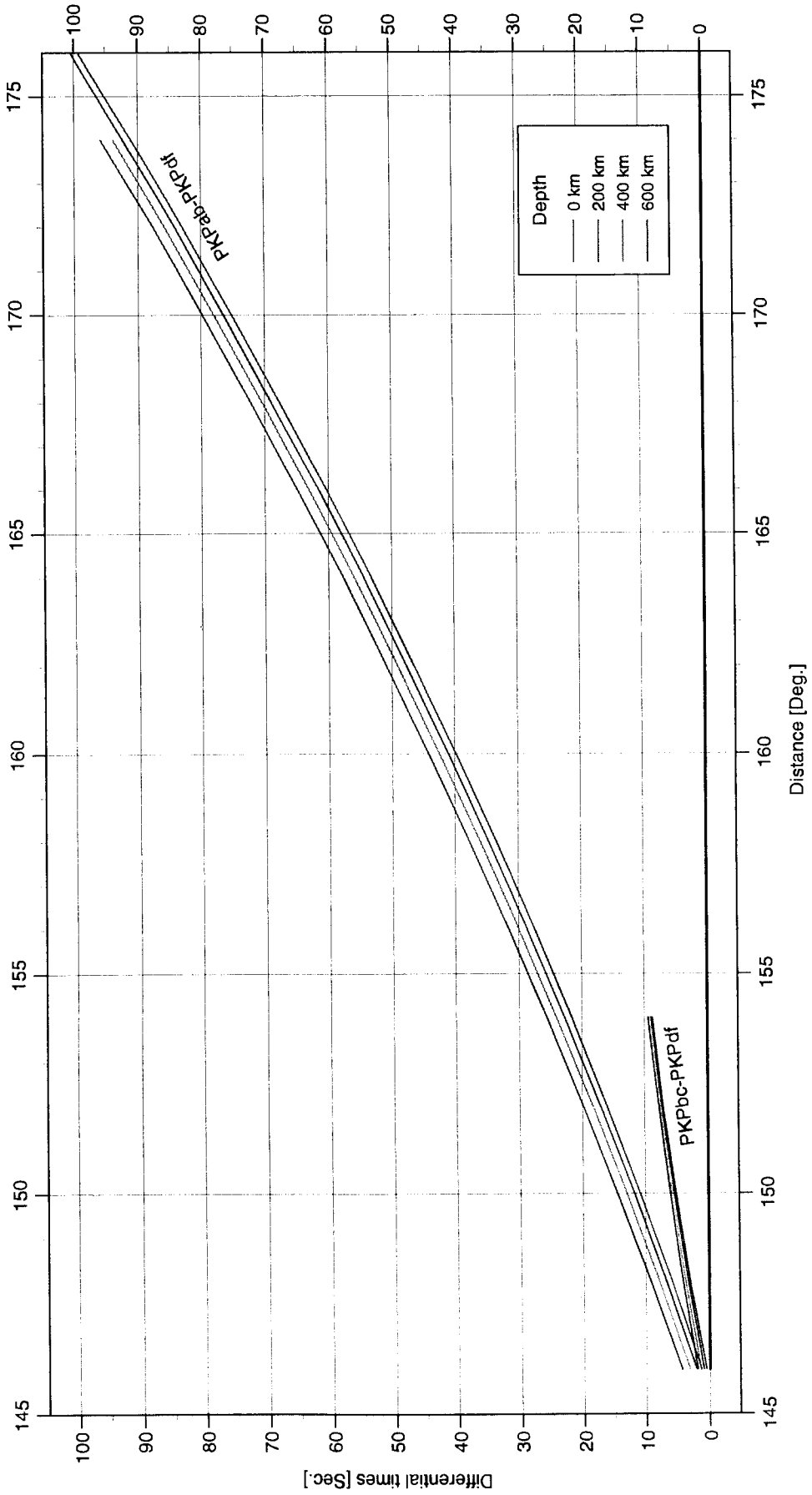


Fig. 12: Depth-dependent travel-time between PKP_{bc}-PKP_{df} and PKP_{ab}-PKP_{df} according to the travel-time tables IASP91 (Kenneth, 1991)

6. REFLECTED CORE PHASES

In case of stronger events, reflected core phases may be observed besides direct ones, sometimes with up to 4 (or even more) repeated reflections. These phases may be observed at practically all teleseismic distances with delays behind the first arriving P or PKP onsets ranging from about 10 minutes up to about 80 minutes depending on the number of multiple reflections. These phases are clearly discernible only in high-magnifying short-period records. Most frequently observable are the single reflection PKKP and PKPPKP, the latter sometimes called P'P' (Fig. 14). The respective n-fold reflections are sometimes annotated for short as PnKP or nPKP, respectively. Fig. 15 shows ray paths for PKKP, PKPPKP and P4KP while Fig. 13 presents a record cut-out with the latter phase, weak but still distinct and superimposed on more long-period "signal noise". The figures illustrate that these phases may indeed erroneously be interpreted by station operators as being P or PKP first arrivals from independent events.

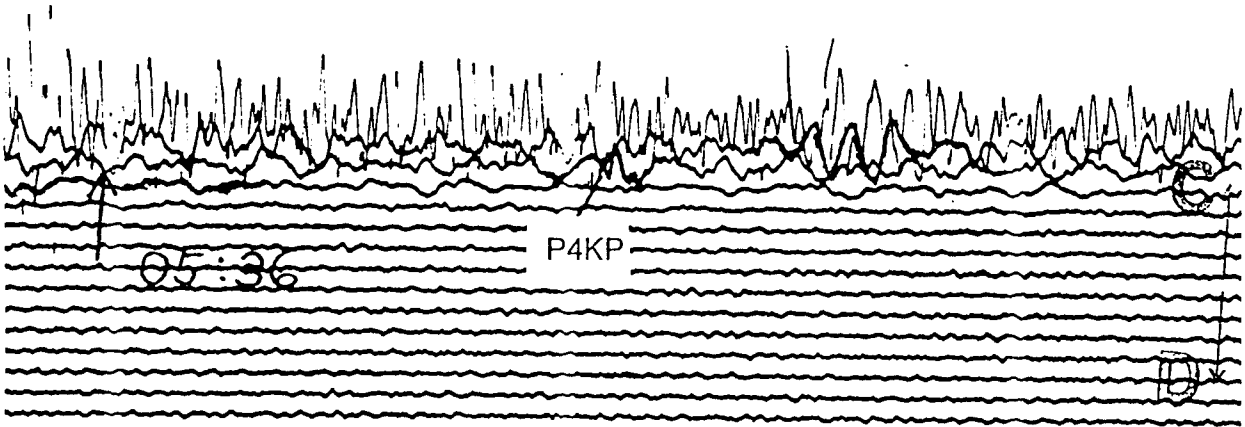
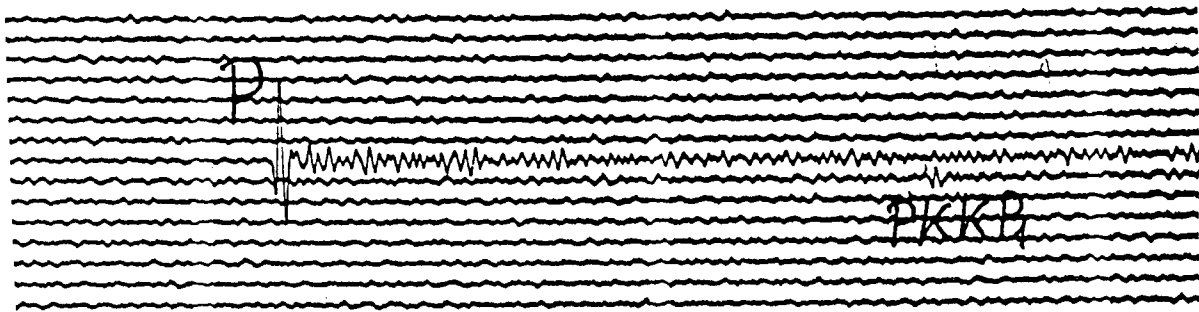


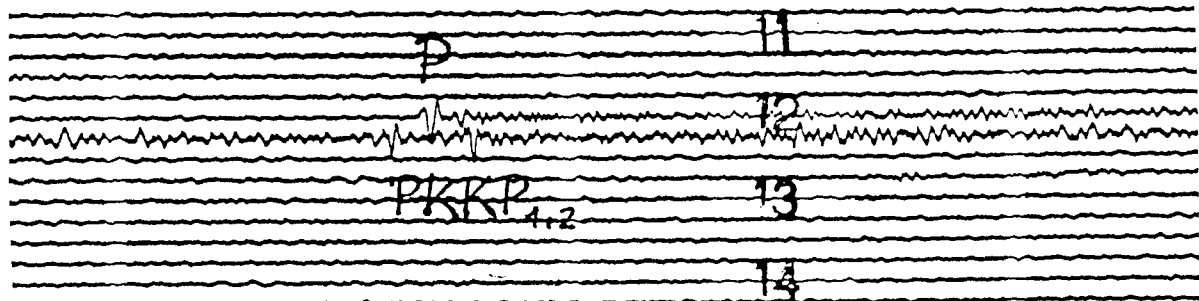
Fig. 13: Weak onset of the multiple reflection P4KP in short-period records of station CLL at the epicentral distance $D = 71^\circ$ from a deep earthquake underneath Sachalin Islands (12.05.1990, $h = 605$ km, $m_b = 6.5$). The related ray path is depicted in the lower part of Fig. 15.

PKKP is observable mainly in the distance range $80^\circ < D < 127^\circ$ with about 13 to 19 min behind P or 9.5 to 12 min behind PKIKP (Fig. 16). PKPPKP is observable between $10^\circ < D \leq 105^\circ$ (Fig. 17). In this range it follows the P-onset after about 40 to 24 min. For more details see the complete IASP91 travel time tables (Kenneth, 1991).

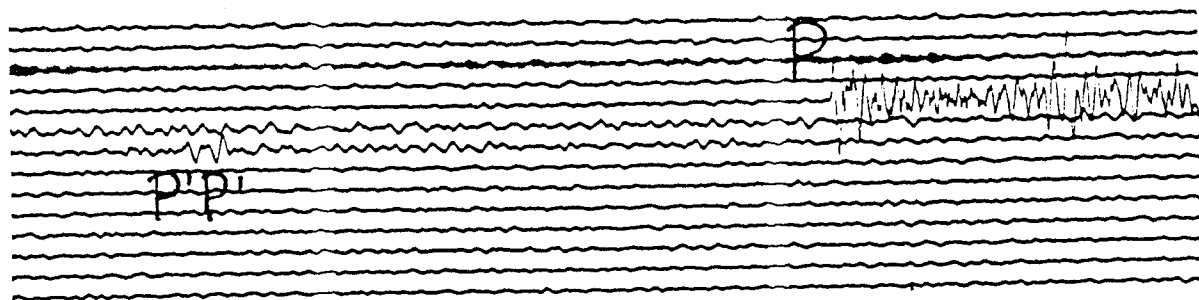
A particular advantage of these phases is again the small depth dependence of their travel-time differences to P and PKP, respectively. Consequently, their identification allows very good distance estimates from single station records even without knowing the source depth. Because of the inverse differential travel-time curves of PKKP and PKPPKP with respect to P and PKP their identification can be facilitated by comparing the onset times at neighbouring stations. An additional interpretation aid is the determination and comparison of the polarisation for both the first arrival and the PKKP or PKPPKP onset, respectively, from 3-component records. According to Fig. 15 their azimuths should be opposite to that of P.



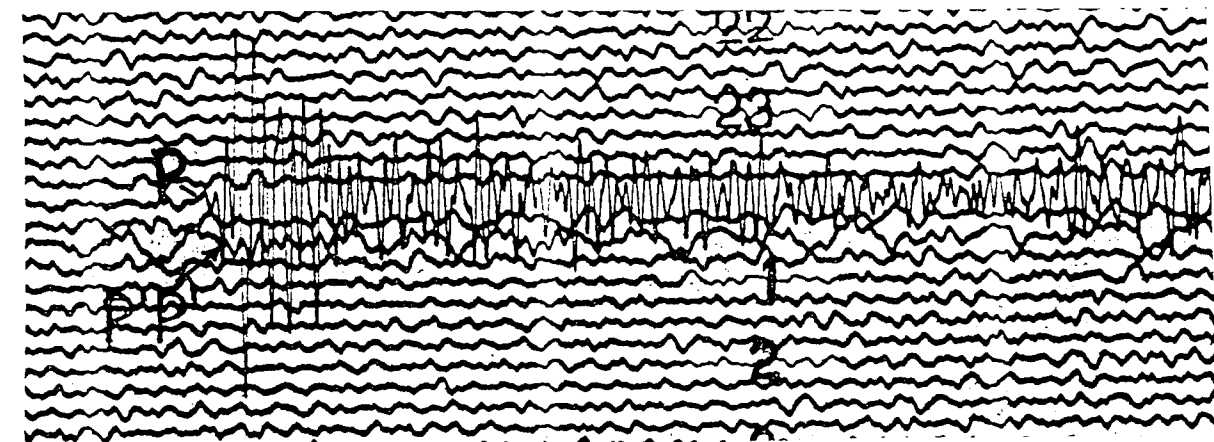
24.08.1995 Mariana Islands: H = 01:55:34.4, D(CLl) = 98.3°, h = 588 km, $m_b = 6.0$



13.07.1994 Banda Sea: H = 11:45:23.4, D(CLl) = 111.2°, h = 159 km, $m_b = 6.5$



08.08.1994 Myanmar: H = 21:08:31.7, D(CLl) = 66.3°, h = 122 km, $m_b = 6.1$



18.02.1996 North of Ascension Island: H = 23:49:27.8, D(CLl) = 57.3°, h = 10 km, $m_b = 6.3$

Fig. 14: Short-period recordings of reflected longitudinal core phases PKKP and PKPPKP (P'P') at station CLL, Germany. Neighbouring traces are 15 min apart from each other!

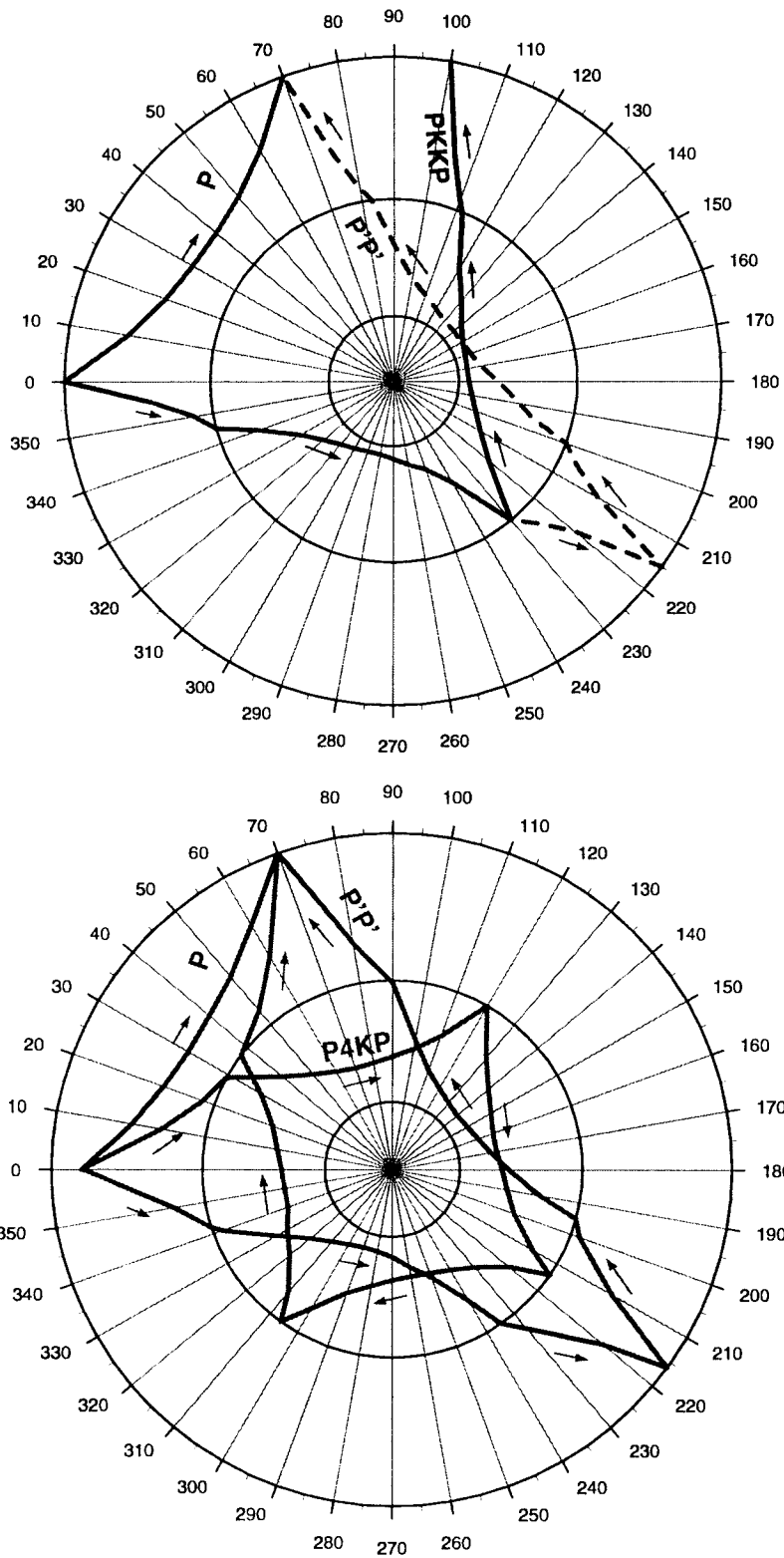


Fig. 15: Ray paths for P, PKKP and PKPPK (P'P') (above) and for P4KP (below).

PKKP - P and PKKP - PKP

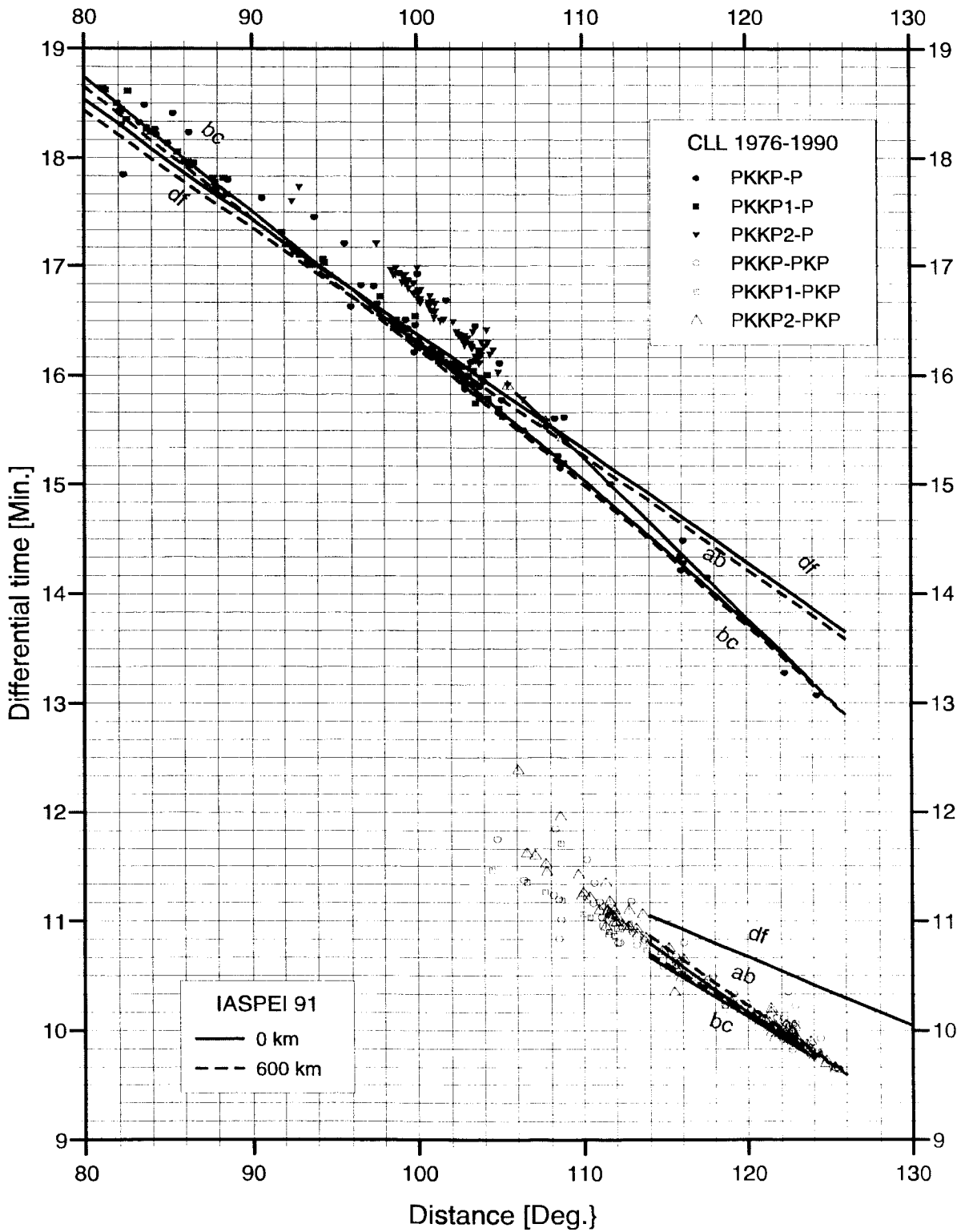


Fig. 16: Comparison between theoretical (IASP91) and observed travel-time differences for PKKP-P and PKKP-PKP at station CLL as a function of epicentral distance and source depth.

PKPPKP - P

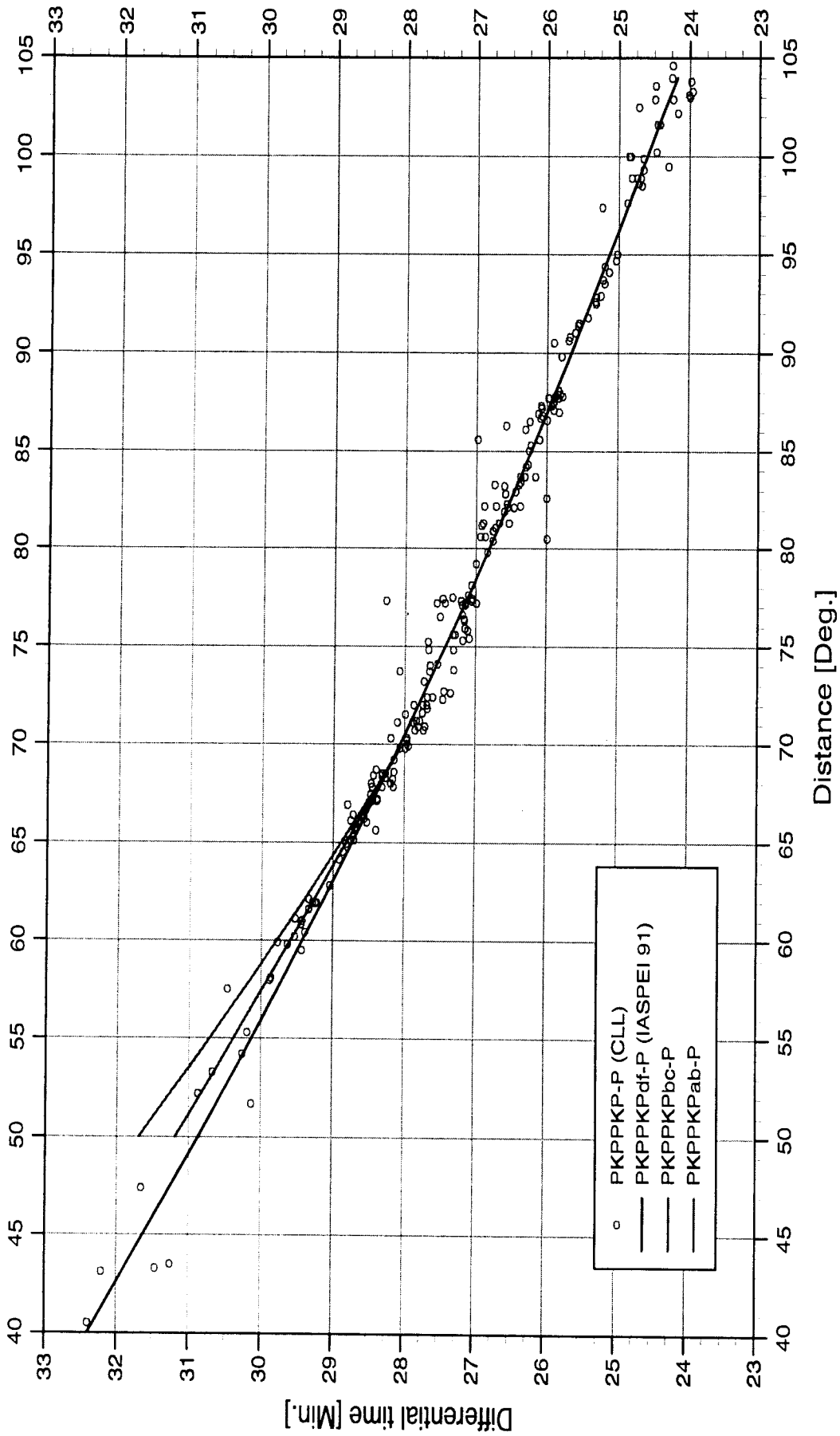


Fig. 17: Comparison between theoretical (IASPEI 91) and observed travel-time differences PKPPKP-P at station CLL depending on epicentral distance.

Multiple reflections from the inner side of the CMB such as P3KP, P4KP and P5KP are observed, if at all, at about 37 ± 1 min after the first arriving wave. The latter is in case of P3KP the P-wave at around 10° epicentral distance, in case of P4KP the P-wave between $45^\circ < D < 75^\circ$ and for P5KP the onset of PKIKP between about $130^\circ < D < 150^\circ$.

Sometimes, also converted core reflections such as SKPPKP or SKKP can be observed in short-period recordings. Contrary to this, converted or reflected core phases which have travelled along both ray segments through the mantle as S-waves are mostly observed in broadband or long-period records.

7. SUMMARY DISCUSSION

From the discussions above, comparing theoretical with experimental travel-time- and amplitude-distance relationships we can conclude:

- 1.) Between about 145° and 160° the longitudinal core phases PKIKP (PKP_{df}), PKP1 (PKP_{bc}) and PKP2 (PKP_{ab}) follow a rather typical distance-dependent travel-time difference and amplitude pattern. This allows to identify these phases and to determine the epicentral distance of the related event with rather high accuracy (better than 1.5°) from short-period records of just a single seismic station. The same applies for using the travel-time differences between P or PKIKP to reflected core phases such as PKKP, PKPPKP or their multiples.
- 2.) This pattern is well developed, especially in case of deep earthquakes when no close-up following depth phases, as in case of crustal earthquakes, interfere with this typical wave group.
- 3.) Experimental data about core phases may still deviate significantly from those predicted on the basis of current best earth models. This highlights not only the urgent need to provide the international data centres with much more carefully identified and measured data about core phases. It also alarms us not to base our interpretations and measurements exclusively on theoretically expected travel-time branches and onset times or amplitude-distance relationships. Distinct and well correlated phases may still exist clearly beyond the limits to which their theoretical travel-time curves, based on ray theory calculations, have been defined, and also their amplitudes may differ significantly from the predicted ones.
- 4.) The depth-dependent magnitude calibration curves as derived from PKP amplitude readings at the station CLL (cf. Fig. 9) allow m_b determinations from core phases with an accuracy of better than ± 0.2 magnitude units. Their applicability should be tested at other stations of the world-wide network.

ACKNOWLEDGEMENT

The authors wish to thank Dr. Bernd Tittel from the Geophysical Observatory Collm (CLL) for valuable discussions and suggestions. He also provided us with Figs. 13 and 15.

REFERENCES

- Bath, M. (1984). Earthquake magnitudes based on PKP and SKP waves. In: The O.G.S. Silver Anniversary Volume, O.G.S. Trieste, p.93-108
- Bolt, B.A. (1964). The velocity of seismic waves near the earth's center. *Bull. Seism. Soc. Am.*, **54**, 1, 191-208.
- Bormann, P. (1967). Aufzeichnungen longitudinaler Kernphasen an der Station Moxa und ihre Interpretation. In: Stelzner, J. und Bormann, P.. *Seismologisches Bulletin 1965 - Station Moxa*. Akademie-Verlag Berlin 1967, 10-15.
- Bormann, P. (1972). A study of relative frequencies of body-wave onsets in seismic registrations of station Moxa. In: Bormann, P. and Stelzner J. (1972). *Seismological Bulletin 1967 - station Moxa (MOX)*, Akademie-Verlag Berlin, 379-396.
- Christoskov, L., Kondorskaya, N.V. and Vanek, J. (1978). Homogeneous magnitude system of the Eurasian continent. *Tectonophysics*, **49**, 131-138.
- Christoskov, L., Kondorskaya, N.V., Vanek, J. (1985). Magnitude calibrating functions for a multidimensional homogeneous system of reference stations. *Tectonophysics*, **118**, 213-226.
- Gutenberg, B. (1913). Über die Konstitution des Erdinnern, erschlossen aus Erdbebenbeobachtungen. *Physik. Zeitschrift* **14**, 1217-1218.
- Haddon, R.A.W. and Cleary, J.R. (1973). Precursors to PKIKP and seismic wave scattering near the mantle-core boundary. *Phys. Earth Planet. Interiors* **7**, 495-497
- Hales, A.L. (1995). Comment on "Amplitudes of core waves near the PKP caustic, from nuclear explosions in the South Pacific recorded at the "Laboratoire de Detection et Geophysique" network in France" by S. Houard et al., *BSSA.*, **85**, 3, 957-958.
- Houard, S., Plantet, J.L., Massot, J.P. and Nataf, H.C. (1993). Amplitudes of core waves near the PKP caustic, from nuclear explosions in the South Pacific recorded at the "Laboratoire de Detection et Geophysique" network in France. *BSSA*, **83**, 6, 1835-1854.
- Janský, J., Ruprechtová, L. and Tittel, B. (1977). Magnitude determination based on short-period core waves. *Studia geoph. et geod.* **21**, 267-273.
- Kulhanek, O. (1990). Anatomy of seismograms. *Developments in Solid Earth Geophysics*, No. 18, Elsevier Science Publishers B.V., Amsterdam-Oxford-New York-Tokyo, 178 pp.
- Kennett, B.L.N. (Editor) (1991). *IASPEI 1991 Seismological Tables*. Research School of Earth Sciences, Australian National University, 167 pp.
- Kowalle, G., Tittel, B. and Bormann, P. (1983). Determination of a magnitude calibration function using short-period readings of PKP. *Tectonophysics*, **93**, 289-294.
- Lehmann, I. (1936). *P'. Bur. Centr. Seismol. Int. A.*, **14**, 87-115.
- Miamura, S. (1974). Determination of body-wave magnitudes for shallow earthquakes in the New Zealand and Macquarie Loop regions using PKP data. *Phys. Earth Planet. Int.*, **8**, 167-176.
- Oldham, R.D. (1899). Report on the great earthquake of 12th June 1897. *Mem. Geol. Survey, India*, **29**, 1-379.
- Schlittenhardt, J. (1996). Array analysis of core-phase caustic signals from underground nuclear explosions: Discrimination of closely spaced explosions. *Bull. Seism. Soc. Am.*, **86**, 1A, 159-171.
- Tittel, B. (1977). Zur Bestimmung von Erdbebenmagnituden aus longitudinalen Kernwellen. *Gerlands Beitr. Geophysik*, **86**, 79-85.
- Wendt, S. and Tittel, B. (1991). Calibration function and station corrections for PKP waves in the vicinity of a caustic. *Studia geoph. et geod.*, **35**, 213-220.

Exercise on local event localisation by means of seismic network recordings: Graphical and PC assisted methods

P. Bormann, M. Baumbach and K. Wylegalla

GeoForschungsZentrum Potsdam,
Telegrafenberg, D-14473 Potsdam

1. Identify the local phases (Pn, Pg, Sn and Sg only) in the records of the Potsdam seismic network shown in Figs. 1 and 2 using the travel-time difference curve shown in Fig. 3 and provided as transparent overlay. Mark the onset-times and annotate them with the respective phase symbols (by weak pencil only!).
2. Write the distance, corresponding to your phase interpretation, on each record and mark also the origin time according to your interpretation with a vertical line on each trace. Determine the average origin time.
3. Use a) the circle and b) the chord method on the map (Fig. 4) to determine the epicenter co-ordinates for both events. As epicenter take the center of gravity of your circle- or chord-crossings, respectively.
4. Carry out the phase interpretation and event localization of several digitally recorded local events by using the PC program **seis89**.

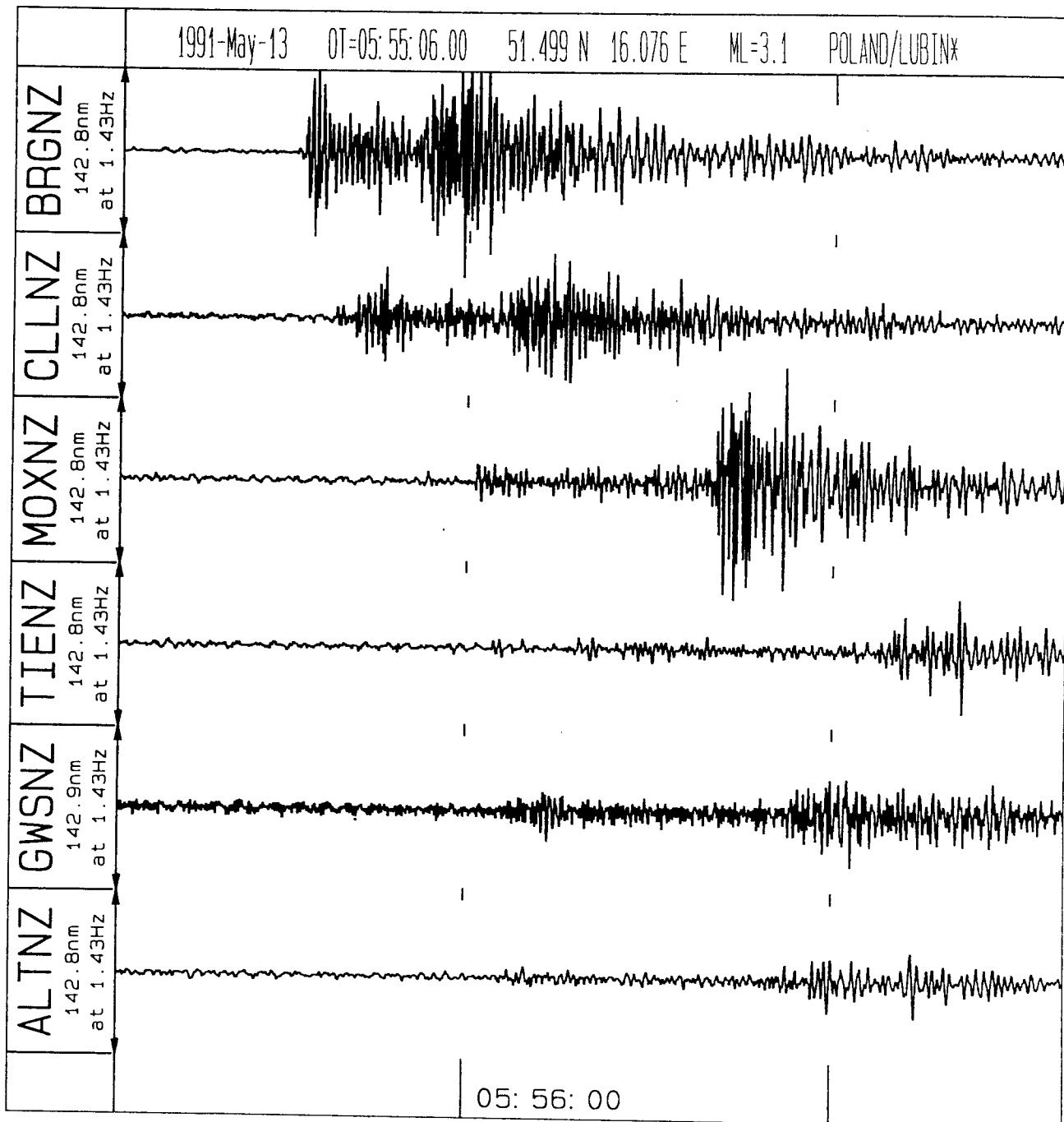


Fig. 1

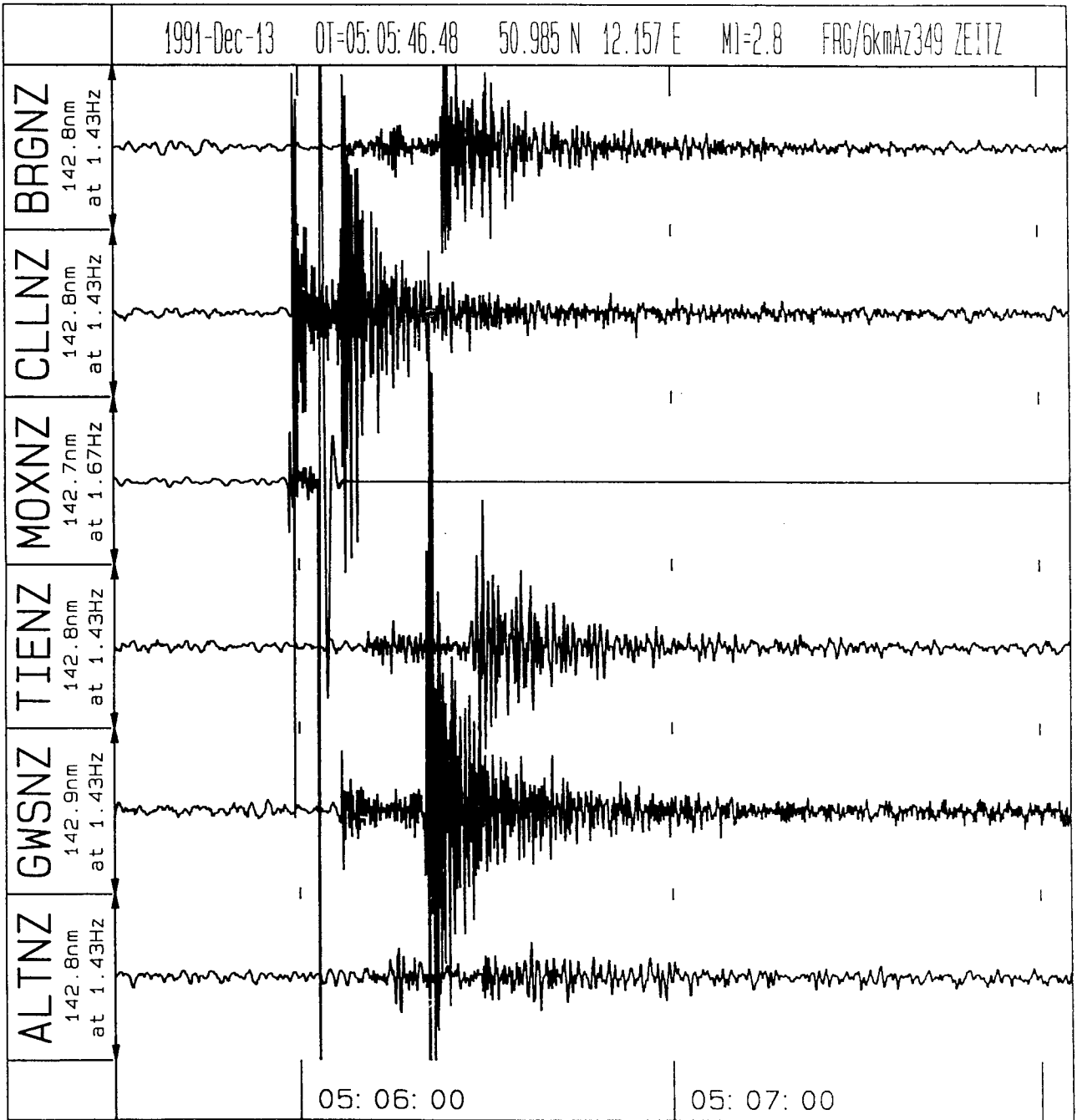


Fig. 2

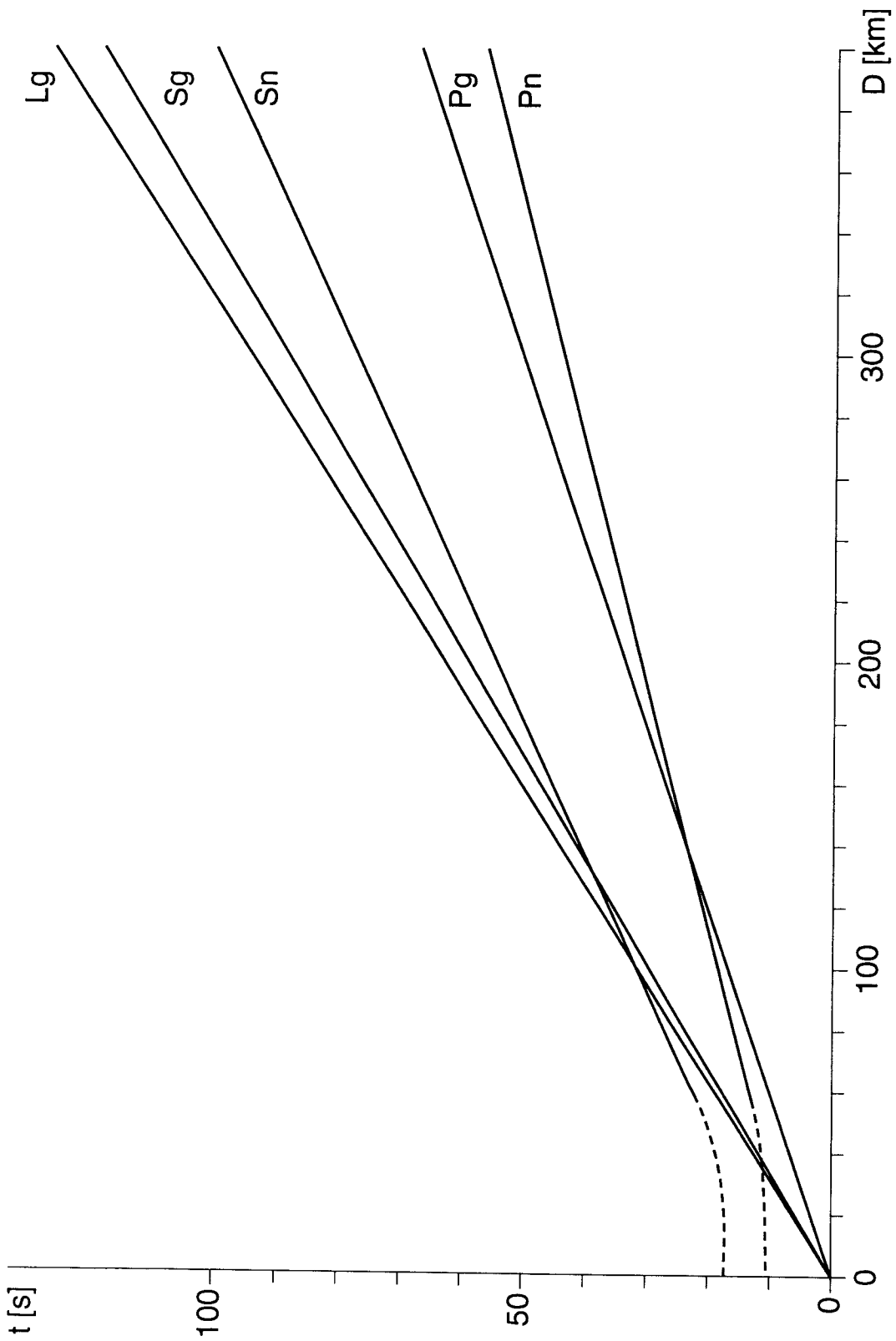


Fig. 3: Local travel-time curves for SE Germany

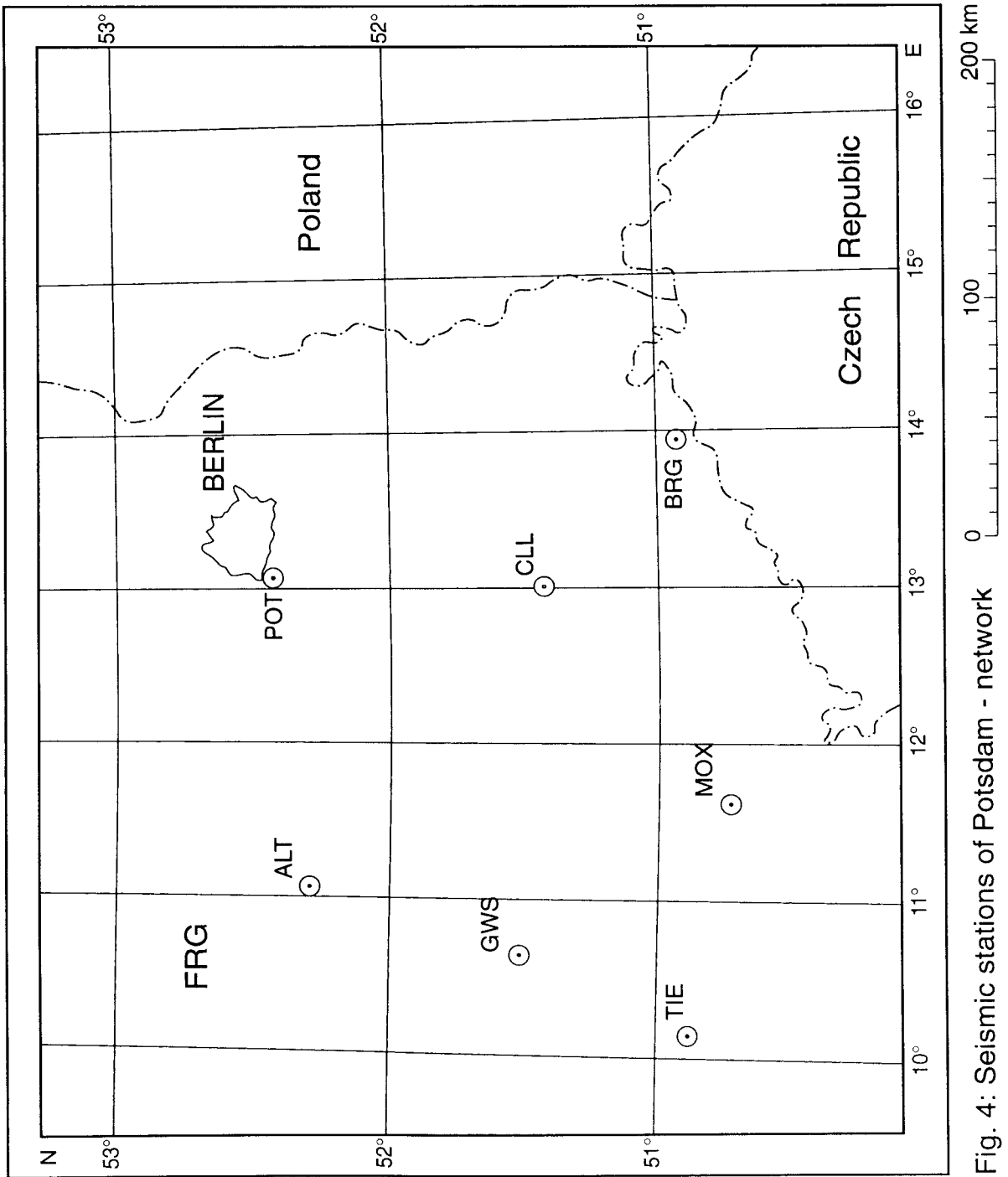


Fig. 4: Seismic stations of Potsdam - network

Exercise on 3-component seismogram interpretation

P. Bormann and K. Wylegalla

GeoForschungsZentrum Potsdam,
Telegrafenberg, D-14473 Potsdam

1. Analyse Fig. 1, i.e.:
- 1.1 Decide whether the earthquake shown is shallow or deep taking into account also Tab. 1 which gives the travel-time difference between the first P-wave onset and the surface Rayleigh-wave maximum R_{\max} .

Tab. 1	Δ°	$t_{R_{\max}} - t_p$ minutes	Δ°	$t_{R_{\max}} - t_p$ minutes	Δ°	$t_{R_{\max}} - t_p$ minutes
	10	4-6	55	26	100	45-46
	15	6-8	60	28-29	105	47-48
	20	9-10	65	31	110	48-50
	25	10-12	70	33	115	53
	30	13-14	75	35	120	55
	35	15-16	80	37	125	57
	40	18-19	85	39-40	130	60
	45	21	90	42	140	64
	50	24	95	43	150	70

- 1.2 Identify the first onset and the largest secondary onset.
- 1.3 Determine the epicentral distance Δ from the S - P times:
 - a) using the "rule of thumb" $\Delta [^\circ] = [t(S-P)_{\text{[min]}} - 2] \times 10$;
 - b) using the Jeffreys-Bullen travel-time difference graph for shallow events shown in Fig. 2 and provided as transparent overlay.
- 1.4 In case you had decided under 1.1 that the event was a deeper one, please try to identify the onset of depth phases (pP and/or sP, respectively) and calculate the focal depth h using Tab. 2 and/or 3.
- 1.5 Calculate the back-azimuth of the event using the following relationship $Az = \arctan(A_E/A_N)$. Be careful in deciding about the proper quadrant in which the azimuth is situated by comparing the polarities in all three components.
- 1.6 Determine the epicentral coordinates and source region of the event shown in Fig. 1 on the global map (Fig. 3).
2. Interpret along the lines outlined under 1. at least one more analog 3-component record given to you. Additionally try to identify as many as possible phases in the record and improve the distance determination by best possible fit of your identified onsets with the detailed travel-time difference graphs available from the exercise assistants.

Note! Please mark and annotate onsets in the seismograms only with weak pencil so as to be erasable.
3. Carry out the phase interpretation, distance and depth determination, polarization analysis and back-azimuth determination as well as event localization for several teleseismic events by using the PC program **seis89** and the global map in Fig. 3.

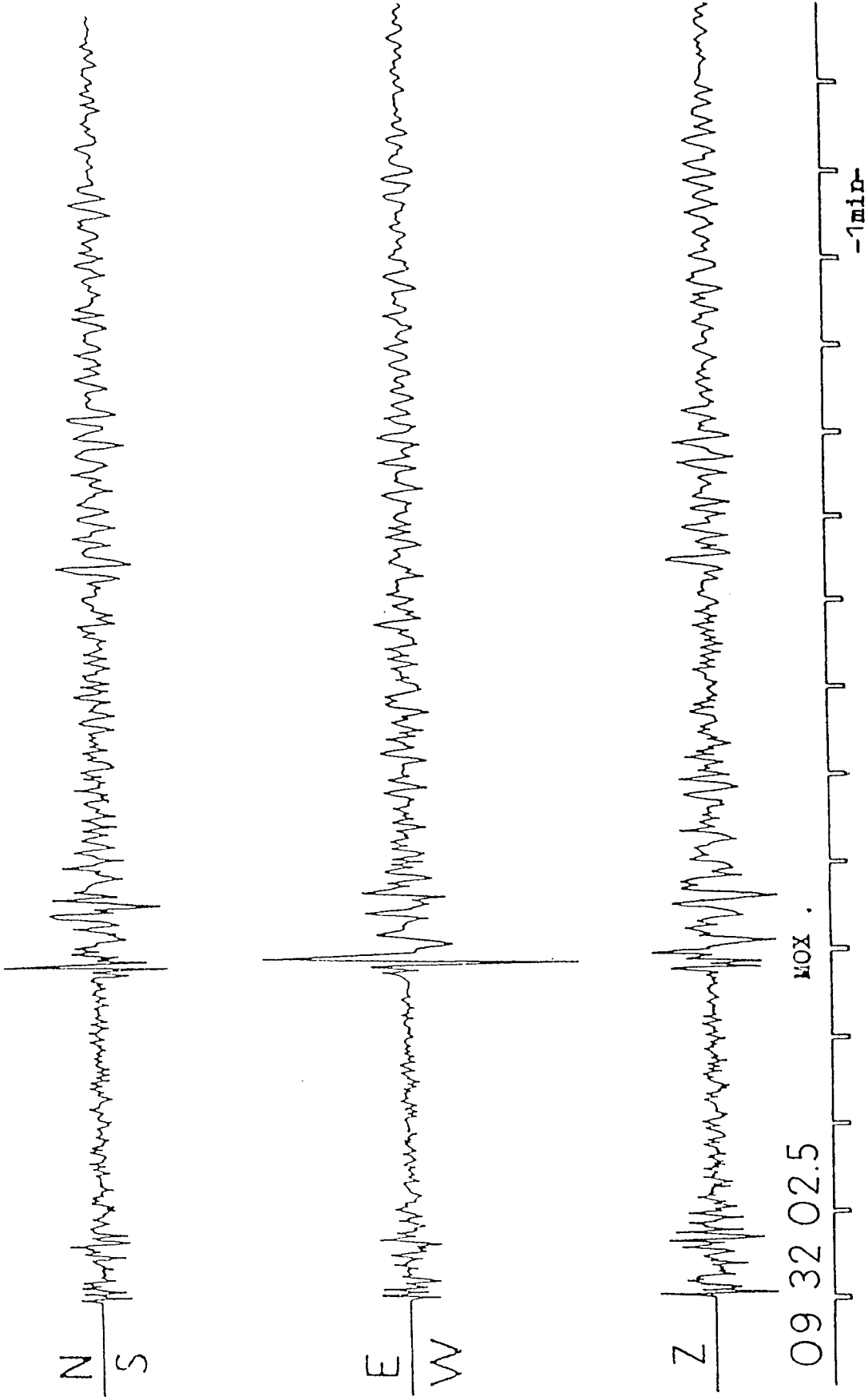
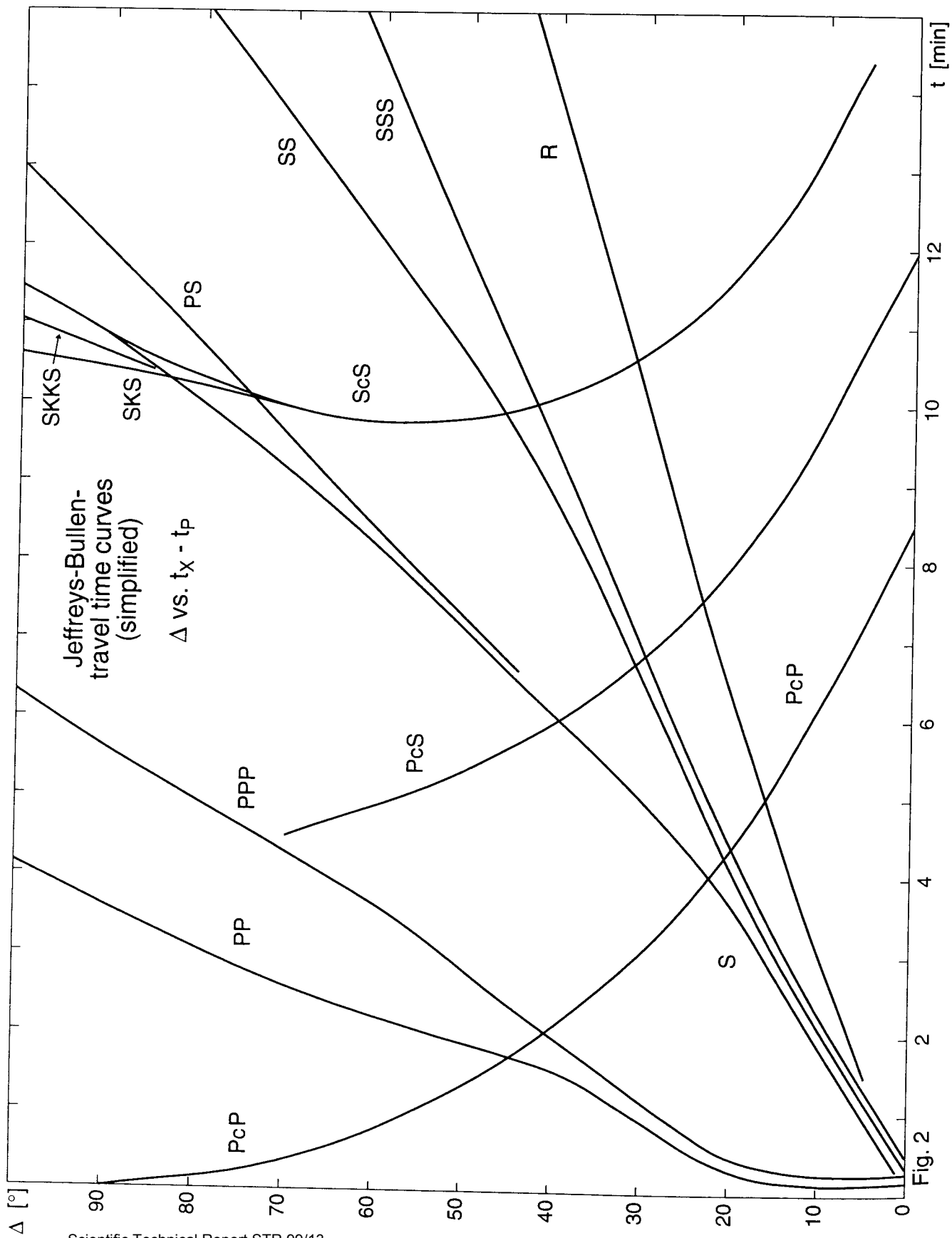
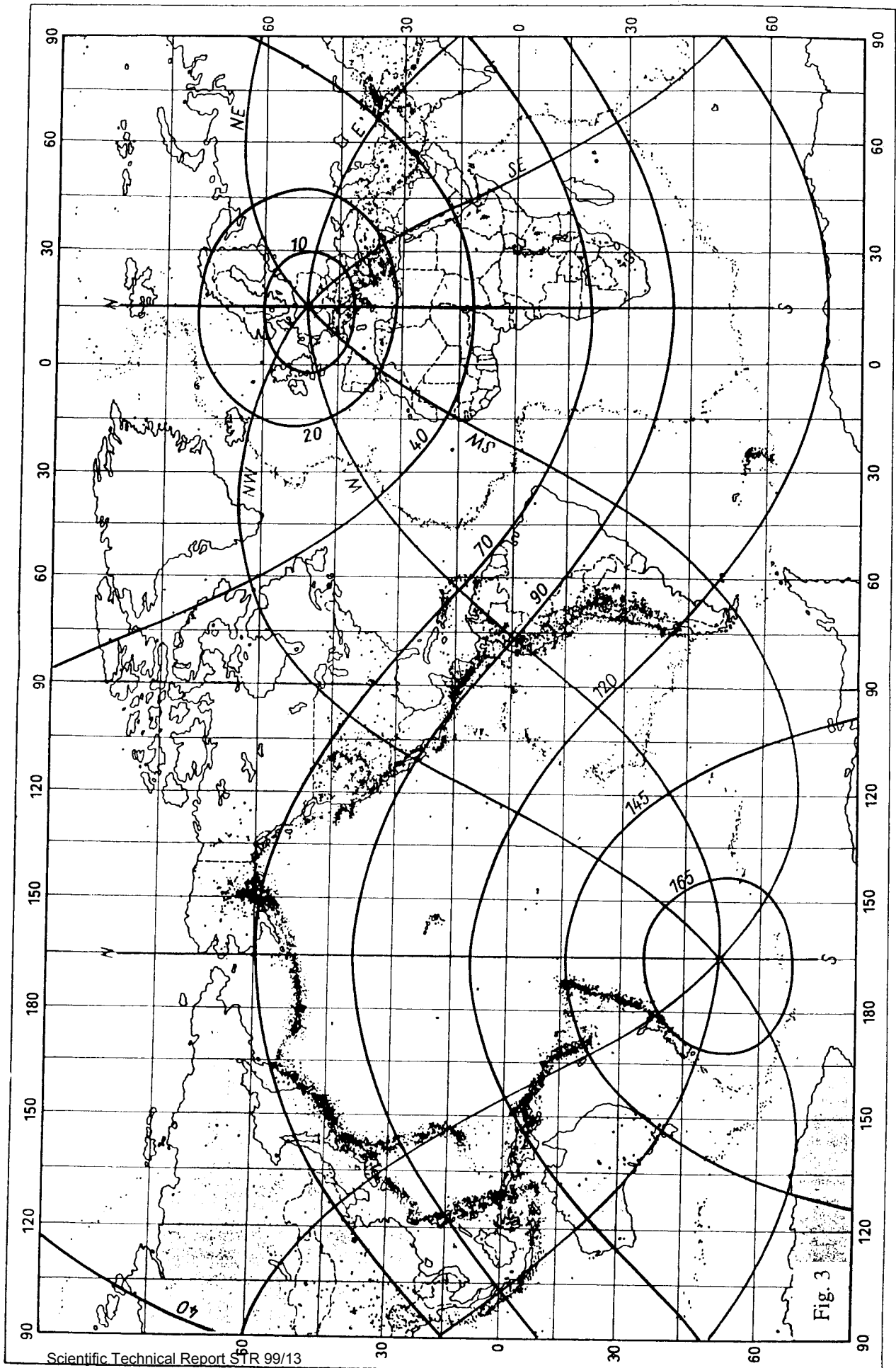


Fig. 1



Tab. 2

pP-P Δ	Depth of source [km]											
	15.	35.	50.	100.	150.	200.	250.	300.	400.	500.	600.	700.
2	3.6	7.5	7.9	20.1	26.2	32.6	38.8					
4	3.6	7.5	8.0	16.2	25.9	33.2	39.6					
6	3.6	7.5	8.3	16.0	25.8	34.4	41.7					
8	3.6	7.5	8.5	16.2	25.9	34.4	41.7					
10	3.6	7.6	8.1	16.2	25.9	34.4	41.7					
12	3.6	7.6	8.3	16.2	25.9	34.4	41.7					
14	3.6	7.6	8.5	16.2	25.9	34.4	41.7					
16	3.6	7.6	8.5	16.2	25.9	34.4	41.7					
18	4.0	8.5	10.1	19.0	26.6	34.4	41.7					
20	4.3	9.2	11.5	20.1	27.5	34.4	41.7					
22	4.3	9.3	11.7	19.4	26.9	34.4	41.7					
24	4.5	10.0	12.7	21.4	29.8	37.8	45.3					
26	4.6	10.0	12.8	22.1	31.3	40.2	48.7					
28	4.6	10.0	12.9	22.3	31.5	40.5	49.1					
30	4.6	10.1	12.9	22.4	31.7	40.8	49.4					
32	4.6	10.1	13.0	22.5	31.9	41.0	49.8					
34	4.6	10.1	13.0	22.6	32.1	41.3	50.1					
36	4.6	10.2	13.1	22.8	32.3	41.6	50.5					
38	4.6	10.2	13.1	22.9	32.6	42.0	51.0					
40	4.7	10.2	13.2	23.1	32.8	42.3	51.4					
42	4.7	10.3	13.3	23.2	33.1	42.7	51.9					
44	4.7	10.3	13.4	23.4	33.4	43.0	52.4					
46	4.7	10.4	13.4	23.6	33.6	43.4	52.8					
48	4.7	10.4	13.5	23.7	33.9	43.7	53.3					
50	4.7	10.5	13.6	23.9	34.1	44.1	53.7					
52	4.8	10.5	13.6	24.0	34.4	44.4	54.2					
54	4.8	10.5	13.7	24.2	34.6	44.8	54.6					
56	4.8	10.6	13.8	24.3	34.8	45.1	55.0					
58	4.8	10.6	13.8	24.5	35.1	45.4	55.4					
60	4.8	10.7	13.9	24.6	35.3	45.7	55.8					
62	4.8	10.7	13.9	24.8	35.5	46.0	56.2					
64	4.9	10.7	14.0	24.9	35.7	46.3	56.5					
66	4.9	10.8	14.1	25.0	35.9	46.5	56.9					
68	4.9	10.8	14.1	25.1	36.1	46.8	57.2					
70	4.9	10.8	14.2	25.3	36.3	47.1	57.6					
72	4.9	10.9	14.2	25.4	36.5	47.3	57.9					
74	4.9	10.9	14.3	25.5	36.7	47.6	58.2					
76	4.9	10.9	14.3	25.6	36.8	47.8	58.6					
78	4.9	11.0	14.4	25.7	37.0	48.1	58.9					
80	5.0	11.0	14.4	25.8	37.2	48.3	59.2					
82	5.0	11.0	14.5	25.9	37.4	48.5	59.5					
84	5.0	11.1	14.5	26.1	37.5	48.8	59.8					
86	5.0	11.1	14.6	26.1	37.7	49.0	60.0					
88	5.0	11.1	14.6	26.3	37.9	49.2	60.4					
90	5.0	11.1	14.6	26.3	37.9	49.3	60.5					
92	5.0	11.1	14.7	26.3	38.0	49.4	60.6					
94	5.0	11.1	14.7	26.4	38.1	49.5	60.6					
96	5.0	11.2	14.7	26.4	38.1	49.5	60.7					
98	5.0	11.2	14.7	26.4	38.1	49.6	60.8					
100	5.0	11.2	14.7	26.5	38.1	49.6	60.9					



Exercise on magnitude determination

P. Bormann and K. Wylegalla

GeoForschungsZentrum Potsdam,
Telegrafenberg, D-14473 Potsdam

1. Determine the surface wave magnitude $M_S = \log (A/T)_{\max} + \sigma (\Delta)$ both from the maximum amplitudes of the vertical (MLV) and horizontal components (MLH) of surface waves in the record given in Fig. 1. Use Tab. 1 for the calibration functions and the epicentral distance Δ and depth h as given on the record. The frequency response of all three seismometer components is identical. The respective magnifications V as a function of the period T are given in the table inserted in Fig. 1.
2. Determine the body wave magnitude $m_B = \log (A/T)_{\max} + Q (\Delta, h)$ for the intermediate deep earthquake shown in Fig. 1 of the exercise on 3-component seismogram interpretation both for the vertical component of P (MPV) and the horizontal component (vector sum!) of S (MSH). As calibration functions use the graphs shown in Fig. 2. As epicentral distance use $\Delta = 20.2^\circ$ and as focal depth $h = 111$ km.
3. Determine the local magnitude ML using the Potsdam magnitude formula developed by WAHLSTROEM and STRAUCH (1984):

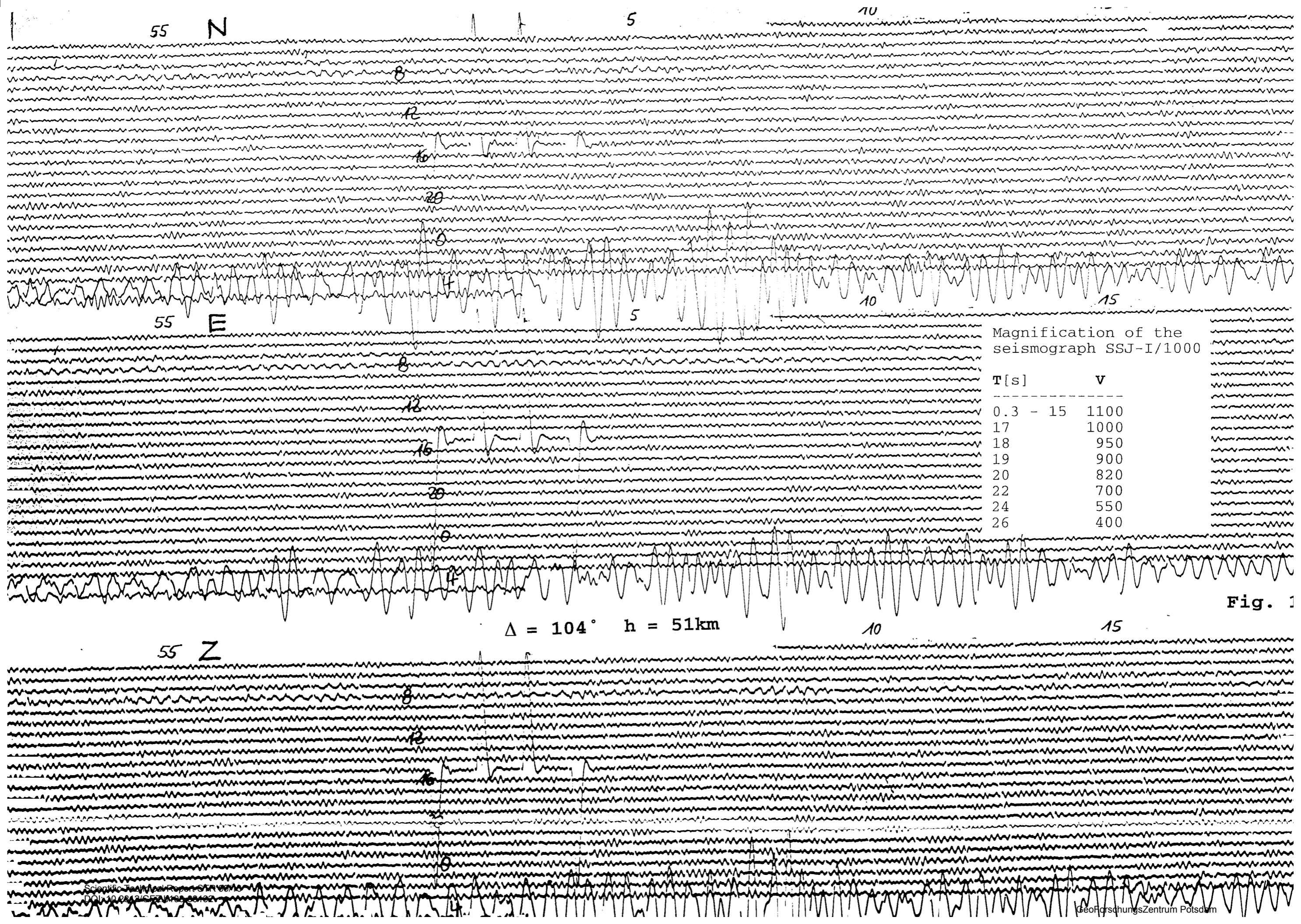
$$ML_{\text{POT}} = \log A - \log V_{\text{net}}(T) + \log V_{\text{WA}}(T) + 0.83 \log D + (0.0017/T) \times (D - 100) + 1.41$$

with **A** - measured seismogram amplitude of Sg wave in mm
V_{net} - amplification of the network seismographs
V_{WA} - amplification of a standard Wood-Anderson seismograph
D - epicentral distance in km
T - measured period in s

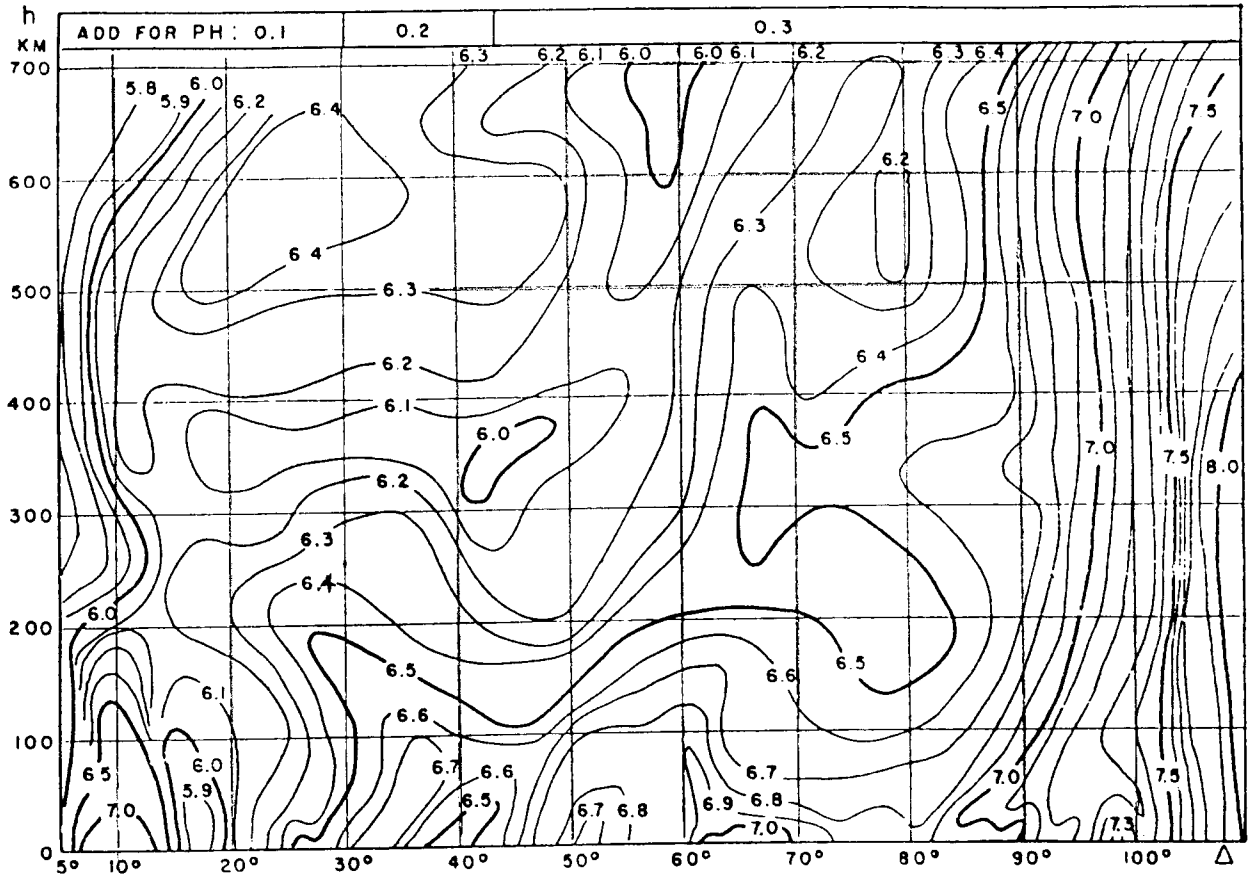
Note! This formula is applicable for distances between $100 \text{ km} < D < 700 \text{ km}$ only.

Determine ML for at least two stations of the Potsdam-network given in Fig. 1 of the exercise on local event localization. Use the maximum amplitude of Sg waves taking into account the event distance **D** as determined from these records. Use the period dependent magnifications **V_{net}(T)** and **V_{WA}(T)** as given below.

T [s]	V _{net}	V _{WA}	T [s]	V _{net}	V _{WA}
0.1	35000	2800	1.1	190000	1100
0.2	92000	2700	1.2	180000	950
0.3	125000	2600	1.3	170000	850
0.4	150000	2400	1.4	155000	750
0.5	170000	2200	1.5	140000	700
0.6	190000	2000	1.6	120000	
0.7	200000	1800	1.7	90000	
0.8	201000	1600	1.8	80000	
0.9	201000	1400	1.9	70000	
1.0	200000	1200	2.0	60000	

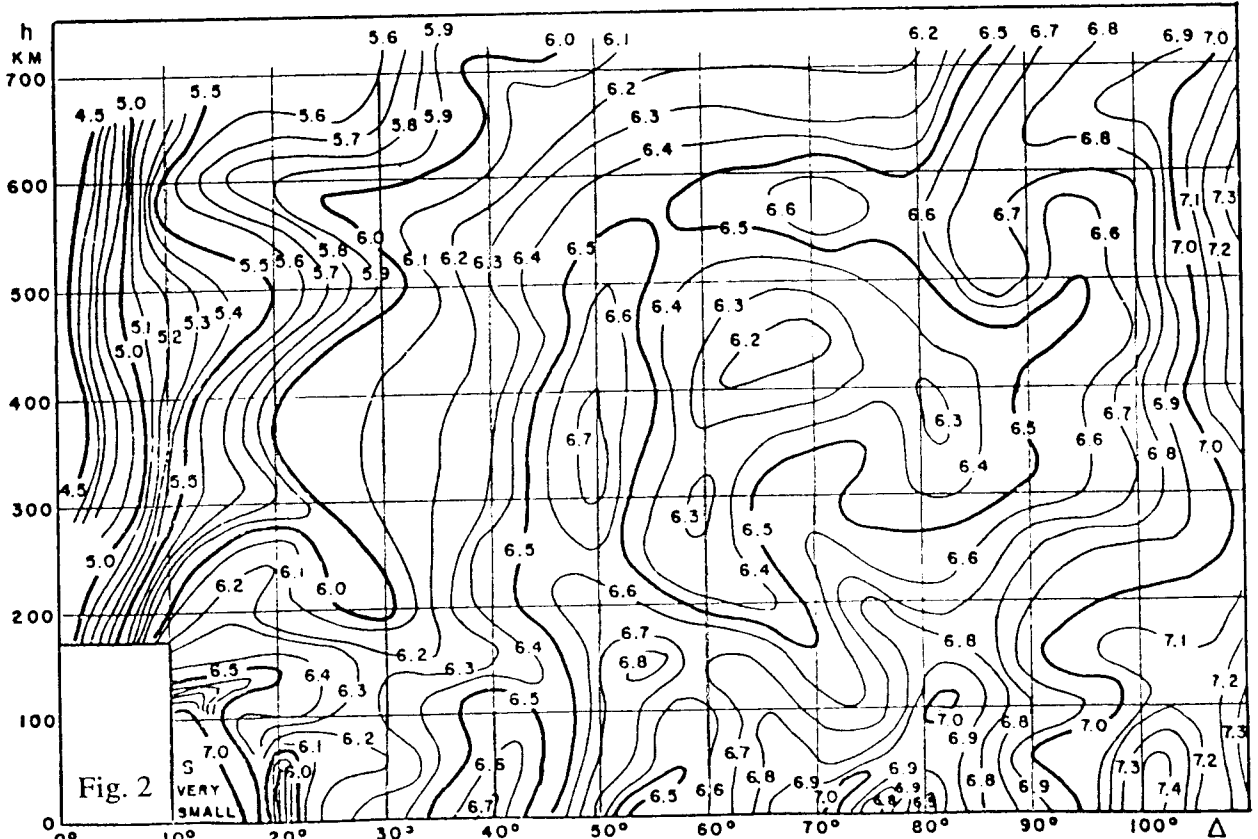


REVISED VALUES OF Q FOR PZ, 1955



GUTENBERG - RICHTER MAGNITUDE, ETC 3 1955

REVISED VALUES OF Q FOR SH 1955



Scientific Technical Report STR 99/13
DOI: 10.2312/GFZ.b103-99132

Δ°	0°		1°		2°		3°		4°		5°		6°		7°		8°		9°	
	H	V	H	V	H	V	H	V	H	V	H	V	H	V	H	V	H	V	H	V
0°			3.30		3.80		4.09		4.30		4.46		4.59		4.70		4.80		4.88	
10°	4.96		5.03		5.09		5.15		5.20		5.25		5.29		5.34		5.38		5.42	
20°	5.46	5.61	5.50	5.64	5.53	5.67	5.56	5.70	5.59	5.72	5.62	5.75	5.65	5.78	5.68	5.80	5.71	5.82	5.73	5.85
30°	5.75	5.87	5.78	5.89	5.80	5.91	5.82	5.93	5.84	5.95	5.86	5.97	5.88	5.98	5.90	6.00	5.92	6.02	5.94	6.03
40°	5.96	6.05	5.98	6.07	5.99	6.08	6.01	6.10	6.03	6.11	6.04	6.13	6.06	6.14	6.07	6.15	6.09	6.17	6.10	6.18
50°	6.12	6.19	6.13	6.21	6.14	6.22	6.16	6.23	6.17	6.24	6.18	6.25	6.20	6.26	6.21	6.28	6.22	6.29	6.24	6.30
60°	6.25	6.31	6.26	6.32	6.27	6.33	6.28	6.34	6.30	6.35	6.31	6.36	6.32	6.37	6.33	6.38	6.34	6.39	6.35	6.40
70°	6.36	6.41	6.37	6.42	6.38	6.42	6.39	6.43	6.40	6.44	6.41	6.45	6.42	6.46	6.43	6.47	6.44	6.48	6.45	6.48
80°	6.46	6.49	6.47	6.50	6.48	6.51	6.49	6.52	6.49	6.52	6.50	6.53	6.51	6.54	6.52	6.55	6.53	6.55	6.54	6.56
90°	6.55	6.57	6.55	6.57	6.56	6.58	6.57	6.59	6.58	6.59	6.58	6.60	6.59	6.61	6.60	6.62	6.61	6.62	6.61	6.63
100°	6.62	6.63	6.63	6.64	6.64	6.65	6.64	6.65	6.65	6.66	6.66	6.67	6.66	6.67	6.67	6.68	6.68	6.68	6.69	6.69
110°	6.69	6.69	6.70	6.70	6.70	6.71	6.71	6.71	6.72	6.72	6.72	6.72	6.73	6.73	6.74	6.73	6.74	6.74	6.75	6.75
120°	6.75	6.75	6.76	6.76	6.76	6.76	6.76	6.77	6.77	6.77	6.77	6.78	6.78	6.78	6.78	6.79	6.78	6.79	6.80	6.80
130°	6.79	6.80	6.79	6.81	6.80	6.81	6.80	6.82	6.80	6.82	6.81	6.83	6.81	6.83	6.81	6.84	6.81	6.84	6.81	6.84
140°	6.82	6.85	6.82	6.85	6.82	6.86	6.82	6.86	6.83	6.87	6.83	6.87	6.83	6.88	6.83	6.88	6.83	6.88	6.83	6.89
150°	6.84	6.89	6.84	6.90	6.84	6.90	6.84	6.91	6.84	6.91	6.84	6.91	6.84	6.92	6.84	6.92	6.84	6.93	6.84	6.93
160°	6.84	6.93	6.84	6.94	6.83	6.94	6.83	6.95	6.83	6.95	6.82	6.95	6.82	6.96	6.82	6.96	6.82	6.96	6.82	6.97
170°	6.81	6.97	6.81	6.98	6.80	6.98	6.79	6.98	6.77	6.99	6.74	6.99	6.71	7.00	6.69	7.00	6.64	7.00	6.59	7.01
180°	6.49	7.01																		180°

Table 1. Magnitude calibration values $\delta(\Delta)$ for surface-waves ($h \leq 50$ km)

REFERENCES

Wahlstroem, R. and Strauch, W. (1984). A regional magnitude scale for Central Europe based on crustal wave attenuation. University of Uppsala, Seismol. Dept., Report No. 5-79, 21 p.

EXERCISES ON EVENT LOCATION AND MAGNITUDE DETERMINATION BY MEANS OF SEISMIC CORE PHASES

Siegfried Wendt¹⁾ and Peter Bormann²⁾

¹⁾ Universität Leipzig, Institut für Geophysik und Geologie, Geophysikalisches Observatorium Collm, D-04779 Wermsdorf, Germany; e-mail: wendt@rz.uni-leipzig.de

²⁾ GeoForschungsZentrum Potsdam, Division 2: Solid Earth Physics and Disaster Research, Telegrafenberg, D-14473 Potsdam, Germany; e-mail: course@gfz-potsdam.de

1. INTRODUCTION

Clear short-period vertical component PKP seismograms of a single station contain all information needed to determine *source depth* h , *epicentral distance* D and *magnitude* m_b , with an accuracy of ± 30 km, better $\pm 1.5^\circ$ and ± 0.3 magnitude units, respectively. In case of strong events and the availability of identically calibrated horizontal components with good signal-to-noise ratio, additionally the source azimuth can be determined with an accuracy of about $\pm 5^\circ$ - 10° and thus the approximate location. As a guideline for the identification of longitudinal core phases may serve the record examples (cf. Figs. 5,6 and 8) given in the chapter *Identification and analysis of longitudinal core phases (IALCP)*. From this it becomes clear that the typical three-phase pattern PKIKP (PKP_{df}), PKP1 (PKP_{bc}) and PKP2 (PKP_{ab}) is only well developed for $D > 147^\circ$. Around 145° all three phases come together forming a rather sharp impulsive onset. At $D < 145^\circ$ small amplitude precursors of waves scattered from the core-mantle boundary (CMB) may occur (phase notation PKHKP or PK(P)).

Note: In case of crustal earthquakes closely following depth phases may complicate the wave pattern and mimic a core phase triplication typical for $D > 146^\circ$. But in case of deeper events with sharp onsets and no or small signal coda the triplication is rather distinct. Depth phases pPKP may follow up to about 2.5 min later in case of a maximum possible source depth of 700 km. When the primary core phases are rather strong, two or three related depth phases may be discernible.

All steps of determining h , D , Az and m_b will be practised in the following based on not annotated copies of records given in Fig. 1. In these records 1 mm corresponds to 1 s. In case of events No. 1 and 2 full minutes start at the left side of the 2 s long gap or „fainting“ of the record traces.

2. EXERCISES

Exercise 1: Depth determination

- Make a table with event No., phase pair, Δt , $h(\Delta t)$, $h(\text{average})$, $h(\text{NEIS})$, δh which is $h(\Delta t)$ or $h(\text{average}) - h(\text{NEIS})$.
- Try, to identify in at least one of the 3 Z-component records of Fig. 1 all three depth phases related to PKIKP, PKP1 and PKP2.

- By using Fig. 11 in the chapter *IALCP* determine $h(\Delta t)$ and $h(\text{average})$, where possible, from all Z-component records shown in Fig. 1. Write your results into the table. You will then be given the values $h(\text{NEIS})$.
- Determine δh and assess the accuracy of your h -determinations as compared to NEIS.

Note: If the pPKP group is less distinct relate its onset to the strongest direct core phase !

Exercise 2: Distance determination

Fig. 11 in chapter *IALCP* gives the IASPEI 91 depth-dependent differential travel-time curves for PKPbc-PKPdf and PKPab-PKPdf, respectively. Thus, having identified two or three of these phases, D can be determined.

- Make a table with event No., time-differences $\Delta t(\text{PKP1-PKIKP})$ and $\Delta t(\text{PKP2-PKIKP})$, h , $D(\Delta t)$, $D(\text{fit})$, $D(\text{NEIS})$ and δD which is $D(\Delta t \text{ or fit}) - D(\text{NEIS})$.
- Measure and write down for each event in Fig. 1 the $\Delta t(\text{PKP1-PKIKP})$ and/or $\Delta t(\text{PKP2-PKIKP})$, if possible with an accuracy of better than 0.5 s.
- Determine $D(\Delta t)$ for all time differences and $D(\text{average})$ for each event in Fig. 1 by taking into account the source depth determined under 1.1.
- Use the transparent overlay of Fig. 12 in chapter *IALCP* and try a best fit with all phases, taking h into account ! Write down your $D(\text{fit})$! You will then be given the values for $D(\text{NEIS})$.
- Determine $\delta D(\Delta t)$ and $\delta D(\text{fit})$ and assess the accuracy of your own distance determinations as compared to NEIS.

The origin time of the event could additionally be determined knowing the absolute onset times measured, h and D as determined above and consulting a published absolute travel-time curve or table (e.g. Kennett 1991).

Exercise 3: Azimuth determination

The back-azimuth in degrees against North can be determined from the relationship $Az = \arctan(A_E/A_N)$ with A_E and A_N as the trace amplitudes measured in mm from the equally calibrated records of the E-W and N-S components.

Note: Be careful in deciding about the proper quadrant in which the determined angle is situated by comparing the polarities in all three records !

- Determine Az from the 3-component records of event No. 3 in Fig. 1 for which you have already determined D ! To ease your task a high time-resolution display is reproduced in Fig. 2.

- Find the source area by using the global map with D and Az isolines centred around station CLL (cf. Fig. 3 in *Exercise on 3-component seismogram interpretation*) ! Write down the name of the source area. You will then be given the name of the source area as determined by NEIS.
- Assess the achievable accuracy of a single station location as compared to NEIS.

Exercise 4: Magnitude determination from direct longitudinal core phases

In the exercise we will use the detailed depth- and distance-dependent functions $Q(D, h)$ given in Fig. 9 of the chapter *IALCP* for all three direct core phases appearing in the range $D = 145^\circ - 164^\circ$. We determine $m_b(\text{PKP})$ by using the relationship:

$$m_b(\text{PKP}) = \log_{10} (A/T) + Q(D, h) \quad (1)$$

with amplitude A in μm (10^{-6} m), period T in s, epicentral distance D in degree and source depth h in km. To determine the „true ground motion“ amplitude A from the measured trace amplitudes we need to correct the latter for the period-dependent magnification of the seismograph. In case of Fig. 1 the records No. 1 and 3 were made with a frequency response according to the magnification values given in the table below while for event No. 2 the magnification was half of these values.

Period (sec)	0.8	1.0	1.2	1.4	1.6	1.8	2.0	2.4
Magnification	54 250	52 440	49 210	44 090	37 550	30 660	24 420	14 000

- Make a table with columns for event No., D , h , phase name, T in s, corresponding magnification value M , amplitude A (trace in mm) and A („true“ in nm), $\log A/T$, $Q(D, h)$, $m_b(\text{phase})$, $m_b(\text{average})$, $m_b(\text{NEIS})$ and δm_b which is $m_b(\text{average}) - m_b(\text{NEIS})$. The $m_b(\text{NEIS})$ -values will be given to you after you have completed your own determinations.
- Determine for the three events in Fig. 1 separately $\log A/T$, $Q(D, h)$, $m_b(\text{phase})$ for all identified phases of direct core phases using the $Q(D, h)$ plots in Fig. 9 of chapter *IALCP*. Then determine $m_b(\text{average})$. You will be given the values of $m_b(\text{NEIS})$.
- Determine δm_b for your own $m_b(\text{phase})$ and $m_b(\text{average})$ determinations. Assess the accuracy of your magnitude determinations from PKP measurements as compared to the global average $m_b(\text{NEIS})$ values determined from teleseismic P-wave readings.

Exercise 5: Distance determinations by using reflected core phases

Reflected longitudinal core phases such as PKKP and PKPPKP (cf. section 6 in chapter *IALCP*) are very suitable for distance determinations at single stations since they are nearly independent of source depth. Fig. 16 in chapter *IALCP* shows both theoretical and observed travel-time differences of PKKP - P and PKKP - PKP depending on epicentral distance D , while Fig. 17 in the same chapter gives the respective relationship for PKPPKP - P.

- Make a table with event No., phase difference, respective time difference Δt , related epicentral distance $D(\text{observed})$, $D(\text{NEIS})$ and δD which is $D(\text{observed}) - D(\text{NEIS})$.

- Determine $\Delta t(\text{PKKP-P or PKP})$ and $\Delta t(\text{PKPPKP-P})$, respectively, for the 4 events shown in Fig. 14 of the chapter *IALCP*. You will then be given the values $D(\text{NEIS})$.
- Calculate δD and assess the accuracy of single station D -determinations using reflected longitudinal core phases.

3. SOLUTIONS

Exercise 1: NEIS calculated for the three events the following hypocentral depths:

No.1	$h = 435 \text{ km}$
No. 2	$h = 235 \text{ km}$
No. 3	$h = 540 \text{ km}$

Your own determinations should be within about $\pm 20 \text{ km}$ to these values.

Exercise 2: NEIS calculated for the stations which recorded these three events the following epicentral distances:

No. 1	$D = 148.5^\circ$
No. 2	$D = 159.5^\circ$
No. 3	$D = 150.0^\circ$

Your own determinations should be within $< \pm 2^\circ$ to these values.

Exercise 3: Event No. 3 was in the Fiji Islands. Its azimuth as seen from the station CLL was

$$Az = 26^\circ.$$

Your own determinations should be within $< \pm 10^\circ$ to this value.

Exercise 4: NEIS determined for the three events from global P-wave data the following body-wave magnitudes:

No. 1	$m_b = 5.0$
No. 2	$m_b = 5.5$
No. 3	$m_b = 5.3$

Your own determinations should be within ± 0.5 magnitude units to these values.

Exercise 5: NEIS determined for the four events the following epicentral distances to CLL:

No. 1	D = 98.3°
No. 2	D = 111.2°
No. 3	D = 66.3°
No. 4	D = 57.3°

Your own determinations should be within $< \pm 2^\circ$ to these values.

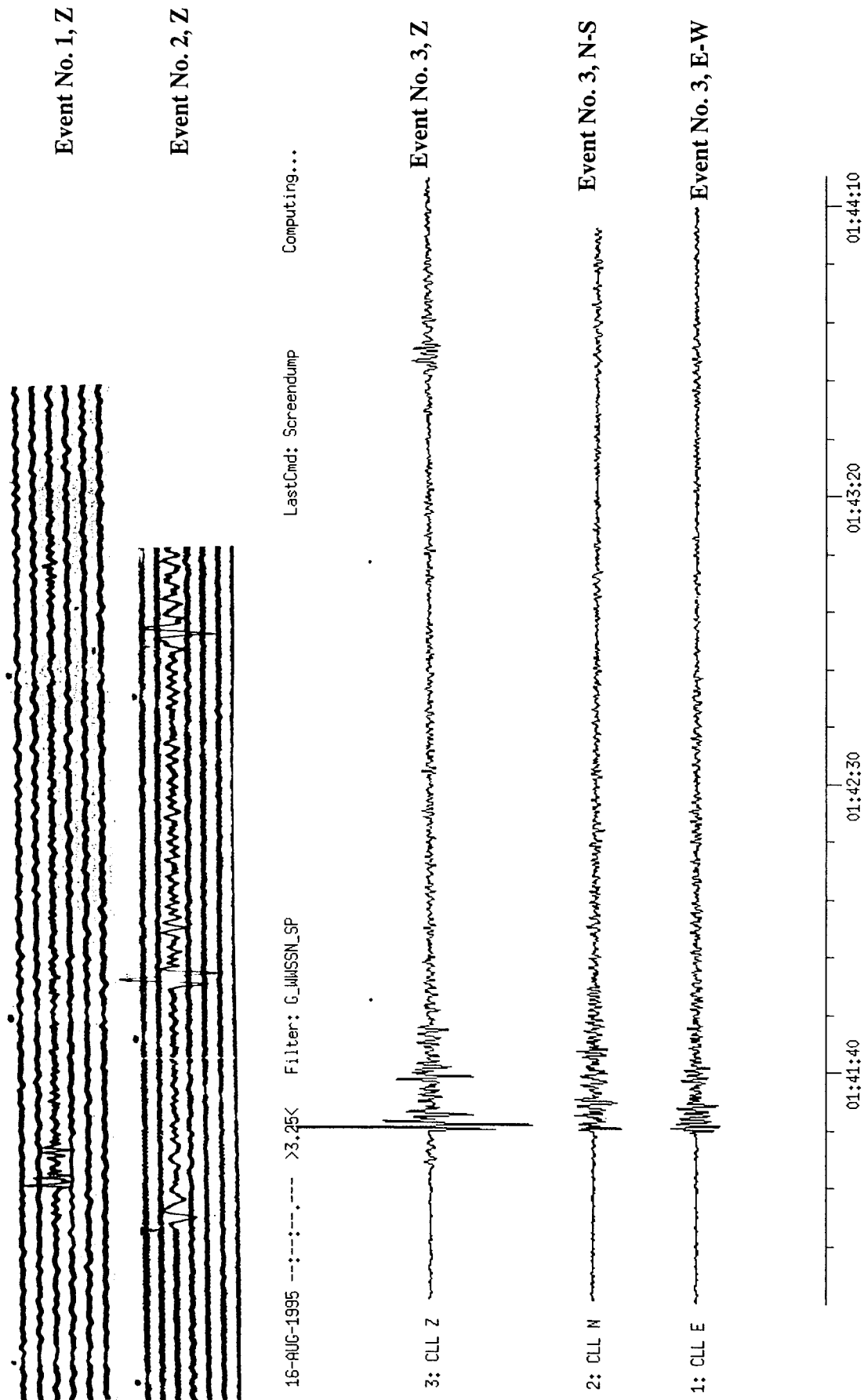
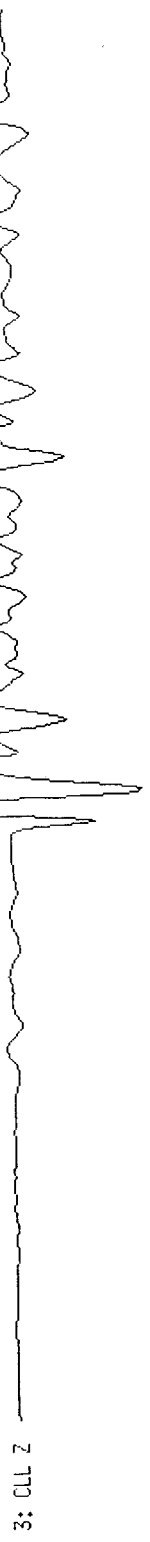


Fig. 1: Recordings of direct longitudinal core phases and related depth phases from records of station

Computing...

16-AUG-1995 --:--:--:-- >0.59K Filter: G_WISSN_SP



01:41:15 01:41:25 01:41:35 01:41:45

Fig. 2: High time resolution of event No. 3 in Fig. 1

EXERCISE ON FAULT PLANE SOLUTIONS

Michael Baumbach and Peter Bormann

GeoForschungsZentrum Potsdam, Division 2: Solid Earth Physics and Disaster Research
Telegrafenberg, D-14473 Potsdam, Germany

1. AIM

The exercise aims at:

- Understanding the effect of the movement on the fault in relation to the polarities of P-waves;
- Understanding the presentation of P-wave polarities in an equal angle (Wulff net) or equal area projection (Lambert-Schmidt net) of the focal sphere;
- Constructing a fault-plane solution and the related parameters (P- and T-axes, displacement vector) for a real earthquake;
- To discuss the fault-plane solution in relation to the tectonic setting of the epicentral area.

2. DATA AND RELATIONSHIPS

Before a fault-plane solution for a teleseismic event can be constructed, the following steps must be completed or data be known:

- a) Interpretation of P-wave first-motion polarities from seismograms at several stations;
- b) Calculation of epicentral distances and source-to-station azimuths for these stations;
- c) Calculation of the take-off angles for the seismic P-wave rays leaving the hypocenter towards these stations. This requires the knowledge of the focal depth and of the P-wave velocity at this depth (cf. *Exercise on take-off angle calculations*).

For the calculations b) and c) standard Earth's velocity models are used (e.g. Kennett, 1991). In case of local events it is necessary to calculate first the ray propagation and to localize the events, if possible with a special layered crustal velocity model for that region. Most of such programs provide both the source-station azimuths and take-off angles in their output files.

The exercise below is based on the definitions, diagrams and relationships given in the chapter *Determination of fault plane solutions*, for short *DFPS*. As an example serve data determined in the steps a)-c), by using the program HYPO71, for a locally recorded aftershock of the Erzincan earthquake in Turkey (Date: 12.04.1992, ML = 2.8, latitude = 39.519° N, longitude = 39.874° E, source depth $h = 3.13$ km; station distance up to 50 km).

Note: The take-off angles θ calculated for a ray arriving at a given seismic station may vary significantly depending on the assumed velocity model in the source region. When considering an average single layer crustal model of 30 to 40 km thickness all rays of P-wave first arrivals reaching stations up to 120 - 200 km distance would have left the upper focal hemisphere only. When using HYPO71 with the average global two-layer crust according to the velocity model IASP91 (Kenneth 1991) also only upper hemisphere take-off angles would have been calculated for the first P-wave arrivals up to distances of 50 km. But in the considered epicentral area a significant velocity increase in the upper crust was found already at 4 km depth (increase of $v_p = 5.3$ km/s to 6.0 km/s). Accordingly, stations up to 50 km distance were reached partially by upper or lower focal sphere rays (cf. Fig. 7 in *DFPS*). Since only lower hemisphere projections will be used in the exercise values for upper hemisphere

rays ($AIN > 90^\circ$) must be corrected according to Fig. 6 in DFPS. **Conclusion:** AIN calculations based on strongly biased velocity models might result in inconsistent fault-plane solutions or not permit a proper separation of polarity readings into quadrants at all!

Tab. 1 gives the needed primary data. They were taken from the output file of the program HYPO71 with which the event was located. The first five columns of this file contain, as an example for the two stations ALI and ESK in Tab. 1, the following data:

STN	DIST	AZM	AIN	PRMK
ALI	3.7	40	130	IPD0	
ESK	22.7	312	62	IPU1	

with STN - station code; DIST - epicentral distance in km; AZM - azimuth towards the station in degree from north; AIN - take-off angle of the ray towards the station as calculated for the given structure-velocity model; PRMK - P-wave reading remarks. In the column PRMK P stands for P-wave onset, I for impulsive (sharp) or E for emergent (less clear) onset, D for clear (or - for poor) dilatational (downward) first motion, U for clear (or + for poor) compressional (upward) first motion. The last character may range between 0 and 4 and is a measure of the quality (clarity) of the onset and thus of the weight given to the reading in the calculation procedure, e.g. 0 for zero and 4 for full weight. In case of the above two stations the values for ALI would need to be corrected to get the respective values for the equivalent lower hemisphere ray, i.e. $AINc = 180^\circ - 130^\circ = 50^\circ$ and $AZMc = 180^\circ + 40^\circ = 220^\circ$ while the values for ESK can be taken unchanged from the HYPO71 output file.

3. TASKS

Task 1:

If in Tab. 1 $AIN > 90^\circ$ then correct take-off angles and azimuths for lower hemisphere projection: $AINc = 180^\circ - AIN$, $AZMc = AZM(<180^\circ) + 180^\circ$ or $AZM(\geq 180^\circ) - 180^\circ$. In case of $AIN < 90^\circ$ the original values remain unchanged.

Task 2:

Place tracing paper or a transparency sheet over the Wulff or Lambert-Schmidt net projection (Fig. 5a or b in DFPS). Mark on it the centre and perimeter of the net as well as the N, E, S and W directions. Pin the marked sheet centre with a needle to the centre of the net.

Task 3:

Mark the azimuth of the station on the perimeter of the transparency and rotate the latter until the tick mark is aligned along an azimuth of 0° , 90° , 180° or 270° . Measure the take-off angle from the centre of the net along this azimuth. This gives the intersection point of the particular P-wave ray with the lower hemisphere. Mark on this position the P-wave polarity with a neat + for compression or o for dilatation (U or D in Tab. 1) using *different colours* for better distinction of closely spaced polarities of different sign. **Note:** The proper distance d of the polarity entry from the centre of the net corresponds to $d = r \times \tan(AINc / 2)$ for the Wulff net and $d = r \times \sin(AINc / 2)$ for the Lambert-Schmidt net with r the radius of the given net.

Task 4:

By rotating the net over the plotted data try to find a great circle which separates as good as possible the expected quadrants with different first motion signs. This great circle represents the intersection trace of one of the possible fault (respectively nodal) planes with the lower half of the focal sphere (FP1). **Note 1:** All N-S connecting lines on both nets are great circles!

Note 2: Switching polarities close to each other may be due to uncertain readings in case of relatively small P-wave amplitudes. The latter is necessarily the case near to the strike direction of the nodal (fault) planes. Accordingly, connecting clusters of nearby switching polarities may guide you in finding the best separating great circle.

Tab. 1: Original and corrected values of ray azimuth (AZM and AZMc) and take-off angles (AIN and AINc) towards stations of a temporary network which recorded the Erzincan aftershock of April 12, 1994. POL - polarity of P-wave first motions.

STA	AZM (degree)	AIN (degree)	POL	AZMc (degree)	AINc (degree)
ALI	40	130	D		
ME2	134	114	D		
KAN	197	112	D		
YAR	48	111	D		
ERD	313	103	D		
DEM	330	102	D		
GIR	301	102	U		
UNK	336	101	D		
SAN	76	62	U		
PEL	327	62	D		
GUN	290	62	U		
ESK	312	62	U		
SOT	318	62	D		
BA2	79	62	U		
MOL	297	62	U		
YUL	67	62	U		
ALT	59	62	D		
GUM	320	62	U		
GU2	320	62	D		
BAS	308	62	D		
BIN	295	62	U		
HAR	24	62	D		
KIZ	311	62	U		
AKS	284	62	D		
SUT	295	62	U		

Task 5:

Mark point A at the middle of FP1 and find, on the great circle perpendicular to it, the pole P1 of FP1, 90° apart (cf. Fig. 9 in the chapter DFPS). All great circles, passing this pole are perpendicular to the great circle of FP1. Since the second possible (auxiliary) fault plane (FP2) must be perpendicular to the FP1, it has to pass P1. Find, accordingly, FP2 which again has to separate areas of different polarity.

Task 6:

Find the pole P2 for FP2 and delineate the equatorial plane EP. The latter is perpendicular to both FP1 and FP2, i.e. a great circle through the poles P1 and P2. The intersection point between FP1 and FP2 is the pole of the equatorial plane (P3).

Task 7:

Mark the position of the pressure and tension axes on the equatorial plane and indicate their direction towards (P) and from the center (T) of the considered net (cf. Fig. 9 of DFPS). Their positions on the equatorial plane lie in the centre of the respective dilatational (-) or compressional (+) quadrant, i.e. 45° away from the intersection points of the two fault planes with the equatorial plane. **Note:**

All angles in the net projections have to be measured along great circles!

Task 8:

Mark the slip vectors, connecting the intersection points of the great circles, representing the fault planes and the equatorial plane, with the centre of the considered net. If the centre lies in a tension quadrant, then the slip vectors point to the net centre. If it lies in a pressure quadrant, then the slip vector points in the opposite direction. The slip vector shows the direction of displacement of the hanging wall.

Task 9:

Determine the azimuth (strike direction ϕ) of both FP1 and FP2. It is the angle measured clockwise against North between the directional vector connecting the centre of the net with the end point of the respective projected fault trace lying towards the right of the net centre.

Task 10:

Determine the dip angle δ (against the horizontal) for both FP1 and FP2 by putting their projected traces on a great circle. Measure δ as the difference angle from the outermost great circle towards the considered fault plane trace.

Task 11:

Determine the slip direction (i.e. the sense of motion along the two possible fault planes. It is obtained by drawing one vector each from the centre of the net the poles P1 and P2 of the nodal planes (or vice versa from the poles to the centre depending on the sign of the rake angle). The vector from the centre to P1 (P2) shows the slip direction along FP2 (FP1). The rake angle λ is positive in case the centre of the net lies in the tension (+) quadrant (i. e. an event with a thrust component) and negative when it lies in the pressure (-) quadrant (event with a normal faulting component). In the first case λ is $180^\circ - \lambda^*$. λ^* has to be measured on

the great circle of the respective fault plane between its crossing point with the equatorial plain and the respective azimuth direction of the considered fault plane (cf. Fig. 9 in DFPS). In the second case $\lambda = -\lambda^*$. For a pure strike slip motion ($\delta = 90^\circ$) $\lambda = 0$ defines a left lateral strike-slip and $\lambda = 180^\circ$ defines a right-lateral strike-slip.

Task 12:

The azimuth of the pressure and the tension axes, respectively, is equal to the azimuth of the line connecting the centre of the net through the P and T point with the perimeter of the net. Their plunge is the respective dip angle of these vectors against the horizontal (to be measured as for δ).

Task 13:

Estimate the parameters of the fault planes and of the stress axes for the Erzincan aftershock and insert your results into Table 2 below:

Tab. 2

	strike	dip	rake
Fault plane, 1			
Fault plane 2			

	azimuth	plunge
Pressure axis		
Tension axis		

Note: The angles may range between:

- $0^\circ < \text{strike} < 360^\circ$
- $0^\circ < \text{azimuth} < 360^\circ$
- $0^\circ < \text{dip} < 90^\circ$
- $0^\circ < \text{plunge} < 90^\circ$
- $-180^\circ < \text{rake} < 180^\circ$

Task 14:

The question of which of the nodal planes was the acting fault plane cannot be answered on the basis of the fault-plane solution alone. Considering the event in its seismotectonic context may give an answer. Therefore, we have marked the epicenter of the event in Fig. 1 with an open star at the secondary fault F2.

- a) Decide which was the likely fault plane (FP1 or FP2)?,
- b) What was the type of faulting?
- c) What was the direction of slip? and
- d) Is your solution compatible with the general sense of plate motion in the area as well with the orientation of the acting fault and the orientation of stress/deformation in the area? (Yes or No)?

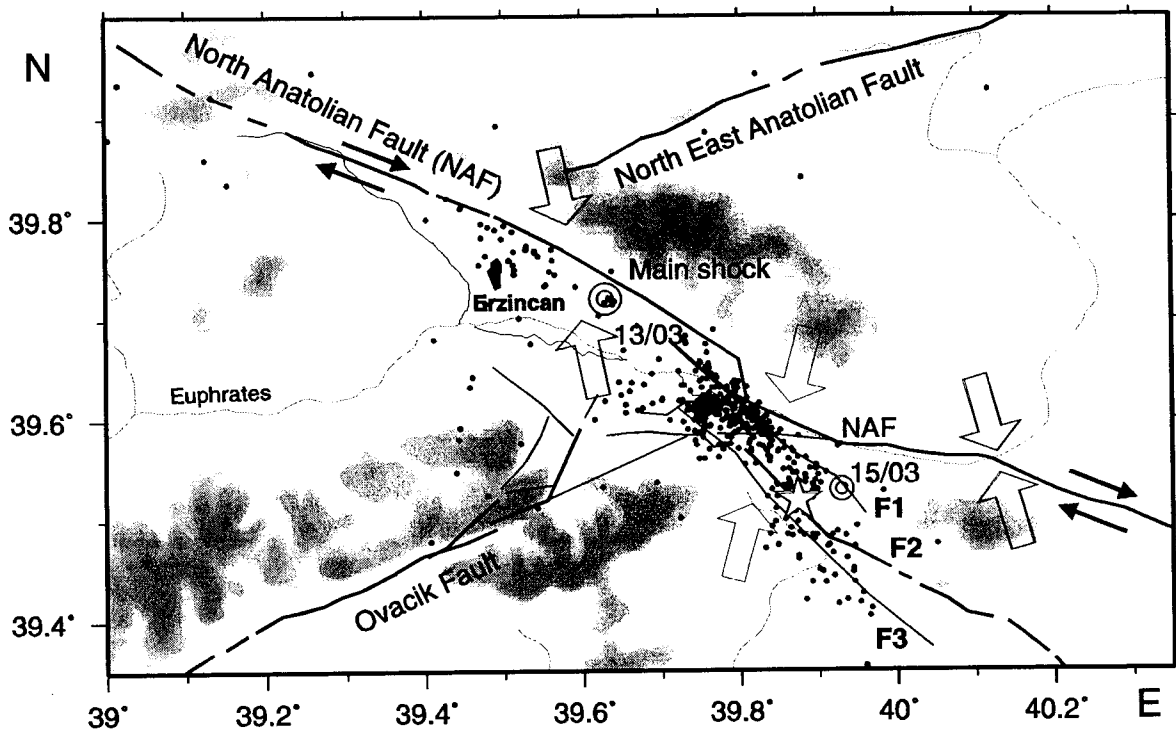


Fig. 1: Epicentres of aftershocks between March 21 and June 16, 1992 of the March 13, 1992 Erzincan earthquake, Turkey. The open circles represent the main shock and its strongest aftershock on March 15, and the open star the analysed aftershock. F1, F2 and F3 are secondary faults to the North Anatolian Fault (NAF). Black arrows - directions of relative plate motion, open arrows - direction of maximum horizontal compression as derived from centroid moment tensor solutions of stronger earthquakes.

4. SOLUTIONS

In the Table 3 below the authors have given the data for their own eye-fitting solution together with the values for the best PC fit to the data (in brackets). If your manually determined results differ by more than about 20° or even show different type of faulting mechanism then you should critically check your data entries and/or fault-plane fits again.

Tab. 3

	strike	dip	rake
Fault plane 1 (FP1)	280° (278.5°)	40° (39.9°)	68° (67.4°)
Fault plane 2 (FP2)	130° (127.0°)	54° (53.7°)	108° (107.8°)

	azimuth	plunge
Pressure axis	205° (204.4°)	7° (7.1°)
Tension axis	90° (88.6°)	73° (74.0°)

The answers to the questions in Task 14 are:

- a) FP2 was more likely the acting fault.
- b) The aftershock was a thrust event with a small right-lateral strike-slip component.
- c) The slip direction is strike direction - rake azimuth, i.e. for FP2 $130^\circ - 108^\circ = 12^\circ$ against north. This is close to the direction of maximum horizontal compression (15°) in the nearby area as derived from centroid moment tensor solutions of stronger events.
- d) The earthquake rupture of this event agreed with the general tendency and direction of plate motion in the area under study.

EXERCISE ON TAKE-OFF ANGLE CALCULATIONS FOR FAULT PLANE SOLUTIONS

Peter Bormann

GeoForschungsZentrum Potsdam, Division 2: Solid Earth Physics and Disaster Research
Telegrafenberg, D-14473 Potsdam, Germany

1. DATA AND RELATIONSHIPS

When localising near events by using HYPO71 or similar programs the values for both the azimuth AZM and for the take-off angles AIN of the rays leaving the source for each station are given in the localisation output file together with the polarity readings (cf. *Exercise fault plane solutions*). When one intends to determine the fault plane solution for seismic events published in the bulletins of the International Seismological Centre (ISC), mainly teleseismic ones, one finds in the ISC bulletins the data for polarity readings at the reporting stations (\uparrow or c for up and \downarrow or d for down in short- or long-period instruments, respectively) and the calculated values AZM for the (back-) azimuth from the event towards the seismic station but not values for AIN. Fig. 1 shows a cut-out example of a typical ISC event-stations report. It gives in its header also the results of seismic moment tensor and fault plane solutions calculated by various international data centres or agencies using different (sometimes automated) procedures. Values for AIN can be calculated by using the relationship

$$\sin \text{AIN} = v_p(h) \times (r_o/r_h) \times S_o(\Delta, h) / 111.11 = (180/\pi) \times (v_p/r_h) \times p(\Delta, h) \quad (1)$$

with p - ray parameter, $S_o(\Delta, h) = dT/d\Delta = p(\Delta, h)$ - slowness observed on the Earth's surface (in units s/deg) at the epicentral distance Δ (in degree) as a function of the hypocentral depth h (in km), $v_p(h)$ - P-wave velocity at the depth h , $r_o = 6371$ km - Earth's radius and $r_h = r_o - h$.

Tabs. 1 and 2 give the respective values $v_p(h)$ and $p(\Delta, h)$ for P-waves.

Tab. 1: $v_p(h)$ according to the IASPEI91 velocity model (Kennett, 1991).

h (km)	v_p (km/s)	h (km)	v_p (km/s)	h (km)	v_p (km/s)
0	5.8000	120	8.0500	471	9.5650
20	5.8000	171	8.1917	571	9.9010
20	6.5000	210	8.3000	660	10.2000
35	6.5000	271	8.5227	660	10.7900
35	8.0400	371	8.8877	671	10.8192
71	8.0442	410	9.0300	760	11.0558
120	8.0500	410	9.3600		

Tab. 2: Slowness values $S_0 = dT/d\Delta = p$ of Pn, P or PKP_{df} first arrivals at the Earth's surface as a function of hypocentral depth h according to IASPEI 1991 Seismological Tables (Kennett, 1991)

Phase	Δ (in deg)	S_0 (s/deg)			
		$h=0$ km	$h=100$ km	$h=300$ km	$h=600$ km
Pn (P)	2	13.75	12.90	7.91	4.01
	4	13.75	13.49	10.96	6.91
	6	13.74	13.58	11.95	8.60
	8	13.72	13.60	12.25	9.48
	10	13.70	13.59	12.26	9.90
	12	13.67	13.29	12.12	10.05
	14	13.64	12.91	11.03	10.06
	16	12.92	12.43	10.91	9.17
	18	12.33	10.97	10.73	9.10
	P	20	10.90	10.81	10.50
22		10.70	10.58	9.12	8.90
24		9.14	9.11	9.03	8.83
26		9.06	9.02	8.91	8.76
28		8.93	8.90	8.83	8.66
30		8.85	8.82	8.75	8.56
32		8.77	8.74	8.65	8.45
34		8.67	8.64	8.54	8.33
36		8.56	8.52	8.42	8.21
38		8.44	8.40	8.29	8.08
40		8.30	8.26	8.16	7.95
42		8.17	8.13	8.03	7.82
44		8.03	7.99	7.89	7.69
46		7.89	7.85	7.75	7.56
48		7.55	7.71	7.61	7.42
50		7.60	7.56	7.47	7.29
52		7.46	7.42	7.33	7.15
54		7.31	7.28	7.19	7.02
56		7.17	7.13	7.05	6.88
58		7.02	6.99	6.90	6.74
60		6.88	6.84	6.76	6.61
62		6.73	6.70	6.62	6.47
64		6.59	6.55	6.48	6.33
66		6.44	6.41	6.33	6.19
68		6.30	6.27	6.19	6.05
70		6.15	6.12	6.05	5.91
72		6.00	5.97	5.90	5.77
74		5.86	5.83	5.76	5.63
76		5.71	5.68	5.61	5.49
78		5.56	5.53	5.46	5.34
80	5.40	5.38	5.31	5.20	

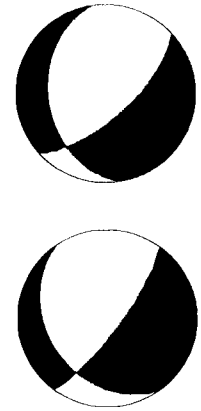
Tab. 2: cont.

Phase	Δ (in deg)	S_0 (in s/deg)			
		h = 0 km	h = 100 km	h = 300 km	h = 600 km
P	82	5.25	5.22	5.16	5.04
	84	5.09	5.07	5.01	4.90
	86	4.94	4.92	4.85	4.72
	88	4.74	4.72	4.69	4.65
	90	4.66	4.65	4.64	4.61
	92	4.61	4.61	4.60	4.57
	94	4.58	4.57	4.55	4.51
	96	4.52	4.51	4.49	4.44
	98	4,45	4.44	4.44	4.44
P_{diff}	100-144	4.44	4.44	4.44	4.44
PKP _{df}	114	1.92	1.92	1.92	1.92
	116-122	1.91	1.91	1.91	1.91
	124-126	1.90	1.90	1.90	1.90
	130	1.88	1.88	1.88	1.88
	136	1.84	1.84	1.84	1.83
	140	1.80	1.79	1.79	1.78
	142	1.76	1.76	1.76	1.75
	144	1.73	(1.72)	(1.72)	(1.71)
	146	1.68	1.68	1.67	1.66
	148	1.63	1.62	1.62	1.60
	150	1.57	1.56	1.55	1.54
	152	1.49	1.49	1.48	1.47
	154	1.42	1.41	1.40	1.39
	156	1.33	1.33	1.32	1.30
	158	1.24	1.23	1.23	1.21
	160	1.14	1.14	1.13	1.11
	162	1.04	1.03	1.03	1.01
	164	0.93	0.93	0.92	0.91
	166	0.82	0.82	0.81	0.80
	168	0.71	0.70	0.70	0.69
	170	0.59	0.59	0.58	0.58
172	0.47	0.47	0.47	0.47	
174	0.36	0.36	0.35	0.35	
176	0.24	0.24	0.24	0.23	
178	0.12	0.12	0.12	0.12	
180	0.00	0.00	0.00	0.00	

NEIC Moment tensor solution: s_{23} , scale 10^{17} Nm; M_{rr} -3.05; $M_{\theta\theta}$ -0.97; $M_{\phi\phi}$ 4.03; $M_{r\theta}$ -2.51; $M_{r\phi}$ -1.95; $M_{\theta\phi}$ 2.71. Depth 272km; Principal axes: T 6.09, Plg17°, Azm117°; N -136, Plg27°, Azm216°; P -4.73, Plg57°, Azm358°; Best double couple: M_0 5.4x10¹⁷Nm; NP1: ϕ_s 172°, δ 36°, λ -140°. NP2: ϕ_s 48°, δ 68°, λ -60°.

HRVD 05^d 13^h 24^m 15^s.7±0^s.2, 39°.10N±°.02x15°.39E±°.02, h295^{km}±.8^{km}, Centroid moment tensor solution. Data used: GDSN; LP body waves: s50, c**; Half duration: 1^s.9. Moment tensor: Scale 10¹⁷Nm; M_{rr} -2.17±.06; $M_{\theta\theta}$ -1.97±.10; $M_{\phi\phi}$ 4.14±.09; $M_{r\theta}$ -3.51±.09; $M_{r\phi}$ -3.29±.09; $M_{\theta\phi}$ 0.01±.09. Principal Axes: T 5.83, Plg27°, Azm103°; N 0.32, Plg30°, Azm210°; P -6.15, Plg48°, Azm339°. Best Double couple: M_0 6.0x10¹⁷Nm, NP1: ϕ_s 146°, δ 33°, λ -157°. NP2: ϕ_s 37°, δ 78°, λ -60°.

ISC 05^d13^h24^m11^s.4±0^s.13, 39.16±0^s.16x15°.18E±°.014, h290^{km}±1.3^{km}, (h286km±2.7^{km}:pP-P), n757, σ 1^s.04/729, Mb5.7/107, 119C-155D, Southern Italy.



OVO Vesuviano	1.77	340	↑P	13 24 57.2	+1.5
MCT Mte Cammarata	1.95	219	P	13 24 57.7	+0.6
FG4 Candela	1.99	8	P	13 24 58.2	+0.9
MEU Monte Lauro	2.07	186	dP	13 24 56.8	-1.3
PZI Palazzolo	2.14	186	eP	13 24 57	-1.7
FAI Favara	2.21	213	dP	13 24 59.5	+0.1
MSC Monte Massico	2.23	336	↑P	13 25 01.1	+1.6
SGG Gregorio Matese	2.30	345	↑P	13 25 01.9	+1.8

Fig. 1: Cut-out of the ISC bulletin (left) with NEIC (National Earthquake Information Center) and Harvard University (HRVD) moment tensor fault plane solutions (right) for the Italy deep earthquake (h = 286 km) of Jan. 05, 1994. In the columns 3 to 5 of the bulletin the following data are given: 3 - epicentral distance in degree, 4 - backazimuth AZM in degree, 5 - phase code and polarity.

Tab. 3 gives respective selected data from the ISC bulletin for five seismic stations at different epicentral distances Δ and back-azimuth AZM for the Italian earthquake shown in Fig. 1. The polarity readings correspond to the first P ($\Delta < 100^\circ$) or PKP ($\Delta < 110^\circ$) onsets.

Tab. 3:

STA	Δ (deg)	AZM (deg)	POL	$v_p(h)$ km/s	v_p/r_b (s ⁻¹)	$S_0(\Delta, h)$ (s/deg)	AIN (deg)	AZMc (deg)	AINc (deg)
SGG	2.30	345	+						
KHC	10.03	354	-						
BTH	12.25	294	+						
ZAK	60.02	48	-						
PAE	154.8	324	-						

2. TASKS

Task 1:

Calculate for the data given in Tab. 3 the missing values in the blank columns for $v_P(h)$, v_P/r_h and $p = S_o(\Delta, h)$ as well as for AIN using the relationship (1) and the values tabulated in Tabs. 1 and 2. If needed, interpolate linearly as a first approximation.

Task 2:

Decide whether your ray has left the upper or lower half of the focal sphere and whether or not you need to calculate AINc and/or AZMc. Complete Tab. 3 accordingly.

Task 3:

Use the values given in Fig. 1 for ϕ and δ for the fault-plane solutions FP1 and FP2 of NEIC and reconstruct in the *Lambert-Schmidt net* (cf. Fig. 4b in DFPS) both nodal (fault) planes by applying the inverse procedure as the one described in the *Exercise on fault plane solutions*. Compare your nodal plane pattern with that of the NEIC "beach-ball" solution (Fig. 1 upper right).

Task 4:

Find the corresponding equatorial plane to your FP1 and FP2 and mark there the penetration points of the P and T axes through the focal sphere. Draw the P and T vectors towards and from the center of the net, determine their azimuth Azm and plunge Plg (equivalent to dip, measured from the horizontal). Compare your respective values with those given bei NEIC in Fig. 1.

Task 5:

Use your values calculated for the P-wave take-off angle AINc and and ray azimuth AZMc to all 5 stations in Tab. 3 and mark the respective polarities and ray penetration points through the focal sphere in the Lambert-Schmidt net. Check whether they fall into the proper T and P quadrants and whether the short-period polarity readings given in Tab. 3 are consistent with the fault plane solution of NEIC which is based on long-period wave-form data.

3. SOLUTIONS AND DISCUSSION

Tab. 4: Solutions for Tasks 1

STA	Δ (deg)	AZM (deg)	POL	$v_P(h)$ km/s	v_P/r_h (s ⁻¹)	$S_o(\Delta, h)$ (s/deg)	AIN (deg)	AZMc (deg)	AINc (deg)
SGG	2.30	345	+	8,57745	1.4096x	8.69	(135.4)	165	44.6
KHC	10.03	354	-		10 ⁻³	12.35	85.9	354	85.9
BTH	12.25	294	+			12.07	71.1	294	77.1
ZAK	60.02	48	-			6.77	33.1	48	33.1
PAE	154.8	324	-			1.37	6.4	324	6.4

Task 2:

Note: Slowness values increasing with Δ (e.g. in Tab. 2 for $h = 300$ km up to $\Delta = 10^\circ$) correspond to seismic rays leaving the source upwards! Consequently, the value $AIN = 44,6^\circ$ calculated with eq. (1) for station SGG corresponds, according to the definition given in Fig. 5 of the chapter DFPS, in fact to an angle of $180^\circ - AIN = 135,4^\circ$. Accordingly, $AZMc$ and $AINc$ for the equivalent lower hemisphere projection of this ray are $345^\circ - 180^\circ = 165^\circ$ and $44,6^\circ$, respectively.

Task 3: Your manually drawn fault-plane solutions should look very similar to that of NEIC in Fig. 1 upper right.

Task 4:

Your manually re-constructed values for Azm and Plg of the P and T axes should agree with the NEIC solution within a few degrees. If not, check your drawing of the three planes, of the related P and T axis and the measured angles.

Task 5:

All your polarities should fall into the proper quadrants. Accordingly, the short-period polarity data used in this exercise are consistent with the fault-plane solution by NEIC solution based on long-period wave-form data.

4. REFERENCES

Kennett, B.L.N. (Editor) (1991). IASPEI 1991 Seismological Tables. Research School of Earth Sciences, Australian National University. 167 pp.

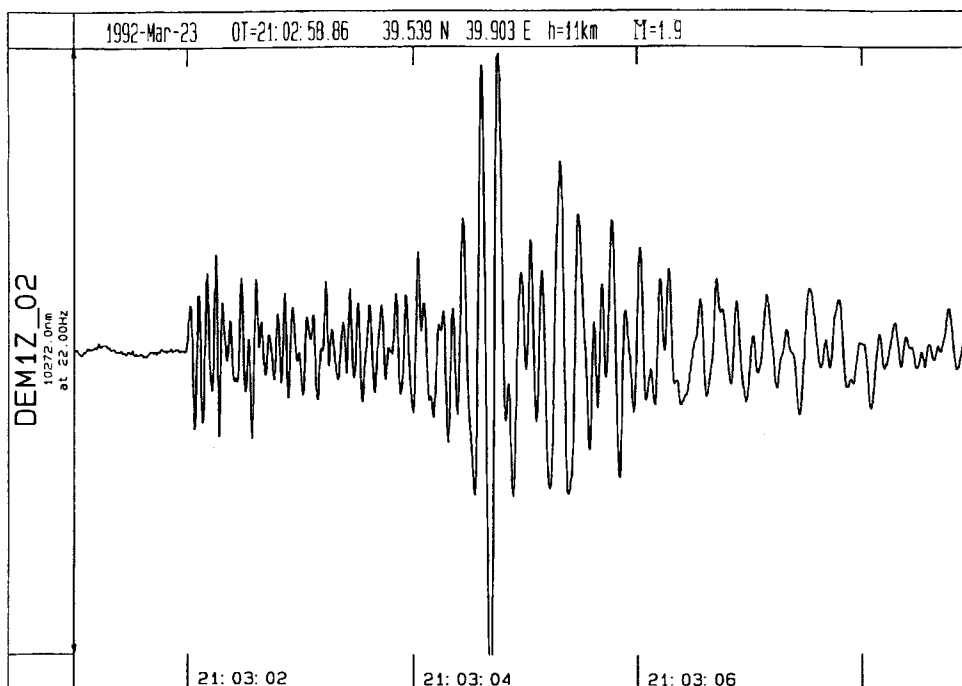


Fig. 1: Record of an Erzincan aftershock (vertical component)

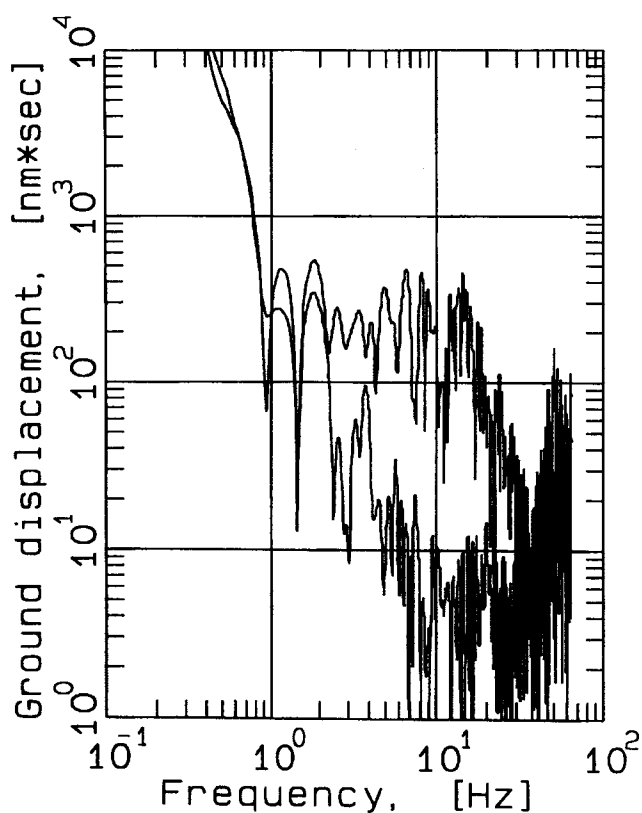


Fig. 2: P-wave (upper curve) and noise spectrum (lower curve) of the record shown in Fig. 1, corrected for the instrument response and frequency attenuation.

2.2 Estimate the low-frequency level u_0 of the spectrum by approximating it with a horizontal line. Note the logarithmic scales and ordinate dimension in $\text{nm s} = 10^{-9} \text{ m s}$.

$u_0 = \dots\dots\dots \text{ m s}$

2.3 Estimate the exponent n of the high frequency decay f^{-n} , mark it by an inclined straight line.

$n = \dots\dots\dots$

2.4 Estimate the corner frequency fc_p (intersection between the two drawn straight lines).

$fc_p = \dots\dots\dots \text{ Hz}$

3. Parameter calculations

3.1 Seismic moment

Under the assumption of a homogeneous Earth model and constant P-wave velocity V_p , M_0 can be determined from the relationship:

$M_0 = 4 \pi r V_p^3 \rho u_0 / (A S_a)$ with: density $\rho = 2.7 \text{ g/cm}^3$

P-wave velocity $V_p = 6 \text{ km/sec}$

source depth $h = 11.3 \text{ km}$

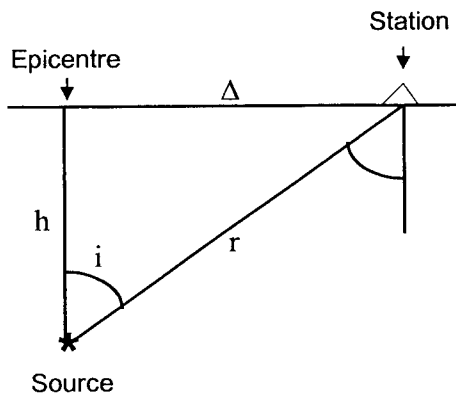
epicentral distance $\Delta = 18.0 \text{ km}$

travel path $r = \sqrt{(h^2 + \Delta^2)}$

incidence angle $i = \arccos(h/r)$

surface amplification S_a

averaged radiation pattern $A = 0.64$



Note the differences in dimensions used! M_0 has to be expressed in the unit $\text{Nm} = \text{kg m}^2 \text{s}^{-2}$. S_a can be determined by linear interpolation between the values given in table 1. It was computed for the above given constant values of V_p and ρ (homogeneous model) and assuming a ratio $V_p / V_s = 1.73$. i is the angle of incidence, measured from the vertical.

Calculate for the above given case the values for r , i , S_a and M_0

$r = \dots\dots\dots \text{ km}$

$i = \dots\dots\dots ^\circ$

$S_a = \dots\dots\dots$

$M_0 = \dots\dots\dots \text{ Nm}$

Table 1: Surface amplification S_a for P-waves; i is the incidence angle

i	S_a	i	S_a	i	S_a
0	2.00	30	1.70	60	1.02
5	1.99	35	1.60	65	0.90
10	1.96	40	1.49	70	0.79
15	1.92	45	1.38	75	0.67
20	1.86	50	1.26	80	0.54
25	1.79	55	1.14	85	0.35

3.2. Size of the rupture plane

For estimating the size of the rupture plane and the source dislocation one has to adopt a kinematic (geometrical) model, describing the rupture propagation and the geometrical shape of the rupture area. For the exercise computations have to be made for three different circular models, which differ in the source time function and the crack velocity V_{cr} . V_s is the S-wave velocity, here, as common, assumed to be $V_s = V_p / \sqrt{3}$.

Table 2: Parameters of some commonly used kinematic rupture models

1. Brune (1970)	$V_{cr} = 0.9 V_s$	$K_p = 3.36$	$K_s = 2.34$
2. Madariaga I . . . (1976)	$V_{cr} = 0.6 V_s$	$K_p = 1.88$	$K_s = 1.32$
3. Madariaga II . . . (1976)	$V_{cr} = 0.9 V_s$	$K_p = 2.07$	$K_s = 1.38$

The source radius R has to be computed by using the formula

$$R = V_s K_{p/s} / 2\pi fc_{p/s}$$

with $fc_{p/s}$ - the corner frequency of the P- or S-waves, respectively, and K_p and K_s being the related model constants. Only K_p has to be used in the exercise (P-wave record!).

The size of the circular rupture plane is $A = \pi R^2$. $\Rightarrow A_1 = \dots\dots m^2$, $A_2 = \dots\dots m^2$, $A_3 = \dots\dots m^2$.

3.3. Source dislocation \bar{D}

The average source dislocation \bar{D} can be computed from the expression $M_0 = \mu \bar{D} A$

with the shear modulus $\mu = V_s^2 \rho$ and $V_s = V_p / 1.73$.

The average dislocation is $\bar{D} = M_0 / (\mu A)$. Determine $\bar{D}_1 = \dots m$, $D_2 = \dots m$, $D_3 = \dots m$.

3.4 Stress drop

The static stress drop $\Delta\sigma$ describes the difference in shear stress on the fault plane before and after the slip. According to Keilis Borok (1959) the following relationship holds for a circular crack with a homogeneous stress drop:

$$\Delta\sigma = 7 M_0 / (16 R^3).$$

The stress drop is expressed in the unit of Pascal $\text{Pa} = \text{N m}^{-2} = \text{kg m}^{-1} \text{s}^{-2} = 10^{-5} \text{ bar}$.

Summarise your results for R , A , \bar{D} and $\Delta\sigma$ according to the circular models given above in the table below.

Model	R [m]	A [m ²]	D [m]	$\Delta\sigma$ [MPa]
1. Brune				
2. Madariaga I				
3. Madariaga II				

Note: Since $\Delta\sigma \sim R^{-3}$ the estimate of stress drop very much depends on f_c , a parameter which can not be estimated very precisely from real spectral data. In case of non-circular, e.g. rectangular fault ruptures, even two corner frequencies may exist which are controlled by the width W and the length L of the rupture plane. Additionally, differences in the assumed mode of crack propagation (e.g. unilateral, bilateral, radial) and crack propagation velocity V_{cr} influence the parameters calculated from spectral data. Accordingly, stress drop values may be uncertain by about two orders of magnitude. Therefore, in studying possible systematic differences in source parameters derived from spectral data for events in a given area for which similar modes of faulting and crack propagation can be assumed with good reason one should always stick to using one type of model.

REFERENCES

- Brune, J. N. (1970). Tectonic stress and the spectra of shear waves from earthquakes. J. Geophys. Res. 75, 4997-5009.
- Keilis Borok, V. I. (1959). On the estimation of the displacement in an earthquake source and of source dimensions. Ann. Geofis. 19, 205-214.
- Madariaga, R. (1976). Dynamics of an expanding circular fault. BSSA 66, 639-666.

SOLUTIONS

Note that individual visual parameter readings from Fig. 2 might be somewhat biased but they should not differ by more than about $\pm 10\%$ from the mean. Acceptable average values for the read and calculated parameters are for:

2.1 $f_1 = 2 \text{ Hz}, \quad f_2 = 30 \text{ Hz}$

2.2 $u_o = 3 \times 10^{-7} \text{ m s}$

2.3 $n = 3$

2.4 $f_{cp} = 14.4 \text{ Hz}$

3.1 $i = 58^\circ, \quad S_a = 1.07, \quad M_o = 6.8 \times 10^{13} \text{ N m}$

3.2 $R_1 = 129 \text{ m}, \quad A_1 = 5.23 \times 10^4 \text{ m}^2$

$R_2 = 72 \text{ m}, \quad A_2 = 1.63 \times 10^4 \text{ m}^2$

$R_3 = 79 \text{ m}, \quad A_3 = 1.96 \times 10^4 \text{ m}^2$

3.3 $\mu = 3.24 \times 10^{10} \text{ kg m}^{-1} \text{ s}^{-2}$

$\bar{D}_1 = 4.0 \times 10^{-2} \text{ m}$

$\bar{D}_2 = 1.3 \times 10^{-1} \text{ m}$

$\bar{D}_3 = 1.1 \times 10^{-1} \text{ m}$

3.4 $\Delta\sigma_1 = 13.8 \text{ MPa}$

$\Delta\sigma_2 = 79.7 \text{ MPa}$

$\Delta\sigma_3 = 60.3 \text{ MPa}$

SEISAN (Version 7.0) INTRODUCTORY TRAINING COURSE

J. Havskov and L. Ottemöller

University of Bergen, Institute of Solid Earth Physics,
Allégaten 41, N-5007 Bergen, Norway
Fax: +47 55 58 96 69; E-mail: jens@ifjf.uib.no

1. INTRODUCTION

This SEISAN training course is intended as a short introduction to SEISAN and how to use it. It assumes some knowledge of basic seismological processing and basic computer knowledge. During the course, the SEISAN manual, version 7.0 (Havskov and Ottemöller, 1999), will be used. The goal of the exercises is to be able to handle the SEISAN database, pick phases, locate the events and display the results. There is also a short exercise in doing fault plane solutions and determining spectral parameters.

SEISAN is a large system with many options and this course will only deal with the most basic operations. However, it should hopefully be sufficient to get started with SEISAN.

2. OVERVIEW OF SEISAN

The main goal of SEISAN is to have a simple system for routine processing of all kinds of seismic observatory data, whether digital, analog, broad band, teleseismic or local data. Another important goal is to be able to store and retrieve all data in a single system so that when one analysis like spectral analysis requires a hypocenter and an attenuation function, these parameters should automatically be available if obtained at some earlier time or already given in a parameter file. In SEISAN, this is achieved by having a simple event oriented database storing all data in chronological order. Once the user has found the relevant event to work with, no other steps are needed to access all data related to this event. This requires that station coordinates, crustal models etc. are stored in a standard way.

Batch processing: Since SEISAN is used for routine observations, there is also a need for processing large data sets in one go. In SEISAN, any part of or all of the database can be reprocessed with new parameters. If e.g. a new crustal model becomes available, a single command will relocate all events in the database and give the changes in location relative to the old model. If trace plots are required for any number of events, this can also be done with one command.

Computer independent: The system operates on UNIX (SunOS, Solaris and Linux) and Windows95/NT and all types of files can be moved between the two systems without any kind of reformatting. It is thus e.g. possible to preprocess data on a PC and move the data to Sun for further processing and storage.

Advanced analysis: By having all parameters collected in a single database, and by adjusting well known analysis programs like PITSA and SAC2000 (both Unix) to SEISAN, further

data analysis becomes much easier compared to having to reformat data for each new analysis tool. Thus SEISAN has a series of well known analysis programs integrated and has as a goal to integrate more to take advantage of the unified database and associated formats in SEISAN.

Learning SEISAN then involves as a first major step to become familiar with the database and how to manipulate data in the database as well of how to input and output data from the database. Once this is mastered, different kinds of analysis can be done following similar steps.

2.1 Installation of SEISAN

If SEISAN already has been installed, skip this section.

SEISAN for PC and Sun is normally distributed on a CD, the alternative is floppies, ZIP drive or tape. Here it is assumed that a CD is available. Normally SEISAN comes in one file, ZIP file for PC and a compressed tar file for Sun.

- Copy the file from the CD to the directory under which SEISAN is going to be installed.
- Follow the instructions in the SEISAN manual section 3. In order to get SEISAN operating with the test data included, the only parameters to set are the paths to the database and software. The remaining parameters can be dealt with later.
- Once the software has been installed and paths set, reboot the computer (on Sun, source the .SEISAN file).
- Give a command (e.g. 'wo' to move to working directory) to check that it is installed. If that works, try command dirf, if no protests, the software is successfully installed.

The testdata set is part of the full distribution, this part is only relevant if a limited version has been installed. To install the testdata, copy the file 'testdata_7.zip' for PC or 'testdata_7.tar.Z' for SUN to the SEISAN_TOP directory and restore the data as described for the SEISAN software. Note that if you get the software on CD, the filename for SUN will be 'testdata_7.z' and you will have to change it to 'testdata_7.tar.Z'. To work with the testdata, it is recommended to change the default database to 'TEST'.

2.2 Basics of the SEISAN database

The data is organized in a database like structure using the file system. The smallest basic unit is a file containing original phase readings (arrival times, amplitude, period, azimuth, apparent velocity) for one event. The name of that file is also the event ID, which is the key to all information about the event in the database. Although the database in reality only consists of a large number of sub-directories and files (all of which the user has access to), the intention is that by using the surrounding software, the user should rarely need to access the files directly, but rather do all work from the user's own directory using the SEISAN software.

The whole SEISAN system is located in sub directories residing under the main directory SEISMO (can have a different name). The database and associated parameter files consist of the following:

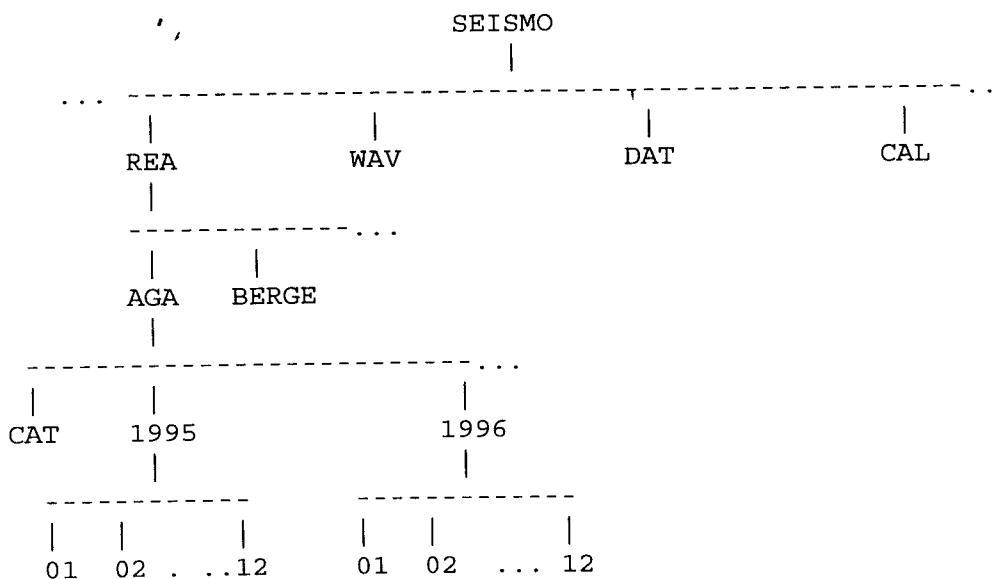
```

REA: Earthquake readings and full epicenter solutions in a database
DAT: Parameter and fixed data files, e.g. station coordinates
WAV: Digital waveform data files
CAL: System calibration files

```

The directory structure is used as a tree like structure for quick access to individual files in the REA directory, which therefore will appear as a simple database to the user. Figure 1 shows the tree structure of the SEISAN database.

Fig. 1: Directory tree structure of SEISAN database part.



2.3 REA directory and database

The REA directory contains phase readings and derived source information like hypocenters, fault plane solutions etc. The REA directory has one or several sub-directories corresponding to separate databases (max 5 characters), for simplicity it is here assumed that only the database AGA is present (see Figure 1). For quick reference and interactive work the events are stored in single files (S-files) in yearly directories and monthly sub-directories. When new data is entered into the database, it is stored as individual event files. However, once the interactive work has finished, the single event files are overwritten with the final location and additionally stored in monthly files, which are only changed when updating the database.

The monthly files, called CAT-files for catalog, are stored separately in the CAT directory and primarily used for quick searching and backup for the single files.

The key files in the database are the S-files. Each S-file contains original phase readings in the Nordic format (see example below) which includes file names of all corresponding waveform files. One event is one file. Each event has an ID line. The ID line contains a unique ID which will follow the event through all following operations. The **Fehler! Textmarke nicht definiert.**ID line also contains status information about the event like last action as e.g. when it was updated.

Table 1: A typical S-file

The first line is the header with origin time, location and magnitudes, in this case 2 magnitudes. The line type (last column) is 1.

The second line gives the event ID, line type I.

The third line gives the name of the associated waveform file, in this case from Sun, line type 6.

The fourth line is a comment line, line type 3.

The fifth line is a header line for the phase lines, line type 7, followed by the phases lines, one per line. The abbreviations are:

Input parameters:

STAT SP : Station and component
 IPHAS : Phase with onset
 W : Phase weight, HYPO71 style
 HRMM SECON : Hour, minute and seconds
 CODA : Coda length (secs)
 AMPLIT PERI: Amplitude (nm) and period (sec)
 AZIM VELO : Azimuth (deg) and apparent velocity of arrival at station
 SNR : Signal to noise ratio for phase

Output parameters:

AR : Azimuth residual
 TRES : Arrival time residual
 W : Weigh used in location
 DIS : Epicentral distance in km
 CAZ : Azimuth from event to station

```

1993 1014 1638 24.1 L 58.285 6.356 16.0 BER 8 .8 2.6CBER 2.3LNAO 1
ACTION:UPD 97-03-25 21:28 OP:jh STATUS: ID:19931014163824 I
1993-10-14-1638-01S.NSN_23 6
535 SOUTHERN NORWAY, this line is comment 3
STAT SP IPHASW D HRMM SECON CODA AMPLIT PERI AZIMU VELO SNR AR TRES W DIS CAZ7
KMY SZ EP 1638 43.75 99 .010 122 328
KMY SZ ES 1638 59.09 .810 122 328
BLS5 SZ EP 1638 44.83 101 .210 127 3
BLS5 SZ ES 1638 59.60 -.210 127 3
ODD1 SZ EP 1638 53.18 122 .910 182 5
EGD SZ EP 1638 57.89 122 -.3 9 230 343
EGD SZ ES 1639 23.23 -.2 9 230 343
BER SZ EP 1638 59.23 105 -.3 9 241 346
ASK SZ EP 1639 0.91 113 -.2 9 254 344
ASK SZ ESG 1639 33.37 -1.9 9 254 344
SUE SN EP 1639 9.70 156 .2 9 322 343
NRA0 S EPn 1639 19.25 20.0 1.7 20.4 9.452.0 -8 -.1 9 401 49

```

NRA0 S	EPg	1639	26.92		228.7	6.7	6.0	0	-1.9	9	401	49
NRA0 S	ESn	1640	01.69		232.3	4.7	3.6	3	1.4	9	401	49
NRA0 S	ELg	1640	15.09		222.4	3.4	6.2	-6	- .4	9	401	49

For more details on the S-file, see p 195 in the SEISAN manual.

The S-files are used as input for location and, when making a permanent update, also for output. Events are classified either as L, R or D for local, regional or distant event respectively. This information is given in the header line of the S-file as well as in the S-file name.

Interactive work with the S-files in the database is done with the program EEV. This program will enable the user to point to any event in the database and to do interactive work with that event.

The catalog in the CAT directory is accessed ONLY with the SELECT command. This command searches the database for events of particular interest. Data in the CAT directory are updated only through the UPDATE program.

2.4. Waveform data, the WAV directory

This directory contains files with digital waveform data. The directory normally has no sub-directories or any other organization since there is only room for a small part of the waveform data corresponding to the entries in the REA database. However, in case of using very large disks, WAV can also, be subdivided (see SEISAN manual).

The S-file will, in addition to seismic parameters, have a list of waveform file names associated with the event (see example above, line type 6 lines). This means that the S-file contains ALL information about available data for a particular event.

The analysis system (like EEV) will always look in the users own directory and then in WAV for a waveform file.

2.5 Calibration data, the CAL directory

The CAL directory contains calibration files, one for each channel of digital data. For details see SEISAN manual. For this exercise, it is assumed that the calibration files are already there.

2.6 Parameter files, the DAT directory

The DAT directory contains station files, program parameter files like channels to be plotted on default. Parameters used for spectral analysis are also stored here as well as map contours. Changes to the files in this directory will only have to be done occasionally, and most often when a new crustal model is to be used or new stations added. It is assumed for this exercise,

that no changes are needed. The station and model file used with these testdata is 'STATIONt.HYP'

3. EXERCISES

In all the following exercises a reference to a page number means reference to SEISAN manual.

Exercise 1: Interactive work with the database using EEV

COMMANDS CAN BE ENTERED IN UPPER OR LOWER CASE EXCEPT ON SUN WHERE PROGRAM NAMES MUST BE GIVEN IN LOWER CASE.

These exercises are based on a set of test data, which are stored in the database TES. Before you start, check that the TEST database is set as default database (p.12-13). Data are available for the following months: September 1993, June 1994, October 1994, August 1995, November 1995, June-July 1996, August 1997 and August 1998.

A list showing location and magnitude for these events is given in the Appendix. Waveform data is available for all events in the test database. For details of EEV, see p 24.

Always work in the work directory seismo\wor, use command 'wo' to get there.

Type 'eev 199606', that points you to the first event for June, 1996. You will see the essential information about the event (p 28) like origin time, location and magnitude. The letters L, R or D indicate whether it is a local, regional or distant event. To move around the data for that month, try the following commands (terminated with a CR)

Return: go to next event
'b' : move back one event
'3': move to event # 3
'd23': move to the first event on the 23rd or later

The event shown, can be operated on with several commands (upper or lower case), try these:

t: type the event (S-file) to see the parameters
tt: ----- only header line
e: edit event file
l: locate event
d: delete event (do not confirm !!)

Note: The editor is NE on PC and vi on Sun. To change to another editor, see p 12.

To see all commands in EEV, type '?'

Question 1.1

How many events does the month have (June 1996) ?

Question 1.2

How many local, regional and distant events are there ?

Question 1.3

What happens when you type return when positioned at the last event of the month ?

Question 1.4

Use event: 7 June 1996, 13:25

Locate event (command 'l') : The last output line gives the location in decimal degrees. How does that location compare to the database location ?

Edit the event (command 'e') and change the P-reading for station KMY by +5 seconds.

Locate again, what is the difference in the location ? Examine the details of the location in file print.out. This can be done from EEV with command 'one print.out' (PC) or 'ovi print.out' (SUN). 'o' in front of 'ne' means giving the command ne to the operating system. How many iterations was used to locate the event ?

Question 1.5

Use event: 5 July 1996, 02:20

Edit the event and add the following readings to the event:

station ASK, component SZ, phase EP, time 0221 0.57, coda 87

station ASK, component SZ, phase ES, time 0221 12.66

Exit from the editor and relocate event. Does the new station appear on the output ? How much did the location change ?

Question 1.5

Try command 'c' (p 26) to copy event file to working directory. Explain what it does and check that it works.

Question 1.6

Try command 'r' (p 26), explain what it does.

If you have SEISAN installed on a Windows95 system, try the same commands, see p 30.

Question 1.7

As mentioned above, all events for June and July 1996 have digital waveform files available. Make a cross-check between the file names of waveform files in the WAV directory (type WA to go there) and the events in the database (check for line type 6 in the S-file). Try the 'w' command in EEV.

Exercise 2: Selecting data from the database and making an epicenter map

An important task is to extract data out of the database for further analysis like epicenter plotting or exchange with other agencies. If the database has been updated, meaning that data is available in the CAT directory, this is most easily done with the SELECT command, otherwise use the COLLECT command (p 93). These commands will extract data out of the database in any given time interval, and the SELECT program can in addition use many selections criteria (magnitude, location etc.) to further limit the data extraction. The data is extracted to one file in the same format with events separated with a blank line. For this exercise, only the SELECT program will be used.

Go back to WOR directory with command 'wo'. Start the select program with command SELECT, use time limits 199309 to 199808 and default database. When menu comes up, select 2 as minimum magnitude(6), make another return (see also p 89). You will now get an output file select.out with selected events. Edit the file to see what it looks like.

Question 2.1

How many events were selected out of the total available ? How many waveform files were available for these events ? How was the distribution of local, regional and distant events ?

Plot the selected events using command EPIMAP. Follow instructions, p 82, use defaults for most parameters and select.out as input epicenter file name. The latitude - longitude range should be 59-63 and 0-10 respectively.

EPIMAP generates a file epimap.cmd with the plot commands every time it runs. This file can be edited to run the same map with e.g. a new input file. Try the command 'epimap epimap.cmd' to plot the same map again without answering questions.

Question 2.2

When the plot is on the screen, try commands 'p' and 'z', explain what they do.

Exercise 3: Putting new data into the database

Data can come into the database in two forms, parameter data and/or waveform data (see exercise 4). For this exercise, it is assumed that parameter data (readings) are available from a different agency. Data can also be manually entered through SEISAN program NEWEVE. For the exercise, a test file with readings from August 1996 is available (file name august.96 in DAT directory). The format is the same as used in all other S-files and CAT files. In order to put the data into the database, the necessary directory structure must be in place. If not already there, create it with command MAKEREA (p 15). Make a directory structure for all of 1996 and use database name TEST.

Question 3.1

How many directories were made with MAKEREA ?

Go to the DAT directory using command 'da' and check that file august.96 is there. Now that the directory structure is in place, the data is put into the database with program SPLIT (p 94), which splits up the input file, containing many events to single S-files in the database.

Question 3.2

Use EEV on the month of August 96, and find how many events there are.

Exercise 4: Plotting digital data

Digital data is plotted and analyzed with program MULPLT. The program is capable of doing general phase picking, correct for instrument response, produce ground corrected seismograms for determining Ml, Mb or Ms, determine azimuth of arrival for 3 component stations and do spectral analysis. The program can also read in theoretical arrival times for global phases to help with the identification of phases.

MULPLT operates either as a database independent program (started with command MULPLT) or in connection with the database (started from EEV with command 'p'). If the program works independently of EEV, it will create an output file mulplt.out in Nordic format with the readings and results of spectral analysis.

Running MULPLT using command MULPLT, the program asks for a file name or file number of a waveform file. To use the number, it is assumed that a list of interesting files has first been created and numbered in a file FILENR.LIS using command DIRF, see p 96. By giving the number, the file corresponding to the number is used. By giving a '?', the list with numbers is displayed and a new number can be given. In the first exercise, MULPLT will be used from EEV.

- Start EEV on June 1996
- Try several events in this month
- Type 'p' to plot. Chose filename if more than one and plot with option '0' (p 52-53), press return for no filter
- When plot comes up try the following:
Get options: Click on the 'MENU' bar. MENU or single letter commands can be used (p 61)

zoom: Put cursor to the left, push left mouse button or space bar, move mouse to the right, repeat
Back to original: Do in reverse order (right - left)
Filter: Click filter limits (e.g. '.1-1.0') 0.1 to 1.0 Hz, click on 'Plot' or push 'x' followed by 'r'
Push 'b', then 'r' (filtered from 5 to 10 hz)

- Select channels: Click on 'Other' and select channels or click on channel name on left hand side and type 'r' or click on 'Plot'
- Plot one channel at a time: Click 'Toggle' or press 't', back to multi trace do the same
- All commands are one key press or click on menu, to see all type '?' or click on 'Help'

- Quit by typing 'q' or click on 'Quit', you are now back to EEV

Plotting events directly with MULPLT without using the database:

- Move to WAV directory : 'wa'
- Make a list of waveform files : 'dirf 199*.*', use all files starting with 199
- Check list of files : 'type filenr.lis', on Sun 'cat filenr.lis'
- Plot event : 'mulplt', give event number e.g. '2', then option '0'
- Plot next event in list : Press 'f' or click on 'Next'

In this way, many events can sequentially be plotted for quick inspection.

Question 4.1: Are all channels available in one waveform file plotted ?

Putting a new digital recorded event into the database:

- Move to DAT directory ('da') and make list of files 'dirf 199*'
- Start MULPLT, when asked about filename, answer '?' to get the event list, select the event from August 96 (1996-08-15-2340-35S.TEST_009), use option '0' to plot the event.
- When event is on the screen, click on 'Regis' and answer questions (event is local) (p 62), then quit.

The event is now put into the database as a new event. Check that it is there by using EEV on August 96.

- change the model used for this event to 't' (p 44, p 196)

Question 4.2

What information is now available for the August event in the database ?

Exercise 5: Phase picking

Phases picked will enter the database and, when plotting from EEV, phases already present in the S-file will be shown on the plot (p 62). In this exercise, phases will be picked and put into the database. Optional phases can be picked in single or multi trace mode, to toggle between the two modes in mulplt press 't'.

Local event

- Start EEV for August 96

- Move to event on August 15 at time 23:40 using the 'd15' command, this event was registered in Exercise 4
- Plot event with 'p'

Question 5.1: Are there phases picked already for this event ?

- Go back to EEV and type the event with command 't'

Question 5.2: Are there readings available in the database (S- file) ?

- If readings are already present, edit the event and delete all phase lines (lines below the phase header line), DO NOT DELETE OTHER LINES.
- Plot event in single trace mode, press return when mulplt asks for plot option. The first trace will be shown on the screen.

It is essential to zoom, this in single trace is done by putting the mouse to the left and pressing the left mouse button and then to the right, but above the trace window. Try to zoom putting the right mouse in or outside the trace window. What is the difference? To zoom out again press 'r' for replot.

Try different filters when picking phases.

When the trace is zoomed, move cursor to the P-phase for the first trace, press '1', move to the S-phase press '8' and to the end of the coda and press 'c' (phase keys are defined on the top of the screen in single trace mode). As the phases are picked, they will be displayed. Pick also phases with polarity (p 63). Go to the next trace pressing 'f' and pick phases, until you get back to eev.

- Check readings available : 't' for type to see readings

Question 5.3: How many phase lines are present in S-file ?

- Locate event : 'l'

Question 5.4: Does the location and magnitude look 'reasonable' (compare with Appendix), how big is the RMS and how large is the largest residual ?

Phases can also be picked in multi trace mode, try. Looking at the phase picks in multi trace mode might be useful to get an overview.

Question 5.5: What is the advantage of using single trace mode compared to multiple trace mode when picking phases ?

- In EEV, use command 'update' (p 28), explain what happens, what changes do you see in the S-file ?

Distant event

- start EEV for August 1998, there is only one event
- plot the waveform file 1998-08-04-1902-47.TEST__011, which has broadband recordings
- in single trace mode, pick the first arriving signal as P ('1') for all traces
- locate event and compare with PDE location, which is given in the S-file

Exercise 6: Magnitude determination

All currently used magnitudes can be determined with SEISAN. In exercise 5, coda magnitude was calculated, here we shall calculate local magnitude M_l , body wave magnitude M_b and surface wave magnitude M_s . In order to determine magnitudes based on amplitudes, response information must be available in the system. The response files have already been installed in the CAL directory for this exercise. The definition of the magnitude scales are given on p 40-41.

Local magnitude M_l

In order to determine M_l , amplitudes must be read on a Wood Anderson seismograph. In SEISAN, the original trace is corrected for instrument response and converted to a synthetic Wood Anderson trace (p 65). Then the maximum amplitude is read.

- Select the August 1996 event from exercise 5, which has a local magnitude of 1.6, plot the event in single trace mode. Select Wood Anderson trace by clicking on 'WA', select a window around the maximum amplitude. The lower trace will now show the Wood Anderson simulated trace with amplitude scale of nanometers. Pick the amplitude (p 63) and store with an E-phase. Do the same for all stations and exit plot.

Question 6.1

Inspect the amplitude readings in the database (S-file), how do the amplitudes vary with distance ?

- Locate the event. At the end of the listing, the magnitudes calculated for each station are shown.

Question 6.2

How well do the M_l values for the different stations agree ?

Body wave magnitude Mb

Mb is defined using SP seismographs with a peak gain around 1 sec. Modern SP instrument have a flat velocity response from 1 to e.g. 20 Hz so, like for MI, SEISAN simulates the old SP response (p 65).

- Select event June 3,1996 at 19:55, plot file '1996-06-03-2002-18S.TEST__012' in single trace mode. Click on 'Mb' button and select a window around the P-phase. On the lower trace, the corrected seismogram will appear. Pick amplitudes for several stations and exit the plot.

- Locate event, the magnitudes will appear for each station

Question 6.3

How well do Mb for different stations agree, how do they agree with PDE magnitude (found in S-file) ?

Surface wave magnitude Ms

Ms is supposed to be read near the 20 sec period. In SEISAN, this is simulated by making the ground correction and filtering between 16 and 24 secs (p 66).

- Select the same event as for Mb, plot file '1996-06-03-1917-52S.TEST__002' in single trace mode. Since this data is from a broad band station, it must be filtered to 'see' the signals. Try with filter 0.01 0.1 Hz on the LZ channel. Click on 'Ms' and select a window around the surface waves. On the lower trace, read the maximum amplitude, go to next trace with 'F' and quit.

Question 6.4

What is the period and amplitude read (remember units) ?

- Locate the event.

Question 6.5

How does your determined Ms compare to the PDE magnitude (found in S-file)?

Exercise 7: Fault plane solution

In SEISAN, the fault plane solution can be determined with first motions (p 122). Polarities are picked by placing the cursor at the top or bottom of the seismogram when the phase is picked (p 63).

- Select one of the events 25 June 1996, 03:37 and 12 August 1997, 08:14 and determine polarities for all stations. The polarities are best seen when using zoom in zoom, in single trace mode. Fix the depth to 15 km (p 44). Then choose option 'f' and proceed with the fault plane solution (p 122).

Question 7.1

How well is the solution constrained ?

Compare your results to (strike: 327, dip: 62, rake: -11) for the first event and (strike: 184, dip: 64, rake: 16) for the second.

Exercise 8: Spectral analysis

The standard displacement spectral analysis determining seismic moment, stress drop and source radius can be done with SEISAN (p 71). As with other parameters, the results of the analysis is stored in the database. In addition to the spectral parameters, the moment magnitude M_w will also be determined using the seismic moment and the hypocentral distance (p 72). It is therefore important, that before doing any spectral analysis, that the database has been updated, meaning that epicentral distances are stored in the database.

- Select the event on 12 August 1997 at 08:14, plot in single trace mode
- Click on 'Spec' on the menu and select a window around the S-waves (about 10 - 20 secs long), select displacement spectrum when question comes up. The displacement spectrum is now displayed. With cursor, select the 3 points defining the spectral level and slope (p 76), enter 'f' and the spectral values are displayed. Enter 'f' again and the values are stored in the S-file. Quit the plotting program. To calculate the average values of the parameters, use the 'update' option in EEV.

Question 8.1

Are the spectral parameters stored in the S-file ?

Question 8.2

How does the M_w magnitude compare to M_l ?

Question 8.3

How big is the stress drop and source radius ?

Exercise 9: Reading global phases using IASPEI91 tables

The IASPEI91 travel time tables can be used to help reading phases (p 64). In order to calculate the theoretical times, the hypocenter and origin time must be known. In SEISAN, this means that the data is available in the S-file in the header line or another hypocenter line (type 1). Chose one of the events, which have broadband and long period data:

29 September 1993, 22:25

16 June 1994, 18:41

4 October 1994, 13:22

10 June 1996, 01:04

4 August 1998, 18:59

- Pick phases for the stations of interest, this could just be E phases.
- Calculate theoretical times: Command 'iasp' from EEV. This will calculate theoretical arrival times for all stations given in the S-file.
- Plot broadband and long period data first in multi and then in single trace mode, use filter 1-5 Hz for broadband and 0.01-0.1 Hz for long period. The theoretical phase will now be displayed with a prefix 'y' and displayed below the trace. There will be very many phases, try to zoom to identify a few. Phases are picked by pressing 'y' and labeled with the name of the closest calculated phase name in time.

Question 9.1

Which phases could be identified ?

Question 9.2

First identify P phases for one of the events June 16, 1994 at 18:41 and June 10, 1996 at 01:04, and locate. Then try to identify pP and sP and relocate. What can you say about the depth (compare to PDE)?

ACKNOWLEDGMENTS

This manuscript was revised by K. Atakan and B. Storheim. B. Storheim also tested all the exercises.

REFERENCES

Havskov, J (1997), editor. The SEISAN earthquake analysis software for the IBM PC and SUN. Version 6.0. Manual, Institute of Solid Earth Physics, University of Bergen, Norway.

Appendix

List of epicenters for which waveform data is available:

1993 929 2225 48.6 D 18.066 76.451 6.8 PDE625 6.3BPDE 6.2SPDE 6.2WGS 1
1994 616 1841 28.3 D -15.250 -70.294199.5 PDE401 5.6BPDE 5.8BBRK 6.0WGS 1
1994 10 4 1322 55.8 D 43.773 147.321 14.0 PDE672 7.3BPDE 8.1SPDE 7.9SBRK1
1995 822 0141 6.5 L* 60.353 2.734 23.0 BER 13 0.8 2.7CBER 2.3LBER 2.2LNAO1
1995 1120 0401 59.4 L* 60.064 5.400 5.0 BER 12 0.8 2.3CBER 2.0LBER 2.1LNAO1
1996 6 3 1955 40.1 D 47.715 153.256 33.0 BER 15 1.1 5.3SBER 6.0BBER 5.6BPDE1
1996 6 6 0648 30.5 L* 62.636 5.064 14.5 BER 13 1.3 3.0CBER 2.9LBER 3.0LNAO1
1996 6 7 1325 29.1 L* 59.841 5.127 12.0 BER 12 1.1 2.2CBER 1.9LBER 2.0LNAO1
1996 610 1 4 47.0 D -13.481 167.130200.1 PDE301 5.8BPDE 5.9SPDE 6.7WGS 1
1996 623 0117 57.8 D 51.636 159.828 33.0 BER 16 0.4 5.4SBER 5.5BBER 5.4BPDE1
1996 625 0337 31.9 L* 61.655 3.368 17.0 BER 35 1.4 3.0CBER 3.2LBER 3.2LNAO1
1996 7 5 0220 47.1 L* 61.264 4.797 20.0 BER 11 1.0 2.2CBER 2.0LBER 1.9LNAO1
1996 713 0556 46.9 L* 61.388 4.048 12.0 BER 9 1.0 2.1CBER 1.5LBER 1.6WBER1
1996 718 0946 51.4 L* 60.156 2.071 15.0 BER 9 1.1 2.5CBER 1.8LBER 2.1WBER1
1996 718 2255 6.0 D 51.438 157.737 29.9 BER 18 0.4 5.7BBER 5.5BPDE1
1996 726 0742 11.9 L* 61.739 2.377 15.0 BER 9 0.4 2.4CBER 1.8LBER 2.0WBER1
1996 815 2341 13.2 L* 59.883 5.745 6.0F BER 12 0.9 2.1CBER 1.6LBER 1.6LNAO1
1997 812 0814 24.1 L* 59.819 6.647 12.0F BER 14 1.0 2.7CBER 2.8LBER 3.4LNAO1
1998 0804 1859 18.2 D -0.551 -80.411 19.0 PDE 6.2BPDE 1

SEIS89 – A PC-TOOL FOR SEISMOGRAM ANALYSIS

M. Baumbach

GeoForschungsZentrum Potsdam,
Telegrafenberg, D-14473 Potsdam, Germany
Fax: +49 331 288 1295; E-mail: baum@gfz-potsdam.de

1. INTRODUCTION

SEIS89 was developed in 1989 for routine analysis of both local and teleseismic events, recorded with local networks or single stations. The basic tools implemented are therefore routines for localisation and magnitude estimation of local and teleseismic events. With time, more specific tools for seismological research were integrated into SEIS89. Much effort was made to create an truly interactive tool with easy access to the records and the estimated parameters.

SEIS89 was written in Turbo-Pascal for DOS-PC's, but it can be used on WINDOWS-PC's in a DOS-window. There is a specific data format for SEIS89. Records of data acquisition systems have to be converted into the SEIS89-format. This requires some programming effort. In the UNESCO course SEIS89 will be used as teaching tool for various seismological routines discussed during the lessons.

2. INSTALLATION OF SEIS89

SEIS89 is shareware. It may be distributed for scientific purposes without limitations. SEIS89 is included in a CDROM with different software tools assembled by Jens Havskov for the UNESCO- Training Course. Insert the CDROM into the corresponding drive, change to the CDROM-directory SEIS89 and type INSTALL. The program asks for the drive (C:, D:, ...) where to install SEIS89. The installation program creates the directory SEIS90 and copies all files supplied into subdirectories of SEIS90. During installation SEIS89 is adapted to the directory structure of the PC. In the directory SEIS90 resides the batch file SEIS89.BAT, which has to be used for calling SEIS89. You may start SEIS89 from this directory, otherwise you have to include the directory name SEIS90 into the path command of the autoexec.bat. When having changed the autoexec.bat reboot the PC. SEIS89 needs some information about the PC-hardware (disk structure, graphics card, plotter type and port and RAM-disk). This information will be stored in SEIS89.DIR (directory UNITS). To specify the necessary parameters call the interactive configuration program by typing SEI89 INSTALL. Indicate only a RAM disk if it's size is sufficiently large (more than 1Mbyte). Don't try to install Turbo-Pascal high resolution graphics drivers on a WINDOWS-PC.

3. RECORD AND PARAMETER FORMATS

Data files: each component (Z, N, E, P, R, T, Q) of a station record is stored in a separate data file. The data files may be stored anywhere on the hard disk, on a diskette or on a CDROM. Records of one event have to reside in the same directory. The records will be loaded by SEIS89 with a routine similar to the Norton Commander.

- There is a strict rule for forming file names: `ssstcxxx.nnn`
 sss: 3-letter station code, e.g. `mox`.
 t: record type (1 letter), e.g. `b` for broad band, `s` for short-period, `l` for long-period... The record type shows the processing history. For instance, a short-period record, filtered from a broadband record gets the record type `s`.
 c: record component (1 letter), e.g. `z`, `n`, `e`, `r` (radial), `t` (transversal in SH-plane), `q` (transversal in SV plane), `p` (rotation into the direction of P-wave polarisation).
 xxx: any 3 optional letters or numbers (a...z,0...9) for additional information
 nnn: file number for the given station and record type nnn: 000 – 999 or 3-letter identification of the event (e.g. `ind` for India)
- Each data file has a 512-byte data header. It includes the station location, the record start time, the record type (acceleration, velocity, displacement, broad-band, short-period...), the event location, the magnitude and a response table consisting of 20 triplets of frequency in Hz, magnification in nm/count and phase shift in degree. The magnification must include both the seismometer response and the filters implemented in the recording system. See Appendix 1 for a detailed format description.
- The time series attached to the data header consists of 2-byte (90dB) integer data samples. When using records of 24-bit high-resolution data acquisition systems one has to reduce the dynamic range in order to fit the maximum amplitude into a 2-byte integer sample. The magnification, given in the response table has to be corrected correspondingly. There is no limitation to the record length, except the size of the hard disk.
- The processing results are stored in ASCII-files. For each processing tool a separate file will be created (e.g. `coda-Q`, spectral analysis, ...). If a file with results derived with a specific tool already exists, the new data will be appended. The directory of these result files may be selected after loading a file set. There is no data bank system implemented in SEIS89.
- For some processing tools specific initialisation files `*.INI` with processing parameters are required. They have to reside in the directory `UNITS`. This is the directory of executables and parameter files necessary to run SEIS89.

4. LOADING RECORDS

After calling SEIS89 the file selection window will be displayed. The file selection procedure is self-explaining. Data files can be selected by a mouse click with the left button on the records of interest. A click on the right mouse button displays information about the record. Further, the files can be specified by hitting `+` and typing the file name (wildcards `?` and `*` are allowed) Take care to load always records of the same event (identical file name extensions). The maximum number of traces displayed is 10. When having records on screen, a new file set may be loaded by hitting **F4**. The traces loaded before may be reloaded by hitting **Strg F4** (last file set) or **Alt F4** (last but one set). Hit **Strg F3** to show a list of all traces loaded and the last and last but one file sets. SEIS89 may create new traces, e.g. by filtering. The new traces will get an entry as last file set to ease their loading. The former last file set will become the last but one. GSE-files (GSETT 1) with calibration section in Poles and Zeros (PAZ) can be loaded by SEIS89. They will be automatically converted into the SEIS89-Format. Fig. 1 shows a plot of loaded teleseismic P-wave network recordings.

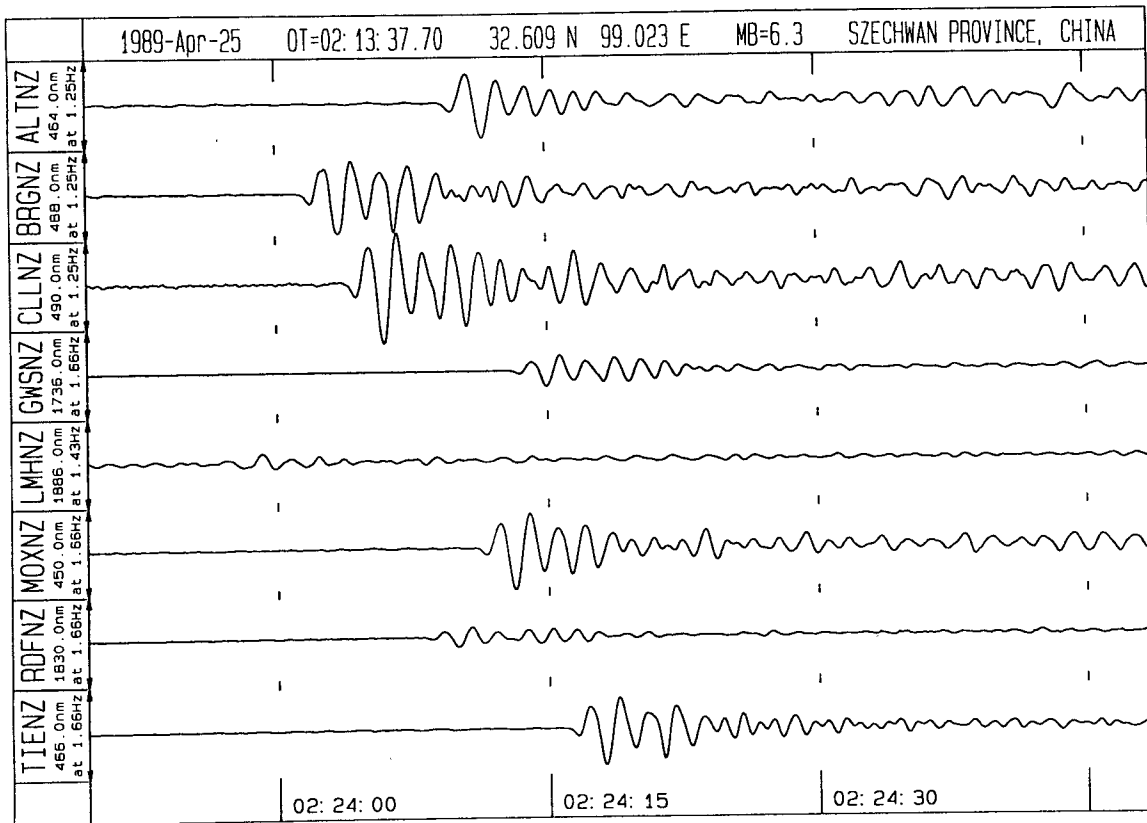


Fig. 1: Plot of short-period P-wave recordings of a teleseismic earthquake in China at a regional seismic station network in East Germany. Event information is given in the head line and the time scale (hours, min., sec. in UT) on the bottom. Station code and component (Z) are written in the boxes on the left side together with the scale of ground-motion amplitudes at given frequencies (corresponding to the length of the arrow-bar in each box).

4.1 Specification of screen trace parameters

After having confirmed the file selection 4 windows appear showing the traces to be displayed, the screen amplification, the trace colour (colour code: 1-15) and necessary directories. The screen amplification may be changed separately for each trace. The larger the value in the "maxcount" table, the smaller the amplitude on screen. A value of 32767 allows to display records with full dynamic range of 90 dB unclipped on screen. The traces of a 3-component record (e.g. Z, N, S) should have always the same screen amplification. The 4th window displays the name of the directory of the currently loaded files, the directory for storing processed files (e.g. filtered, or rotated traces) and the directory for storing parameter data (info directory). The last two directories and the trace parameters can be changed interactively. The bottom window shows the editor commands.

The screen parameters and directories may be specified in SEIS89.INI (directory UNITS):

- Line 1: RECORD LOAD DIRECTORY
- Line 2: RECORD SAVE DIRECTORY
- Line 3: INFO DIRECTORY

Next lines (4-13): filename without filename extension screen amplification colour.
 Supposed, a dataset with the same filenames indicated in SEIS89.INI and any valid file name extension will be selected, then the trace parameters specified will be applied. For changing screen parameters when having records on screen, hit **F3**.

4.2 Loading large 3-component datasets

There is a specific mode for loading large data sets of 3-component records of a local network. The filenames of the traces must be identical except the station name (letters 1-3) and the record component (e,n,z, letter 5). Start SEIS89 with the command **SEIS89 3C**. Load any record of the event data set to be analysed. When having it on screen hit **+**. This results in automatic loading of all traces belonging to the event. Always 3 stations (9 traces) will be displayed together on screen. Hit **ALT n** with $n=1, 2, 3, \dots, 9, 0$ to display all traces in groups of three stations. The maximum number of stations that can be loaded and processed together is 30. Hit **Strg F3** to show all traces loaded. If the events to be processed do have consecutive file name extensions (e.g. 123, 124, 125, ...) then the next event or the last event may be simply loaded by hitting **+** or **-**, respectively.

4.3 Loading data sets of a permanent network or of permanent single stations

This mode of loading files was implemented in order to get a fixed configuration for routine processing and analysis of seismic records. A fixed trace configuration on screen eases the every day routine job. The trace configuration has to be fixed in the file **SAVEFILE.INI** (directory **UNITS**). As an example check this file for a dataset consisting of short-, long- and broadband recordings at the seismic station Moxa. Start SEIS89 by typing **SEIS89 IND**. **IND** is the file name extension of the data files. Another record set with the same configuration may be loaded when indicating the corresponding file name extension. The trace swapping is organised in the same way as described in the previous paragraph (**ALT n**).

4.4 Single trace mode

Out of the traces displayed on screen a single one may be displayed for more detailed examination (e.g. for exact arrival time picking). To do this one has to hit one of the keys **1, 2, 3, \dots, 9, 0**. The traces are counted from the top to bottom. Hit **ESC** to get the complete record set back on screen.

4.5 Screen information

Up to 10 traces can be displayed on screen. The filename (without extension) and component of the trace, the cursor is pointing at, is displayed in the lower left screen corner (see Fig. 2 and Fig. 3 in section 7.3). The cursor time is shown in the lower right corner and the trace amplitude in digital counts in the upper right corner. If a dataset with more than 10 traces is loaded (see previous 2 paragraphs) than the number displayed in the upper left corner is the number $n=1, 2, 3, \dots, 9, 0$ which was used for putting the records on screen with **Alt n**.

The parameters, stored in the data header may be displayed by moving the cursor onto the trace of interest and hitting **F2**.

All processing steps will be started by a mouse click, a mouse menu item or a keyboard command.

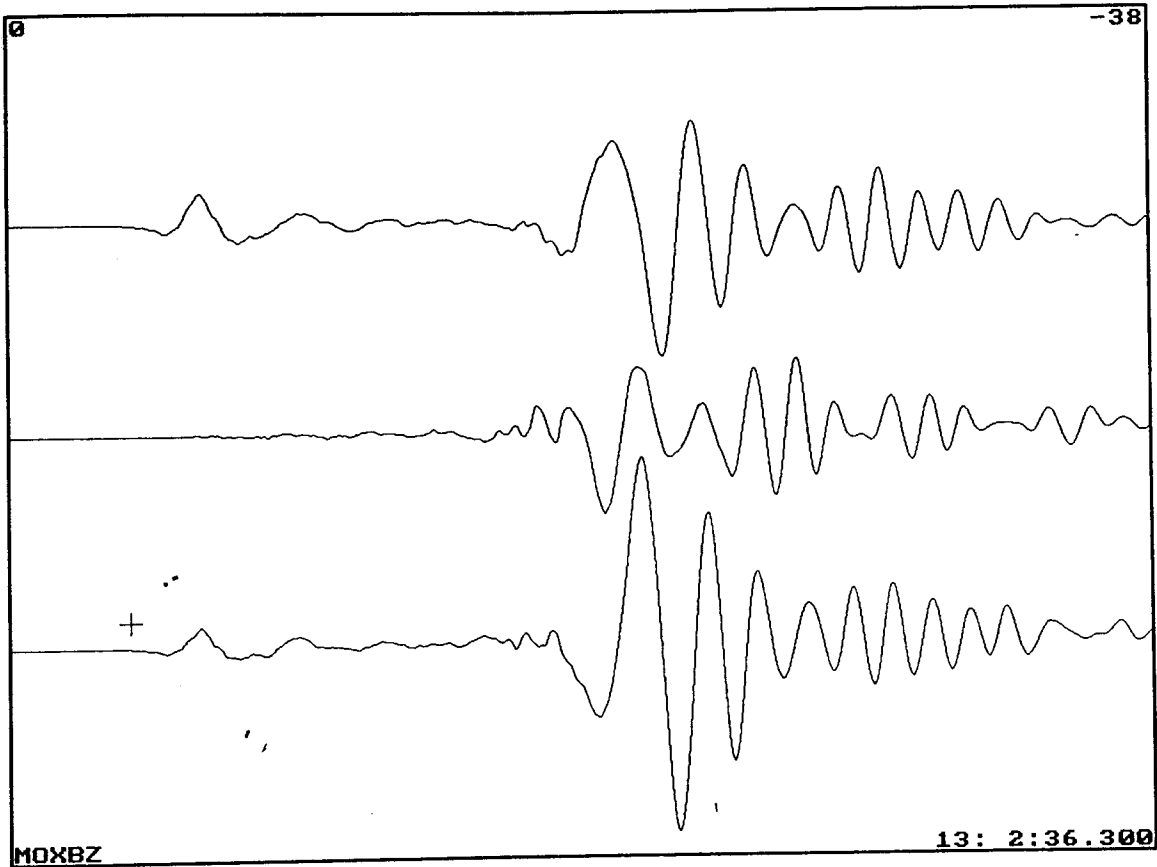


Fig. 2: Screen display of a broadband (B) 3-component record at station Moxa (MOX) of a local seismic event (strong rockburst). The cursor points at the vertical (Z) component.

5. HOW TO GET HELP

SEIS89 includes a lot of subroutines and you need quite a bit of time to get accustomed to it. All available commands are described in help widows. We advise to start SEIS89 with the command SEIS89 3 (3 is the number of the event). Records of a teleseismic event close to Japan will be loaded. On top of the screen you find a small blue window with 4 help items. Move the cursor for the help item of interest into the yellow screen corner as indicated by an arrow in the mentioned top window. A window will open with available commands and processing routines. To get a short description of the help items move the cursor onto the line with the command or routine of interest ending with ... and hit the left mouse button. An additional window appears with more detailed information. The other commands (without ...) are self-explaining. The cursor shows an increased line thickness as long as the help window is active. To deactivate the help window move the cursor out of the window or hit ESC. ESC in addition removes the help window. Test the program options described in the help windows. See Appendix 2 for a list of commands of SEIS89.

6. PROCESSING MODES OF SEIS89

For computation of seismological parameters one or more time markers will be set by clicks with the left mouse button. There are two modes of work with SEIS89:

ONSET-ON: computation of seismological parameters, **ONSET-OFF:** setting time markers. After starting SEIS89 is in the mode ONSET-OFF. Hit F9 to change to ONSET-ON.

ONSET-ON will appear at the screen bottom. Hit **F9** to change back to ONSET-OFF. In detail these two modes of operation provide the following:

ONSET-ON: Move the cursor to the exact time position of the trace where you want to set a marker. Hit the left mouse button and select the desired item from the mouse menu (see Tab. 1). The markers set will get a name, showing the type of parameters computed. The parameters will be stored together with their position in the record (trace and time). **STRG F1** displays the marker list with the parameters computed, **STRG F2** saves the marker list to disk and **ALT F1** clears the marker list. If the number of parameters computed in a subroutine is rather large (e.g. spectral source parameters, coda-Q), only the most important parameters will be kept in the marker list. The complete results will be saved to disk. There is a specific output file for each type of computed parameters. The same parameters estimated for a new record will be appended to an existing output file of the same type. The parameters in the marker list will be used for further calculations (e.g. event localisation with given wave types, onset times, amplitudes ...).

ONSET-OFF: Simple markers without names will be set. No parameters will be computed. This mode will be used for instance for computation and display of a noise power spectrum.

Table 1: **Mouse menu** (only ONSET-ON)

	Explanation
Keyboard input	Input of wave phases, e.g. PKP, SS, ...
P, P, P, P, *)	Multiple P-picks for a network
S, S, S, S, *)	Multiple S-picks for a network
Ampli., Ampl., *)	Multiple amplitude picks for a network
Pn	Pn-Pick
Pg	Pg-Pick
Sn	Sn-Pick
Sg	Sg-Pick
P	P-pick for a single station
S	S-pick for a single station
Amplitude	Ampl.: automatic computation of A and T
Amplitude (T+A)	Separate measurement of A and T
End of Event	Fixing the end of an seismic event
End of Event,	Same but for a network
Polarization	Computation of P- or Rayleigh wave polarisation
P-Moment & fc	Computation of P-spectral parameters
P-noise spectrum	Computation of P-noise spectrum
S-Moment & fc	Computation of S-spectral parameters
S-noise spectrum	Computation of S-noise spectrum
Coda-Q	Computation of Coda-Q
Shift traces	Shift time origin of traces
Begin of section	Select begin of section for processing
End of section	Select end of section for processing

*) The multiple P-, S- and amplitude picks have to be terminated by ENTER

All parameters or functions based on amplitude readings will be automatically corrected for the magnification curve given. Amplitudes will, therefore, be given in the displacement unit of nanometres, displacement spectra in nm·sec and displacement power spectra in nm²/Hz.

7. TOOLS FOR LOCALISATION AND MAGNITUDE DETERMINATION

7.1 Localisation of teleseismic events

There is a teleseismic localisation tool implemented for local to regional network. It is based on the IASPEI-91 velocity model (Kennett, 1991). A standard source depth of 35km is assumed. If there are independent depth estimates from depth phases available, the source depth may be recalculated with an accuracy of about 18 km.

Start SEIS89 and load the vertical component records of the network recordings of the Japan event (directory NET, event number 3). Move the cursor onto the best visible P-onset. Select a **waveform cursor** by hitting **ALT Q** and move the mouse to the right side and finish by clicking the left mouse button. The waveform cursor helps in fixing the correct arrival time by visual correlation of the waveform cursor with the other traces. Match the waveform cursor with a P-wave arrival, click the left mouse button and select **multiple P-picks** from the mouse menu. Finish P-picking by hitting **ENTER**. Estimate the P-amplitudes by **multiple amplitude picking** (see mouse menu). Look for the cycle with the largest difference between maximum and minimum (peak-to-through) amplitude of the given P-trace. Move the cursor close to the zero crossing between the largest and smallest amplitude of the cycle. A left button mouse click at this position starts the amplitude calculation. The cycle used for amplitude estimation will be marked brighter. Finish amplitude picking by hitting **ENTER**. Start epicentre location by hitting **T** (teleseismic location). In the examples used for demonstration data from a network in eastern Germany are used. Note that for this network the localisation routine was optimised by applying empirical station corrections depending on the epicentre region in order to improve location accuracy. Note that SEIS89 calculates for teleseismic events only short period P-wave magnitudes m_b (cf. chapter Magnitude of seismic events, section 2.4.2).

7.2 Localisation of local events based on travel-time curves

This localisation program can be used for location of crustal earthquakes and quarry blasts based on recordings of a sparse local network. Source depth estimations are unreliable because of the large inter-station distances. Therefore, only epicentre co-ordinates are calculated. The travel time curves (Pn, Pg, Sn and Sg velocities and intercept times) are specified in LOC_TT.INI (directory SEIS90\UNITS). Load the files *.0 from the directory SEIS90\NET. Pick the available Pn, Pg, Sn and Sg-arrival times and the maximum Sg-amplitudes. Hit **L** (local event) for location and magnitude calculation.

7.3 Localisation of local events with HYPO71

HYPO71, a program for locating local earthquakes on a mainframe computer was released in 1971 by Lee and Lahr (1972, 1975). The conversion to the PC was made in 1985 by Lee and Valdés. The input to this program keeps to the "card format" with 80 characters per line. Both arrival time readings and processing parameters have to be specified in a single input file. HYPO71 may be used for local event location in SEIS89. The code HYPO71PC.EXE is not supplied with SEIS89. It is available with the IASPEI Software Library Volume 1, edited by W.H.K. Lee (1989). The executable file HYPO71PC.EXE (136 Kbytes) has to be copied into the SEIS89-directory UNITS. To ease the handling of processing parameters they are specified in 5 input files. For each parameter a short description is given in the respective input file. For detailed information read the description given in the IASPEI Software Library Volume 1, p. 203-236.

Check whether the parameters given in the input files are correctly selected with respect to network configuration, crustal structure and distribution of hypocentres. Input files for localisation with HYPO71 reside in the directory UNITS.

HYPO71PC.INI:	- directory for saving localisation results, - map file for plotting epicentres, - magnitude: Iida or Wahlstroem & Strauch (c.f. chapter Magnitude of seismic events, section 2.3.2) - epicentral or hypocentral distance for magnitude calculations - colour code for display of source depth
HYPO71PC.MOD	- velocity model
HYPO71PC.STA	- station data (check whether you have the correct station file for the given network)
HYPO71PC.TST	- test data (one parameter per line)
HYPO71PC.CON	- HYPO71 configuration file

For interactive location your PC should have at least 600 Kbytes of free RAM. Check this by the DOS-command CHKDSK.

Localisation procedure: Call SEIS89 and hit **STRG L** to switch to the HYPO71 phase picking menu. Mark the onset with **P** or **S**, and indicate its characteristics. After picking an arrival a menu is displayed for selecting the necessary parameters. The menu eases the selection of the parameters required. The corresponding HYPO71-code which is shown below in bold characters is used for labelling the P- and S-markers.

- quality of the arrival: **i** for impulsive or **e** for emergent
- first motion: up (**U**), poor up (**+**), down (**D**), poor down (**-**), noisy (**N**)
poor up and poor down are abbreviated in the mouse menu as “(up)” and “(down)”
- weight assigned to the arrival: 1 (**0**), $\frac{3}{4}$ (**1**), $\frac{1}{2}$ (**2**), $\frac{1}{4}$ (**3**), 0 (**4**), S-P difference (**9**).

Note that HYPO71 allows to pick only the first P- and first S-arrival for the velocity model assumed. A high noise level may mask the first arrival or a weak guided wave might be overlooked. Picking of a later arrival as a first arrival will result in large traveltimes residuals and a wrong hypocentres.

Estimate the maximum S-wave amplitudes or the record duration (Marker **EQ-end** in the first line of the phase picking menu) for calculation of magnitudes according to Wahlstroem & Strauch or Iida, respectively. An example of a record set with arrival time and amplitude picks is shown in Fig. 3.

For location hit **L**. The input file for HYPO71 is formatted in SEIS89 by using the arrival time and amplitude picks and the parameters stored in the HYPO71 input files. Further, SEIS89 checks the free RAM of the PC. If there is enough RAM it will start location. Otherwise one has to use HYPO71PC.S89 for offline location with HYPO71PC. The localisation results can be displayed on a map. See Appendix 3 for the format of the map file. New phase readings will be always appended to HYPO71PC.S89. This allows to re-run offline location with modified parameters for a suite of events. To return to the SEIS89 picking menu hit again **STRG L**.

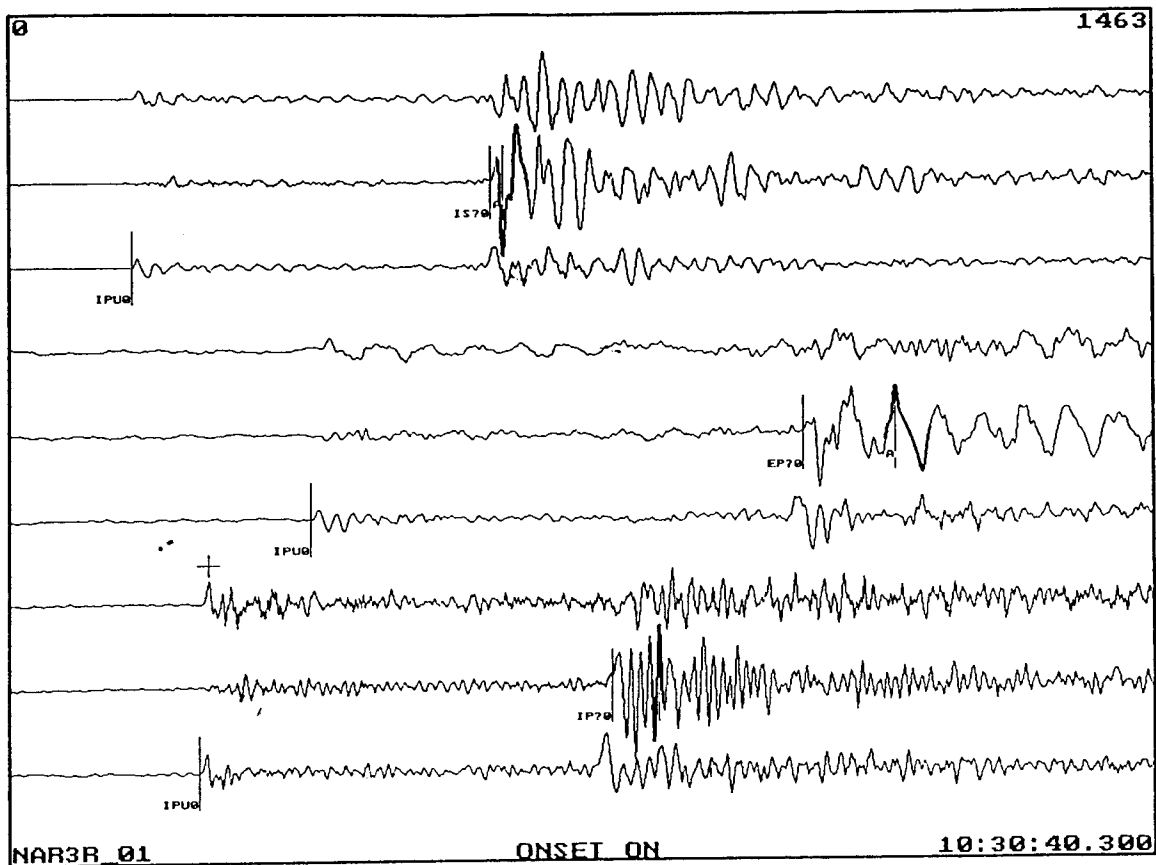


Fig. 3: Displacement records of an aftershock of the September 29, 1993 Killari earthquake in India by stations of a local seismic network. The HYPO71 phase and amplitude picks are indicated.

8. DATA PROCESSING ROUTINES

8.1 Filtering

There are Butterworth filters implemented in SEIS89. The filter parameters (filter order and corner frequency) can be preselected in the initialisation file BUTTER.INI (directory UNITS) and modified interactively. Check BUTTER.INI for how to specify filter parameters. Low-pass, highpass, bandpass and bandstop filters are available.

Mode ONSET-ON: Mark the record section to be filtered with 2 markers: Begin and End.

Mode ONSET-OFF: Mark the record section to be filtered with two time markers (left mouse button). If there are no markers set, the complete record will be filtered.

Start the filter procedure with **F5**. This allows to fix the filter type and the filter parameters interactively. In single trace mode only the record displayed will be filtered. Otherwise, all traces displayed will be processed. The filtered records will be stored in the RECORD SAVE DIRECTORY (see **F3**: screen parameters and directories). Load the filtered traces from disk with **STRG F3**.

Two standard filters may be defined. In this case the records selected will be filtered with the parameters fixed in BUTTER.INI. The type of the two standard filters is indicated in the last parameter line (1: lowpass, 2: highpass, 3: bandpass, 4: bandstop filter).

Example for the last line: 1 2.

In this case the first standard filter is a lowpass, the second one a highpass. Adapt in BUTTER.INI the filter types and filter parameters according to your needs. To start filtering with the first or second standard filter hit **STRG F5** or **ALT F5**, respectively. For all 4 filters the upper corner frequency must be smaller than 0.25 of the sampling frequency. Sometimes, in case of lowpass filtering the sampling frequency may be reduced. An example is the lowpass filtering of a 20 Hz broadband record in order to get a long-period record with a sampling rate of 1 Hz. Take care that the sampling theorem is obeyed (i.e. no signal energy in the spectrum at and above the Nyquist frequency).

8.1 Spectral calculations

Spectral calculations are performed only in the mode ONSET-OFF. All spectra will be computed with the Fast Fourier Transform and corrected for the instrumental response, taken from the trace header (see F2). There are three options for calculating spectra and subsequent plotting. There is a specific menu for formatting the graph before plotting on an IBM-GL plotter or HP-Laserjet.

1. Calculation of displacement spectrum: Mark the begin and the end of the time series to be processed with two markers and hit **F7**. The spectrum will be displayed on screen in double logarithmic scales.
2. Calculation of displacement power spectra: Mark the begin and the end of the time series to be processed and hit **STRG F7**. Try to use a long time series. If it is long enough, a smoothed spectrum may be computed, i.e. spectra of half overlapping time intervals will be computed and averaged (see example in Fig. 4). The power spectrum helps in analysing seismic noise and station quality. The frequency ranges with high natural or technical noise level can be identified. Before installation of a network noise measurements should be undertaken in order to select low noise station sites (cf. chapters *Seismic site quality* and *site selection*).

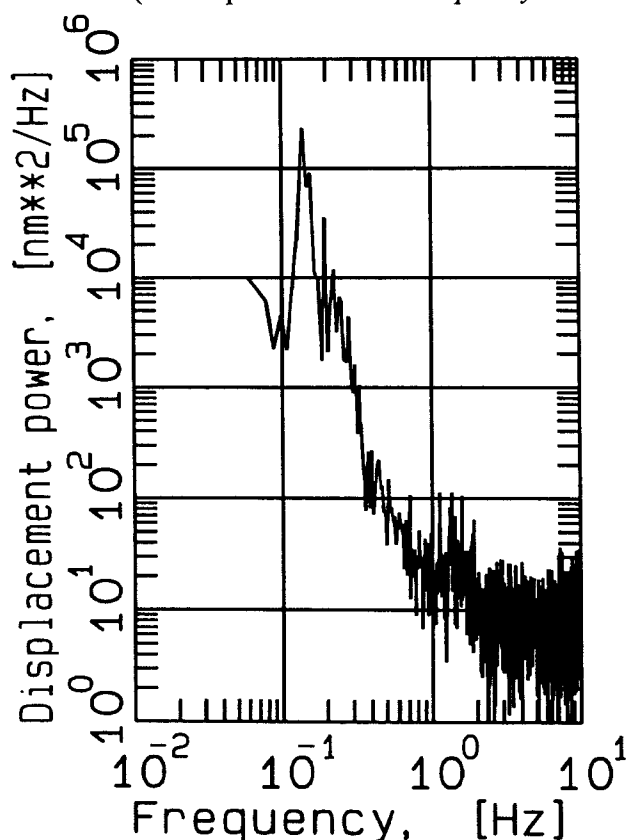


Fig. 4: Displacement power spectrum of a Z-component noise record at station MOX, Germany.

3. Calculation of spectral signal to noise ratio (displacement)

Set three markers and hit **ALT F7**. The first marker defines the begin of a noise section before the signal. The second and third markers define the begin and the end of the signal to be analysed. The time difference between the 1st and 2nd marker must be larger than the time difference between the 2nd and 3rd marker. This is necessary in order to analyse a noise section not superimposed by the signal. The signal-to-noise spectrum helps to identify the frequency range with sufficient signal-to-noise-ratio for analysis. An example is given in Fig. 5.

Note: In order to avoid spectral distortion by arbitrary truncation of the record the markers should be set as follows: First, press **M** to get a horizontal line which should be matched to the imaginary zero line of the record. Then, set markers for the beginning and end of the section to be analysed so that they coincide with a zero-line crossing of the record trace. Then, no additional tapering procedures are required. The computation of power spectra includes tapering with a cosine window. In case of several traces displayed analyse one by one pressing 1, 2, ... 9, 0.

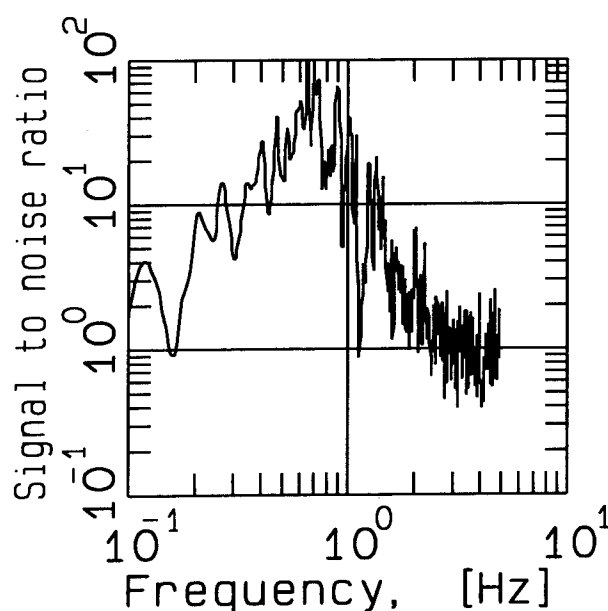


Fig. 5: Spectral signal-to-noise ratio for a P wave trace of a teleseismic earthquake in Japan, recorded at station BRG, Germany.

8.2 Polarisation analysis of P- and Rayleigh waves

P-wave polarisation analysis should be performed for a time interval including a noise section before the P-wave arrival, and the P-wave train itself. A time window will be moved across a 3-component recording within the selected time between the polarisation marker **Pol** and the **End**-marker. For each position the **P-wave back azimuth** (azimuth towards the epicentre as measured from north), the **incidence angle** (as measured from the vertical direction) and the **rectilinearity** are computed. The general assumption is, that particle motion can be approximately described by an ellipsoid. For the selected time window the length and orientation of the particle motion axes are computed. Two graphs show the azimuth (**AZI**) and incidence angle (**INC**) of the three axes for the record section analysed. The largest axis (**L1**) is displayed in red, the smallest (**L3**) in white and the intermediate one (**L2**) in green. The largest axis is assumed to be the P-wave polarisation ray direction. The lower graph shows the rectilinearity (**REC**) which is a measure of linear polarisation:

$$\text{REC} = 1 - (L_2 + L_3) / L_1 \quad (1)$$

In case of a P-wave with both L_2 and $L_3 \ll L_1$ we get a rectilinearity close to 1 (linear polarisation). The azimuth and incidence angle of the largest polarisation axes are shown in bold. The two thin lines in the rectilinearity window show the ratios of the smaller axes to the larger one.

The knowledge of the P-wave backazimuth allows to **rotate the horizontal co-ordinates N and E** into the direction away from the epicentre, i.e. in the direction of wave propagation and perpendicular to it, respectively. In the new co-ordinate system **RTZ** (radial-transversal-vertical) we get the SH- and SV-waves separately on the transversal and respectively the vertical and radial components. The S-wave arrival can be best picked on the transversal component. Polarisation analysis and determination of the a S-P-travel time difference allows roughly to estimate the epicentre of an event by means of travel-time tables or curves.

When rotating the co-ordinate system in both the horizontal (azimuth) and incidence (P) directions (PTQ-system) than a P-wave is shown only in the P-axis, SH in the T-axis and SV in the Q-axis.

A record with strong Rayleigh wave and small Love wave amplitudes may be used to estimate the direction towards the epicentre (backazimuth). Because a Rayleigh wave always shows retrograde particle motion a check of the rotation pattern by the program gives the backazimuth towards the epicentre. Fig. 6 shows a screen hardcopy of P-wave polarisation computed for an $M_b = 5.5$ rockburst in Germany (see Fig. 2).

Start polarisation analysis by moving the cursor to a position before the P- or Rayleigh wave onset, hit the left mouse button and select the menu item **Polarisation**. The next two mouse clicks define the length of the time window to be moved across the record for polarisation analysis. Of importance is not the initial position of these two markers, but only the distance between them which should correspond to at least one up to several periods of the ground oscillation. The length of the noise section before the onset (fixed with the 1st mouse click; **Pol**) should be equal or larger than the width of the moving window. The last mouse click fixes the **END** of the time window to be analysed. All 4 markers set should fit on the screen (no screen scrolling).

Analyse the polarisation parameters displayed as a function of time. You may select the window position which has the most stable or representative polarisation parameters (e.g. for the window position shown in Fig. 6). These data for this position may then be stored by setting a polarisation marker (press F10 or the left mouse button) and used for the rotation of the co-ordinate system (below).

8.3 Rotation of the co-ordinate system

This tool transforms the right hand co-ordinate system ENZ (East, North, Vertical) into the right hand system RTZ or PTQ. The capital letters stand for:

- R - radial component away from the epicentre into direction of P-wave propagation (ray azimuth = back azimuth $\pm 180^\circ$)
- T - transversal component: horizontal component perpendicular to R
- Z - vertical component (is kept unchanged)
- P - component along the P-wave motion (corresponding to the incidence angle of the ray)
- Q - component perpendicular to P and T.

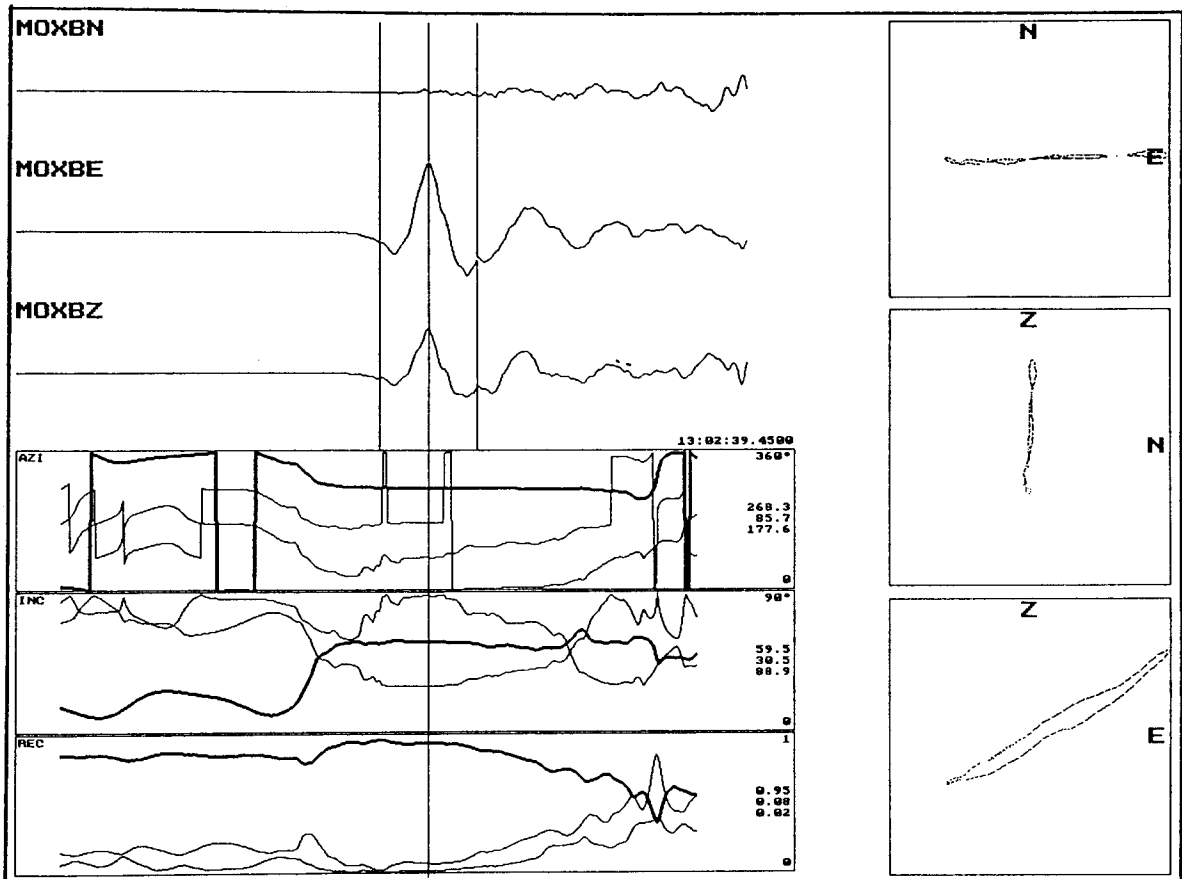


Fig. 6: P-wave polarisation analysis of a 3-component record of the rockburst on March 13, 1989 in Völkershausen, Germany.

Top: N-S, E-W and vertical components of the record.

Bottom: azimuth (AZI), incidence angle (INC) and rectilinearity (REC), estimated for the time window depicted on the record traces and moved across the record.

Right: particle motion plot in the N-E, Z-N and Z-E planes.

Mode ONSET-ON: If there is a polarisation marker for the given 3-component record, the back azimuth and the incidence angle will be used for the transformation of the co-ordinate system. In addition both azimuth and incidence angle can be entered or changed via keyboard input. For horizontal rotation of the co-ordinate system enter an incidence angle of 90° . Two mouse menu markers fixing the length of the record section to be rotated have to be set (Begin and End). The rotated seismograms will be stored in the RECORD SAVE DIRECTORY (see: 4.1 Specification of screen trace parameters).

Mode ONSET-OFF: no polarisation markers are available. This mode may be used for horizontal rotation of the co-ordinate system of each station in order to get individual RTZ-systems of co-ordinates. The required azimuth for each station should be taken from the output of an initial localisation with HYPO71 in the NEZ-system. After rotation the S-wave arrival can be picked more accurately on the transversal (SH) component. A localisation with the updated picks gives in general a better location accuracy.

The rotation of the NEZ system of co-ordinates into a RTZ-system eases the phase recognition of wave phases of teleseismic events too.

8.4 Trigger

Two triggers are implemented in SEIS89:

- **STA/LTA** (short term average/long term average trigger): All traces on screen will be simultaneously triggered. An event will be declared when the STA-LTA ratio exceeds a given threshold.
- **STA/LTA+3C** (combined STA/LTA and 3-component coherence trigger): If there is one 3-component record on screen, it will be triggered. If there are more 3-component records on screen, than that record will be triggered, the cursor is pointing at. It may be any of the 3 components. If no 3-component records are loaded, only the trace the cursor is pointing at will be triggered by a STA/LTA. The trigger criterion will be met if both the coherence and the STA-LTA ratio exceed the respective trigger thresholds.

SEIS89 does not impose any limitation on the length of the record, except hard disk size. In case of quasi continuous records (from some minutes to hours or even days), a trigger should be used to find the events.

8.4.1. Automatic STA/LTA trigger: Call SEIS89 by **SEIS89 nr stalta**

nr is the record number. Filenames have to be specified in SAVEFILE.INI. A trigger list will be compiled during the trigger run and loaded when SEIS89 is started again by SEIS89 nr. ALT F3 displays the trigger list and with the keys Up and Down you can step fort and back from event to event.

The trigger parameters have to be specified in **STALTA3C.INI** (directory UNITS)

- line 1: 1 STA window length in seconds
- 2: 10 LTA window length in seconds
- 3: 4 STA/LTA threshold for N, E and Z
- 4: 3 STA/LTA threshold for Z (3C-trigger)
- 5: 0.6 coherence level for 3C-detection
- 6: 10000 maximum STA for display of STA(t) and LTA(t)
- 7: NO show sta(t)/lta(t) (YES or NO)
- 8: 30 delta-t in seconds: it will be used for automatic triggering.

After declaring an event, the trigger will not be applied to the next delta-t seconds of the record in order to avoid multiple triggering for the same event.

8.4.2. Interactive processing

STRG F8: Start of STA/LTA+3C (trigger parameters will be taken from STALTA3C.INI)

ALT F8: Start of the STA/LTA+3C-trigger with the option to change the trigger parameters interactively. The STA/LTA+3C-trigger includes a separate STA/LTA trigger for each channel. In addition, a 3-component trigger calculates the coherence. The trigger criterion is met, when the coherence exceeds the coherence level specified in STALTA3C.INI and the STA/LTA ratio the threshold for Z.

STRG F6: Start of STA/LTA. All traces displayed on screen will be triggered with the same trigger parameters.

ALT F6: Start of STA/LTA with the option to change trigger parameters interactively.

8.4.3. Graphics option for fixing trigger parameters

Start the trigger in the interactive mode (ALT F6 or ALT F8). Change the parameter "show STA(t)/LTA(t)" to "YES". The STA/LTA-ratio will be displayed for all traces. In addition the coherence will be shown for the 3C-detector. When starting the STA/LTA+3C-trigger without

having loaded a 3-component record, then for the trace, the cursor is pointing at, only the STA(t)/LTA(t) ratio will be displayed.

The graphics option can be used to find the best suitable trigger parameters:

- load the records
- move the cursor to the record start
- increase the trigger threshold to a level which will never be exceeded (e.g. $1e10$)
- change "show STA(t)/LTA(t) to "YES"
- start the trigger by ALT F6 or ALT F8

From the displayed STA/LTA-ratio you should select the best detection threshold. Enter the parameter found in STALTA3C.INI.

The STA/LTA trigger thresholds differ slightly for both trigger types. This is because the code for the respective subroutines are slightly different in order to make the computation as fast as possible.

8.5. Estimation of Coda-Q

Coda waves comprise the tail of a seismogram and usually make up its major part. Coda waves consist of S-waves, backscattered from many randomly distributed heterogeneities in the Earth's crust. The single isotropic scattering model is adopted. It supposes that the coda waves propagate within an unbounded, homogeneous and isotropic medium with randomly distributed scattering sources. The density of scatterers is assumed to be small so that only one encounter with a wave scatterer has to be considered on the wave path from the source to the receiver. The coda waves, arriving at the same time at the station were scattered from heterogeneities located on an ellipsoid expanding with time and having the hypocentre and the

station as foci. The decay of the coda amplitudes for a given record is due to attenuation, increasing travel time for later arriving coda waves and geometrical spreading. Both spreading and travel time effects will be corrected based on the theoretical model adopted. The method allows to compute a frequency dependent coda Q_c by analysing narrow bandpass filtered traces from the available record. The details of the theory were described by Jin and Aki (1986) and Herraiz and Espinosa (1987). In SEIS89 a noise section before the P-wave onset will be treated in the same way as the coda waves. This helps to fix the time range with sufficient signal to noise ratio for estimating Q_c . The noise level will be displayed as light blue line together with the squared coda amplitudes averaged over twice the centre bandpass period as a function of $t-t_s$. t is the travel time of the coda wave and t_s is the travel time of the direct S-wave.

To start calculation of coda-Q move the cursor onto a noise section before the P-arrival. The noise section should have a length of about 5 times the largest period to be analysed. Hit the left mouse button (mode ONSET-ON) and select Coda-Q. You will be requested to mark the P_g and S_g -onset and the end of the coda section to be analysed (left mouse button). The selected frequency range for narrow band filtering will be shown and has to be confirmed. The filtered traces will be displayed. In a next step Q_c will be estimated for each filtered trace. In order to avoid coda distortion by the direct S-wave, the analysis should start only after twice the S-wave travel time which is marked on screen with a white vertical line labelled with " $2t_s$ ". The time interval for analysis has to be selected individually for each filtered channel in dependence on the noise level. In order to fix the begin and the end of the analysis window for estimation of Q_c shift the red vertical mouse line and mark the selection by left mouse button clicks. Take care that the data points of the selected time interval are well above the noise level. They should show a linear decay according to the expected graph $\text{const}-\omega(t-$

$t_s)/(2Q_c)$. Hit the right mouse button to escape from estimation of Q_c for the given filtered trace (e.g. in case of insufficient signal-to-noise-ratio.) The results will be stored in CODA_Q.RES. Fig. 7 shows an example of a least square fit for estimation of coda - Q. The record used for analysis is an aftershock of the 1995 Chile Antofagasta earthquake.

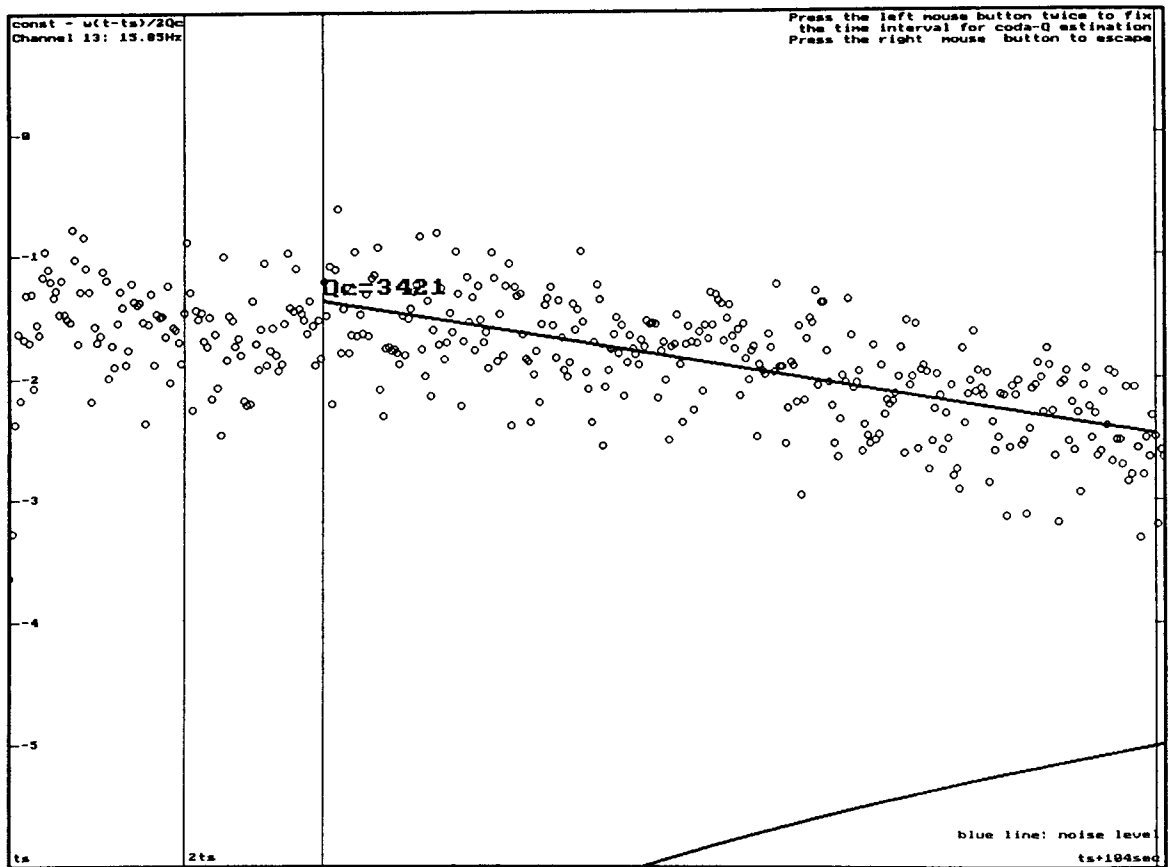


Fig. 7: Estimation of coda-Q: least squares fit of a straight line to corrected, squared and averaged coda amplitudes. Axis of ordinates: normalised coda amplitudes, corrected for wave propagation (logarithmic scale), abscissa: time axis $t-t_s$, t_s : S-wave travel time.

8.6 Estimation of spectral source parameters

This tool allows to calculate spectral source parameters from P- and S-waves of local to regional events for a suit of theoretical shear fault models with circular rupture planes and constant slip direction. In the models used the rupture propagates either from the centre of the circle to its fringe or fault propagation effects are neglected at all (contemporaneous slip on the circular fault plane). The models differ in the source time function, rise time and crack velocity of rupture propagation.

The following requirements have to be met (Brüistle, 1985):

1. Double couple source mechanism;
2. Far field approximation: $r > 5\lambda$ with r : hypocentral distance, λ : wavelength;
3. Teleseismic approximation (assumption of parallel rays): all rays leaving the source towards the station are parallel, i.e. the source size x_{\max} is small compared with the hypocentral distance: $x_{\max} \ll \sqrt{(\lambda r)}$;
4. The source is not a point source: $x_{\max} > 0.1 \lambda$.

Table 2: Parameters of circular source models

Model by	Crack Velocity, V_{cr}	K^P	K^S
Brune (1970)	$0.9 V_s$	3.36	2.34
Savage (1974)	$0.9 V_s$	1.82	0.82
Sato & Hirasawa (1973)	$0.5 V_s$	1.90	1.53
Sato & Hirasawa (1973)	$0.9 V_s$	2.61	1.85
Sato (1978)	$0.5 V_s$	1.95	1.57
Sato (1978)	$0.7 V_s$	2.41	1.81
Sato (1978)	$0.9 V_s$	2.73	1.94
Madariage (1976)	$0.6 V_s$	1.88	1.32
Madariage (1976)	$0.9 V_s$	2.07	1.38

The following formulae will be used for the calculation of source parameters:

$$\text{source radius: } R = K^{P/S} V_s / (2\pi f_c^{P/S}) \quad (2)$$

$$\text{seismic moment: } M_0 = 4\pi \rho U_0 V_{P/S}^3 r / (R^{P/S}(\theta, \varphi) A^{P/S}) \quad (3)$$

$$\text{average slip: } \bar{D} = M_0 / (\pi R^2 V_s^2 \rho) \quad (4)$$

$$\text{stress drop: } \Delta\sigma = 7/16 \cdot M_0 / R^3 \quad (5)$$

- with
- ρ - density in the source area
 - U_0 - low frequency spectral level
 - $V_{P/S}$ - velocity of P or S-wave, respectively
 - r - hypocentral distance
 - $R^{P/S}(\theta, \varphi)$ - radiation pattern for P- or S-waves, respectively (usually the averaged radiation pattern of 0.64 is used)
 - A - surface amplification (2 for vertical incidence)
 - $f_c^{P/S}$ - corner frequency of the P- or S-wave, respectively.

In SEIS89 the inverse of the product of radiation amplitude and surface amplification $(R(\theta, \varphi) \cdot A)^{-1}$ is used as input parameter for the calculation of spectral parameters.

The radius R of the circular rupture plane has to be computed from expression (2). $K^{P/S}$ is a coefficient relating the corner frequency to the source radius. It differs for P- and S-waves and was derived from theoretical calculations of rupture propagation for the models shown in Table 2. Spectral source parameters may be computed with SEIS89 either for all 9 circular models indicated or for one selected model (see SPECTRUM.INI in the directory UNITS).

A correcting factor of 0.8 accounting for the inverse of the product of averaged radiation pattern (0.64) and surface amplification (2 for vertical incidence) will be taken into account. The incidence angle and therefore the surface amplification can be calculated more accurately from the location of the hypocentre and the station. If a fault plane solution is available for the given event, the correct radiation amplitude should be used instead of 0.64.

The input parameters for calculations are stored in SPECTRUM.INI (directory UNITS):

- P- and S-wave velocities: V_P , V_S (approximate average velocities for Earth crust, depending on source depth)

- average crustal attenuation parameters (Quality factors für P- and S-waves):
 $Q_P = Q_{0P} f^{n_P}$, $Q_S = Q_{0S} f^{n_S}$
- density ρ in the source area at hypocenter depth (in $\text{g}\cdot\text{cm}^{-3}$)
- $(R^{P/S}(\theta, \varphi) \cdot A)^{-1}$

The attenuation parameter Q describes the loss of elastic energy caused by internal friction. Q depends in a simple way on the ratio of the energy, dissipated per oscillation to the total energy stored. Expression (6) gives the definition of Q . It holds for weak attenuation, i.e. for high Q values ($Q \gg 1$).

$$\Delta E / E = (\exp(-\omega (t + T) / Q) - \exp(-\omega t / Q)) / \exp(-\omega t / Q) \approx 2\pi / Q \quad (6)$$

E is the initial energy of the system. $T = 2\pi/\omega$ is the period of oscillations. The energy of $\Delta E = E \cdot 2\pi/Q$ is dissipated per cycle. The respective amplitude decrease per cycle is $\exp(-\pi/Q)$. Q is therefore the number of oscillations to reduce the amplitude to $A_0 \cdot \exp(-\pi)$, with A_0 as initial amplitude.

The parameters necessary for the calculation of spectral source parameters have to be specified for the region investigated. A constant P- and S-wave velocity is assumed. The average crustal velocities can be derived from existing layered models by averaging the layer velocities. Attenuation parameters can be derived from Coda- Q studies (see 8.5. Estimation of Coda- Q). The Q_C -values calculated for many events and for a suit of frequency bands gives in double logarithmic scales a linear relation:

$$\log Q_C = \log Q_0 + n \log f \quad \text{that is identical to} \quad Q_C = Q_0 f^n . \quad (7)$$

Both Q_S and Q_C are computed from S-waves, Q_C from scattered and Q_S from direct S-waves. Therefore, it may be assumed, that Q_C agrees with Q_S and may be used in order to correct the S-wave displacement spectrum for attenuation. Q_P may be derived as first approximation from Q_S under the assumption, that the dissipation of compressional wave energy may be neglected compared with the dissipation of shear-wave energy. Under these assumptions one gets for an adopted V_P/V_S -ratio of 1.73

$$Q_P = 2.25 Q_S . \quad (8)$$

If there are Q_P and Q_S -values available from specific Q -studies of P- and S-waves, these data should be used of course.

Steps for calculation of spectral source parameters:

1. Calculation of noise spectra from a noise section before the P-onset: In order to check the signal to noise ratio, the spectra are treated in the same way as the P- and S-wave records. The length of the noise record should be comparable to the length of the P- or S-trace used for spectral calculations. To start noise analysis move the mouse to the begin of the noise section to be processed, hit the left mouse button (ONSET-ON) and select the mouse menu item P-noise spectrum or S-noise spectrum, respectively. The next mouse click (left button) fixes the end of the noise section. The processing parameters, stored in SPEC-TRUM.INI will be displayed (if available). Parameters can be entered or updated via keyboard. If the epicentral distance is stored in the file header, it will be used by the program. Otherwise one has to key it in. The computed spectra can be plotted.

2. Calculation of P- or S-wave spectrum: Move the cursor onto the P- or S-onset and hit the left mouse button. Select the item 'P-moment & f_c ' or 'S-moment & f_c ', respectively. The spectrum is computed with the Fast Fourier Transform and corrected for the station response curve, attenuation, wave propagation (r^{-1} with r as hypocentral distance) and surface amplification and radiation pattern $(R^{P/S}(\theta, \varphi) \cdot A)^{-1}$. The signal spectrum will be displayed together with the noise spectrum, supposed it was computed before. Check, whether there is a sufficiently large signal to noise ratio for estimating source parameters. A typical P- or S-wave spectrum displays a low frequency plateau and a high frequency decay of f^{-2} to f^{-3} . The spectra are displayed in double logarithmic scales. In this representation the high frequency slope f^{-n} is displayed as straight line with a decay of $-n$. The abscissa of the intersection point of both lines (plateau and decay) is the so called corner frequency (see above), which can be used to calculate the source radius. To make the estimation of the low frequency level and the corner frequency rather objective, an automatic procedure was implemented to estimate the low frequency spectral amplitude, the corner frequency and the order of the high frequency decay. Four mouse clicks (left button) have to be made. The first fixes the lower frequency bound for estimating the low frequency amplitude. The next two clicks mark the lower and upper frequency limits for automatic estimation of the corner frequency. The last click fixes the upper frequency bound of the window used for estimation of the high frequency decay. The program fixes the optimum low frequency plateau level and the optimum corner frequency by fitting straight lines to the maximums of the spectrum plateau and the high frequency decay for a suit of corner frequencies. An example of corrected P-wave-and-noise-spectra is shown in Fig. 8. The low-frequency plateau and the high frequency decay are indicated too. The fit can also be corrected or made manually.

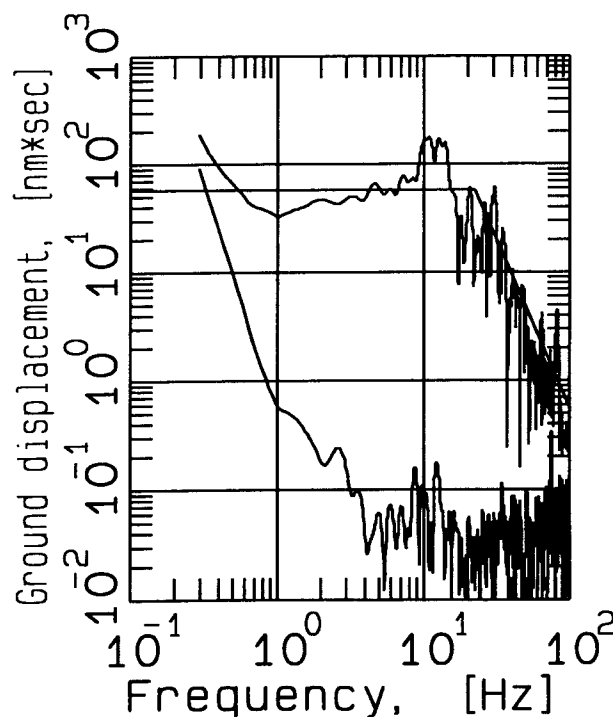


Fig. 8: Corrected P-wave displacement spectrum of an aftershock of the 1993 Killari earthquake and related noise spectrum. The straight-line fits of the low-frequency amplitude level and the high-frequency decay are shown. The peak at 10 Hz is due to surface amplification, caused by a thin low velocity layer.

3. The program calculates from the input parameters, from the low frequency plateau level and the corner frequency the seismic moment M_0 (expression 3), the source radius R (expression 2), the average source slip D (expression 4) and the stress drop (expression 5).
4. The corner frequency and the seismic moment are recorded in the marker list. All results for the different models analysed are stored in the file SPECTRUM.RES (INFO-DIRECTORY). All parameters are given in SI-units (kg, m, sec). The geometry of rupture plane of an earthquake and the rupture propagation (velocity, direction, rise time) is a priori unknown. The range of parameters, estimated for the above given suit of models gives an idea about the accuracy of the estimated source parameters. In general, results for a given model, derived from network recordings of an event may differ by up to a factor of 4. Always the same model should be used for the calculation of spectral source parameters in a given tectonic region. The stress drop is the most uncertain parameter estimated, because the source radius R , derived from eq. (2) enters in the denominator of the expression for calculation of stress drop eq. (5) as R^3 . For an radius error of $\pm\Delta R$ we get an error in R^3 of $\pm 3R^2 \Delta R + 3R \Delta R^2 \pm \Delta R^3$.
5. There may occur problems during calculation of source parameters. The calculation of spectral parameters presumes the so-called far-field approximation: The hypocentral distance r must be large compared with the wave length λ : $r > 5 \lambda$. In this case the near-field terms r^{-2} , r^{-3} and r^{-4} may be neglected. Otherwise, the spectral amplitudes increase with decreasing frequency and prevent to estimate the seismic moment from the low-frequency spectral plateau. Spectra of small events may show an insufficient signal-to-noise-ratio. Additional noise sources close to the station may truncate the spectrum.

8.7 IASPEI-91 travel times: a teaching tool for the analysis of teleseismic records

This tool allows to display all arrivals of seismic waves included in the **IASPEI-91** travel time tables for a teleseismic event with known hypocentre, recorded at a given station. If the hypocentre is unknown, the epicentral distance and the source depth may be estimated by picking the strongest phases (e.g. P and S) and related depth phases, if recognisable. Based on these readings, the program searches for the optimum epicentre distance and source depth. The residuals will be displayed for a grid of epicentral distance Δ and source depth h . The optimum parameters (Δ and h) and the minimum residual will be displayed. For crustal events the computation may be limited to the estimation of only the epicentral distance. With polarisation analysis (see paragraph 8.2) the back azimuth may be estimated in order to locate the epi- or hypocentre.

The accuracy of estimations was limited to 1 degree in epicentral distance and 35 km in source depth in order to save computation time. The travel times are stored on PC in tabulated form. Therefore, this tool may be used rather for learning how to recognise different teleseismic wave phases than for a very accurate estimation of epicentral distance and source depth. The dataset supplied includes 3-component short-period, long-period and broadband records of an earthquake in northern India, recorded at the station MOX in the south-east of Germany. Load this event with the command **SEIS89 IND**. Hit **ALT 2** to load the long period records and switch to processing mode **ONSET-ON (F9)**. The seismogram header includes the epicentre location (zero source depth). Execute the following steps:

8.7.1 Phase picking for an event with given epicentre or hypocentre

Pick the P- and S-onsets on the trace with the largest amplitude: P on the Z-component and S on the horizontal components (N-S or E-W). Move the cursor away from any picked arrival. Hit **O** to display the arrivals. There appears first a window with origin time and epicentre lo-

cation (source depth = 0). Confirm it with the left mouse button click. There will appear another window, showing the names of phases with arrival times within the time range fixed by the length of the record. Select the phases to be displayed by left mouse button clicks. Either individual phases (e.g. PP) or a group of phases (eg. P*, S*, pP*) may be selected. The star indicates, that the phase names start with P, S or pP, respectively). We recommend to select the **basic** phases. These are usually the strongest phases in the record. In addition to the phases given in the IASPEI91 tables we included the arrival times of the Love (LQ) and Rayleigh (LR) waves and the expected time of the maximum Rayleigh wave amplitude (MR). The computed phases will be displayed in red. Compare them with the white user picked phases and pick additional phases with clear onsets. Try to find depth phases (e.g. pP, sP, sS) necessary for depth estimation. Use for input of longer phase names the first line of the mouse menu: **keyboard input**. The used phase names must agree with the generally accepted ones as given in the IASPEI-91 travel-time tables. Try to get a good fit of picked arrival times to computed ones. **ALT O** displays a table with the IASPEI-91 arrival times and **STRG O** deletes the IASPEI-91 onsets.

8.7.2 Estimation of epicentre or hypocentre co-ordinates

Pick clearly visible phases and try to include depth phases as well. Move the cursor onto one of the picked phases, preferably onto the P-onset and hit **O**. A window for input of epicentral distance and hypocentral depth will be displayed. Put a question mark into the first line for epicentre distance and enter the assumed source depth into the second window line in order to compute the epicentral distance for the given source depth. The optimum epicentral distance can be read from the travel-time residual plot with an accuracy of one degree. To display the IASPEI-91 arrival times for the given location select the phases of interest and exit the phase window. The arrival times will be displayed relative to the onset the cursor was moved onto.

An input of question marks in both the 1st and 2nd lines of the input window results in calculation of optimum epicentral distance and optimum source depth. A residual plot for a grid with a spacing of one degree in epicentral distance and 35 km in source depth will be displayed. The theoretical arrival times for the given source location may be displayed as described above.

9. TRACE UTILITIES (F8)

These are utilities for trace editing of the records displayed on screen.

1. Removing DC: A constant amplitude shift (DC-offset) is removed from the record. This is important for automatic estimations of amplitude. If there is an offset, amplitude estimations may fail.
2. Change sign: The trace amplitudes will be multiplied by -1 . The traces can be selected individually.
3. Delete traces: The trace amplitudes will be set to zero.

10. DESPIKER

Spikes in records can be removed with the despiker implemented. Both linear and spike interpolation is implemented. The trace, the cursor is pointing at will be despiked. Hit **D** to start the despiker. A window with the despiker parameters will appear. Adapt the parameters to your records. When specifying "Input of new parameters", the minimum amplitude and the

maximum width of spikes to be corrected can be selected with a mouse resizable rectangle. The detected spikes are displayed in blue. Check the selection and add manually additional spikes to be removed (left mouse button) or delete wrongly detected spikes (right mouse button). Check carefully the result before accepting the changes and storing to the disk. Keep for security a copy of the original record.

11. PRINTING AND PLOTTING

- To print a screen in text mode hit the key **PRINT**.
- To make a hardcopy of the screen in graphics mode hit **STRG PRINT**.
- The graphical output of some tools can be plotted, supposed the printer understands the graphical language. This is the case for most HP-Laserjets.

11.1. Plotting and printing seismograms

All traces to be plotted or printed together have to be loaded (maximum: 10 traces). Mark the begin and the end of the selected record section to be plotted or printed by two time markers in the mode ONSET-OFF or by the markers BEGIN and END in the mode ONSET-ON and hit **P**. The records will appear on screen as they will be plotted or printed afterwards. Hit any key, except **ESC**, to display the print menu. Instead of direct plotting or printing the plot- or print-file may be stored to disk and printed later. This option is useful for PC's not connected to a printer. When selecting from the menu the items **PLOTTER** or **PLOTFILE OUTPUT**, one has to specify the time resolution for the plot from the menu displayed. **AUTO-SCALING** results in a maximum size plot. The plot- and print files are stored in the directory **PLOTTER** and **PRINTER**, respectively.

11.2. Plotting spectra (ONSET-OFF)

The computed signal to noise-spectra, power spectra and displacement spectra may be plotted, printed and also stored as plot- or print file to disk.

11.3 Plotting displacement spectra for estimation of source parameters

First the spectrum of a noise section before the onset has to be computed and plotted. Deny the question for ejecting the paper from the printer. As next step compute the signal spectrum and fit the plateau and the high frequency decay. The signal spectrum and the straight lines, fitting the spectrum will be added to the noise plot. More spectra may be plotted on the same paper sheet when carefully selecting the size of the individual graphs and their position in order to prevent overwriting.

12. STORING RECORDS IN GSE-FORMAT

All records in SEIS89 format may be stored on hard disk in GSE-format. This format was elaborated by the Group of Seismic Experts (GSE) for data exchange in the framework of the Verification of a Nuclear Test Ban Treaty and is now widely used. We used the FAP file format: The station response curve is given as a table of frequency, amplitude and phase angle. The data may be stored as Integer data, 1st or 2nd differences of integer or as compressed 2nd differences of Integer data.

Fix the begin and the end of the record section to be stored by setting two time markers (ONSET-OFF) or 2 markers BEGIN and END (ONSET-ON). Hit **ALT G** and select the compression format. The GSE-files will be stored in the directory GSE_TEXT (subdirectory of SEIS90).

REFERENCES

- Brune, J.N.: Tectonic stress and the spectra of seismic shear waves from earthquakes. *Journ. Geophys. Res.* Vol. 75, No. 26, p. 4997-5009, 1970.
- Brüstle, W.: Der Bruchverlauf im Erdbebenherd – Untersuchung ausgewählter Erdbeben mit beobachteten und synthetischen Seismogrammen. *Berichte des Instituts für Meteorologie und Geophysik der Universität Frankfurt/Main*, Nr. 63, Mai 1985, Eigenverlag des Instituts.
- Herraiz, M., A.F. Espinoza: Coda waves: a review. *PAGEOPH*, 125 (1987) 4, pp. 499-577.
- Jin, A. and K. Aki: Temporal change in coda Q before the Tangshan earthquake of 1976 and the Haicheng earthquake of 1975. *Journ. Geophys. Res.*, 91(1986) B1, pp. 665-674.
- Kennett, B.L.N. (Editor): *IASPEI 1991 Seismological tables*. Research School of Earth Sciences, Australian National University, 1991.
- Lee, W.H.K. (Editor): *Toolbox for seismic data acquisition, processing and analysis*. IASPEI Software Volume 1, published by International Association of Seismology and Physics of the Earth Interior in collaboration with Seismological Society of America, 1989.
- Lee, W.H.K. and J.C. Lahr: *HYPO71: A computer program for determining hypocentre, magnitude, and first motion pattern of local earthquakes*. U.S. Geol. Surv. Open-File Report, 100 pp., 1972
- Lee, W.H.K. and J.C. Lahr: *HYPO71 (REVISED): A computer program for determining hypocentre, magnitude, and first motion pattern of local earthquakes*. U.S. Geol. Surv. Open-File Report, 100 pp., 1972
- Lee, W.H.K. and C.M. Valdés: *HYPO71PC: A personal computer version of the HYPO71 earthquake location program*, U.S. Geol. Surv. Open-File Report 85-749, 43 pp.
- Savage, J.C.: Relation between P- and S-wave corner frequencies in the seismic spectrum. *BSSA* 64, 6, 1621-1627, 1974.
- Sato, T. and T. Hirasawa: Body wave spectra from propagating shear crack. *Journal of Physics of the Earth*, 21, 4, pp. 415-431, 1973.
- Sato, T.: A note on body wave propagation from expanding tension crack. *Tohoku Geophys. Journal* 25, 1, pp. 1-10, 1978.
- Madariaga, R.I.: Dynamics of an expanding shear fault. *BSSA*, 66, 3, pp. 639-666, 1976.

Appendix 1: STRUCTURE OF SEISMOGRAM FILES

Each seismogram trace has to be stored in a separate file. There is a strict rule for creating file names filenames:

character 1-3: station name (e.g. MOX), the same as characters 1-3 of the station name in the header

character 4: record type, any letter e.g. V for velocity, D for displacement, S for short-, L for long-period, B for broadband (the same as character 1 of record type in the header)

character 5: component, (the same as character 1 of header component, e.g. Z = vertical, (UP +, Down -), N = North (+), E = East (+), R = radial (direction away from the epicentre), T – transversal (SH-type motion), P = up-dip direction of the arriving P- wave, Q: perpendicular to P and T.

character 6-8: free, or any information

Filename extension: any number 0-999 (seismogram number) or any 3 characters. All files with the same file name extension belong to the same event (e.g. network recordings, or recordings of a 3-component station).

Example: MOXSZ.1 (station MOX, short period record, vertical component). The filename (without filename extension) will be displayed in SEIS89 on screen and helps in identifying the seismogram traces.

A seismogram file consists of a standard header (512 bytes) followed by the time series stored in INTEGER*2 format (least significant byte, most significant byte).

The program HEAD helps to change/correct the file header or to create the file structure necessary for SEIS89. You will find the header structure in the TURBO-PASCAL source code file GLOBAL.PAS (see TYPE head). If you are going to write your own program for adapting the files of your recording system to the format required in SEIS89 use the subroutine CONVERT_HEADER (file HEADCON.PAS) to convert the header into the format described below. SEIS89 uses a special conversion in order to store REAL data in two INTEGER*2 data to make the seismogram files independent from the computer type used.

Header structure

Abbreviations: char = character, character data must be left justified (!!!)

int=INTEGER*2 (2-byte integer) int4=INTEGER*4, (4-byte integer),

real1,real2: real value, decomposed into two 2byte-integer values I1 and I2:

real1=I1+I2/10000; real2:=I1*10¹²

byte No. type meaning

	1	4 char	network code (e.g. CIPE)
#	5	4 char	station code (e.g. MOX)
#	9	4 real1	geographical latitude [degree] (North +, South -)
#	13	4 real1	geographical longitude [degree] (East +, West -)
	17	4 real1	height above sea level [meters]
#	21	4 char	component (e.g. Z)
#	25	4 real1	sampling rate (samples per second)
-----magnification table: 20 * (frequency, magnification, phase shift)			
#	29	4 real1	frequency(1) [Hz]
#	33	4 real2	magnification(1) [!!! nanometers per count !!!]

```

# 37    4 real1  phase shift(1)  [°]
# 41    4 real1  frequency(2)   [Hz]
. . . . .
# 257   4 real1  frequency(20)
# 261   4 real2  magnification(20)
# 265   4 real1  phase shift(20)
----- start time of record (universal time)
# 269   2 int    year
# 271   2 int    month
# 273   2 int    day of month
# 275   2 int    day of weak
# 277   2 int    hour
# 279   2 int    minute
# 281   2 int    difference local time - UT in hours
# 283   4 real1  seconds
----- event information
# 287   4 real1  geographical latitude
# 291   4 real1  geographical longitude
# 295   2 int    hour of origin time
# 297   2 int    minute of origin time
# 299   4 real1  second of origin time
# 303   4 real1  hypocentre depth [km]
# 307   4 real1  magnitude
# 311   2 char   magnitude identifier (e.g. Mb, Ml)
# 313   28 char  region name (e.g. Northern Italy)
# 341   80 char  any remarks
# 421   4 real1  distance epicentre-station [km] (If zero SEIS89 will compute
it for the given source location)
----- recording system
# 425   4 char   record type (any letter)
# 429   4 char   seismometer code (seismometer type)
# 433   20 byte  free for further developments
----- information about stored time series
# 453   4 int4   number of samples of the time series
# 457   2 int    zero level before removing DC (if any)
# 459   2 int    info-byte, 3 for co-ordinates in degrees, 7 for co-ordinates
in meter (for very small networks, e. g. network in a mine)
# 461   52 bytes preserved for further developments (data compression algorithms)

```

The first 3 characters of the station code must coincide with the first 3 characters of the filename. The first character of the record type must coincide with character 4 of the filename and the first character of the component must coincide with character 5 of the filename. If the record type has changed during work with SEIS89 (e.g. by filtering) its first 3 characters will be shifted one character to the right and a new letter, characterising the new record is stored in character 1 of the character field of the record type. So the character field "record type" shows the history of manipulations with the original time series.

To run SEIS89 only a minimum of the header data (marked with #) has to be specified. Unused numerical fields must be filled with byte zeros, character fields with blanks (!!!).

Event information is useful e.g. for the compilation of an event file library. The magnification table will be interpolated in SEIS89 in double logarithmic scales and the phase shift curve in log-linear scales. The 20 samples should be more or less equally spaced in the logarithmic frequency scale with increasing frequency. No frequency or magnification value must be zero. If no phase shift curve is available, use zeros. Note that the magnification is given in nanometers per digital count.

Appendix 2: COMMANDS OF SEIS89 AND GETTING HELP

Move the cursor into a corner of the screen (marked in yellow). A window with help text for the topics shown in the small window at the top of the screen will be displayed. To get additional help move the cursor in the help window onto a line which ends with ... and press the left mouse button. Exit from HELP: hit ESC or move the cursor out of the help window.

There are two modes of work with SEIS89:

- 1) **ONSETON** (hit F9, **ONSETON** appears on screen bottom): All Markers set with the mouse (e.g. amplitude, period, corner frequency, ...) will get a name, and parameters will be stored together with the marker position (trace and time).
Hit CTRL F1 to see the estimated parameters.
- 2) **ONSETOFF** (F9): simple time markers without names, no computation of seismic parameters. After starting, SEIS89 is in the mode **ONSETOFF**.

F-KEYS	CTRL F-KEYS	ALT F-KEYS
F2 : Trace header	CTRL F1: Marker list	ALT F1: Clear marker list
F3 : Screen parameters	CTRL F2: Save parameters	ALT F2: Save trace
F4 : Load traces	CTRL F3: Show loaded files	ALT F3: Show onset list
F5 : Butterworth filter	CTRL F4: Reload traces	ALT F4: Reload traces
F6 : new co-ordinate system ENZ-->TRZ/TPQ	CTRL F5: Standard filter 1	ALT F5: Standard filter 2
F7 : Spectrum (ONSETOFF)	CTRL F6: STA/LTA/3C- trigger, editing of trigger parameters	ALT F6: STA/LTA/3C- trigger, editing of trigger parameters
F8 : Trace utilities	CTRL F7: Power spectrum (ONSETOFF)	ALT F7: Spectral S/N-ratio (ONSETOFF)
F9 : ONSETON / ONSETOFF	CTRL F8: STA/LTA-trigger	ALT F8: STA/LTA-trigger
F10: Quit SEIS89		

MOUSE: left button (mode **ONSETOFF**): time marker
left button (mode **ONSETON**): marker with name, selected from mouse menu (e.g. name of a seismic onset: Pg, Sg, ... or computation of parameters: amplitude, ...)
right mouse button :
- display traces starting from the current cursor position-
- cursor at left screen side: display preceding seismogram section
- cursor at right screen side: display next seismogram section

KEYS

ESC	screen refreshing, return to all traces mode
1 2 3 4 5 6 7 8 9 0	SINGLE TRACE MODE : show a single trace (1-10, 1 is the uppermost trace)
ALT i (i=1,2,3,4)	Load standard background file set No. i
←	show the preceding trace section
→	show the next trace section
Home(Pos1)	show the begin of the traces
End	show the end of the traces
← → (tabulator)	input of time to show a desired seismogram section +t or -t for relative shift, t for absolute time, format of t: h min sec e.g. 3 216.1 or 30216.1, leading zeros may be omitted
A Up A Down	increase/decrease of the screen amplitudes of all traces by a factor of 2
A PgUp A PgDn	increase/decrease screen amplitudes by a factor of 5
A ESC	initial scaling of screen amplitudes (see screen parameters)
F Dn F Up F i	1 pixel = i*sampling interval i=1..5: Dn : i=i+1; Up : i=i-1
F PgUp F PgDn	PgUp: i=1; PgDn : i=5
F ESC	1 pixel = sampling interval

CTRL S	switch SOUND ON / OFF
CTRL T	time origin switch absolute time / time relative to the last marker set, the cursor must be accurately on this marker
CTRL H	hide / show a small window at the top of the screen with hints for getting help
Q	waveform cursor (maximum length: 100 samples)
ALT Q	waveform cursor (variable length, max 200 samples)
CTRL Q	change cursor: five different cursors are available
H	draw a horizontal line in the middle of the screen (for vertical shift use the mouse) -for keeping the line hit ENTER or the left mouse button -for deleting the line hit ESC or the right mouse button
V	draw a vertical line in the middle of the screen (for horizontal shift use the mouse) -for keeping the line hit ENTER or the left mouse button -for deleting the line hit ESC or the right mouse button
R	resampling mode: display only each i.th sample to get an overview over a longer trace. Use the keyboard for input of i. There is no processing allowed in resampling mode. ESC: exit resampling mode
PRINT	print a textscreen
CTRL PRINT	print the traces or spectra displayed on screen (hardcopy).
P	print or plot traces
D	despike seismograms
S	slowness computation: mark network onsets of the same phase, move the cur- sor on one of these markers and hit S
O	display of onsets of teleseismic waves (IASPEI91-model) cursor on a marked onset: input of epicentre distance and source depth, other- wise input of hypocentre data.
CTRL O	delete red IASPEI onset markers
ALT O	show IASPEI arrival times (after O)
T	localisation of teleseismic events with local to regional networks
L	localisation of local events using travel-time curves or HYPO71
CTRL L	switch between SEIS89-mouse menu and HYPO71-menu
ALT G	save traces in GSE-format
ALT X	QUIT SEIS89
Up	show next triggered event
Dn	show previous triggered event.

Appendix 3: HINTS FOR CREATING MAPS FOR DISPLAYING HYPO71 LOCALISATION RESULTS IN SEIS89

The filename of the map file has to be specified in HYPO71PC.INI (directory X:\SEIS90\UNITS). The map file has to be stored in the directory X:\SEIS90\MAPS (X: is the disk where SEIS98 was installed.)

TURBO-PASCAL colour code:

0=black, 1=blue, 2=green, 3=cyan 4=red, 5=magenta,
6=brown, 7=lightgray, 8=darkgray, 9=lightblue, 10=lightgreen, 11=lightcyan,
12=lightred, 13=lightmagenta, 14=yellow, 15=white

File structure:

Line 1: lo1 lo2 dlo	Line 2: la1 la2 dla	Line 3: fc bc
lo1 = minimum longitude	la1 = minimum latitude	fc = frame colour
lo2 = maximum longitude	la2 = maximum latitude	bc = background colour
dlo = longitude scale unit	dla = latitude scale unit	

Next lines: graphic objects

Objects are separated by one line: 1111 1111

(before the first object, between objects and after the last object)

1. line of each object: c th gt te

c = colour code [0-15],
th = line thickness [th = 1 or 3],
gt = graph type [line = 1, rectangle = 2, circle = 3, star = 4]
te = text line describing this object [No = 0, Yes = 1]

if gt=3 or gt=4 then next line: os

os = object size in pixel (e.g. radius of circle)

if te = 1 then next line: tx ty ts1 ts2 lo la text

lo, la: position of the text (longitude, latitude)

tx, ty: tx and ty describe, how the text is justified relative to lo and la:

tx=0,1,2 (lefttext, centertext, righttext)

ty=0,1,2 (bottomtext, centertext, toptext)

ts1 : textstyle (0,1,2,3)

ts2 : textsize (1,2,3,4,...)

text : text to be plotted on the map

(check the different parameters by testing)

next lines: longitude latitude

for gt = 1 (display of lines) any number of longitude - latitude pairs

Check the parameters by comparing the map displayed when locating Killari aftershocks (Directory X:\SEIS90\NET*.334) with the map file india.txt.

All parameters are integer data, except latitudes and longitudes (float). For displaying localisation results the minimum number of lines in the map files is 3 (minimum/maximum longitude and latitude, scale unit and frame- and background colours).

Appendix 4: DIRECTORY STRUCTURE

(X: is the hard disk where you have installed SEIS89, e.g. C:)

All directories given below are subdirectories of X:\SEIS90\

DRIVERS	graphics drivers and fonts
GSE_TEXT	directory for GSE-files, written by SEIS89 (by ALT G)
HYPO71	directory for HYPO71-onset files and localisation results The directory name has to be entered in line 1 of HYPO71PC.INI (directory UNITS)
MAPS	map files for displaying localisation results
MOXBB	broadband seismogram test files of station MOXA
MOXLP	long-period files
MOXSP	short-period files
NET	network files
NEW	record save directory: directory for storing files created by SEIS89 (e.g. filtered traces or rotated traces)
PLOTTER	directory for plot files (to be plotted after SEIS89 session)
PRINTER	directory for print files (to be printed after SEIS89 session)
README	description (word files)
SEISINFO	directory for storing parameter files (onset data, parameter output of subroutines, e.g. spectral parameters)
SOURCES	source code of SEIS89 (for BORLAND 6.0 compiler)
TEMP	directory for temporary files
UNITS	EXE-, initialisation- and help files
RESPONSE	directory for storing response parameters (frequency- amplitude-phase or poles and zeros for converting GSE-files)
EARTH_M	IASPEI91 travel times

The installation procedure will create this directory structure. The records to be processed may be loaded from any directory. Parameters estimated during processing may be stored in any existing directory. This directory has to be specified in the "SCREEN PARAMETERS and DIRECTORIES" window (F3). The same applies to processed records (filtering, component rotation, ...). The corresponding directory names for the standard installation are written in bold face.

Appendix 5: HIGH RESOLUTION GRAPHICS

The standard graphics resolution for a DOS-PC is 640 x 480 pixels. There are graphics drivers supplied for some high resolution graphics cards. The distance of record samples on screen is just a pixel. Therefore, high resolution graphics allows to display longer time series on screen. There are TURBO-PASCAL drivers supplied for DOS-PC's only. They can't be used on a WINDOWS PC. SEIS89 shows a good performance on DOS-PC's. The code was optimised to make the processing fast. Check your DOS-PC what type of graphics card is installed and check whether a driver is available (directory DRIVERS). Run the SEIS89 configuration program SEIS89 INSTALL to select and install the driver.

Appendix 6: SEIS89: TURBO-PASCAL 6.0 RUNTIME ERRORS

002	File not found	154	CRC error in data
003	Path not found	155	Bad drive request structure length
004	Too many open files	156	Disk seek error
005	File Access denied	157	Unknown media type
006	Invalid file handle	158	Sector not found
012	Invalid file access mode	159	Printer out of paper
015	Invalid drive number	160	Device write fault
016	Cannot remove current directory	161	Device read fault
017	Cannot rename across drives	162	Hardware failure
100	Disk read error	200	Division by zero
101	Disk write error	201	Range check error
102	File not assigned	202	Stack overflow error
103	File not open	203	Heap overflow error
104	File not open for input	204	Invalid pointer operation
105	File not open for output	205	Floating point overflow
106	Invalid numeric format	206	Floating point underflow
150	Disk is write protected	207	Invalid floating point operation
151	Unknown Unit	208	Overlay manager not installed
152	Drive not ready	210	Object not initialised
153	Unknown command	211	Too many nested scopes

INTRODUCTION TO NATURAL DISASTERS AND DISASTER MITIGATION

Peter Bormann

GeoForschungsZentrum Potsdam, Department of Solid Earth Physics and Disaster Research,
Telegrafenberg E428, D - 14473 Potsdam; E-mail: course@gfz-potsdam.de

1. DEFINITION OF TERMS

Disaster aid organisations speak frequently of a **disaster** as soon as an event kills more than 10 people or injures more than 100. But in a wider sense an event becomes a disaster only if it seriously disrupts the functioning of an affected community due to widespread human, material or environmental losses that exceed the community's capability to cope without external relief.

If the latter definition holds then events such as the San Francisco earthquake in 1989 or the winter storms in Central Europe in 1990 could not be considered as real disasters although the damage ranked in the order of 6 and 15 billions US\$, respectively. On the other hand already smaller damages can be terrible disasters to many developing countries because they strip these people of their already meager resources, often disrupt their economies and destroy their limited potential for reconstruction. So, the 1972 Managua earthquake, which killed about 5000 people and left 300.000 homeless, caused estimated economic losses of "only" about 1.3 billion US\$. But this corresponded to roughly 1 year's GNP at the time and Nicaragua was unable to rebuild the centre of its capital till now.

One differentiates between **sudden disasters** and **creeping disasters**. Sudden events hit man unexpectedly or more or less prepared in an instant of seconds or minutes such as earthquakes and avalanches, during hours or days such as storms and storm surges and days or weeks at the most such as violent volcanic eruptions or floods. These sudden events are rare. There may be years, decades, centuries or even millennia before another strong event of the same kind and magnitude strikes the same area or locality again. Contrary to this, creeping disasters, such as desertification, soil erosion and salinization, drought, famine and epidemics develop slowly over months, years or even decades and may last comparably long. Although man has a much larger lead-time to prepare for them and often also possibilities to avoid them at all they have caused most of the disaster victims during this century. More than 8 million, probably more than 10 million people died since 1900 because of drought and famine as compared to about 4 million people killed by sudden disasters of natural origin.

Man-made disasters are directly related to human activities, sometimes deliberate, sometimes unwanted in their detrimental effects, such as wars, explosions, mining collapses, traffic accidents, failure of major technical systems, air, soil and water pollution, uncontrolled deforestation, overgrazing or improper irrigation resulting in soil erosion, desertification etc.

Natural disasters are related to natural phenomena and processes such as earthquakes, tsunamis, avalanches, rock falls, land slides, floods, storms, volcanic eruptions, desert locust infestations etc. Often they give rise to **chains of disasters** with consequences which may go far beyond that of the primary cause of disaster. Thus, earthquakes may trigger rock falls, the outbreak of fire, the generation of tsunamis with related flooding, pollution of potable water

and epidemics. The 1970 Peru off-shore earthquake ($M = 7.8$), e.g. generated a tsunami which killed many people and caused heavy damages in the coastal area. It also triggered a rock and mud avalanche in the Andes about 100 km inland at an epicentral distance of some 130 km which swept away the towns of Yungay and Ranrahirca in an instant, burying another 25.000 to 30.000 people. This debris avalanche also caused the damming of the Rio Santa. When this dam broke a few days later many people were drawn downstream and the flush of water and debris devastated villages and crops in the flood plains along the river course over a distance of about 160 km down to the Pacific coast. Only about half of the 70.000 victims of this event lost their life's due to the primary cause, namely the collapse of their mostly adobe houses under the strong Earth's shaking. About 800.000 people were left homeless. A special issue of BSSA was dedicated to the detailed evaluation of this horrible event and disaster chain (e.g. Cluff 1971). In 1923 the majority of the 143.000 casualties in the Tokyo earthquake were not killed by their collapsing houses but by outbreak of large areal fires in the densely populated city as a consequence of electric shorts, broken fire places and gas pipes. Also, in conjunction with tropical storms, an average of 90 to 95 % of the people is not killed by the strong winds but rather by accompanying storm surges which flood the coastal lowlands, e.g. in the very shallow terrain of Bangladesh.

Due to the ever growing impact of human activities on natural cycles and equilibrium there is an increasing tendency of coupling between man-made and natural disasters. These **mixed disasters** often develop feedback mechanisms of mutual reinforcement (e.g. increased hazard or flooding due to large scale deforestation and soil erosion or aggravation and prolongation of periods of drought due to large scale overgrazing and related regional changes of Earth's albedo).

But rigorously speaking, **the term natural disaster is misleading**. According to the above definition the term disaster has a meaning only with respect to men and human activities. Nature itself does not know about disasters at all. There is nothing but a great variety of natural phenomena and processes of different time, spatial and intensity scale. They all bear witness of our still living planet Earth. Some of them may have an impact on men with disastrous consequences. This may be due to:

- **lacking awareness** of the natural hazard, human vulnerability and related economic and social risks;
- **settlement in risky areas** (e.g. along active faults, in low-level coastal areas, near steep slopes or cliffs, in flood plains or avalanche corridors, on unstable grounds etc.);
- **unknown or ignored natural conditions**, such as ecosystems stability, soil liquifaction potential, sub-soil amplification characteristics, attenuation laws of seismic waves etc.;
- **improper use** of building material and **bad design or execution** of man-made structures such as houses, industrial facilities, infrastructure and life-lines which are not in accordance with the actual hazard and risk;
- **missing or not appropriate land-use regulations**, safety and preparedness measures and **lacking control** of proper execution and **inforcement** of regulations by law, taxes, insurance etc.;

- **ignorance** of human safety interests and long-term needs for sustainable development;
- **lack of well trained** and motivated **man-power** to tackle with the above shortcomings.

Therefore, in the last consequence, the provoking hypothesis is right that

All disasters are man-made!

This necessitates to investigate, first and foremost, the natural hazard, the vulnerability of human lives and structures and the risk or impact of a natural phenomena with disaster potential. Taking recommendations by an UNDRO Expert Meeting on Vulnerability Analysis in July 1979 into account, these terms can be defined as follows:

- Hazard H :** Probability of occurrence of an event with disaster potential within a defined area and interval of time;
- Vulnerability V :** Expected degree of loss ($0 < V < 1$) due to a disaster event;
0 - no loss/ damage, 1 - total loss/ damage;
- Specific Risk SR :** Expected degree of loss due to a particular event i with the probability of occurrence H_i , i.e. $SR_i = V * H_i$;
- Elements of Risk RE :** Endangered elements RE_j ($j = 1...m$) within a defined area, e.g. number of persons, value of property, level of economic activity etc. which constitute the elements of an "exposure model";
- Risk R :** Expected total loss due to a specific type of event i , e.g. earthquakes, i.e.:
- $$R_i = H_i \sum_{j=1}^m RE_j * V_j ;$$
- Cumulative Risk CR :** Expected cumulative loss as a consequence of n different potential disaster events, i.e.:
- $$CR = \sum_{i=1}^n \sum_{j=1}^m RE_{ji} * V_{ji} * H_i$$

From this follows:

High hazard does not necessitate high risk !

The risk will only be high when people, structures and values are exposed to hazard (**exposure model**) and if their **vulnerability** is significant. Low density of population, proper land use, safe constructions, good developed preparedness etc. will result in low risk even in high hazard areas. Consequently, the prime task is to develop, on the basis of scientifically

based deeper understanding of causes and effects, strategies, methods and technologies for the reduction of vulnerability. This can be achieved by:

- 1.) **Prediction** of the location, time of occurrence and strength/ magnitude of an event with disaster potential with a view to take prophylactic measures;
- 2.) **Warning** of the population and/ or governmental, private or public institutions aimed at (in case of early warning systems often automatic) switching-off of critical facilities such as lifeline and transport systems, at mobilising the civil defence, activating emergency and rescue teams or even ordering the evacuation of the population if the prediction is sufficiently accurate and reliable with respect to location, time and magnitude of the forthcoming event;
- 3.) **Prevention or mitigation** of the negative impact of pending disasters particularly by means of proper land use regulations and physical planning (e.g. United Nations 1978), building codes and other disaster related legislation (e.g. United Nations 1980; IAEE 1984) based on **long-term predictions**, hazard, vulnerability and risk analyses. Here one has to differentiate between **corrective measures** with respect to already existing settlements and industrial facilities by means of strengthening and retrofitting on the one hand and prophylactic measures based on comprehensive interdisciplinary planning and execution in connection with the development of new areas (e.g. United Nations 1976 b);
- 4.) **Preparedness** in taking effective countermeasures for the prevention or limitation of damages or injury/ death of people in case of unavoidable disaster events. This requires a developed information/communication systems (e.g. Maskrey, 1997; Whittaker, J.P., 1990), public awareness, conscious and trained personal at all social and regional levels, availability of contingency plans and resources, evacuation schemes etc. (United Nations 1984) taking also social and sociological aspects (United Nations 1986; Mileti and Sorensen, 1990; Mileti and O'Brien, 1992) as well as the result of disaster scenario modelling into account (Tucker, 1998);
- 5.) Quick and realistic **assessment** of the extend of a disaster and the kind of damages/ injuries as a precondition for a quick **emergency response** and the effective execution and co-ordination of national and international **rescue and relief** activities.

2. STATUS OF DISASTER PREDICTION AND HAZARD ASSESSMENT

While most of the above mentioned points are essentially of political, administrative and organisational nature, supported by logistic-technical means, the successful realisation of 1.) and 3.) requires extensive basic and applied geoscientific and civil engineering research, data and skills. The current status may be characterised as follows:

2.1. Deterministic prediction and early warning

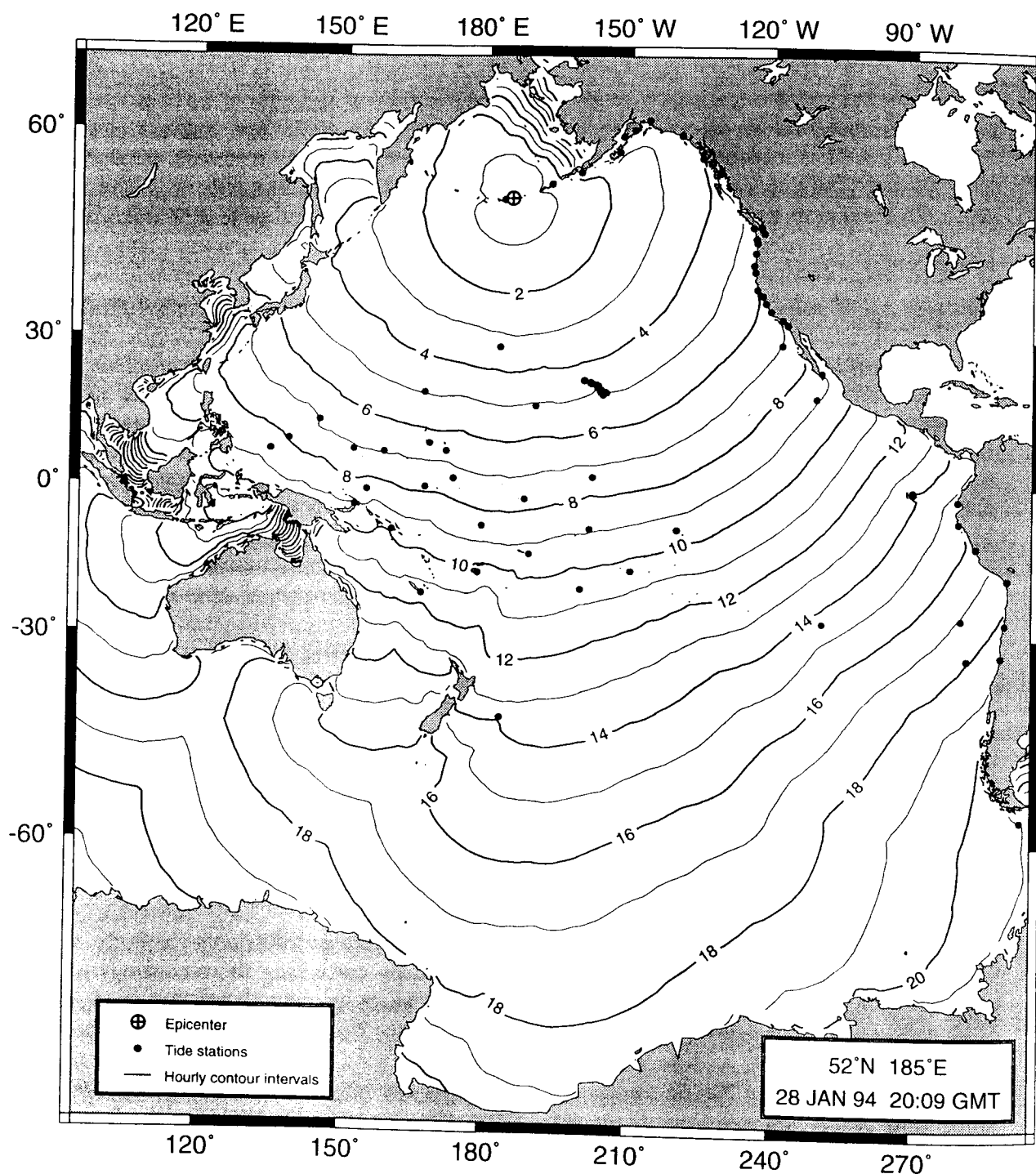
Prediction of future events is at the very heart of science. The reliability of predictions is an effective yardstick to assess the achieved state of knowledge, theory development and their practical handling. One discriminates between **deterministic prediction** of the precise location, time and magnitude of a given event and **probabilistic prediction** that an event of a

given magnitude or magnitude range will occur within a given time window in a considered area (cf. definition hazard H above). The former necessitates the availability of a reliable **deterministic parameter model** of the causing physical process or related phenomena, an **operational monitoring system** which provides the needed multiparameter input data for the model calculations in the required quantity, quality and representativeness, in near real time as well as powerful computers which are able to carry out the calculations within the lead-time required for the practical use of prediction of a forthcoming event in terms of **warning** of the population and the realisation of short-term prevention of mitigation measures such as evacuation, mobilisation of civil defence etc. Even when the prediction problem is solved sufficiently well in academic terms its beneficial practical applicability is not yet assured. The latter does not only necessitate the availability of a well developed communication system for rapid dissemination and assured receipt of warnings by the population at risk but also the availability of well developed and trained response schemes at all administrative levels down to the affected communities. Besides this, public awareness and rational response to such emergency messages and measures are preconditions for avoiding panics or other detrimental social misbehaviour in the wake of published predictions, issued warnings, ordered evacuations or related measures.

Prediction and warning schemes for tropical cyclones are currently most advanced. These storms develop over warm oceans only. They can be detected in time by operational weather satellites and their tracks, velocity of migration and power (maximum wind speeds) be determined sufficiently accurate, also by means of complementary ground-based techniques. This allows to issue and regularly up-date early warnings with days to hours lead-time through established channels of the World Meteorological Organisation's World Weather Watch and Global Telecommunications System as well as other national services (e.g. of the USA). The number of casualties due to such tropical storms could, therefore, already drastically be reduced although the material losses are still dramatic and increasing.

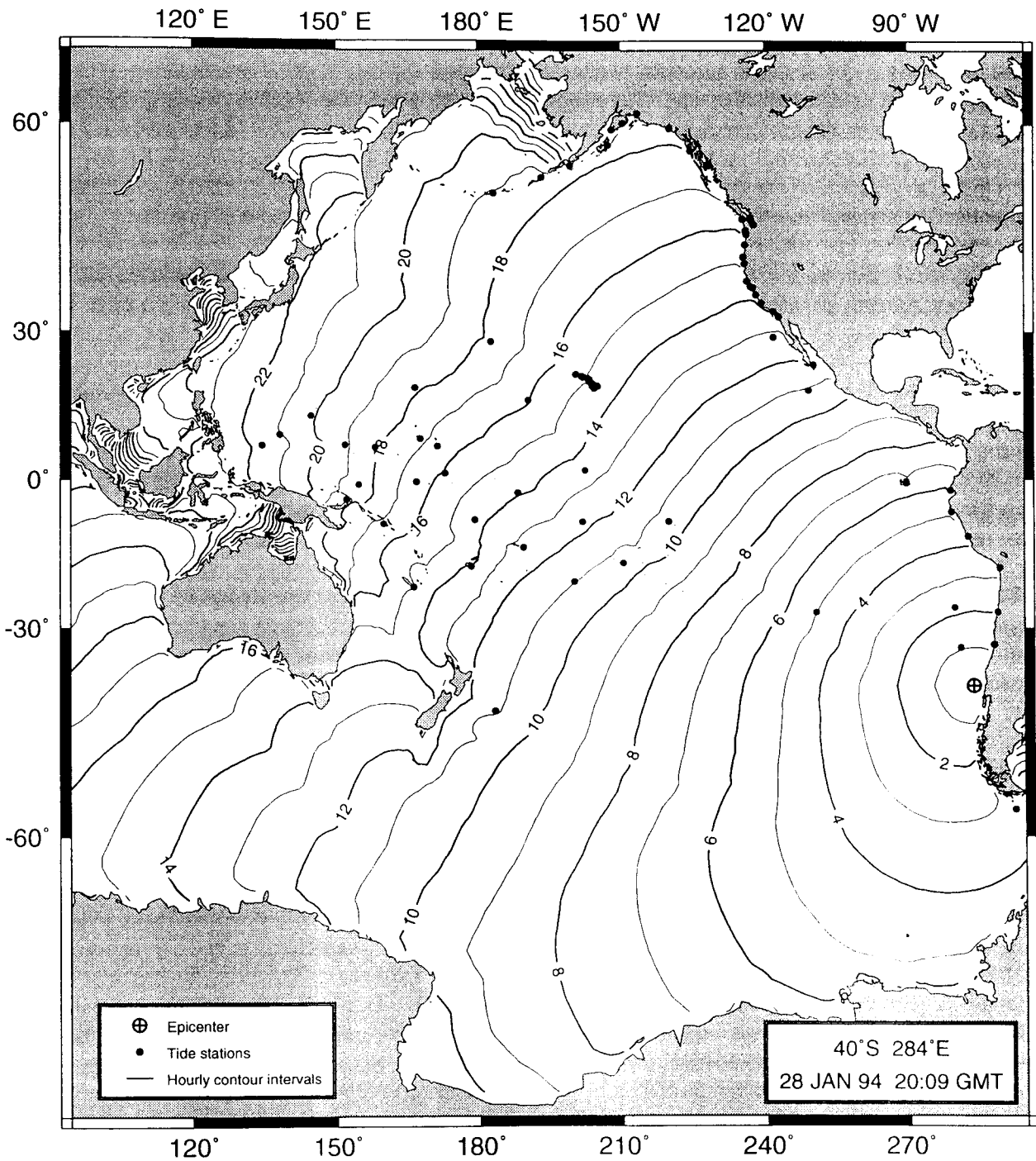
Also rather well developed are operational predictions and warnings of tsunamis by the international Pacific Tsunami Warning Center (PTWC) at Honolulu, Hawaii, but only for coastal areas which are sufficiently far away (several 1000 kms) from the epicentre of the causing earthquake. The PTWC avails of more than a dozen on-line access to 9 USA station on the Aleutian islands, in Alaska and on the USA mainland. It is connected via satellite communications both with the US National Earthquake Informations Center (NEIC) at Boulder and other important centres in Japan (Matsushiro), Alaska, Sachalin, Kamchatka, Hong Kong, Soul, Manila, Port Moresby and Tahiti (French GEOSCOPE network). NEIC reports to the ITWC within 10-15 minutes after a Pacific earthquake with body wave magnitudes $m_b > 6$ their location. It may be improved by consulting the recordings of the PTWC stations. Via satellite further parameter data can be requested and received in an instant from the other centres mentioned above in order to check and refine the location and magnitude of the event. Additionally, via satellite, actual sea level data from more than 100 tidal stations around the Pacific can be acquired. Then, for the given earthquake location, the travel time of the expected tsunami wave front travelling through the whole Pacific Basin are calculated and plotted (Figs. 1a and b). These results are transmitted on request, or in case of $M > 7.5$ at once, to all countries in the Pacific region. This kind of prediction is possible due to the fact that the tsunami wave generated in the ocean by a submarine earthquake is a simple gravity wave. It travels with the speed $v = \sqrt{g \times h}$ (in m/s) with g - gravity and h - water depth in meters, e.g. with $v = 200$ m/s in case of 4000 m water depth and $v = 44$ m/s in case of 200 m water depth. This is about 50 to 200 times slower than the apparent (surface propagation) velocity of teleseismic P-waves. Therefore, the seismic event can first be

located, its magnitude be determined and its tsunami potential be assessed with a sufficient lead-time, in case of distant events about 10 to 20 hours ahead of the arrival of the tsunami wave on far away shores (cf. Figs. 1a and b).



GMT Jan 28 22:17 Courtesy of The Pacific Tsunami Warning Center

Fig. 1: Calculated travel times through the Pacific of tsunami waves generated by earthquakes a) in the central Aleutian Islands and b) off-shore of Chile (courtesy of the Pacific Tsunami Warning Center, Honolulu, Hawaii, 1994).



GMT Jan 28 22:09 Courtesy of The Pacific Tsunami Warning Center

Fig. 1b (for text cf. Fig. 1 above)

But this system fails to provide sufficiently early tsunami warnings for earthquakes off one's own shores although some of the national tsunami warning centres in Alaska, Kamchatka, Japan, Chile and Tahiti struggle currently with the development of some suitable

kind of rapid early warning systems also for that case (e.g. Bernard, 1989; Lander, 1986; Yamazaki et al. 1993; Tsuchiya and Shuto, 1995). Unfortunately, also reliable operational predictions of the expected height of a tsunami wave are not yet possible at the PTWC since the controlling parameters such as earthquake magnitude and source mechanism, ocean bottom relief, coastal profile and shoreline configuration vary too much, are not readily available with sufficient precision or not yet well enough known on a larger scale as to consider them in regional prediction and warning procedures. But local solutions of tsunami heights for particularly tsunamis prone risky shores by detailed tsunami modelling are already practised in Japan, Russia and the USA e.g. and may become more widespread in future.

The relative successful and to a certain extent already operational prediction and early warning systems in case of tsunamis and tropical storms are mainly due to a number of beneficial circumstances. In both cases the source develops out in the sea. It does then, in most cases, not yet constitute an immediate disaster threat to densely populated areas on land. It can be localised with high precision by available operational global monitoring systems (weather satellites or seismographic stations) shortly after its generation with a sufficient lead-time so as to allow ahead warnings. The propagation direction and velocity of the phenomena with disaster potential can either be continuously or in short time-intervals be monitored or, as in the case of the tsunami waves, be calculated on the basis of relatively simple deterministic physical relationships with sufficient precision.

On principally the same grounds earthquake early warning systems are designed, namely, a group of sensors is placed along a fault or around a potential source area at a sufficiently large distance from objects or sites at risk. The sensors will record strong ground motions, may additionally determine the location and size of the causing event and/or the direction of propagation of the fault rupture and will trigger the immediate automatic switching-off of critical lifeline systems, power stations, electricity and gas supplies, will stop trains or road traffic etc. This may drastically reduce electric shorts and the related outbreak of fires, the derauling of trains, the crashing of cars when deriving over collapsing bridges and similar earthquake effects. But since the lead-time before arrival of the strong ground motions at several 10 to some 100 to 300 km from the earthquake epicentre is only in the order of a few seconds to about a minute at the most, deliberate human decision and response is in most cases no longer possible. Such systems are operational already for many years in Japan along the National Railway system. Others are currently proposed, installed, tested or operated along the San Andreas fault in California, in Mexico, in Taiwan, in Romania, in the area of Istanbul, Turkey, or at special high-risk sites such as nuclear power plants (United States Department of the Interior 1990; Toksöz et al. 1990; National Research Council 1991; Espinoza-Aranda et al., 1995; Nanometrics 1994; Nakamura, 1996; Wenzel et al. 1999; Wu et al., 1997, 1999;).

The situation is more complicated with the prediction of with sudden geological events such as earthquakes and volcanic eruptions. They occur in the lithosphere which presents a hierarchy of solid volumes or blocks which move relative to each other (Sadovsky and Pisarenko, 1990; Fig. 2), underlain by the less rigid, partially molten asthenosphere which interacts with the lithosphere. But any such complex multi-parameter system consisting of interacting elements has the tendency of developing into an instable **non-linear chaotic dynamic system of self-organised criticality** (Bak et al. 1988). Earthquakes, volcanic eruptions, rock avalanches etc. are expressions of the "catastrophic" collapse/destabilisation of fractal geological systems (e.g. Bak and Tang 1989; Ito and Matsuzaki 1990; Korvin 1992; Turcotte 1992). Such events cannot precisely be described in deterministic terms but they are

somehow conditioned by the scale-independent selfsimilar internal structuring, the phase composition of the medium as well as by the external acting forces ("deterministic chaos"). Consequently, they develop certain characteristic stochastic patterns of forms, spatial dimensions, frequency of occurrence and energy release. They follow a power law distribution, i.e. logarithmic decay of the frequency of events with increasing size (so-called $1/f$ or "flicker noise" relationship). This applies in the same way to the relationship, e.g., between number and size of trunk, branches and twigs of a tree as to the branching of tectonic faults and fractures at various scales (cf. Fig. 6 in chapter *Introduction to seismic sources and source parameters*). But the accurate size, time and location of the occurrence of the next "avalanche" or branching/ bifurcation/ fracture/ collapse event is generally not deterministically predictable. If at all, prediction can be made only in a probabilistic sense despite of certain typical, conditioned stochastic patterns that may develop prior to a pending major event (e.g. "quiescence" and/or clustering of micro-earthquakes prior to a main shock).

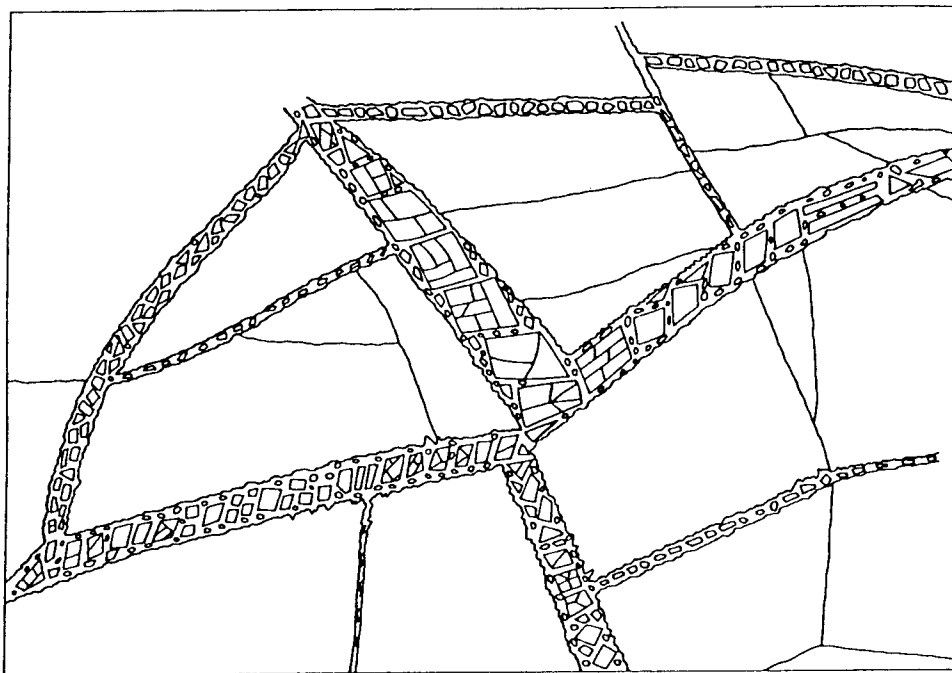


Fig. 2: Schematic depiction of the lithosphere as a hierarchy of volumes or blocks which can move relatively to one another (reprinted from *Physics of the Earth and Planetary Interiors*, Vol. 61, Keilis-Borok: Introduction: Non-linear systems in the problem of earthquake prediction, p.1-7, Copyright 1990, with permission from Elsevier Science).

Earthquake occur along the less rigid boundaries of block structures as shown in Fig. 2. Such fault zones are typically about 10-100 times smaller than the adjacent blocks. The same applies to the internal structuring within such fault zones. They constitute, according to Keilis-Borok (1990), boundary zones which hold blocks together by forces of friction and cohesion. These forces are controlled by internal processes which are confined mainly to the boundary zones, e.g. by interaction with fluids, phases and petrochemical transformations, fracturing etc. These processes can **rapidly and unobtrusively change the friction and cohesion and thus the effective strength** within fault zones by a factor up to $10^5 - 10^6$ (Keilis-Borok 1990). This makes earthquake prediction so difficult a task.

In this context we have to be aware that despite of the existence of some common first order features which allow to classify an object as a "tree" or an event as an "earthquake", there exists a great variety of "species" of trees, earthquakes etc. The latter may vary by orders of magnitude in their relevant parameters such as seismic moment-release, stress drop, depth distribution, magnitude-frequency relationship, average return periods etc. They depend on the given seismotectonic environment (plate boundary or intraplate situation; continent-continent collision, subduction or rifting zones), magnitude and orientation of stresses (compressional, extensional or shearing regime), rock type, crustal rheology etc. This makes it principally impossible to apply - with the hope for assured success - certain systematic precursory patterns or quantified "prediction criteria" as derived from investigations in one earthquake zone to another earthquake area belonging to a different seismotectonic regime. Even within a given area no future earthquake with all its related inter-, pre-, co-, and post-event features will ever be a precise copy of any previous event there, as there is never any oak, birch or pine tree a precise copy of any individual member of its species. Each earthquake somehow changes the conditions and fine structure of a fault zone. Accordingly, subsequent processes of stress redistribution and reloading, re-crystallisation and fracture healing, renewed fracturing etc. will vary with time and never be the same again.

But despite of these remarks, which should make us sober in our expectations and critical against unjustified claims to have already found the key to successful earthquake prediction (e.g. Varotsos and Alexopoulos 1984 a and b) and some recent outright dismissals that earthquake prediction could ever be achieved and become operationally feasible (Geller, 1991, 1997a and b; Geller et al. 1997) the problem is still thought to be not completely hopeless by many researchers, at least with respect to intermediate- and long-term predictions (e.g. Harris, 1998; Sykes, 1996; Brehm and Braile, 1998). The debate is still going on (e.g. Lerner-Lam, 1997; Wyss, 1997; 1998; Silver, 1998; Whiteside, 1998; Crampin, 1999), the more so since in 1997 seven magnitude 6+ earthquakes had rocked Jiashi county in China with 4 predictions and advanced warnings made, out of which apparently three were successes (Hui and Kerr, 1997).

Both earthquakes and volcanic eruptions are connected with preparatory, co- and post-event deformation and fracturing. They are accompanied by plenty of more or less subtle and noisy long-, medium- and short-term changes in related phenomena and other geophysical field parameters (e.g. Mogi 1985; Rikitake 1987 and 1988; Ma Zongijn et al.; Boschi and Dragoni 1992; Gasparini et al. 1992). Their comprehensive complex monitoring with sufficiently dense and precise networks of sensors capable also of recording disturbing influences from other sources (e.g. meteorological, hydrogeological and other effects), which might cause similar anomalies or parameter changes, is an indispensable precondition for any kind of prediction research aimed at physical modelling of parameter changes related to pending earthquakes or volcanic eruptions. But only if the assumed or derived model does indeed, and independent with time, correctly reflect the complex controlling processes and their quantitative interrelationship and provided that the 3-D starting conditions can indeed precisely enough be determined from (in most cases spatially scarce and point-like) surface measurements an effort of deterministic **prediction of future events** (and not retrospective one as usual) could have a chance at all. A critical assessment of retrospective validation of precursors has been given by Mulargia (1997).

In the case of volcanoes such an approach seems to be, at a first glance, most promising. A volcano is a structurally complex 3-phase system with solid, liquid and gaseous phases interacting. Modelling of its active states requires to consider non-linear flows of a two-phase

compressible liquid. But at least the location of the "trouble maker" is known. This enables us to focus the complex monitoring of precursory phenomena on a small area with rather dense networks of sensors. This may be the main reason for several successful predictions of pending eruptions which allowed to issue early warnings and to evacuate the population at risk out of the endangered zones (e.g. in case of Mt. Pinatubo in the Philippines; Punongbayan 1998). In other cases it made possible a full-scale geoscientific monitoring and documentations of the eruptions in all phases as in the case of Mt. St. Helens in 1980 and of several eruptions in Kamchatka, e.g. of the volcano Tolbatschik in 1977. None the less, also for volcanoes, there are no fixed patterns of precursory phenomena which signal a pending eruption. Each volcano has its own life and his signals must be studied individually. Also, there is no assurance that different eruption episodes, often with decades, hundreds or even thousands of years of quiescence in between, will be ushered by the same set and intensity of precursory features since the state of activity of a volcano may change significantly with the time.

There have been, therefore, several false alarms, and evacuations of thousands of people in vain as well, when strong signs of seismic "unrest" or even initial volcanic activity were not followed by larger dangerous eruptions. Examples are the volcano La Soufrière on the island Guadalupe in 1975 (Schick 191) and the volcano Mihara Yama on Izu-Oshima in the Bay of Tokyo in 1986/87 (Schimozuru 1988; Schick 1991). In other cases, completely unexpected strong eruptions of well monitored volcanoes occurred partially without any seismic precursory signals (failure to predict). Examples are the eruptions of the volcano Avachinsky on Kamchatka on 13 January 1991 and of the volcano Galeras in Columbia on 14 January 1993 (Schick 1994).

With reference to earthquakes the situation is still much more complex, especially because of the much more extended and heterogeneous seismogenic zones. The monitoring of the preparatory zones of large earthquakes would require to run permanently dense networks of costly multiparameter sensors covering vast areas of about 10^5 to several 10^6 km². But even then we could not expect to gain from them more reliable and consistent precursory patterns or better ratios for successful predictions against false alarms and failures than in the case of well monitored volcanoes. That is why renown seismologists nowadays share the view that a **deterministic earthquake prediction is not possible** (e.g. Aki 1989; Geller 1997).

There have been several "academic" (e.g. Morgan et al. 1988) and at least one spectacular practical success(es) in earthquake prediction. The latter refers to the prediction of the Haicheng earthquake in 1975 in China (e.g. in Ma Zongjin et al. 1990). Besides this there have been plenty of failures to predict (e.g. Tangshan earthquake 1976, all recent strong California and Japanese events) as well as false alarms, e.g. in case of the expected Parkfield earthquake in California (Bakun et al. 1986; Hellweg 1994) (see also Bormann, 1994). False predictions published in 1978 and 1981, related to strong events to be expected in the Oaxaca province of Mexico and in Peru, respectively, had detrimental economic and social consequences. They upset the local population, caused many people to abandon their home and land and triggered large-scale speculative business transactions. Tourist rates and related income dropped significantly. The overall losses were estimated to be in the order of several 100 Mio US\$, i.e. larger than the real losses due to the earthquakes which followed indeed in these areas with several month of delay and smaller magnitudes than predicted. This should make us aware that even in case of correct predictions they may contribute to the mitigation of disaster losses only if they are sufficiently reliable in space, time and magnitude, if they are issued not earlier than a few days and not later than several hours before the event and if they

meet a well aware and trained population which will consciously and disciplined follow the instructions given by authorities without panic or riots. Otherwise, even successful predictions may turn out to be worse than no predictions at all.

Nevertheless, there are still strong endeavours in some countries, Germany with the GFZ included, in the area of earthquake prediction research. They are first of all aimed at a better understanding of the complexity and interrelationship of the inter-, pre-, co- and post-event phenomena, their causing physical and geochemical processes and their modelling. But globally, spendings on earthquake prediction have - as compared to the seventies and early eighties - been more and more reoriented towards seismic hazard, vulnerability and risk assessment, microzoning of local underground response to strong earthquake shaking, into the development of codes and practices of earthquake resistant design and construction, towards scenario modelling and development of risk management plans (e.g. Anonymous 1994, 1998, 1999), i. e. into practical preparedness and preventive measure based on statistical medium- and long-term predictions of the probability of occurrence of strong earthquake ground motions or underground failures. Therefore, the practice-oriented Potsdam seismology training course, will focus on these topics (see lectures on *Methodology of seismic hazard assessment*, *Approaches to seismic hazard assessment in China*, *Seismic Risk assessment and disaster management* and related exercises).

2.2 Probabilistic prediction and hazard assessment

According to Aki (1989) the ideal prediction in probabilistic terms could be defined as follows: "100 years before a target earthquake with a given magnitude and location we would tell people that probability of the occurrence of this earthquake is one per 100 years. Then, 1 year before the earthquake, the probability rate goes up to one per year, and 1 minute before ... (it) reaches one per minute". Fig. 3 shows this relation between the probability rate and the time before the target earthquake in a log-log plot. For the ideal probabilistic prediction we would get a straight line with the slope 45°. For comparison, several realistic prediction curves are shown which are based on different kind of data and analysis procedures. The horizontal line at the bottom corresponds to the long-term average rate of occurrence as determined from earthquake catalogues or paleoseismological data. Its level of probability is typically rather low. It also differs from region to region according to the level of seismic activity and related mean return periods for events of a given magnitude class. The broken line "gap theory" in Fig. 3 indicates that a probability increase of about one order of magnitude can be achieved when the long-term averages can be related to identified gaps along a given plate boundary. The gap concept was originally proposed by Kelleher et al. (1973) and McCann et al. (1979), It allowed already several successful long-term predictions and has since then further be refined by including information on rates of plate motion, average repeat times, estimates of earthquake size in a probabilistic manner for specific segments of relatively simple major plate boundaries. A comprehensive review of the development of this concept since its introduction, its current state as well as criticism together with many suitable references is given by Nishenko and Sykes (1993),

According to Fig. 3 the achieved prediction probabilities in the intermediate-term range (a few weeks to years) are until now about one to three orders of magnitude below the ideal probabilistic prediction while, partially by chance, the actual short-term prediction probability in the Haicheng case came rather close to that of an ideal prediction. Aki (1989) concluded from this that precursory signals may be significantly stronger immediately prior to an

from this that precursory signals may be significantly stronger immediately prior to an earthquake than at a longer time before. This is also plausible from a physical point of view when considering both the necessary "nucleation" around the starting point of an earthquake rupture and the non-linear acceleration of many related phenomena when approaching the critical state. But the apparently rather high short-term probability in the Parkfield case was a false-alarm. The prediction window is over now for years already without the expected event. The vertical line SCAN in Fig. 3 stands for "Computerised Alert Networks" such as the ones discussed above. But these are no true predictions but rather systems for near real-time early warning and response. They are feasible only for sites at some distance from the event and based on the detection, rapid (automatic) analysis of ground motions of an already ongoing earthquake.

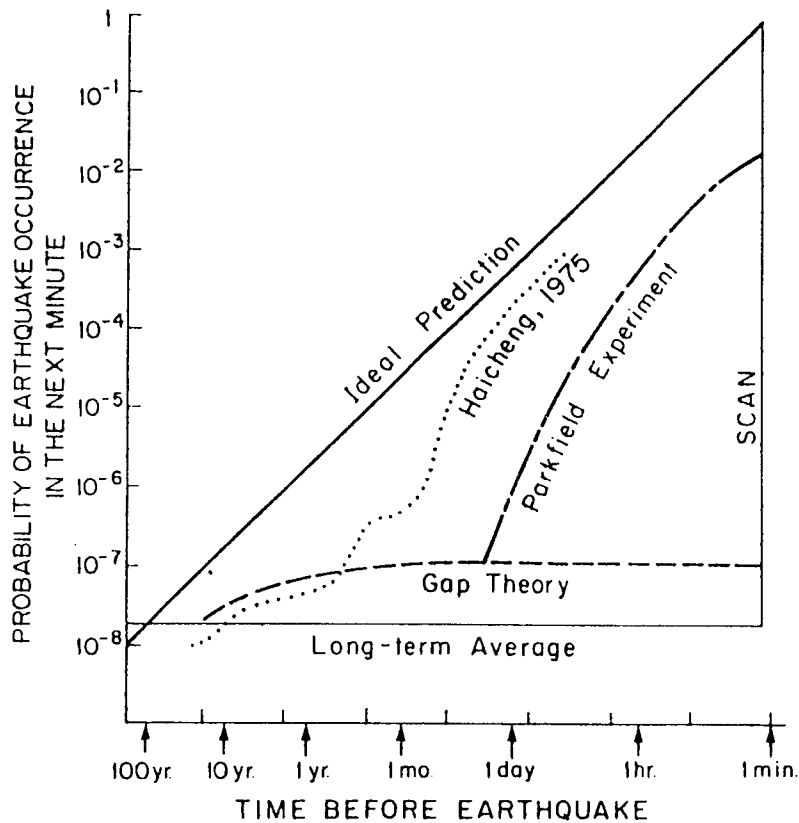
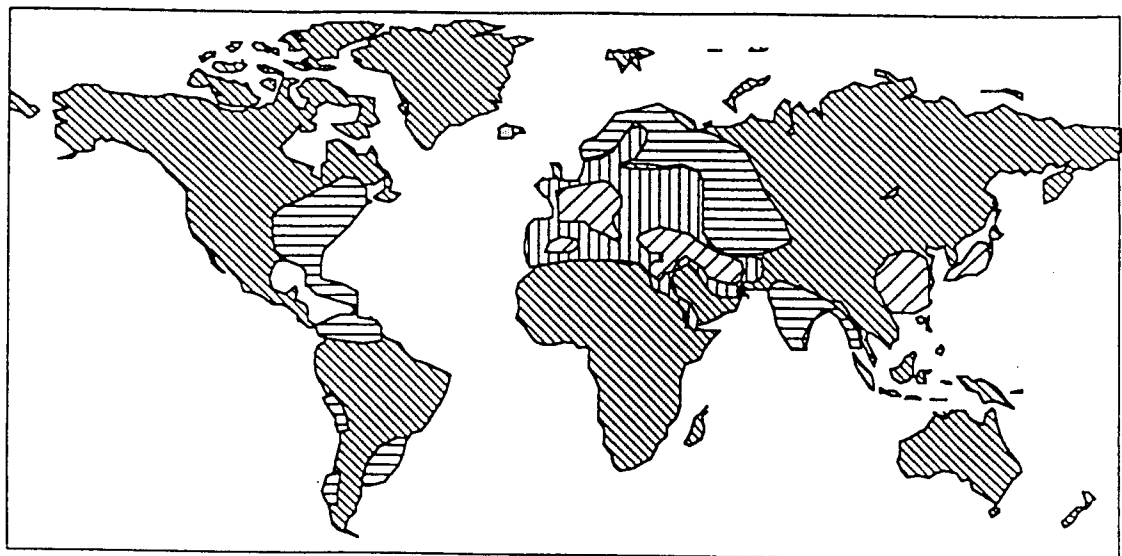


Fig. 3: Probability of earthquake occurrence in the next minute (Reprinted from *Tectonophysics*, Vol. 169, Aki: Ideal probabilistic earthquake prediction, p. 197-198, Copyright 1989, with permission from Elsevier Science).

Also probability predictions are not free from assumptions. In case of long-term predictions it is mostly assumed that the data on which they are based are complete for the considered interval of time, that they include the strongest "characteristic" event in that area or that the strongest possible earthquake can be inferred sufficiently accurate from seismotectonic considerations or paleoseismological data. Besides this, it is mostly assumed that the recurrence intervals between consecutive strong events follow a "normal", i.e. Gaussian distribution and that the frequency of earthquake occurrence is a stationary process which follows a Poissonian distribution. But in reality these assumptions are often not fulfilled. Although Fig. 4 may be debatable in detail it clearly shows that the potential time span for which earthquake catalogues may be complete for events with magnitudes $M > 6$, i.e. for potentially seriously damaging earthquakes, differs significantly from region to region. For

such as sparsely populated areas or only rather recent habitation by population groups capable of and practising careful written reports of unusual events. Only for Japan, parts of China, Europe and the Near East earthquake catalogues are available which cover more than 800 years. If we consider this in the context of Fig. 5 which shows the differences in strain rates of the lithosphere in different tectonic environments as well as the related variability of the duration of seismic cycles we can draw the following conclusions:

- Earthquake catalogues solely based on instrumental records do generally not cover a sufficient time period (< 50 – 100 years) as to cover at least one full seismic cycle but they have the advantage of being more complete for lower magnitudes;
- Along active plate boundaries strain rates are large enough as to cover one or more seismic cycles with complete catalogues dating back for more than one or a few hundred years;
- In active intraplate environments the historical records of only the oldest cultural nations may date sufficiently far back (> 800 years) so as to assure the coverage of one or more seismic cycle(s) containing also the strongest “characteristic” events;
- Only stable continental platforms even the longest catalogues or historical records do not reach back sufficiently far in the past as to assure the coverage of at least one seismic cycle and the strongest possible earthquake in such areas.



Potential duration of earthquake catalogue complete above M6



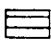

 <200 years	 400-800 years
 200-400 years	 >800 years

Fig. 4: World-wide completeness of earthquake catalogues (after Muir-Wood 1993; with permission of Annali di Geofisica)

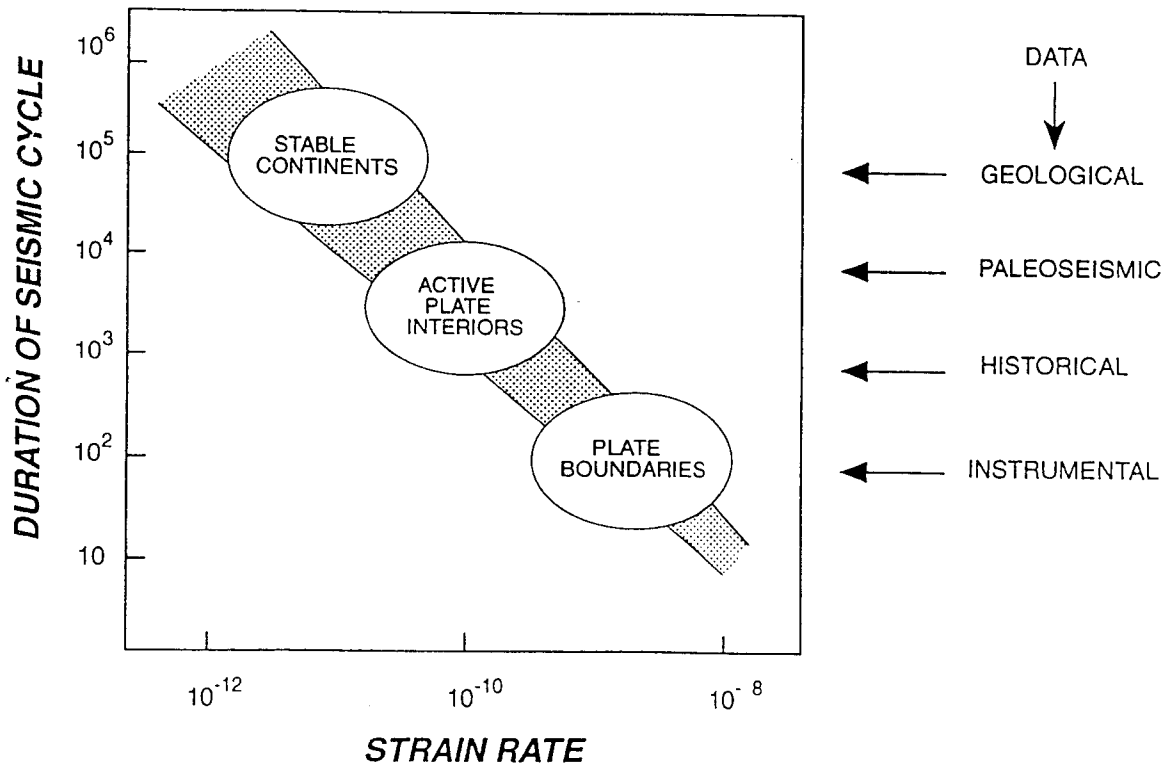


Fig. 5: The duration of seismic cycle (in years) as a function of strain rate (courtesy of D. Giardini 1994)

The last conclusion was dramatically confirmed by the most devastating Haicheng (1975, $M_s = 7.3$, $I_{max} = 9^\circ$ MSK) and Tangshan earthquakes (1976, $M_s = 7.8$, $I_{max} = 11^\circ$ MSK) in China. Both events occurred in regions for which the former Chinese seismic zoning map, based on data of an about 3000 year old earthquake catalogue, assumed only a maximum intensity of ground shaking $I_{max} = 6^\circ$ MSK. Later paleoseismological investigations in the Tangshan area revealed that the two prehistoric events of about the same magnitude as the 1976 event had occurred in this region with an estimated return period of about 3000 years (Wang 1987). The importance and methodology of using both historical and palaeoseismological investigations for the extension of the time window of earthquake catalogues as the indispensable precondition for the more reliable long-term hazard assessments as well summarised, with many suitable references for the further readings, in papers by Vittori et al. (1991), Guidoboni and Stucchi (1993) and Pantosi and Yeats (1993).

But even if we have covered one or more seismic cycles containing also the strongest possible or at least the “characteristically” strongest events probable in the considered region we still have to base our statistical calculations for seismic hazard assessment on other assumptions, e.g. with respect to the statistical distribution of data. The return period of strong events may follow a normal (i.e. Gaussian) or another, e.g. a log-normal distribution. In practice, we have for most regions not enough realisations of strong events in order to derive the most appropriate or “true” distribution model from the data itself. Also, our current understanding of the underlying physical processes that control the recurrence times is not yet good enough as to give us any assurance on whether they distribute normally or log-normally or different from both. But different assumptions on their distribution may have dramatic consequences on the hazard assessment. This was demonstrated by Jacob (1984) who calculated for the

critical gaps along the Aleutian Islands' arc a two to three times lower conditional probability of occurrence of strong events with seismic moment magnitudes $M_w > 7.8$ within the 20 years' interval 1983 – 2003 when assuming a log-normal instead of a normal distribution of the respective recurrence times (Fig. 6). As long as these basic uncertainties remain the long-term probabilities for great earthquakes have to be taken with great caution. This is especially true when considering the possible social impact of such "predictions" as well as the risk assessments based on these probabilities.

Another important finding from old catalogues is that over periods of several hundred or thousand years the seismic activity within a given area varies. Ben-Menahem (1981) derived from the catalogue of the earthquakes in North and Central Israel, which dates back for about

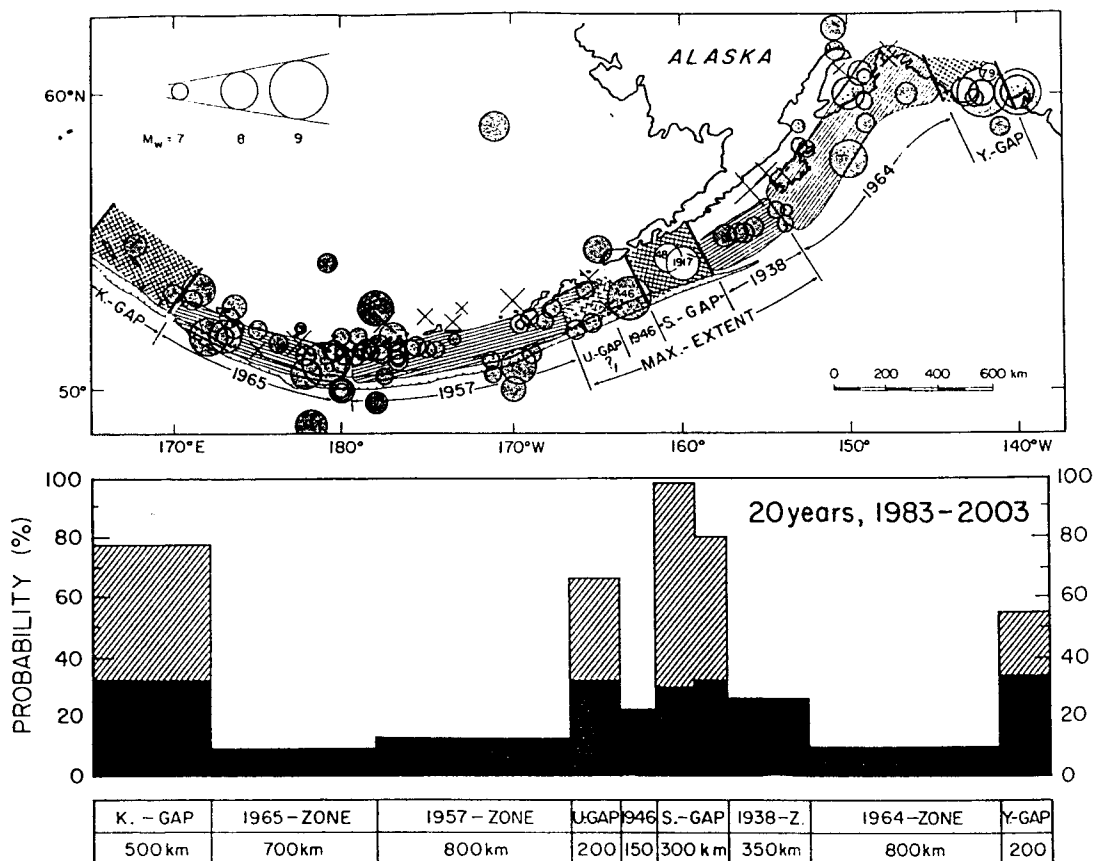


Fig. 6: Top: Instrumental seismicity since 1898 for $M_w > 7.0$ and segmentation into major zones of recent ruptures with $M_w > 8$ as well as seismic gaps.

Bottom: Conditional probabilities for great earthquakes with $M_w > 7.8$ in all major segments of the Aleutian arc for the time window 1983 – 2003 based on normal distribution (hatched columns) or log-normal distribution of recurrence times (solid columns) (after Jacob 1984; with permission of American Geophysical Union).

4000 years, activity maxima with events up to $M = 7 - 7.5$ every 760 ± 40 years while in time intervals between these "peaks" the maximum magnitudes of events reached only values of $M = 6.5 \pm 0.1$. Ambrasseys (1980) could show that phases of higher and reduced earthquake activity may occur alternately in neighbouring seismotectonic zones such as the North

Anatolian and the East Anatolian or Border Zone (Fig. 7). This behaviour resembles the oscillations of a coupled pendulum with a weak connecting spring.

The fundamental precondition for the applicability of the Poisson model in earthquake hazard assessment, namely, that the earthquake generating process is a stationary one, is under such circumstances not strictly applicable. Time-dependent Markov models, considering both the temporal and the magnitude dependence of earthquake recurrence, would then, in principle, better describe the probability distribution of events. But in the case that the instrumental or even the historical record is shorter than the duration of major episodes of increased or reduced activity we will not recognise this variability and cannot evaluate its possible influence on the long-term hazard assessment. Consequently, the latter might turn out to be either too high or too low, i.e. conservative or unconservative.

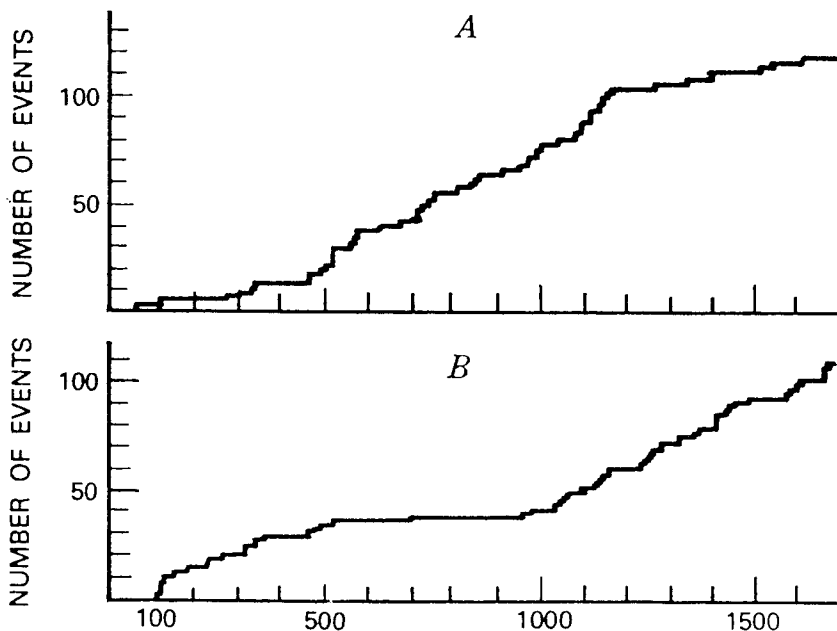


Fig. 7: Cumulative number of damaging earthquakes for the Border zone (A) and the North Anatolian zone (B) between 0 and 1700 AD (after Ambraseys 1980).

But for more short-term hazard assessment as being relevant for many engineering applications with typical time windows of about 50 to 100 years and magnitude levels with an annual exceedance probabilities of 10^{-3} or less (i.e. considering very strong and rare earthquakes) only this is in most cases not critical. According to Cornell and Winterstein (1988) Poisson estimates are insufficient in practice only in cases where the hazard is controlled by single features for which the elapse time since the last significant event exceeds the average time between such events. But the Poisson estimate “will generally be adequate if the mean interevent time between the significant events exceeds the ... elapsed time since the last such event or the length of the historical record, which ever is less”. Consequently, “... a gap with higher than Poisson hazard may be rather unusual in engineering design practice“. This may also be due to the reasonable assumption that the sum of several non-Poissonian processes may be appropriately Poissonian again. Since, in practice, two or more factors will control the hazard at a particular site the combined hazard is, according to Cornell and

Winterstein (1988), better estimated by the Poisson model than by a single feature non-Poisson model one. On the other hand, Muir-Wood (1993) gave a striking example for how strong also short-term hazard assessments may depend on our knowledge of the hazard generating process, i.e. , whether such assessments are based on probabilities derived from historical data only or on seismotectonically constraint or time-dependent probabilistic models (Fig. 8).

But in general, available methodologies for the calculation of seismic hazard are well established. According to McGuire (1993) uncertainties in interpretation can be accounted for by applying multiple hypotheses resulting in uncertainties in the hazard assessment. Being aware of them leads to the most informed decisions for risk mitigation. The training course will, therefore, strongly focus on the fundamentals, data to be used, chief steps to be considered and methods to be applied in seismic hazard assessment as well as on other crucial interdisciplinary questions such as vulnerability and risk assessment which have to be tackled mainly by engineers. Economists, sociologists et al. (see lecture *Seismic risk assessment and disaster management*).

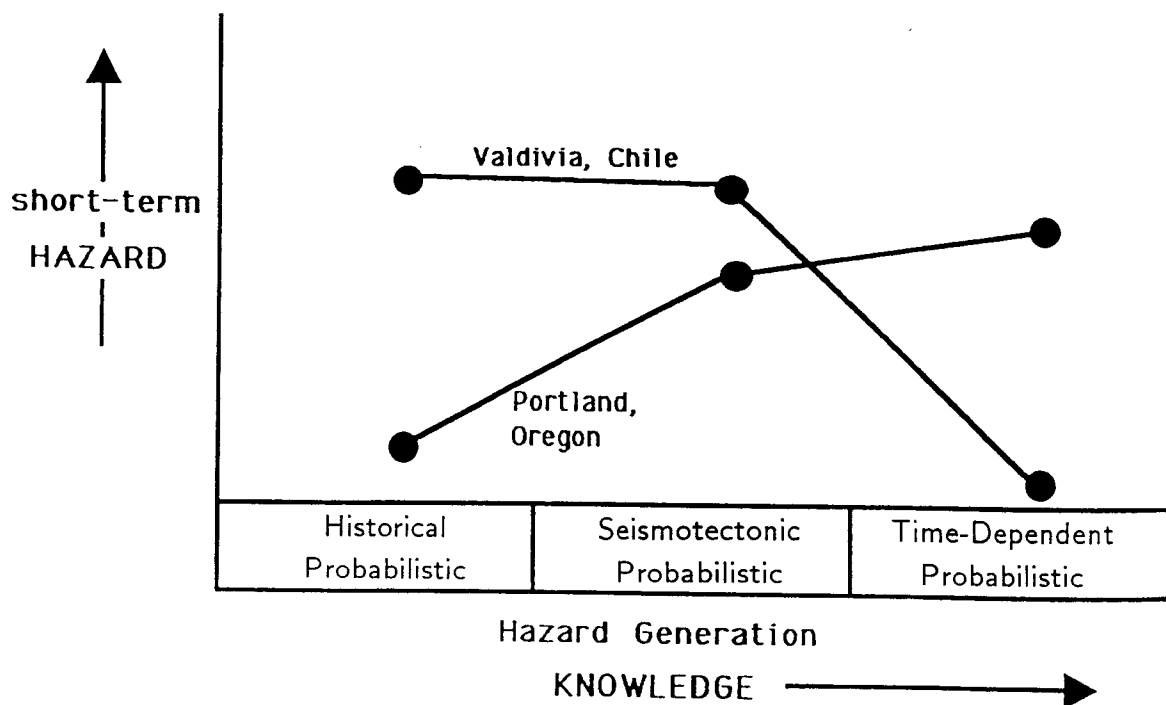


Fig. 8: Dependence of the short-term hazard assessment for the towns of Valdivia, Chile and Portland, Oregon, on the applied probabilistic model (after Muir-Wood 1993; with permission of Annali di Geofisica)

According to Rhoades and Evison (1989) comprehensive and reliable precursory observations may additionally provide a basis for the quantification of time-variable hazard models. But the precondition is that the precursor data are sufficient to allow the derivation of intermediate quantities such as probability distributions for location, magnitude and time of occurrence of events as well as valid false alarm and failure rates. But this is, in the authors opinion, not yet available anywhere in the world for practical applications.

3. A REVIEW OF NATURAL DISASTERS IN THE 20TH CENTURY

Fig. 9 shows the probably most complete compilation of casualties due to natural disasters between 1900 and 1988 (Science Council of Japan 1989). Respective shares given for various kinds of disasters as well as regions differ slightly from source to source, also depending on the time interval considered. Not considered are in Fig. 9 casualties due to drought and famine. They are by far the largest (> 8 to 10 Mio) but at the same time also the least reliable figures. Also not shown in Fig. 9 is the fact that generally the number of people being injured is typically 3 to 10 times and that of those being left homeless about 10 to several 100 times larger. Accordingly, in the preamble of a related resolution of the United Nations General Assembly of December 1987 it is stated, that during the last two decades natural disasters claimed world-wide more than 3 million human lives and affected the life of at least 800 million people. Consequently, the human suffering and tragedy is immense, not to speak of the material losses.

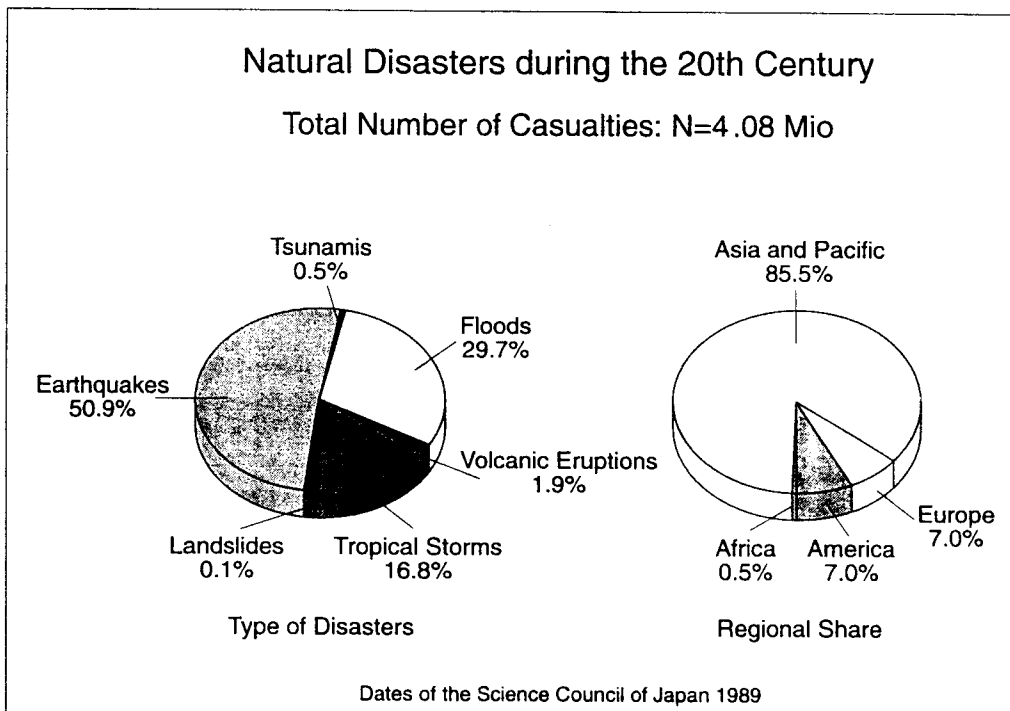


Fig. 9: Number of casualties during the 20th century due to natural disasters (without drought and famine) according to dates of the Science Council of Japan, 1989.

On the basis of still incomplete data published by the German IDNDR-Committee (1994) for disaster events with more than 1000 casualties and complemented by data published in Hurtig and Stiller (1984) for earthquakes and for other types of events by data from another German IDNDR publication (1991), the author compiled Tab. 1. It gives the country-wise percentage of casualties during this century for different kinds of major natural disasters. According to it India/ Bangladesh and China are by far the most disaster stricken countries.

From the various consulted data sources the following conclusions can be drawn:

- Earthquakes have a significant share in the total deaths toll of over 10 Mio. due to natural disasters during this century;

- The frequency of casualties is not uniformly distributed over the various decades (cf. also Fig. 12);
- Within a given decade one or two disaster events may account for over 80 per cent of the total losses due to this type of event

Tab. 1: Natural Disasters 1900 - 1993: Relative death toll due to various types of disasters for the most affected countries.

Type of disaster	Country	% of disaster type total
Drought/ Famine	India/ Bangladesh	75
	USSR	14.6
	Sahel countries	>10
Floods Tropical Storms	China	98.1
	India/ Bangladesh	92.7
	Hong Kong	1.6
	USA	1.5
	Honduras	1.3
	Philippines	1.0
	Earthquakes	China, Taiwan
USSR		10.9
Japan		10.4
Italy		8.0
Iran		7.2
Peru		4.4
Pakistan		4.2
Turkey		3.7
Central America and Mexico		2.8
India		2.6
Chile		2.2
Morocco		0.9
Ecuador		0.5
Argentina		0.3
Philippines		0.3
Algeria		0.2
Indonesia		0.2
Yemen		0.2
Romania		0.2
Papua New Guinea		0.1
USA	0.1	
Yugoslavia	0.1	
Volcanic Eruptions	Martinique	39.0
	Colombia	30.9
	Indonesia	14.0
	Guatemala	8.1
	Papua New Guinea	3.9
	Cameroon	2.3
	Philippines	1.7

A more detailed account of loss of life due to earthquakes between 1900 and 1979 is depicted in Fig. 10 and compared in Fig. 11 with the changes in seismic moment and seismic energy release. Shown are both the respective values for strong individual events and the moving annual averages over intervals of 5-years (according to Kanamori, 1980).

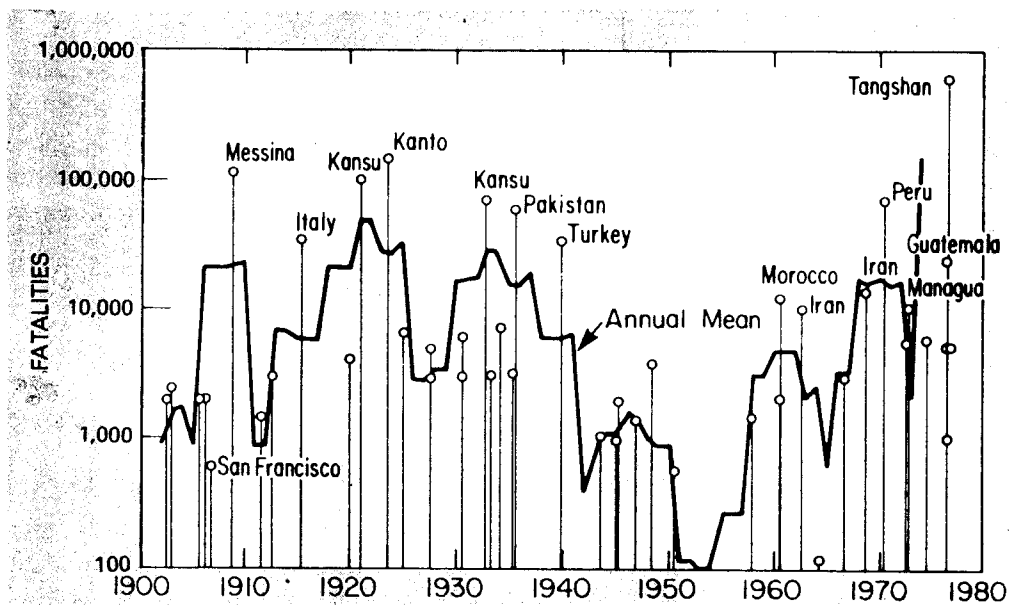


Fig. 10: Loss of life caused by major earthquakes since 1900. Individual events are marked with thin vertical lines and open circles. The solid line is the annual average taken over 5 years at a time (according to Kanamori 1980).

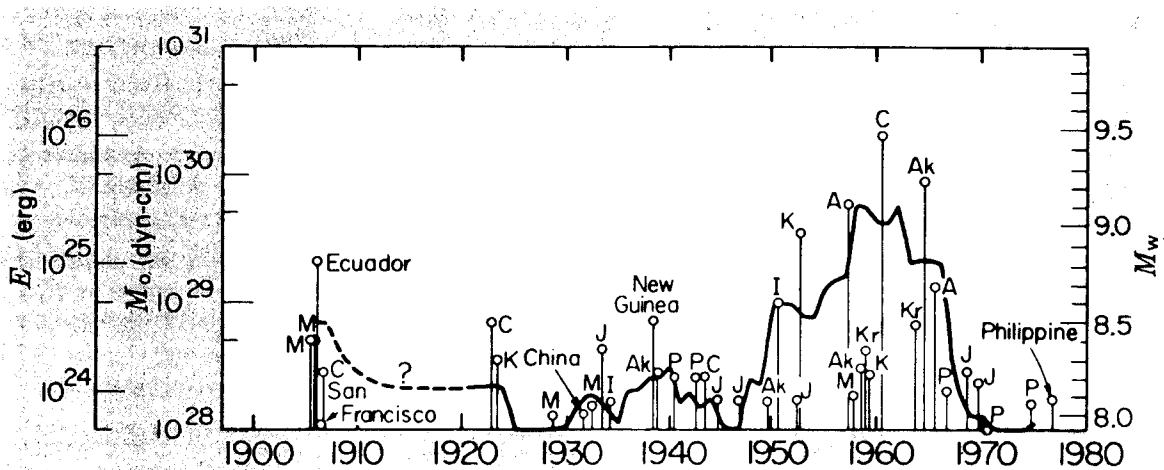


Fig. 11: Seismic moment M_0 , seismic energy E , and moment magnitude M_w for large earthquakes together with the 5-year running annual average of E (solid line). Abbreviations are: A - Aleutian, Ak - Alaska, C - Chile, I - India, J - Japan, K - Kamchatka, Kr - Kuriles, M - Mongolia, P - Peru (from Kanamori 1980).

The comparison reveals that there is no direct correlation between the number of earthquake casualties and the global seismic activity and energy release. A single giant event such as the Chile earthquake 1960 released roughly as much seismic energy as the long-term global cumulative average over 25 years corresponding to about 20 percent of the total annual

energy of lithospheric plate motion. It killed about 3000 people while hitting a sparsely populated area. Contrary to this, the about 300 times weaker event which struck the populated area around the Chinese town of Tangshan in 1976 caused officially quoted 242.000 casualties. Not confirmed earlier estimates spoke even of more than 600.000 deaths (still depicted in Fig. 10).

Figs. 10 and 11 do discard speculations of an escalation of global seismic and volcanic activity due to the underground nuclear testing (UNT) by military superpowers. As large as these explosions are in human terms and as devastating they would be in a targeted military application as small they are still when compared with the energies by global lithospheric plate motions and those released to major earthquakes. UNT reached its climax between 1967 and 1976 with many yields ranging between about 1 and 6 megatons of TNT equivalent. But just during this time window the global curve of seismic energy release shows a dramatic decline. The following increase again coincides with the prohibition of testing of devices with more than 0.150 Mt TNT equivalent. Seismologists should know that even the strongest UNT had a body wave magnitude of about 7 only. Every year there occur about 10 earthquakes of this magnitude and stronger. And the Chile earthquake was about 3.000 times stronger than the strongest UNT and about 200.000 times stronger than the largest tests after 1976. About half of these later test had even yields between about 1 and 20 kt TNT only (magnitudes between 2 and 5.5). Every year there are thousands to hundreds of thousand of natural events in this magnitude range. Although very strong UNTs may trigger hundreds of tectonic aftershocks in an area up to about 20 km radius around the source along pre-existing faults they can neither trigger nor cause earthquakes at significantly larger distances. Beyond 30 to 100 km distance the quasi-static deformations of the Earth's crust after a Mt-UNT do fall already below the periodic deformations due to the gravitational forces of the sun and moon (solid earth tides) which have no proven significant effect on the triggering of earthquakes (cf. Bormann 1990).

Fig. 12 depicts the economic losses due to natural disasters for the time span 1960 to 1998 on the basis of data published by the Munich Reinsurance Company. One recognises, despite of significant annual fluctuations, a striking steadily increasing trend. The global annual mean economic losses per decade (in terms of 1991 values) were about 4 billion US\$ between 1960 and 1969, 7 billion US\$ between 1970 and 1979, 12 billion US\$ between 1980 and 1989 and 52.5 billion US\$ for the first 8 years of the 90s alone.

Note, that the Northridge earthquake in January 1994 (California) accounted for economic losses of about 44 billion US\$ alone and the Kobe earthquake 1995 in Japan even more than 100 billion US\$, respectively. The cumulative economic losses for Europe (with Turkey included), increased from about 0.6 billion US\$ for the decade 1960 - 69 to about 11 billion US\$ for 1980 - 89.

This speaks of a rapidly increasing vulnerability of human society due to population growth, expanding settlements into more and more risky areas and poverty related inappropriate building materials and techniques in developing countries on the one hand and more and more dense and costly settlements, industries, equipment's, infrastructure and life-line systems on the other hand in highly industrialised countries. In the first case the losses are mostly human lifes, in the latter case material values. The United States Agency for International Development (US-AID) estimated for the next decade disaster losses of about 400 billion US\$. It states at the same time that damages of about 280 billion US\$ could be avoided when immediate prophylactic measures were taken. They would cost about 40 billion US\$, i.e. one

seventh only of the expected losses. On the other hand, in a 1989 report, the Tokai Bank of Japan predicted that another earthquake in the Tokyo area comparable with the size of that in 1923 could cause US\$ 650 billion in damage alone. Losses of this order to Tokyo as one of the leading world financial centres are expected to have a detrimental effect on the world economy as a whole.

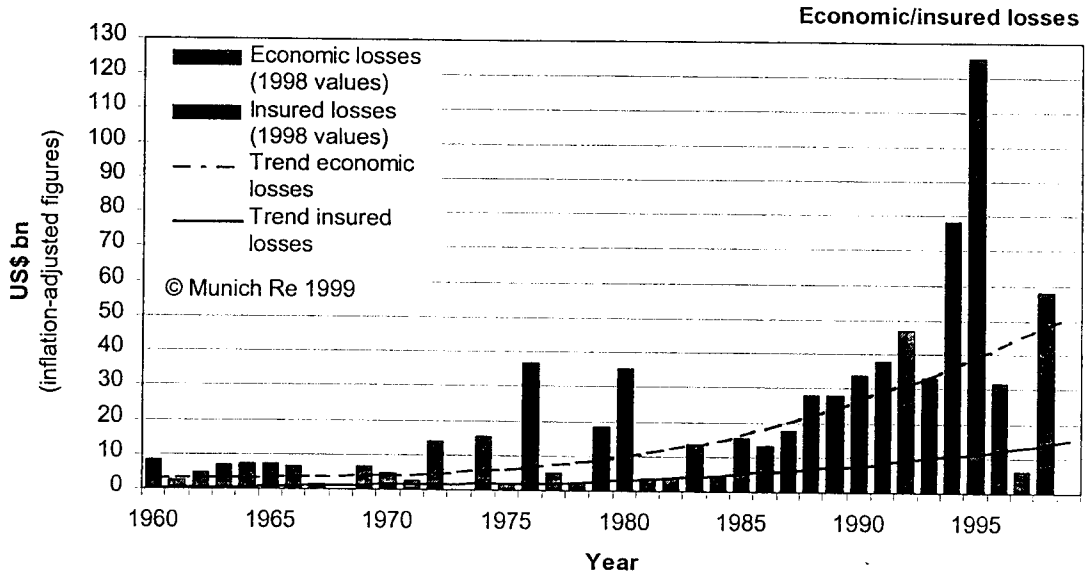


Fig. 12: Economic losses due to great natural disasters (without draught and famine) which far exceed 100 death and/or US\$ 100 millions in claims (according to Munich Reinsurance 1999).

Although as much as three fourth of the global material disaster losses occur in the industrialised countries, the proportional losses in terms of percentage of GNP are much higher in developing countries. The damage caused exceeds by far the total amount of economic assistance which disaster-prone developing countries receive from abroad and cancel out in many of these countries any real economic growth. And their share in human losses is about 95 % of the disaster total. The United Nations Conference on Human Settlement cited in its conference background paper A/Conf. 70/B/7 of 24 February 1976 the result of a case study of the office of the United Nations Economic Commission for Latin America (ECLA). According to this, the estimated disaster damage in the five countries of the Central American Common Market has averaged 2.3 per cent of the gross domestic product in the 15-years period 1960-74, even without taking indirect disaster effects such as disruption of economic activities, soil degradation etc. into account which are most cases higher than the direct material losses. Considering too, that the countries concerned have an average population growth rate of about 3 per cent a year an economic growth rate of at least 5.3 per cent would be necessary in order to remain at a static level of development. Since only a few of these countries achieve this rate most are falling back in relative terms, to a large extent because of the detrimental impact of natural disasters.

These facts demonstrate that disaster prevention of at least the mitigation of their destructive effects must be viewed as a problem of economic and social development, too. Vulnerability studies, hazard and risk assessments and mapping, cost-benefit analyses of various alternative preventive or mitigation measures and pre-disaster planning must be considered, therefore, integral part of any national development strategy and planning in disaster-prone countries.

This the more so if one considers that most developing countries are still at the initial stages of urbanisation and industrialisation and that, according to the United Nations Habitat Conference in Vancouver 1976, "... as many human settlements will have to be made available during the next 25 years as during the whole of man's previous history." To cope with these challenging problems a major joint effort of scientists and educators, development planners, decision makers and community officials is needed. The Global Seismic Hazard assessment project (GSHAP) (Giardini and Basham 1993), proposed by the International Lithosphere Program (ILP) and sponsored by the International Council of Scientific Unions (ICSU) was completed in 1998 and made a major contribution toward these goals and to the interdisciplinary co-operation amongst the concerned scientific disciplines (Fig. 13).

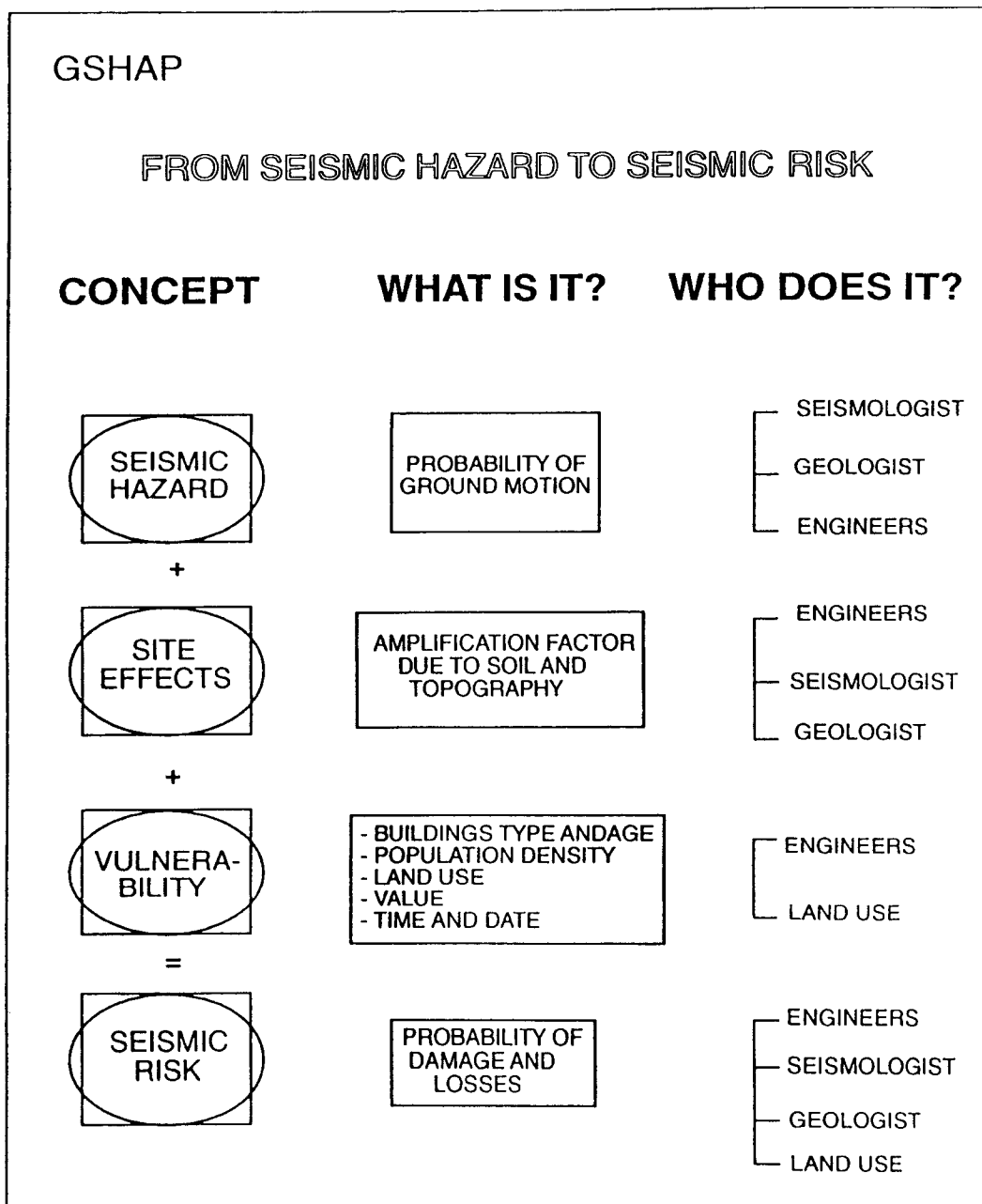


Fig. 13: The GSHAP concept from seismic hazard to seismic risk (courtesy of D. Giardini 1994).

REFERENCES

- Aki, K. (1989). Ideal probabilistic earthquake prediction. *Tectonophysics*, 169, 197-198.
- Ambraseys, N. (1980). Studies in historical seismicity and tectonics. *Earthquake Information Bulletin*, Vol. 12, No. 1, 26-35.
- Anonymous (1994). The Quito, Ecuador, earthquake risk management project. A GeoHazards International Publication, San Francisco, California.
- Anonymous (1998). Kathmandu Valley's earthquake scenario. National Society for Earthquake Technology, Kathmandu, Nepal published with support of GeoHazards International - USA.
- Anonymous (1999). The Kathmandu Valley earthquake risk management action plan. Published by the National Society for Earthquake Technology and GeoHazards International - USA, Kathmandu, Nepal.
- Bak, P., Tang, Ch. And Wiesenfeld, K. (1988). Self-organised criticality. *JGR*, Vol. 94, No. 1, July 1, 364-374.
- Bak, P. and Tang, Ch. (1989). Earthquakes as self-organised critical phenomenon. *JGR*, Vol. 94, No. B11, 15635-15637
- Bakun, W.H., Bredehoeft, J., Burford, R.O., Ellsworth, W.L., Johnson, M.J.S., Jones, L., Lindh, A.G., Mortensen, C., Roeloffs, E., Shulz, S., Segall, P. and Thatcher, W. (1986). Parkfield earthquake prediction scenarios and responses plans. *U.S. Geol. Surv., Open-File rep.*, 86-365.
- Bernard, E.N. (1989). Early warning system for tsunami is tested successfully in Chile. *Earth in Space*, Vol. 1, NO. 9, 7-10.
- Berry, M.J. (Ed.) (1989). Earthquake hazard assessment and prediction. Special issue of *Tectonophysics*, Vol. 167, No. 2-4, 81-364 pp.
- Bormann, P. (1987). Disaster prediction, prevention and mitigation - its scientific, social, economic and organisational aspects. Veröff. Zentralinstituts Physik der Erde, Potsdam, 8th International Training Course on "Seismology, Tectonics and Seismic Risk Assessment", Lectures and Exercises, Vol. II, 302-312.
- Bormann, P. (1990). Können unterirdische Kernwaffentests Erdbeben auslösen? *Wissenschaft und Fortschritt*, 40, 10, 293-286.
- Bormann, P. (1994). Earthquake prediction: Lessons learned from China. In: Internat. Training Course on Seismology and Seismic Hazard Assessment, Lecture and Exercise Material, Vol. II, GeoForschungsZentrum Potsdam, 324-327.
- Boschi, E. and Dragoni, M. (Eds.). (1992). Earthquake prediction. *Il Cigno Galileo Galilei di Arte e Scienza*, Roma, 610 pp.
- Brehm, D. and Braile, L. (1998). Intermediate-term earthquake prediction using precursory events in the New Madrid seismic zone. *Bull. Seism. Soc. Am.*, **88**, 2, 564-580.
- Cluff, J.S. (1971). Peru earthquake of May 31, 1970: Engineering geology observations, *Bull. Seis. Soc. Am.*, 61, 3, 511-534.
- Coontz, R. (1998). Can we ever know in advance when an earthquake will strike? There are no easy answers, but plenty of seismologists want to keep looking. *New Scientist*, October 1998, 36-40.
- Cornell, C.A. and Weinstein, St.R. (1988). Temporal and magnitude dependence in earthquake recurrence models. *BSSA*, Vol. 78, No. 4, 1522-1437.
- Crampin, S. (1999). Stress-forecasting earthquakes. *Seism. Res. Letters*, Vol. 70, No. 3, 291-293.

- Espinoza-Aranda, J.M., Jimenez, A.O.C., Ibarrola, G., Alcantar, F., Aguilar, A., Inostroza, M., Maldonado, S. (1995). Mexico City seismic alert system. *Seismolog. Res. Letters*, Vol. 66, Nr. 6, 42-53.
- Gasparini, P., Scarpa, R. and Aki, K. (Eds.) (1992). *Volcanic Seismology*. Springer Verlag Berlin-Heidelberg, 572 pp.
- Geller, R.J. (1991). Shake-up for earthquake prediction. *Nature*, Vol. 352, 275-276.
- Geller, R.J. (1997a). Earthquake prediction: a critical review. *Geophys. J. Intern.*, **131**, 425-450.
- Geller, R.J. (1997b). Predictable publicity. *Seismol. Res. Letters*, Vol. 68, No. 4, 477-480.
- Geller, R.J., Jackson, D.D., Kagan, Y.Y., Mulargia, F. (1997). Earthquakes cannot be predicted. *Science*, Vol. 275, 1616-1617.
- German IDNDR-Committee (1994). Projects for the understanding and mitigation of natural disasters. *International Decade for Natural Disaster Reduction*; published by Grube & Speck, Karlsruhe, 307 pp.
- Giardini, D. and Basham, P. (Eds.) (1993). *Global Seismic Hazard Assessment Program for the UN/IDNDR*. *Annali di Geofisica*, Vol. XXXVI, No. 3-4, 257 pp.
- Giardini, D. (1994). Personal communication.
- Gu G. & Ma X. (Eds.) (1984). On continental seismicity and earthquake prediction. *Proceedings of an international conference*, Seismological Press, Beijing, 867 pp.
- Guidoboni, E. and Stucci, M. (1993). The contribution of historical records of earthquakes to the evaluation of seismic hazard. *Annali di Geofisica*, Vol. XXXVI, No. 3-4, 201-216.
- Harris, R.A. (1998). Forecasts of the 1989 Loma Prieta, California, earthquake. *Bull. Seism. Soc. Am.*, **88**, 4, 898-916.
- Hellweg, P. (1994). Das Parkfield-Experiment zur Erdbevendevorhersage - Erfolg oder Mißerfolg? Lecture at the GeoForschungsZentrum Potsdam, 13.10.1994.
- Hui, Li and Kerr, R.A. (1997). Warnings precede Chinese tremblors. *Science*, Vol. 276, 526.
- Hurtig, E. and Stiller, H. (1984). *Erdbeben und Erdbebengefährdung*. Akademie-Verlag Berlin, 328 pp.
- International Decade for Natural Disaster Reduction (1991). *Organization and tasks of the German Committee to the IDNDR*, 35 pp.
- IAEE (International Association for Earthquake Engineering) (1984). *Earthquake resistant regulations: A world list - 1984*. Tokyo, 904 pp.
- Ito, K. and Matsuzaki, M. (1990). Earthquakes as self-organized critical phenomena. *JGR*, **95**, B5, 6853-6860.
- Jacob, K. (1984). Estimates of long-term probabilities for future great earthquakes in the Aleutians. *Geophysical Research Letters*, Vol. 11, No. 295-298.
- Kanamori, H. (1980). The size of earthquakes. *Earthquake Information Bulletin*, Jan.-Febr. 1980, Vol. 12, No. 1, 10-15.
- Keilis-Borok, V.I. (1990). Introduction: Non-linear systems in the problem of earthquake prediction. *Physics Earth Planet. Inter.*, **61**, 1-7.
- Kelleher, J., Sykes, L.R. and Oliver, J. (1973). Possible criteria for predicting earthquake locations and their application to major plate boundaries of the Pacific and the Caribbean. *J. Geophys. Res.*, Vol. 78, 2547-2585.
- Korvin, G. (1992). *Fractal Models in the Earth Sciences*. Elsevier, Amsterdam, 396 pp.

- Kitazawa, K. (1982). Earthquake prediction and public response. *Impact of Science on Society*, 32, 29-37.
- Lander, J.F. (1986). THRUST - Final Report. U.S. National Geophysical Data Center, Boulder, Colorado.
- Lerner-Lam, A.L. (1997). Predictable debate. *Seismol. Res. Letters*, Vol. 68, No. 3, 381-382.
- Mark, R.K. and Stuart-Alexander, D.E. (1977). Disasters as a necessary part of benefit-cost analysis. *Science*, 197, 1160-1162.
- Maskrey, A. (1997). Report on national and local capabilities for early warning. Prepared for the IDNDR Secretariat Geneva. Printed by GeoForschungsZentrum Potsdam, Germany, 1999, in conjunction with the International IDNDR-Conference on Early Warning Systems for the Reduction of Natural Disasters (EWC'98), F1-30.
- Ma Zongjin, Fu Zhengxiang, Zhang Yingzhan, Wang Chengmin, Zhang Guomin, Liu Defu (1990). Earthquake prediction - nine major earthquakes in China. Seismological Press Beijing and Springer Verlag Berlin Heidelberg, 332 pp.
- McGuire, R.K. (1993). Computations of seismic hazard. *Annali di Geofisica*, Vol. XXXVI, No. 3-4, 181-200.
- Miletti, D. and Sorensen, J. (1990). Communication of emergency public warnings: A social science perspective and state-of-the-art assessment. Oak Ridge National Laboratory.
- Miletti, D. and O'Brien, P. (1992). Warnings during disaster: normalizing communicated risk. In: *Social Problems*, Vol. 39, No. 1.
- Mogi, K. (1985). Earthquake prediction. Academic Press, Tokyo, 355 pp.
- Morgan, F.D., Wadge, G., Latchman, J., Aspinall, W.P., Hudson, D. and Samstag, F. (1988). The earthquake hazard alert of September 1982 in Southern Tobago. *BSSA*, Vol. 78, No. 4, 1550-1562.
- Muir-Wood, R. (1993). From global seismotectonics to global seismic hazard. *Annali di Geofisica*, Vol. XXXVI, 3-4, 153-168.
- Mulargia, F. (1997). Retrospective validation of the time association of precursors. *Geophys. J. Intern.*, 131, 500-504.
- Nakamura, Y. (1996). Real-time information system for hazards mitigation: UrEDAS, HERAS and PIC. *Quart. Report of Railway Tech. Res. Inst., Japan*, Vol. 37, 112-127.
- Nanometrics (1994). Early warning system for Taiwan. *Nanometrics News*, March 31, Vol. 1.
- National Research Council (1991). Real-time earthquake monitoring, early warning and rapid response. National Academy Press, Washington D.C., 1-52.
- Nishenko, St. P. and Sykes, L.R. (1993). Comment on "Seismic gap hypothesis: Ten years after" by Y.Y. Kagan and D.D. Jackson. *JGR*, Vol. 98, No. B6, 9909-9916.
- Petrovski, J. (1991). Modelling and assessment of seismic vulnerability and risk for earthquake disaster management. *Proc. 1st International Conference on "Seismology and Earthquake Engineering"*, May 27-29, 1991, Teheran, Vol. II, 1209-1225.
- Punongbayan, R.S. (1998). Early warning for the 1991 eruptions of Pinatubo volcano: a success story. Abstract. In: *International IDNDR-Conference on Early Warning Systems for the Reduction of Natural Disasters (EWC'98)*, Potsdam, Germany, 7-11 September 1998, GeoForschungsZentrum Potsdam, Programme and Abstract Volume, p. 34.
- Reiter, L. (1990). Earthquake hazard analysis. Columbia University Press, New York, 254 pp.
- Rhoades, D.A. and Evison, F.F. (1989). Time-variable factors in earthquake hazard. *Tectonophysics*, 167, 201-210.

- Rikitake, T. (1987). Earthquake precursors in Japan: precursors time and detectability. *Tectonophysics* 136, 265-282.
- Rikitake, T. (1988). Earthquake prediction: an empirical approach. *Tectonophysics* 148, 195-210.
- Sadovsky, M.A. and Pisarenko, V.F. (1990). *Seismic process in block medium*, Nauka, Moscow.
- Science Council of Japan (1989). In: *Information Bulletin of the Pacific Science Association*, Honolulu, Vol. 42, No. 1, p. 21.
- Shimozuru, D. (1988). Role of the Co-operating Committee Hazard Mitigation and the evacuation. In: *The 1986-87 eruption of Izu-Oshima volcano*. Earthquake Research Institute, Univ. of Tokyo, 61 pp.
- Silver, P. Why is earthquake prediction so difficult? *Seism. Res. Letters*, Vol. 69, No. 2, 111-113.
- Sykes, L.R. (1996). Intermediate- and long-term earthquake prediction. *Proc. Natl. Acad. Sci. USA*, Vol. 93, 3732-3739.
- Tilling, R.I. (Ed.) (1989). *Volcanic Hazard*. American Geophysical Union, Washington, Short Course in Geology: Vol. 1, 123 pp.
- Toksöz, M.N., Dainty, A.M. and Bullitt, T. (1990). A prototype earthquake warning system for strike-slip earthquakes. *PAGEOPH*, Vol. 133, No. 3, 145-187.
- Turcotte, D.L. (1992). *Fractals and chaos in geology and geophysics*. Cambridge University Press, 211 pp.
- Tsuchiya, Y. and Shuto, N. (1995). *Tsunami: progress in prediction, disaster prevention and warning*. Kluwer Academic Publishers, Dordrecht, *Advances in Natural and Technological Hazards Research*, Vol. 4, 336 pp.
- UNDRO (1979). *UNDRO Expert Group Meeting on Vulnerability Analysis, 9-12 July 1979*, Geneva.
- United Nations (1976 a). *Disaster prevention and mitigation: A compendium of current knowledge*. Vol. 1 - *Volcanological Aspects*. Geneva, 38 pp.
- United Nations (1976 b). *Guidelines for disaster prevention*. Vol. 1: *Pre-disaster physical planning of human settlements*. Geneva, 93 pp.
- United Nations (1976 c). *Conference on Human Settlements*, Vancouver, Canada, Conference background paper A/Conf. 70/B/7, 24 February 1976.
- United Nations (1978). *Disaster prevention and mitigation: A compendium of current knowledge*, Vol. 5 - *Land use aspects*. New York, 61 pp.
- United Nations (1979 a). *Disaster prevention and mitigation: A compendium of current knowledge*, Vol. 7 - *Economic aspects*. 48 pp.
- United Nations (1979 b). *Disaster prevention and mitigation: A compendium of current knowledge*, Vol. 10 - *Public information aspects*. 142 pp.
- United Nations (1980). *Disaster prevention and mitigation: A compendium of current knowledge*, Vol. 9 - *Legal aspects*. New York, 67 pp.
- United Nations (1984). *Disaster prevention and mitigation: A compendium of current knowledge*, Vol. 11 - *Preparedness aspects*. 218 pp.
- United Nations (1986). *Disaster prevention and mitigation: A compendium of current knowledge*, Vol. 12 - *Social and sociological aspects*. 48 pp.
- United Nations (1990). *Resolution A/RES/44/236 on the International Decade for Natural Disaster Reduction*, 20 March 1990.
- United States Department of the Interior (1990). *Early warning alert system*. Geological Survey, Western Region, Menlo Park, California 94025, Release of the public Affairs Office, 3 pp.

- Varatsos, P. and Alexopoulos, K. (1984 a). Physical properties of the variations of the electric field of the Earth preceding earthquakes. Part I. *Tectonophysics*, Vol. 110, 73-98.
- Varatsos, P. and Alexopoulos, K. (1984 b). Physical properties of the variations of the electric field of the Earth preceding earthquakes. Part II Determination of epicentre and magnitude. *Tectonophysics*, Vol. 110, 99-125.
- Vittori, E., Labini, St.S. and Sera, L. (1991). Palaeoseismology: Review of the state-of-the-art. *Tectonophysics*, 193, 9-32.
- Wang, T. (1987): English abstract in *Geology and Seismology*, Beijing.
- Wenzel, F., Oncescu, M.C., Baur, M., Fiedrich, F. (1999). An early warning system for Bucharest. *Seismolog. Res. Letters*, Vol. 70, No. 2, 161-169.
- Whiteside, L.S. (1998). Earthquake prediction is possible. *Seismol. Res. Letters*, Vol. 69, No. 4, 287-286.
- Whittaker, J.P. (1990). Warning systems and information dissemination in a major incident. In: *Disaster Management*, Vol. 3, No. 1.
- Wu, Y.M., Shin, T.C., Chen, C.C., Tsai, Y.B., Lee, W.H.K., and Tang, T.L. (1997). Taiwan rapid earthquake information release system. *Seism. Res. Letters*, Vol. 68, 931-943.
- Wu, Y.M., Chung, J.-K., Shin, T.C., Hsiao, N.C., Tsai, Y.B., Lee, W.H.K., Teng, T. (1999). Development of an integrated seismic early warning system in Taiwan. *Terrestrial, Atmospheric and Oceanic Sciences*, Taiwan, in print.
- Wyss, M. (Ed.) (1991). Earthquake prediction. Special issue of *Tectonophysics*, Vol. 193, No. 4, 253-412.
- Wyss, M. (1997). Cannot earthquakes be predicted? *Science*, Vol. 278, 487.
- Yamazaki, F., Meguro, K. and Katayama, T. (1993). A quick look report on the Hokkaido-Nansei-Oki earthquake, July 12, 1993. Special Issue of INCEDE Newsletter, Institute of Industrial Science, The University of Toyo, 12 pp.

SEISMICITY AND SEISMOTECTONICS IN ASIA

Zhang Peizhen and Chen Yong

China Seismological Bureau, Beijing 100036, China
Fax: +86-10-6821 5973; E-mail:peizhen@public3.bta.net.cn

1. INTRODUCTION

Continental Asia is a region with a high level of seismic hazard (Ma et al., 1989; Zhang, 1993). The tectonic setting of most of the region is intraplate continental interior with the exception of the Himalayan frontal arc that is associated with the collision between Indian plate and Eurasian plate (Molnar and Tapponnier, 1975; Tapponnier and Molnar, 1977). Statistics of global earthquakes from 1900 to 1985 indicate that 13 percent of shallow-depth earthquakes ($M_s \geq 7$) occurred in the interior of the continents (intraplate). Eighty percent of these continental earthquakes occurred in continental China (Feng Hao, 1989). There have been 9 great earthquakes ($M_s \geq 8$) and 80 large earthquakes ($8 > M_s \geq 7$) between 1900 and 1985, which account for more than a 1/3 of the total amount of earthquakes that have occurred in continental Asia between 1900 and 1986.

Although only 13 percent of all global earthquakes occur in the interior of the continents, the resulting social and economic impact are no less than that from the other 87 percent earthquakes occurred along the plate boundaries which commonly occur offshore as subduction zone, middle ocean ridge, and transform fault earthquakes. The continental earthquakes cause widespread loss of life, property damage, and social and economic disruption. For example, the nine $M_s > 7$ earthquakes that successively struck China from 1966 to 1978 (Ma et al., 1989) are a tragic example of seismic disasters. These nine earthquakes occurred in densely populated areas and caused approximately 300,000 casualties and more than 2 billion US dollars in economic damage. Thus, seismic hazards pose a major threat to the social and economic development of China.

2. SEISMOTECTONICS OF CONTINENTAL ASIA

Late Quaternary deformation of continental Asia is distributed over a vast region, and includes a full spectrum of deformational styles and structural orientations. Much, if not all, of the deformation can be attributed to the collision and subsequent penetration of the Indian plate with respect to Eurasia (for example, Molnar and Tapponnier, 1975, 1978; Tapponnier and Molnar, 1977, 1979). The occurrence and distribution of strong earthquakes are the manifestation and result of this deformation. The locations of earthquakes, especially large earthquakes, are not uniformly and randomly distributed -- rather cluster in belts and regions of prominent late Quaternary tectonic activity (Fig.1) (Tapponnier and Molnar, 1977; Molnar and Deng, 1984).

2.1 Himalayan Frontal Arc

Intense seismic activity associated with the Himalayan Frontal Arc affects India, Nepal and Bangladesh. The approximately 2000 km long Himalayan Frontal Arc (from the western syntaxis in Kashmir to the eastern syntaxis in Assam) has been very active seismically (Fig.1). More than a dozen earthquakes of $M_S > 7.5$ have occurred in this region since 1897 (Gupta, 1993). The seismic activity in the Himalayan Frontal Arc is the result of continued collision between the Indian and Eurasian plates (Molnar and Tapponnier, 1975; Tapponnier and Molnar, 1977; Curry et al., 1979; Le Dian et al., 1984; Gupta and Bhatia, 1986). Three fault zones dominate the deformation of the Himalayan frontal Arc: the Main Central Thrust (MCT), the Main Boundary Thrust (MBT), and the Frontal Thrust. It appears that tectonic activity has been shifting from the MCT and MBT in the north to the Frontal Thrust in the south, along which the Indian sub-continent underthrusts beneath the Himalayas (Molnar and Lyne-Caen, 1989).

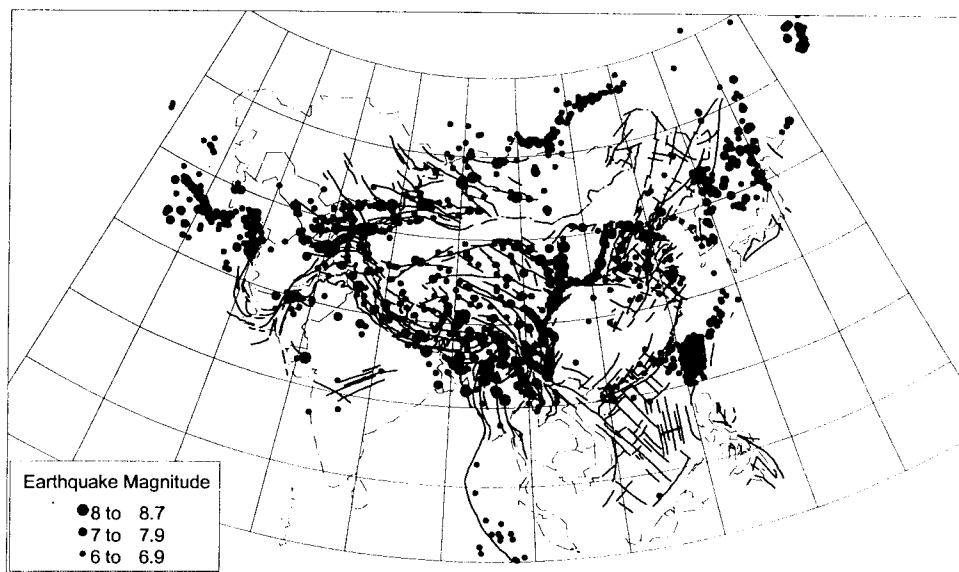


Fig.1: Seismotectonic map of continental Asia. Thin lines are active faults. Solid dots are earthquakes of magnitude equal and greater than 6.0. Lightly shaded areas are the regions discussed in the text. 1 is the Himalayan Frontal Arc region, 2 is the Tibetan Plateau region, 3 is the Northern and eastern margin of the Tibetan Plateau, 4 is the Yunnan and Sichun region, 5 is the Myanmar (Burma) region, 6 is the Northern China region, and 7 is the Pamir-Tianshan-Mongolia region.

The 2000 km long Himalayan Frontal Arc experienced four great earthquakes ($M_S > 8$) in the short span of 53 years (Gupta, 1993): the Shillong earthquake of 1897; the Kangra earthquake of 1905; the Bihar-Nepal earthquake of 1934; and the Assam-Chayu earthquake of 1950. These four earthquakes may have ruptured 1400 km of the Frontal Arc. The remaining 600 km of the Himalayan Frontal Arc were partially, or possibly totally, ruptured by large ($M_S \geq 7$) earthquakes in 1803 and 1833. The extent of this rupture associated with these two

earthquakes is poorly constrained. If these two earthquakes did not rupture the entire 600 km, then the unruptured portion must be considered likely to rupture in the near future, possibly in a great earthquake. Repeat time for an earthquake of $M_S \geq 8$ is estimated to be 200 to 270 years, and the amount of time required for the entire Himalayan Frontal Arc to be ruptured in a series of large or great earthquakes is between 180 and 240 years (Seeber and Ambruster, 1981).

2.2 Tibetan Plateau

Although many great earthquakes have occurred along the margins of the Tibetan plateau, the world's highest plateau itself also has experienced great earthquakes. More than 30 earthquakes with $M_S > 7$ have occurred in the interior of the Tibetan Plateau, and five of them are $M_S \geq 8$ (Gu, 1983; Ma, 1989).

Fault plane solutions of 23 well constrained earthquakes show normal and strike-slip mechanism with consistent T-axes oriented between east-west and northwest-southeast (Chen and Molnar, 1983; Molnar and Lyon-Caen, 1989; Ni and York, 1978). There appears to be geographic variation in the style of faulting. Earthquakes that occurred closest to the highest Himalayas show nearly pure normal faulting, but farther north, strike-slip and normal faulting seem to be equally common (Molnar and Lyon-Caen, 1989). Active fault studies in the central Tibetan Plateau also reveal this pattern of normal and strike-slip faulting (Armijo et al., 1986; Wu et al., 1992). The southern part of the Tibetan Plateau is characterized by a series of north-south trending grabens. Surface ruptures associated with major earthquakes often occur along boundaries of these active grabens. For example, the 1952 Dangxiong, Tibet, earthquake was associated with a 57-km long surface rupture zone along the basin boundary. The maximum displacement was 5.5 m and the horizontal offset was 3.6 m (Wu et al., 1992).

2.3 Northern and eastern margin of the Tibetan Plateau

Crustal shortening is the predominant late Cenozoic tectonic process in this area as the Tibetan Plateau is apparently being overthrust to the north and to the east, with much of this deformation accommodated by several prominent left-lateral strike-slip faults such as the Altyn Tagh and Haiyuan faults (Peltzer and Tapponnier, 1988; Institute of Geology, 1993). Mapped active reverse faults and reverse faults with a strong strike-slip component dominate this belt of deformation. Fault plane solutions of earthquakes also show thrust faulting with a strike-slip component (Molnar and Lyon-Caen, 1989).

Four earthquakes of $M_S > 7$ have occurred in this region during the twentieth century. Each of the earthquakes was associated with surface ruptures of over 100 km in length (Zhang et al., 1987; Peltzer and Tapponnier, 1988; Institute of Geology, 1993). The 1920 Haiyuan earthquake caused 220,000 deaths and destroyed thousands of towns and villages (Zhang et al., 1987). This earthquake had $M_S = 8.6$ and created about 300 km of surface rupturing (Zhang et al., 1987). Only seven years after the Haiyuan earthquake, an earthquake of $M_S = 7.9$ (the Gulang earthquake) occurred in less than 100 km west of the Haiyuan surface rupture zone. This earthquake also resulted in significant casualties and economic losses.

2.4 Yunnan - Sichun

Yunnan - Sichun is another seismically active region. There have been 32 earthquakes with $M_s > 7$ since the beginning of documented history in the region 1500 years ago (Gu, 1983; Ma, 1989). Two events among them have $M_s > 8$. These earthquakes caused a great number of casualties and significant economic damage.

Earthquakes in this region are characterized by shallow strike-slip faulting (focal depths between 10 and 15 km; Allen et al., 1989; Zhou et al., 1984). The seismicity of the region may be divided into two sub-regions, the western Sichun-eastern Yunnan sub-region and the western Yunnan sub-region (Fig.1). Earthquakes in the western Sichun-eastern Yunnan sub-region occur mainly in the northwestern trending Xianshuihe and the north-trending Xiaojiang fault systems. The Xianshuihe fault is a 450 km long left-lateral strike-slip fault with a Holocene slip rate of 13 mm/yr. Nine earthquakes with $M_s > 7$ have occurred along this fault zone. The latest one, the 1973 Luhuo earthquake ($M_s = 7.9$) was associated with 90 km of surface rupture and a maximum left-lateral displacement of 6 meters (Tang et al., 1982). To the south, the Xianshuihe fault, which curves into the north-south trending Xiaojiang fault, also is a source of strong earthquakes. For example, the 1833 Songming earthquake ($M_s = 8$) occurred along this fault.

Earthquakes are widely distributed in the western Yunnan seismic sub-region. Both major active faults with lengths of several hundred kilometers (i.e. the Red River and Jingsha Jiang faults), and short faults with different orientations host occurrences of strong earthquakes in the western Yunnan sub-region (Fig. 1). The frequency of occurrence of earthquakes in this sub-region is the highest within China. This very active seismic sub-region is part of the Assam-Yunnan-Myanmar earthquake region resulting from penetration of the Indian plate into the Eurasian plate (Molnar and Tapponnier, 1975; Tapponnier and Molnar, 1977; Tapponnier et al., 1982; Le Dain et al., 1984; Gupta, 1993).

2.5 Myanmar (Burma) region

Seismotectonic processes in the Myanmar region are very complex (Le Dian et al., 1984). This region accommodates the large strike-slip movement of India with respect to Southeast Asia (Le Dain et al., 1984; Gupta and Bhatia, 1986, 1993). At least nineteen earthquakes of $M_s > 7$ have occurred in the region. The great Arakan earthquake of 1762 caused extensive changes in the level of the Myanmar (Burma) coast (Richter, 1958). The 1878 earthquake caused uplift of 6 m on the west coast of Ramree island, while another island seems to have disappeared (Richter, 1958). Another event in 1843 was associated with the eruption of mud volcanoes.

2.6 North China region

The North China basin is an extensional region of high seismic hazard. Strike-slip and normal faults are the predominant active structures in the North China region (Fig. 1). The regional extension is probably caused, in part, by southeastward extrusion of southeastern Asia with respect to Eurasia (Tapponnier and Molnar, 1977; Peltzer et al., 1988). There have been 6 earthquakes of $M_s \geq 8$ and 16 earthquakes of $M_s \geq 7$ in this region during the past 2000 years (Gu, 1983, Ma, 1988). Major earthquakes generally occur along major active faults that

bound large basins. Fault-plane solutions of earthquakes are commonly right-lateral strike-slip with a normal dip-slip component.

Although earthquake recurrence intervals along any individual fault are relatively long (usually in the range of several thousand years), the composite recurrence interval for the whole region is in the order of a few decades (Ma et al., 1984, 1989). The region is densely populated, and is the cultural and economic center of China. Every earthquake of $M_s \geq 6$ has the potential for causing serious loss of life and economic damage (Ma et al., 1989). Five earthquakes with $M_s > 7$ occurred in this region within the decade between 1966 and 1976. These earthquakes resulted in hundreds of thousands of casualties and significant economic damages. The 1976 Tangshan earthquake is a tragic example of the nature of seismic hazard in this region. During this earthquake, 240 000 people were killed and direct economic losses reached approximate \$ 1 billion RMB.

2.7 Pamir - Tianshan - Mongolia

This seismic belt is situated in the interior of continental Asia (Fig. 1). The Pamir plateau is one of the most seismically active regions in the world. Many earthquakes with $M_s > 7$ occurred in the Pamir since the beginning of this century. A zone of intermediate earthquakes dips south-southeast beneath the Pamir. This is generally taken as evidence for subduction of the cold Tianshan lithosphere beneath the Pamir (Burtman and Molnar, 1994).

Late Quaternary deformation in the Tianshan Mountain is dominated by reverse faulting and crustal shortening and associated with conjugate strike-slip faulting north of the Tianshan. The structural convergence in the Tianshan is also attributed to India's penetration into Eurasia (Nelson et al., 1987; Avouac et al., 1993; Baljinyam et al., 1993). Neotectonics in Mongolia is characterized by strike-slip faulting with thrust dip-slip components. The 1955 Gobi Altai ($M_s = 8$) earthquake was associated with 8 m left-lateral displacement and about 5 m vertical offset (Tapponnier and Molnar, 1979; Molnar and Deng, 1984; Baljinyam et al., 1993). Lake Baikal is tectonically an intracontinental rift system, characterized by normal faulting and crustal extension. There have been nine earthquakes of $M_s \geq 8$ and 22 earthquakes of $M_s \geq 7$ in the Tianshan-Mongolia-Lake Baikal seismic belt. Fault plane solutions of these earthquakes indicate east-trending reverse faulting in the Tianshan, strike-slip faulting in Mongolia, and normal faulting in the Lake Baikal region, consistent with results of late Quaternary deformation in this belt (Chen and Molnar, 1977; Tapponnier and Molnar, 1979; Molnar and Deng, 1984; Nelson et al., 1987).

3. TEMPORAL AND SPATIAL CLUSTERING NATURE OF CONTINENTAL EARTHQUAKES

On the basis of studies of active faults in the Basin and Range province of the United States, Wallace (1984) suggested a long-term pattern of temporal clustering behavior for major surface rupturing earthquakes ($M \geq 6.5$) along an individual fault zone or a seismic region. The recognition of a temporal clustering pattern implies that displacement on fault occurs in a pulse of activity for a limited period in localized belts or subprovinces, while other areas remain relatively quiet in seismicity. After a pulse of major activity in one belt or area, activity shifts to another belt or area in the same tectonic province in some unknown sequence, but does not return to the first belt or area for long time (Wallace, 1984).

The modern seismicity in continental Asia also shows apparent periodicity (temporal clustering); that is, the occurrence of strong earthquakes in a seismic region clustered in a period of time which is followed by a period of seismically quiescence. Analysis of historical earthquakes in China reveals this kind of pattern, with earthquake sequences having approximate return times of 300 years (McGuire, 1979; Ma et al., 1989).

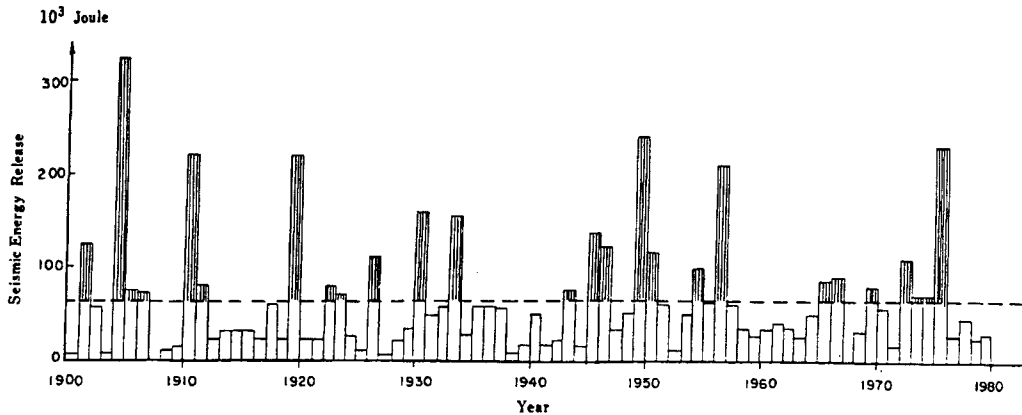


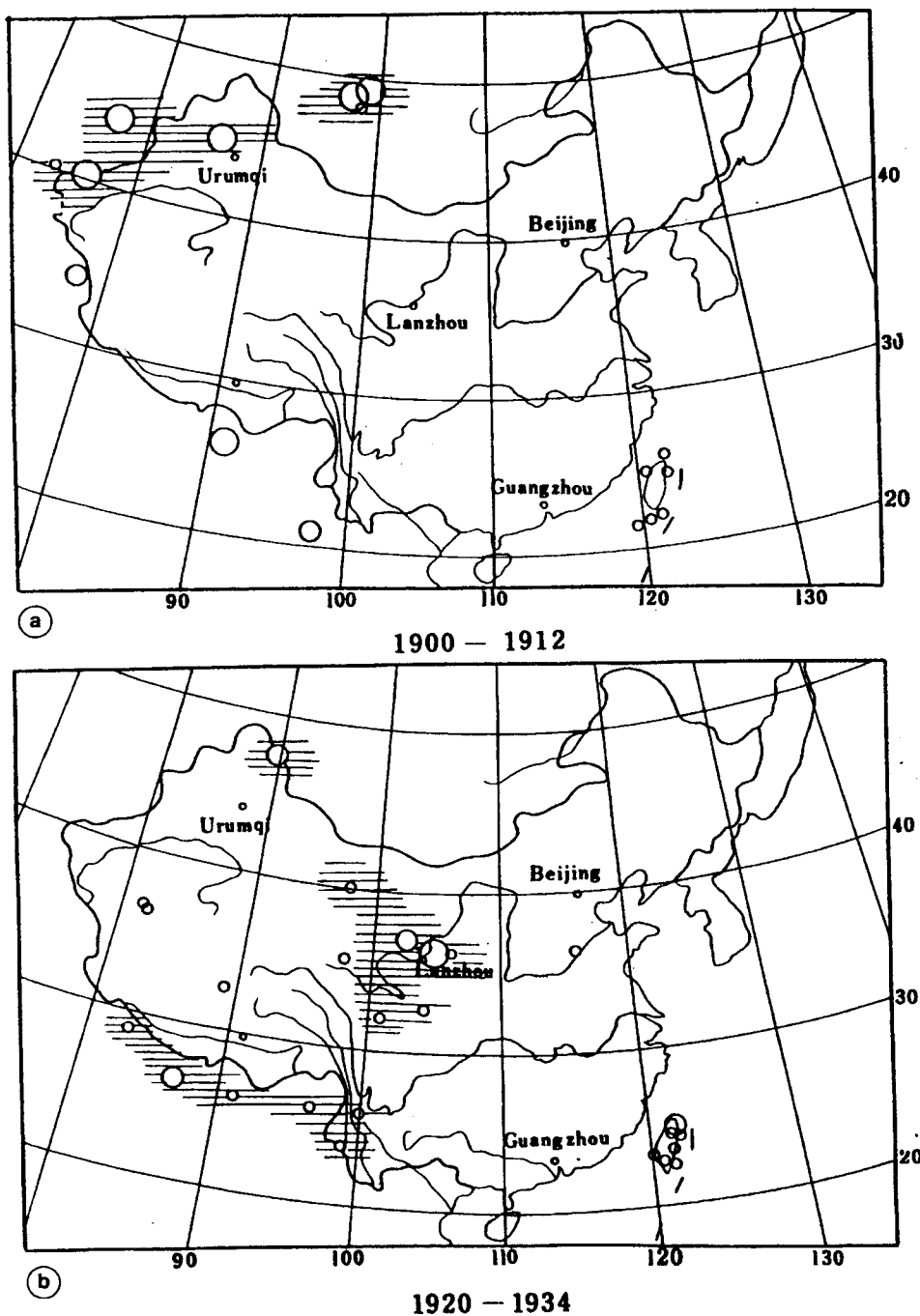
Fig. 2: Distribution of annual seismic energy release as a function of time from 1900 to 1980. The dashed line represents the normal annual seismic energy release. The shadowed bars above the dashed line are the annual seismic energy release in excess of the normal annual seismic energy release. Four episodes of seismic activity can be identified.

Several episodes of seismic activity can be further recognized within a given period of seismic activity (Ma et al., 1989). Earthquakes ($M_s \geq 6.0$) in continental China since the beginning of this century clearly reveal the pattern of clustering / quiescence as showing by seismic energy release distribution as a function of time (Fig. 2). The normal annual seismic energy release is defined as the average annual release over this century. The time episodes when the annual release of seismic energy successively exceeds the normal annual release are recognized as active episodes of seismicity. There have been 4 active episodes of seismicity in continental China since the beginning of this century (Fig. 2). These episodes occurred from 1897 to 1912, 1920 to 1934, 1944 to 1957, 1966 to 1976 with intervals that persist for an average of 13 years. Several earthquakes of $M \geq 8$ occur in each episode of activity.

Great earthquakes in an episode of seismicity mainly concentrate in one or two seismic belts or regions. In the succeeding seismic episode, earthquakes primarily occur in another (different) seismic belt and region. This pattern and behavior is similar to the long-term tectonic activity that Wallace (1984, 1987) recognized in the Basin and Range province.

Great earthquakes in the first recorded active episode of seismicity in China (Ma et al., 1989) mainly occurred in central Asia along the seismic belts of Pamir, Tianshan, and Mongolia (Fig. 3a). In the second seismic episode, earthquakes occurred along the northern and eastern margin of the Tibetan Plateau seismic belt and along the Himalaya seismic belt (Fig. 3b). Earthquakes in the third episode of activity were distributed in the seismic region of southern and eastern Tibet, and several large earthquakes also occurred in the Pamir and Mongolia

seismic regions (Fig. 3c). In the most recent seismic episode, the North China seismic region was the primary target for the occurrence of large earthquakes - the last disastrous earthquake in this episode is the 1976 Tangshan earthquake (Fig. 3d). The 1985 Wuqia earthquake ($M_s=7.4$) in the Tianshan seismic belt probably marks the onset of the fifth, and current, active episode of seismicity. If the duration of past seismic episodes is an indicator, the current episode might persist until 1995 or 2000, and we would anticipate one or more great earthquakes in this time period.



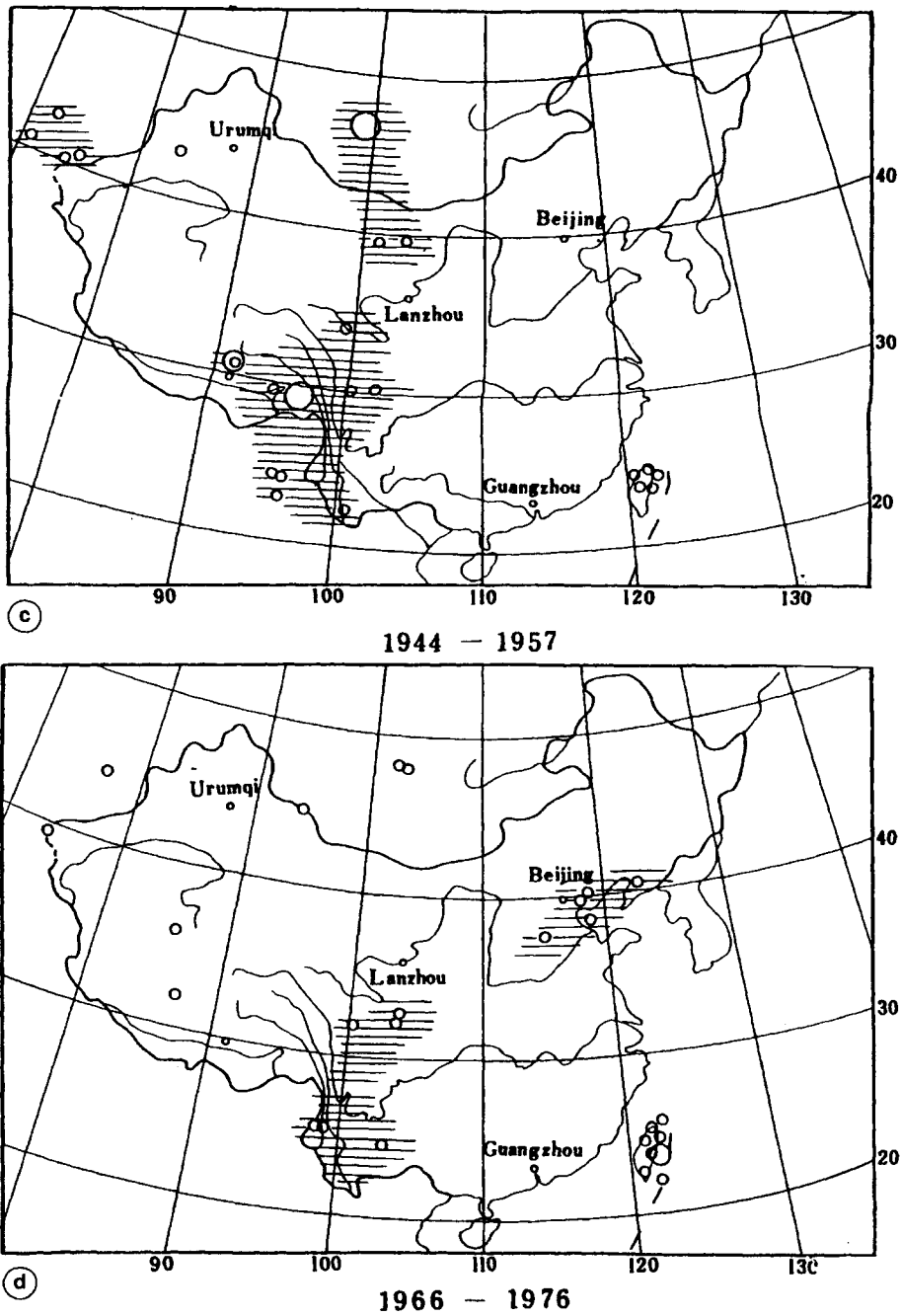


Fig.3: Spatial distribution of earthquakes during the four episodes of seismic activity in China. The shadowed areas are the regions of major earthquakes during each episode of seismic activity. (a) shows the first episode from 1897 to 1912; (b) shows the second episode from 1920 to 1934; (c) shows the third episode from 1944 to 1957, and (d) shows the last episode from 1966 to 1976.

4. CONCLUSION

Major earthquakes are widely distributed over whole China and are intimately tied with style of late Quaternary regional deformation. These earthquakes cause significant casualties and economic losses. Observations in modern pattern of seismicity and paleoseismological studies reveal irregularity of earthquake distribution in both time and space. To realistically assess seismic hazard, the temporal and spatial variations in seismic potential ought to be incorporated. To increase our ability in assessing seismic hazard, we need to incorporate more geological and geophysical information, to enhance international cooperation, to improve seismic models to describe the physical process of earthquake generation, and to use multiple approaches in each step of seismic hazard assessment.

REFERENCES

- Allen, C.R., Luo Zhuoli, Qian Hong, Wen Xueze, Zhou Huwei, and Huang Weishi (1989). Segmentation and rupture history of the Xianshuihe fault, southwestern China. U. S. Geological Survey Open-File Report 89-315, 10-31.
- Armijo, R., Tapponnier, P., Mercier, J. L., and T. Han (1986) Quaternary extension in southern Tibet: field observations and tectonic implications. *J. Geophys. Res.*, 91, 13803-13872.
- Avouac, J. P., Tapponnier, P., et al. (1993). Active Thrusting and folding Along the Northern Tianshan and late Cenozoic Rotation of the Tarim Relative to Dzungaria and Kachakhsfan. *J. G. R.*, 98, 6755-6804.
- Baljinnyam, I., Bayasgalan, B.A., Borisov, B.A., Armando Cisternas, Dem'yanovich, G.G., Ganbaatar, L., Kochetkov, V.M., Kuruchin, R.A., Peter Molnar, Herve Philip, and Vashchilov, Y.Y. (1993). Ruptures of major earthquakes and active deformation in Mongolia and its surroundings. *Geol. Soc. Am. Memoir* 181.
- Burtman, V.S., and Molnar, P. (1994). Geological and geophysical evidence for deep subduction of continental crust beneath the Pamir. *Geological Society of America Special Paper*, 281, 1-75.
- Chen, W. P. and P. Molnar (1983). Focal depths and fault plane solutions of earthquakes under the Tibetan Plateau. *J. Geophys. Res.*, 88, 1180-1196.
- Curry, J.R., Emmel, F.J., Moore, D.G., and R.W. Raitt (1979). Tectonics of the Andaman Sea and Burma. *Am. Assoc. Pet. Geol. Memoir*, 29, 189-198.
- Gu Gongxiu (1983). *Earthquake Catalog of China*. Seismological Press.
- Gupta, H.K., and Bhatia, S.C. (1986). Seismicity in the vicinity of the India and Burma board: evidence for the sinking lithosphere. *J. Geodynamics*, 5, 379-381.
- Gupta, H.K. (1993). Seismic Hazard assessment in the Alpine belt from Iran to Burma. *Annali di Geofisica*, XXXVI, 61-82.
- Institute of Geology, State Seismological Bureau (1993). *Active faults along the Qiliang Shan-Hexi Corridor*. China, Seismological Press.
- Le Dain, A.Y., Tapponnier, P., and P. Molnar (1984). Active faulting and tectonics of Burma and surroundings. *J. Geophys. Res.*, 89, 453-472.
- Ma Zongjin, Fu Zhengxiang, Zhang Yingzhen, Wang Chengmin, Zhang Guomin, Liu Defu (1989). *Earthquake Prediction: nine major earthquakes in China*. Seismological Press and Springer-Verlag.
- Ma Xingyuan (1989). *Lithospheric dynamics atlas of China*. China Cartographic Publishing House, Beijing.
- McGuire, R. K. (1979). Adequacy of simple probability models for calculating felt-shaking hazard, using the Chinese earthquake catalog. *Bull. Seism. Soc. Am.*, 69, 877-892.

- Molnar, P. and Q. Deng (1984). Faulting associated with large earthquakes and average rate of deformation in central and eastern Asia. *J. Geophys. Res.*, 89, 6203-6227.
- Molnar, P. and H. Lyon-Caen (1989). Fault plane solutions of earthquakes and active tectonics of the Tibetan Plateau and its margins. *Geophys. J. Int.*, 99, 123-153.
- Molnar, P. and P. Tapponnier (1975). Cenozoic tectonics of Asia: Effects of a continental collision. *Science*, 189, 419-426.
- Molnar, P. and P. Tapponnier (1978). Active tectonics of Tibet. *J. Geophys. Res.*, 83, 5361-5374.
- Nelson, M.R., McCaffey, R., and P. Molnar (1987). Source parameters for 11 earthquakes in the Tien Shan, Central Asia, determined by P and Sh waveform inversion. *J. Geophys. Res.*, 92, 12629-12648.
- Ni, J., and York, J.E. (1978). Late Cenozoic extension tectonics of the Tibetan Plateau. *J. Geophys. Res.*, 83, 5377-5387.
- Paltzer, G., and Tapponnier, P. (1988). Formation and evolution of strike-slip faults, rifts, and basins during the India – Asia collision: an experimental approach. *J. Geophys. Res.*, 93, 15,085-15,117.
- Richter, C.F. (1958). *Elementary Seismology*, W.H. Freeman, San Francisco.
- Seeber, L., and J.G., Ambruster (1981). Great detachment of earthquakes along the Himalayan arc and long-term forecasting. *American Geoph. Un., Maurice Ewing Series*, 4, 259-277.
- Tang, Rongchan, Huang, Zuzhi, Qian Hong, Deng Tiangang, Jiang Lenqiang, Ge Peiji, Liu Shengli, Cao Yangguo, and Zhang Chenggui (1984). On the recent tectonic activity and earthquake of the Xianshuihe fault zone, in *Collection of Papers of the International Symposium on Continental Seismicity and Earthquake Prediction*. Seismological Press, Beijing, 347-363.
- Tapponnier, P. and P. Molnar (1977). Active faulting and Cenozoic tectonics of China. *J. Geophys. Res.*, 82, 2905-2930.
- Tapponnier, P. and P. Molnar (1979). Active faulting and Cenozoic tectonics of the Tien Shan, Mongolia, and Baikal region. *J. Geophys. Res.*, 84, 3425-3459.
- Tapponnier, P., Peltzer, G., Le Dain, A.Y., Armiji, R., and Cobbold, P. (1982). Propagating extrusion tectonics in Asia: New insights from simple experiments with plasticine. *Geology*, 10, 611-616.
- Wallace, R.E. (1984). Patterns and timing of late Quaternary faulting in the Great Basin Province and relation to some regional tectonic features. *J. Geophys. Res.* 89, 5763-5769.
- Wallace, R.E. (1987). Grouping and migration of surface faulting and variation in slip rate on faults in the Great Basin Province. *Bull. Seismol. Soc. Am.*, 77, 868-876.
- Zhang, W., Jiao, D., Zhang, P., Molnar, P., Burchfiel, B.C., Deng, Q., Wang, Y., and F. Song (1987). Displacement along the Haiyuan fault associated with the great 1920 Haiyuan China, earthquake. *Bull. Seism. Soc. Am.*, 77, 117-131.
- Wu, Z., Cao, Z., Shengto, B., and Deng, Q. (1992). *Active faults in the central Tibet*, Seismological Press.
- Zhang Peizhen, (1993). Seismic hazard assessment in continental Asia. *Annali di Geofisica*, XXXVI, 41-59.
- Zhou Huilan, Liu H.-L., and H. Kanamori (1983). Source processes of large earthquakes along the Xianshuihe fault in southwestern China. *Bull. Seismo. Soc. Am.*, 73, 171-181.

SEISMIC HAZARD IN ASIA: WHAT DO WE KNOW AFTER GSHAP? WHAT REMAINS TO BE DONE?

Chen Yong and Li Juan

China Seismological Bureau, 100036 Beijing, China
Fax: +86-10-6821 5973; E-mail: yongchen@public.bta.net.cn

1. EARTHQUAKE DISASTERS IN ASIA

Throughout the Asian history, earthquake disasters have exacted a heavy toll of death and human suffering (Fig. 1 and Table 1).

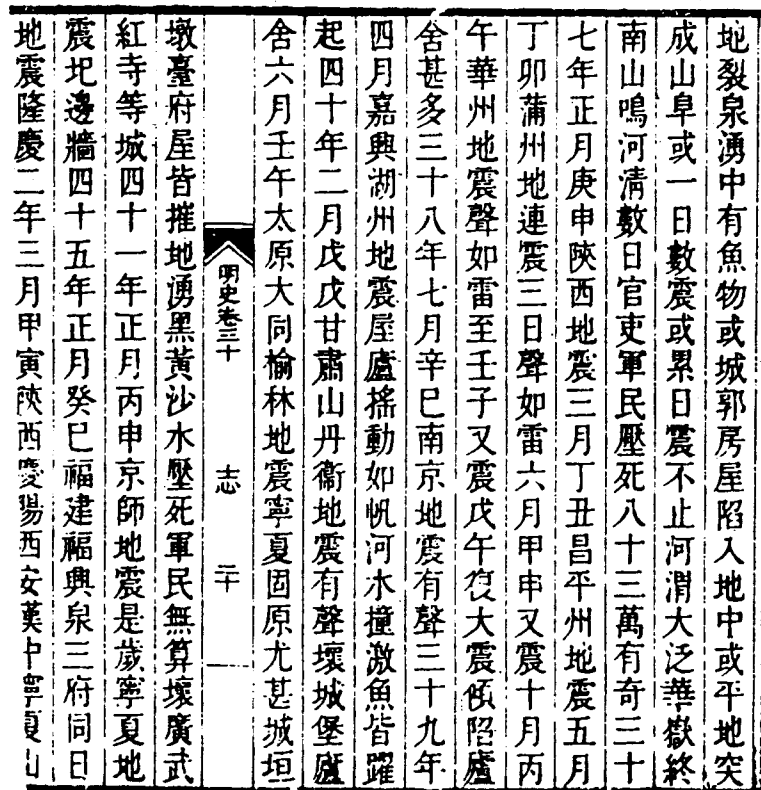


Fig. 1: Historic record: in 1556 (Ming Dynasty of China), a great earthquake occurred in the middle part of China, killed 830,000 people or more.

It can be seen from Table 1 that among the total 44 earthquakes, there are 17 earthquakes occurred in Asia. The ratios of number of death and overall losses of Asia to that of the whole world are 71% and 53% respectively.

Date	Year	Area	No. of Deaths	Overall Losses Mio US \$	Insured Losses Mio US \$
29th Feb.	1960	Marocco	13,100	120	0
21st May	1960	Chile	3,000	880	0
26th July	1963	Yugoslavia	1,070	600	0
28th March	1964	USA	131	540	10
16th June	1964	Japan	26	205	0
31th May	1970	Peru	67,000	500	14
9th Feb.	1971	USA	65	535	50
10th April	1972	Iran	5,400	5	0
23rd Dec.	1972	Nicaragua	5,000	800	100
6th Sept.	1975	Turkey	2,400	17	0
4th Feb.	1976	Guatemala	22,778	1,100	55
6th May	1976	Italy	978	3,600	0
27th July	1976	China	290,000	5,600	0
17th Aug.	1976	Philippines	3,564	120	0
24th Nov.	1976	Turkey	3,626	25	0
4th March	1977	Romania	1,387	800	0
12th Jun.	1978	Japan	28	865	2
16th Sept.	1978	Iran	20,000	11	0
15th April	1979	Yugoslavia	131	2,700	0
10th Oct.	1980	Algeria	2,590	3,000	0
23rd. Nov	1980	Italy	3,114	10,000	40
24th Feb.	1981	Greece	25	900	5
13th Dec.	1982	Yemen	3,000	90	0
31th March	1983	Columbia	250	380	40
26th May	1983	Japan	104	560	26
30th Oct.	1983	Turkey	1,346	0	0
3rd March	1985	Chile	200	1,200	90
19th Sept.	1985	Mexico	10,000	4,000	275
10th Oct.	1986	El Salvador	1,000	1,500	75
2th March	1987	New Zealand	0	350	270
5th March	1987	Ecuador	1,000	700	0
1st Oct.	1987	USA	8	358	73
7th Dec.	1988	Armenia	25,000	14,000	0
17th Oct.	1989	USA	68	6,000	900
28th Dec.	1989	Australia	12	3,200	870
21th June	1990	Iran	40,000	7,000	100
16th July	1990	Philippines	1,660	2,000	200
20th Oct.	1991	India	2,000	100	0
12th Oct.	1992	Egypt	561	300	0
12th Dec.	1992	Indonesia	2,500	100	0
29th Sept.	1993	India	9,475	280	0
17th Jan.	1994	USA	61	44,000	15,300
17th Jan.	1995	Japan	6,348	100,000	3,000
28th May	1995	Russia	1,841	100	0
4.2., 30.5.	1998	Afghanistan	9,100		
Total		560,947	218,821		
In Asia		400,551	116,773		

Table 1: Major disastrous earthquakes of the world during 1980-1998 (Munich Re, Munich, March 1999). The earthquakes occurred in Asia were marked boldly in the table.

A key question that must be addressed in earthquake disaster reduction is: how much loss might a city or region suffer in future earthquakes? There are two components comprising the basic structure of a loss estimate study. One component, the seismic hazard analysis, involves the identification and quantitative description of strong ground motion caused by future earthquakes. The second component, the seismic risk analysis, involves the vulnerability analysis of buildings and other man-made facilities to earthquake damage and the losses that may result from this damage.

The definitions of seismic hazard, vulnerability and seismic risk given by the NUDRO Expert Group (Natural disaster and vulnerability analysis, Report of Expert Group Meeting, 9-12, July, UNDRO, Geneva, 1980) are as follows:

Definition of seismic hazard:

Earthquake hazard is defined as the probability that a certain value of a macroscopic intensity or of a ground motion parameter (i.e. particle acceleration, velocity and displacement) will not be exceeded at a specific site in a specific period of time.

Definition of vulnerability:

Vulnerability is the expected degree of losses within a defined area resulting from the occurrence of earthquakes. Vulnerability is expressed on a scale from 0 (no damage) to 1 (full damage).

Definition of seismic risk:

Seismic risk is the expected degree of losses caused by earthquakes and therefore the product of seismic hazard and vulnerability:

$$\text{Risk} = \text{Hazard} \times \text{Vulnerability}$$

Elements at risk include the number of persons, the value of properties, the level of economic activities such as public service, and so on in a given area.

Seismic hazard describes the potential for dangerous, earthquake-related natural phenomena such as ground shaking, fault rupture, or soil liquefaction. These phenomena could result in adverse consequences to society such as the destruction of buildings or the loss of life. Seismic risk is the probability of occurrence of these consequences. The output of a seismic hazard analysis could be a description of the intensity of shaking of a nearby magnitude eight earthquake or a map which shows level of ground shaking in various parts of the country that have an equal chance of being exceeded.

The results of seismic hazard analysis provide a basis for anti-earthquake design, which is the main engineering measure for the reduction of earthquake disasters. The seismologists

performing seismic hazard analysis are really carrying out one part of an engineering process or one part of a social disaster reduction process. The end product of this analysis is an expression of seismic hazard or threat that is oriented toward some specific use. This product may be expressed in the form of a simple, single-value characterisation of earthquake ground motion, like Modified Mercalli Intensity (MMI), Peak Ground Acceleration (PGA), or more complex, multi-value characterisations, like response spectra. In any case it can be readily used to achieve some practical goal.

2. GSHAP

The Global Seismic Hazard Assessment Program (GSHAP) was launched in 1992 by the International Lithosphere Program (ILP) with the support of the International Council of Scientific Unions (ICSU), and endorsed as a demonstration program in the framework of the United Nations International Decade for Natural Disaster Reduction (UN/IDNDR).

In order to mitigate the risk associated with the recurrence of earthquakes, the GSHAP promotes a regionally co-ordinated, homogeneous approach to seismic hazard evaluation and the ultimate benefits are improved national and regional assessment of seismic hazards, which can be used by national decision makers, engineers in many fields such as land use planning, improved building design and construction et al.

The GSHAP was implemented during the period 1992-1998 and is coming to a conclusion. All regional activities are now completed. The publications of all regional results and of the GSHAP map of global seismic hazard are under way. Regional reports, GSHAP yearly reports, summaries and maps of seismicity, source zones and seismic hazard are on the GSHAP homepage on <http://seismo.ethz.ch/GSHAP/>.

2.1 GSHAP regions, test areas and co-operating projects

To achieve a global dimension, the GSHAP strategy established in Roma in 1992 has been established a mosaic of regions under the co-ordination of chosen regional centres. The goal in the first implementation phase (1993-1995) was to compute the seismic hazard in selected test areas, and then, in the second phase (1995-1997), to apply it to the whole continents and finally the globe. This strategy has been maintained in many of the originally established ten regions, while elsewhere the activities focussed directly on key test-areas under the co-ordination of large working groups. Some areas, specifically the Mediterranean and the Middle East, have been covered by a mosaic of overlapping projects, while elsewhere (i.e. parts of Africa and of the Western Pacific rim) the hazard mapping was obtained only at the end of the program by using published materials.

Following the Rome guidelines in 1992, the general rule has been to establish for each region or test area a working group of national experts covering the different fields required for seismic hazard assessment, to produce common regional catalogues and databases and to assess regional

hazard. GSHAP was globally co-ordinated in the 1992-97 period by ING, Roma, in the final 1997-99 period by ETH, Zurich.

The following lists and map illustrate the global coverage of GSHAP, separating GSHAP Regions, Test Areas and Co-operating Projects.

GSHAP Regions:	GSHAP Test Areas:	Co-operating Projects:
1. Central-North America; 2. South America (CERESIS); 3. Central-Northern Europe; 6. Middle East (Iran); 7. Northern Eurasia; 8. Eastern Asia; 10. South-West Pacific	Northern Andes (PILOTO); Caucasus (CAUCAS); Adriatic Sea (ADRIA); East African Rift; India-China-Tibet-Myanmar- Bangla Dash; Ibero-Maghreb.	Mexico-C. America-Caribbean-S. America (PAIGH-IDRC); Circum Pannonian Basin (EU-QSEZ- CIRPAN); Eastern Mediterranean (RELEMR, USGS/UNESCO); Mediterranean (SESAME, IGCP 382); Turkey and Neighbouring Regions.

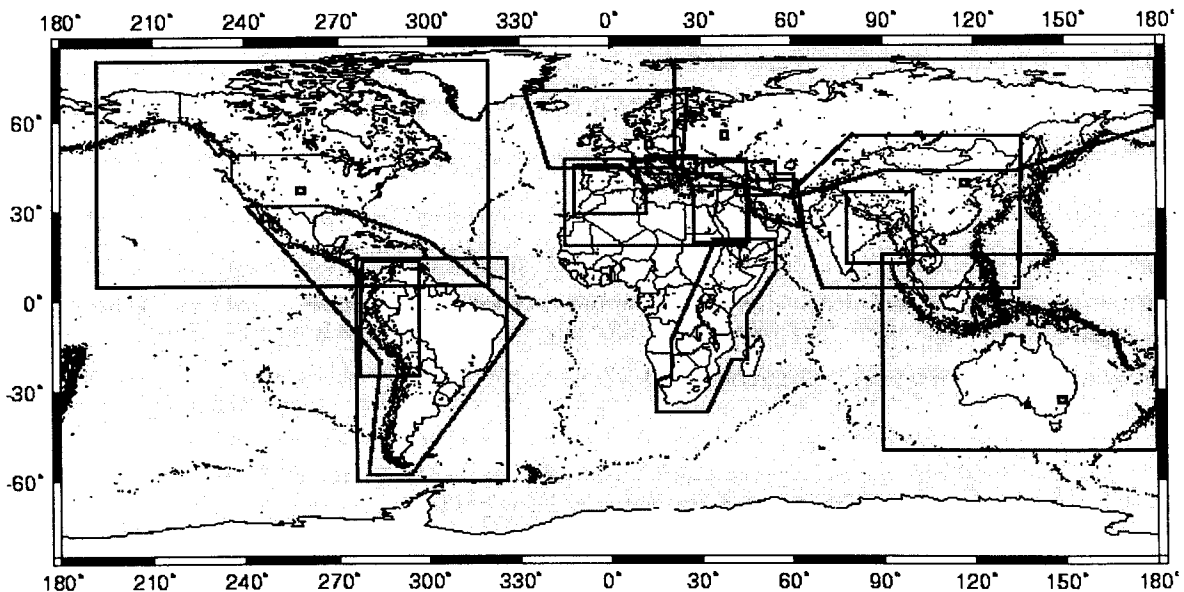


Fig. 2: The regions, test areas and co-operating projects of GSHAP.

2.2 Summary of regional activities related to Asia

Following in the original framework planned in Rome, 1992, the hazard mapping for the whole Eastern Asia originates from the expansion of the test area initially established in the border region of China-India-Nepal-Myanmar-Bangla Dash. The regional mapping has been co-ordinated by the China Seismological Bureau (CSB) Regional Centre in Beijing, in co-ordination with the other Regional Centres (JIPE, Moscow, and AGSO, Canberra) and with the direct assistance of the USGS. All Eastern Asian countries have participated directly in this regional effort, with the exclusion of Japan, for which an existing national hazard map was incorporated. In addition, the "Eastern Asia Natural Hazards Mapping" project, led by the GSJ, has compiled

seismicity maps for the whole Eastern Asia region from China to Japan to Indonesia at 1:5 million scale; planning meetings were held in Tsukuba (6/93) and Yokohama (5/94), and two technical workshops in Tsukuba (9/94, 9/95). The EANHMs project co-ordinated its activities with the GSHAP centres in Asia (SSB) and Australia (AGSO).

China-India-Nepal-Myanmar-Bangla Dash

The GSHAP test area has been established in the border region of China, India, Nepal, Myanmar and Bangla-Dash, the GSHAP Regional Centre and the NGRI of Hyderabad; it is the first time that this type of regional framework is effectively operating in the region. Activities initiated with a planning meeting in Beijing (10/93), followed by the preliminary compilation of regional catalogues and by technical workshops in Beijing (10/94) and Hyderabad (3/96), to produce the final earthquake catalogue, seismic source zoning and SHA presented at the ASC Assembly in Tangshan (8/96) and the 30th International Geological Congress in Beijing (8/96).

2.3 GSHAP global programs

Another key element of the GSHAP implementation is the pursue of activities and tasks devoted to the improvement of the global practice of seismic hazard assessment.

2.3.1 Uniform instrumental global seismic catalogue

With the aim of extending the global instrumental earthquake catalogue and database, now available since 1964 (ISC, NEIC), to cover the whole century, work is in progress at USGS and the University of Colorado, on the digital scanning and processing of the ISS and BCIS Bulletins; the relocation of a uniform global catalogue is under way, using modern travel-times and location procedures used at NEIC (Global Catalogue, E. Engdahl, USGS Boulder. engdahl@gldfs.cr.usgs.gov).

2.3.2 Software for seismic hazard assessment

The goal of across-boundary integration of seismic hazard databases and products was identified in the Rome 1992 planning meeting as crucial to the global implementation of GSHAP. The "seismotectonic probabilistic approach" was selected as a standard for global SHA application, to allow the comparison and integration of regional maps and zonations. To implement this strategy, an integrated software package dealing with all the steps of seismotectonic hazard computation, FRISK88M, has been made available free of charge by Risk Engineering for GSHAP applications to all test areas and regional centres (Software, R. McGuire, Risk Eng. Boulder, USA. m McGuire@riskeng.com; D. Mayer-Rosa, ETH Zurich, CH dieter@seismo.ifg.ethz.ch).

2.3.3 Multidisciplinary approach to seismic hazard assessment

A primary goal of GSHAP has been the implementation of a multidisciplinary approach to seismic hazard assessment introducing the results from geological disciplines dealing with active faulting (neotectonics, paleoseismology, geomorphology, geodesy) to complement the historical and instrumental records of earthquakes. This goal has been pursued with several initiatives.

The adoption of the seismotectonic probabilistic approach for global application reflects the aim to incorporate the geological input to characterise the earthquake recurrence in space and time.

The workshop on "Active Faulting Studies for Seismic Hazard Assessment", held in Erice (Sicily, 9/95), brought together specialists in active faulting studies with seismologists and engineers responsible for developing assessment methodologies and for leading major national seismic hazard programs from all continents, to explore new trends in active faulting studies and verify the extent to which the geological input is being used in seismic hazard assessment practice. The workshop produced a document of recommendations, which is being circulated world-wide.

GSHAP and the ILP Projects "II-2: Maps of major active faults" and "II-3: Earthquakes of the late Holocene" have joint activities under way and scheduled for 1995-97, including the 1996 NATO/ARW "Historical and pre-historical earthquakes in the Caucasus" and the "training course in paleoseismology and active faulting in South America" in 1997.

Scientific articles illustrating strategies and examples in multidisciplinary seismic hazard assessment have been published on proceedings volumes and scientific journals; among these, the GSHAP Volume (Annali di Geofisica, vol. 36-3, 1993) includes seminal papers on the integration of the geological input in seismic hazard assessment.

3. WHAT DO WE KNOW AFTER GSHAP-DISSEMINATION OF PRODUCTS AND RESULTS

3.1 GSHAP on the web

Regional reports, GSHAP yearly reports, summaries and maps of seismicity, source zones and seismic hazard are available freely on the GSHAP homepage on <http://seismo.ethz.ch/GSHAP/>. The page is not final yet, as a few regional products are still missing and the global map will be available in the spring 1999.

3.2 GSHAP summary volume and CD-ROM

The regional reports, detailing the compilation of the databases and of the hazard results in the GSHAP test-areas and regions, are being collected in a special volume, prepared following common guidelines, including also a CD-ROM with the earthquake databases, the seismic source zones and the regional hazard maps. The volume and CD-ROM are scheduled for release in spring 1999, published as a Special Issue of *Annali di Geofisica*.

3.3 Publications

The dissemination and publication of GSHAP ideas and results started with the GSHAP Volume (*Annali di Geofisica*, vol. 36, 3-4, 1993; 2000 copies). GSHAP activities and results have been presented at the major international and regional assemblies and meetings. Research papers and articles describing the program's approach and regional activities have appeared on scientific journals, special volumes and regional bulletins. Sessions dedicated to GSHAP have been hosted by the assemblies of IASPEI, ESC, ASC and SSA and by other international meetings. GSHAP workshops have been organised in all test areas, as listed above.

3.4 Reports

Progress reports and summaries prepared by the Co-ordinating Centre have been distributed world-wide (7/92, 11/92, 12/93, 2/94, 9/94, 6/95, 4/96, 1/97, 1/98). Periodic summaries have appeared on bulletins and newsletter of IASPEI, ICSU, ILP, AGU.

4. SUCCESSES AND EXISTING PROBLEMS

The GSHAP has fulfilled in large part the goals and design principles set in 1992. In addition to the regional and global results and products listed above, the following should be noted:

- The global standards in seismic hazard assessment have markedly improved in the last few years, with specific regards to the implementation of multi-disciplinary information, the refinement of the databases, the standardisation of the knowledge of earthquake hazards.
- National hazard maps have improved in developed countries involved in across-border co-operation (i.e. in Europe) as well as in Third-World countries with no previous experience in SHA (i.e. the African Rift). GSHAP was very aggressive in promoting multi-national co-operation in all continents, with particular emphasis in critical border areas. Some examples: S. Africa worked together with the African Rift framework in a regional scientific program; Russia, Turkey and Iran co-operated together in the Caucasus; China and India co-operated over many years in a sensitive border area; the Andean countries worked together under a unified framework program.
- SHAP was successful in attracting significant funds to regional SHA. Some examples:

NATO financed a scientific meeting in the Caucasus; the first EC-OPA Center was selected in Northern Africa; INTAS and EU funded programs with a large emphasis on coordination.

The GSHAP suffered also setbacks and right criticisms.

It failed to establish efficient large-scale regional programs in areas where significant external funding or local energies were not available (i.e. large parts of the African continent), in areas where the scientific community and the national interests are too strong (N. America), in areas where the political boundaries are still prevailing (Middle East).

- The balance between science and application was difficult to achieve, with criticisms of having chosen low scientific standards (from ICSU) clashing against criticisms of not thinking enough about applications (from the UN/IDNDR) GSHAP often interfered with national agendas and priorities, entering in competition with national programs for funding, hazard standards and agendas; in the end these clashes mostly resulted in improved hazard assessment, but they also created frictions.

- While GSHAP focussed on the establishment on regional working frameworks which were very active during the program implementation, the long term future of this co-operation is often doubtful, in absence of appropriate international frameworks, funding and guidelines.

- Disciplinary boundaries are reduced but remain strong.

- The GSHAP, like other demonstration programs, suffered also from overall limitations in the implementation of the UN/IDNDR program: changing priorities, no inter-project co-ordination, no plans for follow-up projects implementing the results of the demonstration programs in risk mitigation strategies, lack of significant start-up and operational funding. All these elements have resulted in the GSHAP to operate in a rather independent fashion within the seismological and seismic hazard assessment community. A mid-program review conducted by the IDNDR Scientific and Technical Committee helped in focussing the GSHAP results and applications.

5. WHAT REMAINS TO BE DONE?

5.1 Homogeneous approach of SHA and non-homogeneous data sources

GSHAP promotes a regionally co-ordinated, homogeneous approach to seismic hazard evaluation; the ultimate benefits are improved national and regional assessments of seismic hazards. On the other hand, the data, based on which the homogeneous approach was, are geographically distributed non-homogeneously. Let us take the historic earthquake data as an example. Fig. 3 gives the seismicity of the mainland of China since AD 1000. The Chinese earthquake catalogue is based on a rich collection of historical documentation and represents one of the longest seismicity records for an area. Because of its large sample size, it is statistically

suitable for complete analysis use. From Fig. 3 it can be seen that the older records of seismic events since AD 1000 are obviously less complete, confined to a smaller area surrounding culture activity centres, and depleted in earthquake events of small magnitude. Therefore, the historical earthquake catalogues in most regions of the world are incomplete, and the completeness varies from country to country, even from region to region within the same country. Our conclusion is that it is very difficult or very expensive to get detailed data of geological settings, active faults, paleo-seismicity, crustal deformation etc. for constructing the homogeneous SHA model in most regions of the world. We could not develop homogeneous approach of SHA based on non-homogeneous data. A new methodology of SHA should be taken into consideration.

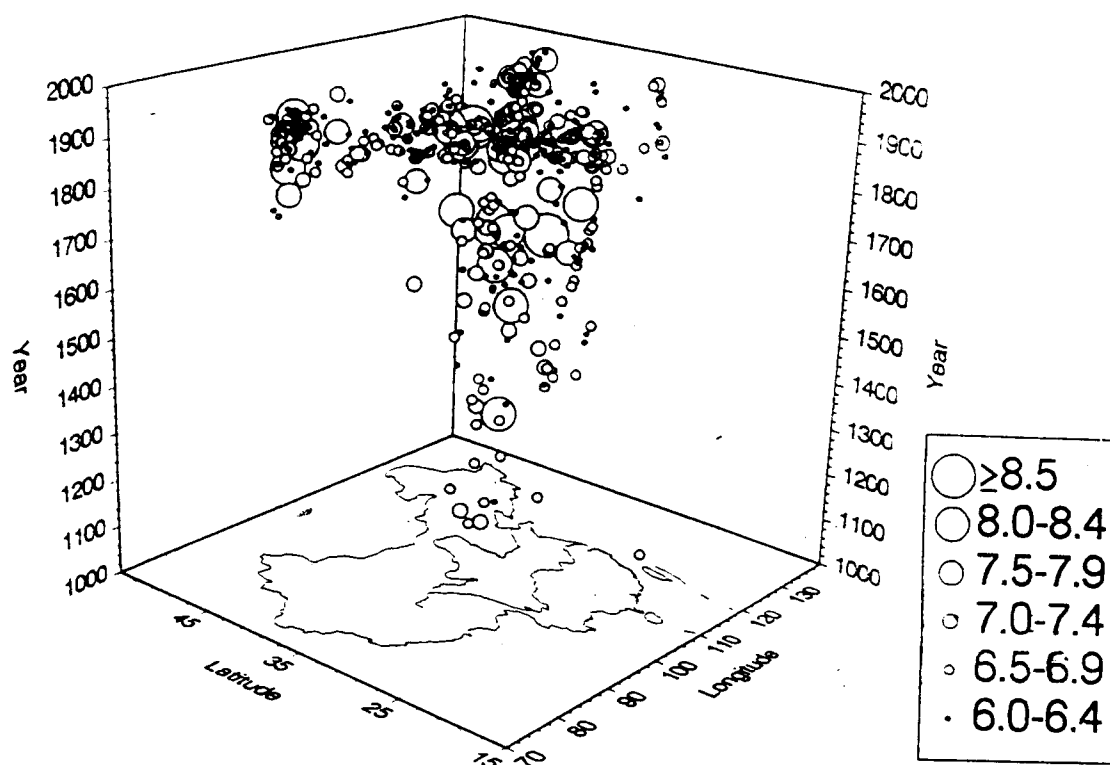


Fig. 3: Incompleteness of historical earthquake catalog: Seismicity of mainland of China since AD 1000 in space-time plot. The vertical axis represents time, both horizontal axis's represent latitudes and longitudes respectively. Magnitudes of earthquakes are expressed by circles with different radius.

5.2 The relation between the existing faults and the occurrence of earthquakes is still an open question

Even since its taking shape, the theory of plate tectonics provided the first scientific framework for the assessment of seismic hazard. Prior to the validation of plate tectonic concepts in 1960s, it was customary for earthquake catalogues to be taken at face value as representative empirical guides to the sources of hazard, future and past. However, given the lack of direct tectonic input,

sole reliance on earthquake data (particular on historical earthquake data) was deprecated by Cornell (1968) on the ground that insufficient weight was given to known corrections between geological structure and most seismic activity.

The concepts of potential earthquake source and the probabilistic approach play very important roles in seismic hazard analysis (SHA). Among the various forms of potential sources, the linear form, namely the fault model is widely used in both deterministic and probabilistic hazard analyses. The fault model, as the linear form of potential earthquake sources, is widely used as the essential basis for both deterministic and probabilistic hazard analyses due to its clear geological background. However, there are some noticeable problems existing in the application of fault model to hazard assessment including the difficulties in data collections, the problem about the unclear earthquake-fault relation (e.g. Tangshan earthquake (1976, China), Coalinga earthquake (1983, US) and North Ridge Earthquake (1994, US), all of these earthquakes did not occur on the well known faults), and the uncertainties from the determination of maximum length of rupture, et al.. Moreover, recent studies also found that neither the uniform seismicity within a zone nor the Euclidean geometry of a zone accord with the fractal spatial distribution of seismicity. Therefore, the construction of zone geometry in fault model may become contentiously subjective, and ambiguities may end up being resolved through consideration appeal to non-scientific rule of conservatism or pragmatism (Woo, 1996).

Considering the above problems in seismic hazard assessment, we need to develop a new methodology of hazard analysis, which must be:

- Simple SHA model
- Available key data
- Testable results

5.3 Quantification of earthquake disaster

The output of a seismic hazard analysis could be a description of the intensity of shaking. The output of a seismic risk analysis could be the probability of damage (in some unit of currency) from nearby magnitude eight earthquake or the probability of fatalities due to seismically induced nuclear power-plant accidents. Seismic risk is a probabilistic expression of the product of seismic hazard and its consequences. One needs to know the seismic hazard in order to calculate the seismic risk. If not already known, defining the seismic hazard become part of the risk estimation process.

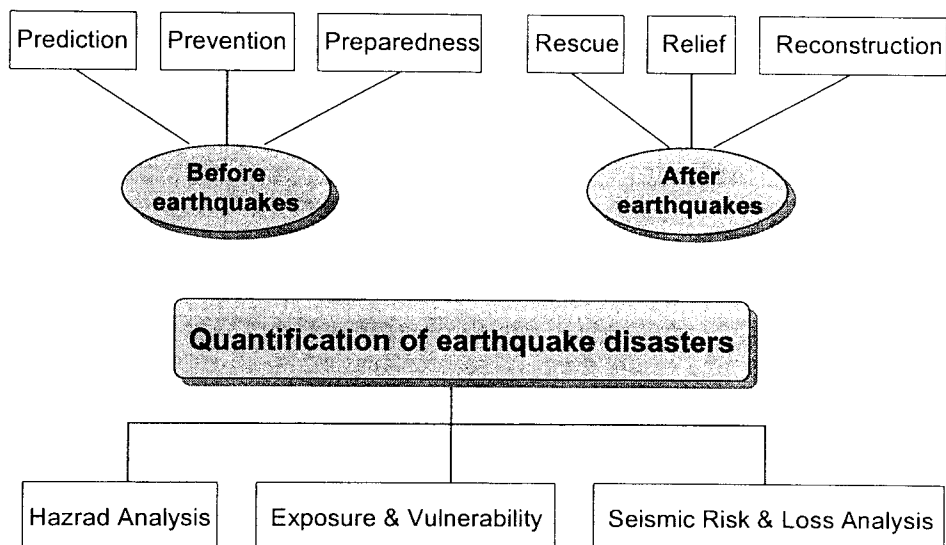


Fig. 4: Qualification of earthquake disaster is an essential scientific problem for IDNDR.

The Quantification of earthquake disasters is the basis for the reduction of natural disasters and the risk management of which the seismic hazard analysis and the seismic risk assessment are the key scientific problems (Fig. 4).

REFERENCES

Note: All the references are from GSHAP Summary Volume (1999). Annali di Geofisica.

The Global Seismic Hazard Assessment Program, D. Giardini.

The compilation of the GSHAP map of global seismic hazard, D. Giardini, D. Mayer-Rosa, K. McCue, R. McGuire, K. Shedlock & P. Zhang.

Seismic Hazard Map of the Western Hemisphere, K. M. Shedlock & J. G. Tanner.

The Seismic Hazard Map of the European-Mediterranean-African region, G. Grünthal, D. Giardini, D. Mayer-Rosa & S. Sellami.

Seismic Hazard Map of North and Central America and the Caribbean (GSHAP Region 1), K. M. Shedlock.

Seismic Hazard of South America - CERESIS (GSHAP Region 2), A. Giesecke.

Seismic Hazard Assessment of Northern Europe (GSHAP Region 3), G. Grünthal.

Seismic Hazard Assessment of Iran (GSHAP Region 6), B. Tavakoli & M. Ghafory-Ashtiani.

Seismic Hazard of Northern Eurasia (GSHAP Region 7), V.I. Ulomov.

Seismic Hazard of Eastern Asia (GSHAP Region 8), P. Zhang & K. Shedlock.

Seismic Hazard Mapping of Australian, the Southwest Pacific and Southern Asia (GSHAP Region 10), K. McCue.

Seismic Hazard Assessment of the Northern Andean region, C. Dimaté, L. Drake, A. Fuenzalida, D. Giardini, G. Gruenthal, L. Ocola, H. Rendon & H. Yepes.

Seismic Hazard Assessment in the Ibero-Maghreb Region, M.-J. Jiménez, M. García-Fernández, M. Chadi, D. El Foul, A. Izquierdo, J.-M. Martínez-Solares, C. Sousa-Oliveira & B.-A. Tadili.

Seismic Hazard Assessment in Eastern and Southern Africa, V. Midzi, D. J. Hlatywayo, L. S. Chapola, F. Kebede, K. Atakan, D. K. Lombe, G. Turyomuru-gyendo & F. A. Tugume.

GSHAP seismic hazard assessment for the Adria region, D. Slejko, R. Camassi, I. Cecic, D. Herak, M. Herak, S. Kociu, V. Kouskouna, J. Lapajne, K. Makropoulos, C. Meletti, B. Muco, C. Papaioannou, L. Peruzza, A. Rebez, P. Scandone, E. Sulstarova, N. Voulgaris, M. Zivcic & P. Zupancic.

Seismic Hazard Assessment of the Circum-Pannonian basin (EU-CIPAR-QSEZ), R. Musson.

Seismic Hazard Assessment of Turkey and the Aegean, M. Erdik.

Seismic Hazard Map of the Near East (RELEMR/SESAME/ESC), A-Q. Amrat, E. Ibrahim, D. Mayer-Rosa, G. Papakyriacou, S. Riad, S. Sellami, A. Shapira, W. Hays, M. Al Haddad & M. El Khoubbi.

Seismic Hazard Assessment for the Caucasus test area, S. Balassanian, D. Giardini, V. Ulomov, T. Ashirov, T. Chelidze, M. Erdik, A. Gassanov, M. Ghafory-Ashtiany, N. Kondorskaya, G. Molchan, B. Pustovitenko & V. Trifonov.

Seismotectonics and Seismic Hazard Assessment of the Mediterranean Region (SESAME, ICTP n.382), D. Giardini, M. Garcia-Fernandez, K. Macropulos, S. Riad, S. Sellami.

The India-China-Tibet GSHAP Test Area, H. Gupta & P. Zhang.

APPENDIX II: List of GSHAP Co-ordination

Coordinator D. Giardini ETH Zurich, CH giardini@seismo.ifg.ethz.ch

Chair, SteerCom H. Gupta NGRI Hyderabad, India director@csngri.ren.nic.in

Test areas and regional centres

South America A. Giesecke CERESIS Lima, Peru giescere@inictel.gob.pe

A.C. Dimaté INGEOMINAS Bogota, Colombia cdimate@esmeralda.ingemin.gov.co

North America K. Shedlock USGS Golden, USA shedlock@gldvxa.cr.usgs.gov

C-N Europe G. Grunthal GFZ Potsdam, DE ggrue@gfz-potsdam.de

Ibero-Maghreb M. Garcia CSIC Barcelona, Spain mgarcia@ija.csic.es

B. Iben Brahim CNCPRST Rabat, Morocco lag@cnr.ac.ma

ADRIA D. Slejko OGS Trieste, Italy dslejko@ogs.trieste.it

C. Pannonian R. Musson BGS Edimburg, UK rmwm@wpo.nerc.ac.uk

Caucasus S. Balassanian NSSP Yerevan, Armenia presidnt@nssp.r.am

N. Eurasia V. Ulomov JIPE Moscow, Russia ulomov@uipe-ras.scgis.ru

Iran M. G. Ashtiany IIEES Tehran, Iran ashtiany@dena.iiees.ac.ir

Africa Rift K. Atakan Bergen Univ. Norway kuvvet@ifjf.uib.no

I. Nyambok Nairobi Univ. Kenya uonseism@arcc.or.ke

C-N Asia P. Zhang SSB Beijing, China peizhen@public3.bta.net.cn

Oceania K. McCue AGSO Canberra, Australia kmccue@agso.gov.au

APPENDIX III. GSHAP History

8.91 following the ICSU request to provide scientific input for IDNDR demonstration activities, ILP initiates the planning and preparation for the GSHAP

3.92 the UN/IDNDR Scientific and Technical Committee endorses the GSHAP as a Decade demonstration project

6.92 the GSHAP is launched with a Technical Planning Meeting in Rome, to focus the consensus of the scientific community on the development of a multi-national and multi-disciplinary approach to seismic hazard assessment, to define schedule and structure of the program

92-93 the first year is devoted to the definition and implementation of the regional and management structure, the establishment of the program in the international scientific and engineering communities, the coordination with other UN/IDNDR activities, the establishment of a funding strategy

7.93 the GSHAP Volume is published (*Annali di Geofisica*, vol. 36, 3-4), containing all program documents, a revision of the existing status-quo in global seismic hazard and the technical guidelines for the GSHAP implementation

93-95 The first implementation phase is devoted to implement the key strategic elements of the program: the operation of regional centres in all continents and the activation of multinational test areas for seismic hazard assessment in regions of high seismotectonic significance

8.95 program evaluation (Boulder, IUGG Assembly)

95-97 the second implementation phase extends the GSHAP coverage to more test areas and regions covering the most of the world

8.97 regional results are presented and evaluated in a special meeting (Thessalonicki, IASPEI Assembly); plans for the final phase of GSHAP are drawn

97-98 the final phase focuses on the completion of regional hazard assessment, on the compilation of all regional databases and results, on the compilation of the GSHAP map of global seismic hazard, on the dissemination of GSHAP products and materials (special volumes, maps, CD-ROM, web)

6.99 publication of the GSHAP Summary volume

7.99 the GSHAP map of global seismic hazard is presented at the IDNDR Closing Conference in Geneva

APPENDIX IV: Design Principle of GSHAP

The GSHAP has been designed as a Decade demonstration project, adopting and implementing the following design principles:

- Hazard assessment is the primary input for the implementation of risk mitigation strategies
- Scientific research is a key to engineering applications
- Maintain high scientific standards
- Ensure consensus and enlarge participation at all levels
- Enforce a multi-disciplinary approach to seismic hazard assessment
- Work across boundaries
- Enhance the role of developing countries
- Ensure technology transfer
- Focus on key geographical and border areas
- Ensure the implementation of regional and global results in national policies

Slide 1 Title of presentation

Figure 1 Historic record: in 1556 (Ming Dynasty of China), a great earthquake occurred in the middle of China, killed 830,000 or more people

Slide 2 Major disastrous earthquakes of the world during 1980-1998 (Munich Re, Munich, March 1999). The earthquakes occurred in Asia were marked with bolt characters in the table. Among the total 44 earthquakes, 17 earthquakes occurred in Asia

Slide 3 Percentage of death and loss of Asia to the world Meeting, 9-12, July, UNDRO, Geneva, 1980) are as follows:

Slide 4 Definition of **seismic hazard**

Slide 5 Definition of **vulnerability**

Slide 6 Definition of **seismic risk**

Seismic risk is the expected degree of losses caused by earthquakes and therefore the product of seismic hazard and vulnerability:

$$\text{Risk} = \text{Hazard} \times \text{Vulnerability}$$

Elements at risk include the number of persons, the value of properties, the level of economic activities such as public service et al. and so on in a given area.

Slide 7 A key question that must be addressed in earthquake disaster reduction is: how much loss might a city or a region suffers in future earthquakes? There are two components comprising the basic structure of a loss estimate study. One component, the seismic hazard analysis, involves the identification and quantitative description of strong ground motion caused by the future earthquakes; The second component, the seismic risk analysis, involves the vulnerability analysis of buildings and other man-made facilities to earthquake damage and the losses that may result from this damage.

Slide 8 The Global Seismic Hazard Assessment Program (GSHAP) was launched in 1992

by the International Lithosphere Program (ILP) with the support of the International Council of Scientific Unions (ICSU), and endorsed as a demonstration program in the framework of the United Nations International Decade for Natural Disaster Reduction (UN/IDNDR).

Figure 2 The Regions, Test Areas, and Co-operating Projects of **GSHAP**

Slide 9 Successes of GSHAP

Slide 10 Shortcome of GSHAP

Slide 11 What remains to be done?

Figure 3 Incompleteness of historical earthquake catalog: Seismicity of mainland of China since AD 1000 in space-time plot. The vertical axis represents time, both horizontal axis's represent latitudes and longitudes respectively. Magnitudes of earthquakes are expressed by circles with different radius

Figure 4 Qualification of earthquake disaster is an essential scientific problem for IDNDR

EARTHQUAKES IN CHINA: A BRIEF INTRODUCTION

Z. L. Wu, Y.-T. Chen and R. F. Liu

Institute of Geophysics, China Seismological Bureau, Beijing 100081, China
Fax: +86-10-68415372; E-mail: wuzl@cdsnmc.css.gov

1. HISTORICAL EARTHQUAKES IN CHINA

1.1 Introduction

China is a country of abundant earthquakes both in history and at present (see Fig. 1). Written historical records are scattered in all kinds of literatures. Compiling of earthquake records can be traced back to early Song Dynasty (about A.D. 1000) when 45 pieces of earthquake record were collected by Li Fang from ancient literatures as a record of 'catastrophe'. Since then compiling of earthquake records have been going on in each dynasty. At the beginning of the 20th century, Chinese earthquake records also caused attention of European, American, and Japanese seismologists. Because of language and culture barriers, too many errors associated with the location and time of earthquakes can be found in their catalogues. As a result, those catalogues compiled by foreign seismologists are seldom used.

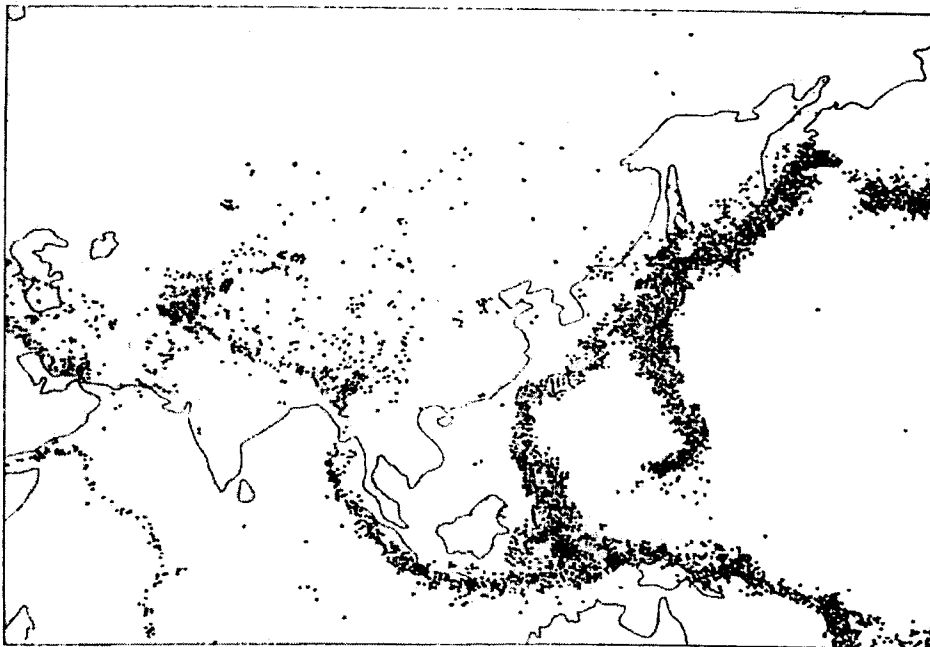


Fig. 1: The epicentre distribution in China and its neighbouring regions (according to Li, 1981).

In the 1950s, to provide the constructions with information of seismic risk, the Chinese Academy of Sciences (CAS) organised a two year project for compiling the historical records of earthquakes in China. As a result, tens of thousands of earthquake records were found from various kinds of historical literatures. Carefully examination of the records lead to the *Chronicle Data of Chinese Historical Earthquakes*. By using the concepts of modern seismology, Li Shanbang (S. P. Lee) et al. determined the parameters of all the destructive earthquakes, which lead to the *Catalogue of Chinese Earthquakes*.

It is well-known that in the evolution of history, names and locations of the places where earthquakes occurred as well as other geographic aspects are changing from time to time. Accordingly there are significant distortions with regard to the location, date and intensity distribution of historical earthquakes. Furthermore, historical records are highly diverse in detailness for different events. Therefore, since the 1950s Chinese seismologists and historians have cooperated in many aspects reexamining the historical materials to make the historical earthquake catalogue more reliable. For some of the earthquakes, field investigation were also carried out to study the destruction and geology of the earthquake. At the mean time, in some regions of minorities, such as in Tibet, literatures in the local languages of minorities are also collected and studied, which contributed much to the compiling of the historical records of earthquakes in China.

The earliest recorded Chinese earthquake is supposed to be that in the 23rd century B.C. about which written literatures recorded that an earthquake occurred in Shanxi Province and caused the emergence of underground water. But these records are indirect ones coming from ancient legends, so it is not regarded as reliable. The earliest reliable recorded Chinese earthquake is believed to be that occurred in the Tai Mountain, Shandong Province in about 1831 B.C. which was recorded by the bamboo-carving records at that time. The first Chinese earthquake whose seismological parameters can be evaluated is that occurred in 780 B.C. in Zhou Dynasty. In the pre-Qin Dynasty before the third century B.C. more than ten destructive earthquakes were recorded. Since the beginning of the Western Han Dynasty in about 200 B.C., in each dynasty, royal historians have been assigned the job to record earthquakes routinely into history books in terms of 'catastrophe' from the Heaven. Since the Song Dynasty, local chronicles have been gradually spread, which promoted to much extent the development of the historical records of earthquakes. The degrees of damage and affected areas, even some plausible precursors, were recorded and narrated, in brief or in detail, in various kinds of literatures, such as academic geography/engineering books, royal history/astronomy books, local/governmental chronicles, private notebooks/diaries, and even poems. In the history of China, over 8000 earthquakes have been recorded, among which more than 880 are destructive ones. Since the foundation of the Ming Dynasty in 1368, catalogue of destructive earthquakes (about magnitude 5 and above) in the eastern part of China has become complete.

1.2 Significant historical earthquakes in China

Gansu, March 1, A.D.138, Eastern Han Dynasty

In A.D. 132, Zhang Heng invented the first seismoscope in the world which can record the azimuth of earthquakes at remote distances. This earthquake is suggested by some seismologists to be the first distant one recorded by the seismoscope. On the other hand, however, historical records are inconsistent with each other. According to the *History of Late Han Dynasty (Hou Han Shu)*, when the earthquake was recorded by the seismoscope, the capital of the Han Dynasty (now Louyang, Henan Province) did not feel the ground motion, causing the scholars in the capital to blame it as a 'false alarm', and the information of the earthquake came to the capital several days after, which is the reason why after the earthquake, the Han Dynasty started to assign an officer to monitor and report the records of the seismoscope. In the same book, however, it is recorded that Longxi, Gansu and Jingshi (capital), Henan were all effected by the earthquake of March 1. The death and lost was significant but hard to evaluate. In Gansu, landslides also occurred during the earthquake. It is worth pointing out that in this book the time of the earthquake recorded by the seismoscope is not specified. Also the ambiguity of record does not exclude the possibility that within the same day, there are two earthquakes occurred separately in Luoyang and Gansu, respectively. Anyway, it is too early to conclude that the earthquake recorded by the Zhang Heng seismoscope is that one on March 1. Probably it is another smaller one in Gansu but not recorded in the literature. The incompleteness of historical recordings leaves a question to future investigation.

Fenhe, Shanxi (37N, 112E), September 17, 1303, Yuan Dynasty, magnitude about 8

According to the historical literatures, this earthquake occurred during night time, causing significant ground fissures. Thousands of Taoist priests were recorded to be killed or injured by building collapse, but the total death toll can not be estimated from historical literatures (most of the recordings wrote 'innumerable') . At that time local chronicles were not developed, therefore the information in the historical recordings was limited. Although the recordings of this earthquake can be found widely in the local chronicles compiled after the Ming Dynasty, such recordings are obviously not independent ones but origins from the literatures and legends in the Yuan Dynasty and therefore are not reliable. The intensity distribution orients along the NNE direction. Later field investigations confirmed the size of the earthquake. (This and other earthquakes from Yuan Dynasty you can see in Fig. 2.)

Huaxian, Shaanxi (34.5N, 109.7E), January 23, 1556, Ming Dynasty, magnitude estimated 8

This earthquake caused over 830,000 deaths, ranking the first in the world on record. The earthquake occurred in the midnight. Landslide and water emergence occurred during the earthquake. Destruction of buildings was serious. Intensity in the mezo-seismal region is XI. The effected area (with intensity above IV) is about 1000 km in size. The distribution of the intensity shows a two-mode orientation pattern with the high intensity area (intensity above

VI) oriented along the NEE direction and the intermediate intensity area (intensity between VI and IV) oriented along its conjugate direction. The very-high intensity area (intensity above VIII) shows a near linear orientation, being consistent with the orientation of the Quaternary graben. The aftershock activity was recorded to last until 1570s, approximately 15 years after the mainshock. Three years after the mainshock, a strong aftershock occurred in the same region, causing significant destruction's. About this earthquake there are many literatures recording the process of earthquake occurrence, destruction, seismic and secondary disasters, as well as the emergency response of the authorities, to some extent in detail. Late field investigation confirmed the records about the site liquefaction and landslide.

Juxian-Tancheng, Shandong (35.0N, 118.6E), July 25, 1668, Qing Dynasty, magnitude estimated 8½

This earthquake is one of the great earthquakes of magnitude 8 and above in China in the 17th century. The earthquake occurred along the Tancheng-Lujiang fault which strikes NNE near to the eastern coast of China spanning thousands of kilometres from the south to the north, being comparable to the San Andreas fault. Over 30,000 people dead of building collapse during the earthquake. The earthquake also caused landslide and large ground fissures. The distribution of intensity is along the NNE direction with the maximum intensity being XI in the Tancheng-Juxian region. The affected area (with intensity IV and above) spans over 1300 km. According to historical literatures, the immediate aftershocks lasted continuously for over 20 hours from the night to the next evening. After the mainshock occurred on July 25, strong aftershocks occurred 1 day, 30 days, 56 days, 61 days, 3 years and 4 years after, respectively, causing further damage. The aftershock sequence was felt to last for over 6 years.

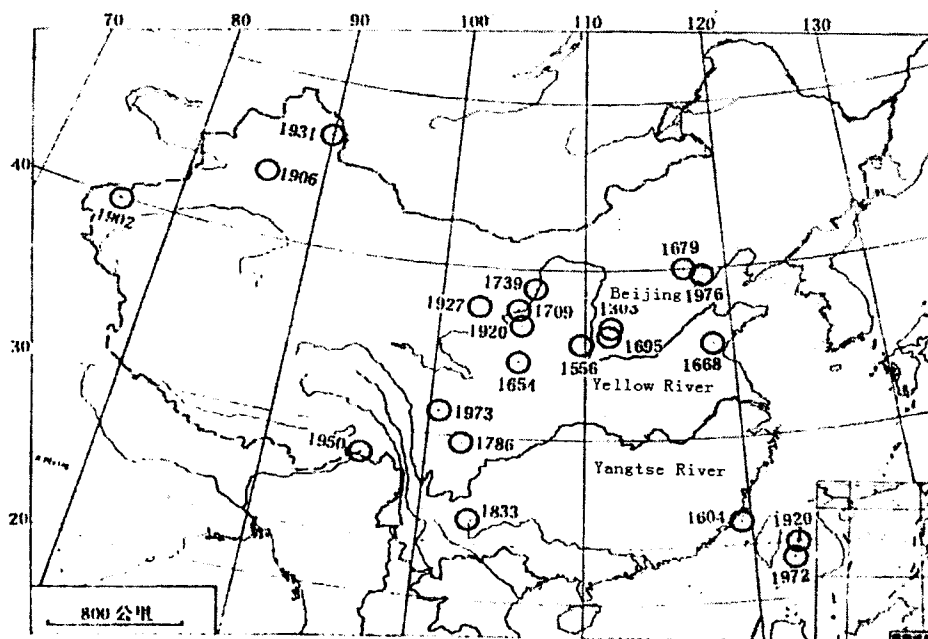


Fig. 2: The epicentre distribution of very big earthquakes with magnitude near or greater than 8.0 from Yuan Dynasty (according to Li, 1981).

Sanhe-Pinggu, Zhili (40.0N, 117.0E), September 2, 1679, Qing Dynasty, magnitude estimated 8

The historical record of this earthquake is interesting to some extent. Because this earthquake occurred very near to the capital of the Qing Dynasty (now Beijing), and at that time earthquakes were widely believed to be a punishment from the Heaven to the Emperor, the record of this earthquake by royal documents was very brief and ambiguous. In contrast, as the affected area of this earthquake was quite large, many detailed records can be found from local chronicles and public literatures. Another characteristics is that while the affected area (with intensity IV and above) spans near to 1000 km, the high intensity area (with intensity larger than VI) is relatively small, concentrating to the Zhili (now Beijing) region. Over 10,000 people dead during the earthquake. According to the historical literatures, another earthquake with comparable magnitude occurred the next day, still the third one with comparable magnitude occurred three days after the first one. Two strong aftershocks occurred 15 days after the mainshock; another two strong aftershocks occurred 27 days after the mainshock. The aftershock activity lasted for about two months. On the other hand, however, it is not easy to draw more detailed information of aftershocks/swarms from historical recordings. It is worth pointing out that although the destruction was serious during the earthquake, some architectures, such as the Guanyin Ge of Dule Shi in Jizhou, Zhili (the Temple of the Guanyin Buddha near to Beijing, the local intensity is between IX and X) kept standing without any destruction's, indicating the experiences in earthquake engineering at that time.

This earthquake as well as the 1668 Juxian-Tancheng, Shandong earthquake all occurred during the rein from 1662 to 1723 of Aixinjueluo Xuanye (the Emperor Kangxi). During this time there were many other strong earthquakes with magnitude 7 and above occurred in China, including the May 18, 1695, Linfen, Shanxi, earthquake and the October 14, 1709, Zhongwei, Ningxia, earthquake with magnitudes near to 8. Near to the capital, there were strong earthquakes with magnitude 6 and above in 1679, 1704 and 1720, respectively. Frequent strong seismic disasters forced the Emperor to study earthquakes rather than simply believe that earthquakes are the punishment of the Heaven. In about 1721 to 1722, Aixinjueluo Xuanye wrote an article explaining the mechanism of earthquakes combining the Chinese concept of Yin Yang and the western concept of 'gas', in which the distribution of Chinese earthquakes were described systematically for the first time.

1.3 Distribution of historical earthquakes in China

The historical records of destructive earthquakes (with magnitude above 5) has been complete for the eastern part of China since the Ming Dynasty (approximately after the 1400s). The 500 year duration of complete historical earthquake recordings before instrumental seismology have provided seismological study with valuable information about the regularity of earthquakes.

To objectively distinguish seismogenic regions is one of the outstanding problems even in modern seismology, especially as the scale under consideration goes smaller. However, for large scales up to thousand of kilometres, the spatial regularity of earthquakes is quite clear. From historical recordings it can be seen that Chinese earthquakes show clustering in space, forming some important seismic zones. The most important seismic zones are (1) the north China seismic zone in the north China as well as the Bohai Sea and the Huanghai Sea; (2) the north-south seismic zone from Yunnan and Sichuan in the south to Gansu and Ningxia in the north; and (3) the Fujian-Taiwan seismic zone. Incompleteness of historical recordings prevent us from recognising the Himalayan seismic zone in Tibet and the north Xinjiang seismic zone from the historical earthquakes.

In a broader perspective, the most important seismic belts around China include (1) the circum-Pacific seismic belt indicating the boundary between the Pacific plate and the Eurasian plate, with the Fujian-Taiwan seismic zone being a part of it; (2) the Himalayan-south Asian seismic belt indicating the boundary between the Eurasian plate and the Indian plate; and (3) the Pamir seismic belt, with the north Xinjiang seismic zone being a part of it. The southern part of the north-south seismic zone belongs partly to the Himalayan-south Asian seismic belt. But the tectonics of the north China seismic zone, the whole north-south seismic zone, and the north Xinjiang seismic zone is still under discussion. In fact, the study of intraplate (continental) earthquakes is one of the challenging problems in seismology and geodynamics.

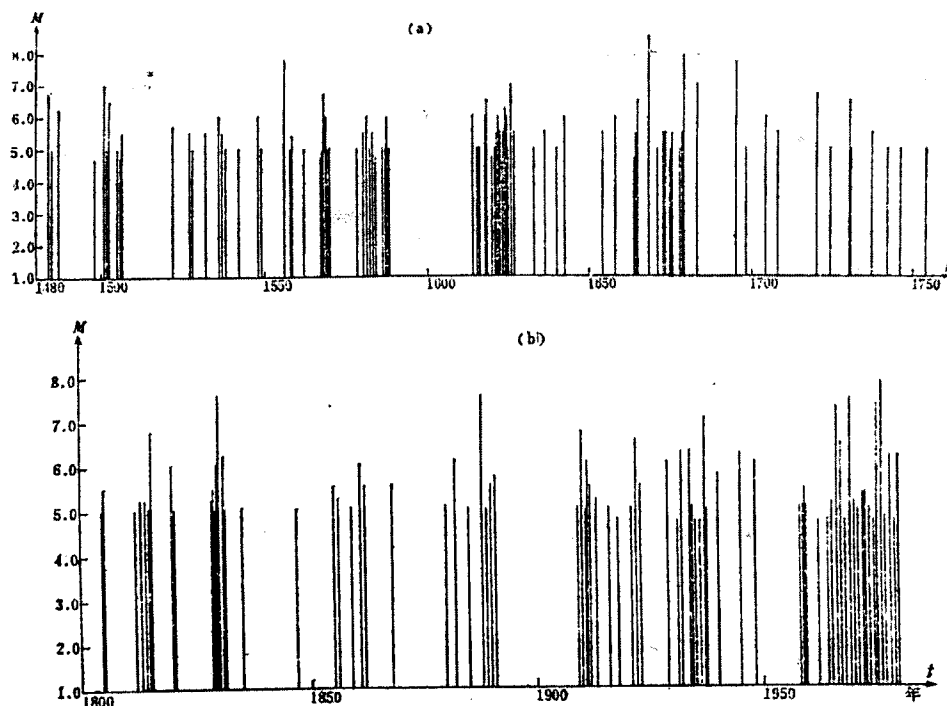


Fig. 3: The time sequence distribution ($M > 4.8$) in North China (a) the third period (1484 - 1730) (b) the fourth period (1815 -) (according to Ma et al., 1982).

The temporal clustering of earthquakes is also evident. Taking the north China seismic zone as an example (see also Fig. 3), active and quiescent periods occurred alternatively. Periodicity of decades is significant in statistics but with considerable fluctuations. The mechanism of such a regularity, however, is still not quite clear in geodynamics. It is also evident that great earthquakes with magnitude 8 and above were active in the 17th century (4 times) comparing to the other centuries (1 or 0 for each century from the 14th to 16th century and 1 for each century in the 18th and 19th century).

2. EARTHQUAKES IN CHINA IN THE 20TH CENTURY

2.1 Seismological observation in China in the 20th century

Modern seismological observation in China started in the turn of the 19th to 20th century when local seismic stations were installed in Taipei (1897), Tainan (1898), Taichong (1902), Taitong (1903), and other places in Taiwan by Japanese seismologists; in Shanghai (1904) by French missionary; in Dalian, Yingkou, Lushun, Shengyang, and Changchun (from 1904 to 1908) by Russian and/or Japanese seismologists; and in Tsingtao (1909) by German experts. Also in Tianjin and Xi'an there used to be seismic stations installed by foreign missionaries, but these stations failed to provide available data. The first seismic stations installed and managed by Chinese seismologists were the Chiufeng station, Peiping (now Beijing), from 1930, and the Peitsike station, Nanking (now Nanjing), from 1931. The two stations operated the Wiechert seismograph and the Galitzin seismograph and exchanged data with the I.S.S. (now I.S.C.). During the World War II both these two stations ceased to work. In 1943 during the war time, Chinese seismologists installed a temporary station, with a simple seismograph designed and made in China, in Peipei, Chongking (now Chongqing). This station was moved back to Nanking (now Nanjing) in 1946 after the world war and started its operation in late 1948. To study the seismicity in China in the early half of the 20th century, the data of I.S.S. (now I.S.C) and B.C.I.S. (now European-Mediterranean Seismological Center) can also be used as a reference.

Since 1954, using Chinese designed horizontal-component 51-seismograph, seismic stations had been installed in Xi'ning, Lanzhou, Yinchuan, Taiyuan, Xi'an, and other places in the Yellow River region and in Changchun, Dalian, Harbin, and Shuihua in the north-eastern China, forming the first nation-wide seismograph network in China. In 1958, Kirnos seismograph had been installed in 12 stations nation-wide including Beijing, Lanzhou, Changchun, Lhasa, Guangzhou, Kunming, Nanjing, Sheshan (Shanghai), Baotou, Xi'an, Chengdu, and Wuhan. In the 1960s to 1970s, Kirnos seismograph had been installed gradually in another 13 stations including Uhrumiqi, Tai'an, Kashi, Gaotai, Guiyang, Dalian, Taiyuan, Mudanjiang, Hailar, Quanzhou, Hohhot, Qiongzong, and Shengyang. These seismic stations formed the national seismograph network in China. At the mean time, regional and local networks are also installed and operated. After the 1966 Xingtai, Hebei Province, earthquake, regional and local networks were developed rapidly, amongst which the

most famous one is the Beijing Regional Telemetered Seismograph Network built in late 1960s. With the development of seismic monitoring, seismographs were also designed and made in China, amongst which the most famous ones are the 763 long-period seismograph and the DD-1 short-period seismograph. At present the Chinese seismograph network includes three levels, namely national, regional, and local networks, which can completely monitor the earthquakes down to M5 nation-wide, down to M4 nation-wide except the Tibetan plateau and the desert area of Xinjiang, down to M3 in the eastern part of China, and down to M1 in some regions such as Beijing.

In 1986, the Sino-American cooperative China Digital Seismograph Network (CDSN) started its operation, which now includes 11 stations: Beijing, Lanzhou, Enshi, Kunming, Qiongzong, Sheshan (Shanghai), Hailar, Mudanjiang, Uhrumuqi, Lhasa, and Xi'an. CDSN is a partner of the IRIS Global Seismograph Network and the global GSETT network for monitoring nuclear tests. Starting from the late 1990s, the China Seismological Bureau (CSB) carried out a project to deploy 49 digital seismic stations nation-wide and 6 regional digital seismic networks.

It is worth pointing out that in the 20th century, after each destructive earthquake whose meioseismal region was accessible, field investigation was carried out routinely to study the destruction and tectonics and to collect the data of plausible precursors. After some of the earthquakes, temporal seismic networks were also deployed to monitor the aftershock activity, study the structure of the source region, and record the strong ground motion data for engineering seismology.

2.2 Significant earthquakes in China in the 20th century

Haiyuan, Ningxia (36.7N, 104.9E), December 16, 1920, 20:05:53 local time, M8.5

This earthquake is significant in three aspects: (1) it is the largest earthquake occurred in the mainland of China in the 20th century, and one of the largest intraplate earthquakes within the Eurasian continent; (2) it caused over 230,000 deaths, being one of the most destructive earthquakes in the history of China; (3) it triggered the modern seismological studies in China.

The affected area ranges from the Eastern China Sea coast in the east to Qinghai and Gansu in the west, from Hong Kong and Vietnam in the south to northern Inner-Mongolia in the north, being the largest one on record. The maximum intensity ranks XII near to Haiyuan. Field investigation found that the maximum horizontal slip is as large as 14 m, and the slip spans 230 km. Due to the earthquake, there occurred large scale landslides, causing serious secondary disasters by flood. Actually besides the collapse of buildings, flood, landslide, and starvation are the main causes to the death toll. Field investigation also determined that the earthquake faulting strikes NWW with dip angles ranging from 30° to 70°. The ratio of horizontal slip versus vertical is about 7:1.

The field investigation of the Haiyuan earthquake is not the first one in the sense of modern seismological studies of China (the first one should be the field investigation of the January 24, 1917, Huoshan, Anhui M6¼ earthquake). But the field investigation of this earthquake is the first one which was systematically conducted and lead to the first research article published by Chinese geologist to international seismological community. After this earthquake, the scientific community of China started to notice the problems of earthquakes in China and organised several projects in seismological studies including the building of the Chiufeng seismic station in Peiping and the Peitsike seismic station in Nanking.

Xingtai, Hebei (37.5N, 115.1E), March 22, 1966, 16:19:27 (BJT), Ms 7.2

On March 8, 1966, an earthquake of M6.8 occurred in Xingtai, Hebei Province. Fourteen days after the first one, another earthquake of M7.2 stroke the same region. The mezoisismal region is about 130 square kilometres with maximum intensity of X. The damage area (intensity VI and above) is about 130,000 square kilometres. The earthquake caused 8,064 people dead and 38,451 people injured. Landslides occurred in the mountainous regions during the earthquake. The isoseismal lines orients NE. P wave first motion data gives that the two conjugate nodal planes are NP I striking 11° dipping SE with dip angle 85°, and NP II striking 282° dipping SW with dip angle 86°, respectively, in which NP I is suggested to be the earthquake fault showing a right-lateral strike-slip motion. Inversion of deformation data obtains that the slip is 1.3 m along the strike and 0.5 m along the dip, producing a mean stress drop of 42 bar and a seismic moment of 5.9×10^{25} dyncm. The aftershock area is about 90 km long and 30 km wide, with the largest aftershock of magnitude 6.2. The aftershock activity lasted for 645 days with the Gutenberg-Richter *b* value of 0.75 and the Omori *p* value of 0.96.

The Xingtai, Hebei, earthquake plays an important role in the development of Chinese seismology because it is the first strong earthquake in the 20th century striking the densely populated north China region. Shortly after the March 8 event, a large research project was organised to investigate the geology, geophysics and possible precursors of the Xingtai earthquake, which stimulated the large scale endeavour in China studying the problems of earthquake prediction.

Haicheng, Liaoning (40.7N, 122.8E), February 4, 1975, 19:36:05.0 (BJT), Ms 7.3

This is the first strong earthquake which was reported to be successfully predicted by seismologists. The intensity shows a two axis distribution with one axis pointing NE and another pointing NWW. P wave first motion data gives that the two conjugate nodal planes are NP I striking 290° dipping NE with dip angle 81°, and NP II striking 23° dipping SW with dip angle 75°, respectively, with NP I being preferred as the earthquake fault, showing a left-lateral strike-slip motion. Body wave spectral analysis gives that the rupture is 54 km long and 24 km wide, showing a symmetric bilateral propagation with velocity of 1.3 km/sec. The dislocation is 1.2 m along the strike and 0.3 m along the dip. The stress drop is 22 bar, and the seismic moment is 5.2×10^{26} dyncm. Aftershocks lasted for 1198 days with the largest aftershock ranking M 6.0. The *b* and *p* value of the aftershock sequence are 0.95 and

0.79, respectively. Because prediction was issued before the earthquake, and evacuation was carried out by the local authorities in the winter time, the death during the earthquake (1328) is only 0.2% of the population living in the area with intensity VII and above. The foreshock swarm for the prediction of the 1975 Haicheng earthquake was evaluated by the IASPEI Committee of Earthquake Prediction as one of the significant precursors.

Tangshan, Hebei (39.4N, 118.0E), July 28, 1976, 03:42:54.2 (BJT), Ms 7.8

This earthquake is the largest one in the eastern China in the 20th century. The area of intensity VII and above is 33,000 square kilometres. The mezo-seismal area is 47 square kilometres, orienting NE with maximum intensity of XI, locating just beneath the urban area of Tangshan. The earthquake caused 242,000 people dead and 164,000 seriously injured, being the most in the world in the 20th century. The earthquake faulting shows a right-lateral strike-slip motion along a SE striking fault. The dislocation is 5m along the strike and 0.5 m along the dip. The seismic moment estimated from ground deformation data is 4.3×10^{27} dynm. The aftershock region spans 145 km in length and 50 km in width, with the largest aftershock ranking M 7.1, 15 hours after the mainshock. The *b* and *p* value of the aftershock sequence are 0.98 and 0.80, respectively. In the mezo-seismal region, there appeared a ground fissure zone of 8 km long and 30 m wide, with right-lateral horizontal torque dislocation up to 1.5 m. During the earthquake almost all of the local and regional seismic recordings were out of scale. Waveform modelling of global teleseismic data and strong motion data reveals that the rupture process of this earthquake is complex.

It is worth pointing out that with the accumulation of seismic data, it is evident that most of the strong earthquakes in the mainland of China show complexity in their rupture processes. Almost all of the strong earthquakes possess strong foreshocks and/or aftershocks with comparable magnitudes. The time interval between the strong foreshocks/aftershocks and the mainshock ranges from several seconds (such as in the 1990 Gonghe, Qinghai earthquake and the 1996 Lijiang, Yunnan earthquake) and several minutes (such as in the 1988 Langcang-Gengma, Yunnan earthquake), to several hours (such as in the 1976 Longling, Yunnan earthquake) and several days (such as in the 1966 Xingtai, Hebei earthquake), to more than one year (such as in the 1989 and 1991 Datong, Shanxi earthquake).

2.3 Seismicity in China in the 20th century

From the distribution of instrumentally determined earthquakes, it can be seen that seismicity in China in the 20th century shows spatial clustering, forming several seismic zones with relatively active seismicity. The main seismic zones include (1) the north-eastern China deep seismic zone with the maximum depth of earthquakes being around 600 km, an extent of the Japan Sea subduction zone; (2) the Fujian-Taiwan seismic zone with strong earthquakes, being a part of the circum-Pacific seismic belt; (3) the north China seismic zone with several strong earthquakes attacking the cities in this area; (4) the north-south seismic zone which keeps active since the ancient time; (5) the Himalayan seismic zone indicating the collision

between the Indian plate and the Eurasian plate; (6) the north Xinjiang seismic zone with several strong earthquakes and earthquake swarms; and (7) the Guangdong-Hainan coast seismic zone with relatively weak but still significant seismicity. Here what is considered is only the apparent clustering of seismicity. Since the relation between seismicity and tectonics is still under discussion, we did not describe the seismic zone in the perspective of tectonics, nor did we sub-divide the large scale seismic zones which may include different tectonic units into smaller zones.

Historical earthquakes shows the north-south seismic zone, the north China seismic zone, and the Fujian-Taiwan seismic zone. The north-eastern China deep seismic zone, the Himalayan seismic zone, and the north Xinjiang seismic zone can be seen only with instrumentally determined catalogues. The Guangdong-Hainan coast seismic zone can also be recognised in historical earthquakes but not so evident. The earthquakes in the north-south seismic zone, the north China seismic zone, the north Xinjiang seismic zone, and the Guangdong-Hainan coast seismic zone belong to intraplate (continental) earthquakes, the tectonics of which is still an open question in geodynamics.

Strong earthquakes in China in the 20th century also show temporal clustering. For example, decade periodicity is significant in statistics. Some other patterns, such as earthquake migration, seismic gap, seismic quiescence, and so on, have also been recognised, yet to be tested by statistics. The mechanism of the decade periodicity is still to be studied in geodynamics. The accumulation of knowledge of earthquakes in the 20th century being considerable, the understanding of the nature of earthquake is still an outstanding question for seismologists both in China and all over the world.

REFERENCES

- Editorial Committee of *China Today* (ed.), 1993. *China Today: Earthquake Hazard Reduction Undertaking*. Publishing House of *China Today*, in Chinese, 462pp.
- Institute of Geophysics of the State Seismological Bureau (ed.), 1987. *Field Investigation of Chinese Earthquakes, vol.1*. Seismological Press, in Chinese, 346pp.
- Institute of Geophysics of the State Seismological Bureau (ed.), 1990. *Field Investigation of Chinese Earthquakes, vol.2*. Seismological Press, in Chinese, 374pp.
- Institute of Geophysics of the State seismological Bureau and Institute of Chinese Historical Geography of Fudan University (eds.), 1986. *Atlas of the Historical Earthquakes in China: The Ming Dynasty Period*. China Cartographic Publishing House, in Chinese, 194pp.
- Institute of Geophysics of the State seismological Bureau and Institute of Chinese Historical Geography of Fudan University (eds.), 1990. *Atlas of the Historical Earthquakes in China: The Qing Dynasty Period*. China Cartographic Publishing House, in Chinese, 244pp.

- Lee, W. H. K., Wu, F. T. and Wang, S. C., 1978. A catalog of instrumentally determined earthquakes in China (Magnitude>6) compiled from various sources. *Bull. Seism. Soc. Amer.*, **68**: 383~398.
- Li Shanbang (Lee, S. P.), 1981. *Earthquakes in China*. Seismological Press, in Chinese, 612pp.
- Ma Zongjin, Fu Zhengxiang, Zhang Yingzhen, Wang Chengmin, Zhang Guomin and Liu Defu, 1982. *Nine Strong Earthquakes in China (1966~1976)*. Seismological Press, in Chinese, 216pp.
- Xie Yushou and Cai Meibiao (eds.), 1983a. *Collection of Historical Data of Chinese Earthquakes, vol. 1, Remote Antiquity to The Yuan Dynasty Period*. Publishing House of Sciences, in Chinese, 227pp.
- Xie Yushou and Cai Meibiao (eds.), 1983b. *Collection of Historical Data of Chinese Earthquakes, vol.2, The Ming Dynasty Period*. Publishing House of Sciences, in Chinese, 949pp.
- Xie Yushou and Cai Meibiao (eds.), 1983c. *Collection of Historical Data of Chinese Earthquakes, vol. 3, The Qing Dynasty Period*. Publishing House of Sciences, in Chinese, 1427pp.

MACROSEISMIC AND STRONG-MOTION PARAMETERS

G. Grünthal

Dept. of Kinematics and Dynamics of the Earth
GeoForschungsZentrum Potsdam, Telegrafenberg C3, D-14473 Potsdam

1. INTRODUCTION

The extensive devastations during catastrophic earthquakes require vigorous investigations to reduce losses of life and in economy. Generally, the better the economy and infrastructure is developed in countries of high seismic activity the greater the efforts of the society towards earthquake protection will be. Particular attention should be payed to the assessment and mitigation of earthquake risk in earthquake struck developing countries where major investments and vital lifeline systems are frequently concentrated in seismically dangerous areas. Especially there the economic losses incurred by a devastating earthquake may result in serious economic disruptions with all its detrimental social consequences. Therefore, regional as well as detailed urban planning in seismic active areas should rest on proper knowledge of:

- Regional geology and tectonics;
- Regional seismicity, earthquake catalogues (especially investigations of major previous events in the region);
- Characteristics of regional seismic activity and strong ground motion;
- Seismic zoning, both on seismological and tectonical data;
- Faulting and permanent ground deformations, landslides, other geological effects of earlier earthquakes;
- Regional distribution of earthquake effects;
- Microzoning of special local areas;
- Engineering aspects of disastrous earthquakes, damage distribution on different structural types;
- Adequacy of existing building codes and regulations;
- General recommendations for retrofitting of existing housing in the area;
- Social and economic implications of earthquakes in the region.

2. MACROSEISMIC PARAMETERS

The first question arising from the topics stated above is how to scale the earthquake effects in its regional distribution. For engineering design the parameters of primary importance are the recorded amplitudes of ground acceleration, velocity and displacement, the frequency content of such records and the duration of strong ground shakings. In the absence of any dense net of strong motion recording sites the macroseismic intensity as a descriptive quantity provides useful information on the regional distribution of earthquake effects, its dependence on distance, focal depth, local ground conditions etc. Because of the lacking of relevant strong-motion data macroseismic intensity has been used in most cases as scaling parameter for seismic hazard studies.

But the intensity will not fully satisfy the requirements of engineers in charge of designing earthquake resistant structures. Nevertheless, macroseismic investigations have been going

through a Renaissance recently because both of their relative simplicity and complexity as well as the necessity of re-evaluation of historical records as a data base for seismic zoning and studies of long term patterns of seismicity. For hazard studies it is necessary to have an as long as possible time span of catalogued earthquake data. These data are macroseismic ones anyhow for times before 1900 and it is not possible to disclaim this part of data, because the better we know the seismic history or past the better we can assess the future process of seismicity.

Macroseismic investigations include the collection of felt perceptions by persons and of damages on structures in a dense net of settlements as well as the compilation of changes in landscape. These non-instrumental macroscopic criteria have to be quantified in grades of intensities according to their definition in an appropriate macroseismic scale. The intensity data depicted in isoseismal maps are analysed with regard to (1) the determination of the epicentre (especially of historical, non-instrumental earthquakes); (2) the attenuation of intensity with distance, (3) peculiarities of isoseismals etc. and their causes.

Problems will arise when comparing the intensity data of different epochs and from different countries owing to the use of different scales and their different versions. Therefore, the knowledge about the used scales since the middle of last century, their relations to each other as well as the underlying predominant opinions and conceptions in quantifying macroseismic observations is indispensable especially where original descriptions of the observed effects are no longer available. Some of the most important scales are the ROSSI-FORREL scale from 1883 (when dealing with historical data), the scale used in Japan (JMA, 1952), the Modified-Mercalli scale (MM; USA, 1931), and the Medvedev-Sponheuer-Karnik scale (MSK) in its versions from 1964, 1981, and 1992.

The wording of the MSK-92 or EMS-92 scale with its detailed definitions of types of structures, classification of damages and quantities is annexed to the lecture notes "The updated MSK intensity scale EMS-92". Fig. 1 presents the relations between individual intensity range of the above mentioned scales.

Global conversion relations of epicentral intensity I_0 , magnitude M and focal depth h [km] as well as for intensity I_n in a hypocentral distance D_n , respectively, are given for shallow earthquakes ($0 < h < 100$) in the nomogram in Fig. 2. But considerable variations of such a "global" relation are known. It is, therefore, essential to apply in a considered region the relation which is valid for that region or relevant subregions. For Europe, e.g., the following relation after Karnik provides the best results:

$$M = 0.5I_0 + \log h + 0.35 \quad [h \text{ in km}].$$

It is well known since the beginning of this century that the focal depth has an important influence on the areal distribution of the severity of shakings. This fact can be used to assess the focal depth from macroseismic data. Based on the fundamental work of Kövesligethy (1907), Sponheuer (1960) presented a set of nomograms (Fig. 3) to determine the focal depth h from the mean isoseismal radii D_i of Intensities I_i according to the following relation:

$$I_0 - I_i = 3 \log \left(\frac{\sqrt{D_i^2 + h^2}}{h} \right) + 3\alpha \log e \left(\sqrt{D_i^2 + h^2} - h \right)$$

Comparison of different macroseismic scales

scale	degrees of intensity											
MSK-64	2	3	4	5	6	7	8	9	10	11	12	
MM	1	2	3	4	5	6	7	8	9	10	11	12
RF	2	3	4	5	6	7	8	9	10			
JMA	1	2	3	4	5	6	7					

Fig. 1 Relations of the intensity ranges of the following macroseismic intensity scales: MSK-64, MM, RF, JMA: modified after Shebalin (1975). Between the different versions of the MSK-scale there are no differences in the assessed intensities.

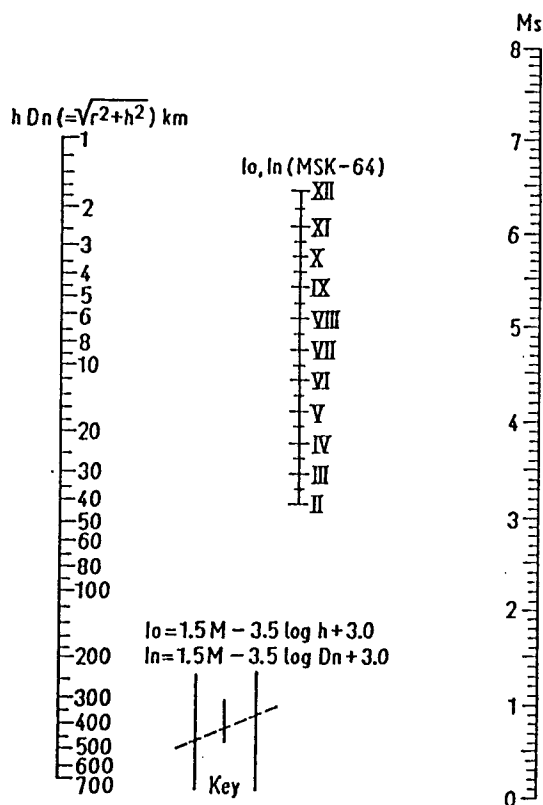


Fig. 2 Nomogram converting M , I_0 and h or M , I_n and D_n (after Shebalin).

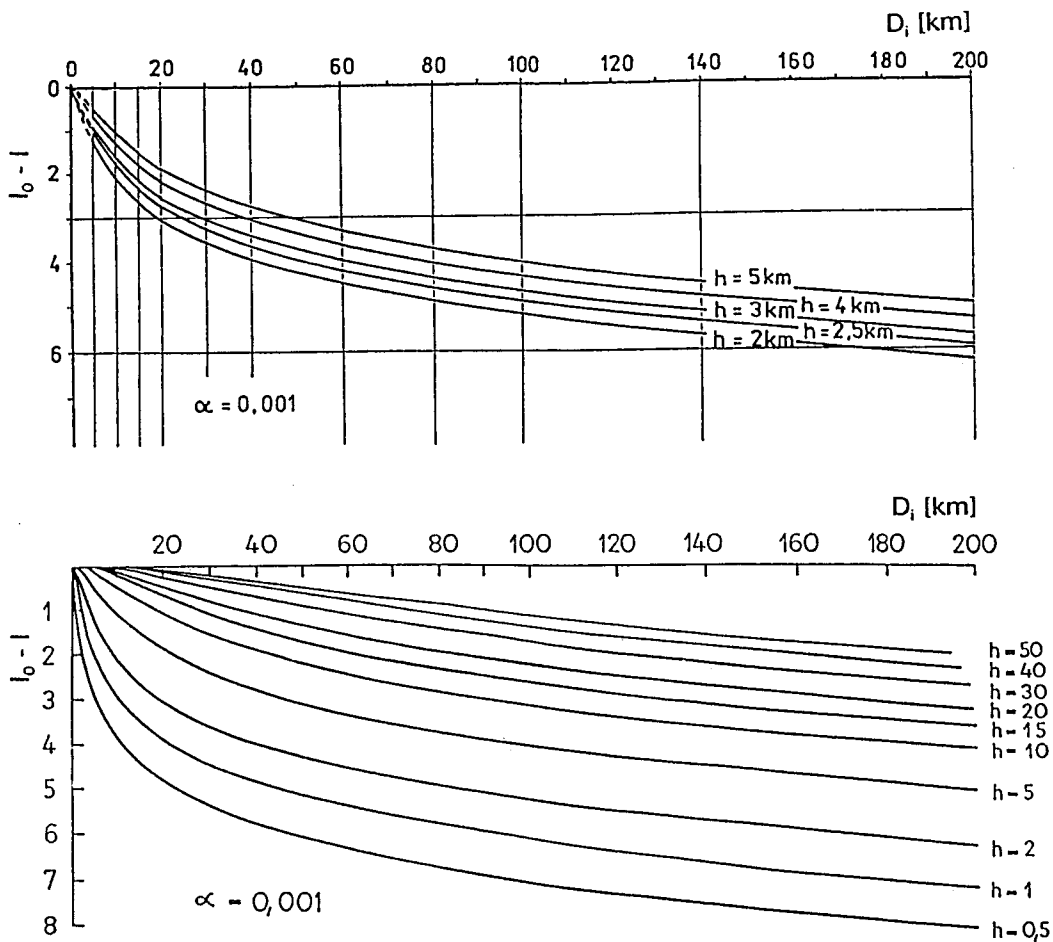


Fig. 3 Diagram for the determination of the focal depth h (in km) from mean isoseismal radii D_i ; based on an attenuation coefficient $\alpha = 0.001 \text{ km}^{-1}$.

3. STRONG-MOTION PARAMETER

3.1 Strong-motion records and different kind of spectral representations

Damage to engineering structures caused by earthquakes is known to depend both on the ground motion characteristics and on the characteristics of structures. For the purpose of engineering design, the characteristics of ground shaking that are of primary importance, are the amplitude, the frequency distribution and the duration of shaking. These characteristics (see scheme of Fig. 4) depend on various factors such as:

- I the earthquake source spectrum depending on the physical source process (the orientation of the site with respect to the source);
- II the filter function of the transfer media (influence of distance, structure, attenuation)
- III the filter function of the local site conditions (the surface topography, the subsurface configuration and attenuation);
- IV the resonance period of structures in relation to the local transfer function of the subsoil
- V the soil-structure interaction.

Remarks on the above mentioned characteristics:

to I: The seismic source spectrum determines the spectral content of the strong-motion records in the following way:

- The extent of the source plane F and the amount of dislocation determine the seismic moment M_0 and influences mainly the long-period spectral part which is decisive for far-field effects.
- The dislocation velocity v_B influences especially the short-period spectral part (the higher v_B the shorter the radiated wave lengths); both v_B and F determine the duration of the source process and in particular the shape of the displacement spectrum.
- The stress drop determines the high frequency part and thus the acceleration spectrum which is most decisive for the near-field effects.
- Additionally the orientation of the source to the site can influence the strong-motion characteristics.
- Also the tectonic regime influences the expected peak accelerations. In thrust fault regimes the maximum accelerations can be higher by the factor 4 than in normal faulting regimes.

to II: The filter function of the transfer medium is characterized by:

- the structure and elastic parameters including attenuation of the media through which the waves propagate;
- the length of the travel path.

to III: The filter function of the local soil conditions is also expressed as soil amplification and is the subject of microzoning studies. It is characterized by:

- the local subsoil (3d) structure and its elastic parameters;
- the angle of incident waves;
- the inelastic behaviour for shakings above a certain level.

The earthquake effects on the ground surface and on structures can be considered as follows:

- **Seismic zoning**, i.e. the definition of ground motion parameters on bedrock;
- **Seismic microzoning**, i.e. the consideration of the modification of the ground motion parameters obtained on bedrock due to the influence of the ground surface;
- **Aseismic design** parameters, i.e. the definition of structural design parameters considering the soil-structure interaction.

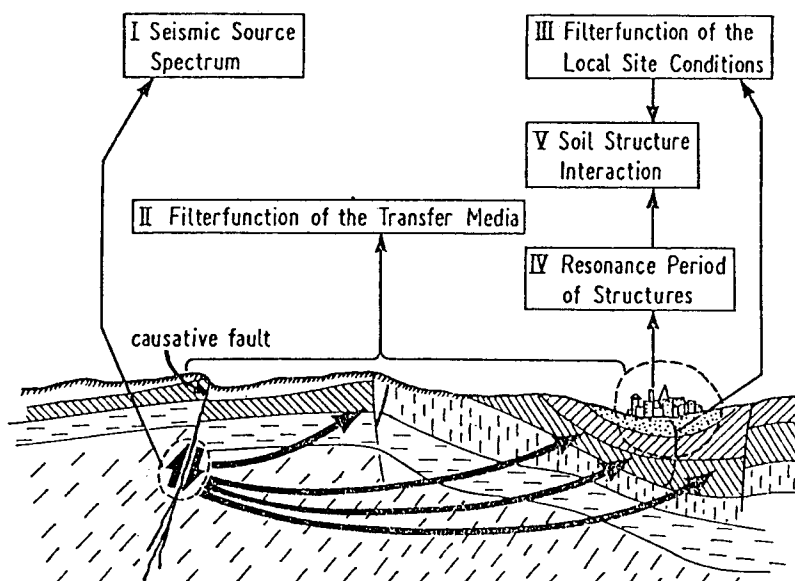


Fig. 4 Schematic illustration of the 5 basic components influencing the damage potential of structures.

The relations between intensity, magnitude and epicentral distance on the one hand and the strong-motion parameters on the other hand (i.e. the absolute peak values or average values of maximum recorded acceleration a , velocity v and displacement d , their frequency spectra, the duration of strong ground motions, the relation between all these parameters and their dependence on the respective soil conditions) are of essential practical importance in hazard assessments. Engineering seismology could be defined as strong-motion seismology which produces results used as input for earthquake engineering, i. e. for earthquake resistant design of structures and appropriate experimental studies.

Fig. 5 shows a typical acceleration record as well as the computed time series of velocity and displacement. The appropriate acceleration response spectra for different structural damping (in percent of the critical damping) is given in Fig. 6. This type of spectra represents the response (maximum amplitude) of a set of single degree of freedom oscillators each characterizing the response of a special natural period excited by the strong-motion record. The principle of the computation of response spectra is shown in Fig. 7.

The velocity response spectrum without damping corresponds with regard to characteristic features with the Fourier acceleration spectrum. The response spectra of acceleration S_a , of velocity (respectively pseudo-velocity) S_{pv} and of displacement S_d are symmetrically according to

$$\frac{T}{2\pi} S_a = S_{pv} = \frac{2\pi}{T} S_d.$$

This distinctive feature leads to the common presentation of smoothed and generalized spectra in special tripartite logarithmic paper (Newmark-spectra or design spectra). Fig. 8 shows such a tripartite spectral presentation in its classical form after Newmark (1973).

The observed strong motion data show a great variation when classified according to intensity, magnitude, distance, type of soil etc. Only a statistical representative data set allows to derive general results.

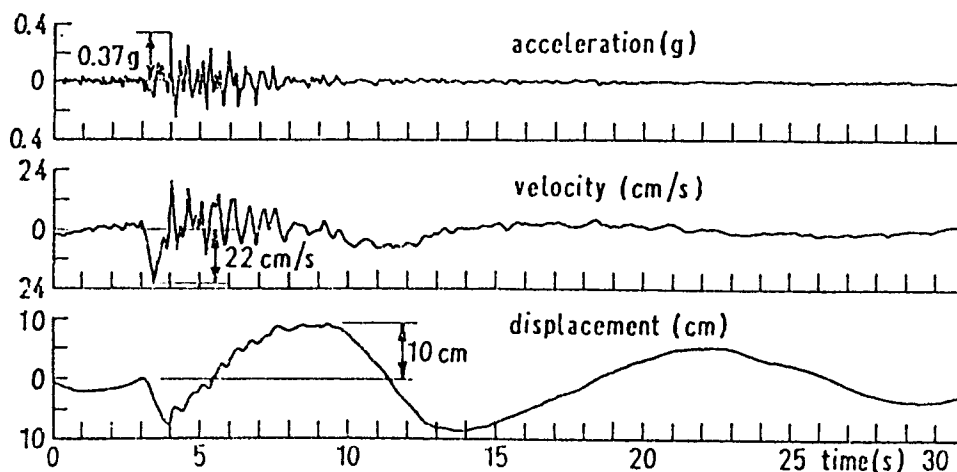


Fig. 5 Acceleration, velocity and displacement (N-S component) recorded at Tolmezzo (N-Italy) at 20h 00m 15s on May 6th, 1976 (15 km epicentral distance, $M = 6.5$, $h = 10$ km, $I_0 = IX - X$); CNEL-ENEL (1976).

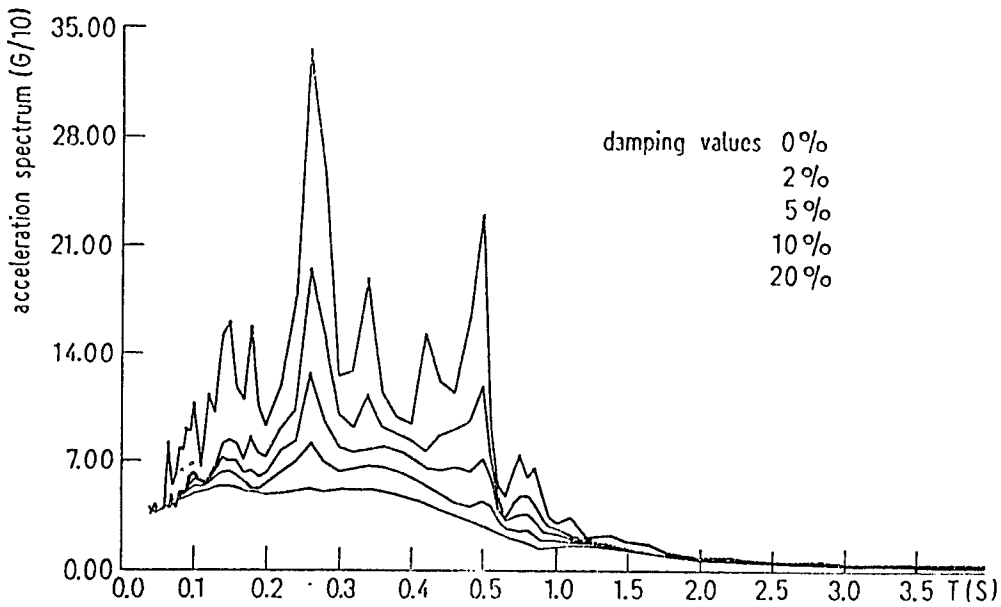


Fig. 6 Acceleration response spectrum corresponding to the record shown in Fig. 5 (CNEL-ENEL, 1967).

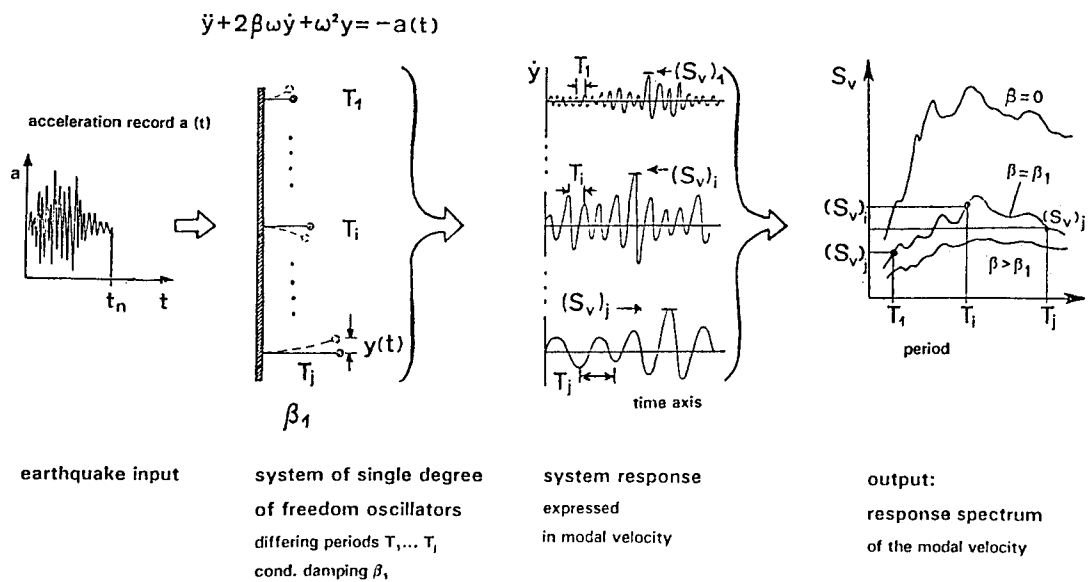


Fig. 7 Schematic presentation of the construction of response spectra.

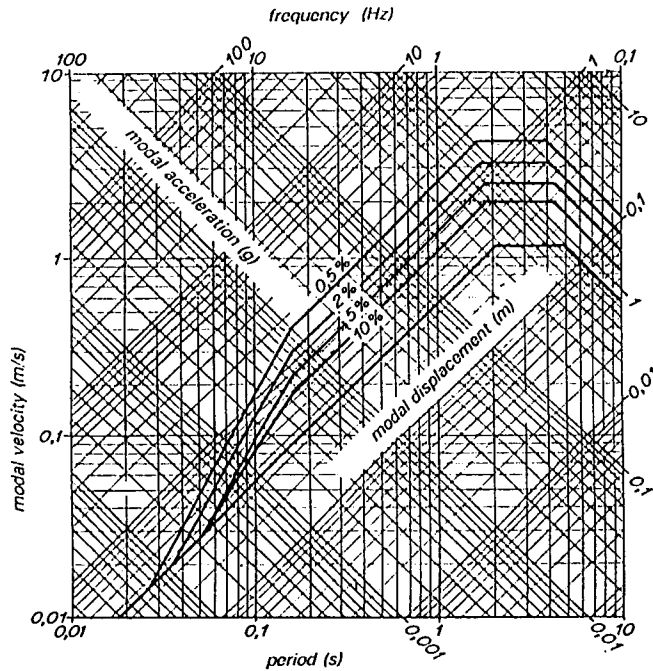


Fig. 8 Tripartite spectral presentation of smoothed design spectra after Newmark (1973) representing intensities of about VII.

3.2 Attempts to correlate intensity with amplitudes of recorded accelerations

From the practical point of view it is often asked to correlate intensity with accelerations. This is a very critical questions and to be answered with caution only.

Fig. 9 shows the observed peak acceleration in relation to intensity for the data from 1933 to 1973. The scatter ranges over two orders in acceleration and illustrates the principal weakness of any correlation attempts of acceleration with intensity. The reasons for this scatter can partly be explained by the various factors influencing the strong-motion characteristics as shown in Fig. 4. But for many practical routine purposes it is sufficient to use a simple intensity-acceleration relation such as the one given by Trifunac and Brady (1975):

$$\log a_{\text{vert.}} = 0.30 I_{\text{MM}} - 0.18$$

$$\log a_{\text{hori.}} = 0.30 I_{\text{MM}} - 0.14$$

$$IV \leq I_{\text{MM}} \leq X$$

with a - acceleration in cm/s^2 .

Another frequently used conversion relation is given by Murphy and O'Brien (1977):

$$\log a = 0.25 I + 0.25;$$

and, when considering especially hypocentral distances smaller than 25km

$$\log a = 0.38 I - 0.56.$$

A relation which allows to take into account soil categories ($s=0$ alluvial, $s=2$ hard rock, $s=1$ intermediate), the component of recording ($v = 0$ horizontal, $v = 1$ vertical), and the chosen confidence interval p ($0 \leq p \leq 1$) has been given by Trifunac (1976):

$$\log \left\{ \begin{matrix} a_{\text{max}, p} \\ v_{\text{max}, p} \\ d_{\text{max}, p} \end{matrix} \right\} = ap + bI_{\text{MM}} + c + ds + ev + fI_{\text{MM}}^2;$$

	a	b	c	d	e	f
a_{\max}	0.942	0.459	-0.047	0.014	-0.270	-0.014
v_{\max}	0.883	0.288	-1.411	0.014	-0.286	0.000
d_{\max}	0.913	0.006	-0.690	-0.059	-0.186	0.019

More modern relations using the magnitude M and the hypocentral distance R or epicentral distance D in km as parameters, respectively, are those of Abrahamson and Litchiser (1989):

$$\log a(g) = -0.62 + 0.177M - 0.982 \log (R + e^{0.284M}) + 0.132F - 0.0008 Er \quad \text{with}$$

F - tectonic regime ($F=1$ thrust faulting, $F=0$ others than thrust)

Er - type of earthquake ($Er = 1$ intraplate earthquakes, $Er = 0$ interplate earthquakes)

$a(g)$ - peak ground acceleration as fraction g (Earth's gravity).

Campbell (1989): $\ln a(g) = -2.501 + 0.623M - 1.0 \ln (D + 7.28)$ for

$$2.5 \leq M \leq 5.0 \quad \text{and} \quad 2 \text{ km} \leq D \leq 25 \text{ km.}$$

Joyner and Boore (1981):

$$\log a(g) = 1.02 + 0.249M - \log R - 0.00255 R$$

Ambraseys and Bommer (1992):

$$\log a(g) = -0.87 + 0.217M - \log R - 0.00117 R$$

as well as many others.

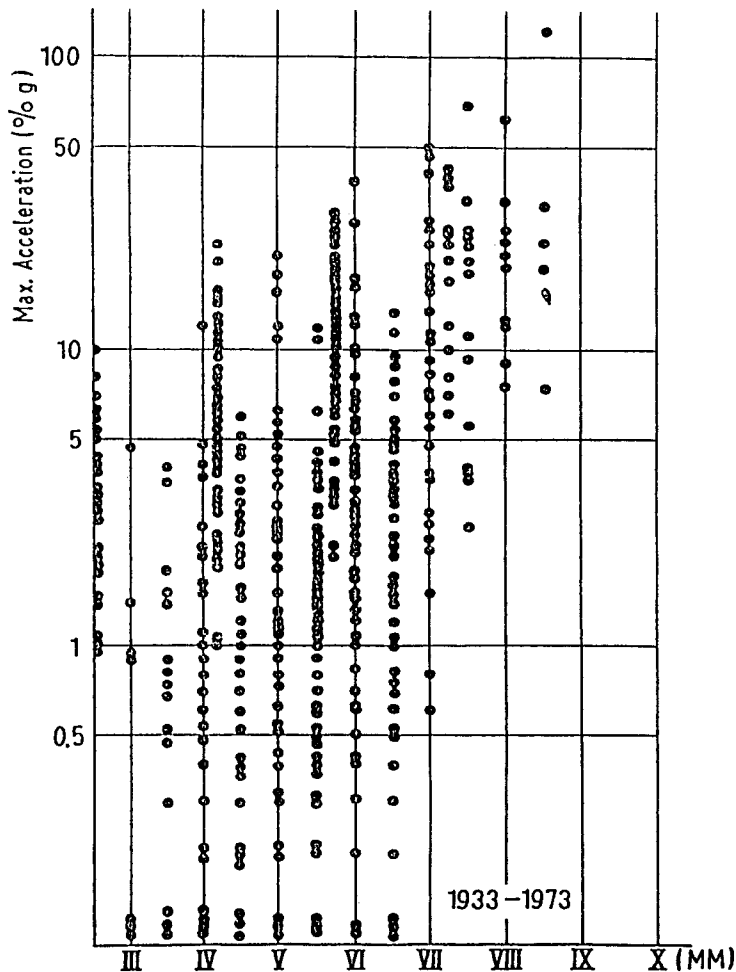


Fig. 9 Recorded maximum acceleration versus reported intensities for the period 1933 - 1973 (Ambraseys, 1974)

Theoretically, the largest possible acceleration in geological media could reach about 2 g (g: Earth's gravity, approx. 981 cm/s^2) (Ambraseys, 1974). The strongest acceleration of 1.49 g shown in Fig. 8 occurred at a site some 2 km from the causative fault during the Oct. 15, 1979, Imperial Valey earthquake (California) with $M = 6.4$. Relatively small shocks can produce rather strong acceleration peaks as well very close to the causative faulting (e. g. Parkfield earthquake, June 27, 1966, $M = 5.6$, $a_{\text{max}} = 0.50 \text{ g}$, distance about 70 m). But the duration of strong shaking is relatively short in such cases so that the intensity which is an integral measure of both acceleration and duration corresponds to the relative small magnitude of these events. A better correlation with intensity shows the velocity (Fig. 10). Here the scatter of data is "only" one order of magnitude. This implies that the velocity is a better measure for intensity and thus for structural damage or human perception, respectively, than acceleration.

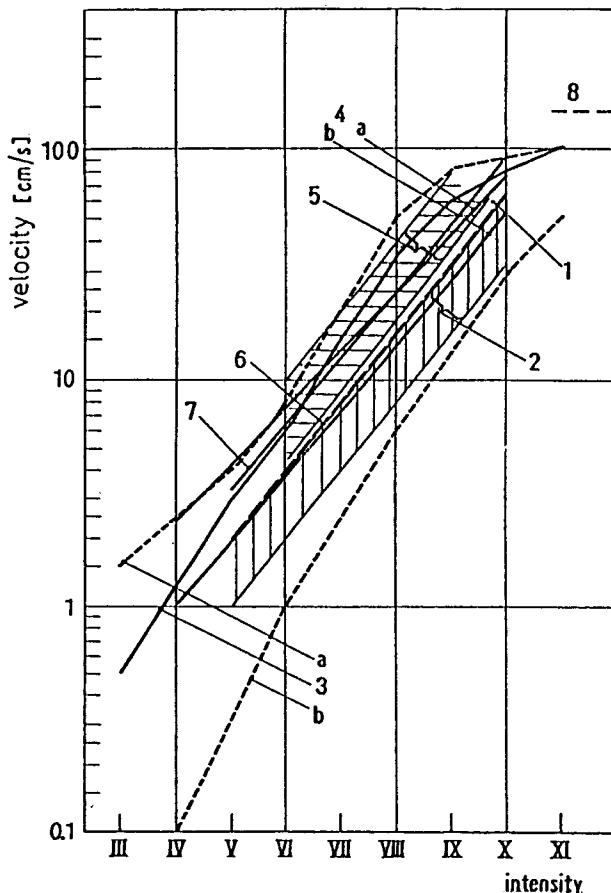


Fig. 10 Relations between recorded maximum soil-velocity and reported intensity: 1 - Neumann (1960); 2 - Medvedev and Sponheuer (1969); 3 - Shebalin (1975) a and b - probable upper and lower bound; 5 - Trifunac and Brady (1975) a - horizontal, b - vertical; 5 - Nazarov and Darbinyan (1975); 6 - Medvedev (1977); 7 - Espinosa (1977); 8 - Ambraseys (1974): expected maximum possible values.

3.3 Generalized spectral presentations

Fig. 11 and 12 show the mean spectral content of acceleration records of horizontal motion for different magnitudes in different epicentral distances for soft soils ($s = 0$) and hard rock ($s=2$). The influence of the type of soil at the recording site depends on frequency. Larger amplitudes (by the factor s) are observed on soft soils for periods greater than 0.2 s.

An interesting spectral feature presents Fig. 13 after Devilliers and Mohammadioun (1981). It shows 7 different spectra for the one intensity level $I_S = VI - VII$. This one intensity level can be produced by different constellations of magnitudes and distances given also in Fig. 13 (i.e. from motions of a $M = 4.6$ earthquake recorded at a distance of $R = 10$ km up to an $M = 7.5$ earthquake recorded at a distance of 200 km, which all yields in the same intensity of $I = VI - VII$). The different shapes of the spectra reflect both the influence of large discrepancies in the source characteristics of such a wide range of earthquake sizes and the influence of considerable differences of seismic wave attenuations along the wave paths ranging from 10 to 200 km.

The influence of different soil conditions on the spectral shape is shown in Fig. 14a and b after Seed et al. (1974) at the example of the best investigated magnitude $6\frac{1}{2}$ earthquakes in two different distances (5 and 20 miles). For short periods (< 0.6 sec) the largest amplitudes can be expected on stiff soils while for larger periods the effects are largest on soft soil conditions. The prediction of such effects is one of the subjects of microzoning.

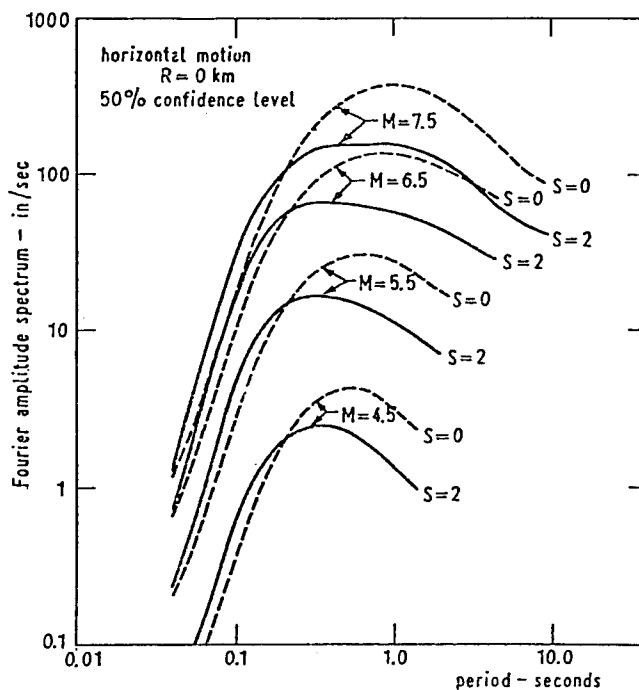


Fig. 11 Mean Fourier amplitude spectra of horizontal acceleration in the epicentre for magnitudes from 4.5 to 7.5 on soft ($s = 0$) and on hard rock ($s = 2$); Trifunac (1976).

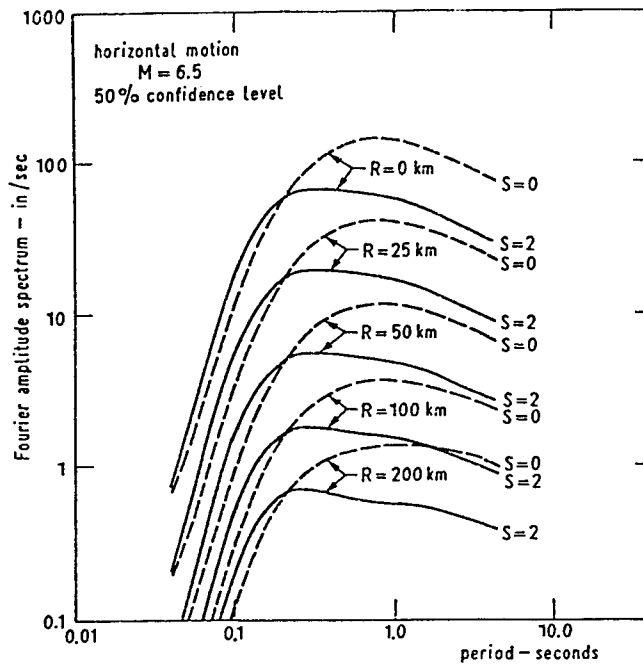


Fig. 12 Mean Fourier amplitude spectra of horizontal acceleration for 6.5 magnitudes in epicentral distances from 0 to 200 km; Trifunac (1976).

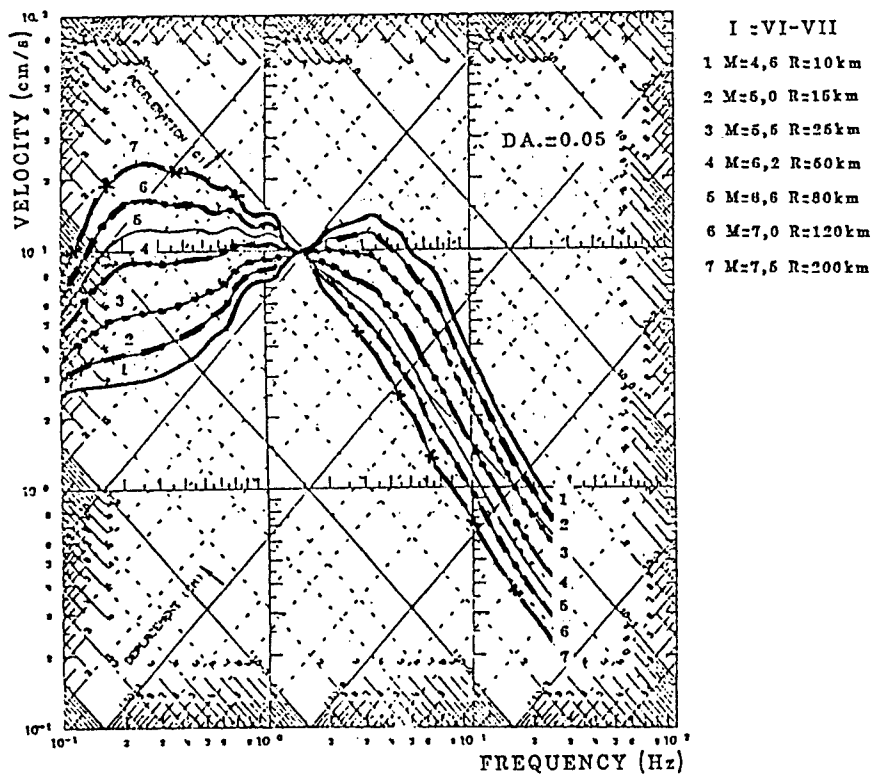


Fig. 13 Variation of spectra corresponding to the intensity VI - VII with magnitude and focal distance.

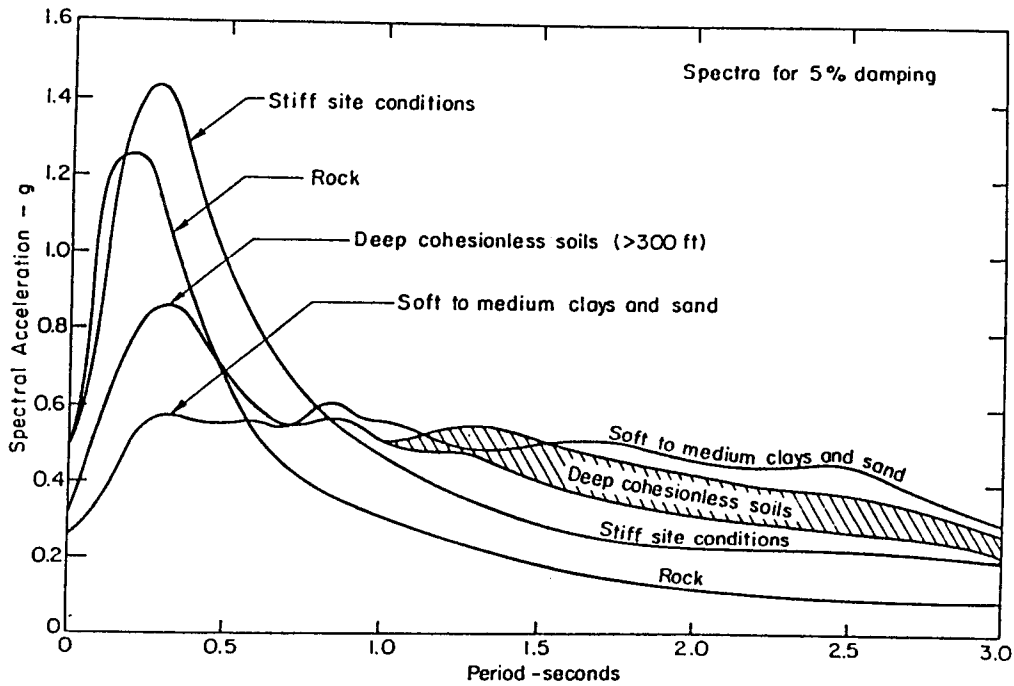


Fig. 14a Anticipated mean spectra for magnitude $6\frac{1}{2}$ earthquakes at a distance of 5 miles (after Seed et al., 1974).

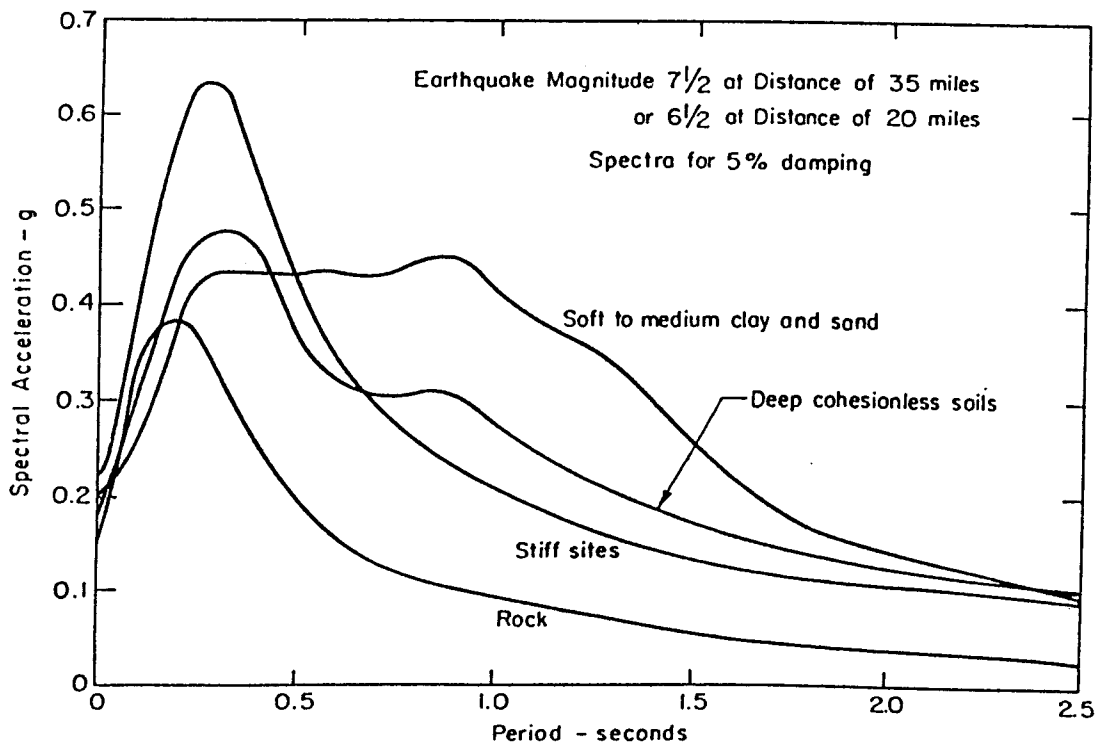


Fig. 14b Anticipated mean spectra for magnitude $6\frac{1}{2}$ earthquakes at a distance of 20 miles (after Seed et al., 1974).

3.4 Attenuation of acceleration with distance and dominating periods of motion

Another important problem concerns the attenuation of acceleration or velocity with distance. The observed peak values with distance show a large variability.

Fig. 15 presents average values of maximum acceleration for different magnitudes as a function of distance in the western United States. It should be noted that the peak acceleration values, e.g. in the Mediterranean region, are in the average by the factor 2 - 3 higher than those in the western United States. This phenomenon can be explained by regional differences in stress drop. Low stress-drop events cause low acceleration records in the epicentral area and vice versa. Further important parameters in engineering seismology are the duration of the strong-motion phase and the dominant periods of motion. The duration increases with magnitude due to the extension of the source process as well as with distance (Tab. 1). The dominant period of strong shaking differs essentially between acceleration, velocity and displacement. Expected mean values for different magnitudes and distances are given for acceleration on rock sites in Tab. 2 and for displacement in Tab. 3.

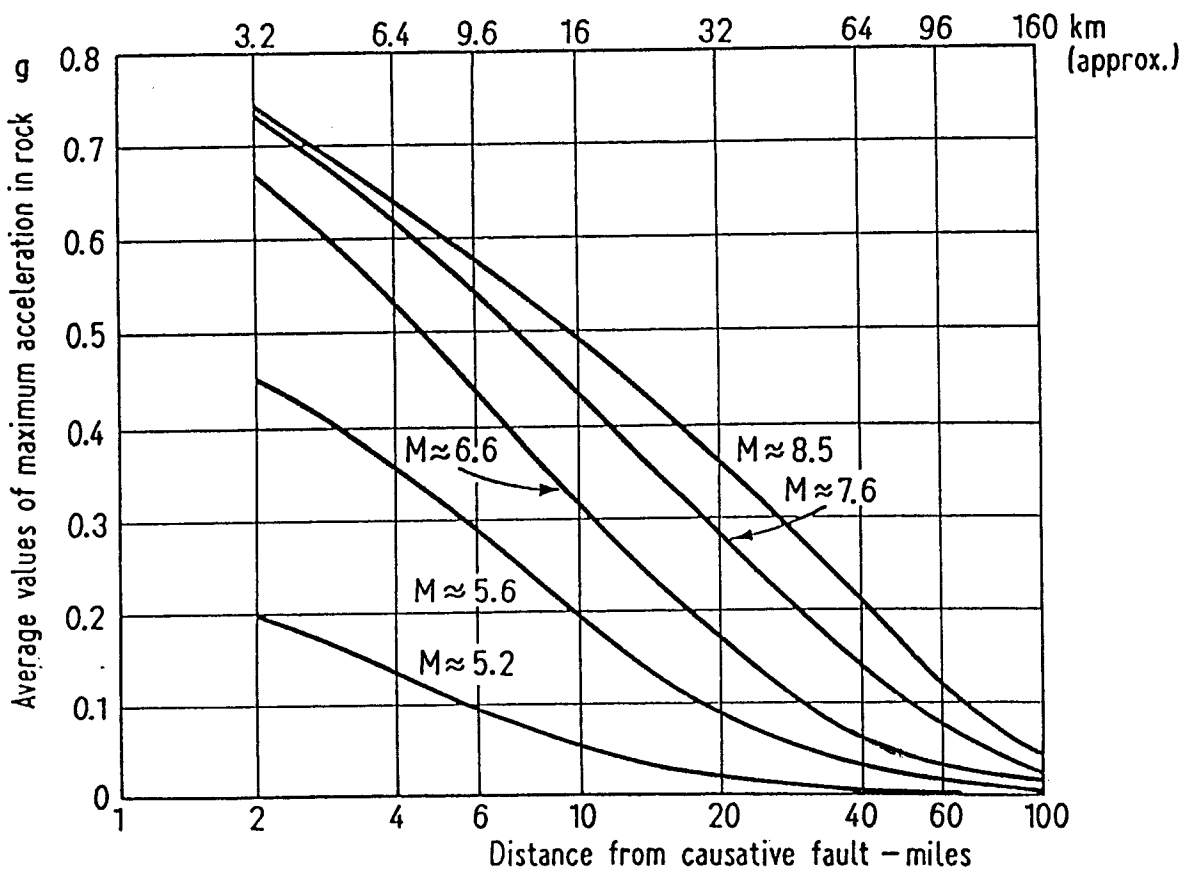


Fig. 15 Average values of maximum acceleration on rock sites versus distance in the western United States (Schnabel and Seed, 1972).

Tab. 1 Duration of strong-motion phase in dependence on magnitude M and distance D in km (Shebalin, 1975).

D \ M	3.3-3.9	4.0-4.6	4.7-5.3	5.4-6.0	6.1-6.7	6.8-7.4	7.5-8.1	8.2
3-7	0.5	1	2	3	5	-	-	-
7-15	0.8	1.5	2	4	7	10	15	-
15-30	1.0	1.5	3	5	9	14	20	30
30-60	1.0	2	3	6	12	20	40	50
60-120	-	2	4	7	14	30	60	100
-250	-	-	4	8	16	40	90	200

Tab. 2: Dominating period of acceleration in dependence on M and D as in Tab. 1 (Shebalin, 1975).

D \ M	3.3-3.9	4.0-4.6	4.7-5.3	5.4-6.0	6.1-6.7	6.8-7.4	7.5-8.1
3-7	0.18	0.21	0.24	0.27	0.29	-	-
7-15	0.20	0.24	0.27	0.30	0.34	0.37	-
15-20	0.22	0.27	0.31	0.35	0.39	0.43	0.43
30-60	0.26	0.31	0.36	0.41	0.45	0.49	0.52
60-120	0.31	0.38	0.42	0.48	0.52	0.57	0.61
250	0.36	0.45	0.50	0.57	0.63	0.70	0.78

Tab. 3: Dominating period of displacement in dependence on M and D as in Tab. 1 (Shebalin, 1975).

D \ M	3.3-3.9	4.0-4.6	4.7-5.3	5.4-6.0	6.1-6.7	6.8-7.4	7.5-8.1	8.2
3-30	0.6	2	3	5	10	-	-	-
30-300	1	2.5	5	9	16	28	40	50

REFERENCES

- Ambraseys, N.N.: Dynamics and response of foundation materials in epicentral regions of strong earthquakes.
- Abrahamson, N.A.; Litehiser, J.J.: Attenuation of vertical peak acceleration. *Bull. Seismol. Soc. Am.* 79/3, 549, 1989.
- Ambraseys, N.N.: Notes on Engineering seismology. In: *Engineering seismology and earthquake engineering*, J. Solnes (ed.)
- Campbell, K.W.: The dependence of peak horizontal acceleration on magnitude, distance, and site effects for small-magnitude earthquakes in California and Eastern North America. *Bull. Seismol. Soc. Am.* 79/5, 1311-1346, 1989.
- CNEN-ENEL: Contribution of the study of Friuli earthquake of May 1976. CNEN-ENEL Publ., Nov. 1976, Rom.
- Devillers, C.; Mohammadioun, B.: 1981. French methodology for determining site adapted SMS (Séisme Majoré de Sécurité) Spectra. Proceedings of the 6th International Conference on Structural Mechanics in Reactor Technology, Paris. Vol K, paper 1/9.
- Espinosa, A.F.: Practice-velocity attenuations relations: San Fernando earthquake of February 9, 1971.
- Joyner, W.B.; Boore, D.M.: Peak horizontal accelerations and velocity from strong-motion recordings including records from the 1979 Imperial Valley, California, earthquake. *Bull. Seis. Soc. Am.* 71, 2011-2038, 1981.
- Kövesligethy, R.V.: Seismischer Stärkegrad und Intensität der Beben. *Gerlands Beitr. Geophys.* 8 (1907), 22-29.
- Medvedev, S.V.: Seismic intensity scale MSK-76. *Publ. Inst. Geophys. Pol. Acad. Sc.*, A-6 (117), 1977, 95-102.
- Medvedev, S.V.; Sponheuer, W.: Scale of seismic intensity. *Proc. IV World Conf. Earthquake Eng.*, Santiago, Chile, A-2 (1969), 143-153.
- Murphy, J.R.; O'Brien, L.J.: The correlation of peak ground acceleration amplitude with seismic intensities and other physical parameters. *Bull. Seism. Soc. Am.* 67 (1977), 877-915.
- Nazarov, A.G.; Darbinyan, S.S.: Škala dlja opredelnija intensivnosti sil'nych zemletrjasenij na količestvennoj osnove. In: *Seismičeskaja škala i metody izmerenija sejsmičeskoj intensivnosti*. Nauka (1975), 40-79.
- Neumann, F.: A Broad formular for estimating earthquake forces on oscillators. *Proc. II World Conf. Earthquake Eng.*; 2 (1960), p. 850, Tokyo.
- Newmark, N.: A study of vertical and horizontal earthquake spectra. *Consulting Engineer Services, Directorate of Licensing, U. S. Atomic Energy Comm. WASH-1255*, Wash. D.C. April 1973.

- Schnabel, B.; Seed, H.B.: Acceleration in rock for earthquakes in the Western United States. Earthqu. Engin. Research Center Rep. No. 72-2 (1972).
- Seed, H.B.; Ugas, C.; Lysmer, J.: Site-dependent spectra for earthquake-resistant design. EERC-Rep. No. 74-12 (1974).
- Shebalin, N.V.: Ob ozenke sejsmičeskoj intensivnosti. In: Sejsmičeskaja škala i metody immerenija sejsmičeskoj intensivnosti (87-109), Nauka 1975.
- Sponheuer, W.: Methoden zur Herdtiefenbestimmung in der Makroseismik. Freib. Forschungsh. C88 (1960), 117 pp.
- Trifunac, M.D.: A note on the range of peak amplitudes of recorded accelerations, velocities and displacements with respect to the Modified Mercalli Intensity Scale. - Earthquake Notes, Vol. 47/1 (1976), 9-24.
- Trifunac, M.D.; Brady, A.G.: On the correlation of seismic intensity scales with the peaks of recorded strong ground motion. Bull. Seis. Soc. Am. 65 (1975), 139-162.

METHODOLOGY OF SEISMIC HAZARD ASSESSMENT

G. Grünthal

Dept. of Kinematics and Dynamics of the Earth
GeoForschungsZentrum Potsdam, Telegrafenberg C3, D-14473 Potsdam

1. INTRODUCTION

In seismically active regions, any decision-making for urban or regional planning should be based on probable characteristics of earthquakes to be expected in future. These features are provided by the procedure usually called "seismic hazard assessment".

The term "seismic hazard" (H) means the probability of occurrence of potentially damaging seismic ground motions at a certain site within a certain time interval. The process of determining seismic hazard in a region is also called "seismic zoning". It has to be stated that this term does not involve a special study, how local surface and subsurface conditions can influence the seismic soil or ground motions. This falls into the domain of seismic microzoning. The main outcome of a seismic zoning procedure are seismic hazard or zoning maps displaying a quantity related to the assessed frequency and severity of shaking due to expected future earthquakes.

The term "seismic risk" is derived from the insurance sector with the meaning that there can be no risk due to natural phenomena if there are no values or works of man exposed to natural hazards. But the usage of the term "risk" is not uniform - therefore it is important to define the meaning in which it is used in the following.

Prior to any evaluation of the seismic risk, the "vulnerability" V has to be determined. The vulnerability is the expected degree of loss within a defined area resulting from the occurrence of a certain earthquake (for assessing the seismic risk) on a scale from 0 (no damage) to 1 (total loss). The vulnerability can be reduced by applying antiseismic measures in civil engineering. The seismic specific risk SR_i is then the product of seismic hazard and vulnerability:

$$SR_i = H_i \cdot V$$

The seismic risk R itself is the sum of all products of the value C_i of the different elements at risk multiplied with the seismic specific risks, i.e.:

$$R = \sum_i (SR_i \cdot C_i)$$

According to the recent security philosophy, different levels of earthquake loading have to be considered. The decision on the probability level to be used in practical seismic hazard applications is rather complex and depends on the final risk that the society is willing to accept. The probabilities of exceedance per year (p.a.) currently used in the design of structures are approximately as follows:

standard buildings: $2 \cdot 10^{-2} - 10^{-3}$ p.a.

important structures: $2 \cdot 10^{-3} - 10^{-4}$ p.a.

nuclear power plants: $10^{-4} - 10^{-6}$ p.a.

2. BASIC DATA

2.1 Seismicity studies

The fundamental basis for any seismic zoning is a carefully compiled earthquake catalogue for the study area. The latter is usually a region of some 200-300 km around the site for which the hazard has to be assessed.

The data on earthquakes should be catalogued backward into history so far as possible. A prerequisite for reliable seismic hazard assessments is the determination of the completeness of data backward into history for different classes of event strength. The primary parameters of earthquake catalogues are the date of an event, the location and a parameter classifying the strength, i.e. the epicentral intensity I_0 or the magnitude M . Appropriate relations between I_0 , M and the focal depth (h) have to be determined for the study region to express the complete data set in terms of a unique strength parameter.

Plots of the epicentres and sizes of earthquakes provide the primary basis for the recognition and delineation of hazardous regions. Significant earthquakes tend to occur repeatedly in certain regions, whereas other regions have experienced few or no events during long historical periods. But one has to be cautious in interpreting epicentre maps, particularly when the depicted time span is short.

2.2 Delineation of seismic source regions

The next step in the preparation of the basic data for seismic hazard assessment concerns the subdivision of the area under investigation into seismic source regions. Within these regions the character of seismic activity should be uniform and the epicentres of expected future events should be likely fall within them. The character of seismic activity within any region is described by the magnitude-frequency relationship according to Gutenberg and Richter (1944):

$$\log N = a - bM.$$

The parameter a describes the level of **seismic activity**; b indicates the proportion of larger to smaller earthquakes and is also called the **seismic regime parameter** of a certain region. The reliable determination of the parameters a and b is of special importance during the zoning procedure. When regions with different slopes of the magnitude frequency graph are combined, this results in a misleading description of a fictitious source region.

In order to increase the reliability of the delineated features, derived purely from historical or previously observed seismicity, it is advisable to include additional data from geology, tectonics, geophysics and geodesy. Especially useful are seismotectonic maps, indicating provinces with different tectonic regimes (normal-, thrust-, or strike-slip-faulting), and

correlations of epicentres with neotectonic fault activity. In this way, it is sometimes possible to delineate rather narrow source zones.

2.3 Estimates of the upper-bound magnitude M_{\max}

For any region there exists a maximum possible magnitude. Its determination, as reliable as possible, is of extreme importance for hazard statements especially for very low occurrence probabilities; i.e. for sites of important structures and nuclear power plant. It has to be stated at the outset that up to now the approaches to determine M_{\max} are not yet well established and a considerable portion of personal judgement is still required. Furthermore, the nature of this problem varies from area to area. The best prerequisite for its estimation is in each case a well recorded earthquake history of the study region. Especially useful is the application of different approaches for one region. Some of the existing possibilities to get a reasonable estimate of M_{\max} or I_{\max} , respectively, are:

- in case of very long and well recorded seismicity observations, simply a certain value should be added to the largest observed intensity;
- to use the GUMBELs type-III extreme value statistics which yields the maximum as an asymptotic value;
- from a cumulative seismic energy release covering at least several centuries, it can be inferred with sufficient reliability;
- to base the estimate on tectonic features, e.g., on the overall length of an active tectonic fault segment.

2.4 Attenuation of ground shaking with distance

The knowledge of attenuation relations - as correct as possible - of that shaking parameter in which the hazard statements will be expressed is also very important for reliable seismic zoning. Appropriate scaling parameters of seismic hazard maps are the macroseismic intensity, the ground acceleration or velocity.

Different versions of algorithms for seismic hazard assessment require either an average attenuation relation for the study region or special relations for the different source regions; additionally, an azimuthal dependence can be introduced.

There are observed large variations in the attenuation pattern - not only on the sub-regional scale due to different subsoil conditions but also from region to region. Therefore, it makes not much sense to transfer any attenuation relation derived for one region to another one without verifying its validity. In order to get reliable seismic hazard maps it is indispensable that the attenuation relations must be based on the detailed analysis of either carefully elaborated macroseismic maps of typical earthquakes or on extensive strong ground-motion recordings in the study region.

3. STATISTICAL BACKGROUND

The tool for the quantitative determination of seismic hazard provides the earthquake statistics. This term means the empirical analysis of the distribution of earthquakes with

regard to their temporal occurrence as well as their energetic classification related to a certain volume of the lithosphere. The necessary assumption for the mostly used approaches on seismic hazard assessment is the random occurrence of earthquakes. But in reality, this assumption has its limitations; i.e. the earthquakes are not fully random - neither in space nor in time.

Seismic hazard assessments are probabilistic. As a numerical value for the statistical probability of the occurrence of an event E, denoted as P(E), the expression

$$P(E) = \frac{\text{number of favourable cases}}{\text{number of possible cases}}$$

can be chosen.

3.1 Temporal occurrence of earthquakes

The frequency of earthquakes above a certain magnitude and within fixed time intervals is fairly good Poissonian when foreshocks and aftershocks are removed from the data set. A random variable N (which can have integer values) is Poissonian with the parameter α if

$$P[N=n] = \frac{\alpha^n}{n!} \exp(-\alpha) \quad (n = 0, 1, 2, \dots)$$

is valid. A suitable estimate for α is the arithmetic mean of the independent realizations of the random variable. This discrete distribution describes many processes in nature (in biology, meteorology, quality control, nuclear physics) and in daily life.

3.2. Frequency distribution of different magnitudes

After Gutenberg and Richter the relation between the number N of earthquakes in a natural sequence, having magnitudes in the interval $m \pm \frac{1}{2} \Delta$, and the magnitude m was given as

$$\log N(m) = a - bm \quad \text{for } m_{\min} < m < m_{\max}$$

This is the non-cumulative magnitude-frequency relation. Of special importance in hazard studies is the cumulative magnitude-frequency; i.e. the plot of the number N^* of earthquakes with a magnitude equal to or larger than $m - \frac{1}{2} \Delta$.

$$\log N^*(m) = a^* - b^* m \quad \text{for } m_{\min} < m < m_{\max}$$

Here N^* is always non-zero as it can happen with the non-cumulative form which makes problems because $\log N$ does not exist for $N=0$. The parameters of both relations are not substantially different for large event populations ($N > 4000$). But caution must be used in applying the cumulative form in case of poor and too small data sets. Then the cumulative format can introduce a bias and can drive completely unsuitable sets of data to a smoothed a priori established pattern.

3.3 Cumulative probability distribution function for magnitudes or intensities

For the lowest magnitude class m_1 included in the data set one gets as the cumulative number N^* of earthquakes, in the following written as N only for simplicity, having magnitudes or intensities greater than m_1

$$\log N(m_1) = a - bm_1 .$$

Normalizing the cumulative magnitude-frequency by $\log N(m_1)$ one gets

$$\frac{N(m)}{N(m_1)} = \exp(-b \cdot \ln 10 \cdot (m - m_1)) .$$

This relation implies the introduction of a probability expression. The probability that the random value M has a value smaller than a real number m , can be denoted as:

$$F_M(m) = P(M < m) = 1 - \exp(-\beta(m - m_1)); \quad \beta = b \cdot \ln 10 .$$

Normalizing this expression by the total number of events in the magnitude range $m_n - m_1$ yields the truncated exponential distribution function with:

$$F_M^T(m) = \frac{1 - \exp(-\beta(m - m_1))}{1 - \exp(-\beta(m_n - m_1))} .$$

3.4 Calculation of seismic hazard

The probability that from any point source the random variable in terms of intensity I (or acceleration) at the site of interest can be larger than any realization i , is expressed as the conditional probability, depending on earthquake size m and distance r

$$P[I > i \mid m, r] .$$

As a mean intensity-attenuation function a relation of the following type can serve :

$$I_{\text{site}}(m, r) = C_1 + C_2 m + C_3 \ln(r + r_0) .$$

The total probability theorem is used to express the probability of occurring or exceeding any ground shaking level at any site considering all surrounding source regions:

$$P[I > i] = \int_r \int_{m_1}^{m_2} P[I > i | m, r] \cdot f_M(m) \cdot f_R(r) \, dm \, dr .$$

$f_M(m)$ is the probability-density function of magnitudes, i.e. the first derivative of the cumulative distribution function $F_M(m)$. $f_R(r)$ denotes the probability-density function of the site-to-source distances and is calculated numerically with appropriate algorithms.

Assuming a Poisson process of earthquake occurrence in the study region, then the selected events, fulfilling the condition of the total probability theorem, are also Poissonian. The probability that these events larger than i will not occur in the time interval 0 to t (usually one year) is:

$$P[N_{t>i} = 0] = \exp(-vt) .$$

The probability of occurring or exceeding any critical i at a site per year - defined as seismic hazard H - is:

$$H = 1 - P[N_{t>i} = 0] = 1 - \exp(-v) .$$

The mean return period of any critical event is the reciprocal value of its total annual occurrence rate. The occurrence probability of an event within its mean return period is $1 - e^{-1} = 63\%$.

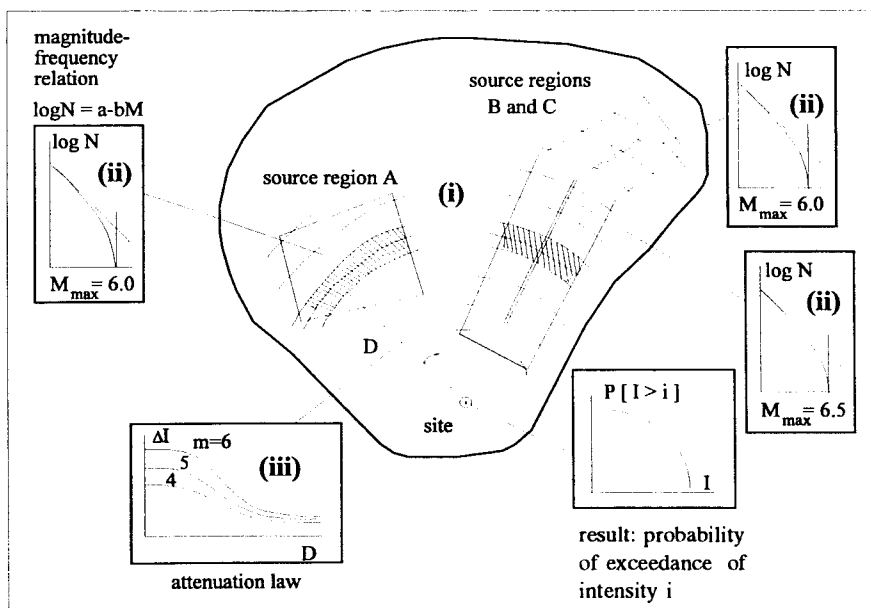


Fig. 1 Scheme illustrating the input data necessary for the process of seismic zoning and the integration procedure over distance and source regions, respectively.

Exercise on assigning seismic intensities¹⁾

G. Grünthal

Dept. of Kinematics and Dynamics of the Earth
GeoForschungsZentrum Potsdam, Telegrafenberg C3, D-14473 Potsdam

1. Intensity assignment based on questionnaire data

The following data are extracted from questionnaires relating to the effects of a magnitude 4.8 earthquake in one town in north-western Europe. The questionnaire was published in local newspapers; readers of the newspaper were invited to fill out the questionnaire and send it in. The questionnaire was not designed with the MSK scale in mind, and therefore not all the questions relate closely to the text of the scale. By way of this this example we show that the scale works well even with data which are not optimal.

For the purposes of this study the city of Carlisle was divided into three areas. The data from the western part of the city will be used in the exercise. The number of questionnaires received was 222.

The time of the earthquake was 03h 57m; almost all observers were indoors and in bed. There were no reports from people outdoors, since the streets were deserted at this time of night.

Question: What did you feel?

87% felt some sort of vibration; 19% described it as strong (though they weren't specifically asked to qualify their description); 1% described it as weak; 11% felt no shaking.

Commentary: the vibration was generally observed and felt as strong by many.

Question: What did others nearby feel or hear?

73% said their neighbours felt or heard the earthquake; 12% said they didn't and the remainder didn't know or didn't answer.

Commentary: the earthquake was felt by... (insert here your conclusion derived from the answers given in the questionnaire with regard to assigning intensity; c.f. commentary given above).

Question: Were you frightened or alarmed?

69% said they were - 18% said they were not. Three people said they ran outdoors, but this information wasn't actually requested by the questionnaire, so more may have done so.

Commentary: So far the intensity looks to be in the range of

Question: Did doors or windows rattle?

54% said yes; 26% said no.

Question: Did anything else rattle?

54% said yes; 19% said no.

Commentary: the intensity is so far at least ... and probably ... or even more from this evidence.

¹⁾ These Examples are based on a compilation prepared by R. Musson (Edinburgh)

Question: Did any hanging objects swing?

14% said yes; 26% said no, and the rest had no hanging objects to observe, or couldn't see in the dark, or didn't answer.

Commentary: since the shaking from a relatively small earthquake at close range (as here) is likely to be of high frequency, it is not to be expected that there will be many observations of hanging objects swinging. In these circumstances the ratio of approximately 1:2 yes:no replies suggests quite strong shaking, i.e. at least intensity

Question: Did anything fall over or upset?

18% said yes; 72% said no.

Commentary: The intensity was at least

Question: Was there any damage?

13% reported damage of some sort; 85% reported no damage. Most of the damage was of cracks to plaster and walls; also fall of slates, fall of chimneys and loose bricks dislodged. In one case it was reported that a gap opened between a garage and a house extension.

Commentary: the type of housing is predominantly brick-built. The damage can be summarised as ... vulnerability class ... buildings suffer damage of grade This does not match exactly the descriptions given in the scale, but is closer to that for degree ... than anything else.

Question: Have you any other observations?

A variety of answers were received. Nine people reported that furniture was shifted, an effect first mentioned at degree 6 of the scale.

Question to be answered: What was the intensity in the respective part of the city? Summarize the main reasons for your conclusion.

2. Intensity assignment based on documentary data

The following two descriptions are of the effects of an earthquake on 7 September 1801 at Comrie, in Scotland. Both are taken from contemporary Edinburgh newspapers. Edinburgh was at that time the nearest place at which newspapers were published. The distance from Comrie to Edinburgh is about 75 km. The time of the earthquake was about 6 am.

The following account was written by an observer in Comrie, on 9 September, two days after the earthquake. It was published in the Edinburgh Advertiser (15 September 1801 p174).

1) The ... shock ... was very great, and alarming beyond expression. ... Slates fell from some houses, and many loose bodies tumbled down with great precipitation. Sonorous bodies were dashed on each other, and rang loudly, such as bottles, glasses, &c. Several large stones and fragments of rocks fell down the sides of the mountains. Pieces of stone dykes fell, and one bank of earth slid from its place. If the shock had had a little more impetus, it is probable, several frail houses would have been thrown down; but, in the kindness of Providence, no farther harm has been done than what is above stated.

The second account was also written at Comrie on 9 September, and was published in the Edinburgh Evening Courant (14 September 1801, p3).

2) ... the noise and shock ... were instantaneous; all those persons who were in bed were terrified that their houses were tumbling down about their ears, and many here and in the neighbourhood jumped out as quickly as possible - its duration might be about five or six seconds, and during all that time the floors, beds, and window shutters shook violently, and the roofs creaked and strained at a great rate. The horses that were grazing seemed much frightened and to listen with their ears pricked up; the cows also that were housed appeared, from their lowing, to be very uneasy, and all the dogs and other animals gave signs of fear. A shepherd, a few miles to the westward, had just separated a flock of cattle, but as soon as the earth began to tremble they all crowded together in a moment.

Question to be answered: What was the intensity at Comrie?

Help: A word needs to be said first about local building type, which would have been predominantly stone-built houses (usually single-storey), with timber roofs covered with slates. These can be considered as vulnerability class B structures. The strength of these buildings is likely to have been quite good, where not affected by disrepair.

The "stone dykes" referred to here are boundary walls. This type of structure is not dealt with by the MSK intensity scale as such, but experience shows that this type of damage begins at intensity 5.

Make an extract of all effects reported that have a relation to intensity assessment. Give comments to all these single effects what intensity range could be related to them.

Note that not all of the given effects are explicitly included in the intensity definitions - the appropriate equivalences have to be found out.

Exercise on incompleteness of a catalogue with respect to the determination of the parameters of the Gutenberg - Richter relation

G. Grünthal

Dept. of Kinematics and Dynamics of the Earth
GeoForschungsZentrum Potsdam, Telegrafenberg C3, D-14473 Potsdam

Task: Determination of the annual intensity-frequency relation

$$\log N_y(I_0) = a - b I_0$$

Input data: Earthquake catalogue. For simplicity the enclosed Table 1 gives only the origin time of events (in years) and their epicentral macroseismic intensities I_0 (in grades of MSK).

Consider the incompleteness of the earthquake catalogue.

Help: - Plot a time-chart of earthquake occurrences for each intensity class.
- Estimate the time span for which you assume a completeness of catalogued data.

Make some statements about the problem how the parameters a and b can depend on personal judgement.

Tab. 1

year	I_0	year	I_0	year	I_0	year	I_0	year	I_0
1025	8,5	1526	7,0	1820	5,0	1915	5,0	1957	3,0
1026	7,5	1531	7,0	1827	5,0	1920	4,5	1960	4,0
1030	7,0	1537	8,5	1837	5,5	1922	4,0	1960	3,5
1070	6,5	1550	6,0	1837	4,5	1925	6,0	1961	3,0
1085	7,0	1575	6,5	1838	7,0	1925	5,0	1962	5,0
1100	5,5	1593	7,0	1845	5,5	1932	5,0	1962	3,5
1150	7,0	1600	6,0	1849	6,0	1935	3,0	1964	3,5
1155	6,0	1625	6,5	1850	4,5	1936	4,5	1964	3,0
1250	7,0	1625	5,5	1850	3,5	1937	6,5	1967	3,0
1260	8,5	1638	6,0	1855	8,5	1937	3,5	1968	4,5
1265	7,0	1650	6,0	1859	5,0	1940	4,0	1968	4,0
1280	6,0	1660	7,0	1859	3,5	1940	3,0	1968	3,5
1350	5,5	1675	4,0	1874	6,5	1943	4,5	1969	5,5
1351	7,5	1677	6,0	1875	5,0	1943	3,0	1969	3,0
1376	5,0	1699	6,5	1876	3,0	1944	5,5	1970	3,5
1378	5,0	1701	4,5	1880	5,5	1944	4,0	1973	3,0
1425	6,5	1715	8,0	1887	5,0	1945	3,5	1975	3,5
1438	5,0	1724	6,5	1887	3,0	1947	3,0	1975	3,0
1450	8,0	1725	5,5	1900	6,0	1949	6,5	1976	4,0
1460	7,0	1751	7,5	1905	4,0	1949	4,0	1977	3,0
1470	6,5	1762	6,0	1906	5,0	1949	3,5	1980	3,5
1475	6,0	1775	6,5	1907	7,5	1951	3,0	1980	3,0
1478	6,0	1800	4,0	1910	4,0	1952	3,5		
1500	6,5	1810	7,0	1912	5,5	1955	7,0		
1501	5,5	1812	5,5	1912	4,5	1955	4,5		
1525	5,0	1820	6,5	1915	4,0	1957	3,5		

Exercise on the determination of the parameters of the Gutenberg-Richter relation $\log N = a - bm$

G. Grünthal

Dept. of Kinematics and Dynamics of the Earth
GeoForschungsZentrum Potsdam, Telegrafenberg C3, D-14473 Potsdam

Use the following data and abbreviations:

Data: m_i	N_i		
2.50	(380)		
2.75	420		
3.00	286	n	- number of classes
3.25	143	m_0	- smallest magnitude considered
3.50	129	m_i	- magnitude of class i events
3.75	66	\bar{m}	- average magnitude in the range of classes $i = 1, \dots, n$
4.00	24		
4.25	15	N_i	- non-cumulative number of events
4.50	4		
4.75	3		

1. Give a graphical presentation of the data given in the table above
2. Make an eye-fit of the data points and determinate the parameters \hat{a} and \hat{b} from the graph according to

$$\hat{b} = \frac{\log N_2 - \log N_1}{m_1 - m_2}, \quad \hat{a} = \log N_2 + m_2 \hat{b}$$

3. Determinate the parameter b by using the preferable maximum likelihood estimate (MLE) (Utsu, 1965; Aki, 1965):

$$b_{MLE} = \frac{\text{loge}}{\bar{m} - m_0} \quad \text{with} \quad \left(\text{loge} = \frac{1}{\ln 10} \right),$$

which yields accurate and unbiased values for $(m_{\max} - m_0) \geq 2$ (otherwise use corrections according to Utsu, 1966) or determine the MLE of the parameter β of the exponential distribution $P(M < m) = 1 - \exp(-\beta m)$, respectively:

$$\beta_{MLE} = (\bar{m} - m_0)^{-1}; \quad \beta_{MLE} = \frac{b_{MLE}}{\text{loge}}.$$

4. Determine the slope parameter b by least-square estimate (LSE) for $\log N = a + bm$:

$$b_{\text{LSE}} = \frac{\sum_{i=1}^n (m_i - \bar{m}) (\log N_i - \overline{\log N})}{\sum_{i=1}^n (m_i - \bar{m})^2}, \quad \bar{m} = \frac{1}{N} \sum_{i=1}^n m_i N_i,$$

$$\overline{\log N} = \frac{1}{N} \sum_{i=1}^n N_i \log N_i.$$

Hint: To perform the LSE use the following table:

m_i	N_i	$N_i m_i$	$\log N_i$	$N_i \log N_i$	$m_i - \bar{m}$	$(m_i - \bar{m})^2$	$\log N_i - \overline{\log N}$

Aki, K., 1965: Maximum likelihood estimation of b in the formula $\log N = a - bM$ and its confidence limits. Bull. of the Earthquake Research Inst. of the Univ. of Tokyo 43, p. 237-239.

Utsu, T., 1965: A method for determining the value of b in a formula $\log N = a - bM$ showing the magnitude-frequency relation for earthquakes. Geophys. Bull., Hokkaido Univ. 13, p. 99-103.

Utsu, T., 1966: A statistical significance test on the difference in b -value between two earthquake groups. Journal of Physics of the Earth 14(2), p. 37-40.

Exercises on earthquake occurrence in time (Poisson distribution)

G. Grünthal

Dept. of Kinematics and Dynamics of the Earth
GeoForschungsZentrum Potsdam, Telegrafenberg C3, D-14473 Potsdam

Check if the data set given below is Poissonian.

Make a plot of the observed numbers N of frequency classes having 0, 1, 2, ... , n earthquakes per time interval t and compare it with the poisson random distribution P . t should be one year.

$n = 0, 1, 2, \dots$;

α - mean occurrence rate per t

$$P(N = n, t) = \frac{(\alpha \cdot t)^n}{n!} \exp(-\alpha \cdot t)$$

For better comparison of the Poisson distribution with the observed numbers plot:

$$K[N = n, t] = k \cdot P[N = n, t]$$

with k - number of time intervals used.

Data: yearly number of shallow earthquakes with $M \geq 7.5$ from 1904 up to 1980 after Abe (1981): Magnitudes of large shallow earthquakes from 1904 to 1980. Phys. Earth Planet. Int. 27, 72-92.

year	No.	year	No.	year	No.	year	No.	year	No.	year	No.
1904	9	1917	4	1930	1	1943	8	1956	2	1969	3
1905	6	1918	6	1931	9	1944	2	1957	5	1970	1
1906	7	1919	3	1932	4	1945	2	1958	2	1971	5
1907	7	1920	4	1933	3	1946	6	1959	2	1972	1
1908	1	1921	2	1934	5	1947	3	1960	3	1973	1
1909	2	1922	2	1935	4	1948	3	1961	1	1974	1
1910	1	1923	3	1936	1	1949	4	1962	-	1975	6
1911	6	1924	2	1937	4	1950	2	1963	1	1976	5
1912	5	1925	-	1938	9	1951	1	1964	2	1977	2
1913	3	1926	2	1939	4	1952	5	1965	3	1978	3
1914	3	1927	2	1940	2	1953	2	1966	5	1979	2
1915	4	1928	6	1941	5	1954	-	1967	1	1980	1
1916	4	1929	4	1942	5	1955	2	1968	5		

Recommendation: Use the following table.

frequency classes n	number of occurring classes N	total number of events within n	K
0	3	0	2.73
1			
2			

(In textbooks on statistics you will find procedures on possibilities about tests of the goodness of fit between observed distribution and theoretical distribution.)

Exercise on the application of extreme value statistics

G. Grünthal

Dept. of Kinematics and Dynamics of the Earth
GeoForschungsZentrum Potsdam, Telegrafenberg C3, D-14473 Potsdam

Make a graph for the data according to the plotting rule given below. Make statements on the expected extremal intensities of mean return periods of 10, 50, 100 and 200 years.

Data: Maximum earthquakes of an area of low seismic activity within 10 year intervals (t):

interval	data	I_0
1800-1809	-	-
10-	1811 Dec. 12	5.5
20-	1821 Oct. 28	5
30-	1831 Nov. 29	4.5
40-	1847 Apr. 7	6.5
50-	1857 Jun. 7	5.5
60-	1862 Jan. 9	5
70-	1872 Mar. 6	7.5
80-	1883 Oct. 20	5.5
90-	1897 Nov. 7	6.5
1900-1909	1908 Nov. 3	6.5
10-	1914 Jun. 27	6
20-	1926 Jan. 28	6
30-	1936 Dec. 2	4.5
40-	1943 Jun. 20	4
50-	1956 Sep. 19	3.5
60-	1962 Sep. 18	5
70-	1979 Sep. 25	5

N - number of intervals; j - rank; P_j - plotting position of the j th observation

Procedure

j	I_0	$P_j = j/(N+1)$	$-1n(-1nP_j)$	$T = (1-P^{1/t})^{-1}$ [years]
1	-	0.0526	-1.080	3.92
2	3.5	0.1053	-0.812	
18	7.5	0.9474	2.918	185.6

Plot I_0 over P_j and use special extreme value paper. If this paper is not available use $-1n(-1nP_j)$ as abscissa with values in units of 3 cm; I_0 as ordinate with values in units of 2 cm.

Exercise on seismic hazard assessment (a simplified approach)

G. Grünthal and Ch. Bosse

Dept. of Kinematics and Dynamics of the Earth
GeoForschungsZentrum Potsdam, Telegrafenberg C3, D-14473 Potsdam

Task: Estimation of site design earthquake (SDE) and safety shutdown earthquake (SSE) on the basis of the cumulative intensity-frequency relation determined at the site

Input data: Let us assume five seismoactive zones characterized by:

- annual intensity-frequency relations, $\log N_n(I_0) = a - b I_0$ which are defined by the coefficients a and b ,
- maximum possible epicentral macroseismic intensities I_{\max} estimated for each zone separately, and
- attenuation values ΔI of intensities determined for the distance of the seismoactive zone to the site.

Seismoactive zone	a	b	I_{\max}	ΔI
1	1.570	0.516	IX-X	1.0
2	0.055	0.335	X	1.3
3	0.387	0.372	XI	2.2
4	-0.394	0.326	IX-X	0.5
5	1.203	0.509	VIII-IX	1.3

Tasks:

1. Compile the cumulative intensity-frequency relation for the site.
2. Estimate the intensity of the SDE and the SSE.
3. What is the maximum possible intensity at the locality?
4. What seismoactive zone is affecting the site most?

Help for answers:

1. $I_{\text{site}} = I_{\max} - \Delta I$
2. Compare the effects caused by the third and by the fourth seismoactive zones at the site.
3. The return period of the SDE is 100 years and that of the SSE is 10 000 years; compare these periods with the present input data (e.g. take into account the Tab. 1 of exercise "Incompleteness of a catalogue and the parameters of the Gutenberg - Richter relation").

Exercise on PC assisted hazard assessment

Ch. Bosse and G. Grünthal

Dept. of Kinematics and Dynamics of the Earth
GeoForschungsZentrum Potsdam, Telegrafenberg C3, D-14473 Potsdam

Task: Create an input-file for the 1976 McGuire program with help of the "GFZ - toolbox on data preprocessing for seismic hazard assessment".

Input data: You will find an earthquake catalogue and its format description at the PC.

1. Start the toolbox program. (The catalogue should be read in automatically.)
2. In order to estimate the completeness of the catalogue do the following:
 - a) delineate a region including the whole catalogue area;
 - b) click into the region area with the left mouse button;
 - c) click "No vs. time" button (number versus time);
 - d) estimate completeness times for the different intensity ranges, note them and remove the region.
3. Define a new completeness table using the noted completeness times.
4. Delineate seismic source areas on the screen. Use the given geological map (Fig. 1).
5. Estimate a characteristic depth for each source region using depth distribution plot of the toolbox (click into the region area with the left mouse button; click "depth distrib.")
6. Create an input file for the 1976 McGuire program with the help of the toolbox (use Output; McGuire 1976; Get all).

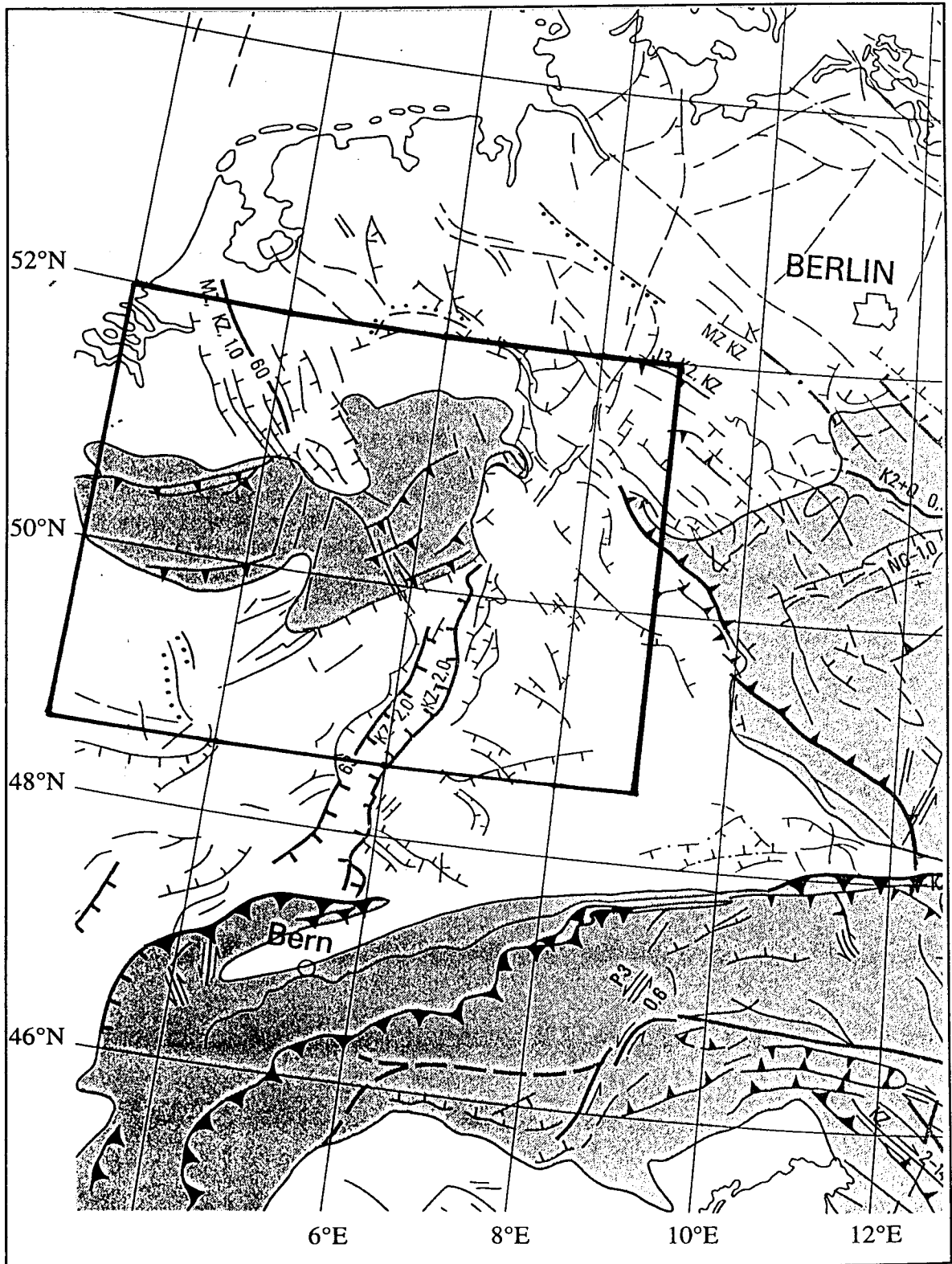


Fig. 1 Map of main tectonic faults (part of Meier, R. et al., Veröff. Zentr.-Inst. Phys. Erde, Potsdam Nr. 47 1976, Materialien zum tekt. Bau von Europa, Tektonische Bruchstörungen Karte 7); conventional signs are made according to the international use

APPROACHES TO SEISMIC HAZARD ASSESSMENT IN CHINA: METHODOLOGY

PART I: ASSESSMENT OF SEISMIC HAZARD BASED ON AREA SOURCE AND SEISMICITY DATA

Chen Yong

China Seismological Bureau, 100036 Beijing, China
Fax: +86-10-6821 5973; E-mail: yongchen@public.bta.net.cn

1. INTRODUCTION

The concept of potential earthquake source first proposed by Cornell (1968) plays a very important role. The potential earthquake sources can be in the form of points, lines and areas. The line model, namely the fault model, has been widely used as the basis for comprehensive analyses of earthquake hazards (McGuire, 1993; Giardini and Basham, 1993). However, it is very difficult in most regions of the world to get sufficiently detailed data of geological settings, faults, paleoseismicity, and crustal structure for the construction of accurate fault models. Also, hidden active faults are common in earthquake-prone terraces; several of the largest earthquakes in recent times, such as Tangshan earthquake (1976, China), Coalinga earthquake (1983, USA) and North Ridge earthquake (1994, USA), all occurred on previously unknown faults. The third question is that of the realistic maximum limit to the fault length that will rupture, i.e. it concerns the related maximum possible earthquake. In attempting to estimate the probability of rupture lengths, geological evidence (such as the identification of fault segments that are separated by such mechanical barriers as changes in fault strike or lateral fault offsets) and seismological evidence (such as historical hypocentral patterns) are used.

We propose a new methodology of seismic hazard analysis by using an area source model defining potential earthquake sources, taking recent instrumental earthquake catalogues as basic data for determining seismicity parameters, and employing Kernel method for estimating the magnitude of maximum earthquake in each source based on historical earthquake data. This method can be used for those regions without detailed geological information or where the relation between existing faults and earthquake occurrence is not clear. Applying this methodology to the available global earthquake catalogue from 1964 to 1994, global seismic hazard map in terms of the exceeding probability of intensity for the forthcoming 50 years has been constructed, and the seismic hazard maps of three countries have also been constructed using the same method. By comparison study, the hazard maps constructed from this study are in good agreement with the existing maps constructed based on the traditional fault model. The results show that the new method can provide a quick means of seismic hazard assessment for various regions world-wide.

2. AREA SOURCE MODEL OF POTENTIAL EARTHQUAKE SOURCES

2.1 Occurrence rate function

To assess the seismic hazard of a given region, first we need to divide this region into square cells of appropriate size, each cell represents a potential earthquake source. In order to assure to get seismicity parameters in each cell, every source cell must be large enough that it contains a sufficient number of earthquake data points, and the statistical error does not exceed a reasonable level. On the other hand, every source cell must also be small enough for getting a high spatial resolution (Kijko and Sellevoll, 1989a, 1989b). To find an acceptable balance between the competing goals of high resolution and small statistical error, we have to choose appropriate size of cells based on the amount of existing data. The key feature of this division, quite different with the fault model, is that potential earthquake sources are defined not according to geological information, but dependent on their geographic co-ordinates as illustrated in Fig. 1.

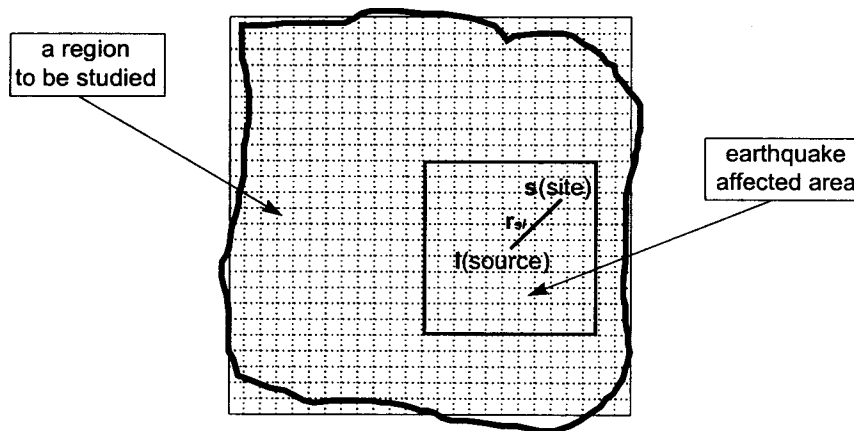


Fig. 1: Area potential earthquake source model.

In order to describe the seismic activity of each cell quantitatively, we introduce the annual earthquake occurrence rate $\nu(\geq m)$ as a basic parameter for seismicity analysis. $\nu(\geq m)$ is defined as the annual occurrence rate of earthquakes with magnitude m or above when the record time length of the catalogue under consideration is infinite long. Obviously, the $\nu(\geq m)$ is a constant rather than a random variable for a given cell.

$$\nu_l(\geq m) = \lim_{T \rightarrow \infty} \frac{N_l(\geq m)}{T} \quad (1)$$

in which the index l refers to the l -th cell, $N_l(\geq m)$ is the number of earthquakes with magnitude $\geq m$ in the l -th cell, and T is the time length of catalog. But in practice, only limited-length earthquake records are available (Chen et al., 1995; Kilko et al., 1989a, 1989b; Tinti et al., 1985). In this case, the annual earthquake occurrence rate $\nu(\geq m)$ can be calculated approximately by the observed annual frequency

$$\nu_l(\geq m) \approx \frac{N_l(\geq m)}{T} \quad (2)$$

where T is finite but long enough. The relation between the annual occurrence rate of earthquake $\nu(\geq m)$ and magnitude m is given by the Gutenberg-Richter (G-R) relation

$$\log \nu(\geq m) = a - bm \quad (3)$$

in which a, b are empirical constants (Gutenberg and Richter, 1956).

A G-R relation has been formulated for each source cell. Taking into account the monitoring capacity of the region containing the cell, the $\nu_l(\geq m)$ of various magnitude for l -th cell can be calculated by the following formula:

$$\nu_l(\geq m) \approx \frac{N_l(\geq m_{min}^l)}{T \cdot 10^{b_l(m-m_{min}^l)}} \quad (4)$$

in which m_{min}^l is the detection magnitude threshold in l -th cell, $N_l(\geq m_{min}^l)$ is the number of earthquakes with magnitude $\geq m_{min}^l$ in the time interval T , and b_l is the b -value in the l -th cell. The relations described above represent an empirical method based on the area source model to formulate the source parameters associated with the earthquake occurrence rate for the source cells. An occurrence rate function can thus be obtained for every source cell in the region, which is considered a distribution function inherent to the cell.

Maximum earthquake is an essential concept in hazard assessment. Considering the insufficient understanding of the earthquake generating process and specific source properties, we use the maximum historic earthquake as the expected maximum earthquake for earthquake sources in the present simplified analysis, and we employ Kernel method for estimating the magnitude of maximum earthquake in each cell (Woo, 1996).

2.2 Attenuation of intensity

The intensity at any site can be similarly described by an intensity distribution function, which must take into account the intensity attenuation over the distance between the site and the source cells. The intensity attenuation relation has been studied by many authors (Howell and Schultz, 1975; Anderson, 1978; Chamdra, 1979). Fig. 2 shows some relation curves obtained previously. From Fig. 2, it can be found that the data exhibiting scattering distribution and most data falling in 100-400 km range while too few in near field. In the present study, we take the average values of that, the bold line in Fig. 2, which represents the intensity attenuation in the western part of the United States:

$$I = I_0 + 3.2 - 0.00106r - 2.7 \lg r \quad (5)$$

in which I_0 is the epicenter intensity and r is the distance from the epicenter. The empirical relation between earthquake magnitude m and epicentre intensity I_0 given by Gutenberg and Richter (1956)

$$m = \frac{2}{3} I_0 + 1 \quad (6)$$

was used in the computation of the epicentre intensity.

Some local intensity attenuation relations are used for special areas, such as

$$I = 5.643 + 1.538m - 2.109 \ln(r + 25) \quad (7)$$

for Western China (Jin, 1992). Obviously, the use of local attenuation relation is necessary if it is available.

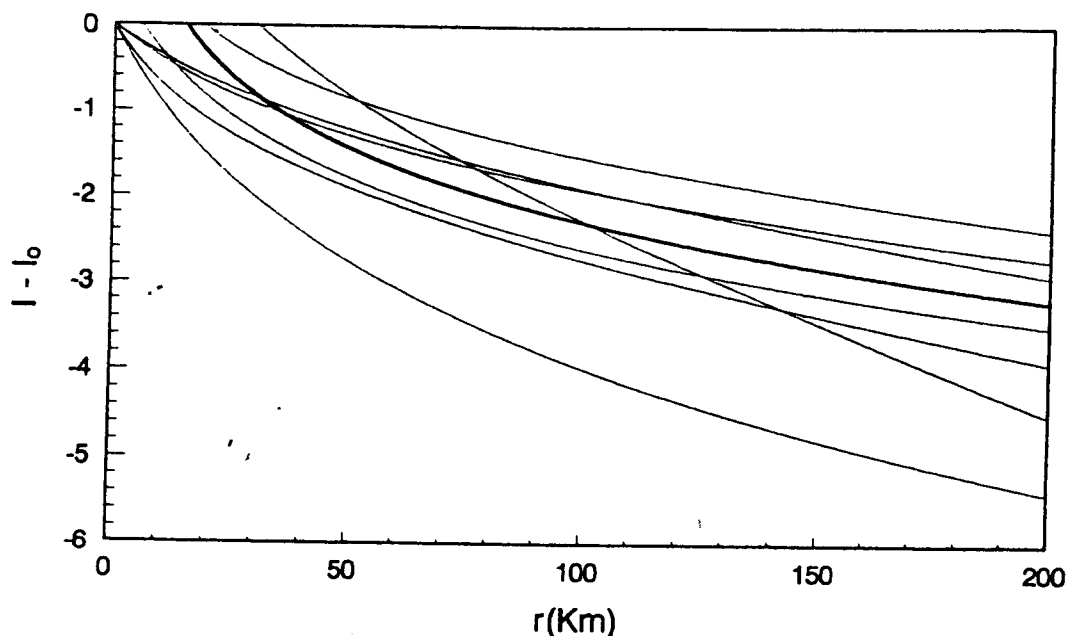


Fig. 2: Intensity attenuation curves obtained by other authors and for various regions. The bold line represents the average values used for most regions in this paper.

3. ANALYSIS OF SEISMIC HAZARD

3.1 Exceeding probability of site intensity

Based on the Poisson model of temporal distribution of seismicity, we can estimate the annual occurrence probability of earthquakes with magnitude $\geq m$, i.e., the exceeding probability, from the annual earthquake occurrence rate $\nu(\geq m)$ function (Hu, 1988).

$$P(\geq m) = 1 - \exp(-\nu(\geq m)) \quad (8)$$

The probability distribution of earthquake intensity at any site in the area source model was determined by integrating the influences of the surrounding source cells. As shown in Fig. 1, consider S as the l -th source cell and r_l as the distance from it to a site. Based on the attenuation of Modified Mercalli intensity

$$I = I(m, r) \quad (9)$$

and (1), the annual exceeding probability of site intensity contributed by the l -th cell, $P_l(I \geq i)$, can be calculated from the following equation (Howell & Schultz, 1975):

$$P_l(I \geq i) = P_l(m \geq m(i, r_l)) = 1 - \exp(-v_l(\geq m(i, r_l))) \quad (10)$$

where $P_l(m \geq m(i, r_l))$ is the annual exceeding probability of earthquakes in the l -th cell with magnitude $\geq m(i, r_l)$, and $m(i, r_l)$ is the magnitude in the l -th source cell calculated from the intensity i at a site and the distance r_l between site and source cell according to (8) (If $m(i, r_l)$ is larger than the magnitude of maximum earthquake in the l -th cell, $v_l(m \geq m(i, r_l))=0$).

In this analysis, the source cells around the site (suppose the total number is N_s) are considered independent of each other and have equal seismic influences on the site. By totalling the influences of all the source cells on a site, the annual exceeding probability of site intensity is obtained by

$$P(I \geq i) = 1 - \prod_{l=1}^{N_s} (1 - P_l(I \geq i)) \quad (11)$$

Substituting equation (10) into equation (11), we obtain:

$$P(I \geq i) = 1 - \exp\left[-\sum_{l=1}^{N_s} v_l(\geq m(i, r_l))\right] \quad (12)$$

The above result yields the one year's exceeding probability of site intensity. If a time interval of T years is used, the T -year exceeding probability can be obtained by

$$\begin{aligned} P_T(I \geq i) &= 1 - (1 - P(I \geq i))^T \\ &= 1 - \exp\left[-T \sum_{l=1}^{N_s} v_l(\geq m(i, r_l))\right] \end{aligned} \quad (13)$$

3.2 Working steps of seismic hazard analysis

For convenient use, we summarise the above-mentioned computing procedure of seismic hazard assessment into four basic steps that are illustrated in the working flow chart (Fig. 3). The analytical steps are comparable with those in the traditional deterministic as well as the probabilistic seismic hazard analysis, but with some considerable differences.

Step 1 is the definition of area potential earthquake sources. The sources are similarly characterised in seismicity as in the probabilistic method, namely they bear uniform potential of earthquake occurrence with a given magnitude; satisfy Gutenberg-Richter relation; and obey Poisson model temporally. However the definition of earthquake sources in the present method is distinguished not according to geological information, but dependent on the current geographic co-ordinates.

Step 2 is to analyse the seismicity of each source that is characteristically described by three parameters: annual occurrence rate, b -value and expected maximum earthquake. For statistical reasons, zoned b -values obtained through G-R analyses in large seismic regions are distributed into their subdivided source cells. Consequently, the annual occurrence rates of different magnitude levels for each source cell are calculated from the so-obtained b -value and the corresponding earthquake frequency of minimum threshold magnitude. It is noticeable

that above analyses are based on instrumental seismic data. On the other hand, according to available historical records and drawing the idea of the Kernel method (Woo, 1996) as reference, a maximum magnitude is chosen for each source which represents the maximum event expected to occur in the forthcoming future.

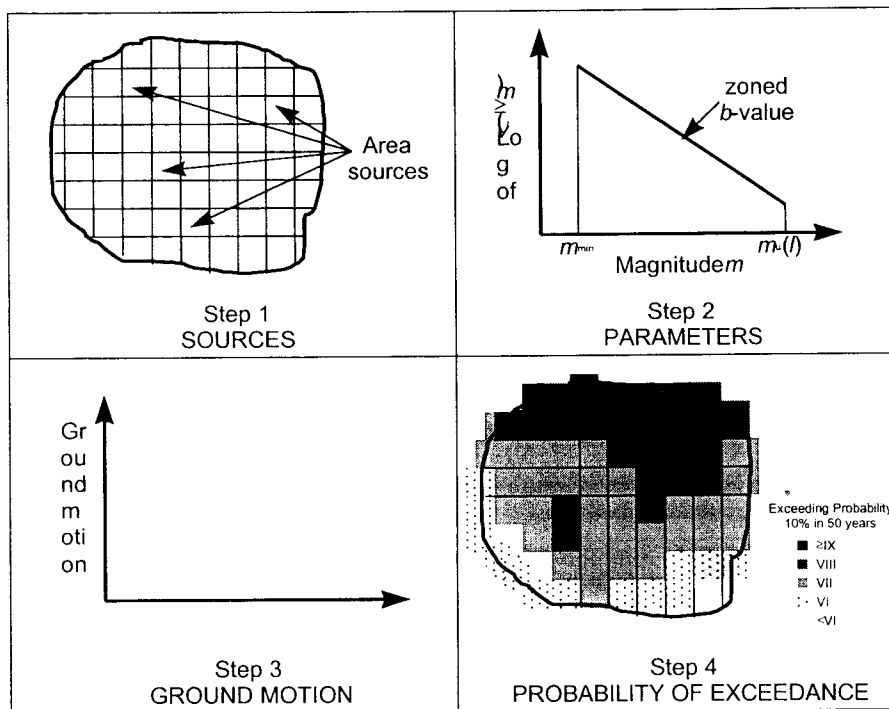


Fig. 3: Basic working steps of the newly developed hazard analysis methodology.

Step 3, estimation of earthquake effect, is similar to those in the deterministic and the probabilistic analyses. Attenuation functions, the most important information required in this step, are constructed either for the whole region to be studied or for each specified smaller area if practical data are available.

Step 4 is the determination of the site hazard, which is basically similar with the procedure used in the probabilistic method. Based on the Poisson assumption of earthquake occurrence both temporally and spatially, the effects of all the earthquakes of different sizes, occurring at different locations in different potential sources with different seismicity degrees are integrated into the probability calculation of exceeding different ground motion levels at the site during a specified period of time.

4. GLOBAL SEISMIC HAZARD MAP

4.1 Earthquake catalogues

Since the turn of this century, especially since 1960's, world-wide seismographic networks are able to provide complete earthquake catalogue in global scale. The seismic data accumulations remarkably increase year by year due to the great improvement of the

earthquake monitoring capacity, which makes it possible to achieve seismic hazard assessment by using earthquake catalogues for seismicity computation.

In the present study, we take the global earthquake catalogue (1964-1994) given by Engdahl (Engdahl, 1995, personal communication) as our original data of estimation of annual earthquake occurrence rate and b -value for each potential earthquake source. After statistical examination of completeness (Chen et al., 1995; Tinti and Mulgarin, 1985), the global earthquake catalogue proved to have the magnitude threshold $m_{\min}=4.5$, which means the global catalogue for earthquakes with magnitude above 4.5 is generally complete during 1964 -1994.

Since deep earthquakes have minor impact on the ground motion, those with depth ≥ 150 km are not taken into account. On the other hand, because of their great influence on seismicity statistics, aftershocks have been removed from the catalogue. The number of events contained in the revised as well as the original global catalogues are listed in Table 1.

Table 1: Global earthquake catalogue from 1964 to 1994.

Magnitude m	$4 \leq m < 4.5$	$4.5 \leq m < 5$	$5 \leq m < 6$	$6 \leq m < 7$	$7 \leq m$	Total
	Number of events					
Data Catalogue						
Original Engdahl data	9338	41677	35210	2177	174	89576
Revised Engdahl data	5524	27699	23265	1578	161	58227

To determine the expected maximum earthquake for each earthquake source, the historical records of earthquakes with magnitude 6.0 or above throughout the world given by USGS (USGS, 1996) are taken into account in the present study. This catalogue includes all available data of historical events occurred in any area of the world in which the earliest record can be traced back to 2150 BC.

4.2 Seismic hazard assessment

Considering the quantity of the data used and the average earthquake location precision world-wide, we divided the world into 0.5° by 0.5° cells as potential earthquake sources.

According to the historical earthquake records all over the world provided by USGS, the expected maximum earthquakes of source cells are determined.

For b -value calculation, we follow the seismic regionalization proposed by Flinn and Engdahl (Flinn, et al., 1974). Considering the 1964-1994 global catalogue, the numbers of earthquakes in most of the 50 seismic regions are more than 1000, statistically suitable for G-R analysis. Thereafter, the b -value of each region is obtained reliably and here given in Fig. 4. Generally speaking, most b -values calculated by this way are ranging from 0.8 to 1.2, which is consistent quite well with the results obtained previously (Evernden, 1970).

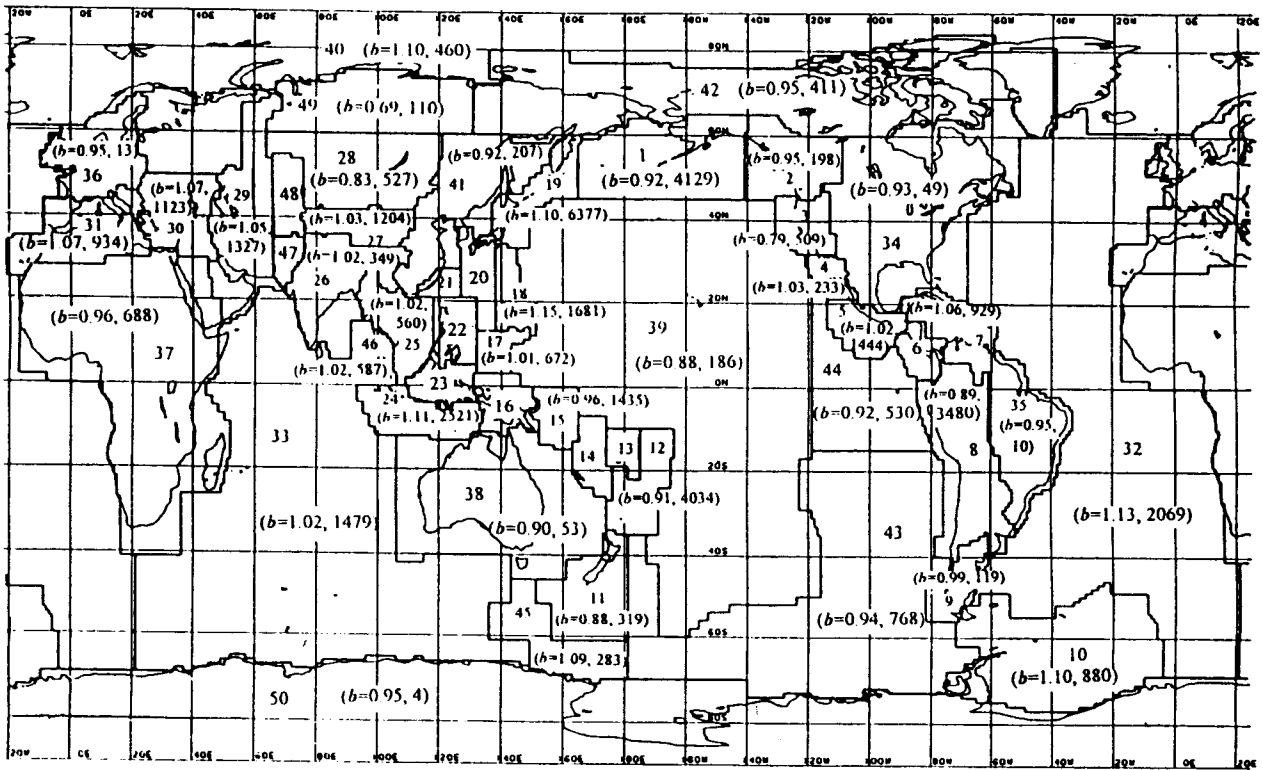


Fig. 4: *b*-value of 50 seismic regions, seismic regionalization is followed with Flinn and Engdahl (Flinn, Engdahl and Hill, 1974).

Based on the results of the above-mentioned steps and given the intensity attenuation relation, the global seismic hazard for the forthcoming 50 years has been estimated objectively and illustrated in Fig. 5.

Fig. 5 refers to average subsoil condition (firm sediments). Local subsoil conditions may lead differences in hazard over relatively small area which can not be shown in a large scale hazard map. However, it is possible to take such small areas into account by means of a local correction, for example, Table 2 indicates the average change in intensity for various subsoil conditions (Munich Re, 1988).

Table 2: Average changes in intensity for various subsoil conditions

Subsoil	Average change in intensity
Rock	-1
Firm sediments	0
Loose sediments(sand, alluvial deposit)	+1
Wet sediments or artificial filled ground	+2

For the intensity value indicated in Fig. 5, the probability that such a degree of intensity will exceed 10% in future 50 years. As various time periods are concerned, the corresponding probability of the same intensity will change accordingly.

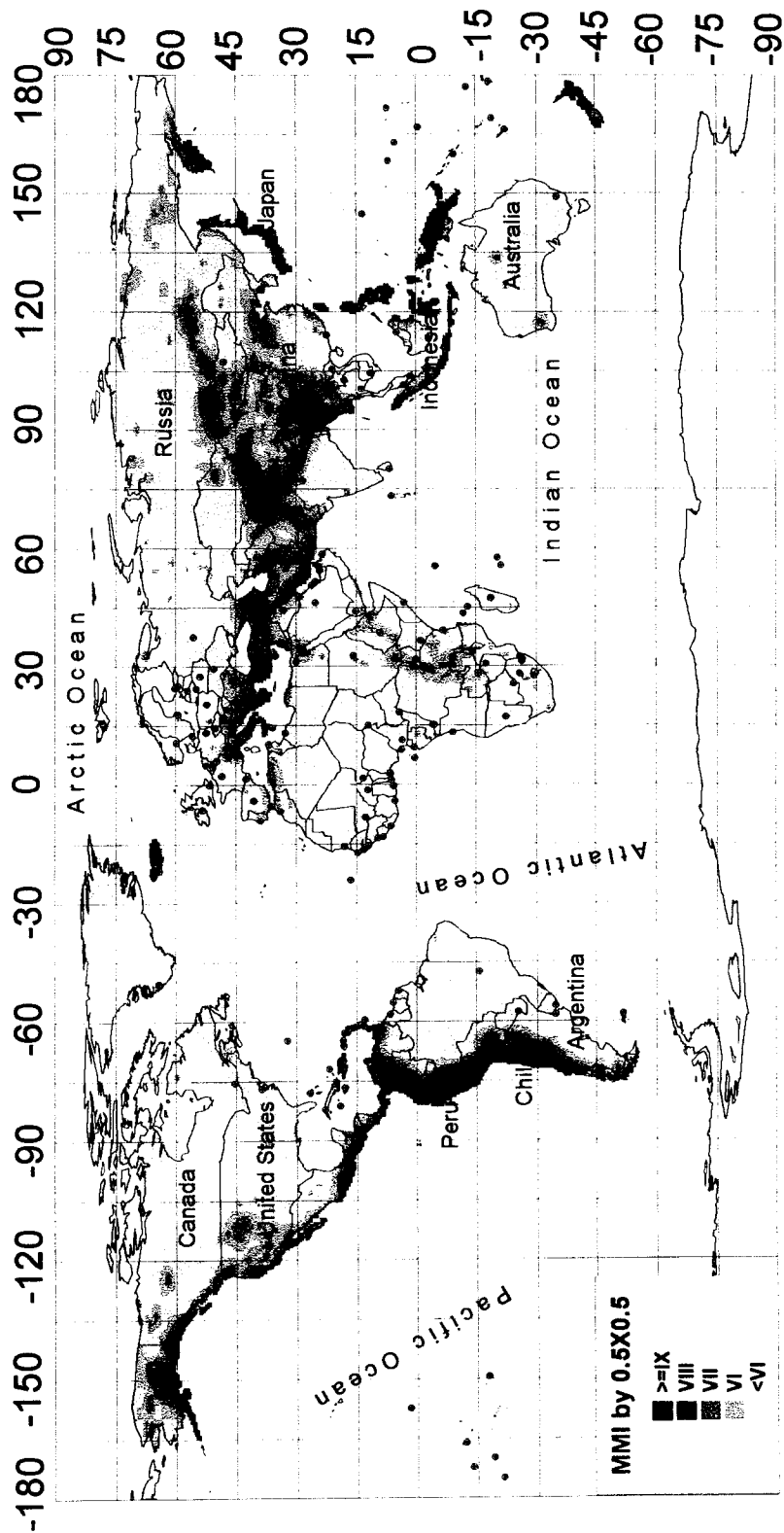


Fig. 5: Global Seismic Hazard Map with probability of exceedance 10% in 50 years.

4.3 Comparison with existing results

Systematic comparisons between the final global seismic hazard map and existing maps should verify that the global hazard map of this study depicts reasonable results. The set of existing maps includes other global maps, as well as more detailed country hazard maps. Through a side-by-side view of general appearance of regions for different intensities, we compare the global hazard maps (Fig. 5) with Munich Re' map (Munich Re, 1988), the similar appearance is obvious. We have also constructed the seismic hazard maps for three countries, China, Romania, and Ethiopia (Fig. 6). The ones obtained in the present study using area source model (have been compared to existing ones presented in the zoning maps by McGuire, et al. (1993). Table 3 shows the comparisons of the country areas for different intensities.

Through these comparisons, we can see that it is possible to estimate seismic hazard by using the area source model and seismicity data. Moreover, through similar computing procedure but inputting other T values in equation (4), seismic hazard for different time scales can also be assessed readily.

Table 3: The distribution of different intensities in area cells of 0.5×0.5 degrees.

Country	Intensity	< VI	VI	VII	VIII	\geq IX
		Number of cells				
China	Zoning Map this study	905	1094	1371	582	169
		934	1194	1256	649	124
Ethiopia	Zoning Map this study	119	149	87	55	3
		160	84	120	51	2
Romania	Zoning Map this study		30	33	11	2
		13	50	36	7	2

5. DISCUSSION

In the present study, a simplified method has been developed for seismic hazard assessment based on the area potential earthquake source model and seismicity data, instrumental as well as historical. The computing procedure of the exceeding probability distribution of the Modified Mercalli intensity has been illustrated and briefly summarised in a readily-used working flow chart. Taking the global seismic hazard map as a practical test of the new methodology, we place a strong emphasis upon the fact that through similar computing process, other regions with various features, big or small, continental or oceanic, seismicity active or inactive, for any specified time duration, can also be studied if their seismicity data required are available. Moreover, with different individual attenuation relations, it is possible to estimate probability distributions of other ground motion parameters, such as peak-ground acceleration (PGA), peak-ground velocity (PGV), or peak-ground displacement (PGD), which are generally more concerned with by engineers than that of intensity. More detailed studies for some countries and regions in terms of intensity and/or PGA have been finished and will be given by other papers.

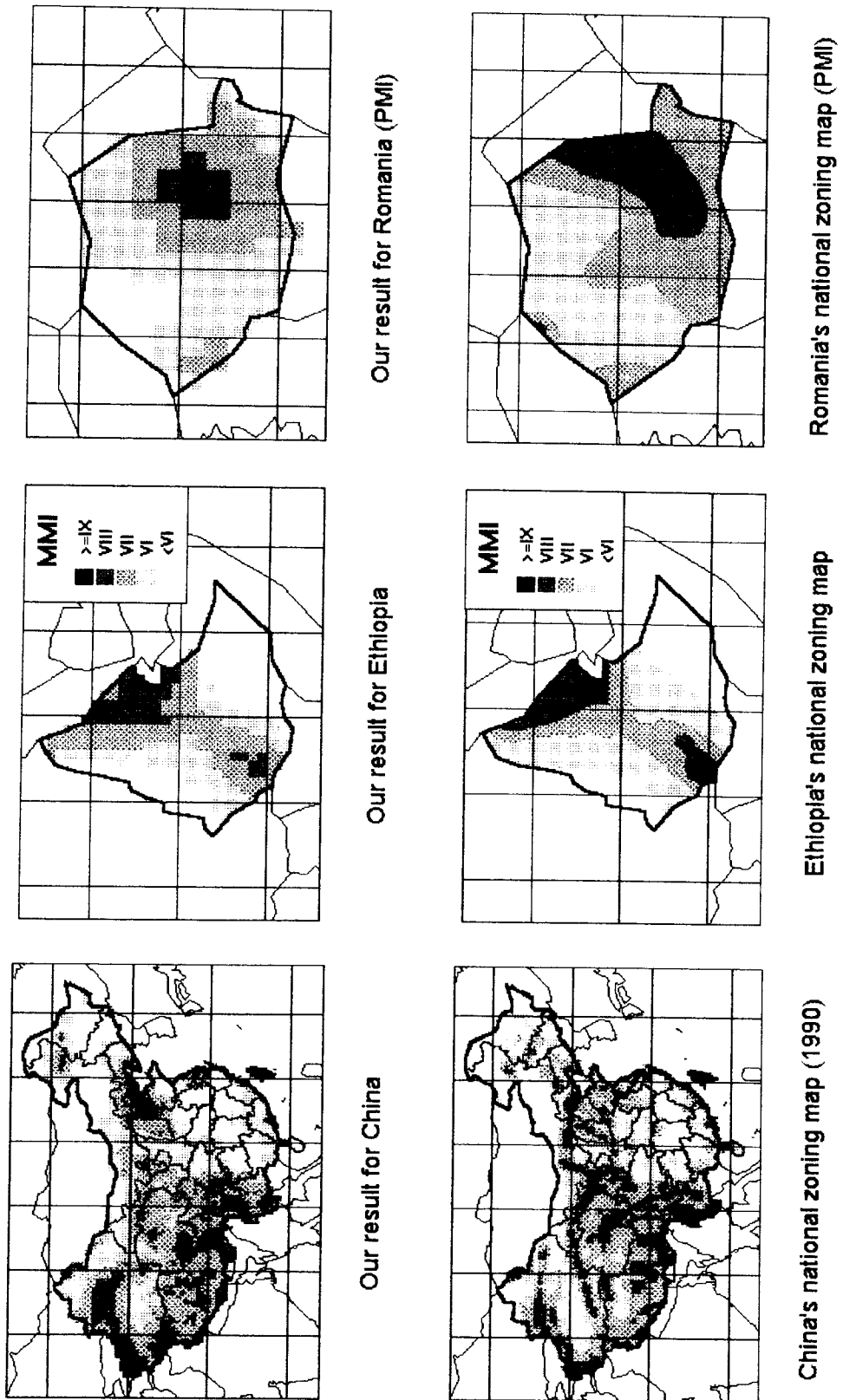


Fig. 6: Comparisons between three national zoning maps with our hazard assessment results.

According to the computation procedure of seismic hazard assessment, it can be seen that factors in calculation contributing to the errors of seismicity analysis come mainly from the estimations of the three important parameters: the annual occurrence rate, the b -value, and the expected maximum magnitude for each seismic potential source cell (in this study, 0.5° by 0.5°). All of the related aspects focus on the data shortage problem. For maximum magnitude estimation, we take the maximum historical event as the maximum one expected to occur in the future because of lack of other valuable data for us to make a reasonable decision. As to the b -value calculation, the amount of earthquake records does not allow us to get the b -values for small but evident seismicity active areas, not to mention those of low seismicity. In such a case, we could only perform G-R analysis for relatively large regions to ensure sufficient data points within each of them considering statistical requirement. However, we are not able to evaluate the errors associated with above two aspects, which may be achieved following further understanding of essential regularities of earthquake occurrence and its relation with geological structures.

On the other hand, the annual earthquake occurrence rate is approximately assessed as the observed annual frequency with limited time length T of records. From a point of view of statistics, such an approximation will enhance inevitably the statistical uncertainty in seismicity analysis and hence will bias the hazard assessment results considerably. From equation (4), an important factor on computing $\nu_l (\geq m)$ is $N_l (\geq m_{\min}^l)$, the number of earthquake with magnitude $\geq m_{\min}^l$ (detection magnitude threshold) in the time interval T . Therefore, in order to assure $\nu_l (\geq m)$ is more accurate, $N_l (\geq m_{\min}^l)$ must be large enough.

ACKNOWLEDGMENTS

Many thanks due to Dr. E. R. Engdahl, Dr. H. Shah and Ms. Jin Anshu for their valuable suggestion and comments. This work is partly sponsored by NSFC and Hong Kong RGC grant while working on this project.

REFERENCES

- Anderson, J.G. (1978). On the attenuation of Modified Mercalli Intensity with distance in the United States, BSSA 68, No.4, 1147-1179.
- Chandra, U. et al. (1979). Attenuation of intensities in Iran, BSSA 69, No.1, 237-250.
- Chen, L., Q. Chen, et al. (1997). Analysis of earthquake occurrence rate and the associated uncertainty of four earthquake catalogues, submitted to Geophysical Res. Lett., in review.
- Chen, Y., Chen, Q. F. (1995). Completeness analysis of the historical earthquake catalog in China, Earthquake Research in China 9, No.4, 365-369.
- Cornell, C. A. (1968). Engineering Seismic Risk Analysis, BSSA 58, No.5, 1583-1606.

- Engdahl, E. R., Castano, J. C. and Berrocal, J. (Editors) (1996). Selected papers from the 1994 Regional Seismological Assembly in South America held in Brasilia, Brazil, *Geofisica International*, 35.
- Evernden, J. F. (1970). Study of regional seismicity and associated problems, *BSSA* 60, No.2, 393-446.
- Flinn, E. A., Engdahl, E. R., and Hill, A. R. (1974). Seismic and geographical regionalization, *BSSA* 64, No.3, 771-774 .
- Gao, M. (1996). Poission-based Probability Model of Seismic Intensity Occurrence, *Earthquake Research in China*, 12, No.2, 195-200.
- Giardini, D. and Basham, P. W. (1993). The ILP's Global Seismic Hazard Assessment. Program for UN/IDNDR, *Annali di Geophysica*, 36, No.3-4, 257.
- Gutenberg, B. and Richter, C.F. (1956). Earthquake magnitude, intensity, energy, and acceleration. *BSSA* 46, No.2, 105-146.
- Howell, B. and Schultz, T. (1975). Attenuation of Modified Mercalli Intensity with the distance from the epicentre, *BSSA* 65, No.3, 651-665.
- Hu, Y. X. (1988). *Seismic Engineering*, Seismological Press, 454.
- Jin, Y. (1992). Attenuation relation of intensity in china, *Earthquake Research in China*, 8, 4, 121-134.
- Kijko, A. and Sellevoll, M.A. (1989a). Estimation of earthquake hazard parameters from incomplete data files. Part I. Utilisation of extreme and complete with different threshold magnitude. *BSSA* 79, 645-654.
- Kijko, A. and Sellevoll, M.A. (1989b). Estimation of earthquake hazard parameters from incomplete data files. Part II. Incorporation of magnitude heterogeneity. *BSSA* 82, 120-134.
- Munich Re. (1988). World map of natural hazard (order No. 1272-V-e).
- McGuire, R. K. (1993). Computation of seismic hazard, *Annali di Geophysica* 36, No.3-4, 181-200.
- Tinti, S. and F. Mulargia (1985).Completeness analysis of seismic catalogue, *Annales Geophysicae* 3, No.3, 407-414.
- Vere-Jones, D., (1992). Statistical methods for the description and display of earthquake catalogues, *Statistics in the environment and earth sciences*, A.T. Walden and P. Guttorp, (Editors), Edward Arnold, London, 220-246
- Woo, G. (1996). Kernel estimation methods of seismic hazard area source model, *BSSA* 86, No.2, 253-362.

APPROACHES TO SEISMIC HAZARD ASSESSMENT IN CHINA: METHODOLOGY

PART II: ANALYSIS OF EARTHQUAKE LOSS BASED ON MACROECONOMIC INDICATORS

Chen Yong, Chen Qifu

China Seismological Bureau, 100036 Beijing, China
Fax: +86-10-6821 5973; E-mail: yongchen@public.bta.net.cn

1. INTRODUCTION

Forecasting probable losses in hypothetical earthquake events is a fundamental exercise for the planning and preparation of mitigation actions by regions with active seismicity.

Most earthquake loss studies use an inventory approach in which predicted damages in various categories of structure and facility in a concerned region are estimated and added together to obtain the total estimated loss for particular intensity ranges. Such an approach requires a detailed inventory database of the structures and facilities in the region, which is not always readily available in many regions of Asia.

We have used an alternative means of estimating earthquake losses based on several macroeconomic indices such as the Gross Domestic Product (GDP) and population. Using published earthquake loss data during 1980-1995, the relations between GDP and earthquake loss have been formulated empirically for several intensity ranges. The global land surface was divided into unit cell $0.5^\circ \times 0.5^\circ$ in size. The GDP of each cell was apportioned based on its population and the GDP per capita of the region to which it belongs. The predicted seismic loss of the cell was then estimated from the seismic hazard probability function, its GDP, and the empirical relation between GDP and seismic loss. A global seismic loss map is then compiled based on the results of seismic hazard analysis in the world. Employing readily available socio-economic data as the basis for the vulnerability analysis, the method enables us to obtain seismic loss estimates for regions without a detailed inventory of exposed structures or the required collateral geological information. Seismic loss estimates can also be upgraded easily with social economic data collection for the fast developing areas of the world.

2. METHODOLOGY OF EARTHQUAKE LOSS ESTIMATE

The prediction of economic impacts can use either a deterministic or a probabilistic approach (Yeats et al., 1997). Most earthquake loss studies employ the former, which requires the specification of a maximum credible earthquake event and the level of ground shaking without being explicit of the probability that those events may occur (Panel on Earthquake Loss Estimation Methodology, 1989). In the probabilistic assessment, on the other hand, considerations are given to the numerical probabilities at which earthquakes occur and their total effects during a specific time period (Yeats et al., 1997). Commonly, the probability

function describing the seismic hazard of a region is combined with a vulnerability analysis of the structures and facilities in the region. The set of guidelines and recommendations for a loss estimation methodology (PELEM, 1989) is primarily based on the method suggested by the Applied Technology Council (1985), generally designated as ATC-13. The ATC-13 method contains two major components: a seismic hazard analysis and a structural vulnerability function. The seismic hazard analysis takes into account the frequency distribution of earthquakes, intensity attenuation, and bedrock or soil conditions of the affected region. The vulnerability analysis requires a detailed inventory of the buildings and facilities in the region, which are categorised according to their structural type or occupational use, and an estimate is made for the average degree of damage in each category during an earthquake event by multiplying the damage ratio of the category, the total value of the buildings in that category, and the probability distribution function of seismic hazards of the region.

An example of loss estimating using this approach is the one carried out by the Research Group of Chinese Earthquake Risk Prediction in China (RG CER, 1995) which was based on a formula modified from ATC-13:

$$L_k = \sum_I \sum_j P(I) P_k(D_j | I) b_k(D_j) B_k \quad (1)$$

Where L_k is the economic loss incurred on buildings of type k during an earthquake event of intensity I , $P(I)$ the probability of earthquake intensity I , $P_k(D_j | I)$ the probability for D_j degree of damage to be incurred on type k buildings in an earthquake of intensity I , $b_k(D_j)$ the ratio of repair cost to rebuilding cost at D_j degree of damage to type k buildings, and B_k the total value of type k buildings (Chen et al., 1992).

The method suffers several major limitations. Firstly, the data collection is obviously laborious and requires painstaking cataloguing of buildings and facilities in the affected regions. In many parts of the world, particularly in Asia, the vast amount of data required for such calculations is difficult to obtain. Regional differences in facility classification schemes also render the compilation of available information into a single consistent database for the whole world difficult. Secondly, it is not always plausible to adhere monetary values to the loss and damage of the facilities. The values of the exposed buildings and facilities fluctuate with the growth and decline of the local economy. Estimates based on current values may become outdated quickly for fast developing regions such as China. Thirdly, such inventory databases generally ignore loss due to business interruption, limiting the loss estimates to visible structural damages. Also, in spite of the complexity of the numerical procedure and the completeness of the inventory databases, it is not unusual for loss estimates to be off by as much as a factor of 10.

3. ECONOMIC LOSS ESTIMATES BASED ON MACROECONOMIC INDICES

The limitations of the conventional method have necessitated the search for an alternative approach. Since the total values of the buildings and facilities as well as deprivation in revenues due to business interruption are all closely related to the economic productivity of the region, the economic loss caused by an earthquake must bear a direct relation with the

state of its economy. The economic condition of a region is commonly measured in terms of its GDP, which is the total newly created social wealth of the region as defined by World Bank (1995). The GDP measures the total output of goods and services for final use from all resident units in the region, including both enterprises and self-employed individuals, of the region during a specific period of time. A similar index, the GNP, includes overseas income earned by the residents of the region. Since such overseas earnings are unlikely affected in an earthquake event, the GDP, if available, is the more appropriate index to be used.

Fig. 1 shows that the GDP and the social wealth in Japan as a function of time from 1955-1993 (Shono, 1995). It can be seen from Fig. 1 that the GDP increases while the total social wealth increases. Fig. 2 shows that there are closely relation between newly increased fixed assets and GDP in the mainland of China. Both of these examples, one in Japan as a representative of developed countries, another in China as a representative of developing countries, show that GDP can be used as a measure of the social wealth.

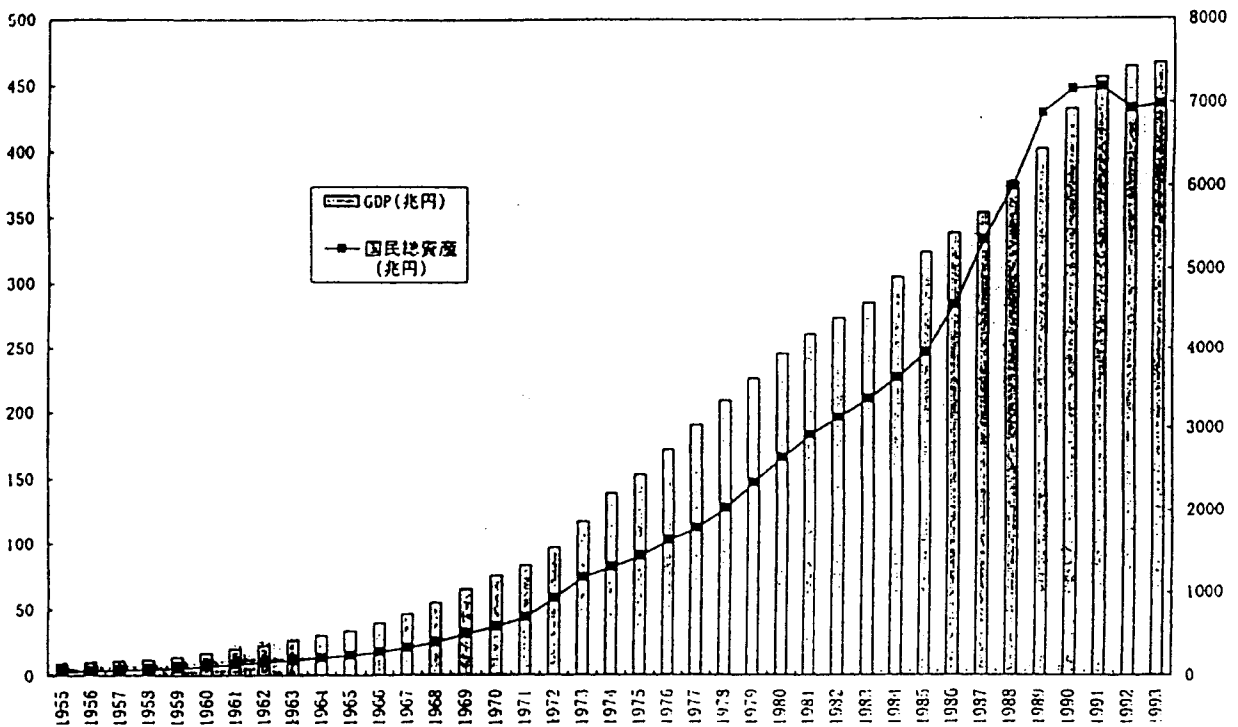


Fig. 1: GDP and total social wealth of Japan during 1955-1993 (Shono, 1995)

In the present method, the estimated economic loss is given by a formula modified from (1). For a given area, the estimated loss is given by

$$L = \sum_I P(I) F(I, GDP) GDP \quad (2)$$

where $F(I, GDP)$ is a measure of the area's vulnerability to earthquake damage. Essentially, the expression for the collective vulnerability of buildings in (1) has been replaced by the area's GDP in (2).

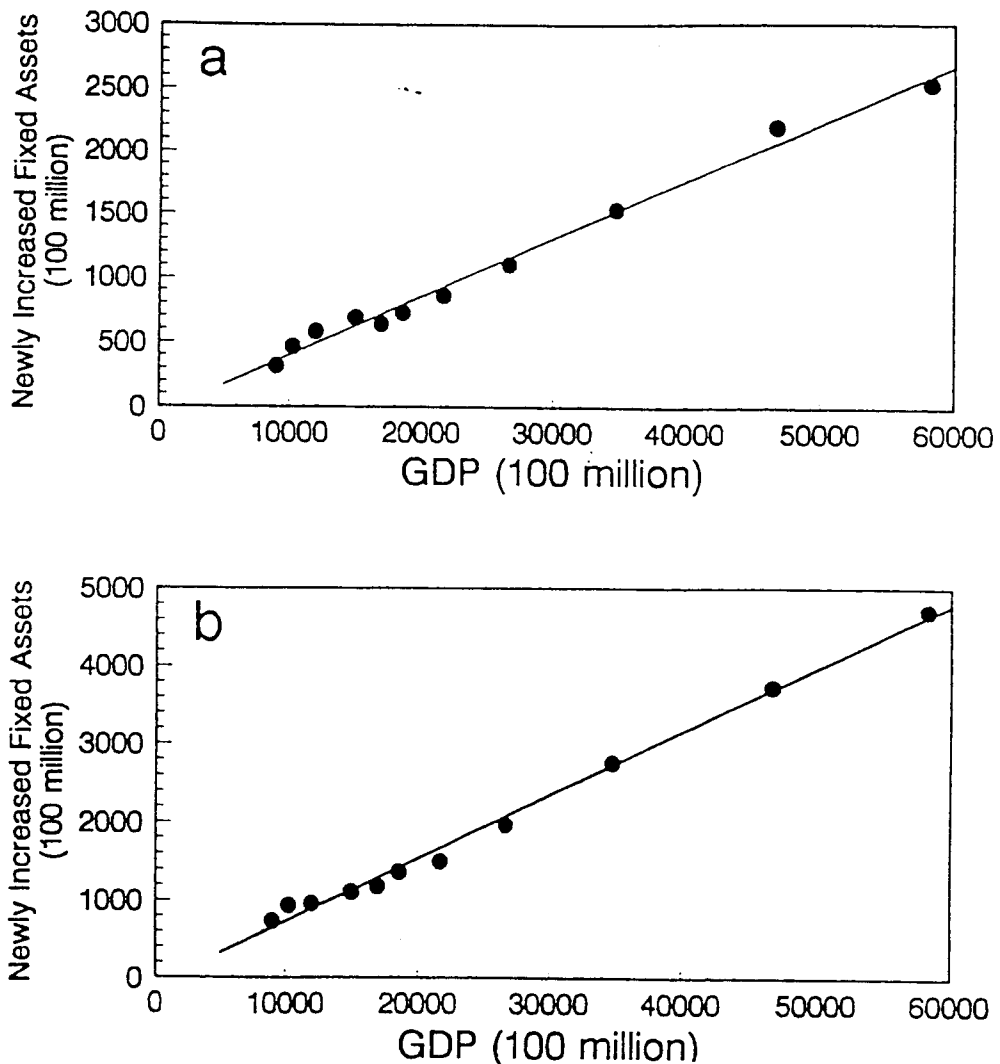


Fig. 2: Relation between GDP and the newly increased assets in the mainland of China (data from the State Statistical Bureau of China, 1996). (a) Newly increase fixed assets through technical updates. (b) Newly increase fixed assets through capital construction.

4. GDP DISTRIBUTION OF THE WORLD

The earthquake loss estimate methodology outlined in (2) requires the formulation of several key components: the seismic hazard and the GDP of the region, and a relation between GDP and seismic loss. GDP is one of the many socio-economic indicators regularly compiled by various agencies and institutions, such as the World Bank, the World Resources Institute, and the United Nations. It is suitably used as a measure of the economic condition of a community. However, the GDP is often given for a nation or a province with no specific reference to its areal extent. The national or provincial GDP must be apportioned over the

nation or province to provide the seismic exposure analysis with the necessary resolution. A mechanism of apportionment is therefore needed to systematically derive the GDPs of the individual zones in the nation or province.

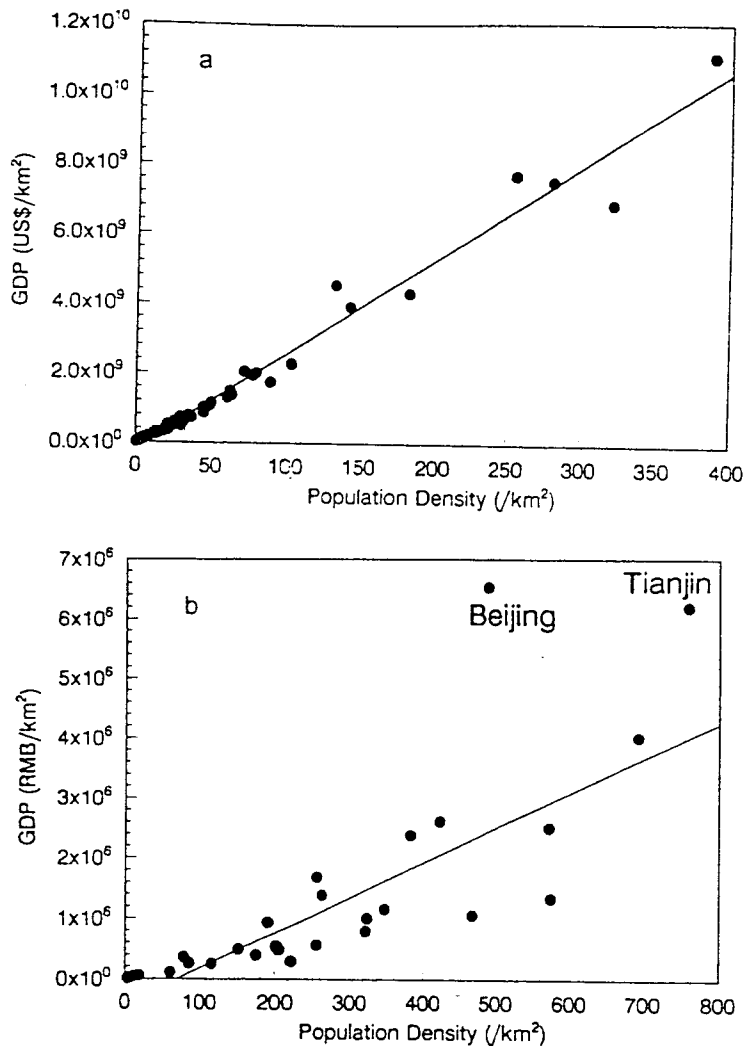


Fig. 3: Correlation between population density and GDP/unit for (a)United States and (b) China

Population probably serves as the most useful basis for the apportionment of the GDP. Fig. 3 shows the correlation between the population and the GDP of the individual states in the United States (California Department of Finance, 1995) and the provinces in China (State Statistical Bureau of China, 1996). In both examples, the GDPs of the individual states or provinces show a strong correlation with population. Fig. 4 shows more relations between GDP and population of provinces in different countries. In these studies, the GDP of an individual unit within a nation was determined according to the following equation:

$$GDP_{Unit} = (GDP_{region}) \cdot \frac{Population_{Unit}}{Population_{region}} \quad (3)$$

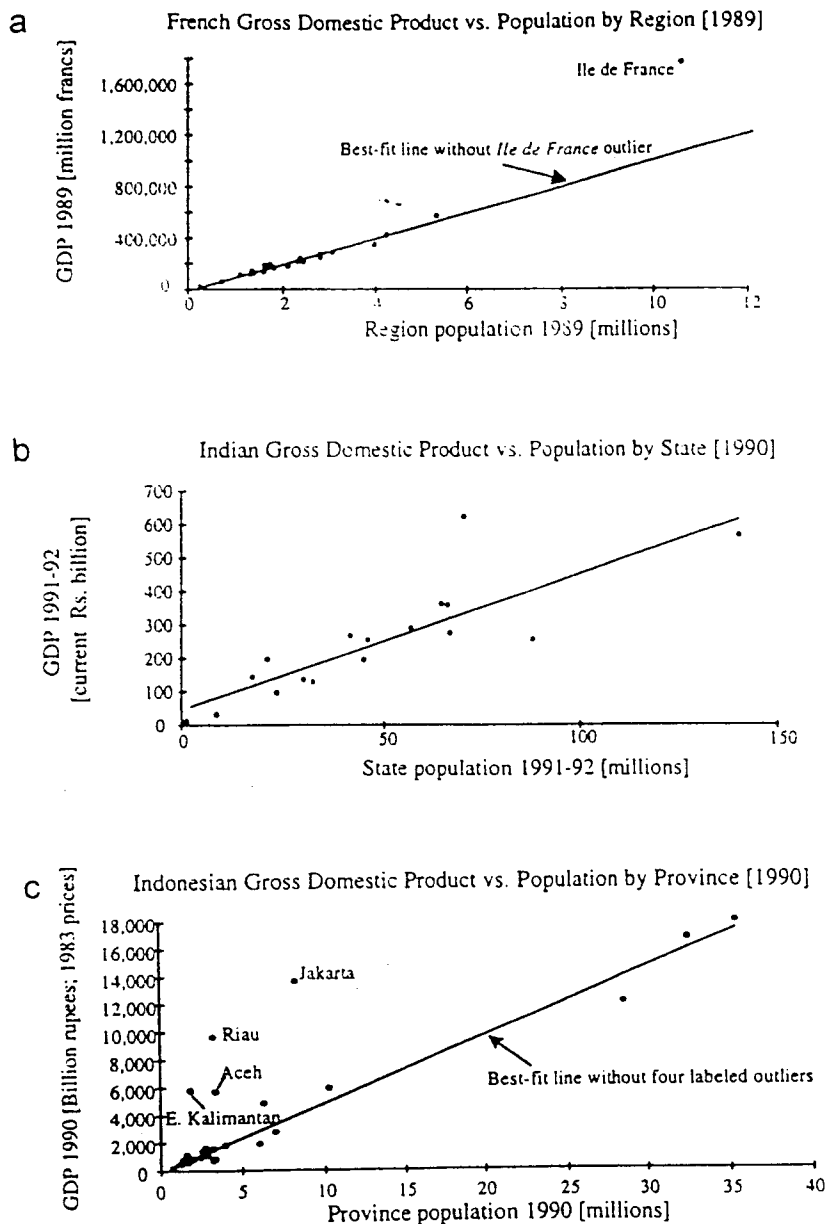


Fig. 4: GDP and population of provinces in different countries (Davidson, 1997).
 (a) France, (b) India, (c) Indonesia

The Consortium for International Earth Science Information Network (CIESIN) and the Environmental Systems Research Institute, Inc. (ESRI) compiled a database containing about 19,000 subnational administrative regions and the associated population for the whole world (Tobler, 1995). The population data, reported at a 5' lat. 5' long. resolution, were used in the present analysis (CIESIN's contribution of data to the current study is gratefully acknowledged by the authors). GDP data were extracted from World Bank (1995). In this study, we have partitioned the Asia's land surface into 0.5° latitude by 0.5° longitude cells. The GDP of each cell was determined based on the GDP and the population of the region to which the cell belong, as well as the population of the cell according to equation (3).

5. RELATION BETWEEN GDP AND EARTHQUAKE LOSS

The second important attribute of the loss estimate in (2) is the relation between potential economic loss and the GDP in earthquake events. The functions $F(I, GDP)$ can plausibly be determined empirically from previous case histories. Unfortunately, reported economic loss figures even for the same event are often inconsistent and are subject to revisions. The catalogues of significant earthquakes presented by Dunbar et al. (1992), Zhao and Chen (1993,1994), and Zhao (1995a,1995b) provide losses of over 500 events, but most of the reported cases did not include any numerical data on loss estimates or epicentral intensity and could not be used in the present computation. From those catalogues, we have 39 earthquakes since 1980 with epicentral MMI greater than VI and for which loss data are available (Table 1).

The mean damage factor for a group of similar structures exposed to the same ground shaking intensity is defined by:

$$\text{Mean Damage Factor (MDF)} = \frac{1}{n} \sum \frac{(\text{Dollar Loss})_i}{(\text{Replacement Value})_i} \quad (4)$$

Where n is the number of structures in the sample. For statistical data sample sets from a given geographical study area, the damage ratio and the mean damage factor can be calculated as mentioned above. Following to the previous philosophy, we define

$$F(I, GDP) = \text{Mean Damage Factor (MDF)} = \frac{1}{n} \sum \frac{(\text{Dollar Loss})_i}{(GDP)_i} \quad (5)$$

The GDP of the epicentral zone was then determined by prorating the GDP of the nation or the region according to (3), based on the population data for the affected zones provided by CIESIN database. The ratios of the reported economic loss to the GDP of the affected zone are also listed in Table 1. The reported losses are plotted against the computed GDPs of the epicentral ones for event with MMI VI in Fig. 5. While both, the loss and GDP are plotted on a logarithmic scale, there is an obvious correlation between the two parameters. The loss-GDP relation may require some modification for nations at different economy level. We have divided the nations in Table 1 into categories of high-income (GDP greater than US \$8,300), medium-income (US \$675-US \$8,300), and low-income (less than US \$675) economies according to their GDPs. The loss/GDP ratios are plotted against the earthquake intensities for the events listed in Table 1. As shown in Fig. 4, the high-income economies generally have lower loss/GDP ratios than the medium- and low-income economies, which is attributed to the better earthquake prevention and earthquake-resistant capacities in the more advanced nations.

Chen, et al. (1998) found that the adobes in Costa Rica have almost the same vulnerability with the old civil houses in China, which represent the vulnerability in worst cases. On the other hand, the high quality buildings in Costa Rica have the same vulnerability with the reinforced concrete buildings in China due to employing the state-of the art-design and construction techniques, which represent the vulnerability of the best cases. The macroeconomic vulnerability defined by Chen, et al. (1998), falls in the middle of the two extreme cases of inventory studies because the total macroscopic loss is the sum of different types of buildings and facilities loss. Therefore the macroeconomic vulnerability must be

greater than that of best cases and less than that of worst cases. The use of macroscopic vulnerability in earthquake loss estimate is easy, simply and feasible. This vulnerability is preliminary in nature and should be refined as additional earthquake loss data.

Date	Lat.	Long.	Depth	M	I ₀	Deaths	Loss*	L/GDP	Location	Income
19800727	38.2N	83.9W	8	5.2	6	0	1	0.0042	USA	HIE
19801123	40.9N	15.3E	10	6.9	9	3114	10000	1.1750	Italy	HIE
19810224	38.2N	22.9E	33	6.8	8	16	900	1.8493	Greece	MIE
19810426	33.1N	115.6W	4	6.0	7	0	1.5	0.0060	USA	HIE
19821017	43.2N	12.7E	20	4.5	6	0	35	0.0355	Italy	HIE
19821213	14.7N	44.3E	10	6.0	8	2800	90	0.1909	Yemen	MIE
19830502	36.2N	120.3W	10	6.5	8	0	31	0.0125	USA	HIE
19831108	50.7N	5.3E	10	4.7	6	2	50	0.0394	Belgium	HIE
19831222	11.9N	13.5W		6.3	7.95	275	10	0.1667	Guinea	MIE
19831230	36.4N	70.7E		6.5	8.25	24	3	0.1452	Afghanistan	LIE
19840429	43.2N	12.5E	7	5.6	7	0	31	0.0084	Italy	HIE
19850510	5.6S	151.1E	27	7.1	8	1	1.0	0.0227	Papua New Guinea	MIE
19850703	4.4S	152.8E	46	7.2	7	0	1	0.0541	Papua New Guinea	MIE
19850729	36.2N	70.9E	99	6.6	8	5	2	0.0968	Afghanistan	LIE
19860405	13.4S	71.8W	55	5.3	6	16	22	0.4809	Peru	MIE
19860721	37.5N	118.4W	9	6.3	6	0	1	0.0457	USA	HIE
19870302	37.9S	176.8E	20	6.8	10	1	200.0	1.3825	New Zealand	HIE
19870306	0.1N	77.8W	10	6.9	9	1000	700.0	4.3750	Ecuador-Colombia	MIE
19871124	33.1N	116.0W	2	6.6	7	0	4.0	0.0161	USA	HIE
19881106	22.8N	99.8E	10	7.6	9.9	930	269	3.4487	China	LIE
19890507	23.5N	99.5E	33	5.7	7	1	54	0.9432	Burma-China	LIE
19891018	37.1N	121.8W	19	7.1	9	62	5600	0.2251	USA	HIE
19900620	37.0N	49.4E	12	7.7	10	55000	500	0.5915	Iran	MIE
19910422	9.9N	82.9W	10	7.6	10	75	43	0.1792	Costa Rica	MIE
19910704	8.1S	124.7E	29	6.5	8.25	23	7.7	0.0601	Indonesia	MIE
19920425	42.0N	123.8W		6.9	8.85	0	66	0.1800	USA	HIE
19920628	35.2N	118.5W	5	7.4	8.6	3	92	0.0518	USA	HIE
19921012	29.7N	31.1E		5.9	8	541	500	0.3561	Egypt	LIE
19930801	15.4N	31.6E		5.2	6.3	2	0.1	0.0667	Sudan	LIE
19930921	42.3N	122.1W		5.8	7	2	7.5	0.0896	USA	HIE
19930929	18.0N	76.4E	6	6.3	8	30000	80	0.3399	India	LIE
19940117	34.2N	118.8W	18	6.8	9	61	15000	0.5083	USA	HIE
19940215	5.1S	104.0E	15	7.0	9	207	170.0	1.1333	Indonesia	MIE
19940602	3.0N	75.9W	9	6.6	8.4	795	100	0.3138	Colombia	MIE
19950116	34.5N	135.0E	16	7.2	10	5502	100000	6.1937	Japan	HIE
19950119	5.1N	72.0W	18	6.6	8	5	2	0.0667	Colombia	MIE
19950514	8.4S	125.1E	33	6.9	8	6	5	0.1136	Indonesia	MIE
19950527	52.6N	142.8E	33	7.6	9.9	1989	110	4.1250	Russia	MIE
19950615	38.4N	22.5E	14	6.5	8	27	7	0.0455	Greece	MIE

* Damaged loss by million US dollar.

* The definition of HIE, MIE and LIE given by World Bank and UN as follows(World Development Report 1994, Oxford):

--High Income Economies are those countries with a GNP per capita of \$8,356 or more in 1993.

--Middle-Income Economies are those countries with a GNP per capita of more than \$675 but less than \$8,356.

--Low-Income Economies are those countries with a GNP per capita of \$675 or less.

Table 1: List of damaged earthquakes during 1980-1995

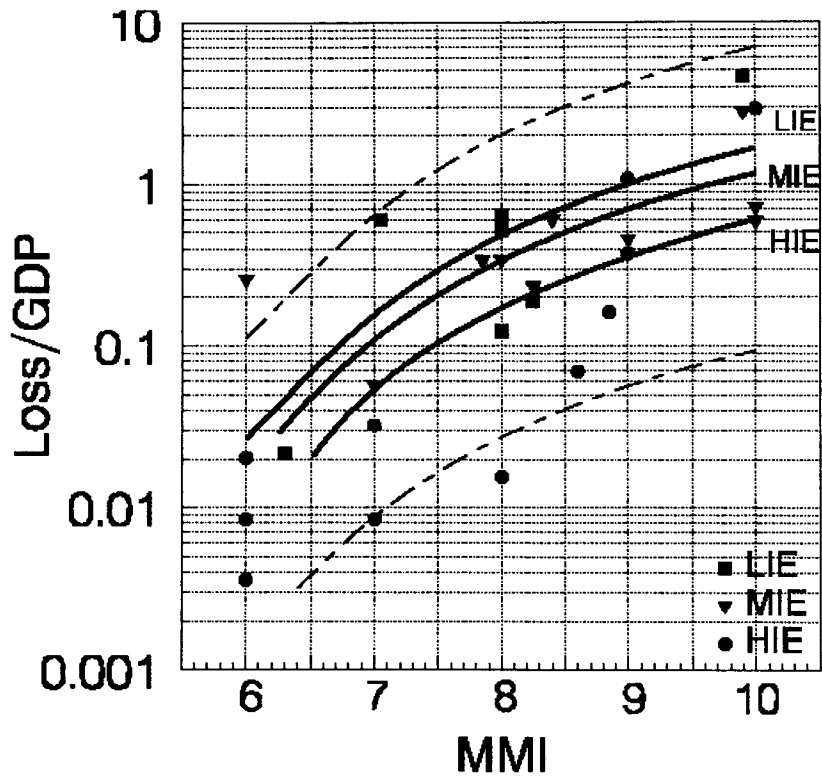


Fig.5: Relation between loss/GDP ratio and earthquake intensity for nations of different economic levels. Solid lines are cubic spline fits for the loss/GDP-intensity relation and dashed lines errors of estimates for the entire dataset.

6. COMPILATION OF GLOBAL LOSS ESTIMATES

In current analysis, we have carried out the estimation of predicted earthquake loss on a global scale based on the global seismic hazard analysis (Chen et al., 1998). The exceeding probability $P(\geq I)$ of earthquake intensity I for a region represents the probability at which an event of a particular intensity or less occurs at the location within the specified duration of time. Based on an earthquake occurrence probability from hazard analysis, the maximum intensity can be obtained for each $0.5^\circ \times 0.5^\circ$ cell over the land surface of the world.

Region or country	Loss
World	949
Asia	563
Europe	184
North America	115
South America	60

Table 2: Expected earthquake loss at 10% probability of exceedance in the next 50 years for some countries and regions (unit: billion USD).

The GDP of each unit cell is obtained from (4), and the projected earthquake loss was obtained by integrating the losses from the intensity lower than the maximum intensity using the hazard-loss relation. The global expected loss distribution is shown in Fig. 6. Table 2 lists the expected loss (in USD) of selected countries and regions for the next 50 years.

Three aspects in the loss equation could have contributed to the errors of the analysis: the seismic hazard probability function, the computed GDP for the individual cells, and the accuracy of the empirical relation between earthquake loss and GDP. Among the three attributes, the seismic hazard was estimated from a large database of earthquakes and unlikely gives rise to large error in loss estimate. We are not able to evaluate the errors associated with the GDP estimates. The strong correlation between population and GDP within a nation suggests that the criterion is appropriate. The largest source of error appears to have arisen from the loss-GDP relation which was derived empirically for each earthquake intensity. The estimated standard errors of the regression lines are about 0.5 for intensities VIII and X, and 0.2 for intensity IX (Table 3). In other words, the loss estimate may commonly deviate from the estimate by half an order of magnitude, or equivalent to a factor of 3. The deviations of the data are probably due to a combination of the errors in the intensity estimates, computed GDP, and the reported losses.

Intensity	Regression*	Standard error	R
8	$L = -0.35 + 0.86 G$	0.50	0.82
9	$L = 0.04 + 0.93 G$	0.25	0.95
10	$L = 0.21 + 1.05 G$	0.48	0.97

*L : Log of loss in \$M G : Log of GDP in \$M

Table 3: Relation between GDP and Economic Loss

In addition, the present analysis has assumed a single size for the epicentral zones for different intensity. Such an assumption likely leads to some bias in view of the variable nature of the geometry and size of epicentral zones. The crude correlation between earthquake loss and GDP, however, suggests that GDP can plausibly be used as a measure of the vulnerability of the structures in the epicentral zones.

7. DISCUSSION AND SUMMARY

In this analysis, we have presented a new method to estimate seismic loss based on GDP and population data. The method may have several limitations. First, the estimate of physical losses may be unsuitable for certain areas with high earthquake resistant capability. Secondly, we do not have the actual GDP data for the individual units; we have only used the population-weighted GDP data in the calculation. Thirdly, the physical loss estimation in the above analysis is given for intensity over VI. It may have been over-estimated the losses for the developed areas with high earthquake resistant capability. A further limitation is that differences in the bedrock geology or site condition have not been taken into account. Also, the empirical relation between the damage loss and GDP obtained in this paper is still preliminary in nature. Better relations can be formulated with more earthquake reports and detailed intensity attenuation studies. More accurate analyses can also be obtained for an individual region if detailed local GDP and population data are available.

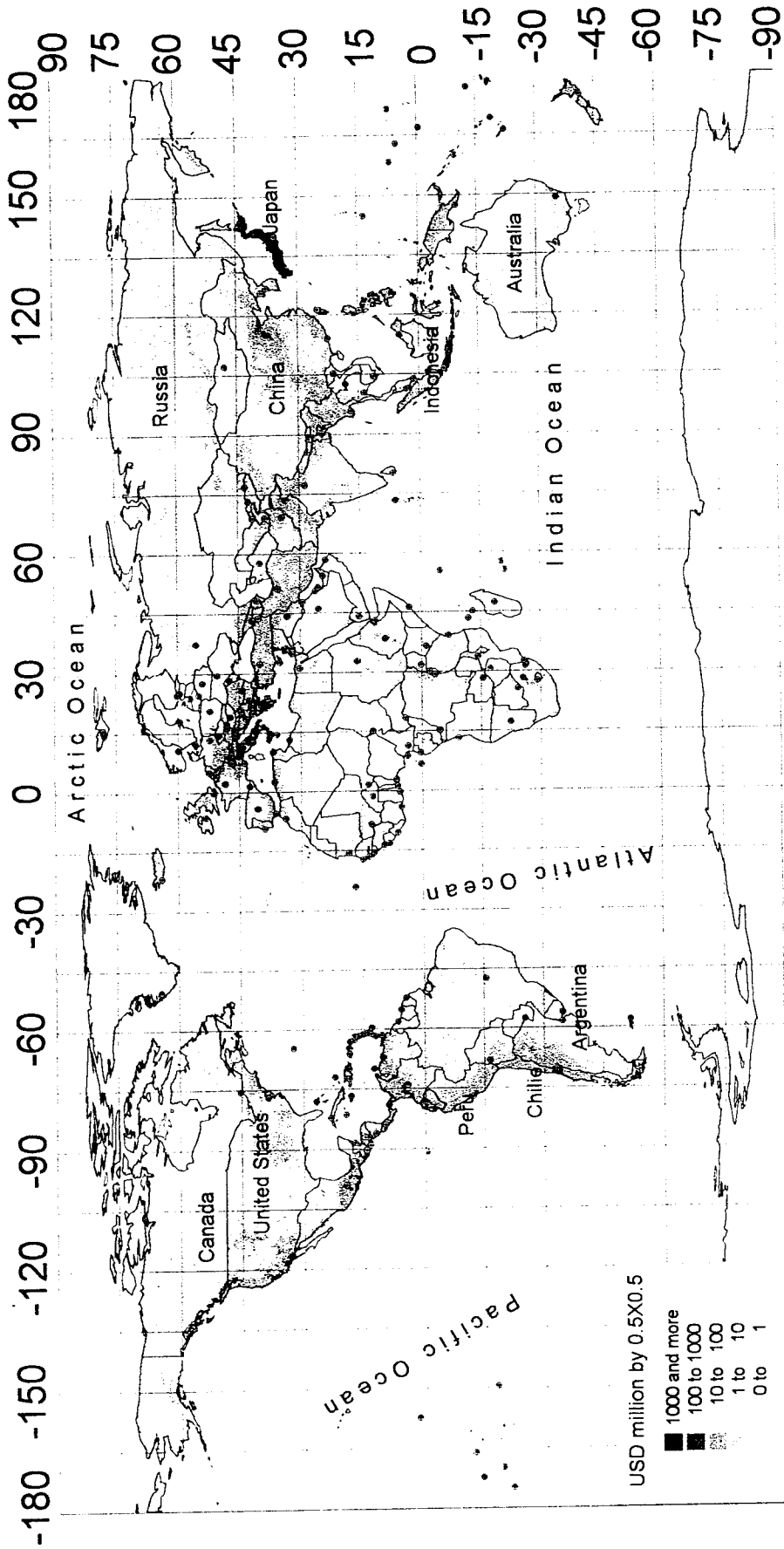


Fig. 6: Expected Earthquake Loss Map(50 years)

According to our computation of the earthquake losses which maybe caused from the earthquakes in the future 50 years, the loss is 565 billion USD for Asia, and 949 billion USD for the world. About 59% earthquake loss will occur in Asia.

In spite of these limitations, the method provides a standard means of estimating earthquake damages and enables assessment of earthquake risk on a global scale with limited inventory data and at a modest cost. Secondly, the data used are readily available, avoiding the painstaking procedure of collecting inventory data. Thirdly, the method is suitable to be used in rapidly developing areas, where values of structures and facilities, as well as indirect losses due to business interruption can escalate in short periods of time. Also, since macroeconomic data are regularly compiled by financial institutes, the earthquake risk estimates can be updated readily. The precision of the method is certainly limited by the accuracy of the macroeconomic data and the accuracy of the loss-GDP relation. The loss estimates are probably accurate within an order of magnitude, which is comparable to the precision of estimates with conventional methods. It may be premature to suggest that the advantages provided by the method outweigh its limitations, but the method certainly provides us with a quick means of earthquake risk assessment, which could be useful for earthquake planning undertaken by governments.

ACKNOWLEDGMENTS

This work was undertaken within the framework of the activities of IASPEI and WSSI task force on "Global Seismic Assessment". It was supported partly by National Science Foundation of China (49574207). We also acknowledge the Consortium for International Earth Science Information Network for providing the population data.

REFERENCES

- Applied Technology Council (1985). Earthquake Damage Evaluation Data for California (ATC-13), Redwood City, California, Applied Technology Commission.
- California Department of Finance (1995). California Statistical Abstract: 1995, Sacramento, California, Issued November, 1995.
- Chen, Y. et al. (1992). Estimating Losses from Earthquakes in China in the Forthcoming 50 Years, Seismological Press, Beijing.
- Chen, Y., Liu, J. et al. (1998). Global Seismic Hazard Assessment Based on Area Source Model and Seismicity Data, *Natural Hazards*, 17, 251-267.
- Chen, Y., Li, G.P., Chen, Q.F. et al. (1998). Earthquake Damage and Loss Estimation with Geographic Information System, *Acta Seismologica Sinica*, 11, 6.
- Dunbar, P.K., Lockridge, P.A., and Whiteside, L.A. (1992). Catalogue of Significant Earthquakes (2150 BC--1991 AD), Report SE-49, World Data Centre A for Solid Earth Geophysics, September 1992.
- PELEM (Panel on Earthquake Loss Estimation Methodology) (1989). Estimating losses from

- future earthquakes, Panel Report, National Academy Press, Washington DC, 57.
- RGCER (Research Group of Chinese Earthquake Risk Prediction in Ten Years) (1995). Atlas of Earthquake Risk Prediction in China, Science Press, Beijing, 46.
- State Statistical Bureau of China (1996). Statistical Yearbook of China 1996, China Statistical Publishing House, Beijing, China.
- Tobler, W. et al. (1995). The Global Demography Project, Technical Report TR-95-6 National Center for Geographic Information and Analysis, Department of Geography, University of California, Santa Barbara.
- World Bank (1995). World Development Report 1994: Infrastructure for Development, Oxford University Press.
- Yeats, R.S., Sieh, K., and Allen, C.R. (1997). Geology of Earthquakes, Oxford, New York, 568.
- Zhao, R. and Chen, Y.(1993). The global seismicity and earthquake disasters in 1992, Recent Developments in World Seismicity, 4, 1-6.
- Zhao, R., and Chen, Y. (1994). Outline of world-wide earthquakes disasters in 1993, Recent Developments in World Seismicity, 8, 12-15.
- Zhao, R. (1995a). Overview of World-wide damaging Earthquakes in 1994, Recent developments in World Seismicity, 8, 12-15.
- Zhao, R. (1995b). Overview of World-wide damaging Earthquakes occurring in the half of 1995, Recent developments in World Seismicity, 11, 14-19.

INTRODUCTION TO CAPSeis

Li MinFeng and Li Shengqiang

Center for Analysis and Prediction, China Seismological Bureau ,
No. 63, Fuxing Avenue, Beijing, 100036, China,
Fax: +86 10 88015480, Email: Li minfeng@seism.ac.cn

1. INTRODUCTION

The Software System for Seismic Data Management and Analysis named CAPSeis is a software package for catalogue management, data processing, spatial-temporal parameters analysing and graph processing, which includes almost all the approaches for long-term, immediate-term, short-term and imminent seismic activity analysis, and tools for trend decision in situ after a large earthquake. In order to make users comprehensively understand this software package, we are planning to introduce it as follows:

The running environment of the CAPSeis system requires as follows: 1) PC386 and above, VGA graphical mode for Display and above; 2)MS-DOS 6.0 and above, Windows 3.x or Windows 9x; and 3) at least 450K EMS Memory and at least 1MB Basic Expanded Memory.

2. DIRECTIONS FOR GENERAL MODULES

CAPSeis is a software system fully controlled by functional modules, which is easily used by users. This part shows you the construction of user interfaces, and how to input parameters as well as how to print graphs, display maps and transfer map formats.

2.1 Selection Menu contains main menu, pull-down menu in DOS text format and menu in graph pattern.

2.2 File Selecting Windows consist of two kinds of file selecting windows, one is used to select only one file (SSM) and can be closed with Enter, the other is used to select more than 1 files (MSM), which must be closed with Esc.

2.3 Parameter Input Window are the useful interfaces for users to input parameters. A common window usually includes 3 blocks, i.e., parameter input section with some selection bars, OK icon and Cancel icon.

2.4 Graph Operation Status When the cursor appears as a cross and the mouse appears with an arrow in the graph mode, you are in the graph operation status.

2.5 Graph Scale and Graph Superposition will be introduced from 1) Graphs of geological co-ordinates and 2) Graphs of time co-ordinates.

2.6 Graph Output and Display includes 1) Format transformation, 2) Graph display, and 3) Graph printing.

3. CATALOGUE MANAGEMENT

The “Catalogue Management” on the main menu is to deal with catalogues and its submenus include Format Transformation, Catalogue Combination, Catalogue Arrangement, Catalogue Display, Catalogue Compiling and Catalogue Selection in rectangle area, circle area or polygon area etc. This module is used to prepare data for other modules and to prepare catalogues for researchers.

3.1 Catalogue Format

Each records of a catalogue in CAPSeis contains year, month, day, hour, minute, second, latitude, longitude, magnitude, depth, serial number of seismic sequences, which can be in ASCII system (*.eqt) and binary system (*.eq2). Any of the two formats of catalogues can be used in CAPSeis.

3.2 Format Transformation This item is to introduce how to convert seismic catalogues from user’s own format to the one that can be supported by CAPSeis system.

3.3 Catalogue Combination

Two catalogues can be combined into one file with this function provided by CAPSeis. The two files can be in either ASCII format or binary format and the final file is in the same format as the first catalogue.

3.4 Catalogue Arrangement CAPSeis can automatically arrange catalogues according time. The function of “arrange” is set just for users to deal with catalogue files in ASCII format.

3.5 Catalogue Display is designed to list the catalogues.

2.6 Catalogue Selection This module includes rectangle selection, circle selection and polygon selection, which are different in the geometry of the area within which the shocks are selected.

3.7 Aftershock Deletion The module of aftershock deletion is designed to delete the aftershocks for all the shocks in the catalogue based on a model of diffusion chains,

which can also be used to deal with seismic swarms and to delete foreshocks.

3.8 Catalogue Breaking The sub-choice of Breaking can divide a large catalogue into several smaller ones, which can be used directly without decompressing.

3.9 Catalogue Editing Shocks in a catalogue in EQT or EQ2 format can be inserted, rewritten, deleted and added with the sub-choice of "Editing" function.

4. BASIC SETUP OF THE SYSTEM

The choice of System on the main menu is to set up system parameters for CAPSeis.

4.1 Graph Mode on the Screen

The pictures provided with CAPSeis system are in VGA format, but for special users, higher-resolution formats such as SVGA are also provided with CAPSeis, which can only be displayed on newer screens with VGSA stand.

4.2 Basic Parameters of the System

If you choose the "Parameter" of the "System" menu, a popup window will appear on the screen, which contains many items including the basic parameters for projection map, the colour parameters, the saving paths for system procedures and for system fonts, and the parameters for the size of shock marks.

4.3 Quit CAPSeis If you want to exit the CAPSeis system, please choose this item.

5. ANALYSIS OF SHOCK IMAGES

The contents introduced above are prepared for processing earthquake data, creating shock images and analysing their mechanisms. The main functional modules of CAPSeis include almost all the approaches for seismic activity analysis such as spatial distribution module, seismic sequence module, temporal scanning module, spatial scanning module etc.

5.1 Spatial image of Shocks (Chart)

This module is used to do spatial analysis for earthquakes, such as seismic gap, seismic belt, seismic immigration, and so on. **This module consists of "Shock Map", "R-t Map", "D-t Chart", "Low Seismic Belt", "Migration", "Depth Profile" and "FMS Map"**. The function of "Shock map" is very useful for researchers to analyze spatial features of earthquakes. It is a very useful module to display shock distribution and to select shocks.

An R-t map is used to investigate the relationship between the shock time and the distance between every two shocks. A D-t map is used to investigate the relationship between the shock time and the shock depth.

5.2 Seismic Sequence

This module is used to **calculate and analyse lgN-M, b value, h value, U value, K value, value and waiting time**. It is also used to check earthquake sequence types. The **sequence catalogues** used in this module are provided with the “Catalogue” of the main menu.

5.3 Temporal Scanning (T-scan)

The module of “T-scan” is used to deal with the seismic parameters that change with time, including **frequency (N-t), creep, energy, b value, shock absence, value, Rm value, A(b)-N, M-t, Depth-t, general T-curves, and SEISMOLAP value**. The first subchoice of “**General Condition**” is used for all other temporal scanning methods.

5.4 Spatial Scanning (S-scan)

The module of “S-scan” is used to deal with the seismic parameters that change with space, including **frequency (N-t), creep, energy, b value, shock absence, value, and Rm value**. The first subchoice of “**General Condition**” is used for all other spatial scanning methods. The last choice of “Graphic output” under this module is used to draw the pictures whose parameters match to the above subchoices.

Additionally, the software package of CAPSeis also provides the help function, which includes the two choices of “Manual” and “Show file.” the contents provided by this package can not only be read through the Display, but also be printed through the Printers. And the system provides the extended module that users can add their executable programs into the CAPSeis system by modification of the file of “capseis.con”.

PC ASSISTED EXERCISES IN SEISMIC HAZARD ASSESSMENT BASED ON DATA FROM THE COUNTRIES OF PARTICIPANTS

Chen Yong, Chen Qifu and Chen Ling

China Seismological Bureau, 100036 Beijing, China
Fax: +86-10-6821 5973; E-mail: yongchen@public.bta.net.cn

1. INTRODUCTION TO WORLDRISK

WorldRisk is a software package for Seismic Hazard and Risk Analysis. WorldRisk is a GIS (Geographic Information System)-based application program designed to analyse and demonstrate seismic hazard and risk through the simplified methodology introduced in the Part I and II of the lecture "Approach to assessment of seismic hazard in China: Methodology". WorldRisk is a program running in Windows environment, therefore it is easy to learn and operate for users who have Windows experiences.

The following world-wide databases have been included in WorldRisk already:

- Historic earthquake catalogue (USGS, since 1800 BC)
- Instrumental earthquake catalogue ($M_{\min}=4.5$, 1964-1996)
- Population data (resolution $0.5^\circ \times 0.5^\circ$, 1995)
- Average attenuation of intensity or Peak Ground Acceleration (PGA)
- National Gross Domestic Product (GDP, 1996)
- World-wide earthquake loss data (1960 - 1998)

The advantage of WorldRisk is that it can provide a reasonable assessment of global as well as regional seismic hazard and risk only by using limited data through our simplified method. A key contribution of WorldRisk is the series of global or regional seismic hazard and risk (loss estimate) maps that can be produced and updated periodically with new and refined information. Now the following lists of quantitative products and information of seismic hazard and risk have been provided:

- The probability that a certain value of a macroseismic intensity or of a ground motion parameter (i.e. particle acceleration, velocity or displacement) will not be exceeded **at any site (oceanic or continental) in the world in various periods of time.**
- The expected loss caused by future earthquakes **at any site in the world in various periods of time.**
- Assess the seismic hazard and loss impact from **earthquake scenario** in the world (or in a specific region).
- Incorporate the results with GIS for specific output maps.

The GIS-based WorldRisk offers a new approach modelling earthquake loss estimates and earthquake scenarios.

2. GEOGRAPHIC INFORMATION SYSTEM (GIS)

A Geographic Information System (GIS) is a computer-based tool for mapping and analysing existing data sets such as earthquake events happened or expected to happen on Earth. GIS is, as the name implies, an information system specially designed for handling of geographic, location or spatial information. GIS comprises all the usual components of any information system, including system analysis and design, information management procedures, data conversion, analysis and maps output etc.

What places GIS apart from traditional information system is that they have special characteristics (such as map and image output, spatial analysis algorithms and ability to handle map projections) that enable them to work with location and spatial references. GIS technology integrates common database operations such as query and statistical analysis with the unique visualisation and geographic analysis benefits offered by maps. These abilities distinguish GIS from other information systems and make it valuable to a wide range of users. Based on GIS, the spatial analysis becomes feasible and the results of such analysis can be displayed in the form of thematic and other types of maps.

2.1. How GIS works

A GIS stores information as a collection of thematic layers that can be linked together by geography. This simple but extremely powerful and versatile concept has proven invaluable for solving many real-world problems from tracking delivery vehicles, atmospheric circulation to seismic hazard assessment.

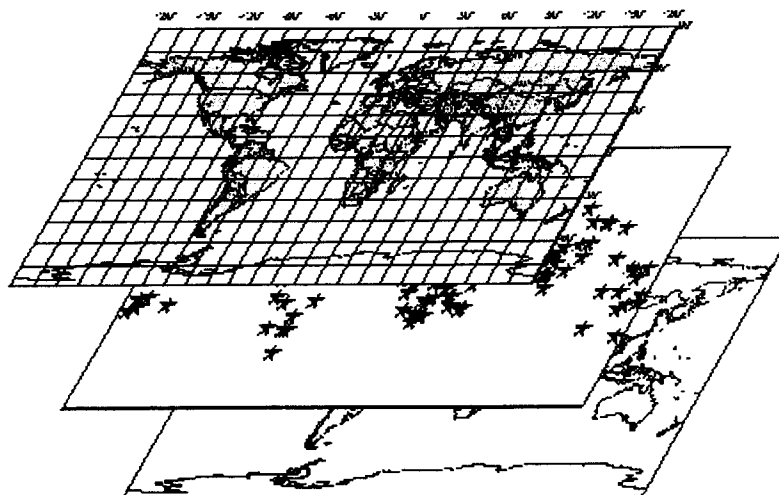


Fig. 1: Thematic layers of WorldRisk

Using the GIS technology, WorldRisk can be regarded as an integration of some basic thematic layers:

- World map (including nation's boundaries)
- World historic earthquake distribution map
- Expected maximum earthquake distribution
- Recent instrumental earthquake distribution (1964-1996)
- Seismic regionalization and *b* value distribution
- Destructive earthquakes and damage data
- Seismic hazard maps of the world for various periods of time
- Seismic risk maps of the world for various periods of time
- World expected earthquake loss maps for various periods of time
- GDP of countries
- World GDP distribution
- World population distribution (1994 data)

Geographic information contains either an explicit geographic reference such as latitude and longitude or national grid co-ordinate, or an implicit reference such as an address, a postal code, a census tract name, a forest stand identifier, or a road name. An automated process called geocoding is used to create explicit geographic references (multiple locations) from implicit references (descriptions such as address). These geographic references allow you to locate features such as business of forest stand and events such as earthquake on the Earth's surface to analyse.

2.2 GIS-based WorldRisk components

WorldRisk is GIS-based system, which integrates four key components: hardware, software, data, and methods.

2.2.1 Hardware

The WorldRisk **hardware** means the computer system on which GIS software and applications operate plus various peripherals. The simplest GIS's hardware can be implemented in a standard personal computer, often having a direct link to printing or plotting facilities. Sometimes, such systems also have input facilities (such as scanner or digitizer). The minimum requirements for **hardware** of WorldRisk are:

Personal computer:	Intel-based Pentium or compatible computer
Memory:	16 megabytes of RAM, strongly recommend 32 megabytes or above
Disk space:	300 megabytes for basis data
Monitor:	VGA or better resolution monitor
Operation environment:	Microsoft Windows 95 or later

WorldRisk hardware, like every other computer system, is affected by the advance in technology that seem to become more frequent each year. The suppliers of these systems try to make them evolutionary rather than revolutionary, so that development can progress quickly and steadily.

2.2.2 Software - MapInfo

The GIS software means the programs that give a computer the four basic capacities essential to handle geo-referenced data: input, data storage and retrieval (data management), spatial manipulation analysis, and output and presentation. The following Table 1 gives the most common GIS software.

Software	Company	Operation environment	
		DOS/Windows	UNIX
ARC/INFO ArcView	Environmental System Research Institute (ESRI), Inc.	Yes	Yes
Modular GIS Environment	Intergraph Corp. Generation 5 Tech. Inc.	Yes	Yes
MapInfo	MapInfo Corporation	Yes	Yes
Altas GIS	Strategic Mapping	Yes	No

Table 1: GIS Software

The detailed description of these popular GIS softwares can be found in the following books:

- Inside Arc/Info(includes CD), Onword Press, 1996.
- Inside ArcView(includes CD), Onword Press, 1996.
- Inside MapInfo (includes CD), Onword Press, 1996.

The simplest software of GIS is the ArcView Version 1.0 for Windows. ArcView Version 1.0 for Windows is very popular as an easy-to-use query and display tool for geographic information. Tens of thousands of copies are in use around the world today. Product features include

- An Intuitive, Menu-Driven Interface;
- An Easy data display and query;
- An Integrated raster and vector data display.

By visiting the following address, the free software of ArcView 1.0 can be obtained on INTERNET: <http://www.esri.com>.

The software of MapInfo Professional 4.5 is used in WorldRisk, and it provides the basic functions and tools required to store, analyse and display geographic information of seismic hazard and risk analysis. The key components are:

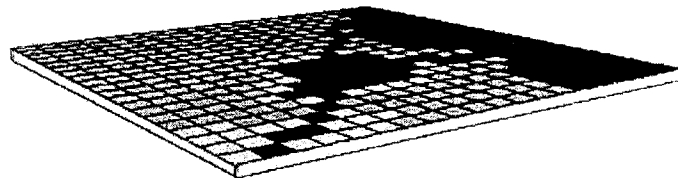
- a database management system (DBMS);
- tools that support geographic query, analysis and visualisation;
- a graphic user interface for easy access to tools.

2.2.3 Basic data

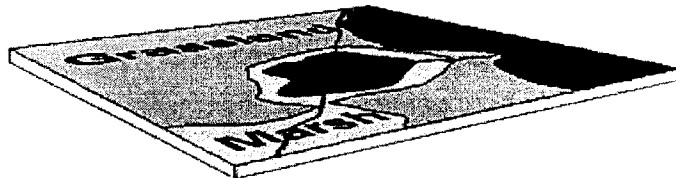
The Data required by GIS can be divided into two groups, the first group is related to the geographic maps, and the second one related to some specific requirements, for example the seismicity data, attenuation data etc. in seismic hazard analysis and risk assessment respectively.

Most maps used in GIS are originally generated from paper drawings. They are transferred to the computer by digitising or scanning and can be stored as two basic forms: raster or vector. Raster maps are faithful pictorial copies of the paper and are generated on a dot-for-dot basis across the whole sheet. The user can control the coarseness of the copy, however 200 dots per inch (dpi) usually provides a good visual representation of the original paper map. Raster maps are quick and cheap to transfer to computer, as all that is required, is a good paper copy of the area. Therefore, raster maps have a wide range of uses in the GIS world. By translating each of the lines in a map into computer data, vector maps are much more difficult to obtain. Yet it is more flexible, and compared with raster map it requires less computer storage for the same geographical area. With the increasing power of modern computers it is becoming more and more feasible to work with graphic data in both styles.

Raster



Vector



Real World

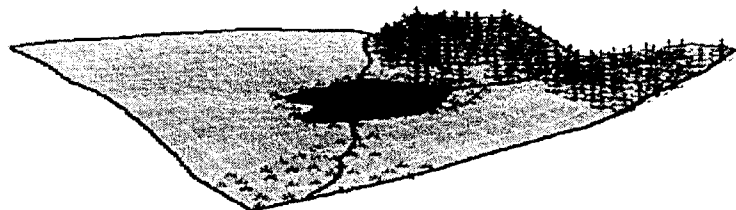


Fig. 2: Raster and Vector maps

Geographic data and related tabular data can be collected in-house or purchased from a commercial data provider. A GIS will integrate spatial data with other data resources even like DBMS, used by most users to organise and maintain their data, to manage spatial data.

Before geographic data can be used in a GIS, the data must be converted into a suitable digital format. The process of converting data from paper map into computer files is called digitising. Modern GIS technology has the capability to automate this process fully for large projects using scanning technology; small jobs may require some manual digitising. Today many types of geographic data already exist in GIS-compatible formats. These data can be obtained from data suppliers and loaded directly into GIS.

The second group of data, related closely to the seismic hazard and risk assessment, should be collected according to specific mission. Most data and information in seismic hazard analysis and seismic risk assessment are related closely to geographic co-ordinates which describe the location on the ground. Generally, the most data required for global seismic hazard and risk analysis are available in WorldRisk.

However, when doing seismic hazard and risk analysis on a regional or national scale supplementary data are needed.

2.2.4 Analysis method

A successful GIS operates according to a well designed plan and rules, which are the models and operating practices unique to each user.

In the present method, seismic hazard assessment by using area model and seismicity data and seismic risk analysis by using GDP and population data are proposed, which provide the scientific basis for construction the GIS's model. Based on this model, we summarise the whole computing procedure of seismic hazard assessment and seismic risk analysis in brief as the following working flow chart (Fig. 3).

2.3 What can GIS do for seismic hazard and risk assessment?

- Using GIS makes it much easier to update all the data required than with previous traditional analysis method and mapping procedure. This favours keeping data current, particularly for the exposure and vulnerability data. Only few working hours and smaller portions of the budget are required to add new data.
- It is much easier to produce reports and maps that are tailored to the user's need. The GIS can produce maps at any scale, any time length interested in risk assessment, any exceeding probability, with any combination of map themes, and for any area of the world. Furthermore, it is no longer necessary to work back and forth between separate map sheets, since GIS can display two adjacent maps simultaneously.

- The GIS enables to perform seismic risk analyses that were not feasible before, usually because the uniformed format of data was not available, the computer software was not available, or the analysis required too much time. One example is the determination of vulnerable region based on seismic risk analysis.
- User-friendly computer techniques, which may be implemented on PCs use integrated GIS software. Based on GIS, the seismic hazard and risk assessment method will be modular and accommodate improvement to modules as earthquake loss estimation research progresses. Therefore, the state-of-art-methodology will be used.

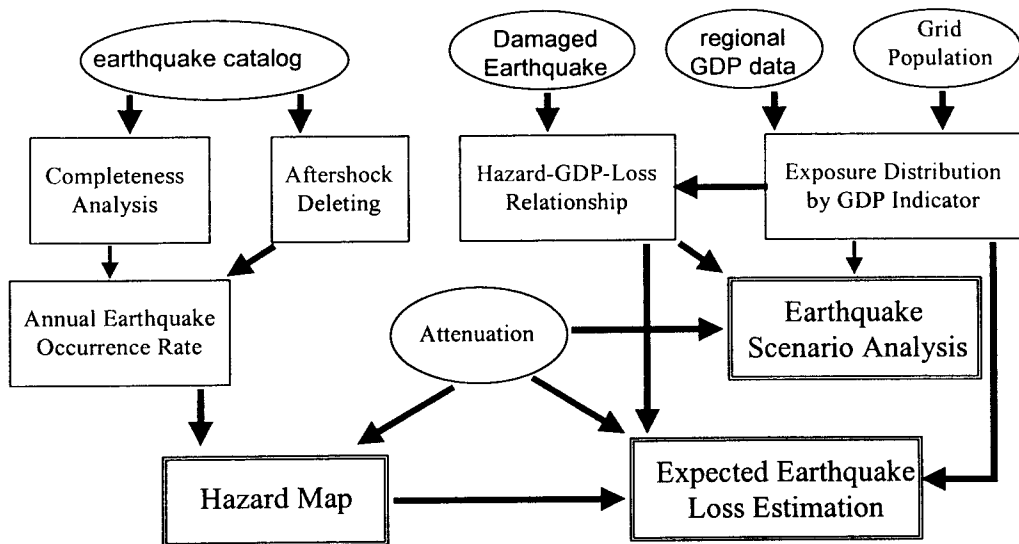


Fig. 3: Working flow chart of WorldRisk for seismic hazard and risk analysis

3. EXERCISES

WorldRisk installation is described below. If you have not already installed MapInfo, please install MapInfo before you install WorldRisk.

1. Run the Windows program manager.
2. Place the WorldRisk CD-ROM in your CD drive.
3. Double-click to run INSTALL.EXE on your CD drive.
4. Specify the directory where WorldRisk will set up. The default is C:\WRISK. If you prefer another directory, type the desired drive letter and/or directory path.
5. When the "Installation successful" message appears, click OK. WorldRisk is now installed on your system.

To start WorldRisk, click on Windows 95' **Start**, point to **Run** and select **WorldRisk.EXE** from the drive and directory where the WorldRisk was installed beforehand. Alternatively, double-click the icon **WorldRisk** on the Windows 95 desktop. Thus the WorldRisk application will appear on screen.

Exercise 1: Viewing the following information of your country

- Historic earthquake catalogue;
- Instrumental earthquake catalogue for a given time period;
- Population census data;
- Latest GDP for provinces or counties (as detailed as possible);
- Others, such as the *b*-value and maximum earthquake.

Exercise 2: Viewing the seismic hazard and risk results of your country

From the WorldRisk main menu choose EqRisk and Earthquake Risk, then single-click World or China item, the results of seismic hazard and risk world-wide or for China will be presented. The results are given with several maps named seismic hazard, expected earthquake losses etc.

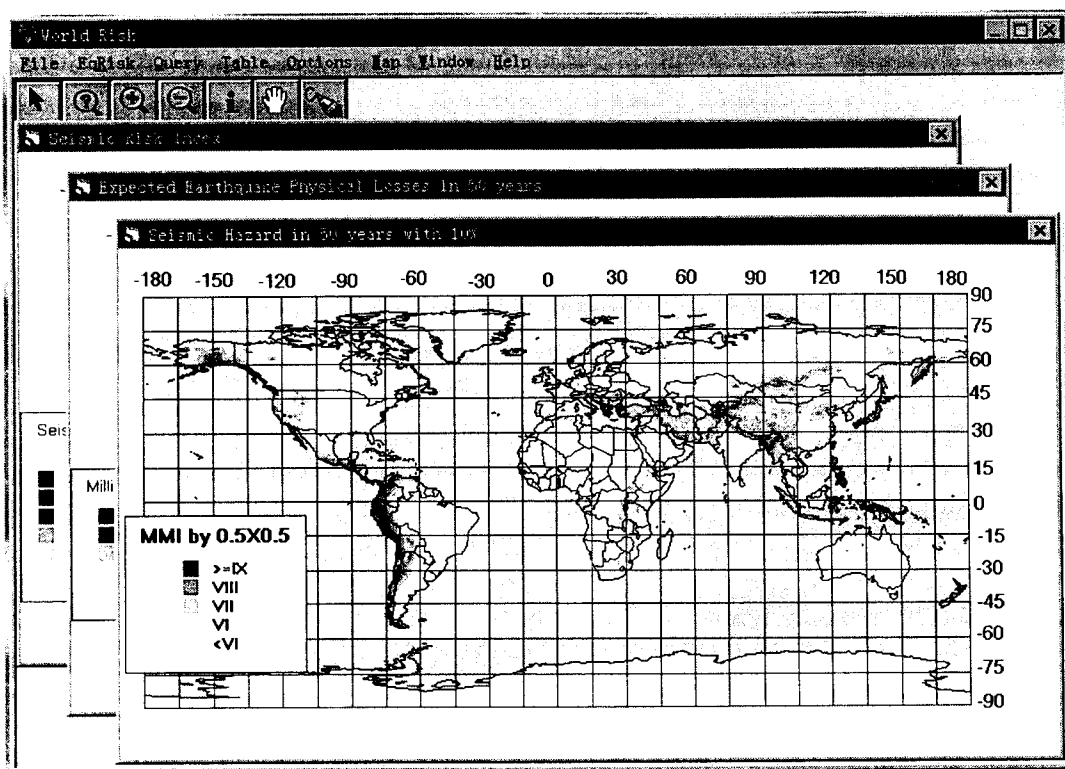


Fig. 4: Viewing seismic hazard and risk results

You can view those results in three formats: Map windows, Browsers, and Graph windows. The querying capabilities for those results range from simple selections such as a single file to complex SQL queries, which comprise one or more files. The query result can be saved as another MapInfo table for your specific work with MapInfo feature File Save As. You can extract results from interesting areas or regions as primary maps to perform geographic analysis, geocoding and other MapInfo operations. See MapInfo Reference for those operations.

Exercise 3: Earthquake scenario analysis

The earthquake scenario analysis allows you to simulate the calculation of the expected physical loss with a possible earthquake occurrence or to estimate the possible physical loss for an occurred earthquake. The analysis is based on $0.5^{\circ} \times 0.5^{\circ}$ population-weighted GDP data with the new methodology given in the Part II of “Approach to seismic hazard assessment in China: Methodology”.

Choose Scenario from EqScenario sub-menu. Then the Earthquake scenario analysis dialog displays. This dialog is waiting for you to input the location (Latitude and Longitude) and magnitude or intensity of earthquake for scenario analysis. Click the Calculate button, and the scenario calculation will begin on the basis of $0.5^{\circ} \times 0.5^{\circ}$ population-weighted GDP data.

From the City drop-down, the user can just choose some cities (Beijing, Istanbul, Lisbon, Mexico City, Rome, Los Angeles, San Francisco and Tokyo, etc.) which affected by historical earthquakes to input the location of those cities. The parameter of average annual GDP growth rate is set to estimate the possible earthquake loss at present time based on the data in 1996.

WorldRisk is only designed for the new methodology and its results are presented with the powerful GIS desktop MapInfo. It still needs improvement through different applications by different users. The scenario analysis results become more reasonable with updated GDP and population data as well as the availability of regional intensity attenuation and hazard-loss-GDP relations.

Exercise 4: Calculate the seismic hazard and risk of your country by using your data

- Historical earthquake catalogue (as long as possible);
- Instrumental earthquake catalogue (the magnitude threshold as small as possible);
- Local attenuation relation;
- National Gross Domestic Product for small administration unit or area;
- Earthquake loss data (if available).

SEISMIC RISK ASSESSMENT AND DISASTER MANAGEMENT

Yuxain Hu

Institute of Geophysics, China Seismological Bureau
5 Minzu-Xueyuan South Road, Beijing, 100081, China
e-mail: huyuxian@public.bta.net.cn

1. GENERAL FRAMEWORK OF SEISMIC RISK ASSESSMENT (SRA)

1.1 Strong earthquake --- a rare and sudden disaster

There are two kinds of natural disasters. One is the result induced by a gradually occurred and slow natural process such as heavy rainfall, flood and drought, which take at least a few days to cause disaster. The other is the result induced by a suddenly coming and violent natural process such as strong earthquake, and perhaps, typhoon. Strong earthquakes take only a few minutes or even less to cause a great loss with casualty of more than 10 thousands of human lives and an economic loss of over a billion US dollars. For the first kind of disaster, temporary measures can usually be taken to release or even prevent the disaster, at least to save human lives. But for the second kind of disaster, because of no pre-warning, there is no time to take effective measures to save the buildings and human lives. The best we can do after the attack of a strong earthquake is to rescue the people trapped under the collapsed buildings or to ask the people stay out of the damaged buildings to prevent further losses. Because of the poor standard of the construction and the fast urbanisation, the big cities in the developing countries are most vulnerable to this kind of natural disaster.

1.2 General framework of seismic risk assessment (SRA)

The general framework of SRA and disaster mitigation may be given in Eq. (1.1) as an equation or in Fig. 1.1 as a flow chart (Hu, Liu, Dong, 1996; Yin, 1999; Kiremidjian, 1998).

$$SRA = D \times [L(D) + IL(D)] \quad (1.1A)$$

$$D = SHA \times VUL \times EXP \quad (1.1B)$$

where D is damage, L and IL are respectively direct and indirect loss, VUL is the vulnerability of the exposure EXP , and SRA and SHA are respectively the seismic risk and hazard. All terms used here are vectors or matrices and will be defined in Section 1.3 and some necessary explanations are given in the following sections.

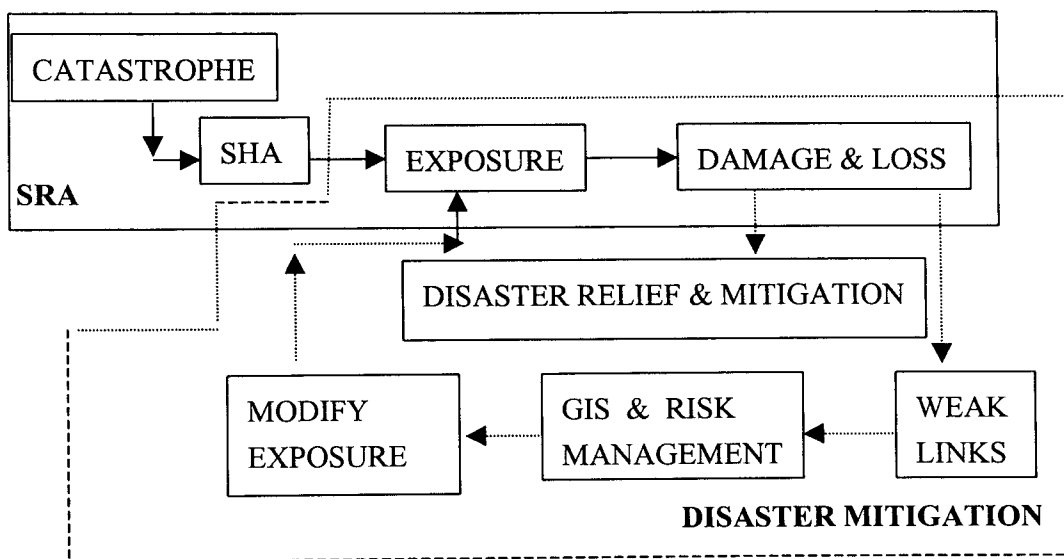


Fig. 1.1: General framework of seismic assessment and disaster mitigation.

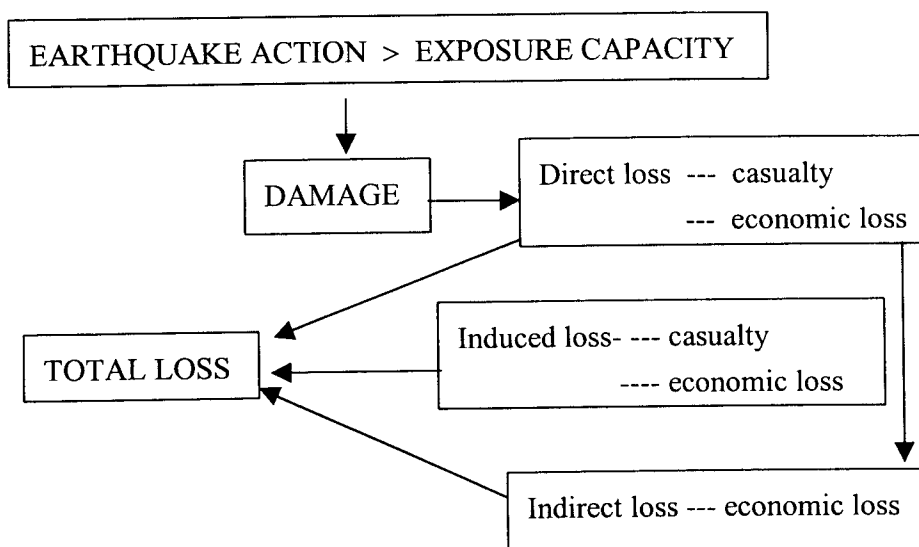


Fig. 1.2: Relationship between earthquake damages and losses.

Generally speaking, damage-related problems are of cause-effect nature. When some action (earthquake ground motion or an enemy) acts on an exposure (a building or a person), the effect of the exposure will be intact if the strength of the exposure is stronger than the action, or damaged if the strength is less than the action. The damage causes may be classified into two: the external cause is the strength or intensity of the action and the internal cause is the weakness of the strength or the resistance of the subject. Damage occurs if the intensity of the external action is greater than the resistance of the internal capacity, as defined in Fig. 1.2.

The flow chart given by Whitman et al. (1997) for a FEMA project [RMS, 1997] in the United States is shown in Fig. 1.3. It is quite similar to Fig. 1.2.

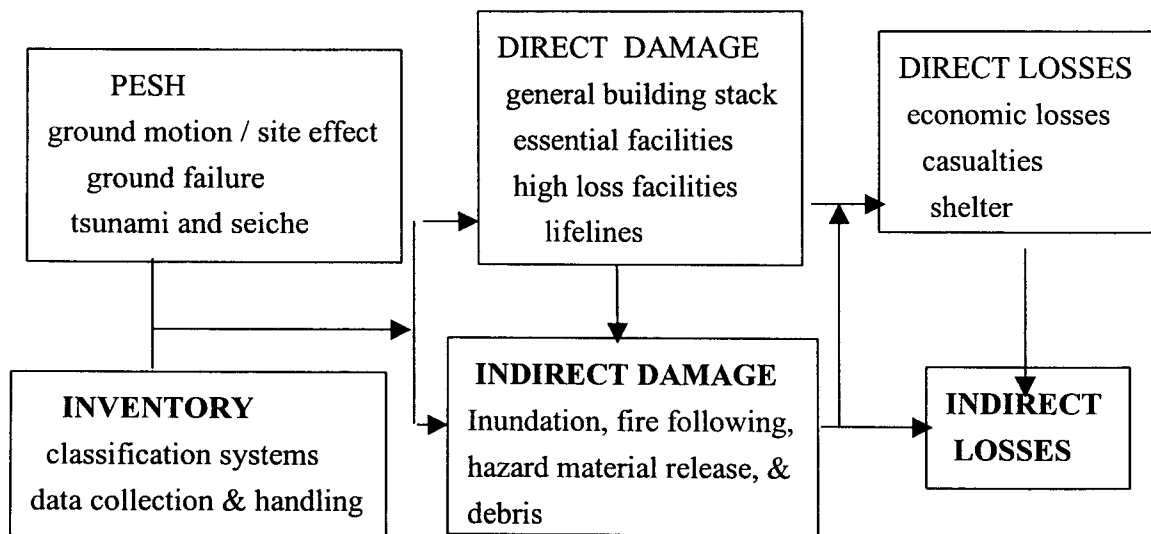


Fig. 1.3: Components of the earthquake loss estimation methodology.

It is clear how damage is related to losses (direct, induced and indirect, casualty and economic), and how losses are related to mitigation measures before, during and after a strong earthquake will be decided on the basis of the damage and loss evaluation made before or after the earthquake as shown in Figs. 1.1 – 1.3. The induced loss includes those losses from fire following, inundation, hazard-material release; and indirect loss includes those from loss of labour, business interruption and capital investment.

The whole process of seismic risk management is usually now carried out through a geographic information system (GIS) (ESRC et al., 1997; Shakhramanjan, 1998). This new technique provides a quick means to provide the following features important in practical application: (1) a dynamic or updated modification of the data bank of the exposure in big cities, (2) an easy modification of the damage and loss assessment for various possible scenario earthquakes, (3) a quick retrieval of the condition of any single item of exposure during an earthquake and the losses induced from its damage, and also (4) a quick visual display of formation of the disaster and the effects of a suggested disaster mitigation decision.

1.3 Technical terms

To make things clear, some technical terms used in this note are defined as follows.

DISASTER ----- damage and loss caused by the natural phenomenon, or the earthquake, but not the natural phenomenon itself.

HAZARD ----- the natural phenomenon, or the earthquake itself, but not the damage nor loss (Hu, Liu, Dong, 1996; EERI Comm. on Seismic Risk, 1987; Coburn and Spence, 1992).

HAZARD ACTION ----- the action, such as the earthquake ground motion due to the hazard. In engineering field, the term “action” is used for various kinds of load, such as snow load, wind load, dead load (weight of the structure), traffic load from trains and automobiles, etc.; but in seismic design field, the term “load” was replaced a few decades ago by the term “action” because it was realised that the parameters considered in seismic design are not force but ground motion. And for those responses of internal forces and deformation in the structure by the earthquake ground motion, the term “effect” is used.

HAZARD ACTION PARAMETER, Y ----- parameters of the hazard action, such as acceleration, effective or peak, velocity or response spectrum, is the specific physical quantity used in the seismic design or damage assessment. Although macroseismic intensity is now not commonly used in seismic design code, but it is in risk damage or assessment of earthquakes almost in the whole world.

HAZARD ACTION INTENSITY ----- the strength or level of the hazard action parameter.

CATASTROPHE ----- the occurrence of the natural hazard, including the magnitude and location of the earthquake.

SCENARIO CATASTROPHE ----- considered typical catastrophe.

EXPOSURE ----- any thing that is exposed to the damage of the earthquake. It includes buildings and other man-made structures, lifeline systems (pipelines, transportation, commercial, communication, and management), infrastructures, natural resources.

FUNCTION OF EXPOSURE ----- each item of the exposure serves the mankind or the society by its functions in the society.

DAMAGE ----- various levels of loss of function of the exposure. For a building, it may range from slight or repairable damage to complete collapse.

DAMAGE STATE, D ----- simplified classification of damage level, ranging from intact, slight, moderate, heavy, partial collapse and up to complete collapse.

CAPACITY or RESISTANCE ----- capacity or resistance of the item of the exposure against earthquake action.

VULNERABILITY ----- usually a matrix of probability $P[D|Y]$, which gives the probability of one item of the exposure of being in a damage state D when subject to an earthquake action Y.

LOSS ----- direct, induced and indirect losses, including casualty and economic losses. Other kind of losses, such as political loss, may be included, but it is not easy to evaluate.

RISK ----- commonly used as a probabilistic measure of the expected damage and loss.

SHA ----- seismic hazard assessment, commonly used as a probabilistic measure of the seismic hazard at a given site or region.

SRA ----- seismic risk assessment, commonly used as a probabilistic measure of the seismic risk of a city of a region.

2. VULNERABILITY ASSESSMENT

2.1 Exposure

The term “exposure” is used to include all items, which are important to human beings or the society. It includes most importantly the engineering works, such as houses, factories, hydraulic works, lifeline systems and infrastructures. Lifeline system is usually defined as those inter-connected networks, which are needed most strongly during and after a strong earthquake to limit the losses to a minimum. One lifeline system or network consists of many links and nodes, such as underground pipelines for water supply and sewerage in a city, and other kind of lifelines for energy supply, highway, railway, waterway and airline systems for transportation, and also information-transfer networks which have only stations as nodes. The term “infra-structure” is popularly used in this decade to mean those fundamental systems important to a large city or society, which include also lifeline systems and may also include other kinds of economic, political and management networks, especially those related to disaster relief and safety insurance.

In addition to engineering works, exposure includes also natural resources, such as fields, farms, rivers and slopes. Their damage induces also losses to a society. Foundation may be considered as part of an engineering work.

2.2 Inventory of exposure (ATC-13, 1985; ATC-21, 1988; ATC-21-1, 1988; Yin, 1996)

2.2.1 Specific need of exposure for SRA

For the need of the GIS-based SRA, there should be a map of the region on which all details of the exposure should be indicated and this map including all of its details should be stored in the GIS-based computer and later be analysed there. With the geographic coordinates of latitude and longitude all data are stored in the computer in "layers". There are in general the following layers. (1) Sectional boundaries of the region and its subdivisions or blocks. These Census blocks may be city and town or ZIP codes, within which exposures of engineering works and population may be grouped. (2) Geologic and geographic data, including active faults and tectonic movement, topography, site soil deposits, and soil properties together with boring data and dynamic properties. (3) Seismological data, including historical earthquakes and their intensity distributions, potential source zones together with their seismicity descriptions, and results from seismic zonation, micro-zonation and seismic hazard evaluation of engineering sites. (4) Strong motion observation data. (5) Exposure data, including all details of each item of each category of the inventory, as described in Sect.2.1 and Sect.2.2.2, related with its location, retrieval, damage and losses induced. One layer is used in the GIS for each category of the exposure. Items of exposure in a region or city should be classified into categories, according to their use or occupancy and also their structural systems so that their vulnerability matrices and thus damage and loss possibilities can be estimated accordingly. There should be at least three levels of exposure classification as follows. The first level for a very general classification of exposure may be engineering work, natural environment, and society organisation. Under each of the first level class, the second level, taking the engineering work as an example, may be residential building, commercial building, industrial building, agricultural building, facility, bridge, dam, harbour, tunnel, pipeline, road, tower, etc. Under each of the second level, taking residential building as an example, the third level may be adobe, plain masonry, reinforced masonry, masonry with frames, timber frame, reinforced concrete frame, reinforced concrete shear wall, shear wall with ductile bending frames, steel bending frame, steel frame with diagonal bracing. Of course, under the third level, a fourth level may be considered, for example, single story, multi-story, or high-rise buildings; precasted or cast-in-place concrete; regular or irregular in plan and elevation. The lowest level is termed as category here.

The principle of classification of the exposure is to facilitate the evaluation of the vulnerability. Those items of the exposure of same or similar vulnerability should be classified in one group. In classification, the following facts should be noted. (1) Only those items in the considered region will be classified. Some special items particular in the region may be added and very popular items in the region may be classified further in detail. (2) The functioning of the items should be considered, because the vulnerability and damage are defined on the basis of loss of functions.

The exposure may be classified according to two different principles, one for the social function of the item and another for the engineering function. The social function is related closely with the economic and societal losses and the engineering requirement with the damage and vulnerability evaluation. The first and second levels of classification given at the beginning of this section are classifications of the social functions and the third level there is a classification of the engineering function. Example may be found from ATC-13 (1985). Under the category of “structure”, there are the following two classifications.

(1) For the social function classification --- Important for indirect economic loss

- Residential buildings
- Commercial buildings
- Industrial buildings
- Critical facilities
- Lifeline facilities

(2) Under the engineering function classification (important for structural damage estimate), the following engineering characteristics should be considered

- Location and street address
- Material and construction type
- Soil foundation
- Structural foundation
- Height or number of stories, configuration and structural continuity
- Structural framing
- Design and construction quality
- Construction date
- Design standard
- Proximity to other structures

(3) Special attentions should be given to those structures of very low earthquake-resistant strength in the developing regions. This category of buildings is usually made of mud, adobe, or irregular pieces of stones or gravel, depending on the materials available in local regions. It is well known that buildings made of these kinds of materials are not earthquake-resistant, but it is inevitable because of economic reasons.

2.2.2 Collection of inventory data

Inventory required for damage-loss assessment be a detailed, classified and itemised list of all data related to the vulnerability or earthquake-resistance of each item of the exposure in a region. It may be obtained from various sources, such as city government, County Tax Assessor's Office, post office, and insurance office. It may be easy to obtain the required details of one item of one category in the inventory, but for the ordinary structures such as residential buildings and underground pipelines it is difficult to obtain a complete and accurate set of data. It is important then for each city under study to collect first all available data from city government and other offices, and then to complete the data by field investigation under the help of the related local offices.

2.3 Seismic vulnerability matrix (Whitman et al., 1997; ATC-13, 1985)

2.3.1 Damage of each item of the exposure

Damage means the loss of some function of the item and any item of the exposure has a certain function in the society. The function of a residential building is to house a group of persons. A network of underground water supply pipeline is to supply clean water to the people in the society.

Damage or loss of function is usually classified in to several grades or states, such as intact, slight, moderate, heavy and total. For buildings, the following classification has been popularly used.

Intact --- no damage

Slight damage --- only the non-structural members damaged

Moderate damage --- repairable damage of some structural members and the building may be used after adequate repairing

Heavy damage --- non-repairable damage of the structural members but no collapse of the main structure

Total damage --- collapse of the main frames supporting the whole structure

2.3.2 Definition of vulnerability matrix for building

Vulnerability matrix $P[D|Y]$ is defined as a matrix of probability P of being in a damage state D of some item of the exposure when subject to an earthquake action of Y where Y may be earthquake intensity I or peak ground motion acceleration A . Table 2.1 is an example suggested by R. Whitman (Whitman, 1997) and given in ACT-13 (1985).

Table 2.1: A sample for vulnerability matrix for building

Damage State	DF		Damage probability (%) for given intensity I						
	range	mean	VI	VII	VIII	IX	X	XI	XII
None	0	0	95	49	30	14	3	1	0.4
Slight	0-1	0.5	3	38	40	30	10	3	0.6
Light	1-10	5	1.5	8	18	24	30	10	1
Moderate	10-30	20	0.4	2	8	16	26	30	3
Heavy	30-60	45	0.1	1.5	3	10	18	30	18
Serious	60-100	80	--	1	2	4	10	18	39
Collapse	100	100	--	0.5	1	2	3	8	38

In this table, the damage factor (DF) and its mean (MDF) are defined as

$$DF = \text{damage factor} = \text{dollar loss} / \text{replacement value}$$

$$MDF = (1/n) \Sigma (DF)$$

and the summation Σ is taken over the total number n of the structure in the sample.

2.3.3 Methods of vulnerability matrix assessment (ATC-13, 1985)

The methods of vulnerability matrix assessment can be classified into two categories, the empirical and the analytical. The empirical method is based entirely on damage data of similar structures from past strong earthquakes and the analytical one is based on both the damage data and the analytical assessment of the earthquake-resistant capacity of the structure. The following sections will be dedicated to their explanation, together with some examples.

2.3.3.1 The empirical method (Kircher et al., 1997; Yin, 1995, 1996; Coburn and Spence, 1992)

The oldest and the most commonly applied method is the empirical method, which derives the vulnerability matrix from past earthquake damage data by regression analysis and the results are those similar to Table 2.1. In this method, the earthquake action is always macro-seismic intensity I. Firstly, enough damage data of each category of structure should be collected from past earthquakes to cover the whole range of possible damage states from intact to complete collapse. Because of the large uncertainties involved in the level of earthquake resistant capacity of the same category and the details of earthquake action or intensity, the damage state of each item of the same structural category usually varies for the same intensity. The damage matrix is then a full matrix as shown in Tables 2.1 and 2.8. If there is no uncertainty considered, the relation between damage state D and intensity I will be definite, and the

damage matrix will have only diagonal terms with all the non-diagonal terms being zero, as given in Tables 2.2 – 2.7 and 2.10 (Li, 1995; ATC-13, 1985; Yin, 1995, 1996).

Table 2.2: Vulnerability matrices of transportation system components mean damage ratios (%)

Intensity NMI	Bridges	Major roadways	Railway tracks	Runways/ terminal	Ports
VI	<1	0	0	2	0
VII	3	0	0	6	1
VIII	10	<1	<1	11	4
IX	27	6	11	22	18
X	56	19	29	44	45

Table 2.3: Mean damage ratios (%) of vulnerability of utility system components

Intensity MMI	Generation Plants	High Volt. Substations	Refineries/ Tank Farms	Oil Pipelines	Processing Plants	Gas Pipelines	Treatment Plants
VI	1	<1	<1	0	1	0	<1
VII	6	4	4	0	6	0	2
VIII	16	17	14	17	18	17	10
IX	37	48	35	77	38	77	30
X	72	81	66	97	62	97	60

Table 2.4: Vulnerability matrices (in %) of adobe houses obtained from the Xingtai Earthquake in 1966

Intensity	Collapse	Heavy	Moderate	Slight	Almost Intact	Total no. buildings
IX	79.2	13.4	5.1	1.5	0.7	4251
VIII	29.4	44.6	24.8	2.0	1.0	18742

Table 2.5: Vulnerability matrices (in %) of adobe houses obtained from the Xingtai Earthquake in 1966

Intensity	Collapse	Heavy	Moderate	Slight	Almost Intact	Total no. buildings
IX	79.2	13.4	5.1	1.5	0.7	4251
VIII	29.4	44.6	24.8	2.0	1.0	18742

Table 2.6: Vulnerability matrices (in %) of adobe houses obtained from the Tangshan Earthquake in 1976 (Liu, 1985)

Intensity	Collapse	Heavy	Moderate	Slight	Almost Intact	Total no. buildings
IX	100.0	0	0	0	0	36
VIII	23.0	11.2	57.1	8.7	0	617

Table 2.7: Vulnerability matrices (in %) of adobe cave houses for intensity VII obtained from the Xiji Earthquake in 1966

Type of cave	Collapse	Heavy--Moderate	Slight	Almost Intact	Total no. caves
Loess cave	43	14	13	30	45
Arch cave	64	24	3	9	259

Table 2.8: Vulnerability matrices (in %) of adobe cave houses obtained from the Datong-Yanggao Earthquake in 1989

Intensity	Collapse	Heavy	Moderate	Slight	Almost Intact	Total no. buildings
VIII	80.8	17.0	3.0	0	0	100
VII	31.6	40.6	13.9	11.9	2.0	200
VI	3.0	24.2	32.3	27.3	13.1	400
V	2.0	11.1	15.2	24.2	47.5	1800

Vulnerability matrices for some types of these low-quality buildings and structures popularly used in some developing regions in China have been estimated from past earthquakes and are given in Tables 2.4 – 2.10. Data in these tables show that there are very large uncertainties in the results, especially when the samples are not large enough, such as that for intensity IX in Table 2.6 and those in Tables 2.9 and 2.10 for the same type of smokestacks.

Table 2.9: Vulnerability matrices (in %) of the isolated unreinforced brick smokestacks obtained from the Haicheng Earthquake in 1975

Intensity	Collapse	Heavy	Moderate	Slight	Almost Intact	Total no. Smokestacks
IX	48.2	23.5	9.4	10.6	8.2	85
VIII	42.0	30.0	10.0	16.0	2.0	50
VII	15.5	14.4	9.3	21.6	39.1	97

Table 2.10: Vulnerability matrices (in %) of the isolated unreinforced brick smokestacks obtained from the Tangshan Earthquake in 1976 (Liu,1987)

Intensity	Collapse	Heavy	Moderate	Slight	Almost Intact	Total no. Smokestacks
XI	100	0	0	0	0	18
X	83.5	12.4	5.1	0	0	137
IX	87.9	6.1	3.0	3.0	0	33
VIII	53.3	17.8	11.1	17.8	0	45
VII	18.8	24.8	9.0	4.0	41.6	101
VI	0.3	1.8	4.8		93.1	6000

This method can be applied only to common old-type buildings, of which there are enough past earthquake damage data. When data are not enough, estimates of mean damage ratios may be used on the basis of expert opinion or capacity analysis, which can be used for engineering structures with no past damage data. The expert opinion approach has been used for the California cases in ATC-13 report, and the capacity analysis approach has been recently suggested in 1997 in HAZUS97. Table 2.2 gives the vulnerability matrices of transportation systems and Table 2.3 for utility systems, both from HAZUS97 (RMS, 1997).

Table 2.11 gives the vulnerability matrices of building, bridge and dam for California, given in ATC-13 (1985), where the damage factor is another way of specifying the damage state D (Rojahn et al., 1986).

Table 2.11: Damage probability (in %) matrices on expert opinion
(ATC-13, 1985)

Central Damage factor	Modified Mercalli Intensity						
	VI	VII	VIII	IX	X	XI	XII
Conventional Continuous-Span Bridges (Less than 500-ft span)							
0	93.6	8.1	0.9	***	***	***	***
0.5	6.4	77.8	17.6	***	***	***	***
5	***	14.1	78.6	56.	***	***	***
20	***	***	2.9	43.5	1.8	1.2	0.7
45	***	***	***	***	98.2	36.8	5.7
80	***	***	***	***	***	61.9	39.1
100	***	***	***	***	***	0.1	54.5
Earthfill and Rockfill Dams							
0	50.9	***	***	***	***	***	***
0.5	49.1	86.6	20.0	1.1	***	***	***
5	***	13.4	80.0	88.9	62.5	7.8	***
20	***	***	***	10.0	37.5	71.1	21.4
45	***	***	***	***	***	21.1	74.1
80	***	***	***	***	***	***	4.5
100	***	***	***	***	***	***	***

*** Very small probability

2.3.3.2 The analytical method --- The single parameter approach (Yin, 1995, 1996)

There are currently two kinds of analytical methods, the single parameter approach of earthquake action and the earthquake spectrum approach, which will be illustrated in the following paragraphs.

The Chinese approach (Yin,1996) will be given in the following as an example of this kind.

(1) In the first step in this approach, the earthquake resistant capacity is evaluated. For example of un-reinforced masonry building, the earthquake resistant capacity R may be

$$R = \alpha [\sum F_k / (2A_s)] R_\tau (1+C_i) \quad (2.1)$$

where

- F_k --- the cross-sectional area of the k-th wall on the s-th floor;
- Σ --- over all walls on the m-th floor;
- A_s --- the constructional area of the s-th floor of the building;
- C_i --- a reduction factor to consider the quality of the building, varying from -0.2 to $+0.3$;
- R_τ --- the shearing strength of the walls on the s-th floor and may be given approximately by the following formula

$$R_\tau = 0.14 (n-m+1) + 0.014 R_m + 0.5 \quad (2.2)$$

where R_m is the mortar strength;

α --- the factor of the earthquake shear on the s-th floor as given below

$$\alpha = (2n+1) / (3\sum i) \quad (2.3)$$

where the summation is from the s-th floor to the top of the building.

(2) The second step of this approach is to evaluate the relation between the capacity R or the ductility factor μ ($\mu = \text{max. story drift to elastic-limit story drift}$) and the damage state D on the basis of damage data of the considered kind of building from the past earthquakes.

From the damage data of several thousand buildings of various damage states, these relations among the building shearing force capacity R or the ductility factor μ , the damage state D , and the earthquake intensity I were obtained as shown in Figs. 2.1 and 2.2 (Yin et al., 1990; Yin, 1996). The uncertainty of these relations may be considered as normal distribution. Similar results have been obtained for ductility factor μ of the weakest story of R.C. buildings as shown in Table 2.5.

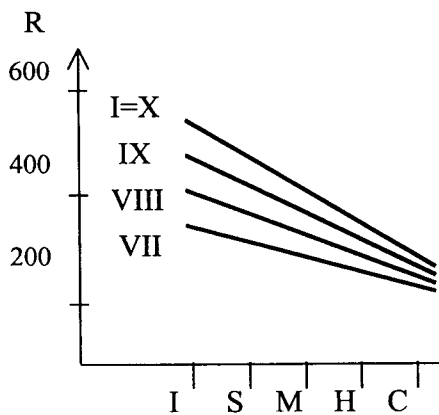


Fig. 2.1: Masonry Building
(D = I---intact S—slight M—moderate H—heavy C—complete collapse)

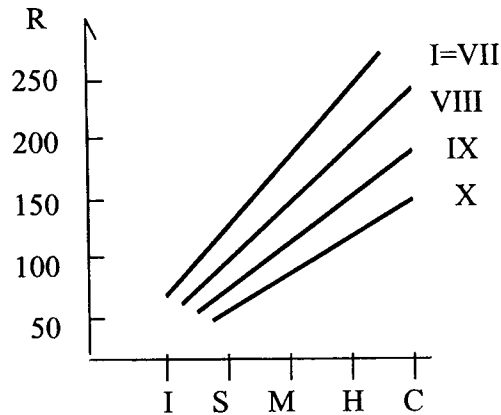


Fig. 2.2: Single-story factory with R.C. Columns
(D = I---intact S—slight M—moderate H—heavy C—complete collapse)

Table 2.12: Relation between damage state D and mean ductility factor μ for R.C. buildings

μ \ D	intact	slight	moderate	heavy	complete collapse
building					
Framed bldg	< 1	2	4.5	8	> 10
Shear-wall bldg	< 1	1.3	2.5	4	> 4

2.3.3.3 The analytical method --- The spectral approach (Mahaney et al.,1993; Calvi,1998)

An analytical method is developed in the late 90's and later applied as a basic method of vulnerability matrix assessment in HAZUS97 (RMS,1997). This method considers the response spectrum as the earthquake action and develops the structural earthquake resistance or capacity from the analytical or experimental pushover curves in terms of force and displacement as shown in Fig. 2.3.

In Fig. 2.3, the ordinate A represents force applied on the structure. For earthquake action, A may be obtained from the design acceleration spectrum, or the demand curve; and the period T of the spectrum is transformed into a displacement D from the following relationship between the acceleration response spectrum $S_a(T)$ and the displacement response spectrum

$$S_d(T) = (T/(2\pi))^2 S_a(T) \quad (2.4)$$

The characteristic points of the capacity curve have some physical meaning. The point Y(A_y , D_y) is the end of elastic behaviour or the starting point of initial yield, beyond which the structure works in partial yield condition until the complete yield point U(A_u , D_u) is reached.

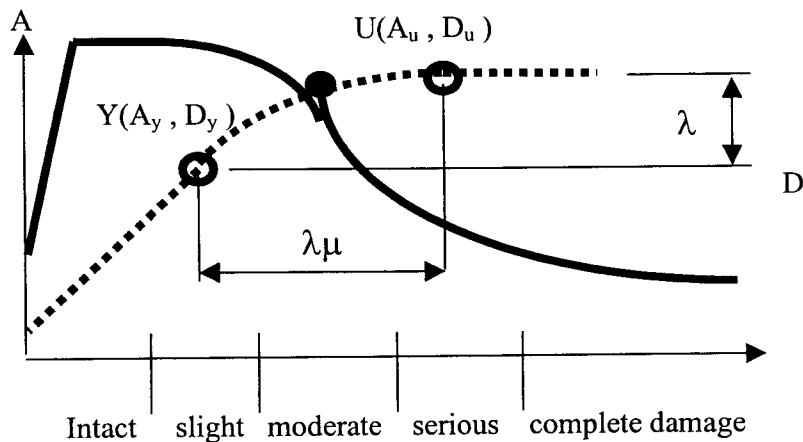


Fig. 2.3: Analytical damage assessment

..... Building capacity curve — Demand spectrum

Between these two points, the structure behaves with partial restraint. After the complete yield, the structure becomes like a mechanism, i.e., yields with no restraint. The damage state or grade D is defined by the capacity curve. When the demand A is much less than the elastic limit A_y of the capacity curve, or when the displacement demand D is much less than the elastic limit D_y of the capacity curve, the structure is considered to be intact or with no damage. When the demand is well above the corresponding ultimate value of the capacity, the structure is considered completely damaged or collapsed. For the case shown in the figure, the damage is moderate. Table 2.13 shows an example used to define structural damage states by Kircher et al. (1997) based on the values of the inter-story drift ratio for several common building types of different design standards.

There are several ways of using and defining the damage state D . The way showing in Fig. 2.3 may be used to estimate the possible damage in terms of the response of a structure in future earthquakes through analysis. Another way suggested by ATC-13 (1985) suggests defining the damage states in terms of the percentage of the replacement cost, which may be used to estimate the direct economic loss. A third way is that used in some Intensity Scales, such as the European Macroseismic Scale (EMS) or the up-dated MSK Scale in 1992, which assigns the intensity to a site in terms of the damage after an earthquake according to the damage matrix observed at the site. Different definition has its own way of application; but attention has to be paid is that any such definition related to qualitative terms as moderate damage, serious damage, and repair needed, is by nature a fuzzy term, which must be dealt with care when quantified to a certain number.

In Table 2.13, under the building type, the first part W1 means wood frame, S1 steel moment frame, C2 concrete shear walls, and URM unreinforced masonry bearing walls; the last part L, M or H means low-, mid- or high-rise.

Table 2.13 Typical drift ratios to define structural damage states

design level	building type	drift ratio at the threshold of structural damage			
		slight	moderate	extensive	complete
high code	W1	0.004	0.012	0.040	0.100
	S1L	0.006	0.012	0.030	0.080
	S1M	0.004	0.008	0.020	0.053
	S1H	0.003	0.006	0.015	0.040
	C2L	0.004	0.010	0.030	0.080
moderate code	W1	0.004	0.010	0.031	0.075
	S1L	0.006	0.010	0.024	0.060
	C2L	0.004	0.008	0.023	0.060
low code	W1	0.004	0.010	0.031	0.075
	S1L	0.006	0.010	0.020	0.050
pre-code	C2L	0.004	0.008	0.020	0.050
	URML	0.003	0.006	0.015	0.035
	W1	0.003	0.008	0.025	0.060
	S1L	0.005	0.008	0.016	0.040
	C2L	0.003	0.006	0.016	0.040
	URML	0.002	0.005	0.012	0.028

Figs. 2.1-2.2 gives an example of vulnerability curves of two common building types in a way somewhat different from the vulnerability matrix. The differences are (1) continuously varying peak ground acceleration PGA is used for earthquake action instead of discrete intensity I and (2) probability of exceedance is used in this figure instead of probability of occurrence.

Fig. 2.4 gives an example of vulnerability curves of two common building types in a way somewhat different from the vulnerability matrix. The differences are: (1) continuously varying peak ground acceleration PGA is used for earthquake action instead of the discrete intensity I and (2) probability of exceedance is used in this figure instead of the probability of occurrence.

This method has been used mostly for modern structures with few earthquake damage data.

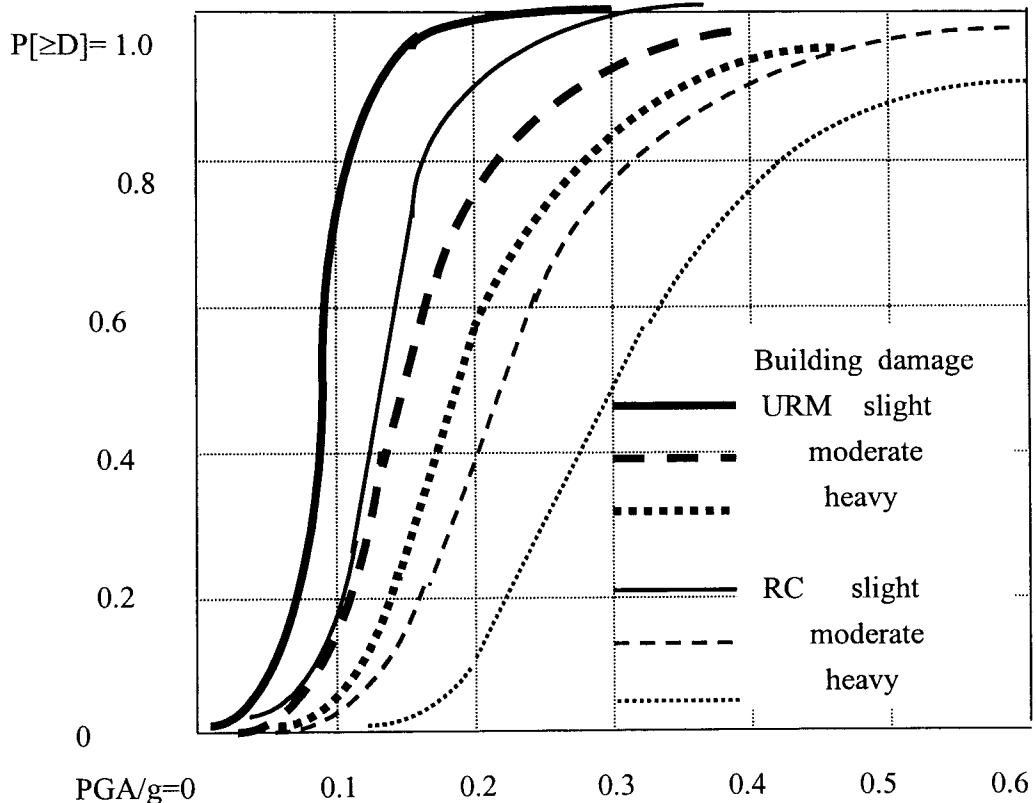


Fig.2.4: Samples of vulnerability curves for some common buildings

2.3.4 The Urumqi case

In the case of Urumqi City, the Chinese method suggested by Professor Z.Q.Yin (1996) is followed. Roughly 8000 buildings were inspected building by building by the local technicians, with the assistants from research engineers. Vulnerability matrices were given, district by district (part of the city), for different categories of ordinary engineering structures and building by building for important structures. Tables 2.14 –2.15 are examples for District N for various categories of engineering structures (ESRC et al.,1997; Yang, Du, Li, 1999).

It is important to realise that the vulnerability matrix may be different for different districts in one city, for different sub-districts in one district, and even different for different buildings of the same category in one sub-district. Table 2.15 gives the vulnerability matrix of unreinforced multi-story masonry buildings of a sub-district in the District N. For the case of Urumqi City, where individual building inspection has been carried out, the damage state of

Table 2.14: Vulnerability matrices, in %, of engineering structures
in district N (ESRC,1997)

Damage State D	I	S	M	H	C
Intensity I					
(1) Multi-story masonry building					
VI	92.22	7.78	0	0	0
VII	90.00	4.44	5.56	0	0
VIII	48.89	32.22	13.33	5.56	0
IX	18.89	28.89	22.22	24.44	5.56
X	2.22	8.89	13.33	43.33	32.23
(2) Single-story factory					
VI	69.57	30.43	0	0	0
VII	28.17	40.85	22.74	8.24	0
VIII	3.44	24.73	46.38	17.75	7.70
IX	0	12.41	29.98	37.68	19.93
X	0	0.45	11.96	28.17	59.42
(3) Multi-story R.C. building					
VI	100	0	0	0	0
VII	85.62	14.38	0	0	0
VIII	36.60	44.44	13.73	5.23	0
IX	7.19	29.41	35.95	22.22	5.23
X	0	7.19	12.42	43.14	37.25
(4) Inner-frame(R.C.)					
VI	72.22	27.78	0	0	0
VII	47.22	36.11	16.67	0	0
VIII	11.11	36.11	36.11	0	0
IX	5.56	6.94	29.17	48.61	9.72
X	0	2.78	5.55	43.06	48.61

(to be continued)

Table 2.14: Vulnerability matrices of engineering structures in district N (continued).

Damage State D	I	S	M	H	C
Intensity I					
(5) Single-story large-span building					
VI	77.91	22.09	0	0	0
VII	44.17	33.74	19.02	3.07	0
VIII	9.20	34.97	38.65	14.11	3.07
IX	0	22.86	44.17	23.31	11.67
X	0	1.84	19.02	41.10	38.04
(6) Smokestack					
VI	81.40	18.60	0	0	0
VII	43.04	38.37	16.28	2.33	0
VIII	12.79	30.23	38.37	18.61	0
IX	0	12.79	22.09	37.21	27.91
X	0	2.32	17.44	23.26	56.98
(7) Elevated water-tower					
VI	66.67	33.33	0	0	0
VII	27.27	39.40	33.33	0	0
VIII	6.06	21.21	39.40	33.33	0
IX	0	9.09	18.18	39.40	33.33
X	0	0	12.12	15.15	72.73

buildings of the same category in one sub-district may vary from intact to complete collapse. Comparing vulnerability matrices given for the same category of building in Table 2.15 and No.(1) of Table 2.14, one can see the difference here also. It is quite easy to accept such big difference, if one realise the big possible range of variation of quality of two buildings which are built even according to the same blue print but by different construction teams. Big scattering comes from differences in details, dimensions, quality of construction and maintenance, location and site conditions, and many others. No one will expect that students in one class in primary school, even of the same age, will be of the same health, same nature.

It is quite common that twin brothers may behave differently after a few years old.

Table 2.15: Vulnerability matrices of masonry building in a sub-district of district N.

Damage State D	I	S	M	H	C
Single-story large-span building					
Intensity I					
VI	80.65	16.13	3.22	0	0
VII	69.35	13.71	13.71	3.23	0
VIII	22.58	29.02	30.65	14.52	3.23
IX	11.29	10.48	12.91	45.97	19.35
X	0.81	3.23	7.26	20.97	67.73

In the Urumqi case, both individual sampling and district sampling have been compared with average case. Table 2.16 gives the results of building-by-building sampling (total number of building for this sub-district is 354) and sub-district sampling (total number of building is 45) of multi-story R.C. buildings (Yang, Du, Li, 1999). From them, together with that of No.(3) of Table 2.14 for the whole district N, it can be seen that the values are somewhat different, but are comparable.

Table 2.16: Comparison of results from different samples.

Damage State D	I	S	M	H	C
Intensity I					
(3) Multi-story R.C. building (from Table 2.14)					
VI	100	0	0	0	0
VII	85.62	14.38	0	0	0
VIII	36.60	44.44	13.73	5.23	0
IX	7.19	29.41	35.95	22.22	5.23
X	0	7.19	12.42	43.14	37.25
Individual sampling					
VI	100	0	0	0	0
VII	87.29	12.71	0	0	0
VIII	40.40	40.11	14.97	4.52	0
IX	5.56	34.75	34.18	20.90	4.52
X	0	5.65	16.38	45.48	32.49
Sub-district sampling					
VI	100	0	0	0	0
VII	93.33	6.67	0	0	0
VIII	40.00	44.45	13.33	2.22	0
IX	8.89	31.11	37.78	20.00	2.22
X	0	8.89	11.11	51.11	28.89

2.4 Consideration of site effects on damage

It is well known that site condition has a strong influence on structural damage in the following two aspects: the ground failure and the ground motion. I am glad to mention here that the Chinese code in 1964 was leading in the specifying in the code that the main effect of site condition on ground motion is the widening of the design spectrum for softer sites to the longer period side, as shown in Fig. 2.5 and Table 2.17. Both the Japanese code and the United State code made similar specifications about 10 years later. In the former China code in 1959, the site effect was considered by modifying the design intensity, which is transferred to design acceleration $k = a/g$ and the design acceleration k is used as a multiplier to the standard design spectrum $\beta(T)$, or $k\beta(T)$ (Hu, Liu, Dong, 1996).

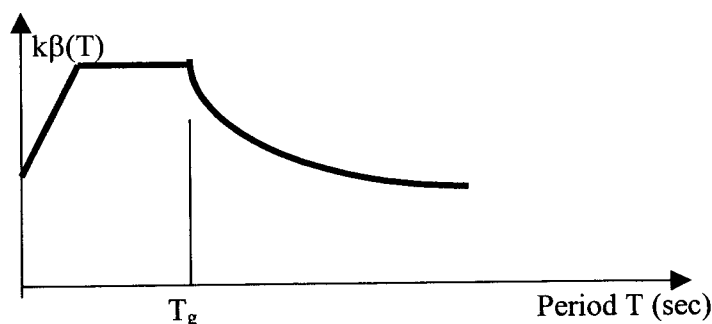


Fig. 2.5: Design spectrum in building code.

2.4.1 Site effect on intensity

Roughly before the seventies, the qualitative quantity of intensity was almost the only earthquake action used to evaluate the damage, and thus the vulnerability. In this case the two effects of site condition, i.e. the effect on ground motion and the effect on ground failure, were integrated in one with no need of their distinction. It is very simple, but rough. The site effect is then to increase the intensity on soft sites and decrease on rock sites, compared with the stiff soil sites. In the 1959 China seismic design code, following the former Soviet Union codes, the increase or decrease is one intensity grade in a 12 grade intensity scale, and one grade difference means a difference of a factor 2 in design values over the whole design spectrum $k\beta(T)$. If compared with the difference of the site effect on ground motion in the later codes as shown in Table 2.16, the codes before 1964 did not consider the difference of site effect on long or short periods of the spectrum.

In general, intensity estimation is made on some given intensity attenuation curves, which are derived from past earthquake intensity data. Those intensity data are usually given in a form of isoseismals of past earthquakes, with sometimes several intensity-abnormal regions, and nothing is mentioned about the site conditions of each intensity rating spot, usually a town, a

Table 2.17: Site dependant design spectra in China building codes (IAEE,1996).

Site	Description of site	Bearing power (T/m^2)	Predominant period (sec)	Tg (sec)
The 1964 China code				
I	Stable rock	> 40	< 0.2	0.2
II	Ordinary soil	15 – 40	0.15 – 0.50	0.3
III	Soft soil	8 – 15	0.35 – 0.70	0.5
IV	Very soft soil	< 8	> 0.60	0.7
The 1981 Japan code				
1	bedrock, tertiary			0.4
2	diluvium			0.6
3	alluvium			0.8
4	fill; thick alluvium			---
The 1976 ATC 3-06 code and the 1991 UBC in USA				
1	rock and stiff soils			0.40
2	deep cohesionless or stiff clay soils			0.57
3	soft to medium clays and sands			0.90
The current China building code (1989)				
			Tg (sec) near earthquake	Tg (sec) far
earthquake				
1	hard		0.20	0.25
2	moderately hard		0.30	0.40
3	moderately soft		0.40	0.55
4	soft		0.65	0.85

village or a part of a city. Judging from the geographical condition of the region, a general idea may be obtained of the overall background of the shaken area, such as a diluvium or alluvium plain, or a mountainous region. For the general intensity attenuation relationship, such abnormal intensity regions are usually ignored and many of the abnormal are due to very stiff or very soft sites. If there are local intensity attenuation relations can be used, it may contain the overall site conditions there, and modifications of intensity may only be considered for special sites, especially soft and especially stiff in the region. If intensity

attenuation relations of other regions are used, it is better to find out if there is any difference in general geographical background also.

2.4.2 Site effect on ground motion and ground failure

In case a refined SRA is required, two effects of site effect should be considered. In big cities where boring data can be collected, ground failure vulnerability of slopes and grounds of weak soil deposit underneath can be estimated on the basis of past experience. Particular attention should be given to sites with liquefiable sand layers within 15 meters from surface or highly compressive layers of very soft muddy clay.

Based on the collection of boring data of the region, the site effect on ground motion can also be evaluated. The following conclusions were verified both by empirical data from past strong earthquakes and by theoretical studies.

- (1) Ground motion at a site should be expressed in spectrum, not only by peak acceleration.

The softer the site, the larger is the long period ground motion, which is usually shown in ground motion velocity and displacement but not the acceleration. The design spectra given in codes (IAEE,1996) in Table 2.16 reveal this fact. It is important in many big cities in the world, such as Shanghai, Tianjin and Teipei in China and Mexico City and Tokyo in other countries, to consider these. Effects. The predominant ground period of these cities is close to 1 sec. In this case, where very tall buildings and other structures of long period are constructed more and more now days, the long period motion effect due to the double resonance from site ground motion and from the long-period structures may increase the damage. The Mexico City had such experience.

It is almost universally understood that the so-called soft site means that the soil is both soft and deep. A soft soil layer, if the depth is only a meter or two, its predominant period under weak motion may not be long and its effect on ground motion will be in the short period range, say 0.1 to 0.3 sec.

- (2) The soft soil site has a strong non-linear effect. Site amplification of short period motion may be very large, say 3 or 5 times, for weak motion of peak acceleration 0.05g or less, but may be decreased to 1, or even a reduction by a factor of 2, instead of amplification, for strong motion of peak acceleration 0.5g or larger. The soft site effect of long period motion is always amplified due to non-linearity of the soil material. It can be easily understood if the transfer idea is applied here for the soil layer.

In the frequency domain, the site spectrum $Y(i\omega)$ may be expressed as the product of the input or the bedrock spectrum $X(i\omega)$ and the transfer function $H(i\omega)$ of the site is then

$$Y(i\omega) = H(i\omega) X(i\omega) \quad (2.5)$$

where $i = (-1)^{1/2}$ and ω is the circular frequency. For a given input motion from the earthquake to the bedrock under the site, $X(i\omega)$ is constant. The site transfer function $H(i\omega)$ changes by

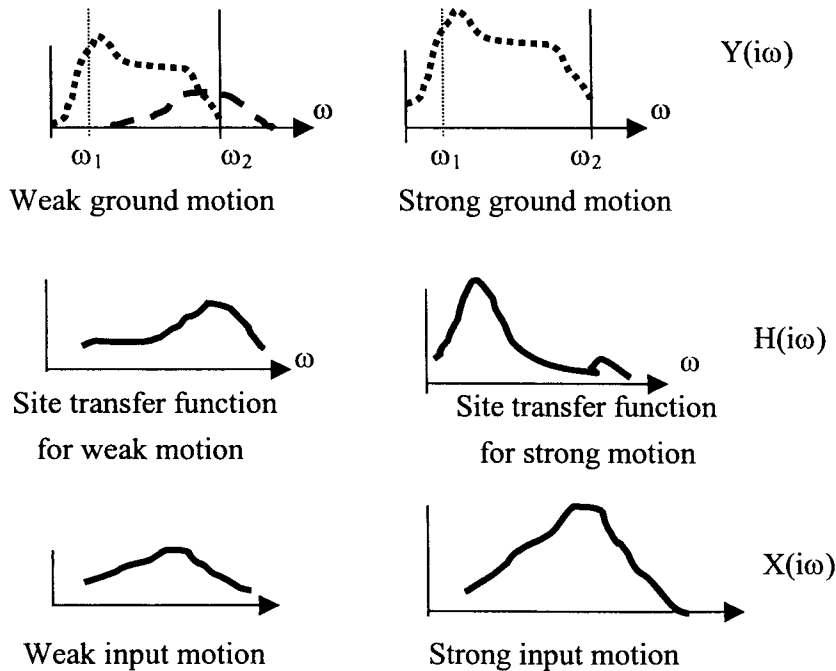


Fig. 2.6: Softening effect of site due to non-linearity of site soils.

to the bedrock under the site, $X(i\omega)$ is constant. The site transfer function $H(i\omega)$ changes by increasing the long period components and decreasing the short period ones, the result is then a corresponding change of the spectrum $Y(i\omega)$ of the site ground motion, as shown in Fig. 2.6, where the site spectrum for strong motion is shifted to the long period or the low frequency range. For a stiffer building of larger natural frequency ω_2 , the site ground motion for strong input may be amplified as much as that for weak input; but for a tall building of smaller natural frequency ω_1 , the site ground motion is always amplified more than the weak motion, because the transfer function increases at the lower frequency ω_1 . This situation may be stated briefly as follows: soft sites amplifies the longer period components motion, and non-linear effect of soil deposit helps the amplification of the longer period components (Hu, Liu, Dong, 1996).

(3) Liquefaction of a sandy soil layer will prevent the shear wave transmission and thus the horizontal motion of the ground above the liquefied layer may be reduced after liquefaction, though the chance of settlement of the ground increases.

3. SEISMIC RISK ASSESSMENT (SRA)

3.1 Damage-loss relations (Whitman et al., 1997; Kiremidjian, et al., 1998; Yin, 1999; Hu, 1998; Brookshire, 1997)

As mentioned in Fig. 1.2 of Section 1.4, Total loss includes direct loss, induced loss and indirect loss. And all kinds of losses are related directly or indirectly to damage or loss of functions of some item of the exposure. This chapter will start firstly from a brief discussion of the damage-loss relationship and then the losses themselves.

Damage and loss relations are usually expressed in terms of loss ratios and they are usually estimated from loss data collected from past earthquakes. These damage-loss relations are by nature, empiric. Gross loss ratios may also be obtained from reconstruction fees and relief funds. Table 3.1 shows a comparison of direct economic loss and relief and reconstruction fee of some strong earthquakes (Li, 1995).

Table 3.1: Direct economic loss and reconstruction-plus-relief (R+R) fee

Eqk date	Earthquake place	Direct economic loss	R+R fee	Note
1975.02	Haicheng, China	0.81 billion RMB	0.446	Tangshan city only
1976.07	Tangshan, China	~6	5.243	
1979.07	Liyang, China	0.195	0.137	
1964.03	Alaska, USA	0.311 billion, USD	0.414	San Fernando city only
1971.02	San Fernando, USA	0.50	0.556	

The extent of loss, or loss ratio ξ , is usually expressed in terms of a fraction of the full replacement cost W , not the original construction cost, of the item as shown in the following expression

$$\xi = \Delta W/W \text{ or } \Delta W = \xi W \quad (3.1)$$

There are enough damage data to derive the extent loss as a function of damage state D for ordinary buildings. Table 3.2 gives some typical samples of the direct loss ratios for several building types used popularly in China (Yin, 1995,1998, 1999; Li, 1995; EERC et al., 1997). Table 3.3 gives similar data used in USA (Kircher et al., 1997). These values are by nature only some rough average estimate; if applied to individual cases, the variance can be very large.

Table 3.2: Direct loss ratios (%) of buildings and contents used in China

Loss Ratio Structure	Damage				
	Intact	slight	moderate	heavy	collapse
R.C. bldg.	0	5 – 10	10 – 40	40 – 80	80 - 100
Masonry bldg.	0	5 – 10	10 – 40	40 – 70	70 - 100
Single story factory	0	4 – 8	8 – 35	35 – 70	70 - 100
Adobe	0	2 – 12	12 – 45	45 – 80	80 - 100
Content	0	0	0	20 – 40	40 - 95

Table 3.3: Direct economic loss (%)

Damage State D	Structural System	Non-structural (drift sensitive)	Non-structural (acceleration sensitive)	Contents
Slight	2	2	2	1
Moderate	10	10	10	5
Extensive	50	50	50	25
Complete	100	100	100	50

3.2 Loss assessment

Losses may be computed from Eq.1.1 given in Section 1.2

$$SRA = D \times [L(D) + IL(D)] \quad (1.1A)$$

$$D = SHA \times VUL \times EXP \quad (1.1B)$$

if all of the following quantities

$$D = [D_i] = [D_1, D_2, \dots, D_i, \dots, D_n] \quad (3.2a)$$

$$SHA = P[D|Y] = [P_{ij}] \quad (3.2b)$$

$$Y = [Y_j] = [Y_1, Y_2, \dots, Y_j, \dots, Y_m] \quad (3.2c)$$

$$L = L(D) = [L_1, L_2, L_3] \quad (3.2d)$$

$$IL = IL(D) [IL_1, IL_2, IL_3] \quad (3.2e)$$

$$SR = [SR_1, SR_2, SR_3] \quad (3.2f)$$

$$EXP = [[EXP_1, EXP_2, \dots, D_k, \dots, EXP_1] \quad (3.2g)$$

are known numerically.

The losses and seismic risk are usually considered as vectors of three elements as shown in the foregoing equations and there are number of death, heavy injury or homeless, and money loss. The damage D, as shown in examples given in Sect.2.3.2, may be a vector of 5 to 7 elements. For earthquake action Y, number of elements may be around 5, in case of intensity, they may be VI, VII, VIII, IX and X, because they are possible and may introduce damage and loss. For exposure EXP vector, its number of elements is equal to the number of classification of the exposure, which is usually very large.

3.3 Direct loss

Direct loss include the losses from the direct damage caused by the earthquake, such as the direct damage of items of the exposure due to earthquake shock, which includes engineering damage, slope slides, and ground liquefaction, etc. Death or injury from damage of a building or frightening of the shock and the economic loss of the direct damage are direct losses.

3.4 Induced loss

Induced losses are those losses from damage induced by the direct earthquake damage, such as fire ignition and spreading by the damage of gas or electricity system in a house damaged by the earthquake, inundation due to dam water release, death or injury due to hazardous materials release from a storage tank damaged by the earthquake, losses from tsunami, seiches and landslides induced by the earthquake. Induced loss is a part of the indirect loss and sometimes referred to as secondary loss. Probabilistic or rough average estimates may be made here on the basis of case studies from past earthquake experience. Chance of occurrence of induced loss is usually considered as proportional to the damage level and number of the structures. The number of casualty and injury are strongly dependent on many un-predictable conditions, such as the season and the hour of the day of the earthquake occurrence. The induced disasters of fires and hazardous material release are strongly related to the natural conditions of wet or dry and wind speed and direction for the fire ignition and spread or hazardous material release. Since all these conditions are unpredictable, it is common then to make only average or rough average assessments.

3.5 Indirect loss

Indirect loss, as shown in Figs. 1.2 and 1.3, includes two kinds of loss. One is the induced loss, such as fires, flood and hazardous material release after earthquake, which can also be considered as disaster by itself. The other one is the indirect loss, mainly a chain-action economic losses, such as the commercial effect of the close-up of one plant to the other and the reduction of production due to loss of labour and capital input. Indirect loss in highly developed commercial regions may be very high even for a moderate earthquake at a close distance. For example, it was reported that the economic loss of the 1989 Loma Prieta Earthquake of magnitude 7.1 reached 6 billion US dollars, and that of the 1994 North Ridge Earthquake of magnitude 6.7 reached 17 billions, but the casualty amounts only 60 to 70. It is quite possible that the indirect economic loss in a well-developed region from a strong earthquake may be as high as, or even more than the direct economic loss.

Table 3.4: Interruption of function caused by structural damage

% of structural damage D	0	10	25	75	100
outage period	0	1-2 days	2 wk – 3 mo	3 mo – 1 yr	up to 2 yr

3.6 Loss due to business interruption

It is possible to estimate the time of business interruption due to damage of a structure. The simplest way is to estimate the time needed to recover the entire function of the structure and a more complex but reasonable way is to consider the functional recovery function, which shows the percentage of recovery as a function of time. For this purpose, it is necessary first to estimate the time of business interruption or the outage as a function of damage state D. Table 3.4 shows such a table from ATC-13.

Indirect loss can be evaluated by following up the path of their formation sequence. For example, the damage (A) of one pipeline may cause the interruption (B) of gas supply of some days to the factories and homes inside a district, and this interruption may cause a reduction (C) of production of some products, etc. The sequence is then A to B to C. In some cases. This procedure is at least theoretically possible, and in some cases, it is indeed possible when there are enough data to evaluate some useful numerical averages. But in many cases, these numerical data are not complete or enough; even in some cases there are data, but different cases may provide quite different data, and we have to accept some rough average estimates. For example, number of death in a building completely or partially collapsed may vary by more than 10 times because there are some many chance factors involved.

Discussion of other indirect economic loss is also given in Sect.4.4.

3.7 Loss and risk

It is used here as defined by the United Nations Office of the Co-ordinator of Disaster Relief (UNDRO), Fournier d'Albe and EERI (1987) in the United States that earthquake risk refers to the expected losses to a given element at risk, over a specified future time period, which is a probabilistic assessment of loss. Because there are so many uncertainties involved in the process of loss assessment of future earthquakes, any single deterministic estimate will be considered good if it is within 50% error. In this case, one way of making an estimate is to give an estimate with a possible range; another way is to give a probabilistic estimation. The probabilistic way is perhaps more popularly used.

4. EARTHQUAKE LOSSES ESTIMATION

4.1 Losses (Whitman et al.,1997; Brookshire,1997; ESRC,1997)

Earthquake loss may be classified into direct, secondary or induced, and indirect losses in its sequence, and into casualty (injury and death) and economic losses in its final measures. Fires, flood and ground failures induced by a strong earthquake are the common secondary disasters. Direct loss includes casualty and economic losses directly from the earthquake damage of the exposure items and also the direct loss from induced disasters. The direct losses are usually expressed as a vector, composed of both casualty and economic loss as its elements, and casualty may be expressed by two elements: the number of heavy injury and the death. Heavy injury means hospital treatment is required and that will mean a temporary loss of labour. Light injury may not be considered because it costs almost no economic loss. Indirect loss is only economic loss due to loss of labour, energy supply, material supply and capital investment. Indirect loss may come from regions far away, if those regions are commercially connected to the region subjected to earthquake damage. In addition to the losses mentioned above, there might be other losses such as political effect from a sudden and heavy loss and a great disorder in the capital of a nation, but it will not be discussed here. It is also possible that a strong earthquake disaster may in some cases bring a temporary increase of the demand of a certain branch of business, for example, the construction business because of the emergent need of reconstruction of damaged buildings and the added investments from the recovery and reconstruction financial aids allocated by the government, but it costs a loss of investment in other part of the nation.

4.2 Direct loss-damage relations DL(D)

Direct loss DL due to damage of an item of the exposure is related directly to the damage state D and the type and the cost or value of the item. For example, if a schoolhouse is damaged at school time, the casualty will be high; and for a warehouse, there will be little

change of loss of life.

Direct loss ratio has been defined in Eq. (3.1) and examples are given in Tables 3.1 and 3.2 in Sect.3.1. Other data are given in Table 4.3. It should be mentioned here that loss ratios may also be given to intensity I . For one intensity, the structures may be damaged to different damage state, because of various uncertainty factors existed in quality of structure and site intensity. An overall loss ratio for a given intensity of a certain type of structure is then defined as the sum of the loss ratios of all damage states possible for a given intensity [Yin 1995].

4.3 Direct losses DL(D) --- casualty and direct economic loss

Once the direct loss ratios are estimated, the direct loss estimation will be only a pure mathematical computation by summing up all items of exposures in the region. Several points should be mentioned in this respect as follows.

- (1) Number of persons inside a house is time-dependent. During school hours, schools will be full of students; during working hours, offices will be full of workers; in the evening, theatres may be full of audience. It is then necessary to find out the time-dependent ratio of people in a house.
- (2) For an old building, depreciation of the cost should be considered.
- (3) Estimation of casualty is very uncertain. Different estimates may vary by an order of magnitude.
- (4) Estimation of direct loss ratios is also uncertain and it varies from region to region.

Direct loss ratios may be evaluated from past earthquake experience. Table 4.1 is an example.

One additional economic loss is sometimes considered as direct economic loss, such as the building repair time, relocation, property income, and function recovery, but we think it is better to consider them in indirect economic loss.

4.4 Indirect economic loss IL(D) (EERC, 1997; Brookshire, 1997)

Indirect economic loss includes the economic losses in addition to the direct loss of repairing the damaged exposures to their original condition. It includes all other losses to rebuild the society to its original economic condition, such as the following items:

- (1) Chain-linked business loss. For example, the reduction of labour due to casualty and heavy injury, the reduction of supply from other business influenced by the earthquake, the reduction of need, etc.
- (2) Debris removal and interruption of transportation.
- (3) Interruption of information and communication.
- (4) Shortage of supply of daily needs
- (5) Fire and inundation

In indirect economic loss, chain action of loss is common, especially in big cities, from the reduction of labour and capital investments and from the malfunctioning of some links in a large network of the commercial, communication and productive chains. The links of the chain may be a highway and railway, may be a communication line, may be a computer, or may even be some personal connection. The scope is not limited within the earthquake-damaged region, and it may reach other cities in other nations. In developed country, this kind of economic network is also highly developed. Just to think of the recent economic disturbance in the South-eastern Asia region, its economic disturbance wave propagated almost to the whole world.

Indirect economic loss is very important for mega-cities but not easy to be estimated after a strong earthquake with reasonable accuracy, say 100%, and even much more difficult to predict before the earthquake. All we can do is to make very rough estimations.

There are two kinds of indirect economic loss estimate approaches, the detail and the overall estimates, as discussed in the following.

4.4.1 Detail estimate of indirect economic loss

The approach tries to follow the loss formation. Indirect economic loss of some branches of production is induced by the loss of functions of some other system due to structural damage. The economic loss of the item of exposure directly damaged by earthquake is considered as direct economic loss. For example, when a cement production factory is damaged by an earthquake, the direct economic loss is taken as the fee required to rebuild it or to repair it to its original earthquake resistant capacity. This factory will produce no or less cement for a period of time, or the amount and period of business interruption, which will cause a reduction of some business of other factories or shops. The economic loss of other factories or shops is the indirect economic loss. The detail estimate approach follows this process of indirect loss formation and makes some estimates. Economic loss of exposures of any kind of business due to landslides, ground failure from liquefaction, earthquake induced fires, tsunami, reduction of labour due to death and heavy injuries, interruption of transportation and information exchanges, are all considered as indirect economic loss. Indirect economic loss of from some business may cause another indirect loss. It is a forward linkage chain-type action. Fortunately, the chain effect attenuates when distance increases, when time goes by. The direct loss is limited to the region attacked by the earthquake, but indirect economic

losses are not confined and may happen thousands of kilometres away from the centre of the earthquake. It was reported that the business in other parts of the world suffers heavy indirect losses too. It is quite easy to understand this situation. For example, if production is reduced in Kobe after the 1995 Earthquake, the export business will be reduced accordingly and the harbour business in other countries may suffer losses too. In short, the indirect economic loss transmitted throughout the regional economy.

The extent of indirect loss depends on several factors of business interaction, such as length of time of production interruption, alternative or redundant links of business connection (sources of supply and markets for products), etc. HAZUS97 (RMS, 1997) suggested a model, based on data from input-output business interaction, accumulated for many years in a region. Helps from business experts are necessary. But the generally applied method is to obtain a rough estimate of the indirect economic loss based on interruption time estimation and a rough guess of the loss on the basis of available disaster data.

To estimate the indirect economic loss by detail follow-up approach, it is necessary to have the so-called functionality restoration function or restoration curve as shown in Fig. 3.1. This kind of functions can be obtained from other disasters or business changes and they will differ for a similar business relation but in different locations. There are examples given in reports listed in the References (ATC-13, RMS1997).

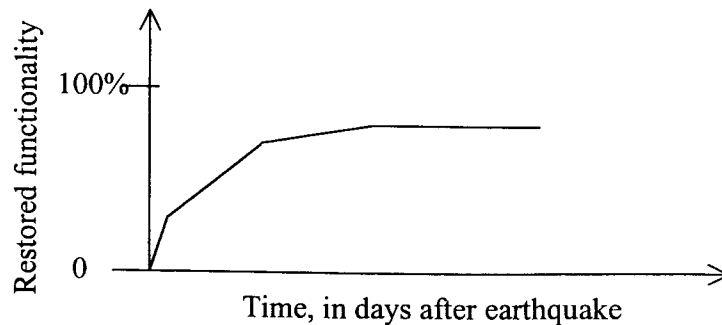


Fig. 4.1: Sketch of functionality restoration function

The indirect economic loss is important but it is difficult to estimate with good accuracy. Theoretically, it is not difficult to formulate the chain economic interaction of business relationship of a society; but the difficulty lies in the lack of data to obtain useful the necessary coefficients of the interrelated chain relationship. The simplest one of such relationship may be the Cobb-Douglas production function

$$Y(K,L) = AK^\alpha L^\beta \tag{4.1}$$

where Y is the total production or output of a system, K and L are respectively the capital and labour inputs, and A, α , and β are numerical constants to be estimated from the input-output

data of the interrelated economic system considered. After a strong earthquake, there will be reduction or loss of capital and labour inputs, ΔK and ΔL or the ratios $\Delta K/K$ and $\Delta L/L$, and the consequent reduction of the product or output ΔY or the ratio $\Delta Y/Y$ can be estimated through the following equation

$$\Delta Y/Y = \alpha \Delta K/K + \beta \Delta L/L \quad (4.2)$$

With adequate input-output data of many years published by the regional government, coefficients α and β may be obtained for each economic system of the region. In general, a

simplified relation may be adopted, i.e.

$$\alpha + \beta = 1.0 \quad (4.3)$$

and the numerical values of α and β usually vary in the ranges of $\alpha = 0.05 - 0.60$ and $\beta = 0.95 - 0.40$, depending on cities and industries. In China, α is small in agriculture, and it is large in industries.

Table 4.1 shows this kind of input-output data obtained in one year in some city in China. With many years data like this, the coefficients α and β can be estimated with acceptable results, as shown in Equation (4.1) and in Fig. 4.2 for input-output relation of agriculture.

$$Y = 4.3623 L^{0.412164} K^{0.587836} \quad (4.4)$$

with $\alpha = 0.41$ and $\beta = 0.59$. Similar relations have been obtained for other branches.

Similar data of input-output relations have been obtained from other cities in China, which give similar results as shown here. Variations will be very large if data are not long enough. In these cases, the relationships obtained are not good and quite doubtful. In case that data are enough and of several tens of years, the coefficients α and β may be considered as time-dependent and the sum of these two coefficients may be different from 1.

Table 4.1: Input/output data between economic items in some city (million Yuan, RMB)

output	item 1	item 2	item 3	item 4	item 5	item 6	final	total
input							product	
item 1	17.39	616.48	0.05	0	32.95	1.84	-307.52	361.20
item 2	111.50	4498.99	1151.01	385.86	349.40	931.66	1640.97	9069.39
item 3	0	0.88	1.41	7.47	32.72	78.94	2146.10	2267.51
item 4	4.58	400.54	144.38	19.17	23.16	120.23	687.88	1399.94
item 5	11.86	274.51	121.31	27.63	61.30	99.30	2054.19	2650.10
item 6	5.25	297.85	75.05	129.04	456.93	401.24	2928.67	4294.02
created	210.62	2980.13	774.30	830.77	1693.84	2660.82		
total	361.20	9069.39	2267.51	1399.94	2650.10	4294.02		

item 1 agriculture item 2 industry
 item 3 construction item 4 transportation
 item 5 commerce item 6 non-material production

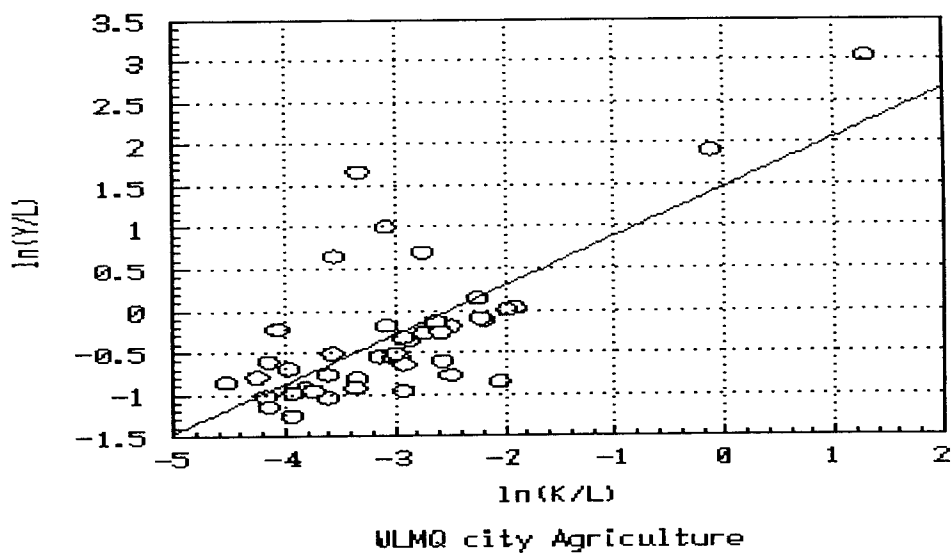


Fig. 4.2: Regression or Cobb-Douglas Function

It is clear from Fig. 4.2 that the scattering of data is large, which is typical of this kind. It is clear also from data given in Table 4.1, where the final product for agriculture in that year is even negative.

4.5 Secondary or induced disasters

Secondary disaster includes fires ignition and spreading, hazardous material storage release, inundation due to dam water release, and field damage due to liquefaction or landslides. Probabilistic estimates have to be made here on the basis of averages from past earthquakes, since fire ignition depends on many chance factors of the timing of earthquake. Earthquake occurs just before dining and with weak gas pipe connection will increase the chance of fire ignition; wind speed and direction will change the fire spreading. These can hardly be predicted with deterministic result and we are forced to accept a probabilistic approach.

Secondary or induced losses will be larger, of course, for those buildings of heavier damage and of relative easiness of being induced to disasters. For example, buildings with wooden walls and floors will be much easier to have secondary fires induced.

4.6 Lifeline system

Lifeline system includes at least the following:

- Railway and highway systems, including bridges,
- Electricity distribution systems,
- Water supply systems,
- Gas supply systems.

And, recently they should include airlines, tele-communication systems, such as telephone, computer network and internets; financial systems such as stocks. A lifeline system or network usually consists of links and nodes and a node is the joint of a number of links, such as the common joint of three water pipes, or a relay station to receive and send electricity of signals.

The direct loss from the damage of a link or a node can be found from the cost of rebuilding it but there are important aspects of losses due to the mal-functioning of the network.. The new problem comes from the function of a network of transferring people, goods, and energy of daily life importance, which introduces a new problem of **connectivity and flow rate**. Connectivity means the possibility of flow from one node in the network to other nodes, while flow rate means the rate of transferring or the amount of materials to be transferred. For example, for an underground water pipeline system in a city, the problem is: (1) can water be delivered to a factory, (2) how much water can be delivered, and (3) if less than normal, how long can it be recovered to normal supply of water after the earthquake. The indirect economic loss or the production of the factory after the earthquake depends on these factors. The bigger and the more developed is the city, the heavier will be the indirect economic loss, and the increment will be highly non-linear. For a small city, the indirect loss may be less

than the direct loss; but for a mega-city, the indirect loss is certainly many times higher than the direct loss in many cases.

4.7 Total loss

The total loss will be the sum of all the losses, direct and indirect, casualty and economic, see Eqs 1.1 and 2.1. It is pointed out here again that the total loss will be given in a vector, with three elements: injury, death and monetary loss. A fictitious numerical example is given here to illustrate the process of damage-loss estimation process. Suppose there are only three multi-story unreinforced brick buildings, 1, 2 and 3, of the exposure in a region with no specific seismic design, subjected to a strong earthquake with intensity IX in the region.

Table 4.2: Vulnerability matrix for multi-story unreinforced brick buildings, $P(R,D | I=7)$ in %

damage state	Intact D ₁	Slight D ₂	Moderate D ₃	Serious D ₄	Partial collapse D ₅	Collapse D ₆
Intensity IX	1.3	6.8	34.3	32.5	9.9	5.2
Bldg. loss (D)	0	5--10	10--40	40--70	70--100	
Content loss (D)	0	0	0	20-40	40--95	
Casualty death ratio	0	0	0	1/40000	1/10000	100
injury ratio	0	0	1/10000	1/5000	1/1000	1/500

Table 4.3: Values of the buildings and contents inside the buildings

	bldg. value	person	content value
building 1	W ₁	N ₁	C ₁
2	W ₂	N ₂	C ₂
3	W ₃	N ₃	C ₃

The vulnerability matrixes VUL of these three items are given in Table 4.2 from Table 3.2. Let then the current values of both the buildings and the contents (number of people N and value C of other contents) inside the buildings are those given in Table 4.2.

In Table 4.3, some loss ratios are assumed.

Suppose that building 2 may be on fire with a chance of 0.5 when building 1 is seriously damaged and that chance will increase to 0.8 when building 1 is partially collapsed or completely collapsed. From data given in Table 4.2, the following data can be obtained by taking the averages of some given ranges in the tables related.

$$SH(P | I) = SH(P | I=IX) = 1.0 \text{ and } SH(P | I I X) = 0$$

The vulnerability and loss ratios for bldg. 1, 2, and 3 are given in Table 4.2.

Table 4.4: Vulnerability and loss ratios for bldg..1, 2, and 3

	D ₁	D ₂	D ₃	D ₄	D ₅	D ₆
VUL(D/I=IX)	0.013	0.068	0.343	0.325	0.099	0.152
building loss ratio (D)	0	0.075	0.25	0.55	0.70	1.0
content loss ratio (D)	0	0	0	0.30	0.60	0.95
death ratio	0	0	0	0.0025	0.01	0.2
injury ratio	0	0	0.0001	0.0002	0.0010	0.001

With all data given above, the direct loss can be calculated according to Eqs.3.2 as follows.

$$SR = SH(P | I) * [VUL(D | I) * (DL(D) * SL(D)) * (1+ID) * EXP] \quad (4.5)$$

$$= [(SR(1) \quad SR(2) \quad SR(3))]$$

SR(1) is the total economic loss, SR(2) the total injuries, and SR(3) the total death.

For the first element (monetary) of the direct loss [VUL(D | I) * DL(D) * EXP]

$$DL(1) = (0.013*0 + 0.068*0.075 + 0.343*0.25 + 0.325*0.55 + 0.099*0.70 +$$

$$0.15*1.0) * (W_1 + W_2 + W_3) + (0 + 0 + 0 + 0.325*0.30 + 0.099*0.60 +$$

$$0.152*1.0) * (C_1 + C_2 + C_3)$$

$$= 0.4889(W_1 + W_2 + W_3) + 0.3090(C_1 + C_2 + C_3)$$

for the second element (injury) of the direct loss

$$DL(2) = (0 + 0 + 0.343*0.01 + 0.325*0.02 + 0.099*0.10 + 0.152*1.0) * (N_1 + N_2 + N_3)$$

$$= 0.16193 (N_1 + N_2 + N_3)$$

$$SR(2) = DL(2) * (1 + ID)$$

for the third element (death) of the direct loss

$$DL(3) = (0 + 0 + 0 + 0.325*0.0025 + 0.099*0.01 + 0.152*0.2) * (N_1 + N_2 + N_3)$$

$$= 0.0401 (N_1 + N_2 + N_3)$$

$$SR(3) = DL(3) * (1 + ID)$$

for the secondary or induced fire loss (monetary) [$VUL(D|I) * DL(D) * (1 + SL(D)) * EXP$]

$$SL(1) = SH(P|I) * [VUL(D/I) * DL(D) * SL(D) * EXP]$$

$$= (0 + 0.325*0.5 + 0.099*0.8 + 0.15*0.8) * W_2 + [0.325*(1-0.30) + 0.099*(1-0.60)] * C_2$$

$$= 0.36178W_2 + 0.02671C_2$$

$$SR(1) = (DL(1) + SL(1)) * (1 + ID)$$

4.8 Scales of seismic risk assessment

SRA may be classified into four different scales: the world or national scale, regional scale, city scale and individual scale, according to the level of details required. The procedure and data required may be quite different, as shown in table 4.6 below. The world or national scale will be described in some details in the later sections, the city scale is the main concern of this lecture, and the other two scales will be mentioned briefly in this section.

The regional scale SRA is actually something in-between those of the world scale and the city scale, with details varying according to the results required and the information and data available.

The individual scale SRA is actually a dynamic analysis of the structure. Because the structure is very important, such as a historic museum or the key buildings of a nuclear power plant, all possible cases of SHA inputs and consequently their results are investigated. In this case, a probabilistic assessment and scenario earthquakes are usually considered together with the possible variations of the structure. In special cases, model tests may also be considered to help and supplement the computation. The important issue is that the structure should be thoroughly checked for its weak links in design, construction and maintenance so that the structure can be rightly modelled for both linear and non-linear (up to failure) response analysis

Table 4.5: Input and Output of SRA for Different Scales

Scale	input SHA	input EXP	output SRA
World	M	population	global loss
Regional	zonation map scenario earthquake	population & statistics	damage & global loss
City	probabilistic SHA intensity or spectrum	detail EXP with samples	damage & loss distribution & global losses
Individual	spectrum and time history	individual inspection & design drawings	damage detail & dynamic responses

The current standard in non-linear dynamic analysis allows us to obtain a reasonably good answer, as long as the structure is well modelled. The prediction of the seismic ground motion is not very good and full of uncertainties of course, but the responses under the given ground motion can be obtained with some accuracy. If the structure is wrongly modelled, no response can be obtained with any accuracy at all.

For structures of moderate importance, no individual non-linear analysis is necessary, but a check with the vulnerability damage matrix by analytical method with given site-specific spectrum is needed to ensure the correct selection of the empirical estimation.

4.8.1 The world scale of SRA (Chen, 1997; Chan, Chen, Chen, et al. 1998)

Professor Chen (Chen, 1997; Chan, Chen, Chen, et al. 1998) started first to offer a smart and easy way to provide a useful rough assessment of seismic risk for large regions, such as for the whole world or a nation. The main idea is to obtain a rough estimation of the exposure from population and a rough estimation of the seismic hazard from the scenario earthquake.

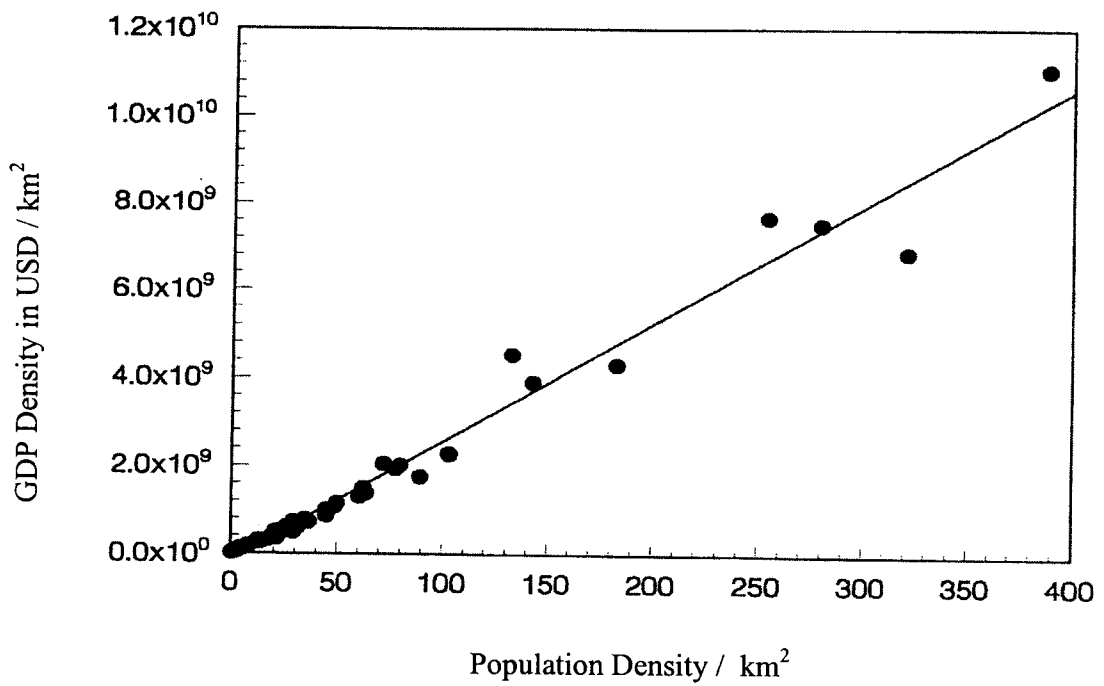


Fig. 4.3: Relationship between population density and GDP in USA (after Chen, 1997).

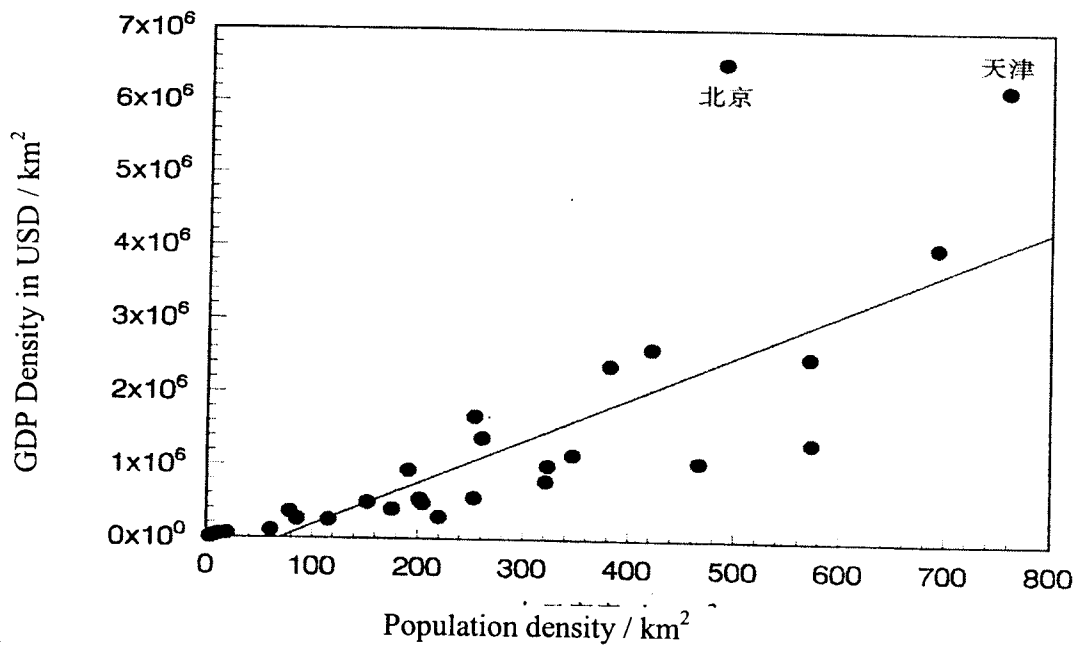


Fig. 4.4: Relationship between population density and GDP in USA (after Chen, 1997).

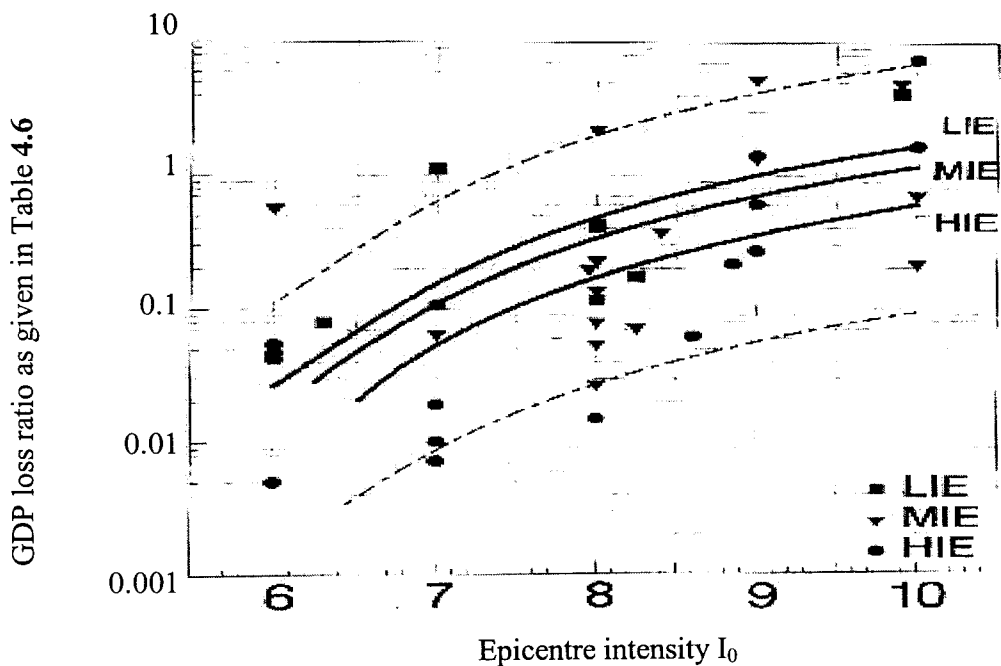


Fig. 4.5: Relationship between the epicentre intensity I_0 and the GDP loss ratio in the world (after Chen, 1997).

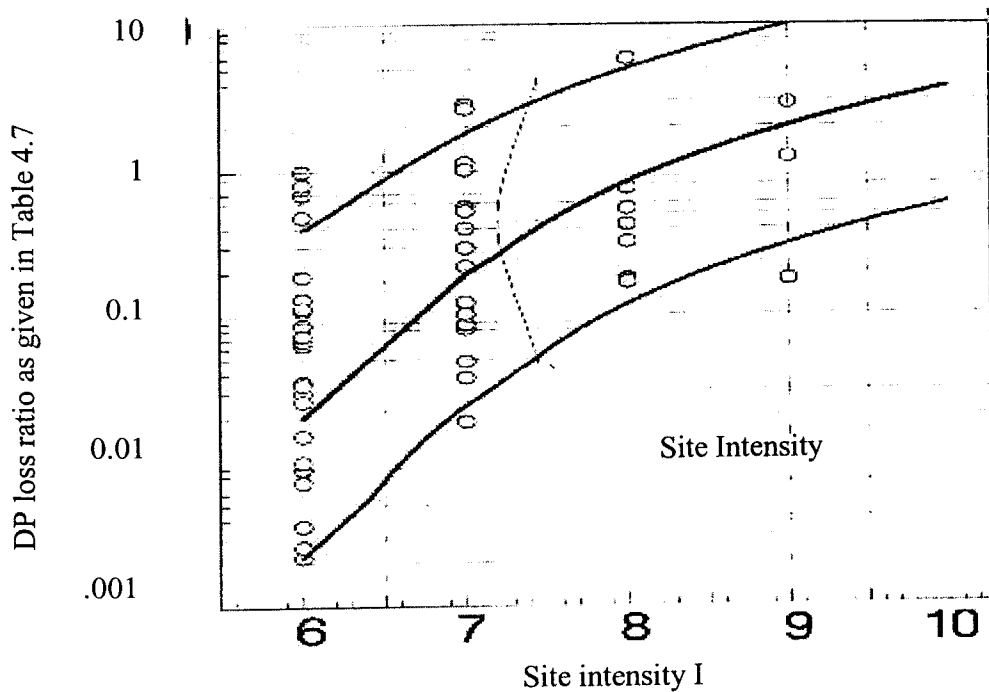


Fig. 4.6: Relationship between GDP loss ratio and earthquake site intensity in China (after Chen, 1997).

Table 4.6: Disaster data of earthquakes in 1980-1995 for establishing $f(I_0, L)$

Date	Latitude	Longitude	M	I_0	Death	Loss L*	LR	Location	Income
19800727	38.2N	83.9W	5.2	6	0	1	0.0042	USA	HIE
19801123	40.9N	15.3E	6.9	9	3114	10000	1.1750	Italy	HIE
19810224	38.2N	22.9E	6.8	8	16	900	1.8493	Greece	MIE
19810426	33.1N	115.6W	6.0	7	0	1.5	0.0060	USA	HIE
19821017	43.2N	12.7E	4.5	6	0	35	0.0355	Italy	HIE
19821213	14.7N	44.3E	6.0	8	2800	90	0.1909	Yemen	MIE
19830502	36.2N	120.3W	6.5	8	0	31	0.0125	USA	HIE
19831108	50.7N	5.3E	4.7	6	2	50	0.0394	Belgium	HIE
19831222	11.9N	13.5W	6.3	8	275	10	0.1667	Guinea	MIE
19831230	36.4N	70.7E	6.5	8	24	3	0.1452	Afghanistan	LIE
19840429	43.2N	12.5E	5.6	7	0	31	0.0084	Italy	HIE
19850510	5.6S	151.1E	7.1	8	1	1	0.0227	New Guinea	MIE
19850703	4.4S	152.8E	7.2	7	0	1	0.0541	New Guinea	MIE
19850729	36.2N	70.9E	6.6	8	5	2	0.0968	Afghanistan	LIE
19860405	13.4S	71.8W	5.3	6	16	22	0.4809	Peru	MIE
19860721	37.5N	118.4W	6.3	6	0	1	0.0457	USA	HIE
19870302	37.9S	176.8W	6.8	10	1	200	1.3825	New Zealand	HIE
19870306	0.1N	77.8W	6.9	9	1000	700	4.3750	Ecuador	MIE
10871124	33.1N	116.0W	6.6	7	0	4	0.0161	USA	HIE
19881106	22.8N	99.8E	7.6	10	930	269	3.4487	China	LIE
19890507	23.5N	99.5E	5.7	7	1	54	0.9432	China-Burma	LIE
19891018	37.1N	121.8W	7.1	9	62	5600	0.2251	USA	HIE
19900620	37.0N	49.4E	7.7	10	55000	500	0.5915	Iran	MIE
19910422	9.9N	82.9W	7.6	10	75	43	0.1792	Costa Rica	MIE
19910704	8.1S	124.7E	6.5	8	23	7.7	0.0601	Indonesia	MIE
19920425	42.0N	123.8W	6.9	9	0	66	0.1800	USA	HIE
19920628	35.2N	118.5W	7.4	9	3	92	0.0518	USA	HIE
19921012	29.7N	31.1E	5.9	8	541	500	0.3561	Egypt	LIE
19930801	15.4N	31.6E	5.2	6	2	0.1	0.0667	Sudan	LIE
19930921	42.3N	122.1W	5.8	7	2	7.5	0.0896	USA	HIE
19930929	18.0N	76.4E	6.3	8	30000	80	0.3399	India	LIE
19940117	34.2N	118.8W	6.8	9	61	15000	0.5083	USA	HIE
19940215	5.1S	104.0E	7.0	9	207	170	1.1333	Indonesia	MIE
19940602	3.0N	75.9W	6.6	8	795	100	0.3138	Columbia	MIE
19950116	34.5N	135.0E	7.2	10	5502	100000	6.1937	Japan	HIE
19950119	5.1N	72.0W	6.6	8	5	2	0.0667	Columbia	MIE
19950514	8.4S	125.1E	6.9	8	6	5	0.1136	Indonesia	MIE
19950527	52.6N	142.8E	7.6	10	1989	110	4.1250	Russia	MIE
19950615	38.4N	22.5E	6.5	8	27	7	0.0455	Greece	MIE

* loss in million USD

Table 4.7: Ratios L_0/L of loss L_0 in epicentre to total loss L

No. of earthquake	M	Intensity range	L	L ₀	Ratio L ₀ /L	Average	
			in 10 ⁴ RMB			I ₀	L ₀ /L
1	6.5	IX – VI	45116	6601	14.6	≥ VIII	0.15
2	6.3	VIII—VI	6720	647	9.6		
3	5.8	VIII—V	10214	828	8.1		
4	5.6	VII – VI	590	380	64.4	VII	0.40
5	5.5	VII – IV	1057	249	23.6		
6	5.7	VII – VI	1903	512	31.4		
7	5.2	VI – V	205	40	19.5	VI	0.80
8	5.1	VI –	730	730	100		
9	5.1	VI –	1481	1481	100		
10	5.3	VI –	165	69	41.8		
11	5.0	VI –	194	194	100		

The idea is carried out first by obtaining a relationship between the GDP (gross domestic product) or GNP (gross national product) and population such as those shown in Fig. 4.3 and Fig. 4.4 respectively for the USA and the mainland of China [Chen, 1997]. Similar relations have been given for other cases and the results are similar to those in Figs. 4.3-4.4. All of them show some linear relationship except for big cities where special modifications are needed. It is possible to obtain the population distribution in the world and in a nation, from which GDP and GNP distributions may be derived.

The second step of this approach is to establish a relationship $f(I_0, L)$ between the epicenter intensity I_0 and the total loss L of the earthquake on the basis of some recent strong earthquakes occurred in the period of 1980 and 1995 in the world as shown in Table 4.7 below. For those earthquakes given in Table 4.7 whose epicenter intensities are not given, they are converted from the magnitude M . The data given in Table 4.7 can then be plotted as shown in Fig. 4.6. Both in Table 4.7 and Fig. 4.6, it is considered that the relationship $f(I_0, L)$ is also a function of the economic development level. The levels used by the World Bank are adopted, where one of three levels is assigned to each country: HIE for high level of development, MIE for moderate and LIE for low. The effect of economic development level can be seen clearly in Fig. 4.5; of course, these curves represent just an average trend, and individual cases may be widely scattered. It should be emphasized again that what is aimed at by this method, perhaps also by all other methods, is but a good average.

The result obtained from the second step is a rough estimation of the total loss of an earthquake of known epicenter intensity I_0 or magnitude. But Professor Chen's group suggested also one step forward, the third step, to derive a relation between economic loss L and local intensity I on the basis of recent earthquakes in China as shown in Table 4.8. In this table, only building losses were considered. The results show very large variation, of course,

but some average values were recommended. The economic loss ratio can then be converted to GDP loss ratio and the final loss function for various intensities.

Dr. Chen (Chen, 1997) obtained similar result on the basis of 55 earthquakes of magnitudes from 4.5 to 6.9 and epicenter intensities from VI to IX, occurred in the mainland of China in the period of 1990 to 1995 and the final result is shown in Fig. 4.6. It can be seen clearly that the variation may be very large; for the same intensity, the loss ratio may vary by two orders of magnitude.

The fourth step is to estimate the seismic hazard of the region from small earthquake data, which are much easier to have than strong earthquakes. For a region of $3^{\circ} \times 3^{\circ}$, the return period of earthquake of magnitude 3 is about 0.07 year, but the return period for magnitude 5 is about 7 years and that for magnitude 7 is about 700 years. Professor Chen's group suggested that it is quite possible to make use of earthquake catalog of magnitude 3. They obtained such a map for China and compared it with the 1990 intensity zonation map, they claim the two maps are quite similar.

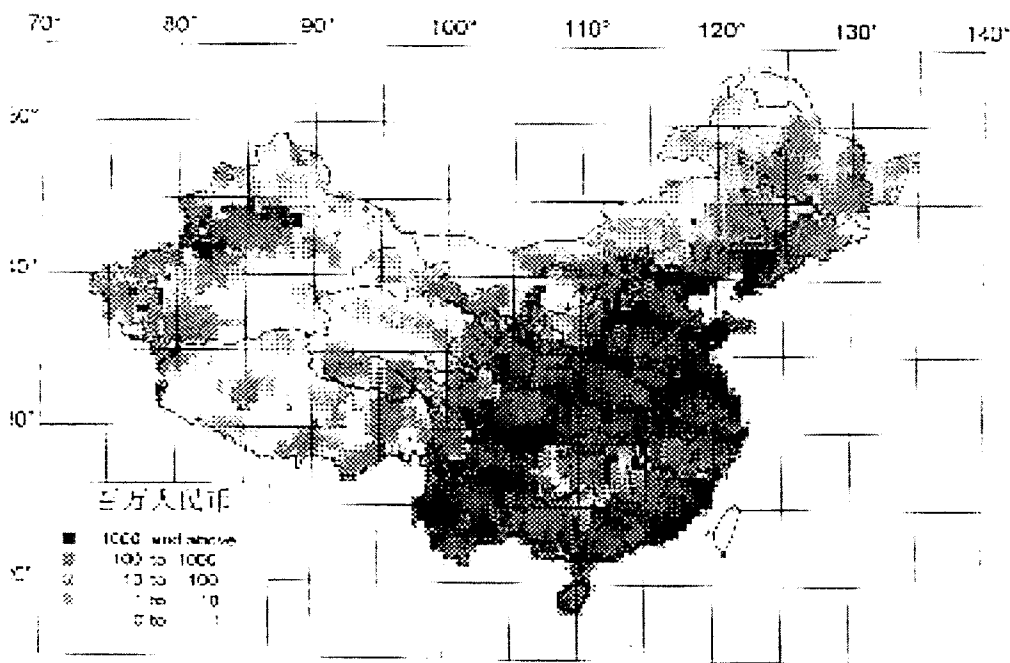


Fig. 4.7: Part of expected seismic direct economic loss from buildings before 2005
(after Chen et al., 1995)
(loss in 10000 Yuan RMB)
(data for Taiwan not included here)

With the seismic hazard map in the fourth step, it is easy to obtain the intensity distribution in the region. And then together with the exposure in terms of GDP distribution in the first step, and the GDP loss ration in the third step, the total loss of the region can then be obtained. Fig. 4.7 shows the loss prediction they obtained for China for a 10 years period from 1995 (Chen, 1997).

The advantage of this approach is its ease and simplicity; its shortcoming is too rough both in its estimation of exposure and in its way of seismic hazard assessment.

4.8.2 The individual scale of SRA

The individual scale is the most detailed way of seismic risk assessment. This approach considers exposures one by one and is applied only to important items, such as nuclear power plant, very high dam, very long bridge, important communication center, and other hazardous material container, arm and other government headquarters. For any one of them, both the seismic hazard and exposure vulnerability should be estimated with all effort.

For seismic hazard, both scenario earthquakes and probabilistic presentation of earthquake are required. The output of the earthquake hazard will be more than a single intensity estimate, ground motion parameters such as peak acceleration, spectrum, strong motion duration and acceleration time histories are sometimes also needed (Hu, 1994, 1996). When it is for long span bridges, special requirement of input ground motion, such as long-period motion and differential motion of pier supports, is also considered.

For site condition, nothing is mentioned in the world scale, but the so-called average site condition is usually taken for granted implicitly because the intensity attenuation relationship is usually based on intensity data obtained on such sites. For the case of individual scale study, the specific site condition should be considered, especially when the site is soft all liable to ground failure due to liquefaction of slope slide. Special studies of possible amplification due to resonance effect are necessary. Permanent ground deformation is an important input required for underground structures, such as underground pipelines and tunnels, and for bridges and other transportation systems.

For the important items, design drawings and in-situ inspection of the structure are required. For very important items, where seismic dynamic behavior is not known, both theoretical and experimental studies are also considered.

When the items are not very important, the requirement may be less strong than what mentioned above, but in-situ inspection of the item is needed to find out the quality of maintenance. And careful estimation of its vulnerability is usually carried out by comparing the results from different methods, such as from experience from past earthquake damage data and also from capacity analysis of its nonlinear response to strong earthquake motion.

4.9 Loss evaluation after a strong earthquake

It is an important job to evaluate the losses caused by a strong earthquake. The total loss evaluated is required to allocate the relief effort as an emergent help to the damaged society; it is also needed for loss estimation or prediction before earthquakes. There are two differences between evaluation and prediction. Firstly, for loss prediction, it is necessary to estimate the possible future earthquakes. It is not easy to make a reasonably good prediction of future earthquake, and that is why one or several scenario earthquakes are usually considered. Secondly, for loss prediction, it is necessary to estimate the vulnerability or the earthquake-resistant capacity of each kind of the exposure, which is not an easy job either. The working procedure for loss evaluation after a strong earthquake is outlined in Chapter 3. A real

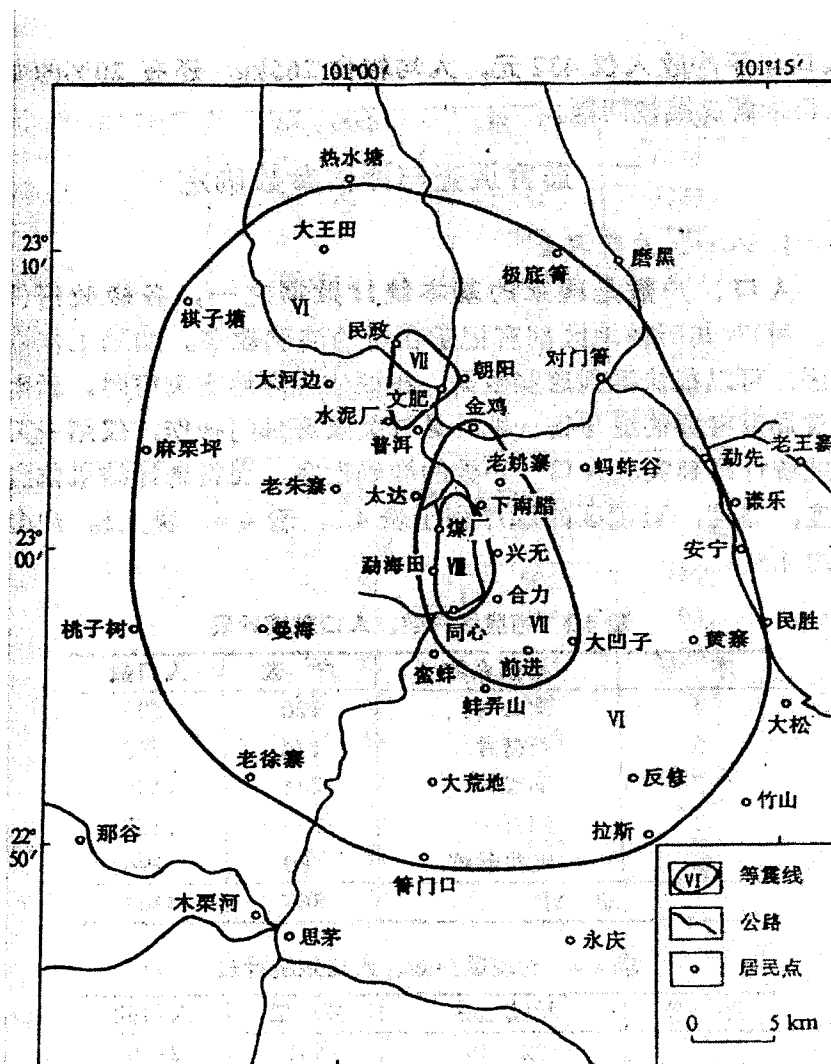


图 4.3 1993 年 1 月 27 日云南普洱 6.3 级地震等震线图

Fig.4.8: Isoseismals of the 1993 Pu-Er Earthquake
(after State Seismological Bureau and State Statistical Bureau, 1996)

example of the Pu-Er earthquake of magnitude 6.3 occurred on 4:32 am of January 27, 1993 in Yuan-Nan Province of Southwest China is shown here (State Seismological Bureau and State Statistical Bureau, 1996; Li, 1995).

The isoseismal lines of this earthquake are shown in Fig. 4.8. The epicenter intensity is VIII of the Chinese Intensity Scale, which is roughly similar to MMI and MSK or the new EMS. The focal depth is 14km. Areas of intensities VIII, VII and VI are respectively 20, 113 and 1174 km², and the total area of disaster is then 1307 km². In the two counties inside the disaster region, the population is roughly 79,000, and more than 80% of them are farmers.

The loss evaluation is carried out separately in the three regions of intensities VI, VII, and VIII, and the economic loss is evaluated by samplings.

4.9.1. Some basic data

The basic parameters for loss evaluation include the total number of buildings or building construction area, population or number of families, average unit prices of buildings and average content values inside the buildings in the region and loss ratios. They can be estimated in some way similar to those given in the following steps for Pu-Er case.

4.9.1.1 Average areas A_s and total areas T_s of building construction in a region

On the basis of data of population and number of families obtained from the local government, the total building construction area can be estimated from the following empiric relation

$$T_s = \xi A_s H_s \quad (4.6)$$

where ξ - an empiric coefficient for buildings of public use, usually varying in the range of 1.0 – 1.2;

A_s - the average construction area per family. This is a very important factor and may be obtained from sampling inspection or from local authorized sources; $A_s = 125 \text{ m}^2$ per family is used here for Pu-Er case;

H_s - the total number of family;

s - a subscript for the type of building.

For the case of Pu-Er, it is obtained then for the region of intensity VIII

$$T_s = 1.2 \times 125 \times 869 = 130,350 \text{ m}^2$$

4.9.1.2 Number of buildings in each intensity region

Number of families and number of buildings can be obtained from the local government in

China, but modifications may be needed to make it up to date. For Pu-Er case, these numbers in three intensity regions are shown in Table 4.9.

Table 4.8: Populations and building areas in various regions of intensity.

Intensity I	No. of Families	Population	Building Area (m ²)
VIII	869	4,363	130,350
VII	4,028	17,667	604,200
VI	12,432	57,281	1,864,800

Table 4.9: Age reduction coefficient C_i.

age (year)	1—10	11—25	26—50	more than 50
i	1	2	3	4
C _i	0.9—1.0	0.7—0.9	0.5—0.7	0.2—0.5

4.9.1.3 Unit price B_s of building

Unit price B_s of building type s may be estimated by the following empiric relation

$$B_s = C \times BD \quad (4.7)$$

where BD - the unit price obtained on the basis of sampling or from local authorities;

C - an average coefficient of the age reduction of price, obtained from the following formula:

$$C = C_1 B_1 + C_2 B_2 + C_3 B_3 + C_4 B_4 \quad (4.8)$$

Where C_i and B_i --- respectively the reduction factor and the fraction of the building of age i in the group. The coefficient C_i can be found from Table 4.10 for the Pu-Er case. In this table, the percentages of buildings of each age group are also given.

For the Pu-Er case, values in Table 4.10 are used and the average unit price is then

$$C = 0.4 \times 1.0 + 0.3 \times 0.8 + 0.2 \times 0.6 + 0.1 \times 0.4 = 0.8$$

If the average construction cost now in that region is taken as 200 Yuan/m², the current average value of the building will finally be

$$B_s = C \times BD = 0.8 \times 200 = 160 \text{ Yuan/m}^2.$$

4.9.1.4 Loss ratios of contents inside buildings

Content loss ratios are evaluated on the basis of samplings. Sampling is usually concentrated on buildings subjected to heavy damage and collapse, because slight damage and moderate

Table 4.10: Age reduction coefficient C_i used for Pu-Er.

age (year)	1—10	11—25	26—50	more than 50
age group i	1	2	3	4
C_i	1.0	0.8	0.6	0.4
% of buildings	40	30	20	10

damage causes usually no content loss. Tables 3.2 and 4.2 list some values obtained from past earthquakes in China.

4.9.2 Loss ratios η for Pu-Er case

Referring to data obtained from previous earthquakes, such as those given in Table 4.1 and considering the local situation, loss ratios given in Table 4.12 are used for the Pu-Er wooden buildings.

Table 4.11: Loss ratio η_j for wooden building in Pu-Er.

Damage state D_j	Collapse	Heavy	Moderate	Slight	Intact
j	1	2	3	4	5
Loss ratio %	80	40	20	5	0

4.9.3 Damage ratios for the wooden buildings in Pu-Er (State Seismological Bureau and State Statistical Bureau, 1996; Li, 1995)

Damage ratio is defined as the ratio of number of buildings suffered a damage state $\lambda_j =$ to the total number of buildings in a region, or

$$\text{Damage ratio } \lambda_j = \text{No. buildings of damage state } D_j / \text{No. all buildings} \quad (4.9)$$

On the basis of sampling on-situ, values obtained for Pu-Er case are given in Table 4.12. Note here that for higher intensities, the percentages of heavy damages are increasing. It is a

distribution of damage ratios of various damage states in a region of given intensity.

Table 4.12: Distribution of damage ratio λ_j in % in regions of various intensities

Intensity	$D_j = \text{Collapse}$	Heavy	Moderate	Slight	Intact
VIII	0.99	41.60	37.78	17.39	2.24
VII	0	14.85	33.38	39.12	12.65
VI	0	4.20	13.76	44.28	37.76

4.9.4 Construction area of buildings of a damage state

The total construction area of buildings of a damage state D_j in region of all intensities from VI to VIII in Pu-Er case can be easily calculated. For example, the total area of heavy damage ($j=2$) is

$$DT_{j=2} = \Sigma \text{Total construction area} \times \lambda_{j=2}$$

$$= 130.350 \times 0.416 + 604,200 \times 0.1485 + 1,864,800 \times 0.042 = 22271 \text{ m}^2$$

The summation is taken over all regions of intensity VI, VII and VIII here for PU-Er case. The final result of construction areas of buildings suffering all damage states is given in Table 4.13 below for the Pu-Er case.

Table 4.13: Areas of buildings of different damage states for Pu-Er

Damage state D_j	collapse	heavy	moderate	slight
Area (m^2)	1,290	22,271	507,898	1,084,764

4.9.5 Number of homeless residents

Residents in buildings damaged to a state of collapse or heavy are considered homeless and those in buildings damaged to moderately damage state are considered to have a 50% chance to live in temporarily.

Taking construction area being $1.2 \times 125 = 150 \text{ m}^2$ and 4 persons per family, the number M of homeless persons is then

$$M = (1290 + 22,271 + 507,898 \times 1/2) / 150 = 12,734$$

4.9.6 Total economic loss from damaged buildings L_B

The total economic loss from damaged buildings L_B is calculated as the sum of losses of buildings of all damage states, of all types of buildings, and in regions of all intensities as given by the following formula

$$L_B = \gamma \sum \sum \sum [\lambda_j (s, I) \eta_j (s) B_s T_s (I)] \quad (4.10)$$

where subscript j --- for damage state

s --- for building type

I --- earthquake intensity

λ --- damage ratio

η --- loss ratio

γ --- a modification factor to consider other factors not considered

and the three summations are taken over damage states j , building types s and intensity I . Taking $\gamma=1.2$, the final loss is then

$$\begin{aligned} L_B &= 1.2 \times 160 \times 130350 \times (0.8 \times 0.099 + 0.4 \times 0.4160 + 0.2 \times 0.3778 + 0.05 \times 0.1739 + 0 \times 0.0224) \\ &\quad + 1.2 \times 160 \times 624200 \times (0.8 \times 0 + 0.4 \times 0.1485 + 0.2 \times 0.3338 + 0.05 \times 0.3912 + 0 \times 0.1265) \\ &\quad + 1.2 \times 160 \times 1864800 \times (0.8 \times 0 + 0.4 \times 0.0420 + 0.2 \times 0.1376 + 0.05 \times 0.4428 + 0 \times 0.3776) \\ &= 47,197,300 \text{ Yuan} \\ &= 4.7 \text{ million Yuan} \end{aligned}$$

4.9.7 Economic loss of other engineering works

There are other kinds of engineering works in Pu-Er region. The losses of these items of exposure were evaluated item by item. The results are listed in Table 4.15 below.

Table 4.14: Direct economic losses of other engineering works in Pu-Er.

Engg Work	Town House	Industrial	Hydraulic	Army	Lifeline
Loss in 10^4 Yuan	601	798	367	84	100

4.9.8 Total economic loss

$$\begin{aligned} L_T &= 4719.73 + 801 + 798 + 367 + 84 + 100 \\ &= 6869.73 \times 10^4 \text{ Yuan} = 6.9 \text{ million Yuan} \end{aligned}$$

4.9.9 Death and injury

No death was reported in this earthquake and heavy injury reaches 24 persons.

4.9.10 Softwares for SHA and SRA

The first published and widely used software, a FORTRAIN program for probabilistic seismic hazard assessment (SHA) is perhaps that by McGuire, but the modern software means usually not a FORTRAIN program, but a whole set of software, including geographic information system (GIS) of data base, data formation, retrieval, analysis and display of SHA and SRA. The first and popularly used one of this kind is perhaps the commercial software IRAS on MAPINFO by Prof. H. Shah of RMS.

There are many software packages for both SHA and SRA available in the world now. The first published and widely used software, a FORTRAIN program for probabilistic seismic hazard assessment (SHA) is perhaps that by McGuire, but the modern software means usually not a FORTRAIN program, but a whole set of software, including geographic information system (GIS) of data base, data formation, retrieval, analysis and display of SHA and SRA. The first and popularly used one of this kind is perhaps the commercial software IRAS on MAPINFO by Prof. H. Shah of RMS.

There are many FORTRAN programs in China now for SHA, either for zonation and/or for individual engineering sites. There are also several programs for SRA or damage-loss assessment, most of which are referred to direct damage and losses based on average estimations of vulnerability of ordinary buildings. Starting from the Urumqi case study, individual assessment of important items of engineering works has been considered.

5. RISK MANAGEMENT

5.1 Risk management

Risk management usually means a government or societal action, which aims at reduction of possible losses before earthquake attacks a region. There is enough experience for ordinary hazard and risk management, such as traffic, fire and flood, but not so for earthquakes, which may happen daily, monthly or every decade. But for earthquake, it may not happen once in a lifetime in a region and people easily forget its harm and are not willing to take counter-measures. Especially in developing regions, people care first of their daily lives before they have enough money for better earthquake-resistant buildings. People, at least the engineers and government officials, in developing regions of seismically active area know that masonry is not good at all, but they can not afford to have steel and reinforced concrete for their

houses. There will be an important problem then for us to pay special attention to earthquake risk management.

Risk management is a kind of counter-measure of safeguarding the people from the rare but dangerous attack of strong earthquakes. It tries to estimate first the probable earthquake risk in a region, and then to suggest possible ways to mitigate the risk as much as necessary and possible with possible financial and technical support.

Traditional risk management, a decade ago, was to have some report made before earthquakes, which may not be easy for government officials to read and make decisions. With the modern development of technology of GIS, the risk management today has the following advantages: (1) easy to understand and apply with visual and sound facilities, (2) easy to find out quickly the results of their decisions, (3) easy to modify and update quickly their societal wealth (building, road, utility, population, etc.), and (4) easy to combine the earthquake risk management with their daily risk management.

5.2 Laws and standards

For earthquake risk management, there are laws for a nation and its provinces and also standards or requirements to be followed. For example, in the United States of America there were Federal Acts and Public Laws on mitigation of earthquake disasters since 1977 and its revised editions in later years. Earthquake related technical problems are generally managed by FEMA (Federal Emergency Management Agency) and studied by NSF (National Science Foundation), USGS (U. S. Geological Survey) and other institutions. FEMA has many contracts with other institutions to carry out studies on specific topics, Among them, NEHRP(National Earthquake Hazards Reduction Program) deserves particular attention in providing model seismic design code for the safety of new buildings and also in drafting provisions for the safety assessment and rehabilitation of existing buildings. The recently completed HAZUS97 for earthquake loss estimation methodology is the product of a contract from FEMA and NIBS (National Institute of Building Sciences). In Japan there are similar laws and provisions. If the United States of America emphasized on the disaster mitigation measures before earthquake, then Japan emphasized also the disaster mitigation during and immediately after a strong earthquake.

5.2.1 The Chinese efforts on earthquake disaster mitigation

5.2.1.1 Development of practical implementation of earthquake disaster mitigation in China

Since the seventies, earthquake disaster mitigation was considered primarily through earthquake capacity assessment and strengthening of existing structures in many cities, such as Beijing, Xi'an and Tianjin, as well as of structures in large factories and enterprises in regions of high seismicity. In the nineties, following the trend of the world, such as the call

for an International Decade for Natural Disaster Reduction, earthquake disaster mitigation plans of whole cities are carried out in China. In this period, losses of all kinds of structures in the city and indirect economic losses are considered, together with the application of high-technology such as the geographical information system (GIS) to facilitate the implementation by the government.

5.2.1.2 Relevant laws, acts and standards in China

There are laws, acts and standards in China for earthquake disaster mitigation. The highest level laws are from the Standing Committee of the People's Republic of China and the State Council, below that there are laws, orders and standards from the Provincial Governments and Ministries. The following laws and standards are closely related to earthquake disaster mitigation.

5.2.1.3 National laws and standards

Law of the People's Republic of China on Protecting against and Mitigating Earthquake Disasters, 1998

Seismic design code of buildings GBJ 11-89, 1989

Seismic design code of structures GB 50191-93, 1993

5.2.1.4 Province and ministry regulations

(a) of the China Seismological Bureau-----

Seismic intensity zoning map, 1990 (currently required)

Seismic ground motion parameter zoning map (in preparation)

Handbook for earthquake disaster prediction and evaluation (1993)

Regulations for information management system of earthquake disaster prediction and evaluation in cities (in preparation)

Working manual for earthquake safety assessment of engineering sites, DB 001-94, 1994

(b) of the Ministry of Construction-----

Management regulations for earthquake disaster resistance of building structures, 1994

Temporary regulations for drafting of earthquake disaster mitigation zonation, 1996

5.2.2 Law of the People's Republic of China on protecting against and mitigating earthquake disasters, 1998

Contents:

- Chapter I General Provisions
- Chapter II Earthquake Monitoring and Prediction
- Chapter III Protection against Earthquake Disasters
- Chapter IV Measures for Earthquake Emergencies
- Chapter V Post-earthquake Relief and Reconstruction
- Chapter VI Legal Liability
- Chapter VII Supplementary Provisions

This law specifies clearly the four components of earthquake disaster protection and mitigation, i.e. the earthquake prediction, measures taken before, during and after the earthquake. The last three components are common in the world and will be introduced in the following sections, but the first is not commonly emphasized in the world that will not be discussed further in this lecture.

5.3 The pre-stage --- mitigation planning

The most important thing for mitigating the earthquake disaster is to have a mitigation plan for all the three stages of earthquake disaster mitigation and to implement it in later years. Before the earthquake, there should be a mitigation plan made for and to be implemented by an executive committee. This committee should be powerful to force the city or the country not only to follow the seismic safety requirements in building their city but also to have some emergent organizations ready to act immediately when a strong earthquake occurs. The whole idea is that every thing that can and should be done to mitigate the losses of the considered region should be planned and improved before the earthquake and be ready to implement it when an earthquake is coming. Of course, this plan will be modified according to the real damage cases, which are usually somewhat different from those predicted before the earthquake.

In addition to the loss assessment, the pre-stage plan includes also all measures to mitigate the expected losses. The mitigation measures include engineering measures and non-engineering measures, such as pre-earthquake warning, if possible, and life-saving measures of training and education on earthquake rescuing and emergency management and insurance.

The work should be carried out before the earthquake may be illustrated by quoting the relevant articles of the Chinese Law mentioned in Section 5.2.2 in the following.

In Chapter III, it reads as follows:

“Article 17 The projects built, expanded or rebuilt shall meet the requirements for seismic resistance.”

“Construction projects other than the ones mentioned in paragraph 3 of this Article shall be fortified against earthquakes in compliance with the seismic-resistance requirements specified in the seismic intensity zoning map or the ground motion parameter zoning map issued by the State.”

“Seismic safety shall be evaluated for major construction projects and the construction projects which may induce serious secondary disasters. The requirements for fortification against earthquakes, drawn up on the basis of the results of seismic safety evaluation, shall be fulfilled.”

“The major construction projects mentioned in this Law refer to projects which are of great value to or have a vital bearing on the society. The construction projects which may induce serious secondary disasters mentioned in this Law refer to construction projects which may, as a result of earthquake damage, lead to flood, fire, explosion, leak of a large amount of hypertoxic or strong corrosive materials and other serious secondary disasters, including such projects as large dams, embankments, petroleum and gas tanks and the facilities storing inflammables or explosive substances, hypertoxic or strong corrosive materials, and other construction projects which may induce serious secondary disasters.

“For the construction projects such as nuclear power plants and nuclear facilities, which may lead to serious secondary disasters due to radioactive contamination in the wake of earthquake damage, seismic safety shall be evaluated carefully and the projects shall be fortified against earthquakes strictly in accordance with law.”

“Article 18 The competent administrative department for seismic work under the State Council shall be responsible for drawing up the seismic intensity zoning motion or the ground motion parameter zoning map and for examining and granting approval of seismic safety evaluation results.

“The competent administrative department for construction under the State Council shall be responsible for drawing up the seismic intensity zoning map or the ground motion parameter zoning map and for examining and granting approval of seismic safety evaluation results. “The competent administrative department for construction under the State Council shall be responsible for working out the standard aseismatic design for construction projects of all kinds of houses and buildings and the facilities attached to them and of the urban utilities, except as otherwise provided for in paragraph 3 of this Article:

“The competent administrative departments for railways, communications, civil aviation

and water conservancy and other specialized departments concerned under the State Council shall be responsible for working out the standard aseismatic design for construction projects of railways, highways, ports, wharfs, airports, water conservancy and other special projects respectively.

“**Article 20** The following buildings and structures without the necessary fortifications against earthquakes shall be appraised for their earthquake-resistance capability in accordance with relevant State regulations, and the necessary measures of reinforcement shall be taken:

(1) buildings and structures, which come under the category of, major construction projects,

(2) buildings and structures which may induce serious secondary disasters,

(3) buildings and structures which are of great cultural relic value and are memorable, and

(4) buildings and structures which are located in the key areas under surveillance for and protection against earthquakes.

“**Article 21** The local people's governments concerned shall take appropriate and effective measures against sources of the secondary disasters, such as fires, floods, landslides, radioactive contamination and epidemic diseases, that may occur in the wake of earthquakes.

“**Article 22** The competent administrative department for seismic work under the State Council and the administrative departments or institutions for seismic work under the local people's governments at or above the county level shall, together with the departments concerned at the corresponding level, work out plans for protecting against and mitigating earthquake disasters on the basis of the prediction of the possible earthquake situation and earthquake

It may be mentioned here that the so-called “The competent administrative department for seismic work under the State Council” in Article 18 is the China Seismological Bureau, and “The competent administrative department for construction under the State Council” is the Ministry of Construction.

All the articles quoted above are to be done in the Pre-stage, as discussed in Section 5.3. Chapter 4 of this law is for the on-stage measures and will be discussed in Section 5.5. Chapter 5 is for the post-stage and will be discussed in Section 5.6.

5.4 Weak-link analysis

The purpose of carrying the pre-stage of disaster mitigation. The role of weak-link analysis in risk management is quite similar to the diagnosis in health care of disease treatment. It is important to find out first the health condition of a person and the cause of the trouble, if any, before the suggestion of a prescription. The first step of risk management is to run a SRA and

find out the weak links of the society against the earthquake attack and mitigation plans will be made accordingly to achieve maximum gain for a given amount of input. The seismic weak links of the society are those items of the exposure, whose damage contributes most for the risk. For risk mitigation, there may be various considerations of making the best benefit of the mitigation effort, but the economic principle of seismic mitigation is to make the net gain E a maximum, or

$$E = \text{net gain} = \text{gain} - \text{cost of mitigation} = \text{max.} \quad (5.1)$$

This principle is certainly right, at least in principle. But there are very large uncertainties involved in the estimation of the loss and gain (reduction of the loss) from the modification of the weak link. Usually, the seismic weak links are the old houses, especially those made of adobe or unreinforced masonry, those with no seismic design consideration, and those built on unstable foundations. It is important to notice that the importance of a structure is not measured only on its constructional cost, but also on the induced casualty and indirect losses once it is damaged.

5.5 The on-stage

During a strong earthquake, it is important to save the injured people and to restore the normal life of the society. Technically, it is important to know how well are the lifeline systems behaving so that smooth communication and transportation are possible. New high technology such as GIS, GPS and RS can help.

On-stage mitigation measures include implementation of mitigation plan, rescue of injuries, provision of temporary houses and daily necessities, and restore of emergency communication. All these can be done with a high-tech tool GIS as discussed in the next chapter. The fundamental methodology is try to find satisfactory way to distribute injuries and goods to some place as quickly as possible, which is referred to as “barrier and shortest route analysis”. After a strong earthquake, road and bridges may be damaged and blocked. To send the injuries to the nearest and available hospital as soon as possible, to fight with earthquake-induced fires or hazardous material release, or to distribute appropriate amount of daily needs can be done with the help of GIS.

The newly implemented Law in China gives an overall review of what are usually required at this stage, except that insurance is not mentioned because there is no such policy yet in China for earthquake disasters. It is quite possible to be added to the next edition of this law.

“Article 26 The competent administrative department for seismic work under the State Council shall, together with the departments concerned under the State Council, draw up national emergency preplans for destructive earthquakes and submit them to the State Council for approval.

“The departments concerned under the State Council shall formulate their own emergency preplans for destructive earthquakes in accordance with the national emergency preplans for destructive earthquakes and submit them to the competent administrative department for seismic work under the State Council for the record.

“The competent administrative departments or institutions for seismic work under the local people's governments at or above the county level in areas where destructive earthquakes may occur shall, together with the departments concerned, work out emergency preplans for destructive earthquakes in their own administrative areas in the light of the national emergency preplans for destructive earthquakes and submit them to the said people's governments for approval. All such emergency preplans for provinces, autonomous regions and cities with a population of over one million shall, in addition, be submitted to the competent administrative department for seismic work under the State Council for the record.
.....

“Article 27 The State encourages and gives aid to research and development of technology and equipment for earthquake emergency and rescue.

“Article 28 An emergency preplan for a destructive earthquake mainly includes the following :

- (1) composition and functions and duties of an emergency institution;
- (2) guarantee of emergency telecommunications,
- (3) preparation of manpower, funds and materials for rescue and disaster relief;
- (4) preparation of emergency and rescue equipment;
- (5) preparation for disaster evaluation, and
- (6) a plan for emergency actions.

“Article 30 After the occurrence of a severely destructive earthquake which causes tremendous losses, the State Council shall set up headquarters for resisting the earthquake and providing disaster relief, which shall mobilize the departments concerned to implement the emergency preplan for destructive earthquakes. An office of the said headquarters shall be setup in the competent administrative department for seismic work under the State Council.

“After the occurrence of a destructive earthquake, the local people's governments at or above the county level concerned shall set up headquarters for resisting earthquake and providing disaster relief, which shall mobilize the departments concerned to implement the emergency preplan for destructive earthquakes.

“Article 32 After the occurrence of a severely destructive earthquake, the State Council or the people's governments of provinces, autonomous regions and municipalities directly under the Central Government may take the following emergency measures in the earthquake-

stricken areas in order to deal with the emergency, provide disaster relief and maintain public order:

- (1) traffic control;
- (2) centralized provision and distribution of basic daily necessities such as foods,
- (3) temporary requisition of houses, transportation vehicles and telecommunications equipment, etc.;and
- (4) other necessary emergency measures.

5.6 The post-stage

Temporary living arrangements and medical care of the injuries are the main job immediately after a strong earthquake and reconstruction of houses and the whole city may have to wait for weeks or months later.

“Article 33 After the occurrence of a destructive earthquake, the local people's governments at all levels in the earthquake-stricken areas shall mobilize forces from all quarters to rescue people and mobilize grassroots units and personnel for self and mutual-rescue. The local people's governments at all levels in non-earthquake-stricken areas shall mobilize people from all sectors of society to provide aid to the earthquake-stricken areas in the light of the earthquake situation and the disasters inflicted.

“After the occurrence of a severely destructive earthquake, the State Council shall provide aid to the earthquake-stricken areas and charge the competent department for comprehensive management of the economy with the duty of coordinating the efforts for disaster relief in an all-round way and, together with the relevant departments under the State Council, making an overall plan for the distribution of relief funds and materials.

“Article 34 The local people's governments at or above the county level in earthquake-stricken areas shall mobilize health and medical institutions and other departments or units concerned to provide medical aid to the wounded and do a good job of sanitation and epidemic prevention.

“Article 35 The local people's governments at or above the county level in earthquake-stricken areas shall mobilize the civil affairs authorities and other departments or units concerned to lose no time in setting up shelters and stations for the supply of relief goods and materials, make proper arrangements for the daily life of the victims, and help them to evacuate and settle down in new places.”

In addition to the above mentioned Law, there other two regulations to be followed right after a strong earthquake, which are:

Handbook for earthquake disaster prediction and evaluation (1993)

“The departments concerned under the State Council shall formulate their own emergency preplans for destructive earthquakes in accordance with the national emergency preplans for destructive earthquakes and submit them to the competent administrative department for seismic work under the State Council for the record.

“The competent administrative departments or institutions for seismic work under the local people's governments at or above the county level in areas where destructive earthquakes may occur shall, together with the departments concerned, work out emergency preplans for destructive earthquakes in their own administrative areas in the light of the national emergency preplans for destructive earthquakes and submit them to the said people's governments for approval. All such emergency preplans for provinces, autonomous regions and cities with a population of over one million shall, in addition, be submitted to the competent administrative department for seismic work under the State Council for the record.
.....

“Article 27 The State encourages and gives aid to research and development of technology and equipment for earthquake emergency and rescue.

“Article 28 An emergency preplan for a destructive earthquake mainly includes the following :

- (1) composition and functions and duties of an emergency institution;
- (2) guarantee of emergency telecommunications,
- (3) preparation of manpower, funds and materials for rescue and disaster relief;
- (4) preparation of emergency and rescue equipment;
- (5) preparation for disaster evaluation, and
- (6) a plan for emergency actions.

“Article 30 After the occurrence of a severely destructive earthquake which causes tremendous losses, the State Council shall set up headquarters for resisting the earthquake and providing disaster relief, which shall mobilize the departments concerned to implement the emergency preplan for destructive earthquakes. An office of the said headquarters shall be setup in the competent administrative department for seismic work under the State Council.

“After the occurrence of a destructive earthquake, the local people's governments at or above the county level concerned shall set up headquarters for resisting earthquake and providing disaster relief, which shall mobilize the departments concerned to implement the emergency preplan for destructive earthquakes.

“Article 32 After the occurrence of a severely destructive earthquake, the State Council or the people's governments of provinces, autonomous regions and municipalities directly under the Central Government may take the following emergency measures in the earthquake-

stricken areas in order to deal with the emergency, provide disaster relief and maintain public order:

- (1) traffic control;
- (2) centralized provision and distribution of basic daily necessities such as foods,
- (3) temporary requisition of houses, transportation vehicles and telecommunications equipment, etc.;and
- (4) other necessary emergency measures.

5.6 The post-stage

Temporary living arrangements and medical care of the injuries are the main job immediately after a strong earthquake and reconstruction of houses and the whole city may have to wait for weeks or months later.

“Article 33 After the occurrence of a destructive earthquake, the local people's governments at all levels in the earthquake-stricken areas shall mobilize forces from all quarters to rescue people and mobilize grassroots units and personnel for self and mutual-rescue. The local people's governments at all levels in non-earthquake-stricken areas shall mobilize people from all sectors of society to provide aid to the earthquake-stricken areas in the light of the earthquake situation and the disasters inflicted.

“After the occurrence of a severely destructive earthquake, the State Council shall provide aid to the earthquake-stricken areas and charge the competent department for comprehensive management of the economy with the duty of coordinating the efforts for disaster relief in an all-round way and, together with the relevant departments under the State Council, making an overall plan for the distribution of relief funds and materials.

“Article 34 The local people's governments at or above the county level in earthquake-stricken areas shall mobilize health and medical institutions and other departments or units concerned to provide medical aid to the wounded and do a good job of sanitation and epidemic prevention.

“Article 35 The local people's governments at or above the county level in earthquake-stricken areas shall mobilize the civil affairs authorities and other departments or units concerned to lose no time in setting up shelters and stations for the supply of relief goods and materials, make proper arrangements for the daily life of the victims, and help them to evacuate and settle down in new places.”

In addition to the above mentioned Law, there other two regulations to be followed right after a strong earthquake, which are:

Handbook for earthquake disaster prediction and evaluation (1993)

Regulations for information management system of earthquake disaster prediction and evaluation in cities (in preparation)

The purpose of carrying out a quick in-situ investigation of the earthquake-stricken region is to evaluate roughly the losses so that the government can take adequate emergency measures accordingly, such as providing adequate amount of food, temporary housing, and other daily needs, to the region. Remember that there is almost no earthquake insurance policy in China now, the government aid and voluntary help are all sources for the emergent relief of the disaster.

The regulation for information management system of earthquake disaster prediction and evaluation in cities (in preparation) is a new effort trying to make better assessment of damage and losses through the application of geographic information systems and other high technology for the whole country.

6. GEOGRAPHIC INFORMATION SYSTEM (GIS)

6.1 What is GIS

Geographic information system (GIS) is a computer-oriented information management system of data of a huge amount related to geography. It takes the earth surface, or the latitude and longitude, and, if needed, the altitude, as the coordinates, and stores all kinds of data on earth accordingly. All data, including diagram, picture or map, are digitized and stored in the computer and managed by software, which can then be analyzed in various ways to show the inter-relationship of the elements stored in the computer. All results can finally be displayed in the all forms of geographically referenced information as a movie. Because the data are managed in computer, it is appropriate for emergency management of huge amount of data, such as that in seismic risk assessment and disaster mitigation problem of big cities.

6.2 Features of GIS

GIS has the following features:

(1) GIS provides a link between data and map. All kinds of information of the hazards and exposures in a region are managed in one GIS, such as the distribution or the location of all buildings, infra-structures and lifelines, together with the properties of each of them, including their vulnerability matrices, the contents, and their possible damage conditions under given future earthquake attack are managed in one GIS. Because of this link between data and map, the risk assessment and disaster mitigation measures can then be analyzed and managed inside the GIS.

(2) GIS provides a tool of emergency management. Because of the possibility of rapid analysis and display in computer, fast analysis can be made to assess the damage and losses of a region right after a strong earthquake, and also the corresponding disaster mitigation measures and the effectiveness of the measures.

(3) GIS provides immediate video display to facilitate the executives to make quick decisions of disaster mitigation right after a damaging earthquake.

(4) GIS provides easy dynamic risk management. Here the word “dynamic” means quick and easy update modification of the society exposure and on-line damage and loss analysis and prediction. Big cities develop very rapidly and old structures are replaced by new structures continuously. Buildings, lifelines, roads as well as population are increasing almost daily. Updating is certainly required.

(5) GIS provides a ready extension with other hi-tech methodology such as the global positioning system (GPS) and remote sensing (RS) to facilitate the data possession and a quick assessment of disaster management.

6.3 Contents of GIS

6.3.1 GIS platform

The GIS platform consists of both the software and the hardware. The hardware consists of computer and other accessories, such as digitizer, video- and acoustic-parts. Both PC computer and workstation have been popularly used. The most popularly used software for GIS are ARC/INFO, such as that used in USGS and for HAZUS, and MAPINFO, such as that used at RMS, both in USA. The MAPINFO is much easier to use and cheaper, but the ARC/INFO is more powerful to make spatial analysis of the data stored in GIS. In China, both are popularly adopted now.

6.3.2 Functional requirements

A GIS for risk management should possess the following data or functions.

(1) Basic information data base of necessary three dimensional maps to show the location of all elements or items of the exposure, including roads, buildings and other structures, lifeline systems, seismic and geological conditions, and economic, informational and societal networks.

(2) SHA data, to show the effect of possible or scenario earthquake sources and their effects.

(3) SRA assessment, including possible damage of all items of the exposure and loss estimations, including induced and indirect economic losses. After a prediction or occurrence of a strong earthquake, SRA can be made right away through the GIS with basic information of that region.

(4) Disaster mitigation measures before, during and after a strong earthquake ready to be implemented.

(5) Updating of the platform as well as of the database to follow the fast development of the city or the region.

6.3.3 Framework of GIS

A GIS should be able to accomplish the following duties:

- (1) Display and retrieval of basic data
- (2) SHA
- (3) SRA
- (4) Disaster mitigation measures
- (5) Demonstration of the whole process

6.4 The risk management software system

Risk management may be classified into three stages as: before, during and after a strong earthquake. The pre-stage includes all means to reduce the disaster or risk, such as laws to limit the seismic disaster, land planning, earthquake prediction, earthquake zonation, seismic design and construction, SRA, earthquake insurance, education of people on earthquake protection, and mitigation planning. The on-stage includes implementation of mitigation plan, rescue of injuries, provision of temporary houses and daily necessities, and emergency communication. The post-stage is the reconstruction and restoration of the society with necessary improvements.

6.4.1 Introduction

Generally, a GIS project can be organized into a series of steps or modules. The general sequence may be as follows: design the project and the framework, design the database, input the spatial data, edit and create topology; input the attribute data, manage and manipulate the data, analyze the data, present the results, check the process with examples, and prepare a demo. This process will be generally followed in the following example of the Seismic Disaster Assessment and Mitigation Management of the Urumqi City, completed in 1997 in

China, which is the first one of this kind of a whole city through GIS application. After it, there were several other ones completed or going to be completed for other cities by other institutions, with some modifications.

6.4.2 System demand–supply analysis --- design the project

The purpose of the demand-supply analysis is to select a database of the system, which includes the input-output requirements and the functioning requirements of the database. The input- output requirement analysis of data includes those for graphic display and those for disaster assessment. The graphic data are used mainly to supply data for disaster assessment and base maps for result display. Data for disaster assessment are used directly for numerical computation in the computer. The functioning requirement analysis of the system includes a module analysis to divide the project into several steps or modules and define clearly the content of each module and the inter-relations between the modules.

It is important to notice that there are two main parts of the whole GIS project: the database and the software, which will be described in the following sections for those considered in the Urumqi case. Many other subjects may be added if needed. For example, the site effect analysis and ground failure assessments of slope slide, liquefaction of sandy soils, and relative displacement of active faults. In case of Urumqi City, no such possibilities are considered, partially because of the good site conditions there.

As shown in Fig. 6.1, there are five modules considered: the base map data, earthquake prediction, damage and loss assessment, disaster mitigation, and the system display.

6.4.3 Building the GIS database

(1) The design of the GIS database:

- Boundaries of the study region
- Selection of the coordinates
- The primary data layers
- Feature type of each data layer
- Attribute information of each map feature
- Coding schemes for the map feature and its attribute information
- etc.

(2) Input of the GIS data:

GIS data include two parts, the spatial data and the attribute data, which are held in two different files. The spatial data are the spatial coordinates, on which the attribute data are related. To obtain the spatial data, the maps should be pretreated before sampling; digitization is then followed to obtain the map data in digitized data. This set of files is usually referred to as location data files. The base map is then completed.

The second step is to input the attribute data, which are the necessary to state the characteristics of the map feature described by numbers or characters. The attribute data are usually stored in tabular format, and linked to the feature by an assigned identifier. To input the attribute data, the attribute terms should be determined first. For example, the attributes of a site soil condition, represented by a point on the map, may include the depth, soil type, the shear-wave velocity, etc. Or for a building, its attributes may include the owner, address, type of the building, number of stories, plan area, the date built, the earthquake-resistant capacity or the vulnerability matrix, the design level, etc. This set of files is usually referred to as feature attribute data files.

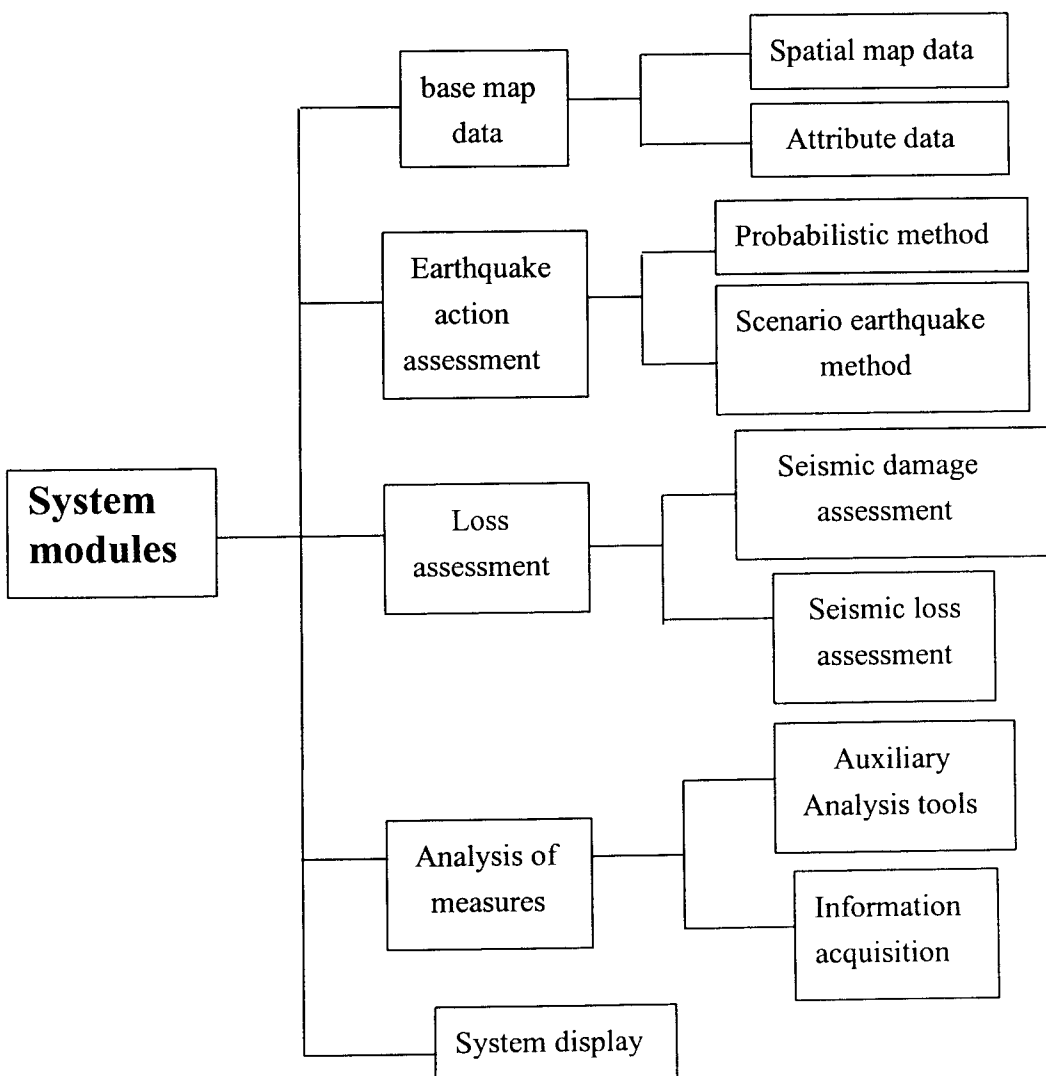


Fig. 6.1: System framework for seismic risk management

(3) Check of the data input

It is necessary to have a careful check of the data input. What have been done for the Urumqi case is as follows:

Spatial data: missing data, extra data, position and shape of the map features, coordinates of sampling points and shape spatial relation of the map features

Attribute data: legal and logic check, for example, if the attribute values out of the assigned scope.

Matching checks of spatial data and attribute data:

This check is based on the uniqueness of the feature coding to check the match between the spatial data and the attribute data to discover if there is any missing feature data.

6.4.4 Building the information system software

(1) The software platform
(omitted)

(2) Main functions of the system:

- Graphic Database: display, retrieval, output and formation of maps
- Earthquake and earthquake action assessment
- Damage and loss assessment
- Disaster mitigation measures
- System display

6.5. Computer programs

In carrying out seismic risk assessment, it is necessary to have some computer programs to estimate the seismic hazard (SHA) for possible future earthquakes and, then to combine with the vulnerability of the exposure, to estimate the seismic risk (SRA), as explained in Section 1.2. There are many computer programs for both SHA and SRA.

Since SHA will be covered by other lectures in this workshop, only those for SRA will be discussed here.

As given in Section 1.2, the SRA is obtained from eq. (1.1)

$$SRA = D \times [L(D) + IL(D)] \quad (1.1A)$$

$$D = SHA \times VUL \times EXP \quad (1.1B)$$

These equations show clearly that the main job of computer part of the SRA is

$$\text{SRA} = \text{SHA} \times \text{VUL} \times \text{EXP} \times [\text{L}(\text{D}) + \text{IL}(\text{D})] \quad (6.1\text{A})$$

for given probabilistic assessment of SHA, or

$$\text{SRA} = \text{P}(\text{I}) \times \text{VUL} \times \text{EXP} \times [\text{L}(\text{D}) + \text{IL}(\text{D})] \quad (6.1\text{B})$$

for a given scenario earthquake of the probability $\text{P}(\text{I})$ of some intensity I for the given region equal to 1, or

$$\text{P}(\text{I}) = 1$$

Once the losses $\text{L}(\text{I})$ for given intensities $\text{I} = \text{VI}, \text{VII}, \text{VIII}, \text{IX}, \text{X}, \dots$ are computed, it is very simple then to compute the losses for given probabilistic hazard assessment simply by a vector multiplication

$$\text{SRA} = \text{SHA} \times \text{L}(\text{I}) = \sum \text{P}(\text{I}) \times \text{L}(\text{I})$$

$$\begin{aligned} \text{SRA} = & \text{P}(\text{VI}) \times \text{D}(\text{VI}) + \text{P}(\text{VII}) \times \text{D}(\text{VII}) + \text{P}(\text{VIII}) \times \text{D}(\text{VIII}) + \\ & + \text{P}(\text{IX}) \times \text{D}(\text{IX}) + \text{P}(\text{X}) \times \text{D}(\text{X}) + \dots \dots \dots \end{aligned} \quad (6.2)$$

6.6 EDEP-03 ----- A computer program for assessment of scenario earthquake losses

In 1993, a FORTRAN computer program EDEP-93 has been adopted in China for rapid loss assessment after a strong earthquake [Li, 1995]. In this case, the exposure and the damage are all known and the only requirement is to evaluate the total loss.

The program consists of a main program EDEP of 280 sentences and a subroutine DALOSS of 61 sentences. Their flow diagrams are given in Fig. 6.2 and Fig. 6.3 respectively. This program has been applied in China to evaluate the total loss in-situ.

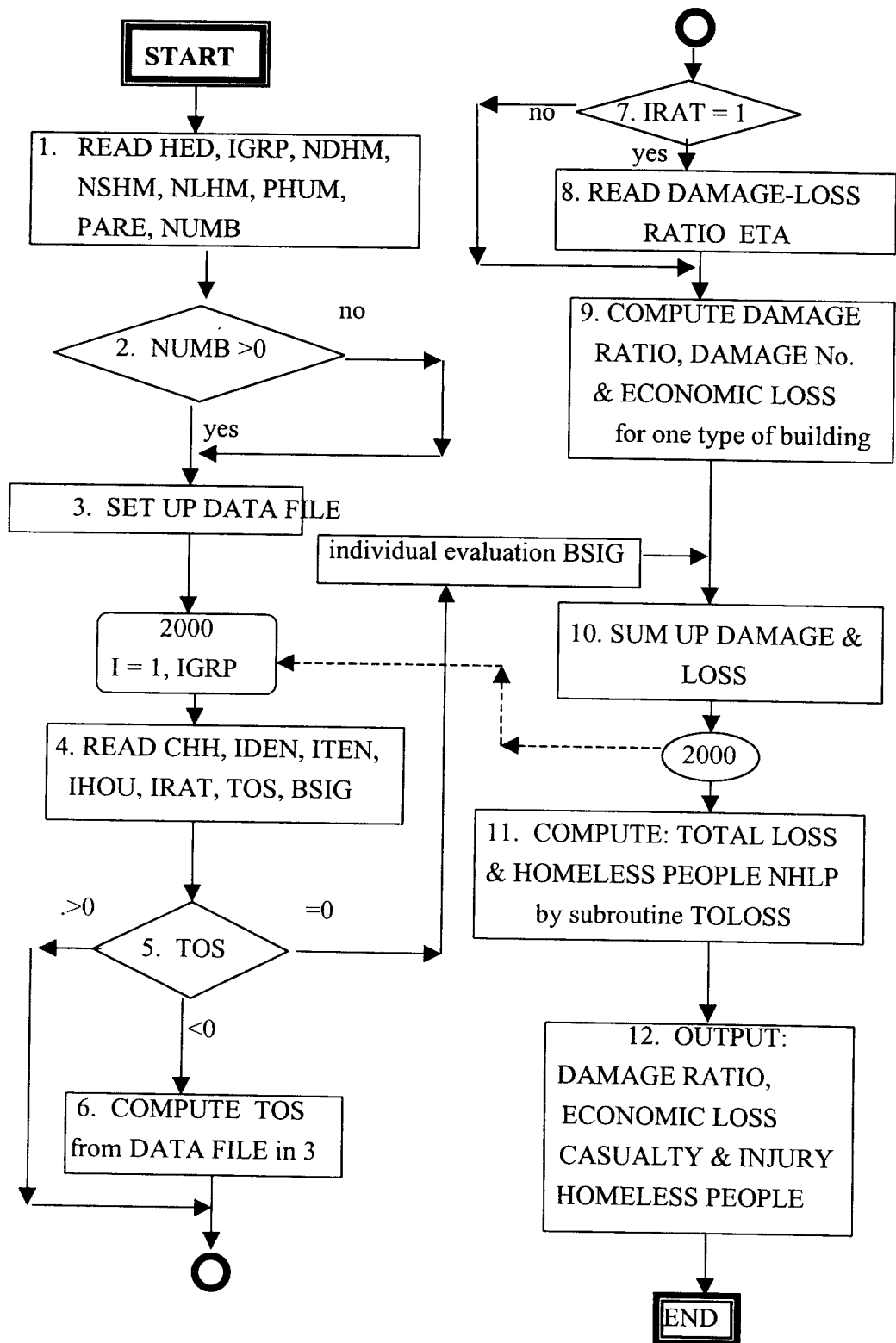


Fig. 6.2: Flow diagram of EDEP-93

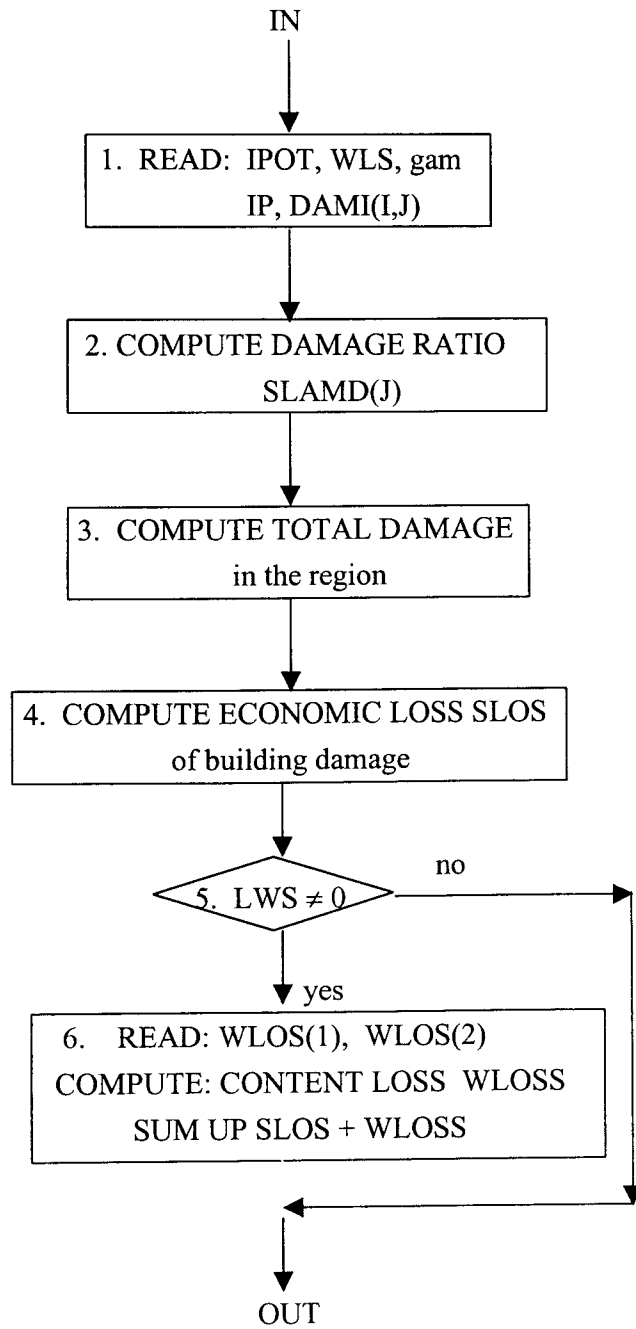


Fig. 6.3: Flow diagram of subroutine DALOSS

REFERENCES

- ATC-13 (1985). Earthquake damage evaluation data for California, Applied Technology Council, FEMA Contract No.EMW-C-0912, Redwood City, California, USA.
- ATC-21 (1988). Rapid visual screening of buildings for potential seismic hazards: A handbook, Applied Technology Council, FEMA-154, Redwood City, California, USA.
- ATC-21-1 (1988) Rapid visual screening of buildings for potential seismic hazards: Supporting Documentation, Applied Technology Council, FEMA-155, Redwood City, California, USA, Earthquake Spectra, v.13, n.4, 1997 Theme Issue: Loss Estimation.
- Brookshire, D.S., et al.(1997). Direct and indirect economic losses from earthquake damage. Earthquake Spectra, v.13, n.4, 683-701.
- Calvi, G.M. (1998). Performance-based approaches for seismic assessment of existing Structures. Proc. Eleventh European conf. on earthquake engineering. 3-19.
- Chan, L.S., Chen, Y., Chen, Qifu, et al. (1998). Assessment of global seismic loss based on Macro-economic indicators, Natural Hazards, v.17, 269-283.
- Chen, Qifu (1997). Seismic Risk Analysis---Simplified Approach, Dr. Thesis, Institute of Geophysics, CSB (in Chinese).
- Coburn, A. and Spence, R. (1992). "Earthquake Protection", John Wiley & Sons
- EERI Committee on Seismic Risk.(1989). The basics of seismic risk analysis, Earthquake Spectra, v.5, n.4.
- Engineering Seismological Research Center (ESRC), et al. (1997). Report of loss evaluation and disaster mitigation of Urumqi City.
- Feng, Qi-Min (Chief Ed.). (1999). Specifications for management and information system of earthquake disaster assessment and evaluation in cities, China Seismological Bureau (in preparation).
- Hu, Yu-Xian (1988). Earthquake disaster mitigation and engineering seismology, IUGG/SSB International Training Course on Continental Earthquakes and Seismic Hazard, 1988, Beijing, China
- Hu, Yu-Xian (Chief ed.). (1994) Working regulation for seismic safety assessment of engineering sites--- DB 001-94. Seismological Press (to be issued as a national standard).
- Hu, Yu-Xian (Chief ed.). (1996). Notes on "Working regulation for seismic safety assessment of engineering sites". Seismological Press.
- Hu, Y.X., Liu,S.C. and Dong,W.M. (1996). "Earthquake Engineering". E&FN, An Imprint of Chapman & Hall.
- IAEE (International Association for Earthquake Engineering). (1996). Regulations for seismic design. A world list -- 1996.
- Kircher, C.A., Reitherman, R.K., Whitman, R.V., Arnold,C.(1997). Estimation of earthquake losses to buildings, Earthquake Spectra.v.13, no.4, 703-720.

- Kiremidjian, A.S. (1998). Multiple earthquake event loss estimation methodology. Proc. Eleventh European conf. on earthquake engineering. 151-160.
- Li, Shu-Zhen. (1995) Earthquake Disaster Evaluation, Seismological Press.
- Liu, H.X. (Chief Editor) (1985). "Damage of Tangshan Earthquake", (in Chinese 1985; English edition to be published soon), Four Volumes.
- Mahaney, J.A., et al. (1993). The capacity spectrum method for evaluating structural response during the Loma Prieta earthquake, National Earthquake Conference, Proc. V.II, 501-510.
- RMS (Risk Management Solutions). (1997). HAZUS97, Technical manual, earthquake loss estimation methodology, FEMA, National Institute of Building Sciences.
- Rojahn, C. et al. (1986). Earthquake damage and loss evaluation for California, Earthquake Spectra, v.2, n.4.
- Shakhramanjan, G.M. et al. (1998). GIS application for vulnerability and seismic risk assessment for some Northern Caucasian cities. Proc. Eleventh European conf. on earthquake engineering. 351-360.
- State Seismological Bureau and State Statistical Bureau. (1996). Collection of earthquake disaster and losses evaluations on the China Continent in 1990-1995, 1996
- Whitman, R.V., et al. (1997). Development of a national earthquake loss estimation methodology, Earthquake Spectra 13, 643-661.
- Yang, Y.D., DuJ, L., and Li, G.R. (1999). Study of sampling in seismic damage prediction. Earthquake engineering and engineering vibration 19, 76-80.
- Yin, Zhi-Qian. (1996). Methodology of evaluation of earthquake damage and loss, earthquake Earthquake Press, 1996.
- Yin, Zhi-Qian. (1995). Content of analyzing earthquake losses in city and the process of countermeasures: Decision-making for disaster mitigation, Journal of Natural Disasters, v.4, n.1, 1995.
- Yin, Zhi-Qian, (1999). Basic framework of urban earthquake risk analysis. Earthquake Engineering and Engineering Vibration v.19, n.1, 70-75 (in Chinese, with English abstract).

METHOD ON PHYSICAL DAMAGE PREDICTION OF BRICK BUILDINGS

Feng Qimin

Institute of Engineering Mechanics, CSB,
29 Xue Fu Road, Harbin, 150080, China
Fax: 86 0451 6664755; E-mail: iem @ public. hr. hl. cn

1. INTRODUCTION

In this century alone, nearly three million people have been killed by the destructive force of earthquakes. The collapse of existing buildings, particularly unreinforced, lightly reinforced masonry construction or brick houses, is the cause of the vast majority of these deaths. Masonry is the world's most common building material and masonry buildings are the most vulnerable to severe damage during seismic events.

Low-Strength masonry (LSM) is a general classification for weak, primarily unreinforced buildings. The three major types of LSM materials are fired brick, stone and adobe (unfired brick). Because the building materials for LSM are readily available and very expensive, LSM is perhaps the most common and often used material by many of the country's citizens.

The collapse of LSM buildings must be prevented to reduced the large number of lives lost in earthquakes. Because of the low strength and large mass of LSM materials; buildings made with these materials sustain substantial damage during large seismic events. The risk of collapse can be reduced with proper detailing and construction techniques. Even through LSM materials are weak and brittle, the structural system of LSM buildings does not have to perform in a brittle manner.

Simple improvement techniques can be used to substantially reduce the risk of collapse. While it is true that extensive cracking will occur in LSM buildings during a major seismic event, structural collapse can be delayed considerable by the inclusion of well designed construction details. The effective design of an LSM buildings can only be performed with knowledge of how construction details to limit the progression of damage and prevent the principal modes of failure.

For the collapse resistance of LSM buildings, good construction details are more important than the elastic strength of the structural elements. In analysing the post-elastic response, it is important to understand that forces required to prevent wall overturning and to hold the broken sections of a wall in place are relatively small. Construction details that have little or no effect on the elastic responses can play a major role in the post-elastic performance and in the ability of on LSM buildings to resist collapse.

In the destructive earthquakes, we had often observed that the most often observed mode of failure of LSM buildings is wall overturned. Because walls are substantial structural components bearing earthquake loads. Walls overturned often could cause collapse of the building. Linear-elastic analysis technique can be used to determine early stages of damage

but can not predict the behaviour of a building as it approaches collapse. Once cracks have occurred, the dynamic response of the a discontinuous masonry building is impossible to predict with presently available analytical tools.

A method on predicting physical damage of LSM buildings is presented in the lecture. The method is based on synthesising analysis and results of damage degree of brick houses observed in several great earthquakes in China. Firstly finding the major parameters which affect on earthquake resistant capability of substantial structure components, the corresponding relation between these parameters and damage degree can statistically calculated. Then construction site condition and construction details can be considered to modify the predicted results. The damage degree could be predicted by these ultimate parameters.

2. PHYSICAL DAMAGE PREDICTION OF MULTI STORY BRICK BUILDINGS

For the brick building, major components to bear earthquake loads are its walls. The roof of the building may be constructed with reinforced concrete slabs or wood frame. Most of the brick buildings in China have 2 to 7 stories, a small amount of the brick buildings has 8 stories, their walls are made of brick materials named as brittle structures.

2.1 Damage types observed in earthquakes

The reasons resulting in the damage of brick buildings come from both aspects: one is the strong ground motion, other is the damage of ground surface such as settlement, liquefaction and ground surface faults.

Only the physical damage caused by strong ground motion will be discussed here. The breaking of wall and collapse of the building have two types: shear type and overturned type.

Most of the buildings would have shear type damage which can be divided into three types:

Inclined tensile damage, firstly inclined crevices caused by positive stresses occur in the walls bearing loads, then slide, stagger, breakdown and falling in occur in succession until the collapse.

The horizontal breaking damage, The horizontal crevices occur along the mortar joint plane of the walls, then horizontal stagger and slide occur.

The last one is bending shear damage, the horizontal crevices frequently occur in both ends of the wall, particularly, in higher wall between windows and doors of the house.

The overturned damage type of building is caused by collapse of the side longitudinal walls.

2.2 definition of the earthquake resistant coefficient

The damage types of the buildings show that the earthquake resistant capability of the brick building depends on the capability of the walls to resist shear loads. Firstly we assume that walls along earthquake direction majority bear earthquake loads, the walls along other direction can be neglected, considering them not to bear any loads. Therefore we adopt many degree freedom mode to simulate the multi story brick building, mass of the each story can be concentrated the its floor position. The horizontal earthquake force of the i th mass and j th modal can be written as the following:

$$F_{ji} = \alpha_j \gamma_j X_{ji} G_i \quad \begin{cases} i = 1, 2, \dots, n \\ j = 1, 2, \dots, m \end{cases} \quad (1)$$

where

F_{ji} - horizontal earthquake force

α_j - affected coefficient corresponding to j th modal

X_{ji} - horizontal relative displacement of j th modal and i th mass

γ_j - participant factor of j th modal

$$\gamma_j = \frac{\sum_{i=1}^n X_{ji} G_i}{\sum_{i=1}^n X_{ji}^2 G_i}$$

G_i - gravity of the i th mass

If the floor slabs have only horizontal movement, the earthquake loads bearded by the walls between both floors can be considered as the distribution according to the section area of the walls, the larger of the section area of the wall is, the larger of the earthquake load bearded by the wall.

The shear resistant strength of the wall under combining horizontal and vertical earthquake loads can be calculated as the following:

$$f_{VE} = 1.1 \zeta_N f_N \quad (2)$$

where

f_{EV} - shear resistant strength of wall

ζ_N - affected factor of positive stresses to design strength, value of the factor.

ζ_N can be selected from the following the table 1.

Table 1

σ_0 / f_N	0.0	1.0	3.0	5.0	7.0	10.0	15.0
ζ_N	1.0	1.20	1.53	1.80	2.04	2.35	2.80

f_N - shear resistant strength of the wall without earthquake resistant design. The value of f_N can be adopted as the table 2.

Table 2

Mortar scale R	150	100	75	50	25	10	4
f_N	2.2	1.8	1.6	1.3	0.9	0.6	0.4

The high of the each story of the brick building can approximately be considered as the equal and the mass is equal also, the primary modal of the building can be defined as the straight line, the relative displacement of the each mass is in proportion to its elevation.

Following mentioned above, the calculation of the earthquake force of the building can be estimated only by the value of the primary modal. So formulation (1) can be rewritten:

$$F_{li} = \alpha_1 r_1 X_{li} G_i$$

$$= \alpha_1 \frac{\sum_{i=1}^n i}{\sum_{i=1}^n i^2} G$$

The shear force of the sth floor of the building with n stories can be calculated as the following formulation:

$$V_s^n = \sum_{i=s}^n F_{li} = \alpha_1 \sum_{i=1}^n i \cdot \frac{\sum_{i=1}^n i}{\sum_{i=1}^n i^2} G \quad (3)$$

the strength of the walls of the each story should satisfy the following equation:

$$V_s^n \leq \frac{f_{VE} A}{\varepsilon \cdot \gamma_{RE}} \quad (4)$$

V_s^n - shear force of the S th floor of the building with n stories.

f_{VE} - shear resistant design strength of the wall

A - section area of the wall

ε - non-uniform coefficient of the shear force distribution

r_{RE} - safety adjustment factor

Following the table 2, we can find that relation between mortar scale R and shear resistant strength f_N , the relation shows a straight line

The formulation of this straight line is:

$$f_N = \frac{R + 35}{70} \quad (5)$$

Similarly the relation between σ_σ / f_N and ζ_N from table 2 can also be simulated with straight line.

The equation of the straight line is:

$$\zeta_N = \frac{\sigma_0}{7f_N} + 1 \quad (6)$$

Substitute equation (5) into equation (6) and (2), we obtain:

$$\begin{aligned} f_{VE} &= 1.1\zeta_N f_N \\ &= 1.1\left(\frac{\sigma_0}{7f_N} + 1\right) \cdot f_N \\ &= 1.1\left(\frac{\sigma_0}{7} + \frac{R+35}{70}\right) \end{aligned} \quad (7)$$

The positive stress σ_0 in the wall of equation (6) only considers static load, not includes added vertical stresses caused by earthquake. σ_0 should be calculated by the following formulation:

$$\sigma_0 = 0.9(n-s+1) \quad (8)$$

where

S - is the floor

N - total number story of the building.

Substitute equation (8) into equation (7), we have the following equation:

$$\begin{aligned} f_{VE} &= \left[\frac{0.9(n-s+1)}{7} + \frac{R+35}{70} \right] \cdot 1.1 \\ &= 0.14(n-s+1) + 0.015R + 0.55 \end{aligned} \quad (9)$$

Substitute equation (3) in to equation (4), we obtain the following equation:

$$\alpha_1 \sum_{s=1}^n i \frac{\sum_{i=1}^n i}{\sum_{i=1}^n i^2} G \leq \frac{f_{VE} A}{\varepsilon \gamma_{RE}} \quad (10)$$

G in the equation (10) can be taken as an average gravity of the each story:

$$G = \rho F$$

where

ρ - average gravity of the floor area per unit

F - floor area

So equation (10) becomes the following:

$$\begin{aligned} \alpha_1 \sum_s^n i \frac{\sum_1^n i}{\sum_1^n i^2} \rho \cdot F &\leq \frac{f_{VE} A}{\varepsilon r_{RE}} \\ \frac{A}{F} f_{VE} \frac{\sum_1^n i^2}{\sum_s^n i \sum_1^n i} &\geq \alpha_1 \cdot \rho \cdot \varepsilon \cdot r_{RE} \end{aligned} \quad (11)$$

Substitute equation (9) into right side of formulation (11), we have the following formulation:

$$\frac{A}{F} [0.14(n-s+1) + 0.015R + 0.55] \cdot \frac{\sum_{i=1}^n i^2}{\sum_{i=1}^n i \sum_{i=1}^n i} \geq \alpha_1 \rho_E \tau_{RE} \quad (12)$$

Lets the right side of the formulation (12) equal to K_s^n ,

$$K_s^n = \frac{A}{F} \cdot \frac{\sum_{i=1}^n i^2}{\sum_{i=1}^n i \sum_{i=1}^n i} [0.14(n-s+1) + 0.015R + 0.55] \quad (13)$$

We can see from formulation (13) that K_s^n defines the average shear resistant strength per unit section area of wall and K_s^n has the dimension of shear resistant strength. K_s^n depends on the section area of wall, shear resistant strength f_{VE} , number story of the building and floor number. If K_s^n is the larger, the earthquake resistant capability of the building also is the larger. If we know the construction area of the building, section area of the walls and story number of the building, we can easily calculate the K_s^n . Next we will give the relation between earthquake resistant coefficient K_s^n and damage degrees of building.

2.3 classification of damage degree of brick buildings

Damage degree of brick buildings can be divided into five degrees: intact, slight damage, moderate damage, severe damage and collapse as shown in table 3.

Table 3: Damage Degrees

Intact	Structural components are intact, non-structural components may be slight damage, building can still normally be used without repaired
Slight	Structural components are intact, non-structural components have slight damage and need simply repaired
Moderate	Structural components have breaking or larger displacement, can not be normally used and need repaired
Severe	Structural components have many breaking or stagger, can not be used and need completely repaired
Collapse	Walls are collapse, building need reconstruction

We collected the data of 434 brick houses damaged in different intensity 7 to 10 region in Tonghai Haicheng, Tangshan earthquakes, and divided them into 5 types according to the classification damage degree defined above, calculated coefficient K_s^n of each house using formulation (13), statistically calculated the probabilistic distribution of the K_s^n according to different earthquake intensity and different damage degrees. The statistical results show that

the earthquake resistant coefficient K_s^n of the each damage degree accords with probabilistic normal distribution.

The mean value and standard deviation of the K_s^n of the each damage degree and probabilities can be obtained. The tables 4 to 7 list the occurrence probability of the K_s^n under intensity 7 to 10 region according to different damage degrees. From these table, we can recognize that if K_s^n is less, the damage degree is more severe. A brick building may have several stories, each story have own K_s^n respectively, selecting the minimum K_s^n among all stories as the earthquake resistant coefficient of the building to estimate the damage degree depending on maximum damage probability value.

Table 4: Damage Probability (%) for Intensity 7 area

K_s^n damage degree	0 50	50 100	100 150	150 200	200 250
Collapse	100	85	63	39	14
Severe		15	27	36	31
Moderate			10	21	34
Slight				4	15
Intact					6

Table 5: Damage Probability (%) for Intensity 8 area

K_s^n damage degree	250 300	300 350	350 400	400 450	>450
Collapse	3				
Severe	13	2			
Moderate	26	11			
Slight	34	39	30	14	
Intact	24	48	70	86	100

Table 6: Damage Probability (%) for Intensity 9 area

K_s^n damage degree	100	100 150	150 200	200 250	250 300	300 350	350 400	400 450	450 500	>500
Collapse	100	87	69	36	12					
Severe		13	27	47	38	13	2			
Moderate			4	17	40	39	16	4		
Slight					10	32	44	35	21	
Intact						16	38	61	79	100

Table 7: Damage Probability (%) for Intensity 10 area

damage degree	K_s^n	<200	200	250	300	350	400	450	500	550	600	650	>650
			250	300	350	400	450	500	550	600	650		
Collapse		100	89	64	24	5							
Severe			11	36	66	53	16						
Moderate					10	42	67	41	10				
Slight							17	47	51	33	16		
Intact								12	39	67	84	100	

We are known that site condition of the building, construction detail design and high or low of construction quality significantly affect on the damage degree of the building. Therefore modification must be done by multiplying some modified factors based on the K_s^n calculated above. Modified earthquake resistant coefficient K_s can be obtained by the following formulation:

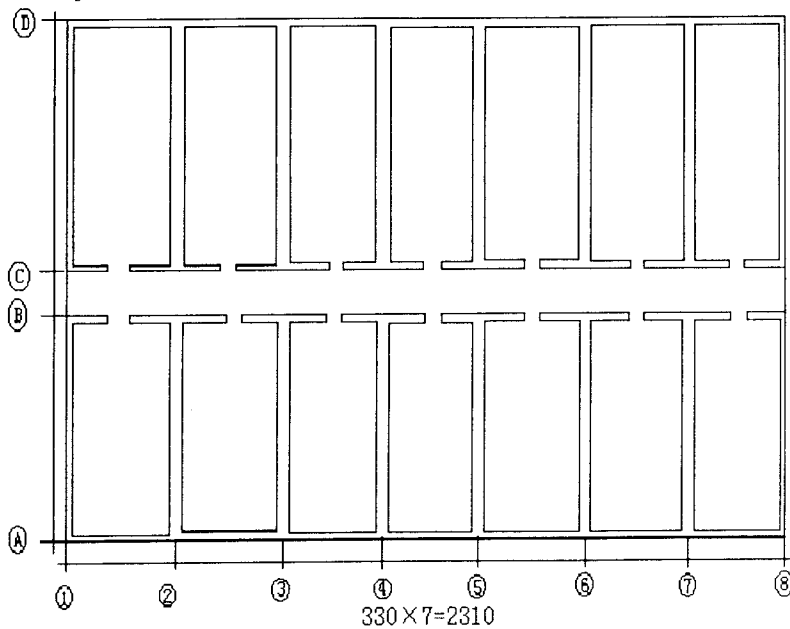
$$K_s = K_s^n \left(1 + \sum_{i=1}^4 c_i \right) \quad (14)$$

where c_i - modified factors. The value of c_i can be obtained from table 8.

Table 8: Values of c_i

Conditions	c_i	
	yes	no
The size of the span between the walls accords with design demands	0	-0.1
The floor slabs have enough stiffness	0	-0.15
The construction technique quality not have any problem	0	-0.2
The design accords with the Building earthquake resistant code	0.2	-0.10

After calculating k_s , the damage degree can be judged by method mentioned above.



Plane of the 4 story house

3. AN EXAMPLE FOR PREDICTION OF THE DAMAGE DEGREE OF A BRICK HOUSE

A brick house has 4 stories with RC floor slab, thickness of the walls are 24cm. Mortar scale is 50 for 1 and 2 story, mortar scale is 25 for 3 and 4 story. The house is designed to resist intensity 8.

First, calculate lateral walls:

$$\frac{A}{F} = \frac{24 \times 15}{4620} \times 0.84 \times 10^4 = 654.5$$

$$K_s^n = \frac{A}{F} \cdot \frac{\sum_1^n i^2}{\sum_1^n i \sum_s^n i} \cdot (0.14(n-s+1) + 0.015R + 0.5)$$

So

$$\begin{aligned} K_1^4 &= 654.5 \cdot \frac{1^2 + 2^2 + 3^2 + 4^2}{(1+2+3+4)(1+2+3+4)} \\ &\quad \cdot (0.14 \times 4 + 0.015 \times 50 + 0.5) \\ &= 645.5 \times 0.3 \times 1.76 \\ &= 345.6 \end{aligned}$$

$$\begin{aligned} K_2^4 &= 645.5 \cdot \frac{30}{(1+2+3+4)(2+3+4)} \\ &\quad \cdot (0.14 \times 3 + 0.015 \times 50 + 0.5) \\ &= 654.5 \times 0.333 \times 1.62 \\ &= 353.4 \end{aligned}$$

$$\begin{aligned} K_3^4 &= 654.5 \times \frac{30}{10 \times (6+4)} \cdot (0.14 \times 2 + 0.015 \times 25 + 0.5) \\ &= 654.5 \times 0.4286 \times 1.13 \\ &= 317.0 \end{aligned}$$

$$\begin{aligned} K_4^3 &= 654.5 \times \frac{30}{10 \times 4} \cdot (0.14 \times 1 + 0.015 \times 25 + 0.5) \\ &= 654.5 \times 0.75 \times 0.99 \\ &= 485.9 \end{aligned}$$

then, calculate the longitudinal walls:

$$\frac{A}{F} = \frac{24 \times 4}{1220} \times 0.68 \times 10^4 = 535.1$$

$$\begin{aligned} K_1^3 &= 535.1 \times 0.3 \times 1.76 \\ &= 282.5 \end{aligned}$$

$$K_2^3 = 535.1 \times 0.333 \times 1.62 \\ = 288.6$$

$$K_3^3 = 535.1 \times 0.4286 \times 1.13 \\ = 259.2$$

$$K_4^4 = 535.1 \times 0.75 \times 0.99 \\ = 397.3$$

Therefore, consider the mean value of longitudinal wall and lateral wall of the first story as the earthquake resistant coefficient $K_c(1)$ of first story of the house.

$$K_c(1) = \frac{1}{2}(345.6 + 282.5) = 314.1$$

similarly,
$$K_c(2) = \frac{1}{2}(353.4 + 289) = 321.2$$

$$K_c(3) = \frac{1}{2}(317.0 + 259.2) = 288.1$$

$$K_c(4) = \frac{1}{2}(485.9 + 397.3) = 441.6$$

Comparing $K_c(1)$, $K_c(2)$, $K_c(3)$, $K_c(4)$, minimum value $K_c(3)$ will be earthquake resistant coefficient of the brick house and be modified, because the building had been designed with earthquake resistant design code of the buildings, here modified resistant earthquake coefficient will be:

$$K_c(3) = K_c(3)(1 + 0.2) \\ = 288.1 \times 1.2 \\ = 345.7$$

Because $K_c(3)$ is 345.7 and the house locates in intensity 8 area, so we should look up the table 5, severe damage probability is 2%, moderate damage probability is 11%, slight damage probability is 39%, intact probability is 48%, so this brick building will be slight damage or intact under intensity 8.

REFERENCES

- Yin Zhiqian, Lishuzhen, Zhaozhi "Prediction of Earthquake Disaster and Disaster Degree" Earthquake Research in China, Vol.7, No.1, 1991.
- Zhao Zhi, "Method on Predicting Damage Degree of Brick Building" Dissertation for Master's degree, Institute Engineering Mechanics, CSB, 1992.
- Feng Qimin, "Prediction of Structural Damage due to Earthquake" Research Report of Institute Engineering Mechanics, May, 1993.